RECENT ADVANCES IN GEOMICROBIOLOGY OF THE OCEAN CRUST

EDITED BY: Beth N. Orcutt, Jason B. Sylvan and Cara M. Santelli

PUBLISHED IN: Frontiers in Microbiology

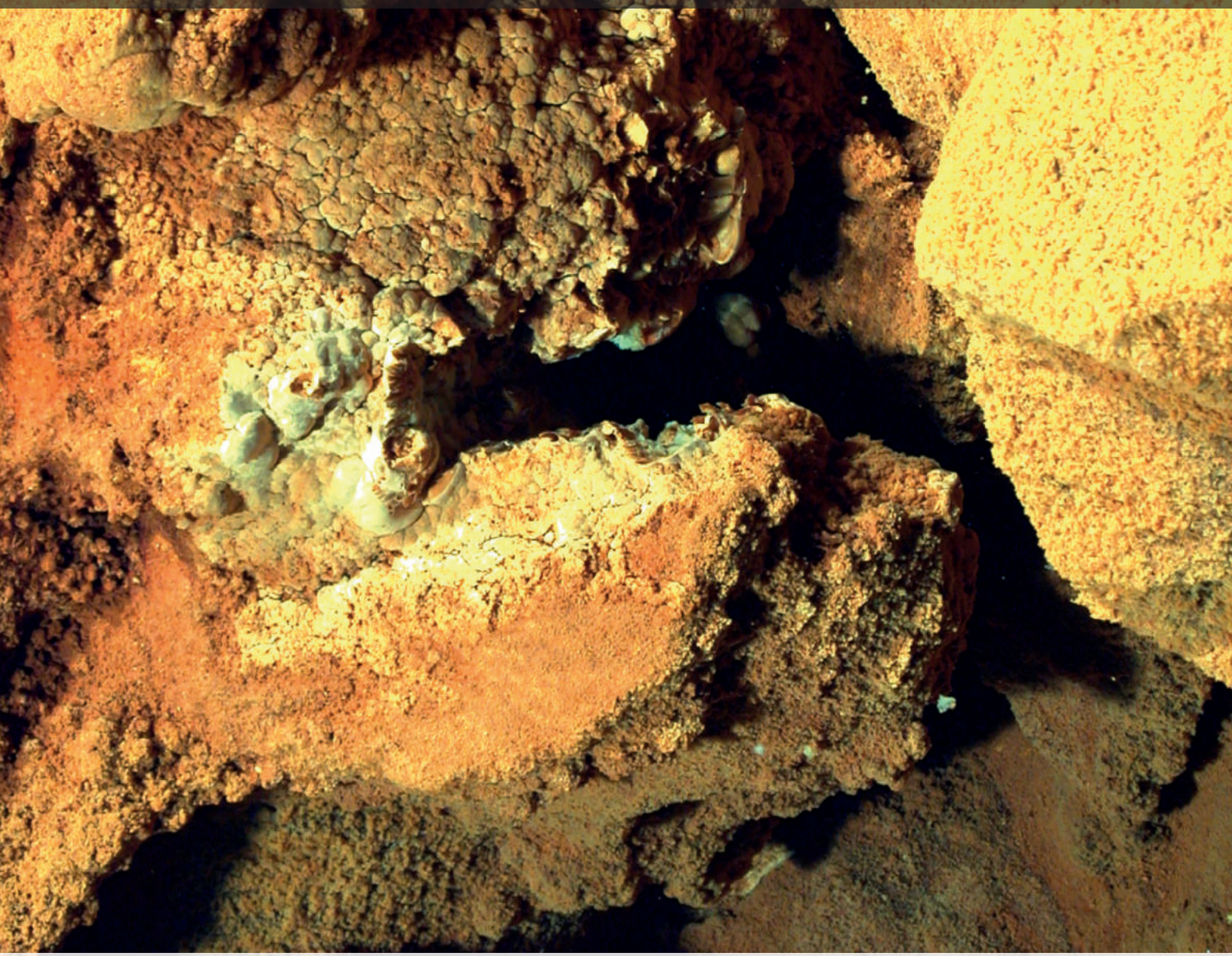

frontiers Research Topics

ISSN 1664-8714
ISBN 978-2-88945-283-5
DOI 10.3389/978-2-88945-283-5

About Frontiers

Frontiers is more than just an open-access publisher of scholarly articles: it is a pioneering approach to the world of academia, radically improving the way scholarly research is managed. The grand vision of Frontiers is a world where all people have an equal opportunity to seek, share and generate knowledge. Frontiers provides immediate and permanent online open access to all its publications, but this alone is not enough to realize our grand goals.

Frontiers Journal Series

The Frontiers Journal Series is a multi-tier and interdisciplinary set of open-access, online journals, promising a paradigm shift from the current review, selection and dissemination processes in academic publishing. All Frontiers journals are driven by researchers for researchers; therefore, they constitute a service to the scholarly community. At the same time, the Frontiers Journal Series operates on a revolutionary invention, the tiered publishing system, initially addressing specific communities of scholars, and gradually climbing up to broader public understanding, thus serving the interests of the lay society, too.

Dedication to Quality

Each Frontiers article is a landmark of the highest quality, thanks to genuinely collaborative interactions between authors and review editors, who include some of the world's best academicians. Research must be certified by peers before entering a stream of knowledge that may eventually reach the public - and shape society; therefore, Frontiers only applies the most rigorous and unbiased reviews.
Frontiers revolutionizes research publishing by freely delivering the most outstanding research, evaluated with no bias from both the academic and social point of view.
By applying the most advanced information technologies, Frontiers is catapulting scholarly publishing into a new generation.

What are Frontiers Research Topics?

Frontiers Research Topics are very popular trademarks of the Frontiers Journals Series: they are collections of at least ten articles, all centered on a particular subject. With their unique mix of varied contributions from Original Research to Review Articles, Frontiers Research Topics unify the most influential researchers, the latest key findings and historical advances in a hot research area! Find out more on how to host your own Frontiers Research Topic or contribute to one as an author by contacting the Frontiers Editorial Office: **researchtopics@frontiersin.org**

RECENT ADVANCES IN GEOMICROBIOLOGY OF THE OCEAN CRUST

Topic Editors:
Beth N. Orcutt, Bigelow Laboratory for Ocean Sciences, United States
Jason B. Sylvan, Texas A & M University, College Station, United States
Cara M. Santelli, University of Minnesota, United States

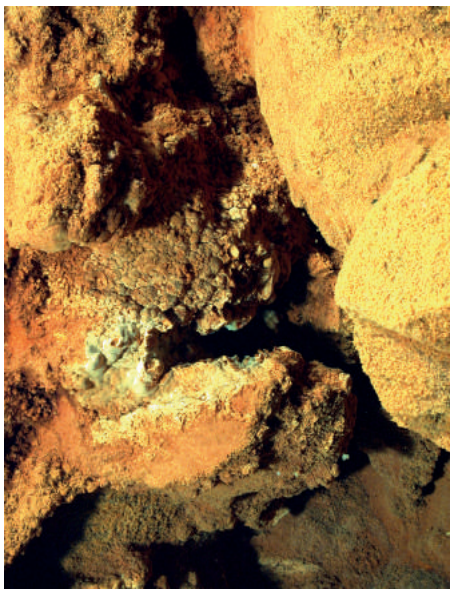

Mat of iron oxyhydroxides and iron oxidizing bacteria at a hydrothermal vent at the Loihi Seamount offshore Hawai'i.
Image taken by the ROV Jason on cruise KM09-23, chief scientist Hubert Staudigel and courtesy of Woods Hole Oceanographic Institute

Igneous oceanic crust is one of the largest potential habitats for life on earth, and microbial activity supported by rock-water-microbe reactions in this environment can impact global biogeochemical cycles. However, our understanding of the microbiology of this system, especially the subsurface "deep biosphere" component of it, has traditionally been limited by sample availability and quality. Over the past decade, several major international programs (such as the Center for Dark Energy Biosphere Investigations, the current International Ocean Discovery Program and its predecessor Integrated Ocean Drilling Program, and the Deep Carbon Observatory) have focused on advancing our understanding of life in this cryptic, yet globally relevant, biosphere. Additionally, many field and laboratory research programs are examining hydrothermal vent systems –a seafloor expression of seawater that has been thermally and chemically altered in subseafloor crust – and the microbial communities supported by these mineral-rich fluids. The

papers in this special issue bring together recent discoveries of microbial presence, diversity and activity in these dynamic ocean environments. Cumulatively, the articles in this special issue serve as a tribute to the late Dr. Katrina J. Edwards, who was a pioneer and profound champion of studying microbes that "rust the crust". This special issue volume serves as a foundation for the continued exploration of the subsurface ocean crust deep biosphere.

Citation: Orcutt, B. N., Sylvan, J. B., Santelli, C. M., eds. (2017). Recent Advances in Geomicrobiology of the Ocean Crust. Lausanne: Frontiers Media. doi: 10.3389/978-2-88945-283-5

Table of Contents

frontiers in Microbiology

EDITORIAL
published: 21 July 2017
doi: 10.3389/fmicb.2017.01368

Editorial: Recent Advances in Geomicrobiology of the Ocean Crust

Beth N. Orcutt[1]*, *Jason B. Sylvan*[2] *and Cara M. Santelli*[3]

[1] *Bigelow Laboratory for Ocean Sciences, East Boothbay, ME, United States,* [2] *Department of Oceanography, Texas A&M University, College Station, TX, United States,* [3] *Department of Earth Sciences, University of Minnesota, Minneapolis, MN, United States*

Keywords: geomicrobiology, deep biosphere, IODP, ocean crust, iron oxidation

Editorial on the Research Topic

Recent Advances in Geomicrobiology of the Ocean Crust

Igneous oceanic crust is one of the largest potential habitats for life on earth (Orcutt et al., 2011), and microbial activity supported by rock-water-microbe reactions in this environment can impact global biogeochemical cycles (Bach and Edwards, 2003). However, our understanding of the microbiology of this system, especially the subsurface "deep biosphere" component of it, has traditionally been limited by sample availability and quality. Over the past decade, several major international programs (such as the Center for Dark Energy Biosphere Investigations, the current International Ocean Discovery Program, and its predecessor Integrated Ocean Drilling Program, and the Deep Carbon Observatory) have focused on advancing our understanding of life in this cryptic, yet globally relevant, biosphere. Additionally, many field and laboratory research programs are examining hydrothermal vent systems—a seafloor expression of seawater that has been thermally and chemically altered in subseafloor crust—and the microbial communities supported by these mineral-rich fluids. The papers in this special issue bring together recent discoveries of microbial presence, diversity, and activity in these dynamic ocean environments.

Starting at the seafloor where igneous rocks are directly exposed to oxic, bottom seawater, two papers in this special issue address the microbial diversity (Lee et al.) and metagenomic characteristics (Singer et al.) of seafloor basalts. Going deeper below the seafloor where cool, oxic fluids circulate through fractures in the lithosphere, two papers document the biomass and structure (Jørgensen and Zhao) and metabolic potential (Zhang et al.) of biofilms on subsurface basalts from the western flank of the Mid-Atlantic Ridge at a site known as North Pond. A companion project at this same site used a new *in situ* spectral imaging tool to assess biofilms and biomass in the crustal subsurface (Salas et al.). Basalts from the seafloor and this oxic subsurface environment were used in a survey to assay the magnitude of microbial carbon fixation on basalts, and to identify microbial groups potentially involved in this process (Orcutt et al.). Isolation and description of bacteria from the overlying sediment at North Pond provides a comparison between the crustal microbial communities and those detected in the sediment lying just above (Russell et al.).

Comparing these oxic and cool subsurface crustal fluids with warmer and anoxic subsurface crustal fluids from the eastern flank of the Juan de Fuca Ridge, a new nanocalorimetry approach documents the energy available to subsurface crustal fluid communities (Robador et al.). These new approaches help to validate theoretical models of energy availability in the crustal subsurface, such as new work in this special issue on hydrogen production from water-rock reactions (Bach) and radiolysis (Dzaugis et al.). Finally, new time series data from a crustal observatory at the Juan de Fuca Ridge flank reveals the importance of redox conditions and temperature on structuring biofilms forming on crustal rocks (Baquiran et al.).

OPEN ACCESS

Edited by:
Axel Schippers, Federal Institute for Geosciences and Natural Resources, Germany

Reviewed by:
Timothy Ferdelman, Max Planck Institute for Marine Microbiology (MPG), Germany

***Correspondence:**
Beth N. Orcutt
borcutt@bigelow.org

Specialty section:
This article was submitted to Extreme Microbiology, a section of the journal Frontiers in Microbiology

Received: *31 May 2017*
Accepted: *05 July 2017*
Published: *21 July 2017*

Citation:
Orcutt BN, Sylvan JB and Santelli CM (2017) Editorial: Recent Advances in Geomicrobiology of the Ocean Crust. Front. Microbiol. 8:1368. doi: 10.3389/fmicb.2017.01368

FIGURE 1 | Dr. Katrina J. Edwards (1968–2014), a visionary geomicrobiologist who promoted the study of microbes that "rust the crust," breaking open a seafloor basalt from the North Pond study site in 2012. Photograph by Beth Orcutt.

The Juan de Fuca Ridge and flank environment are also loci of recent efforts to cultivate thermophilic organisms. Thermophilic sulfate reducing bacteria were isolated from deep sediment on the ridge flank influenced by the diffusion of sulfate and heat from the underlying igneous basement (Fichtel et al.), and multivariate laboratory experiments were conducted to determine controls on thermophilic sulfate reduction in the hydrothermal sulfide chimney structures nearer to the ridge axis (Frank et al.). The genomes of isolates of *Thermococcus* from the Juan de Fuca were compared to isolates from other hydrothermal systems to explore thermophile biogeography and adaptation (Price et al.).

Moving to a more organic-rich hydrothermal setting, two papers in the special issue explore the microbial residents in the Guaymas Basin in the Gulf of California. A "hiking guide" of Guaymas documents the connection of surface patterns in microbial mats to subsurface gradients in temperature and porewater chemistry (Teske et al.). Honing in on the surface microbial mats, and the resident giant sulfur bacteria therein, an exploration of genomes from these organisms reveals intriguing hints about their possible transcriptional regulation mechanisms (MacGregor).

Given that oceanic crust is composed of igneous rocks (e.g., basalt, gabbro, peridotite) enriched in reduced iron, chemosynthetic iron oxidation received focused attention in this special issue. The growth of chemoorganotrophic (Sudek et al.) and chemolithoautotrophic (Henri et al.) iron-oxidizing bacteria in the presence of basalt was investigated with interdisciplinary approaches. Two studies show the early colonization by marine Zetaproteobacteria—neutrophilic, microaerophilic iron-oxidizing bacteria—on surfaces containing reduced iron (Henri et al.; McBeth and Emerson). Zetaproteobacteria also colonize reduced iron substrates in freshwater systems (McBeth and Emerson), and genomes of freshwater iron oxidizing bacteria reveal similarities and differences to their marine cousins (Kato et al.). An exploration of the architecture of the microbial mats generated by freshwater and marine iron-oxidizing bacteria reveals the ecosystem structuring performed by these lithotrophs (Chan et al.). Finally, an intense investigation of the alteration products in active and inactive hydrothermal chimneys reveals diverse signatures of microbial iron oxidation and reduction (Toner et al.).

Cumulatively, the articles in this special issue serve as a tribute to the late Dr. Katrina J. Edwards (**Figure 1**), who was a pioneer and profound champion of studying microbes that "rust the crust" (Bach and Edwards, 2003; Edwards et al., 2003, 2005, 2011a,b, 2012a,b). As co-author on five of the twenty-two papers in this special issue (Lee et al.; Salas et al.; Singer et al.; Baquiran et al.; Toner et al.), and an acknowledged inspiration of several others, Katrina's influence on the field has a lasting legacy. This legacy is eloquently captured in an award-winning feature length documentary about the North Pond ocean drilling project (https://vimeo.com/117447690), a long-term observatory project that Katrina initiated to study deep biosphere crustal microbes (Edwards et al., 2012c). Her legacy lives on in the various collaborators that continue to study microbes that rust the crust, as well as in the scientists that passed through her lab and are now running their own labs, including the editors of this volume. This special issue volume serves as a foundation for the continued exploration of the subsurface ocean crust deep biosphere.

AUTHOR CONTRIBUTIONS

All authors listed have made a substantial, direct and intellectual contribution to the work, and approved it for publication.

FUNDING

This work was supported by Center for Dark Energy Biosphere Investigations (C-DEBI), National Science Foundation Science and Technology Center (NSF award OCE-0939564), and the Deep Carbon Observatory supported by the Alfred P. Sloan Foundation.

REFERENCES

Bach, W., and Edwards, K. J. (2003). Iron and sulfide oxidation within the basaltic ocean crust: implications for chemolithoautotrophic microbial biomass production. *Geochim. Cosmochim. Acta* 67, 3871–3887. doi: 10.1016/s0016-7037(00)00304-1

Edwards, K. J., Bach, W., and McCollom, T. M. (2005). Geomicrobiology in oceanography: microbe-mineral interactions at and below the seafloor. *Trends Microbiol.* 13, 449–456. doi: 10.1016/j.tim.2005.07.005

Edwards, K. J., Becker, K., and Colwell, F. (2012a). The deep, dark biosphere: intraterrestrial life on Earth. *Annu. Rev. Earth Planet. Sci.* 40, 551–568. doi: 10.1146/annurev-earth-042711-105500

Edwards, K. J., Fisher, A. T., and Wheat, C. G. (2012b). The deep subsurface biosphere in igneous ocean crust: frontier habitats for microbiological exploration. *Front. Microbiol.* 3:8. doi: 10.3389/fmicb.2012.00008

Edwards, K. J., Glazer, B. T., Rouxel, O., Bach, W., Emerson, D., Davis, R. E., et al. (2011a). Ultra-diffuse hydrothermal venting supports Fe-oxidizing bacteria and massive umber deposition at 5000m off Hawaii. *ISME J.* 5, 1748–1758. doi: 10.1038/ismej.2011.48

Edwards, K. J., Rogers, D. R., Wirsen, C. O., and McCollom, T. M. (2003). Isolation and characterization of novel, psychrophilic, neutrophilic, Fe-oxidizing, chemolithoautotrophic alpha- and gamma-Proteobacteria from the deep sea. *Appl. Environ. Microbiol.* 69, 2906–2913. doi: 10.1128/AEM.69.5.2906-2913.2003

Edwards, K. J., Wheat, C. G., and Sylvan, J. B. (2011b). Under the sea: microbial life in volcanic oceanic crust. *Nat. Rev. Microbiol.* 9, 703–712. doi: 10.1038/nrmicro2647

Edwards, K. J., Wheat, C. G., Orcutt, B. N., Hulme, S., Becker, K., Jannasch, H., et al. (2012c). "Design and deployment of borehole observatories and experiments during IODP Expedition 336 Mid-Atlantic Ridge flank at North Pond," in *Proc. IODP.* eds K. J. Edwards, W. Bach, A. Klaus and Expedition336Scientists (Tokyo: Integrated Ocean Drilling Program Management International, Inc.), 336.

Orcutt, B. N., Sylvan, J. B., Knab, N. J., and Edwards, K. J. (2011). Microbial ecology of the dark ocean above, at, and below the seafloor. *Microbiol. Mol. Biol. Rev.* 75, 361–422. doi: 10.1128/MMBR.00039-10

Conflict of Interest Statement: The authors declare that the research was conducted in the absence of any commercial or financial relationships that could be construed as a potential conflict of interest.

frontiers in Microbiology

ORIGINAL RESEARCH
published: 23 December 2015
doi: 10.3389/fmicb.2015.01470

Microbial Communities on Seafloor Basalts at Dorado Outcrop Reflect Level of Alteration and Highlight Global Lithic Clades

Michael D. Lee[1], *Nathan G. Walworth*[1], *Jason B. Sylvan*[1,2], *Katrina J. Edwards*[1†] *and Beth N. Orcutt*[3*]

[1] Department of Biological Sciences, University of Southern California, Los Angeles, CA, USA, [2] Department of Oceanography, Texas A&M University, College Station, TX, USA, [3] Bigelow Laboratory for Ocean Sciences, East Boothbay, ME, USA

Areas of exposed basalt along mid-ocean ridges and at seafloor outcrops serve as conduits of fluid flux into and out of a subsurface ocean, and microbe–mineral interactions can influence alteration reactions at the rock–water interface. Located on the eastern flank of the East Pacific Rise, Dorado Outcrop is a site of low-temperature (<20°C) hydrothermal venting and represents a new end-member in the current survey of seafloor basalt biomes. Consistent with prior studies, a survey of 16S rRNA gene sequence diversity using universal primers targeting the V4 hypervariable region revealed much greater richness and diversity on the seafloor rocks than in surrounding seawater. Overall, Gamma-, Alpha-, and Deltaproteobacteria, and Thaumarchaeota dominated the sequenced communities, together making up over half of the observed diversity, though bacterial sequences were more abundant than archaeal in all samples. The most abundant bacterial reads were closely related to the obligate chemolithoautotrophic, sulfur-oxidizing *Thioprofundum lithotrophicum*, suggesting carbon and sulfur cycling as dominant metabolic pathways in this system. Representatives of Thaumarchaeota were detected in relatively high abundance on the basalts in comparison to bottom water, possibly indicating ammonia oxidation. In comparison to other sequence datasets from globally distributed seafloor basalts, this study reveals many overlapping and cosmopolitan phylogenetic groups and also suggests that substrate age correlates with community structure.

Keywords: basalt, geomicrobiology, oceanic crust, microbe–mineral interactions, biogeography

OPEN ACCESS

Edited by:
Axel Schippers, Federal Institute for Geosciences and Natural Resources (BGR), Germany

Reviewed by:
Takuro Nunoura, Japan Agency for Marine-Earth Science and Technology, Japan
Gordon Webster, Cardiff University, UK

***Correspondence:**
Beth N. Orcutt
borcutt@bigelow.org

[†] *Deceased.*

Specialty section:
This article was submitted to Extreme Microbiology, a section of the journal Frontiers in Microbiology

Received: *28 September 2015*
Accepted: *07 December 2015*
Published: *23 December 2015*

Citation:
Lee MD, Walworth NG, Sylvan JB, Edwards KJ and Orcutt BN (2015) Microbial Communities on Seafloor Basalts at Dorado Outcrop Reflect Level of Alteration and Highlight Global Lithic Clades. Front. Microbiol. 6:1470. doi: 10.3389/fmicb.2015.01470

INTRODUCTION

Areas of exposed oceanic lithosphere comprise a substantial proportion of the seafloor. The global mid-ocean ridge system generates new crust at an average rate of ~3.3 km^2 $year^{-1}$ (German and Von Damm, 2004). This contributes to ridge flanks having constantly-replenished, large stretches of unsedimented basalt totaling more than 10^6 km^2 worldwide (Edwards et al., 2005). Dwarfing this, however, are the estimated millions of seamounts and outcrops >100 m in relief that extend above sedimentation lines (Wessel et al., 2010). Conservative estimates including only those taller than 1 km pin this area at nearly 30 × 10^6 km^2 worldwide, providing a potential biome larger than

the global continental shelf (Etnoyer et al., 2010). These regions also serve as conduits of fluid flux into and out of a subsurface ocean (Edwards et al., 2005), facilitating ongoing exchanges between the crust and seawater that contribute as much chemically-altered fluid to the ocean as the totality of global riverine inputs (Elderfield and Schultz, 1996; Wheat and Mottl, 2000).

At the rock–water interface, chemically-reduced substrates hosted by basalts meet an oxidative ocean, supporting spontaneous oxidation–reduction (redox) reactions. These reactions cause slow weathering of basalts at low temperatures, granting microorganisms the opportunity to manipulate this energy transfer, accelerating redox processes by unknown magnitudes and forming a chemolithotrophic foundation for basalt-hosted biomes. Accounting for Fe and S oxidation alone, the most dominant reduced substrates found in basalt, it has been estimated that this trophic foundation may extend 500 m down into the crust and can theoretically support the production of as much as 10^{11} g of fixed C per year (Bach and Edwards, 2003; Orcutt et al., 2015) In addition to Fe and S, basaltic crust hosts reduced Mn as well as P, Ni, and other trace elements integral to microbial processes (Staudigel et al., 2008). Driven by redox reactions, as fresh seafloor basalts weather, an outer rind develops that is primarily composed of Mn and Fe (>30%) and other elements sourced from the basalt itself; however, similar to ferromanganese nodules found throughout the seafloor, these outer rinds also serve as nuclei that continue to accrete additional biologically significant metals including Co, Cu, Mo, Zn, Pb, and others as the basalt ages (Mero, 1962). Some have argued this fluid-delivery mechanism is actually the primary source of support for basalt-hosted microbial communities (Templeton et al., 2009).

Although ocean crust comprises a significant fraction of the seafloor, the microbial communities resident within and on these rocks—and likely involved in the rock alteration processes described above—are poorly understood. Culturing efforts have yielded otherwise unknown Mn oxidizers (Templeton et al., 2005) and Fe oxidizers (Edwards et al., 2003, 2004; Rogers et al., 2003; Daughney et al., 2004), suggesting that these microorganisms may play a role in the weathering of rock at the seafloor. Culture-independent molecular techniques aimed at phylogeny have also been successful in probing the microbial communities of seafloor basalts. Sequences from the Knipovich Ridge in the Atlantic Arctic have revealed Gamma-, Alpha-, Delta-, and Epsilonproteobacteria, as well as Actinobacteria, Chloroflexi, Firmicutes, and Bacteroidetes within Bacteria, and Marine Group I Crenarchaeota (now known as Thaumarchaeota; Brochier-Armanet et al., 2008) within the Archaea (Thorseth et al., 2001; Lysnes et al., 2004). Samples from the Juan de Fuca Ridge (JdF) were found to contain Gamma-, Beta-, and Epsilonproteobacteria (Rogers et al., 2003). In addition to these previously mentioned taxa, two other studies with samples from the East Pacific Rise (EPR), Loihi Seamount, and JdF also recovered Gemmatimonadetes, Nitrospirae, Planctomycetes, and Verrucomicrobia (Santelli et al., 2008; Mason et al., 2009). Larger clone libraries revealed basalts host extremely diverse microbial communities and suggested that rock alteration positively correlated with richness and diversity (Santelli et al., 2009). A study looking at very young, newly erupted samples (<10 years) from Vailulu'u Seamount in the southwest Pacific identified Alpha-, Beta-, Delta-, Epsilonproteobacteria, and Bacteroidetes (Sudek et al., 2009), while a survey of a relatively much older site, Takuyo Seamount (∼80 mya) near Japan, detected all of the taxa mentioned above and additionally Caldithrix, Chlamydiae, and clones belonging to the groups BRC1, KSB, NKB19, OP11, OP3, SAR406, and SBR1093, and suggested that aged basalts with developed Mn crusts are as or more diverse than younger basalts (Nitahara et al., 2011). Generally consistent findings of these prior phylogenetic surveys include that these substrates host some of the most diverse communities known, are more abundantly characterized by bacteria over archaea [though quantitative Polymerase Chain Reaction (qPCR) has yielded at least one exception to this; Nitahara et al., 2011], and are consistently dominated by Gamma- and Alphaproteobacteria. The broad similarities detected in communities over large geographic stretches has led some to suggest there are conserved major taxa that are ubiquitous with regard to seafloor basalts (Mason et al., 2007, 2009; Santelli et al., 2008).

Previous studies of microbial diversity hosted on seafloor basalts have focused on either relatively young (<∼3 mya; Thorseth et al., 2001; Rogers et al., 2003; Lysnes et al., 2004; Santelli et al., 2008; Mason et al., 2009; Sudek et al., 2009) or old (∼80 mya; Nitahara et al., 2011) ocean crust, precluding an assessment of how microbial communities may develop with age of the seafloor. Moreover, prior work has focused on basalts from actively venting high-temperature (>200°C) hydrothermal environments (Rogers et al., 2003) or quiescent seafloor habitats (Thorseth et al., 2001; Lysnes et al., 2004; Santelli et al., 2008; Mason et al., 2009; Sudek et al., 2009; Nitahara et al., 2011), but nothing is known about microbial community structure on basalts from low-temperature (<25°C) venting environments postulated to be abundant seafloor features (Elderfield and Schultz, 1996; Wheat and Mottl, 2000; Wessel et al., 2010).

Located 200 km west of Costa Rica on the eastern flank of the East Pacific Rise, Dorado Outcrop (**Figure 1A**) is an environment that allows assessment of both of these conditions as it is comprised of 23 Ma seafloor (Wheat and Fisher, 2008) where cool (10–20°C) hydrothermal fluids were predicted to be venting after transiting from nearby Tengosed Seamount located ∼20 km away (Hutnak et al., 2008; Wheat and Fisher, 2008). Sediment porewater chemistry from on and around Dorado Outcrop indicates minimally altered fluids exiting the seafloor (i.e., nitrate is present at 42.3 μmol/kg in bottom water and estimated at 40.9 μmol/kg in venting fluids; Wheat and Fisher, 2008). This is in contrast to mid-ocean ridge and hotspot volcanoes, where the chemical composition of diffuse flow vent fluids is very different from background seawater. Here, we analyze 16S rRNA gene sequences (focusing on the V4 hypervariable region) from basalts collected from Dorado Outcrop to provide the first survey of microbial communities inhabiting basalts recovered from a low-temperature venting, "middle-aged" outcrop. Building upon previous work investigating the biogeography of seafloor-exposed basalts, we further elucidate globally distributed monophyletic clades, supporting the observation that the

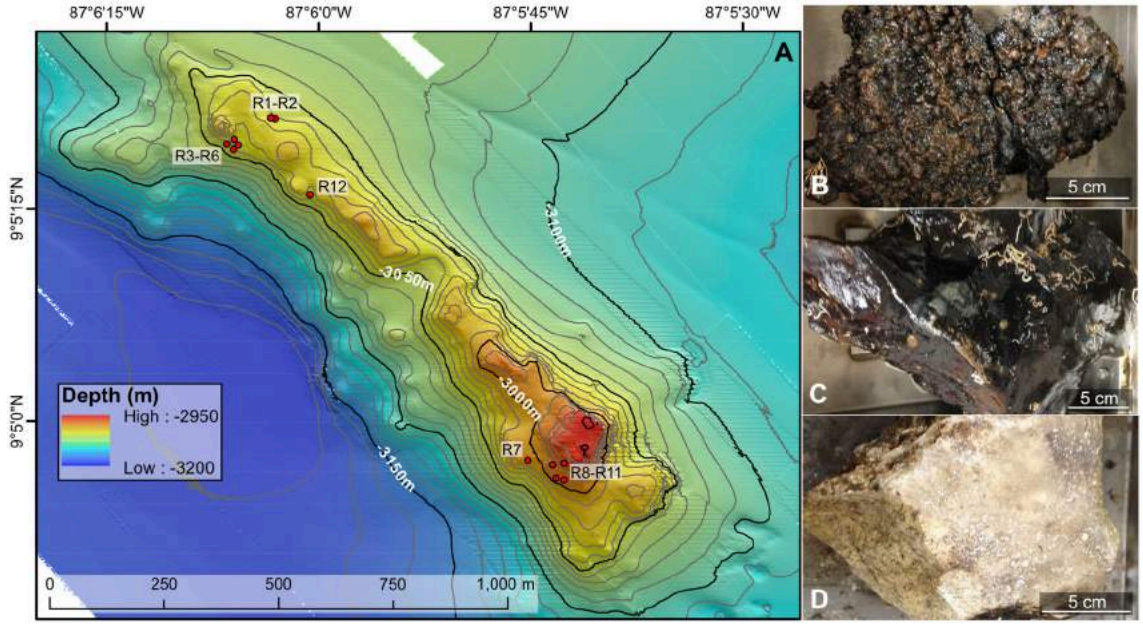

FIGURE 1 | Bathymetric map (A) and example rock types (B–D) collected from the Dorado Outcrop offshore Costa Rica in the Pacific Ocean. (A) Locations of the 12 rock samples examined in this study are indicated with red circles. The underlying north–south oriented map was created shipboard by Samuel Hulme and Chris Treboal from bathymetric data collected by the AUV *Sentry* at heights of 5, 30, and 60 m above bottom, with 10 m water depth contours (data are publicly available through the National Oceanic and Atmospheric Administration's National Centers for Environmental Information database). **(B–D)** Examples of highly oxidized, manganese encrusted basalt **(B)**, less altered basalt **(C)**, and lithified carbonate **(D)** rock types examined in this study, with scale bars to indicate size. Photographs by Michael Lee.

composition of deep-sea mineral substrates plays a larger role than other factors (e.g., geography, temperature, depth) in determining mineral-attached microbial community structure (Santelli et al., 2008; Mason et al., 2009; Toner et al., 2013) and further support the notion of a crust-associated clade within the Thaumarchaeota as has been put forward previously (Mason et al., 2007).

MATERIALS AND METHODS

Sample Collection

Dorado Outcrop (**Figure 1A**) is located 200 km west of Costa Rica on the Cocos Plate (Wheat and Fisher, 2008). Its surface is ∼3000–3100 m below the sea surface and rises to a height of ∼80 m above the surrounding seafloor (Wheat and Fisher, 2008). Over the span of December 7–23, 2013, 12 seafloor rock samples (11 basalts and 1 lithified carbonate, hereafter R1–R12; **Table 1**, Figure S1) were collected from across Dorado Outcrop while aboard *R/V Atlantis* during cruise AT26-09 following previously developed protocols (Santelli et al., 2008). Immediately prior to collection, the temperature of fluids venting from cracks in the outcrop was measured using the "high temperature" thermocouple available from the *ROV Jason II*. Using the *ROV*, all samples were placed in plastic "bioboxes" that were sealed at depth to maintain them in seawater from where they were collected. Once onboard the ship, samples were immediately photographed and processed in a flame-sterilized steel box with a flame-sterilized hammer and chisel. Most samples possessed visibly altered outer rinds that were chiseled off for molecular analysis. For those lacking an altered rind (namely the lithified carbonate sample), the exterior was targeted to chip off small fragments of rock. Samples for DNA analysis were placed in either sterile whirl-pak bags or centrifuge tubes and frozen at −80°C. Locations of the collection sites are marked on **Figure 1A** and coordinates can be found in **Table 1**. In addition to the basalts, two bottom water samples were collected using a Niskin bottle mounted to an elevator, and 1.25 L were filtered onto 0.2 μm pore size polycarbonate Nucleopore filters that were then frozen at −80°C.

DNA Extraction and Sequencing of the 16S rRNA Gene

Frozen rock pieces were crushed in a flame-sterilized impact mortar into sand-sized grains which were then transferred to sterile plastic centrifuge tubes and stored at −80°C until DNA extractions were performed. DNA extractions were carried out with the FastDNA Spin Kit for Soil (MP Biomedicals, Santa Ana, CA, USA) following the manufacturer's specifications. About 0.5 g of crushed material were placed directly into the lysis tubes of the kit, as were the bottom water filters. Protocol blanks were performed with each extraction (no samples or DNA added to lysis tubes) to track the potential for contamination. DNA concentrations were quantified with the Qubit HS dsDNA Assay

TABLE 1 | Characteristics of the rock and background seawater samples investigated in this study including sample description, ROV *Jason-II* dive number, Dorado Outcrop site marker classification, latitude, longitude, water depth, and water temperature.

ID	Description	Dive	Site	Lat. (N)	Lon. (W)	Water depth (m)	Water temp[a] (°C)
R1	Altered basalt, >1 cm thick black Mn rind	J2-752	14	9.089	87.101	3039	8.6
R1A*	Replicate extraction of above	J2-752	14	9.089	87.101	3039	8.6
R2	Altered basalt, >1 cm thick black Mn rind	J2-752	14	9.089	87.101	3039	8.6
R3	Altered basalt, >1.5 cm thick black Mn rind	J2-752	A	9.089	87.102	3041	12.7
R4	Altered basalt, >1 cm thick black Mn rind	J2-752	A	9.089	87.102	3041	12.7
R5	Altered basalt, >1.5 cm thick black Mn rind	J2-752	A	9.089	87.102	3041	12.7
R6	Altered basalt, >1 cm thick black Mn rind	J2-752	A	9.089	87.102	3041	12.7
R7	Lithified carbonate	J2-757	M	9.099	87.096	3011	n.d.
R8	Glassy basalt, 1 cm thick black and orange rind	J2-757	D	9.082	87.095	3007	13.5
R9	Glassy basalt, 1 cm thick black Mn rind	J2-757	K	9.082	87.095	3007	13.7
R10	Glassy basalt, thin black and orange rind	J2-757	K	9.082	87.095	3007	13.7
R11	Glassy basalt, thin black and orange rind, green veneer	J2-757	F	9.082	87.095	3007	7.3
R12	Basalt, thin black rind	J2-757	B	9.088	87.101	3024	n.d.
R11-BF	Green veneer from R-11	J2-757	F	9.082	87.095	3007	7.3
BW-1	1.25 L Bottom seawater (elevator Niskin)	n.a.	n.a.	9.083	87.103	3183	2.0
BW-2	1.25 L Bottom seawater (elevator Niskin)	n.a.	n.a.	9.081	87.101	3176	2.0

Sample marked with asterisk indicates a technical replicate of sample R1—a separate part of the outer rind was analyzed. n.a., not applicable; n.d., not determined. [a]Measurements were made with an uncalibrated thermocoupler (Jason II), and bottom water temperature was ~2°C.

kit with a Qubit 2.0 Fluorometer (Life Technologies, Carlsbad, CA, USA) according to manufacturer protocols.

DNA extracts from the 12 rock samples (plus one technical replicate from the same sample), one green-colored, potential biofilm sample from R11 (Figure S2), two bottom water samples, and four protocol blanks for a total of 20 samples (**Table 2**) were sent for DNA sequencing by a commercial vendor (Molecular Research LP; MR DNA; Shallowater, TX, USA). Illumina MiSeq paired-end (2 × 300 base pair) tag sequencing was carried out using the Earth Microbiome Project universal primers 515f (5′-GTG CCA GCM GCC GCG GTA A-3′) and 806r (5′-GGA CTA CHV GGG TWT CTA AT-3′; Caporaso et al., 2012), which flank the V4 region of the 16S rRNA gene. Library preparation and sequencing was carried out at the facility. In brief, the 515f/806r PCR primers with 8-base barcodes on the forward primer were used in a PCR reaction with the HotStarTaq Plus Master Mix Kit (QIAGEN:USA, Valencia, CA, USA) under the following conditions: 94°C for 3 min, followed by 28 cycles of 94°C for 30 s, 53°C for 40 s, and 72°C for 1 min, and a final elongation step at 72°C for 5 min. PCR products were then run on a 2% agarose gel to check amplification and relative intensity of bands. Based on their DNA concentrations and molecular weight, multiple samples were pooled together in equal proportions, purified with Ampure XP beads, and then used to prepare the library by following the Illumina TruSeq DNA library preparation protocol.

In addition to MiSeq tag sequencing, one near-full-length 16S rRNA clone library was prepared from sample R5. Following extraction as noted above, DNA was amplified with GoTaq Green Master Mix (Promega, Madison, WI, USA) using universal bacterial primers B27f (5′-AGA GTT TGA TCM TGG CTC AG-3′) and U1492r (5′-GGT TAC CTT GTT ACG ACT T-3′; Lane, 1991). The PCR was performed as follows: 95°C for 5 min, then 30 cycles of 95°C for 30 s, 55°C for 30 s, and 72°C for 90 s, followed by a final 72°C for 10 min. After amplification, PCR product was purified with the QiaQuick PCR Purification Kit (QIAGEN:USA, Valencia, CA, USA), and cloned into the pCR 4 TOPO vector using the TOPO TA Cloning Kit (Invitrogen, Grand Island, NY, USA). Transformants were plated on LB agar containing 100 μg mL^{-1} ampicillin as per the manufacturer's instructions and incubated overnight. Ninety-six colonies were then selected and grown overnight in liquid culture. These were sent for Sanger sequencing at Beckman Coulter Genomics in Danvers, MA, USA and resulted in the recovery of 67 near full-length 16S rRNA gene sequences.

Sequence Data Analysis

Tag data curation and processing were carried out using *mothur* v.1.34.4 (Schloss et al., 2009) following the *mothur* Illumina MiSeq Standard Operating Procedure (Kozich et al., 2013). Briefly, paired reads were joined into contigs and any sequences with ambiguous base calls or homopolymers longer than 8 bp were removed. These merged contigs were aligned to the mothur-recreated Silva SEED database from release v119 (Yarza et al., 2008). Sequences were then pre-clustered at a near 1% dissimilarity by ranking the sequences by abundance and merging the most rare with the most abundant using

TABLE 2 | DNA extraction and 16S rRNA gene sequencing characteristics of the rock and background seawater samples investigated in this study, including mass or volume of sample extracted for DNA, DNA concentration (in ng DNA g^{-1} or ng DNA ml^{-1}), number of 16S rRNA gene sequence reads before and after filtering and removal of sequences from the protocol blanks, and number of predicted operational taxonomic units (OTUs) defined at the 97% or greater sequence similarity level before and after filtering and blank removal.

ID	Sample extracted (g or ml)	ng DNA g^{-1} or ng ml^{-1}	Number of QC reads	Number of OTUs	Number of reads after filtering	Number of OTUs after filtering
R1	0.38	572	155,483	10,893	135,466	1376
R1A*	0.40	343	207,831	13,329	178,760	1433
R2	0.45	105	239,591	11,203	210,764	1464
R3	0.39	212	225,789	13,111	195,939	1464
R4	0.43	5.9	243,465	9123	215,990	1249
R5	0.42	404	232,055	14,432	198,281	1517
R6	0.77	438	194,066	11,023	166,608	1412
R7	0.59	3.8	110,382	4272	93,015	1069
R8	0.57	14	166,861	5933	150,118	1190
R9	0.50	91	118,960	5647	109,163	1205
R10	0.55	196	159,781	4956	146,733	1141
R11	0.50	36	115,105	6297	103,064	1263
R12	0.43	422	197,018	16,553	164,991	1460
R11-BF	n.d.	n.d.	121,025	4103	110,244	810
BW-1	1250	b.d.l.	32,354	1031	21,218	381
BW-2	1250	b.d.l.	84,314	2328	70,775	577
Blank-1	n.a.	b.d.l.	24,651	425	n.a.	n.a.
Blank-2	n.a.	b.d.l.	9354	173	n.a.	n.a.
Blank-3	n.a.	b.d.l.	8008	159	n.a.	n.a.
Blank-4	n.a.	b.d.l.	7823	227	n.a.	n.a.

Sample marked with asterisk indicates a technical replicate of sample R1. b.d.l., below detection limit; BF, biofilm; BW, bottom water; n.a., not applicable; n.d., not determined; OTU, Operational Taxonomic Unit; QC, quality controlled.

the *pre.cluster* command with diffs = 2, as this step has been shown to mitigate the generation of spurious sequences (Kozich et al., 2013). Chimeras were screened with UCHIME using *de novo* mode (Edgar et al., 2011) and removed from further processing and analysis. Sequences were clustered into Operational Taxonomic Units (OTUs) at 3% or less sequence dissimilarity using the average neighbor method. These are referred to throughout as OtuXXXXXX.

Treatment of Extraction Blanks and OTU Filtering

OTUs recovered from the four protocol blank samples (which may reflect over-amplification of contaminant DNA from the DNA extraction or sequencing kit reagents, as has been observed previously (Champlot et al., 2010), or cross-contamination from actual samples during sample handling) were statistically treated to determine if the sequences should be removed from the actual sample datasets, based on the proportional abundance of the reads. For example, OTUs with only a few reads in the blank samples but a higher abundance of reads in the actual samples were not removed from the dataset, as they likely reflected "real" sequences that resulted in the blanks from cross-contamination. To be rigorous in the application of this cutoff criterion, the OTUs from the four blanks were combined and compared against all of the samples combined together and normalized (divided by four to account for the difference in sample numbers). If any OTU was represented by at least 50 sequences in the sample dataset and had at least an order of magnitude or more reads than in the blank dataset, it was retained. Otherwise, the OTU was removed from the dataset, as it was likely a result of kit contaminant amplification. Following removal of blank sequences, the dataset was filtered using a conservative minimum OTU abundance cutoff threshold of 0.005% of total reads, as has been recommended when a mock community is not incorporated with sequencing in order to further mitigate the generation of spurious OTUs (Bokulich et al., 2013). This precludes, however, performing any richness estimator calculations such as the Chao1 abundance estimator or the abundance-based coverage estimator (ACE), as these utilize singletons in their calculations.

OTU Matrix Visualizations and Statistics

Visualizations, tests of significance, analysis of similarities (ANOSIM), and permutational analysis of variance (ANOVA)

tests of the final OTU abundance matrix were carried out in *RStudio* version 0.98.1091 (Racine, 2012) using the package *vegan* version 2.3-0 (Oksanen, 2015) with default settings unless otherwise noted. Hierarchical clustering analyses were performed with Bray-Curtis, Jaccard, and Yue-Clayton dissimilarity indices. Non-metric multidimensional scaling (NMDS) ordinations were carried out using the function *metaMDS*(). Redundancy analysis (RDA), ANOSIM, and permutational ANOVA were performed to test for any correlations between community composition and sample collection location, groupings of basalts by level of alteration, or observed venting temperature at time of collection using the functions *rda*(), *anosim*(), and *adonis*() with 10,000 permutations. In the case of the RDA ordination, because ecological data containing very high abundances as well as many rare abundances can be misleading when calculating Euclidean distances on raw values, the data were first Hellinger transformed as this has been shown to be effective in ameliorating this problem (Legendre and Gallagher, 2001).

Clone Library Processing

For the clone library, near full-length contigs were assembled using *Geneious* v6.1.8 (Kearse et al., 2012). Sequences were oriented and trimmed manually and then screened for chimeras using the online program *Decipher* version 1.14.4 (Wright et al., 2012). The resulting sequences were used in phylogenetic tree construction and submitted to BLAST (Altschul et al., 1990) to search for nearest cultured neighbors as well as environmental samples.

Incorporation of Other Seafloor Basalt Studies

Multiple studies of seafloor basalts that contained clone sequence data for the 16S rRNA gene were examined in context with the MiSeq tag data generated by this study in an effort to delineate any globally distributed clades. This effort follows up on previous work (Mason et al., 2007) with data now available from more geographically disparate sites. The sites incorporated here include: a recently erupted sample (2004) from the Vailulu'u Seamount in the Southern Pacific Ocean, near American Samoa (Sudek et al., 2009); a sample from the East Pacific Rise from a recent eruption (1991), designated as 9N in this study (Mason et al., 2009); samples from the Loihi Seamount and South Point near the big island of Hawaii (labeled collectively as Loihi herein) that are <1000 years old (Santelli et al., 2008); older samples from the East Pacific Rise at <18,000 years labeled here as EPR (Santelli et al., 2008); samples from the Juan de Fuca Ridge (JdF) in the Northern Pacific that are 100 kya and 3.3 mya (Mason et al., 2009); Mn crusts from the 80 mya Takuyo-Daigo Seamount in the Northwest Pacific (Nitahara et al., 2011); basalts from Lau Basin (Sylvan et al., 2013); and basalts from an Arctic spreading ridge in the northern Atlantic (Thorseth et al., 2001; Lysnes et al., 2004). Sequences were gathered from GenBank and used for identifying overlapping OTUs and generating phylogenetic trees. Previous studies were selected for comparison only if they had sequence information that spanned the V4 region used in this study. To find overlapping OTUs between the Dorado tag OTUs recovered in this study and clones from other sites, clones that spanned the V4 region were trimmed down to cover only that region within *mothur* and were then aligned with the OTUs called from the tag data. These were then binned into OTUs at the 3% sequence dissimilarity level using *mothur*'s cluster command with the average neighbor algorithm. The percent shared OTUs was calculated by dividing the total number of shared OTUs between the Dorado tag OTUs and each site by the total number of OTUs at that respective site. For example, 196 OTUs were identified in the Santelli et al. (2008) dataset from the EPR basalts, and 115 were shared with the Dorado tag OTUs, representing 58.67% shared OTUs between Dorado and EPR—i.e., 58.67% of the OTUs recovered at EPR were also recovered at Dorado.

Phylogenetic Tree Construction

For phylogenetic tree construction, OTUs from this study, as well as the full-length sequences available from the above mentioned studies, were aligned using the *ARB-Silva* online SINA aligner (Pruesse et al., 2012) and imported into *ARB* (Ludwig et al., 2004) for identifying nearest neighbors using the SILVA Release v119 database. Where numerous OTUs from this study's tag data grouped with each other in a monophyletic clade, the most abundant OTU was selected as the representative sequence for that clade and the total number of reads for all encompassing OTUs was assigned to it. Groupings of Archaeal, Alpha-, Gamma-, and Deltaproteobacterial sequences were exported in an unaligned fasta format. GeneiousR6 (Kearse et al., 2012) was then used to align these subsets using MUSCLE (Edgar, 2004). These were exported from Geneious and, using only the near full-length reference and environmental sequences to facilitate the construction of robust reference trees, RAxML (Stamatakis, 2014) was used to generate 1000-bootstrap maximum likelihood trees under the General Time Reversible evolution model using a gamma distribution. The short tag reads from this study and short reads from the Arctic ridge study were then added to these trees using Phylogenetic Placer (pplacer) (Matsen et al., 2010). It is worth noting that because of this process, any branches solely containing these short reads from the current study or the Arctic study do not have any statistical branch support as they are simply inserted as a "best fit" within the bootstrapped maximum likelihood reference tree.

Accession Numbers

The clone sequences recovered from this project are publicly available through NCBI′s GenBank, accession numbers KT748562–KT748628, and the raw tag data are available through NCBI′s Sequence Read Archive under project accession number SRP063681. Additionally, a fasta-formatted file containing the representative OTU sequences identified is available as a Datasheet 2 in Supplementary Material.

RESULTS

Sample Description

Twelve seafloor rock samples were collected from across Dorado Outcrop (**Figure 1A**), denoted herein as R1–R12 (R1A is a technical replicate of R1, where two different areas of the same outer rind were sampled; **Table 1**). The rock samples originated from two different regions of Dorado Outcrop (**Figure 1A**), most

from areas where fluids seeping from cracks in the outcrop had elevated temperatures as compared to bottom seawater (**Table 1**). It should be noted the venting temperatures recorded are snapshots of venting conditions only at the time of sample collection, and returning to the same site on a different day often yielded different conditions or even no observable venting; detailed examination of these venting fluctuations was beyond the scope of this study.

Of the 12 samples recovered, one sample was a lithified carbonate (R7), and 11 of the samples (R1–R6 and R8–R12) were basalts with varying degrees of alteration ranging from highly altered, with thick (>1 cm), rough outer rinds (samples R1–R6 and R12) of a black material that resembled manganese oxides, to those with less altered, glassy, thin outer rinds (samples R8–R11). These groups will be referred to hereafter as the "more altered" (samples R1–R6 and R12) and "less altered" (samples R8–R11) sample sets. **Figures 1B–D** shows an example of each of these major three types (Figures S1, S3 contain images of all 12 samples). One of the rocks collected, R11, had a bright green veneer on the outside (Figure S2) that was scraped off and analyzed separately.

DNA Extraction, Sequencing, and OTU Clustering

The more altered basalts ($n = 8$) generally yielded more nucleic acid biomass than the less altered samples ($n = 4$), with 313 ± 190 ng DNA g^{-1} rock (mean ± 1 standard deviation) from the more altered basalts vs. 84 ± 81 in the less altered basalts (**Table 2**). The large standard deviations are mostly due to lone outliers in each group: R4 in the highly altered group with only 5.9 ng DNA g^{-1} rock recovered, and R10 in the less altered group with 196 ng DNA g^{-1} rock (**Table 2**). A Mann–Whitney (Wilcoxon rank sum) test was carried out to test the significance of this observation [due to the few samples and uneven group sizes, both of which are known to lower the power of a standard *T*-test (Zimmerman, 1987)], resulting in a $p = 0.07$.

Initial processing of the Illumina MiSeq tags resulted in 2,653,916 reads found in 72,965 OTUs (defined as 3% or less sequence dissimilarity) across the entire sample set including the two bottom water samples and the protocol blanks ($n = 20$; **Table 2**). The protocol blanks contained 816 OTUs, 561 of which met the criteria for removal from the sample dataset (see Section Materials and Methods). NMDS analysis of the pre-filtered dataset showed clear separation of all rock samples from the two collected bottom water samples and four extraction blanks (Figure S4), supporting our treatment of the protocol blanks' sequences. Bray–Curtis and Jaccard outputs were identical, with only minor differences in Yue–Clayton clustering (Figure S5); ultimately, Bray-Curtis dissimilarities were used in any applicable downstream analyses.

Filtering the data with a conservative 0.005% OTU abundance cutoff threshold to minimize the presence of spurious OTUs (see Section Materials and Methods) resulted in the removal of any OTU with <129 reads cumulatively (across all samples). The final data matrix used for all subsequent analyses contained 1595 OTUs comprised of 2,271,129 reads and is provided in Supplementary Materials along with a fasta-formatted file containing these representative OTU sequences (selected as the most abundant in an OTU cluster). The number of tag reads for each rock sample after processing ranged from 93,015 to 215,990 (**Table 1**). Despite initial DNA concentrations from the rock samples ranging across two orders of magnitude (from 4 to 600 ng DNA per gram rock), the number of OTUs per rock sample was rather consistent at 1336 ± 145 OTUs (average ± one standard deviation, $n = 13$; **Table 2**). The green veneer from R11 had a slightly lower OTU count of 810, whereas the bottom water samples contained <600 OTUs each.

Basalt Microbial Community Structure

Hierarchical cluster analysis and constrained ordination of the filtered basalt sequence dataset (**Figures 2A,B**) revealed robust groupings that statistically correlate with rock alteration characteristics and geography (although the effects of each could not be separated as alteration and geography correlate in this sample set, as discussed below). Namely, the less altered samples (R8–R11), group together to the exclusion of the more highly altered samples (R1–R6 and R12) and the lithified carbonate sample R7 (**Figure 2A**). As mentioned, the major dendrogram clusters and apparent levels of alteration also support a geographic relationship between the samples, as the less altered basalts were all collected from the southern end of the outcrop (**Figure 1A**). This end was found to be more hydrothermally active during our exploration, with more venting areas and higher temperatures detected at those areas.

Redundancy analysis supported the same sample-clustering pattern as the dendrogram (**Figure 2B**). The constraining variables used included location, as a binary input, for collection from the north or south end of the outcrop—a clear distinction as can be seen in **Figure 1A**—and the temperature of venting fluids at the time of collection (**Table 1**). Location was found to explain ∼25% of the variance with a significant $p = 0.002$, while temperature was found to explain ∼10% of the variance, however without any notable significance. An analysis of similarities test (ANOSIM, see Section Materials and Methods above) was carried out to test if the groupings by level of alteration (also being consistent with the north/south delineation) were statistically different and yielded a significant $p = 0.001$. A permutational ANOVA-test was also carried out to test the likelihood of this north/south delineation explaining the hierarchical clustering results occurring by chance; the correlation was supported ($p = 0.0002$). A second permutational ANOVA-test was run to test the ability of the observed venting temperatures at time of sample collection (**Table 1**) to explain the communities recovered and was also found significant, though much less so ($p = 0.0472$). However, it should be stated again that venting was observed to be variable (though consistently more active on the southern end) and these relationships should be interpreted with caution. We note that while there can be variation across the exterior of each sample (Figure S1) the grouping together of technical replicates R1 and R1A (**Figures 2A,B**) provides some confidence that the variation between rocks is likely stronger than the heterogeneity that may be found within one sample.

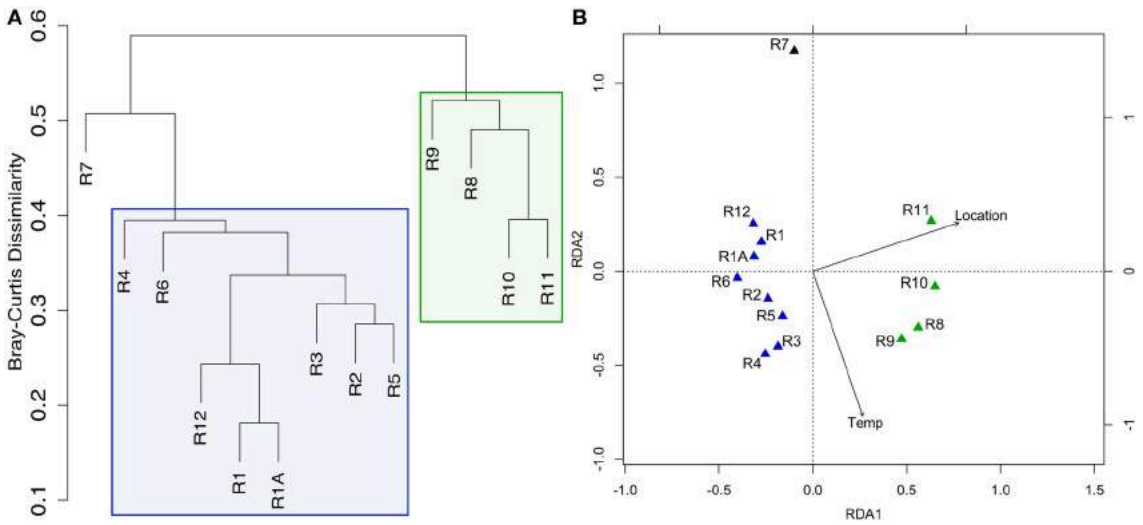

FIGURE 2 | Clustering of Dorado Outcrop sample microbial community 16S rRNA gene sequences as analyzed by (A) hierarchical clustering of community membership similarity based on the Bray-Curtis dissimilarity index and (B) redundancy analysis (RDA). (A) Microbial communities harbored by highly-altered basalt with thick Mn rinds (R1–R6, R12) group together in exclusion to less altered basalts (R8–R11), with the lithified carbonate hosting a dissimilar microbial community. **(B)** RDA showing the same clustering pattern.

To examine relative diversity between samples, rarefaction curves generated by subsampling to the depth of the sample with the least number of reads in the dataset (a bottom water sample, BW1, with 21,218 reads) show three major groupings of the samples (**Figure 3**). Of the observed communities retained after subsampling, the two bottom water samples were found to be much less diverse than the rock samples. And with the exception of R4, the more altered basalts (R1–R6 and R12) have distinct rarefaction curves from the less altered basalts, revealing the more highly altered basalts host more complex communities (**Figure 3**). A more detailed analysis of alpha diversity of the samples is not possible due to the filtering of the dataset to remove possible spurious sequences, as this eliminated any singletons and doubletons (see Section Materials and Methods).

Major Phylogenetic Groups on Dorado Outcrop Basalts

The relative sequence abundances of major microbial phyla were rather consistent across the basalt samples with some notable exceptions (**Figure 4**, Figure S6). Overall, Bacteria dominated the rock sequence libraries, making up ∼86% of the observed communities. The most abundant Bacteria class on the basalts was Gammaproteobacteria, comprising an average of ∼23% of sequences from each rock (**Figure 4**), mostly dominated by the order Chromatiales (**Figure 5**). The sample with the highest percentage of Gammaproteobacteria was R9 (43% of sequences), followed by R11 (38%) and R10 (31%). All three of these samples were basalts that appeared to be glassier/less altered and had thinner exterior rinds as compared to the rest of the samples collected, suggesting the less altered basalts ($n = 4$) host more Gammaproteobacteria relative to the more altered samples ($n = 8$; see **Figure 1C** for an image of basalt R9 and Figure S1 for all others). A Mann–Whitney U test found this difference to be significant ($p = 0.024$).

Of the 213 OTUs assigned to the Gammaproteobacteria (out of 1595 total OTUs in the filtered dataset, **Figure 4**), 178 fall within or near the orders Alteromonadales, Chromatiales, Legionalles, Methylococcales, Oceanospiralles, Pseudomonadales, and Thiotrichales (**Figure 6**). The most abundant bacterial OTUs recovered (totaling ∼15% of all reads collected from the rock samples) were most closely related to the obligate chemolithoautotrophic, sulfur-oxidizing *Thioprofundum* isolates within the Chromatiales as determined by BLAST sequence alignment. Representative sequences Otu000002 (192,401 sequences from rocks), Otu000003 (69,037 sequences), and Otu000016 (52,265 sequences) were 95, 96, and 93% similar to *T. lithotrophicum* and 94, 95, and 93% similar to *T. hispidum*, respectively. These species were isolated from deep-sea hydrothermal environments and are known to oxidize sulfur with oxygen and/or nitrate (Takai et al., 2009; Mori et al., 2011). These phylogenic groups are also commonly observed on basalts from other environments (**Figure 6**). Although the clade labeled Otu000002 in **Figure 6** groups nearer to *Oceanococcus atlanticus* than to *Thioprofundum* spp., a BLAST alignment shows this OTU is only 87% similar to *Oceanococcus* as compared to 94–95% similarity to *Thioprofundum* spp. This discrepancy between BLAST alignment and tree topology is likely due to the difference between a simple pairwise alignment and using an evolutionary model as applied in tree construction (trees were built with the general time reversible model, and tests using the Jukes-Cantor model revealed the same clustering). This may also be partly due to the lower resolution resulting from the V4 region of the 16S rRNA gene; however, the near full-length EPR sequence within

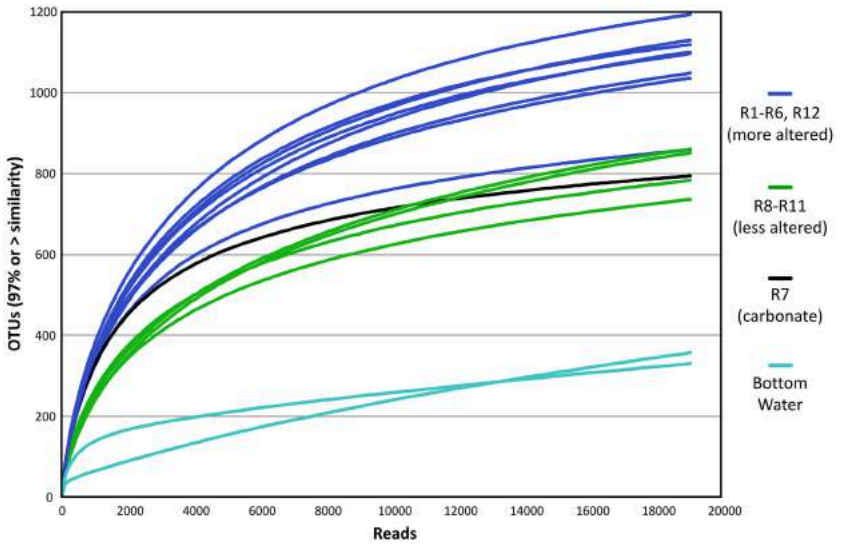

FIGURE 3 | Estimation of diversity between sample types as shown by rarefaction analysis of rock microbial community 16S rRNA gene sequence data, with each sample set subsampled to the size of the smallest dataset from bottom seawater sample. x-Axis shows number of sequences and y-axis indicates estimated number of operational taxonomic units (OTUs) defined at the 97% or greater sequence similarity level. Blue represents the more altered basalts, green the less altered, black the lithified carbonate sample, and aqua the two bottom water samples.

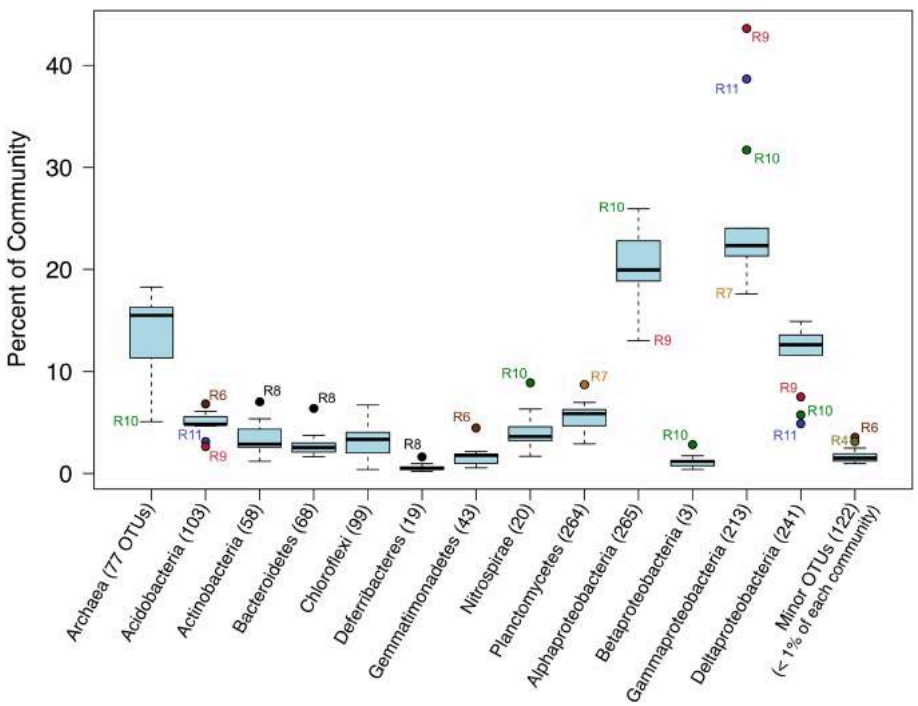

FIGURE 4 | Box-and-Whisker plot of median, upper and lower quartiles, and maximum and minimum percent abundance of 16S rRNA gene sequences from major taxa across all Dorado Outcrop basalt samples. Outliers depicted with filled circle symbols. Number of operational taxonomic units (OTUs, defined at 97% or greater sequence similarity) in each taxonomic group indicated in parentheses.

the compressed clade including Otu000002 was found to be 90% similar to *T. lithotrophicum*, 89% similar to *T. hispidum,* and 88% similar to *O. atlanticus*, showing this clustering is not solely an artifact of the short sequence length of the tag data (data not shown). It has been shown before that the Chromatiales are not monophyletic and splitting of this order has been supported by

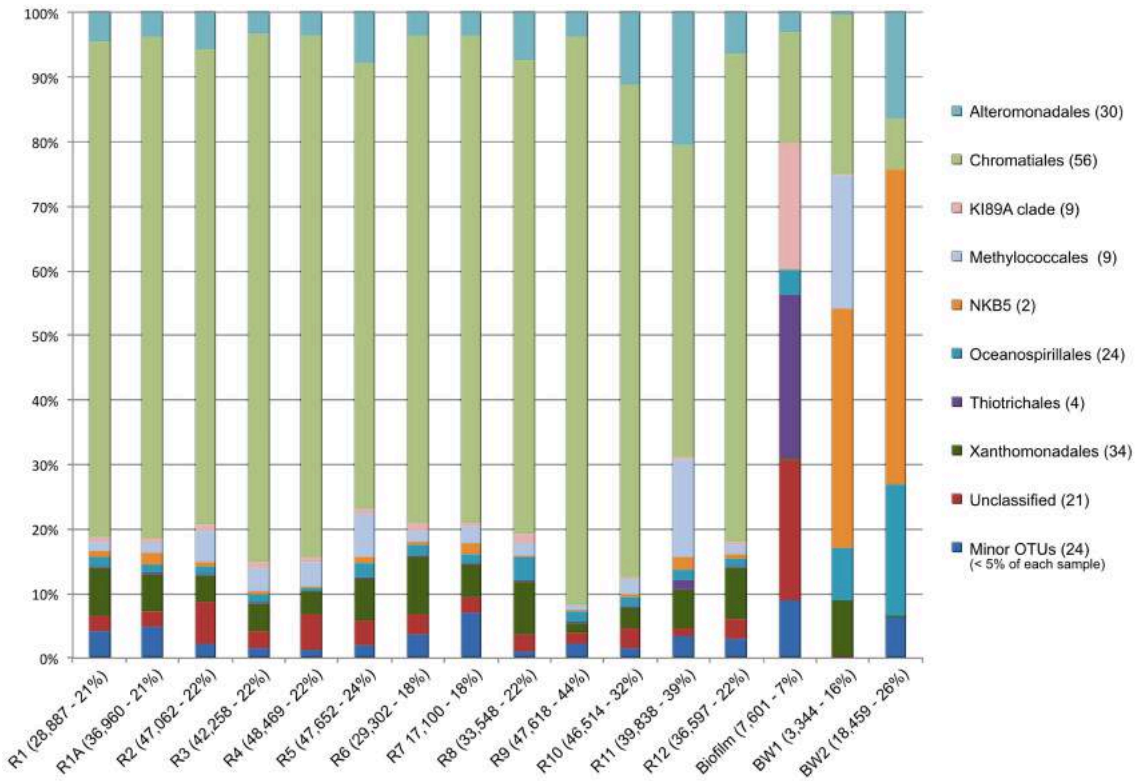

FIGURE 5 | Breakdown of Gammaproteobacteria by order. In parentheses next to sample names on the x-axis are the total number of reads for each sample and the percentage of that sample's total they represent. In parentheses next to each taxon is the number of OTUs (97% similarity or greater) recovered in that taxon.

phylogenetic trees built with hundreds of concatenated protein sequences (Williams et al., 2010).

Alphaproteobacteria was the next most abundant bacterial class, making up ∼20% of each rock community on average, with 265 OTUs at the 3% dissimilarity level (**Figure 4**, Figure S6). The dominant orders identified were Rhodospirillales and Rhizobiales (**Figure 7**, Figure S7), with a significantly greater proportion of Rhodospirillales being found on the more altered basalts (60.5% of Alphaproteobacteria) than on the less altered (42.2%; Mann–Whitney U test, $p = 0.006$). The dominant Alphaproteobacteria groups on rock samples were also found in the water samples, though in much lower relative abundance, indicating some connectivity between these environments. The most prominent representative OTU within the Rhodospirillales, Otu000013, was found by BLAST alignment to be 99% similar to an unpublished environmental clone obtained from sediment within the Barents Sea (GenBank accession number FJ800194) and 92% similar to *Pelagibius litoralis*, an isolate from seawater off the coast of Korea (Choi et al., 2009). Otu000059 is 95% similar to the same cultured isolate. Although *P. litoralis* is a common water column bacterium, the proportion of these reads found on basalt samples as compared to the proportion recovered from the water samples grants some confidence they may be predominantly rock-hosted organisms. For example, in examining the normalized dataset, Otu000013 had over 6000 rock sample sequences and only 18 water sample sequences, and Otu000059 had 472 sequences from rock samples and only three from water samples. Otu000011 in the Rhizobiales order is 97% similar to cultured *Hyphomicrobium* spp. and is also relatively more abundant on the rocks (2500 reads or 0.12% of rock sequences) than in the water (11 reads or 0.01% of water samples).

The green veneer scraped off of sample R11 (Figure S2) was almost entirely comprised of Alphaproteobacteria (∼80% of sequences, Figure S6), with the majority of sequences (∼40% of total community) grouping by the SB1-18 clade (Figure S7). This Otu000024 was only distantly related (<90% similarity) to the any cultured isolates while environmental BLAST hits included 98% similarity to endosymbionts recovered from the bone-eating worm *Osedax mucofloris* collected from a whale-fall in the North Atlantic (Verna et al., 2010), and 98% similar to clones recovered from sunken wood in the Mediterranean Sea (Bessette et al., 2014). This OTU was much more rare in the rock (0.06% of sequences) and water samples (0.01%).

Deltaproteobacteria made up roughly 12% of the rock communities on average, with 241 OTUs being called at the 3% dissimilarity level (**Figure 4**), with sequences grouping within the Myxococcales, Desulfobacterales, Syntrophorhabdaceae, Desulfarculales, and Desulfuromonadales (Figures S8, S9).

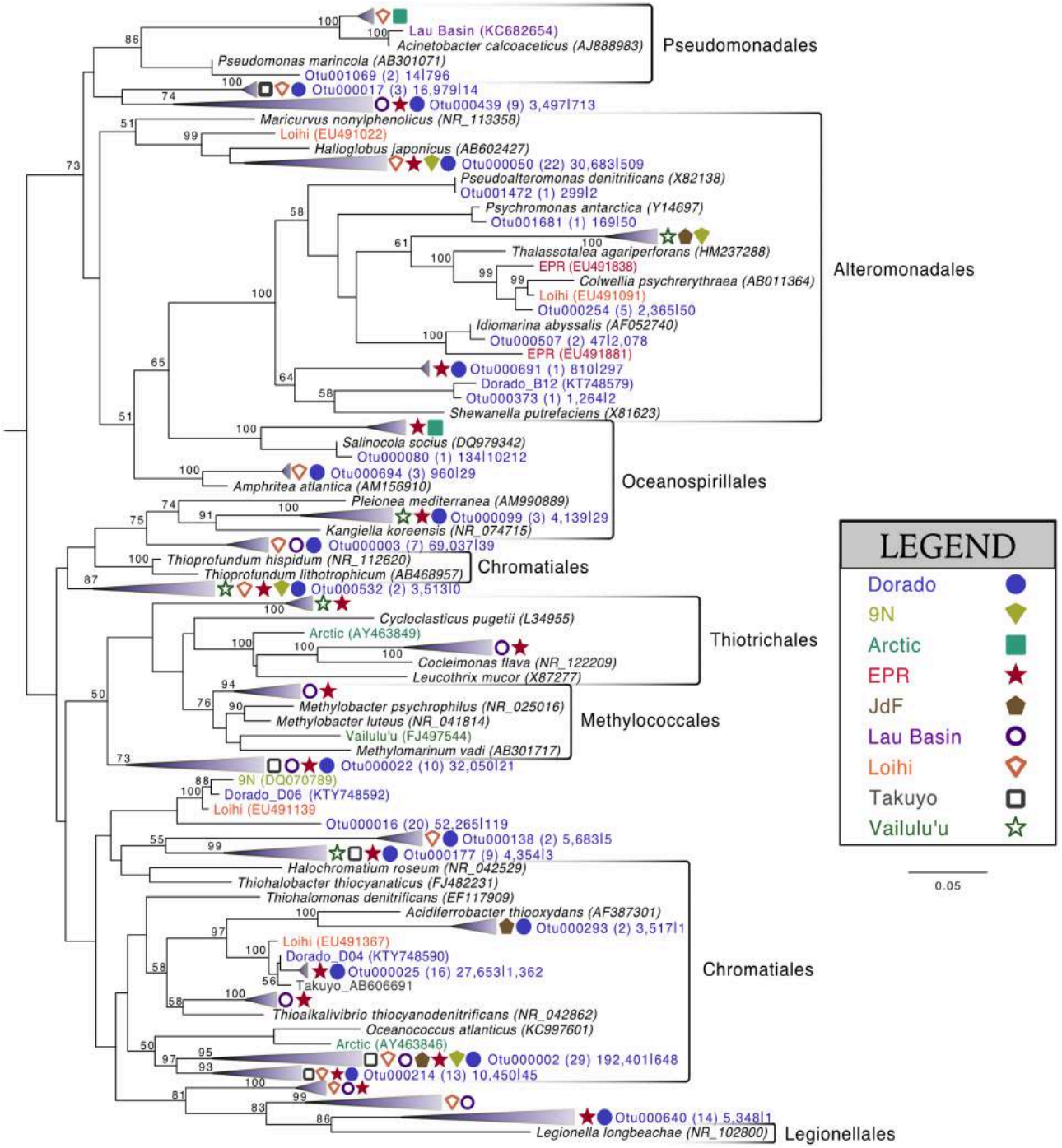

FIGURE 6 | Phylogenetic tree of seafloor basalt Gammaproteobacteria based on the hypervariable V4 region of the 16S rRNA gene. Tree topology determined using publicly available nearly full-length sequences from environmental samples or cultivated representatives (GenBank accession number listed in parentheses), with representatives of shorter tag OTUs from this study inserted with pplacer (Matsen et al., 2010). Closely related OTUs from this study are grouped together into fans, with number of Dorado tag OTUs indicated in parentheses followed by number of sequences from all rock samples ($n = 13$) |bottom seawater samples ($n = 2$). Sequences from other seafloor basalt samples that group most closely to OTU fans indicated by symbols shown in legend. Support for branching patterns of the maximum likelihood tree from 1000 bootstraps reported at the nodes. *Mariprofundus ferrooxydans* was used as the outgroup (not shown).

The same group of less altered basalts that had a significantly higher proportion of Gammaproteobacteria as compared to the more altered samples also had a lower proportion of Deltaproteobacteria (**Figure 4**), though not found to be significantly different when including R8 in the test (Mann–Whitney U test, $p = 0.11$).

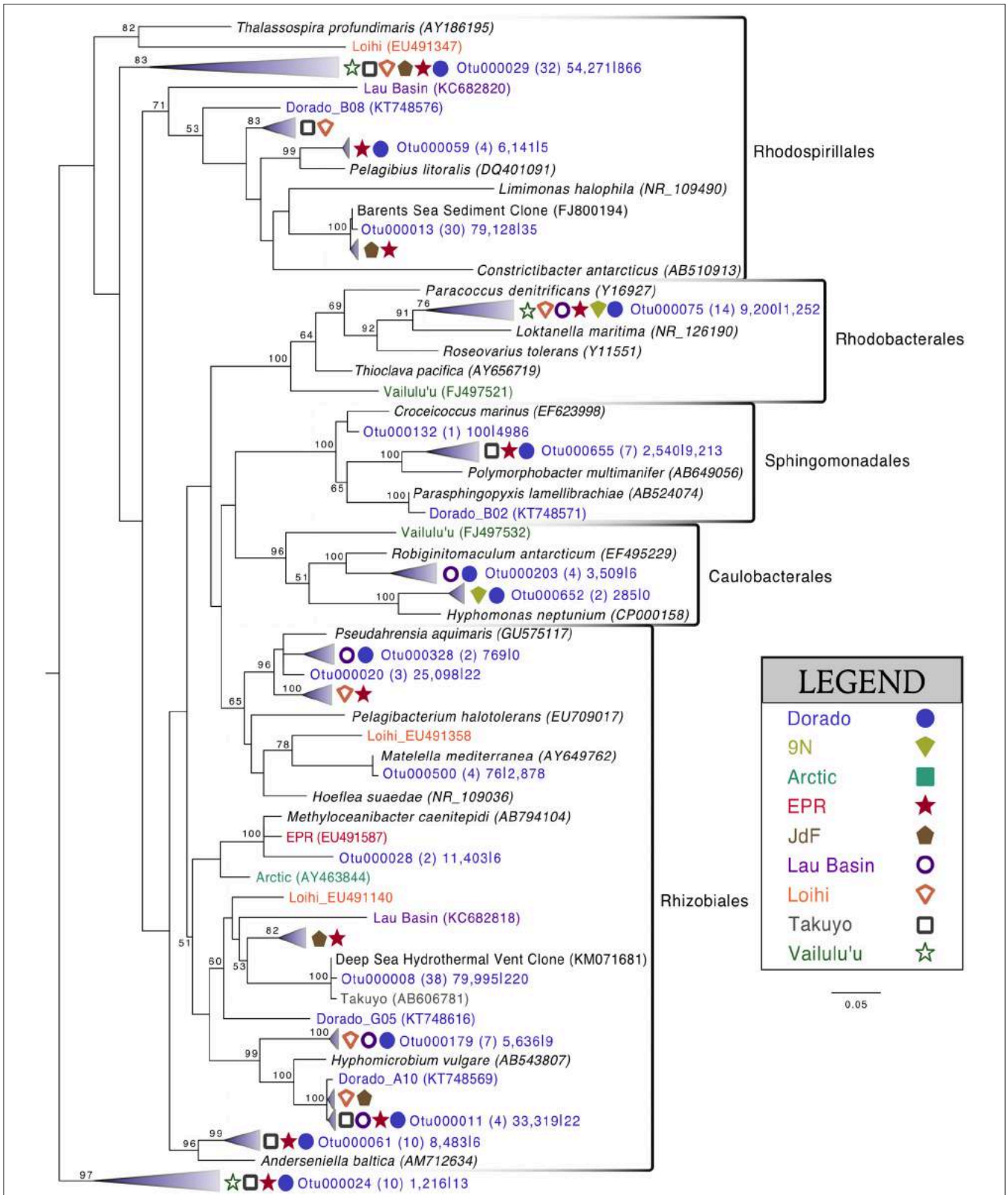

FIGURE 7 | Phylogenetic tree of seafloor basalt Alphaproteobacteria based on the hypervariable V4 region of the 16S rRNA gene, created using similar conditions as listed for Figure 6.

Major bacterial groups recovered outside of the Proteobacteria phylum included, by order of relative abundance (**Figure 4**), Planctomycetes, Acidobacteria, Nitrospirae, Actinobacteria, Gemmatimonadetes, and Chloroflexi, all of which have been identified in basalt samples from previous studies (Lysnes et al., 2004; Mason et al., 2009; Nitahara et al., 2011; Sylvan et al., 2013). All together these make up <20% of each community of the rocks sampled.

Archaeal reads averaged about 15% of total communities on the basalts collected, with significantly fewer being found on the less altered samples (an average of 8.5%) than on the more altered basalts (15.7%; Mann–Whitney U test, $p = 0.02$). Though Bacteria overall are more dominant than Archaea, the most abundant OTU in the entire dataset was archaeal. Otu000001 (167,020 sequences from rocks) groups near the cultured Marine Group I Thaumarchaeota *Nitrosopumilus maritimus* and *Nitrosopumilus koreensis* (**Figure 8**), with BLAST alignments of 97% similarity to both. Members of this genus are globally-distributed, known chemolithoautotrophic ammonia-oxidizers suspected to play an integral role in carbon and nitrogen cycling (Walker et al., 2010). While the genus *Nitrosopumilus* is ubiquitous in deep marine waters, some of the OTUs appear to have a preference for basalts as opposed to water. For example, Otu000001 represents 8.1% of the total reads recovered from the rock communities, and only 0.7% of the water communities, whereas, for example, Otu000039 that groups closer to *Nitrosopumilus* spp. represents 0.2% of the rock communities and 10% of the water samples.

Similarity of Dorado Outcrop Basalt Communities to Other Basalt Samples

Comparison of the Dorado Outcrop tags and clone library sequences with other previously published basalt sample clone datasets revealed several monophyletic clades of basalt-derived sequences. For example, within the Gammaproteobacteria, the collapsed clade labeled as Dorado tag Otu000002 (**Figure 6**) contains clones from six out of the eight other sites included in the analysis (the only exceptions being the young Vailulu'u seamount and the Arctic Ridge, which has a clone very near). This was the most abundant bacterial OTU recovered in this study, totaling over 10% of all reads collected, and is only 95% similar to the cultured obligate chemolithoautotrophic, sulfur-oxidizing *Thioprofundum* spp. As another example, within Rhodospirillales of the Alphaproteobacteria, Otu000029 contains sequences from Takuyo, Loihi, JdF, and EPR, with a Vailulu'u clone branching nearby (**Figure 7**). This representative Dorado tag OTU, Otu000029, contained about 2.5% of all sequences recovered from the 12 rock samples and has only 93% sequence similarity to *Limimonas halophile*, a chemoheterotroph isolated from a hypersaline lake (Amoozegar et al., 2013). Together with closely related Otu000013, these two OTUs make up over 6.5% of total sequences recovered in this study, and they have near neighbors that were recovered from five out of the eight other sites examined, suggesting a global distribution of this clade. Another Alphaproteobacteria clade containing Otu000075 within the Rhodobacterales also has clones from Vailulu'u, Loihi, Lau Basin, EPR, and 9N. These are most closely related to the cultured representative *Loktanella maritima* (96% similarity), which was recently isolated from shallow sediments in the Sea of Japan (Tanaka et al., 2014). Within the Rhizobiales order there are numerous clades branching out around the cultured *Hyphomicrobium vulgare*, containing sequences recovered from every site except the very young Vailulu'u and 9N samples (being from recent eruptions about 10 and 20 years ago, respectively). Within the Deltaproteobacteria, a large monophyletic clade is found between the orders Desulfarculales and Desulfuramonadales that contains basalt sequences from many sites (Figure S8) with no closely related cultured representatives (<86% similarity to *Geobacter* spp.). Similarly, another basalt clade found within the Deltaproteobacteria is represented by Otu000057 and has near neighbors from Loihi, EPR, Takuyo, and the Atlantic Arctic Ridge. Additionally, a large clade of Thaumarchaeota comprised of basalt and sediment environmental sequences was observed grouping near *Nitrosopumilus* spp. (**Figure 8**).

At a broader taxonomic level, all basalt samples examined in this study, as well as previous studies, are dominated by Gamma-, Alpha-, and Delta-proteobacteria (**Figure 9**). In alignment with results of this study, wherein the less altered basalts were found to have a greater proportion of Gammaproteobacteria and lower proportion of Deltaproteobacteria than in the more altered samples (**Figure 4**), the proportions of Gammaproteobacteria appear to decrease while Deltaproteobacteria increase as age increases in basalts (**Figure 9**). Additionally, Bacteroidetes have been recovered from every site, as were Planctomycetes and Acidobacteria (with the exception of the very newly erupted Vailulu'u sample), whereas other bacterial phyla do not have consistent trends. However, sequence library size may play a factor in this interpretation, with sample sets ranging from only 32 clones up to 470. The use of different DNA extraction methods, primer sets, and sequencing technologies may also skew these interpretations. As one measure of this, the single clone library constructed from Dorado sample R5 was compared to the Dorado tag sequence library. Only 61% of OTUs identified in the clone library (33 out of 54 total clone OTUs) were shared with OTUs from the tag library, even though these were from the same site. It should be noted this may also be due to the tag dataset having already been clustered into OTUs at the 3% dissimilarity level. While these differences prohibit any quantitative analyses between sites, it still allows a conservative window into the presence or absence of specific OTUs globally. Following these caveats, an analysis of the Dorado Outcrop basalt tag OTU library with clone libraries from other geographically-disparate studies reveals a significant trend of an increasing proportion of shared OTUs with sample set age ($p = 0.006$; **Figure 10**).

DISCUSSION

As a low-temperature (5–15°C) venting site likely representative of millions of similar features on the seafloor (Etnoyer et al., 2010; Wessel et al., 2010), Dorado Outcrop represents a new end-member in the global survey of hydrothermal systems and basalt biomes that has heretofore not been examined. Our analysis of 16S rRNA genes from Dorado Outcrop basalts confirms the

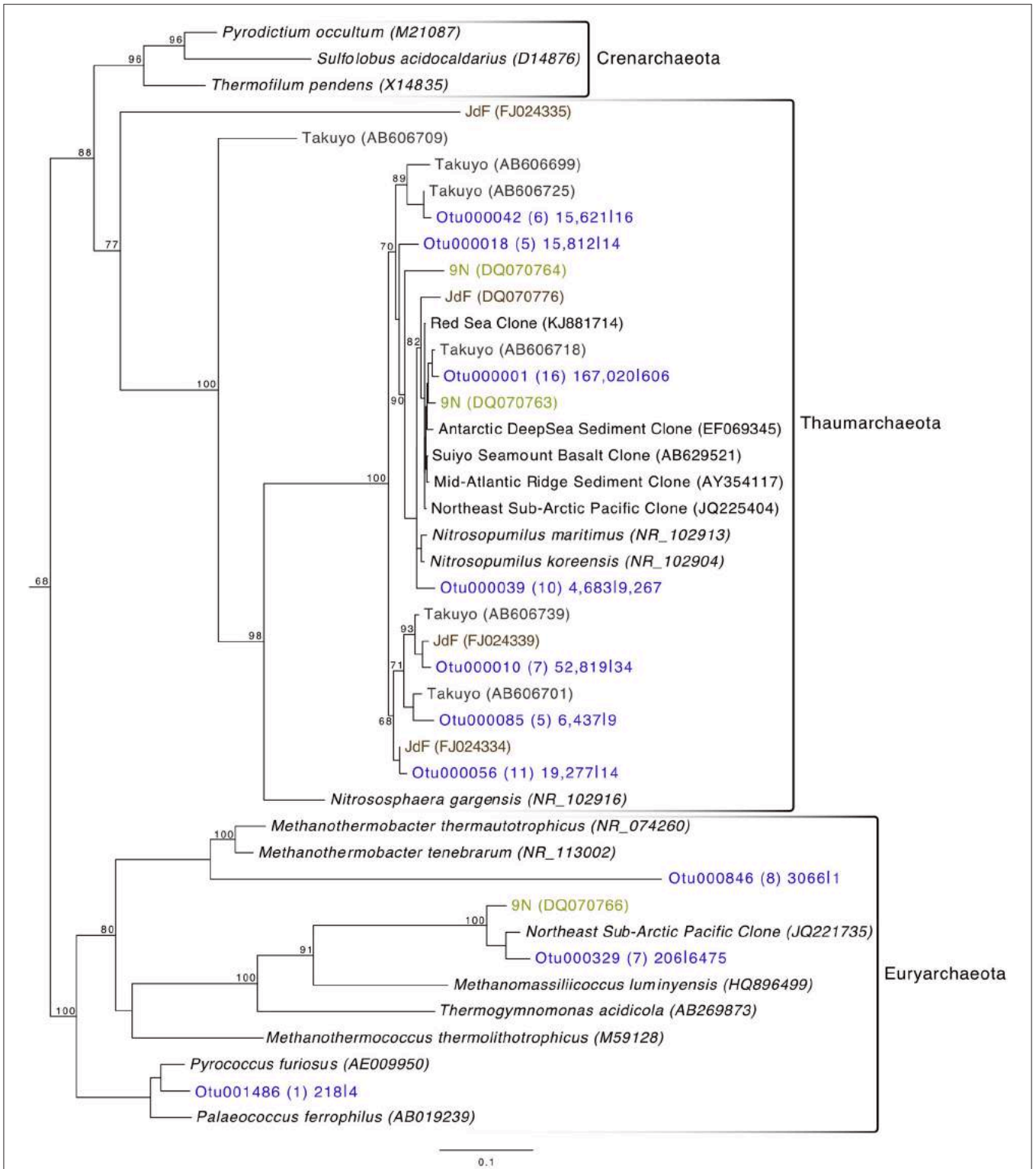

FIGURE 8 | Phylogenetic tree of seafloor basalt Archaea based on the hypervariable V4 region of the 16S rRNA gene, created using similar conditions as listed for Figure 6.

pattern of overall basalt microbial community dominance by Gamma-, Alpha-, and Deltaproteobacteria (**Figure 4**), consistent with previous surveys of much younger and older basalts from geographically distant locations (**Figure 9**). Furthermore, this new sequence study provides further support for the idea put forward previously (Mason et al., 2009) that there is a clade

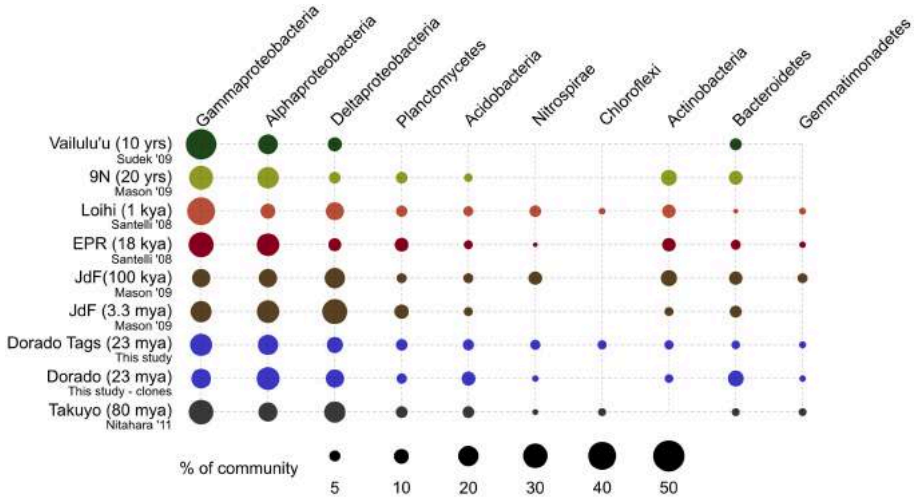

FIGURE 9 | Comparison of major bacterial taxa abundances between Dorado Outcrop rocks and other seafloor basalt sample sets. Proportions of 16S rRNA gene sequences in each taxonomic group indicated by size of circles, as shown in legend. Dorado Outcrop dataset from tag sequencing of V4 hypervariable region, while other sample sets are clone library data of nearly full-length 16S rRNA gene sequences. Ages of samples sets are listed in parentheses. From top to bottom: n = 142, 35, 470, 352, 25, 32, 2,068,892, 67, 86.

of basalt-hosted Thaumarchaeota very closely related to the genus *Nitrosopumilus* (**Figure 8**). There also appears to be an age correlation in the overlap of microbial community membership, with increasing similarity of communities with age (**Figure 10**), suggesting that species endemism on young basalts possibly diminishes with aging, yielding to a shifting community dynamic that may eventually stabilize to reflect a more global seafloor basalt biome.

Diversity and Potential Function of Microbial Communities on Dorado Outcrop Basalts

The majority of sequences recovered were bacterial, dominating samples about 85–15% over Archaea (**Figure 4**). Previous studies have ranged from finding <0.02% Archaea ($n = 7$) through qPCR on samples dredged up from the Knipovich Ridge up in the Atlantic–Arctic Ocean (Einen et al., 2008), to 4–12% ($n = 5$) on samples collected directly from the seafloor at the EPR (Santelli et al., 2008), to 65% ($n = 1$) on a sample collected from the seafloor at Takuyo Seamount near Japan, though clone libraries from the same study yielded 17% Archaea with the discrepancy suspected by the authors to be due to PCR bias (Nitahara et al., 2011). The Arctic Ridge samples varied in age from <30 years to 100 kya, the EPR samples were estimated at <18 kya, and Takuyo at ∼80 mya. Due to the overlap in age between the Arctic and EPR samples, a simple correlation with age to explain the drastic shift in proportion of Archaea recovered does not suffice. However, data from this study suggest that more altered basalts host a higher proportion of Archaea than those that are less altered (16.7% as compared to 8.5%, Mann–Whitney U, $p = 0.02$).

The most abundant individual OTU recovered across all rock samples in the current study (making up just over 5% of all reads recovered) was comprised of sequences representative of Thaumarchaeota most closely related to two isolates of the *Nitrosopumilus* genus. Though *N. maritimus* is commonly found in the water column (Karner et al., 2001), *N. koreensis* was isolated through enrichment cultures of Arctic sediment (Park et al., 2010). And while 16S rRNA gene similarities (99%) group these species very near each other (**Figure 8**), genomic analysis has identified that outside of core genes involved in ammonia oxidation and lithotrophy, 30% of *N. koreensis's* genes are unique with respect to *N. maritimus*, demonstrating these species may possess more differences than their ribosomal phylogeny would suggest alone (Park et al., 2012). This gives confidence to the idea of a crust-specific clade of *Nitrosopumilus*, just as *N. koreensis* appears to be a sediment-specific clade. We suggest that Otu000001 (**Figure 8**) represents a rock-associated *Nitrosopumilus* as it comprises 8.1% of the rock communities recovered, and only 0.7% of the water communities, whereas, in contrast, Otu000039 makes up only 0.2% of the rock communities, and 10% of the water communities. Given their abundance and global distribution as chemolithoautotrophic ammonia-oxidizers, it is likely these organisms play a key role in C and N cycling in the global basalt biome in addition to the sediment and water column.

It is likely that S and C cycling, and possibly N cycling, are partially mediated by the highly abundant OTUs that are most closely related to *Thioprofundum lithotrophicum* and *Thioprofundum hispidum* (95–96% similar) within the Gammaproteobacteria. These are known chemolithoautotrophic sulfur-oxidizers that utilize nitrate and oxygen as electron acceptors, and they are commonly observed on globally distributed basalts (**Figure 6**). *Thioprofundum* group within the Chromatiales order, which has previously been indicated as a group involved in carbon fixation on seafloor basalts via

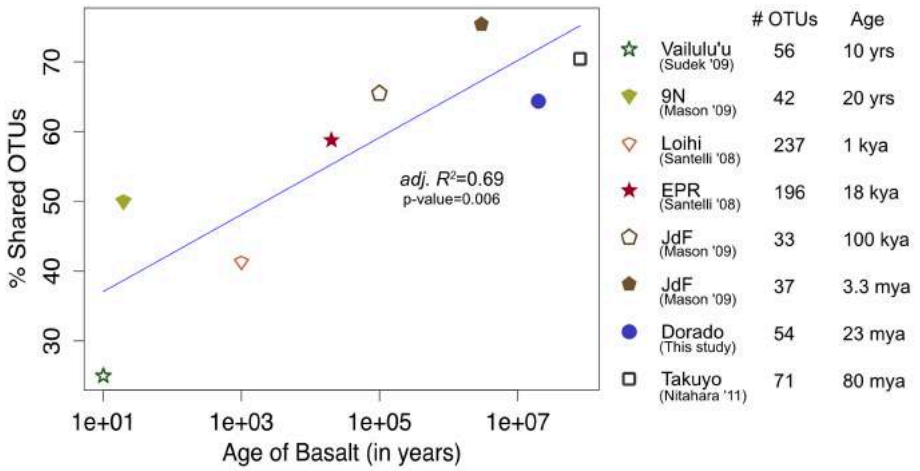

FIGURE 10 | Bacterial community overlap between Dorado Outcrop 16S rRNA gene V4 hypervariable region sequence OTUs from this study in comparison to clone library sequences from other seafloor basalt samples trimmed to the same region, as based on percent of shared operational taxonomic units (OTUs) defined at the 97% or greater sequence similarity level, and plotted in relation to site age. From top to bottom in the legend, number of samples available from each study that contributed to the clone libraries: 1, 1, 4, 6, 1, 1, 1, 1.

the Calvin cycle using RuBisCO form II (Orcutt et al., 2015). Microarray analysis of a seafloor basalt sample from JdF revealed RuBisCO genes (Mason et al., 2009), and quantitative PCR of globally distributed basalts revealed a higher abundance of Calvin cycle genes compared to other carbon cycling pathways (Orcutt et al., 2015). Thus, we propose that the *Thioprofundum*-related OTUs observed in this study, and commonly observed on basalts, are likely major contributors to carbon cycling on basalts, gaining energy from the oxidation of reduced sulfur with either oxygen or nitrate. Although Deltaproteobacteria are commonly known to be involved in sulfur cycling in the marine environment, sequences recovered from this study were only 86% similar to cultivated species, making any assignment of function tenuous. Relative abundance of the Deltaproteobacteria indicates that they may be restricted to anaerobic microniches within the basalt rind that builds up over time, since their sequences are more abundant in altered basalts (∼13% of sequences) than on less altered basalts (∼8%), and since sequence abundance seems to be lowest on the youngest basaltic substrates (**Figure 9**).

Many of the basalts recovered in this study had thick manganese oxide rinds with visible iron oxide staining, indicating that manganese and/or iron cycling may support chemolithotrophy in these samples. Within the Alphaproteobacteria, the relatively abundant Otu000011 (with 1.5% of total sequences from rocks) is 95% similar to *Hyphomicrobium vulgare*, a known manganese oxidizer. Within the Gammaproteobacteria, Otu001472, though low in abundance, is 100% similar to the known manganese oxidizer *Pseudoalteromonas denitrificans* (**Figure 6**). Observation of these groups indicates the possibility of Mn oxidation occurring on the basalts. Otu000652, within the Alphaproteobacteria, groups near the known iron-oxidizer *Hyphomonas neptunium* at 96% sequence similarity (BLAST alignment; **Figure 7**). Possible iron-reducers can be found within the Alteromonadales clade, with Otu000373 closely related to *Shewanella putrefaciens* (97% similarity according to BLAST alignment; **Figure 6**). Notably, no sequences from the known marine neutrophilic iron oxidizing Zetaproteobacteria, commonly found in areas with relatively high concentrations of dissolved reduced iron (Emerson et al., 2007), were detected in this study. Thus, the identities of potential iron oxidizing bacteria on the Dorado Outcrop basalts are unclear, as it often the case in other studies of basalt microbial communities (Mason et al., 2007, 2009; Santelli et al., 2009).

Biogeography of Clades Enriched on Basalt

As has been investigated previously (Mason et al., 2007, 2009), phylogenetic trees constructed with 16S rRNA gene sequences recovered from multiple studies of geographically distinct seafloor basalts, nearest cultured and environmental samples, and this study elucidate many lithic clades that appear ubiquitous in their distribution. One example includes the highly abundant Gammaproteobacteria most closely related to members of the genus *Thioprofundum* represented by Otu000002 (**Figure 6**). The abundance of these sequences recovered from Dorado Outcrop and its presence in almost every other dataset support that this is likely a globally-significant basalt ecotype that may play a role in C, S, and potentially N cycling at the seafloor. Similarly, several monophyletic clades consisting of basalt sequences from all sites examined can be found within the Deltaproteobacteria, e.g., those surrounding Otu000027, Otu000037, Otu000057, and Otu000074 (Figure S8). Furthermore, all basalt studies that have recovered Archaeal sequences (Thorseth et al., 2001; Lysnes et al., 2004; Mason et al., 2007, 2009; Nitahara et al., 2011) have observed the Thaumarchaeota clade that has been suggested to be ocean-crust specific (Mason et al., 2009), and that is the single most abundant OTU in the Dorado Outcrop dataset (**Figure 8**). Considering the close sequence similarity of this clade to *N.*

maritimus and *N. koreensis*, it is likely these organisms play an important role in ammonia oxidation and C cycling at the seafloor. While this clade is also found in the water column, the much higher relative abundance of this group in the basalt samples suggested that it has a lithic niche. Supporting the idea of lithic niches for *Nitrosopumilus*-related groups, subaerial ferromanganese deposits in terrestrial caves have been found to host abundant Thaumarchaeota (Northup et al., 2003) with 86–90% sequence similarity to *Nitrosopumilus* and Otu000001 and Otu000010 from this study.

The common appearance of such abundant clades on globally distributed seafloor basalts begs the question of what drives these similarities. The relationship of increasing diversity correlating with increasing levels of alteration has been put forward before (Lysnes et al., 2004; Mason et al., 2009; Santelli et al., 2009), and this premise is supported by rarefaction analysis of the Dorado Outcrop basalts (**Figure 3**). In many cases, such as in the present study, detailed chemical composition data of the basalts is not available, preventing an analysis of how much rock composition drives these similarities. As a proxy for rock composition and alteration state, we examined the similarity of basalt microbial communities based on the approximate age of the basalts. By calculating the percent of shared OTUs between this study's tag data and other sites' clones to further investigate any presence/absence relationships of specific OTUs, a strong positive correlation between percent OTUs shared and increasing age of basalt emerged (adj. $R^2 = 0.69$, $p = 0.006$, **Figure 10**). However, the largest difference, and much of the support of the regression, seems to be due to the three youngest data points (from Vailulu, 9N, and Loihi); when these sites are removed from the analysis, the correlation is no longer significant (adj. $R^2 = 0.10$, $p = 0.31$, data not shown). Also, although the regression based on age is strong ($R^2 = 0.69$) with a significant relationship ($p = 0.006$), the low number of available sequences from some samples/sites and the methodology of comparing tag sequence data to clones further convolutes this apparent relationship to an unknown degree. For example, when performing the same analysis with only the clone data from this study ($n = 67$ sequences) compared to the clones from other sites, the correlation disappears (data not shown). This is likely due to insufficient data as a result of the relatively shallow depth offered by clone libraries. Nevertheless, while the correlation of shared communities with regard to age requires deeper examination, the percentage of OTUs from other sites that were also observed at Dorado Outcrop ranges from 25 to 75%, with more overlap being found at older sites.

Due to Dorado being 23 million years old and having the most overlap with "older" sites (>1000 years), this suggests there may be a broader relationship underlying the available data wherein very young, glassier basalts (<1000 years old in this case) host unique communities as compared with those >1000 years old. Pitting of fresh, glassy basalt surfaces as a result of biological activity has been observed in the lab to occur within weeks, showing fresh basalts can be, and likely are, immediately colonized after formation at the seafloor (Staudigel et al., 1995, 1998; Thorseth et al., 1995). This initial environment, composed solely of newly solidified basalt conditions, may provide only a relatively narrow range of distinct habitats for microorganisms. Aged basalts, in contrast, accrete organics and allochthonous, biologically-significant metals during the course of abiotic/biotic alterations, and develop stratified outer rinds with cracks and fissures providing aerobic/anaerobic microniches with a greater availability of energy sources (Mero, 1962; Zinger et al., 2012). Thus, they may come to host extremely diverse, though globally ubiquitous, communities.

CONCLUSIONS

This work provides the first community assessment of a new basalt biome—with regard to age and hydrothermal properties—that is likely representative of millions of outcrops globally. In alignment with previous studies, Gamma-, Alpha-, and Deltaproteobacteria seem to dominate the lithic communities, and greater biodiversity was found on basalts with more highly altered outer rinds. We identified several shared OTUs between global seafloor basalt studies that appear to form monophyletic clades to the exclusion of other environments. This conservation of certain taxa colonizing seafloor basalts is likely due to the selective geochemical environment and to there being virtually no dispersal limitation for microbes throughout the oceans. Of these globally ubiquitous clades, particularly of note are abundantly recovered OTUs from this study that are closely related to sulfur-oxidizing, chemolithoautotrophic Gammaproteobacteria, as well as what appear to be crust-specific ammonia-oxidizing archaea. The cosmopolitan distributions, high proportions, and lineages of these organisms suggest they may play substantial roles in C, N, and S cycling globally, and identifies them as clear subjects for future, targeted metagenomic and metatranscriptomic efforts. Our analysis also reveals a significant correlation between basalt age and microbial community membership. From the limited available data, it appears that upon initial formation basalts host distinct communities as compared to those greater than a few thousand years old. Moreover, it appears the communities may stabilize somewhat over time as the proportion of shared OTUs between Dorado (23 mya) did not greatly fluctuate between those that are ∼18 kya to a site that is ∼80 mya. It seems as though the initial environment, driven primarily by only those substrates sourced from the basalt itself, selects for a founding population that over time begins to shift, giving way to a much more diverse lithic community. Mechanisms that may be involved with driving this shift include the persistent accretion of metals and organics through fluid-deposition, the accumulation of breakdown products, and the spawning of various microniches coincident with ongoing biotic/abiotic weathering and development of an outer alteration rind that is ultimately likely to be more indicative of the global seafloor basalt biome.

AUTHOR CONTRIBUTIONS

BO, KE, and ML conceived the study; BO and ML collected the samples; and ML carried out all laboratory analyses. ML

performed all data analysis with support from NW and JS. ML wrote the manuscript with input from all authors.

ACKNOWLEDGMENTS

We thank the science party and ship crew of the RV *Atlantis* cruise AT26-09, and the crews of the ROV *Jason-II* and AUV *Sentry* (Woods Hole Oceanographic Institution), for assistance with sample recovery. In particular, we thank Samuel Hulme and Chris Treboal for generating bathymetric maps. We also thank Grayson Chadwick for computational assistance and direction. Funding for this work was provided in part by NSF (OCE-1233226 to BO) and the NSF-funded Center for Dark Energy Biosphere Investigations Science and Technology Center (C-DEBI, OCE-0939564). Ship time was supported in association with NSF-funding to C. Geoff Wheat, Andrew T. Fisher, and Samuel Hulme (OCE-1260548 and linked proposals). This is C-DEBI contribution 286. This manuscript is dedicated to the memory of co-author KE, who inspired this project.

SUPPLEMENTARY MATERIAL

The Supplementary Material for this article can be found online at: http://journal.frontiersin.org/article/10.3389/fmicb.2015.01470

REFERENCES

Altschul, S. F., Gish, W., Miller, W., Myers, E. W., and Lipman, D. J. (1990). Basic local alignment search tool. *J. Mol. Biol.* 215, 403–410. doi: 10.1016/S0022-2836(05)80360-2

Amoozegar, M. A., Makhdoumi-Kakhki, A., Ramezani, M., Nikou, M. M., Fazeli, S. A., Schumann, P., et al. (2013). *Limimonas halophila* gen. nov., sp. nov., an extremely halophilic bacterium in the family Rhodospirillaceae. *Int. J. Syst. Evol. Microbiol.* 63, 1562–1567. doi: 10.1099/ijs.0.041236-0

Bach, W., and Edwards, K. J. (2003). Iron and sulfide oxidation within basalt ocean crust: implications for chemolithoautotrophic microbial biomass production. *Geochim. Cosmochim. Acta* 67, 3871–3887. doi: 10.1016/S0016-7037(03)00304-1

Bessette, S., Fagervold, S. K., Romano, C., Martin, D., Le Bris, N., and Galand, P. E. (2014). Diversity of bacterial communities on sunken woods in the mediterranean sea. *J. Mar. Sci. Technol.* 22, 60–66. doi: 10.6119/JMST-013-0829-2

Bokulich, N. A., Subramanian, S., Faith, J. J., Gevers, D., Gordon, J. I., Knight, R., et al. (2013). Quality-filtering vastly improves diversity estimates from Illumina amplicon sequencing. *Nat. Methods* 10, 57–59. doi: 10.1038/NMETH.2276

Brochier-Armanet, C., Boussau, B., Gribaldo, S., and Forterre, P. (2008). Mesophilic Crenarchaeota: proposal for a third archaeal phylum, the Thaumarchaeota. *Nat. Rev. Microbiol.* 6, 245–252. doi: 10.1038/nrmicro1852

Caporaso, J. G., Lauber, C. L., Walters, W., Berg-Lyons, D., Huntley, J., and Fierer, N., et al. (2012). Ultra-high-throughput microbial community analysis on the Illumina HiSeq and MiSeq platforms. *ISME J.* 6, 1621–1624. doi: 10.1038/ismej.2012.8

Champlot, S., Berthelot, C., Pruvost, M., Bennett, E. A., Grange, T., and Maria Geigl, E. M. (2010). An efficient multistrategy DNA decontamination procedure of PCR reagents for hypersensitive PCR applications. *PLoS ONE* 5:e13042. doi: 10.1371/journal.pone.0013042

Choi, D. H., Hwang, C. Y., and Cho, B. C. (2009). *Pelagibius litoralis* gen. nov., sp. nov., a marine bacterium in the family Rhodospirillaceae isolated from coastal seawater. *Int. J. Syst. Evol. Microbiol.* 59, 818–823. doi: 10.1099/ijs.0.002774-0

Daughney, C., Rioux, J., Fortin, D., and Pichler, T. (2004). Laboratory investigation of the role of bacteria in the weathering of basalt near deep sea hydrothermal vents. *Geomicrobiol. J.* 21, 21–31. doi: 10.1080/01490450490253437

Edgar, R. C. (2004). MUSCLE: a multiple sequence alignment method with reduced time and space complexity. *BMC Bioinformatics* 5:113. doi: 10.1186/1471-2105-5-113

Edgar, R. C., Haas, B. J., Clemente, J. C., Quince, C., and Knight, R. (2011). UCHIME improves sensitivity and speed of chimera detection. *Bioinformatics* 27, 2194–2200. doi: 10.1093/bioinformatics/btr381

Edwards, K. J., Bach, W., and McCollom, T. M. (2005). Geomicrobiology in oceanography: microbe-mineral interactions at and below the seafloor. *Trends Microbiol.* 13, 449–456. doi: 10.1016/j.tim.2005.07.005

Edwards, K. J., Bach, W., McCollom, T. M., and Rogers, D. R. (2004). Neutrophilic iron-oxidizing bacteria in the ocean: their habitats, diversity, and roles in mineral deposition, rock alteration, and biomass production in the deep-sea. *Geomicrobiol. J.* 21, 393–404. doi: 10.1080/01490450490485863

Edwards, K. J., Rogers, D. R., Wirsen, C. O., and McCollom, T. M. (2003). Isolation and characterization of novel psychrophilic, neutrophilic, Fe-oxidizing, chemolithoautotrophic alpha- and gamma-proteobacteria from the deep Sea. *Appl. Environ. Microbiol.* 69, 2906–2913. doi: 10.1128/AEM.69.5.2906-2913.2003

Einen, J., Thorseth, I. H., and Ovreås, L. (2008). Enumeration of archaea and bacteria in seafloor basalt using real-time quantitative PCR and fluorescence microscopy. *FEMS Microbiol. Lett.* 282, 182–187. doi: 10.1111/j.1574-6968.2008.01119.x

Elderfield, H., and Schultz, A. (1996). Mid-ocean ridge hydrothermal fluxes and the chemical composition of the ocean. *Annu. Rev. Earth Planet. Sci.* 24, 191–224. doi: 10.1146/annurev.earth.24.1.191

Emerson, D., Rentz, J. A., Lilburn, T. G., Davis, R. E., Aldrich, H., Chan, C., et al. (2007). A novel lineage of proteobacteria involved in formation of marine fe-oxidizing microbial mat communities. *PLoS ONE* 2:e667. doi: 10.1371/journal.pone.0000667

Etnoyer, P., John, W., and Shirley, T. (2010). How large is the seamount biome? *Oceanography* 23, 206–209. doi: 10.5670/oceanog.2010.96

German, C. R. and von Damm, K. L. (2004). Hydrothermal processes. *Treat. Geochem.* 6, 181–222. Available online at: http://www.sciencedirect.com/science/referenceworks/9780080437514

Hutnak, M., Fisher, A. T., Harris, R., Stein, C., Wang, K., Spinelli, G., et al. (2008). Large heat and fluid fluxes driven through mid-plate outcrops on ocean crust. *Nat. Geosci.* 1, 611–614. doi: 10.1038/ngeo264

Karner, M. B., DeLong, E. F., and Karl, D. M. (2001). Archaeal dominance in the mesopelagic zone of the pacific ocean. *Nature* 409, 507–510. doi: 10.1038/35054051

Kearse, M., Moir, R., Wilson, A., Stones-Havas, S., Cheung, M., Sturrock, S., Buxton, S., et al. (2012). Geneious basic: an integrated and extendable desktop software platform for the organization and analysis of sequence data. *Bioinformatics* 28, 1647–1649. doi: 10.1093/bioinformatics/bts199

Kozich, J. J., Westcott, S. L., Baxter, N. T., Highlander, S. K., and Schloss, P. D. (2013). Development of a dual-index sequencing strategy and curation pipeline for analyzing amplicon sequence data on the Miseq Illumina sequencing platform. *Appl. Environ. Microbiol.* 79, 5112–5120. doi: 10.1128/AEM.01043-13

Lane, D. J. (1991). "16S/23S rRNA Sequencing," in *Nucleic Acid Techniques in Bacterial Systematics* (Wiley), 125–175. Available online at: http://ci.nii.ac.jp/naid/10008470323/en/

Legendre, P., and Gallagher, E. D. (2001). Ecologically meaningful transformations for ordination of species data. *Oecologia* 129, 271–280. doi: 10.1007/s004420100716

Ludwig, W., Strunk, O., Westram, R., Richter, L., Meier, H., Yadhukumar, A., et al. (2004). ARB: a software environment for sequence data. *Nucleic Acids Res.* 32, 1363–1371. doi: 10.1093/nar/gkh293

Lysnes, K., Thorseth, I. H., Steinsbu, B. O., Øvreås, L., Torsvik, T., and Pedersen, R. B. (2004). Microbial community diversity in seafloor basalt from the arctic spreading ridges. *FEMS Microbiol. Ecol.* 50, 213–230. doi: 10.1016/j.femsec.2004.06.014

Mason, O. U., Di Meo-Savoie, C. A., van Nostrand, J. D., Zhou, J., Fisk, M. R., and Giovannoni, S. J. (2009). Prokaryotic diversity, distribution, and insights into their role in biogeochemical cycling in marine basalts. *ISME J.* 3, 231–242. doi: 10.1038/ismej.2008.92

Mason, O. U., Stingl, U., Wilhelm, L. J., Moeseneder, M. M., Di Meo-Savoie, C. A., Fisk, M. R., et al. (2007). The phylogeny of endolithic microbes associated with marine basalts. *Environ. Microbiol.* 9, 2539–2550. doi: 10.1111/j.1462-2920.2007.01372.x

Matsen, F. A., Kodner, R. B., and Armbrust, E. V. (2010). Pplacer: linear time maximum-likelihood and bayesian phylogenetic placement of sequences onto a fixed reference tree. *BMC Bioinformatics* 11:538. doi: 10.1186/1471-2105-11-538

Mero, J. (1962). Ocean-floor manganese nodules. *Econ. Geol.* 57, 747–767. doi: 10.2113/gsecongeo.57.5.747

Mori, K., Ichiro Suzuki, K., Urabe, T., Sugihara, M., Tanaka, K., Hamada, M., et al. (2011). *Thioprofundum hispidum* sp. nov., an obligately chemolithoautotrophic sulfur-oxidizing Gammaproteobacterium isolated from the hydrothermal field on Suiyo Seamount, and proposal of Thioalkalispiraceae fam. nov. in the order Chromatiales. *Int. J. Syst. Evol. Microbiol.* 61, 2412–2418. doi: 10.1099/ijs.0.026963-0

Nitahara, S., Kato, S., Urabe, T., Usui, A., and Yamagishi, A. (2011). Molecular characterization of the microbial community in hydrogenetic ferromanganese crusts of the Takuyo-Daigo Seamount, Northwest Pacific. *FEMS Microbiol. Lett.* 321, 121–129. doi: 10.1111/j.1574-6968.2011.02323.x

Northup, D. E., Barns, S. M., Yu, L. E., Spilde, M. N., Schelble, R. T., Dano, K. E., et al. (2003). Diverse microbial communities inhabiting ferromanganese deposits in lechuguilla and spider caves. *Environ. Microbiol.* 5, 1071–1086. doi: 10.1046/j.1462-2920.2003.00500.x

Oksanen, J. (2015). *Vegan: Community Ecology Package*. Available online at: http://cran.r-project.org/package=vegan

Orcutt, B. N., Sylvan, J. B., Rogers, D. R., Delaney, J., Lee, R. W., and Girguis, P. R. (2015). Carbon fixation by basalt-hosted microbial communities. *Front. Microbiol.* 6:904. doi: 10.3389/fmicb.2015.00904

Park, B. J., Park, S. J., Yoon, D. N., Schouten, S., Damsté, J. S. S., and Rhee, S. K. (2010). Cultivation of autotrophic ammonia-oxidizing archaea from marine sediments in coculture with sulfur-oxidizing bacteria. *Appl. Environ. Microbiol.* 76, 7575–7587. doi: 10.1128/AEM.01478-10

Park, S.-J.,Kim, J.-G., Jung, M.-Y., Kim, S.-J., Cha, I.-T., Kwon, K., et al. (2012). Draft genome sequence of an ammonia-oxidizing archaeon, 'Candidatus Nitrosopumilus Koreensis' AR1, from marine sediment. *J. Bacteriol.* 194, 6940–6941. doi: 10.1128/JB.01857-12

Pruesse, E., Peplies, J., and Glöckner, F. O. (2012). SINA: accurate high-throughput multiple sequence alignment of ribosomal RNA genes. *Bioinformatics* 28, 1823–1829. doi: 10.1093/bioinformatics/bts252

Racine, J. (2012). RSTUDIO: a platform-independent IDE for R and Sweave. *J. Appl. Econ.* 27, 36–37. doi: 10.1002/jae.1278

Rogers, D. R., Santelli, C. M., and Edwards, K. J. (2003). Geomicrobiology of deep-sea deposits: estimating community diversity from low-temperature seafloor rocks and minerals. *Geobiology* 1, 109–117. doi: 10.1046/j.1472-4669.2003.00009.x

Santelli, C. M., Edgcomb, V. P., Bach, W., and Edwards, K. J. (2009). The diversity and abundance of bacteria inhabiting seafloor lavas positively correlate with rock alteration. *Environ. Microbiol.* 11, 86–98. doi: 10.1111/j.1462-2920.2008.01743.x

Santelli, C. M., Orcutt, B. N., Banning, E., Bach, W., Moyer, C. L., Sogin, M. L., et al. (2008). Abundance and diversity of microbial life in ocean crust. *Nature* 453, 653–656. doi: 10.1038/nature06899

Schloss, P. D., Westcott, S. L., Ryabin, T., Hall, J. R., Hartmann, M., Hollister, E. B., et al. (2009). Introducing mothur: open-source, platform-independent, community-supported software for describing and comparing microbial communities. *Appl. Environ. Microbiol.* 75, 7537–7541. doi: 10.1128/AEM.01541-09

Stamatakis, A. (2014). RAxML Version 8: a tool for phylogenetic analysis and post-analysis of large phylogenies. *Bioinformatics* 30, 1312–1313. doi: 10.1093/bioinformatics/btu033

Staudigel, H., Chastain, R. A., Yayanos, A., and Bourcier, W. (1995). Biologically mediated dissolution of glass. *Chem. Geol.* 126, 147–154. doi: 10.1016/0009-2541(95)00115-X

Staudigel, H., Furnes, H., McLoughlin, N., Banerjee, N. R., Connell, L. B., and Templeton, A. (2008). 3.5 Billion years of glass bioalteration: volcanic rocks as a basis for microbial life? *Earth Sci. Rev.* 89, 156–176. doi: 10.1016/j.earscirev.2008.04.005

Staudigel, H., Yayanos, A., and De Baar, H. (1998). Biologically Mediated dissolution of volcanic glass in seawater. *Earth Planet. Sci. Lett.* 164, 233–244. doi: 10.1016/S0012-821X(98)00207-6

Sudek, L., Templeton, A. S., Tebo, B. M., and Staudigel, H. (2009). Microbial ecology of Fe (hydr)oxide mats and basaltic rock from Vailulu'u seamount, American Samoa. *Geomicrobiol. J.* 26, 581–596. doi: 10.1080/01490450903263400

Sylvan, J. B., Sia, T. Y., Haddad, A. G., Briscoe, L. J., Toner, B. M., Girguis, P. R. et al. (2013). Low temperature geomicrobiology follows host rock composition along a geochemical gradient in Lau basin. *Front. Microbiol.* 4:61. doi: 10.3389/fmicb.2013.00061

Takai, K., Miyazaki, M., Hirayama, H., Nakagawa, S., Querellou, J., and Godfroy, A. (2009). Isolation and physiological characterization of two novel, piezophilic, thermophilic chemolithoautotrophs from a deep-sea hydrothermal vent chimney. *Environ. Microbiol.* 11, 1983–1997. doi: 10.1111/j.1462-2920.2009.01921.x

Tanaka, N., Romanenko, L. A., Kurilenko, V. V., Svetashev, V. I., Kalinovskaya, N. I., Mikhailov, V. V. (2014). *Loktanella maritima* sp. nov. isolated from shallow marine sediments. Int. J. Syst. Evol. Microbiol. 64, 2370–2375. doi: 10.1099/ijs.0.061747-0

Templeton, A. S., Knowles, E. J., Eldridge, D. L., Arey, B. W., Dohnalkova, A. C., et al. (2009). A seafloor microbial biome hosted within incipient ferromanganese crusts. *Nat. Geosci.* 2, 872–876. doi: 10.1038/ngeo696

Templeton, A. S., Staudigel, H., and Tebo, B. M. (2005). Diverse Mn(II)-oxidizing bacteria isolated from submarine basalts at loihi seamount. *Geomicrobiol. J.* 22, 127–139. doi: 10.1080/01490450590945951

Thorseth, I. H., Furnes, H., and Tumyr, O. (1995). Textural and chemical effects of bacterial activity on basaltic glass: an experimental approach. *Chem. Geol.* 119, 139–160. doi: 10.1016/0009-2541(94)00098-S

Thorseth, I. H., Torsvik, T., and Torsvik, V. (2001). Diversity of life in ocean floor basalt. *Earth Planet.* 194, 31–37. doi: 10.1016/S0012-821X(01)00537-4

Toner, B. M., Lesniewski, R. A., Marlow, J. J., Briscoe, L. J., Santelli, C. M., Bach, W., et al. (2013). Mineralogy drives bacterial biogeography of hydrothermally inactive seafloor sulfide deposits. *Geomicrobiol. J.* 30, 313–326. doi: 10.1080/01490451.2012.688925

Verna, C., Ramette, A., Wiklund, H., Dahlgren, T. G., Glover, A. G., Gaill, F., et al. (2010). High symbiont diversity in the bone-eating worm *Osedax mucofloris* from shallow whale-falls in the north atlantic. *Environ. Microbiol.* 12, 2355–2370. doi: 10.1111/j.1462-2920.2010.02299.x

Walker, C. B., de la Torre, J. R., Klotz, M. G., Urakawa, H., Pinel, N., Arp, D. J., et al. (2010). Nitrosopumilus maritimus genome reveals unique mechanisms for nitrification and autotrophy in globally distributed marine crenarchaea. *Proc. Natl. Acad. Sci. U.S.A.* 107, 8818–8823. doi: 10.1073/pnas.0913533107

Wessel, P., Sandwell, D., and Kim, S. (2010). The global seamount census. *Oceanography* 23, 24–33. doi: 10.5670/oceanog.2010.60

Wheat, C. G., and Fisher, A. T. (2008). Massive, low-temperature hydrothermal flow from a basaltic outcrop on 23 Ma seafloor of the cocos plate: chemical constraints and implications. *Geochem. Geophys. Geosyst.* 9:Q12014. doi: 10.1029/2008GC002136

Wheat, C. G., and Mottl, M. J. (2000). Composition of pore and spring waters from baby bare: global implications of geochemical fluxes from a ridge

flank hydrothermal system. *Geochim. Cosmochim. Acta* 64, 629–642. doi: 10.1016/S0016-7037(99)00347-6

Williams, K. P., Gillespie, J. J., Sobral, B. W., Nordberg, E. K., Snyder, E. E., Shallom, J. M., et al. (2010). Phylogeny of gammaproteobacteria. *J. Bacteriol.* 192, 2305–2314. doi: 10.1128/JB.01480-09

Wright, E. S., Yilmaz, L. S., and Noguera, D. R. (2012). DECIPHER, a search-based approach to chimera identification for 16S rRNA sequences. *Appl. Environ. Microbiol.* 78, 717–725. doi: 10.1128/AEM.06516-11

Yarza, P., Richter, M., Peplies, J., Euzeby, J., Amann, R., Schleifer, K. H., et al. (2008). The all-species living tree project: a 16S rRNA-based phylogenetic tree of all sequenced type strains. *Syst. Appl. Microbiol.* 31, 241–250. doi: 10.1016/j.syapm.2008.07.001

Zimmerman, D. (1987). Comparative power of Student T Test and Mann-Whitney U Test for unequal sample sizes and variances. *J. Exp. Edu.* 55, 171–174. doi: 10.1080/00220973.1987.10806451

Zinger, L., Gobet, A., and Pommier, T. (2012). Two decades of describing the unseen majority of aquatic microbial diversity. *Mol. Ecol.* 21, 1878–1896. doi: 10.1111/j.1365-294X.2011.05362.x

Conflict of Interest Statement: The authors declare that the research was conducted in the absence of any commercial or financial relationships that could be construed as a potential conflict of interest.

frontiers in Microbiology

ORIGINAL RESEARCH
published: 16 December 2015
doi: 10.3389/fmicb.2015.01409

Similar Microbial Communities Found on Two Distant Seafloor Basalts

Esther Singer[1], Lauren S. Chong[2], John F. Heidelberg[3] and Katrina J. Edwards[2,3†]*

[1] Joint Genome Institute, Walnut Creek, CA, USA, [2] Department of Earth Sciences, University of Southern California, Los Angeles, CA, USA, [3] Department of Marine Environmental Biology, University of Southern California, Los Angeles, CA, USA

The oceanic crust forms two thirds of the Earth's surface and hosts a large phylogenetic and functional diversity of microorganisms. While advances have been made in the sedimentary realm, our understanding of the igneous rock portion as a microbial habitat has remained limited. We present the first comparative metagenomic microbial community analysis from ocean floor basalt environments at the Lō'ihi Seamount, Hawai'i, and the East Pacific Rise (EPR; 9°N). Phylogenetic analysis indicates the presence of a total of 43 bacterial and archaeal mono-phyletic groups, dominated by *Alpha-* and *Gammaproteobacteria,* as well as *Thaumarchaeota*. Functional gene analysis suggests that these *Thaumarchaeota* play an important role in ammonium oxidation on seafloor basalts. In addition to ammonium oxidation, the seafloor basalt habitat reveals a wide spectrum of other metabolic potentials, including CO_2 fixation, denitrification, dissimilatory sulfate reduction, and sulfur oxidation. Basalt communities from Lō'ihi and the EPR show considerable metabolic and phylogenetic overlap down to the genus level despite geographic distance and slightly different seafloor basalt mineralogy.

Keywords: seafloor basalt, metagenome, thaumarchaeota, microbe-rock interactions, oceanic crust

OPEN ACCESS

Edited by:
Cara M. Santelli, University of Minnesota, USA

Reviewed by:
Takuro Nunoura, Japan Agency for Marine-Earth Science and Technology, Japan
Heather Fullerton, Western Washington University, USA

****Correspondence:***
Esther Singer
esinger@lbl.gov

† Deceased

Specialty section:
This article was submitted to Extreme Microbiology, a section of the journal Frontiers in Microbiology

Received: *01 September 2015*
Accepted: *27 November 2015*
Published: *16 December 2015*

Citation:
Singer E, Chong LS, Heidelberg JF and Edwards KJ (2015) Similar Microbial Communities Found on Two Distant Seafloor Basalts. Front. Microbiol. 6:1409. doi: 10.3389/fmicb.2015.01409

INTRODUCTION

Oceanic basalts cover approximately 60% of the Earth's surface. Due to their high permeability, these volcanic rocks are greatly influenced by infiltration and circulation of seawater (Fisher, 1998; Fisher and Becker, 2000). The rock-seawater interaction results in a flux of energy and solutes between basalt crust and the overlying seawater (Fisher, 1998). Micro-niches on and inside basalts support both autotrophic and heterotrophic microbial growth. Lava surfaces are predominantly composed of volcanic glass, harboring reduced elemental species, including iron, sulfur, and manganese (Alt, 1995). These constituents can be oxidized by chemoautotrophic microorganisms with oxygen and nitrate to fix CO_2 (Edwards et al., 2003b). Furthermore, ferromanganese crust formation on the glassy rims of pillow basalts can give rise to the formation of microbial biofilms, which use these secondary minerals for energy metabolism (Templeton et al., 2009).

Cell densities in volcanic glasses from the East Pacific Rise (EPR) were estimated to amount to 10^5–10^9 cells g^{-1} basalt based on qPCR results (Einen et al., 2008; Santelli et al., 2008). Cell densities and community compositions are hypothesized to be linked to the alteration state of the source rock: younger basalts generally host less diverse communities that are more similar to their source environments (e.g., surrounding water), whereas older basalts (>20,000 years) usually

display richer communities adapted to the mineralogical composition of the rock (Santelli et al., 2008). Fe(II)-reducing bacteria alone were estimated to amount to 10^3 cells ml^{-1} at the Lō'ihi Seamount (Emerson, 2009). While the origin of these seafloor basalt microbial communities may be the surrounding seawater and/or sediments, over time (thousands of years), they appear to become distinct from the surrounding habitat, so that mineralogy – rather than geographical setting – ultimately determines the community structure (Santelli et al., 2008; Toner et al., 2013). While deep-sea basalts host a greater phylogenetic diversity of bacteria and archaea than other deep-sea environments, community structures on basalts of similar mineralogical composition resemble each other when compared to other environments (Huber et al., 2003; Santelli et al., 2008). In fact, shared operational taxonomic unit (OTU) richness and community membership between the EPR and Hawai'i suggest that there is a basalt biome which positively correlates with seafloor basalt characteristics (Santelli et al., 2009). Microbial community richness is most likely supported by the wide variety of micro-niches that allows diverse redox reactions and metabolic pathways (e.g., heterotrophic, anaerobic, and reductive) within small spatial scales (Santelli et al., 2008; Shi et al., 2012).

Thus far, the limited number of existing molecular microbial community studies on seafloor basalts exposed to seawater have all relied on PCR-biased results. Thorseth et al. (2001) investigated samples from Knipovich Ridge and observed bacteria belonging to the *Proteobacteria, Bacteroidetes,* and archaea. Lysnes et al. (2004) studied Hawaiian basalts and determined that the microbial community was dominated by bacteria and was structurally dependent on rock age. Santelli et al. (2008) found 10^5–10^6 cells almost exclusively from the bacterial domain in the glassy rind of seafloor basalts from the Norwegian/Greenland sea and did not find a correlation between community structure and rock age. The large diversity and richness of microbial communities on seafloor basalts from various locations was first emphasized in studies from Mason et al. (2007, 2009), Santelli et al. (2008), and microbial community structures appeared comparable between geographically distant sites. Santelli et al. (2008) and Mason et al. (2009) found similar relative abundances of *Proteobacteria* (56–68%), *Planctomycetes* (5–8%), *Actinobacteria* (7–9%), *Bacteroidetes* (1–10%), *Acidobacteria* (3–6%) at Lō'ihi, the EPR, and the Juan de Fuca Ridge. Archaea were found to be ubiquitous in seafloor basalts, although estimates of archaeal relative abundance are discrepant, ranging from 0.02 to 25% (Einen et al., 2008; Santelli et al., 2008; Mason et al., 2009).

Since metabolic functions are difficult to construe from 16S rRNA phylogeny, it is unclear how functional gene patterns compare among rocks from geographically different locations. Functional surveys conducted at the Lō'ihi Seamount and the EPR, to date, include isolate studies (Templeton et al., 2005; Emerson, 2009), synchrotron-based X-ray microprobe mapping (Templeton et al., 2009), enzyme assays (Jacobson Meyers et al., 2014), and stable isotope incubations of crustal samples (Orcutt et al., 2015). These studies have helped characterize the extent of some of the main microbial metabolic activities supported at these sites. While these studies elegantly investigated specific metabolic pathways, studies of the pathway diversity present at seafloor basalts are scarce. Mason et al. (2009) have provided the only broad functional gene analysis at the EPR and the Juan de Fuca Ridge using GeoChip. The authors detected genes for carbon fixation, methane oxidation, methanogenesis, and nitrogen fixation on rocks from the EPR and the Juan de Fuca Ridge (Mason et al., 2009). In order to further test the hypothesis (while avoiding PCR-bias) that the phylogeny and functional gene set of microbial communities is comparable between seafloor basalts of similar age and mineralogy, we conducted the first comprehensive metagenomic study of seafloor basalts. We describe the phylogenetic and metabolic characteristics of the basalt-hosted microbial communities from the Lō'ihi Seamount and the EPR, and provide links to the mineralogy of the seafloor basalts and parameters of the surrounding environment.

MATERIALS AND METHODS

Rock Collection and Analysis

One sample of seafloor basalt (AT11-07_3968_B_OF5) was collected from the EPR (9° 43.8′ N, 104° 9.6′ W) from a depth of 2,674 m aboard the R/V Atlantis using the submarine Alvin (cruise AT11-07) in 2004. Two seafloor basalt samples (J2-243 R2-F, J-246 R2) were collected from the Lō'ihi Seamount (18° 28.2′ N, 155° 10.8′ W) at a depth of 5,000 m aboard the R/V Melville using the ROV Jason II in 2006 (**Figure 1**). All seafloor basalts were stored frozen at −80°C for XRD analysis and DNA extraction. Bulk mineralogy analysis, i.e., quantitative determination of rock-forming minerals and total clay minerals, was determined on all three seafloor basalts via X-ray Diffraction (XRD) analysis at KT GeoServices, Inc. Detection limits were at 1–5 wt%. The two Lō'ihi seafloor basalts were combined for analysis.

DNA Extraction and Sequencing

DNA was extracted from basalt chips using a phenol-chloroform extraction with a negative control (NC). DNA extracts from the two Lō'ihi seafloor basalt samples were combined. Since the amount of DNA was <1 μg on all seafloor basalts, DNA was amplified using the illustra GenomiPhi V2 DNA Multiple Displacement Amplification (MDA) kit (GE Healthcare Life Sciences, Pittsburgh, PA, USA). The NC sample was also processed with the MDA kit in the same reaction as the seafloor basalt samples. Final DNA samples and the control were sent to the core genomics center at the University of Pennsylvania for whole genome shotgun sequencing on a Roche GS-FLX Titanium 454 sequencer (454 Life Sciences, Branford, CT, USA).

Sequence Processing and Assembly

Raw sequence reads were evaluated with FastQC version 0.11.3 (Schmieder and Edwards, 2011a), quality trimmed (minimum quality score–25, maximum length–450 bp, maximum homopolymer length–9 bp, max N-tail–1 bp),

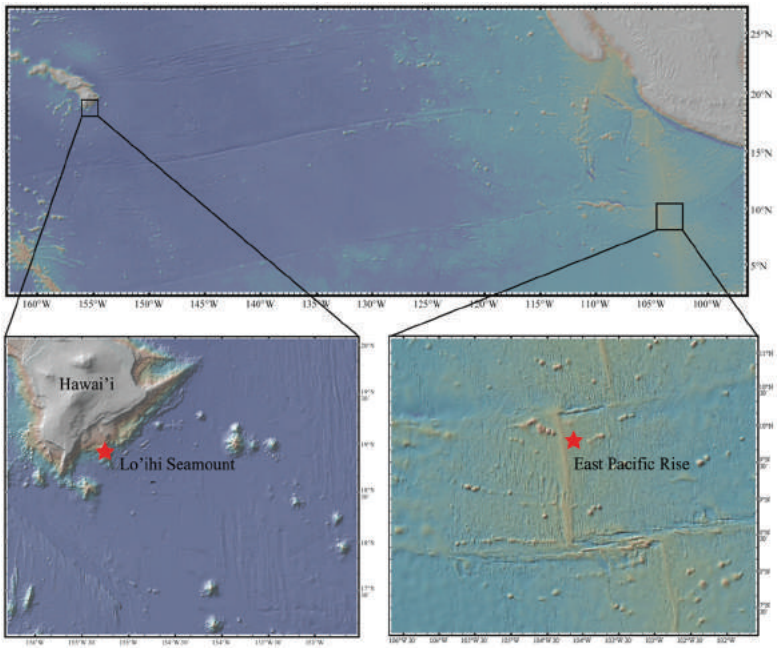

FIGURE 1 | Map of study sites.

and filtered (removal of technical duplicates, minimum length–60 bp) with Prinseq 0.20.4 (Schmieder and Edwards, 2011b) and MG-RAST (Meyer et al., 2008). We obtained 1,102,191 sequences in the Lō'ihi dataset, 1,191,651 sequences in the EPR dataset, and 58,188 sequences in the NC dataset. Quality-filtered reads were assembled *de novo* using standard 454 settings in mira 3.4.1.1 (Chevreux et al., 1999). Padded (i.e., including potential gaps) contigs >500 bp were filtered using mira 3.4.1.1 (convert_project; Chevreux et al., 1999).

Seafloor basalt contigs were screened for contamination using a combination of BBMap (bbduk.sh with parameters $mcf = 0.25$, $k = 31$) and the BLASTN algorithm (Altschul et al., 1990). The BBMap algorithm identified 10 potentially contaminant contigs in the Lō'ihi (total of 12,423 bp) and four potentially contaminant contigs in the EPR metagenome dataset (total of 4,290 bp). For the Lō'ihi dataset, the BLAST alignment results for the identified contaminant contigs rendered ≥84% identity over ≥28% of the seafloor basalt contig length. For the EPR dataset, the BLAST alignment results for the contaminant contigs rendered ≥86% identity over ≥8% of the seafloor basalt contig length. Contig statistics are displayed in **Table 1** and in **Supplementary Figure S1**. All sequences are available online at http://www.bco-dmo.org/dataset/616326.

Gene Annotation

Contigs >500 bp were annotated by using the BLASTX algorithm in diamond v0.79 (Buchfink et al., 2014) against the Refseq non-redundant database (Pruitt et al., 2011) and analyzed

TABLE 1 | Sequence, assembly, and annotation statistics of metagenome datasets.

Sequences: post QC

Sample	Depth (m)	Total reads	Sequence total (Gbp)	Avg. sequence length (bp)	Average %GC
Lō'ihi	5,000	1,055,848	~268	253 ± 110	45
EPR	2,540	1,191,651	~233	195 ± 102	48
NC	N/A	58,188	~10	177 ± 93	51

Contig statistics

Sample	# of reads assembled	Avg. total coverage	# of contigs	N50 [bp]	Contigs >500 bp	BLAST hits*	Pfam hits*
Lō'ihi	245,493	3.94	17,080	877	11,617	9,154	8,668
EPR	89,245	3.43	9,541	763	6,440	5,440	4,377
NC	51,089	6.73	1,080	2638	1,009	1,008	839

**Filtered BLASTX and Pfam hits as described in section "Materials and Methods."*

in MEGAN5 (Huson and Weber, 2013). Relative abundance comparison of phylogenies between seafloor basalt datasets was achieved by normalizing to total read length (Lō'ihi: 6,738,682 bp, EPR: 3,508,565 bp). Further functional prediction of contigs was performed by alignment against Pfam-A regions from the Pfam version 27.0 database (Finn et al., 2013) using prodigal 2.50 (Markowitz, 2006). Pfam hits with *e*-value $<10^{-5}$ and pfam score >50 were retained. Contig fractions encoding for small subunit (SSU) ribosomal genes were retrieved with RNAmmer-1.2 (Lagesen et al., 2007) and classified using the SINA aligner (Pruesse et al., 2012).

Phylogenetic Reconstruction and Statistical Analysis

Community richness was estimated using the Chao1 index, and diversity analysis was calculated using the Shannon index in QIIME 1.9.1 (alpha_diversity.py) based on BLASTX assignments of contigs. Phylosift was used to assess community diversity using the core molecular marker set of genes, which includes ∼40 three-domain protein coding genes, single-copy eukaryote specific nuclear orthologs, ribosomal RNA genes (16S/18S), mitochondrial genes (mtDNA markers), and plastid and viral markers identified through Markov-clustering algorithms applied to genome datasets (Darling et al., 2014). *D*-score calculations of functional categories in Supplementary Table S2 were calculated as previously described (Markowitz et al., 2007).

RESULTS

Mineralogy

Bulk mineralogy of the basalt from both sites is shown in **Table 2**. Considerable amounts of glass (amorphous), containing ∼10 wt% iron, were identified in both samples. The volcanic glass was mainly composed of silica (≥70%), but also harbored magnesium and iron in the form of Fe_3O_4 (magnetite), i.e., Fe^{2+} and Fe^{3+} ions, which is readily oxidized to hematite with oxygen. The Lō'ihi basalt sample additionally contained significant amounts of pyroxene and olivine, which typically consist of ∼6 and 8–34 wt% Fe(II), respectively. Overall, the mineralogies observed were representative of typical basalt compositions (Yoder, 1976).

Phylogeny

Phylogenetic analysis using 180 identified molecular marker genes in seafloor basalt metagenomes from Lō'ihi and 125 from the EPR resulted in 13 and 17 monophyletic groups, respectively (**Figure 2A**). At Lō'ihi, *Gamma-* and *Alphaproteobacteria* accounted for nearly 80% of total abundance, with *Thaumarchaeota* (13%) representing the third most abundant phylogenetic group. Besides *Verrucomicrobia* (4.5%) and *Planctomycetes* (1.3%), all other phyla accounted for less than 1% of the total prokaryotic community. The EPR community displayed more evenness; *Bacteroidetes*, *Thaumarchaeota,* and *Proteobacteria* together held similar shares, comprising over 60% of the total community (**Figure 2A**). Phylogenetic classification of all contigs resulted in 7,841 (67.2% of total) and 4,566 (77.2% of total) contigs assigned to 44 and 34 bacterial and archaeal phyla in the Lō'ihi and EPR datasets, respectively (**Figure 2B**) The community diversity and richness was estimated to be comparable between the two seafloor basalt communities, while being considerably larger than those of subsurface sediment samples (Chao1: ∼63–188; Shannon: 3.3–3.8 at genus-level; Biddle et al., 2011), and approaching those of soil samples (Chao1: 1,400; Shannon: 1.3–4.0; Pearce et al., 2012) (**Figure 2B** – table inset). The microbial community represented by contigs with taxa assignment was dominated by *Gamma-* and *Alphaproteobacteria,* and *Thaumarchaeota* (together 68.6 and 49.6% of total bp at Lō'ihi/EPR, respectively). The *Gammaproteobacterial* class was mostly composed of the ubiquitous marine order *Alteromonadales* (6.6%, 1.0% of total bp at Lō'ihi/EPR), which was previously shown to be among the most abundant orders on seafloor basalts (Jacobson Meyers et al., 2014). *Alphaproteobacteria* was mainly comprised of *Rhizobiales* (0.6 and 0.2% at Lō'ihi/EPR), *Rhodospirillales* (0.2 and 0.02% at Lō'ihi/EPR), *Rhodobacterales* (0.1 and 0.2% at Lō'ihi/EPR), and *Sphingomonadales* (0.2 and 0.1% at Lō'ihi/EPR), which include known seafloor basalt occupying genera (Mason et al., 2007; Jacobson Meyers et al., 2014). The relative abundance of *Thaumarchaeota* sequence assigned by BLAST (12.3 and 26.8% at Lō'ihi/EPR) as well as molecular marker genes (12.8 and 16.0% at Lō'ihi/EPR) was relatively high compared to previous PCR-based seafloor basalt community analyses. Quantitative analyses of microbial communities on the surface of and inside seafloor basalts have reported a ubiquitous but minor presence of archaea, although estimates of archaeal abundance are disparate, ranging from <0.02% at Knipovich Ridge (Einen et al., 2008), 4–12% at Hawai'i, the EPR and the Juan de Fuca Ridge (JdF; Santelli et al., 2008) to 10.6–25.3% at the EPR and the JdF (Mason et al., 2009).

At the EPR, 9.0% of classified contigs were assigned to the *Planctomycetes*, which thereby represent the fourth most abundant phylum (**Figure 2B**). The contigs assigned to the *Planctomycetes* only account for ∼1.0% in the Lō'ihi dataset. Other less represented phyla and *Proteobacterial* classes (1–5%) at both sites include *Betaproteobacteria* (4.0 and 3.4% at Lō'ihi/EPR), *Bacteroidetes* (2.0 and 4.4% at Lō'ihi/EPR), *Delta-/Epsilonproteobacteria* (2.0 and 4.0% at Lō'ihi/EPR), *Firmicutes* (0.9 and 1.5% at Lō'ihi/EPR), *Cyanobacteria* (0.8 and 1.4% at Lō'ihi/EPR), *Verrucomicrobia* (0.6 and 1.1% at Lō'ihi/EPR), as well as *Nitrospirae* (0.1 and 1.5% at Lō'ihi/EPR; Supplementary Table S1). Several phyla were only present at one site: 15 phyla accounting for 0.5% of the total community were only found at the Lō'ihi site, while four phyla accounting for 0.1% were

TABLE 2 | X-ray Diffraction analysis data of bulk seafloor mineralogy.

XRD#	Lō'ihi (wt%)	East Pacific Rise (EPR; wt%)
Quartz	1.5	1.7
Pyroxene	37.5	7.1
Olivine	12.5	0
Amorphous	48.5	91.2

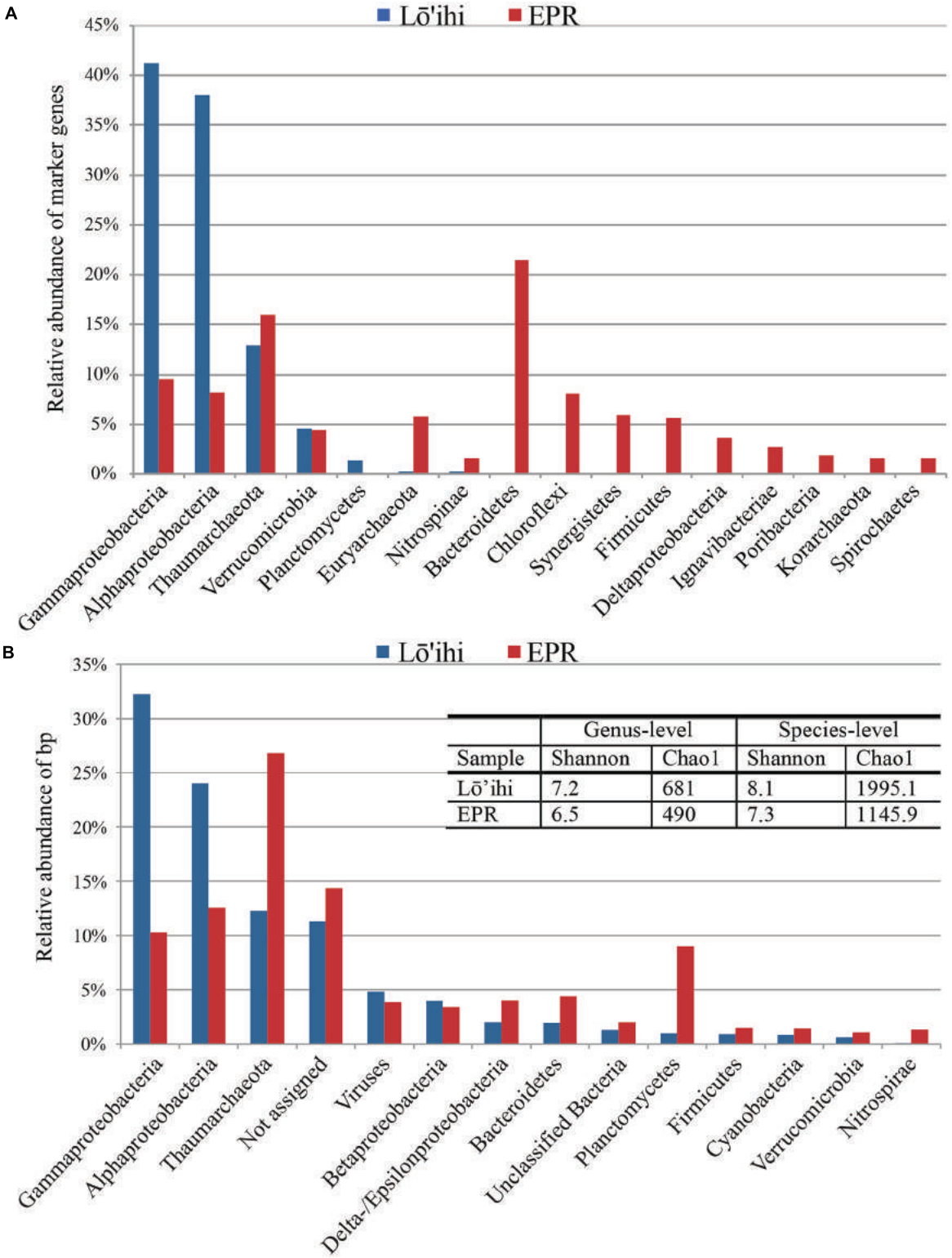

	Genus-level		Species-level	
Sample	Shannon	Chao1	Shannon	Chao1
Lō'ihi	7.2	681	8.1	1995.1
EPR	6.5	490	7.3	1145.9

FIGURE 2 | Phyla classification of taxonomy assignments based on molecular marker genes (A) and BLAST assignments (B). *Proteobacteria* were split into classes due to their inherent diversity. Only phyla/*Proteobacterial* classes with relative abundance >1% are listed. The Lō'ihi community is dominated by few phyla/*Proteobacterial* classes compared to a more even taxa distribution at the EPR **(A)**. Community structure based on BLAST assignment supports the dominance of *Gamma-* and *Alphaproteobacteria* at Lō'ihi, but also displays comparable evenness and diversity to the EPR community. The barplot shows percentages of total identifiable hits to phyla and *Proteobacteria* classes normalized by read length and with relative abundance >1% (Lō'ihi: 6,738,682 bp; EPR: 3,508,565 bp; **B)**.

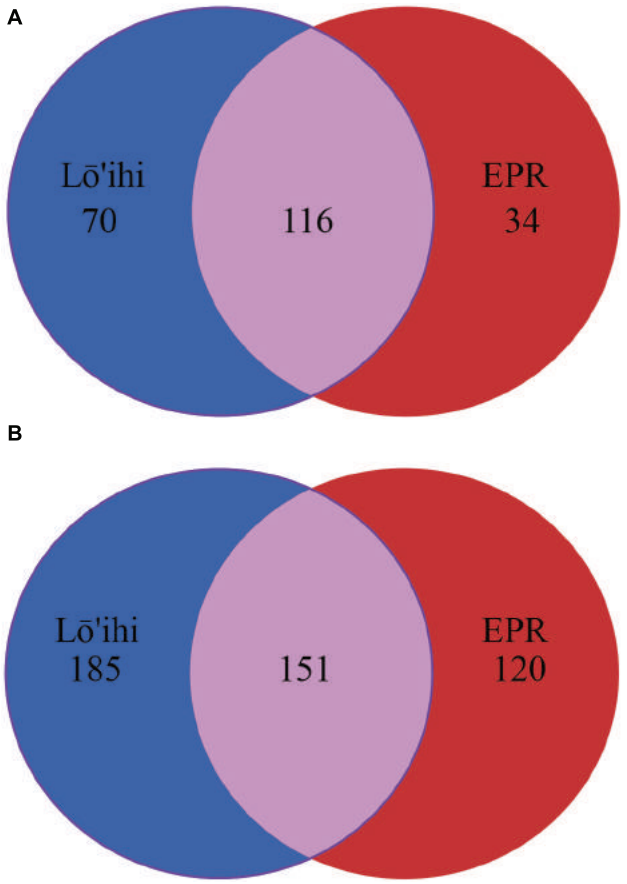

FIGURE 3 | Venn diagram at family (A) and genus (B) level. Numbers represent individual taxonomic groups at their respective phylogenetic rank. Unclassified sequences are excluded from this analysis.

exclusively present at the EPR site. The contigs representing the 'rare biosphere' (<1% of total community) are more diverse at Lō'ihi and incorporate 35 phyla (total of 5.1% of total community; Supplementary Table S1). The rare biosphere at the EPR includes 24 phyla representing 4.0% of the total community. At the family level, 18.6 and 27.1% of all Lō'ihi and EPR contigs were classifiable and >50% of all family OTUs overlapped between the two metagenome datasets. At the genus level, 11.8 and 16.5% of all Lō'ihi and EPR contigs were classifiable and >30% of all genus OTUs overlapped between Lō'ihi and EPR (**Figure 3**).

Functional Genes

The diversity of the microbial communities observed on these seafloor basalts suggests the possibility of the co-occurrence of various nutrient cycles. Functions discussed here were annotated using KEGG Orthology (KO; Supplementary Table S2) and shows that broad categories did not significantly differ in relative abundance between the seafloor basalt metagenome datasets (Supplementary Table S3). In order to determine potential microbial metabolic activities occurring on basalts leading to alteration reactions, we were interested in the type of carbon and energy metabolisms that are predicted by our basalt metagenomes. Since our datasets only represent a fraction of the complete metagenome at Lō'ihi and the EPR, we focused our analysis on the pathways that are present and will rely on future, more comprehensive, gene and pathway studies to resolve ecologically important metabolic functions absent from our dataset.

The transformation potential for organic matter on seafloor basalts was previously estimated to be comparable to that of continental shelf sediments and larger than that in the water column (Jacobson Meyers et al., 2014). Key enzymes involved in carbon fixation, e.g., the large and small subunits of Ribulose-1,5-biosphosphate carboxylase oxygenase (RuBisCo) Form I and II, are assumed to play a dominant role in the accumulation of biomass on basalt surfaces, because carbon concentrations are typically low there (Edwards et al., 2003a). Both, the Lō'ihi and the EPR seafloor basalt metagenomes harbor genes mediating the Calvin-Benson-Bassham (CBB) cycle for autotrophic carbon assimilation, though the ribulose 1,5-biphosphate carboxylase/oxygenase (RuBisCo) gene (*cbbM*) is only present in the Lō'ihi dataset (Supplementary Table S4). The corresponding gene sequence encodes for RuBisCo Form II, which functions at $[CO_2] > 1.5\%$, and shares closest similarity to that from *Candidatus Ruthia magnifica*, a sulfur-oxidizing endosymbiont retrieved from the deep-sea hydrothermal vent clam *Calyptogena magnifica* (Newton et al., 2007). We also identified a citrate lyase (beta subunit) in the Lō'ihi dataset, which enables the reverse tricarboxylic acid (TCA) cycle. The presence of these genes supports an autotrophic lifestyle on basalts at Lō'ihi. Autotrophy was recently experimentally demonstrated to occur on seafloor basalts from the Lō'ihi Seamount, as well as from North Pond and the Juan de Fuca Ridge via ^{13}C incubation experiments (Orcutt et al., 2015). Carbon fixation rates across global oceanic crust were estimated to be 10^9–10^{12} g C yr^{-1}, thereby likely supporting heterotrophic organisms (Orcutt et al., 2015). Genes involved in heterotrophic carbon metabolism are present in both datasets and include chitinases, which degrade chitin, starch phosphorylases, which catalyze phosphorolytic degradation of starch, and beta-1,4-endoglucanases, which hydrolyze cellulose (Supplementary Table S4). Since some of these genes share highest similarity with organisms that are also expected to perform carbon fixation, e.g., starch phosphorylase in *Nitrosomonas cryotolerans*, mixotrophy appears to be a possible alternative lifestyle on seafloor basalts.

In both datasets, we found bacterial and archaeal genes encoding for various aerobic and anaerobic steps in the nitrogen cycling pathways (**Figure 4**, Supplementary Table S4). These include the complete pathways for dissimilatory nitrate reduction to ammonia (*narGHJ*/*nirB*) and denitrification of nitrate to nitrogen gas (*nirK*, *norBC*, *nosZ*). Organisms predicted to be involved in these pathways span *Alpha-*, *Beta-*, and *Gammaproteobacteria*, as well as *Nitrospirae,* and *Thaumarchaeota* (Supplementary Table S4). The archaeal gene *nirK* shows closest sequence similarity to *nirK* from *Candidatus Nitrosoarchaeum limnia* SFB1 (Lō'ihi) and

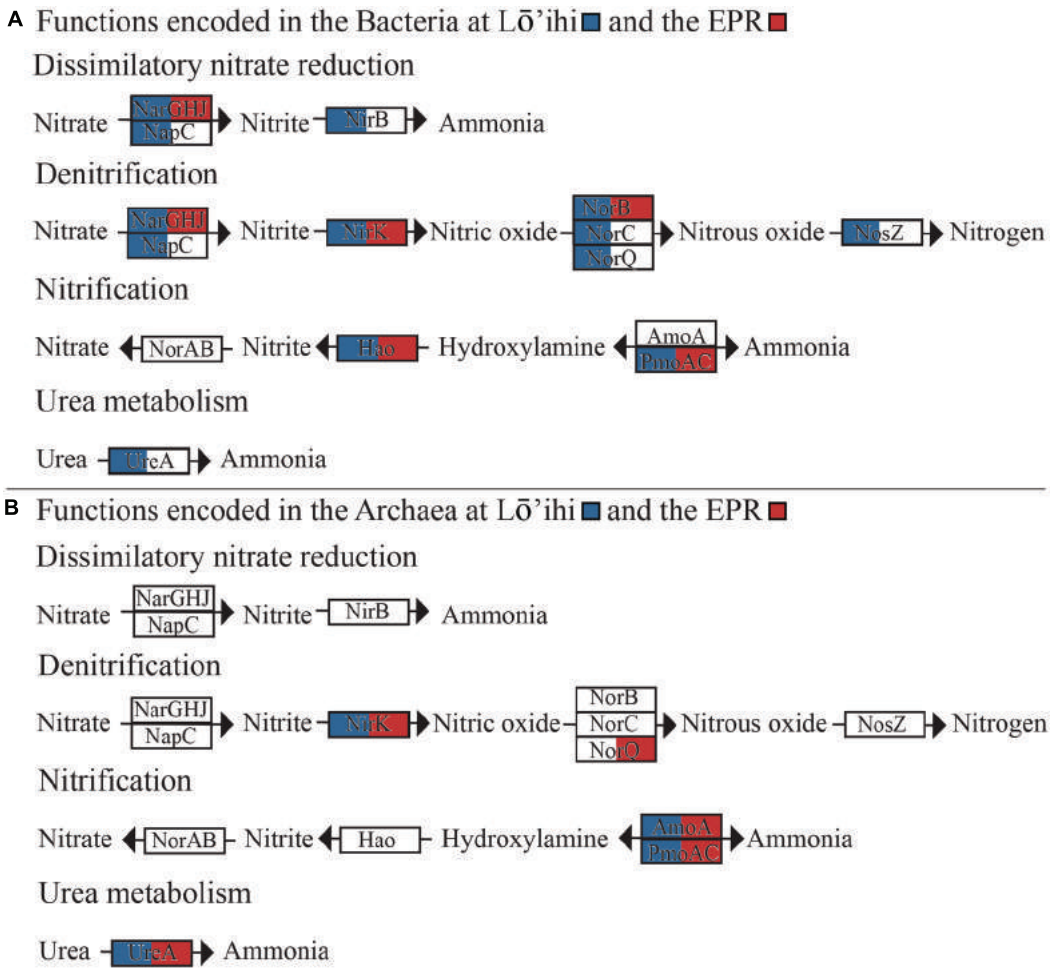

FIGURE 4 | Nitrogen metabolism pathways encoded in the Lō'ihi and EPR metagenomes attributed to bacteria (A) and archaea (B). Genes present in either metagenome dataset are indicated by coloration of the respective gene boxes (Lō'ihi – blue; EPR – red).

Candidatus Nitrosopumilus koreensis (EPR), therefore likely representing the AnirKa variant (Lund et al., 2012). This variant was previously shown to be more common in the epipelagic to mesopelagic water horizons, but the presence of *nirK* in our deep-sea datasets is an indication of AnirKa in the bathypelagic.

Nitrification is encoded by ammonia monooxygenase subunit C (*amoAC*), hydroxylamine oxidase (*hao*), and nitric oxide reductase (*norAB*). The oxidation of ammonia to hydroxylamine is encoded by *amoC* genes with closest similarity to *Nitrosopumilus sp.* SJ and *Nitrosospira multiformis* in the Lō'ihi as well as the EPR dataset, indicating that both *Thaumarchaeota* and *Betaproteobacteria* may be involved in ammonia oxidation. Pfam motif search also resulted in indications of fractions of *amoA* genes with closest similarity to *amoA* from *Nitrosospira lacus* (56% coverage, 91% identity) and an *amoA* gene from *Thaumarchaeota archaeon* MY2 (78% cov., 96% id.). These findings further support the co-existence of bacterial and archaeal ammonia oxidizing organisms (AOB and AOA) on both host seafloor basalts. Most archaeal contigs with genes involved in nitrogen cycling returned best BLAST hits to members of *Nitrosopumilus* and *Nitrosoarchaeum*, two ubiquitous phyla in the open ocean and coastal waters (Hatzenpichler, 2012), which may significantly contribute to the nitrification process in the deep ocean. Contigs assigned completely to the *Thaumarchaeota* did not harbor any other genes known to facilitate energy metabolism pathways besides those for ammonia oxidation. While genes encoding nitrite reduction and nitrogen fixation to ammonia were not detected in either dataset, we found urease genes with high sequence similarity to urease alpha subunit (*ureA*) genes from bacteria (*Nitrospina, Pseudomonas, Spiribacter*) and archaea (*Nitrosopumilus, Nitrososphaera*). Urea may represent an alternative ammonia source. For example, the soil AOA *Nitrososphaera viennensis* is capable of growth on urea (Tourna et al., 2011). Other studies have suggested that the excess ammonia available for nitrification may be derived from nitrogen fixation (Cowen et al., 2003). However, N_2 fixation genes were not found in our seafloor basalt metagenomes. Nif protein encoding genes were previously found in basalt microbial communities (Mason et al., 2009) and in crustal fluids attributed

to nitrogen fixing, non-methanogenic archaea (Mehta et al., 2005) at the Juan de Fuca Ridge. It is thus likely that nitrogen fixation provides ammonia on seafloor basalts, although this cannot be concluded from our datasets.

Sulfur cycling is a process known to occur in porous basalts due to biological activity (Rouxel et al., 2008). Various gene fractions of *dsrC* and the *dsrEFH* complex were identified with closest similarity to members of the *Proteobacteria*, known to participate in sulfur oxidation, e.g., *Marichromatium purpuratum* (Prange et al., 1999) (Supplementary Table S4). While all sulfate-reducing organisms with *dsrAB* [catalyzing the reduction of sulfite to sulfide (Wagner et al., 1998)], also possess *dsrC,* which interacts with *dsrAB*, DsrC is also a homolog to TusE, a sulfur transfer protein, which can act in a sulfur relay system assumed to be important during sulfur oxidation (Cort et al., 2008). Indeed, DsrC was shown to interact with DsrEFH, and *dsrEFH* genes are specific to sulfur-oxidizing bacteria containing *dsrAB* and do not occur in sulfate-reducers (Cort et al., 2008). Since we did not find any *dsrAB* genes or motifs in either seafloor basalt metagenome, and the gene motif search results in ambiguous annotations, we can only speculate about the simultaneous presence of sulfur oxidation and dissimilatory sulfate reduction reactions on seafloor basalts as previously identified using GeoChip (Mason et al., 2009). As basalts have low concentrations of sulfate, microbial sulfate reduction typically utilizes sulfate from the surrounding seawater. Sulfate reduction and a potential influx of hydrothermal fluids from the underlying crust introduces sulfide into this habitat, which can then abiotically react with ferrous iron to form pyrite (FeS_2) at low temperatures (Berner, 1964). Although pyrite (FeS_2) was not detected in basalts from either Lō'ihi or EPR, sulfur oxidation genes, including *dsrEFH* (e.g., from *M. purpuratum* and *Sulfuricella denitrificans*) and molecular marker genes from sulfur-oxidizing as well as sulfate-reducing organisms (e.g., *Sulfitobacter* sp. Bio 11, *Geobacter sulfurreducens, Desulfomonile tiedjei, Thermodesulfobium narugense*) were detected at both sites, supporting the potential for biological sulfate reduction and sulfide oxidation.

Chemolithoautotrophic microbial biomass production in marine basalts has furthermore been attributed to methanogenesis and Fe(II) oxidation (Bach and Edwards, 2003). Genes involved in methanogenesis or methanotrophy were not detected, but we found several species based on molecular marker gene search that are known for methane production under various conditions. These include *Methanocaldococcus* sp., (Jeanthon et al., 1998, 1999; Bellack et al., 2011), *Methanococcus voltae* (Whitman et al., 1982), *Methanothermococcus thermolithotrophicus* (Huber et al., 1982). Species predicted to be capable of methylotrophic growth found in our seafloor basalt datasets include *Methylotenera versatilis* (Kalyuzhnaya et al., 2012), and *Methylophaga* sp., (Kim et al., 2007; Villeneuve et al., 2013). Similarly, although none of the recently identified candidate genes in neutrophilic Fe(II)-oxidation (Barco et al., 2015) were detected in our dataset, a few gene sequences on ambiguously classified contigs showed closest relatedness to sequences from various *Zetaproteobacteria* sp. (0.3%, 0.02% at Lō'ihi/EPR), a group of marine organisms present and often dominant in Fe-rich ecosystems and speculated to contribute a large amount of Fe(III)-oxides to the global oceans (Singer et al., 2011; Barco et al., 2015).

DISCUSSION

Ecology studies of seafloor basalts attempting to link phylogenetic players to metabolic function are scarce to date. Seafloor basalts have previously been recognized to host a microbial phylogenetic diversity that is richer than the typical surrounding seawater and to show considerable taxonomic overlap between basalt sites of similar age and alteration state (Santelli et al., 2008). It seems that the geographical location of seafloor basalts only initially influences microbial community composition, and that mineralogy is the driving force that determines how a community structure develops and catalyzes the weathering of its host rock (Toner et al., 2013). Seafloor basalts from both sites discussed here were formed at approximately the same time (∼20,000 years ago) and were selected to confirm the hypothesis of community similarity among like basalts. XRD analysis confirmed an average mineralogical composition, with Lō'ihi being enriched in olivine and pyroxene, and generally containing higher Fe(II) compared to the EPR. Phylogenetic analysis demonstrated considerable overlap between Lō'ihi and EPR on various phylogenetic levels and even showed matches to many of the same dominant species, including members of the *Thaumarchaeota*. The large relative abundance of archaea detected in our datasets is comparable between sites and slightly higher compared to those of previous (PCR-dependent) studies. In fact, in the EPR dataset, *Thaumarchaeota* represented the second most abundant phylum with 12–27% of total sequence volume.

Predicted metabolic functions display comparable diversity and suggest that lithoautotrophic and heterotrophic lifestyles occur next to each other on the host seafloor basalts. The potential for exposed basalts to transform organic matter was previously shown to be substantial, confirming this environment is a major player in benthic biogeochemical processes (Jacobson Meyers et al., 2014; Orcutt et al., 2015). Basalt mineralogy is not likely to fuel all of the encoded metabolic activities, but may support, for instance, sulfate-reducing organisms during the interaction with seawater in reducing micro-niches on and inside the seafloor basalt. The genetic potential for the co-existence of aerobic and anaerobic metabolic processes, e.g., denitrification and nitrification, has been observed in various marine environments, such as oil seeps (Hawley et al., 2014), oxygen minimum zones (Yan et al., 2012; Kalvelage et al., 2013), and deep-sea sedimentary environments (Nunoura et al., 2013). Nitrogen cycling, especially the aerobic oxidation of ammonia, is more commonly encoded in the archaeal fraction of the metagenomes compared to the other studied processes and shows the potential for competition between bacteria and archaea for ammonia. The relative importance of AOA in nitrification as compared to AOB has been debated in other environments (Hatzenpichler, 2012), and similarly requires more quantitative data for the seafloor basalt environment. Interestingly, there were

no entire contigs that could be unambiguously assigned to the *Zetaproteobacteria,* and BLAST searches of known genes involved in Fe(II)-oxidation at circumneutral pH did not return any hits in our dataset. While previous studies identified *Zetaproteobacteria* as abundant, and sometimes dominant Fe(II)-oxidizing members of the seafloor basalt community, e.g., (McAllister et al., 2011), *Zetaproteobacteria* sequences may not have been assembled into contigs in our datasets because of low relative abundance, high diversity of *Zetaproteobacteria* genomic information and/or MDA bias. Testing the latter would be useful for future low biomass metagenomic studies on seafloor basalts that are assumed to host a significant abundance of *Zetaproteobacteria*.

This study is a first attempt at characterizing the seafloor basalt environment using a metagenome approach. The insights gained here contribute to addressing the question of 'who is doing what?', which remains a challenge, as many sequences are novel compared to what is in our current databases and are consequently assembled or functionally placed with low confidence. It appears that a broad range of bacterial phyla gives rise to a similarly broad range of metabolic gene potentials, whereas archaeal functional genes were mainly found to encode ammonia and methane oxidation. Our qualitative and quantitative interpretation of the results is certainly subject to the incompleteness of our datasets as well as the bias associated with the MDA process (Yilmaz et al., 2010). Hence, further examination of organisms responsible for seafloor basalt alteration and general redox reactions can be achieved in more detail with more in-depth sequencing and upon the availability of more genomes that are environmentally significant in the seafloor basalt habitat.

ACKNOWLEDGMENTS

We would like to thank Dr. John Fleming for helpful comments. This work was supported by the NSF Science and Technology Center for Dark Biosphere Investigations (C-DEBI) (Award 0939564). This is C-DEBI Contribution 296.

SUPPLEMENTARY MATERIAL

The Supplementary Material for this article can be found online at: http://journal.frontiersin.org/article/10.3389/fmicb.2015.01409

FIGURE S1 | Contig length by sample. (A) Lō'ihi **(B)** EPR **(C)** NC.

REFERENCES

Alt, J. C. (1995). "Subseafloor processes in mid-ocean ridge hydrothermal systems," in *Seafloor Hydrothermal Systems: Physical, Chemical, Biological, and Geological Interactions*, eds S. E. Humphris, R. A. Zierenberg, L. S. Mullineaux, and R. E. Thomson (New York City, NY: Wiley Online Library).

Altschul, S. F., Gish, W., Miller, W., Myers, E. W., and Lipman, D. J. (1990). Basic local alignment search tool. *J. Mol. Biol.* 215, 403–410. doi: 10.1016/S0022-2836(05)80360-2

Bach, W., and Edwards, K. J. (2003). Iron and sulfide oxidation within the basaltic ocean crust: implications for chemolithoautotrophic microbial biomass production. *Geochim. Cosmochim. Acta* 67, 3871–3887. doi: 10.1016/S0016-7037(03)00304-1

Barco, R. A., Emerson, D., Sylvan, J. B., Orcutt, B. N., Jacobson Meyers, M. E., Ramírez, G. A., et al. (2015). New insight into microbial iron oxidation as revealed by the proteomic profile of an obligate iron-oxidizing chemolithoautotroph. *Appl. Environ. Microbiol.* 81, 5927–5937. doi: 10.1128/AEM.01374-15

Bellack, A., Huber, H., Rachel, R., Wanner, G., and Wirth, R. (2011). *Methanocaldococcus villosus* sp. nov., a heavily flagellated archaeon that adheres to surfaces and forms cell-cell contacts. *Int. J. Syst. Evol. Microbiol.* 61, 1239–1245. doi: 10.1099/ijs.0.023663-0

Berner, R. A. (1964). Iron sulfides formed from aqueous solution at low temperatures and atmospheric pressure. *J. Geol.* 72, 293–306. doi: 10.1086/626987

Biddle, J. F., White, J. R., Teske, A. P., and House, C. H. (2011). Metagenomics of the subsurface Brazos-Trinity Basin (IODP site 1320): comparison with other sediment and pyrosequenced metagenomes. *ISME J.* 5, 1038–1047. doi: 10.1038/ismej.2010.199

Buchfink, B., Xie, C., and Huson, D. H. (2014). Fast and sensitive protein alignment using DIAMOND. *Nat. Methods* 12, 59–60. doi: 10.1038/nmeth.3176

Chevreux, B., Wetter, T., and Suhai, S. (1999). "Genome sequence assembly using trace signals and additional sequence information," in *Computer Science and Biology: Proceedings of the German Conference on Bioinformatics (GCB)*, 99, Hanover, 45–56.

Cort, J. R., Selan, U., Schulte, A., Grimm, F., Kennedy, M. A., and Dahl, C. (2008). Allochromatium vinosum DsrC: Solution-State NMR structure, redox properties, and interaction with DsrEFH, a protein essential for purple sulfur bacterial sulfur oxidation. *J. Mol. Biol.* 382, 692–707. doi: 10.1016/j.jmb.2008.07.022

Cowen, J. P., Giovannoni, S. J., Kenig, F., Johnson, H. P., Butterfield, D., Rappé, M. S., et al. (2003). Fluids from aging ocean crust that support microbial life. *Science* 299, 120–123. doi: 10.1126/science.1075653

Darling, A. E., Jospin, G., Lowe, E., Matsen, F. A. IV, Bik, H. M., and Eison, J. A. (2014). PhyloSift: phylogenetic analysis of genomes and metagenomes. *Peer J.* 2:e243. doi: 10.7717/peerj.243/table-1

Edwards, K. J., Bach, W., and Rogers, D. R. (2003a). Geomicrobiology of the ocean crust: a role for chemoautotrophic Fe-bacteria. *Biol. Bull.* 204, 180–185. doi: 10.2307/1543555

Edwards, K. J., Rogers, D. R., Wirsen, C. O., and McCollom, T. M. (2003b). Isolation and characterization of novel psychrophilic, neutrophilic, Fe-oxidizing, chemolithoautotrophic α-and γ-*Proteobacteria* from the deep sea. *Appl. Environ. Microbiol.* 69, 2906–2913. doi: 10.1128/AEM.69.5.2906-2913.2003

Einen, J., Thorseth, I. H., and Øvreås, L. (2008). Enumeration of Archaea and Bacteria in seafloor basalt using real-time quantitative PCR and fluorescence microscopy. *FEMS Microbiol. Lett.* 282, 182–187. doi: 10.1111/j.1574-6968.2008.01119.x

Emerson, D. (2009). Potential for iron-reduction and iron-cycling in iron oxyhydroxide-rich microbial mats at loihi seamount. *Geomicrobiol. J.* 26, 639–647. doi: 10.1080/01490450903269985

Finn, R. D., Bateman, A., Clements, J., Coggill, P., Eberhardt, R. Y., Eddy, S. R., et al. (2013). Pfam: the protein families database. *Nucleic Acids Res.* 42, D222–D230. doi: 10.1093/nar/gkt1223

Fisher, A. T. (1998). Permeability within basaltic oceanic crust. *Rev. Geophys.* 36, 143–182. doi: 10.1029/97RG02916

Fisher, A. T., and Becker, K. (2000). Channelized fluid flow in oceanic crust reconciles heat-flow and permeability data. *Nature* 403, 71–74. doi: 10.1038/47463

Hatzenpichler, R. (2012). Diversity, physiology, and niche differentiation of ammonia-oxidizing archaea. *Appl. Environ. Microbiol.* 78, 7501–7510. doi: 10.1128/AEM.01960-12

Hawley, E. R., Piao, H., Scott, N. M., Malfatti, S., Pagani, I., Huntemann, M., et al. (2014). Metagenomic analysis of microbial consortium from natural crude

oil that seeps into the marine ecosystem offshore Southern California. *Stand. Genomic Sci.* 9, 1259–1274. doi: 10.4056/sigs.5029016

Huber, H., Thomm, M., König, H., and Thies, G. (1982). Methanococcus thermolithotrophicus, a novel thermophilic lithotrophic methanogen. *Arch. Microbiol.* 132, 47–50. doi: 10.1007/BF00690816

Huber, J. A., Butterfield, D. A., and Baross, J. A. (2003). Bacterial diversity in a subseafloor habitat following a deep-sea volcanic eruption. *FEMS Microbiol. Ecol.* 43, 393–409. doi: 10.1111/j.1574-6941.2003.tb01080.x

Huson, D. H., and Weber, N. (2013). Microbial community analysis using MEGAN. *Methods Enzymol.* 531, 465–485. doi: 10.1016/B978-0-12-407863-5.00021-6

Jacobson Meyers, M. E., Sylvan, J. B., and Edwards, K. J. (2014). Extracellular enzyme activity and microbial diversity measured on seafloor exposed basalts from loihi seamount indicate the importance of basalts to global biogeochemical cycling. *Appl. Environ. Microbiol.* 80, 4854–4864. doi: 10.1128/AEM.01038-14

Jeanthon, C., L'Haridon, S., Reysenbach, A. L., Corre, E., Vernet, M., Messner, P., et al. (1999). *Methanococcus vulcanius* sp. nov., a novel hyperthermophilic methanogen isolated from East Pacific Rise, and identification of *Methanococcus* sp. DSM 4213T as *Methanococcus fervens* sp. nov. *Int. J. Syst. Bacteriol.* 49(Pt 2), 583–589. doi: 10.1099/00207713-49-2-583

Jeanthon, C., L'Haridon, S., Reysenbach, A. L., Vernet, M., Messner, P., Sleytr, U. B., et al. (1998). *Methanococcus infernus* sp. nov., a novel hyperthermophilic lithotrophic methanogen isolated from a deep-sea hydrothermal vent. *Int. J. Syst. Bacteriol.* 48, 913–919. doi: 10.1099/00207713-48-3-913

Kalvelage, T., Lavik, G., Lam, P., Contreras, S., Arteaga, L., Löscher, C. R., et al. (2013). Nitrogen cycling driven by organic matter export in the South Pacific oxygen minimum zone. *Nat. Geosci.* 6, 228–234. doi: 10.1038/ngeo1739

Kalyuzhnaya, M. G., Beck, D. A. C., Vorobev, A., Smalley, N., Kunkel, D. D., Lidstrom, M. E., et al. (2012). Novel methylotrophic isolates from lake sediment, description of *Methylotenera versatilis* sp. nov. and emended description of the genus Methylotenera. *Int. J. Syst. Evol. Microbiol.* 62, 106–111. doi: 10.1099/ijs.0.029165-0

Kim, H. G., Doronina, N. V., Trotsenko, Y. A., and Kim, S. W. (2007). *Methylophaga aminisulfidivorans* sp. nov., a restricted facultatively methylotrophic marine bacterium. *Int. J. Syst. Evol. Microbiol.* 57, 2096–2101. doi: 10.1099/ijs.0.65139-0

Lagesen, K., Hallin, P., Rodland, E. A., Staerfeldt, H. H., Rognes, T., and Ussery, D. W. (2007). RNAmmer: consistent and rapid annotation of ribosomal RNA genes. *Nucleic Acids Res.* 35, 3100–3108. doi: 10.1093/nar/gkm160

Lund, M. B., Smith, J. M., and Francis, C. A. (2012). Diversity, abundance and expression of nitritereductase (nirK)-like genes in marine thaumarchaea. *ISME J.* 6, 1966–1977. doi: 10.1038/ismej.2012.40

Lysnes, K., Thorseth, I. H., Steinsbu, B. R. O., Ã VreÃ, L., Torsvik, T., and Pedersen, R. B. (2004). Microbial community diversity in seafloor basalt from the Arctic spreading ridges. *FEMS Microbiol. Ecol.* 50, 213–230. doi: 10.1016/j.femsec.2004.06.014

Markowitz, V. M. (2006). The integrated microbial genomes (IMG) system. *Nucleic Acids Res.* 34, D344–D348. doi: 10.1093/nar/gkj024

Markowitz, V. M., Ivanova, N. N., Szeto, E., Palaniappan, K., Chu, K., Dalevi, D., et al. (2007). IMG/M: a data management and analysis system for metagenomes. *Nucleic Acids Res.* 36, D534–D538. doi: 10.1093/nar/gkm869

Mason, O. U., Di Meo-Savoie, C. A., Van Nostrand, J. D., Zhou, J., Fisk, M. R., and Giovannoni, S. J. (2009). Prokaryotic diversity, distribution, and insights into their role in biogeochemical cycling in marine basalts. *ISME J.* 3, 231–242. doi: 10.1038/ismej.2008.92

Mason, O. U., Stingl, U., Wilhelm, L. J., Moeseneder, M. M., Di Meo-Savoie, C. A., Fisk, M. R., et al. (2007). The phylogeny of endolithic microbes associated with marine basalts. *Environ. Microbiol.* 9, 2539–2550. doi: 10.1111/j.1462-2920.2007.01372.x

McAllister, S. M., Davis, R. E., McBeth, J. M., Tebo, B. M., Emerson, D., and Moyer, C. L. (2011). Biodiversity and emerging biogeography of the neutrophilic iron-oxidizing Zeta*proteobacteria*. *Appl. Environ. Microbiol.* 77, 5445–5457. doi: 10.1128/AEM.00533-11

Mehta, M. P., Huber, J. A., and Baross, J. A. (2005). Incidence of novel and potentially archaeal nitrogenase genes in the deep Northeast Pacific Ocean. *Environ. Microbiol.* 7, 1525–1534. doi: 10.1111/j.1462-2920.2005.00836.x

Meyer, F., Paarmann, D., D'Souza, M., Olson, R., Glass, E. M., Kubal, M., et al. (2008). The metagenomics RAST server – a public resource for the automatic phylogenetic and functional analysis of metagenomes. *BMC Bioinform.* 9:386. doi: 10.1186/1471-2105-9-386

Newton, I. L. G., Woyke, T., Auchtung, T. A., Dilly, G. F., Dutton, R. J., Fisher, M. C., et al. (2007). The Calyptogena magnifica chemoautotrophic symbiont genome. *Science* 315, 998–1000. doi: 10.1126/science.1138438

Nunoura, T., Nishizawa, M., Kikuchi, T., Tsubouchi, T., Hirai, M., Koide, O., et al. (2013). Molecular biological and isotopic biogeochemical prognoses of the nitrification-driven dynamic microbial nitrogen cycle in hadopelagic sediments. *Environ. Microbiol.* 15, 3087–3107. doi: 10.1111/1462-2920.12152

Orcutt, B. N., Sylvan, J. B., Rogers, D. R., Delaney, J., Lee, R. W., and Girguis, P. R. (2015). Carbon fixation by basalt-hosted microbial communities. *Front. Microbiol.* 6:904. doi: 10.3389/fmicb.2015.00904

Pearce, D. A., Newsham, K. K., Thorne, M. A. S., Calvo-Bado, L., Krsek, M., Laskaris, P., et al. (2012). Metagenomic analysis of a southern maritime Antarctic soil. *Front. Microbiol.* 3:403. doi: 10.3389/fmicb.2012.00403

Prange, A., Arzberger, I., Engemann, C., Modrow, H., Schumann, O., Trüper, H. G., et al. (1999). In situ analysis of sulfur in the sulfur globules of phototrophic sulfur bacteria by X-ray absorption near edge spectroscopy. *Biochim. Biophys. Acta* 1428, 446–454. doi: 10.1016/S0304-4165(99)00095-1

Pruesse, E., Peplies, J., and Glockner, F. O. (2012). SINA: accurate high-throughput multiple sequence alignment of ribosomal RNA genes. *Bioinformatics* 28, 1823–1829. doi: 10.1093/bioinformatics/bts252

Pruitt, K. D., Tatusova, T., Brown, G. R., and Maglott, D. R. (2011). NCBI Reference Sequences (RefSeq): current status, new features and genome annotation policy. *Nucleic Acids Res.* 40, D130–D135. doi: 10.1093/nar/gkr1079

Rouxel, O., Shanks, W. C. III, Bach, W., and Edwards, K. J. (2008). Integrated Fe- and S-isotope study of seafloor hydrothermal vents at East Pacific Rise 9-10° N. *Chem. Geol.* 252, 214–227. doi: 10.1016/j.chemgeo.2008.03.009

Santelli, C. M., Edgcomb, V. P., Bach, W., and Edwards, K. J. (2009). The diversity and abundance of bacteria inhabiting seafloor lavas positively correlate with rock alteration. *Environ. Microbiol.* 11, 86–98. doi: 10.1111/j.1462-2920.2008.01743.x

Santelli, C. M., Orcutt, B. N., Banning, E., Bach, W., Moyer, C. L., Sogin, M. L., et al. (2008). Abundance and diversity of microbial life in ocean crust. *Nature* 453, 653–656. doi: 10.1038/nature06899

Schmieder, R., and Edwards, R. (2011a). Fast identification and removal of sequence contamination from genomic and metagenomic datasets. *PLoS ONE* 6:e17288. doi: 10.1371/journal.pone.0017288.t002

Schmieder, R., and Edwards, R. (2011b). Quality control and preprocessing of metagenomic datasets. *Bioinformatics* 27, 863–864. doi: 10.1093/bioinformatics/btr026

Shi, L., Rosso, K. M., Zachara, J. M., and Fredrickson, J. K. (2012). Mtr extracellular electron-transfer pathways in Fe (III)-reducing or Fe (II)-oxidizing bacteria: a genomic perspective. *Biochem. Soc. Trans.* 40, 1261–1267. doi: 10.1042/BST20120098

Singer, E., Emerson, D., Webb, E. A., Barco, R. A., Kuenen, J. G., Nelson, W. C., et al. (2011). *Mariprofundus ferrooxydans* PV-1 the first genome of a marine Fe(II) oxidizing *Zetaproteobacterium*. *PLoS ONE* 6:e25386. doi: 10.1371/journal.pone.0025386

Templeton, A. S., Knowles, E. J., Eldridge, D. L., Arey, B. W., Dohnalkova, A. C., Webb, S. M., et al. (2009). A seafloor microbial biome hosted within incipient ferromanganese crusts. *Nat. Geosci.* 2, 872–876. doi: 10.1038/ngeo696

Templeton, A. S., Staudigel, H., and Tebo, B. M. (2005). Diverse Mn(II)-oxidizing bacteria isolated from submarine basalts at loihi seamount. *Geomicrobiol. J.* 22, 127–139. doi: 10.1080/01490450590945951

Thorseth, I. H., Torsvik, T., Torsvik, V., and Daae, F. L. (2001). Diversity of life in ocean floor basalt. *Earth Plan. Sci. Lett.* 194, 31–37. doi: 10.1038/nature06899

Toner, B. M., Lesniewski, R. A., Marlow, J. J., Briscoe, L. J., Santelli, C. M., Bach, W., et al. (2013). Mineralogy drives bacterial biogeography of hydrothermally inactive seafloor sulfide deposits. *Geomicrobiol. J.* 30, 313–326. doi: 10.1080/01490451.2012.688925

Tourna, M., Stieglmeier, M., Spang, A., Konneke, M., Schintlmeister, A., Urich, T., et al. (2011). Nitrososphaera viennensis, an ammonia oxidizing archaeon from soil. *Proc. Natl. Acad. Sci. U.S.A.* 108, 8420–8425. doi: 10.1073/pnas.1013488108

Villeneuve, C., Martineau, C., Mauffrey, F., and Villemur, R. (2013). *Methylophaga nitratireducenticrescens* sp. nov. and *Methylophaga frappieri* sp. nov., isolated from the biofilm of the methanol-fed denitrification system treating the seawater at the Montreal Biodome. *Int. J. Syst. Evol. Microbiol.* 63, 2216–2222. doi: 10.1099/ijs.0.044545-0

Wagner, M., Roger, A. J., Flax, J. L., Brusseau, G. A., and Stahl, D. A. (1998). Phylogeny of dissimilatory sulfite reductases supports an early origin of sulfate respiration. *J. Bacteriol.* 180, 2975–2982.

Whitman, W. B., Ankwanda, E., and Wolfe, R. S. (1982). Nutrition and carbon metabolism of *Methanococcus* voltae. *J. Bacteriol.* 149, 852–863.

Yan, J., Haaijer, S. C. M., den Camp, H. J. M., van Niftrik, L., Stahl, D. A., Könneke, M., et al. (2012). Mimicking the oxygen minimum zones: stimulating interaction of aerobic archaeal and anaerobic bacterial ammonia oxidizers in a laboratory-scale model system. *Environ. Microbiol.* 14, 3146–3158. doi: 10.1111/j.1462-2920.2012.02894.x

Yilmaz, S., Allgaier, M., and Hugenholtz, P. (2010). Multiple displacement amplification compromises quantitative analysis of metagenomes. *Nat. Methods* 7, 943–944. doi: 10.1038/nmeth1210-943

Yoder, H. S. J. (1976). *Generation of Basaltic Magma*. Washington, DC: National Academy of Sciences.

Conflict of Interest Statement: The authors declare that the research was conducted in the absence of any commercial or financial relationships that could be construed as a potential conflict of interest.

frontiers in Microbiology

ORIGINAL RESEARCH
published: 27 May 2016
doi: 10.3389/fmicb.2016.00820

Microbial Inventory of Deeply Buried Oceanic Crust from a Young Ridge Flank

*Steffen L. Jørgensen * and Rui Zhao*

Department of Biology, Centre for Geobiology, University of Bergen, Bergen, Norway

The deep marine biosphere has over the past decades been exposed as an immense habitat for microorganisms with wide-reaching implications for our understanding of life on Earth. Recent advances in knowledge concerning this biosphere have been achieved mainly through extensive microbial and geochemical studies of deep marine sediments. However, the oceanic crust buried beneath the sediments, is still largely unexplored with respect to even the most fundamental questions related to microbial life. Here, we present quantitative and qualitative data related to the microbial inventory from 33 deeply buried basaltic rocks collected at two different locations, penetrating 300 vertical meters into the upper oceanic crust on the west flank of the Mid-Atlantic spreading ridge. We use quantitative PCR and sequencing of 16S rRNA gene amplicons to estimate cell abundances and to profile the community structure. Our data suggest that the number of cells is relatively stable at $\sim 10^4$ per gram of rock irrespectively of sampling site and depth. Further, we show that *Proteobacteria*, especially *Gammaproteobacteria* dominate the microbial assemblage across all investigated samples, with Archaea, in general, represented by <1% of the community. In addition, we show that the communities within the crust are distinct from the overlying sediment. However, many of their respective microbial inhabitants are shared between the two biomes, but with markedly different relative distributions. Our study provides fundamental information with respect to abundance, distribution, and identity of microorganisms in the upper oceanic crust.

Keywords: deep biosphere, oceanic crust, geobiology, cell abundance, community structure, endolitihic community

OPEN ACCESS

Edited by:
Beth Orcutt,
Bigelow Laboratory for Ocean Sciences, USA

Reviewed by:
William Brazelton,
East Carolina University, USA
Hazel Barton,
University of Akron, USA

****Correspondence:***
Steffen L. Jørgensen
steffen.jorgensen@bio.uib.no

Specialty section:
This article was submitted to Extreme Microbiology, a section of the journal Frontiers in Microbiology

Received: *09 January 2016*
Accepted: *13 May 2016*
Published: *27 May 2016*

Citation:
Jørgensen SL and Zhao R (2016) Microbial Inventory of Deeply Buried Oceanic Crust from a Young Ridge Flank. Front. Microbiol. 7:820. doi: 10.3389/fmicb.2016.00820

INTRODUCTION

Every day ~100 billion cubic meters of bottom seawater are transported down into the permeable upper oceanic crust. Within this gigantic aquifer system oxic seawater circulates and reacts with reduced igneous rocks before eventually recharging back into the oceans 10^3–10^4 years later (Wheat et al., 2003; Orcutt et al., 2011). Consequently, the chemical composition of fluids and rocks are strongly altered, with wide-reaching ramifications throughout the marine system (Fisher and Becker, 2000; Bach and Edwards, 2003; Bach et al., 2004). Strong evidence exist for an abundant microbial community residing within this subsurface crustal basaltic aquifer (Giovannoni et al., 1996; Torsvik et al., 1998; Fisk et al., 2003; Lysnes et al., 2004; Orcutt et al., 2011; Nigro et al., 2012; Lever et al., 2013) where microbial activity is believed to influence basalt alteration and mineral dissolution

rates (Thorseth et al., 1995; Fisk et al., 1998; Furnes et al., 2001b; Storrie-Lombardi and Fisk, 2004; Kruber et al., 2008).

Endolithic microorganisms in subsurface basalt were first reported two decades ago from a drilling expedition to the Costa Rica Rift zone (Ocean Drilling Program Leg, ODP Leg 148). The presence and activity of microorganisms were inferred via detection of biosignatures including: (i) microscopic tubular structures in which DNA could be detected by staining (Thorseth et al., 1995; Giovannoni et al., 1996), (ii) targeting and localization of intact and active cells via *in situ* fluorescent hybridization (FISH) (Torsvik et al., 1998), and (iii) site-specific nitrogen and carbon enrichment in the altered tubular structures (Giovannoni et al., 1996; Torsvik et al., 1998). These results were later supported by drilling in the Australian Antarctic Discordance (ODP Leg 187) where, in addition to corroborating textural, geochemical, and molecular observations (Furnes et al., 2001a,b; Thorseth et al., 2003), microbial DNA (16S rRNA genes) from subsurface samples was for the first time successfully amplified and sequenced (Lysnes et al., 2004). Despite limited sequencing depth, this analysis revealed a unique microbial population dominated by the bacterial phyla *Gammaproteobacteria*, *Actinobacteria*, *Bacteroidetes*, *Chloroflexi,* and *Firmicutes*, and different from those in the above sediment and seawater.

Besides the pioneering work outlined above only a few additional microbial studies have directly investigated native subsurface igneous rocks (Fisk et al., 2003; Mason et al., 2010; Lever et al., 2013; Orcutt et al., 2015). Thus, this habitat is heavily under-studied, a fact that can be largely attributed to the immense technical and economic challenges involved in the sampling of deeply buried oceanic crust. Consequently, most of our knowledge about the crustal biosphere originates from samples exposed at the seafloor (Orcutt et al., 2011; Edwards et al., 2012b; Orcutt and Edwards, 2014). Seafloor-derived samples, however, are not representative of the subseafloor crustal environment and constitute only a small fraction of the 10^9 km^3 of the upper oceanic crust that has been suggested to be habitable (Heberling et al., 2010). In an effort to address these concerns, *in situ* subseafloor observatories, installed primarily at Juan de Fuca Ridge (JdFR), have expanded our understanding of subseafloor water–rock–microbe interactions in a more representative setting (Orcutt et al., 2011). Despite such technological advancement, a number of basic questions cannot easily be inferred from subseafloor observatories, including cell abundances and community structure in native material.

The first dedicated microbial investigation of a low-temperature young ridge flank system was undertaken by the International Ocean Drilling Program (IODP) expedition 336 to North Pond in the North Atlantic gyre (Expedition 336 Scientists, 2012e). The basement in North Pond is covered by a sediment layer (up to 300 m) and is characterized by vigorous crustal fluid circulation driven mainly by advection (Edwards et al., 2012a). The fast fluid circulation results in relatively low fluid temperatures (10–15°C) and seawater-like fluid chemistry, such as high dissolved oxygen concentration at discharge zones [55–191 μM] (Orcutt et al., 2013). Further, a recent study revealed an active and distinct bacterial community in the crustal fluids underneath North Pond (Meyer et al., 2016).

In the present study, we analyse the abundance and structure of microbial communities in deeply buried basaltic rocks in a total of 33 different samples retrieved from the basement underneath North Pond and compare these to the communities in the above sediments. We analyse the samples by means of 16S rRNA gene amplicon libraries and quantitative PCR (qPCR). Our results are among the first to quantify microbial abundances in native subsurface basalt, thus guiding biomass constrains for this globally significant system. Furthermore, our data elucidate the taxonomic identity of native microbial inhabitants suggesting a community capable of facilitating a diverse range of redox reactions. Lastly, we provide evidence that the dispersal scenarios of the sedimentary and crustal microbial inhabitants are intertwined and potentially closely linked.

MATERIALS AND METHODS

Sample Location, Collection, and Description

We investigated a total of 33 subsurface samples (27 from igneous crust and 6 from a sedimentary breccia) collected from North Pond on the west flank of the Mid-Atlantic Ridge. Samples originate from Holes 1382A (22°45.353′N, 46°04.891′W) and 1383C (22°48.1241′N, 46°03.1662′W; **Figure 1**), both were retrieved using rotary core barrel (RCB) coring. Florescent microspheres were added to the drilling fluid in order to assess potential contamination as described in details elsewhere (Expedition 336 Scientists, 2012d). In order to remove potential contamination introduced during drilling operation, all samples were washed three times in sterile seawater on-board before being sub-sampled into smaller pieces using a chisel and hammer under sterile conditions, as described in details elsewhere (Expedition 336 Scientists, 2012c). The presence of fluorescent microspheres in the wash solution was investigated by microscopy after the last wash. Subsamples (∼2 cm^3) were placed in sterile Whirlpak bags and immediately frozen at −80°C before further processing at the home institute.

Samples follow a depth gradient ranging from ∼110 to 200 meter below seafloor (mbsf) in Hole 1382A (16 samples) and 70 to 300 mbsf in Hole 1383C (17 samples). The igneous crust at the two sites likely originates from different volcanic centers fed by a mantle source of variable composition (Expedition 336 Scientists, 2012c). A short overview of sample depths and lithological characteristics can be found in **Table 1**. For a comprehensive description the reader is recommended to consult the IODP proceedings volume 336 (http://publications.iodp.org/proceedings/336/336title.htm). Following is a brief characterization of each site.

In Hole 1382A basement was located 90 mbsf, however the interval from 93 to 99 mbsf are inferred to be sedimentary (Expedition 336 Scientists, 2012e). A total of 32 meter of upper crustal material was recovered between 110 and 210 mbsf (recovery 32%). From this material we analyzed 16 samples covering six of the eight lithological units encountered in this

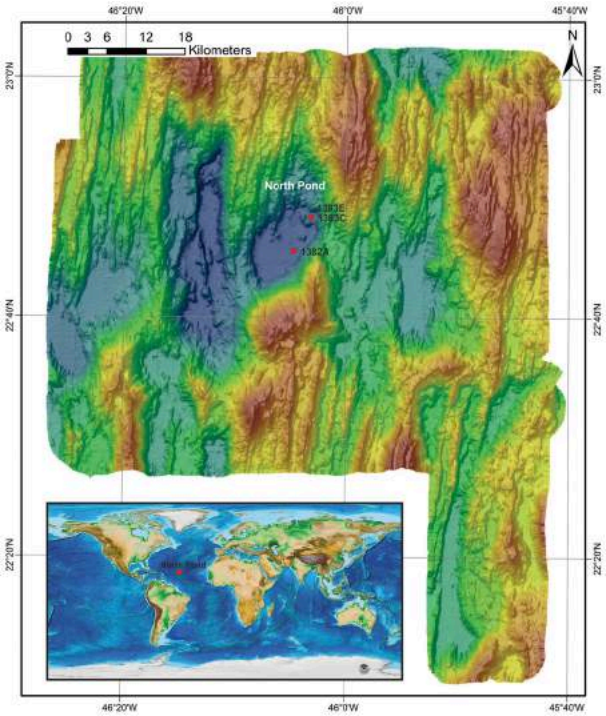

FIGURE 1 | Bathymetric map with the location of the investigated sites. Red circles indicate the geographic location of the investigated sites. Insert: global map indicating the position of North Pond in the Mid-Atlantic Ocean (Source: National Centers for environmental Information - NCEI). Modified from Bach (2012).

Hole (I, II, IV, V, VI, and VII). Unit V consist of sedimentary breccia; likely as a result of a rock slide deposit, whereas all other units are represented by basalt, either as varying volcanic pillow basalt or massive flows with geochemical and petrographic distinct characteristics. Rock alteration can be assigned to low temperature processes.

In Hole 1383C the sediment/basement interface was found at 38.3 mbsf and 50.3 meter of hard rock was recovered from the interval between 69.5 and 331.5 mbsf (recovery 19%). The 17 samples investigated from this Hole are glassy to fine-grained basalts with variable content of phenocrysts, which divides them into three major lithological units (I, II, and III).

DNA Extraction

Small pieces of sample material was pulverized in a flame sterilized steel mortar and ∼0.5 g (0.49–0.91 g) from each sample was subjected to genomic DNA extraction using the FastPrep soil DNA isolation kit (MP Biomedicals) following the manufacturer's instruction with two modifications. First, we used a special bead coating, similar to the G2 DNA/RNA enhancer (Amplicon A/S, Odense, Denmark, available from June 2016) that increases yield, by reducing DNA binding to the beads (Baælum and Jacobsen, 2010; Bælum et al., 2013; Hjelmso et al., 2014). Next, 200 μg of sterile filtered polyadenylic acid (PolyA; Sigma) was added to each lysis mixture prior to bead beating, to avoid DNA binding to the sample matrix (Hugenholtz et al., 1998). Bead beating was performed using the MP-Biomedical FastPrep®-24 for 45 s (speed setting 6). DNA was finally eluted into 75 μl PCR-grade double-distilled water (ddH_2O), and preserved at −80°C until further analysis. In order to assess potential contamination introduced from the extraction kit, two blank extractions were included using the same batch of chemical reagents as for the samples.

Quantitative PCR

Bacterial and Archaeal 16S rRNA genes were quantified individually using quantitative real time PCR applying the StepOne Real Time PCR system (Applied Biosystems). All samples and standards were run in triplicates using SYBR Green Hot Start master mixture (Qiagen) and with the standards, primers, and thermal conditions described in details elsewhere (Jørgensen et al., 2013). In short, a dilution series (10–10^6 target copies) containing *Escherichia coli* PCR amplified full-length 16S rRNA genes and a linearized archaeal fosmid (54d9) was used as bacterial and archaeal standards, respectively. Bacterial SSU rRNA genes were targeted with the primers bac341F (5′-CCTACGGGWGGCWGCA) and 518R (5′-ATTACCGCGGCTGCTGG). For archaeal SSU rRNA gene amplification the primers Un515F (5′-CAGCMGCCGCGGTAA) and Arc908R (5′-CCCGCCAATTCCTTTAAGTT) were used. All R^2 were >0.95 and the amplification efficiency between 90 and 104%.

Ion Torrent SSU rRNA Amplicon Library Preparation and Sequencing

All DNA extracts were PCR amplified in duplicates with the SSU rRNA gene specific primers 519f (5′-CAGCMGCCGCGGTAA) and 805r (5′-GACTACHVGGGTATCTAATCC) in order to generate an amplicon library for subsequent sequencing using the Ion Torrent PGM Personal Genome Machine (PGM) platform technology (Life Technologies). We used a two-step amplification approach as described by Berry et al. (2011), to minimize bias introduced by the long adaptor sequence. The first-round PCR was carried out in duplicate for each sample, to minimize PCR drifting, and each reaction (20 μl) contained 10 μl 2x HotStarTaq® master mixture (Qiagen), 0.2 μl of each primer (100 μM stock), 2 μl template and ddH_2O. The PCR program was initiated with a hot start activation step for 15 min at 95°C followed by an optimized number of PCR cycles (36–37) of 95°C for 30 s, 56°C for 30 s, and 72°C for 30 s. The duplicate PCR products were pooled and purified using QIAquick PCR purification kit (Qiagen). In the second-round PCR attaching the Multiplex Identifiers (MIDs), seven cycles were run, where each reaction (25 μl) contained 12.5 μl 2x HotStarTaq® master mixture (Qiagen), 0.2 μl 806r-B-Key (100 μM stock), and 2 μl 519f MID primer (10 μM stock), with 5 μl of purified PCR products from first-round amplification as the template, according to the Ion Torrent protocol. The PCR amplicons were purified using AMPure XP bead Purification Kit (Agencourt), following manufactures protocol, before all samples were pooled in equimolar concentrations (26 pmol). We note, that due to the PCR and the subsequent equimolar pooling, the

TABLE 1 | General sample description including depth, lithological unit, onboard sample description, and in which group in the hierarchical cluster analysis the microbial community is located.

Sample	Depth (mbsf)	Unit	Specific sample description	Cluster
1382A				
2R_1C	110	I	Massive, minor red-yellow-brown alteration	4
3R_2B	115	I	Massive, yellow-white-brown alteration in vein	4
3R_3A	117	I	Massive, patchy orange-brown alteration	4
3R_4B	117	I	Massive, mostly brown oxidized halo	4
4R_1B	123	II	Aphyric cryptocrystalline basalt, gray-brown alteration	4
5R_1B	133	II	Massive, aphyric, red alteration	4
6R_1A	142	II	Aphyric, cryptocrystalline, less vesicular, patchy alteration	4
7R_2B	153	III	Aphyric, glassy margin, red, and orange-brown alteration	4
8R_1A	161	IV	Ultramafic, pyroxene, evidence of low-temperature alteration	1
8R_1B	161	IV	Porphyritic basalt	4
8R_2F	162	IV	Orange-brown sediment with small (<1 mm) basalt clasts	2
8R_3G	163	IV	Gray-brown + orange-brown sediment with small (<1 mm) basalt clasts	1
8R_4D	163	IV	Sedimentary breccia with basalt clasts, rusty colored, extensive carbon	2
9R_1C	172	IV	Sediment near serpentinized breccia	3
10R_3D	183	V	Medium-grained basalt, massive, porphyritic, pervasive alteration	4
12R_1A	199	VI	Porphyritic basalt, minor alteration	4
1383C				
2R_2E	72	I	Aphyric basalt, highly altered, vein with red alteration, light brown alteration	5
3R_1B	77	I	Aphyric basalt, slight alteration, tan alteration deposits	4
4R_1B	87	I	Light tan micrite breccia with altered glass clasts	4
5R_1B_I	97	I	Aphyric basalt, moderately altered, vein with red alteration	5
5R_1B_II	97	I	Aphyric basalt, moderately altered	5
6R_1A	105	I	Aphyric basalt, slight alteration, altered chilled margin, ochre alteration	6
10R_1A	144	II	Light tan micrite with large clasts of altered glass	5
10R_1D	145	II	Phyric basalt, moderately altered, multiple veins, slight red alteration	5
11R_1C	154	II	Phyric basalt, extensive alteration, orange, and olive alteration	5
19R_1B	212	III	Aphyric basalt, highly oxidized, light brown alteration, relatively brittle	5
19R_1A	212	III	Two small pieces, mostly glass, rust alteration	5
20R_1A	219	III	All basalt glass, rust alteration	5
24R_1B	257	III	Aphyric basalt, oxidized, dark orange-brown alteration, fractured	5
24R_1A	256	III	Aphyric basalt glass with rust alteration, vesicles	5
27R_1A	285	III	Aphyric massive basalt, alteration	4
29R_1A	300	III	Aphyric basalt, highly oxidized, thin carbonate veins	6
30R_1A	304	III	Aphyric basalt, oxidized, some fractures, dark orange alteration	5

*Cluster number corresponds to numbers in **Figure 4**. The sample description presented here is modified from IODP 336 site summaries (Expedition 336 Scientists, 2012a,b).*

number of reads do not reflect the original concentration of DNA, which based on gel band intensity after PCR was much higher in the samples than in the blank extractions. Raw reads generated in this study were deposited at the NCBI Sequence Read Archive under the project number SRP070121.

OTU Filtering, Clustering, and Taxonomic Assignment

Sequence reads obtained from the Ion Torrent sequencing were cropped at 220 bp and quality filtered with a 0.5 quality cut-off, chimera checked, and Operational Taxonomic Units (OTUs) clustered (97% similarity) using UPARSE/USEARCH (Edgar, 2013). The resulting OTUs were taxonomically assigned using the CREST software, with a lowest common ancestor algorithm implementing the SilvaMod reference database (Lanzen et al., 2012). A fasta sequence file of the represented OTUs can be found in the Supplementary Material (Data sheet S2).

Contamination Assessment of Sequence Pool

Contamination issues have previously hampered progress in deep marine research. In an attempt to avoid such obstacles this study applies several measures to prevent and assess the degree of potential contamination, as outlined in the sample handling and collection section above. Further, as a broad reaching contamination control for drilling protocols we extracted and

sequenced DNA from the drill mud and a recovered microsphere bag (exposed to bottom seawater, drill fluid, and mud). The purpose of this control is to address potential inadvertent contamination of samples introduced during standard IODP drilling protocols. The results allow estimating the ratio of the inferred natural community that is likely to arise from contamination. Any OTU present in the control and in the native sample material was removed from the dataset. We note that true overlap between communities in the control and native samples may exist, which would lead to culling of legitimate sequences. Additionally, in order to assess potential contamination in the 16S rRNA gene amplicon preparation procedure two blank extractions (no sample material) were subjected to the same amplification protocol as the samples. Amplified DNA from these blanks may represent contamination originating from DNA extraction kit and/or PCR mix reagents (Champlot et al., 2010; Lusk, 2014; Salter et al., 2014). Therefore, any OTU found in both the extraction blanks and the native sample material was removed prior to any further downstream analysis, with the exception of OTUs that was found to be more than 50 times as abundant in the basalts than in the above-described controls. These were retained in the dataset, due to the plausible scenario of cross-contamination from controls to samples. This approach is similar to that described by Lee et al. (2015) with modified increased stringency addressing the assumed lower biomass in our sample set. However, in order to evaluate the impact of this stringent filtering, ordination, and clustering were likewise performed on the full dataset prior to the above described filtering.

Ordination and Hierarchical Clustering Analysis

The relative abundances of individual OTUs in each sample were clustered based on unconstrained Bray-Curtis, Jaccard, and Dice dissimilarity index using the software PAST version 3.08 (Hammer et al., 2001), before and after removal of potential contaminant reads. The basalt-hosted microbial communities were compared to those in the overlying sediments (Hole 1383E), using non-metric dimensional scaling (NMDS) applying Bray-Curtis dissimilarity. The data from the sediment samples was generated following identical protocols (e.g., the same primers, extraction kit, PCR mix), sequencing platform and downstream analysis, thereby enabling a valid comparison. The concentrations of major and trace elements from rocks provided by the IODP data report (Expedition 336 Scientists, 2012a,b) originating from the same core sections, but separated from the samples used for microbiology (between 20 and 70 cm distance), were used in cluster analysis using Bray-Curtis and Jaccard.

RESULTS

16S rRNA Gene Abundance

The total abundance of 16S rRNA gene copy numbers (Archaea plus Bacteria) estimated by qPCR varies between 0.3 and 8.3 $\times$ 10^4 copies per gram in Hole 1382A and 0.6–3.9 $\times$ 10^4 copies per gram in 1383C (**Table 2**), with the majority of all samples (80%) falling within the range of 1.9–5.8 $\times$ 10^4 copies. Three samples from the sedimentary breccia between 162.8 and 163.8 mbsf in Hole 1382A (8R-2F, 8R-3G, and 8R-4D) had notably lower numbers (0.3–0.6 $\times$ 10^4 copies per gram) than the remaining samples from this site. Based on our quantification the 16S rRNA genes are predominantly of bacterial origin, comprising between 92.6–100% and 91–100% in Hole 1382A and 1383C, respectively (**Table 2**). Assuming an average copy number per genome of 4.2 for Bacteria and 1 for Archaea (Stoddard et al., 2015), these copy numbers suggests cell abundances ranging ~0.1–2 $\times$ 10^4 per gram of sample material (average 0.71 $\times$ 10^4).

Sequence Reads, Filtering, and OTU Clustering

The total number of sequence reads per sample after filtering and potential contaminants removal (OTUs present in the four controls) varied between 8598 and 25,841 with an average of 17,649 (**Table 2**). A total of 1,804 OTUs (>97% sequence similarity) were found across all samples, of which 1,643 OTUs (91% of total OTUs) were assigned to the bacterial domain, 44 OTUs (2.5% of total OTUs) to the archaeal domain, while 60 OTUs (3.4% of total OTUs) were Eukaryotic. The remaining 57 OTUs were classified as "no hits" which means that the sequence is <80% similar to any in the database (Data sheet S1). The number of OTUs in the individual samples varied between 16 and 371 (**Table 2**). Blank extractions contained a combined total of 221 OTUs of which 142 were removed according to the criteria outlined in the Materials and Methods Section. An additional 50 OTUs were removed from the original data, as they were present in either the drill mud and/or on the recovered microsphere bag (12 and 46 OTUs, respectively).

Microbial Community Composition

As the microbial communities are spread across 41 different phyla, 73 classes, 155 orders, and 218 families, it is far beyond the scope of this work to address the community composition in all samples in detail. Therefore, only the results of the most abundant groups are listed here. However, a full list of OTUs present and their taxonomic assignments can be found in the Supplementary Material (Data sheet S1). In general the communities are relatively homogenous on higher taxonomic level across all samples, however in the sedimentary breccia the diversity of microorganisms and number of OTUs are extraordinarily low, especially in the middle section of that lithological unit (**Figure 2** and **Table 2**), in many ways causing these samples to deviate substantially from the rest.

All samples are dominated by *Proteobacteria* (35–99% of the total communities) of which the class of *Gammaproteobacteria* is the most abundant, followed by *Alphaproteobacteria*, *Deltaproteobacteria,* and *Betaproteobacteria*, respectively (**Figure 2A** and Data sheet S1). Only very low abundances, if any, were assigned to the class of *Epsilonproteobacteria* and *Zetaproteobacteria*. Analysing the different classes of *Proteobacteria* with higher taxonomic resolution show that many (average 60%) of the *Gammaproteobacteria* could not be assigned below class level (**Figure 2B**). The majority of these were represented by OTU5, which showed high similarity (100%) to *Pseudomonas* when performing NCBI blast search. The limited taxonomic resolution of OTU5 in our analysis is

TABLE 2 | General molecular characteristic of the samples investigated.

Sample ID	Depth (mbsf)	Unit	16S rRNA copies (× 10^4)	% Bacteria		Reads after filtering	OTU #	Shared with sediment	
				qPCR	Amplicon			OTUs	Reads of total %
U1382A									
2R_1C	110	I	5.7	98	100	8,598	371	198	72
3R_2B	115	I	8.3	100	100	12,966	174	114	81
3R_3A	117	I	2.7	100	99	16,574	96	66	80
3R_4B	117	I	2.4	100	100	11,349	224	133	81
4R_1B	123	II	4.8	96	97	15,330	215	128	78
5R_1B	133	II	3.9	92	99	19,517	279	168	83
6R_1A	142	II	2.1	100	100	20,437	175	101	69
7R_2B	153	IV	3.8	100	100	10,968	193	127	85
8R_1A	161	V	1.8	100	100	23,251	42	23	80
8R_1B	161	V	4.1	95	100	12,495	261	142	80
8R_2F	162	V	0.3	100	100	19,858	16	10	99
8R_3G	163	V	0.5	100	100	19,145	25	18	22
8R_4D	163	V	0.6	100	86	25,028	27	20	31
9R_1C	172	V	4.2	92	99	16,873	314	185	82
10R_3D	183	VI	5.8	97	99	18,080	283	148	79
12R_1A	199	VII	3.0	92	98	19,506	273	153	75
U1383C									
2R_2E	72	I	2.8	99	100	19,163	319	165	63
3R_1B	77	I	3.1	98	100	18,240	141	75	75
4R_1B	87	I	1.9	98	97	19,144	124	72	72
5R_1BI	97	I	3.1	91	96	15,164	177	124	77
5R_1BII	97	I	2.6	99	99	19,553	330	168	75
6R_1A	105	I	2.2	100	100	23,627	243	146	71
10R_1A	144	II	2.1	90	100	25,841	158	99	86
10R_1D	145	II	2.9	98	100	17,447	326	161	83
11R_1C	154	II	1.7	99	100	24,686	204	116	87
19R_1B	212	III	3.0	98	100	19,107	264	130	84
19R_1A	212	III	3.3	99	100	18,946	126	81	88
20R_1A	219	III	2.9	100	100	3916	148	90	81
24R_1B	257	III	1.9	100	100	12,775	162	99	86
24R_1A	256	III	3.2	100	100	20,900	213	121	86
27R_1A	285	III	3.9	99	100	9,811	162	113	87
29R_1A	300	III	0.6	100	98	11,218	69	48	82
30R_1A	304	III	3.3	100	100	22,903	229	117	88

Including gene copy numbers of total prokaryotic 16S rRNA gene copies per gram of sample material. Percent of the total community related to the domain Bacteria reported both from the qPCR and the amplicon library. The total number of reads after filtering. Number of OTUs in each sample (97% similarity). The number of OTUs and the % of total read that is shared with the samples in the above sediment from North Pond (1383E).

likely due to the high stringency used by the lowest common ancestor algorithm applied to assign taxonomy. Most of the reminding *Gammaproteobacteria* in Hole 1382A belonged to the two orders *Oceanospirillales*, mainly affiliated with the SAR86 clade and *Pseudmonadales*, (largely divided between the families *Moraxellaceae* and *Pseudomonadaceae*). In contrast, the most abundant Gammaproteobacterial order from Hole 1383C is *Alteromonadales*, whereof most can only be assigned to family level (*Alteromonadaceae*) and to a lesser extent *Marinobacter* (<1% of total community). Although, abundance-variation between samples is present within the *Alphaproteobacteria*, as for all taxonomic groups, *Rhizobiales*, *Rhodobaceriales,* and *Rhodospirilialles* were in general the most abundant orders (**Figure 2C**). At both sites, *Burkholderiales* was by far the most prominent member of the *Betaproteobacteria* at the order level, with the genus *Variovorax* accounting for approximately half of this group and the family *Oxalobacteraceae* representing the other half (**Figure 2D** and Data sheet S1). The overall abundance of *Deltaproteobacteria* was relatively low and in Hole 1382A it was dominated primarily by *Myxococcales* and the *SAR324* clade whereas *Bdellovibrionales* and *Desulfobacterales* were the most abundant orders in Hole 1383C (**Figure 2E**). In addition

to the mentioned members of the *Proteobacteria* the following phyla were found in relatively high abundances; *Actinobacteria*, *Firmicutes*, *Bacteroidetes*, and *Acidobacteria* along with a number of less abundant groups, but still representing more than 1% of all reads in one or more samples, such as *Planctomycetes* and *Chloroflexi* (see **Figure 2A**).

The archaeal community constitute only a minor fraction of the entire community (max. 5%, avg. 0.6% of all reads) and is represented by five phyla; *Ancient Archaeal Group* (AAG), *Crenarchaeota*, *Euryarchaeota*, *Thaumarchaeota,* and the newly proposed *Lokiarchaeota* (Spang et al., 2015; **Figure 2A** and Data sheet S1). Of these, Thaumarchaeal *Marine Group I* is by far the most abundant.

A comparison between the rank abundance of the 576 OTUs shared between the basalt and the overlying sediment was performed using the average abundances of the OTUs across all basalt and across all sediment samples, excluding the sedimentary breccia from Hole 1384A (**Figure 5**). The shared OTUs represented between 63 and 86% (average 80%) of all reads in the basalt and 44–71% (average 58%) in the sediments, but show a markedly different rank abundance distribution (**Table 2** and **Figure 5**).

Ordination and Clustering Analysis

The variation in the microbial community structure (relative abundance of OTUs) found in the basaltic samples beneath North Pond was compared to the composition in a number of sedimentary horizons in Hole 1383E directly overlying the basaltic crust by means of NMDS. The sedimentary community was investigated at 17 different depths, spanning from the top of the sediment to a few meters above the sediment basement interface and clearly shows a separation from those observed in the underlying upper crust (**Figure 3**). The microbial composition in the sedimentary breccia (lithological unit V) in Hole 1382A are markedly different from the rest of the samples from this sites and also from the basaltic rocks from Hole 1383C, causing these samples to cluster alone, with the exception of sample 8R_1B (the only basalt sample within the breccia unit). An NMDS analysis was also carried out on the full dataset, before removal of any of the OTUs found in the four controls, as described in the Materials and Methods Section. This result shows the same pattern, as with the "cleaned" dataset presented in **Figure 3**, and verifies that all control samples are markedly different from any of the indigenous samples (Figure S1).

In order to investigate any link between community composition and lithology a hierarchical clustering analysis based on the relative abundance of OTUs was executed. The results show several minor (group 1, 2, 3, 6) and two major (group 4 and 5) clusters separated by high bootstrap value (**Figure 4**). The major clusters largely distinguish the two sites from one another. However, three samples from Hole 1383C cluster within 1382A. The bootstrap values are generally low and clustering according to lithology or depth cannot be inferred. The clustering using the full dataset, before removal of potential contaminant reads in general shows the same clustering pattern, however a higher degree of mixing between the two sites is observed (Figure S2). The results from clustering based on Jaccard and Dice dissimilarity indexes, showed no clear difference in clustering pattern as compared to Bray-Curtis (data not shown). Using the geochemical data (major and trace elements) from the same core sections as those used for microbiology, in a hierarchical clustering, shows only very small variation in composition. No clear clustering pattern between sites or lithology could be observed and most branching points were unsupported (Figure S3).

Contamination Control

The presence of fluorescent microspheres in the sterile seawater used to wash the basalt rock surface was investigated on board the ship. After three washing rounds, microspheres were detected in 36% of the samples (**Figure 4**) and more frequently observed in Hole 1383C than 1382A.

Drill mud and the microsphere bag yielded a total of ∼47,500 high-quality reads comprising a number of different bacterial taxa (Data sheet S1). After removal of extraction blanks, 12 OTUs were obtained from the drill mud and 46 from the microsphere bag, most of these were affiliated with *Streptococcus*, a group that are often associated with human pathogens. A larger number of OTUs were obtained from the microsphere plastic bag, many of which were affiliated with different SAR clades. However, also here a number of reads were associated with bacterial groups often associated with humans (e.g., *Streptococcus* and *Dermabacter*; Data sheet S1). Standard drilling protocols inevitably introduce contaminants to drilling components and we propose this as an explanation for the detection of human associated taxa.

Extraction blanks were represented by ∼16,000 reads whereof the vast majority could be assigned to the following three taxonomic groups: *Ralstonia*, *Enterobacteriaceae,* and *Methylobacterium*. On average 38% of all reads were removed during the cleaning procedure (total of 158 OTUs) highlighting the importance of performing operation controls and analysing blank extractions, especially when working with low biomass sample material (Data sheet S1).

DISCUSSION

Microbial Abundances in Subsurface Basaltic Crust

Based on our qPCR results of prokaryotic 16S rRNA gene abundances, we estimate that the samples contain $\sim 10^4$ cells per gram of rock sample, with *Bacteria* outnumbering *Archaea* in all samples (**Table 2**). However, as with all cell estimates based on a primer-based approach it is prone to bias and the numbers should be evaluated with this in mind. It is difficult to compare our estimates with earlier reports since, to the best of our knowledge, only one previous study has been conducted in which direct cell abundances were estimated from native cold subsurface basalt (Fisk et al., 2003). Based on amino acid concentration they suggest $\sim 10^5$ cells per gram sample. A recent study estimated cell numbers in the basaltic fluids from both investigated sites, to be between 1.4 and 2.2×10^4 per ml fluid, based on direct cell counts (Meyer et al., 2016). Considering the average basaltic porosity of 4% and assuming a density of 3, implies that our quantification

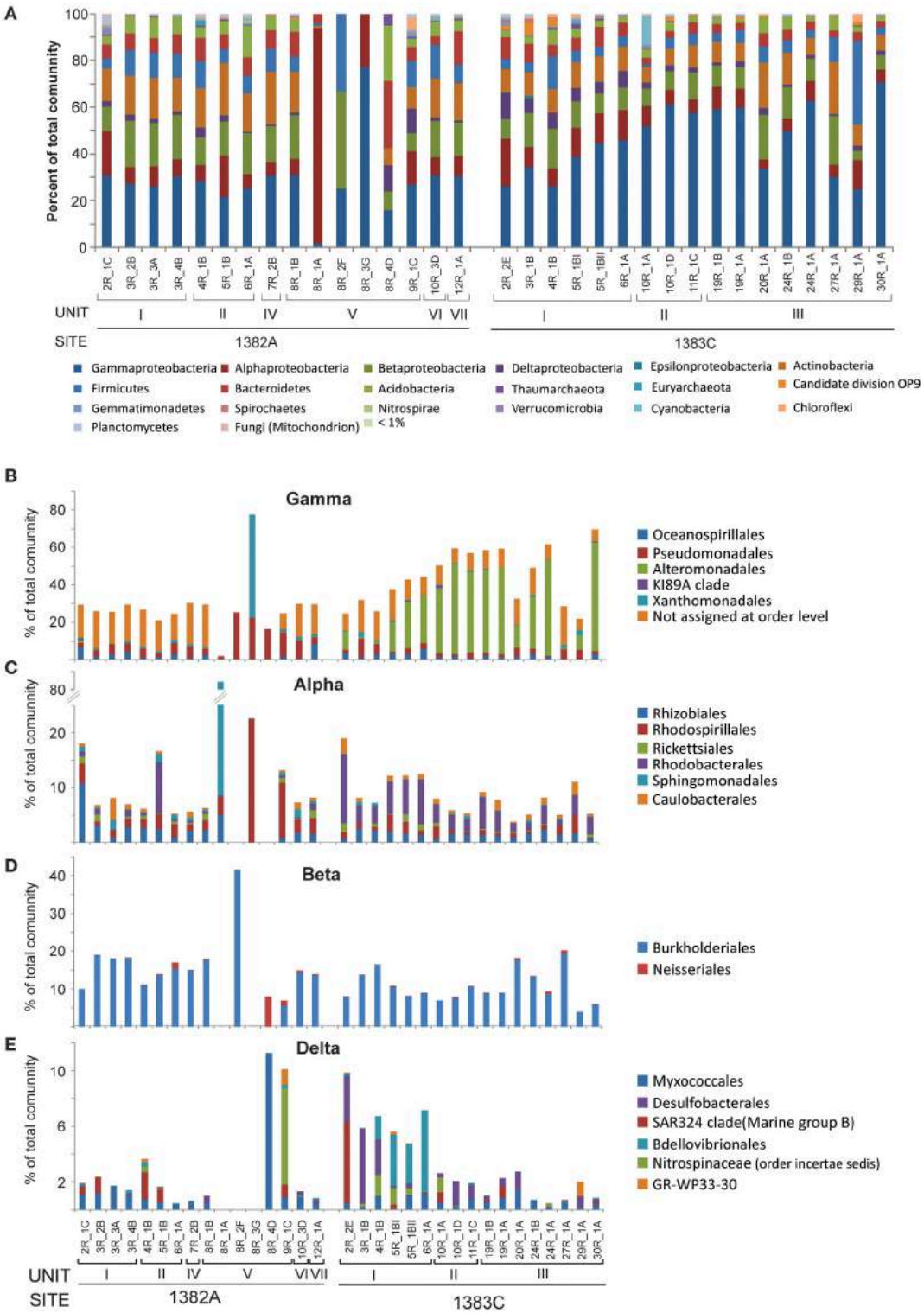

FIGURE 2 | Relative abundance of taxonomic groups. (A) Class level abundances of *Proteobacteria* and phylum level for all other groups comprising more than 1% of total community in one or more samples. Abundances for the taxonomic orders representing more than 1% of total community of **(B)** *Gammaproteobacteria*, **(C)** *Alphaproteobacteria*, **(D)** *Betaproteobacteria*, and **(E)** *Deltaproteobacteria*.

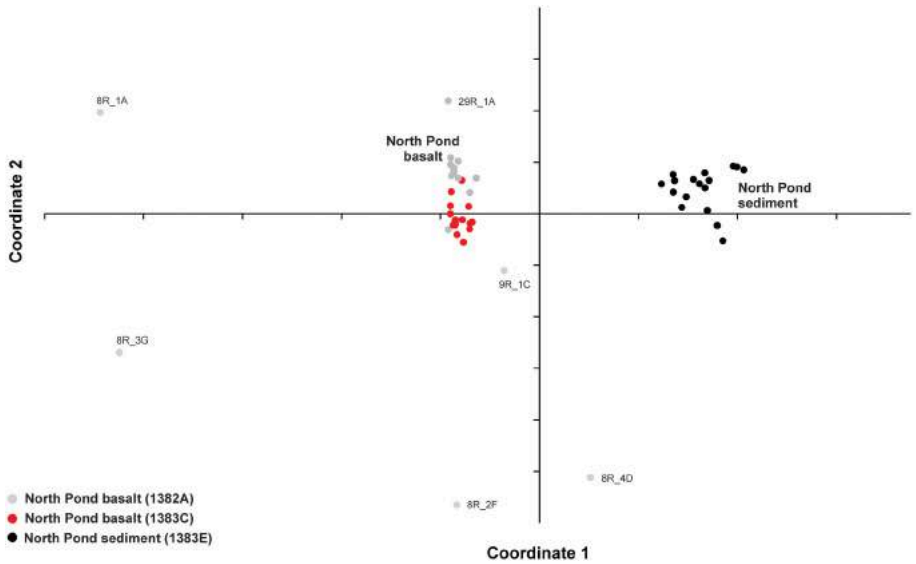

FIGURE 3 | Comparison between community structures. Relative abundance of OTUs in each sample was used to compare the variation between the basalt-hosted communities and the sediment-hosted communities by means of non-metric multidimensional scaling (NMDS). Samples are color coded gray: Hole 1382A, red: 1383C, black: North Pond sediment from Hole 1383E.

is not merely representing cells in the fluid, but that the majority must be attached to the rock surfaces.

Due to the restricted number of sites in our study we have restrained ourselves from the tantalizing prospect of extrapolating the cell abundance to global biomass. However, we note that a previous estimate based on thermodynamic and bioenergetic models was suggested to translate into $\sim 10^7$–10^9 cells per gram rock (Santelli et al., 2008). In other words, 3–5 orders of magnitudes off our estimations. In support of a lower cell abundance is the relatively low oxygen consumption (<1 nmol O_2 cm^{-3} rock d^{-1}) estimated beneath North Pond (Orcutt et al., 2013). Another interesting observation related to the cell numbers is the relative consistency across all samples, which suggest that the cells are limited by a common vital anabolic or catabolic resource.

Microbial Community Composition in Subsurface Basaltic Crust

Based on the 16S rRNA amplicon libraries the microbial communities in the subsurface basalt in North Pond are all dominated by Bacteria, in general leaving the archaeal domain represented by <1%. Although, our qPCR estimations vary slightly from this, both analyses confirm the bacterial dominance (**Table 2**). By far the most abundant phylum was *Proteobacteria*, with *Gamma-*, *Beta-*, and *Alphaproteobacteria* constituting the majority within this phylum. In addition *Actinobacteria*, *Firmicutes*, *Bacteroidetes*, and *Acidobacteria* were all represented by relatively high abundances. To the best of our knowledge, only one previous published study has successfully amplified DNA from native subsurface material and determined the community composition (Lysnes et al., 2004). By means of DGGE that study reported sequences related to *Gammaproteobacteria*, *Actinobacteria*, *Bacteroidetes*, *Chloroflexi,* and *Firmicutes*, of which *Gammaproteobacteria* was the most abundant. A more recent study compiled taxonomic data from a number of studies regarding surface-exposed basalts and identified a set of commonly found abundant microbial groups, including *Gamma-*, *Alpha-*, and *Deltaproteobacteria*, as well as *Actinobacteria*, *Bacteroidetes*, *Acidobacteria*, *Planctomycetes*, *Gemmatimonadetes,* and *Nitrospirae* (Lee et al., 2015). Finally, the microbial community composition in the fluids underneath North Pond has revealed a similar dominance of *Proteobacteria,* also with *Gammaproteobacteria* being most abundant, then followed by *Alpha-*, *Epsilon-*, *Beta-*, and *Deltaproteobacteria* (Meyer et al., 2016). Further, relative high abundances of *Actinobacteria*, *Bacteroidetes*, *planctomycetes, Gemmatimonadetes,* and *Chloroflexi* were observed. Based on this it is tempting to suggest that a basalt-hosted taxonomic core group exists, including surface, subsurface fluids, and hard rocks. However, it is important to stress that the similarity of microbial groups in all cases is based on high taxonomic rank and future in-depth phylogenetic comparison, founded on full-length 16S rRNA sequences, are needed to resolve this issue.

The origin of the subsurface oceanic crustal community is an open question and different scenarios have been debated, one of them being that dispersion may occur via the above sediment column (Huber et al., 2006; Schrenk et al., 2010). When we compared the relative community composition in the basaltic rocks with that in overlying sediment striking differences were observed (**Figure 3**). However, this is by no means indicative of community isolation between the crust and sediment. On the contrary, a high degree of overlap was revealed from the OTUs distribution pattern. Of the 1,802 OTUs

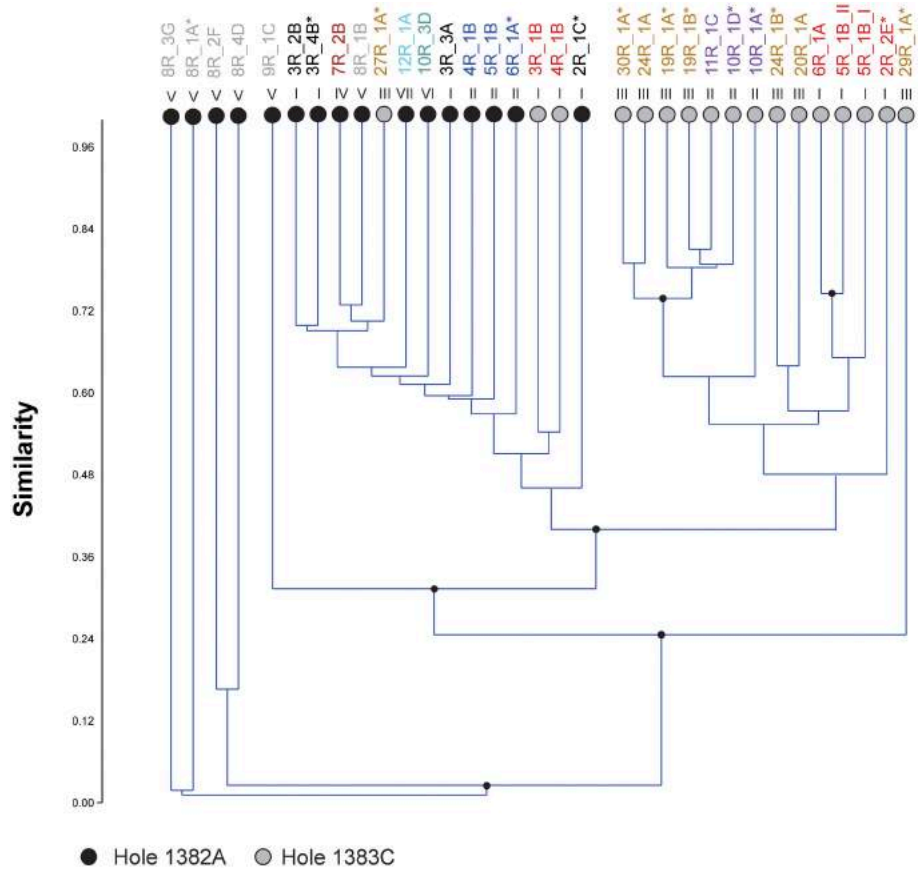

FIGURE 4 | Microbial community clustering. Relative abundance of OTUs in each sample was used to cluster the different communities within the crustal samples from North Pond by means of Bray-Curtis distance calculations. Circles at the end of each branch indicates sampling site; gray: Hole 1383C, black; Hole 1382A. Roman numerals above the branches indicate the lithological unit, also indicated by colors in the sample name above. Asterisk indicates presence of microspheres in the wash fluids after last washing. Numbers above sample name indicates clusters supported by high bootstrap values (> 90) and are identical to numbers used in **Table 2**.

found across all 33 crustal samples, 576 OTUs were shared with the sedimentary habitat above, comprising as much as 63–86% (average 80%) of all reads in the basaltic samples. However, the relative distributions of the shared OTUs in the two environments are markedly different, which might reflect environment-specific taxon recruitment based on availability of electron donors and acceptors (**Figure 5**). Based on these results the two components of the deep biosphere do indeed share many of their microbial inhabitants. Although, the dynamics and mechanisms of taxon dispersal between the crustal and sedimentary subseafloor regimes is beyond the scope of this study, we note that a recent study support the dispersal of sedimentary bacteria via the ocean (Walsh et al., 2016).

Regarding the heterogeneity of crust-associated microbial communities beneath North Pond, we note that although the communities from the two different sites to a large degree cluster together, (**Figure 3**), there are also clear differences (**Figure 4**). Two major clusters, supported by high bootstrap values (> 90) were found, largely separating the two investigated sites from one another. Notable differences are the presence of a few highly abundant OTUs affiliating with an uncultured *Alteromonas* lineage (*Gammaproteobacteria*) in Hole 1383C and a much higher occurrence of *Rhodobacterales* (*Betaproteobacteria*) in Hole 1383C than in Hole 1382A. The significance of this is not known, but it is possible that the physico-chemical nature, and associated redox coupling, of advective crustal fluids, drive community differentiation.

Potential Metabolic Traits and Dominant Groups

The vast majority of lineages reported here do not group within taxonomic clades with known metabolism, and therefore their potential role in the ecosystem is unresolved. However, a number of less abundant groups with relatively constrained metabolic potential are present, thereby allowing us to assign their function with some degree of certainty. For example, as putative sulfate reducers in other environments a number of different genera were observed, including, *Desulfotomaculum*, *Desulfurispora*, *Desulfosporosinus*, *Desulfobaca*, *Desulfobulbus*, *Desulforomonas*, *Desulfovibrio,* and *Desulfobacula*, suggesting that at least the potential for active sulfate reduction is present. The classical sulfur oxidizers (mainly within *Epsilonproteobacteria*), on the

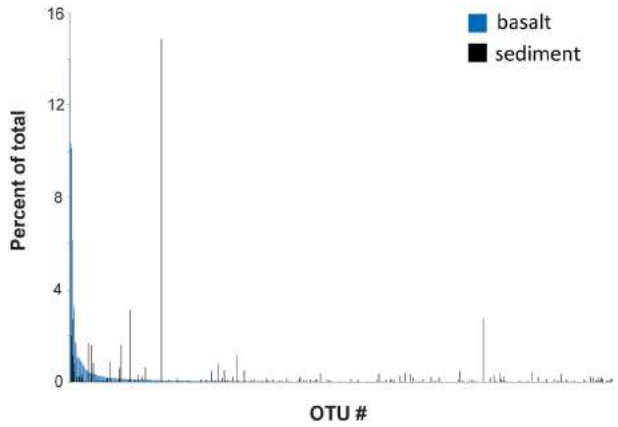

FIGURE 5 | OTU rank abundance. Comparing the rank abundance of OTUs shared between the basalt-hosted community (Holes 1382A and 1383C) and the sediment-hosted (1383E). The abundance of each OTU across all basalt-hosted samples and across all sediment samples was compiled and the average abundance used (excluding the sedimentary breccia in Hole 1382A).

other hand, were only sporadically observed. This observation is worth mentioning in the context of the relatively high abundances of sulfur oxidizers found in the fluids by Meyer et al. (2016) and in the overlying sediments, suggesting different functions between the free-living and the surface-attached communities.

Iron and hydrogen (beside sulfur) has been proposed to be important electron donors in this type of habitat (Bach and Edwards, 2003; Edwards et al., 2005). However, known metal reducers such as, *Marinobacter, Shewanella*, *Geobacter,* and *Ferruginibacter* made up only a minor fraction of the entire community (*Marinobacter* up to 0.3%). Hydrogen utilization is another widespread trait that is difficult to pinpoint based on taxonomy alone, hence we could only assign this to *Hydrogenophilus*, *Hydrogenophaga,* and *Paracoccus,* all represented in the dataset, but in low abundances.

Finally, we observe a number of groups with the ability to transform nitrogen compounds. This includes members of the putative ammonium-oxidizing archaeal Marine Group I (<5% of total community) and nitrifiers (*Nitrospira)*, which was detected in discrete samples up to 0.5%. Despite, the relative low abundances, their presence suggest an active nitrogen cycle, which is in congruence with the low concentration of organic carbon measured in this environment (Orcutt et al., 2015; Sakata et al., 2015).

Contamination Control

A great concern related to investigations of subsurface crustal material (and the deeply buried biosphere in general) has been the challenge of overcoming issues related to contamination constrains (Lever et al., 2006; Santelli et al., 2010). In order to delineate potential sources of contamination (acquired during drilling or subsequent sample processing) we analyzed two sample processing controls (extraction blanks) and two drilling operation controls (drill mud and a recovered empty microsphere bag). Designation of potential contaminants facilitates the tracking of their source in addition to their downstream removal from the bioinformatic pipeline as described before. As more reads were removed from the native samples due to their overlap with extraction blanks rather than with the drill mud and microsphere bag, we conclude that more contamination was introduced during DNA extraction and amplification than from the actual drilling procedure. However, we acknowledge that contamination could have originated from drilling or downstream procedures not accounted for by our contamination controls.

Despite, the observed contamination, several lines of evidence suggest that the final community structure is not corrupted: (i) the bifurcation of community structure of the two crustal sites, (ii) drastic differences between the composition and structure of sedimentary and crustal samples, despite equally low biomass, (iii) congruence between our results and taxonomic identity of enriched organisms from independent studies at this site, including *Pseudomonas, Burkholderia, Bacillus, Salinibacterium, Sphingomonas, Moraxella,* and *Methylobacterium* (Hirayama et al., 2015), (iv) agreement with core-taxa hitherto identified in basalt hosted environments (Lysnes et al., 2004; Lee et al., 2015) and in the fluids under North Pond (Meyer et al., 2016).

In sum, the data shows that contamination in low abundance habitats is a concern, and we encourage that both extraction and operation controls are performed. If such measures are taken the influence of contamination in data analysis seems manageable.

We also note that the presence of microspheres, a general measure of contamination deployed during IODP drilling operations, does not seem to be reflected in the magnitude of contamination in the 16S rRNA gene libraries (measured as number of reads removed in the filtering due to drill mud contamination).

CONCLUSIONS

Our study gives some of the first insights into the microbial inventory of the subsurface oceanic crust in a young cool ridge flank system and show a community dominated by *Proteobacteria* (*Gammaproteobacteria*, *Alphaproteobacteria,* and *Betaproteobacteria*), followed by *Actinobacteria*, *Firmicutes*, *Bacteroidetes*, and *Acidobacteria*. In general, the same phyla are present in high abundances on seafloor-exposed basalts and in the crustal fluids, suggesting the possibility for a common basalt-hosted microbial biome. However, more data is needed to establish if a core group also exist at deeper taxonomic levels. Within the crustal communities we find microbial representatives that are likely to be involved in iron, sulfur, hydrogen, and nitrogen cycling but all in relative low abundances. However, the activity levels might be considerably higher than what the relative abundance implies.

Our estimated cell abundances are on average 0.7×10^4 cells per gram of igneous rock, several orders of magnitude lower than what has been found on seafloor-exposed basalt (e.g., Einen et al., 2008; Santelli et al., 2008). The abundance is relatively consistent across all samples and we therefor speculate that the available

energy is equal across the different samples and/or cell numbers are limited by a common nutrient factor.

Further, the variations in community structure between the samples do, to a large extent, separate the two investigated sites (1382A and 1383C) into two major clusters with no apparent link to differences in lithology. Comparing the basalt-hosted community structure to the overlying sediment using the relative distribution of individual OTUs clearly separates the two environments. However, ∼1/3 of all OTUs in the basalt, representing an average of 80% of all sequences, were also present in the overlying sediment, indicating coupling between the two compartments of the deep biosphere. This observation is interesting with respect to the origin of the microorganisms inhabiting the crustal aquifer, however, deciphering the direction of cell dispersal, the source and the nature and underlying mechanisms of such links needs further investigation.

AUTHOR CONTRIBUTIONS

SJ designed the research; SJ and RZ performed the research; SJ and RZ analyzed the data; and SJ and RZ wrote the manuscript.

ACKNOWLEDGMENTS

This article is dedicated to the late Katrina Edwards. We thank the entire scientific party, especially the basaltic sampling crew and all crewmembers onboard Joides Resolution during IODP expedition 336, for their help and expertise. Co-chief scientists Katrina Edwards and Wolfgang Bach were instrumental in realizing this great undertaking, and are gratefully acknowledged. We thank Håkon Dahle for helping to develop the bioinformatic pipeline. The comments and suggestions from Gustavo Ramirez on the final version of this article are much appreciated. This study used samples and data provided by the IODP and was funded by the Norwegian Research Council through the Centre for Geobiology, University of Bergen.

SUPPLEMENTARY MATERIAL

The Supplementary Material for this article can be found online at: http://journal.frontiersin.org/article/10.3389/fmicb.2016.00820

REFERENCES

Baælum, J., and Jacobsen, C. S. (2010). *Pre-treating DNA/RNA Adsorbing Matrix Sample for Extracting Cell-derived Target DNA/RNA, by Isolating Sample of DNA/RNA Adsorbing Matrix and Contacting Sample with DNA of Natural Origin in Fragmented Form*. Patent No. WO2010146026-A1, US2012094353-A1, EP2443251-A1.

Bach, W. (2012). *Borehole Microbial Observatory Science in Basaltic Ocean Crust: The North Pond Area on the Western Mid-Atlantic Ridge Flank at 23° N*. Cruise Report MSM20/5, DFG Senatskommission für Ozeanographie, Freeport. doi: 10.2312/cr_msm20_5

Bach, W., and Edwards, K. J. (2003). Iron and sulfide oxidation within the basaltic ocean crust: implications for chemolithoautotrophic microbial biomass production. *Geochim. Cosmochim. Acta* 67, 3871–3887. doi: 10.1016/S0016-7037(03)00304-1

Bach, W., Garrido, C. J., Paulick, H., Harvey, J., and Rosner, M. (2004). Seawater-peridotite interactions: First insights from ODP Leg 209, MAR 15 degrees N. *Geochem. Geophys. Geosys.* 5:Q09F26. doi: 10.1029/2004gc000744

Bælum, J., Chambon, J. C., Scheutz, C., Binning, P. J., Laier, T., Bjerg, P. L., et al. (2013). A conceptual model linking functional gene expression and reductive dechlorination rates of chlorinated ethenes in clay rich groundwater sediment. *Water Res.* 47, 2467–2478. doi: 10.1016/j.watres.2013.02.016

Berry, D., Ben Mahfoudh, K., Wagner, M., and Loy, A. (2011). Barcoded primers used in multiplex amplicon pyrosequencing bias amplification. *Appl. Environ. Microbiol.* 77, 7846–7849. doi: 10.1128/AEM.05220-11

Champlot, S., Berthelot, C., Pruvost, M., Bennett, E. A., Grange, T., and Geigl, E.-M. (2010). An efficient multistrategy DNA decontamination procedure of PCR reagents for hypersensitive PCR applications. *PloS ONE* 5:e13042. doi: 10.1371/journal.pone.0013042

Edgar, R. C. (2013). UPARSE: highly accurate OTU sequences from microbial amplicon reads. *Nat. methods* 10, 996–998. doi: 10.1038/nmeth.2604

Edwards, K. J., Bach, W., and McCollom, T. M. (2005). Geomicrobiology in oceanography: microbe-mineral interactions at and below the seafloor. *Trends Microbiol.* 13, 449–456. doi: 10.1016/j.tim.2005.07.005

Edwards, K. J., Becker, K., and Colwell, F. (2012b). The deep, dark energy biosphere: intraterrestrial life on earth. *Annu. Rev. Earth Planet. Sci.* 40, 551–568. doi: 10.1146/annurev-earth-042711-105500

Edwards, K. J., Fisher, A. T., and Wheat, C. G. (2012a). The deep subsurface biosphere in igneous ocean crust: frontier habitats for microbiological exploration. *Front. Microbiol.* 3:8. doi: 10.3389/fmicb.2012.00008

Einen, J., Thorseth, I. H., and Ovreas, L. (2008). Enumeration of Archaea and Bacteria in seafloor basalt using real-time quantitative PCR and fluorescence microscopy. *FEMS Microbiol. Lett.* 282, 182–187. doi: 10.1111/j.1574-6968.2008.01119.x

Expedition 336 Scientists (2012a). "Site U1382," in *Proc IODP, 336,* eds K. J. Edwards, W. Bach, A. Klaus, and The Expedition 336 Scientists (Tokyo: Integrated Ocean Drilling Program Management International, Inc.).

Expedition 336 Scientists (2012b). "Site U1383," in *Proc IODP, 336,* eds K. J. Edwards, W. Bach, A. Klaus, and The Expedition 336 Scientists (Tokyo: Integrated Ocean Drilling Program Management International, Inc.).

Expedition 336 Scientists (2012c). "Methods," in *Proc IODP, 336,* eds K. J. Edwards, W. Bach, A. Klaus, and The Expedition 336 Scientists (Tokyo: Integrated Ocean Drilling Program Management International, Inc.).

Expedition 336 Scientists (2012d). "Sediment and basement contact coring," in *Proc IODP, 336,* eds K. J. Edwards, W. Bach, A. Klaus, and The Expedition 336 Scientists (Tokyo: Integrated Ocean Drilling Program Management International, Inc.).

Expedition 336 Scientists (2012e). "Expedition 336 summary", in *Proc IODP, 336,* eds K. J. Edwards, W. Bach, A. Klaus, and The Expedition 336 Scientists (Tokyo: Integrated Ocean Drilling Program Management International, Inc.).

Fisher, A. T., and Becker, K. (2000). Channelized fluid flow in oceanic crust reconciles heat-flow and permeability data. *Nature* 403, 71–74. doi: 10.1038/47463

Fisk, M. R., Giovannoni, S. J., and Thorseth, I. H. (1998). Alteration of oceanic volcanic glass: textural evidence of microbial activity. *Science* 281, 978–980. doi: 10.1126/science.281.5379.978

Fisk, M. R., Storrie-Lombardi, M. C., Douglas, S., Popa, R., McDonald, G., and Di Meo-Savoie, C. (2003). Evidence of biological activity in Hawaiian subsurface basalts. *Geochem. Geophys. Geosyst.* 4:1103. doi: 10.1029/2002gc000387

Furnes, H., Muehlenbachs, K., Torsvik, T., Thorseth, I. H., and Tumyr, O. (2001a). Microbial fractionation of carbon isotopes in altered basaltic glass from the Atlantic Ocean, Lau Basin and Costa Rica Rift. *Chem. Geol.* 173, 313–330. doi: 10.1016/S0009-2541(00)00285-0

Furnes, H., Staudigel, H., Thorseth, I. H., Torsvik, T., Muehlenbachs, K., and Tumyr, O. (2001b). Bioalteration of basaltic glass in the oceanic crust. *Geochem. Geophy. Geosy.* 2:1049. doi: 10.1029/2000gc000150

Giovannoni, S., Fisk, M., Mullins, T., and Furnes, H. (1996). Genetic evidence for endolithic microbial life colonizing basaltic glass/sea water interfaces. *Ocean Drill. Prog.* 148, 207–214. doi: 10.2973/odp.proc.sr.148.151.1996

Hammer, Ø., Harper, D., and Ryan, P. (2001). PAST: Paleontological statistics software package for education and data analysis. *Palaeontol. Electron.* 4, 9. Available online at: http://palaeo-electronica.org/2001_1/past/issue1_01.htm

Heberling, C., Lowell, R. P., Liu, L., and Fisk, M. R. (2010). Extent of the microbial biosphere in the oceanic crust. *Geochem. Geophys. Geosyst.* 11:Q08003. doi: 10.1029/2009gc002968

Hirayama, H., Abe, M., Miyazaki, J., Sakai, S., Nagano, Y., and Takai, K. (2015). "Data report: cultivation of microorganisms from basaltic rock and sediment cores from the North Pond on the western flank of the Mid-Atlantic Ridge, IODP Expedition 336," in *Proc IODP, 336,* eds K. J. Edwards, W. Bach, A. Klaus, and The Expedition 336 Scientists (Tokyo: Integrated Ocean Drilling Program Management International, Inc.).

Hjelmso, M. H., Hansen, L. H., Baelum, J., Feld, L., Holben, W. E., and Jacobsen, C. S. (2014). High-resolution melt analysis for rapid comparison of bacterial community compositions. *Appl. Environ. Microbiol.* 80, 3568–3575. doi: 10.1128/AEM.03923-13

Huber, J. A., Johnson, H. P., Butterfield, D. A., and Baross, J. A. (2006). Microbial life in ridge flank crustal fluids. *Environ. Microbiol.* 8, 88–99. doi: 10.1111/j.1462-2920.2005.00872.x

Hugenholtz, P., Pitulle, C., Hershberger, K. L., and Pace, N. R. (1998). Novel division level bacterial diversity in a Yellowstone hot spring. *J. Bacteriol.* 180, 366–376.

Jørgensen, S. L., Thorseth, I. H., Pedersen, R. B., Baumberger, T., and Schleper, C. (2013). Quantitative and phylogenetic study of the Deep Sea Archaeal Group in sediments of the Arctic mid-ocean spreading ridge. *Front. microbiol.* 4:229. doi: 10.3389/fmicb.2013.00299

Kruber, C., Thorseth, I. H., and Pedersen, R. B. (2008). Seafloor alteration of basaltic glass: textures, geochemistry, and endolithic microorganisms. *Geochem. Geophys. Geosyst.* 9:Q12002. doi: 10.1029/2008gc002119

Lanzen, A., Jorgensen, S. L., Huson, D. H., Gorfer, M., Grindhaug, S. H., Jonassen, I., et al. (2012). CREST–classification resources for environmental sequence tags. *PLoS ONE* 7:e49334. doi: 10.1371/journal.pone.0049334

Lee, M. D., Walworth, N. G., Sylvan, J. B., Edwards, K. J., and Orcutt, B. N. (2015). Microbial communities on seafloor basalts at Dorado Outcrop reflect level of alteration and highlight global lithic clades. *Front. Microbiol.* 6:1470. doi: 10.3389/fmicb.2015.01470

Lever, M. A., Alperin, M., Engelen, B., Inagaki, F., Nakagawa, S., Steinsbu, B. O., et al. (2006). Trends in basalt and sediment core contamination during IODP Expedition 301. *Geomicrobiol. J.* 23, 517–530. doi: 10.1080/01490450600897245

Lever, M. A., Rouxel, O., Alt, J. C., Shimizu, N., Ono, S., Coggon, R. M., et al. (2013). Evidence for microbial carbon and sulfur cycling in deeply buried ridge flank basalt. *Science* 339, 1305–1308. doi: 10.1126/science.1229240

Lusk, R. W. (2014). Diverse and widespread contamination evident in the unmapped depths of high throughput sequencing data. *PLoS ONE* 9:e110808. doi: 10.1371/journal.pone.0110808

Lysnes, K., Torsvik, T., Thorseth, I. H., and Pedersen, R. B. (2004). "Microbial populations in ocean floor basalt: results from ODP Leg 187," in *Proceedings of the Ocean Drilling Program, Scientific Results*, Vol. 187, eds R. B. Pedersen, D. M. Christie, and D. J. Miller (College Station, TX: Ocean Drilling Program), 1–27. doi: 10.2973/odp.proc.sr.187.203.2004

Mason, O. U., Nakagawa, T., Rosner, M., Van Nostrand, J. D., Zhou, J., Maruyama, A., et al. (2010). First investigation of the microbiology of the deepest layer of ocean crust. *PLoS ONE* 5:e15399. doi: 10.1371/journal.pone.0015399

Meyer, J. L., Jaekel, U., Tully, B. J., Glazer, B. T., Wheat, C. G., Lin, H.-T., et al. (2016). A distinct and active bacterial community in cold oxygenated fluids circulating beneath the western flank of the Mid-Atlantic ridge. *Sci. Rep.* 6:22541. doi: 10.1038/srep22541

Nigro, L. M., Harris, K., Orcutt, B. N., Hyde, A., Clayton-Luce, S., Becker, K., et al. (2012). Microbial communities at the borehole observatory on the Costa Rica Rift flank (Ocean Drilling Program Hole 896A). *Front. Microbiol.* 3:232. doi: 10.3389/fmicb.2012.00232

Orcutt, B. N., Bach, W., Becker, K., Fisher, A. T., Hentscher, M., Toner, B. M., et al. (2011). Colonization of subsurface microbial observatories deployed in young ocean crust. *ISME J.* 5, 692–703. doi: 10.1038/ismej.2010.157

Orcutt, B. N., and Edwards, K. J. (2014). "Life in the ocean crust: lessons from subseafloor laboratories," in *Earth and Life Processes Discovered from Subseafloor Environments: A Decade of Science Achieved by the Integrated Ocean Drilling Program (IODP),* Vol. 7, eds R. Stein, D. Blackman, K. F. Inagaki, and H.-C. Larsen (Amsterdam: Elsevier), 175–196.

Orcutt, B. N., Sylvan, J. B., Knab, N. J., and Edwards, K. J. (2011). Microbial ecology of the dark ocean above, at, and below the seafloor. *Microbiol. Mol. Biol. Rev.* 75, 361–422. doi: 10.1128/MMBR.00039-10

Orcutt, B. N., Sylvan, J. B., Rogers, D., Delaney, J., Lee, R. W., and Girguis, P. R. (2015). Carbon fixation by basalt-hosted microbial communities. *Front. Microbiol.* 6:904. doi: 10.3389/fmicb.2015.00904

Orcutt, B. N., Wheat, C. G., Rouxel, O., Hulme, S., Edwards, K. J., and Bach, W. (2013). Oxygen consumption rates in subseafloor basaltic crust derived from a reaction transport model. *Nat. Commun.* 4:2539. doi: 10.1038/ncomms3539

Sakata, K., Yabuta, H., Ikehara, M., and Kondo, T. (2015). "Data report: carbon content and isotopic composition of basalts and sediments in North Pond, Expedition 336," in *Proc IODP*, Vol. 336, eds K. J. Edwards, W. Bach, A. Klaus, and the Expedition 336 Scientists (Tokyo: Integrated Ocean Drilling Program Management International, Inc.), 1–8. doi: 10.2204/iodp.proc.336.203.2015

Salter, S. J., Cox, M. J., Turek, E. M., Calus, S. T., Cookson, W. O., Moffatt, M. F., et al. (2014). Reagent and laboratory contamination can critically impact sequence-based microbiome analyses. *BMC Biol.* 12:87. doi: 10.1186/s12915-014-0087-z

Santelli, C. M., Banerjee, N., Bach, W., and Edwards, K. J. (2010). Tapping the subsurface ocean crust biosphere: low biomass and drilling-related contamination calls for improved quality controls. *Geomicrobiol. J.* 27, 158–169. doi: 10.1080/01490450903456780

Santelli, C. M., Orcutt, B. N., Banning, E., Bach, W., Moyer, C. L., Sogin, M. L., et al. (2008). Abundance and diversity of microbial life in ocean crust. *Nature* 453, U653–U657. doi: 10.1038/nature06899

Schrenk, M. O., Huber, J. A., and Edwards, K. J. (2010). Microbial provinces in the subseafloor. *Annu. Rev. Mar. Sci.* 2, 279–304. doi: 10.1146/annurev-marine-120308-081000

Spang, A., Saw, J. H., Jorgensen, S. L., Zaremba-Niedzwiedzka, K., Martijn, J., Lind, A. E., et al. (2015). Complex archaea that bridge the gap between prokaryotes and eukaryotes. *Nature* 521, 173–179. doi: 10.1038/nature14447

Stoddard, S. F., Smith, B. J., Hein, R., Roller, B. R. K., and Schmidt, T. M. (2015). rrnDB: improved tools for interpreting rRNA gene abundance in bacteria and archaea and a new foundation for future development. *Nucleic Acids Res.* 43, D593–D598. doi: 10.1093/nar/gku1201

Storrie-Lombardi, M. C., and Fisk, M. R. (2004). Elemental abundance distributions in suboceanic basalt glass: evidence of biogenic alteration. *Geochem. Geophys. Geosys.* 5:Q10005. doi: 10.1029/2004gc000755

Thorseth, I. H., Pedersen, R. B., and Christie, D. M. (2003). Microbial alteration of 0-30-Ma seafloor and sub-seafloor basaltic glasses from the Australian Antarctic Discordance. *Earth Planet. Sci. Lett.* 215, 237–247. doi: 10.1016/S0012-821X(03)00427-8

Thorseth, I. H., Torsvik, T., Furnes, H., and Muehlenbachs, K. (1995). Microbes play an important role in the alteration of oceanic crust. *Chem. Geol.* 126, 137–146. doi: 10.1016/0009-2541(95)00114-8

Torsvik, T., Furnes, H., Muehlenbachs, K., Thorseth, I. H., and Tumyr, O. (1998). Evidence for microbial activity at the glass-alteration interface in oceanic basalts. *Earth Planet. Sci. Lett.* 162, 165–176. doi: 10.1016/S0012-821X(98)00164-2

Walsh, E. A., Kirkpatrick, J. B., Rutherford, S. D., Smith, D. C., Sogin, M., and D'Hondt, S. (2016). Bacterial diversity and community composition from seasurface to subseafloor. *ISME J.* 10, 979–989. doi: 10.1038/ismej.2015.175

Wheat, C. G., Jannasch, H. W., Kastner, M., Plant, J. N., and DeCarlo, E. H. (2003). Seawater transport and reaction in upper oceanic basaltic basement:

chemical data from continuous monitoring of sealed boreholes in a ridge flank environment. *Earth Planet. Sci. Lett.* 216, 549–564. doi: 10.1016/S0012-821X(03)00549-1

Conflict of Interest Statement: The authors declare that the research was conducted in the absence of any commercial or financial relationships that could be construed as a potential conflict of interest.

frontiers in Microbiology

ORIGINAL RESEARCH
published: 18 March 2016
doi: 10.3389/fmicb.2016.00363

Diversity and Metabolic Potentials of Subsurface Crustal Microorganisms from the Western Flank of the Mid-Atlantic Ridge

*Xinxu Zhang[1,2], Xiaoyuan Feng[1] and Fengping Wang[1,2]**

[1] State Key Laboratory of Microbial Metabolism, School of Life Sciences and Biotechnology, Shanghai Jiao Tong University, Shanghai, China, [2] State Key Laboratory of Ocean Engineering, School of Naval Architecture, Ocean and Civil Engineering, Shanghai Jiao Tong University, Shanghai, China

Deep-sea oceanic crust constitutes the largest region of the earth's surface. Accumulating evidence suggests that unique microbial communities are supported by iron cycling processes, particularly in the young (<10 million-year old), cool (<25°C) subsurface oceanic crust. To test this hypothesis, we investigated the microbial abundance, diversity, and metabolic potentials in the sediment-buried crust from "North Pond" on western flank of the Mid-Atlantic Ridge. Three lithologic units along basement Hole U1383C were found, which typically hosted $\sim 10^4$ cells cm^{-3} of basaltic rock, with higher cell densities occurring between 115 and 145 m below seafloor. Similar bacterial community structures, which are dominated by Gammaproteobacterial and Sphingobacterial species closely related to iron oxidizers, were detected regardless of variations in sampling depth. The metabolic potentials of the crust microbiota were assayed by metagenomic analysis of two basalt enrichments which showed similar bacterial structure with the original sample. Genes coding for energy metabolism involved in hydrocarbon degradation, dissimilatory nitrate reduction to ammonium, denitrification and hydrogen oxidation were identified. Compared with other marine environments, the metagenomes from the basalt-hosted environments were enriched in pathways for Fe^{3+} uptake, siderophore synthesis and uptake, and Fe transport, suggesting that iron metabolism is an important energy production and conservation mechanism in this system. Overall, we provide evidence that the North Pond crustal biosphere is dominated by unique bacterial groups with the potential for iron-related biogeochemical cycles.

Keywords: comparative metagenomics, deep biosphere, geomicrobiology, iron metabolism, oceanic crust

OPEN ACCESS

Edited by:
Jason B. Sylvan, Texas A&M University, USA

Reviewed by:
Jens Kallmeyer, Helmholtz Zentrum Potsdam – Deutsches GeoForschungsZentrum, Germany
Julie L. Meyer, University of Florida, USA

****Correspondence:***
Fengping Wang
fengpingw@sjtu.edu.cn

Specialty section:
This article was submitted to Extreme Microbiology, a section of the journal Frontiers in Microbiology

Received: *08 August 2015*
Accepted: *07 March 2016*
Published: *18 March 2016*

Citation:
Zhang X, Feng X and Wang F (2016) Diversity and Metabolic Potentials of Subsurface Crustal Microorganisms from the Western Flank of the Mid-Atlantic Ridge. Front. Microbiol. 7:363. doi: 10.3389/fmicb.2016.00363

INTRODUCTION

Oceanic crust microbiology has long been ignored and is not well studied due to technical constraints; however, the crust has been assumed to harbor active microorganisms that may significantly contribute to global biogeochemical cycles and weathering of the seafloor landscape (Schrenk et al., 2010; Wang et al., 2013). Several lines of evidence have revealed the presence of microorganisms in this dark, oligotrophic biosphere (Fisk et al., 1998; Cowen et al., 2003; Santelli et al., 2008; Lever et al., 2013); however, some fundamental questions remain, including (1) how

much microbial biomass is present in the oceanic crust, (2) where do the microorganisms originate, and (3) what are their metabolic functions.

The recent Integrated Ocean Drilling Program (IODP) expeditions dedicated to microbiology (Expedition 327 Scientists, 2010; Expedition 329 Scientists, 2011; Expedition 330 Scientists, 2011; Expedition 336 Scientists, 2012b) support the investigation of the basalt-hosted oceanic crust and the collection of uncontaminated samples for microscopic and molecular analysis. Previous studies attempted to count cells from seafloor-exposed basalts (Einen et al., 2008; Santelli et al., 2008; Jacobson Meyers et al., 2014), subsurface gabbros (Mason et al., 2010) and crustal fluids (Jungbluth et al., 2013). The results showed that cell densities in the seafloor-exposed crust were between 10^6 and 10^9 cells cm^{-3}, while those in the subsurface had lower cell densities ($<10^5$ cell cm^{-3}). Diverse microbial communities from crustal environments have been detected by culture-dependent and -independent techniques spanning a large range of bacterial phyla. For example, Deltaproteobacteria, Firmicutes, Gammaproteobacteria, and Bacteroidetes are present in the flanks of the Juan de Fuca Ridge (JdFR) and the Costa Rica Rift (Nigro et al., 2012; Jungbluth et al., 2013, 2014). Seafloor basaltic glass from the East Pacific Rise (Santelli et al., 2008, 2009) and the Arctic spreading ridges (Lysnes et al., 2004), altered basalts from the Hawaiian Loihi Seamount (Templeton et al., 2005; Santelli et al., 2008; Jacobson Meyers et al., 2014) and the Mid-Atlantic Ridge (Rathsack et al., 2009; Mason et al., 2010) are dominated by Gammaproteobacteria and Alphaproteobacteria. Extracellular enzyme activity tests, functional gene analysis, carbon and sulfur isotopic signatures and laboratory incubations demonstrated the presence of active microorganisms involved in methane- and sulfur-cycling and organic matter transformations (Mason et al., 2010; Lever et al., 2013; Jacobson Meyers et al., 2014; Robador et al., 2015; Supplementary Table S1). However, these studies were restricted to seafloor-exposed basaltic habitats (Templeton et al., 2005; Einen et al., 2008; Santelli et al., 2008), subsurface crustal environments with high temperature basalts (Nigro et al., 2012; Jungbluth et al., 2013), and mantle-type rock (Brazelton et al., 2010; Mason et al., 2010). The microbial life of the young, cool subsurface basalts in ridge flank systems, which represent a more common hydrologically active type of ocean crust (Edwards et al., 2012), has not been characterized yet.

Integrated Ocean Drilling Program Expedition 336 drilled the basaltic basement at "North Pond" (NP), which is located on the western flank of the Mid-Atlantic Ridge (Expedition 336 Scientists, 2012b). Numerous hydrological, geological, and geochemical data have been collected at this site from previous ocean drilling (Becker et al., 2001) and site surveys (Langseth et al., 1992; Picard and Ferdelman, 2011; Ziebis et al., 2012). The data indicated that this area was characterized by vigorous, oxic seawater circulation within the young basaltic crust under a <300 m sedimentary pile (Expedition 336 Scientists, 2012b; Ziebis et al., 2012). NP was thus suggested as a model system for studying subsurface basalt-hosted microorganisms (Bach and Edwards, 2003; Edwards et al., 2012). Modeling approaches suggested the presence of significant biotic oxygen consumption in the upper oceanic crust (Orcutt et al., 2013b). Collectively, the few explorations of the NP crustal biosphere suggested the existence of a unique subsurface biosphere in this system, probably supported by energy produced through iron cycling processes (Thorseth et al., 2001; Bach and Edwards, 2003; Edwards et al., 2012; Scott et al., 2015). To test these assumptions, we analyzed the microbial abundance, diversity and metagenomic properties of basalts collected from basement Hole U1383C with a penetration depth of 324 m below seafloor (mbsf). This is the first study of the vertical distribution of microbial communities in the cool, oxic subsurface oceanic crust, and it provides direct evidence to support the hypothesis that the NP crust hosts a unique biosphere with iron metabolizing potential.

MATERIALS AND METHODS

Sample Collection and Incubation

Basaltic basement samples were collected from North Pond on the western flank of the Mid-Atlantic Ridge during IODP Expedition 336 (Supplementary Figure S1). The methods for collecting and processing the samples, including quality and contamination assessments, are detailed in the Supplementary Material and elsewhere (Expedition 336 Scientists, 2012a). Briefly, samples were checked for the presence of fluorescent microspheres used during coring according to the protocol of Smith et al. (2000), and a drilling mud sample was collected to assess the possibility of contamination from drilling. Only interior pieces of rock were selected for microbiological study to avoid potential drilling mud contamination as recommended elsewhere (Expedition 330 Scientists, 2012; Lever et al., 2013). Samples used for cell enumeration were fixed with paraformaldehyde directly on shipboard. In total, 23 basalt samples that passed the contamination tests from Hole U1383C were used for cell enumeration, seven basalt samples were used for 16S rRNA gene sequencing, and one basalt sample was used for enrichment culturing. Properties of these samples, including porosity and P_2O_5 content of the basaltic rocks, are described in more detail elsewhere (Expedition 336 Scientists, 2012c) and the Supplementary Material.

A series of enrichments with the addition of a carbon substrate (sodium bicarbonate, sodium acetate or methane) and/or a nitrogen substrate (ammonium chloride or sodium nitrate) were set up to stimulate the growth of the microorganisms. Briefly, 2 cm^3 of each rock sample was mixed with 5 mL of 0.22 μm-mesh filtered seawater (collected on site at a water depth of ∼100 m) in a sterile 18 mm × 150 mm glass tube, and each substrate was added at a final concentration of 1.5–3 mM or 20% [vol/vol] headspace. The tube was capped with a butyl rubber stopper and an aluminum seal with filter-sterilized air in the headspace. After 6 months of incubation at 10°C in the dark, 2 mL of thoroughly mixed slurry, which contained suspended rock particles and seawater, was transferred and preserved in an equal volume of 1x phosphate buffered saline (PBS)/ethanol

at –20°C until analysis. A parallel incubation was conducted with a double autoclaved basalt sample and incubated in the same conditions as the sterile control. The latter control showed no amplification of bacterial/archaeal 16S rRNA genes and no microbial cells by epi-fluorescence microscopy, which indicated that in this study, 0.22-μm mesh was appropriate for seawater media sterilization, a result similar to those in previous reports (Meron et al., 2011; Zeng and Chisholm, 2012; Reveillaud et al., 2014).

Cell Enumeration

Cell enumeration was performed after cell extraction, which was conducted following a protocol of Kallmeyer et al. (2008) with a few modifications. Each reagent used before the cell enumeration steps was filter sterilized through a 0.22 μm-mesh membrane filter (Millipore, Billerica, MA, USA). The cell enumeration blank was performed without a sample and processed with the same steps as the basalt samples. Each sample was extracted and counted in triplicate. An average of 200 fields of view was counted for each membrane. The area of each field of view was set at 10,000 μm^2, and the detection limit was $\sim 10^3$ cells cm^{-3} for a 95% probability of detecting at least 1 cell as described by Kallmeyer et al. (2008). Details of the method are provided in the Supplementary Material.

DNA Extraction and 16S rRNA Gene Sequencing

DNA was extracted using a FastDNA^{TM} SPIN Kit for Soil (MP Biomedicals, Santa Ana, CA, USA) according to the manufacturer's instructions with a few modifications. Approximately 0.5 g of rock was ground into powder with a double flame-sterilized mortar and pestle. To the powder, 5 μg of clean, UV-irradiated poly-dIdC (Sigma–Aldrich, St. Louis, MO, USA) was added to increase the yield of DNA for low-biomass rock samples according to Barton et al. (2006). Three parallel extractions were performed for each sample, and the DNA extracts were pooled for subsequent PCR amplification. All procedures were performed in a laminar flow hood with 70% ethanol decontaminated pipettes, autoclaved filter pipette tips and UV-irradiated reagents. The V4 region of the bacterial 16S rRNA gene was amplified using the multi-tag primers 520F and 802R (Supplementary Table S2), and ∼240 bp amplicons were generated. The PCR program involved an initial denaturation step at 95°C for 10 min, followed by 30 cycles of denaturation at 95°C for 45 s, annealing at 55°C for 1 min, and extension at 72°C for 1 min, with a final extension at 72°C for 5 min. Three parallel PCR amplifications were performed for each sample and pooled for subsequent sequencing. The DNA blank extraction was performed without a sample and processed with the same DNA extraction and PCR amplification kits as the basalt samples. DNA extraction and PCR amplification were considered free of contamination if no target PCR band of approximately 240 bp was seen on an agarose gel for the blank DNA extraction and the PCR negative control.

The 16S rRNA gene amplicons containing unique 8-mer barcodes used for each sample were pooled at equal concentrations, and sequenced on an Illumina MiSeq platform using 2 × 250 bp cycles and the MiSeq Reagent Kit v2 (500 cycle, Illumina, USA) according to manufacturer's instructions. Raw reads were removed if they contained a 50 bp continuous fragment with an average quality score less than 30 and/or any ambiguities. Filtered reads were merged together using FLASH (Magoč and Salzberg, 2011; Version 1.2.6). Merged sequences were removed if they contained more than six identical bases occurred continuously and/or any ambiguities, or the sequence length was <200 bp. Clean sequences were demultiplexed using the QIIME software pipeline (Caporaso et al., 2010b; Version 1.9.0) with a mapping file containing the sample ID, barcode and primer sequence. Three sets of archaeal primers were tested using conditions described elsewhere (see Supplementary Table S2), but no positive PCR bands were observed.

Bacterial Community Composition and Phylogenetic Analysis

Sequences were aligned with PyNAST (Caporaso et al., 2010a; Version 1.2.2) and clustered into operational taxonomic units (OTUs) at 97% sequence similarity cutoff using usearch61 (Edgar, 2010) with default parameters in the QIIME software pipeline (Caporaso et al., 2010b; Version 1.9.0). OTUs were assigned to taxa based on the Greengenes database (DeSantis et al., 2006; Version gg_13_5). Chimeric sequences were detected with the UCHIME program (Edgar et al., 2011; Version 4.2) using default parameters, and they were removed from further analysis. Cluster analysis of the microbial community structure was performed in *R* based on a Bray–Curtis matrix using average linkage (R Core Team, 2015; Version 3.2.0). Phylogenetic trees were constructed in QIIME using the FastTree method, and the Shimodaira–Hasegawa test was used to estimate the reliability of each branch with 1000 resamples (Price et al., 2010; Version 2.1.3). Sequences covering the V4 region of the 16S rRNA gene from type species (downloaded from GenBank) and species from the crustal environments of the Mid-Atlantic Ridge (Rathsack et al., 2009; Mason et al., 2010), the JdFR (flanks; Mason et al., 2007, 2009; Orcutt et al., 2011a; Smith et al., 2011; Jungbluth et al., 2013, 2014), the Costa Rica Rift flank (Nigro et al., 2012), the East Pacific Rise (Mason et al., 2007; Santelli et al., 2008, 2009), the Hawaiian Seamounts (Templeton et al., 2005; Santelli et al., 2008; Edwards et al., 2011), and the Takuyo-Daigo Seamount (Nitahara et al., 2011) with sequence similarity to the North Pond sequences were included in the trees. FigTree[1] was used to modify the phylogenetic trees. In the phylogenetic trees, a representative sequence for each OTU (the most abundant one) is shown rather than all the sequences due to the high sequence number. For the Venn diagram, sequences were rarefied to an even depth (7952 reads; **Table 1**) by random sampling using QIIME. Sample 5R-1B and 20R-2C were excluded from the diagram due to (1) the limit of the Venn diagram presentation and (2) the similarity of their bacterial community compositions to those of 2R-2E and 6R-1A, respectively. The Venn diagram was created with a web

[1]http://tree.bio.ed.ac.uk/software/figtree/

TABLE 1 | Number of high quality bacterial 16S rRNA gene sequences used in this study.

Sample ID	Depth (mbsf)	Description†	Number of sequences	OTUs (97% cutoff)
2R-2E	72	Aphyric basalt, highly altered	7952	562
5R-1B	97	Aphyric basalt, moderately altered	10472	646
6R-1A	105	Aphyric basalt, slight alteration	9936	548
9R-2C	137	Phyric basalt, extensive alteration	9922	691
10R-1B	145	Phyric basalt, highly altered	10366	754
20R-2C	221	Aphyric basalt, extremely hard	16122	734
30R-1A	304	Aphyric basalt, fractured	16146	596
10R-1B-1	145	Bicarbonate + Ammonium	16283	714
10R-1B-2	145	Bicarbonate + Nitrate	20477	803

†*Described by Expedition 336 Scientists (2012c).*

tool provided by the Bioinformatics and Systems Biology of Gent[2].

To assess potential contaminating sequences from the reagent kits, a low-biomass contaminant database was constructed using sequences from Tanner et al. (1998), Kulakov et al. (2002), and Barton et al. (2006). All of the OTUs that were assigned to the same taxa with the contaminating sequences were used to construct phylogenetic trees using the same method as described above. A representative set of sequences for each OTU (the most abundant one) were used due to the high sequence number. If an OTU was closely related to sequences of the low-biomass contaminant database, it was further compared with the contaminating sequence using ClustalW Alignment (Thompson et al., 1994; Version ClustalW2) to give a sequence similarity value.

Metagenomic Sequencing and Analysis

Metagenomic sequencing of the original basalt from 145 mbsf (10R-1B) and its two enrichments (10R-1B-1, sodium bicarbonate + ammonium chloride; 10R-1B-2, sodium bicarbonate + sodium nitrate) which showed the best stimulation of cell growth were performed. To obtain sufficient amounts of DNA for sequencing, whole genome amplification of the total DNA was performed with REPLI-g Mini Kits (Qiagen, Hilden, Germany) following the manufacturer's protocol. Amplified DNA was further purified using QIAamp DNA Mini Kit (Qiagen, Hilden, Germany) according to the manufacturer's recommendations. The amplification was conducted in five separate reactions, and they were pooled for subsequent sequencing to reduce amplification biases. Parallel blank controls, including sampling, DNA extraction and amplification controls, were performed with 0.22 μm-mesh membrane filtered Milli-Q water (18.2 MΩ; Millipore, Billerica, MA, USA). Sequencing was performed on HiSeq 2000 platform (Illumina, San Diego, CA, USA) using 2 × 100 bp pair-end technology. Due to the challenging nature of sample retrieval and DNA recovery, replication of the metagenomes was not possible. Raw reads that passed the quality control were assembled into contigs by SOAPdenovo2 (Luo et al., 2012; Version 2.0.4). Gene prediction, annotation, and taxonomic assignments were performed as described previously (He et al., 2013b; Wang et al., 2014). Statistical significance between samples was analyzed by SPSS 13.0 software using the Mann–Whitney *U* test.

Comparing the Relative Abundances of Iron-Related Pathways

Metagenomes were subject to tBLASTn (Altschul et al., 1990) searches against an iron uptake and transport-related gene database, which was collected from Hopkinson and Barbeau (2012) and Toulza et al. (2012). Matched genes, with a maximum *e*-value of 10^{-5} and minimum identity of 30%, were assigned to specific pathways. The abundance of each pathway is the total count of hits that matched the database, except for the NP and JdFR flank fluid metagenomes, which were adjusted by using the average read depth of the corresponding contig as described elsewhere (He et al., 2013a). The relative abundance of each iron-related pathway among the metagenomes was normalized by estimating the number of sequenced genome equivalents with a set of 30 essential single-copy genes (Nayfach and Pollard, 2015; MicrobeCensus Version 1.0.4). The statistical significance between samples was analyzed by SPSS 13.0 software using the Mann–Whitney *U* test.

Accession Number

All sequence data have been deposited in the National Center for Biotechnology Information (NCBI) Sequence Read Archive under the accession number SRP042264.

RESULTS

Microbial Abundance

In general, the microbial abundances in the basalts at basement Hole U1383C were between $<1.0 \times 10^3$ and 6.1×10^4 cells cm^{-3} (**Figure 1**). The highest densities of microorganisms in the basalt occurred between 115 and 145 mbsf, and the biomass was distributed heterogeneously above or below detection at the other depths, with those above detection being $\sim 1–3 \times 10^4$ cells cm^{-3}. Samples from the top and the bottom sections gave similar, low values (for example 72 mbsf and 324 mbsf, 1.2×10^4 – 1.4×10^4 cells cm^{-3}, respectively), although some samples were near or below the detection limit ($\sim 10^3$ cells cm^{-3}).

[2]http://bioinformatics.psb.ugent.be/webtools/Venn/

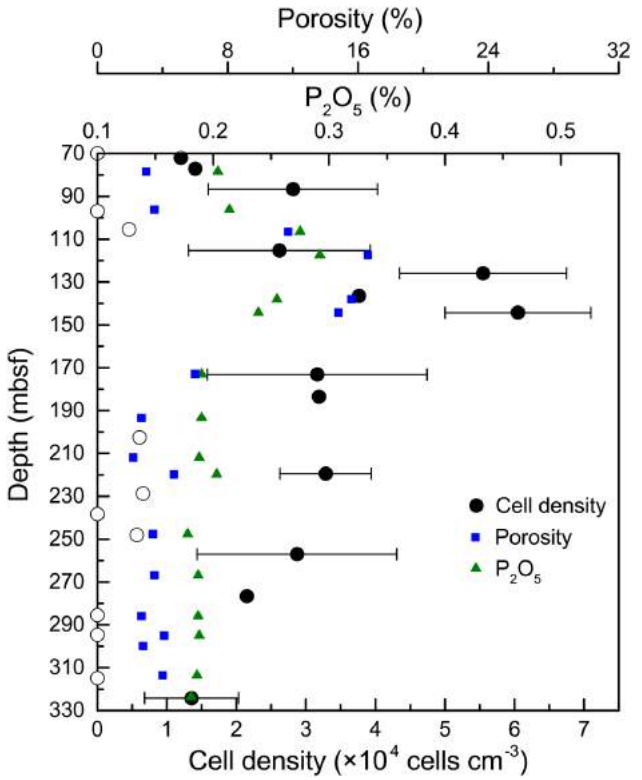

FIGURE 1 | Microbial abundance in basalt samples from Hole U1383C. The cell counting data are averages of three determinations. The error bars indicate the standard deviations of the cell counts. Open circles indicate suspicious values near or below the detection limit (~10^3 cells cm^{-3}). Porosity and P_2O_5 content of the basalts are from Expedition 336 Scientists (2012c).

Microbial Community Structure

Seven basalt samples from 72 to 304 mbsf were used for microbial community structure characterization (**Table 1**). Across all the basalt samples, no archaeal 16S rRNA gene bands were amplified using different archaeal primer sets (see the section "Materials and Methods"). This indicated a low abundance of archaea, if present, which was consistent with previous studies in other oceanic crust environments (Einen et al., 2008; Santelli et al., 2008; Mason et al., 2010). The number of high quality bacterial 16S rRNA gene sequences obtained by high-throughput sequencing were between 7,952 and 16,146, resulting in more than 548 OTUs at 97% SSU rRNA gene sequence similarity. Alpha-diversity analysis showed that the rarefaction curves for all of the samples did not plateau at this sequencing depth (Supplementary Figure S2A), but the Shannon Diversity indices were stable (Supplementary Figure S2B). This indicated that major bacterial communities had largely been covered, although rare new phylotypes could still appear upon further sequencing.

To assess the potential contamination of rocks from the drilling mud during sampling (Lever et al., 2006) and the potential contaminating sequences from commercial kits used for DNA extraction (Salter et al., 2014), we conducted a comparative taxonomic/phylogenetic analysis of the 16S rRNA gene sequences from this study and those from the procedural controls (see the section "Materials and Methods" for more details). First, no sequences of common surface seawater bacteria (e.g., Cyanobacteria) were recovered in the sequence library, indicating that surface seawater derived drilling fluids did not contaminate the rocks. Second, comparative taxonomic analysis of the sequences from this study with those from the drilling mud sample revealed a distinct separation of rock-hosted microorganisms from drilling mud influence (J. Meyer, J. Huber, personal communication). Third, a comparison of the phylogenetic analysis of the sequence library with a known low-biomass contaminant database (Tanner et al., 1998; Kulakov et al., 2002; Barton et al., 2006) was conducted. As suggested by Barton et al. (2006), any sequences that demonstrated >98% sequence similarities to the contaminant database were flagged as possible contaminants. Six OTUs (representing <11.8% of the total quality-screened sequences) were identified as having 98% or greater sequence similarity to known contaminating sequences, including those from *Acinetobacter*, *Bradyrhizobium*, *Curvibacter*, *Ralstonia*, *Sphingomonas*, and *Stenotrophomonas* (Supplementary Figure S3; Supplementary Table S3). However, cultures from the genera *Ralstonia*, *Sphingomonas*, and *Comamonas* (*Acidovorax*) have recently been reported from basalts collected from this same expedition (Hirayama et al., 2015), and their 16S rRNA genes showed high sequence similarity with those from this study, indicating that removal of these flagged sequences from the library may not be warranted. Thus, sequences identified as possible sequence contaminants are retained in the library but are highlighted in the overall description of the community structure.

In general, Gammaproteobacteria dominated the bacterial community, ranging from 54.9 to 69.3% at different depth intervals (**Figure 2A**). The greatest abundance of Gammaproteobacteria occurred at 137 mbsf, whereas samples from the top and bottom sections gave similar but lower values. The second most abundant group was Sphingobacteria, showing a relative abundance between 21.8 and 30.0%. Alphaproteobacteria and Cytophagia were generally less than 10% in relative abundance. Other groups with >0.5% relative abundance were Betaproteobacteria, Flavobacteria, Fimbriimonadia, and Deltaproteobacteria. As the microbial biomass in the rocks was low (**Figure 1**), it was not yet clear if and how much the PCR primers preference, and the number of 16S rRNA gene copies in different microbial cells may influence the 16S rRNA gene abundance in the samples (Vetrovsky and Baldrian, 2013). Therefore, we did not tend to compare the differences in the percentages of bacterial 16S rRNA gene sequences in different samples, as the abundance of the bacterial groups were likely under- or overrepresented through the present PCR sequencing methods. We then listed the microbial groups with >1% abundance as major groups in the samples. The microbial community structures shared much in common at different depth intervals, as shown by a Venn diagram (**Figure 2B**). The overlapping groups covered more than 99.8% of the total bacterial community within each sample (Supplementary Table S4). At the genus level, the major groups in the basalts included *Marinobacter*,

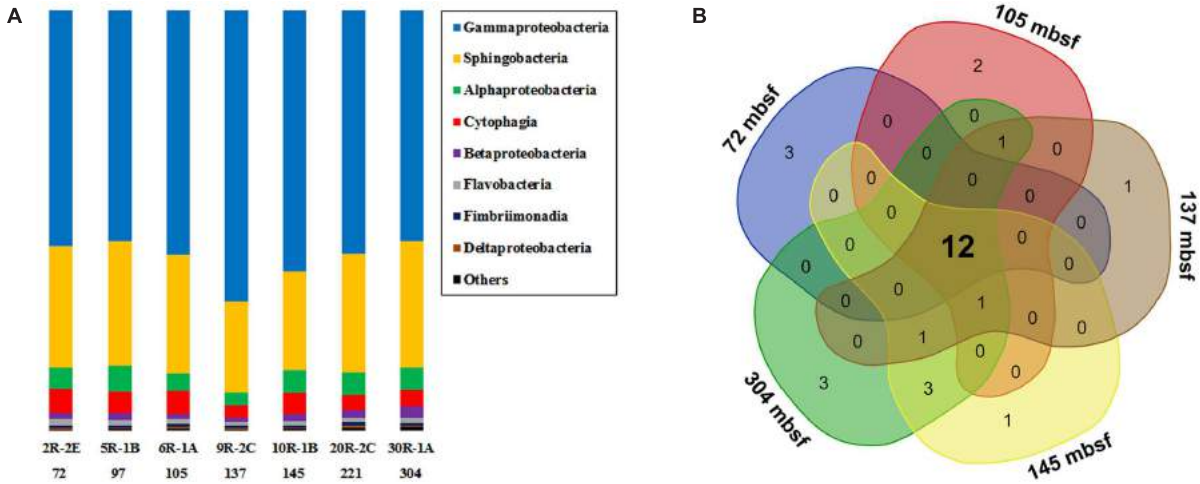

FIGURE 2 | (A) The bacterial community composition of basalt samples (at class level). Colored bars indicate the percentage of the designated group within each sample. Only those with >0.5% class abundance are listed. The remaining sequences are grouped to "Others." The number indicates sample depth, mbsf. **(B)** A Venn diagram showing the distribution of shared bacterial groups (at class level) in samples from 72, 105, 137, 145, and 304 mbsf.

Sediminibacterium, *Comamonas*, *Marivirga*, *Alcanivorax*, *Alteromonas*, *Pseudomonas*, *Methylophaga*, *Oleibacter*, and *Halomonas* (Supplementary Figure S4). The overlapping groups at the genus level covered ∼99% of the total sequences within each sample, regardless of the sample types and depths. Cluster analysis revealed that the samples from 72, 97, 105, and 221 mbsf grouped together based on a Bray–Curtis matrix. Samples from 145 and 304 mbsf formed monophyletic lineages separately, and they were adjacent to the sample from 221 mbsf. The basalt at 137 mbsf formed a distant lineage; however, the community structure was similar to those of other samples, showing a maximum dissimilarity of 0.18 with the sample at 304 mbsf (Supplementary Figure S4).

Spearman's correlation analysis was performed to identify the distribution of specific crustal bacterial species that was affected by depth. Correlations between OTU abundance and depth were considered significant when $P < 0.05$ and $|R| > 0.6$. In general, 75 OTUs showed positive correlations with depth and 24 OTUs showed the opposite trend, covering a large species diversity within major groups (Supplementary Table S5).

Phylogeny

Phylogenetic analysis revealed a single cluster that was closely related to a cultured neutrophilic Fe-oxidizing bacterium isolated from weathering deposits of the JdFR axis (Edwards et al., 2003; designated *Marinobacter* Group IV; **Figure 3**). The most diverse subcluster within the genus *Marinobacter* was *Marinobacter* Group II in the Gammaproteobacteria. Sequences related to this group included an iron oxidizing bacterium isolated from 304 mbsf (30R-1A) of U1383C (GenBank accession number KJ914666; unpublished), and a manganese oxidizing bacterium from the basalts of the Hawaiian Loihi Seamount (Templeton et al., 2005). *Marinobacter* Group III is characterized as a common lineage in marine basaltic habitats, including the JdFR flanks, the Mid-Atlantic Ridge and the Hawaiian Loihi Seamount. Some cultured strains of this group have been demonstrated to oxidize iron under neutrophilic conditions (Smith et al., 2011). One of these strains was also a known hydrocarbon degrader (Huu et al., 1999). Seven OTUs from Group I of *Marinobacter* formed a monophyletic lineage that was distinct from any cultured *Marinobacter* species, with the best BLAST hit (identity < 97%) to a recently identified *Marinobacter* species from the Sea of Japan (Ng et al., 2014). OTUs that were assigned to *Pseudomonas*, *Alcanivorax*, *Halomonas*, and *Alteromonas* were closely related to Fe/Mn oxidizers isolated from subsurface crustal fluids of the JdFR flank and/or seafloor basalts near Hawaii, and some of them also clustered with environmental gene clones from the Mid-Atlantic Ridge (Atlantis Massif) and/or the East Pacific Rise. In addition, OTUs that may participate in iron reduction and iron assimilation were detected and showed close relationships to known iron reducers, including *Alteromonas* (Lovley et al., 1989), *Shewanella* (Wu et al., 2013), and siderophore producing *Pseudomonas* (Paulsen et al., 2005). A single OTU related to *Methylophaga* was unique to NP basalts and indicated the potential to use one-carbon compounds (Villeneuve et al., 2013).

Some Alphaproteobacterial OTUs from *Roseovarius* and *Sulfitobacter* clustered with Mn oxidizers recovered from the Loihi Seamount and South Point near Hawaii (**Figure 4**), although they were generally present in low relative abundance (<1%). The *Bacteriovorax*-related sequences were the only identified Deltaproteobacterial OTU, and they shared 100% sequence similarity with *Bacteriovorax marinus*, a marine bacterium that preys upon Gram-negative bacteria (Baer et al., 2004).

Sequences that were assigned to *Sediminibacterium* were closely related to environmental clones recovered from crustal fluids of the JdFR flank and an enrichment clone from iron pipes of a water distribution system (Wang et al., 2012) (**Figure 5**). Other abundant OTUs were generally related to

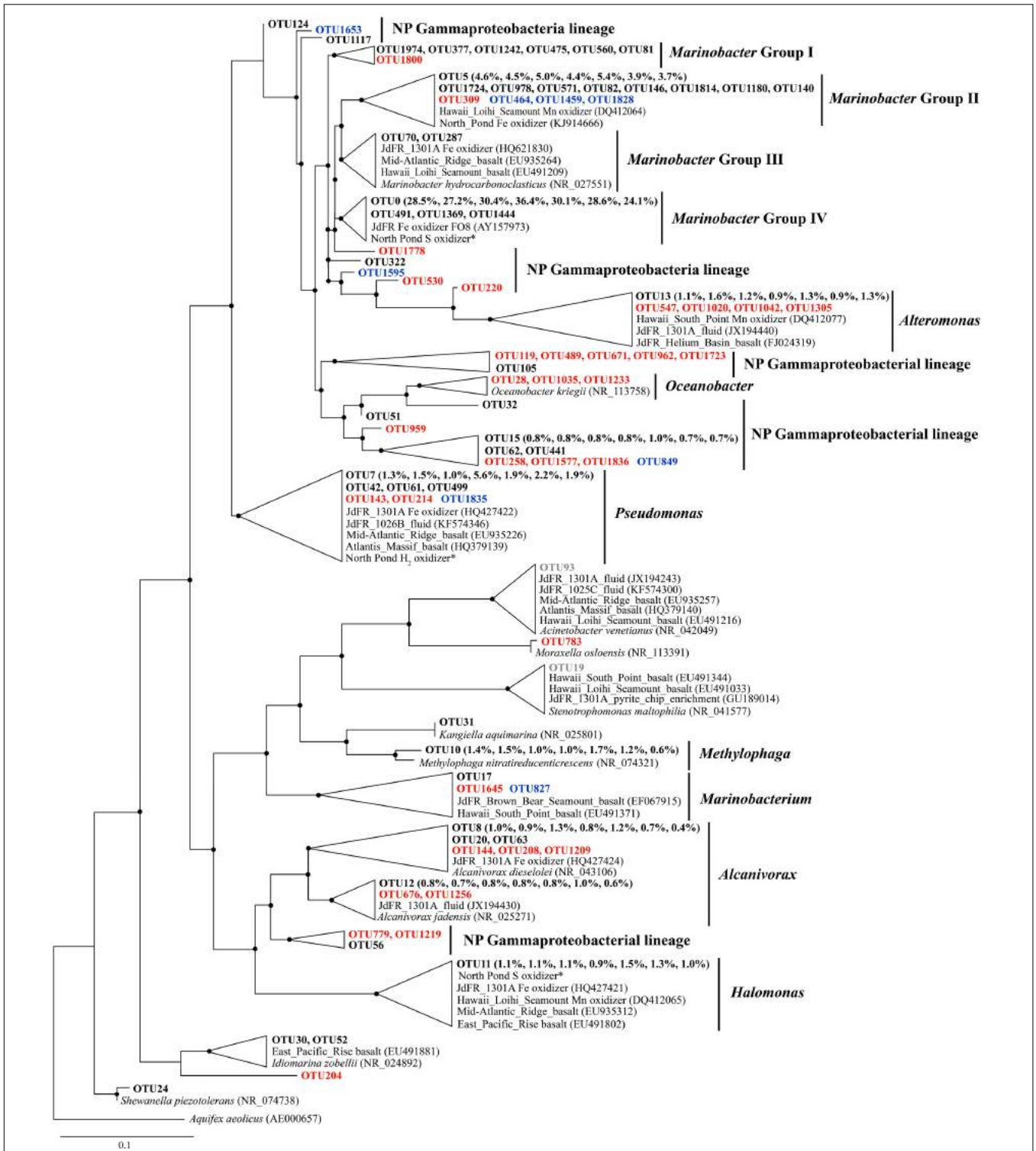

FIGURE 3 | The Phylogenetic tree of Gammaproteobacterial-related OTUs from seven basalt samples. Sequences recovered in this study are highlighted in bold font. The numbers in parentheses indicate percentage of the designated reads clustered in 97% cutoff OTUs in the order 72, 97, 105, 137, 145, 221, and 304 mbsf. Sequences in red are positively correlated with depth, those in blue are negatively correlated with depth, and those in gray are potential contaminants. * indicates sequences from Hirayama et al. (2015). Only those with >70 local support values are shown as filled circles at each branch. Only those with >0.1% OTU abundance within each sample and a representative sequence for each OTU (the most abundant one) are used due to the large number of sequences. The 16S rRNA gene of *Aquifex aeolicus* (AE000657) is used as the outgroup. The scale bar indicates 0.1 nucleotide substitutions per site.

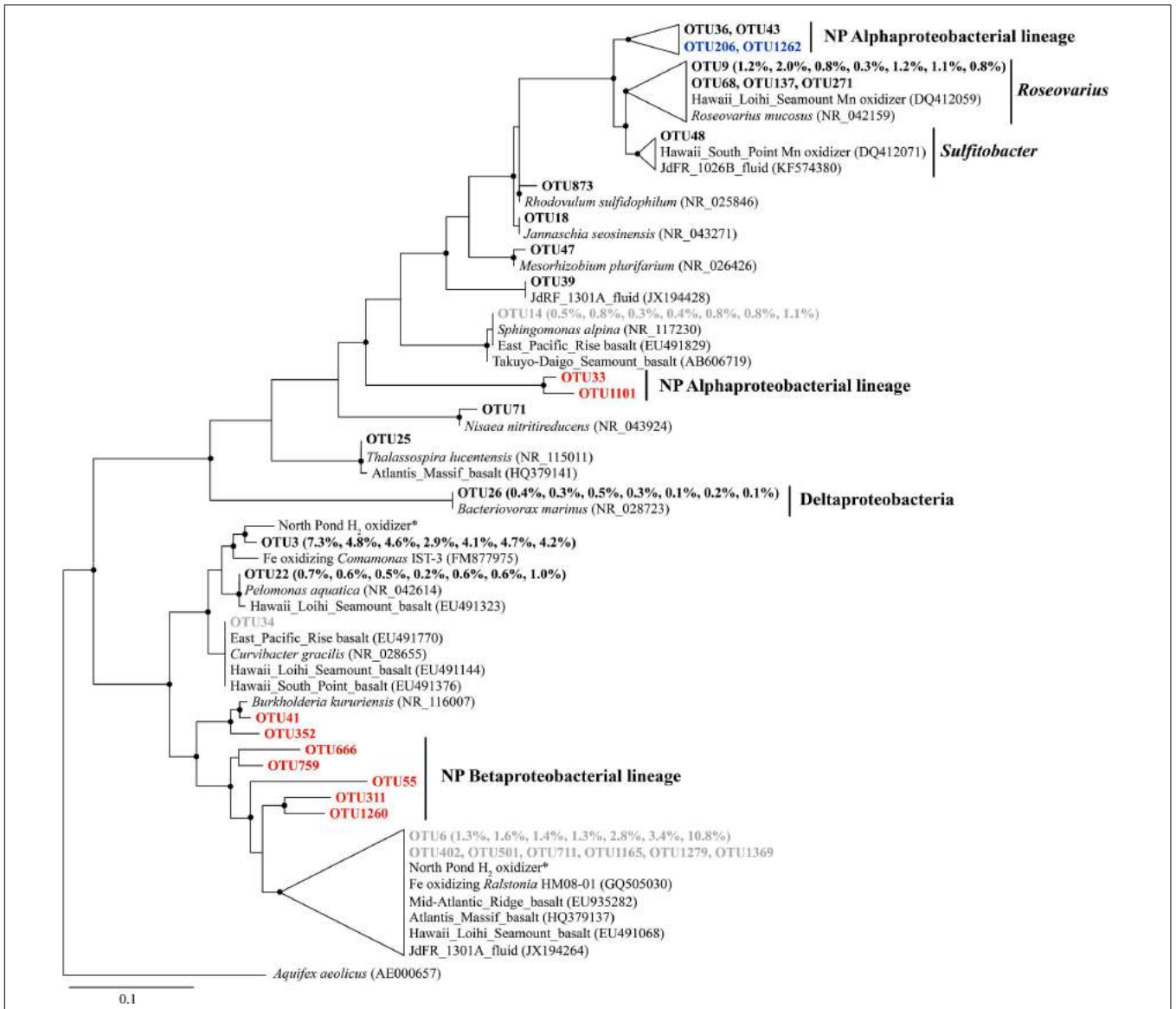

FIGURE 4 | The phylogenetic tree of Beta-, Alpha-, and Delta-proteobacterial-related OTUs from seven basalt samples. Sequences recovered in this study are highlighted in bold font. The numbers in parentheses indicate the percentage of the designated reads clustered in 97% cutoff OTUs in the order 72, 97, 105, 137, 145, 221, and 304 mbsf. Sequences in red are positively correlated with depth, those in blue are negatively correlated with depth, and those in gray are potential contaminants. * indicates sequences from Hirayama et al. (2015). Only those with >70 local support values are shown as filled circles at each branch. Only those with >0.1% OTU abundance within each sample and a representative sequence for each OTU (the most abundant one) are used due to the large number of sequences. The 16S rRNA gene of *Aquifex aeolicus* (AE000657) is used as the outgroup. The scale bar indicates 0.1 nucleotide substitutions per site.

aerobic heterotrophs, including *Marivirga* and *Ekhidna*, which were isolated from marine environments and characterized by gliding motility (Lewin and Lounsbery, 1969; Alain et al., 2010).

Metabolic Potential

Metagenomic sequencing of the original basalt from 145 mbsf (10R-1B) and its two enrichments were performed as described in the Section "Materials and Methods." Unfortunately, the assembly of the original basalt sample resulted in only ~1 Mbp, and, although multiple assembly software applications were tested [including SOAPdenovo2 (Luo et al., 2012; Version 2.0.4), Velvet (Zerbino and Birney, 2008; Version 1.2.09), ABySS (Simpson et al., 2009; Version 1.5.1), and SPAdes (Bankevich et al., 2012; Version 3.5.0)], it had to be excluded from further analysis. In general, more than 99.3% of the total number of sequences were assigned to bacteria [rules for taxonomic assignment were detailed by He et al. (2013b)]. The archaeal sequences were present at less than 0.2% in the two metagenomes (Supplementary Table S6), which was consistent with previous results. The taxonomic composition of these two basalt enrichments based on 16S rRNA gene amplification revealed that they shared much similarity with those in the

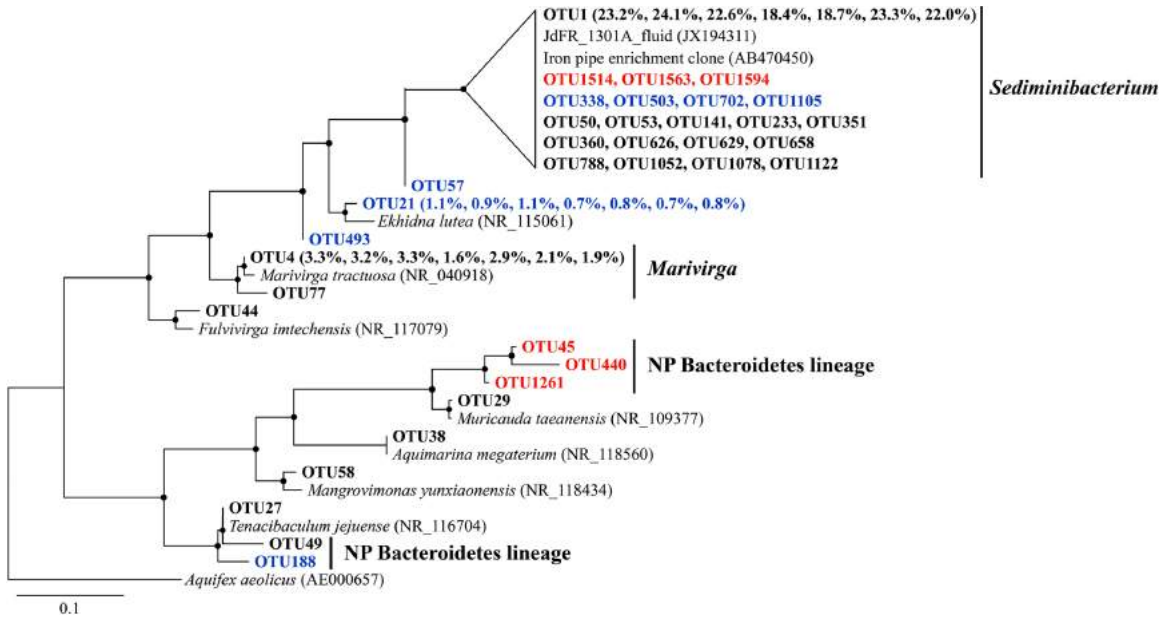

FIGURE 5 | The phylogenetic tree of Bacteroidetes-related OTUs from seven basalt samples. Sequences recovered in this study are highlighted in bold font. The numbers in parentheses indicate the percentage of the designated reads clustered in 97% cutoff OTUs in the order 72, 97, 105, 137, 145, 221, and 304 mbsf. Sequences in red are positively correlated with depth, those in blue are negatively correlated with depth. Only those with >70 local support values are shown as filled circles at each branch. Only those with >0.1% OTU abundance within each sample, and a representative sequence for each OTU (the most abundant one) is used due to the large number of sequences. The 16S rRNA gene of *Aquifex aeolicus* (AE000657) is used as the outgroup. The scale bar indicates 0.1 nucleotide substitutions per site.

original rock (Supplementary Figure S4). Integrated study of these two metagenomes may shed some light on the potential functions of the indigenous microbiome in the basalt, although they were not representative of the *in situ* environment.

The proteins predicted from the metagenomes of the NP basalt enrichments were classified into functional gene categories based on the Subsystems database (Overbeek et al., 2005). Hierarchical clustering was conducted by comparing metagenomes from diverse environments, including two subsurface crustal fluids from the JdFR flanks (GOLD ID: Gs0090290; Reddy et al., 2015), a carbonate chimney from the Lost City (Brazelton and Baross, 2009), a sulfide chimney from the JdFR (Xie et al., 2011), an oil-immersed chimney from the Guaymas Basin (He et al., 2013b), an iron oxide mat from the Loihi Seamount (Singer et al., 2013), three water samples from the Sargasso Sea (MG-RAST ID: 4539502.3, 4539504.3, 4539507.3; Meyer et al., 2008), two subseafloor sediments from the Peru Margin (Biddle et al., 2008) and two pyrite sediments from California acid mine drainage (Tyson et al., 2004; Lo et al., 2007).

The metagenomes of the NP basalt enrichments clustered closely with samples from the subsurface crustal fluids of the JdFR flanks, the iron mat from the Loihi Seamount and the Lost City carbonate chimney (Supplementary Figure S5). When we considered those samples as Group 1 and the rest of the samples as Group 2, Group 1 was significantly enriched in functional categories, including flagellar motility, fatty acids, branch-chain amino acids, siderophores ($P < 0.05$), and it was depleted in ATP synthases, quorum sensing, and biofilm formation ($P < 0.05$). Variability in these functional categories appeared to drive this clustering. In addition, the two metagenomes from the NP basalts were enriched in functional categories, including resistance to antibiotics and toxic compounds, fermentation, peripheral pathways for catabolism of aromatic compounds, phospholipids, osmotic stress and tricarboxylate transporter ($P < 0.05$) compared with the rest of the metagenomes. The metagenomes of two subsurface pyrite sediments from California acid mine drainage were adjacent to NP enrichments, indicating their microbial functional similarity with basalt-hosted environments.

To determine the metabolic potentials of the microorganisms in NP basalts involved in carbon, nitrogen, hydrogen, and iron processes, key genes were searched in the assembled contigs. Genes, including those coding for alkane monooxygenase, cytochrome P450, flavin-binding monooxygenase and catechol-2,3-dioxygenase were identified (**Table 2**), suggesting that the microorganisms could degrade hydrocarbons. Carbon fixation via the reductive TCA cycle and the reductive acetyl-CoA cycle (Hugler and Sievert, 2011) were identified but were incomplete; however, key genes, including carbon monoxide dehydrogenase were present in both metagenomes. RuBisCO genes of the Calvin–Benson–Bassham cycle were not detected. In nitrogen metabolism, the complete pathways of dissimilatory nitrate reduction to ammonium (DNRA) and denitrification were both present in the two metagenomes (**Table 2**). However, genes for ammonia oxidation, anaerobic ammonium oxidation (Anammox) and nitrogen fixation

TABLE 2 | Key genes involved in carbon, nitrogen and hydrogen metabolism.

Pathway	Enzyme	Best hit Contig ID		Best Blastp hit organism	Similarity (%)
		10R1B-1	10R1B-2		
Dissimilatory nitrate reduction to ammonium	Nitrate reductase alpha subunit, NarG	NP-10R-1B-1_contig4398	NP-10R-1B-2_contig245	*Marinobacter manganoxydans* MnI7-9	99
	Nitrite reductase [NAD(P)H] large subunit, NirB	NP-10R-1B-1_contig29	NP-10R-1B-2_contig1171	*Marinobacter manganoxydans* MnI7-9	99
Denitrification	Nitrite reductase (NO-forming), NirK	NP-10R-1B-1_contig5784	NP-10R-1B-2_contig5271	*Alcanivorax dieselolei* B5	99
	Nitric oxide reductase subunit B, NorB	NP-10R-1B-1_contig2504	NP-10R-1B-2_contig240	*Marinobacter hydrocarbonoclasticus* ATCC 49840	95
	Nitrous oxide reductase, NosZ	NP-10R-1B-1_contig7092	NP-10R-1B-2_contig6914	*Marinobacter manganoxydans* MnI7-9	99
Nitrogen assimilation	Assimilatory nitrate reductase, NasA	NP-10R-1B-1_contig28	NP-10R-1B-2_contig1171	*Marinobacter manganoxydans* MnI7-9	99
	Glutamine synthetase, GlnA	NP-10R-1B-1_contig1716	NP-10R-1B-2_contig1000	*Marinobacter algicola* DG893	99
	Glutamate synthase alpha subunit, GltB	NP-10R-1B-1_contig3559	NP-10R-1B-2_contig709	*Marinobacter algicola* DG893	99
H_2 oxidation	[NiFe]-hydrogenase large subunit	NP-10R-1B-1_contig3091	ND	Gamma proteobacterium HIMB30	80
Hydrocarbon degradation	Alkane monooxygenase, AlkB	NP-10R-1B-1_contig7840	NP-10R-1B-2_contig151	*Marinobacter manganoxydans* MnI7-9	99
		NP-10R-1B-1_contig3498	NP-10R-1B-2_contig4917	*Alcanivorax dieselolei* B5	99
	Cytochrome P450	NP-10R-1B-1_contig1835	NP-10R-1B-2_contig1725	*Alcanivorax hongdengensis* A-11-3	95
		NP-10R-1B-1_contig10204	NP-10R-1B-2_contig1585	*Marinobacter manganoxydans* MnI7-9	99
	Flavin-binding monooxygenase, AlmA	NP-10R-1B-1_contig909	NP-10R-1B-2_contig4078	*Alcanivorax dieselolei* B5	99
	Catechol-2,3-dioxygenase	NP-10R-1B-1_contig7526	NP-10R-1B-2_contig859	*Marinobacter algicola* DG893	97

ND, not detected.

pathways were absent. Other genes in the assimilatory nitrate reduction (nitrate reductase, NasA) and ammonia assimilation pathways (glutamine synthetase and glutamate synthase) were identified. Three [NiFe]-hydrogenase genes were identified in the metagenome 10R1B-1 (**Table 2**), indicating that cells may gain energy by the oxidation of hydrogen gas (H_2).

In particular, a comparison of the relative gene abundances for cellular iron uptake and transport pathways within metagenomes from diverse marine environments and a subsurface pyrite-hosted acid mine drainage was conducted by using a database collected from Hopkinson and Barbeau (2012) and Toulza et al. (2012). The results showed that genes for Fe^{3+} uptake, siderophore synthesis and uptake, and unspecified Fe transport were significantly enriched in the basalt-hosted environments (Loihi Seamount and NP) and the deep-sea hydrothermal chimneys (JdFR, Guaymas Basin and Lost City), with p-values < 0.05 (Supplementary Figure S6). Cluster analysis further revealed that these samples grouped together (except for those from the Guaymas Basin) and were distinct from the metagenomes of the Peru margin sediments and Sargasso seawater. The subsurface crustal fluids of the JdFR flanks and the pyrite sediments of the California acid mine drainage formed a distant subcluster, which showed a relatively low abundance of iron-related genes. In total, genes involved in Fe^{3+} uptake were always the most abundant in NP basalts, whereas siderophore synthesis and uptake pathways prevailed in an iron oxide microbial mat from the Loihi Seamount.

DISCUSSION

Using microscopic cell enumeration and molecular techniques, we characterized the microbiota of subsurface basalts from the young, cool oceanic crust at NP. Our results demonstrate that the microbial abundances in the basalts are less than 6.1×10^4 cells cm^{-3}, with the microbial communities dominated by Gammaproteobacteria and Sphingobacteria (**Figures 1** and **2**). The microbial abundances of the NP basalts are similar to those of previous measurements of cell densities on subsurface basaltic environments (Fisk et al., 2003; Mason et al., 2010; Jungbluth et al., 2013), which are more than two orders of magnitude lower than those on seafloor-exposed basalts (Einen et al., 2008; Santelli et al., 2008; Jacobson Meyers et al., 2014). Higher cell densities are observed at 115–145 mbsf, indicating potential

correlations with *in situ* physical and geochemical characteristics as discussed below. The basalt bacterial community structures at different sampling depths are relatively uniform with numerous bacterial species closely related to cultured iron/manganese oxidizers and environmental clones from various oceanic crustal habitats. Moreover, we identified some bacterial lineages that appear to be localized in NP, indicating that a unique microbial biosphere is hosted in this system. Finally, we suggest that iron-related metabolisms are significant processes in basalt-hosted environments based on comparative metagenomics.

Distribution of Microbial Abundance and Composition

In contrast to previous studies (e.g., Santelli et al., 2008; Jungbluth et al., 2013), we provide a more detailed characterization of microbial life in the subsurface oceanic crust across a 254 m core. The distribution of microbial abundance in Hole U1383C did not follow the general trend observed in global subsurface marine sedimentary environments, where cell densities decrease logarithmically with increasing sediment depth (Kallmeyer et al., 2012). This trend in sediments was principally controlled by the availability of energy sources, including buried organic matter (D'Hondt et al., 2004; Lipp et al., 2008). Along the core analyzed in our study, higher cell densities were found at depths where higher contents of phosphorus oxide (P_2O_5) and porosity occurred in the rock (**Figure 1**). For example, the cell density at 145 mbsf was fivefold higher than in the top sample at 72 mbsf and the bottom sample at 324 mbsf; the content of P_2O_5 and the porosity of the basalt at this depth reached 0.3 and 16.6%, respectively, which were among the highest values in the core (Expedition 336 Scientists, 2012c). The co-occurrence of higher cell densities and P_2O_5 at 115–145 mbsf suggests that phosphorus is an important nutrient that may control the endolithic microbial biomass. Phosphorus is known to be an essential element for microbial growth. This is consistent with recent observations of low phosphate content in subsurface crustal fluids compared to bottom seawater, suggesting that phosphorus is a limiting nutrient in the subsurface crustal biosphere (Lin et al., 2012). Meanwhile, the co-occurrence of higher cell densities and porosity at these depth intervals could be explained by the fact that (1) high porosity provides more potential surface area available for microbial colonization (Nielsen and Fisk, 2010), and (2) high porosity facilitates higher rates of fluid flow through the basalts (Orcutt et al., 2013b), supplying higher contents of bioavailable nutrients and/or energy from crustal fluids or bottom seawater.

In summary, we see a strong correlation of microbial abundance with basalt P_2O_5 and porosity, which suggests that the variation in microbial abundance in subsurface basalts is controlled by geochemical and/or physical changes. However, we cannot preclude the possibility of other parameters *in situ*, due to the challenges of obtaining samples and collecting data as well as the heterogeneous nature of the basalts. For example, because the nitrogen content in the basalt is extremely low (<0.01%; Marty, 1995; Busigny et al., 2005), nitrogen in the crustal fluids, which is the main source of nitrogen, may decrease over time due to consumption to levels that limit microbial growth. Nitrogen limitation is also indicated in altered basalts from Costa Rica Rift (Torsvik et al., 1998).

Considering the large volume of the oceanic crustal habitats (Orcutt et al., 2011b), even the relatively low microbial abundances determined in this study suggest that basalt-hosted microorganisms contribute significantly to global biogeochemical cycles. Extrapolating from this limited dataset of microbial abundance on seafloor-exposed basalts and in subsurface basalts (Supplementary Table S1) to the global volume of this habitat, we estimate that the total microbial biomass could match or exceed the total cells estimated in subseafloor sediments (Kallmeyer et al., 2012), which is consistent with a recent hypothesis (Orcutt et al., 2013a). Modeling approaches based on assumptions of assumed pore space available in the crust suggest that a much higher cell density in the global crust is possible (Heberling et al., 2010), but more investigations of microbial abundance in the crust are needed to constrain these estimates, including microbiological samples from a broader range of crust type, crustal age and permeability conditions.

A similar microbial community was found colonizing the basaltic crust of NP regardless of variations in sampling depth (**Figure 2**). This result was suggested from a previous study of the subsurface gabbroic crust at the Atlantis Massif (Mason et al., 2010), although the study used a low resolution method based on Denaturing Gradient Gel Electrophoresis (DGGE). This suggests that (1) the geochemical redox zonations of the basaltic rock and its surrounding crustal fluids are similar, showing relatively stable ratios of major electron donors (e.g., reduced iron, hydrogen gas and trace amount of dissolved organic carbon) and acceptors (e.g., oxygen and nitrate; Expedition 336 Scientists, 2012c; Ziebis et al., 2012; Orcutt et al., 2013b); (2) the microbial communities are homogeneously distributed within the porous and permeable basaltic crust by the advection dominated crustal fluid flow at NP (Edwards et al., 2012), where the basalts are continuously seeded with microbial cells by crustal fluids; (3) the dominance of these groups showed their potential importance to the dynamics of the basaltic microbial community.

In addition, we retrieved sequences that are not found in other crustal environments and/or without any cultured representatives (the "NP lineage" in the tree), covering diverse bacterial groups (**Figures 3**–**5**). This is mainly owing to the recent high-throughput sequencing technology, which substantially extended our view of microbial diversity and potential metabolic functions inhabiting the cool, oxic subsurface basalt-hosted biosphere. For example, we identified a single lineage of *Marinobacter* Group I, which is distinct from any cultured *Marinobacter* species, indicating a unique lineage localized in the NP basalts. The first detection of *Bacteriovorax*-related sequences provides clues that the predatory lifestyle may be an important survival strategy and contribute to microbial biogeochemical cycles in nutrient-starved environments exemplified by NP. Furthermore, the identification of some OTUs that show positive correlation with sampling depth may suggest that they are characteristic of deep biosphere lineages, especially

for those forming monophyletic lineages without cultured representatives.

Carbon and Energy Metabolism in the Cool, Oxic Subsurface Crust

The exact mechanism of autotrophic fixation of CO_2 by basalt microorganisms is uncertain due to the lack of key genes involved in the main autotrophic carbon fixation pathways (Hugler and Sievert, 2011). The presence of O_2 and the δ^{13}C-TOC values of basalts (approximately –25‰; Sakata et al., 2015) suggest carbon fixation by the Calvin–Benson–Bassham cycle, an aerobic pathway found in most Fe oxidizers (Emerson et al., 2010; Lever et al., 2013). However, based on the detection of carbon monoxide dehydrogenase, phosphoenolpyruvate (PEP) carboxylase and pyruvate carboxylase, together with the dominance of facultative chemoautotrophs/mixotrophs, we speculate that the subsurface microorganisms at NP use a mixotrophic pathway to assimilate CO_2 into cellular materials, as proposed elsewhere (Swingley et al., 2007).

The metagenomes from the basalt-hosted environments (e.g., Loihi Seamount, JdFR, and NP) are enriched in genes for Fe^{3+} uptake, siderophore synthesis and uptake, and unspecified Fe transport pathways (Supplementary Figure S6), suggesting that iron-related metabolism could be significant processes supporting life in subsurface basalts from the cool, oxic subsurface crust at NP. Notably, iron oxidation could be an important energy producing process in the basalts. Our diversity analysis showed that some OTUs obtained from NP basalts were closely related to cultured iron oxidizers (**Figures 3–5**; Edwards et al., 2003; Blothe and Roden, 2009; Smith et al., 2011; Swanner et al., 2011; Wang et al., 2012; Hirayama et al., 2015). For example, a monophyletic clade, *Marinobacter* Group II, may represent Fe-oxidizing facultative chemoautotrophs based on the phylogenetic data here and elsewhere (Kaye et al., 2011), and an iron-oxidizing *Marinobacter* strain was isolated from 30R-1A basalts at 304 mbsf (GenBank accession number KJ914666), although known iron oxidation genes [e.g., *iro*, *fox, cyc1*, *cyc2*, *cox*, *pio*, and *rus* (as summarized by Ilbert and Bonnefoy, 2013)] and potential candidate genes [e.g., *mtoA* (Liu et al., 2012), *actB* (Refojo et al., 2012), and $cyc2_{PV-1}$ (Barco et al., 2015)], were not detected in the metagenomes. If iron oxidation is a dominant process as discussed previously, aqueous Fe^{2+} is transformed to Fe^{3+} at the outer membrane or in the periplasm of microbial cells (Emerson et al., 2010; Ilbert and Bonnefoy, 2013). Abundant genes involved in Fe^{3+} uptake, siderophore uptake and unspecified Fe transport may facilitate the transport of the Fe^{3+} into intracellular materials or the binding to organic complexes, including siderophores (Sandy and Butler, 2009). This may avoid the accumulation of insoluble Fe oxyhydroxide and sulfide minerals on the surface of microbial cells due to the rapid chemical precipitation of Fe^{2+} at circumneutral pH. Excess Fe minerals would cause encrustation and cell death for lack of energy and nutrient availability. Moreover, the relatively high abundances of siderophore synthesis genes in basalt-hosted metagenomes helps to produce more siderophores, which would facilitate the dissolution of solid-phase iron minerals (Kraemer et al., 2005) and, in turn, provide more bioavailable iron for microbial energy-yielding activities. Previous work hypothesized that a significant fraction of the iron oxidation in the young upper oceanic crust (<20 million-year old) could support microbial biomass production in subsurface basalts, given that (1) iron is assumed to be the quantitatively most important bioavailable element in the basalt (8 wt%; Melson et al., 2002), and (2) the kinetic favorability in low-temperature ridge flank systems (Bach and Edwards, 2003; Edwards et al., 2012).

Other energy producing processes may also exist in this system. The detection of a hydrogen oxidation gene in the 10R-1B-1 metagenome (**Table 2**) indicates that microbial life is supported by H_2 sources generated from water-rock reactions (e.g., serpentinization; McCollom and Bach, 2009). Heterotrophic metabolism is predicted by our metagenome data. Notably, genes involved in hydrocarbon degradation (e.g., alkane monooxygenase, cytochrome P450, flavin-binding monooxygenase, and catechol-2,3-dioxygenase) were identified, indicating that the microorganisms could use hydrocarbons that originated from crustal fluids or bottom seawater (Lin et al., 2012), diffusion from the overlying sediment (D'Hondt et al., 2009), serpentinization reactions (Proskurowski et al., 2008) or even cell lysates (Jover et al., 2014). In addition, heterotrophic metabolism is supported by the enrichment of functional categories, including fermentation and catabolism of aromatic compounds in NP basalts compared to the rest of the metagenomes listed in Supplementary Figure S5. Heterotrophy is also suggested by previous observations of depleted dissolved organic carbon in subsurface crustal fluids compared with the surrounding bottom seawater in the JdFR flank (Lin et al., 2012) and the detection of hydrocarbon degradation genes in the subsurface gabbroic crust at the Atlantis Massif (Mason et al., 2010).

In summary, this study demonstrates that similar microbial communities with relatively low abundance are colonizing the cool, oxic subsurface oceanic crust at NP. Unique microbial communities dominated by Gammaproteobacteria and Sphingobacteria have the potential to play a major role in iron metabolism, which appears to be a significant process in this ecosystem. Although the correlation between microbial abundance and *in situ* physical and geochemical characteristics is indicated in this study, it is still an open question due to the limited data. In addition, the specific contributions of autotrophy versus heterotrophy in the crustal biosphere are still unclear. Ongoing studies at NP (including laboratory incubations, CORK borehole observatory, RNA-based microbial diversity analyses) and future expeditions [e.g., IODP Expedition 357 at the Atlantis Massif (Früh-Green et al., 2015)] may elucidate the variability of microbial abundance and diversity and the balance of autotrophy versus heterotrophy in the oceanic crustal biosphere.

AUTHOR CONTRIBUTIONS

FW and XZ designed and performed the experiments, analyzed the data and wrote the manuscript. XF analyzed the data. All authors commented on the manuscript.

ACKNOWLEDGMENTS

Thanks are given to the entire shipboard party of IODP Expedition 336 for assistance in collecting, processing, and shipping the samples. Special thanks to the late Katrina J. Edwards for assistance with this project. We thank Ying He, Vengadesh Perumal Natarajan, and Jiahua Wang for assistance in sequencing and metagenomic analysis. This work has been financially supported by the Natural Science Foundation of China (grant 41525011, 91228201, 91428308), China Ocean Mineral Resources R&D Association (grant DY125-15-T-04).

SUPPLEMENTARY MATERIAL

The Supplementary Material for this article can be found online at: http://journal.frontiersin.org/article/10.3389/fmicb.2016.00363

REFERENCES

Alain, K., Tindall, B. J., Catala, P., Intertaglia, L., and Lebaron, P. (2010). *Ekhidna lutea* gen. nov., sp. nov., a member of the phylum Bacteroidetes isolated from the South East Pacific Ocean. *Int. J. Syst. Evol. Microbiol.* 60, 2972–2978. doi: 10.1099/ijs.0.018804-0

Altschul, S. F., Gish, W., Miller, W., Myers, E. W., and Lipman, D. J. (1990). Basic local alignment search tool. *J. Mol. Biol.* 215, 403–410. doi: 10.1016/S0022-2836(05)80360-2

Bach, W., and Edwards, K. J. (2003). Iron and sulfide oxidation within the basaltic ocean crust: implications for chemolithoautotrophic microbial biomass production. *Geochim. Cosmochim. Acta* 67, 3871–3887. doi: 10.1016/s0016-7037(03)00304-1

Baer, M. L., Ravel, J., Piñeiro, S. A., Guether-Borg, D., and Williams, H. N. (2004). Reclassification of salt-water *Bdellovibrio* sp. as *Bacteriovorax marinus* sp. nov. and *Bacteriovorax litoralis* sp. nov. *Int. J. Syst. Evol. Microbiol.* 54, 1011–1016. doi: 10.1099/ijs.0.02458-0

Bankevich, A., Nurk, S., Antipov, D., Gurevich, A. A., Dvorkin, M., Kulikov, A. S., et al. (2012). SPAdes: a new genome assembly algorithm and its applications to single-cell sequencing. *J. Comput. Biol.* 19, 455–477. doi: 10.1089/cmb.2012.0021

Barco, R. A., Emerson, D., Sylvan, J. B., Orcutt, B. N., Meyers, M. E. J., Ramírez, G. A., et al. (2015). The proteomic profile of an obligate iron-oxidizing chemolithoautotroph reveals new insight into microbial iron oxidation. *Appl. Environ. Microbiol.* 81, 5927–5937. doi: 10.1128/aem.01374-15

Barton, H. A., Taylor, N. M., Lubbers, B. R., and Pemberton, A. C. (2006). DNA extraction from low-biomass carbonate rock: an improved method with reduced contamination and the low-biomass contaminant database. *J. Microbiol. Methods* 66, 21–31. doi: 10.1016/j.mimet.2005.10.005

Becker, K., Bartetzko, A., and Davis, E. E. (2001). "Leg 174B synopsis: revisiting Hole 395A for logging and long-term monitoring of off-axis hydrothermal processes in young oceanic crust," in *Proceedings of the Ocean Drilling Program/Scientific Results 174B*, eds K. Becker and M. J. Malone (College Station, TX: Ocean Drilling Program), 1–12. doi: 10.2973/odp.proc.sr.174b.130.2001

Biddle, J. F., Fitz-Gibbon, S., Schuster, S. C., Brenchley, J. E., and House, C. H. (2008). Metagenomic signatures of the Peru Margin subseafloor biosphere show a genetically distinct environment. *Proc. Natl. Acad. Sci. U.S.A.* 105, 10583–10588. doi: 10.1073/pnas.0709942105

Blothe, M., and Roden, E. E. (2009). Microbial iron redox cycling in a circumneutral-pH groundwater seep. *Appl. Environ. Microbiol.* 75, 468–473. doi: 10.1128/Aem.01817-08

Brazelton, W. J., and Baross, J. A. (2009). Abundant transposases encoded by the metagenome of a hydrothermal chimney biofilm. *ISME J.* 3, 1420–1424. doi: 10.1038/ismej.2009.79

Brazelton, W. J., Ludwig, K. A., Sogin, M. L., Andreishcheva, E. N., Kelley, D. S., Shen, C. C., et al. (2010). Archaea and bacteria with surprising microdiversity show shifts in dominance over 1,000-year time scales in hydrothermal chimneys. *Proc. Natl. Acad. Sci. U.S.A.* 107, 1612–1617. doi: 10.1073/pnas.0905369107

Busigny, V., Laverne, C., and Bonifacie, M. (2005). Nitrogen content and isotopic composition of oceanic crust at a superfast spreading ridge: a profile in altered basalts from ODP Site 1256, Leg 206. *Geochem. Geophys. Geosyst.* 6:Q12O01. doi: 10.1029/2005gc001020

Caporaso, J. G., Bittinger, K., Bushman, F. D., DeSantis, T. Z., Andersen, G. L., and Knight, R. (2010a). PyNAST: a flexible tool for aligning sequences to a template alignment. *Bioinformatics* 26, 266–267. doi: 10.1093/bioinformatics/btp636

Caporaso, J. G., Kuczynski, J., Stombaugh, J., Bittinger, K., Bushman, F. D., Costello, E. K., et al. (2010b). QIIME allows analysis of high-throughput community sequencing data. *Nat. Methods* 7, 335–336. doi: 10.1038/nmeth.f.303

Cowen, J. P., Giovannoni, S. J., Kenig, F., Johnson, H. P., Butterfield, D., Rappe, M. S., et al. (2003). Fluids from aging ocean crust that support microbial life. *Science* 299, 120–123. doi: 10.1126/science.1075653

DeSantis, T. Z., Hugenholtz, P., Larsen, N., Rojas, M., Brodie, E. L., Keller, K., et al. (2006). Greengenes, a chimera-checked 16S rRNA gene database and workbench compatible with ARB. *Appl. Environ. Microbiol.* 72, 5069–5072. doi: 10.1128/aem.03006-05

D'Hondt, S., Jorgensen, B. B., Miller, D. J., Batzke, A., Blake, R., Cragg, B. A., et al. (2004). Distributions of microbial activities in deep subseafloor sediments. *Science* 306, 2216–2221. doi: 10.1126/science.1101155

D'Hondt, S., Spivack, A. J., Pockalny, R., Ferdelman, T. G., Fischer, J. P., Kallmeyer, J., et al. (2009). Subseafloor sedimentary life in the South Pacific Gyre. *Proc. Natl. Acad. Sci. U.S.A.* 106, 11651–11656. doi: 10.1073/pnas.0811793106

Edgar, R. C. (2010). Search and clustering orders of magnitude faster than BLAST. *Bioinformatics* 26, 2460–2461. doi: 10.1093/bioinformatics/btq461

Edgar, R. C., Haas, B. J., Clemente, J. C., Quince, C., and Knight, R. (2011). UCHIME improves sensitivity and speed of chimera detection. *Bioinformatics* 27, 2194–2200. doi: 10.1093/bioinformatics/btr381

Edwards, K. J., Fisher, A. T., and Wheat, C. G. (2012). The deep subsurface biosphere in igneous ocean crust: frontier habitats for microbiological exploration. *Front. Microbiol.* 3:8. doi: 10.3389/fmicb.2012.00008

Edwards, K. J., Glazer, B. T., Rouxel, O. J., Bach, W., Emerson, D., Davis, R. E., et al. (2011). Ultra-diffuse hydrothermal venting supports Fe-oxidizing bacteria and massive umber deposition at 5000 m off Hawaii. *ISME J.* 5, 1748–1758. doi: 10.1038/ismej.2011.48

Edwards, K. J., Rogers, D. R., Wirsen, C. O., and McCollom, T. M. (2003). Isolation and characterization of novel psychrophilic, neutrophilic, Fe-oxidizing, chemolithoautotrophic α- and γ-proteobacteria from the deep sea. *Appl. Environ. Microbiol.* 69, 2906–2913. doi: 10.1128/aem.69.5.2906-2913.2003

Einen, J., Thorseth, I. H., and Ovreås, L. (2008). Enumeration of Archaea and Bacteria in seafloor basalt using real-time quantitative PCR and fluorescence microscopy. *FEMS Microbiol. Lett.* 282, 182–187. doi: 10.1111/j.1574-6968.2008.01119.x

Emerson, D., Fleming, E. J., and McBeth, J. M. (2010). Iron-oxidizing bacteria: an environmental and genomic perspective. *Annu. Rev. Microbiol.* 64, 561–583. doi: 10.1146/annurev.micro.112408.134208

Expedition 327 Scientists (2010). *Juan de Fuca Ridge-flank Hydrogeology: The Hydrogeologic Architecture of Basaltic Oceanic Crust: Compartmentalization, Anisotropy, Microbiology, and Crustal-scale Properties on the Eastern Flank of Juan de Fuca Ridge, Eastern Pacific Ocean*. IODP Preliminary Report, 327. Tokyo: Integrated Ocean Drilling Program Management International, Inc. doi: 10.2204/iodp.pr.327.2010

Expedition 329 Scientists (2011). *South Pacific Gyre Subseafloor Life*. IODP Preliminary Report, 329. Tokyo: Integrated Ocean Drilling Program Management International, Inc. doi: 10.2204/iodp.pr.329.2011

Expedition 330 Scientists (2011). *Louisville Seamount Trail: Implications for Geodynamic Mantle Flow Models and the Geochemical Evolution of Primary*

Hotspots. IODP Preliminary Report, 330. Tokyo: Integrated Ocean Drilling Program Management International, Inc. doi: 10.2204/iodp.pr.330.2011

Expedition 330 Scientists (2012). "Methods," in *Proceedings of the Integrated Ocean Drilling Program 330*, eds A. A. P. Koppers, T. Yamazaki, J. Geldmacher, and the Expedition 330 Scientists (Tokyo: Integrated Ocean Drilling Program Management International, Inc.). doi: 10.2204/iodp.proc.330.102.2012

Expedition 336 Scientists (2012a). "Methods," in *Proceedings of the Integrated Ocean Drilling Program 336*, eds K. J. Edwards, W. Bach, A. Klaus, and the Expedition 336 Scientists (Tokyo: Integrated Ocean Drilling Program Management International, Inc.). doi: 10.2204/iodp.proc.336.102.2012

Expedition 336 Scientists (2012b). *Mid-Atlantic Ridge Microbiology: Initation of Long-Term Coupled Microbiological, Geochemical, and Hydrological Experimentation within the Seafloor at North Pond, Western Flank of the Mid-Atlantic Ridge*. IODP Preliminary Report, 336. Tokyo: Integrated Ocean Drilling Program Management International, Inc. doi: 10.2204/iodp.pr.336.2012

Expedition 336 Scientists (2012c). "Site U1383," in *Proceedings of the Integrated Ocean Drilling Program 336*, eds K. J. Edwards, W. Bach, A. Klaus, and the Expedition 336 Scientists (Tokyo: Integrated Ocean Drilling Program Management International, Inc.). doi: 10.2204/iodp.proc.336.105.2012

Fisk, M. R., Giovannoni, S. J., and Thorseth, I. H. (1998). Alteration of oceanic volcanic glass: textural evidence of microbial activity. *Science* 281, 978–980. doi: 10.1126/science.281.5379.978

Fisk, M. R., Storrie-Lombardi, M. C., Douglas, S., Popa, R., McDonald, G., and Di Meo-Savoie, C. (2003). Evidence of biological activity in Hawaiian subsurface basalts. *Geochem. Geophys. Geosyst.* 4:1103. doi: 10.1029/2002gc000387

Früh-Green, G. L., Orcutt, B. N., and Green, S. (2015). *Expedition 357 Scientific Prospectus: Atlantis Massif Serpentinization and Life*. Tokyo: International Ocean Discovery Program. doi: 10.14379/iodp.sp.357.2015

He, S., Ivanova, N., Kirton, E., Allgaier, M., Bergin, C., Scheffrahn, R. H., et al. (2013a). Comparative metagenomic and metatranscriptomic analysis of hindgut paunch microbiota in wood- and dung-feeding higher termites. *PLoS ONE* 8:e61126. doi: 10.1371/journal.pone.0061126

He, Y., Xiao, X., and Wang, F. (2013b). Metagenome reveals potential microbial degradation of hydrocarbon coupled with sulfate reduction in an oil-immersed chimney from Guaymas Basin. *Front. Microbiol.* 4:148. doi: 10.3389/fmicb.2013.00148

Heberling, C., Lowell, R. P., Liu, L., and Fisk, M. R. (2010). Extent of the microbial biosphere in the oceanic crust. *Geochem. Geophys. Geosyst.* 11:Q08003. doi: 10.1029/2009gc002968

Hirayama, H., Abe, M., Miyazaki, J., Sakai, S., Nagano, Y., and Takai, K. (2015). "Data report: cultivation of microorganisms from basaltic rock and sediment cores from the North Pond on the western flank of the Mid-Atlantic Ridge, IODP Expedition 336," in eds K. J. Edwards, W. Bach, A. Klaus, and the Expedition 336 Scientists (Tokyo: Integrated Ocean Drilling Program Management International, Inc.). doi: 10.2204/iodp.proc.336.204.2015

Hopkinson, B. M., and Barbeau, K. A. (2012). Iron transporters in marine prokaryotic genomes and metagenomes. *Environ. Microbiol.* 14, 114–128. doi: 10.1111/j.1462-2920.2011.02539.x

Hugler, M., and Sievert, S. M. (2011). Beyond the Calvin cycle: autotrophic carbon fixation in the ocean. *Annu. Rev. Mar. Sci.* 3, 261–289. doi: 10.1146/annurev-marine-120709-142712

Huu, N. B., Denner, E. B. M., Ha, D. T. C., Wanner, G., and Stan-Lotter, H. (1999). *Marinobacter aquaeolei* sp. nov., a halophilic bacterium isolated from a Vietnamese oil-producing well. *Int. J. Syst. Bacteriol.* 49, 367–375. doi: 10.1099/00207713-49-2-367

Ilbert, M., and Bonnefoy, V. (2013). Insight into the evolution of the iron oxidation pathways. *Biochim. Biophys. Acta* 1827, 161–175. doi: 10.1016/j.bbabio.2012.10.001

Jacobson Meyers, M. E., Sylvan, J. B., and Edwards, K. J. (2014). Extracellular enzyme activity and microbial diversity measured on seafloor exposed basalts from Loihi seamount indicate the importance of basalts to global biogeochemical cycling. *Appl. Environ. Microbiol.* 80, 4854–4864. doi: 10.1128/aem.01038-14

Jover, L. F., Effler, T. C., Buchan, A., Wilhelm, S. W., and Weitz, J. S. (2014). The elemental composition of virus particles: implications for marine biogeochemical cycles. *Nat. Rev. Microbiol.* 12, 519–528. doi: 10.1038/nrmicro3289

Jungbluth, S. P., Grote, J., Lin, H. T., Cowen, J. P., and Rappe, M. S. (2013). Microbial diversity within basement fluids of the sediment-buried Juan de Fuca Ridge flank. *ISME J.* 7, 161–172. doi: 10.1038/ismej.2012.73

Jungbluth, S. P., Lin, H. T., Cowen, J. P., Glazer, B. T., and Rappe, M. S. (2014). Phylogenetic diversity of microorganisms in subseafloor crustal fluids from Holes 1025C and 1026B along the Juan de Fuca Ridge flank. *Front. Microbiol.* 5:119. doi: 10.3389/fmicb.2014.00119

Kallmeyer, J., Pockalny, R., Adhikari, R. R., Smith, D. C., and D'Hondt, S. (2012). Global distribution of microbial abundance and biomass in subseafloor sediment. *Proc. Natl. Acad. Sci. U.S.A.* 109, 16213–16216. doi: 10.1073/pnas.1203849109

Kallmeyer, J., Smith, D. C., Spivack, A. J., and D'Hondt, S. (2008). New cell extraction procedure applied to deep subsurface sediments. *Limnol. Oceanogr. Methods* 6, 236–245. doi: 10.4319/lom.2008.6.236

Kaye, J. Z., Sylvan, J. B., Edwards, K. J., and Baross, J. A. (2011). Halomonas and *Marinobacter* ecotypes from hydrothermal vent, subseafloor and deep-sea environments. *FEMS Microbiol. Ecol.* 75, 123–133. doi: 10.1111/j.1574-6941.2010.00984.x

Kraemer, S. M., Butler, A., Borer, P., and Cervini-Silva, J. (2005). Siderophores and the dissolution of iron-bearing minerals in marine systems. *Rev. Mineral. Geochem.* 59, 53–84. doi: 10.2138/rmg.2005.59.4

Kulakov, L. A., McAlister, M. B., Ogden, K. L., Larkin, M. J., and O'Hanlon, J. F. (2002). Analysis of bacteria contaminating ultrapure water in industrial systems. *Appl. Environ. Microbiol.* 68, 1548–1555. doi: 10.1128/aem.68.4.1548-1555.2002

Langseth, M. G., Becker, K., Von Herzen, R. P., and Schultheiss, P. (1992). Heat and fluid flux through sediment on the western flank of the Mid-Atlantic Ridge: a hydrogeological study of North Pond. *Geophys. Res. Lett.* 19, 517–520. doi: 10.1029/92gl00079

Lever, M. A., Alperin, M., Engelen, B., Inagaki, F., Nakagawa, S., Steinsbu, B. O., et al. (2006). Trends in basalt and sediment core contamination during IODP Expedition 301. *Geomicrobiol. J.* 23, 517–530. doi: 10.1080/01490450600897245

Lever, M. A., Rouxel, O., Alt, J. C., Shimizu, N., Ono, S., Coggon, R. M., et al. (2013). Evidence for microbial carbon and sulfur cycling in deeply buried ridge flank basalt. *Science* 339, 1305–1308. doi: 10.1126/science.1229240

Lewin, R. A., and Lounsbery, D. M. (1969). Isolation, cultivation and characterization of flexibacteria. *J. Gen. Microbiol.* 58, 145–170. doi: 10.1099/00221287-58-2-145

Lin, H.-T., Cowen, J. P., Olson, E. J., Amend, J. P., and Lilley, M. D. (2012). Inorganic chemistry, gas compositions and dissolved organic carbon in fluids from sedimented young basaltic crust on the Juan de Fuca Ridge flanks. *Geochim. Cosmochim. Acta* 85, 213–227. doi: 10.1016/j.gca.2012.02.017

Lipp, J. S., Morono, Y., Inagaki, F., and Hinrichs, K. U. (2008). Significant contribution of Archaea to extant biomass in marine subsurface sediments. *Nature* 454, 991–994. doi: 10.1038/nature07174

Liu, J., Wang, Z., Belchik, S. M., Edwards, M. J., Liu, C., Kennedy, D. W., et al. (2012). identification and characterization of MtoA: a decaheme c-type cytochrome of the neutrophilic Fe(II)-oxidizing bacterium Sideroxydans lithotrophicus ES-1. *Front. Microbiol.* 3:37. doi: 10.3389/fmicb.2012.00037

Lo, I., Denef, V. J., VerBerkmoes, N. C., Shah, M. B., Goltsman, D., DiBartolo, G., et al. (2007). Strain-resolved community proteomics reveals recombining genomes of acidophilic bacteria. *Nature* 446, 537–541. doi: 10.1038/nature05624

Lovley, D. R., Phillips, E. J. P., and Lonergan, D. J. (1989). Hydrogen and formate oxidation coupled to dissimilatory reduction of iron or manganese by *Alteromonas putrefaciens*. *Appl. Environ. Microbiol.* 55, 700–706.

Luo, R. B., Liu, B. H., Xie, Y. L., Li, Z. Y., Huang, W. H., Yuan, J. Y., et al. (2012). SOAPdenovo2: an empirically improved memory-efficient short-read de novo assembler. *Gigascience* 1:18. doi: 10.1186/2047-217X-1-18

Lysnes, K., Thorseth, I. H., Steinsbu, B. O., Ovreas, L., Torsvik, T., and Pedersen, R. B. (2004). Microbial community diversity in seafloor basalt from the Arctic spreading ridges. *FEMS Microbiol. Ecol.* 50, 213–230. doi: 10.1016/j.femsec.2004.06.014

Magoč, T., and Salzberg, S. L. (2011). FLASH: fast length adjustment of short reads to improve genome assemblies. *Bioinformatics* 27, 2957–2963. doi: 10.1093/bioinformatics/btr507

Marty, B. (1995). Nitrogen content of the mantle inferred from N2-Ar correlation in oceanic basalts. *Nature* 377, 326–329. doi: 10.1038/377326a0

Mason, O. U., Di Meo-Savoie, C. A., Van Nostrand, J. D., Zhou, J., Fisk, M. R., and Giovannoni, S. J. (2009). Prokaryotic diversity, distribution, and insights into their role in biogeochemical cycling in marine basalts. *ISME J.* 3, 231–242. doi: 10.1038/ismej.2008.92

Mason, O. U., Nakagawa, T., Rosner, M., Van Nostrand, J. D., Zhou, J., Maruyama, A., et al. (2010). First investigation of the microbiology of the deepest layer of ocean crust. *PLoS ONE* 5:e15399. doi: 10.1371/journal.pone.0015399

Mason, O. U., Stingl, U., Wilhelm, L. J., Moeseneder, M. M., Di Meo-Savoie, C. A., Fisk, M. R., et al. (2007). The phylogeny of endolithic microbes associated with marine basalts. *Environ. Microbiol.* 9, 2539–2550. doi: 10.1111/j.1462-2920.2007.01372.x

McCollom, T. M., and Bach, W. (2009). Thermodynamic constraints on hydrogen generation during serpentinization of ultramafic rocks. *Geochim. Cosmochim. Acta* 73, 856–875. doi: 10.1016/j.gca.2008.10.032

Melson, W. G., O'Hearn, T., and Jarosewich, E. (2002). A data brief on the Smithsonian Abyssal Volcanic Glass Data File. *Geochem. Geophys. Geosyst.* 3, 1–11. doi: 10.1029/2001gc000249

Meron, D., Atias, E., Iasur Kruh, L., Elifantz, H., Minz, D., Fine, M., et al. (2011). The impact of reduced pH on the microbial community of the coral *Acropora eurystoma*. *ISME J.* 5, 51–60. doi: 10.1038/ismej.2010.102

Meyer, F., Paarmann, D., D'Souza, M., Olson, R., Glass, E. M., Kubal, M., et al. (2008). The metagenomics RAST server – a public resource for the automatic phylogenetic and functional analysis of metagenomes. *BMC Bioinformatics* 9:386. doi: 10.1186/1471-2105-9-386

Nayfach, S., and Pollard, K. (2015). Average genome size estimation improves comparative metagenomics and sheds light on the functional ecology of the human microbiome. *Genome Biol.* 16, 51. doi: 10.1186/s13059-015-0611-7

Ng, H. J., López-Pérez, M., Webb, H. K., Gomez, D., Sawabe, T., Ryan, J., et al. (2014). *Marinobacter salarius* sp. nov. and *Marinobacter similis* sp. nov., isolated from sea water. *PLoS ONE* 9:e106514. doi: 10.1371/journal.pone.0106514

Nielsen, M. E., and Fisk, M. R. (2010). Surface area measurements of marine basalts: implications for the subseafloor microbial biomass. *Geophys. Res. Lett.* 37:L15604. doi: 10.1029/2010gl044074

Nigro, L. M., Harris, K., Orcutt, B. N., Hyde, A., Clayton-Luce, S., Becker, K., et al. (2012). Microbial communities at the borehole observatory on the Costa Rica Rift flank (Ocean Drilling Program Hole 896A). *Front. Microbiol.* 3:232. doi: 10.3389/fmicb.2012.00232

Nitahara, S., Kato, S., Urabe, T., Usui, A., and Yamagishi, A. (2011). Molecular characterization of the microbial community in hydrogenetic ferromanganese crusts of the Takuyo-Daigo Seamount, northwest Pacific. *FEMS Microbiol. Lett.* 321, 121–129. doi: 10.1111/j.1574-6968.2011.02323.x

Orcutt, B. N., Bach, W., Becker, K., Fisher, A. T., Hentscher, M., Toner, B. M., et al. (2011a). Colonization of subsurface microbial observatories deployed in young ocean crust. *ISME J.* 5, 692–703. doi: 10.1038/ismej.2010.157

Orcutt, B. N., LaRowe, D. E., Biddle, J. F., Colwell, F. S., Glazer, B. T., Reese, B. K., et al. (2013a). Microbial activity in the marine deep biosphere: progress and prospects. *Front. Microbiol.* 4:189. doi: 10.3389/fmicb.2013.00189

Orcutt, B. N., Sylvan, J. B., Knab, N. J., and Edwards, K. J. (2011b). Microbial ecology of the dark ocean above, at, and below the seafloor. *Microbiol. Mol. Biol. Rev.* 75, 361–422. doi: 10.1128/Mmbr.00039-10

Orcutt, B. N., Wheat, C. G., Rouxel, O., Hulme, S., Edwards, K. J., and Bach, W. (2013b). Oxygen consumption rates in subseafloor basaltic crust derived from a reaction transport model. *Nat. Commun.* 4:2539. doi: 10.1038/ncomms3539

Overbeek, R., Begley, T., Butler, R. M., Choudhuri, J. V., Chuang, H.-Y., Cohoon, M., et al. (2005). The subsystems approach to genome annotation and its use in the project to annotate 1000 genomes. *Nucleic Acids Res.* 33, 5691–5702. doi: 10.1093/nar/gki866

Paulsen, I. T., Press, C. M., Ravel, J., Kobayashi, D. Y., Myers, G. S. A., Mavrodi, D. V., et al. (2005). Complete genome sequence of the plant commensal *Pseudomonas fluorescens* Pf-5. *Nat. Biotechnol.* 23, 873–878. doi: 10.1038/nbt1110

Picard, A., and Ferdelman, T. G. (2011). Linking microbial heterotrophic activity and sediment lithology in oxic, oligotrophic subseafloor sediments of the North Atlantic Ocean. *Front. Microbiol.* 2:263. doi: 10.3389/fmicb.2011.00263

Price, M. N., Dehal, P. S., and Arkin, A. P. (2010). FastTree 2 – approximately maximum-likelihood trees for large alignments. *PLoS ONE* 5:e9490. doi: 10.1371/journal.pone.0009490

Proskurowski, G., Lilley, M. D., Seewald, J. S., Fruh-Green, G. L., Olson, E. J., Lupton, J. E., et al. (2008). Abiogenic hydrocarbon production at Lost City hydrothermal field. *Science* 319, 604–607. doi: 10.1126/science.1151194

R Core Team (2015). *R: A Language and Environment for Statistical Computing*. Vienna: R Foundation for Statistical Computing.

Rathsack, K., Stackebrandt, E., Reitner, J., and Schumann, G. (2009). Microorganisms isolated from deep sea low-temperature influenced oceanic crust basalts and sediment samples collected along the mid-atlantic ridge. *Geomicrobiol. J.* 26, 264–274. doi: 10.1080/01490450902892456

Reddy, T. B. K., Thomas, A. D., Stamatis, D., Bertsch, J., Isbandi, M., Jansson, J., et al. (2015). The Genomes OnLine Database (GOLD) v.5: a metadata management system based on a four level (meta)genome project classification. *Nucleic Acids Res.* 43, D1099–D1106. doi: 10.1093/nar/gku950

Refojo, P. N., Teixeira, M., and Pereira, M. M. (2012). The Alternative complex III: properties and possible mechanisms for electron transfer and energy conservation. *Biochim. Biophys. Acta* 1817, 1852–1859. doi: 10.1016/j.bbabio.2012.05.003

Reveillaud, J., Maignien, L., Eren, A. M., Huber, J. A., Apprill, A., Sogin, M. L., et al. (2014). Host-specificity among abundant and rare taxa in the sponge microbiome. *ISME J.* 8, 1198–1209. doi: 10.1038/ismej.2013.227

Robador, A., Jungbluth, S. P., LaRowe, D., Bowers, R., Rappe, M., Amend, J., et al. (2015). Activity and phylogenetic diversity of sulfate-reducing microorganisms in low-temperature subsurface fluids within the upper oceanic crust. *Front. Microbiol.* 5:748. doi: 10.3389/fmicb.2014.00748

Sakata, K., Yabuta, H., Ikehara, M., and Kondo, T. (2015). "Data report: carbon content and isotopic composition of basalts and sediments in North Pond, Expedition 336," in *Proceedings of the Integrated Ocean Drilling Program 336*, eds K. J. Edwards, W. Bach, A. Klaus, and the Expedition 336 Scientists (Tokyo: Integrated Ocean Drilling Program Management International, Inc.). doi: 10.2204/iodp.proc.336.203.2015

Salter, S. J., Cox, M. J., Turek, E. M., Calus, S. T., Cookson, W. O., Moffatt, M. F., et al. (2014). Reagent and laboratory contamination can critically impact sequence-based microbiome analyses. *BMC Biol.* 12:87. doi: 10.1186/s12915-014-0087-z

Sandy, M., and Butler, A. (2009). Microbial iron acquisition: marine and terrestrial siderophores. *Chem. Rev.* 109, 4580–4595. doi: 10.1021/cr9002787

Santelli, C. M., Edgcomb, V. P., Bach, W., and Edwards, K. J. (2009). The diversity and abundance of bacteria inhabiting seafloor lavas positively correlate with rock alteration. *Environ. Microbiol.* 11, 86–98. doi: 10.1111/j.1462-2920.2008.01743.x

Santelli, C. M., Orcutt, B. N., Banning, E., Bach, W., Moyer, C. L., Sogin, M. L., et al. (2008). Abundance and diversity of microbial life in ocean crust. *Nature* 453, 653–656. doi: 10.1038/nature06899

Schrenk, M. O., Huber, J. A., and Edwards, K. J. (2010). Microbial provinces in the subseafloor. *Annu. Rev. Mar. Sci.* 2, 279–304. doi: 10.1146/annurev-marine-120308-081000

Scott, J. J., Breier, J. A., Luther, G. W., and Emerson, D. (2015). Microbial iron mats at the Mid-Atlantic Ridge and evidence that Zetaproteobacteria may be restricted to iron-oxidizing marine systems. *PLoS ONE* 10:e0119284. doi: 10.1371/journal.pone.0119284

Simpson, J. T., Wong, K., Jackman, S. D., Schein, J. E., Jones, S. J. M., and Birol, I. (2009). ABySS: a parallel assembler for short read sequence data. *Genome Res.* 19, 1117–1123. doi: 10.1101/gr.089532.108

Singer, E., Heidelberg, J. F., Dhillon, A., and Edwards, K. J. (2013). Metagenomic insights into the dominant Fe(II) oxidizing Zetaproteobacteria from an iron mat at Loi'hi, Hawai'I. *Front. Microbiol.* 4:52. doi: 10.3389/fmicb.2013.00052

Smith, A., Popa, R., Fisk, M., Nielsen, M., Wheat, C. G., Jannasch, H. W., et al. (2011). In situ enrichment of ocean crust microbes on igneous minerals and glasses using an osmotic flow-through device. *Geochem. Geophys. Geosyst.* 12:Q06007. doi: 10.1029/2010gc003424

Smith, D. C., Spivack, A. J., Fisk, M. R., Haveman, S. A., Staudigel, H., and the Leg 185 Shipboard Scientific Party (2000). Methods for quantifying potential microbial contamination during deep ocean coring. *ODP Tech. Note* 28, 19. doi: 10.2973/odp.tn.28.2000

Swanner, E. D., Nell, R. M., and Templeton, A. S. (2011). Ralstonia species mediate Fe-oxidation in circumneutral, metal-rich subsurface fluids of Henderson mine, CO. *Chem. Geol.* 284, 339–350. doi: 10.1016/j.chemgeo.2011.03.015

Swingley, W. D., Sadekar, S., Mastrian, S. D., Matthies, H. J., Hao, J., Ramos, H., et al. (2007). The complete genome sequence of *Roseobacter denitrificans* reveals a mixotrophic rather than photosynthetic metabolism. *J. Bacteriol.* 189, 683–690. doi: 10.1128/jb.01390-06

Tanner, M. A., Goebel, B. M., Dojka, M. A., and Pace, N. R. (1998). Specific ribosomal DNA sequences from diverse environmental settings correlate with experimental contaminants. *Appl. Environ. Microbiol.* 64, 3110–3113.

Templeton, A. S., Staudigel, H., and Tebo, B. M. (2005). Diverse Mn(II)-oxidizing bacteria isolated from submarine basalts at Loihi seamount. *Geomicrobiol. J.* 22, 127–139. doi: 10.1080/01490450590945951

Thompson, J. D., Higgins, D. G., and Gibson, T. J. (1994). CLUSTAL W: improving the sensitivity of progressive multiple sequence alignment through sequence weighting, position-specific gap penalties and weight matrix choice. *Nucleic Acids Res.* 22, 4673–4680. doi: 10.1093/nar/22.22.4673

Thorseth, I. H., Torsvik, T., Torsvik, V., Daae, F. L., and Pedersen, R. B. (2001). Diversity of life in ocean floor basalt. *Earth Planet. Sci. Lett.* 194, 31–37. doi: 10.1016/S0012-821X(01)00537-4

Torsvik, T., Furnes, H., Muehlenbachs, K., Thorseth, I. H., and Tumyr, O. (1998). Evidence for microbial activity at the glass-alteration interface in oceanic basalts. *Earth Planet. Sci. Lett.* 162, 165–176. doi: 10.1016/S0012-821X(98)00164-2

Toulza, E., Tagliabue, A., Blain, S., and Piganeau, G. (2012). Analysis of the global ocean sampling (GOS) project for trends in iron uptake by surface ocean microbes. *PLoS ONE* 7:e30931. doi: 10.1371/journal.pone.0030931

Tyson, G. W., Chapman, J., Hugenholtz, P., Allen, E. E., Ram, R. J., Richardson, P. M., et al. (2004). Community structure and metabolism through reconstruction of microbial genomes from the environment. *Nature* 428, 37–43. doi: 10.1038/nature02340

Vetrovsky, T., and Baldrian, P. (2013). The variability of the 16S rRNA gene in bacterial genomes and its consequences for bacterial community analyses. *PLoS ONE* 8:e57923. doi: 10.1371/journal.pone.0057923

Villeneuve, C., Martineau, C., Mauffrey, F., and Villemur, R. (2013). *Methylophaga nitratireducenticrescens* sp. nov. and *Methylophaga frappieri* sp. nov., isolated from the biofilm of the methanol-fed denitrification system treating the seawater at the Montreal Biodome. *Int. J. Syst. Evol. Microbiol.* 63, 2216–2222. doi: 10.1099/ijs.0.044545-0

Wang, F. P., Lu, S., Orcutt, B. N., Xie, W., Chen, Y., Xiao, X., et al. (2013). Discovering the roles of subsurface microorganisms: progress and future of deep biosphere investigation. *Chin. Sci. Bull.* 58, 456–467. doi: 10.1007/s11434-012-5358-x

Wang, F. P., Zhang, Y., Chen, Y., He, Y., Qi, J., Hinrichs, K.-U., et al. (2014). Methanotrophic archaea possessing diverging methane-oxidizing and electron-transporting pathways. *ISME J.* 8, 1069–1078. doi: 10.1038/ismej.2013.212

Wang, H., Hu, C., Hu, X., Yang, M., and Qu, J. (2012). Effects of disinfectant and biofilm on the corrosion of cast iron pipes in a reclaimed water distribution system. *Water Res.* 46, 1070–1078. doi: 10.1016/j.watres.2011.12.001

Wu, W. F., Wang, F. P., Li, J. H., Yang, X. W., Xiao, X., and Pan, Y. X. (2013). Iron reduction and mineralization of deep-sea iron reducing bacterium *Shewanella piezotolerans* WP3 at elevated hydrostatic pressures. *Geobiology* 11, 593–601. doi: 10.1111/gbi.12061

Xie, W., Wang, F. P., Guo, L., Chen, Z., Sievert, S. M., Meng, J., et al. (2011). Comparative metagenomics of microbial communities inhabiting deep-sea hydrothermal vent chimneys with contrasting chemistries. *ISME J.* 5, 414–426. doi: 10.1038/ismej.2010.144

Zeng, Q., and Chisholm, S. W. (2012). Marine viruses exploit their host's two-component regulatory system in response to resource limitation. *Curr. Biol.* 22, 124–128. doi: 10.1016/j.cub.2011.11.055

Zerbino, D. R., and Birney, E. (2008). Velvet: algorithms for de novo short read assembly using de Bruijn graphs. *Genome Res.* 18, 821–829. doi: 10.1101/gr.074492.107

Ziebis, W., McManus, J., Ferdelman, T., Schmidt-Schierhorn, F., Bach, W., Muratli, J., et al. (2012). Interstitial fluid chemistry of sediments underlying the North Atlantic gyre and the influence of subsurface fluid flow. *Earth Planet. Sci. Lett.* 323, 79–91. doi: 10.1016/j.epsl.2012.01.018

Conflict of Interest Statement: The authors declare that the research was conducted in the absence of any commercial or financial relationships that could be construed as a potential conflict of interest.

frontiers in Microbiology

METHODS
published: 12 November 2015
doi: 10.3389/fmicb.2015.01260

In situ Detection of Microbial Life in the Deep Biosphere in Igneous Ocean Crust

Everett C. Salas[1,2], Rohit Bhartia[1], Louise Anderson[3], William F. Hug[2], Ray D. Reid[2], Gerardo Iturrino[4†] and Katrina J. Edwards[5†]*

[1] Jet Propulsion Laboratory, Planetary Chemistry and Astrobiology, California Insitute of Technology, Pasadena, CA, USA, [2] Photon Systems, Inc., Covina, CA, USA, [3] Department of Geology, University of Leicester, Leicester, UK, [4] Lamont-Doherty Earth Observatory, Marine Geology and Geophysics, Palisades, NY, USA, [5] Department of Biological Sciences and Earth Sciences, University of Southern California, Los Angeles, CA, USA

The deep biosphere is a major frontier to science. Recent studies have shown the presence and activity of cells in deep marine sediments and in the continental deep biosphere. Volcanic lavas in the deep ocean subsurface, through which substantial fluid flow occurs, present another potentially massive deep biosphere. We present results from the deployment of a novel *in situ* logging tool designed to detect microbial life harbored in a deep, native, borehole environment within igneous oceanic crust, using deep ultraviolet native fluorescence spectroscopy. Results demonstrate the predominance of microbial-like signatures within the borehole environment, with densities in the range of 10^5 cells/mL. Based on transport and flux models, we estimate that such a concentration of microbial cells could not be supported by transport through the crust, suggesting *in situ* growth of these communities.

Keywords: deep subsurface biosphere, microbial life, deep UV fluorescence, *in situ* life detection, North Pond, borehole

OPEN ACCESS

Edited by:
Cara M. Santelli, University of Minnesota, USA

Reviewed by:
Hugh Morgan, University of Waikato, New Zealand
Xi-Ying Zhang, Shandong University, China

***Correspondence:**
Rohit Bhartia
rbhartia@jpl.nasa.gov

†Deceased

Specialty section:
This article was submitted to Extreme Microbiology, a section of the journal Frontiers in Microbiology

Received: *30 August 2015*
Accepted: *29 October 2015*
Published: *12 November 2015*

Citation:
Salas EC, Bhartia R, Anderson L, Hug WF, Reid RD, Iturrino G and Edwards KJ (2015) In situ Detection of Microbial Life in the Deep Biosphere in Igneous Ocean Crust. Front. Microbiol. 6:1260. doi: 10.3389/fmicb.2015.01260

INTRODUCTION

The deep marine biosphere is reportedly a massive scale suite of microbial provinces (Schrenk et al., 2010). It is known that microbial life is metabolically active (D'Hondt, 2002), to varying degrees, and extends at least 1.6 km into subsurface sediments (Roussel et al., 2008; D'Hondt et al., 2009). By comparison with what we know for the sedimentary deep biosphere habitats, however, very little is known about the size, function, and activity of microbial life in igneous ocean crust—or even if it truly exists. Igneous ocean crust harbors the largest aquifer on Earth, most of which is hydrologically active (Stein and Stein, 1994; Fisher and Becker, 2000), providing the possibility that microbial life may extend well underground in this habitat as well.

In microbial ecology, scientists are challenged to make even the most basic microbial cell enumerations—this is particularly true in the igneous ocean crust as cells likely exist in biofilms associated with volcanic surfaces in the porous aquifer. The diminutive size and transparency of microbes necessitates the use of stains and fluorescence (Daley and Hobbie, 1975; Giovannoni et al., 1988) for detection on opaque surfaces, such as igneous crust. However, while these methods have enabled detection, visualization and some characterization, the organic and chemical variability of natural samples can lead to confounding results where tags and stains non-specifically bind to background structures (Nadeau et al., 2008). Further, the substrates can produce their own

fluorescence from the near UV (>300 nm) and visible excitation wavelengths used to excite the tags, leading to false positives (Bhartia et al., 2010).

We have developed and applied a novel tool for the *in situ*, rapid detection of microorganisms in the igneous marine deep biosphere by capitalizing on intrinsic fluorescence of bound and free aromatic amino acids; tryptophan, phenylalanine, and tyrosine. Excitation with a <250 nm source enables a means to use these compounds to detect potential signatures of microbial life in these environments. Deep UV excitation results in fluorescence spectral features that can be used to distinguish biological samples from other naturally occurring or anthropomorphically generated fluorophores. This capability to differentiate microbial cells from organic matter is a result of a cell having a high concentration of proteins containing strongly fluorescing bound aromatic amino acids, free amino acids, redox-active membrane proteins and other aromatic compounds (e.g., flavins, NADH). While some bacterial cells can extend the range of fluorescence to beyond 400 nm, most of the unique fluorescence signature associated to all known bacterial cells or spores ranges between 270 and 400 nm. The spectral feature is similar, but not identical to the fluorescence feature of tryptophan, tyrosine, or phenylalanine and can be differentiated from organic matter in the environment (Bhartia et al., 2008, 2010). The Deep Exploration Biosphere Investigative tool (DEBI-t), is based on the use of deep ultraviolet (<250 nm) native fluorescence for rapid, non-contact detection and localization of microbial communities against opaque mineralogical backgrounds (Bhartia et al., 2010). Although the DEBI-t instrument does not have the spatial resolution to determine whether detected spectral signatures are definitively cellular features, the bulk signature analysis shows a consistent ability to differentiate between organics and lab grown microbes and microbes from the terrestrial environment.

DEBI-t was deployed as a wireline tool via logging operations in Hole 395A, a Deep Sea Drilling Program legacy borehole that was drilled in 1974-75. Hole 395A, located at the North Pond site in the western flank of the Mid-Atlantic Ridge (**Figure 1**), was sealed at the seafloor using a circulation obviation retrofit kit (CORK; Becker and Davis, 2005) in 1998 (Becker et al., 2001), and then reopened in September 2011 during IODP Expedition 336 with the goal of deploying DEBI-t and installing a modernized CORK.

DEBI-t relies on a deep UV (<250 nm) laser induced native fluorescence spectroscopy, which enables the detection of microbial cells and organics without tagging or staining.

DEBI-t utilizes a 224.3 nm HeAg hollow cathode laser used to induce fluorescence of organics and microbes. The instrument uses a "soft pulse" of 600 nJ/100 μs pulse to avoid damage or alteration of the materials and operates at a frequency of 4 Hz. The exits the instrument via a deep UV transmissive sapphire window, with a 20 mm clear aperture, seated at the front of the housing. A turning mirror within the sonde directs light to and from the sidewall (Figure S1). Fluorescence emissions are detected using a 150 mm focal length lens coupled to with linear dichroic filter stack that splits the collected light into 7 spectral bands, each with a discrete photomultiplier tube (PMT) coupled

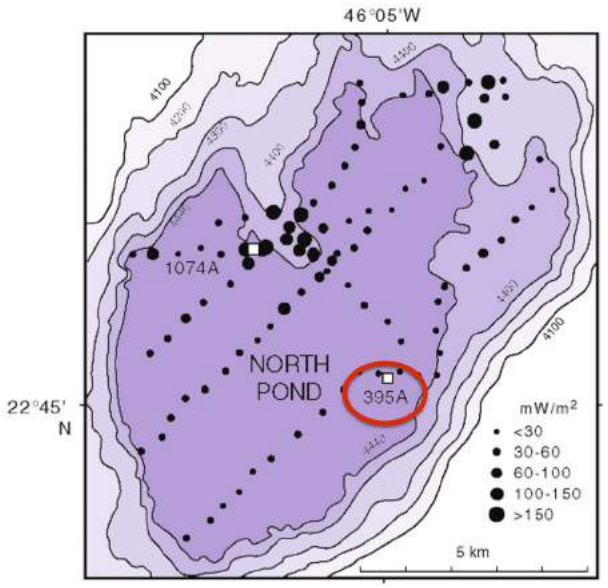

FIGURE 1 | Bathymetric map of North Pond showing the location of Hole 395A. The black circles represent a heat flow survey conducted during DSDP 78B (Langseth et al., 1992). Hole 395A was drilled during DSDP 45, and is located about 1 Km from the southeastern edge of North Pond (red circle).

to a filter and focusing lens. The optical design has a depth of field from the wall of the instrument to 16″ from the instrument. The bandpass filters associated with each PMT was used to detect fluorescence emissions from the 280 to 455 nm with 20 nm bandwidths (full-width-half-max). The center wavelengths are set at 280, 300, 320, 340, 360, 380, and 455 nm. The instrument is also equipped with a pinhole camera that records video of the downhole logging operation to provide spatial context to the fluorescence information. Additional tool specifications are given in Table S1.

RESULTS

DEBI-t was deployed as part of what was designated the microbiology combination tool string, with sondes that recorded 3-axis downhole acceleration, 3-axis magnetic field, temperature and total and spectral (Th, U, K) gamma-ray measurements (Figure S2). These measurements were used to correlate fluorescence data to physical properties collected for Hole 395A during previous expeditions. The instrument utilized a "fire and forget" methodology, in which the embedded control software directed the instrument to fire the laser, collect data and transmit information uphole when power was supplied. Power and real-time telemetry were supplied via a 24 V power supply in the multi-function telemetry module (MFTM). During logging operations, DEBI-t transmitted real-time clock, laser power and detector status to provide the operators on the ship with information regarding downhole *in situ* conditions.

The microbiology combo string was deployed immediately after removal of the old CORK, to minimize introduction of bottom water contaminants. During logging operations at Hole

395A, the instrument acquired native fluorescence data during two complete passes of the borehole, where logs were obtained in both the downhole and uphole directions. Comparison of DEBI-t with mid-Atlantic ocean water and bacterial standards showed a unique spectral signature for the borehole data that was distinct from ocean water (Figure S3).

Data collected in 395A was analyzed using a Support Vector Machine (SVM). SVMs are supervised learning algorithms, which find an optimum hyperplane that maximizes the separation, or margin, between two classes. The function used to describe this hyperplane can be specified by a training set, known as support vectors. For this investigation, the two classes used were "microbe" and "non-microbe." A library of "microbe" data was constructed from spectral information collected using bacteria, bacterial spores and archaea, while tryptophan, phenylalanine and tyrosine mixtures were used to construct the "non-microbe" dataset. The library data used to train the SVM was acquired using the DEBI-t with the same acquisition parameters used for the logging data. Because the chemical information in the standards produced a library that was non-linear (**Figure 2**) a Laplacian kernel was used to optimize the hyperplane. The DEBI-t logging data from 395A was then input into the SVM to be classified as "microbe" or "non-microbe." A conservative value of 95% confidence was used categorize data points as microbial. Results of logging data for Hole 395A demonstrated a significant presence data points that were consistent with microbial signals. Data for the first downhole pass indicated an increase in the detected biomass, with the biggest change occurring below 450 m below sea floor (**Figure 3**). Data from the subsequent uphole and downhole passes showed an increased homogenization of this signal, suggesting disturbance of the hole resulting from the tool string's movement through the borehole. The collected video data (Movie M1) showed an abundance of orange particulate material within the borehole, which may be interpreted as aggregated iron hydroxide particles and microbial flocs.

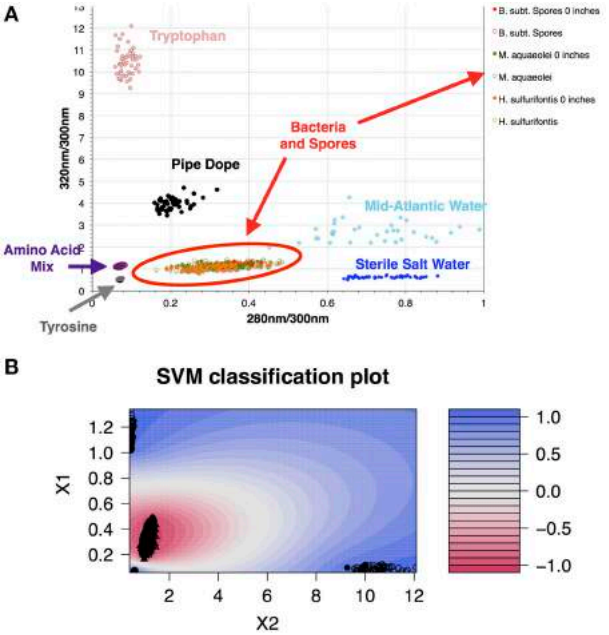

FIGURE 2 | A library of organics and microbes was used to classify data collected at Hole 395A. The database was classified in a binary form: "microbe" and "organic." **(A)** Scatter plot of the standards used for classifying the data collected with DEBI-t. Because the instrument had a long depth of focus, the data was collected at two distances: just in front of the turning mirror (0 inches); and 10 inches from the turning mirror. Fluorescence spectra from all bacterial standards collected at both distances clustered in the same location (red oval); **(B)** SVM contour plot with the fitted decision values using the library. A semi-supervised Laplacian kernel was used to train the SVM. The scale (right) shows the decision boundary values for the two sets, with −1 denoting the "most microbe-like," and +1 denoting the "most organic-like," or "least microbe-like."

DISCUSSION

Using published data for the fluorescence cross-section of microbes with deep UV excitation and the instrument optical parameters (Faris et al., 1997; Bhartia et al., 2010), we can estimate that the bioload within Hole 395A is approximately 10^4–10^5 cells per mL (**Figure 3**), which is greater than the reported cell density of the overlying bottom water (Meyer et al., 2012). The calculated density is dependent on the effective view volume of the instrument. Although DEBI-t has a nominal view volume of 1–2 ml assuming the full depth of field of the instrument. However, particulate matter, evident in the video data collected in line with the spectral data (Movie M1), indicate that the effective view volume was significantly reduced and a majority of the signal was collected from around the focused spot, which we estimate to be between ca. 10 ∼ 200 uL. This suggests that the bulk of the signal originated within the water column, not the wall, and were either planktonic microbes or attached to the particulates.

To ascertain the possibility that the detected signals were the result of cells transported through the crust, a simple box model was used to estimate the discharge of cells into the borehole. The transport and filtration of microbes through subsurface environments has been extensively studied, but the factors contributing to this process are still poorly constrained (Tufenkji, 2007). Several aspects can influence adhesion of a microbe onto a surface: substrate surface charge, microbial-surface zeta potential, nutrient availability, fluid flow, among others (Harvey et al., 2002; Tufenkji, 2007; Boks et al., 2008). However, while transport and accumulation behavior is still under intensive investigation, classical colloid filtration theory (CFT) is currently used by researchers to model and evaluate microbial subsurface transport (Ginn et al., 2002; Tufenkji, 2007). Under CFT, adhesion of bacteria onto a surface can be reduced to a few parameters that make up the following equations:

$$\ln(C_x) = \ln(C_0) - K \quad (1)$$

$$K = \frac{K_d L}{V} \quad (2)$$

$$K_d = \frac{3}{2}\frac{(1-\theta)}{d}\eta\alpha U \quad (3)$$

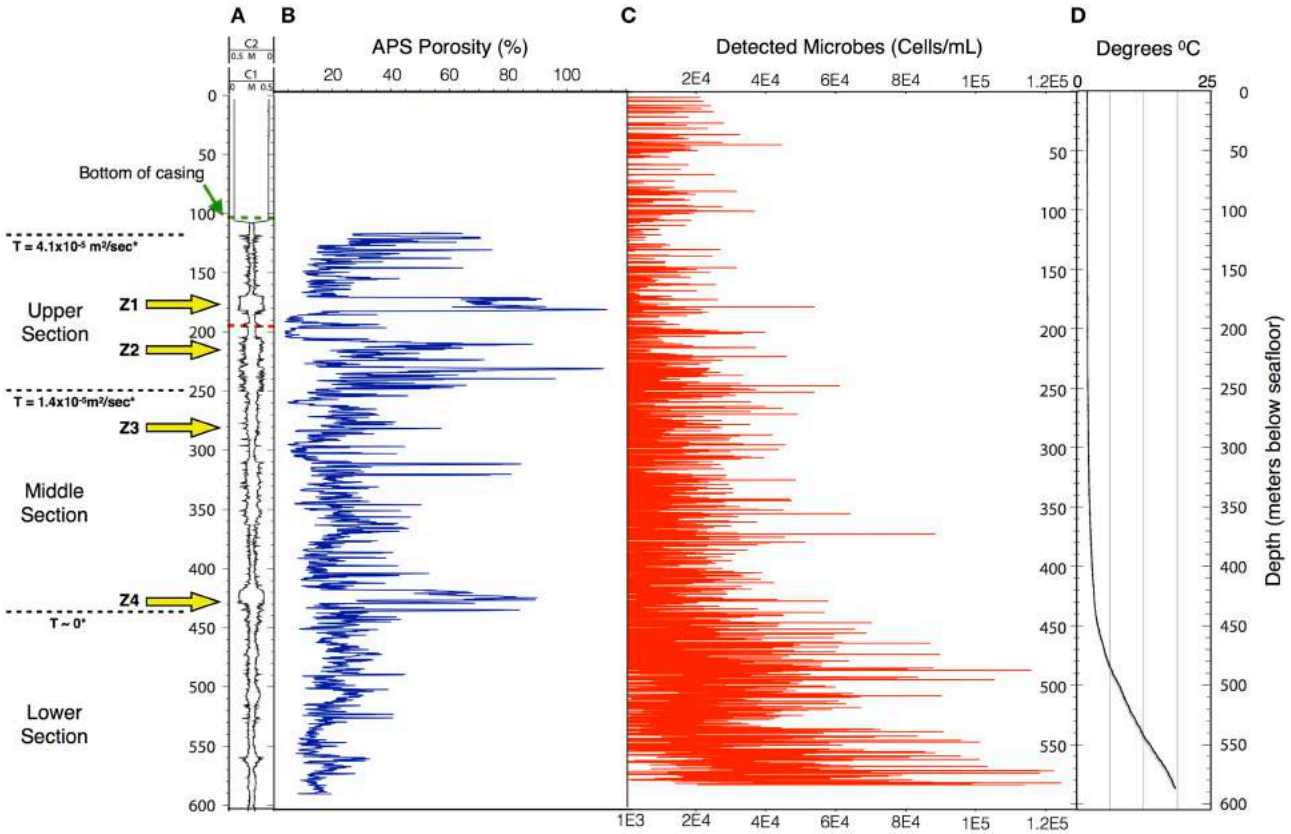

FIGURE 3 | The structure of the microbe-like signature within Hole 395A appears to be indicative of settling. The overall density of microbes increases with depth in Hole 395A. **(A)** Caliper data taken for Hole 395A during ODP Leg 174B; C1 = FMS pass 1, C2 = FMS pass 2; green hash line = location of bottom of casing, red hash line = location of drill pipe for second logging attempt during IODP Expedition 336; location of inflow zones (yellow arrows) is based on spontaneous potential log from Hole 395A collected during ODP Leg 174B; T = hydraulic transmissivity from Morin et al. (1992); based on transmissivity values, the hole was portioned into three sections. **(B)** APS porosity data collected during ODP Leg 174B. **(C)** Scatter plot showing the density range of detected spore signals during the first downlog; the density range is dependent on the excitation source's depth of penetration through the water column; red circles = upper estimate, black circles = lower estimate.; for modeling purposes. **(D)** Temperature profile of Hole 395A. Data is from ODP Leg 174B and IODP Expedition 336. The temperature profile suggests a hydrologically isolated lower portion, which would be consistent with the observed structure of the microbial signatures.

where C_x = concentration of particles at some distance from the recharge zone, C_0 = the concentration of particles at the recharge zone, L = distance from the recharge zone, V = laminar flow velocity of the fluid, θ = porosity, d = grain diameter, η = contact efficiency, i.e., the rate at which a particle strikes a substrate divided by the rate at which the particle moves toward the substrate, α = attachment/filtration efficiency, i.e., the ratio between the number of collisions that succeed in producing attachment of a particle to a substrate divided by the total number of collisions, K_d = filtration coefficient, K = the reduction in particle number, and U = particle velocity/substrate porosity. In these models, adhesion is considered to be irreversible (Yao et al., 1971; Chang et al., 1983; Tong et al., 2005; Tufenkji, 2007). Assuming a particle diameter of 1 μm, η can be estimated to be approximately 10^{-2}–10^{-3} (Yao et al., 1971; Harvey and Garabedian, 1991), while fieldwork has produced values of α on the order of 7×10^{-3} for microbes (Harvey and Garabedian, 1991; Schijven et al., 2000). Filtration efficiencies for endospores are, on average, about 1/3 those of vegetative cells (Chang et al., 1983; Schijven et al., 2000). It is unclear where the recharge zones for North Pond are located; however, subsurface flow is thought to flow from southeast to northwest (Becker et al., 2001, 2012). For simplicity, we assume that recharge occurs in the exposed basalt approximately 1100 m to the southeast of North Pond. Finally, cell concentrations in Mid-Atlantic Ocean Bottom Water are estimated to be on the order of 10^4 cells/mL (Meyer et al., 2012).

The resulting filtration model suggests that cells would be filtered out of the porewater long before arrive at the location of 395A (**Figure 4**). Although the lack of constraints leads to a wide scope of concentrations as a function of distance, the general trend remains the same. Given the known hydrology of Hole 395A (Langseth et al., 1984; Morin et al., 1992; Becker et al., 2001), it was assumed that the bulk of fluids discharged into the hole came from 4 inflow zones (**Figure 3**). A simple box model (Supplementary Material) was constructed to estimate the expected concentration of cells within the borehole after 13 years of isolation from the overlying bottom

water (**Table 1**). Fluid velocities through these inflow regions were estimated to be approximately 100 m per year (Wheat, personal communication). Results from these models suggest that transport could not lead to the observed cell densities (**Figure 3**).

TABLE 1 | Assumptions used for calculating microbial transport model.

Estimated cell density in Mid-Atlantic Ocean Bottom Water (cells/mL)	$\sim 10^{4}$*
Estimated spore density in Mid-Atlantic Ocean Bottom Water (spores/mL)	$\sim 10^{3}$*
ESTIMATED CELL FLUX FROM EACH INFLOW ZONE (cells*m^{-2}*yr^{-1})	
Inflow Zone 1	2.4×10^{8}
Inflow Zone 2	1.5×10^{8}
Inflow Zone 3	1×10^{8}
Inflow Zone 4	6×10^{7}
ESTIMATED SPORE FLUX FROM EACH INFLOW ZONE (spores*m^{-2}*yr^{-1})	
Inflow Zone 1	2.4×10^{9}
Inflow Zone 2	2.4×10^{9}
Inflow Zone 3	2×10^{9}
Inflow Zone 4	1.5×10^{9}
Estimated vertical velocity for spores and cells (m*yr^{-1})	31.5**

*Cell densities are estimated from work carried out during Maria S. Merian Expedition 20/5 (Meyer et al., 2012). Discharge numbers for cells and spores were calculated using estimates from the transport model and laminar flow calculations based on data collected during ODP Leg 174B. **Vertical transport velocity calculated from published work measuring settling rates of spore and spore-like particles (Kempf et al., 2005).*

Analysis of geophysical data also failed to correlate a relationship between areas of high inflow along the borehole sidewall and locations where biomass was detected. Porosity, density, and total gamma ray values where compared to microbial signals from DEBI-t using an iterative, non-hierarchical cluster analysis (**Figure 5**). Areas of higher porosity, lower density, and lower gamma radiation would be indicative of regions with potentially higher lateral fluid flow (Crosby and Anderson, 1971; Helm-Clark et al., 2004). However, the variability in these parameters did not correlate with detected microbial fluorescence signals.

An alternative possibility is that the detected microbes were produced, *in situ*, by active communities residing along the borehole wall. In this case, the transport of microorganisms through the igneous crust could lead to the establishment of communities located within the outflow zones. Although the communities located on the outer walls would have been scraped off during drilling and subsequent reaming, the communities within the crust surrounding the borehole should have remained intact. Further, introduction of the CORK would have provided another substrate for microbes to attach to. The removed CORK was well oxidized, and given the microbial genomic data collected from other basalt zones (Emerson et al., 2007), there is the possibility that iron oxidizers were able to use the CORK as a potential energy source. If the detected signals within Hole 395A represent cells that detached and subsequently reattached to

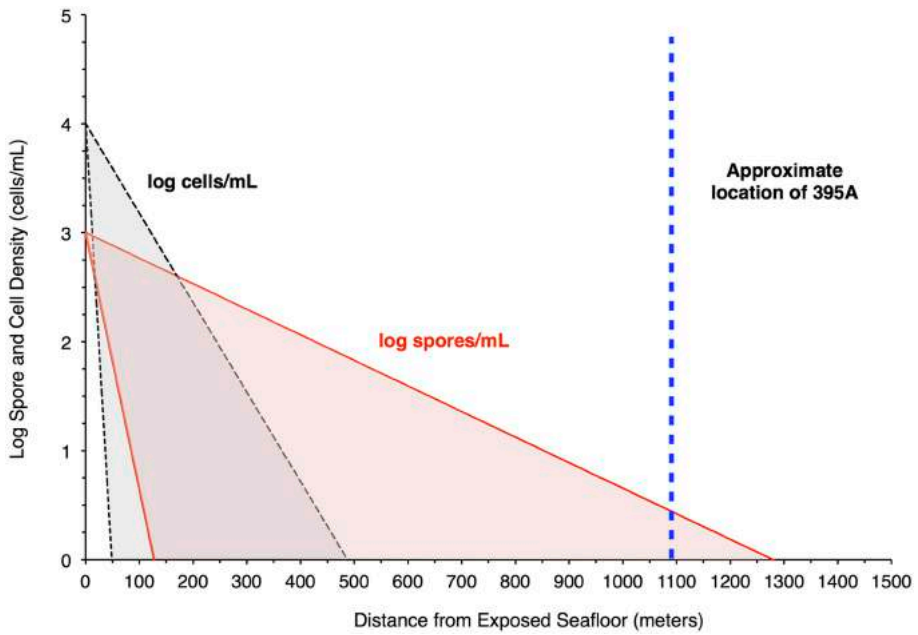

FIGURE 4 | Filtration of bacteria in the crust would produce higher spore densities in pore water 1 Km from a putative recharge zone. The plot shows results from a model that attempts to assess the likelihood of seeing a greater concentration of spores relative to bacteria in pore water at the location of Hole 395A. The red shaded area bordered by the red solid lines indicates the concentration of spores in pore fluids, while the gray shaded area bordered by the black hashed lines indicates the concentration of cells in pore fluids. The blue, hashed line is the location of Hole 395A relative to the exposed ocean crust southwest of North Pond, which serves as a putative recharge zone for purposes of modeling. The model suggests that spore densities will drop off less rapidly than cell densities in the pore fluids.

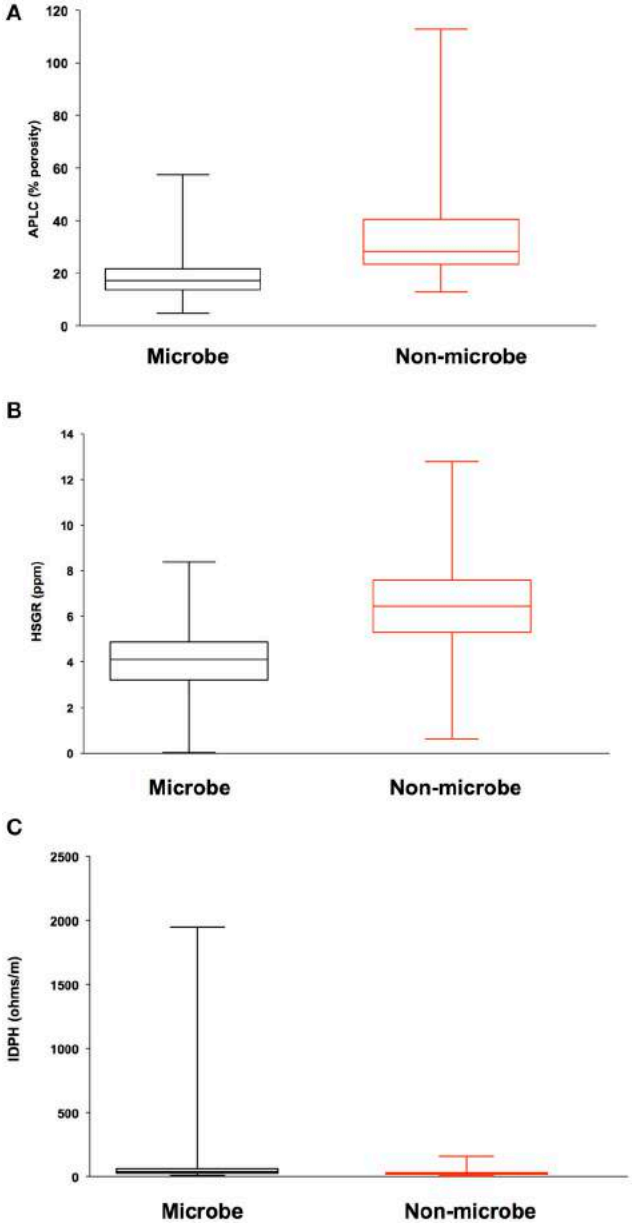

FIGURE 5 | Iterative Non-hierarchical Cluster Analysis (INCA) indicates no relationship between the structure of the detected microbial signatures and the lithological properties within 395A. Briefly, INCA is a variation on K-means clustering, in which objects are moved into and out of clusters, the number of which has been defined by the user (Harvey et al., in prep). The objective is to minimize the variability within clusters, while maximizing the variability between clusters. Resistivity, porosity, and gamma ray profiles for 395A were compared to the distribution of microbial signatures to determine if there was a relationship between the shape of the microbial data and the lithology of 395A. Results from INCA indicate no relationship between the observed structure of the microbial signals, and the lithology of 395A. Data are presented as box and whisker plots for simplicity, and indicate overlap with all physical properties data between the two categories (microbe and non-microbe) used in the analysis. **(A)** Accelerator porosity sonde; provides porosity information for the borehole wall; **(B)** hostile natural gamma ray sonde; used to provide information on lithology, e.g., rock vs. clay; **(C)** dual induction resistivity tool; provides spontaneous potential data that can be used to elucidate density, porosity, and lithologic boundaries.

particles within the borehole water column, then the population attached to the walls or CORK may be on the order of 10^4–10^5 cells/cm^3 in the upper portion of the hole, with the lower portion being comprised of material which settled to the bottom. Vertical transport of particle-attached microbes would be consistent with what is known about the physical nature of 395A, as the lowest 150 m of the hole is thought to be relatively impermeable (Langseth et al., 1992).

The presence of microbial cells in igneous oceanic crust has been previously inferred from petrographic observations of alteration textures in basaltic glass (Fisk et al., 1998), measurements of the presence of chemicals that are consistent with biology (carbon, nitrogen, phosphorous), observed the presence of morphological features interpreted as bacterial cell shapes (Banerjee and Muehlenbachs, 2003), and via molecular analysis of cored materials (Bach and Edwards, 2003). However, neither chemical nor trace fossil evidence can unequivocally prove the existence of microbial life in igneous ocean crust, nor demonstrate the timing of any inferred microbiological activities. Previous theoretical work on bioenergetics of alteration reactions has suggested that microbial communities should be supported as a result of water-rock reactions that occur in young igneous oceanic crust (Bach and Edwards, 2003). Despite these evidences, prior data establishing the *in situ* presence of microbial biomass in the oceanic crustal environment has been scant. Three previous studies have recovered, isolated, and analyzed DNA data from rocks recovered in the Atlantic and Pacific Oceans (Bach and Edwards, 2003; Mason et al., 2010; Santelli et al., 2010) and one has analyzed similar data from novel *in situ* rock colonization experiments conducted in young igneous oceanic crust (Orcutt et al., 2010). These studies have not established the ubiquity or abundance of life in the crust.

The deep marine biosphere has been hypothesized to potentially harbor up to 2/3 of the prokaryotic biomass on Earth, or 1/3 of the total biomass carbon (Whitman et al., 1998). Recent studies have called into question such estimates (D'Hondt et al., 2007; Kallmeyer et al., 2012), pointing out the fact that most data collected for the deep marine biosphere have been rendered largely from continental slopes and margins, which are organic-rich provinces on a global basis compared to the volumetrically more abundant open ocean provinces. Furthermore, it has been suggested that activity levels for the deep marine biosphere are exceptionally slow, with potential turnover rates of 1000 years (Jørgensen and D'Hondt, 2006). It is important to recognize, however, that all data collected to date that are considered as part of this ongoing census of deep life derives from marine sediments. No studies have considered cellular abundances or activities in the hard rock provinces below deeply buried sediments. It has been hypothesized, however, that any biosphere in the igneous ocean crust would have to be characterized by exceptionally low abundances and low activity owing to the fact that energy and nutrient resources in these provinces should be low (Jørgensen and D'Hondt, 2006). However, one recent study examining colonization of native rocks and minerals in the crust as well as the data presented herein suggest another interpretation is possible, and that the igneous oceanic crust may represent a vibrant and dynamic

deep biosphere (Orcutt et al., 2010). Further studies that employ technologies that enable enumeration and activity measurements in other crustal provinces are required to address this enigma.

MATERIALS AND METHODS

Bacterial Cultures

Bacteria were inoculated from frozen stocks into Luria-Bertani (LB) broth and grown overnight at 25°C, shaking at approximately 125 rpm. Archaeal cultures were provided by Victoria Orphan at Caltech. Spore samples were prepared as described in Kwan et al. (2011) and Kempf et al. (2005). All samples were washed 3 times in sterile 1% saline solution to remove all traces of growth media and other organics. Cells were then placed into 100 mm cuvettes containing a sterilized salt solution (36 per ml) at concentrations of approximately 10^5 cells/mL for data collection using DEBI-t.

Amino Acid Standards

HPLC-grade amino acids (Sigma-Aldrich) were used to create the amino acid standards. 1 mM stocks of tryptophan and tyrosine were prepared using 18 MOhm water. These stocks were then diluted to 100 uM concentrations in 100 mm cuvettes containing sterilized salt water.

Bench Setup for Library Standards

Because the penetration depth of the excitation source was not certain, a 100 mm cuvette was used to collect spectral information for standards (Figure S4). Data was collected at two positions; right behind the turning mirror, and 10 inches from the turning mirror. This was to ascertain any potential variation in the structure of the fluorescence spectra as a function of being in front of or behind the focal point. Result from this work indicated that there was no significant variation in the signals (**Figure 2**).

SIGNIFICANCE STATEMENT

This study describes the predominance of microbes within a marine borehole and postulates as to the potential source of this biomass. To the best of our knowledge, it represents the first set of microbial data collected *in situ*, and in real-time.

DEDICATION

This work is dedicated to the memory of Katrina Edwards and Gerardo (Gerry) Iturrino. The successful deployment of this instrument would not have been possible without their efforts. We are glad to have known them as colleagues and friends. Although we mourn their passing, we celebrate their lives and contributions, whose impacts will be felt for years to come.

ACKNOWLEDGMENTS

This research used data provided by the Integrated Ocean Drilling Program (IODP). Funding for this work was provided by the National Science Foundation, Sloan Foundation, NASA Astrobiology Institute (Icy Worlds 13NAI720024 and Life Underground NNA13AA92A publication #067) and NASA Astrobiology Science and Instrument Development (GURILA NNH10ZDA001N). The authors would like to thank Wolfgang Bach, C. Geoff Wheat, Clayton Furman, Eric Meissner and Tania Lado-Insua for logistical and analytical support during the deployment of DEBI-t. Part of this research was carried out at the Jet Propulsion Laboratory, California Institute of Technology, under a contract with the National Aeronautics and Space Administration. This work was supported by the NSF Science and Technology Center for Dark Biosphere Investigations (C-DEBI) (Award 0939564). Raw data is archived at the IODP-USIO Science Services website, administered by Texas A&M University.

SUPPLEMENTARY MATERIAL

The Supplementary Material for this article can be found online at: http://journal.frontiersin.org/article/10.3389/fmicb.2015.01260

REFERENCES

Bach, W., and Edwards, K. J. (2003). Iron and sulfide oxidation within the basaltic ocean crust: implications for chemolithoautotrophic microbial biomass production. *Geochim. Cosmochim. Acta* 67, 3871–3887. doi: 10.1016/S0016-7037(03)00304-1

Banerjee, N. R., and Muehlenbachs, K. (2003). Tuff life: bioalteration in volcaniclastic rocks from the Ontong Java Plateau. *Geochem. Geophys. Geosyst.* 4, 1037. doi: 10.1029/2002GC000470

Becker, K., Bartetzko, A., and Davis, E. E. (2001). Leg 174B synopsis: revisiting Hole 395A for logging and long-term monitoring of off-axis hydrothermal processes in young oceanic crust. *Proc. Ocean Drill. Progr. Sci. Res.* 174B, 1–13. doi: 10.2973/odp.proc.sr.174b.130.2001

Becker, K., and Davis, E. E. (2005). A review of CORK designs and operations during the Ocean Drilling Program. *Proc. Integr. Ocean Drill. Progr.* 301, 1–28. doi: 10.2204/iodp.proc.301.104.2005

Becker, K., Villinger, H. W., and Davis, E. E. (2012). *Initial Pressure Data from the IODP Expedition 336 CORKs at North Pond. 2012 American Geophysical Union* (San Francisco, CA), 1–2.

Bhartia, R., Hug, W. F., Salas, E. C., Reid, R. D., Sijapati, K. K., Tsapin, A., et al. (2008). Classification of organic and biological materials with deep ultraviolet excitation. *Appl. Spectrosc.* 62, 1070–1077. doi: 10.1366/000370208786049123

Bhartia, R., Salas, E. C., Hug, W. F., Reid, R. D., Lane, A. L., Edwards, K. J., et al. (2010). Label-free bacterial imaging with deep-UV-laser-induced native fluorescence. *Appl. Environ. Microbiol.* 76, 7231–7237. doi: 10.1128/AEM.00943-10

Boks, N. P., Norde, W., Van der Mei, H. C., and Busscher, H. J. (2008). Forces involved in bacterial adhesion to hydrophilic and hydrophobic surfaces. *Microbiology* 154, 3122–3133. doi: 10.1099/mic.0.2008/018622-0

Chang, P. W., Findley, J. E., and Yen, T. F. (1983). Selection of bacteria with favorable transport properties through porous rock for the application of microbial-enhanced oil recovery. *Appl. Environ. Microbiol.* 46, 1066–1072.

Crosby, J. W., and Anderson, J. V. (1971). Some applications of geophysical well logging to basalt hydrogeology. *Ground Water* 9, 12–20. doi: 10.1111/j.1745-6584.1971.tb03562.x

Daley, R. J., and Hobbie, J. E. (1975). Direct counts of aquatic bacteria by a modified epifluorescence technique. *Limnol. Oceanogr.* 20, 875–882. doi: 10.4319/lo.1975.20.5.0875

D'Hondt, S. (2002). Metabolic activity of subsurface life in deep-sea sediments. *Science* 295, 2067–2070. doi: 10.1126/science.1064878

D'Hondt, S., Abrams, L., Ferdelman, T. G., Fischer, J., Hasiuk, F., Kallmeyer, J., et al. (2007). Life in subseafloor sediments of the South Pacific Gyre. AGU Fall Meeting Abstracts 1:08.

D'Hondt, S., Spivack, A. J., Pockalny, R., Ferdelman, T. G., Fischer, J. P., Kallmeyer, J., et al. (2009). Subseafloor sedimentary life in the South Pacific Gyre. *Proc. Natl. Acad. Sci. U.S.A.* 106, 11651–11656. doi: 10.1073/pnas.0811793106

Emerson, D., Rentz, J. A., Lilburn, T. G., Davis, R. E., Aldrich, H., Chan, C., et al. (2007). A novel lineage of proteobacteria involved in formation of marine fe-oxidizing microbial mat communities. *PLoS ONE* 2:e667. doi: 10.1371/journal.pone.0000667

Faris, G. W., Copeland, R. A., Mortelmans, K., and Bronk, B. V. (1997). Spectrally resolved absolute fluorescence cross sections for bacillus spores. *Appl. Opt.* 36, 958–967. doi: 10.1364/AO.36.000958

Fisher, A. T., and Becker, K. (2000). Channelized fluid flow in oceanic crust reconciles heat-flow and permeability data. *Nature* 403, 71–74. doi: 10.1038/47463

Fisk, M. R., Giovannoni, S. J., and Thorseth, I. H. (1998). Alteration of oceanic volcanic glass: textural evidence of microbial activity. *Science* 281, 978–980. doi: 10.1126/science.281.5379.978

Ginn, T. R., Wood, B. D., Nelson, K. E., Scheibe, T. D., Murphy, E. M., and Clement, T. P. (2002). Processes in microbial transport in the natural subsurface. *Adv. Water Resour.* 25, 1017–1042. doi: 10.1016/S0309-1708(02)00046-5

Giovannoni, S. J., DeLong, E. F., Olsen, G. J., and Pace, N. R. (1988). Phylogenetic group-specific oligodeoxynucleotide probes for identification of single microbial cells. *J. Bacteriol.* 170, 720–726.

Harvey, R. W., and Garabedian, P. S. (1991). Use of colloid filtration theory in modeling movement of bacteria through a contaminated aquifer. *Environ. Sci. Technol.* 25, 178–185 doi: 10.1021/es00013a021

Harvey, R. W., Harms, H., and Landkamer, L. (2002). *Transport of Microorganisms in the Terrestrial Subsurface: In situ and Laboratory Methods. Manual of Environmental Microbiology*, *2nd Edn*. Washington, DC: ASM Press.

Helm-Clark, C. M., Rodgers, D. W., and Smith, R. P. (2004). Borehole geophysical techniques to define stratigraphy, alteration and aquifers in basalt. *J. Appl. Geophys.* 55, 3–38. doi: 10.1016/j.jappgeo.2003.06.003

Jørgensen, B. B., and D'Hondt, S. (2006). Ecology. A starving majority deep beneath the seafloor. *Science* 314, 932–934. doi: 10.1126/science.1133796

Kallmeyer, J., Pockalny, R., Adhikari, R. R., Smith, D. C., and D'Hondt, S. (2012). Global distribution of microbial abundance and biomass in subseafloor sediment. *Proc. Natl. Acad. Sci. U.S.A.* 104, 16213–16216. doi: 10.1073/pnas.1203849109

Kempf, M. J., Chen, F., Kern, R., and Venkateswaran, K. (2005). Recurrent isolation of hydrogen peroxide-resistant spores of Bacillus pumilus from a spacecraft assembly facility. *Astrobiology* 5, 391–405. doi: 10.1089/ast.2005.5.391

Kwan, K., Cooper, M., La Duc, M. T., Vaishampayan, P., Stam, C., Benardini, J. N., et al. (2011). Evaluation of procedures for the collection, processing, and analysis of biomolecules from low-biomass surfaces. *Appl. Environ. Microbiol.* 77, 2943–2953. doi: 10.1128/AEM.02978-10

Langseth, M. G., Hyndman, R. D., Becker, K., and Hickman, S. H. (1984). The hydrogeological regime of isolated sediment ponds in mid-oceanic ridges. *Init. Rep. Deep Sea Drill. Proj.* 78, 825–837.

Langseth, M. G., Becker, K., Herzen Von, R. P., and Schultheiss, P. (1992). Heat and fluid flux through sediment on the western flank of the Mid-Atlantic Ridge: a hydrogeological study of North Pond. *Geophys. Res. Lett.* 19, 517–520. doi: 10.1029/92GL00079

Mason, O. U., Nakagawa, T., Rosner, M., Van Nostrand, J. D., Zhou, J., Maruyama, A., et al. (2010). First Investigation of the microbiology of the deepest layer of ocean crust. *PLoS ONE* 5:e15399. doi: 10.1371/journal.pone.0015399

Meyer, J. L., Jaekel, U., Girguis, P. R., Glazer, B. T., and Huber, J. A. (2012). *Microbial life in Cold, Hydrologically Active Oceanic Crustal Fluids. 2012 American Geophysical Union* (San Francisco, CA), 1–2.

Morin, R. H., Hess, A. E., and Becker, K. (1992). *In situ* measurment of fluid flow in DSDP Holes395A and 534A: results from the dianaut program. *Geophys. Res. Lett.* 19, 509–512. doi: 10.1029/91GL02947

Nadeau, J. L., Perreault, N. N., Niederberger, T. D., Whyte, L. G., Sun, H. J., and Leon, R. (2008). Fluorescence microscopy as a tool for *in situ* life detection. *Astrobiology* 8, 859–874. doi: 10.1089/ast.2007.0043

Orcutt, B. N., Bach, W., Becker, K., Fisher, A. T., Hentscher, M., Toner, B. M., et al. (2010). Colonization of subsurface microbial observatories deployed in young ocean crust. *ISME J.* 5, 692–703. doi: 10.1038/ismej.2010.157

Roussel, E. G., Cambon Bonavita, A. M., Querellou, J., Cragg, B. A., Webster, G., Prieur, D., et al. (2008). Extending the sub-sea-floor biosphere. *Science* 320, 1046–1046. doi: 10.1126/science.1154545

Santelli, C. M., Banerjee, N. R., Bach, W., and Edwards, K. J. (2010). Tapping the subsurface ocean crust biosphere: low biomass and drilling-related contamination calls for improved quality controls. *Geomicrobiol. J.* 27, 158–169. doi: 10.1080/01490450903456780

Schijven, J. F., Medema, G., Vogelaar, A. J., and Hassanizadeh, S. M. (2000). Removal of microorganisms by deep well injection. *J. Contam. Hydrol.* 44, 301–327. doi: 10.1016/S0169-7722(00)00098-X

Schrenk, M. O., Huber, J. A., and Edwards, K. J. (2010). Microbial provinces in the subseafloor. *Ann. Rev. Mar. Sci.* 2, 279–304. doi: 10.1146/annurev-marine-120308-081000

Stein, C. A., and Stein, S. (1994). Constraints on hydrothermal heat flux through the oceanic lithosphere from global heat flow. *J. Geophys. Res.* 99, 3081–3081. doi: 10.1029/93JB02222

Tong, M., Camesano, T. A., and Johnson, W. P. (2005). Spatial variation in deposition rate coefficients of an adhesion-deficient bacterial strain in Quartz Sand. *Environ. Sci. Technol.* 39, 3679–3687. doi: 10.1021/es048850s

Tufenkji, N. (2007). Modeling microbial transport in porous media: traditional approaches and recent developments. *Adv. Water Resour.* 30: 1455–1469. doi: 10.1016/j.advwatres.2006.05.014

Whitman, W. B., Coleman, D. C., and Wiebe, W. J. (1998). Prokaryotes: the unseen majority. *Proc. Natl. Acad. Sci. U.S.A.* 95, 6578–6583. doi: 10.1073/pnas.95.12.6578

Yao, K. M., Habibian, M. T., and O'Melia, C. R. (1971). Water and waste water filtration. Concepts and applications. *Environ. Sci. Technol.* 5, 1105–1112. doi: 10.1021/es60058a005

Conflict of Interest Statement: The authors declare that the research was conducted in the absence of any commercial or financial relationships that could be construed as a potential conflict of interest.

frontiers in Microbiology

ORIGINAL RESEARCH
published: 07 September 2015
doi: 10.3389/fmicb.2015.00904

Carbon fixation by basalt-hosted microbial communities

Beth N. Orcutt[1,2], Jason B. Sylvan[2], Daniel R. Rogers[3,4], Jennifer Delaney[3], Raymond W. Lee[5] and Peter R. Girguis[3]**

[1] Bigelow Laboratory for Ocean Sciences, East Boothbay, ME, USA, [2] University of Southern California, Los Angeles, CA, USA, [3] Biological Laboratories, Harvard University, Cambridge, MA, USA, [4] Stonehill College, North Easton, MA, USA, [5] School of Biological Sciences, Washington State University, Pullman, WA, USA

OPEN ACCESS

Edited by:
Jennifer F. Biddle, University of Delaware, USA

Reviewed by:
Takuro Nunoura, Japan Agency for Marine-Earth Science and Technology, Japan
Mustafa Yucel, GEOMAR – Helmholtz Centre for Ocean Research Kiel, Germany
Arthur J. Spivack, University of Rhode Island, USA

***Correspondence:**
Beth N. Orcutt, Bigelow Laboratory for Ocean Sciences, 60 Bigelow Drive, P.O. Box 380, East Boothbay, ME 04544, USA borcutt@bigelow.org;
Peter R. Girguis, Biological Laboratories, Harvard University, Room 3085, 16 Divinity Avenue, Cambridge, MA 02138, USA pgirguis@oeb.harvard.edu

Specialty section:
This article was submitted to Extreme Microbiology, a section of the journal Frontiers in Microbiology

Received: *13 April 2015*
Accepted: *19 August 2015*
Published: *07 September 2015*

Citation:
Orcutt BN, Sylvan JB, Rogers DR, Delaney J, Lee RW and Girguis PR (2015) Carbon fixation by basalt-hosted microbial communities. Front. Microbiol. 6:904. doi: 10.3389/fmicb.2015.00904

Oceanic crust is a massive potential habitat for microbial life on Earth, yet our understanding of this ecosystem is limited due to difficulty in access. In particular, measurements of rates of microbial activity are sparse. We used stable carbon isotope incubations of crustal samples, coupled with functional gene analyses, to examine the potential for carbon fixation on oceanic crust. Both seafloor-exposed and subseafloor basalts were recovered from different mid-ocean ridge and hot spot environments (i.e., the Juan de Fuca Ridge, the Mid-Atlantic Ridge, and the Loihi Seamount) and incubated with ^{13}C-labeled bicarbonate. Seafloor-exposed basalts revealed incorporation of ^{13}C-label into organic matter over time, though the degree of incorporation was heterogeneous. The incorporation of ^{13}C into biomass was inconclusive in subseafloor basalts. Translating these measurements into potential rates of carbon fixation indicated that 0.1–10 nmol C g^{-1}_{rock} d^{-1} could be fixed by seafloor-exposed rocks. When scaled to the global production of oceanic crust, this suggests carbon fixation rates of 10^9–10^{12} g C $year^{-1}$, which matches earlier predictions based on thermodynamic calculations. Functional gene analyses indicate that the Calvin cycle is likely the dominant biochemical mechanism for carbon fixation in basalt-hosted biofilms, although the reductive acetyl-CoA pathway and reverse TCA cycle likely play some role in net carbon fixation. These results provide empirical evidence for autotrophy in oceanic crust, suggesting that basalt-hosted autotrophy could be a significant contributor of organic matter in this remote and vast environment.

Keywords: geomicrobiology, biogeochemistry, microbial ecology, ocean crust, basalt, deep biosphere, carbon fixation

Introduction

Oceanic crust is the largest aquifer on Earth, with the entire volume of the ocean circulating through the crust on the order of every 10^5–10^6 years (Fisher and Becker, 2000). This "subsurface ocean" within the oceanic crust is a site of geologically rapid chemical exchange between the crust and the oceans, which has ramifications on global chemical cycles (Edmond and Von Damm, 1983; Stevens and McKinley, 1995; Alt and Mata, 2000; Bach and Edwards, 2003; Bach et al., 2004). Moreover, this aquifer comprises a massive potential habitat for microbial life, yet very little is known about the rates of microbial activity in this environment (Orcutt et al., 2011b). Knowledge of metabolic reactions occurring in the oceanic crust is sparse because accessing pristine samples

for microbiological investigation from this environment is technologically challenging. Most information about microbial activity in ocean crust comes from (i) the quantity and speciation of chemical constituents within rocks or fluids collected from the subsurface or at the seafloor (e.g., Bach and Edwards, 2003; Wheat et al., 2003; Rouxel et al., 2008; Wheat et al., 2010), (ii) functional genes observed in environmental DNA (Mason et al., 2010), or (iii) incubations of mineral substrates in the environment or in the laboratory as a proxy for natural processes (Edwards et al., 2003a,b; Templeton et al., 2009; Toner et al., 2009; Orcutt et al., 2011a). Two recent studies provided the first empirical assessment of microbial sulfate reduction activity in hot and anoxic subsurface ocean crust settings (Lever et al., 2013; Robador et al., 2014).

Determination of rates of microbial activity is essential for evaluating the impact of crustal biosphere microbial activity on global elemental budgets and for understanding the mechanisms for growth and survival of life in this environment. In particular, the sources, sinks, and cycles of carbon in the crustal biosphere are important to understand, since (i) carbon is the primary building block for life, (ii) igneous oceanic crust is a sink for carbon from the oceans (Alt and Teagle, 1999), and (iii) the crustal reservoir is immense (Orcutt et al., 2011b). The potential impact of microbial carbon fixation in the crustal biosphere is unknown, however, as empirical assessments of rates of autotrophy are lacking. One recent study suggests that organic matter in hot and anoxic ocean crust is chemosynthetic in origin (McCarthy et al., 2011), while another recent study suggests that this system is net heterotrophic (Lin, 2013); however, rates of carbon cycling are unconstrained. Are there significant rates of endogenous carbon fixation that alter the inorganic carbon budget in the crust, therefore impacting the sink of inorganic carbon in vein formation? Or, conversely, are the rates of autotrophic carbon production overshadowed by heterotrophic consumption of carbon?

Using theoretical modeling, Bach and Edwards (2003) predicted that aerobic and anaerobic (NO_3-dependent) Fe- and S-oxidation could support $\sim 50 \times 10^{10}$ g C year^{-1} of autotrophic primary production in oceanic crust, with H_2-based sulfate reduction and methanogenesis supporting an additional $1–10 \times 10^{10}$ g C year^{-1} (assuming production of hydrogen from water-rock reactions). Furthermore, these calculations suggest that H_2 reduction of Fe oxides, nitrate, and oxygen could also support $10^{10}–10^{12}$ g C year^{-1} each, assuming available hydrogen and oxidized species are present. These autotrophic primary production rates of $>10^{12}$ g cellular carbon per year are similar in magnitude to the rate of heterotrophic organic consumption in sediment, indicating that autotrophic processes in the oceanic crust could be significant contributors to the local, and potentially global, C cycle.

A survey of environmental DNA from seafloor-exposed basalt collected from the Juan de Fuca Ridge revealed the presence of genes for proteins involved in carbon fixation processes (RuBisCO, ATP citrate lyase, and methyl-coenzyme M reductase; Mason et al., 2009), providing further support for the existence of autotrophy in this environment. Other recent work demonstrates significant extracellular enzyme activity for organic substrates from seafloor-exposed basalt-hosted microbial communities, with activities that are comparable to other marine environments such as marine sediment, marine snow particles, and mangroves (Jacobsen Meyers et al., 2014). However, the methodology in that study could not distinguish between autotrophic and heterotrophic activity, leaving relative rates of autotrophic activities on basalt unknown. Thus, to our knowledge, there are no empirical measurements of carbon fixation activity from either seafloor-exposed or subsurface ocean basalts.

To constrain the potential for chemoautotrophic carbon fixation by basalt-hosted microbial communities, and to identify microbial groups involved in autotrophy, we conducted incubation experiments with stable isotope tracers, as well as quantitative analysis of target gene abundance, with seafloor basalt samples collected from a mid-ocean ridge seamount (the Axial Seamount on the Juan de Fuca Ridge, NE Pacific Ocean), a mid-plate hotspot (Loihi Seamount, offshore Hawaii), and on the flank of a mid-ocean ridge (North Pond, Mid-Atlantic Ridge, Atlantic Ocean; **Figure 1**). Subsurface basalt samples from North Pond collected during scientific ocean drilling were also included in the experiments, to examine the potential for this process in the crustal deep biosphere. Basalt samples with a range of alteration from these different locations were incubated with ^{13}C-labeled sodium bicarbonate over the course of hours to days to months, and incorporation of ^{13}C into organic matter was evaluated using isotope ratio mass spectrometry (IRMS) as a proxy for carbon fixation activity. Our results reveal the potential for autotrophic carbon fixation in basalt biofilms, as demonstrated by the enrichment of ^{13}C-label of organic matter over time. We compare these potential rates of carbon fixation to recently available data on extracellular enzyme activity of basalt-hosted microbial communities to surmise the relative contribution of autotrophic processes to fueling the basalt biosphere. When one considers the relatively large volume of this habitat, even the modest carbon fixation rates determined in this study suggest that basalt-hosted autotrophy may be a significant source of fixed carbon for the deep ocean environment.

Materials and Methods

Sample Collections and Descriptions

Nine different basalt samples were used in this study, collected from three different crustal formation areas (**Figure 1A**; **Table 1**). One glassy, seafloor-exposed basalt came from the ASHES vent field in the Axial Seamount volcano caldera on the Juan de Fuca Ridge off the western coast of North America (**Figure 1C**). The sample was collected in 2009 with the *Alvin* submersible during dive AD-4527 on RV *Atlantis* cruise AT15-51 (Sample JdF2009). The basalt piece had a thick (up to 1 cm depth) glassy rim overlying moderately to sparsely vesicular cryptocrystalline groundmass (**Figure 1D**). A film of iron oxide discoloration was evident in the contact between the glass and groundmass. Two altered, seafloor-exposed basalts were collected from the Loihi Seamount off the coast of the big

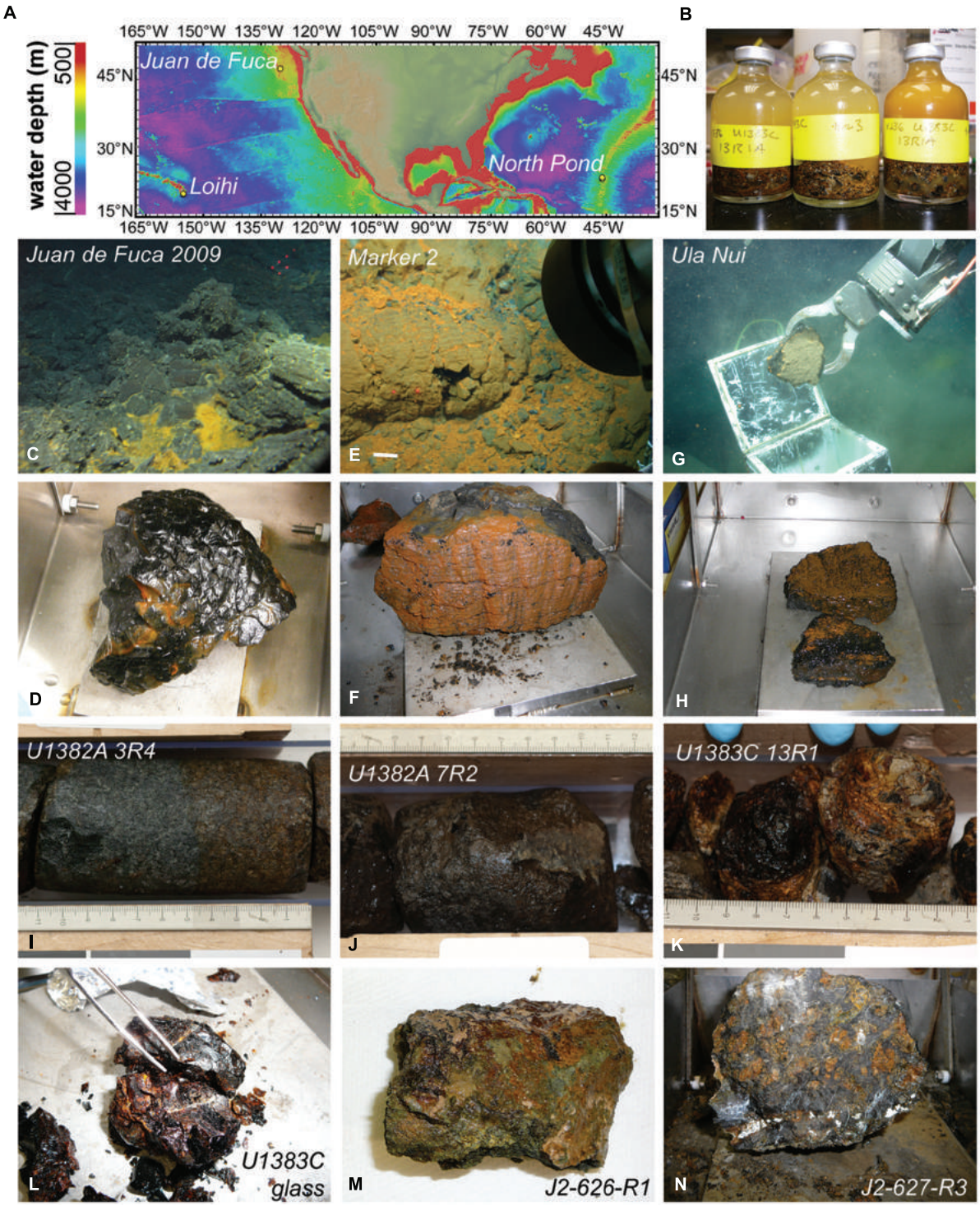

FIGURE 1 | Locations and photographs of samples used in the study. (A) Location map with bathymetry contours created using GeoMapApp (Ryan et al., 2009). **(B)** Example of sample incubation set up. **(C)** Location of glassy basalt (in **D**) collected from the Juan de Fuca Endeavor Ridge. **(E)** Iron oxide stained basalts (in **F**) collected from within Pele's Pit on the summit of the Loihi Seamount offshore Hawai'i. **(G)** Collection of iron oxide stained basalt (in **H**) from the Ula Nui ultradiffuse hydrothermal vent site at the base of the Loihi Seamount. Massive basalts with pervasive oxidation were collected from Hole U1382A sections 3R **(I)** and 7R **(J)** at North Pond, whereas glassy basalts were collected from Hole U1383C sections 13R **(K)** and 19-21R **(L)**. Manganese encrusted altered basalts were collected from the seafloor of North Pond on dives J2-626 **(M)** and J2-627 **(N)**. Photos in **(B,D,F,H,L–N)** by B. Orcutt; photos in **(C,E,G)** are copyright Woods Hole Oceanographic Institution; photos in **(I–L)** previously published (Expedition 336 Scientists, 2012c,d) and reprinted here with permission of the Integrated Ocean Drilling Program.

TABLE 1 | Characteristics of the basalt samples used in this study, including date of collection, cruise and dive number of collection, water depth of sample, depth below seafloor, latitude, longitude, and weight percent organic carbon (OC; listed as average ± 1 standard deviation; *n* = 3–12).

Sample ID	Date	Cruise/dive	Water depth [m]	Depth [mbsf]	Lat.	Lon.	OC [%]
JdF 2009	2009-08-22	AT15-51/AD4527	1545	0	45.934	−130.014	0.030 ± 0.007
Ula Nui	2009-10-07	KM09-23/J2-477	4987	0	18.707	−155.184	0.058 ± 0.022
Marker 2	2009-10-12	KM09-23/J2-481	1178	0	18.909	−155.257	0.058 ± 0.024
U1382A 3R4	2011-10-06	IODP X336/NA	4483	118	22.589	−46.082	0.045 ± 0.024
U1382A 7R2	2011-10-06	IODP X336/NA	4483	154	22.589	−46.082	0.023 ± 0.017
U1383C 13R1	2011-10-25	IODP X336/NA	4414	173	22.802	−46.053	0.018 ± 0.001
U1383C glass	2011-10-25	IODP X336/NA	4414	∼220	22.802	−46.053	0.025 ± 0.016
J2-626-R1	2012-04-23	MSM20-5/J2-626	3949	0	22.469	−46.036	0.053 ± 0.036
J2-627-R3	2012-04-24	MSM20-5/J2-627	3875	0	22.751	−46.056	0.024 ± 0.006

AD, HOV Alvin dive; AT, R/V Atlantis; J2, ROV Jason II dive; KM, R/V Kilo Moana; IODP, Integrated Ocean Drilling Program; mbsf, meters below seafloor; MSM, R/V Maria S. Merian; NA, not applicable.

island of Hawai'i in October 2009 by *ROV Jason-II* during the FeMO2009 cruise on the R/V *Kilo Moana* (cruise KM09-23): one from "Marker 2" in Pele's Pit on the summit of the Loihi Seamount (**Figure 1E**, Sample Marker 2), and one from the Ula Nui vent field at the base of the Loihi Seamount (**Figure 1G**, Sample Ula Nui). Sample Ula Nui, collected on dive J2-477, was glassy, highly vesicular, and friable, contained ∼3 mm olivine phenocrysts, and displayed visible iron oxide staining (**Figure 1H**). Sample Marker 2, collected on dive J2-481 from an area away from diffuse venting, was pillow basalt with an altered rind (**Figure 1F**). Both of the Loihi basalts used in this study were also used in a recent study to examine extracellular enzymatic activity by basalt-hosted microbial communities (Jacobsen Meyers et al., 2014). The remaining six basalts were collected from "North Pond," a small sediment pond located to the west of the Mid-Atlantic Ridge (**Figure 1A**). Four subsurface samples were collected in October 2011 during scientific ocean drilling on Integrated Ocean Drilling Program (IODP) Expedition 336 from Hole U1382A Sections 3R4 (**Figure 1I**) and 7R2 (**Figure 1J**), and from Hole U1383C Section 13R1 (**Figure 1K**) and a mixture of altered glassy basalt from sections 19R-21R (**Figure 1L**). Samples U1382A 3R4 and U1382A 7R2 were phyric massive basalts with varying degrees of oxidation, while the samples from U1383C were extrusive glassy basalts with abundant iron oxide staining (Expedition 336 Scientists, 2012c,d). Finally, two seafloor-exposed rocks were collected from outcrops surrounding North Pond in April 2012 by ROV *Jason-II* on dives J2-626 (**Figure 1M**) and J2-627 (**Figure 1N**) during the MSM20-5 cruise on the R/V *Maria S. Merian*. The J2-626-R1 rock was a breccia of mm- to cm-sized clasts of aphanitic basalt in a greenish-gray matrix, while the J2-627-R3 rock was a highly serpentinized harzburgite (25–30% orthopyroxene surrounded by completely serpentinized olivine and with chrysotile-filled veins; W. Bach, personal communication).

Incubations

Upon retrieval of the samples on board the research vessel, all seafloor-exposed rocks and surrounding water from the plastic sampling containers ("bioboxes") were immediately transferred to glass jars and placed at 4°C until processing, as described elsewhere (Santelli et al., 2008). Basalts were then transferred to ethanol- and flame-sterilized steel processing trays and subsampled with ethanol- and flame-sterilized chisels and tweezers. The experiments utilized the glassy rims of the basalts, which were removed, broken into smaller pieces (<1 cm diameter) and transferred to sterile glass serum vials (30–100 ml volume, depending on experiment) containing 0.2-mm-mesh filter-sterilized oxic bottom seawater. All samples were maintained at 4°C.

The subsurface basalts from North Pond were collected by extended core barrel (XCB) coring as described in detail elsewhere (Expedition 336 Scientists, 2012a,b). Briefly, samples were transferred from the core barrel into sterile plastic bags using 500°C heat-sterilized aluminum foil. Samples were rinsed three times with 0.2-μm-mesh filter-sterilized, autoclaved seawater to remove potential exterior contamination (Expedition 336 Scientists, 2012c,d), as XCB cores are often contaminated on recovery (Smith et al., 2000); this may have also removed some surface-exposed biofilm microbes. Contamination testing with fluorescent microspheres indicated a lack of contamination of all rocks after washing, with the exception of some of the U1383C glassy basalts, as described in detail elsewhere (Expedition 336 Scientists, 2012c,d). Samples were broken apart in a flame-sterilized, stainless steel processing tray as above, then crushed into smaller fragments in a flame-sterilized mechanical metal rock mill.

Basalt fragments (5–20 cm^3) were transferred to sterile and baked glass serum vials (to remove organics, vials had been heated to 500°C for 2 h), which were filled to overflowing with sterile oxic seawater then sealed with autoclaved butyl rubber septa and aluminum crimp seals. Multiple replicate bottles were prepared for each sample to enable as many time series as possible with the limited sample volume, including a no-tracer-addition control.

Time series samples were injected with a small volume of 0.2-μm filter-sterilized ^{13}C-bicarbonate-labeled solution (in sterile filtered seawater) to achieve the following starting concentrations: JdF2009 incubations received a final concentration of 0.75 mM ^{13}C-labeled bicarbonate against a background of seawater bicarbonate (∼2 mM, or, 27% ^{13}C label); the Ula Nui and Marker 2 rock incubations received

a final concentration of 2.7 mM ^{13}C-labeled bicarbonate in background bottom seawater (57% ^{13}C label); the subsurface North Pond basalt incubations contained a final concentration of 1 mM ^{13}C-labeled bicarbonate in background surface seawater (33% ^{13}C label); and the seafloor-exposed North Pond basalt incubations contained a final concentration of 4.5 mM ^{13}C-labeled bicarbonate in surface seawater (69% ^{13}C label). Vials were incubated in the dark at 4°C until sampling. At each time point, the vials were opened and rock fragments were transferred to sterile plastic centrifuge tubes and frozen for shore-based DNA and organic carbon extraction and analysis. For the JdF2009, Marker 2, and Ula Nui samples, time series were stopped after 1 h, 1 day, and 1 week of incubation. The North Pond samples were incubated for 2-weeks, 2-months, and 4-months intervals. Final concentrations of dissolved inorganic carbon were not measured, as rates of carbon consumption were presumed to be significantly slow compared to the bulk pool size, which is supported by our results.

Organic Carbon Quantification, Carbon Stable Isotopic Analysis, and Potential Fixation Rates

The carbon content and stable carbon isotopic composition of biofilms on the incubated basalts were determined by IRMS analysis of subsamples of the basalts that had been stored frozen. Aliquots of the basalt were bathed in acidified deionized water (pH 3, with HCl) in acid-cleaned glassware, with addition of fresh solution repeated after 1 h, to remove any traces of carbonate. Remaining rock residue was dried under vacuum at 60–70°C, then pulverized in an acid-cleaned mortar and pestle to a sand-like granularity. Aliquots were transferred to acid-washed glass vials or aluminum foil prior to analysis. Dried samples of basalt (20–70 mg) were placed into tin foil capsules for isotopic analysis of ^{13}C/^{12}C ratios. Samples were analyzed using a Costech elemental analyzer in line with a Micromass Isoprime continuous flow stable isotope mass spectrometer. The zero-blank autosampler was purged with helium gas to reduce background atmospheric contamination. Sample size was optimized to gain a sample peak equivalent or higher to reference material with 0.08 mg of carbon used to calibrate sample runs. Results are presented in the standard δ notation, where isotopic ratios (R) are expressed in per mil (‰) differences relative to the conventional standard, the PeeDee Belemnite limestone where (Eq. 1):

$$\delta = \left(\frac{R_{sample}}{R_{standard}} - 1\right) \times 1000$$

The isotopic ratio (^{13}C/^{12}C) of the standard reference material (R_{standard}) was 0.0111796, and routine precision for δ^{13}C was 0.3‰ based on the standard deviation of ten replicate measurements of reference material.

Potential carbon fixation rates were determined based on ^{13}C-bicarbonate label uptake into organic matter over time. First, the isotopic ratio of the sample (R_{sample}) was calculated by rearranging Eq. 1. The mass change in carbon labeling between time points and the time zero sample was calculated based on the change in isotopic ratios (Δ ^{13}C/^{12}C) and grams of carbon per gram rock (from the average organic carbon percentage of the sample set; averages and 1 standard deviation reported in **Table 1**), assuming no change in the quantity of organic matter between time points. The rate of change, expressed as nmol C incorporated $g^{-1}{}_{rock}$ d^{-1}, was then calculated by dividing the mass change by the time period and correcting for the ratio of ^{13}C-label in the substrate pool. Thus, the degree of incorporation, or isotopic composition, will depend on the moles of labeled carbon incorporated into biomass and the pre-existing quantity of organic carbon. Due to very small and inconsistent changes in the carbon ratio as well as very low organic carbon content in the subsurface North Pond basalts (as described below, and see **Table 1**), rates were only calculated for seafloor-exposed basalts. Furthermore, although the instrument precision was established as 0.3‰, rates of change were conservatively assumed to be robust if there was more than a 2‰ difference between samples; values less than 2‰ difference are reported as below the detection limit (b.d.l.).

DNA Extraction and Quantitative Polymerase Chain Reaction (qPCR) Analysis of Genes

DNA was extracted from aliquots of the incubated basalts from the JdF2009, Ula Nui and Marker 2 samples that had been stored frozen (−80°C) until analysis. Upon thawing on ice, roughly 0.5–1 g of basalt fragments were transferred via a sterile spatula and roughly ground in a sterilized mortar. DNA was extracted from roughly 0.5 g of this material using the PowerSoil® DNA Isolation Kit (MO BIO Laboratories, Inc.) with the following modifications to the manufacturer's protocol: the cell lysis procedure consisted of two rounds of heating the sample (80°C for 5 min) and then bead beating (6 m/s for 60 s on a FastPrep-24™ Instrument, MP Biomedicals). DNA was eluted in 100 μL of solution C6 (10 mM Tris) according to the manufacturer protocols. DNA concentrations were determined by fluorometry using the Qubit dsDNA® HS Assay kit (Life Technologies Corporation) following the manufacturer instructions.

The abundance of taxonomic marker (i.e., 16S rRNA gene) and various functional genes for carbon cycling pathways was quantified by qPCR using the primer combinations outlined in **Table 2**. QPCR was performed on a Stratagene MX3005P using the iTaq Universal SYBR Green mix (Biorad Inc.). Bacterial 16S rRNA genes, RuBisCO form II enzyme genes of the reductive pentose phosphate cycle/Calvin-Benson-Bassham cycle (*cbbM*), methyl coenzyme M reductase genes of the reductive acetyl-CoA pathway (*mcrA*), and ATP citrate lyase genes of the reverse TCA cycle (*aclB*) were successfully amplified. Attempts to amplify archaeal 16S rRNA genes with multiple primer sets (**Table 2**) were not successful. Appropriate standard and negative controls were constructed from StrataClone vectors (Agilent Technologies), following manufacturer protocols, and linearized using a Hind III (New England Biolabs) restriction digest. QPCR protocols consisted of 180 s denaturation at 94°C, followed by 40 cycles of 60 s at 94°C, 60 s at the annealing temperature (**Table 2**), 45 s at 72°C, and 15 s at 80°C, at the end of which fluorescence was measured. The efficiencies of all reactions were between 96 and 103%. For the *mcrA* gene analyses, the amplicon size was verified.

TABLE 2 | Oligonucleotide primers and conditions used in this study for quantitative PCR analysis.

Category	Target gene	Forward primer (nM)	Reverse primer (nM)	Positive control	Ta	Reference
Calvin Benton Bassham	*RuBisCO* form II	*cbbM591F* (200) TTC TGG CTG GGB GGH GAY TTY ATY AAR AAY GAC GA	*cbbM918R* (200) CCG TGR CCR GCV CGR TGG TAR TG	*Thiomicrospira crunogena* (DMS No. 12353)	55	Campbell and Cary (2004)
rTCA	*ATP citrate lyase*	*aclB892F (200)* TGG ACM ATG GTD GCY GGK GGT	*aclB1204R* (200) GTT GGG GCC RCC WCK KCK NAC	*Sulfurovum denitrificans* (DMS No. 1251)	55	Takai et al. (2005)
Methano genesis	*Methyl CoM reductase*	*qmcrAF-alt (150)* GAR GAC CAC TTY GGH GGT TC	*ML-R (200)* TTC ATT GCR TAG TTW GGR TAG TT	*Methanosarcina acetivorans, Methanococcus jannaschii*	55	Luton et al. (2002), Ver Eecke et al. (2012)
Bacteria	16S rRNA	*Bact1369F* (1000) GTT GGG GCC RCC WCK KCK NAC	*Prok1541R* (1000) CGG TGA ATA TGC CCC TGC	*Arcobacter nitrofigulis*	59	Suzuki et al. (2001)
Archaea	16S rRNA	*Arch1-1369F* (500) CGG TGA ATA CGT CCC TGC + *Arch2-1369F* (500) *CGG TGA ATA TGC CCC TGC*	*Prok1541R* (1000) CGG TGA ATA TGC CCC TGC	*Ferroplasma acidarmonas Fer1*	59	Suzuki et al. (2001)
Archaea	16S rRNA	*Arch349F(500)* GYG CAS CAG KCG MGA AW	*Arch806R (500)* GGA CTA CVS GGG TAT CTA AT	*Ferroplasma acidarmonas Fer1*	54	Takai and Horikoshi (2000)

Ta, annealing temperature during QPCR reaction.

Screening of Microbial Genes Associated with the Potential to Fix Carbon

Although 16S rRNA gene sequencing was beyond the scope of the present study, a parallel study determined the bacterial community composition of the same two Loihi basalts based on Ion Torrent sequencing of the V6 hypervariable region of the 16S rRNA gene (Jacobsen Meyers et al., 2014). To determine which of the bacterial orders recovered from the two Loihi basalts were potentially capable of carbon fixation via the pathways targeted with the qPCR analysis, we searched the Integrated Microbial Genomes (IMG) database (Markowitz et al., 2006) for genomes within the orders previously detected on these samples (Jacobsen Meyers et al., 2014) using the "Find Functions" search and the "Enzymes (list)" filters. EC 4.1.1.39 was used to search for the *cbbM* gene, and EC 2.3.3.8 was used to search for the *aclB* genes (analysis done 07-09 October 2014). Genomes were scored as positive if they contained either the *cbbM* or *aclB* gene, and then the number of genes within the order was tallied to calculate the percentage of genomes within that order capable of producing each enzyme. This analysis depends on the assumptions that: (a) if an organism is a member of a clade in which a specific enzyme is found more frequently in genomes from that clade, then that organism is more likely to have the enzyme, (b) the annotations in IMG are reliable.

Results

^{13}C-Enrichment of Organic Matter

The average organic carbon content of the basalts used in this study was quite low, in all cases less than 0.1 weight percent, and with several less than 0.02 weight percent (**Tables 1** and **3**). These values are lower than has been measured for North Pond basalts previously based on loss-on-ignition measurements (Expedition 336 Scientists, 2012c,d). It is probable that the acid-washing step to remove unincorporated ^{13}C-bicarbonate resulted in the physical removal of some organic matter. If so, we posit that it did not impact the carbon isotope ratio of the residual material, as bulk erosion of a biofilm is not likely to selectively remove organic constituents. Highly oxidized basalt (i.e., Ula Nui, Marker 2, J2-626-R1, U1382A 3R4, U1382A 7R2) had slightly higher organic carbon content (average $\pm$ 1 standard deviation of 0.050 $\pm$ 0.028 wt %, $n = 42$ samples) than the glassy basalt samples (0.027 $\pm$ 0.010, $n = 14$ samples), which is consistent with previous observations of higher organic carbon in altered basalt from North Pond (Expedition 336 Scientists, 2012c,d). These low values required sensitive detection methods for determining stable isotopic composition of organic carbon by IRMS. A few samples ($n = 5$ out of 56 total) did not have enough carbon to enable a robust isotopic determination; these samples are not included in the following analyses.

The JdF2009, Marker 2, and Ula Nui samples, which were incubated for up to a week, all showed some degree of ^{13}C enrichment of organic matter over time (**Figure 2A**; **Table 3**). The JdF2009 glassy basalt had the largest heterogeneity in isotopic values between samples, which may have been affected by the relatively low organic carbon concentration in this sample set (**Tables 1** and **3**), allowing minor amounts of carbon uptake to skew the isotopic ratio to a greater degree than in samples with higher organic carbon pools. Some of the North Pond basalts, which were incubated for a much longer period of time, showed significant incorporation of ^{13}C into organic matter over

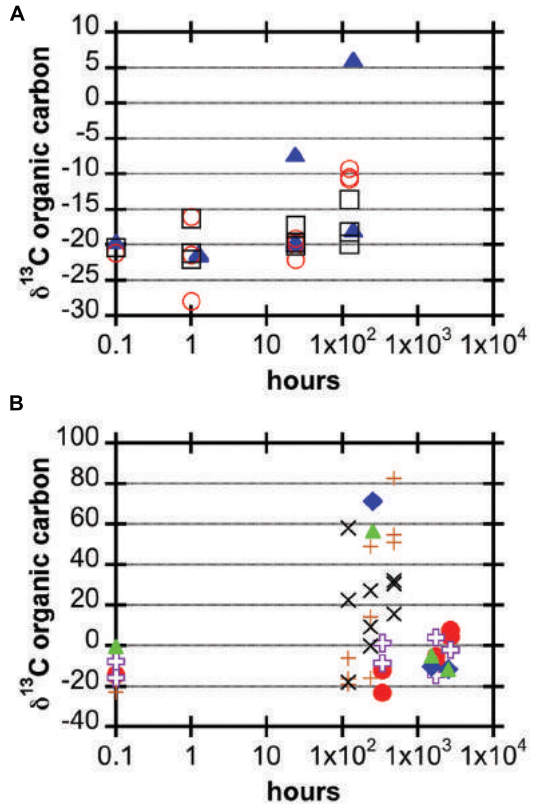

FIGURE 2 | Carbon stable isotopic composition of organic matter in basalt samples after incubation, expressed in the delta notation of per mil (note logarithmic time scale). (A) JdF2009 (blue filled triangles), Ula Nui (black open squares), and Marker 2 (red open circles). **(B)** U1382A 3R4 (purple open crosses), U1382A 7R2 (red filled circles), U1383C 13R1 (blue filled diamonds), U1383C glass (green filled triangles), J2-626-R1 (brown plus signs), J2-627-R3 (black x's).

time, while others did not exhibit a strong trend (**Figure 2B**). The two seafloor-exposed North Pond rocks—J2-626-R1 and J2-627-R3—had the highest incorporation of ^{13}C into organic matter by the end of the incubations. The glassy subsurface basalts from Hole U1383C—U1383C glass and U1383C 13R1—also exhibited some incorporation of ^{13}C into organic matter over time, whereas the massive basalts from Hole U1382A did not show significant incorporation of ^{13}C over time. Again, the degree of incorporation in the glassy basalts could have been skewed by the relatively low organic carbon concentration of these samples. However, it should be noted that some of the Hole U1383C glassy basalts had positive signs of contamination based on fluorescent microsphere tracer tests, and it is possible the contaminant organisms could have been responsible for some degree of carbon uptake.

Conversion of carbon isotope ratios into potential rates of carbon fixation revealed that all of the seafloor-exposed rocks supported potential carbon fixation rates in the range of 0.1–10 nmol C g^{-1}_{rock} d^{-1}, with the samples from the Loihi seamount having a few outliers with rates near 100 nmol C g^{-1}_{rock} d^{-1} from samples incubated for a relatively short period of time (**Figure 3**; **Table 3**). However, four of the five seafloor-exposed basalt incubations contained at least one sample that did not have detectable incorporation of ^{13}C-label into organic matter during the course of the incubations (**Table 3**), based on a conservative requirement of a 2‰ or greater difference between the time zero and samples to define a change in isotopic composition. This emphasizes the heterogeneity of the organic carbon content and likely of the biofilm distributions between samples in the incubations. It should be noted that the relatively low organic carbon content in the samples affects the calculation of potential rates and represents a potentially low end-member if some of the organic carbon was lost during acid-washing steps.

Microbial Abundance and Functional Potential

DNA was successfully extracted from roughly 0.5 g samples of seafloor-exposed basalts from the JdF2009, Marker 2, and Ula Nui samples, resulting in yields between 2 and 31 ng DNA g^{-1}_{rock} (based on Qubit®dsDNA HS Assay concentration assays; data not shown). Quantitative PCR assays with high efficiencies were possible from the DNA extractions without any further purification steps.

Bacterial 16S rRNA gene copy numbers per gram of basalt ranged from roughly 10^7–10^9 for the Marker 2 and JdF2009 incubations, with lower values of 10^5–10^7 for all but two of the Ula Nui incubations (**Figure 4**). These gene copy densities are quite consistent with those reported for other seafloor exposed basalts (Santelli et al., 2008). There was no apparent increase or decrease in cell density between the sample time points, as time point replicates displayed similar ranges of variations as between time points. Assuming roughly four copies of the 16S rRNA gene per cell, these values would translate to approximately 10^6–10^8 cells g^{-1}_{rock} for the Marker 2 and JdF2009 basalts, and 10^5–10^6 cells g^{-1}_{rock} for the Ula Nui basalt. These values are in the same range as those reported for the Ula Nui and Marker 2 basalts in another study (Jacobsen Meyers et al., 2014), although the earlier study did not demonstrate a higher cell density on the Marker 2 samples versus the Ula Nui samples as is potentially evident here. In the present study, archaeal 16S rRNA genes could not be quantified. A previous study documented that archaea made up only 1–2% of the total microbial community on Ula Nui and Marker 2 basalts (Jacobsen Meyers et al., 2014), which is consistent with other studies of seafloor-exposed basalt microbial communities (Santelli et al., 2008).

Genes involved in carbon fixation pathways were detected in all of the samples analyzed, although in different relative amounts (**Figure 4**). The RuBisCO form II enzyme gene *cbbM* was predominantly the most abundant carbon fixation gene in all of the samples, often by several orders of magnitude (**Figure 4**). The *cbbM* gene was most abundant in the Marker 2 basalt samples, ranging from 10^5 to 10^7 *cbbM* gene copies g^{-1}_{rock} (**Figure 4**). Notably, this gene was less abundant in the JdF2009 basalt samples (10^4–10^6 gene copies g^{-1}_{rock}). The abundance of the *cbbM* gene in the Ula Nui samples was erratic, ranging from below detection limit (<1000 gene copies g^{-1}_{rock}) to nearly 10^6 gene copies g^{-1}_{rock}. Although archaeal 16S rRNA genes were not detected, methyl coenzyme M reductase (*mcrA* gene) was

TABLE 3 | Summary of organic carbon content and stable carbon isotope composition of seafloor basalt samples after incubation.

ID	Time (h)	OC wt %	δ^{13}C-OC (‰)	(^{13}C/^{12}C) × 10^2	Δ ^{13}C/^{12}C	Δ ng ^{13}C/g_{rock}	Δ nmol C/g_{rock}/d
JdF2009	*T_0*	*0.040*	*−19.5*	*1.096*	*n.a.*	*n.a.*	*n.a.*
	1.25	0.032	−21.4	1.094	b.d.l.	–	–
	1.25	0.034	−21.1	1.094	b.d.l.	–	–
	23.75	0.028	−19.5	1.096	b.d.l.	–	–
	23.75	0.022	−7.2	1.110	1.4×10^{-4}	41	12.7
	23.75	0.027	−19.9	1.096	b.d.l.	–	–
	139.75	0.023	6.1	1.125	2.9×10^{-4}	86	4.5
	139.75	0.043	−17.9	1.098	1.9×10^{-5}	6	0.3
Ula Nui	*T_0*	*0.044*	*−20.4*	*1.095*	*n.a.*	*n.a.*	*n.a.*
	1	0.113	−22.1	1.093	b.d.l.	–	–
	1	0.061	−21.2	1.094	b.d.l.	–	–
	1	0.041	−16.3	1.100	4.6×10^{-5}	27	92.5
	24.25	0.050	−17.2	1.099	3.5×10^{-5}	21	3.0
	24.25	0.059	−19.6	1.096	b.d.l.	–	–
	24.25	0.040	−20.1	1.095	b.d.l.	–	–
	124.25	0.043	−19.9	1.096	b.d.l.	–	–
	124.25	0.057	−13.6	1.103	7.6×10^{-5}	44	1.2
	124.25	0.074	−18.2	1.098	2.5×10^{-5}	15	0.4
Marker 2	*T_0*	*0.043*	*−21.1*	*1.094*	*n.a.*	*n.a.*	*n.a.*
	1	0.078	−21.4	1.094	b.d.l.	–	–
	1	0.086	−16.1	1.100	5.7×10^{-5}	33	114.3
	24	0.035	−22.1	1.093	b.d.l.	–	–
	24	0.042	−19.1	1.097	2.3×10^{-5}	13	1.9
	24	0.063	−19.7	1.096	b.d.l.	–	–
	124.25	0.029	−9.3	1.108	1.3×10^{-4}	77	2.2
	124.25	0.052	−10.5	1.106	1.2×10^{-4}	69	1.9
	124.25	0.095	−10.8	1.106	1.2×10^{-4}	67	1.9
J2-626-R1	*T_0*	*0.027*	*−22.9*	*1.092*	*n.a.*	*n.a.*	*n.a.*
	118.5	0.032	−16.3	1.100	7.4×10^{-5}	39	1.0
	118.5	0.012	−6.1	1.111	1.9×10^{-4}	100	2.4
	118.5	0.027	−19.1	1.097	4.2×10^{-5}	23	0.6
	237	0.102	14.3	1.134	4.2×10^{-4}	220	2.7
	237	0.032	−16.0	1.100	7.7×10^{-5}	41	0.5
	237	0.105	49.1	1.173	8.0×10^{-4}	426	5.2
	480	n.d.	82.6	1.210	1.2×10^{-3}	625	3.8
	480	0.101	51.1	1.175	8.3×10^{-4}	438	2.6
	480	0.043	54.8	1.179	8.7×10^{-4}	461	2.8
J2-627-R3	118.5	0.024	−18.0	1.098	b.d.l.	–	–
	118.5	0.027	22.6	1.143	4.5×10^{-4}	109	2.7
	118.5	0.020	58.1	1.183	8.5×10^{-4}	204	5.0
	237	0.020	−0.1	1.118	2.0×10^{-4}	48	0.6
	237	0.022	27.2	1.148	5.1×10^{-4}	121	1.5
	237	0.019	9.3	1.128	3.1×10^{-4}	73	0.9
	480	0.019	32.4	1.154	5.6×10^{-4}	135	0.8
	480	0.021	15.6	1.135	3.8×10^{-4}	90	0.5
	480	0.038	30.5	1.152	5.4×10^{-4}	130	0.8

b.d.l., below detection limit; n.a., not applicable; n.d., not determined. See text for details.

detected in all of the samples at 10^3–10^5 gene copies g^{-1}_{rock} (**Figure 4**), and the size of the amplicon matched the expected product size of the primer set (∼265 bp). The *aclB* gene for ATP citrate lyase was observed in the Marker 2 and Ula Nui basalt samples but was undetectable in the JdF2009 basalt samples. This gene was consistently abundant at 10^3–10^4 gene copies g^{-1}_{rock}

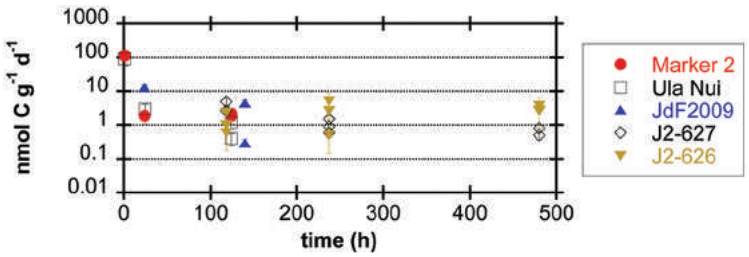

FIGURE 3 | Potential rates of carbon fixation by seafloor-exposed basalt-hosted microbial communities (expressed as nmol C incorporated g^{-1}_{rock} d^{-1}) as a function of incubation time, based on incubation experiments of basalt samples with ^{13}C-labeled bicarbonate. Error bars represent the range of the coefficient of variance from the measurement of organic carbon weight percent, since the mean value for each sample set was applied to all samples in that set (see Materials and Methods); in some cases, data symbol is larger than the error bar range. Samples with isotopic composition differences of less than 2‰ from the time zero sample (**Table 3**) were assumed to be below the limit of detection of the method (see Materials and Methods) and are not reported here.

in the Marker 2 samples, but ranged from 10^2 to 10^6 gene copies g^{-1}_{rock} in the Ula Nui samples.

We determined the bacterial orders putatively responsible for the carbon fixation detected on the Ula Nui and Marker 2 basalts by searching the IMG database (Markowitz et al., 2006) for the presence of *cbbM* and *aclB* in sequenced genomes from all bacterial orders previously detected on these samples (**Figure 5**), using a similar approach as reported elsewhere (Jacobsen Meyers et al., 2014). The presence of *cbbM* was distributed widely in the bacterial orders detected, while *aclB* was detected only in the orders Chlorobiales, Nitrospirales, Desulfobacterales, and Campylobacterales. Although *cbbM* is present in many orders, it is common (present in ≥50% of the genomes queried) in only a few orders: Acidimicrobiales, Chlorobiales, Caldilineales, Gemmatimonadales, Nitrospirales, Nitrosomonadales, Acidithiobacillales, Chromatiales, and Mariprofundales. Of these, Acidimicrobiales, Nitrospirales, Acidithiobacillales, Chromatiales, and Mariprofundales are the most abundant orders, indicating that these groups potentially contribute most significantly to overall rates of basalt carbon fixation in the Loihi basalts, assuming equal rates for all active groups. The presence of *aclB* was common in the Nitrospirales and Chlorobiales.

Discussion

Using stable carbon isotope incubation experiments, we demonstrate autotrophic carbon fixation by basalt-hosted biofilm communities, with consistent potential carbon fixation rates of 0.1–10 nmol C g^{-1}_{rock} d^{-1} in the seafloor-exposed basalts examined in this study (**Figures 2** and **3**; **Table 3**). Notably, subsurface basalts exhibit markedly lower and/or undetectable carbon assimilation (**Figure 2**). The potential rates of carbon fixation are similar to or lower than recently available measurements of total community microbial activity on seafloor-exposed basalts (Jacobsen Meyers et al., 2014). This suggests that the heterotrophic incorporation of exogenous organic carbon may be playing a significant role in this habitat, which is consistent with recent observations of depleted organic carbon content in subsurface crustal fluids as compared to bottom seawater (Lin et al., 2012). Nevertheless, when scaling the potential carbon fixation rates measured in this study to the global reservoir of the oceanic crustal environment, these results support earlier predictions on the magnitude of carbon fixation in oceanic crust (Bach and Edwards, 2003), as discussed below. We note that the rates presented here do not preclude the possibility of elevated rates of basalt-hosted autotrophy *in situ*, nor do they definitively establish the relative proportions of autotrophy versus heterotrophy among deep-sea basalts. Finally, the Calvin cycle appears to be the dominant autotrophic process used in seafloor-exposed basalt based on gene abundance (**Figure 4**). Based on the presence of these genes in microbial groups common on seafloor-exposed basalts (**Figure 5**), we suggest that bacteria in the orders Acidimicrobiales, Acidithiobacillales, Chromatiales, and Mariprofundales are potentially the most active carbon-fixing bacteria in seafloor-exposed basalts.

Carbon Fixation Potential and Rates

Our stable carbon isotope experiments provide the first empirical documentation of potential carbon fixation by basalt-hosted microbial communities (**Figures 2** and **3**; **Table 3**). Potential carbon fixation rates of 0.1–10 nmol C g^{-1}_{rock} d^{-1} were consistently observed under oxic conditions for seafloor basalts sourced from several deep-sea environments (**Figure 3**; **Table 3**). Higher potential rates near 100 nmol C g^{-1}_{rock} d^{-1} were calculated for some of the shorter (1 h) seafloor-exposed basalt incubations, while the 0.1–10 nmol C g^{-1}_{rock} d^{-1} range was fairly consistent in longer incubation periods. This may suggest diminishing carbon fixation potential influenced by incubation effects such as decreased pressure from *in situ* conditions, decreased oxidant availability, nutrient limitation, or other factors. High potential rates may also reflect the impact of relatively small additions in ^{13}C-labeled molecules into very organic poor samples having a strong impact on the overall isotopic composition of the sample. Conversely, four out of the five seafloor-exposed basalts also contained at least one sample that exhibited no detectable shift in carbon isotopic composition over the course of incubation (based on a conservative limit

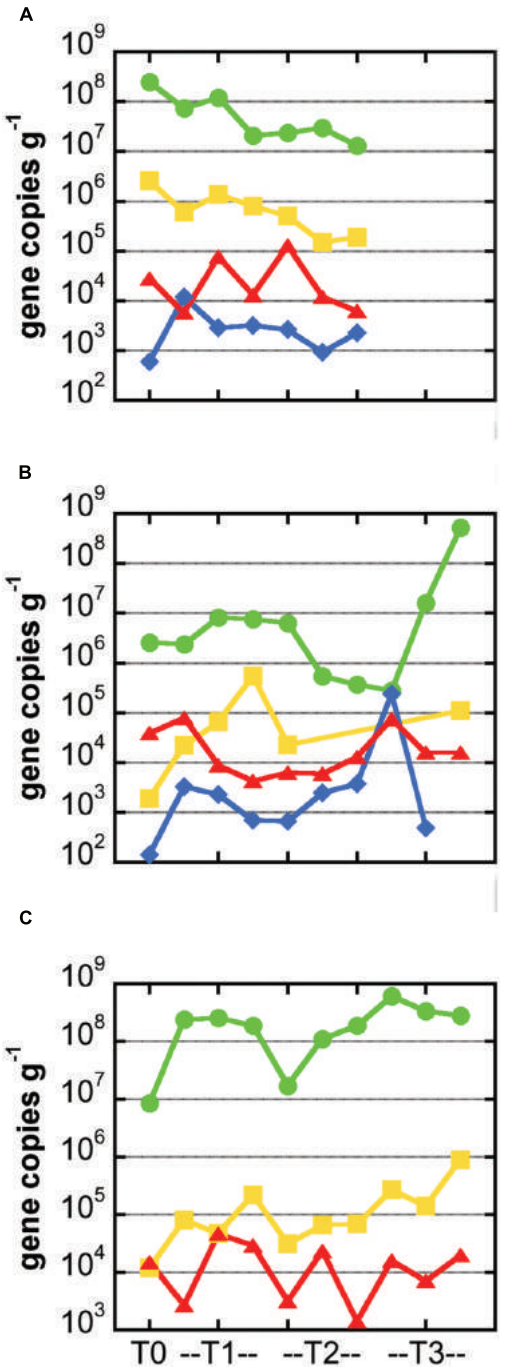

FIGURE 4 | Abundance of carbon cycling functional genes in microbial communities hosted in basalts samples from the Marker 2 (A), Ula Nui (B), and JdF2009 (C) sample sets. In all panels, gene abundance for each sample is presented as number of gene copies per gram of rock. Green circles: bacterial 16S rRNA gene; yellow squares: RuBisCO form II gene *cbbM* from Calvin Benton Bassham pathway; red triangles, methyl coenzyme M reductase gene *mcrA* from methane cycling pathways; blue diamonds, ATP citrate lyase gene *aclB* from reverse TCA process. Note missing symbols in **(A)** indicate samples that were not available for analysis, while missing symbols in **(B,C)** indicate values that were not above the limit of detection (~10^3 gene copies per gram for *cbbM* and ~10^2 gene copies per gram for *aclB*). Lines connecting symbols are for esthetic purpose and convey no meaning.

of 2‰ or greater isotopic change; **Table 3**). This likely reflects patchiness and heterogeneity of biofilm distribution in the pieces of basalt used in the incubation.

Notably, these potential carbon fixation rates are similar to or smaller than the maximum potential rates of extracellular enzyme activity measured for basalts from the Loihi seamount, which ranged from 10 to 1,500 $nmol_{substrate}\ g^{-1}{}_{rock}\ d^{-1}$ (Jacobsen Meyers et al., 2014). However, higher enzyme activities are to be expected for several reasons. First, the two enzymes assayed—alkaline phosphatase and leucine aminopeptidase—are present in both autotrophic and heterotrophic lineages, and therefore the community exoenzyme pool is likely larger than the community pool of proteins involved in autotrophic carbon fixation. Second, the exoenzyme assays were conducted at saturating substrate concentrations, leading to maximum potential rates, while the ^{13}C-bicarbonate assays analyzed here were not at saturation. Third, carbon fixation by basalt biofilm microbial communities is related to anabolic metabolic reaction whereas the extracellular enzyme assays are related to catabolic processes. Finally, the possibility for loss of biofilms from the acid-washing steps used to prepare the samples may have lead to underestimates of the potential carbon fixation rates.

Scaling the potential rates of carbon fixation measured here (range of 0.1–10 nmol C $g^{-1}{}_{rock}\ d^{-1}$ with outliers of ~100 nmol C $g^{-1}{}_{rock}\ d^{-1}$; **Figure 3**; **Table 3**) to the size of the surface crustal reservoir as calculated elsewhere (Bach and Edwards, 2003), we extrapolate that roughly 10^9–10^{12} g C $year^{-1}$ could be fixed in this ecosystem, which matches the earlier predictions of 10^{11}–10^{12} g C $year^{-1}$ based on thermodynamic and bioenergetics considerations (Bach and Edwards, 2003). The match between empirical measures of potential microbial activity in oceanic crust and theoretical estimations provides support that the potential rates measured here are indeed reflective of processes in the environment. Moreover, the overlap between measured and theoretical values further supports the hypothesis that water-rock reactions can support significant microbial life in ridge flank hydrothermal systems (Bach and Edwards, 2003).

Potential carbon fixation rates were generally below detection in subseafloor basalts (**Figure 2**), suggesting (1) that autotrophy is not a dominant metabolic pathway in the subsurface; (2) that bulk rates are too low to detect, regardless of their dominance in the ecosystem; or (3) that incubation conditions were not conducive to activity as compared to *in situ* conditions (such as lower pressure; Nagata et al., 2010). Another possible complicating factor is that these incubations were performed in oxic seawater. While the North Pond crustal subsurface is oxic (Orcutt et al., 2013), warranting the experimental approach, it is possible that inclusion of anoxic incubations may have increased the total rate. The presence of *mcrA* genes in our analysis of seafloor rocks (**Figure 4**) indicates that some anoxic carbon fixation is possible in anaerobic microniche within the rocks. Recent work demonstrates that anoxic, hydrothermal subsurface crustal fluids are depleted in organic carbon compared to bottom seawater, suggesting that the subsurface is net heterotrophic and reliant on organic carbon from outside (Lin et al., 2012). By contrast, however, fluids from the same anoxic system revealed indications of autotrophic production of dissolved organic

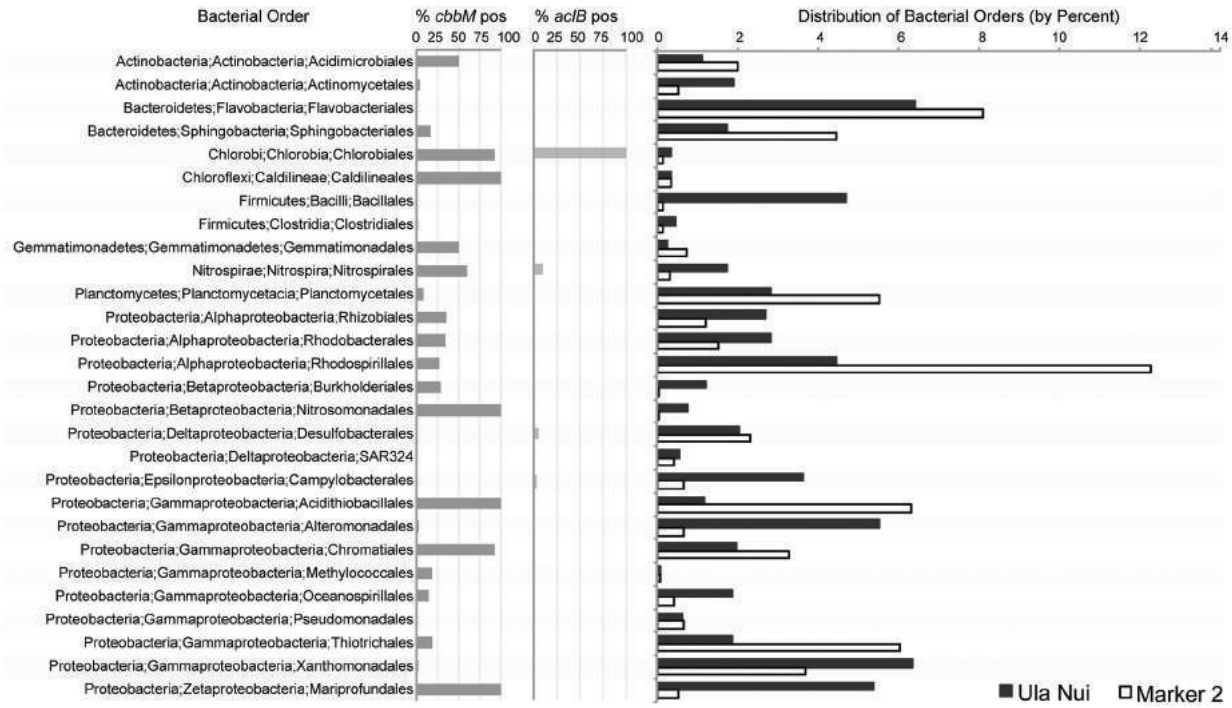

FIGURE 5 | Percent abundance of bacterial orders detected by Ion Torrent sequencing of the V6 region of the 16S rRNA gene from environmental DNA extracts from the Ula Nui and Marker 2 Loihi seafloor basalts versus the percent abundance of publically available genomes from the same orders with evidence of *cbbM* or *aclB* genes. Percent abundance of bacterial orders has been published previously (Jacobsen Meyers et al., 2014) and is used here with permission.

carbon (McCarthy et al., 2011). The balance of autotrophy versus heterotrophy in the crustal biosphere is yet to be resolved.

Microbial Groups Involved in Carbon Fixation on Basalts

The RuBisCO form II *cbbM* gene was the most abundant carbon fixation gene in the all of the samples investigated (**Figure 4**), as compared to methyl coenzyme M reductase *mcrA* gene or the *aclB* gene for ATP citrate lyase, suggesting that the Calvin cycle is the dominant pathway for carbon fixation in these basalt-hosted biofilms. Bacteria within the phylum Nitrospirae, genus *Nitrospira*, and the Gammaproteobacterial order Chromatiales, are recovered consistently from seafloor-exposed basalts (Mason et al., 2009; Santelli et al., 2009; Sylvan et al., 2013) and were present on the Loihi basalts used in this study (Jacobsen Meyers et al., 2014). The majority of sequenced genomes from these groups contain *cbbM* genes (**Figure 5**). This indicates they may participate in autotrophic carbon fixation and are potentially important primary producers on seafloor-exposed basalts. In the case of Nitrospirales, however, the *cbbM* gene is a form IV version of the protein not functional in carbon fixation (Goltsman et al., 2009; Lücker et al., 2010), and this gene may instead be used for sulfur metabolism (Ashida et al., 2005). Likewise, the orders Acidimicrobiales, Acidithiobacillales, and Mariprofundales were also abundant on the Loihi samples, are likely to contain *cbbM* genes, and are therefore likely significant contributors to basaltic carbon fixation as well. Acidimicrobiales is an order within the Actinobacteria into which the Ocean Crust Clade XIII falls; this group consists of organisms detected only in basalt samples (Mason et al., 2009). This suggests that these putative carbon fixers are likely widespread on seafloor-exposed basalts. Acidithiobacillales and Mariprofundales have not previously been detected on seafloor basalts (Jacobsen Meyers et al., 2014), possibly due to the shallow sequencing depth typical of clone libraries (Santelli et al., 2008, 2009; Mason et al., 2009; Sylvan et al., 2013).

The only bacterial order detected on Loihi basalts that has a high percentage of genomes containing *aclB* genes is the Chlorobiales (**Figure 5**), although this group is generally not present in high abundances on basalts (as cited above) and thus likely plays a minor role. While only a small proportion of Campylobacterales genomes encode for *aclB* (**Figure 5**), the Campylobacterales genera most likely to be detected on basalts (i.e., *Sulfuricurvum*, *Sulfuriminas*, *Thiovulum,* and *Nitratifractor*) all contain the rTCA cycle. However, the vast majority of sequenced genomes from this order belong to *Campylobacter* and *Helicobacter*, which are of medical interest but do not carry out carbon fixation via the rTCA cycle. Similarly, while only a small percentage of Nitrospirales genomes contain *aclB* (**Figure 5**), we posit that basalt-hosted Nitrospirales are also likely fixing carbon via the rTCA pathway based on two arguments. First, while members of the genus *Nitrospira* are the only members of the Nitrospirales that contain *aclB* (Lücker et al., 2010), members of the genus *Leptospirillum* seem to universally have an alternative

pathway to cleave citrate using citryl-CoA synthetase and citryl-CoA lyase (Levicán et al., 2008; Goltsman et al., 2009). Therefore, two the three genera within the order Nitrospirales fix carbon using the rTCA cycle (the third genus, *Thermodesulfovibrio*, are heterotrophs). Second, out of the three genera in the order, *Nitrospira* are common in marine systems (Lücker et al., 2010) while the other two are not; therefore, the Nitrospirales on basalts are likely to be *Nitrospira*. It should also be noted that the order Desulfobacterales, which was abundant on the Loihi basalts (**Figure 5**), likely utilizes the acetyl-CoA pathway for carbon fixation (Kuever et al., 2005), but that was not tested here.

Interestingly, *mcrA*, which is associated with the anaerobic production and consumption of methane, was detected in all three incubations assayed (**Figure 4**), even though the incubations were conducted under oxic conditions. Despite the difficulty in detecting Archaea based on the 16S rRNA gene, the presence of methyl coenzyme M reductase indicates that Archaea were present in seafloor-exposed basalts. Two lines of evidence indicate that, while methane cycling may not be a quantitatively large metabolic process on seafloor-exposed basalts (although this remains to be tested), methanogenesis is likely happening to some degree on seafloor and subseafloor basalts. First, *mcrA* genes were detected on seafloor (Mason et al., 2009) and subseafloor (Lever et al., 2013) basalts from the Juan de Fuca Ridge and ridge flank. Second, incubations with seafloor and subseafloor basalts resulted in production of measurable methane (Lysnes et al., 2004; Lever et al., 2013). The presence of *mcrA* genes, indicative of an anaerobic process, indicates that there are anaerobic microniches in the pits and pockets of the basalt rocks, even when exposed to oxic seawater, as posited previously (Edwards et al., 2005) and owing to the presence of genes related to methanogenesis, denitrification, and sulfate reduction on basalt from the Juan de Fuca Ridge (Mason et al., 2009).

This stable carbon isotope study provides empirical evidence for the potential for carbon fixation by basalt-hosted microbial communities in the deep-sea. Though local carbon fixation rates are small in comparison to highly productive photosynthetic regions, the globally scaled rates of 10^9–10^{12} g C fixed per year nevertheless indicate autotrophy as an important metabolism in the oceanic crust and the broader deep-sea ecosystem. These rates of net production are especially important in the dark ocean, which is devoid of photosynthesis. This study does not definitely identify which basalt biofilm microorganisms are involved in carbon fixation, yet functional gene abundance suggests that the Calvin cycle is the primary biochemical mechanism used by basalt microbial communities to fix carbon. While potential carbon fixation rates were quantifiable for seafloor-exposed rocks, carbon fixation activity in deeper basalts was not resolvable with the approach used in this study and warrants further investigation, as the size of the subsurface crustal reservoir is significantly larger than seafloor-exposed basalts.

Acknowledgments

The authors would like to thank the crews of the AT15-51, FeMO2009, MSM20-5, and IODP Expedition 336 cruises for their efforts at sea. In particular, we thank the pilots of the HOV *Alvin* and ROV *Jason-II* for expert sample collection; H. Mills, F. Wang, J. Russell, S. Leth Jørgensen, K. Edwards, A. Haddad, and H. Hirayama for assistance with subsurface basalt collection; and W. Bach for assisting with rock descriptions. Lisa Ledwidge and Pengfei Song are also thanked for assistance in sample preparation. This work would not have been possible without the generous support and encouragement of the late Katrina J. Edwards to BO and JS to participate in fieldwork for this project. BO also thanks Bo Barker Jørgensen for supporting time to participate in fieldwork for this project. This research used samples and data provided by the Integrated Ocean Drilling Program (IODP). Funding for this work was provided in part by NSF (OCE-1233226 to BO and OCE-1344241 to PG), the Integrated Ocean Drilling Program, the NSF-funded Center for Dark Energy Biosphere Investigations Science and Technology Center (C-DEBI, OCE-0939564), the Danish National Research Foundation, the Max Planck Society, and the German Science Foundation (DFG).

References

Alt, J. C., and Mata, P. (2000). On the role of microbes in the alterations of submarine basaltic glass: a TEM study. *Earth Planetary Sci. Lett.* 181, 301–313. doi: 10.1016/S0012-821X(00)00204-1

Alt, J. C., and Teagle, D. A. H. (1999). The uptake of carbon during alteration ocean crust. *Geochim. Cosmochim. Acta* 63, 1527–1535. doi: 10.1016/S0016-7037(99)00123-4

Ashida, H., Danchin, A., and Yokota, A. (2005). Was photosynthetic RuBisCO recruited by acquisitive evolution from RuBisCO-like proteins involved in sulfur metabolism? *Res. Microbiol.* 156, 611–618. doi: 10.1016/j.resmic.2005.01.014

Bach, W., and Edwards, K. J. (2003). Iron and sulfide oxidation within the basaltic ocean crust: implications for chemolithoautotrophic microbial biomass production. *Geochim. Cosmochim. Acta* 67, 3871–3887. doi: 10.1016/s0016-7037(00)00304-301

Bach, W., Humphris, S., and Fisher, A. T. (2004). Fluid flow and fluid-rock interaction within ocean crust: reconciling geochemical, geological, and geophysical observations. *Am. Geophys. Union* 144, 99–117.

Campbell, B. J., and Cary, S. C. (2004). Abundance of reverse tricarboxylic acid cycle genes in free-living microorganisms at deep-sea hydrothermal vents. *Appl. Environ. Microbiol.* 70, 6282–6289. doi: 10.1128/AEM.70.10.6282-6289.2004

Edmond, J. M., and Von Damm, K. L. (1983). Hot springs on the ocean floor. *Sci. Am.* 248, 78–93. doi: 10.1038/scientificamerican0483-78

Edwards, K. J., Bach, W., and Mccollom, T. M. (2005). Geomicrobiology in oceanography: microbe–mineral interactions at and below the seafloor. *Trends Microbiol.* 13, 449–456. doi: 10.1016/j.tim.2005.07.005

Edwards, K. J., Mccollom, T. M., Konishi, H., and Buseck, P. R. (2003a). Seafloor bioalteration of sulfide minerals: results from in-situ incubation studies. *Geochim. Cosmochim. Acta* 67, 2843–2856. doi: 10.1016/S0016-7037(03)00089-9

Edwards, K. J., Rogers, D. R., Wirsen, C. O., and Mccollom, T. M. (2003b). Isolation and characterization of novel, psychrophilic, neutrophilic, Fe-oxidizing, chemolithoautotrophic alpha- and gamma-Proteobacteria from the deep sea. *Appl. Environ. Microbiol.* 69, 2906–2913. doi: 10.1128/AEM.69.5.2906-2913.2003

Expedition 336 Scientists. (2012a). "Methods," in *Proceedings of the Integrated Ocean Drilling Program*, Vol. 336, eds K. J. Edwards, W. Bach, A. Klaus,

and Expedition 336 Scientists (Tokyo: Integrated Ocean Drilling Program Management International, Inc.). doi: 10.2204/iodp.proc.336.102.2012

Expedition 336 Scientists. (2012b). "Sediment and basement contact coring," in: *Proceeding of the Integrated Ocean Drilling program*, Vol. 336, eds K. J. Edwards, W. Bach, A. Klaus, and Expedition 336 Scientists (Tokyo: Integrated Ocean Drilling Program Management International, Inc.).

Expedition 336 Scientists. (2012c). "Site U1382," in *Proceedings of the Integrated Ocean Drilling Program*, Vol. 336, eds K. J. Edwards, W. Bach, A. Klaus, and Expedition 336 Scientists (Tokyo: Integrated Ocean Drilling Program Management International, Inc.).

Expedition 336 Scientists. (2012d). "Site U1383," in *Proceedings of the Integrated Ocean Drilling Program*, Vol. 336, eds K. J. Edwards, W. Bach, A. Klaus, and Expedition336scientists (Tokyo: Integrated Ocean Drilling Program Management International, Inc.).

Fisher, A. T., and Becker, K. (2000). Channelized fluid flow in oceanic crust reconciles heat-flow and permeability data. *Nature* 403, 71–74. doi: 10.1038/47463

Goltsman, D. S., Denef, V. J., Singer, S. W., Ver Berkmoes, N. C., Lefsrud, M., Mueller, R. S., et al. (2009). Community genomic and proteomic analyses of chemoautotrophic iron-oxidizing Leptospirillum rubrum (Group II) and Leptospirillum ferrodiazotrophum (Group III) bacteria in acid mine drainage biofilms. *Appl. Environ. Microbiol.* 75, 4599–4615. doi: 10.1128/AEM.02943-08

Jacobsen Meyers, M. E., Sylvan, J. B., and Edwards, K. J. (2014). Extracellular enzyme activity and microbial diversity measured on seafloor exposed basalts from Loihi Seamount indicate importance of basalts to global biogeochemical cycling. *Appl. Environ. Microbiol.* doi: 10.1128/AEM.01038-1014

Kuever, J., Rainey, F. A., and Widdel, F. (2005). "Class IV. Deltaproteobacteria *class nov*.," in *Bergey's Manual of Systematic Bacteriology*, 2nd Edn, eds D. J. Brenner, N. R. Krieg, and J. T. Staley (New York, NY: Springer-Verlag), 922–1144.

Lever, M. A., Rouxel, O. J., Alt, J. C., Shimizu, N., Ono, S., Coggon, R. M., et al. (2013). Evidence for microbial carbon and sulfur cycling in deeply buried ridge flank basalt. *Science* 339, 1305–1308. doi: 10.1126/science.1229240

Levicán, G., Ugaide, J. A., Ehrenfeld, N., Maass, A., and Parada, P. (2008). Comparative genomic analysis of carbon and nitrogen assimilation mechanisms in three indigenous bioleaching bacteria: predictions and validation. *BMC Genomics* 9:581. doi: 10.1186/1471-2164-9-581

Lin, H.-T. (2013). *Biogeochemistry of Basement Fluids From the Sediment-Buried Juan de Fuca Ridge flanks*. Ph.D., University of Hawaii, Hilo, HI.

Lin, H.-T., Cowen, J. P., Olson, E. J., Amend, J. P., and Lilley, M. D. (2012). Inorganic chemistry, gas compositions and dissolved organic carbon in fluids from sedimented young basaltic crust on the Juan de Fuca Ridge flanks. *Geochim. Cosmochim. Acta* 85, 213–227. doi: 10.1016/j.gca.2012.02.017

Lücker, S., Wagner, M., Maixner, F., Pelletier, E., Koch, H., Vacherie, B., et al. (2010). A Nitrospira metagenome illuminates the physiology and evolution of globally important nitrite-oxidizing bacteria. *Proc. Natl. Acad. Sci. U.S.A.* 107, 13479–13484. doi: 10.1073/pnas.1003860107

Luton, P. E., Wayne, J. M., Sharp, R. J., and Riley, P. W. (2002). The mcrA gene as an alternative to 16S rRNA in the phylogenetic analysis of methanogen populations in landfill. *Microbiology* 148, 3521–3530.

Lysnes, K., Thorseth, I. H., Steinsbu, B. O., Øvreås, L., Torsvik, T., and Pedersen, R. B. (2004). Microbial community diversity in seafloor basalt from the Arctic spreading ridges. *FEMS Microbiol. Ecol.* 50, 13–230. doi: 10.1016/j.femsec.2004.06.014

Markowitz, V. M., Korzeniewski, F., Palaniappan, K., Szeto, E., Werner, G., Padki, A., et al. (2006). The integrated microbial genomes (IMG) system. *Nucleic Acids Res.* 34, D344–D348. doi: 10.1093/nar/gkj024

Mason, O. U., Di Meo-Savoie, C. A., Van Nostrand, J. D., Zhou, J., Fisk, M. R., and Giovannoni, S. J. (2009). Prokaryotic diversity, distribution, and insights into their role in biogeochemical cycling in marine basalts. *ISME J.* 3, 231–242. doi: 10.1038/ismej.2008.92

Mason, O. U., Nakagawa, T., Rosner, M., Van Nostrand, J. D., Zhou, J., Maruyama, A., et al. (2010). First investigation of the microbiology of the deepest layer of ocean crust. *PLoS ONE* 5:e15399. doi: 10.1371/journal.pone.0015399

McCarthy, M. D., Beaupré, S. R., Walker, B. D., Voparil, I., Guilderson, T. P., and Druffel, E. R. M. (2011). Chemosynthetic origin of 14C-depleted dissolved organic matter in a ridge-flank hydrothermal system. *Nat. Geosci.* 4, 32–36. doi: 10.1038/ngeo1015

Nagata, T., Tamburini, C., Arístegui, J., Baltar, F., Bochdansky, A. B., Fonda-Umani, S., et al. (2010). Emerging concepts on microbial processes in the bathypelagic ocean - ecology, biogeochemistry, and genomics. *Deep Sea Res. Part II Top. Stud. Oceanogr.* 57, 1519–1536. doi: 10.1016/j.dsr2.2010.02.019

Orcutt, B. N., Bach, W., Becker, K., Fisher, A. T., Hentscher, M., Toner, B. M., et al. (2011a). Colonization of subsurface microbial observatories deployed in young ocean crust. *ISME J.* 5, 692–703. doi: 10.1038/ismej.2010.157

Orcutt, B. N., Sylvan, J. B., Knab, N. J., and Edwards, K. J. (2011b). Microbial ecology of the dark ocean above, at, and below the seafloor. *Microbiol. Mol. Biol. Rev.* 75, 361–422. doi: 10.1128/MMBR.00039-10

Orcutt, B. N., Wheat, C. G., Rouxel, O. J., Hulme, S., Edwards, K. J., and Bach, W. (2013). Oxygen consumption rates in subseafloor basaltic crust derived from a reaction transport model. *Nat. Commun.* 4, 2539. doi: 10.1038/ncomms3539

Robador, A., Jungbluth, S. P., Larowe, D. E., Bowers, R. M., Rappé, M. S., Amend, J. P., et al. (2014). Activity and phylogenetic diversity of sulfate-reducing microorganisms in low-temperature subsurface fluids with the upper oceanic crust. *Front. Microbiol.* 5:748. doi: 10.3389/fmicb.2014.00748

Rouxel, O. J., Ono, S., Alt, J., Rumble, D., and Ludden, J. (2008). Sulfur isotope evidence for microbial sulfate reduction in altered oceanic basalts at ODP Site 801. *Earth Planetary Sci. Lett.* 268, 110–123. doi: 10.1016/j.epsl.2008.01.010

Ryan, W. B. F., Carbotte, S. M., Coplan, J. O., O'hara, S., Melkonian, A., Arko, R., et al. (2009). Global multi-resolution topograpjy synthesis. *Geochem. Geophys. Geosyst.* 10:Q03014. doi: 10.1029/2008GC002332

Santelli, C. M., Edgcomb, V. P., Bach, W., and Edwards, K. J. (2009). The diversity and abundance of bacteria inhabiting seafloor lavas positively correlate with rock alteration. *Environ. Microbiol.* 11, 86–98. doi: 10.1111/j.1462-2920.2008.01743.x

Santelli, C. M., Orcutt, B. N., Banning, E., Bach, W., Moyer, C. L., Sogin, M. L., et al. (2008). Abundance and diversity of microbial life in ocean crust. *Nature* 453, 653–656. doi: 10.1038/nature06899

Smith, D. C., Spivack, A. J., Fisk, M. R., Haveman, S. A., Staudigel, H., and Party, L. S. S. (2000). Methods for quantifying potential microbial contamination during deep ocean coring. *ODP Technical. Note* 28. doi: 10.2973/odp.tn.28.2000

Stevens, T. O., and McKinley, J. P. (1995). Lithoautotrophic microbial ecosystems in deep basalt aquifers. *Science* 270, 450–454. doi: 10.1126/science.270.5235.450

Suzuki, M. T., Béjà, O., Taylor, L. T., and Delong, E. F. (2001). Phylogenetic analysis of ribosomal RNA operons from uncultivated coastal marine bacterioplankton. *Environ. Microbiol.* 3, 323–331. doi: 10.1046/j.1462-2920.2001.00198.x

Sylvan, J. B., Sia, T. Y., Haddad, A. G., Briscoe, L. J., Toner, B. M., Girguis, P. R., et al. (2013). Low temperature geomicrobiology follows host rock composition along a geochemical gradient in Lau Basin. *Front. Microbiol.* 4:61. doi: 10.3389/fmicb.2013.00061

Takai, K., Campbell, B. J., Cary, S. C., Suzuki, M., Oida, H., Nunoura, T., et al. (2005). Enzymatic and genetic characterization of carbon and energy metabolisms by deep-sea hydrothermal chemolithoautotrophic isolates of Epsilonproteobacteria. *Appl. Environ. Microbiol.* 71, 7310–7320. doi: 10.1128/AEM.71.11.7310-7320.2005

Takai, K., and Horikoshi, K. (2000). Rapid detection and quantification of members of the archaeal community by quantitative PCR using fluorogenic probes. *Appl. Environ. Microbiol.* 66, 5066–5072. doi: 10.1128/AEM.66.11.5066-5072.2000

Templeton, A. S., Knowles, E. J., Eldridge, D. L., Arey, B. W., Dohnalkova, A. C., Webb, S. M., et al. (2009). A seafloor microbial biome hosted within incipient ferromanganese crusts. *Nat. Geosci.* 2, 872–876. doi: 10.1038/NGEO696

Toner, B. M., Santelli, C. M., Marcus, M. A., Wirth, R., Chan, C. S., Mccollom, T. M., et al. (2009). Biogenic iron oxyhydroxide formation at mid-ocean ridge hydrothermal vents: juan de Fuca Ridge. *Geochim. Cosmochim. Acta* 73, 388–403. doi: 10.1016/j.gca.2008.09.035

Ver Eecke, H. C., Butterfield, D. A., Huber, J. A., Lilley, M. D., Olson, E. J., Roe, K. K., et al. (2012). Hydrogen-limited growth of hyperthermophilic

methanogens at deep-sea hydrothermal vents. *Proc. Natl. Acad. Sci. U.S.A.* 109, 13674–13679. doi: 10.1073/pnas.1206632109

Wheat, C. G., Jannasch, H. W., Fisher, A. T., Becker, K., Sharkey, J., and Hulme, S. (2010). Subseafloor seawater-basalt-microbe reactions: continuous sampling of borehole fluids in a ridge flank environment. *Geochem. Geophys. Geosyst.* 11:Q07011. doi: 10.1029/2010GC003057

Wheat, C. G., Jannasch, H. W., Kastner, M., Plant, J. N., and Decarlo, E. H. (2003). Seawater transport and reaction in upper oceanic basaltic basement: chemical data from continuous monitoring of sealed boreholes in a ridge flank environment. *Earth Planetary Sci. Lett.* 216, 549–564. doi: 10.1016/S0012-821X(03)00549-1

Conflict of Interest Statement: The authors declare that the research was conducted in the absence of any commercial or financial relationships that could be construed as a potential conflict of interest.

frontiers in Microbiology

ORIGINAL RESEARCH
published: 10 May 2016
doi: 10.3389/fmicb.2016.00678

Deep Subsurface Life from North Pond: Enrichment, Isolation, Characterization and Genomes of Heterotrophic Bacteria

*Joseph A. Russell[1], Rosa León-Zayas[1], Kelly Wrighton[2] and Jennifer F. Biddle[1]**

[1] College of Earth, Ocean and Environment, University of Delaware, Lewes, DE, USA, [2] Department of Microbiology, The Ohio State University, Columbus, OH, USA

Studies of subsurface microorganisms have yielded few environmentally relevant isolates for laboratory studies. In order to address this lack of cultivated microorganisms, we initiated several enrichments on sediment and underlying basalt samples from North Pond, a sediment basin ringed by basalt outcrops underlying an oligotrophic water-column west of the Mid-Atlantic Ridge at 22°N. In contrast to anoxic enrichments, growth was observed in aerobic, heterotrophic enrichments from sediment of IODP Hole U1382B at 4 and 68 m below seafloor (mbsf). These sediment depths, respectively, correspond to the fringes of oxygen penetration from overlying seawater in the top of the sediment column and upward migration of oxygen from oxic seawater from the basalt aquifer below the sediment. Here we report the enrichment, isolation, initial characterization and genomes of three isolated aerobic heterotrophs from North Pond sediments; an *Arthrobacter* species from 4 mbsf, and *Paracoccus* and *Pseudomonas* species from 68 mbsf. These cultivated bacteria are represented in the amplicon 16S rRNA gene libraries created from whole sediments, albeit at low (up to 2%) relative abundance. We provide genomic evidence from our isolates demonstrating that the *Arthrobacter* and *Pseudomonas* isolates have the potential to respire nitrate and oxygen, though dissimilatory nitrate reduction could not be confirmed in laboratory cultures. The cultures from this study represent members of abundant phyla, as determined by amplicon sequencing of environmental DNA extracts, and allow for further studies into geochemical factors impacting life in the deep subsurface.

Keywords: deep biosphere, bacteria, cultivation, genome, amplicon

OPEN ACCESS

Edited by:
Beth Orcutt, Bigelow Laboratory for Ocean Sciences, USA

Reviewed by:
Donato Giovannelli, Rutgers University, USA
Stephanie Ann Carr, Colorado School of Mines, USA
Caroline Sara Fortunato, Marine Biological Laboratory, USA

****Correspondence:***
Jennifer F. Biddle
jfbiddle@udel.edu

Specialty section:
This article was submitted to Extreme Microbiology, a section of the journal Frontiers in Microbiology

Received: *04 January 2016*
Accepted: *26 April 2016*
Published: *10 May 2016*

Citation:
Russell JA, León-Zayas R, Wrighton K and Biddle JF (2016) Deep Subsurface Life from North Pond: Enrichment, Isolation, Characterization and Genomes of Heterotrophic Bacteria. Front. Microbiol. 7:678. doi: 10.3389/fmicb.2016.00678

INTRODUCTION

The marine environment harbors numerous uncultivated microbes with estimates of culturable marine bacteria around 0.01 to 0.1% of cells present (Kogure et al., 1979; Connon and Giovannoni, 2002). The "great plate count anomaly" (Staley and Konopka, 1985) extends into the marine deep biosphere, yet there is still a need for cultivation-based research to better fill critical knowledge gaps, transforming our understanding of the biogeochemical impacts in the deep biosphere (Parkes et al., 2009; Fichtel et al., 2012; Lomstein et al., 2012; Lever et al., 2013; Ciobanu et al., 2014). Cultivated microbes from the deep marine subsurface have often come from anoxic sediments,

including anaerobes such as *Desulfovibrio profundus* (Bale et al., 1997) and *Methanoculleus submarinus* (Mikucki et al., 2003). Facultative anaerobes (*Shewanella profunda,* Toffin et al., 2004) and numerous aerobes have been retrieved from anaerobic sediments (D'Hondt et al., 2004; Biddle et al., 2005). Overall, most isolates from the deep biosphere have poor environmental context to date, and few isolated aerobes have originated from aerobic sediments.

The collection of deep biosphere sediment and basalt via drilling during International Ocean Drilling Program (IODP) Expedition 336 to North Pond offered an opportunity to initiate cultivation studies across several subsurface environments: young aerobic sediments, older anoxic sediments, still older aerobic sediments, and 7-million-year-old ridge flank basalt (Expedition 336 Scientists, 2012). North Pond is a sediment-filled basin between exposed basalt outcrops, where temperature differences exist between warmer out-crops closer to tectonic activity at the Mid-Atlantic Ridge and colder outcrops further away at the southwest section of the basin (Langseth et al., 1992; Edwards et al., 2012). In the colder, southwest corner of the basin, Site U1382 was drilled to a depth of 210 m below seafloor (mbsf), including 90 m of sediment from Hole U1382B and 120 m of basement from Hole U1382A (Expedition 336 Scientists, 2012; **Figure 1**).

At Site U1382, oxygen penetrated the sediment to approximately 4 mbsf and returned at approximately 68 mbsf due to flow from the underlying basalt (Orcutt et al., 2013). In addition to oxygen, other electron acceptors such as nitrate are reported (Edwards et al., 2012; Wankel et al., 2015). While electron acceptor concentrations are similar at these depths, the buried organic carbon at 68 mbsf is over 6 million years older than at 4 mbsf and has presumably undergone some level of remineralization given that oxygen is used up in the middle of the sediment column (Burdige, 2007). Currently, our knowledge of oxygen- and nitrogen-cycling heterotrophy in North Pond sediments are based on modeling of nitrogen isotopes and the examination of sediment slurries with labeled carbon substrates (Picard and Ferdelman, 2011; Wankel et al., 2015). Physical characteristics of the sediment that enhance the delivery of nutrient/electron-acceptor rich pore-water are more important than indigenous carbon substrates for constraining heterotrophy (Picard and Ferdelman, 2011). Active nitrogen cycling in North Pond sediments does not follow canonical patterns of redox separation between consumption and regeneration of nitrate, with overlapping zones of aerobic (nitrification) and anaerobic (denitrification) processes (Wankel et al., 2015). North Pond sediments are likely to be representative of a majority of the global seafloor, as oligotrophic water columns such as those overlying North Pond comprise a majority of the global ocean (D'Hondt et al., 2009).

Here we report the enrichment, isolation, initial characterizations and genomes of three isolated aerobic heterotrophs from North Pond sediments; an *Arthrobacter* species from 4 mbsf, and *Paracoccus* and *Pseudomonas* species from 68 mbsf. Dissimilatory nitrate reduction could not be induced under laboratory conditions of all three isolates, however, genomic data suggests a metabolic capability for denitrification in the *Arthrobacter* isolate from 4 mbsf and *Pseudomonas* isolate from 68 mbsf at U1382B, depths where we expect this metabolism to be occurring (Wankel et al., 2015). Based on amplicon sequencing abundances, these isolates are rare members of abundant phyla in the environment. To our knowledge, these are the first aerobic isolates reported from oxygenated deep marine sediments.

MATERIALS AND METHODS

Sampling

Samples were acquired from the scientific drilling vessel *JOIDES Resolution* during IODP Expedition 336 in November, 2011 (**Figure 1**). Samples were taken from Holes U1382A, U1382B, U1383C, U1383E, and U1384A (Supplementary Table S1). Whole round core sections were sampled at 10 m intervals when available. Samples for DNA extraction were immediately stored at −80°C and kept at this temperature for the remainder of the cruise and during shipping to shore-based laboratory. Samples for cultivation were stored at 4°C for no longer than 2 h before being inoculated into enrichment media. Enrichment media was prepared from literature-sourced recipes to attempt to cultivate aerobic heterotrophs (GYPS; Burgaud et al., 2009), sulfate reducers (Pfennig et al., 1981), methanogens (Wolfe et al., 2011), sulfide oxiders (Nelson et al., 1986), iron reducers (Wrighton et al., 2011) iron oxidizers/nitrate reducers (Straub and Buchholz-Cleven, 1998), Mn oxiders (Krumbein and Altmann, 1973), and Mn reducers (Burdige and Nealson, 1985) from both sediments and basalts. Numerous enrichments were prepared across different samples and depths with negative controls of uninoculated broth (Supplementary Table S1). However, confirmed growth was only observed in the aerobic heterotroph enrichments from sediments taken by Advanced Piston Coring (APC) at Site U1382B at 22°45.353′N, 46°04.891′W; as such, this is the only enrichment we will report in detail.

Culture Media, Growth Conditions, and Growth Measurements

Original GYPS media for aerobic heterotrophs was prepared in 1 L batches onboard the *JOIDES Resolution* (JR) and consisted of the following; 1 g each of glucose, peptone, starch, and yeast extract, 1 L filtered/autoclaved seawater (Burgaud et al., 2009). Media was then autoclaved for 1 h. After autoclaving and allowing 30 min for cooling, 5 mL Wolfe's vitamins and 5 mL Wolfe's minerals was added and 40 mL was aseptically dispensed in autoclaved 60 ml glass vials and capped with rubber septa, which were removed during sample addition and every week after to reoxygenate the media. This dispensing, and all sediment additions, were performed in the sterile flow hood aboard the JR. The top 3–5 mm of sediment from each whole round core section was removed with a flame-sterilized spatula to reduce any potential drilling contamination and 3 cubic centimeter samples were taken from the center of the core using sterilized cut-off syringes. Care was taken to sample from the *interior* of the core to avoid sampling sediment contaminated with seawater during the drilling process. This drilling-induced seawater contamination

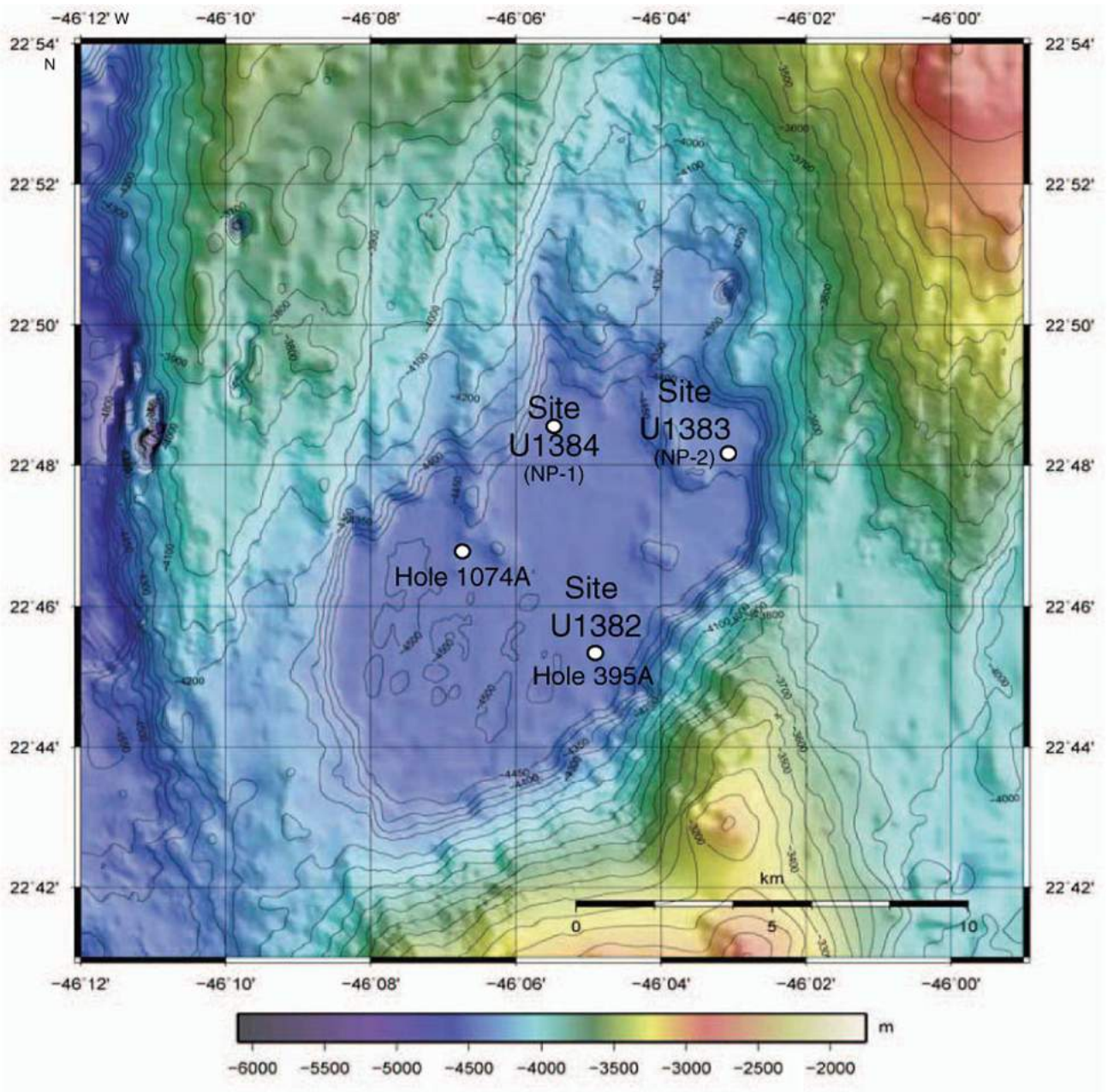

FIGURE 1 | Bathymetric map of North Pond in the Atlantic Ocean, showing drill sites (from Expedition 336 Scientists, 2012). Isolates in this paper are from Site U1382, Hole U1382B and enrichments were also started from Hole U1382A, Site U1383 (Holes U1383C and U1383E) and Site U1384 (Hole 1384A; Supplementary Table S1). Sites from IODP Expedition 336 are shown (Site #, NP #), as are holes previously drilled in the area (DSDP Hole 395A, ODP Hole 1074A).

was monitored using the fluorescent microsphere method, as described previously (Smith et al., 2000). Microsphere data for sediment horizons from which isolates derived is <1 microsphere per field of view for interior core samples, indicating a very low risk that isolates originated from seawater (Expedition 336 Scientists, 2012). Basalt whole-round core samples were broken into smaller pieces with a flame-sterilized chisel in a flame-sterilized steel rock processing box. After processing, 2–3 g of basalt chips were used as inoculum in enrichment media. The sediment and basalt subsamples were immediately inoculated into enrichment vials aerobically and the vials were capped with rubber septa and stored at 4°C. Growth was observed by turbidity of media from sediment samples from 4 and 68 mbsf (section 1 and 8H) within 2 days and transfers into new media were done every 5 days for the remainder of the cruise. At the end of the cruise, culture vessels were crimp-sealed for shipping to the Biddle Lab at 4°C. Once on shore, enriched heterotrophs were plated on Difco Marine Agar 2216 plates and placed at

10°C under aerobic conditions. Individual colonies were picked and streaked on new plates in five successive rounds of isolation at 10°C. Culture media for anaerobic growth on NO_3^- was composed of the following, in 500 mL dH_2O; 0.75 g of KH_2PO_4, 0.15 g of NH_4Cl, 1 g of KNO_3, 5 mM $(NH_4)_2Fe(SO_4)_2{\cdot}6H_2O$, 0.5 mg resazurin, 4% w/v Sigma sea salts, 10 mM glucose, 1 g peptone (Samuelsson, 1985). Culture media for Mn(II) oxidation was prepared as described previously (Krumbein and Altmann, 1973), in 1 L; 75% natural seawater, 25% dH_2O, 20 mM HEPES, 2 g peptone, 0.5 g yeast extract, 1 mM $MnCl_2$ (Templeton et al., 2005). Transfers were performed by growing isolates to late log phase in Difco Marine Broth 2216C at 10°C and 100 μl of this culture was used as inoculum to 40 mL of NO_3^- and 40 mL of Mn(II) oxidizing media (Krumbein and Altmann, 1973) in 60 ml glass vials, capped with rubber septa. Cultivation on nitrate and manganese media was attempted three times for each isolate. Growth temperature tests were initially performed at 4, 12, 22, 37, 42, and 50°C on solid Difco Marine 2216C agar media. Due to equipment limitations on shaking incubators, we only measured growth rates at temperatures starting at 12°C. For growth rate measurements, cells were grown in liquid Difco Marine Broth with shaking and 500 μl timepoints were taken to measure optical density in reference to uninoculated media at 600 nm wavelength on a Nanodrop 2000c (ThermoFisher Scientific). Glycerol stocks of each isolate were prepared and frozen at −80°C for long term archiving. They are available to researchers upon request.

DNA Extractions and Sequencing

Isolates were grown to late stationary phase in 5 ml of media. Cultures were centrifuged for 10 min at 4000 rpm to generate a cell pellet. The cell pellet for each isolate was re-suspended in 500 μl dH_2O and DNA was extracted using the UltraClean Microbial DNA Isolation Kit from MoBIO Laboratories, Inc. (Carlsbad, CA, USA). Full-length 16S rRNA amplicons were generated with bacterial primers 8F/1492R (Eden et al., 1991) with the following PCR protocol; 94°C for 2 min, (94°C for 30 s, 59°C for 1 min, 68°C for 2 min) × 30 cycles, 68°C for 5 min, then cloned with the TOPO TA Cloning Kit for Sequencing (Life Technologies Inc., Grand Island, NY, USA). Ten clones per isolate were picked and sent for Sanger sequencing at GeneWiz Inc., (South Plainfield, NJ, USA) to confirm culture purity. Full length 16S rRNA DNAs are deposited under NCBI accession numbers KU707917–KU707919. Genomic DNA was sent to the United States Department of Energy's Joint Genome Institute for full genome sequencing. Isolate genomes and raw sequencing data are available from the GOLD database via accession numbers: *Pseudomonas stutzeri* NP_8HT: Gp0114906, *Arthrobacter subterraneus* NP_1H: Gp0115197, *Paracoccus* sp. NP_8HO: Gp0114905 and under NCBI project ID: 303658. For total microbial community analysis at both depths (4 and 68 mbsf), 10 g of sediment from each depth was processed with the PowerMax Soil DNA Isolation Kit from MoBio Laboratories, Inc. (Carlsbad, CA, USA). Total bacterial community was amplified from 2 ng template DNA using 16S rRNA primers 27F/338R via PCR protocol: 95°C for 2 min, (95°C for 30 s, 60°C for 1 min, 72°C for 2 min) × 35 cycles, 72°C for 5 min. An extraction blank was processed with the samples. All PCR products, including the one from the extraction blank, were sent for Illumina library prep and sequencing at Next Generation Sequencing Services (Shallowater, TX, USA). This involved a nested PCR approach, resulting in a minimal number of cycles occurring after initial PCR amplification, which may slightly reduce the diversity of the environmental samples. Amplicon sequencing data is available under NCBI accession numbers SRS1277883–SRS1277884.

Sequence Data Processing and Analysis

The raw data from 16S rRNA gene amplicon Illumina reads were converted to a fastq file in QIIME version 1.8 (Caporaso et al., 2010) with the *convert_fastaqual_fastq.py* script. Primers and barcodes were extracted with the *extract_barcodes.py* script and sequences were de-multiplexed via *split_libraries_fastq.py* and an in-house perl script. 1,846 operational taxonomic unit (OTUs) were shared between the extraction blank and the section 1H sample. 1,446 OTUs were shared between the extraction blank and the section 8H sample. The most abundant taxa associated with these OTUs were from families often observed as common kit contaminants, such as *Propionibacteriaceae, Enterobacteriaceae, Ralstoniaceae,* and *Bradyrhizobiaceae* (Salter et al., 2014). Several proteobacterial OTUs, including *Pseudomonas* and *Paracoccus* genera, were observed in the extraction blank. No *Arthrobacter*-related OTUs were observed in the blank. All OTUs shared between samples and the extraction blank were removed before further analysis. Sequences were then uploaded to the SILVA NGS pipeline[1] (Quast et al., 2013) where default quality-trimming parameters were used, sequences were aligned with the SINA aligner (Pruesse et al., 2012), and OTU clustering was performed at 98% sequence identity. Taxonomy was called against the SILVA database (Quast et al., 2013). OTUs identified in the extraction blank sample that were also seen in sediment samples were removed from further analysis. The resulting OTU table was used for creation of taxonomy figures. Full-length 16S rRNA gene amplicon data was trimmed in Sequencher v.5.0.1 (GreenCodes Corp., Ann Arbor, MI, USA), sequences aligned with the online SINA aligner[2] and manually refined within ARB (Ludwig et al., 2004). Phylogenetic analysis was performed using ARB via a neighbor-joining method with 1000 bootstrap replicates on the highest quality clone sequence from each isolate. Genomes were quality trimmed using Nesoni[3]. We then assembled these genomes using SPAdes 3.1.1 in multi cell mode (Bankevich et al., 2012). The – – careful flag was used to reduce the number of mismatches and short indwells and to run error correction in the assembly. The assembly iteratively used kmers 21, 33, 55, and 77. PHRED quality offset for the input reads was set at 33. During assembly and initial annotation, we found that the raw data for the *Pseudomonas* isolate also included the *Paracoccus* genome. Therefore, after assembly by SPAdes, we separated the genomes using MaxBin (Wu et al., 2014), evaluated bin validity with VizBin (Laczny et al., 2015) and CheckM (Parks et al., 2015) and deposited

[1]https://www.arb-silva.de/ngs

[2]www.arb-silva.de/aligner

[3]https://github.com/Victorian-Bioinformatics-Consortium/nesoni

the new genomes in the integrated microbial genomes (IMG) database (Markowitz et al., 2012; Accession numbers 74356, 79457, and 79456; **Table 1**). Genomes were annotated by Prokka (Seeman, 2014). Genes for nitrogen cycling were extracted from the Prokka output and annotations were double checked via manual BLAST analysis against the NCBI nr database[4] and the Interpro protein domain database[5]. Additional genes found via IMG annotation were also added. Proteins annotated as active subunits of significant enzymes were aligned with close relatives of the nr database via MUSCLE (Edgar, 2004) and visually inspected and trimmed with Jalview software (Waterhouse et al., 2009). Trees were made using maximum likelihood in FastTree (Price et al., 2009). Carbohydrate active enzymes were identified by comparison with the Carbohydrate Active Enzymes database[6] (Cantarel et al., 2009) via pFAM scan (Mistry et al., 2007).

RESULTS AND DISCUSSION

Isolation and Phylogeny of Heterotrophs

Only the heterotrophic enrichments yielded observable growth from these deep samples, despite the media being quite high in carbon compared to the *in situ* environment (Edwards et al., 2012). A single colony morphotype was observed on Difco marine agar media during successive rounds of isolation from the 4 mbsf sample (section 1H); a light tan color with moderate EPS production. Two separate morphologies were identified from the 68 mbsf sample (section 8H). The first colony morphotype was light tan colored with moderate EPS production. The second was a bright orange color colonies with low EPS production. Full-length 16S rRNA gene sequencing indicates the section 1H isolate as an *Arthrobacter* species from the *Micrococcaceae* within the *Actinobacteria*, the orange 8H isolate as a *Paracoccus* species from the *Rhodobacteraceae* within the *Alphaproteobacteria*, and the tan 8H isolate as a *Pseudomonas* species from within the *Gammaproteobacteria* (**Figure 2**). The isolates were all related to species found previously in the subsurface and sediments.

The section 1H *Arthrobacter* sp. isolate was closely related to *Arthrobacter* species retrieved from deep subsurface water in South Korea (*A. subterraneus*) and Himalayan ice (*Arthrobacter* sp. zf-IIRIt1), as well as marine sediment off Svalbard, Norway (*Arthrobacter* sp. SH-61B; **Figure 2**). The closest relative (96.7% 16S rRNA gene identity) is *A. flavus*, a psychrophile isolated from a cyanobacterial mat in a pond in the McMurdo Dry Valley, Antarctica (Reddy et al., 2000). This isolate is the most novel based on distance from known relatives, in terms of 16S rRNA identity of the three we cultivated. It had a typical rod/coccus morphology depending on growth stage, with diameters ranging from 0.9 to 2 μm.

Clone A45 from the orange 8H isolate branched close to *Paracoccus* species previously isolated from Korean salt marsh sediments (*Paracoccus* sp. HZ04), Chinese salt deposits (*Paracoccus* sp. Y13), and deep sediments of the Arctic Ocean (*Paracoccus* sp. BSi20509). It is most closely related (99.2% 16S rRNA gene identity) to *Paracoccus carotinifaciens*, an aerobic, orange-pigmented, Gram-negative, rod-shaped microbe originally isolated from soil (Tsubokura et al., 1999; **Figure 2**). Our isolate stained gram-negative and exhibited a primarily coccoid shape (average diameter of 0.85 μm) though some rod shapes were observed, indicating a potential for growth related morphological changes.

Clone A25 from the tan 8H isolate branched close to *Pseudomonas* species previously isolated from South China Sea sediments (*Pseudomonas* sp. CF14-10), sediments of the southwest Pacific Ocean (*Pseudomonas* sp. 76, *Pseudomonas* sp. hyss58), and its closest relative was isolated from East Pacific Rise hydrothermal sediments, *Pseudomonas* sp. EPR 12 (Vetriani et al., 2005; 99% 16S rRNA gene identity; **Figure 2**). The isolate was rod-shaped and approximately 0.9 to 1.5 μm long.

Amplicon Sequencing from Enviromental Samples

To determine relative abundance of our isolates in the context of the greater microbial community from which they were collected from, we generated 16S rRNA gene amplicon libraries from frozen samples of sections 1 and 8H (**Figure 3**). Our enrichments had generated isolates from the *Actinobacteria* in the shallow sample (1H) and *Proteobacteria* from the deeper sample (8H). Consistent with the enrichments, the *Actinobacteria* and *Proteobacteria* were the dominant phyla represented in 1 and 8H microbial communities. *Actinobacteria*, which includes *Arthrobacter*, were 36.7 and 14.8% of the population at 1 and 8H, respectively. *Proteobacteria* were 29.1 and 29.4% of the population at 1 and 8H, respectively. However, the isolates were in extremely low abundance with *Arthrobacter* sp. 1H comprising <0.1% of the population at section 1H (**Table 2**). At section 8H, *Paracoccus* sp. 8HO was 0.1% of the population and *Pseudomonas* sp. 8HT was 1.5% (**Figure 3**; **Table 2**). Since the primers used in this analysis were much less discriminatory than those used to verify the identity of the isolates (310 and 1484 bp PCR products, respectively, whereas full length 16S rRNA gene

[4]http://blast.ncbi.nlm.nih.gov/Blast.cgi

[5]www.ebi.ac.uk/interpro

[6]www.cazy.org

TABLE 1 | Genome statistics of three heterotrophic aerobic isolates from sediment of Hole U1382B collected during IODP Expedition 336.

Organism	Sediment depth (mbsf)	Genome size (Mb)	Contigs*	Number of predicted genes	%GC	% completeness*
Arthrobacter sp. NP1H	4	3.90	99	3674	65	99.1
Pseudomonas sp. NP8HT	68	4.74	24	4353	60	100.0
Paraccocus sp. NP8HO	68	3.32	21	3193	68	99.7

**Reported statistics are based on contigs >500 bp, completeness from CheckM calculation.*

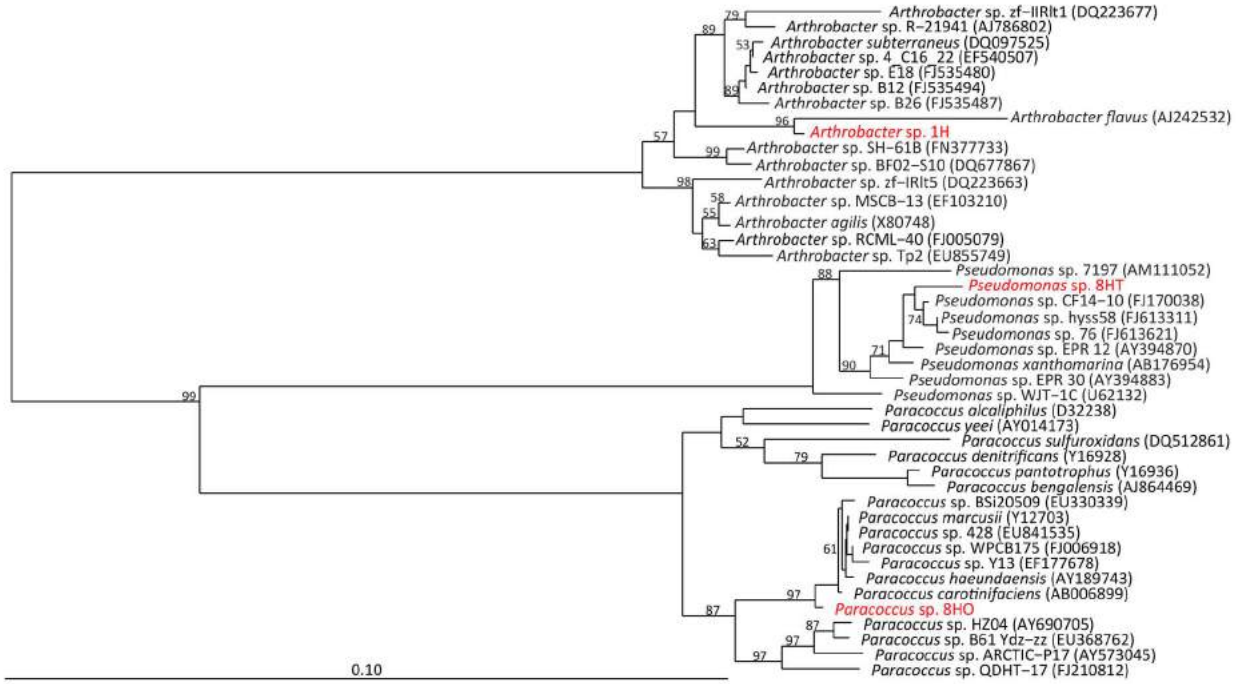

FIGURE 2 | Neighbor-joining tree of full length 16S rRNA gene sequences of isolates (red) to nearest database neighbors (black), based on 1000 bootstrap replicates. Bootstrap values >50% are shown.

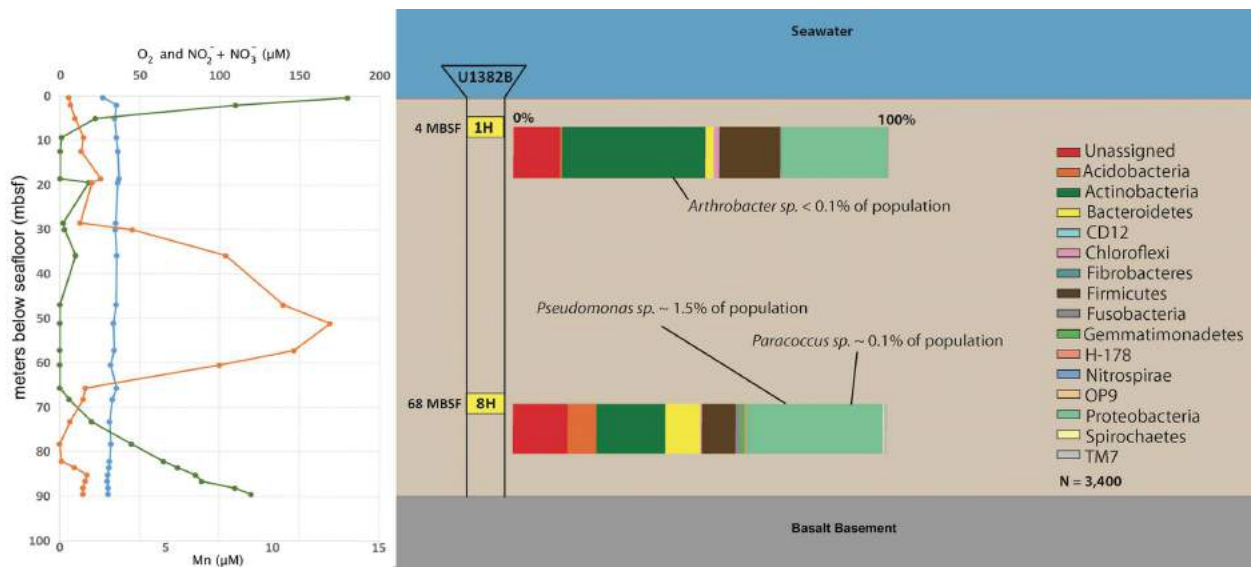

FIGURE 3 | Down-core O_2 (green), Mn (orange), and $NO_3 + NO_2$ (blue) concentrations (from Expedition Expedition 336 Scientists, 2012 and Orcutt et al., 2013) and 16S rRNA gene taxonomic profile, by phyla, for bacteria in frozen sediments of sections 1H (4 mbsf) and 8H (68 mbsf). Each amplicon sample was rarified to 3400 sequences for analysis. Notations regarding the percentage of isolate signatures are listed **(Table 2)**.

primers were used for isolate identification), and this involved a nesting priming approach, the abundances could increase if longer sequences were clustered for the environmental sample. Considering the relationship to other subsurface and sediment relatives that were also isolated, these organisms may not be numerous in these environments, but widely disbursed across these environments and respond well to cultivation. The same OTUs are found at different depths (**Table 2**), which correspond to different ages of sediment. Notably, the *Arthrobacter* is not found at 68 mbsf, which corresponds with the overall decrease

TABLE 2 | Abundances of isolate small subunit ribosomal (rRNA) signatures *in situ*.

Depth (mbsf)	*Arthrobacter* isolate	*Pseudomonas* isolate	*Paracoccus* isolate
4	3 (0.001)	67 (0.025)	6 (0.002)
68	0	52 (0.02)	3 (0.001)

First number is amount of sequences detected. Percent abundance is indicated in parentheses.

of members of *Actinobacterium* phylum at depth (**Figure 3**). We presume that organisms are deposited at the surface of the sediment column, and that the *Actinobacter* may not survive the lowest oxygen portion of the sediment column as well as the *Proteobacteria*, which results in the abundance shift at depth (**Table 2**; **Figure 3**).

Cultivation Responses of Cultivated Bacteria

The response of the isolates to varying temperatures (4, 12, 22, 37, 42, and 50°C) was measured on Difco marine broth agar, using organic carbon as an electron donor and O_2 as an electron acceptor. For all three isolates, growth was very slow but detected at 4°C. No growth was detected at 50°C. Slow growth at 42°C was only seen for the *Pseudomonas* sp. and *Arthrobacter* sp.. Growth rates were measured for three temperatures using equivalent methods across temperatures (12, 22, and 37°C). The *Arthrobacter* sp. had the highest growth rate at 37°C (0.36 h^{-1}), as did the *Pseudomonas* sp. (0.48 h^{-1}). The *Paracoccus* isolate had the highest growth rate at 22°C (0.24 h^{-1}; **Figure 4**). Growth across a wide range of temperatures has been seen for previous isolates of deep subsurface heterotrophs (Biddle et al., 2005). Additionally, we saw low temperatures induce the production of extra polymeric substances, or EPS, which can be seen in the growth curves that do not plateau (**Figure 4**). This response may be induced *in situ*, which may allow greater survival in an environment such as North Pond, as the development of EPS around a cell can allow for carbon resources to be consumed in the oligotrophic conditions of a sediment core, and also allow for maintained water availability as the deeper sediments are under greater pressure and typically have less pore fluid than shallow ones (Marx et al., 2009).

Given the reasonably high pore water NO_3^- concentrations (up to 35 μM) at 4 and 68 mbsf at U1382B and the very low O_2 concentration (under 20 μM) at these depths (**Figure 3**, Expedition 336 Scientists, 2012; Orcutt et al., 2013), we tested growth of isolates in anaerobic, heterotrophic, nitrate-reducing media. Also tested was fermentation capability, with the same media as for nitrate-reduction, without nitrate amendment. No growth was observed in either anaerobic media. Our findings are not consistent with the documented nitrate-reducing capabilities of all three isolate genera (Alefounder et al., 1983; Carlson and Ingraham, 1983; Eschbach et al., 2003). An anomalous sharp peak in Mn(II) was measured in porewaters of sediments from just below 50 mbsf at Hole U1382B (**Figure 3**). Given that the *Pseudomonas* and *Paracoccus* isolates originated near the Mn(II) peak at U1382B, we also evaluated our isolates for the capacity to aerobically oxidize Mn(II). Members of the *Actinobacteria* and *Pseudomonas* are known to oxidize Mn(II) (Okazaki et al., 1997; Tebo et al., 2005). Growth was observed from all three isolates, but no Mn-oxides were visually precipitated, indicating a lack of Mn-oxidation capability. These tests were performed after the isolates had been in culture for over a year and thus it is possible that Mn-oxidation capacity was lost as previously reported (Gregory and Staley, 1982).

Genome Sequencing of Cultivated Bacteria

Isolates genomes were sequenced to validate our physiological data and compare these subsurface isolates to surface relatives. The *Arthrobacter* draft genome assembled into 99 contigs, with a total genome size estimated at 3.9 Mb with a GC content of 65% (**Table 1**). The *Pseudomonas* isolate genome assembled into 24 contigs, with an estimated genome size of 4.7 Mb and a GC content of 60% (**Table 1**). The *Paracoccus* genome assembled into 21 contigs, with an estimated genome size of 3.3 Mb and a GC content of 68% (**Table 1**). All genomes have over 99% completeness, based on the detection of marker genes, and are representative of only one organism. Based on average nucleotide identity (ANI) of equal to or greater than 90% ANI with other genomes, two of these genomes formed cliques with other marine and extreme environment isolates. The *Paracoccus* genome formed a genome clique with *Paracoccus* sp. 361 (Gp0119386) from the Baltic Sea; the *Arthrobacter* formed a clique with *Arthrobacter* sp. 35/47 (Ga0012047) from Antarctic soils. The *Pseudomonas* isolate did not form any cliques, which is typical for this group of microbes, despite the high number of closely related genomes based on ribosomal sequences (25 complete or draft genomes in IMG; Markowitz et al., 2012; database accessed on December 28, 2015).

The *Arthrobacter* sp. 1H isolate from 4 mbsf possessed a denitrifying nitrate reductase gene cluster (Supplementary Table S2; **Figure 5**). Specifically, *narG*, *narH*, *narJ*, and *narI* were all detected, suggesting a capability for the dissimilatory reduction of nitrate (NO_3^-) to nitrite (NO_2^-). This genome also possesses the genes for nitrite reductase (NADH) small and large subunits (*nirD* and *nirB,* respectively), completing the dissimilatory reduction pathway to ammonia. The nitrite reductase NO-forming enzyme (*nirK*) is also encoded within the genome, which performs the second step in the denitrification pathway to nitrogen. The ability to reduce nitrate is not widespread in the *Arthrobacter* genus, with only 8 of the 75 available full to draft genomes available in IMG encoding similar genes, including this North Pond isolate (Markowitz et al., 2012; database accessed on December 28, 2015). Previous detection of nitrate reduction in *Arthrobacter* noted the difficulties of getting the cells to activate the denitrification pathway in culture, and our cultivation setup may not have enabled the shift of the cells into denitrification (Eschbach et al., 2003). Besides the ability of dissimilatory reduction of nitrate, the *Arthrobacter* isolate also encodes genes for the assimilatory nitrate reductase enzymes (the catalytic *nasA* and electron

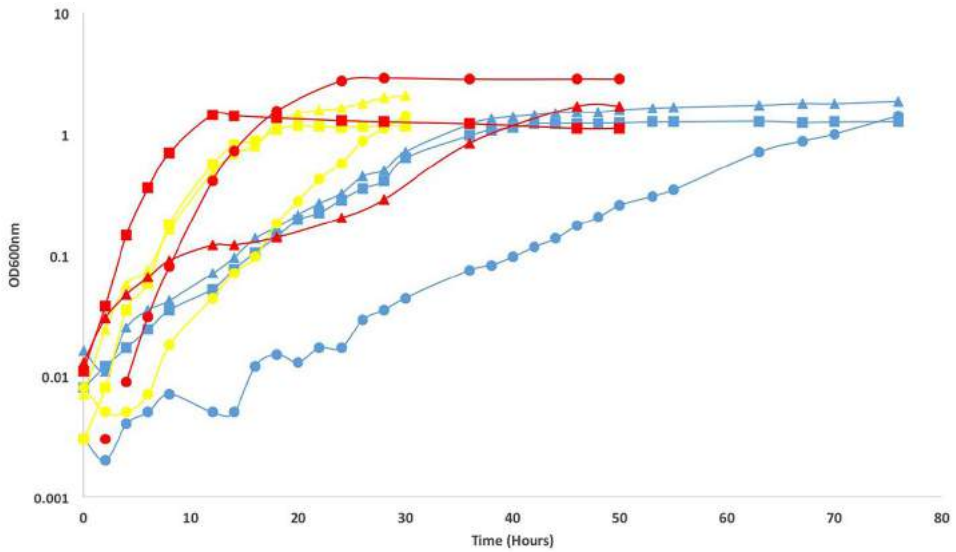

FIGURE 4 | Growth curves and calculated growth rates in parentheses (h^{-1}) of North Pond isolates *Paracoccus* sp. 8HO (triangles), *Arthrobacter* sp. 1H (circles) and *Pseudomonas* sp. 9HT(squares) at 12°C (blue), 22°C (yellow), and 37°C (red). *Paracoccus* sp. 8HO growth rates were 0.12, 0.24, and 0.06, per hour, at 12, 22, and 37°C, respectively. *Arthrobacter* sp. 1H growth rates were 0.06, 0.24, 0.36 and *Pseudomonas* sp. 8HT growth rates were 0.06, 0.24, and 0.48. Curves without a plateau, seen in *Paracoccus* sp. 8HO at 12°C may be caused by a build up in EPS material, not cell division, since cultures became sticky with increasing time, resulting in difficulty pipetting. This was not confirmed by direct cell counts.

transfer *nasB* subunits). Alcohol dehydrogenase and lactate dehydrogenase were present, but we were unable to map the entire mixed acid fermentation previously proposed for *A. globiformis* (Eschbach et al., 2003). In general, the genome showed a high degree of auxotrophy, unable to biosynthesize 6 amino acids and coenzyme A, which may explain why this organism in particular was the one isolated from the enrichment procedure in rich media. No genes for motility or urease were observed.

The *Paracoccus* sp. 8HO genome contained multiple genes involved with nitrate processing including *nasA, nasE, nasD* and regulation genes such as *nirQ* (Supplementary Table S2). It contains the genes for nitrite reductase (NADH) small and large subunits (*nirD* and *nirB,* respectively) to ammonia. Although *P. denitrificans* is the canonical organism for the study of denitrification in this group and many other *Paracoccus* species can denitrify via the nap pathway, we did not find good genomic evidence of a dissimilatory nitrate reduction pathway, and interpret the nitrate reduction genes seen as playing a mostly assimilatory role (Supplementary Table S2; **Figure 5**; Alefounder et al., 1983). Considering our inability to activate dentrification activity in culture, along with the genomic evidence, we presume this organism is not capable of conserving energy through nitrate reduction. This genome was also auxotrophic for eight amino acids, perhaps explaining its success in complex media cultivation and contained genes for α, β, γ urease subunits and formate dehydrogenase, suggesting that ammonia recycling and potential for anaerobic activity exist. This genome contained 44 genes from KEGG pathways for cell motility, including genes for flagellar assembly and chemotaxis (Che A, B, D, W, X, Y). Motility requires a high level of electron flow for its operation, and while motility has been suggested in the subsurface (Orsi et al., 2013), it is unknown if the system would operate in this organism *in situ*.

The genome of the *Pseudomonas* sp. 8HT isolate from 68 mbsf contained the nitrate-reducing genes seen in *Paracoccus* sp. 8HO, as well as those genes necessary for reduction of NO to N_2O (*norE*, *norF*, *norC*, *norB*, *norQ*, and *norD*), and N_2O to N_2 (*nosR*, *nosZ*, *nosD*, *nosF*, *nosY*, and *nosL*) and periplasmic nitrate reductase genes *napA* and *napB* (Supplementary Table S2; **Figure 5**). *P. stutzeri* is a well-known denitrifying bacterium, and this isolate genome contains the transcriptional regulator, NirQ, suggesting activity should be able to be stimulated in proper growth conditions (Supplementary Table S2; Berks et al., 1995). We anticipate that further lab work would be able to induce the expression of these genes in laboratory culture, but for now, the presented genomic information is the only evidence of potential dissimilatory nitrate reduction. Genes are present for β, γ urease subunits (not the catalytic α subunit), formate dehydrogenase and lactate dehydrogenase, suggesting as with *Paracoccus* that potential for ammonia recycling and anaerobic activity exist. The genome is also auxotrophic for 12 amino acids and coenzyme A biosynthesis, which may be why it grew in complex cultivation media. Over 117 genes were mapped to cellular motility pathways, including multiple copies of chemotaxis proteins and flagellar synthesis, as stated before, it is unknown if these would be used *in situ*, however, they could be advantageous for finding food in a limited physical environment.

We investigated the three genomes for genes known to be involved in manganese oxidation, considering its increase in this environment (**Figure 3**), searching for genes previously implicated in the process (Brouwers et al., 1999; Dick et al., 2006, 2008). There were no genes annotated as *mnxG*, and at first

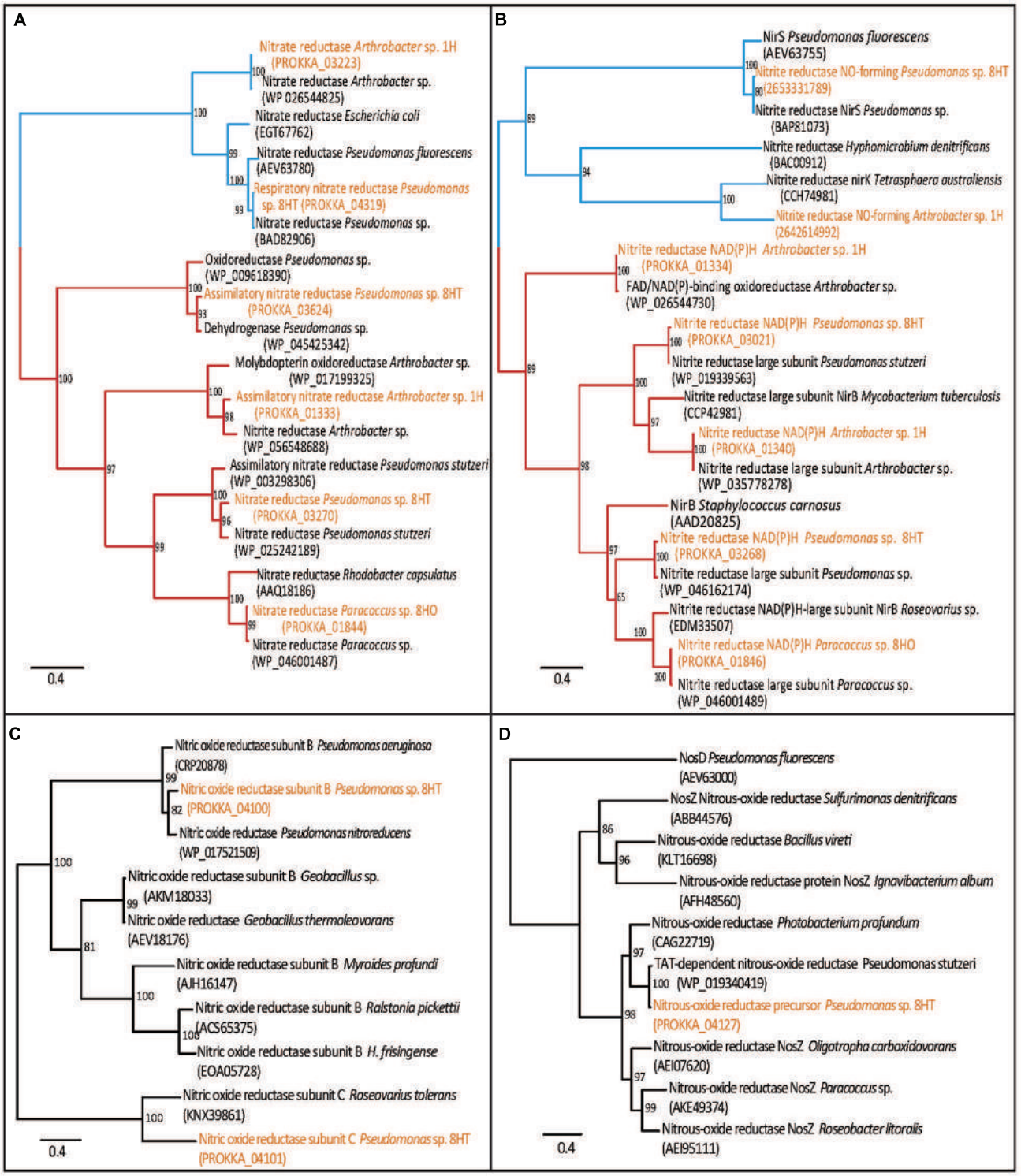

FIGURE 5 | Maximum-likelihood trees of nitrogen cycle proteins present in genomes, with dissimilatory branches in blue and assimilatory branches in red. (A) Nitrate reductase; showing *Arthrobacter* sp. 1H and *Pseudomonas* sp. 8HT have dissimilatory nitrate reductase, narG, and also assimilatory types (*Pseudomonas* sp. 8HT has two separate types). *Paracoccus* sp. 8HO and *Arthrobacter* sp. 1H each have one type of assimilatory nitrate reductase. **(B)** Nitrite reductase; showing all isolates have assimilatory type nitrite reductases. **(C)** Nitric oxide reductase; only the *Pseudomonas* sp 8HT isolate contains one, subunits **(B)** and **(C)** are shown **(D)** Nitrous oxide reductase; only found in *Pseudomonas* sp. 8HT. Proteins found in the genomes are highlighted in orange. Confidence values are located at the branch nodes.

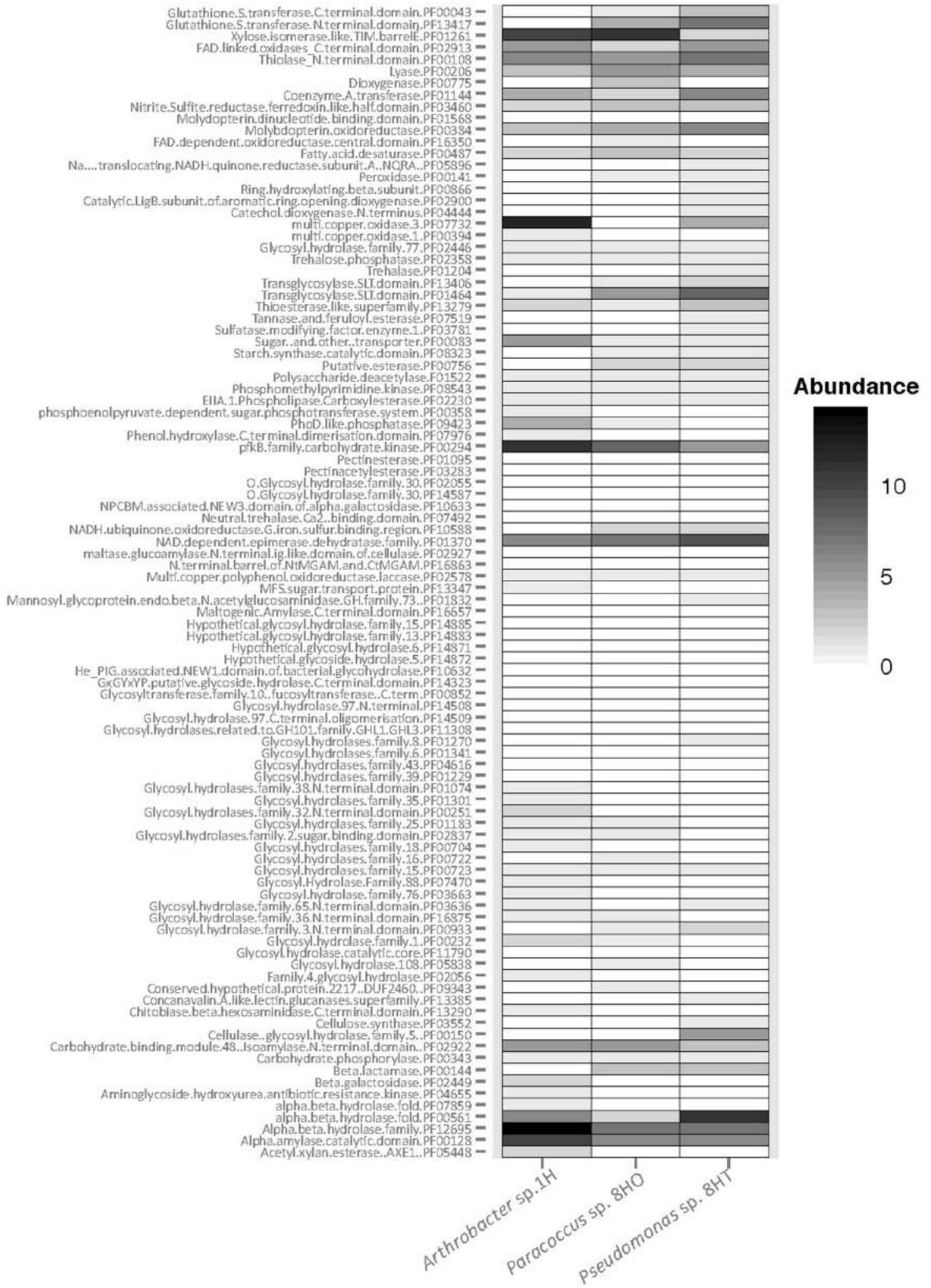

FIGURE 6 | Abundance of carbohydrate-active enzymes by protein family (pfam) across the three isolate genomes: *Arthrobacter* sp. 1H, *Paracoccus* sp. 8HO, *Pseudomonas* sp. 8HT. Black indicates more abundant genes, white indicates absence of genes. Categories without matches are not shown.

glance, none annotated as *cumA*. However, when we investigated for more general multicopper oxidase annotations, we did find a gene in the *Pseudomonas* isolate genome that was 96% similar to CumA-like oxidase, which is suggested to be the gene responsible for Mn oxidation in *P. putida* (Brouwers et al., 1999). Considering the negative result in the culture screening, we cannot confirm this gene confers the ability to oxidize manganese.

We examined all three isolates for carbohydrate-active enzymes (CAZy: Cantarel et al., 2009). As anticipated for aerobic heterotrophs, numerous genes were found, including 144 in *Arthobacter* sp. 1H, 140 in *Pseudomonas* sp. 8HT and 113 in *Paracoccus* sp. 8HO (**Figure 6**). The shallow isolate, *Arthrobacter* sp. 1H, contained abundant genes for glycosyl hydrolases and carbon processing compared to the deeper isolates. It had a higher number of α/β hydrolase (PF12695) and α amylase (PF00128) genes compared to the deeper isolates (**Figure 6**). Many genes are shared between all isolates, but only a few categories were present in abundance in the deeper isolates, *Paracoccus* and *Pseudomonas* and not the shallow *Arthrobacter* sp. (**Figure 6**). This includes β-lactamase (PF00144), a putative esterase (PF00756) and glutathione *S*-transferase (GST) in both C and N terminal domains (PF13417, PF00043), which has 10 total genes in *Pseudomonas* sp. 8HT and 5 in *Paracoccus* sp. 8HO, but none in *Arthrobacter* sp. 1H. These genes are noted for conferring the ability to survive oxidative stress (Vuilleumier and Pagni, 2002). We make the presumption that the sediment column is seeded from the overlying water, and when deposited, the *Arthrobacter* sp. 1H has a higher ability to utilize sugars. However, as the sediment column builds on top of it, it and the rest of its phylum will be pushed to lower depths of sediment, where they encounter the low oxygen zone that exists mid-sediment column (**Figure 3**). Our 16S rRNA gene amplicon sequencing of environmental DNA shows that there is a decrease in *Actinobacteria* and an increase in *Proteobacteria* when the sediment is reintroduced to oxygen diffusing up from flow above the basalt layer (**Figure 3**). The *Proteobacteria* have been noted to possess a greater abundance of GSTs than other bacterial phyla (Allocati et al., 2009), which could confer on them a greater ability to recover from the oxidative stress that can be caused from a reintroduction of oxygen after existence in a low or no-oxygen mid sediment column. This, of course, is speculation and should be investigated further using these laboratory cultures or environmental metagenomic data. Overall, we do not see clear indication in a differential ability to utilize carbon sources from these isolates dependent on depth of recovery, but we suggest the ability to withstand oxidative stress may be more crucial in survival downcore at this site.

Summary

The discrepancy between physiological characterization and genomic data hints at the difficulty of using single cultivation strategies. Given the presence of genes, it is likely that *Arthrobacter* and *Pseudomonas* isolates are capable of nitrate reduction *in situ*. This finding is particularly compelling since the geochemical profiles of their respective isolation depths suggested this metabolic versatility may be important in these low oxygen, nitrate containing porewaters. Recent work has indicated the importance of microbial nitrogen cycling in North Pond sediments (Wankel et al., 2015). In areas of low oxygen, high rates of denitrification were measured. Despite the presumed slow growth rate of organisms in these sediments, isotopic evidence was seen for the energetically costly pathways of nitrate assimilation, nitrification and dentrification (Wankel et al., 2015). The previous work postulates that greater regulation of these processes should be needed in an oligotrophic sedimentary setting such as North Pond. However, our study shows that recoverable isolates are quite similar to species in higher energy environments (**Figures 2**, **3**, and **5**), yet cultivation work suggests that metabolisms beyond aerobic heterotrophy are difficult to induce. The distribution of carbohydrate-active enzymes suggests that genes for oxidative stress may play a role in determining if cells can recover when reintroduced to oxygen in this sediment column (**Figure 6**). With genomes in hand, further investigations can be taken to examine additional metabolic controls and usage of carbon substrates by these isolates, which provide deep subsurface species on which future adaptation or metabolic tests may be performed.

CONCLUSION

We present the enrichment and isolation of three species of aerobic heterotrophs from the shallow and deep micro-aerobic zones of the U1382B sediment column. The three isolates were detected in very low relative abundance at their respective sediment depths according to culture-independent molecular analysis. This phenomenon of culturable microbes often being 'rare' community members is common across many environments (Shade et al., 2012), including the marine deep biosphere (Teske, 2006). However, these isolates, examined in pure culture and through genomics, have traits such as genes for nitrate reduction and denitrification, that would aid their survival in this environment where models have shown these activities to be important. These isolates can serve as type-species for investigations into adaptations for life in the deep biosphere.

AUTHOR CONTRIBUTIONS

JR: performed research, analyzed data, wrote paper. RL-Z: analyzed data, wrote paper. KW: funded research, wrote paper. JB: funded research, analyzed data, wrote paper.

FUNDING

JR was supported by CDEBI (OCE-0939564) and Schlanger Ocean Drilling graduate fellowships (SAF-12-05). RL-Z was funded by a CDEBI Postdoctoral Fellowship (OCE-0939564). Research was supported by a postcruise award to JR and JB through the Consortium for Ocean Leadership. A portion of this research was performed under the JGI-EMSL Collaborative Science Initiative awarded to Wrighton and used resources at the DOE Joint Genome Institute, which are DOE Office of Science User Facilities. JGI is sponsored by the Office of Biological and

Environmental Research and operated under Contract Nos. DE-AC02-05CH11231.

ACKNOWLEDGMENTS

We gratefully acknowledge the co-chiefs, staff, and scientists aboard IODP Expedition 336, of which JR was a member. We thank Rebecca Daly for assistance with interfacing with JGI and Richard Wolfe for CaZy assistance. Research was supported by a postcruise award to JR and JB through the Consortium for Ocean Leadership. This is CDEBI publication 326.

SUPPLEMENTARY MATERIAL

The Supplementary Material for this article can be found online at: http://journal.frontiersin.org/article/10.3389/fmicb.2016.00678

REFERENCES

Alefounder, P. R., Greenfield, A. J., McCarthy, J. E., and Ferguson, S. J. (1983). Selection and organisation of denitrifying electron-transfer pathways in *Paracoccus* denitrificans. *Biochim. Biophys. Acta (BBA)-Bioenergetics* 724, 20–39. doi: 10.1016/0005-2728(83)90022-1

Allocati, N., Federici, L., Masulli, M., and Di Illio, C. (2009). Glutathione transferases in bacteria. *FEBS J.* 276, 58–75. doi: 10.1111/j.1742-4658.2008.06743.x

Bale, S. J., Goodman, K., Rochelle, P. A., Marchesi, J. R., Fry, J. C., Weightman, A. J., et al. (1997). *Desulfovibrio profundus* sp. nov., a novel barophilic sulfate-reducing bacterium from deep sediment layers in the Japan Sea. *Int. J. Syst. Evol. Bacteriol.* 47, 515–521. doi: 10.1099/00207713-47-2-515

Bankevich, A., Nurk, S., Antipov, D., Gurevich, A. A., Dvorkin, M., Kulikov, A. S., et al. (2012). SPAdes: a new genome assembly algorithm and its application to single-cell sequencing. *J. Comput. Biol.* 19, 455–477. doi: 10.1089/cmb.2012.0021

Berks, B. C., Ferguson, S. J., Moir, J. W. B., and Richardson, D. J. (1995). Enzymes and associated electron transport systems that catalyse the respiratory reduction of nitrogen oxides and oxyanions. *Biochim. Biophys. Acta* 1232, 97–173. doi: 10.1016/0005-2728(95)00092-5

Biddle, J. F., House, C. H., and Brenchley, J. E. (2005) "Enrichment and cultivation of microorganisms from sediment from the slope of the Peru Trench (ODP Site 1230)," in *Proceedings of the ODP, Science Results, 201*, eds B. B. Jørgensen, S. L. D'Hondt, and D. J. Miller (College Station, TX: Ocean Drilling Program), 1–19. doi: 10.2973/odp.proc.sr.201.107.2005

Brouwers, G. J., de Vrind, J. P. M., Corstjens, P. L. A. M., Cornelis, P., Baysse, C., and de Vrind-de Jong, E. W. (1999). cumA, a gene encoding a multicopper oxidase, is involved in Mn+2 oxidation in *Pseudomonas putida* GB-1. *Appl. Environ. Microbiol.* 54, 1762–1768.

Burdige, D. J. (2007). Preservation of organic matter in marine sediments: controls, mechanisms and an imbalance in sediment organic carbon budgets? *Chem. Rev.* 107, 467–485. doi: 10.1021/cr050347q

Burdige, D. J., and Nealson, K. H. (1985). Microbial manganese reduction by enrichment cultures from coastal marine sediments. *Appl. Environ. Microbiol.* 50, 491–497.

Burgaud, G., Le Calvez, T., Arzur, D., Vandenkoornhuyse, P., and Barbier, G. (2009). Diversity of culturable marine filamentous fungi from deep-sea hydrothermal vents. *Environ. Microbiol.* 11, 1588–1600. doi: 10.1111/j.1462-2920.2009.01886.x

Cantarel, B. L., Coutinho, P. M., Rancurel, C., Bernard, T., Lombard, V., and Henrissat, B. (2009). The carbohydrate-active enzymes database (CAZy): an expert resources for glycogenomics. *Nucleic Acids Res.* 37, D233–D238. doi: 10.1093/nar/gkn663

Caporaso, J. G., Kuczynski, J., Stombaugh, J., Bittinger, K., Bushman, F. D., Costello, E. K., et al. (2010). QIIME allows analysis of high-throughput community sequencing data. *Nat. Methods* 7, 335–336. doi: 10.1038/nmeth.f.303

Carlson, C. A., and Ingraham, J. L. (1983). Comparison of denitrification by *Pseudomonas* stutzeri, *Pseudomonas aeruginosa*, and *Paracoccus denitrificans*. *Appl. Environ. Microbiol.* 45, 1247–1253.

Ciobanu, M. C., Burgaud, G., Dufresne, A., Breuker, A., Rédou, V., Maamar, S. B., et al. (2014). Microorganisms persist at record depths in the subseafloor of the Canterbury Basin. *ISME J.* 8, 1370–1380. doi: 10.1038/ismej.2013.250

Connon, S. A., and Giovannoni, S. J. (2002). High-throughput methods for culturing microorganisms in very-low-nutrient media yield diverse new marine isolates. *Appl. Environ. Microbiol.* 68, 3875–3885. doi: 10.1128/AEM.68.8.3878-3885.2002

D'Hondt, S., Jørgensen, B. B., Miller, D. J., Batzke, A., Blake, R., Cragg, B. A., et al. (2004). Distributions of microbial activities in deep subseafloor sediments. *Science* 306, 2216–2221. doi: 10.1126/science.1101155

D'Hondt, S., Spivack, A. J., Pockalny, R., Ferdelman, T. G., Fischer, J. P., Kallmeyer, J., et al. (2009). Subseafloor sedimentary life in the South Pacific Gyre. *Proc. Natl. Acad. Sci. U.S.A.* 106, 11651–11656. doi: 10.1073/pnas.0811793106

Dick, G. J., Lee, Y. E., and Tebo, B. M. (2006). Manganese(II)-oxidizing *Bacillus* spores in guaymas basin hydrothermal sediments and plumes. *Appl. Environ. Microbiol.* 72, 3184–3190. doi: 10.1128/AEM.72.5.3184-3190.2006

Dick, G. J., Podell, S., Johnson, H. A., Rivera-Espinoza, Y., Bernier-Latmani, R., McCarthy, J. K., et al. (2008). Genomic insights into Mn(II) oxidation by the marine Alphaproteobacterium *Aurantimonas* sp. Strain DI85-9A1. *Appl. Environ. Microbiol.* 74, 2646–2658.

Eden, P. A., Schmidt, T. M., Blakemore, R. P., and Pace, N. R. (1991). Phylogenetic analysis of *Aquaspirillum magnetotacticum* using polymerase chain reaction-amplified 16S rRNA specific DNA. *Int. J. Syst. Bacteriol.* 41, 324–325. doi: 10.1099/00207713-41-2-324

Edgar, R. C. (2004). MUSCLE: multiple sequence alignment with high accuracy and high throughput. *Nucleic Acids Res.* 32, 1792–1797. doi: 10.1093/nar/gkh340

Edwards, K. J., Becker, K., and Colwell, F. (2012). The deep, dark energy biosphere: intraterrestrial life on earth. *Annu. Rev. Earth Planet. Sci.* 40, 551–568. doi: 10.1146/annurev-earth-042711-105500

Eschbach, M., Möbitz, H., Rompf, A., and Jahn, D. (2003). Members of the genus Arthrobacter grow anaerobically using nitrate ammonification and fermentative processes: anaerobic adaptation of aerobic bacteria abundant in soil. *FEMS Microbiol. Lett.* 223, 227–230. doi: 10.1016/S0378-1097(03)00383-5

Expedition 336 Scientists (2012). *Mid-Atlantic Ridge Microbiology: Initiation of Long-Term Coupled Microbiological, Geochemical, and Hydrological Experimentation Within the Seafloor at North Pond, Western Flank of the Mid-Atlantic Ridge.* IODP Prel. Rept. College Station, TX: Integrated Ocean Drilling Program, 336. doi: 10.2204/iodp.pr.336.2012

Fichtel, K., Mathes, F., Könneke, M., Cypionka, H., and Engelen, B. (2012). Isolation of sulfate-reducing bacteria from sediments above the deep-subseafloor aquifer. *Front. Microbiol.* 3:65. doi: 10.3389/fmicb.2012.00065

Gregory, E., and Staley, J. T. (1982). Widespread distribution of ability to oxidize manganese among freshwater bacteria. *Appl. Environ. Microbiol.* 44, 509–511.

Kogure, K., Simidu, U., and Taga, N. (1979). A tentative direct microscopic method for counting living marine bacteria. *Can. J. Microbiol.* 25, 415–420. doi: 10.1139/m79-063

Krumbein, W. E., and Altmann, H. J. (1973). A new method for the detection and enumeration of manganese oxidizing and reducing microorganisms. *Helgol. Wiss. Meeresunters.* 25, 347–356. doi: 10.1007/BF01611203

Laczny, C. C., Sternal, T., Plugaru, V., Gawron, P., Atashpendar, A., Margossian, H. H., et al. (2015). VizBin – an application for reference-independent visualization and human-augmented binning of metagenomic data. *Microbiome* 3:1. doi: 10.1186/s40168-014-0066-1

Langseth, M. G., Becker, K., Von Herzen, R. P., and Schultheiss, P. (1992). Heat and fluid flux through sediment on the western flank of the mid-atlantic ridge:

a hydrogeological study of north pond. *Geophys. Res. Lett.* 19, 517–520. doi: 10.1029/92GL00079

Lever, M. A., Rouxel, O., Alt, J. C., Shimizu, N., Ono, S., Coggon, R. M., et al. (2013). Evidence for microbial carbon and sulfur cycling in deeply buried ridge flank basalt. *Science* 339, 1305–1308. doi: 10.1126/science.1229240

Lomstein, B. A., Langerhuus, A. T., D'Hondt, S., Jørgensen, B. B., and Spivack, A. J. (2012). Endospore abundance, microbial growth and necromass turnover in deep subseafloor sediment. *Nature* 484, 101–104. doi: 10.1038/nature10905

Ludwig, W., Strunk, O., Westram, R., Richter, L., Meier, H., Yadhukumar, et al. (2004). ARB: a software environment for sequence data. *Nucleic Acids Res.* 32, 1363–1371. doi: 10.1093/nar/gkh293

Markowitz, V. M., Chen, I. M., Palaniappan, K., Chu, K., Szeto, E., Grechkin, Y., et al. (2012). IMG: the integrated microbial genomes database and comparative analysis system. *Nucleic Acids Res.* 40, D115–D122. doi: 10.1093/nar/gkr1044

Marx, J. G., Carpenter, S. D., and Deming, J. W. (2009). Production of cryoprotectant extracellular polysaccharide substances (EPS) by the marine psychrophilic bacterium *Colwellia psychrerythraea* strain 34H under extreme conditions. *Can. J. Microbiol.* 55, 63–72. doi: 10.1139/W08-130

Mikucki, J. A., Liu, Y., Delwiche, M., Colwell, F. S., and Boone, D. R. (2003). Isolation of a methanogen from deep marine sediments that contain methane hydrates, and description of Methanocullus submarinus sp. nov. *Appl. Environ. Microbiol.* 69, 3311–3316. doi: 10.1128/AEM.69.6.3311-3316.2003

Mistry, J., Bateman, A., and Finn, R. D. (2007). Predicting active site residue annotations in the Pfam database. *BMC Bioinformatics* 8:298. doi: 10.1186/1471-2105-8-298

Nelson, D. C., Jørgensen, B. B., and Revsbech, P. (1986). Growth pattern and yield of a chemoautotrophic *Beggiatoa* sp. in oxygen-sulfide microgradients. *Appl. Environ. Microbiol.* 52, 225–233.

Okazaki, M., Sugita, T., Shimizu, M., Ohode, Y., Iwamoto, K., De Vrind-De Jong, E. W., et al. (1997). Partial purification and characterization of manganese oxidizing factors of *Pseudomonas* fluorescens GB-1. *Appl. Environ. Microbiol.* 63, 4793–4799.

Orcutt, B. N., Wheat, C. G., Rouxel, O., Hulme, S., Edwards, K. J., and Bach, W. (2013). Oxygen consumption rates in subseafloor basaltic crust derived from a reaction transport model. *Nat. Commun.* 4:2539. doi: 10.1038/ncomms3539

Orsi, W. O., Christman, G., Edgcomb, V. E., and Biddle, J. F. (2013). Gene expression in the deep biosphere. *Nature* 499, 205–208. doi: 10.1038/nature12230

Parkes, R. J., Martin, D., Amann, H., Anders, E., Holland, M., Schultheiss, P. J., et al. (2009). "Technology for high-pressure sampling and analysis of deep-sea sediments, associated gas hydrates, and deep- biosphere processes," in *Natural Gas Hydrates - Energy Resource Potential and Associated Geologic Hazards: AAPG Memoir 89*, eds T. Collett, A. Johnson, C. Knapp, and R. Boswell (Tulsa, OK: American Association of Petroleum Geologists), 672–683.

Parks, D. H., Imelfort, M., Skennerton, C. T., Hugenholtz, P., and Tyson, G. W. (2015). CheckM: assessing the quality of microbial genomes recovered from isolates, single cells, and metagenomes. *Genome Res.* 25, 1043–1055. doi: 10.1101/gr.186072.114

Pfennig, N., Widdel, F., and Trüper, H. G. (1981). *The Dissimilatory Sulfate-Reducing Bacteria. The Prokaryotes*. Berlin: Springer, 926–940.

Picard, A., and Ferdelman, T. G. (2011). Linking microbial heterotrophic activity and sediment lithology in oxic, oligotrophic sub-seafloor sediments of the North Atlantic Ocean. *Front. Microbiol.* 2:263. doi: 10.3389/fmicb.2011.00263

Price, M. N., Dehal, P. S., and Arkin, A. P. (2009). FastTree: computing large minimum evolution trees with profiles instead of a distance matrix. *Mol. Biol. Evol.* 26, 1641–1650. doi: 10.1093/molbev/msp077

Pruesse, E., Peplies, J., and Glöckner, F. O. (2012). SINA: accurate high- throughput multiple sequence alignment of ribosomal RNA genes. *Bioinformatics* 28, 1823–1829. doi: 10.1093/bioinformatics/bts252

Quast, C., Pruesse, E., Yilmaz, P., Gerken, J., Schweer, T., Yarza, P., et al. (2013). The SILVA ribosomal RNA gene database project: improved data processing and web-based tools. *Nucleic Acids Res.* 41, D590–D596.

Reddy, G. S., Aggarwal, R. K., Matsumoto, G. I., and Shivaji, S. (2000). Arthrobacter flavus sp. nov., a psychrophilic bacterium isolated from a pond in McMurdo Dry Valley, Antarctica. *Int. J. Syst. Evol. Microbiol.* 50, 1553–1561. doi: 10.1099/00207713-50-4-1553

Salter, S. J., Cox, M. J., Turek, E. M., Calus, S. T., Cookson, W. O., Moffatt, M. F., et al. (2014). Reagent and laboratory contamination can critically impact sequence-based microbiome analysis. *BMC Biol.* 12:87. doi: 10.1186/s12915-014-0087-z

Samuelsson, M. O. (1985). Dissimilatory nitrate reduction to nitrate, nitrous oxide, and ammonium by *Pseudomonas* putrefaciens. *Appl. Environ. Microbiol.* 50, 812–815.

Seeman, T. (2014). Prokka: rapid prokaryotic genome annotation. *Bioinformatics* 30, 2068–2069. doi: 10.1093/bioinformatics/btu153

Shade, A., Hogan, C. S., Klimowicz, A. K., Linske, M., McManus, P. S., and Handelsman, J. (2012). Culturing captures members of the soil rare biosphere. *Environ. Microbiol.* 14, 2247–2252. doi: 10.1111/j.1462-2920.2012.02817.x

Smith, D. C., Spivack, A. J., Fisk, M. R., Haveman, S. A., and Staudigel, H. (2000). Tracer-based estimates of drilling-induced microbial contamination of deep sea crust. *Geomicrobiol. J.* 17, 207–219. doi: 10.1080/01490450050121170

Staley, J. T., and Konopka, A. (1985). Measurement of in situ activities of nonphotosynthetic microorganisms in aquatic and terrestrial habitats. *Annu. Rev. Microbiol.* 39, 321–346. doi: 10.1146/annurev.mi.39.100185.001541

Straub, K. L., and Buchholz-Cleven, B. E. E. (1998). Enumeration and detection of anaerobic ferrous iron-oxidizing, nitrate-reducing bacteria from diverse European sediments. *Appl. Environ. Microbiol.* 64, 4846–4856.

Tebo, B. M., Johnson, H. A., McCarthy, J. K., and Templeton, A. S. (2005). Geomicrobiology of manganese (II) oxidation. *TRENDS Microbiol.* 13, 421–428. doi: 10.1016/j.tim.2005.07.009

Templeton, A. S., Staudigel, H., and Tebo, B. M. (2005). Diverse Mn (II)-oxidizing bacteria isolated from submarine basalts at Loihi Seamount. *Geomicrobiol. J.* 22, 127–139. doi: 10.1080/01490450590945951

Teske, A. P. (2006). Microbial communities of deep marine subsurface sediments: molecular and cultivation surveys. *Geomicrobiol. J.* 23, 357–368. doi: 10.1080/01490450600875613

Toffin, L., Bidault, A., Pignet, P., Tindall, B. J., Slobodkin, A., Kato, C., et al. (2004). *Shewanella profunda* sp. nov., isolated from deep marine sediment of the Nankai Trough. *Int. J. Syst. Evol. Bacteriol.* 54, 1943–1949. doi: 10.1099/ijs.0.03007-0

Tsubokura, A., Yoneda, H., and Mizuta, H. (1999). *Paracoccus carotinifaciens* sp. nov., a new aerobic Gram-negative astaxanthin- producing bacterium. *Int. J. Syst. Evol. Bacteriol.* 49, 277–282. doi: 10.1099/00207713-49-1-277

Vetriani, C., Chew, Y. S., Miller, S. M., Yagi, J., Coombs, J., Lutz, R. A., et al. (2005). Mercury adaptation among bacteria from a deep-sea hydrothermal vent. *Appl. Environ. Microbiol.* 71, 220–226. doi: 10.1128/AEM.71.1.220-226.2005

Vuilleumier, S., and Pagni, M. (2002). The elusive roles of bacterial glutathione S-transferases: new lessons from genomes. *Appl. Microbiol. Biotechnol.* 58, 138–146. doi: 10.1007/s00253-001-0836-0

Wankel, S. D., Buchwald, C., Ziebis, W., Wenk, C. B., and Lehmann, M. F. (2015). Nitrogen cycling in the deep sedimentary biosphere: nitrate isotopes in porewaters underlying the oliogtrophic North Atlantic. *Biogeosciences* 12, 7483–7502. doi: 10.5194/bg-12-7483-2015

Waterhouse, A. M., Procter, J. B., Martin, D. M. A., Clamp, M., and Barton, G. J. (2009). Jalview version 2 - a multiple sequence alignment editor and analysis workbench. *Bioinformatics* 25, 1189–1191. doi: 10.1093/bioinformatics/btp033

Wolfe, R. S., Amy, C. R., and Stephen, S. R. (2011). Techniques for cultivating methanogens. *Methods Enzymol.* 494, 1–22. doi: 10.1016/B978-0-12-385112-3.00001-9

Wrighton, K. C., Thrash, J. C., Melnyk, R. A., Bigi, J. P., Byrne-Bailey, K. G., Remis, J. P., et al. (2011). Evidence for direct electron transfer by a Gram-positive bacterium isolated from a microbial fuel cell. *Appl. Environ. Microbiol.* 77, 7633–7639. doi: 10.1128/AEM.05365-11

Wu, Y.-W., Tang, Y.-H., Tringe, S. G., Simmons, B. A., and Singer, S. W. (2014). MaxBin: an automated binning method to recover individual genomes from metagenomes using an expectation-maximization algorithm. *Microbiome* 2:26. doi: 10.1186/2049-2618-2-26

Conflict of Interest Statement: The authors declare that the research was conducted in the absence of any commercial or financial relationships that could be construed as a potential conflict of interest.

frontiers in Microbiology

ORIGINAL RESEARCH
published: 05 April 2016
doi: 10.3389/fmicb.2016.00454

Nanocalorimetric Characterization of Microbial Activity in Deep Subsurface Oceanic Crustal Fluids

Alberto Robador[1], Douglas E. LaRowe[2], Sean P. Jungbluth[3,4†], Huei-Ting Lin[3†], Michael S. Rappé[4], Kenneth H. Nealson[2,5] and Jan P. Amend[2,5]*

[1] Center for Dark Energy Biosphere Investigations, NASA Astrobiology Institute, University of Southern California, Los Angeles, CA, USA, [2] Department of Earth Sciences, University of Southern California, Los Angeles, CA, USA, [3] Department of Oceanography, School of Ocean and Earth Science and Technology, University of Hawaii at Manoa, Honolulu, HI, USA, [4] Hawaii Institute of Marine Biology, School of Ocean and Earth Science and Technology, University of Hawaii at Manoa, Kaneohe, HI, USA, [5] Department of Biological Sciences, University of Southern California, Los Angeles, CA, USA

OPEN ACCESS

Edited by:
Cara M. Santelli, University of Minnesota, USA

Reviewed by:
Mayumi Seto, Nara Women's University, Japan
Christopher Kenneth Algar, Marine Biological Laboratory, USA

****Correspondence:***
Alberto Robador
robadora@usc.edu

†Present address:
Sean P. Jungbluth
Center for Dark Energy Biosphere Investigations, University of Southern California, Los Angeles, CA, USA;
Huei-Ting Lin
Institute of Oceanography, National Taiwan University, Taipei, Taiwan

Specialty section:
This article was submitted to Extreme Microbiology, a section of the journal Frontiers in Microbiology

Received: *12 January 2016*
Accepted: *21 March 2016*
Published: *05 April 2016*

Citation:
Robador A, LaRowe DE, Jungbluth SP, Lin H-T, Rappé MS, Nealson KH and Amend JP (2016) Nanocalorimetric Characterization of Microbial Activity in Deep Subsurface Oceanic Crustal Fluids. Front. Microbiol. 7:454. doi: 10.3389/fmicb.2016.00454

Although fluids within the upper oceanic basaltic crust harbor a substantial fraction of the total prokaryotic cells on Earth, the energy needs of this microbial population are unknown. In this study, a nanocalorimeter (sensitivity down to 1.2 nW ml^{-1}) was used to measure the enthalpy of microbially catalyzed reactions as a function of temperature in samples from two distinct crustal fluid aquifers. Microorganisms in unamended, warm (63°C) and geochemically altered anoxic fluids taken from 292 meters sub-basement (msb) near the Juan de Fuca Ridge produced 267.3 mJ of heat over the course of 97 h during a step-wise isothermal scan from 35.5 to 85.0°C. Most of this heat signal likely stems from the germination of thermophilic endospores (6.66×10^4 cells $ml^{-1}{}_{FLUID}$) and their subsequent metabolic activity at temperatures greater than 50°C. The average cellular energy consumption (5.68 pW $cell^{-1}$) reveals the high metabolic potential of a dormant community transported by fluids circulating through the ocean crust. By contrast, samples taken from 293 msb from cooler (3.8°C), relatively unaltered oxic fluids, produced 12.8 mJ of heat over the course of 14 h as temperature ramped from 34.8 to 43.0°C. Corresponding cell-specific energy turnover rates (0.18 pW $cell^{-1}$) were converted to oxygen uptake rates of 24.5 nmol O_2 $ml^{-1}{}_{FLUID}$ d^{-1}, validating previous model predictions of microbial activity in this environment. Given that the investigated fluids are characteristic of expansive areas of the upper oceanic crust, the measured metabolic heat rates can be used to constrain boundaries of habitability and microbial activity in the oceanic crust.

Keywords: calorimetry, crustal fluids, microbial energy turnover, subsurface biosphere, cell-specific metabolic rates

INTRODUCTION

Low to moderate temperature (<100°C) fluids circulating within the uppermost basaltic ocean crust are known for their contribution to global biogeochemical cycling (Bach and Edwards, 2003; Orcutt et al., 2011; Robador et al., 2015), and for harboring an expansive microbial biosphere distinct from marine sediments (Jungbluth et al., 2016). Knowledge of the metabolic reactions supporting life in these habitats, however, is sparse and limited to specific respiration processes such

as oxygen consumption, methane cycling, and sulfate reduction (Lever et al., 2013; Orcutt et al., 2013b; Robador et al., 2015). A better understanding of the metabolic activity in deep subseafloor fluids is handicapped by several technical challenges, including access to these habitats and the suspected slow growth rates of microorganisms in such low-energy environments (Cowen, 2004).

The physiological state of microbial communities in low-energy systems is manifestly different than those observed in laboratory cultures, which are characterized by rapid growth, high metabolic rates, and high cell densities (Neidhardt et al., 1990). Natural, energy-starved microbial communities are typically associated with a minimal array of functions required to sustain a metabolically active state, or basal maintenance power (Hoehler and Jørgensen, 2013). As a result, it becomes difficult to determine whether microorganisms in energy-limiting environments are alive and active (Jørgensen, 2011). Therefore, one corresponding research challenge is the development of technical approaches wherein microbial metabolism can be characterized. Current techniques for the quantification of microbial activities rely on the identification of specific turnover processes that often occur simultaneously (e.g., methanogenesis and sulfate reduction, Lovley et al., 1982) at rates below detection limits (Adhikari and Kallmeyer, 2010).

An alternative approach to determining the metabolic rate of microorganisms in low-energy settings is to measure the energy dissipated by all biological activities using direct calorimetry (Brown et al., 2004). This approach has been used to accurately measure the heat generated from metabolic activity in microbial cultures (Winkelmann et al., 2004; Braissant et al., 2010) but, despite recent advances in quantifying microbial respiration rates in the environment (Djamali et al., 2012; Mukhanov et al., 2012), technical limitations such as low sensitivities and slow responses have limited the application of calorimetry for these measurements (Karl, 2014).

Calorimetry is based on the assumption that heat is the direct product of all metabolic functions (Russell, 1986; Russell and Cook, 1995). Calorimetry data provide direct heat measurements, which are indicative of the change in enthalpy associated with microbial activity, therefore, allowing for a direct quantification of microbial energy turnover. So far, microbial energy consumption in low-energy environments has been estimated from the turnover rates of an electron donor or acceptor and the calculated Gibbs free energy yield of the predicted reaction (Orcutt et al., 2013a; Lin et al., 2014; LaRowe and Amend, 2015a,b). Calorimetry measurements, however, are not confounded by certain problems of Gibbs free energy calculations (Russell and Cook, 1995) such as those resulting from uncertainties in the exact stoichiometry of the reaction, in the concentrations of reactants and products, and in the estimation of activity coefficients and thermodynamic properties for all individual chemical species.

In this study, we measured the change in enthalpy as a function of temperature by direct nanocalorimetry in order to quantify and interpret microbial energy requirements in natural subseafloor igneous crustal fluids from two aquifers that differ with respect to their *in situ* physicochemical conditions. Warm (>60°C) anoxic fluids are common in all ocean basins (Davis et al., 1997); however, the majority of the upper oceanic crust experiences much cooler (<20°C, Johnson and Pruis, 2003) and presumably oxic conditions (Ziebis et al., 2012; Orcutt et al., 2013b). Therefore, we examined the metabolic heat production rates of microorganisms in highly geochemically altered fluids that are characteristic of the Juan de Fuca Ridge (JFR) in the eastern Pacific Ocean, but focused on fresh-to-moderately altered fluids from a site known as North Pond (NP) in the northern Atlantic Ocean (**Figure 1**), which may be more informative ecologically to constrain the global rates of microbial activity in deep basaltic ocean crust.

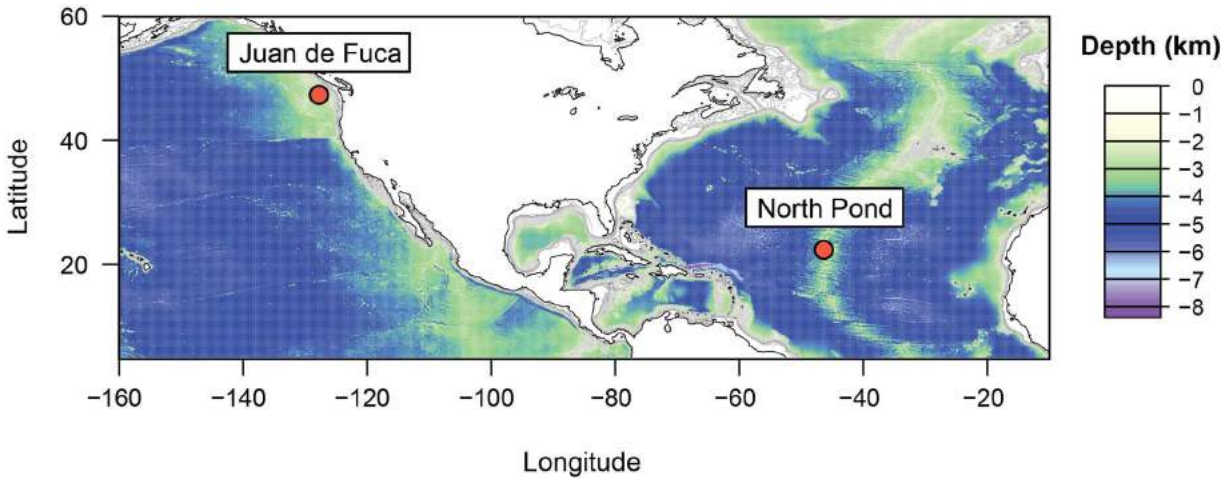

FIGURE 1 | Location of CORK observatory sampling sites on the Juan de Fuca Ridge flank, Pacific Ocean (47°45.6′N, 127°45.6′W) and the North Pond, Atlantic Ocean (22°48.1′N, 46°03.2′W).

MATERIALS AND METHODS

Sampling

Crustal fluids were collected from subseafloor Circulation Obviation Retrofit Kit (CORK) observatories installed within boreholes drilled several hundred meters into the ocean crust, preventing circulation between the open hole and ocean bottom water and allowing access to deep crustal fluids. Samples from the eastern flank of the JFR were obtained in August 2014 from a CORK observatory at borehole U1362A (47°45.6′N, 127°45.6′W) using the ROV *Jason II* deployed from the R/V *Atlantis* (cruise AT 26-18). NP crustal fluids were sampled in April of 2012 from a CORK observatory at Hole U1383C (22°48.1241′N, 46°03.1662′W) using the ROV *Jason II* (WHOI) deployed from the R/V *Maria S. Merian* (cruise MSM 20-5). Both boreholes (U1362A and U1383C) are instrumented with multilevel CORK observatories (Fisher et al., 2011; Edwards et al., 2014), which allow the sampling at different depth intervals using umbilicals with non-reactive tubing (Teflon® and Tefzel®, DuPont™, for U1362A and U1383C respectively). The CORK observatory at borehole U1362A (JFR) is situated at 2661 m below sea level, penetrating 236 m of sediment and the upper 292 m of basement. The CORK observatory at borehole U1383C (NP) is located at 4425 m below sea level and penetrates the upper 293 m of basement through 38 m of sediment. Samples from the deepest horizons were collected at the seafloor into sampling bags of Tedlar polyvinyl fluoride (PVF) film (Midan Co., Chino, CA, USA) as previously described (Robador et al., 2015) and returned to the ship using an independent elevator. Whole crustal fluids were subsequently transferred by gravity feed to 2 L glass bottles (previously cleaned and combusted at 480°C for 6 h) sealed with butyl rubber stoppers and stored at 4°C until further processing.

Crustal Fluids

Crustal fluids circulating through the eastern flank of the JFR system are warm (63°C) and characterized by a steep chemical gradient; the dominant oxidant changes from oxygen to sulfate, which is accompanied by a decrease in organic matter concentration and an increase in the reduced species hydrogen sulfide and methane (Robador et al., 2015). Crustal fluids within upper basaltic basement at NP on the other hand are younger, much cooler (3.8°C), and oxic (Meyer et al., 2016). Fluids collected from CORK observatories at boreholes U1362A and U1383C were analyzed for the major and minor chemical constituents in seawater. Analytical data used in this study are compiled in **Table 1**. Additional original data, including analytical methods, are published elsewhere (Edwards et al., 2014; Lin et al., 2014; Meyer et al., 2016).

TABLE 1 | Chemical compositions of basaltic crustal fluids collected from CORK observatories at boreholes U1362A and U1383C.

	U1362A[a]	U1383C[b]
Temperature (°C)	63	3.8
Pressure (kpa)	~27,071	~46,815
pH	7.9	7.6
Dissolved constituents		
Ca^{2+} (mM)	55.1	10.1
$SO_4{}^{2-}$ (mM)	18.0	27.6
Na^{+} (mM)	463.2	459
K^{+} (mM)	6.4	10
Mg^{2+} (mM)	2.2	52.4
Total organic carbon (μM)	15.5	24.2
Total nitrogen (μM)	112.0	24
Si (μM)	1176.0	120
NO^{3-} (μM)	<0.1	21.8
O_2 (μM)	<0.5	213

[a] *This study.*
[b] *Data from Edwards et al. (2014) and Meyer et al. (2016).*

Nanocalorimetry Experiments

Metabolic heat production rates in crustal fluids were measured using a thermal activity monitor model TAM III equipped with a nanocalorimeter (TA Instruments, Lindon, UT, USA). The TAM III coupled to the nanocalorimeter offers the maximum sensitivity of most commercial isothermal calorimeters (Braissant et al., 2010). These metabolic heat production rates are measured in a pair of sealed glass ampules (up to 4 ml) as the difference in heat flow between the sample and a reference.

Two-step isothermal experiments were performed on the same sample at different temperatures (15–100°C for JFR and 30–85°C for NP). These temperature ranges extend beyond the upper and lower limits of observed microbial activity. To ensure that the samples were in thermal equilibrium with the calorimeter and that the collected data corresponded to that at the true transition temperatures, a very slow scan rate (0.5°C h^{-1}) was used. Thermal equilibrium is not always achieved when differential scanning calorimetry data are collected using far higher scanning rates (often 15–60°C h^{-1}, Hansen and Criddle, 1990; Mukhanov et al., 2012).

Calorimetry experiments consisted of 2 ml of unamended crustal fluids and 2 ml of headspace in glass ampules (previously cleaned and combusted at 480°C for 6 h), crimped and sealed with butyl rubber stoppers. To prevent contamination of the JFR flank anoxic fluids with oxygen, the ampules were prepared in an anaerobic chamber (<5 ppm oxygen and 5% hydrogen gas mix, COY Laboratory Products Inc., Grass Lake, MI, USA). The reference ampule consisted of 2 ml filter-sterilized (0.2 μm) crustal fluids and 2 ml of headspace. Sample and reference ampules were prepared at the same time (i.e., a new reference was used for each measurement) and pre-incubated in the calorimeter at the operating temperature for 24 h prior to each experiment. This minimized potential changes in heat flow associated with, for example, differences in temperature between sample and nanocalorimeter and stresses related to sample preparation.

Two independent nanocalorimeters were used simultaneously to run parallel blank experiments, which consisted of 0.2 μm filter-sterilized crustal fluids in both the sample and reference ampules. An initial baseline correction was done by subtracting the blanks from the sample heat-flow profiles. After identification of upper and lower temperatures of measurable metabolic heat

rates, a second baseline correction was drawn manually between these temperatures using the TAM III Lab Assistant Software (V1.3.0.153, TA Instruments, Lindon, UT, USA) to obtain final data on microbial activity.

Quantifying Spore-Forming Bacteria

Endosporulation allows certain bacteria to persist as dormant cells in adverse conditions, such as prolonged exposure to the low (4°C) storage temperatures (Hubert et al., 2009). In order to quantify the numerical contribution of spore-forming bacteria in our experiments, 150 ml of JFR and NP fluids were pasteurized at 80°C for 2 h and incubated at 50°C for 48 h to induce germination of spores as previously described (Müller et al., 2014). Germinated cells were subsequently quantified as described below.

Total Cell Counts

Cell counts, in triplicate, were performed as previously described for marine planktonic environments (Patel et al., 2007). In short, 10–150 ml of crustal fluids were sampled and fixed in 0.2 μm filtered formalin [37–39% (wt/vol) formaldehyde solution] overnight at 4°C. Samples were then filtered onto polycarbonate membrane filters (type, GTBP; pore size, 0.2 μm; diameter, 2.5 mm; Sartorius, Göttingen, Germany) and stained with SYBR Green I (1:400 dilution from stock solution; Life Technologies, Carlsbad, CA, USA). Filters were mounted onto microscope glass slides with 0.1% (vol/vol) *p*-phenylenediamine anti-fade mounting medium and visualized using a Nikon Eclipse Ti-E inverted microscope (Nikon, Tokyo, Japan) equipped with a drift correction unit (Nikon Perfect Focus System) for maintaining focus at the coverslip-filter interface during imaging. Fluorescence imaging of SYBR Green I was done in the FITC (Nikon filter set B-2E/C). At least 1000 cells stained with SYBR Green I were counted per sample using the scientific image analysis and visualization program *DAIME* (Daims et al., 2006).

Thermodynamic Calculations

Enthalpies (ΔH_r) of organic matter oxidation with the dominant available terminal electron acceptor (SO_4^{2-} for JFR and O_2 for NP) were calculated as a function of temperature for the reactions

$$4C_5H_9NO_2 + 11SO_4^{2-} + 8H_2O \rightarrow 11HS^- + 20HCO_3^- + 5H^+ + 4NH_4^+ \quad (1)$$

and

$$2C_5H_9NO_2 + 11O_2 + 4H_2O \rightarrow 10HCO_3^- + 8H^+ + 2NH_4^+ \quad (2)$$

or

$$2C_5H_9NO_2 + 15O_2 + 2H_2O \rightarrow 10HCO_3^- + 12H^+ + 2NO_3^- \quad (3)$$

respectively (see **Figure 2**). Proline ($C_5H_9NO_2$) was used as a proxy for organic matter since its nominal carbon oxidation state (−0.4, see LaRowe and Van Cappellen, 2011) is the same as that of the dissolved organic carbon in JFR fluids (personal communication, Boris Koch). Values of ΔH_r were calculated as a function of temperature using the revised HKF equations of state (Helgeson et al., 1981; Tanger and Helgeson, 1988; Shock et al., 1992), the SUPCRT92 software package (Johnson et al., 1992), and thermodynamic data taken from the literature (Shock and

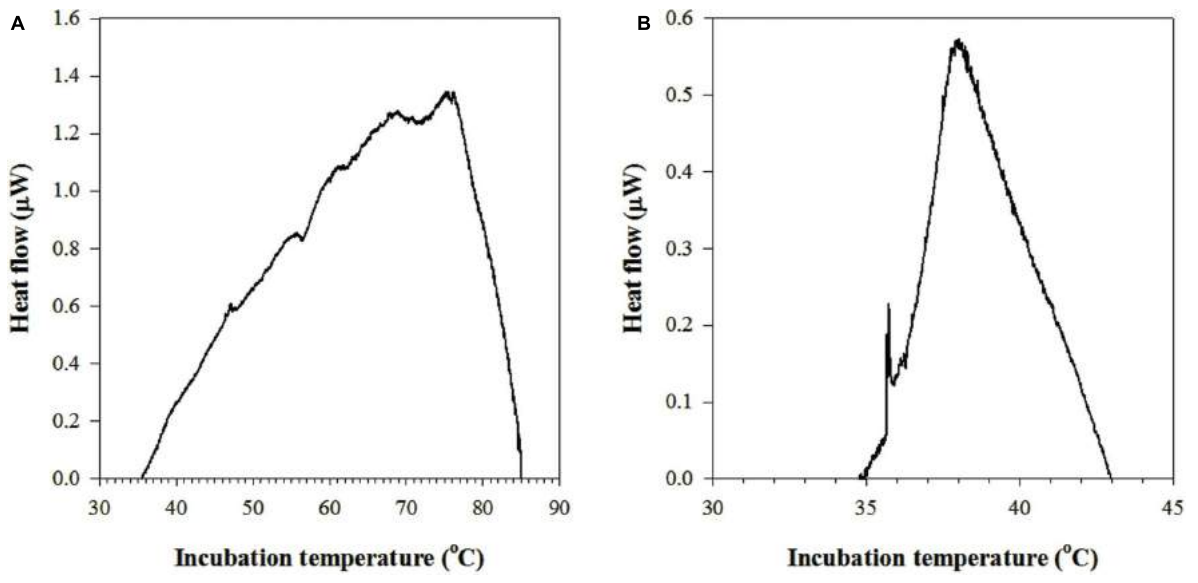

FIGURE 2 | Metabolic heat rates as a function of temperature as measured by two-step isothermal nanocalorimetry in subseafloor crustal fluids of (A) Juan de Fuca Ridge flank and (B) North Pond. An initial baseline correction was performed by subtracting blanks from sample heat-flow profiles. After identification of upper and lower temperatures of measurable metabolic heat rates, a second baseline correction was performed manually between these temperatures.

Helgeson, 1988, 1990; Shock et al., 1989; Shock, 1995; Amend and Helgeson, 1997; Amend and Plyasunov, 2001; Dick et al., 2006).

RESULTS

Metabolic heat production rates were measured in crustal fluids by two-step isothermal nanocalorimetry (**Table 2**) as watts of heat flow. The watt unit is defined as the energy consumption rate of one joule per second. Standard deviation of initial and final isothermal measurements provided an estimate of baseline reproducibility of 2.7 nW ml^{-1} and 1.2 nW ml^{-1} in fluids from the JFR flank and NP, respectively. These data were used to determine the detection limit of microbial metabolic heat production rates on crustal fluids and to delimit the minimum temperature (T_{min}) and maximum temperature (T_{max}) of activity, which were established as 36–85°C in JFR flank fluids and at 34–43°C in NP fluids. The resulting values of ΔH_r for Reaction (1) were −12.7 to −13.7 kJ (mol SO_4^{2-})$^{-1}$ from 36 to 85°C, those for Reaction (2) were −444 to −447 kJ (mol O_2)$^{-1}$ from 34 to 43°C, while those for Reaction (3) were −371 to −373 kJ (mol O_2)$^{-1}$ from 34 to 43°C.

During the transition between initial and final isothermal measurements, metabolic heat production rates increased through a maximum, followed by a continuous decrease (**Figure 2**). Maximum heat production rates of 1.27 μW were determined at a temperature optimum (T_{opt}) of 73.5°C in JFR flank fluids, while 0.57 μW were measured at T_{opt} 38°C in NP fluids. Both of these values are ∼15°C above their respective *in situ* temperatures.

The energy turnover per cell was calculated by dividing the total heat produced during the course of the nanocalorimetry experiment by the number of cells in each fluid sample. Integration of the heat flow temperature plots showed that 267.3 mJ were produced by microbial metabolism in JFR fluids and 12.8 mJ were produced in NP fluids, over 97 and 14 h, respectively. Cellular enumeration within crustal fluids from the JFR flank and NP revealed concentrations of 8.67×10^2 and 6.88×10^5 cells ml^{-1} respectively. However, germination experiments revealed 6.66×10^4 cells ml^{-1} after the pasteurization and incubation of JFR fluids at 50°C (**Figure 3**). Taking into consideration the potential contribution of germinating cells to the measured metabolic heat rates, the cell-specific energy turnover rate in JFR fluids was estimated at 5.68 pW $cell^{-1}$ (**Table 2**). No germinating cells were detected in NP fluids and the cell-specific energy turnover rate was estimated at 0.18 pW $cell^{-1}$ (**Table 2**).

DISCUSSION

The rate of heat production measured in the nanocalorimeter is equivalent to the heat produced by the sum of all of the reactions occurring in the sample chamber. Essentially, the signal shown in **Figure 2** is the sum of the enthalpies of all of the reactions catalyzed by microorganisms. These heat signals can be combined with computed enthalpies of reactions that are thought to be

TABLE 2 | Metabolic heat rates measured by two-step isothermal nanocalorimetry.

Crustal fluids	Cardinal temperatures of microbial metabolic heat rates (°C)			Maximum metabolic heat rate[a]	Detection limit	Enthalpy change (ΔH_r)	Cell abundance	Spore-forming cell abundance	Energy turnover[b]
	T_{min}	T_{max}	T_{opt}	(nW ml^{-1})	(nW ml^{-1})	(mJ)	(cells ml^{-1})	(cells ml^{-1})	(pW ml^{-1})
Juan de Fuca Ridge (Borehole U1362A)	35.5	85.0	76.2	672	2.7	267.3	8.67*E* + 02	6.66*E* + 04	5.68
North Pond (Borehole U1383C)	34.8	43.0	38.0	285	1.2	12.8	6.88*E* + 05	Not detected	0.18

[a] *Measured at T_{opt}.*
[b] *Calculated from the total metabolic heat generated over the temperature transition time.*

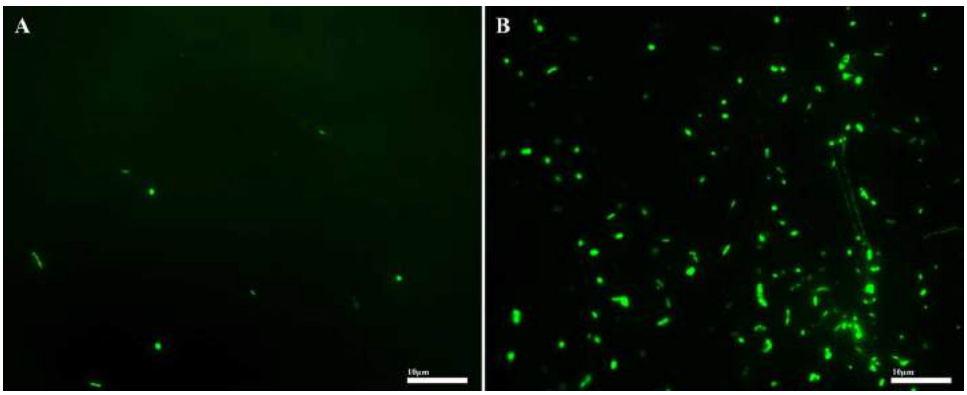

FIGURE 3 | Epifluorescence-microscopy image of basaltic crustal fluid samples from JFR filtered onto a Whatman 0.2 μm Anodisc filter stained with SYBR Green I, before (A) and after (B) induction of spore germination by pasteurization and 48 h of incubation at 50°C. Scale bar 10 μm.

catalyzed by microorganisms *in situ* to infer rates of metabolic activity. The amount of heat detected in fluids taken from the subseafloor at the JFR flank and at NP differ considerably (**Figure 2**), indicating different underlying processes.

Given that fluids sampled years earlier from the same JFR CORK (Robador et al., 2015) revealed genetic signatures and potential rates of microbial sulfate reduction, it is likely that the heat signals shown in **Figure 2A** are at least partially due to the enthalpy of this process. However, using the range of ΔH_r values calculated for Reaction (1) and assuming that the total amount of heat measured in the JFR flank sample, 267.3 mJ, was due to sulfate-reduction, the corresponding rates would be 2.4–2.6 $\times$ 10^3 nmol^{-1} ml$^{-1}{}_{FLUID}$ d^{-1}, far greater than the gross rates of sulfate reduction previously measured in JFR fluids, ∼0.01 nmol ml$^{-1}{}_{FLUID}$ d^{-1} (Robador et al., 2015). We attribute this large difference in sulfate reduction rates to the germination of thermophilic endospores (6.66×10^4 cells ml$^{-1}{}_{FLUID}$). In fact, thermophilic spore-forming bacteria, including close relatives to members of the sulfate-reducing *Firmicutes* phylum and *Candidatus* Desulforudis lineage, have been reported from these fluids (Robador et al., 2015). Not only can the process of germination potentially add to the heat signal measured, but once these organisms are functional, they can contribute to hydrolytic and fermentative activities which could in turn mediate the production of organic matter and further stimulate the rates of sulfate reduction (Hubert et al., 2009, 2010; de Rezende et al., 2013). Measured heat production rates in this study demonstrate that warm, anaerobic crustal fluids can support a large and active population of these thermophilic bacteria. Given that the entire volume of seawater is estimated to cycle through the ocean crust about every 100,000 years (Johnson and Pruis, 2003), the detection of active marine microorganisms with enhanced survival capacities demonstrates not only the importance of circulating crustal fluids for the passive dispersal on marine microbial biogeography (Müller et al., 2014), but also underscores the physiological potential of cells in crustal fluids to migrate and become established in a new location.

In contrast, the smaller heat signal measured in fluids taken from NP, 12.8 mJ, and narrower thermal range of metabolic activity, 34.8–43.0°C, indicate lower levels of microbial activity than in JFR fluids and a predominately mesophilic community. Although it is noteworthy that a metabolic heat signal was not detected at the *in situ* NP crustal temperature, 3.8°C, metabolic rates at this temperature might be too slow to be measured in the calorimeter. In addition, bacteria are known to be active at temperatures that are greater than those associated with the environment in which they were found by generating sufficient energy from respiration to repair or regenerate temperature-denatured enzymes, ribosomes, etc. (Isaksen and Jørgensen, 1996). Nonetheless, the total heat measured from the NP sample (12.8 mJ) and a median value of ΔH_r for Reaction (2) show oxygen respiration rates of 24.5 nmol O_2 ml$^{-1}{}_{FLUID}$ d^{-1}. Furthermore, other metabolic processes, i.e., nitrification, which describes the oxidation of NH_4^+ to ultimately NO_3^-, could also influence oxygen dynamics in NP fluids (Cowen, 2004). Assuming the ΔH_r values calculated for Reaction (3), the increase in oxygen respiration due to nitrification would yield rates of 29.3 nmol O_2 ml$^{-1}{}_{FLUID}$ d^{-1}. Altogether, these rates validate previous model predictions of microbial activity (0.1 to ∼100 nmol O_2 ml$^{-1}{}_{FLUID}$ d^{-1}, Orcutt et al., 2013b) in the same environmental setting.

It should be noted that when activities of natural populations of bacteria are estimated in terms of sulfate reduction or oxygen consumption, only the energy turnover of respiration is calculated, but there are also energetic costs—and thus heat signals—associated with other cellular processes such as anabolism. In the case of microorganisms in energy-limited environments, anabolic activity is mostly associated with the energy demand for the repair of accumulated damage to key macromolecules, i.e., DNA and housekeeping proteins (Russell and Cook, 1995; Johnson et al., 2007; van Bodegom, 2007), the energetics of which vary considerably depending on the environmental conditions (LaRowe and Amend, 2015c). Differences in cell-specific energy turnover between measured rates in fluids from JFR and NP (5.68 and 0.18 pW cell^{-1}, respectively) and compiled cell-specific respiratory rates for anaerobic and aerobic microbes in other deep subsurface

environments, $\sim 3 \times 10^{-3 \text{ to } -8}$ pW cell^{-1} and $\sim 1 \times 10^{-1 \text{ to } -8}$ pW cell^{-1}, respectively (Lever et al., 2015), could partly reflect the product of the minimal complement of functions required to sustain a metabolically active state, the basal power requirement (Hoehler and Jørgensen, 2013). Measurements of heat production by direct nanocalorimetry should allow a straightforward interpretation of the basal power requirements of microbes harbored in deeply buried basaltic crustal fluids.

AUTHOR CONTRIBUTIONS

AR designed and performed experiments, analyzed data, and wrote the paper. AR performed and analyzed calorimetry data. DL contributed to the analysis of calorimetry data, performed thermodynamic calculations, and contributed to the preparation of the manuscript. SJ, H-TL, and MR were instrumental in the acquisition of fluid samples. AR and JA conceived the study, and JA and KN supported the study. All authors discussed the results and implications and commented on the manuscript at all stages.

ACKNOWLEDGMENTS

We are very grateful to Julie Huber, Peter R. Girguis, and Chih-Chiang Hsieh for fluid samples. We thank the captain and crew on-board R/V *Atlantis* cruise AT 26-18 and R/V *Maria S. Merian* cruise MSM 20-5, along with the pilots and crew of ROV *Jason II* for their help. This research was funded by NSF grants (C-DEBI award 1207880 and 1207874 to JA and OCE-1260723 to MR) and the NASA Astrobiology Institute under Cooperative Agreement No. NNA13AA92A issued through the Office of Space Science.

REFERENCES

Adhikari, R. R., and Kallmeyer, J. (2010). Detection and quantification of microbial activity in the subsurface. *Chem. Erde Geochem.* 70, 135–143. doi: 10.1016/j.chemer.2010.05.003

Amend, J. P., and Helgeson, H. C. (1997). Calculation of the standard molal thermodynamic properties of aqueous biomolecules at elevated temperatures and pressures. 1. L-α-amino acids. *J. Chem. Soc. Faraday Trans.* 93, 1927–1941. doi: 10.1039/A608126F

Amend, J. P., and Plyasunov, A. V. (2001). Carbohydrates in thermophile metabolism: calculation of the standard molal thermodynamic properties of aqueous pentoses and hexoses at elevated temperatures and pressures. *Geochim. Cosmochim. Acta* 65, 3901–3917. doi: 10.1016/S0016-7037(01)00707-4

Bach, W., and Edwards, K. J. (2003). Iron and sulfide oxidation within the basaltic ocean crust: implications for chemolithoautotrophic microbial biomass production. *Geochim. Cosmochim. Acta* 67, 3871–3887. doi: 10.1016/s0016-7037(03)00304-1

Braissant, O., Wirz, D., Gopfert, B., and Daniels, A. U. (2010). Use of isothermal microcalorimetry to monitor microbial activities. *FEMS Microbiol. Lett.* 303, 1–8. doi: 10.1111/j.1574-6968.2009.01819.x

Brown, J. H., Gillooly, J. F., Allen, A. P., Savage, V. M., and West, G. B. (2004). Toward a metabolic theory of ecology. *Ecology* 85, 1771–1789. doi: 10.1890/03-9000

Cowen, J. P. (2004). The microbial biosphere of sediment-buried oceanic basement. *Res. Microbiol.* 155, 497–506. doi: 10.1016/j.resmic.2004.03.008

Daims, H., Lücker, S., and Wagner, M. (2006). daime, a novel image analysis program for microbial ecology and biofilm research. *Environ. Microbiol.* 8, 200–213. doi: 10.1111/j.1462-2920.2005.00880.x

Davis, E. E., Fisher, A. T., Firth, J. V., and the Shipboard Scientific Party (1997). Hydrothermal circulation in the oceanic crust and its consequences on the eastern flank of the Juan de Fuca Ridge. *Proc. ODP Init. Repts* 168, 7–21. doi: 10.2973/odp.proc.ir.168.101.1997

de Rezende, J. R., Kjeldsen, K. U., Hubert, C. R. J., Finster, K., Loy, A., and Jørgensen, B. B. (2013). Dispersal of thermophilic *Desulfotomaculum* endospores into Baltic Sea sediments over thousands of years. *ISME J.* 7, 72–84. doi: 10.1038/ismej.2012.83

Dick, J. M., LaRowe, D. E., and Helgeson, H. C. (2006). Temperature, pressure and electrochemical constraints on protein speciation: group additivity calculation of the standard molal thermodynamic properties of ionized unfolded proteins. *Biogeosciences* 3, 311–336. doi: 10.5194/bg-3-311-2006

Djamali, E., Nulton, J. D., Turner, P. J., Rohwer, F., and Salamon, P. (2012). Heat output by marine microbial and viral communities. *J. Non Equilib. Thermodyn.* 37, 291–313. doi: 10.1515/jnetdy-2011-0235

Edwards, K., Bach, W., Klaus, A., and the Iodp Expedition 336 Scientific Party (2014). Mid-Atlantic Ridge microbiology: initiation of long-term coupled microbiological, geochemical, and hydrological experimentation within the seafloor at North Pond, western flank of the Mid-Atlantic Ridge. *IODP Prel. Rept.* 336. doi: 10.2204/iodp.pr.336.2012

Fisher, A., Tsuji, T., Petronotis, K., and the Expedition 327 Scientists (2011). Site U1362. *Proc. IODP* 327. doi: 10.2204/iodp.proc.327.103.2011

Hansen, L. D., and Criddle, R. S. (1990). Determination of phase-changes and metabolic rates in plant-tissues as a function of temperature by heat-conduction DSC. *Thermochim. Acta* 160, 173–192. doi: 10.1016/0040-6031(90)80257-y

Helgeson, H. C., Kirkham, D. H., and Flowers, G. C. (1981). Theoretical prediction of thermodynamic behavior of aqueous electrolytes at high pressures and temperatures: 4. Calculation of activity coefficients, osmotic coefficients, and apparent molal and standard and relative partial molal properties to 600°C and 5 kb. *Am. J. Sci.* 281, 1249–1516. doi: 10.2475/ajs.281.10.1249

Hoehler, T. M., and Jørgensen, B. B. (2013). Microbial life under extreme energy limitation. *Nat. Rev. Microbiol.* 11, 83–94. doi: 10.1038/nrmicro2939

Hubert, C., Arnosti, C., Brüchert, V., Loy, A., Vandieken, V., and Jørgensen, B. B. (2010). Thermophilic anaerobes in Arctic marine sediments induced to mineralize complex organic matter at high temperature. *Environ. Microbiol.* 12, 1089–1104. doi: 10.1111/j.1462-2920.2010.02161.x

Hubert, C., Loy, A., Nickel, M., Arnosti, C., Baranyi, C., Brüchert, V., et al. (2009). A constant flux of diverse thermophilic Bacteria into the cold Arctic seabed. *Science* 325, 1541–1544. doi: 10.1126/science.1174012

Isaksen, M. F., and Jørgensen, B. B. (1996). Adaptation of psychrophilic and psychrotrophic sulfate-reducing bacteria to permanently cold marine environments. *Appl. Environ. Microbiol.* 62, 408–414.

Johnson, H. P., and Pruis, M. J. (2003). Fluxes of fluid and heat from the oceanic crustal reservoir. *Earth Planet. Sci. Lett.* 216, 565–574. doi: 10.1016/s0012-821x(03)00545-4

Johnson, J. W., Oelkers, E. H., and Helgeson, H. C. (1992). SUPCRT92–A software package for calculating the standard molal thermodynamic properties of minerals, gases, aqueous species, and reactions from 1 bar to 5000 bar and 0oC to 1000°C. *Comput. Geosci.* 18, 899–947. doi: 10.1016/0098-3004(92)90029-Q

Johnson, S. S., Hebsgaard, M. B., Christensen, T. R., Mastepanov, M., Nielsen, R., Munch, K., et al. (2007). Ancient bacteria show evidence of DNA repair. *Proc. Natl. Acad. Sci. U.S.A.* 104, 14401–14405. doi: 10.1073/pnas.0710637105

Jørgensen, B. B. (2011). Deep subseafloor microbial cells on physiological standby. *Proc. Natl. Acad. Sci. U.S.A.* 108, 18193–18194. doi: 10.1073/pnas.1115421108

Jungbluth, S. P., Bowers, R., Lin, H.-T., Cowen, J. P., and Rappé, M. S. (2016). Novel microbial assemblages inhabiting crustal fluids within mid-ocean ridge flank subsurface basalt. *ISME J.* doi: 10.1038/ismej.2015.248 [Epub ahead of print].

Karl, D. M. (2014). Solar energy capture and transformation in the sea. *Elem. Sci. Anth.* 2, 000021. doi: 10.12952/journal.elementa.000021

LaRowe, D. E., and Amend, J. P. (2015a). Catabolic rates, population sizes and doubling/replacement times of microorganisms in natural settings. *Am. J. Sci.* 315, 167–203. doi: 10.2475/03.2015.01

LaRowe, D. E., and Amend, J. P. (2015b). Power limits for microbial life. *Front. Microbiol.* 6:718. doi: 10.3389/fmicb.2015.00718

LaRowe, D. E., and Amend, J. P. (2015c). The energetics of anabolism in natural settings. *ISME J.* doi: 10.1038/ismej.2015.227 [Epub ahead of print].

LaRowe, D. E., and Van Cappellen, P. (2011). Degradation of natural organic matter: a thermodynamic analysis. *Geochim. Cosmochim. Acta* 75, 2030–2042. doi: 10.1016/j.gca.2011.01.020

Lever, M. A., Rogers, K. L., Lloyd, K. G., Overmann, J., Schink, B., Thauer, R. K., et al. (2015). Life under extreme energy limitation: a synthesis of laboratory- and field-based investigations. *FEMS Microbiol. Rev.* 39, 688–728. doi: 10.1093/femsre/fuv020

Lever, M. A., Rouxel, O., Alt, J. C., Shimizu, N., Ono, S. H., Coggon, et al. (2013). Evidence for microbial carbon and sulfur cycling in deeply buried ridge flank basalt. *Science* 339, 1305–1308. doi: 10.1126/science.1229240

Lin, H.-T., Cowen, J. P., Olson, E. J., Lilley, M. D., Jungbluth, S. P., Wilson, S. T., et al. (2014). Dissolved hydrogen and methane in the oceanic basaltic biosphere. *Earth Planet. Sci. Lett.* 405, 62–73. doi: 10.1016/j.epsl.2014.07.037

Lovley, D. R., Dwyer, D. F., and Klug, M. J. (1982). Kinetic-analysis of competition between sulfate reducers and methanogens for hydrogen in sedimetns. *Appl. Environ. Microbiol.* 43, 1373–1379.

Meyer, J. L., Jaekel, U., Tully, B. J., Glazer, B. T., Wheat, C. G., Lin, H. T., et al. (2016). A distinct and active bacterial community in cold oxygenated fluids circulating beneath the western flank of the Mid-Atlantic ridge. *Sci. Rep.* 6:22541. doi: 10.1038/srep22541

Mukhanov, V. S., Hansen, L. D., and Kemp, R. B. (2012). Nanocalorimetry of respiration in micro-organisms in natural waters. *Thermochim. Acta* 531, 66–69. doi: 10.1016/j.tca.2012.01.001

Müller, A. L., De Rezende, J. R., Hubert, C. R. J., Kjeldsen, K. U., Lagkouvardos, I., Berry, D., et al. (2014). Endospores of thermophilic bacteria as tracers of microbial dispersal by ocean currents. *ISME J.* 8, 1153–1165. doi: 10.1038/ismej.2013.225

Neidhardt, F. C., Ingraham, J., and Schaechter, M. (1990). *Physiology of the Bacterial Cell: A Molecular Approach*. Sunderland, MA: Sinauer Associates.

Orcutt, B. N., LaRowe, D. E., Biddle, J. F., Colwell, F. S., Glazer, B. T., Reese, B. K., et al. (2013a). Microbial activity in the marine deep biosphere: progress and prospects. *Front. Microbiol.* 4:189. doi: 10.3389/fmicb.2013.00189

Orcutt, B. N., Sylvan, J. B., Knab, N. J., and Edwards, K. J. (2011). Microbial ecology of the dark ocean above, at, and below the seafloor. *Microbiol. Mol. Biol. Rev.* 75, 361–422. doi: 10.1128/mmbr.00039-10

Orcutt, B. N., Wheat, C. G., Rouxel, O., Hulme, S., Edwards, K. J., and Bach, W. (2013b). Oxygen consumption rates in subseafloor basaltic crust derived from a reaction transport model. *Nat. Commun.* 4, 3539. doi: 10.1038/ncomms3539

Patel, A., Noble, R. T., Steele, J. A., Schwalbach, M. S., Hewson, I., and Fuhrman, J. A. (2007). Virus and prokaryote enumeration from planktonic aquatic environments by epifluorescence microscopy with SYBR Green I. *Nat. Protoc.* 2, 269–276. doi: 10.1038/nprot.2007.6

Robador, A., Jungbluth, S. P., LaRowe, D., Bowers, R., Rappé, M., Amend, J., et al. (2015). Activity and phylogenetic diversity of sulfate-reducing microorganisms in low-temperature subsurface fluids within the upper oceanic crust. *Front. Microbiol.* 5:748. doi: 10.3389/fmicb.2014.00748

Russell, J. B. (1986). Heat production by ruminal bacteria in continuous culture and tis relationship to maintenance energy. *J. Bacteriol.* 168, 694–701.

Russell, J. B., and Cook, G. M. (1995). Energetics of bacterial growth: balance of anabolic and catabolic reactions. *Microbiol. Rev.* 59, 48–62.

Shock, E. L. (1995). Organic acids in hydrothermal solutions–Standard molal thermodynamic properties of carboxylic acids and estimates of dissociation constants at high temperatures and pressures. *Am. J. Sci.* 295, 496–580. doi: 10.2475/ajs.295.5.496

Shock, E. L., and Helgeson, H. C. (1988). Calculation of the thermodynamic and transport properties of aqueous species at high pressures and temperatures–Correlation algorithms for ionic species and equation of state predictions to 5 kb and 1000°C. *Geochim. Cosmochim. Acta* 52, 2009–2036. doi: 10.1016/0016-7037(88)90181-0

Shock, E. L., and Helgeson, H. C. (1990). Calculation of the thermodynamic and transport properties of aqueous species at high pressures and temperatures–Standard partial molal properties of organic species. *Geochim. Cosmochim. Acta* 54, 915–945. doi: 10.1016/0016-7037(90)90429-O

Shock, E. L., Helgeson, H. C., and Sverjensky, D. (1989). Calculation of the thermodynamic and transport properties of aqueous species at high pressures and temperatures–Standard partial molal properties of inorganic neutral species. *Geochim. Cosmochim. Acta* 53, 2157–2183. doi: 10.1016/0016-7037(89)90341-4

Shock, E. L., Oelkers, E., Johnson, J., Sverjensky, D., and Helgeson, H. C. (1992). Calculation of the thermodynamic properties of aqueous species at high pressures and temperatures: effective electrostatic radii, dissociation constants and standard partial molal properties to 1000°C and 5 kbar. *J. Chem. Soc. Faraday Trans.* 88, 803–826. doi: 10.1039/FT9928800803

Tanger, J. C., and Helgeson, H. C. (1988). Calculation of the thermodynamic and transport properties of aqueous species at high pressures and temperatures–Revised equations of state for the standard partial molal properties of ions and electrolytes. *Am. J. Sci.* 288, 19–98. doi: 10.2475/ajs.288.1.19

van Bodegom, P. (2007). Microbial maintenance: a critical review on its quantification. *Microb. Ecol.* 53, 513–523. doi: 10.1007/s00248-006-9049-5

Winkelmann, M., Hüttl, R., and Wolf, G. (2004). Application of batch-calorimetry for the investigation of microbial activity. *Thermochim. Acta* 415, 75–82. doi: 10.1016/j.tca.2003.08.028

Ziebis, W., Mcmanus, J., Ferdelman, T., Schmidt-Schierhorn, F., Bach, W., Muratli, J., et al. (2012). Interstitial fluid chemistry of sediments underlying the North Atlantic gyre and the influence of subsurface fluid flow. *Earth Planet. Sci. Lett.* 323, 79–91. doi: 10.1016/j.epsl.2012.01.018

Conflict of Interest Statement: The authors declare that the research was conducted in the absence of any commercial or financial relationships that could be construed as a potential conflict of interest.

frontiers in Microbiology

ORIGINAL RESEARCH
published: 09 February 2016
doi: 10.3389/fmicb.2016.00107

Some Compositional and Kinetic Controls on the Bioenergetic Landscapes in Oceanic Basement

Wolfgang Bach[1,2]*

[1] MARUM and Geoscience Department, University of Bremen, Bremen, Germany, [2] Centre of Excellence in Geobiology and Department of Earth Sciences, University of Bergen, Bergen, Norway

This contribution assesses the availability of catabolic energy for microbial life during water–rock reactions in the flanks of mid-ocean ridges, where basaltic and ultramafic rocks interact with circulating seawater. In addition to equilibrium thermodynamic computations, results for kinetic reaction paths are presented. In these calculations, it is assumed that dissolution of olivine and basalt glass control the rates of hydrogen forming reactions in ultramafic and basaltic rocks, respectively. The results suggest that all ocean crust basement rocks release enough hydrogen (H_2,aq) to support hydrogenotrophic life at low water-to-rock ratios. Olivine dissolution rate control imposes a stronger effect on hydrogen production than phase equilibrium controls, indicating that magnetite formation is not a requirement for production of large amounts of hydrogen in ultramafic rocks. The formation of non-tronite and celadonite are primarily responsible for the formation of the moderate amounts of hydrogen (H_2,aq) expected in basaltic ridge flanks. Under conditions of large seawater fluxes required to account for the great global convective heat flow in ridge flanks, however, hydrogen production in basaltic ridge flanks is insufficient for supporting hydrogenotrophic life. It is hence proposed that the role of Fe oxidation in basaltic ridge flanks is greater than previously suggested. A standing stock of $2.4*10^{28}$ cells may be supported by Fe oxidation in basaltic ridge flanks, equivalent of about 10% of the sedimentary deep biosphere. The size of a hydrogenotrophic biomass within the ocean crust is more difficult to estimate because the rates and processes of hydrogen release are insufficiently constrained. In any case, hydrogenotrophy in the ocean crust should be of key importance only in olivine-rich basement rocks and in sedimented ridge flanks with low time-integrated seawater fluxes.

Keywords: ocean crust, ridge flanks, seawater circulation, water–rock interactions, subseafloor life, bioenergetics

OPEN ACCESS

Edited by:
Jason B. Sylvan,
Texas A&M University, USA

Reviewed by:
Alexis Templeton,
University of Colorado, USA
William E. Seyfried,
University of Minnesota Twin Cities, USA

***Correspondence:**
Wolfgang Bach
wbach@uni-bremen.de

Specialty section:
This article was submitted to Extreme Microbiology, a section of the journal Frontiers in Microbiology

Received: *01 October 2015*
Accepted: *20 January 2016*
Published: *09 February 2016*

Citation:
Bach W (2016) Some Compositional and Kinetic Controls on the Bioenergetic Landscapes in Oceanic Basement. Front. Microbiol. 7:107. doi: 10.3389/fmicb.2016.00107

INTRODUCTION

Seawater flows in aquifers within the seafloor at rates so large that it takes only few 100s of 1000s years to process the entire volume of the oceans through the permeable ocean crust (e.g., Elderfield and Schultz, 1996; Fisher, 2005). This tremendous flux, coupled with exchange reactions between the crust and the circulating seawater, is critical in global budgets of ocean-lithosphere exchange. Important types of reactions include the removal of Mg^{++} and HCO_3^- by minerals (smectite,

carbonate) that fill fracture and void space within the crust. Alteration of basaltic glass removes Ca^{++} and SiO_2 from the crust into the oceans, where these components are taken up in algal and protozoan tests. These processes play a central role in the silicate–carbonate loop of the Earth's carbon cycle (e.g., Arvidson et al., 2006). Alteration reactions also consume oxygen, which makes them a crucial sink for oxidizing power that is continuously produced in the carbon cycle by burial of organic matter (Hayes and Waldbauer, 2006). In addition, the ocean crust may harbor microbial life, which possibly impacts these global scale carbon and redox budgets. Perhaps more importantly, microbial activity within the ocean crust likely affects the rates and pathways of reactions governing exchange between seawater and oceanic basement.

Most of the seawater circulation takes place in ridge flanks, where temperatures are low and the rates of water–rock reaction are slow. The low to moderate temperatures in the ridge flank settings and the sluggish kinetics of abiotic water–rock reactions allow chemolithoautotrophic microorganisms to harness the Gibbs energy ($\Delta_r G$) associated with redox reactions during alteration. An initial appraisal of the potential size of biomass living in these rocky habitats suggests that the cell numbers may resemble those in the sedimentary deep biosphere (Bach and Edwards, 2003).

The principal energy sources (electron donors) are divalent iron (Fe^{+2}) and sulfide (S^{-2}) dissolved in basaltic glass or forming minerals in volcanic and mantle rocks. These reduced constituents of rocks are oxidized in alteration reactions. If the interacting fluid is oxygenated seawater, oxygen is consumed. Different electron acceptors (NO_3^-, SO_4^{2-}, HCO_3^-, ferric hydroxide, etc.) are used in anoxic ridge flank environments (Boettger et al., 2013). Tectonic denudation of olivine-dominated rocks (dunites, peridotites, troctolites) are common along mid-ocean ridges and as much as 50% of the seafloor created along slow and ultraslow spreading ridges may expose these rock types (Escartin et al., 2008; Cannat et al., 2010). Olivine-rich rocks undergo fairly rapid reactions with seawater (serpentinization), during which hydrogen (H_2,aq) may form (McCollom and Bach, 2009; Nakamura et al., 2009; Klein et al., 2013). The reducing potential of micromolal quantities of H_2 is large enough to drive e^- transfers to all electron acceptors, including CO_2. Again, these transfers are sluggish in the abiotic world at low temperatures, but H_2 is turned over very quickly by microorganisms under these conditions (e.g., Hoehler et al., 2001). High hydrogen-yields in serpentinization are contrasted by very low H_2 production related to radiolysis in the subseafloor. But even such small quantities of H_2 are utilized by aerobic microorganisms in energy-starved sedimentary environments with exceedingly low flux of reducing power (Blair et al., 2007).

In this communication, I examine some energetic constraints pertinent to the potential abundance and functioning of microbial life in the oceanic basement (Orcutt et al., 2011; Edwards et al., 2012), where basalt and peridotite are the principal sources of reducing power. In the kinetics calculations, I focus on reactions involving basaltic glass and olivine, as rate data are available for these two substrates, which are abundant phases in volcanic and ultramafic ridge flank environments, respectively.

MATERIALS AND METHODS

Thermodynamic reaction path modeling using both arbitrary and true kinetics mode was conducted to examine the roles of substrate composition, secondary mineral compositions, and rates of primary mineral dissolution on the extent and timing of hydrogen (H_2,aq) release from water rock reactions in the seafloor. The thermodynamic calculations of hydrogen yields were conducted using the EQ3/6 code (Wolery and Jarek, 2003) if solid solution compositions were permitted. Ideal solid solution compositions as in Klein et al. (2013) were allowed to form in these reaction paths, in which rock was added incrementally to decrease water–rock ratios. The REACT code of Geochemist's Workbench (GWB; Bethke, 1996) was used for computing most of the kinetic reaction path models in which basalt glass or olivine dissolution was the rate-limiting step. I used 500-bar databases compiled from SUPCRT92 (Johnson et al., 1991) for these model calculations. Included in the GWB database was mid-ocean ridge basalt glass as a phase, for which thermodynamic properties were calculated with entropy, volume, and free energy data from Chermak and Rimstidt (1989) and Holland (1989) using a polyhedral approach (cf. Oelkers and Gislason, 2001). The composition of the glass ($Ca_{0.25174}Na_{0.0977}K_{0.0013}Fe^{++}{}_{0.1464}Fe^{+++}{}_{0.01627}Mg_{0.2585}Al_{0.3844}Si_{1.0000}O_{3.3566}$) was calculated from average oxide concentrations of mid-Atlantic Ridge basalt reported by Klein (2004). The same basalt composition – added as "special reactant" – was used in the EQ6 model run presented in **Figure 1**. Also included were secondary Fe-phases, such as Fe–Al celadonite, ripidolite, and goethite (Wolery, 2004). Basalt glass dissolution rates at 25°C of 10^{-15} mol cm^{-2} s^{-1} (Oelkers, 2001) and 10^{-7} mol cm^{-2} s^{-1} at 90°C (Daux et al., 1997) were used to estimate a 10°C rate of 10^{-16} mol cm^{-2} s^{-1}. Olivine dissolution rates of 10^{-14} mol cm^{-2} s^{-1} for 25°C and neutral pH were taken from Pokrovsky and Schott (2000). A pH-dependency of reaction rates was not applied. Arrhenius parameters for dissolution of olivine, orthopyroxene, and clinopyroxene were provided in Seyfried et al. (2007). The peridotite composition used in the EQ6 thermodynamic calculations was assumed 70% olivine, 25% orthopyroxene, and 5% clinopyroxene, with X_{Mg} set to 0.9 in all these phases. A specific surface area (SSA) of 1 m^2 g^{-1} was assumed in all kinetics calculations, as it may serve as good approximation for the SSA of fresh basaltic crust (Nielsen and Fisk, 2010).

It should be noted that the presented results of predicted hydrogen levels have large uncertainties due to poorly known thermodynamic properties for some secondary minerals and largely unknown concentration-activity relations in the solid solution phases at low temperatures. The effect of variations in pressure and primary mineral compositions is small by comparison. The calculation results can hence be applied to seafloor systems with <5000 m water depth (i.e., 500 bar pressure) and to basalt and peridotite with compositions that deviate slightly from those used in the calculations. The time values in the true kinetics calculations are plagued by an even larger ambiguity, because the uncertainties in the rate constants and the SSAs of fractured rocks are very large.

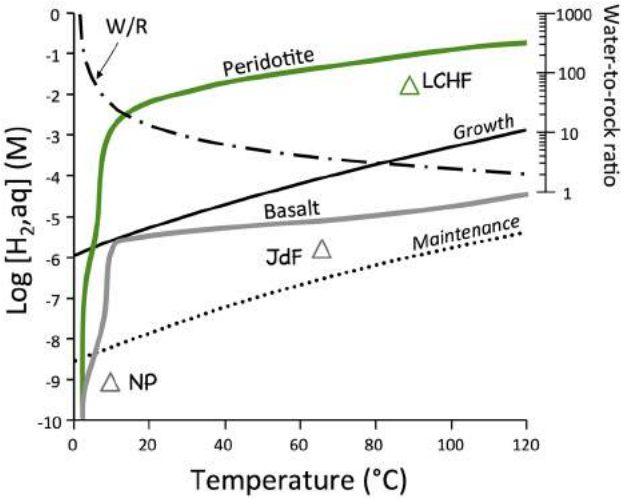

FIGURE 1 | Equilibrium thermodynamic calculation of potential hydrogen supply by water–rock reactions and hydrogen demand by hydrogenotrophic microorganisms (Hoehler, 2004). Off-axis systems in basalt (NP = North Pond; JDF = Juan de Fuca ridge flank) in gray and the Lost City Hydrothermal Vent Field (LHVF) are also shown. Calculations were conducted with EQ3/6 along a path that had water–rock ratios decrease from infinity to two as temperatures increased from 2 to 120°C.

For instance, if average SSAs of partially altered oceanic crust of 3.4 m^2 g^{-1} (Nielsen and Fisk, 2010) were used, all calculated rates would be 3.4 times faster. Therefore, the true kinetics calculation results merely have order-of-magnitude-type accuracies as far as predicted time scales are concerned.

RESULTS

Equilibrium Thermodynamic Computations of Hydrogen Release

The first set of computations examines the differences in the hydrogen generating potentials between basalt and peridotite, the two most abundant rock types in the oceanic basement. The reaction paths were selected such that recharge of seawater into basement and concomitant heating of the water is represented. Consequently, temperatures go up along the reaction paths as water-to-rock ratios decrease. The results of these computations are compared with the demands of hydrogen in maintenance and growth of hydrogenotropic microbial communities (Hoehler, 2004). The results presented in **Figure 1** indicate that basalt–seawater reactions in off-axis environments can provide enough hydrogen for maintenance of hydrogenotrophic communities. Peridotites are predicted to produce hydrogen levels that are 3 to 4 orders of magnitude greater than during basalt–seawater interactions under identical conditions of temperature and water-to-rock ratios. These quantities of hydrogen are sufficient to allow growth of hydrogenotrophic communities across a large range of temperatures.

Kinetic–Thermodynamic Computations of Hydrogen Release

A number of computations were conducted to examine the temporal evolution of water–rock systems assuming that the dissolution of mafic minerals in a peridotite and glass in the basaltic crust are the rate-limiting step in the overall reactions.

Production of hydrogen during low-temperature interactions between seawater and peridotite were examined in **Figure 2**. The evolution of hydrogen in the intergranular fluid of peridotite is predicted to increase in a step-wise fashion, from concentrations <1 nM in the first years to concentration >10 μM after more than 50 years. An interesting discrepancy develops in the period 5 to 50 years between a model run in which serpentine solid solutions were allowed and another run that had solid solutions suppressed. These results suggest that the formation of serpentine with ferric iron dissolved in the tetrahedral and octahedral sites may facilitate rapid generation of hydrogen.

Hydrogen production is also strongly dependent on temperature and is predicted to change from sluggish at 10°C to rapid at 110°C (**Figure 3**). These predicted fast rates at temperatures of 50°C and greater are inconsistent with experimental results (Mayhew et al., 2013), indicating that either dissolution rates of olivine are over-predicted at higher temperatures by the model or that processes other than olivine dissolution are rate-limiting.

Another set of reaction paths were computed to investigate the role of the nature of secondary Fe(III) mineral phase in hydrogen production (**Figure 4**). The interesting observation here is that the type of secondary Fe(III) mineral is only of secondary importance, if olivine dissolution is the rate-limiting step. These results suggest that magnetite is not required to explain hydrogen production. More oxidized phases like hematite and goethite can cause just as much hydrogen production in the kinetically controlled intial phase of peridotite–water interaction. Hydrogen production is predicted to be somewhat retarded, when oxides are not allowed to form and Fe(III)-bearing serpentine (cronstedtite, $Mg_2Fe^{II}SiFe^{III}O_5(OH)_4$) forms instead.

Basalt glass is predicted to dissolve more slowly (10^{-15} mol cm^{-2} sec^{-1}) than olivine (10^{-14} mol cm^{-2} sec^{-1} at 25°C). It is also expected to yield overall lower amounts of aqueous hydrogen upon water–rock reactions when compared with olivine-rich lithologies (**Figure 1**). The predicted evolution of hydrogen in waters interacting with basalt glass at 10 and 30°C is shown in **Figure 5**. Although slower than peridotite (cf. **Figure 3**), basalt glass is predicted to produce nanomolal to micromolal quantities of aqueous hydrogen in the course of a 100,000 years.

Basaltic rocks often have olivine crystals distributed within a glassy mesostasis. An additional set of reactions paths were computed to determine the difference between olivine-bearing glassy basalt and pure basalt glass in the intial 1000 years of alteration. The results (**Figure 6**) show that a moderate proportion of olivine (10%) in a glassy basalt does increase the predicted hydrogen production markedly relative to olivine-free basalt, although it falls short of that predicted for an olivine rock (dunite). The increased hydrogen production is due to the faster dissolution rate of olivine compared to the glass. If the two phases dissolved at the same rate, the presence of olivine in the basalt

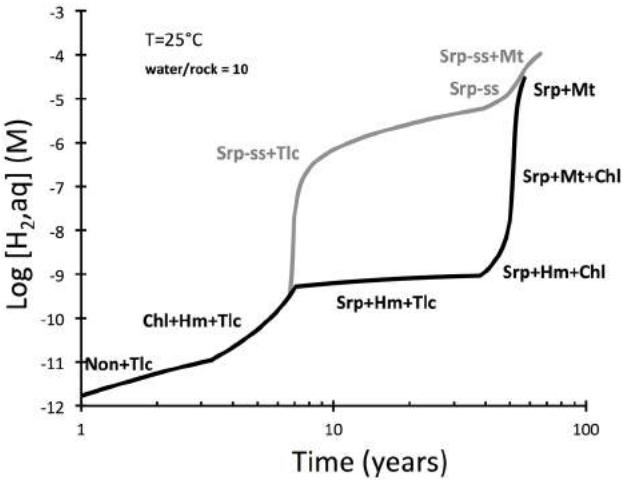

FIGURE 2 | Predicted hydrogen yields during serpentinization of peridotite and considering dissolution rates of olivine and pyroxenes (EQ6). The upper curve represents results of a calculation that allowed serpentine solid solutions (serp-ss) to form. Those were not allowed to from in a second calculation represented by the lower curve. Talc formation early in the reaction path is from loss of silica dissolved in seawater to the rock. Note that the curves merge when magnetite is predicted to become stable.

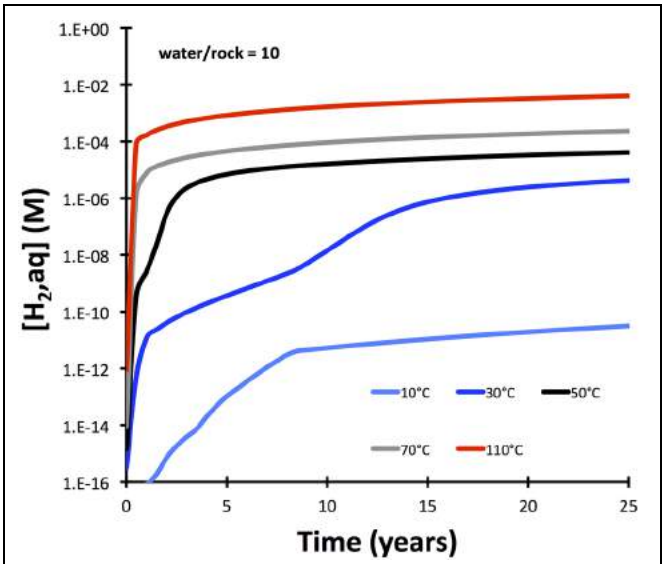

FIGURE 3 | Temperature dependency of hydrogen release from serpentinization of olivine (Fo90) with dissolution of olivine as rate-limiting step. The model (calculated with GWB) is simplified compared to the one presented in **Figure 2** in that solid solutions are not allowed.

would not increase hydrogen production at all, since ferroan smectite (and not serpentine and oxide) is predicted to form.

A comprehensive reaction path model was computed for low-temperature (10°C) alteration of basalt glass over the course of 10 million years (**Figure 7**). The model predicts that nontronite ($Na_{0.33}Fe^{III}{}_2Al_{0.33}Si_{3.67}O_{10}(OH)_2$)*$nH_2O$ and celadonite ($KAlFe^{III}Si_4O_{10}(OH)_2$) drive most of the hydrogen production. Predictions of the quantities of hydrogen in ridge flanks depend heavily on the assumed fluxes (time-integrated water-to-rock ratios). High water-to-rock ratios (e.g., open circulation) does not result in noticable accumulations of hydrogen in volcanic ridge flank settings (**Figure 8**).

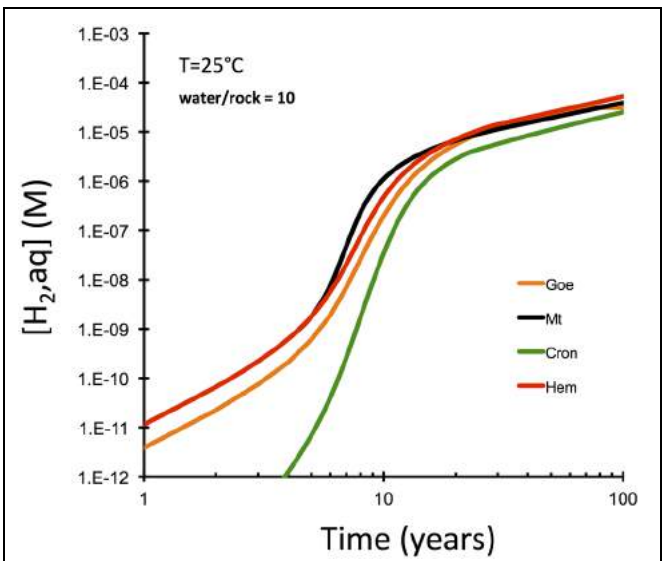

FIGURE 4 | Computational results for olivine-dissolution controlled serpentinization kinetics examining the role of the nature of secondary Fe(III) phase (GWB). Note that magnetite does not produce hydrogen faster than other oxide/oxyhydroxides along this kinetically controlled reaction path.

DISCUSSION

I examined water–rock reactions and energetic implications for related microbial life in three different ridge flank (*sensu lato*) habitats: (i) open circulation of oxygenated seawater (e.g., the North Pond site; Edwards et al., 2012; Orcutt et al., 2013), (ii) closed-system circulation of suboxic to anoxic seawater (eastern flank of the Juan de Fuca Ridge; Fisher et al., 2005), and (iii) seawater interaction with mantle peridotite in fracture zones and off-axis oceanic core complexes (e.g., Kelley et al., 2001). The effects of variable rock composition (e.g., basaltic glass vs. olivine-phyric basalt vs. peridotite) are examined as well as the consequences of variable dissolution and precipitation reactions.

Dissolved hydrogen (H_2,aq) has long been known to be one of the most potent energy sources for chemolithoautotrophic microorganisms in the deep sea (e.g., Edwards et al., 2005). It has been demonstrated that different rock types have strongly variable abilities to release hydrogen upon water–rock reactions. It has been shown that peridotites can generate 100s of millimoles of hydrogen per kg of water in the course of high-temperature (200–300°C) serpentinization reactions (e.g., McCollom and Bach, 2009). The results presented above show that peridotites have much greater potential for producing hydrogen than basalts. This difference may account for the fact that isotopic evidence for sulfate reduction is very commonly found in mantle peridotites (e.g., Alt and Shanks, 1998, 2003;

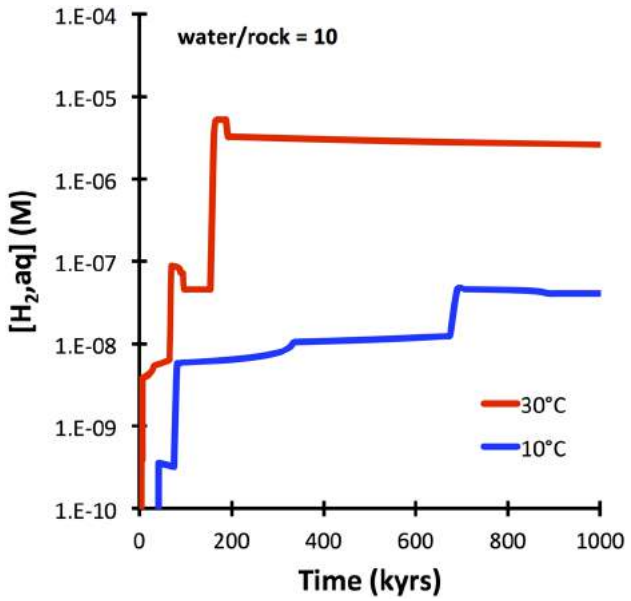

FIGURE 5 | Hydrogen production predicted for basalt-seawater interactions at 10 and 30°C (GWB). Kinetics is controlled by dissolution of basalt glass with an SSA of 1 m^2 g^{-1} (see text).

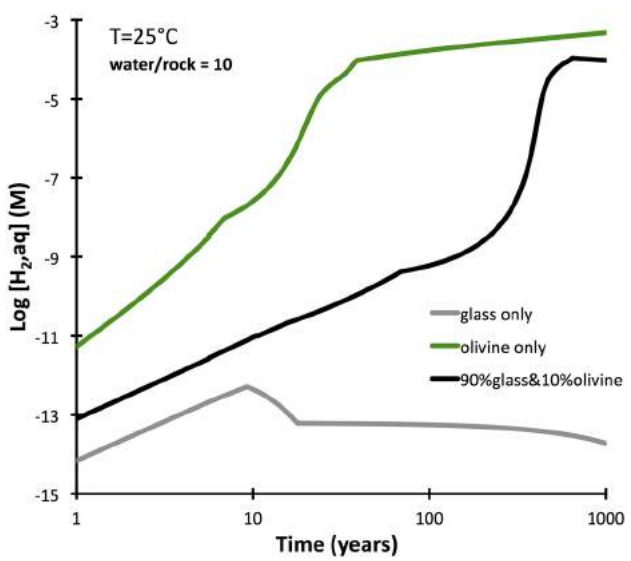

FIGURE 6 | Dissolution-controlled kinetic reaction paths from pure olivine (dunite) and basalt glass in comparison with an olivine basalt, composed for 90% basalt glass and 10% olivine (Fo_{80}). Calculations were conducted by GWB, and forsterite dissolution rates are used.

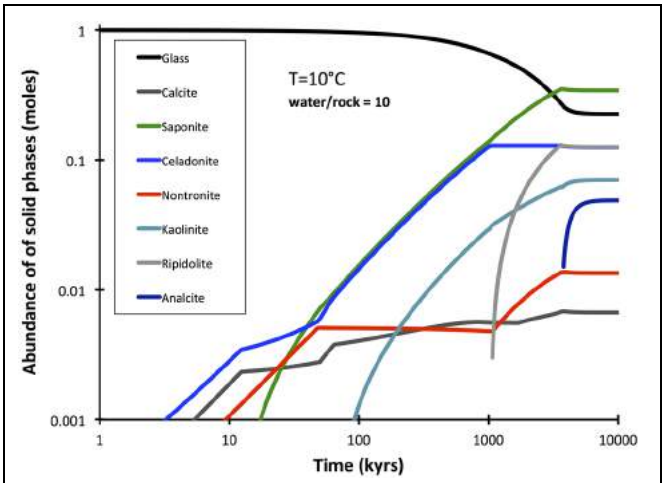

FIGURE 7 | Predicted reaction extent and products in the course of 10 Myrs of alteration at low water-to-rock ratios (10). The computation was conducted with GWB.

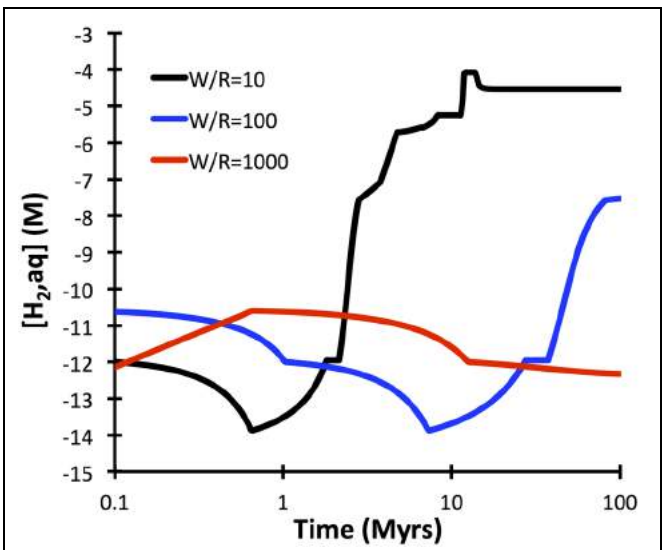

FIGURE 8 | Dependency of hydrogen release kinetics as a function of water-to-rock ratios. Note that at high water-to-rock ratios hydrogen concentrations >1 nM are not predicted to develop. The computations were conducted with GWB for a temperature of 10°C.

Alt et al., 2007) than in basalt. The hydrogen contents of intergranular fluids during serpentinization are high enough under a large range of conditions, even at low temperatures, to allow for hydrogenotrophic sulfate reductions. The drive for hydrogenotrophic sulfate reduction is smaller in basalt systems, but may facilitate maintenance of sulfate reducing communities. The sulfate-reducing bacteria identified in the Juan de Fuca Ridge flank (Lever et al., 2013) may hence be supported by hydrogen (Boettger et al., 2013), although it is also possible that organic carbon compounds are used as electron donor.

Equilibrium thermodynamic predictions of hydrogen yields during low-temperature water–rock reactions are of limited use, because these reactions commonly do not reach the state of equilibrium due to sluggish reaction kinetics. We do not currently have a good understanding of what the rate-limiting steps in production of hydrogen in water–rock reactions are. Most of the calculations presented above work on the assumption that olivine dissolution is an important rate-limiting in the overall reactions

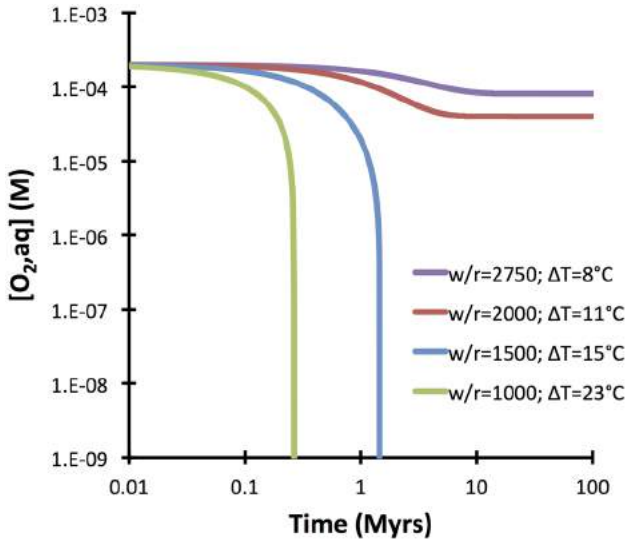

FIGURE 9 | Predicted evolution of dissolved oxygen in the course of water–basalt interactions at different water-to-rock ratios. These ratios correspond to temperature anomalies (ΔT) required for circulating seawater in order to account for a global heat flow of 7 TW in ridge flanks. The computations were conducted with GWB for temperatures as indicated in the inset. Note that warm flanks with decreased ventilation by seawater are predicted to turn anoxic after a few million years. Ridge flanks with higher flux rates of seawater (w/r > 2000), in contrast, may stay oxygenated throughout their evolution.

that release hydrogen. However, the levels of hydrogen predicted to develop within a few years during peridotite-water interactions greatly exceed the hydrogen yields observed in experiments conducted by Mayhew et al. (2013) at temperatures of 55 and 100°C. These authors suggested that the transfer of electrons from silicates to oxides is the rate-limiting step. If so, then apparently the dissolution of olivine may, though part of reaction sequence, not control the rate of this overall transfer. More experiments like those by Mayhew et al. (2013) will be required to decipher the pathways and rates of hydrogen generating reactions. In the meantime, I suggest that simplified kinetic–thermodynamic modeling may provide useful insights that go beyond what can be achieved by equilibrium thermodynamic computations.

The computational results presented above suggest that the nature of the Fe(III) bearing minerals (e.g., hematite vs. goethite vs. magnetite vs. cronstedtite) is of secondary importance in terms of hydrogen yields at low temperatures when dissolution of olivine is the rate-limiting step (**Figure 4**). This result is surprising, because it is commonly assumed that serpentinization of olivine and production of magnetite are required to have high hydrogen yields. Of course, the equilibrium hydrogen concentrations are greatest, when the fluid equilibrates with magnetite, brucite, and serpentine. But other reaction pathways that lead to the production of more oxidized phases like hematite and goethite are apparently able to produce similar quantities of hydrogen as magnetite, as long as the pace of the reaction is determined by the rate of olivine dissolution. On the other hand, should the rates of Fe(III)-mineral precipitation be slower than the rate of olivine dissolution, then the magnitude of the difference in the rates should play a dominant role in controlling hydrogen production. Figuring out those relative rate differences in the critical reaction steps is an import challenge for future experimental work.

The computations also show that when olivine in a basalt dissolves at a rate similar to basalt glass, it does not develop the same reducing power as it does during serpentinization, because ferroan smectite – and not serpentine + ferric oxide – will form. Only if olivine reacts at rates that are an order of magnitude greater than those of the other phases will olivine-bearing basalts yield more hydrogen than basalt free of olivine. These results lend tentative support to the proposal by Lever et al. (2013), who suggested that alteration of olivine may have played an important role in producing hydrogen for sulfate reducing bacteria in the Juan de Fuca ridge flank system. However, better constraints on the relative rates of alteration of basalt glass and olivine are required to further test this idea.

The computations presented indicate that fresh basalt reacting with seawater may yield micromolal quantities of hydrogen at somewhat elevated temperatures and when water-to-rock ratios are small (e.g., 10). The quantities of hydrogen analyzed in the 60°C Juan de Fuca system (1 μM; Boettger et al., 2013) can easily by produced in basement that is largely isolated from the open ocean, even at temperatures below 60°C (**Figure 5**). Hydrogen production in basaltic ridge flank settings can yield levels high enough to support microbial life (i.e., quantities of several nanomoles per kg water; e.g., Hoehler et al., 2001), if time-integrated water-to-rock ratios are <1000 (by mass). We can assess what this flux number implies in terms of alteration temperature, because we have a tight constraint on the amount of heat (about 7TW) that is lost by circulation of seawater in ridge flanks (Stein and Stein, 1994). Most of that circulation takes place within the uppermost 300 m of basement where permeability is high enough to facilitate fluid flow in the absence of large pressure gradients (Fisher and Becker, 2000). Given that 3 km^2 of seafloor are generated anually, roughly $2*10^{12}$ kg yr^{-1} of basaltic upper basement is newly subjected to ridge flank circulation. If this basement is exposed to a 1000-fold greater mass flux of seawater in its lifetime, we arrive at $2 * 10^{15}$ kg of circulating seawater per year. For this mass flux (F), the circulating water must be heated by 21°C (ΔT) to transport 7 TW of heat (Q), given a heat capacity of water (Cp) of 4184 J kg^{-1} $°C^{-1}$ ($F = Q/(Cp * \Delta T)$; Elderfield and Schultz, 1996). Smaller fluxes of water would come with higher hydrogen concentrations in basaltic ridge flank systems, e.g., at a w/r of 100 (**Figure 8**), but then ΔT would have to be an unreasonable 210°C to account for the 7TW heat loss at a global scale. These results lead me to suggest that hydrogen generation in basaltic ridge flank crust on a global scale is negligible, although it may happen regionally in virtually closed circulation systems (e.g., at the eastern flank of the Juan de Fuca Ridge). Oxidatively altered basalt has an even lower potential of yielding hydrogen by hydrolysis reactions, but radiolytic hydrogen production may play a role in the maturing ocean crust (Türke et al., 2015; Dzaugis et al., 2016).

How do these new assessments influence the validity of the bioenergetic calculations presented by Bach and Edwards (2003)? The iron oxidation rate estimated by these authors (1.7 ± 1.2*10^{12} moles yr^{-1}) was recently confirmed by a newer compilation of iron redox state in upper ocean crust (Rutter, 2015). The bioenergetics parameter, e.g., a $\Delta_r G$ of 66 kJ mol^{-1} for iron oxidation and 292 kJ gC^{-1} cellular carbon are also still valid. Bach and Edwards (2003) assumed that only half of the ferrous iron was oxidized to ferric iron by oxygen, the other half, they suspected, is oxidized by water and releases hydrogen. These authors calculated that an energy flux of 0.85*10^{12} moles yr^{-1} * 66 kJ mol^{-1} = 6 * 10^{13} kJ yr^{-1} can fix 2 * 10^{11} gC biomass yr^{-1}. The remaining Fe, they assumed, gives rise to the generation of 0.45 * 10^{12} moles of hydrogen yr^{-1}, which could support twice the amount of biomass by iron reduction.

I suggest considering those 50% of oxidation of ferrous iron by water as absolute maximum value. The computations presented above indicate that hydrogen production from hydrolysis may actually be quite minimal in open ridge flank systems, where time-integrated fluid fluxes are large. The North Pond system in the western flank of the mid-Atlantic Ridge is such an open system, where hydrogen in basement fluids is <1 nM and oxygen is still present, although it is respired along the flow path of seawater (Orcutt et al., 2013). In those kind of systems, iron oxidation by oxygen plays a much larger role, and at time-integrated water-to-rock ratios of >2000 (corresponding to a ΔT of 11°C), oxygen is not even the restricting compound (**Figure 9**). In other words, there is more oxygen fluxed those open ridge flanks than is required to account for the amount of Fe oxidation observed. If we assume that all iron in basaltic basement was oxidized by oxygen, the amount of biomass potentially fixed by iron oxidation in basaltic ridge flank aquifers is up to two times higher (i.e., 4 * 10^{11} gC biomass yr^{-1}) than suggested before. In computing the standing stock of cells (using a maintenance energy of 200 J gC^{-1} yr^{-1} and a cell weight of 26 fg; Whitman et al., 1997) that could be supported by the maximum energy flux related to aerobic iron oxidation (12 * 10^{13} kJ yr^{-1}), we arrive at 6 * 10^{14} gC or 2.4 * 10^{28} cells. This is as much as 10% of the sedimentary biomass (Kallmeyer et al., 2012), indicating that iron oxidation in the basaltic aquifer remains one of key potential drivers supporting microbial communities in the basaltic basement.

Hydrogen plays a role where ultramafic and other olivine-rich rocks interact with seawater. This is case in oceanic detachment fault setting, transform faults, bend faults, and in sedimented ridge flanks such as the eastern of the Juan de Fuca Ridge are the Costa Rica Rift Zone. Globally, a hydrogen-fuelled biophere in the oceanic basement may be as large (or larger) as the cold basaltic ridge flank system that runs primarily on Fe-oxidation. In the aging basaltic ridge flanks, Fe oxidation will be slowed as alteration rinds armor the fresh glass and slow down reactions. Strong enrichments of U and K in the alteration rinds, however, give rise to hydrogen production from radiolysis, which may become increasingly important relative to Fe-oxidation in old seafloor (Türke et al., 2015). For a better assessment of the size of a potential hydrogenotrophic subseafloor biosphere, a more detailed understanding of the critical reaction rates and pathways is needed.

AUTHOR CONTRIBUTIONS

The author confirms being the sole contributor of this work and approved it for publication.

ACKNOWLEDGMENTS

I thank Katrina Edwards for getting me interested in deep biosphere research and being such a great collaborator and friend for many years. MARUM and DFG (grant BA1605/11) as well as the Research Council of Norway (project code 179560) are thanked for financial support.

REFERENCES

Alt, J. C., and Shanks, W. C. (1998). Sulfur in serpentinized oceanic peridotites: serpentinization processes and microbial sulfate reduction. *J. Geophys. Res.* 103, 9917–9929. doi: 10.1029/98JB00576

Alt, J. C., and Shanks, W. C. (2003). Serpentinization of abyssal peridotites from the MARK area, Mid-Atlantic Ridge: Sulfur geochemistry and reaction modeling. *Geochim. Cosmochim. Acta* 67, 641–653. doi: 10.1016/S0016-7037(02)01142-0

Alt, J. C., Shanks, W. C. III, Bach, W., Paulick, H., Garrido, C. J., and Beaudoin, G. (2007). Hydrothermal alteration and microbial sulfate reduction in peridotite and gabbro exposed by detachment faulting at the Mid-Atlantic Ridge, 15°20′N (ODP Leg 209): a sulfur and oxygen isotope study. *Geochem. Geophys. Geosyst.* 8:Q08002. doi: 10.1029/2007GC001617

Arvidson, R. S., Mackenzie, F. T., and Guidry, M. (2006). MAGic: a phanerozoic model for the geochemical cycling of major rock-forming components. *Am. J. Sci.* 306, 135–190. doi: 10.2475/ajs.306.3.135

Bach, W., and Edwards, K. J. (2003). Iron and sulfide oxidation within the basaltic ocean crust: implications for chemolithoautotrophic microbial biomass production. *Geochim. Cosmochim. Acta* 67, 3871–3887. doi: 10.1016/S0016-7037(03)00304-1

Bethke, C. M. (1996). *Geochemical Reaction Modeling*. New York, NY: Oxford University Press.

Blair, C. C., D'Hondt, S., Spivack, A. J., and Kingsley, R. H. (2007). Radiolytic hydrogen and microbial respiration in subsurface sediments. *Astrobiology* 7, 951–970. doi: 10.1089/ast.2007.0150

Boettger, J., Lin, H.-T., Cowen, J. P., Hentscher, M., and Amend, J. P. (2013). Energy yields from chemolithotrophic metabolisms in igneous basement of the Juan de Fuca ridge flank system. *Chem. Geol.* 33, 11–19. doi: 10.1016/j.chemgeo.2012.10.053

Cannat, M., Fountaine, F., and Escartin, J. (2010). "Serpentinization and associated hydrogen and methane fluxes at slow-spreading ridges," in *Diversity of Hydrothermal Systems on Slow Spreading Ocean Ridges*, eds P. Rona, C. Devey, J. Dyment, and B. J. Murton (Washington, DC: American Geophysical Union), 241–264.

Chermak, J. A., and Rimstidt, J. D. (1989). Estimating the thermodynamic properties (ΔGf and ΔHf) of silicate minerals at 298 K from the sum of polyhedral contributions. *Am. Mineral.* 74, 1023–1031.

Daux, V. C., Guy, T., Advocat, J.-L., Crovisier, J., and Stille, M. (1997). Kinetic aspects of basaltic glass dissolution at 90°C: role of silicon and aluminum. *Chem. Geol.* 142, 109–128. doi: 10.1016/S0009-2541(97)00079-X

Dzaugis, M. E., Spivack, A. J., Dunlea, A. G., Murray, R. W., and D'Hondt, S. (2016). Radiolytic hydrogen production in the subseafloor basaltic aquifer. *Front. Microbiol.* 7:76.

Edwards, K. J., Bach, W., and McCollom, T. M. (2005). Geomicrobiology in oceanography: mineral-microbe interactions in the deep-Sea. *Trends Microbiol.* 13, 449–456. doi: 10.1016/j.tim.2005.07.005

Edwards, K. J., Fisher, A. T., and Wheat, C. G. (2012). The deep subsurface biosphere in igneous ocean crust: frontier habitats for microbial exploration. *Front. Microbiol.* 3:8. doi: 10.3389/fmicb.2012.00008

Elderfield, H., and Schultz, A. (1996). Mid-ocean ridge hydrothermal fluxes and the chemical composition of the ocean. *Annu. Rev. Earth Planet. Sci.* 24, 191–224. doi: 10.1146/annurev.earth.24.1.191

Escartin, J., Smith, D. K., Cann, J., Schouten, H., Langmuir, C. H., and Escrig, S. (2008). Central role of detachment faults in accretion of slow-spreading oceanic lithosphere. *Nature* 455, 790–795. doi: 10.1038/nature07333

Fisher, A. T. (2005). Marine hydrogeology: recent accomplishments and future opportunities. *Hydrogeol. J.* 13, 69–97.

Fisher, A. T., and Becker, K. (2000). Channelized fluid flow in oceanic crust reconciles heat-flow and permeability data. *Nature* 403, 71–74. doi: 10.1038/47463

Fisher, A. T., Urabe, T., Klaus, A., Wheat, C. G., Becker, K., Davis, E. E., et al. (2005). IODP Expedition 301 installs three borehole crustal observatories, prepares for three-dimensional, cross-hole experiments in the northeastern Pacific Ocean. *Sci. Drill.* 1, 6–11. doi: 10.5194/sd-1-6-2005

Hayes, J. M., and Waldbauer, J. R. (2006). The carbon cycle and associated redox processes through time. *Philos. Trans. R. Soc. B* 361, 931–950. doi: 10.1098/rstb.2006.1840

Hoehler, T. M. (2004). Biological energy requirements as quantitative boundary conditions for life in the subsurface. *Geobiology* 2, 205–215. doi: 10.1111/j.1472-4677.2004.00033.x

Hoehler, T. M., Alperin, M. J., Albert, B., and Martens, C. S. (2001). Apparent minimum free energy requirements for methanogenic Archaea and sulfate-reducing bacteria in an anoxic marine sediment. *FEMS Microbiol. Ecol.* 38, 33–41. doi: 10.1111/j.1574-6941.2001.tb00879.x

Holland, T. J. B. (1989). Dependence of entropy on volume for silicate and oxide minerals: a review and a predictive model. *Am. Mineral.* 74, 5–13.

Johnson, J. W., Oelkers, E. H., and Helgeson, H. C. (1991). SUPCRT92: a software package for calculating the standard molal thermodynamic properties of minerals, gases, aqueous species, and reactions from 1-5000 bars and 0-1000°C. *Comput. Geosci.* 18, 899–947. doi: 10.1016/0098-3004(92)90029-Q

Kallmeyer, J., Pockalny, R., Adhikari, R. R., Smith, D. C., and D'Hondt, S. (2012). Global distribution of microbial abundance and biomass in subsea!oor sediment. *Proc. Natl. Acad. Sci. U.S.A* 109, 16213–16216. doi: 10.1073/pnas.1203849109

Kelley, D. S., Karson, J. A., Blackman, D. K., Früh-Green, G. L., Butterfield, D. A., Lilley, M. D., et al. (2001). An off-axis hydrothermal vent field near the Mid-Atlantic Ridge at 30°N. *Nature* 412, 127–128. doi: 10.1038/35084000

Klein, E. M. (2004). "Geochemistry of the igneous oceanic crust," in *Treatise on Geochemistry*, eds H. D. Holland and K. K. Turekian (Amsterdam: Elsevier), 433–463.

Klein, F., Bach, W., and McCollom, T. M. (2013). Compositional controls on hydrogen generation during serpentinization of ultramafic rocks. *Lithos* 178, 55–69. doi: 10.1016/j.lithos.2013.03.008

Lever, M. A., Rouxel, O., Alt, J. C., Shimizu, N., Ono, S., Coggon, R. M., et al. (2013). Evidence for microbial carbon and sulfur cycling in deeply buried ridge flank basalt. *Science* 339, 1305–1308. doi: 10.1126/science.1229240

Mayhew, L. E., Ellison, E. T., McCollom, T. M., Trainor, T. P., and Templeton, A. S. (2013). Hydrogen generation from low-temperature water–rock reactions. *Nat. Geosci.* 6, 478–484. doi: 10.1038/ngeo1825

McCollom, T. M., and Bach, W. (2009). Thermodynamic constraints on hydrogen generation during serpentinization. *Geochim. Cosmochim. Acta* 73, 856–879. doi: 10.1126/science.aaa4326

Nakamura, K., Morishita, T., Bach, W., Klein, F., Hara, K., Okino, K., et al. (2009). *Serpentinized troctolites* exposed near the Kairei hydrothermal fluid supporting a unique microbial ecosystemhydrothermal field, central indian ridge: insights into the origin of the kairei . *Earth Planet. Sci. Lett.* 280, 128–136. doi: 10.1016/j.epsl.2009.01.024

Nielsen, M. E., and Fisk, M. R. (2010). Surface area measurements of marine basalts: implications for the subseafloor microbial biomass. *Geophys. Res. Lett.* 37:15. doi: 10.1029/2010GL044074

Oelkers, E. H. (2001). General kinetic description of multioxide silicate mineral and glass dissolution. *Geochim. Cosmochim. Acta* 65, 3703–3719. doi: 10.1016/S0016-7037(01)00710-4

Oelkers, E. H., and Gislason, S. R. (2001). The mechanism, rates and consequences of basaltic glass dissolution: I. An experimental study of the dissolution rates of basaltic glass as a function of aqueous Al, Si and oxalic acid concentration at 25°C and pH = 3 and 11. *Geochim. Cosmochim. Acta* 65, 3671–3681. doi: 10.1016/S0016-7037(01)00664-0

Orcutt, B. N., Sylvan, J. B., Knab, N. J., and Edwards, K. J. (2011). Microbial ecology of the dark ocean above, at, and below the seafloor. *Microbiol. Mol. Biol. Rev.* 75, 361–422. doi: 10.1128/MMBR.00039-10

Orcutt, B. N., Wheat, C. G., Rouxel, O., Hulme, S., Edwards, K. J., and Bach, W. (2013). Oxygen consumption rates in subseafloor basaltic crust derived from a reactive transport model. *Nat. Commun.* 4:2539. doi: 10.1038/ncomms3539

Pokrovsky, O. S., and Schott, J. (2000). Kinetics and mechanism of forsterite dissolution at 25°C and pH from 1 to 12. *Geochim. Cosmochim. Acta* 64, 3313–3325. doi: 10.1016/S0016-7037(00)00434-8

Rutter, J. (2015). *Characterising Low Temperature Alteration and Oxidation of the Upper Oceanic Crust*, Doctoral Thesis, University of Southampton, Earth and Ocean Sciences, Southampton.

Seyfried, W. E. Jr., Foustoukos, D. I., and Fu, Q. (2007). Redox evolution and mass transfer during serpentinization: an experimental and theoretical study at 200°C, 500 bar with implications for ultramafic-hosted hydrothermal systems at Mid-Ocean Ridges. *Geochim. Cosmochim. Acta* 71, 3872–3886. doi: 10.1016/j.gca.2007.05.015

Stein, C. A., and Stein, S. (1994). Constraints on hydrothermal heat flux through the oceanic lithosphere from global heat flow. *J. Geophys. Res.* 99, 3081–3095. doi: 10.1029/93JB02222

Türke, A., Nakamura, K., and Bach, W. (2015). Palagonitization of basalt glass in the flanks of mid-ocean ridges: implications for the bioenergetics of oceanic intracrustal ecosystems. *Astrobiology* 15:10. doi: 10.1089/ast.2014.1255

Whitman, W. B., Coleman, D. C., and Wiebe, W. J. (1997). Prokaryotes: the unseen majority. *Proc. Natl. Acad. Sci. U.S.A.* 95, 6578–6583. doi: 10.1073/pnas.95.12.6578

Wolery, T. J. (2004). *Qualification of Thermodynamic Data for Geochemical Modeling of Mineral-Water Interactions in Dilute Systems. ANL-WIS-GS-000003 REV 00.* Las Vegas: Bechtel SAIC.

Wolery, T. J., and Jarek, R. L. (2003). *Software User's Manual EQ3/6 (version 8.0)*. New Mexico: Sandia National Laboratories Albuquerque.

Conflict of Interest Statement: The author declares that the research was conducted in the absence of any commercial or financial relationships that could be construed as a potential conflict of interest.

frontiers in Microbiology

ORIGINAL RESEARCH
published: 04 February 2016
doi: 10.3389/fmicb.2016.00076

Radiolytic Hydrogen Production in the Subseafloor Basaltic Aquifer

Mary E. Dzaugis[1], Arthur J. Spivack[1], Ann G. Dunlea[2], Richard W. Murray[2] and Steven D'Hondt[1]*

[1] Graduate School of Oceanography, University of Rhode Island, Narragansett, RI, USA, [2] Department of Earth and Environment, Boston University, Boston, MA, USA

Hydrogen (H_2) is produced in geological settings by dissociation of water due to radiation from radioactive decay of naturally occurring uranium (^{238}U, ^{235}U), thorium (^{232}Th) and potassium (^{40}K). To quantify the potential significance of radiolytic H_2 as an electron donor for microbes within the South Pacific subseafloor basaltic aquifer, we use radionuclide concentrations of 43 basalt samples from IODP Expedition 329 to calculate radiolytic H_2 production rates in basement fractures. The samples are from three sites with very different basement ages and a wide range of alteration types. U, Th, and K concentrations vary by up to an order of magnitude from sample to sample at each site. Comparison of our samples to each other and to the results of previous studies of unaltered East Pacific Rise basalt suggests that significant variations in radionuclide concentrations are due to differences in initial (unaltered basalt) concentrations (which can vary between eruptive events) and post-emplacement alteration. However, there is no clear relationship between alteration type and calculated radiolytic yields. Local maxima in U, Th, and K produce hotspots of H_2 production, causing calculated radiolytic rates to differ by up to a factor of 80 from sample to sample. Fracture width also greatly influences H_2 production, where microfractures are hotspots for radiolytic H_2 production. For example, H_2 production rates normalized to water volume are 190 times higher in 1 μm wide fractures than in fractures that are 10 cm wide. To assess the importance of water radiolysis for microbial communities in subseafloor basaltic aquifers, we compare electron transfer rates from radiolysis to rates from iron oxidation in subseafloor basalt. Radiolysis appears likely to be a more important electron donor source than iron oxidation in old (>10 Ma) basement basalt. Radiolytic H_2 production in the volume of water adjacent to a square cm of the most radioactive SPG basalt may support as many as 1500 cells.

Keywords: radiolysis, hydrogen, basalt, ocean crust, geochemistry, deep biosphere

OPEN ACCESS

Edited by:
Jason B. Sylvan,
Texas A&M University, USA

Reviewed by:
Craig Lee Moyer,
Western Washington University, USA
Wolfgang Bach,
University of Bremen, Germany
Lisa Mayhew,
University of Colorado Boulder, USA

****Correspondence:***
Mary E. Dzaugis
mdzaugis@uri.edu

Specialty section:
This article was submitted to Extreme Microbiology, a section of the journal Frontiers in Microbiology

Received: *01 September 2015*
Accepted: *15 January 2016*
Published: *04 February 2016*

Citation:
Dzaugis ME, Spivack AJ, Dunlea AG, Murray RW and D'Hondt S (2016) Radiolytic Hydrogen Production in the Subseafloor Basaltic Aquifer. Front. Microbiol. 7:76. doi: 10.3389/fmicb.2016.00076

INTRODUCTION

The oceanic basement contains the largest aquifer on Earth. Its fractured rock contains nearly 2% of Earth's total volume of seawater (Johnson and Pruis, 2003). Although the extent of life and microbial activity in oceanic basement is not well known, a variety of evidence suggests that microbes reside within the aquifer (Cowen et al., 2003; Edwards et al., 2012; Jungbluth et al., 2013; Lever et al., 2013; Orcutt et al., 2013). Fisk et al. (1998) and Staudigel et al. (2008) report weathering

textures suggestive of microbial alteration in subseafloor basaltic glass. Microorganisms have been found in fluid flowing through 3.5 million year old basalt on the Juan de Fuca ridge flank (Cowen et al., 2003). DNA and isotopic signatures of mineral alteration provide evidence of microbes and microbial activity in ridge-flank basalt (Lever et al., 2013).

Physical and chemical properties limit microbial habitability of the oceanic basement. For example, habitability within subseafloor basalt is constrained by availability of electron donors [e.g., organic carbon, ferrous iron (Fe^{2+}), and hydrogen (H_2)] and electron acceptors [e.g., oxygen (O_2), nitrate (NO_3^-), and sulfate (SO_4^{2-})] (Madigan et al., 2000; Bach and Edwards, 2003; D'Hondt et al., 2004). A number of studies have suggested that microbial life in igneous-rock aquifers may be supported by oxidation of electron donors native to the rock or produced by water–rock interactions (Pedersen, 1993; Stevens and McKinley, 1995; Kelley et al., 2001; Chapelle et al., 2002; Bach and Edwards, 2003; Edwards et al., 2005). For example, basement basalt has high concentrations of reduced elements, specifically iron (Fe) and sulfur (S) (Bach and Edwards, 2003). Oxidation of these elements with O_2 or NO_3^- in the seawater provides energy that microorganisms might utilize. Water–rock interactions that can produce electron donors in the form of molecular H_2 include serpentinization (Kelley et al., 2001) and radiolysis of water due to radioactive decay of radionuclides within the rock (Pedersen, 1993; Lin et al., 2005a,b; Blair et al., 2007; D'Hondt et al., 2009, 2015; Edwards et al., 2011; Lollar et al., 2014). Water radiolysis within subseafloor basalt is the focus of this study.

Water radiolysis is the decomposition of water molecules by ionizing radiation produced during the decay of radioactive elements (Debierne, 1914; Le Caër, 2011). The principal radioactive elements that produce ionizing radiation in basalt are uranium (^{238}U and ^{235}U), thorium (^{232}Th), and potassium (^{40}K), which collectively emit alpha (α), beta (β), and gamma (γ) radiation as they and their daughter nuclides decay. Transfer of energy from this radiation excites and ionizes water molecules, producing several chemical species: e_{aq}^-, HO•, H•, HO_2•, H_3O^+, OH^-, H_2O_2, and H_2 (Spinks and Woods, 1990; Le Caër, 2011). The distribution and rate of formation of these products depends on the linear energy transfer (LET) of the radiation (the amount of energy deposited by the radiation along its path). Low-LET radiation (γ-rays and β particles) ionizes water discretely along the radiation path. High-LET radiation (e.g., α particles) deposits energy densely along the particles' track. The radiolytic yields of the radicals decline with LET. The radicals are short-lived and highly reactive; they recombine in the radiation track to produce stable decomposition products (H_2 and H_2O_2). Production of H_2 and H_2O_2 increases with increasing LET (Pastina and LaVerne, 2001; Le Caër, 2011).

For subseafloor environments, we are particularly interested in the production of the reductant H_2. Many organisms catabolically utilize H_2, including methanogens, sulfate-reducers, iron reducers, and nitrate reducers (Fang and Zhang, 2011). There is evidence that some of these organisms, specifically sulfate reducers and methanogens, are active in subseafloor basalt (Lever et al., 2013). Radiolysis undoubtedly occurs in subseafloor basalt, as both water and radiation are present. Edwards et al. (2012) suggested that in the old and relatively weathered basaltic basement of the South Pacific Gyre (SPG), radiolytic H_2 may be the dominant electron donor.

The potential of radiolytic H_2 as an electron donor has been studied for other environments, such as continental crust (Pedersen, 1993; Lin et al., 2005a,b) and deep-sea sediment (Blair et al., 2007). In these environments, water radiolysis supplies H_2 that may support microbial communities. In deep-sea sediment, H_2 may be especially important to microbial communities where organic carbon availability is very low (Blair et al., 2007; D'Hondt et al., 2009).

Here, we focus on calculating the rate of radiolytic H_2 production in oceanic basement. More specifically, we use our recently published water radiolysis model to calculate H_2 production rates in fractures of South Pacific subseafloor basalt (Dzaugis et al., 2015). Our model more accurately quantifies radiolytic H_2 production in fractured hard rock then previous models, which are more appropriate for physically homogenous environments where solid particles are small compared to the distance that the ionizing radiation travels, such as deep-sea sediment.

To determine variations in radionuclide concentrations of relatively old SPG basalt, we analyzed basalt samples from three SPG sites with basement ages of circa 13 to 100 Ma. Our samples include a wide variety of alteration types. To identify effects of basement age, initial composition, and alteration on radiolysis rates, we compare our H_2 production calculations for these samples to calculations for which we use previously published U, Th, and K data from young basalt samples on the East Pacific Rise (EPR) (Gale et al., 2013). In addition, we quantify the effect of fracture width on the H_2 production rates. We assess the possible significance of radiolytic H_2 production for microbial communities in subseafloor basaltic aquifers by comparing the electron transfer flux from radiolytic H_2 to the electron transfer flux from iron oxidation in the basalt. Finally, we estimate the number of cells that might be supported by radiolysis in the basement.

MATERIALS AND METHODS

Materials

Integrated Ocean Drilling Program (IODP) Expedition 329 collected subseafloor basalt samples at three sites (Sites U1365, U1367, U1368; **Figure 1**). We analyzed 43 samples from these sites to determine the range of U, Th, and K concentrations in SPG basalt.

Site U1365 is located in the western part of the SPG, where the seafloor is approximately 5695 m below sea level (Expedition 329 Scientists, 2011a). At this location, basement is mainly composed of massive lava flows that are approximately 100 Ma (Dunlea et al., 2015a). Recovery of cored basalt was 74.6% at this site. Throughout the cored sequence, alteration extent of the recovered basalt varies between 2 and 95%, with alteration mainly associated with veins and vesicles near flow margins and breccias (Expedition 329 Scientists, 2011a). We analyzed 17 samples from Site U1365 for this study.

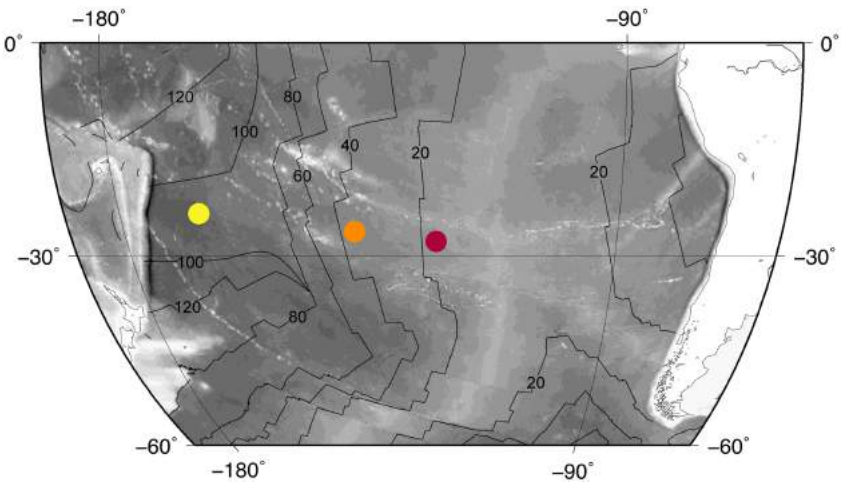

FIGURE 1 | Site locations. Colored dots mark site locations: Site U1365 (yellow), Site U1367 (orange), Site U1368 (red). The site localities are superimposed on a bathymetry map with the East Pacific Rise in light gray. Black lines indicate basement age (20 Myr contours).

The second site, U1367, is east of Site U1365, with seafloor approximately 4288 m below sea level (Expedition 329 Scientists, 2011b). The basement is younger at this site, with an approximate age of 33.5 Ma. The uppermost basement is mostly composed of fractured pillow fragments with a small thin flow at the base of the recovered basalt. Due to the fractured nature of the basalt cored at this site, core recovery was low (11.2%). The extent of alteration in recovered basalt from this site varies between 2 and 25%. Most basalt alteration at Site U1367 occurs around vein-filled fractures of chilled margins (Expedition 329 Scientists, 2011b). We analyzed five samples from Site U1367.

Site U1368 is the eastern-most site of Expedition 329. Seafloor here is 3740 m below sea level (Expedition 329 Scientists, 2011c). Basement at Site U1368 is approximately 13.5 Ma. Core recovery was 27.6%. The recovered portion of the basement is dominantly composed of pillow basalt. Basalt alteration at this site is mainly in veins, vesicles, along chilled margins, and within volcaniclastic breccias. The recovered basalt varies in alteration extent from 2 to 60% (Expedition 329 Scientists, 2011c). There are 21 samples from Site U1368 used in this study.

Alteration Categories

Our 43 samples are characterized by wide ranges of alteration extent and alteration type. We assign samples to the following rock types based on macroscopic visual appearance; brown halos, dark gray halos, carbonate veins, iron oxyhydroxide (Fe) stained, breccia, mixed alteration, and minimally altered. The term brown halo refers to all halos that vary from red to brown in color. Similarly, dark gray halo refers to halos ranging from very dark gray to dark green in color. Fe staining includes samples with iron oxyhydroxide staining of secondary minerals or filling of veins and vesicles. Iron oxyhydroxides leave behind a bright red-orange color. We define samples as mixed-alteration when they are visibly altered but without a dominant single alteration type, such as samples with veins and vesicles filled with carbonate, clays and iron oxyhydroxides and have secondary mineral emplacement. Finally, we classify all aphyric samples without visibly altered regions as minimally altered.

Where possible, we analyzed samples of different visibly altered regions within the same basaltic rock to compare the radioactive element concentrations of the different alteration zones. For example, we took two samples from a piece of light gray basalt with a brown halo. For all analyses of alteration halos and carbonate veins, we separated each alteration type from the rest of the rock. Other alteration categories included a mixture of altered rock and background basalt, as they could not be fully separated. We analyzed the 43 samples for their U, Th, and K concentrations.

U, Th, K Measurements

We used well-established protocols to measure concentrations of U, Th, and K in the 43 samples by inductively coupled plasma-emission spectrometry (ICP-ES) and inductively coupled plasma-mass spectrometry (ICP-MS; Dunlea et al., 2015b). We analyzed these samples at Boston University with a VG PlasmaQuad Excell ICP-MS for U and Th concentrations, and a Jobin-Yvon (JY) Ultima-C ICP-ES for K concentrations. Based on replicate analysis, U and Th precision was 2 and 1%, respectively, of their measured values. The K measurements were within 1% of the measured value. To assess analytical accuracy, we analyzed BHVO-2 Standard Reference Material independently from our calibrations. The measured values agree with the reported accepted values within the analytical precision (Jochum et al., 2005). We list all U, Th, and K data in Supplementary Table S1.

Radiolytic H_2 Production Model

Our radiolysis model calculates production rates in water near a radionuclide-containing solid (Dzaugis et al., 2015). Previous models, such as those used in sediment (Blair et al., 2007), are not applicable to basalt, because studies of basalt cannot assume homogenous porosity or grain/crystal size smaller than

the stopping distance of the radiation. Dzaugis et al. (2015) gives a detailed description of the model that we apply to our samples. In this section, we describe the inputs and assumptions that we used to calculate radiolytic H_2 production rates in fractures.

There are four dominant parent radionuclides in basalt: ^{238}U, ^{235}U, ^{232}Th, and ^{40}K. When these nuclides decay, α, β, and/or γ radiation is emitted. Each type of radiation has different properties that affect radiolytic yield. For example, α particles travel short distances (10s of μm) but have high initial energies and produce the most H_2 molecules per unit of energy absorbed. Our calculations assume that the entire decay series of ^{238}U, ^{235}U, and ^{232}Th are in secular equilibrium. This assumption is valid for basalt older then 377,000 years (five half-lives of ^{230}Th; LaTourrette et al., 1993). However, younger basalt is characterized by isotopic disequilibrium within the ^{238}U-decay series, because fractionation during partial melting leads to excess ^{230}Th relative to ^{238}U (LaTourrette et al., 1993). Due to this ^{230}Th enrichment, we slightly underestimate radiolytic H_2 production rates when we assume secular equilibrium for young basalt.

The distance that α or β radiation travels before losing all of its kinetic energy is called its stopping distance (Spinks and Woods, 1990). Gamma radiation loses energy exponentially with distance and therefore is not assigned a specific stopping distance. Instead, we use the maximum distance traveled by γ-rays to be 10 half-distances, at which point less then 0.1% of their initial energy remains. Stopping distance and γ travel distance depend on the matrix; for example, a 5 MeV α particle will travel about 20 μm in basalt but 40 μm in water. If radiation is emitted from a radionuclide farther from the water interface than the stopping distance, it does not contribute to water radiolysis. Once radiation reaches the basalt-water interface, it continuously ionizes water along its path until it reaches its stopping distance (Le Caër, 2011) or re-enters basalt from the water. Our model incorporates radioactivity, decay energy of each radionuclide, and how each type of radiation attenuates energy along its path. It sums all of the radiation that is absorbed in a fracture. Consequently, the inputs to our model are U, Th, and K concentration, initial energy for all radiation emitted from the isotopes, energy-range relationships for α, β, and γ radiation in basalt and water, H_2 yield per unit energy for each type of radiation, and distance the radiation travels through water. For the calculations in this paper, we assume there is one centimeter of basalt on either side of the fracture, unless noted otherwise.

We used the data in Supplementary Table S1 to calculate the radioactivity of our SPG basalt samples for ^{238}U, ^{235}U, ^{232}Th, and ^{40}K. We used published radionuclide data (Gale et al., 2013) to calculate the radioactivity of EPR basalt at its time of formation. We used the program RadDecay (Hacker, 1997) to find the initial energy for all radiation emitted from radionuclides in basalt. We calculated stopping distances of α and β particles and half-distances of γ-rays for basalt and water using the energy-range data from the ASTAR, ESTAR (Berger et al., 2005), and X-ray Attenuation (Hubbell and Seltzer, 2004) programs in the NIST database. To determine stopping distances in basalt, we used energy-range data for borosilicate glass (in the NIST database, borosilicate glass is the material with electron density most similar to oceanic basalt). Using these relationships, we developed equations to calculate travel distance given an initial energy. Supplementary Table S2 summarizes the equations we use in this study.

Using radioactivity, energy and range data, and how many H_2 molecules are produced per 100 eV (*G*-values), we calculated volume-normalized H_2 production rates for basalt fractures of widths between 1 um and 1 m. These rates assume (i) basalt of the same composition on both sides of a fracture and (ii) homogeneous distribution of the radionuclides throughout the basalt.

RESULTS

South Pacific H_2 Production Rates

We calculated radiolytic H_2 production rates as a function of fracture width for all 43 samples. We show the results of these calculations separately for each site in **Figure 2**. Volume-normalized H_2 production decreases greatly as fracture width increases (from 1μm to 1 m in width; **Figure 2**). For each width, the differences in H_2 yields between samples are due to variations in radioactive element concentrations. Site U1365 contains the oldest and generally most altered basalt of the three sites (Expedition 329 Scientists, 2011a). It exhibits the lowest H_2 production rates (**Figure 2A**), while Site U1368, with the youngest basalt age, generally has the highest rates (**Figure 2C**). The SPG sample with the lowest H_2 production rate (approximately 3X lower then other samples) is from Site U1365 with a Th concentration below the detection limit (0.01 ppm). We calculated the radiolytic H_2 production rate for this sample using the below detection limit value.

Radionuclide Compositional Variance

U and K variance in basalt is due to geochemical composition at the time of basalt formation (initial composition) and post-emplacement alteration. In contrast, Th is not significantly modified during post-emplacement alteration (Kelley et al., 2005). We use Th to constrain abundance variations due to initial composition and U/Th ratios to constrain the magnitude of U alteration.

In our samples, Th ranges from below the detection limit (0.01 ppm) to 1.17 ppm. This range is comparable to the entire range of values observed in unaltered basalt glass from the EPR (compositional data from Gale et al., 2013). The U/Th ratios of our samples range from 0.32 to 4.1 (excluding samples with Th below detection limit). This is much greater than ratios observed in unaltered EPR basaltic glass (Gale et al., 2013). However, it is similar to the range in altered material from other studies (e.g., Kelley et al., 2003). About 1/3 of our samples have U/Th ratios that fall within two standard deviations of the mean U/Th ratio in unaltered EPR glass samples. Most of the SPG samples that fall into this category are from the site with youngest basement age, U1368 (11 samples). Only one and two samples at Site U1367 and U1365, respectively, have U/Th ratios indicative of unaltered composition.

H_2 Yields and Alteration

We separately describe the calculated radiolytic rates of the three SPG sites because they have different geographic origins, different eruptive histories, and different degrees of deviation from the mean U/Th ratio of unaltered EPR glass. Site U1365 exhibits a 21-fold range in rates, whereas Sites U1367 and U1368 show 7- to 8-fold ranges. Overall, Site U1365 has the lowest rates, while Site U1368 has the highest (**Figure 2**).

Our samples show no clear relationship between alteration type and H_2 production rates. The H_2 production rates calculated for all alteration categories, including minimally altered samples, seem to span the entire range; no alteration type exhibits a significantly different range of H_2 production rates than the others (**Figure 3**). There is some separation of alteration types within the individual sites. At Site U1365, iron stained samples tend to have higher rates, while at Site U1368 the mixed alteration samples and the breccia are highest (**Figure 3**). Two of the three mixed alteration samples at U1368 have U/Th ratios within the unaltered range indicating that the high range may not completely be due to alteration. Many of the H_2 production rates for the different samples overlap; the rates calculated for each sample at the basalt-water interface are given in Supplementary Figure S1.

To further investigate the impact of alteration, we calculate the U due to alteration (U_{alt}) as

$$U_{alt} = U_{meas} - \left(\frac{U}{Th}\right)_{unalt} * Th_{meas}$$

where the subscript *meas* refers to measured values and $\left(\frac{U}{Th}\right)_{unalt}$ is the average ratio in unaltered EPR basalt (0.37 ± 0.08). We then calculate H_2 yield due to U_{alt} and determine its fractional contribution to the total yield. There are 27 samples that have excess U that is significantly (more then two standard deviations) different than zero. For these samples, the H_2 yield based on U_{alt} ranges from 0 to $4.9 \times 10^{-1} \pm 1.5 \times 10^{-2}$ nM H_2 yr^{-1}, and can contribute up to $85 \pm 3\%$ of the radiolytic H_2 produced (average of $31 \pm 7\%$ for all samples with altered U/Th ratios).

Influence of Fracture Width and Basalt Width on H_2 Production Rates

While compositional variation leads to a large range of radiolytic H_2 production rates (almost two orders of magnitude within the SPG samples), fracture width has an even greater effect on volume-normalized H_2 production (moles per vol. of water per time). The production rate per volume of water decreases as fracture width increases. This decline in volume-normalized rates is most pronounced after α and β particles run out of energy. To illustrate this effect, we calculated volume-normalized production rates for a range of fracture widths that occur in basement basalt (1 μm to 1 m). Volume-normalized H_2 production rates are highest in microfractures (<10 μm), regardless of radionuclide concentration, and strongly decrease as fracture width increases (**Figure 2**). Production rates in 1 μm wide fractures differ by more than three orders of magnitude from rates in 1 m wide fractures. Volume-normalized H_2 production rates are highest at the rock–water interface, due to high dose rates. However, if production rate is normalized to the surface area of fractures, it increases with fracture width as more radiation, especially

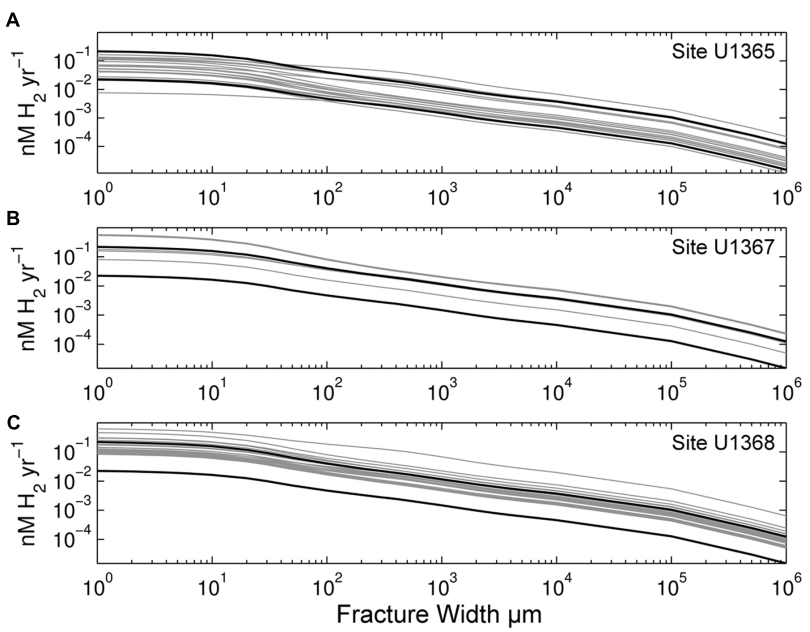

FIGURE 2 | Radiolytic H_2 production rates calculated from radionuclide concentrations of our SPG samples. Volume-normalized rates are shown as a function of fracture width for **(A)** Site U1365, **(B)** Site U1367, and **(C)** Site U1368. Black lines mark maximum and minimum rates calculated from EPR glass samples (Gale et al., 2013). Note that both axes are log scale.

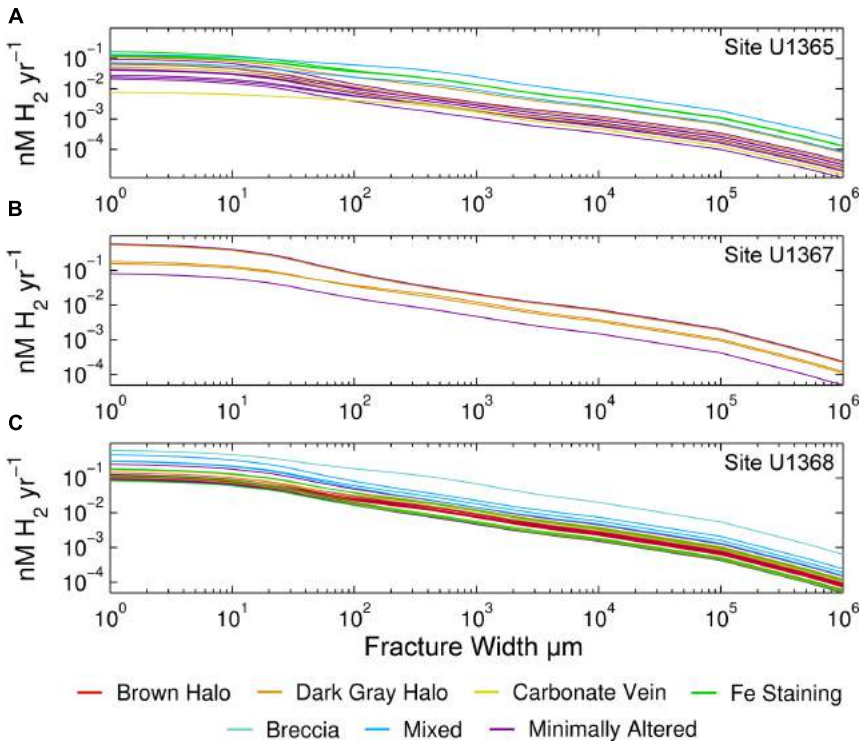

FIGURE 3 | Relation of rock alteration to radiolytic H_2 production rates. Volume-normalized rates are given for Sites **(A)** U1365, **(B)** U1367, **(C)** U1368. Colors show the alteration type to which we assigned each sample. Note that both axes are log scale. As in **Figure 2**, rates are given as a function of fracture width.

from γ-rays, is absorbed in wider fractures than narrower fractures.

Radiolytic H_2 production rates also vary with the thickness of basalt that abuts a fracture (**Figure 4**). To illustrate this effect, we calculated production rates based on a single SPG sample and three different thicknesses: 1 m, 1 cm and 100 μm. Thickness affects the amount of radiation emitted to water. One meter of basalt is approximately equivalent to an infinite basalt thickness because less than 0.1% of the radiation travels beyond a meter (10 half-distances of γ-rays); the amount of energy that reaches the water approaches its maximum at about a meter of basalt.

This dependence on basalt thickness is clearly illustrated by comparing H_2 production by β and γ radiation with 100 μm thick basalt (**Figure 4C**) to H_2 production by β and γ radiation with 1 cm thick or 1 m thick basalt (**Figures 4A,B**). The decrease in thickness from 1 m to 100 μm of basalt causes a 20% decrease in β-produced H_2 and a 98.9% decrease in γ-produced H_2. Because the stopping distance for β and γ radiation is much greater than 100 μm in basalt, the change in thickness greatly impacts the number of β particles and γ-rays emitted from the basalt. Despite these effects of basalt thickness on H_2 production by β and γ radiation, total radiolytic H_2 production rate is not greatly affected by basalt thickness because α radiation is responsible for most radiolytic H_2 production in our examples (**Figure 4**). Total H_2 production rate is only 4% less with 1 cm of basalt and 10% less with 100 μm than 1 m of basalt. In all three cases, α-dose rate is the same, because α particles penetrate no more than 50 μm of basalt (25 μm on average). Therefore, in all three scenarios, all the α radiation that can reach fracture water does.

DISCUSSION

In this section, we discuss (i) factors that impact radiolytic H_2 production rates, (ii) their potential importance to electron donor fluxes in subseafloor basalt, and (iii) the number of cells that might be supported by rates of radiolytic H_2 production in representative fractures. We first consider the fractured nature of oceanic basement and how both fracture width and basalt thickness affect radiolysis rates. We address how source-melt composition and subsequent low-temperature alteration play a role in determining the distribution of radionuclides in our sample set and rates of radiolytic H_2 production. We then compare electron donor fluxes from radiolytic H_2 production and from iron oxidation. Finally, we estimate numbers of cells that might be supported by radiolysis in SPG basaltic fractures, based on comparison to per-cell O_2 consumption rates in SPG sediment.

Factors that Influence H_2 Production

We focused this study on radiolysis in fractures because most of the water in oceanic basement resides in, and travels through, fractures (Fisher, 1998). The three primary categories of porosity

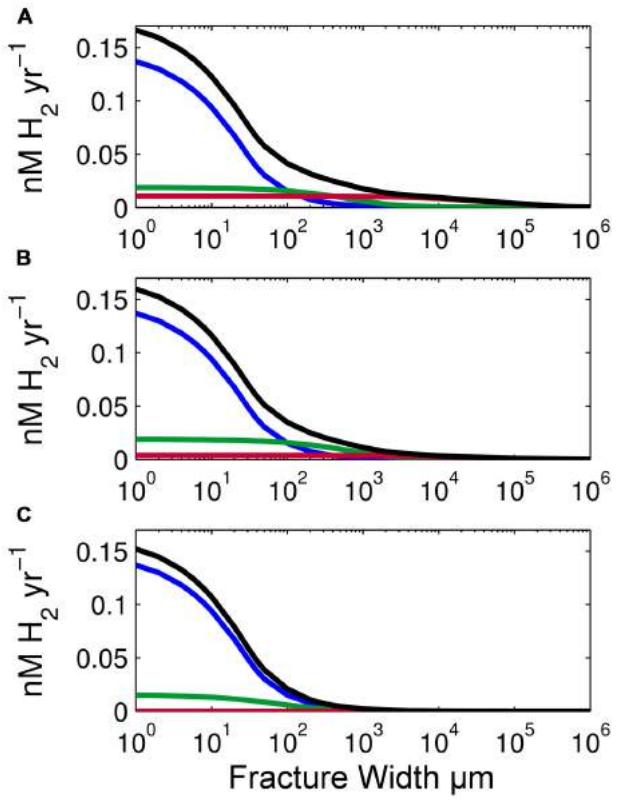

FIGURE 4 | Effect of basalt thickness on radiolytic H_2 production rates. **(A)** Volume-normalized radiolytic H_2 production for 1-m thick basalt using an average SPG composition of our samples, **(B)** 1-cm thick basalt, and **(C)** 100-μm thick basalt. Total production rates are shown as black lines. Rates due to α radiation are shown in blue, β radiation in green and γ radiation in red. *X*-axis is log scale.

in oceanic crust are (i) macroscopic features, such as lithological boundaries (e.g., surfaces of lava flows), voids associated with pillow basalts, and collapse structures; (ii) microcracks which have narrow widths and limited lateral extent, and (iii) vesicles and other primary porosity, which we do not consider since they are typically disconnected and isolated. Of these three categories, the first is most closely related to formation-scale permeability (Fisher, 1998). Fluid flow in the igneous basement is mostly through interconnected fractures in the oceanic basement (Wang, 2004), e.g., through fractures between pillow basalts and along the margins of lava flows. This relationship between fluid flow and interconnected fractures is apparent in the distribution of alteration halos, which are mainly associated with veins in the basalt, indicating that chemical transport is very limited in the low porosity, impermeable basalt matrix (Bach and Edwards, 2003).

Our focus on quantifying radiolytic rates in fractures differs from previous studies of radiolysis in continental crust (e.g., Lin et al., 2005a), which assume porosity to be homogenously distributed throughout the rock. Such an assumption is very problematic for estimating radiolytic H_2 production in hard-rock aquifers, where most porosity is in heterogeneously distributed fractures and much of the radiation emitted from radionuclides in the rock will never reach water. As we discussed in Section "Results," properties that most affect H_2 production rates in hard-rock aquifers include fracture width, rock thickness and rock composition. Of these properties, fracture width and rock composition are the most important.

Fracture width greatly influences radiolytic H_2 production rates (**Figures 2–4**) because volume-normalized H_2 production rapidly decreases with distance from the rock-water interface. This decrease in H_2 production is due to the limited ranges of α and β radiation and increased volume of water. Of the three types of radiation, α radiation has the highest initial energy and highest *G*-value at 1.2 molecules H_2 per 100 eV (Pastina and LaVerne, 2001). However, it also has the shortest range. Consequently, H_2 production by α radiation extends only several tens of microns into fracture water. Beta and gamma radiation have lower *G*-values (0.6 and 0.45 molecules H_2 100 eV^{-1}, respectively) than α particles (Kohan et al., 2013; Mustaree et al., 2014), but β particles can travel 1000s of μm in water and γ-rays travel for tens of cm. Consequently, α radiation dominates total radiolytic H_2 production near the rock-water interface, while γ-produced H_2 is highest in fractures greater than 1 cm (**Figure 4**). Due to the very high rate of H_2 production from α radiation, volume-normalized H_2 production rates in 1 μm fractures are on average 190 times higher than fractures 10 cm in width and 1.6×10^3 times higher than in 1 m fractures. In short, microfractures are hotspots of radiolytic H_2 production.

To a much lesser extent, total radiolytic H_2 production varies with the thickness of the abutting rock (**Figure 4**). Over a four-order magnitude of change in basalt thickness (from 100 μm to 1 m of basalt), H_2 production rates change by only 10% at the rock–water interface. This change is due to differences in the absorbed doses of β and γ radiation. This change is small because α radiation from deeper in the rock does not penetrate to the surface. If the thickness of basalt facing a fracture is less than 50 μm, the rates will drop more dramatically due to a lower absorbed α-dose rate.

Along with microfractures, high concentrations of U, Th, and K create hotspots of radiolytic H_2 production. Uranium, Th, and K concentrations differ widely from sample to sample within and between the three sites. To illustrate the range of H_2 yields due to initial composition variance, we show a H_2 production range for unaltered basaltic EPR glass samples (Gale et al., 2013). The range of calculated H_2 production at the basalt-water interface is approximately 10-fold for the group of EPR samples with Th composition within two standard deviations of the mean (∼90% of the samples) (black lines, **Figure 2**). The range is much greater (93-fold) if we consider all EPR glass measurements reported by Gale et al. (2013), which include measurements of enriched mid-ocean ridge basalt (E-MORB) that have much higher U and Th concentrations. Basement comprised of E-MORB will have higher radiolytic yields than normal ocean basalt.

The 10-fold difference in H_2 yields from EPR data suggests that basaltic source-melt composition has a significant effect on radiolytic rates. Given the wide range of compositions exhibited by the EPR samples, we expect variation in radiolytic H_2

production rates from one SPG site to another, as they all have different geographic locations and ages of origin (**Figure 1**). In addition, the basalt at Site U1365 has a very different eruption history than the basalt at Sites U1367 and U1368. The basalt drilled at Site U1365 was accreted during medium to fast spreading and is comprised mostly of large sheet flows. In contrast, the basalts drilled at Sites U1367 and U1368 are predominantly pillow basalt, and were likely produced during slower spreading than at Site U1365 (Zhang et al., 2013; Zhang and Smith-Duque, 2014).

Site U1365 has lower radiolytic H_2 production rates than Sites U1367 and U1368, despite having the oldest and most altered basalt (**Figure 2**). This can be attributed to low initial concentrations, as indicated by Th values. Thorium concentrations of U1365 samples are all below 0.2 ppm. These concentrations are lower than those in the samples from the other localities and fall into the bottom half of EPR Th data from Gale et al. (2013). Even with enrichment of U during alteration (indicated by high U/Th ratios) at Site U1365, the radiolytic rates are low compared to the other localities indicating that they are greatly affected by initial radioisotope concentrations. This variation in source-melt composition is consistent with the results of Zhang and Smith-Duque (2014), who used differences in initial composition to explain geochemical variance between Sites U1365 and U1368. In addition, there is also likely vertical variation at each site due to changes in source composition between eruptive events (e.g., Bergmanis et al., 2007). Zhang et al. (2013) reported some vertical variation at Site U1368. Using U, Th and K from Zhang et al. (2013) results in a 6X difference in radiolytic rates between their lowest normal-MORB sample and the sample they suggest was influenced by an enriched-MORB source. This difference is similar to the sevenfold range in rates calculated from our radioisotope concentration data for this site.

Concentrations of U and K often increase with alteration (e.g., Staudigel et al., 1996; Teagle et al., 1996; Kelley et al., 2003). We use U/Th ratios to constrain how much excess U a sample contains. We don't calculate excess values for K, because K/Th ratios in fresh basalt are not consistent enough to calculate excess K in this manner. Potassium is typically concentrated in such alteration minerals as smectite and zeolite, as well as K-feldspar (Alt and Teagle, 2003; Bartetzko, 2005). Shipboard logs of natural gamma radiation (NGR) show clear evidence of such K concentration at alteration fronts in Site U1365 basalt (D'Hondt et al., 2011, 2013). However of the three radionuclides, K contributes the least to total H_2 production because it only produces β and γ radiation when it decays. Using an average concentration for the SPG samples, K contributes 13% to total production at the basalt–water interface. Uranium and Th decay series account for 65 and 22% of the H_2 produced, respectively. Of our SPG basalt samples, K decay dominates H_2 production in only one sample (U1365E-3R-4W 25/30), where it accounts for 48% of the total H_2 yield.

The U decay series is overwhelmingly the largest contributor to H_2 production. Uranium enrichment often occurs in carbonate veins and at oxidation/reduction fronts during basalt alteration (Alt et al., 1992; Farr et al., 2001; Kelley et al., 2003). Twenty-seven of our SPG samples exhibit U/Th ratios that indicate U enrichment, excluding the sample with Th below the detection limit. In these twenty-seven samples, U enrichment ranges up to a 10X increase, with an average U/Th ratio indicating a 2X increase in U. Our samples bracket the typical enrichment value of 5X for altered basalt when compared to unaltered glass (Kelley et al., 2003). The samples with excess U increase H_2 yields on average by 29 $\pm$ 6%, 60 $\pm$ 3%, and 23 $\pm$ 10% at Sites U1365, U1367, and U1368, respectively. Therefore, the variation in radiolytic H_2 production rates that we calculate for bulk basalt likely accounts for much of the variation that would be seen in the oceanic crust.

As shown by the variety of visual alteration categories and the wide range of U/Th ratios exhibited by our SPG samples, the kind, and extent of alteration vary greatly on a variety of spatial scales. The most intensely altered samples are likely those with most U enrichment; however that does not mean that they have the highest radionuclide concentrations. This can make links between alteration extent and radiolytic yields difficult to clearly identify. Separation of samples by alteration category or by U/Th ratios does not result in obvious patterns, suggesting that there is no simple relationship between radiolytic rates and alteration. Visual inspection of the samples is not enough to fully assess the impact of alteration on radiolytic rates. For example, some of the SPG samples with brown and dark gray alteration halos have U/Th ratios that indicate no U enrichment. Other studies, such as the SPG study of Zhang and Smith-Duque (2014) and the western Pacific study of Kelley et al. (2003) have shown U enrichment especially within these zones. Much closer analysis of mineral and chemical composition would be needed to fully assess effects of alteration on radionuclide concentrations and radiolytic H_2 production rates of SPG basalt.

The rates we calculate are based on bulk-rock analyses and may underestimate radiolytic H_2 production associated with specific alteration phases. For localized mineral phases with high U, Th, or K concentrations rates will be much higher. Staudigel et al. (2008) suggest that weathering of basaltic glass is the dominant process of chemical exchange between basalt and seawater. Alteration of basaltic glass produces palagonite (Staudigel et al., 2008; Türke et al., 2015), a very porous mineral ($\sim$14–38 wt% H_2O; Pauly et al., 2011) with high concentrations of radioactive elements (Türke et al., 2015).

Palagonite is of special interest for studies of radiolytic H_2 production in subseafloor basalt because its porous nature and its enriched radionuclide concentrations must result in high radiolytic rates (Türke et al., 2015). Türke et al. (2015) calculated H_2 production rates within palagonite rims and show that H_2 can accumulate to minimum concentrations needed for hydrogentrophy at North Pond (on the western flank of the Mid-Atlantic Ridge). For their calculations, Türke et al. (2015) used a porosity model based on protocols from Lin et al. (2005a) and Blair et al. (2007). Because palagonite is so porous, these models' assumptions of fine grain size and homogeneously distributed porosity are broadly relevant for palagonite calculations. However, these models' assumption that all of the radiation interacts with water is not appropriate for relatively thin palagonite occurrences. Türke et al. (2015) note this issue and calculate yields assuming 1% efficiency. However,

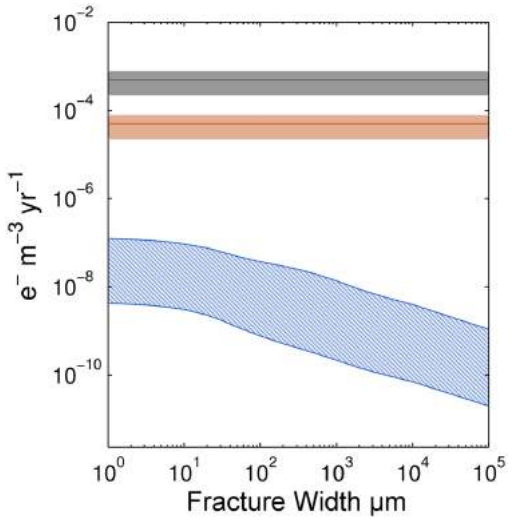

FIGURE 5 | Comparison of electron transfer rates supportable by Fe oxidation and radiolytic H_2 production. Ranges of electron (e^-) transfer rates due to Fe oxidation are shown for basalt of two different ages, 1 and 10 Ma shown by the gray and orange shading, respectively. The blue-hatched region indicates the range of electron transfer supportable by radiolytic H_2 production.

there is no explicit way to calculate the actual efficiency using their model. The average H_2 production rates calculated by Türke et al. (2015) are about four times higher than average SPG rates in microfractures. Consequently, palagonite and other similarly porous alteration minerals may significantly increase radiolytic H_2 production relative to neighboring basalt.

Calculating the global rate of radiolytic H_2 production in oceanic basement requires firm constraints on the distribution of fracture widths in the basement, mean concentrations of U, Th and K in the basalt, and porosity and abundance of alteration minerals in the basement. Mapping the horizontal and vertical distribution of radiolytic H_2 production rates in subseafloor basalt requires information beyond the mean, including knowledge of horizontal and vertical variation in fracture width and number, radionuclide (U, Th, and K) concentrations, and porosity of alteration phases. Spatial variation in radionuclide concentrations is especially difficult to constrain, because it in turn depends on both (i) initial composition (which can vary from region to region, and even between successive eruptive events at the same location; Bergmanis et al., 2007) and (ii) alteration history (including the extent and kinds of secondary mineralization; Alt, 2004).

Comparison of Electron Donor Fluxes from Radiolytic H_2 Production and Iron Oxidation

To assess the potential importance of radiolytic H_2 production for microbial communities in subseafloor basalt, we compare our calculated radiolytic H_2 production rates to iron oxidation rates calculated from Fe(III)/ΣFe ratios compiled by Bach and Edwards (2003; **Figure 5**).

To compare these rates, we convert them to electron transfer rates per unit volume. For Fe oxidation, one electron is transferred during oxidation of Fe(II) to Fe(III); for H_2, two electrons are transferred for each H_2 molecule produced. For direct comparison, we assume a cubic meter of basalt with 10% porosity, density of 2950 kg/m^3 and 8 wt.% Fe (Bach and Edwards, 2003). We use an initial Fe(III)/ΣFe ratio of 0.15 ± 0.05 for fresh basalt and a final ratio of 0.45 ± 0.15 for basalt greater than 10 Ma (Bach and Edwards, 2003). These values include the variation associated with the average Fe(III)/ΣFe ratios at

TABLE 1 | Numbers of cells that might be supported by radiolytic H_2 production in SPG basalt.

	Least radioactive SPG basalt sample		Most radioactive SPG basalt sample	
Fracture Width (µm)	e^- flux per area of fracture surface (mol e^-/cm^2/yr)	Number of cells that might be supported by this flux	e^- flux per area of fracture surface (mol e^-/cm^2/yr)	Number of cells that might be supported by this flux
10^0	7.65E-19	1.1E-04 ± 2E-05 to 1.8E-02 ± 1E-02	6.25E-17	9.2E-03 ± 2E-03 to 1.5E+00 ± 9E-01
10^1	6.50E-18	9.6E-04 ± 2E-04 to 1.6E-01 ± 1E-01	4.72E-16	7.0E-02 ± 1E-02 to 1.1E+01 ± 7E+00
10^2	3.82E-17	5.6E-03 ± 1E-03 to 9.2E-01 ± 6E-01	1.86E-15	2.8E-01 ± 5E-02 to 4.5E+01 ± 3E+01
10^3	1.08E-16	1.6E-02 ± 3E-03 to 2.6E+00 ± 2E+00	6.80E-15	1.0E+00 ± 2E-01 to 1.6E+02 ± 1E+02
10^4	3.53E-16	5.2E-02 ± 1E-02 to 8.5E+00 ± 5E+00	1.99E-14	2.9E+00 ± 5E-01 to 4.8E+02 ± 3E+02
10^5	9.90E-16	1.5E-01 ± 3E-02 to 2.4E+01 ± 1E+01	5.45E-14	8.1E+00 ± 1E+00 to 1.3E+03 ± 8E+02
10^6	1.16E-15	1.7E-01 ± 3E-02 to 2.8E+01 ± 2E+01	6.35E-14	9.4E+00 ± 2E+00 to 1.5E+03 ± 1E+03

Electron fluxes are calculated from radiolytic H_2 production rates for 1 sq. cm of basalt for the least radioactive and most radioactive SPG basalt samples. The ranges of cell numbers that might be supported are calculated from minimum and maximum O_2 consumption rates that are distinguishable from zero within subseafloor SPG sediment (D'Hondt et al., 2015).

their respective basalt ages. Given these ratios, we calculate a mean oxidation rate of 0.19 ± 0.1 mol Fe oxidized kg basalt^{-1} Myr^{-1} for the first 10 Myr of the basalt's existence. Considerable variability in the Fe(III)/ΣFe ratios given by Bach and Edwards (2003) indicates that different regions within the basement have higher, or lower, Fe oxidation rates. For H_2 calculations, we assume that each unique fracture width makes up the 10% porosity in the basalt. For example, there are one thousand 100 μm fractures or one 10 cm fracture in our calculations to account for the correct water-rock ratio.

Given these assumptions, for oceanic crust younger than 10 Ma, calculated electron transfer rates (mol e^- per m^3 rock per year) due to Fe oxidation are about three orders of magnitude higher than electron transfer rates associated with radiolytic H_2 production (**Figure 5**). However, after circa 10 Ma, mean Fe(III)/ΣFe ratios appear to plateau, suggesting that all available Fe has been oxidized (Bach and Edwards, 2003). This means that Fe oxidation rates in basalt older than circa 10 Ma are near zero. In this older basalt, radiolytic H_2 may be more important than Fe(II) as an electron donor for microbial communities.

This change from Fe(II) to radiolytic H_2 as the predominant electron donor is consistent with the palagonite-based conclusion of Türke et al. (2015). In young ridge flanks, Fe oxidation is a main source of energy for microorganisms due to interaction of seawater with fresh basalt in fractures. However, in older crust, after permeability decreases and access to fresh basalt is prevented by alteration phases, the availability of Fe decreases and the dominant electron donor may be radiolytic H_2 (Türke et al., 2015).

Numbers of Cells that Might be Supported by Radiolytic H_2 Production in Fractures

To estimate how many cells might be supported by oxidation of radiolytic H_2, we divide the radiolytic H_2 flux for different fracture widths by the net per-cell oxygen reduction rates in SPG sediment (**Table 1**). As with our comparison to Fe(II) oxidation, we convert both radiolytic H_2 production rates and oxygen reduction rates to electron transfer rates. Net per-cell oxygen reduction rates in subseafloor SPG sediment range between $4.2 \times 10^{-17} \pm 2.6 \times 10^{-17}$ mol e^- cell^{-1} yr^{-1} and $6.8 \times 10^{-15} \pm 1.3 \times 10^{-15}$ mol e^- cell^{-1} yr^{-1} (D'Hondt et al., 2015). Using these maximum and minimum oxygen reduction rates and the radiolytic electron fluxes (mol e^- cm^{-2} yr^{-1}) for discrete fracture widths in our least and most radioactive basalt samples, we can estimate the number of cells that might be supported by H_2 production. If the cells respire at the same rate as the aerobic communities in subseafloor SPG sediment, radiolytic H_2 production in the volume of water adjacent to a square cm of the least radioactive SPG basalt might support up to 30 cells. H_2 production in the same volume of water adjacent to a square cm of the most radioactive SPG basalt might support up to 1500 cells.

CONCLUSION

The extent of life in oceanic crust must depend in large part on the availability of electron donors and acceptors. Water radiolysis produces H_2, which can be metabolized by microorganisms. Microfractures and local maxima in radionuclide concentrations serve as hotspots for radiolytic H_2 production and may also act as hotspots for microbial life. Differences in initial melt composition and low-temperature alteration by seawater affect concentrations and distributions of U, Th, and K within the basement, and consequently also change radiolytic H_2 production rates. Our calculations suggest that in young (less than 10 Ma) basalt, oxidizable Fe(II) is a far more abundant electron donor than radiolytic H_2. However, in older seafloor, where little Fe is accessible to oxidants in the formation water, radiolytic H_2 may be the dominant electron donor. Radiolytic H_2 in the water adjacent to a square cm of SPG basaltic fracture may support up to 10^3 cells if the cells respire at the same rate as net per-cell oxygen reduction in subseafloor SPG sediment.

AUTHOR CONTRIBUTIONS

All authors listed, have made substantial, direct, and intellectual contribution to the work, and approved it for publication.

ACKNOWLEDGMENTS

We thank the reviewers for helpful comments. We thank the National Aeronautics and Space Administration (grant NNX12AD65G) and the U.S. National Science Foundation (grant NSF-OCE-1130735 to SD and NSF OCE1130531 to RM, and through the Center for Dark Energy Biosphere Investigations; grant NSF-OCE-0939564 to SD) for funding this study. Portions of this material are based upon work supported while RM was serving at the National Science Foundation. This is C-DEBI publication number 287.

SUPPLEMENTARY MATERIAL

The Supplementary Material for this article can be found online at: http://journal.frontiersin.org/article/10.3389/fmicb.2016.00076

REFERENCES

Alt, J. C. (2004). "Alteration of the upper oceanic crust: mineralogy, chemistry, and processes," in *Hydrogeology of the Oceanic Lithosphere*, eds E. E. Davis and H. Elderfield (New York, NY: Cambridge University Press), 497–595.

Alt, J. C., and Teagle, D. A. (2003). Hydrothermal alteration of upper oceanic crust formed at a fast-spreading ridge: mineral, chemical, and isotopic evidence from ODP Site 801. *Chem. Geol.* 201, 191–211. doi: 10.1016/S0009-2541(03)00201-8

Alt, J. C., France-Lanord, C., Floyd, P. A., Castillo, P., and Galy, A. (1992). "Low-temperature hydrothermal alteration of Jurassic ocean crust, Site 801,"

in *Proceeding of the Ocean Drilling Program Scientific Results*, Vol. 129, eds R. L. Larson and Y. Lancelot (College Station, TX: Ocean Drilling Program), 415–427.

Bach, W., and Edwards, K. (2003). Iron and sulfide oxidation within the basaltic ocean crust: implications for chemolithoautotrophic microbial biomass production. *Geochim. Cosmochim. Acta* 67, 3871–3887. doi: 10.1016/S0016-7037(03)00304-1

Bartetzko, A. (2005). Effect of hydrothermal ridge flank alteration on the in situ physical properties of uppermost oceanic crust. *J. Geophys. Res. Solid Earth* 110:B06203. doi: 10.1029/2004JB003228

Berger, M. J., Coursey, J. S., Zucker, M. A., and Chang, J. (2005). *ESTAR, PSTAR, and ASTAR: Computer Programs for Calculating Stopping-Power and Range Tables for Electrons, Protons, and Helium Ions (version 1.2.3)*. Gaithersburg, MD: National Institute of Standards and Technology. Available at: http://physics.nist.gov/Star [accessed on December 30, 2015].

Bergmanis, E. C., Sinton, J., and Rubin, K. H. (2007). Recent eruptive history and magma reservoir dynamics on the southern east pacific rise at 17°30′S. *Geochem. Geophys. Geosyst.* 8:Q12O06. doi: 10.1029/2007GC001742

Blair, C. C., D'Hondt, S., Spivack, A. J., and Kingsley, R. H. (2007). Radiolytic hydrogen and microbial respiration in subsurface sediments. *Astrobiology* 7, 951–970. doi: 10.1089/ast.2007.0150

Chapelle, F. H., O'Neill, K., Bradley, P. M., Methe, B. A., Ciufo, S. A., Knobel, L. L., et al. (2002). A hydrogen-based subsurface microbial community dominated by methanogens. *Nature* 415, 312–314. doi: 10.1038/415312a

Cowen, J. P., Giovannoni, S. J., Kenig, F., Johnson, H. P., Butterfield, D., Rappé, M. S., et al. (2003). Fluids from aging ocean crust that support microbial life. *Science* 299, 120–123. doi: 10.1126/science.1075653

Debierne, A. (1914). Recherches sur les gaz produits par les substances radioactives. Décomposition de l'eau. *Ann. Phys. (Paris)* 2, 97–127.

D'Hondt, S., F. Inagaki, C., Zarikian, A., and the IODP Expedition. 329 Scientists (2013). IODP Expedition 329: life and habitability beneath the seafloor of the South Pacific Gyre. *Sci. Drill.* 15, 4–10.

D'Hondt, S., Inagaki, F., Alvarez Zarikian, C., Abrams, L. J., Dubois, N., Engelhardt, T., et al. (2015). Presence of oxygen and aerobic communities from seafloor to basement in deep-sea sediment. *Nat. Geosci.* 8, 299–304. doi: 10.1038/NGEO2387

D'Hondt, S. F., Inagaki, C. A. Zarikian, A., and the Expedition Scientists (2011). "South Pacific Gyre Subseafloor Life," in *Proceeding of the Ocean Drilling Program, 329*, Tokyo: Integrated Ocean Drilling Program Management International, Inc.

D'Hondt, S., Jørgensen, B. B., Miller, D. J., Batzke, A., Blake, R., Cragg, B. A., et al. (2004). Distributions of microbial activities in deep subseafloor sediments. *Science* 306, 2216–2221. doi: 10.1126/science.1101155

D'Hondt, S., Spivack, A. J., Pockalny, R., Ferdelman, T. G., Fischer, J. P., Kallmeyer, J., et al. (2009). Subseafloor sedimentary life in the South Pacific Gyre. *Proc. Natl. Acad. Sci. U.S.A.* 106, 11651–11656. doi: 10.1073/pnas.0811793106

Dunlea, A. G., Murray, R. W., Sauvage, J., Pockalny, R. A., Spivack, A. J., Harris, R. N., et al. (2015a). Cobalt-based age models of pelagic clay in the South Pacific Gyre. *Geochem. Geophys. Geosyst.* 16, 2694–2710. doi: 10.1002/2015GC005892

Dunlea, A. G., Murray, R. W., Sauvage, J., Spivack, A. J., Harris, R. N., and D'Hondt, S. (2015b). Dust, volcanic ash, and the evolution of the South Pacific Gyre through the Cenozoic. *Paleoceanography* 30, 1078–1099. doi: 10.1002/2015PA002829

Dzaugis, M. E., Spivack, A. J., and D'Hondt, S. (2015). A quantitative model of water radiolysis and chemical production rates near radionuclide-containing solids. *Radiat. Phys. Chem.* 115, 127–134. doi: 10.1016/j.radphyschem.2015.06.011

Edwards, K. J., Bach, W., and McCollom, T. M. (2005). Geomicrobiology in oceanography: microbe–mineral interactions at and below the seafloor. *Trends Microbiol.* 13, 449–456. doi: 10.1016/j.tim.2005.07.005

Edwards, K., Fisher, A., and Wheat, C. (2012). The deep subsurface biosphere in igneous ocean crust: frontier habitats for microbiological exploration. *Front. Microbiol.* 3:8. doi: 10.3389/fmicb.2012.00008

Edwards, K. J., Wheat, C. G., and Sylvan, J. B. (2011). Under the sea: microbial life in volcanic oceanic crust. *Nat. Rev. Microbiol.* 9, 703–712. doi: 10.1038/nrmicro2647

Expedition 329 Scientists (2011a). "Site U1365," in *Proceeding of the Integrated Ocean Drilling Program Management International, 329*, eds S. D'Hondt, F. Inagaki, C. A. Alvarez Zarikian, and the Expedition 329 Scientists (Tokyo: Integrated Ocean Drilling Program Management International, Inc.).

Expedition 329 Scientists (2011b). "Site U1367," in *Proceeding of the Integrated Ocean Drilling Program Management International*, 329, eds S. D'Hondt, F. Inagaki, C. A. Alvarez Zarikian, and the Expedition 329 Scientists (Tokyo: Integrated Ocean Drilling Program Management International, Inc.).

Expedition 329 Scientists (2011c). "Site U1368," in *Proceeding of the Integrated Ocean Drilling Program Management International*, 329, eds S. D'Hondt, F. Inagaki, C. A. Alvarez Zarikian, and the Expedition 329 Scientists (Tokyo: Integrated Ocean Drilling Program Management International, Inc.).

Fang, J., and Zhang, L. (2011). Exploring the deep biosphere. *Sci. China Earth Sci.* 54, 157–165. doi: 10.1007/s11430-010-4148-z

Farr, L. C., Plank, T., Kelley, K., and Alt, J. C. (2001). U mineral hosts and enrichment processes in altered oceanic crust. *AGU Fall Meet. Abstr.* 1:0926.

Fisher, A. T. (1998). Permeability within basaltic oceanic crust. *Rev. Geophys.* 36, 143–182. doi: 10.1029/97RG02916

Fisk, M. R., Giovannoni, S. J., and Thorseth, I. H. (1998). Alteration of oceanic volcanic glass: textural evidence of microbial activity. *Science* 281, 978–980. doi: 10.1126/science.281.5379.978

Gale, A., Dalton, C. A., Langmuir, C. H., Su, Y., and Schilling, J. G. (2013). The mean composition of ocean ridge basalts. *Geochem. Geophys. Geosyst.* 14, 489–518. doi: 10.1029/2012GC004334

Hacker, C. (1997). *Radiation Decay (RadDecay) Code, Version 4*. Queensland, QLD: Engineering and Applied Science, Griffith University.

Hubbell, J. H., and Seltzer, S. M. (2004). *Tables of X-Ray Mass Attenuation Coefficients and Mass Energy-Absorption Coefficients (version 1.4)*. Gaithersburg, MD: National Institute of Standards and Technology. Available at: http://physics.nist.gov/xaamdi [accessed on January 13, 2016].

Jochum, K. P., Nohl, U., Herwig, K., Lammel, E., Stoll, B., and Hofmann, A. W. (2005). GeoReM: a new geochemical database for reference materials and isotopic standards. *Geostand. Geoanalyt. Res.* 29, 333–338. doi: 10.1111/j.1751-908X.2005.tb00904.x

Johnson, H. P., and Pruis, M. J. (2003). Fluxes of fluid and heat from the oceanic crustal reservoir. *Earth Planet. Sci. Lett.* 216, 565–574. doi: 10.1016/S0012-821X(03)00545-4

Jungbluth, S. P., Grote, J., Lin, H.-T., Cowen, J. P., and Rappé, M. S. (2013). Microbial diversity within basement fluids of the sediment-buried juan de fuca ridge flank. *ISME* 7, 161–172. doi: 10.1038/ismej.2012.73

Kelley, D. S., Karson, J. A., Blackman, D. K., Früh-Green, G. L., Butterfield, D. A., Lilley, M. D., et al. (2001). An off-axis hydrothermal vent field near the mid-atlantic ridge at 30° N. *Nature* 412, 145–149. doi: 10.1038/35084000

Kelley, K. A., Plank, T., Farr, L., Ludden, J., and Staudigel, H. (2005). Subduction Cycling of U, Th, and Pb. *Earth Planet. Sci. Lett.* 234, 369–383. doi: 10.1016/j.epsl.2005.03.005

Kelley, K. A., Plank, T., Ludden, J., and Staudigel, H. (2003). Composition of altered oceanic crust at ODP Sites 801 and 1149. *Geochem. Geophys. Geosyst.* 4, 1–21. doi: 10.1029/2002GC000435

Kohan, L. M., Sanguanmith, S., Meesungnoen, J., Causey, P., Stuart, C. R., and Jay-Gerin, J. (2013). Self-Radiolysis of Tritiated Water. 1. A comparison of the effects of 60Co Γ-Rays and Tritium β-particles on water and aqueous solutions at room temperature. *RSC Adv.* 3:19282. doi: 10.1039/c3ra42984a

LaTourrette, T. Z., Kennedy, A. K., and Wasserburg, G. J. (1993). Thorium-uranium fractionation by garnet: evidence for a deep source and rapid rise of oceanic basalts. *Science* 261, 739–742. doi: 10.1126/science.261.5122.739

Le Caër, S. (2011). Water radiolysis: influence of oxide surfaces on H2 production under ionizing radiation. *Water* 3, 235–253. doi: 10.3390/w3010235

Lever, M. A., Rouxel, O., Alt, J. C., Shimizu, N., Ono, S., Coggon, R. M., et al. (2013). Evidence for microbial carbon and sulfur cycling in deeply buried ridge flank basalt. *Science* 339, 1305–1308. doi: 10.1126/science.1229240

Lin, L.-H., Slater, G. F., Lollar, B. S., Lacrampe-Couloume, G., and Onstott, T. C. (2005a). The yield and isotopic composition of radiolytic H_2, a potential energy source for the deep subsurface biosphere. *Geochim. Cosmochim. Acta* 69, 893–903. doi: 10.1016/j.gca.2004.07.032

Lin, L.-H., Hall, J., Lippmann-Pipke, J., Ward, J. A., Sherwood Lollar, B., DeFlaun, M., et al. (2005b). Radiolytic H_2 in continental crust: nuclear power for deep subsurface microbial communities. *Geochem. Geophys. Geosyst.* 6, 7. doi: 10.1029/2004GC000907

Lollar, B. S., Onstott, T. C., Lacrampe-Couloume, G., and Ballentine, C. J. (2014). The contribution of the Precambrian continental lithosphere to global H_2 production. *Nature* 516, 379–382. doi: 10.1038/nature 14017

Madigan, M. T., Martinko, J. M., and Parker, J. (2000). *Brock Biology of Microorganisms*. Carbondale, IL: Southern Illinois University Carbondale.

Mustaree, S., Meesungnoen, J., Butarbutar, S. L., Causey, P., Stuart, C. R., and Jay-Gerin, J. P. (2014). Self-radiolysis of tritiated water. 3. The OH scavenging effect of bromide ions on the yield of H_2O_2 in the radiolysis of water by 60Co γ-rays and tritium β-particles at room temperature. *RSC Adv.* 4, 43572–43581. doi: 10.1039/C4RA06707J

Orcutt, B. N., Wheat, C. G., Rouxel, O., Hulme, S., Edwards, K. J., and Bach, W. (2013). Oxygen consumption rates in subseafloor basaltic crust derived from a reaction transport model. *Nat. Commun.* 4:2539. doi: 10.1038/ncomms3539

Pastina, B., and LaVerne, J. A. (2001). Effect of molecular hydrogen on hydrogen peroxide in water radiolysis. *J. Phys. Chem. A* 105, 9316–9322. doi: 10.1021/jp012245j

Pauly, B. D., Schiffman, P., Zierenberg, R. A., and Clague, D. A. (2011). Environmental and chemical controls on palagonitization. *Geochem. Geophys. Geosyst.* 12, 1–26. doi: 10.1029/2011GC003639

Pedersen, K. (1993). The deep subterranean biosphere. *Earth Sci. Rev.* 34, 243–260. doi: 10.1016/0012-8252(93)90058-F

Spinks, J. W. T., and Woods, R. J. (1990). *An Introduction to Radiation Chemistry*, 3rd Edn. New York, NY: John Wiley and Sons Inc.

Staudigel, H., Furnes, H., McLoughlin, N., Banerjee, N. R., Connell, L. B., and Templeton, A. (2008). 3.5 billion years of glass bioalteration: volcanic rocks as a basis for microbial life? *Earth Sci. Rev.* 89, 156–176. doi: 10.1016/j.earscirev.2008.04.005

Staudigel, H., Plank, T., White, B., and Schmincke, H. U. (1996). "Geochemical fluxes during seafloor alteration of the basaltic upper oceanic crust: DSDP Sites 417 and 418," in *Subduction Top to Bottom,* eds G. E. Bebout, D. W. Scholl, S. H. Kirby, and J. P. Platt (Washington, DC: American Geophysical Union), 19–38.

Stevens, T. O., and McKinley, J. P. (1995). Lithoautotrophic microbial ecosystems in deep basalt aquifers. *Science* 270, 450–454. doi: 10.1126/science.270.5235.450

Teagle, D. A., Alt, J. C., Bach, W., and Erzinger, J. (1996). "Alteration of upper ocean crust in a ridge-flank hydrothermal upflow zone: mineral, chemical, and isotopic constraints from Hole 896-A," in *Proceedings of the Ocean Drilling Program, Scientific Results*, Vol. 148 (Texas, TX: Ocean Drilling Program, College Station), 119–150.

Türke, A., Nakamura, K., and Bach, W. (2015). Palagonitization of basalt glass in the flanks of mid-ocean ridges: implications for the bioenergetics of oceanic intracrustal ecosystems. *Astrobiology* 15, 793–803. doi: 10.1089/ast. 2014.1255

Wang, K. (2004). "Applying fundamental principles and mathematical models to understand processes and estimate parameters," in *Hydrogeology of the Oceanic Lithosphere*, eds E. E. Davis and H. Elderfield (New York, NY: Cambridge University Press), 497–595.

Zhang, G.-L., Chen, L.-H., and Li, S.-Z. (2013). Mantle dynamics and generation of a geochemical mantle boundary along the east pacific rise – pacific/antarctic ridge. *Earth Planet. Sci. Lett.* 383, 153–163. doi: 10.1016/j.epsl.2013.09.045

Zhang, G.-L., and Smith-Duque, C. (2014). Seafloor basalt alteration and chemical change in the ultra thinly sedimented South Pacific. *Geochem. Geophys. Geosyst.* 15, 3066–3080. doi: 10.1002/2013GC005141

Conflict of Interest Statement: The authors declare that the research was conducted in the absence of any commercial or financial relationships that could be construed as a potential conflict of interest.

frontiers in Microbiology

ORIGINAL RESEARCH
published: 31 March 2016
doi: 10.3389/fmicb.2016.00396

Temperature and Redox Effect on Mineral Colonization in Juan de Fuca Ridge Flank Subsurface Crustal Fluids

Jean-Paul M. Baquiran[1†], Gustavo A. Ramírez[1†], Amanda G. Haddad[2], Brandy M. Toner[3], Samuel Hulme[4], Charles G. Wheat[5], Katrina J. Edwards[1,2‡] and Beth N. Orcutt[6]*

[1] Department of Biological Sciences, University of Southern California, Los Angeles, CA, USA, [2] Department of Earth Sciences, University of Southern California, Los Angeles, CA, USA, [3] Department of Soil, Water and Climate, University of Minnesota, St. Paul, MN, USA, [4] Moss Landing Marine Laboratories, Moss Landing, CA, USA, [5] School of Fisheries and Ocean Sciences, University of Alaska Fairbanks, Fairbanks, AK, USA, [6] Bigelow Laboratory for Ocean Sciences, East Boothbay, ME, USA

OPEN ACCESS

Edited by:
Michael Rappe,
University of Hawaii at Manoa, USA

Reviewed by:
Craig Lee Moyer,
Western Washington University, USA
Bert Engelen,
University of Oldenburg, Germany

***Correspondence:**
Beth N. Orcutt
borcutt@bigelow.org

[†] These authors contributed equally to this work and should be considered co-first-authors.
[‡] Deceased.

Specialty section:
This article was submitted to Extreme Microbiology, a section of the journal Frontiers in Microbiology

Received: *08 September 2015*
Accepted: *14 March 2016*
Published: *31 March 2016*

Citation:
Baquiran J-PM, Ramírez GA, Haddad AG, Toner BM, Hulme S, Wheat CG, Edwards KJ and Orcutt BN (2016) Temperature and Redox Effect on Mineral Colonization in Juan de Fuca Ridge Flank Subsurface Crustal Fluids. Front. Microbiol. 7:396. doi: 10.3389/fmicb.2016.00396

To examine microbe-mineral interactions in subsurface oceanic crust, we evaluated microbial colonization on crustal minerals that were incubated in borehole fluids for 1 year at the seafloor wellhead of a crustal borehole observatory (IODP Hole U1301A, Juan de Fuca Ridge flank) as compared to an experiment that was not exposed to subsurface crustal fluids (at nearby IODP Hole U1301B). In comparison to previous studies at these same sites, this approach allowed assessment of the effects of temperature, fluid chemistry, and/or mineralogy on colonization patterns of different mineral substrates, and an opportunity to verify the approach of deploying colonization experiments at an observatory wellhead at the seafloor instead of within the borehole. The Hole U1301B deployment did not have biofilm growth, based on microscopy and DNA extraction, thereby confirming the integrity of the colonization design against bottom seawater intrusion. In contrast, the Hole U1301A deployment supported biofilms dominated by Epsilonproteobacteria (43.5% of 370 16S rRNA gene clone sequences) and Gammaproteobacteria (29.3%). Sequence analysis revealed overlap in microbial communities between different minerals incubated at the Hole U1301A wellhead, indicating that mineralogy did not separate biofilm structure within the 1-year colonization experiment. Differences in the Hole U1301A wellhead biofilm community composition relative to previous studies from within the borehole using similar mineral substrates suggest that temperature and the diffusion of dissolved oxygen through plastic components influenced the mineral colonization experiments positioned at the wellhead. This highlights the capacity of low abundance crustal fluid taxa to rapidly establish communities on diverse mineral substrates under changing environmental conditions such as from temperature and oxygen.

Keywords: deep biosphere, geomicrobiology, oceanic crust, microbe-mineral interactions

INTRODUCTION

The deep subsurface biosphere represents a vast and relatively unknown environment. While this deep biosphere is estimated to comprise a significant fraction of the Earth's total biomass (Whitman et al., 1998; Kallmeyer et al., 2012), most investigations have focused on the marine sedimentary realm (Parkes et al., 2000; D'hondt et al., 2004; Biddle et al., 2006; Jørgensen and Boetius, 2007; Teske and Sørensen, 2008; Lever et al., 2010). Our understanding of microbial life within igneous oceanic crust, a potentially far larger habitat than marine sediment (Orcutt et al., 2011a,b), is slowly growing. So far, results indicate that the deep subsurface rock-hosted biosphere is different from overlying sediment in terms of the abundance and distribution of biological taxa (Thorseth et al., 2001; Cowen et al., 2003; Lysnes et al., 2004; Mason et al., 2010; Edwards et al., 2011a; Orcutt et al., 2011a; Jungbluth et al., 2013). Fluids within this highly porous and permeable crust are exchanged via advection with the overlying oceans, resulting in a flux of chemicals to and from the oceans that are significant to global geochemical budgets for some elements (Elderfield and Schultz, 1996; Wheat et al., 2003b). Such chemical exchange reactions are the foundation for chemolithotrophic microbial life (Bach and Edwards, 2003); however, factors controlling substrate colonization, bioalteration, microbial proliferation, and ecosystem establishment in crustal aquifer environments are largely unknown (Edwards et al., 2012b).

A major challenge when examining subsurface crustal microorganisms is the collection of pristine samples during drilling operations (Lever et al., 2006; Santelli et al., 2010), although there are recent examples of the possibility to detect *in situ* microbial communities with this approach (Mason et al., 2009; Lever, 2013). One method to overcome the challenge of sample recovery through drilling is through the use of CORKs (Circulation Obviation Retrofit Kits), which are subsurface observatory systems in which a borehole is cased after drilling and the hydrologic reservoir is allowed to recover to pre-drilling conditions (Davis et al., 1992; Becker and Davis, 2005; Fisher et al., 2011; Wheat et al., 2011; Edwards et al., 2012a). Long-term sampling and experimentation with CORKs is possible through a combination of fluid sampling at the seafloor wellhead, which samples fluids that originate from depth within the oceanic crust, and by the deployment of experiments within the borehole (Fisher et al., 2005; Wheat et al., 2010; Orcutt et al., 2011a; Cowen et al., 2012). Thus, CORKs offer an opportunity to access the crustal subsurface to collect fluid samples and conduct experiments.

One recent type of deep biosphere experiment enabled by CORKs is mineral colonization experiments, where sterile minerals are incubated within CORKs to examine microbe-mineral interactions. For example, flow-through osmotic colonization systems (FLOCS) enable examination of microbe-mineral interactions by slowly and continuously pumping crustal fluids over mineral substrates housed in an *in situ* growth chamber (Jannasch et al., 2004; Orcutt et al., 2010; Wheat et al., 2010). The concept of the FLOCS microbial colonization was established by incubating different minerals with fluids from a hydrothermal vent (Orcutt et al., 2010), and validation of the downhole colonization concept was achieved during a 4-year *in situ* incubation within CORKs (Orcutt et al., 2011a). Similar approaches have been used by other investigators in ocean crust (Smith et al., 2011) and in the terrestrial deep biosphere (Pedersen and Ekendahl, 1992; Pedersen et al., 2008).

Initial CORK-based investigations, focused on a CORK network on the eastern flank of the Juan de Fuca Ridge (**Figure 1**), indicated that microbial communities hosted by the hydrothermal basaltic subsurface are distinct from other deep-sea environments, such as hydrothermal plumes, deep seawater, or seafloor-exposed basalts (Edwards et al., 2011b; Orcutt et al., 2011a,b). Moreover, microbial communities that colonize minerals are dynamic in structure and establish with relative rapidity (Orcutt et al., 2011a). Mineral composition seems to play a role in determining surface-attached microbial community structure (Orcutt et al., 2011a; Smith et al., 2011). Minerals incubated at depth within these crustal fluids were subsequently shown to enrich for microbial groups capable of iron oxidation (Smith et al., 2011). Crustal fluids collected from these CORK observatories host an order of magnitude lower cell density relative to surrounding deep seawater (Jungbluth et al., 2013), and microbial sulfate reduction coupled to organic matter oxidation is possible in these fluids (Robador et al., 2014).

The first microbe-mineral interaction studies from the Juan de Fuca Ridge flank subsurface, from experiments conducted at depth within CORKs at Integrated Ocean Drilling Program (IODP) Holes 1026B and U1301A from 2004 to 2008 (Orcutt et al., 2011a; Smith et al., 2011), offered initial insight into the microbial colonization of minerals incubated subseafloor in crustal aquifer fluids, but they were relatively limited in sample volume for deeper examination of patterns. Incubation of mineral colonization experiments at depth within a borehole has some limitations, including size restrictions to fit within the CORK, and the requirement to open the CORK to remove the instrument string at the end of the experiment, which can perturb the hydrologic system (Wheat et al., 2011). Thus, mineral colonization experiments at the CORK wellhead, where incubations are exposed to fluids rising to the seafloor from depth in the crust, were established as an alternative to the downhole incubation concept (Wheat et al., 2011; Orcutt and Edwards, 2014). While the wellhead incubation approach offers easier access for exchanging experiments and minimizes restrictions for experimental size, it was unknown if incubation at seafloor temperatures or other factors would influence the development of mineral microbial communities when compared to similar experiments deployed within a borehole.

Here, we report the first results from CORK wellhead microbial colonization experiments, which allow examination of how wellhead conditions and/or mineral compositions influence

Abbreviations: CORK, Circulation Obviation Retrofit Kit (a borehole observatory); FLOCS, Flow-through Osmo Colonization System (a flow-through chamber for examining microbe-mineral interactions, where fluid is pulled through by the action of an attached OsmoSampler osmotic pump); IODP, Integrated Ocean Drilling Program; mbsf, meters below seafloor.

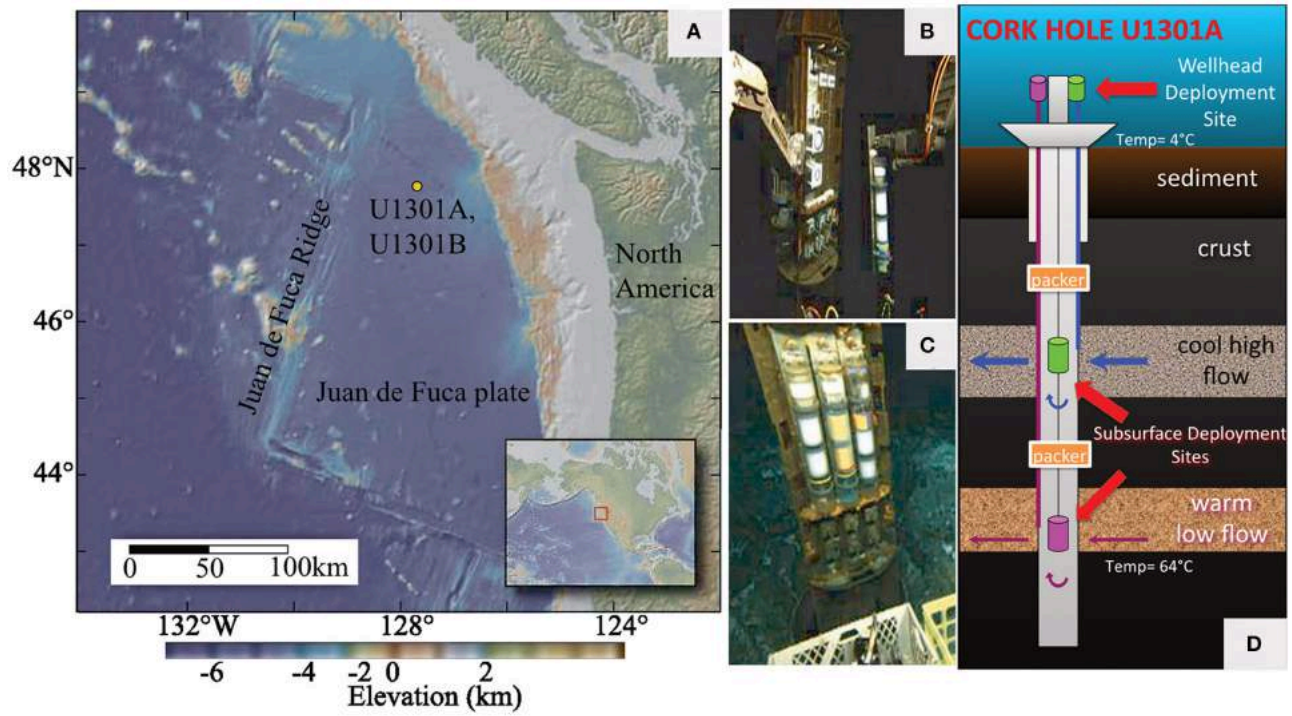

FIGURE 1 | Overview of CORK observatory experiments. (A) Location of CORK observatories at Holes U1301A and U1301B on the Juan de Fuca Ridge flank, northeastern Pacific Ocean (modified from Fisher et al., 2011); **(B,C)** Wellhead FLOCS experiments at IODP Hole U1301A manipulated by the ROV *Jason II* robotic arms. **(D)** Hole U1301A CORK diagram highlighting wellhead seafloor deployment site (modified from Orcutt et al., 2010 and used here with permission). Photos in **(B,C)** reproduced with permission of Woods Hole Oceanographic Institution.

microbe-mineral interactions in the volcanic portion of the oceanic biosphere. In this experiment, FLOCS chambers were placed for 1 year at the wellhead of IODP Hole U1301A on the eastern flank of the Juan de Fuca Ridge (**Figure 1**). An identical deployment at the wellhead of nearby Hole U1301B served as a control, as neither subsurface fluids nor bottom seawater was introduced into the FLOCS chambers during the deployment, and there was no evidence for biofilm formation. Fluid chemical data documents that minerals deployed at Hole U1301A were exposed to fluids sourced from the igneous crustal reservoir approximately 270 m below seafloor (mbsf). 16S rRNA genes recovered from mineral substrates (i.e., basalts, sulfides, iron oxyhydroxides) in this experiment were compared to those of previous colonization experiments at depth within the borehole (Orcutt et al., 2011a) and from crustal fluids (Cowen et al., 2003; Jungbluth et al., 2013), as well as to other environmental sample sets. The wellhead colonization experiments from Hole U1301A hosted microbial communities that differed from previous analyses of this subsurface environment, reflecting psychrophilic and aerobic conditions as opposed to the thermophilic and anoxic conditions found at depth. The results highlight limitations of this experimental approach for studying microbial community structure and function of a warm and anoxic subsurface crustal system, although this wellhead incubation approach may have more success in studying cooler subsurface environments. Nevertheless, such experiments are valuable for highlighting underlying mechanisms that drive microbial colonization and succession patterns on mineral substrates.

MATERIALS AND METHODS

FLOCS Chamber Design, Deployment, and Recovery

The overall design principal of the mineral incubation devices (i.e., FLOCS) is described in detail elsewhere (Orcutt et al., 2010). The Hole U1301A deployment differed from the previous design in that the chambers were constructed of 1.5-inch schedule 40 polyvinyl chloride (PVC) plastic pipe instead of Teflon or polycarbonate (**Figure 2**). FLOCS chambers (sleeves) were assembled onsite, with one FLOCS chamber consisting of cassettes containing glass wool (as a means to maximize surface area for colonization) with an olivine-rich basalt from the Loihi Seamount (GW + basalt in **Table 1**) in Sleeve 2; cassettes of pyrite (FeS_2) and of massive basalt previously collected from the Juan de Fuca Ridge flank subsurface at IODP Hole U1301B ("Basalt" in **Table 1**) in Sleeves 5 and 1; and hematite (Fe_2O_3) and goethite [FeO(OH)] in Sleeves 5 and 1, respectively (**Figure 2**). Minerals and FLOCS components were autoclaved prior to assembly, and flushed with ethanol and ultrapure deionized water after assembly, then flushed with commercially available sterile-filtered seawater (Sigma-Aldrich, product number S9148).

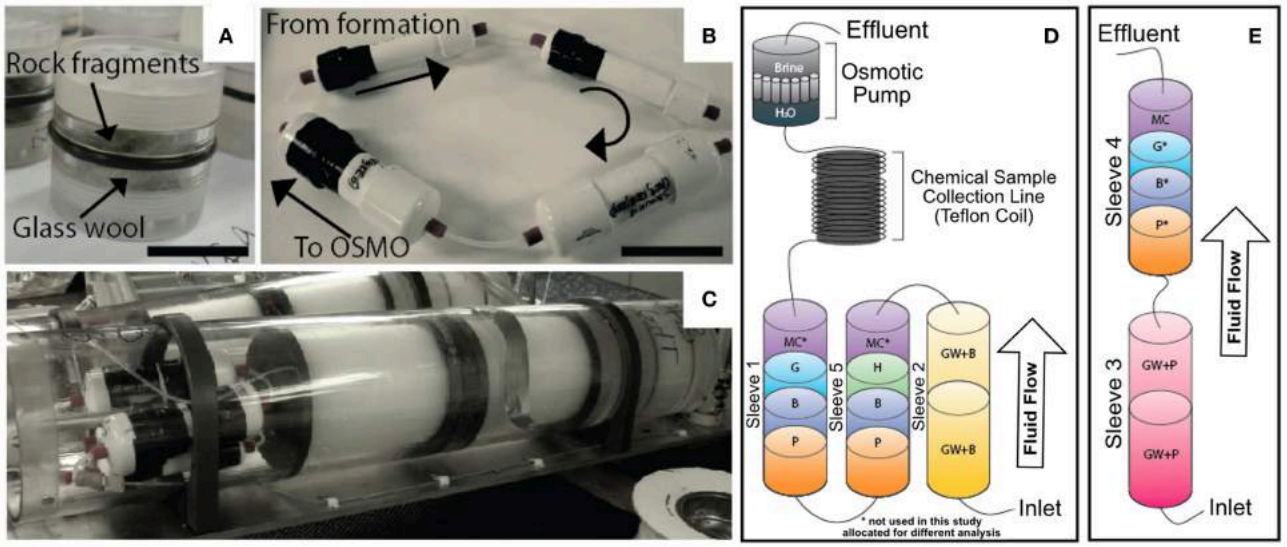

FIGURE 2 | Overview of the FLOCS experiments used in this study. (A) Polycarbonate cassettes containing >250 μm crushed mineral substrates, with ventilated caps and o-ring seal on outside. **(B)** The FLOCS (PVC) sleeves deployed in the negative control at Hole U1301B connected in series illustrating direction of fluid flow. **(C)** The FLOCS sleeves mated to the Teflon tubing coils and osmotic pumps inside the plates to be attached to the wellhead. **(D)** Schematic of FLOCS experimental design deployed at Hole U1301A, where substrates are listed in order of fluid flow: GB, Glass wool and Basalt; P, Pyrite; B, Hole U1301B Basalt; H, Hematite; MC*, cm^2 mineral chips; G, Goethite (*denotes substrates that were not used in this study and allocated for other analyses). **(E)** Hole U1301A passive flow (no OSMO pump) deployment labeled with identical substrate abbreviations as **(D)**.

FLOCS chambers, containing a 1:1 mixture of sterile deionized water and sterile seawater, were connected in series to a fluid sample coil (300-m-long, 1.2 mm outer diameter coil of Teflon tubing initially filled with deionized water), which was connected to an osmotic pump (Jannasch et al., 2004) with 13 semi-permeable membranes that pulled fluids through the FLOCS at ∼1 ml d^{-1} at bottom seawater temperatures (**Figure 2**). The inlet of the FLOCS chamber was connected via gas-impermeable PEEK tubing and union fittings to a stainless steel tube that is part of the wellhead. This tubing extends to 270 mbsf into the upper volcanic crust. A separate FLOCS sleeve containing only glass wool and pyrrhotite [$Fe_{(1-X)}S$ (x = 0–0.2)] was linked to the same stainless steel tubing and allowed to freely vent (i.e., no osmotic pump was connected), allowing subsurface fluids to flow through the sleeve at an unknown rate due to overpressure of the subsurface fluids compared to bottom seawater (**Figure 2E**). The FLOCS sleeves were bundled in custom plates (Wheat et al., 2010) for deployment by the ROV *Jason II* on expedition AT15-66 (R/V *Atlantis*; Woods Hole Oceanographic Institution) in summer 2010. The plate was connected to the right bay of the Hole U1301A CORK wellhead during dive J2-498.

In parallel, a replicate set of FLOCS chambers were attached to the wellhead at Hole U1301B, 300 m from Hole U1301A. Here the stainless steel umbilicals that reach to the volcanic reservoir at depth are obstructed, preventing the exchange of borehole fluids with the FLOCS during the course of the deployment. Moreover, during deployment the tubing connecting the pump to the Teflon coil on the outflow of the FLOCS chambers was accidentally disconnected, preventing the pumping of any fluids into the FLOCS chamber and coil. Thus, this deployment was used as a control that (1) verifies the absence of inadvertent contamination during FLOCS assembly/deployment/collection, (2) provides confirmation of the sterility of filtered seawater used in the FLOCS sleeves during deployment, and (3) confirms the physical integrity of colonization design against background seawater intrusion. Thus, Hole U1301B results verify that observations on the Hole U1301A materials resulted from exposure to volcanic reservoir fluids.

The FLOCS experiments were recovered during ROV *Jason II* dive J2-566 on cruise AT18-07 (R/V *Atlantis*) in summer 2011. Immediately after recovery, FLOCS sleeves were disassembled with ethanol and flame-sterilized tools, and samples were stored for shore-based DNA and microscopy analysis at −80°C.

Chemical Analysis of Fluids Exiting the FLOCS Experiments

In principle, during the deployment of the Hole U1301A FLOCS experiment, fluids sourced from the subsurface mixed with the FLOCS contents, eventually flushing out the initial chamber fluids and replacing it with subsurface-origin fluids. These mixed fluids would then be continuously collected in the sampling coil attached to the outflow end of the FLOCS experiments (**Figure 2D**). Thus, a record of the history of dissolved fluid chemistry in the FLOCS experiment can be obtained by sectioning the Teflon tubing attached downstream of the FLOCS, as described in detail elsewhere (Wheat et al., 2010). Here, the Teflon coils attached to the Hole U1301A and U1301B FLOCS were separated shipboard in 1-m intervals to collect the FLOCS effluent for bulk chemical analyses; these subsamples were then acidified according to established protocols (Wheat

TABLE 1 | Abundance and taxonomic classification of 16S rRNA gene sequence clone groups (focusing on classes of Proteobacteria) from each mineral from Hole U1301A, with an operational taxonomic unit (OTU) defined as 97% or higher sequence similarity.

Group	OTU ID	% of clones	# clones	GW and Basalt	Basalt	GW and Pyrrhotite	Pyrite	Hematite	Goethite	Closest relative—environment (Accession #)	%	References
Alpha	21	6.8	25	25	–	–	–	–	–	*Roseobacter*—Lost City hydrothermal (DQ270648)	97	Brazelton et al., 2006
	18	2.4	9	3	–	1	4	1	1	*Thalassospira*—ridge flank crustal fluids (DQ490020)	99	Huber et al., 2006
	3	2.2	8	–	3	–	–	5	–	*Parvibaculum*—Deepwater Horizon spill (JN018430)	99	Redmond and Valentine, 2012
	23	0.3	1	–	–	–	1	–	–	*Parvibaculum*—borehole crustal fluid (GQ903365)	96	Nigro et al., 2012
	12	1.1	4	–	2	1	1	–	–	Alphaproteobacteria—ocean water (JN717169)	96	Luan et al., unpublished
	9	0.3	1	–	1	–	–	–	–	Alphaproteobacteria—deep ocean (HM798889)	96	Eloe et al., 2011
Beta	15	1.9	7	6	1	–	–	–	–	*Deftia sp.* (NR_074626)	99	Lucas et al., unpublished
	7	0.8	3	2	1	–	–	–	–	*Ralstonia picketti* (CP001645)	99	Lucas et al., unpublished
	14	0.8	3	1	1	1	–	–	–	*Ralstonia solanacearum* (EF016365)	98	Albequrque et al., unpublished
Gamma	1	12.7	47	5	19	4	8	8	3	*Shewanella*—deep-sea surface sediment (AM997576)	98	Schauer et al., 2010
	2	11.1	41	–	21	2	–	18	–	*Neptunamonas*—deep-sea whale fall (AY549004)	99	Goffredi et al., 2005
	8	4.1	15	1	11	–	–	3	–	*Colwellia psychrerythraea 34H* (CP000083)	99	Methé et al., 2005
	16	1.4	5	4	–	1	–	–	–	deep-sea *Pseudomonas sp.* (AM410618)	99	Zhang et al., unpublished
Epsilon	4	27.3	101	–	8	11	34	20	28	*Arcobacter*—Black sea shelf sediment (AJ271654)	95	Thamdrup et al., 2000
	11	12.4	46	–	2	–	17	–	27	*Arcobacter sp.* From North Sea (AF235110)	95	Eilers et al., 2000
	13	3.5	13	–	1	–	1	11	–	Black sea shelf sediment *Arcobacter sp.* (AJ271654)	96	Thamdrup et al., 2000
	5	0.3	1	–	1	–	–	–	–	*Sulfurimonas*—hydrothermal vent (FN554112)	97	Schauer et al., 2011
Other	17	0.3	1	–	–	1	–	–	–	*Mariprofundus*—hydrothermal sulfides (JQ287464)	99	Sylvan et al., 2012
	6	4.9	18	–	6	–	5	–	7	Flavobacteraceae—Japan trench cold seep (AB015261)	99	Li et al., 1999
	19	3.0	11	1	–	1	7	1	1	Bacteriodetes—hydrothermal sediment (AF419687)	98	Teske et al., 2002
	10	1.1	4	1	1	–	–	2	–	*Lutibacter*—Arctic Ocean sediment (EU287256)	99	Li et al., 2009
	22	0.3	1	1	–	–	–	–	–	*Lactobacillus perolens* (NR_029360)	95	Buck et al., unpublished
	20	0.8	3	–	–	–	2	–	1	Unclassified ridge flank crustal fluid (AY704403)	97	Huber et al., 2006
	24	0.3	1	–	–	–	1	–	–	Unclassified hydrothermal sulfide (JQ287080)	95	Sylvan et al., 2012
	25	0.3	1	–	–	–	1	–	–	Unclassified cold marine seep (FJ814754)	94	Buck et al., unpublished
		Total	370	50	79	23	82	69	67			

Closest environmental sequence relatives determined are shown with Genbank accession number and percent sequence similarity.

et al., 2011). Since the fluids were not preserved *in situ* with acid to dissolve metal-containing compounds that precipitate upon exposure to oxic conditions (i.e., the Teflon tubing allows penetration of oxygen; Wheat et al., 2010), particle formation in the sampling coil may have skewed the time-series of redox sensitive elements. Major and minor ion concentrations were measured on select samples using inductively coupled plasma mass spectrometry (ICP-MS) following established procedures (Wheat et al., 2010).

DNA Extraction, 16S rRNA Gene Clone Library Construction, and Sequence Analysis

DNA was extracted from roughly 2 g of crushed mineral chips from each substrate using the FastDNA® Spin Kit for Soil (MP Biomedicals) according to the manufacturer's protocols. DNA was quantified using a Qubit 2.0 fluorometer with HS DNA reagent kit (Invitrogen). Due to low biomass yields (i.e., DNA concentrations below detection limit, no PCR bands directly from DNA extracts), environmental DNA was amplified using the illustra GenomiPhi V2 DNA Amplification Kit (GE Healthcare) according to manufacturer's protocols. The amplified DNA was then used as a template for PCR amplification of the full-length 16S rRNA gene using the universal primers B27F and U1492R (Weisburg et al., 1991). PCR reaction parameters are found elsewhere (Baquiran et al., 2012). The resulting PCR products were purified using the QIAquick PCR Purification Kit (Qiagen), then ligated and cloned using the TOPO TA Cloning® Kit (Invitrogen). Clone libraries from each substrate were constructed and sequenced by Beckman Coulter Genomics. Sequences were assembled using *Geneious R6* and then aligned with the *MAFFT* alignment program (Desantis et al., 2006; Schloss, 2009; Drummond et al., 2012). Chimeric sequences were removed using *Bellerophon*, phylogenetic trees were constructed using *PhyML 3.0* and community dendograms were made with *mothur* version 1.35.1 (Guindon and Gascuel, 2003; Huber et al., 2004; Schloss, 2009; Drummond et al., 2012). Classifications of 16S rRNA gene sequences were performed with the *Silva* ribosomal RNA database using the *SINA* v1.2.11 aligner and the NCBI database using the BLAST algorithm (Altschul et al., 1997; Schloss, 2009; Pruesse et al., 2012). OTUs were arbitrarily numbered according to the order of detection from clone libraries. Additional sequences used for phylogenetic and community analyses were accessed from GenBank. Sequence data were submitted to GenBank under accession numbers KC682104–KC682473.

To examine the microbial community structure of the Hole U1301A wellhead minerals to previous examinations of mineral biofilm community composition, we calculated membership-based pairwise similarity matrix indices between the Hole U1301A wellhead FLOCS clone sequences with clone sequences from inactive seafloor sulfides from the East Pacific Rise (Sylvan et al., 2012), a mineral biofilm collected from a CORK at Hole 896A on the Costa Rica Rift (Nigro et al., 2012), East Pacific Rise seafloor basalts (Santelli et al., 2008), a 3-year time series of crustal fluids from Hole U1301A (Jungbluth et al., 2013), and a mineral colonization experiment incubated at depth in Hole U1301A at 64°C (Orcutt et al., 2011a). Pairwise community comparisons for shared community composition and species richness where performed using the following *mothur* calculators: J_{class}, J_{est}, Kulczynski, Lennon and Anderberg (Schloss, 2009), and cladograms from each metric were compared to examine trends.

Scanning Electron Microscopy

To assess for biofilms on the control incubation minerals from Hole U1301B, scanning electron microscopy was conducted on select mineral substrates (basalt and pyrite) from the experiment, following approaches published previously (Orcutt et al., 2011a). Mineral coupons were thawed to room temperature and mounted on carbon tape and coated with approximately 30 μm of graphite to reduce charging. Images were obtained using a JSM 6610 low-vacuum SEM (JEOL USA, Inc.) at 5 kV and a working distance of 10 mm with a point-to-point resolution of 3 nm in the Center for Electron Microscopy and Microanalysis (University of Southern California). Similar analyses were not possible on Hole U1301A incubated minerals due to consuming all available material for DNA-based analyses.

RESULTS

Fluid Composition

Previous long-term chemical records of fluids at Hole U1301A indicate upper basement fluids (∼300 mbsf) are typically warm (64°C) and anoxic yet relatively high in sulfate and calcium (Wheat et al., 2010; Lin et al., 2012), with the elevated calcium indicative of hydrothermal fluid-rock interactions. In this study, the fluids that bathed the rock substrates evolved over time due to flushing out of the initial chamber contents (a mixture of sterile seawater and deionized water) with the deep-sourced crustal fluids (**Figure 3**). Notably, calcium concentrations increased monotonically from the concentration of distilled water that initially filled the sample tubing before deployment and reaches an asymptote concentration near 56 mmol kg^{-1} after 5 months of deployment (**Figure 3A**), which agrees with regional Ca concentrations in upper basement (Wheat et al., 2010). Concentrations of dissolved silica (Si) also increased throughout the experiment, with a maximum of 1160 μmol kg^{-1}. This is about the same concentration of borehole fluids 3 years after the initial drilling (Wheat and Mottl, 2000; Wheat et al., 2003a, 2010). Concentrations of magnesium changed with time to reach 1.7 mmol kg^{-1} by the end of the experiment (**Figure 3B**), approaching the crustal fluid composition of 1.9 mmol kg^{-1} (Wheat et al., 2010). Sulfate and strontium concentrations increased to 18 mmol kg^{-1} and 110 μmol kg^{-1}, respectively (**Figure 3C**), consistent with earlier results (Wheat et al., 2010). Measured dissolved iron concentrations are not reliable because precipitation in the sample coil is possible during the deployment, since the FLOCS effluent was not preserved with acid during collection.

Manganese initially increased within the first few months to over 12 μmol kg^{-1} (**Figure 3B**), then decreased with time to approach low values (<0.001 μmol kg^{-1}) observed in both

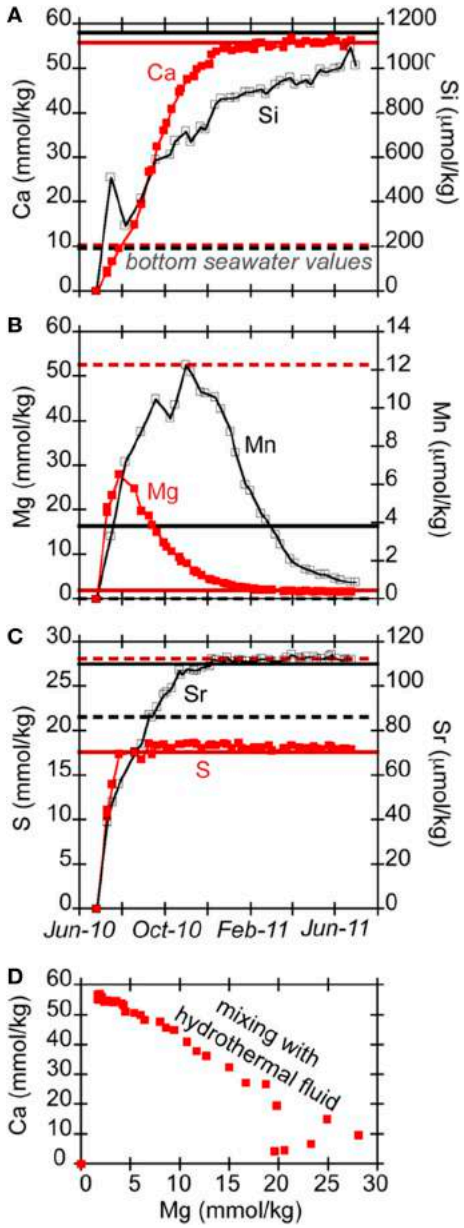

FIGURE 3 | Ion concentrations [(A) Ca (red filled squares) and Si (black open circles); (B) Mg (red filled squares) and Mn (black open circles); (C) S (red filled squares) and Sr (black open circles)] in Hole U1301A FLOCS experiment plotted as a function of time, showing the chemical evolution of the FLOCS experiment from initial conditions when filled with diluted sterile seawater to an eventual replacement with crustal fluids sourced from the volcanic crust. Dashed and solid horizontal lines in **(A–C)** indicate concentrations of ions in bottom seawater and Hole U1301A crustal fluids, respectively, as presented in Wheat et al. (2010). **(D)** presents the Ca vs. Mg concentrations for these samples, demonstrating the mixing of different end member fluids.

bottom seawater and borehole fluids (Wheat et al., 2010). Possible oxidants of Mn, such as oxygen and nitrate, are missing from the source hydrothermal fluids (Mottl et al., 1998), which led us to explore the possibility for oxygen intrusion into the experiment. The PVC plastic used in the construction of the FLOCS is permeable to bottom seawater oxygen. Assuming a 5% decrease per degree Celsius change in the oxygen permeability of PVC at standard state, and given the surface area for each FLOCS chamber, we calculate that roughly 350 nanomole of oxygen per day could penetrate into a PVC FLOCS chamber at the seafloor (at a maximum, as this rate would decrease with a decreasing gradient in oxygen across the plastic). Given the variable FLOCS chamber volume occupied by fluid (as opposed to solid rocks) and the pumping speed of the attached OsmoSampler pump, we estimate that it would take roughly 4 weeks for the oxygen concentration in the FLOCS to reach background seawater oxygen concentrations (∼100 micromolar; Brian Glazer, personal communication) if no oxygen removal processes occurred within the FLOCS.

As expected, the Teflon coil connected to the FLOCS experiment at Hole U1301B contained distilled water, as determined by initial refractometer measurements of the fluids (data not shown), indicating that no fluids (seawater or crustal) had passed through this experiment. Thus, further chemical analyses were not performed.

Bacterial Diversity and Membership Analyses

To evaluate microbial colonization patterns on the different mineral substrates, environmental DNA was extracted from the samples, and then 16S rRNA genes of Bacteria were amplified, cloned and sequenced. Original DNA concentrations were below detection limit, so DNA was amplified with Phi29 Polymerase, then the 16S rRNA gene was amplified with bacterial specific primers via PCR. Hole U1301A minerals produced visible bands on an agarose gel, and the product was used for further cloning, whereas the Hole U1301B minerals did not generate visibly amplified DNA and no further cloning attempts were made. In total, 370 nearly full-length 16S rRNA gene sequences were obtained from Hole U1301A minerals, ranging from 23 to 82 clones per substrate (**Table 1**). At the 97% or greater sequence similarity operational taxonomic unit (OTU) classification level, there were a total of 25 unique OTUs from the 370 16S rRNA gene sequences (**Table 1**, **Figure 4**).

An overview of the OTU diversity and abundance from the Hole U1301A minerals reveals that sequences grouping within the Epsilonproteobacteria were the most abundant in the clone libraries (161 of 370 sequences; **Table 1**, **Figure 4**). OTU4 was the most prevalent clone sequence in the library (27.3% of all clones), and it was detected in all samples except the glass wool + basalt sample (**Table 1**). OTU4 is most closely related to the *Arcobacter* genus (**Table 1**, **Figure 4**). OTU11, the third most abundant clone type, is also closely related to species from the *Arcobacter* genus. This phylotype was abundant in the pyrite and goethite samples but absent or low count in clones from other samples (**Table 1**). OTU13 was also *Arcobacter* related and found predominantly on hematite (**Table 1**). The only other Epsilonproteobacteria-related OTU was related to the *Sulfurimonas* genus and was observed on the basalt sample. In summary, *Arcobacter sp.* related clones were the dominant group in the Hole U1301A FLOCS (43.2% of all

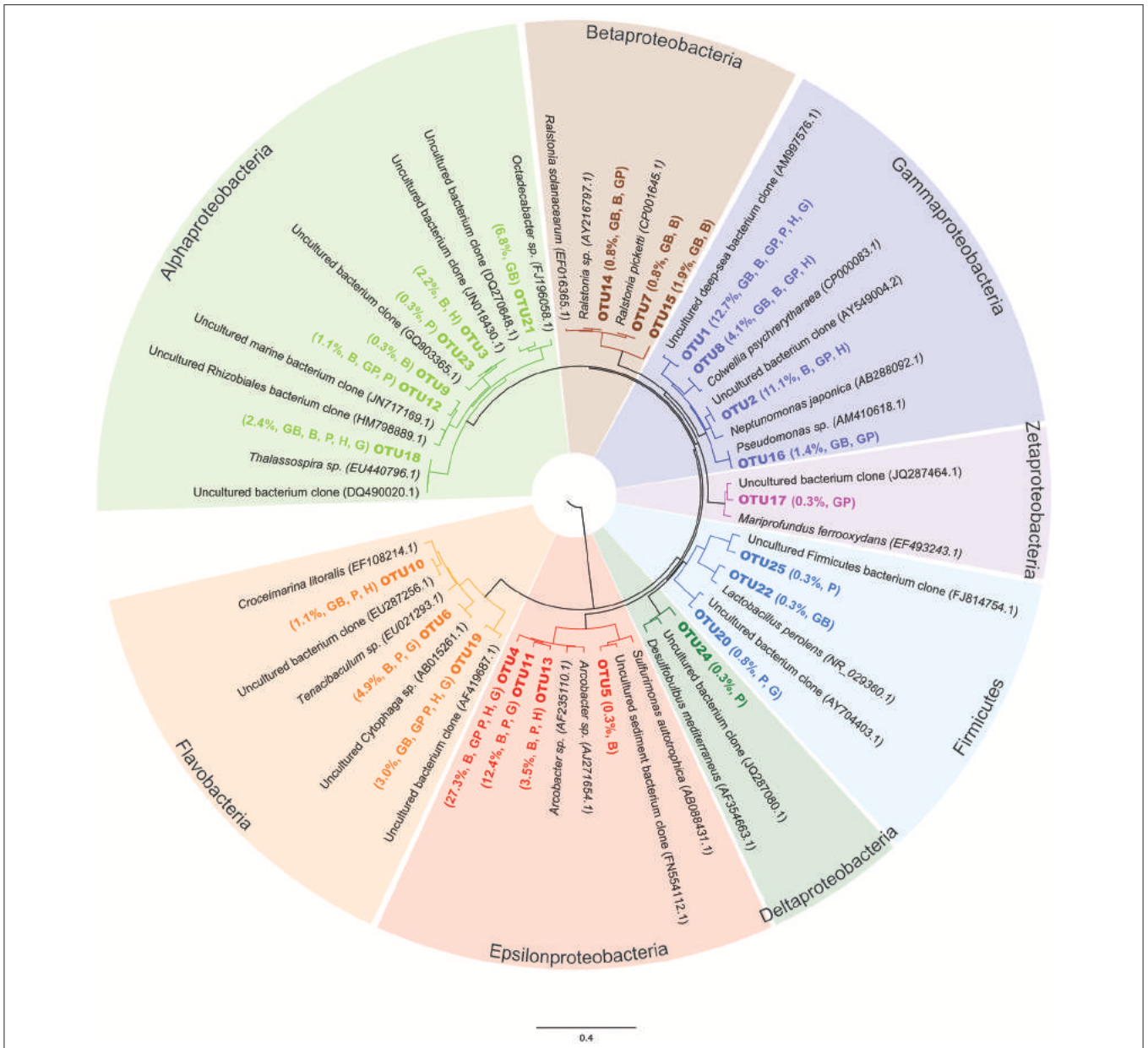

FIGURE 4 | Bacterial 16S rRNA gene neighbor-joining phylogenetic analysis of representative OTU sequences compared to close environmental sequence relatives from the Silva database. OTUs in this study are labeled in bold. Relative abundance of the OTU in the entire sequence library (i.e., percent out of 370 clones) and abbreviation of sample type that the OTU was found in listed in parentheses after each OTU name, using the same sample code as listed in **Figure 2**.

clones), and these were abundant on the iron oxides (hematite, goethite) and iron sulfides (pyrite, pyrrhotite) but less abundant on the basalt samples (**Table 1**).

Gammaproteobacteria related sequences were the second most abundant clone library group (108 clones, 29.3% of all clones; **Table 1**, **Figure 4**). OTU1 was classified within the *Shewanella* genus and was the only clone type present in every substrate of this experiment. OTU2, represented by 41 clones with high relative abundances in hematite and basalt, also groups with Gammaproteobacteria close to *Neptunamonas*-related spp. from deep-sea whale falls. OTU8 is most closely related to the *Colwellia* genus and was most abundant on basalt. Lastly, *Pseudomonas*-related OTU16 in the Gammaproteobacteria was only amplified from the glass wool + mineral substrates. Collectively, four different Gammaproteobacteria phylotypes were observed with high relative abundance in basalt mineral substrates and lower abundance on the sulfides.

Of the remaining sequence groups, 48 clones were classified as Alphaproteobacteria, with the majority of these (25 clones)

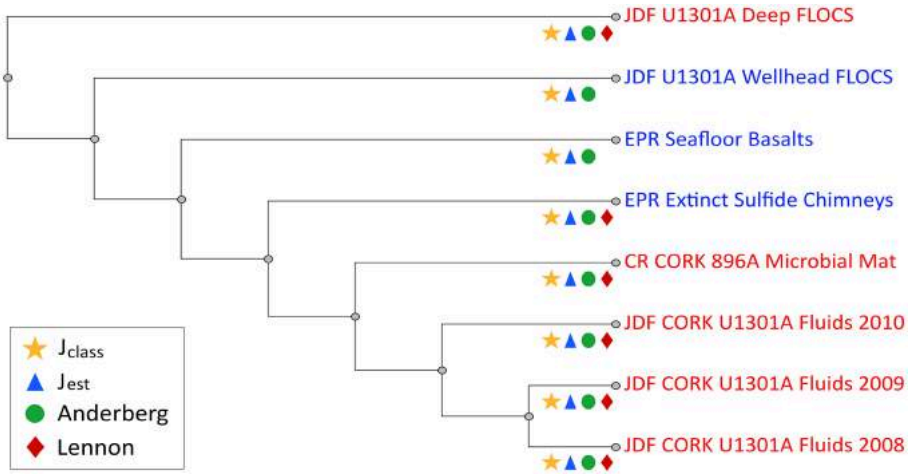

FIGURE 5 | Kulczynski cladogram summarizing results of four other pairwise similarities in community membership calculators (J_{class}, J_{est}, Anderberg, and Lennon) comparing combined OTUs to various environmental sites. Site names, depicted as cladogram leaves, are color coded in red and blue to indicate warm (58–64°C; Hole U1301A Deep, Hole U1301 2008-2010 Crustal fluids, Costa Rica Hole 896A CORK Microbial Mat) and cold (seafloor, ~4°C; Hole U1301A Wellhead FLOCS, East Pacific Rise seafloor Basalts, Extinct Sulfide Chimney) incubation environments, respectively. Symbols on each branch indicate which community membership calculators supported this branching order, as shown in legend.

being closely related to *Roseobacter* from hydrothermal fluids and found exclusively on the glass wool + basalt sample (**Table 1**, **Figure 4**). Other Alphaproteobacteria-related sequences were found on multiple sample types but in relatively low abundance. Three low abundance Betaproteobacteria related phylotypes were observed on the glass wool and basalt substrates and grouped most closely with the *Ralstonia* genus. One clone from pyrite, OTU24, grouped with unclassified Deltaproteobacteria from deep-sea hydrothermal sulfides. One *Mariprofundus*-related sequence within the Zetaproteobacteria was documented from the glass wool + pyrrhotite sample. Two Flavobacteria-related phylotypes were amplified from each of the substrates at low relative abundances.

Community similarity based on sequence membership, as evaluated by several different indices, consistently clustered Hole U1301A wellhead FLOCS mineral microbial communities as branching between Hole U1301A borehole-incubated minerals and seafloor-exposed minerals (basalts and sulfides), with Hole U1301A fluids and a mineral biofilm from Hole 896A grouping more distantly (**Figure 5**).

Mineral Alteration Products

To examine whether microbial biofilms formed on the surface of minerals incubated in the Hole U1301B FLOCS, mineral coupons were examined by SEM. No alteration products or microbial biofilms were observed on Hole U1301B mineral coupons via SEM (**Figure 6**). SEM revealed thin filaments on the basalt coupon. These are most likely fragments of the glass wool from the FLOCS that the mineral chips were embedded within. The basalt coupon had scant amorphous particulate matter (**Figures 6A,B**). The pyrite coupon was devoid of secondary minerals on the surface (**Figures 6C,D**).

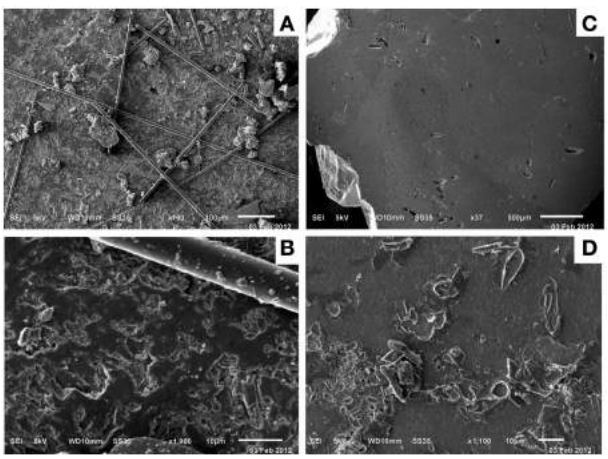

FIGURE 6 | Scanning electron microscopy of control Hole U1301B FLOCS minerals revealed limited evidence for biofilms or secondary mineral alteration. Basalt mineral coupon SEM **(A,B)** revealed thin filaments, most likely fragments of glass wool from the FLOCS experiment. Pyrite mineral coupon SEM **(C,D)** revealed a paucity of particles or alteration. Scale bars lengths are 100 **(A)**, 10 **(B)**, 500 **(C)**, and 10 μm **(D)**.

DISCUSSION

In the quest to study microbial life supported by the deep crustal biosphere—a major focus of the international ocean drilling program (Iodp 2003-2013 Initial Science Plan, 2001)—this experiment set out to examine the utility of deploying mineral colonization experiments at the wellheads of crustal subsurface borehole observatories (i.e., CORKs) as an alternative to downhole deployments (**Figure 2**). The motivation for such deployments is the relative ease of replacing wellhead

experiments using ROVs or submersibles without opening the borehole to remove experiments, which can disturb the system. To this end, mineral colonization experiments were deployed at the wellheads of two CORKs on the Juan de Fuca Ridge flank that permit access to anoxic, warm (64°C) crustal fluids (**Figure 1**). Here, we show that microbial communities sourced from subsurface crustal fluids at Hole U1301A can colonize minerals incubated at seafloor CORK wellheads within a 1-year period, and that the wellhead incubation concept is robust against the intrusion of bottom seawater (based on a control experiment at Hole U1301B). Colonization occurs despite crustal fluids from this region containing approximately an order of magnitude lower cell densities compared to bottom seawater (Jungbluth et al., 2013), and relatively slow fluid flushing rates of the experiments (∼1 ml d^{-1}), both of which exacerbate low biomass conditions.

The results reveal that temperature and physico-chemical conditions at the wellhead have a strong influence on the structure of microbial communities that develop on mineral surfaces. For instance, wellhead-incubated minerals bathed in crustal subsurface fluids at bottom seawater temperature hosted microbial communities dominated by Epsilonproteobacteria and Gammaproteobacteria related to sulfur and iron oxidizing bacteria (**Figures 4**, **5**), whereas anoxic and warm minerals and fluids from depth in the crust at this location harbor microbial communities with significantly different membership and structures dominated by thermophilic, spore-forming Firmicutes and sulfate-reducing bacteria (Orcutt et al., 2011a; Smith et al., 2011; Jungbluth et al., 2013). The wellhead-incubated minerals hosted microbial communities reminiscent of seafloor-exposed rocks that are bathed in cold oxygen-rich seawater, suggesting cold and oxic conditions in the wellhead FLOCS experiment structured the microbial community that colonized the minerals. Thus, although these experiments have limited utility for the intended purpose of understanding the dominant microbe-mineral interactions in the warm and anoxic subsurface at Juan de Fuca, they do have utility for examining the adaptive capacity of subseafloor microbial communities under changing environmental conditions (for example, where hydrothermal fluids mix with oxic seawater near hydrothermal vents). Moreover, temperature and physical-chemical influences may not be an issue when conducting wellhead experiments in cool and oxic ridge flank systems, such as at similar CORKs on the flanks of the Mid-Atlantic Ridge (Edwards et al., 2012b; Orcutt et al., 2013a). Hence, these results highlight the capacity for adaptation for subsurface crustal microbial communities to respond to changing environmental conditions, and will guide future experiments to examine microbe-mineral interactions in the subsurface.

Development of Wellhead FLOCS Chemical Conditions in Comparison to the Borehole Environment

Collectively, the chemical data from the Hole U1301A FLOCS experiment indicate simple three-component mixing upon which reactions are exposed (**Figure 3D**). Given a sample coil that is initially filled with distilled water and FLOCS chambers that are filled with a mixture of sterile-filtered seawater and distilled water, the initial fluids recovered in the sample coil reflect a mixture of these two solutions, consistent with the initial increase in Mg concentrations. As the hydrothermal fluid is pulled into the FLOCS, mixing occurs between the initial FLOCS fluid and this hydrothermal fluid, also producing a linear (conservative) mixing trend (e.g., Ca vs. Mg). This mixing continues until the fluid in the FLOCS is similar to the composition of the crustal fluid (e.g., asymptote for Ca and Mg vs. time). Notably, the major ion chemistry confirms that the Hole U1301A FLOCS were exposed to crustal fluids and not bottom seawater.

In contrast, Mn data do not follow such trends (**Figure 3B**), suggestive of reaction within the FLOCS. Mn is leached from rock substrates, as has been observed previously (Orcutt et al., 2010), either from abiotic or biotic processes. With time, Mn values decrease to concentrations below the basement fluid concentration, consistent with Mn removed from solution. A simple model of oxygen diffusion across the PVC plastic used in the experiment suggests that the interior of the FLOCS experiment became oxic within a few weeks, despite the slow pumping of initially anoxic crustal fluids through the experiment. Thus, use of PVC FLOCS chambers for wellhead mineral colonization experiments compromises an essential chemical condition for studying the anoxic Juan de Fuca Ridge flank environment. Therefore, the structure of mineral-attached microbial communities in the wellhead experiments cannot be extrapolated to the subsurface environment at this site. Nonetheless, the experiments do allow assessment of biological adaption to changing environmental conditions (i.e., warm and anoxic vs. cool and oxic). To match subsurface conditions, future wellhead colonization experiments at this site should be placed within the open borehole which vents anoxic crustal fluids at ∼62°C (Wheat et al., 2004, 2010; Fisher et al., 2012), or they should be constructed of gas-impermeable materials, such as the Teflon-lined stainless steel devices used in the terrestrial subsurface (Pedersen, 2012).

Comparison of Microbial Communities on Wellhead, Borehole, and Seafloor-Exposed Minerals

Comparison of microbial community structure based on amplified DNA can be challenging due to possible amplification biases. In addition to biases associated with any PCR primer set (Suzuki and Giovannoni, 1996), bulk genomic DNA amplification prior to 16S rRNA gene PCR may introduce additional representational inconsistencies. Because the amount of original template DNA prior to multiple displacement amplification was very low in our experiments (<1 ng ml^{-1}) with a relatively diverse community, the representational biases are assumed to be minimal (Suzuki and Giovannoni, 1996; Binga et al., 2008). Thus, we assume that the abundance of clones generated from different minerals can be compared to assess relative abundance.

The combined effects of low temperature and aerobic conditions influenced the wellhead mineral colonization

microbial community structure relative to similar mineral substrates incubated at depth under warm and strictly anoxic conditions (**Figure 5**). Previous experiments showed that incubation of mineral substrates in anoxic crustal fluids at 64°C resulted in microbial communities indicative of anaerobic, thermophilic, and spore-forming organisms (Orcutt et al., 2011a), similar to microbial communities observed in the anoxic fluids sampled from this environment (Jungbluth et al., 2013; Robador et al., 2014). In contrast, microbial communities established on similar minerals incubated in the same crustal fluid source but under low temperature and oxic conditions at the wellhead were dominated by members reflecting aerobic, microaerophilic, or facultatively anaerobic lifestyles (**Table 1**, **Figure 4**). The most prevalently recovered 16S rRNA gene sequences were classified as *Arcobacter* spp. (**Table 1**), members of the Epsilonproteobacteria known for sulfur oxidation metabolic capacity. While Epsilonproteobacteria-related sequences have not previously been found in the anoxic borehole environment of the Juan de Fuca Ridge flank subsurface (Cowen et al., 2003; Orcutt et al., 2011a; Smith et al., 2011; Jungbluth et al., 2013), they have been detected in the mixed hydrothermal fluids that vent from springs on Baby Bare outcrop, about 50 km to the south along the same crustal fluid flow path as Hole U1301A (Huber et al., 2006), suggesting that these low abundance members (Sogin et al., 2006) of the warm and anoxic crustal subsurface can proliferate under suitable cooler and/or oxic environmental conditions. Similar Epsilonproteobacteria have been detected on seafloor-exposed basalt and sulfide minerals near other hydrothermal systems (Orcutt et al., 2010; Sylvan et al., 2012; Toner et al., 2013), suggesting a widespread distribution of mineral-dependent Epsilonproteobacteria.

At a broader level, examining the wellhead FLOCS microbial community structure as a whole in comparison to other environmental studies reveals the blending of the wellhead FLOCS microbial community between subsurface, warm, anoxic conditions with seafloor, cool, oxic conditions (**Figure 5**). Community membership calculators predict intra-community similarities for Hole U1301A crustal fluids, while all other communities are independent branches with no additional significant intra-community similarities but defined inter-community membership patterns. A temperature structure exists; however, downhole FLOCS incubations appear to be an exception. Crustal fluids (64°C) sampled from Hole U1301A during three consecutive years are most similar to a microbial mat collected from the exterior of a sub seafloor observatory port venting 58°C fluids into the surrounding bottom water (Hole 896A CORK). All 4°C environment communities (i.e., extinct sulfide chimneys, seafloor basalts, and wellhead Hole U1301A FLOCS) consistently group together as similar in inter-community membership with deep independent branching relative to the 58°C venting CORK fluid biofilm and 64°C crustal fluid communities. All community calculators used here placed Hole U1301A FLOCS incubated downhole as the outgroup, implying that, in addition to temperature, other variables, such as the lack or presence of dissolved oxygen, must be considered to more accurately explain community membership similarity observations.

Recent studies have suggested that the deep oceanic crustal biosphere has a dynamic nature, where the structure of microbial communities can change on a relatively rapid timescale, reflecting changes in chemical and thermal conditions (Orcutt et al., 2011a; Jungbluth et al., 2013). One unknown in that phenomenon is the rate and extent at which microbes can grow and respond to physico-chemical changes in substrate-attached dark ecosystems. Temperature differences probably result in drastically different selection criteria for enzymes suited for temperature-specific biochemical activity and associated taxon recruitment and/or subsequent biological succession shifts. Here, analyses of mineral colonization FLOCS experiments deployed at a CORK wellhead, sampling fluids sourced from 270 mbsf, indicate that relatively diverse assemblages of bacteria sourced from sub seafloor aquifer fluids can colonize sterile mineral surfaces at both 64°C under anoxia (Orcutt et al., 2011a) and at 4°C under aerobic conditions (this study) within a year. Combined, these observations highlight the dynamic and environmentally responsive nature of microbial assemblages endogenous to crustal fluids at Hole U1301A. The colonization rapidity and thermal/redox selectivity suggests that subseafloor aquifer-hosted microbial assemblages are sufficiently diverse to adapt to a range of redox conditions, selecting favorable environment-dictated bacterial community membership across a 60°C temperature range within relatively short biological temporal scales (<1 year).

In the Hole U1301A incubation, similar taxa prevailed across mineral substrates (**Table 1**), suggesting that mineral composition was not a primary driver of microbial community structure in this 1-year experiment. The close physical association of the minerals in serially connected cassettes within the FLOCS experiment may have allowed crossover between treatments, thus allowing overprinting and blending between treatments that could not be resolved with this approach. Regardless, the dominant, primarily Epsilonproteobacteria taxa may have had an adaptive strategy for harnessing reduced elements from either the mineral surfaces or dissolved in the crustal fluids, despite the mineral composition.

The Potential for S and Fe Oxidation by Subsurface Microbial Communities under Changing Environmental Conditions

The most prevalent taxa observed in the wellhead colonization experiments were the Epsilonproteobacteria, which are capable of carbon fixation via sulfide oxidation (Wirsen et al., 2002) and are known to be the predominant organisms found in hydrothermal environments (Nakagawa et al., 2005; Huber et al., 2007). Epsilonproteobacteria are also detected on seafloor exposed massive sulfides (Sylvan et al., 2012; Toner et al., 2013). The most prevalent species observed in the FLOCS was OTU4 (101 of 370 clones), classified as *Arcobacter*, but with only 95% sequence similarity to other known *Arcobacter* species (**Table 1**, **Figure 4**). This OTU was primarily found on pyrite, goethite, hematite and the glass wool + pyrrhotite, but also on basalt (**Table 1**). Other *Arcobacter*-related OTUs were also observed (**Table 1**, **Figure 4**). *Arcobacter sp.* are capable of sulfide oxidation (Wirsen et al., 2002) and it is possible that these organisms

utilize leaching sulfur species from pyrite and pyrrhotite with oxygen present within the FLOCS chambers. We hypothesize, based on the high prevalence of 16S rRNA genes classified as Epsilonproteobacteria, that sulfur oxidation is a key metabolic pathway supporting mineral-microbe communities under cool and oxic conditions. Given that such Epsilonproteobacteria are known to use the reverse tricarboxylic acid (rTCA) cycle for carbon fixation (Hugler et al., 2005), it is possible that autotrophic metabolisms are also supported in this system by this cohort.

Under the cool and presumably oxic conditions of the wellhead FLOCS experiment, oxidation of sulfur and iron are thermodynamically favorable (Orcutt et al., 2011a). Only one 16S rRNA gene sequence from this study was associated with known iron oxidizing bacteria of the Zetaproteobacteria (**Table 1**), suggesting that iron oxidation may not have been a prominent metabolic process in the wellhead FLOCS environment at the time of collection. The low abundance of known iron oxidizing bacteria in the wellhead FLOCS clone libraries is consistent with previous studies from other iron-oxidizing mineral systems (Thorseth et al., 2001; Edwards et al., 2003; Santelli et al., 2008; Sylvan et al., 2012). This suggests either that (i) known iron oxidizers (i.e., Zetaproteobacteria) make up a small fraction of the microbial community; (ii) that multiple displacement amplification and/or primers used to construct clone libraries are biased against the proportional representation of known iron oxidizers; (iii) that iron oxidation may only be significant under a brief time window early in the experiment, leaving only fossil biominerals by the time of collection, as suggested previously (Orcutt et al., 2011a), or (iv) that iron oxidation was mediated by other unknown groups within the microbial community. Importantly, the observation of any known iron oxidizing bacteria or biomineral markers of their activity is again reflective of the presence of oxygen in the wellhead FLOCS experiments, as these microorganisms are not known from anoxic environments (Emerson et al., 2010).

We stress that observations regarding S and Fe cycling in this study are only applicable to our incubation conditions (i.e., the oxic and cold conditions of the FLOCS at the wellhead environment) and thus do not necessarily reflect subseafloor microbial activities at this site; however, our results show an adaptive response to changing thermal and redox regimes, and suggest an effective adaptation capacity potential for the colonization of mineral substrates by subseafloor crustal fluid biota.

CONCLUSIONS AND RECOMMENDATIONS

As a tool for examining mineral-microbe interactions in the warm (64°C) and anoxic crustal subsurface, deployment of mineral colonization experiments at the wellhead of crustal borehole observatories must be configured to mimic conditions at depth. This can be conducted in multiple ways; however the easiest means is to place such experiments within the open borehole of overpressured observatories from which hydrothermal fluids vent freely (Fisher et al., 2011). Our approach has value for studying cooler and oxic subsurface crustal communities, which are widespread (Edwards et al., 2012a,b; Orcutt et al., 2013b). Results of our experiment illustrate that low abundance members of Juan de Fuca crustal fluids, particularly low abundance crustal taxa classified as Epsilonproteobacteria, proliferate under changing environmental conditions and become dominant members of the microbial community on substrates incubated for a year in the cool and oxic bottom water-hosted system at the CORK wellhead. Different mineral surfaces inoculated with Juan de Fuca crustal fluids do not induce growth of specific communities within a 1-year timeframe. Redox conditions (oxic/anoxic) and temperature (4/64°C) dictate substrate colonization and community succession, and are proposed as major ecological drivers in environments where crustal fluids interact with minerals. Thus, to further the quest of explaining the establishment, adaptation, and activities of microbial life in the marine deep biosphere, future FLOCS experiments can be designed to elucidate mechanisms and/or rate of specific mineral-microbial interactions under a range of thermal and chemical conditions.

AUTHOR CONTRIBUTIONS

All authors contributed to the design of the experiment. KE and SH deployed the experiment; KE, GR, BO, SH, GW recovered the experiment. JB, GR, and AH analyzed samples, and all authors contributed to data analysis. JB, GR, KE, AH, and BO wrote the paper with input from all authors.

ACKNOWLEDGMENTS

We thank the science parties and ship crew of the *R/V Atlantis* cruises AT15-66 and AT18-07 for assistance with sample deployment, recovery, and processing, and the pilots and crew of the ROV *Jason II* (Woods Hole Oceanographic Institute) for enabling the deployment and recovery of the FLOCS experiments. We acknowledge Katherine Inderbitzen and Andrew R. Gross for assistance during deployments/collections, Don Wiggins and the USC Machine Shop for building FLOCS components, John Curulli (Center for Microscopy and Microanalysis at the University of Southern California) for his assistance with SEM analyses, Colleen L. Hoffman for her assistance collecting the micrographs, Roman Barco for insightful conversations about Fe-oxidation, Hector Monterrosa for his constructively critical set of eyes, Elaine Krebs for illustrations and Michael Lee for support and inspiration. We thank all of our reviewers for their comments that lead to an improved manuscript. Support for this work came from NSF awards OCE-1030061 (to CW), OCE-0939564 (to KE), and OCE-123326 (to BO). This is C-DEBI contribution 285. This manuscript is dedicated to the memory of co-author Katrina J. Edwards.

REFERENCES

Altschul, S. F., Madden, T. L., Schaffer, A. A., Zhang, J. H., Zhang, Z., Miller, W., et al. (1997). Gapped BLAST and PSI-BLAST: a new generation of protein database search programs. *Nucleic Acids Res.* 25, 3389–3402. doi: 10.1093/nar/25.17.3389

Bach, W., and Edwards, K. J. (2003). Iron and sulfide oxidation within the basaltic ocean crust: implications for chemolithoautotrophic microbial biomass production. *Geochim. Cosmochim. Acta* 67, 3871–3887. doi: 10.1016/S0016-7037(03)00304-1

Baquiran, J. P., Thater, B., Songco, K., and Crowley, D. E. (2012). Characterization of culturable PAH and BTEX degrading bacteria from heavy oil of the Rancho La Brea tarpits. *Poly Aromat. Comp.* 32, 600–614. doi: 10.1080/10406638.2011.651678

Becker, K., and Davis, E. E. (2005). "A review of CORK designs and operations during the ocean drilling program," in *Proceedings of the IODP,* eds A. T. Fisher, T. Urabe and A. Klaus. (College Station, TX: Integrated Ocean Drilling Program Management International Inc.). doi: 10.2204/iodp.proc.301.104.2005

Biddle, J. F., Lipp, J. S., Lever, M. A., Lloyd, K. G., Sørensen, K. B., Anderson, R., et al. (2006). Heterotrophic archaea dominate sedimentary subsurface ecosystems off Peru. *Proc. Natl. Acad. Sci. U.S.A.* 103, 3846–3851. doi: 10.1073/pnas.0600035103

Binga, E. K., Lasken, R. L., and Neufeld, J. D. (2008). Something from (almost) nothing: the impact of multiple displacement amplification on microbial ecology. *ISME J.* 2, 233–241. doi: 10.1038/ismej.2008.10

Brazelton, W. J., Schrenk, M. O., Kelley, D. S., and Baross, J. A. (2006). Methane- and sulfur-metabolizing microbial communities dominate the Lost City hydrothermal field ecosystem. *Appl. Environ. Microbiol.* 72, 6257–6270. doi: 10.1128/AEM.00574-06

Cowen, J. P., Copson, D. A., Jolly, J., Hsieh, C. C., Lin, H. T., Glazer, B. T., et al. (2012). Advanced instrument system for real-time and time-series microbial geochemical sampling of the deep (basaltic) crustal biosphere. *Deep Sea Res. Part I Oceanogr. Res. Papers* 61, 43–56. doi: 10.1016/j.dsr.2011.11.004

Cowen, J. P., Giovannoni, S. J., Kenig, F., Johnson, H. P., Butterfield, D., Rappe, M. S., et al. (2003). Fluids from aging ocean crust that support microbial life. *Science* 299, 120–123. doi: 10.1126/science.1075653

Davis, E. E., Becker, K., Pettigrew, T., Carson, B., and Macdonald, R. (1992). "CORK: a hydrologic seal and downhole observatory for deep ocean boreholes," in *Proceedings of ODP, Initial Reports, Ocean Drilling Program,* eds E. E. Davis, M. Mottl and A. T. Fisher (College Station, TX). doi: 10.2973/odp.proc.ir.139.103.1992

Desantis, T. Z., Hugenholtz, P., Larsen, N., Rojas, M., Brodie, E. L., Keller, K., et al. (2006). Greengenes, a chimera-checked 16S rRNA gene database and workbench compatible with ARB. *Appl. Environ. Microbiol.* 72, 5069–5072. doi: 10.1128/AEM.03006-05

D'hondt, S., Jorgensen, B. B., Miller, D. J., Batzke, A., Blake, R., Cragg, B. A., et al. (2004). Distributions of microbial activities in deep subseafloor sediments. *Science* 306, 2216–2221. doi: 10.1126/science.1101155

Drummond, A. J., Ashton, B., Buxton, S., Cheung, M., Cooper, A., Duran, C., et al. (2012). *Geneious v5.6*. Biomatters Ltd.

Edwards, K. J., Bach, W., Wheat, C. G., Orcutt, B. N., Hulme, S., Becker, K., et al. (2012a). "Design and deployment of borehole observatories and experiments during IODP Expedition 336, Mid-Atlantic Ridge flank at North Pond," in *Proceedings of the IODP,* eds K. J. Edwards, W. Bach, A. Klaus and E. Scientists (Tokyo: Integrated Ocean Drilling Program Management International Inc.). doi: 10.2204/iodp.proc.336.109.2012

Edwards, K. J., Fisher, A. T., and Wheat, C. G. (2012b). The deep subsurface biosphere in igneous ocean crust: frontier habitats for microbiological exploration. *Front. Microbiol.* 3:8. doi: 10.3389/fmicb.2012.00008

Edwards, K. J., Glazer, B. T., Rouxel, O. J., Bach, W., Emerson, D., Davis, R. E., et al. (2011a). Ultra-diffuse hydrothermal venting supports Fe-oxidizing bacteria and massive umber deposition at 5000m off Hawaii. *ISME J.*, 1748–1758. doi: 10.1038/ismej.2011.48

Edwards, K. J., Mccollom, T. M., Konishi, H., and Buseck, P. R. (2003). Seafloor bioalteration of sulfide minerals: results from *in situ* incubation studies. *Geochim. Cosmochim. Acta* 67, 2843–2856. doi: 10.1016/S0016-7037(03)00089-9

Edwards, K. J., Wheat, C. G., and Sylvan, J. B. (2011b). Under the sea: microbial life in volcanic oceanic crust. *Nat. Rev. Microbiol.* 9, 703–712. doi: 10.1038/nrmicro2647

Eilers, H., Pernthaler, J., Glöckner, F. O., and Amann, R. (2000). Culturability and in situ abundance of pelagic bacteria from the North Sea. *Appl. Environ. Microbiol.* 66, 3044–3051. doi: 10.1128/AEM.66.7.3044-3051.2000

Elderfield, H., and Schultz, A. (1996). Mid-ocean ridge hydrothermal fluxes and the chemical composition of the ocean. *Annu. Rev. Earth Planet. Sci.* 24, 191–224. doi: 10.1146/annurev.earth.24.1.191

Eloe, E. A., Malfatti, F., Gutierrez, J., Hardy, K., Schmidt, W. E., Pogliano, K., et al. (2011). Isolation and characterization of a psychropiezophilic alphaproteobacterium. *Appl. Environ. Microbiol.* 77, 8145–8153. doi: 10.1128/AEM.05204-11

Emerson, D., Fleming, E. J., and Mcbeth, J. M. (2010). Iron-oxidizing bacteria: an environmental and genomic perspective. *Annu. Rev. Microbiol.* 64, 561–583. doi: 10.1146/annurev.micro.112408.134208

Fisher, A. T., Tsuji, T., Petronotis, K., and Scientists, E. (2011). "Design, deployment and status of borehole observatory systems used for single-hole and cross-hole experiments, IODP Expedition 327, eastern flank of the Juan de Fuca Ridge," in *Proceedings of the IODP,* Vol. 327. (Tokyo), doi: 10.2204/iodp.proc.327.107.2011

Fisher, A. T., Tsuji, T., Petronotis, K., Wheat, C. G., Becker, K., Clark, J. F., et al. (2012). IODP Expedition 327 and Atlantis Expedition AT 18-07:Observatories and Experiments on the Eastern Flank of the Juan de Fuca Ridge. *Sci. Drill.* 13, 4–11. doi: 10.5194/sd-13-4-2012

Fisher, A. T., Wheat, C. G., Becker, K., Davis, E. E., Jannasch, H., Schroeder, D., et al. (2005). "Scientific and technical design and deployment of long-term subseafloor observatories for hydrogeologic and related experiements, IODP Expedition 301, Eastern flank of the Juan de Fuca Ridge," in *Proceedings of the IODP,* eds A. T. Fisher, T. Urabe and A. Klaus (College Station, TX: Integrated Ocean Drilling Program Management International Inc.), 1–39. doi: 10.2204/iodp.proc.301.103.2005

Goffredi, S. K., Orphan, V. J., Rouse, G. W., Jahnke, L., Embaye, T., Turk, K., et al. (2005). Evolutionary innovation: a bone-eating marine symbiosis. *Environ. Microbiol.* 7, 1369–1378. doi: 10.1111/j.1462-2920.2005.00824.x

Guindon, S., and Gascuel, O. (2003). A simple, fast, and accurate algorithm to estimate large phylogenies by maximum likelihood. *Syst. Biol.* 52, 696–704. doi: 10.1080/10635150390235520

Huber, J. A., Johnson, H. P., Butterfield, D. A., and Baross, J. A. (2006). Microbial life in ridge flank crustal fluids. *Environ. Microbiol.* 8, 88–99. doi: 10.1111/j.1462-2920.2005.00872.x

Huber, J. A., Mark Welch, D., Morrison, H. G., Huse, S. M., Neal, P. R., Butterfield, D. A., et al. (2007). Microbial population structures in the deep marine biosphere. *Science* 318, 97–100. doi: 10.1126/science.1146689

Huber, T., Faulkner, G., and Hugenholtz, P. (2004). Bellerophon: a program to detect chimeric sequences in multiple sequence alignments. *Bioinformatics* 20, 2317–2319. doi: 10.1093/bioinformatics/bth226

Hugler, M., Wirsen, C. O., Fuchs, G., Taylor, C. D., and Sievert, S. M. (2005). Evidence for autotrophic CO2 fixation via the reductive tricarboxylic acid cycle by members of the epsilon subdivision of proteobacteria. *J. Bacteriol.* 187, 3020–3027. doi: 10.1128/JB.187.9.3020-3027.2005

Jannasch, H. W., Wheat, C. G., Plant, J. N., Kastner, M., and Stakes, D. S. (2004). Continuous chemical monitoring with osmotically pumped water samplers: OsmoSampler design and applications. *Limnol. Oceanogr. Methods* 2, 102–113. doi: 10.4319/lom.2004.2.102

Jørgensen, B. B., and Boetius, A. (2007). Feast and famine–microbial life in the deep-sea bed. *Nat. Rev. Microbiol.* 5, 770–781. doi: 10.1038/nrmicro1745

Jungbluth, S. P., Grote, J., Lin, H., Cowen, J. P., and Rappe, M. S. (2013). Microbial diversity within basement fluids of the sediment-buried Juan de Fuca Ridge flank. *ISME J.* 7, 161–172. doi: 10.1038/ismej.2012.73

Kallmeyer, J., Pockalny, R., Adhikari, R. R., Smith, D. C., and D'hondt, S. (2012). Global distribution of microbial abundance and biomass in subseafloor sediment. *Proc. Natl. Acad. Sci. U.S.A.* 109, 16213–16216. doi: 10.1073/pnas.1203849109

Lever, M. A. (2013). Functional gene surveys from ocean drilling expeditions - a review and perspective. *FEMS Microbiol. Ecol.* 84, 1–23. doi: 10.1111/1574-6941.12051

Lever, M. A., Alperin, M., Engelen, B., Inagaki, F., Nakagawa, S., Steinsbu, B. O., et al. (2006). Trends in basalt and sediment core contamination during IODP Expedition 301. *Geomicrobiol. J.* 23, 517–530. doi: 10.1080/01490450600897245

Lever, M. A., Alperin, M. J., Teske, A., Heuer, V. B., Schmidt, F., Hinrichs, K. U., et al. (2010). Acetogenesis in deep subseafloor sediments of The Juan de Fuca Ridge Flank: a synthesis of geochemical, thermodynamic, and gene-based evidence. *Geomicrobiol. J.* 27, 183–211. doi: 10.1080/01490450903456681

Li, L., Kato, C., and Horikoshi, K. (1999). Microbial diversity in sediments collected from the deepest cold-seep area, the Japan trench. *Mar. Biotechnol.* 1, 391–400.

Li, H., Yu, Y., Luo, W., Zeng, Y., and Chen, B. (2009). Bacterial diversity in surface sediments from the Pacific Arctic Ocean. *Extremophiles* 13, 233–246. doi: 10.1007/s00792-009-0225-7

Lin, H. T., Cowen, J. P., Olson, E. J., Amend, J. P., and Lilley, M. D. (2012). Inorganic chemistry, gas compositions and dissolved organic carbon in fluids from sedimented young basaltic crust on the Juan de Fuca Ridge flanks. *Geochim. Cosmochim. Acta* 85, 213–227. doi: 10.1016/j.gca.2012.02.017

Lysnes, K., Thorseth, I. H., Steinsbu, B. O., Ovreas, L., Torsvik, T., and Pedersen, R. B. (2004). Microbial community diversity in seafloor basalt from the Arctic spreading ridges. *FEMS Microbiol. Ecol.* 50, 213–230. doi: 10.1016/j.femsec.2004.06.014

Mason, O. U., Di Meo-Savoie, C. A., Van Nostrand, J. D., Zhou, J., Fisk, M. R., and Giovannoni, S. J. (2009). Prokaryotic diversity, distribution, and insights into their role in biogeochemical cycling in marine basalts. *ISME J.* 3, 231–242. doi: 10.1038/ismej.2008.92

Mason, O. U., Di Meo-Savoie, C. A., Van Nostrand, J. D., Zhou, J., Fisk, M. R., and Giovannoni, S. J. (2010). Spatial structure and activity of sedimentary microbial communities underlying a *Beggiatoa* spp. mat in a Gulf of Mexico hydrocarbon seep. *PLoS ONE* 5:e8738. doi: 10.1371/journal.pone.0008738

Methé, B. A., Nelson, K. E., Deming, J. W., Momen, B., Melumud, E., Zhang, X., et al. (2005). The psychrophilic lifestyle as revealed by the genome sequence of Colwellia psychrerythraea 34H through genomic and proteomic analyses. *Proc. Nat. Acad. Sci. U.S.A.* 102, 10913–10918. doi: 10.1073/pnas.0504766102

Mottl, M. J., Wheat, G., Baker, E., Becker, N., Davis, E., Feely, R., et al. (1998). Warm springs discovered on 3.5 Ma oceanic crust, eastern flank of the Juan de Fuca Ridge. *Geology* 26, 51–54.

Nakagawa, S., Takai, K., Inagaki, F., Chiba, H., Ishibashi, J., Kataoka, S., et al. (2005). Variability in microbial community and venting chemistry in a sediment-hosted backarc hydrothermal system: impacts of subseafloor phase-separation. *FEMS Microbiol. Ecol.* 54, 141–155. doi: 10.1016/j.femsec.2005.03.007

Nigro, L. M., Harris, K., Orcutt, B. N., Hyde, A., Clayton-Luce, S., Becker, K., et al. (2012). Microbial communities at the borehole observatory on the Costa Rica Rift flank (Ocean Drilling Program Hole 896A). *Front. Microbiol.* 3:232. doi: 10.3389/fmicb.2012.00232

Orcutt, B. N., Bach, W., Becker, K., Fisher, A. T., Hentscher, M., Toner, B. M., et al. (2011a). Colonization of subsurface microbial observatories deployed in young ocean crust. *ISME J.* 5, 692–703. doi: 10.1038/ismej.2010.157

Orcutt, B. N., and Edwards, K. J. (2014). "Life in the oceanic crust: lessons from subseafloor laboratories," in *Earth and Life Processes Discovered from Subseafloor Environments: A Decade of Science Achieved by the Integrated Ocean Drilling Program (IODP)*, eds R. Stein, D. K. Blackman, F. Inagaki, and H.-C. Larsen (Amsterdam; New York, NY: Elsevier Science), 175–196.

Orcutt, B. N., Larowe, D. E., Biddle, J. F., Colwell, F. S., Glazer, B. T., Reese, B. K., et al. (2013a). Microbial activity in the marine deep biosphere: progress and prospects. *Front. Microbiol.* 4:189. doi: 10.3389/fmicb.2013.00189

Orcutt, B. N., Sylvan, J. B., Knab, N. J., and Edwards, K. J. (2011b). Microbial ecology of the dark ocean above, at, and below the seafloor. *Microbiol. Mol. Biol. Rev.* 75, 361–422. doi: 10.1128/MMBR.00039-10

Orcutt, B. N., Wheat, C. G., Rouxel, O., Hulme, S., Edwards, K. J., and Bach, W. (2013b). Oxygen consumption rates in subseafloor basaltic crust derived from a reaction transport model. *Nat. Commun.* 4:2539. doi: 10.1038/ncomms3539

Orcutt, B., Wheat, C. G., and Edwards, K. J. (2010). Subseafloor ocean crust microbial observatories: development of FLOCS (FLow-through Osmo Colonization System) and evaluation of borehole construction materials. *Geomicrobiol. J.* 27, 143–157. doi: 10.1080/01490450903456772

Parkes, R. J., Cragg, B. A., and Wellsbury, P. (2000). Recent studies on bacterial populations and processes in subseafloor sediments: a review. *Hydrogeol. J.* 8, 11–28. doi: 10.1007/PL00010971

Pedersen, K. (2012). Subterranean microbial populations metabolize hydrogen and acetate under *in situ* conditions in granitic groundwater at 450 m depth in the Aspo Hard Rock Laboratory, Sweden. *FEMS Microbiol. Ecol.* 81, 217–229. doi: 10.1111/j.1574-6941.2012.01370.x

Pedersen, K., Arlinger, J., Eriksson, S., Hallbeck, A., Hallbeck, L., and Johansson, J. (2008). Numbers, biomass and cultivable diversity of microbial populations relate to depth and borehole-specific conditions in groundwater from depths of 4-450 m in Olkiluoto, Finland. *ISME J.* 2, 760–775. doi: 10.1038/ismej.2008.43

Pedersen, K., and Ekendahl, S. (1992). Incorporation of CO2 and introduced organic compounds by bacterial populations in groundwater from the deep crystaline bedrock of the Stripa mine. *J. Gen. Microbiol.* 1992, 369–376. doi: 10.1099/00221287-138-2-369

Pruesse, E., Peplies, J., and Glockner, F. O. (2012). SINA: accurate high-throughput multiple sequence alignment of ribosomal RNA genes. *Bioinformatics* 28, 1823–1829. doi: 10.1093/bioinformatics/bts252

Redmond, M. C., and Valentine, D. L. (2012). Natural gas and temperature structured a microbial community response to the Deepwater Horizon oil spill. *Proc. Natl. Acad. Sci. U.S.A.* 109, 20292–20297. doi: 10.1073/pnas.1108756108

Robador, A., Jungbluth, S. P., Larowe, D. E., Bowers, R. M., Rappe, M. S., Amend, J. P., et al. (2014). Activity and phylogenetic diversity of sulfate-reducing microorganisms in low-temperature subsurface fluids within the upper oceanic crust. *Front. Microbiol.* 5:748. doi: 10.3389/fmicb.2014.00748

Santelli, C. M., Banerjee, N. R., Bach, W., and Edwards, K. J. (2010). Tapping the subsurface ocean crust biosphere: low biomass and drilling-related contamination calls for improved quality controls. *Geomicrobiol. J.* 27, 158–169. doi: 10.1080/01490450903456780

Santelli, C. M., Orcutt, B. N., Banning, E., Bach, W., Moyer, C. L., Sogin, M. L., et al. (2008). Abundance and diversity of microbial life in ocean crust. *Nature* 453, 653–656. doi: 10.1038/nature06899

Schloss, P. D. (2009). A high-throughput DNA sequence aligner for microbial ecology studies. *PLoS ONE* 4:e8230. doi: 10.1371/journal.pone.0008230

Iodp 2003-2013 Initial Science Plan (2001). *Scientific Investigation of the Earth System Using Multiple Drilling Platforms and New Technologies, Integrated Ocean Drilling Program Initial Science Plan 2003-2013*. International Working Group Support Office, Integrated Ocean Drilling Progam, Washington DC.

Schauer, R., Bienhold, C., Ramette, A., and Harder, J. (2010). Bacterial diversity and biogeography in deep-sea surface sediments of the South Atlantic Ocean. *ISME J.* 4, 159–170. doi: 10.1038/ismej.2009.106

Schauer, R., Røy, H., Augustin, N., Gennerich, H.-H., Peters, M., Wenzhoefer, F., et al. (2011). Bacterial sulfur cycling shaped microbial communities in surface sediments of an ultramafic hydrothermal vent field. *Environ. Microbiol.* 13, 2633–2648.

Smith, A., Popa, R., Fisk, M., Nielsen, M., Wheat, C. G., Jannasch, H., et al. (2011). *In situ* enrichment of ocean crust microbes on igneous minerals and glasses using an osmotic flow-through device. *Geochem. Geophys. Geosyst.* 12, 1525–2027. doi: 10.1029/2010GC003424

Sogin, M. L., Morrison, H. G., Huber, J. A., Mark Welch, D., Huse, S. M., Neal, P. R., et al. (2006). Microbial diversity in the deep sea and the underexplored "rare biosphere." *Proc. Natl. Acad. Sci. U.S.A.* 103, 12115–12120. doi: 10.1073/pnas.0605127103

Suzuki, M. T., and Giovannoni, S. J. (1996). Bias cuased by template annealing in the amplification of mixtures of 16S rRNA genes by PCR. *Appl. Environ. Microbiol.* 62, 625–630.

Sylvan, J. B., Toner, B. M., and Edwards, K. J. (2012). Life and death of deep-sea vents: bacterial diversity and ecosystem succession on inactive hydrothermal sulfides. *MBio* 3, e00279–e00211. doi: 10.1128/mBio.00279-11

Teske, A., Hinrichs, K. U., Edgcomb, V., De Vera Gomez, A., Kysela, D., Sylva, S. P., et al. (2002). Microbial diversity of hydrothermal sediments in the guaymas basin: evidence for anaerobic methanotrophic communities. *Appl. Environ. Microbiol.* 68, 1994–2007. doi: 10.1128/aem.68.4.1994-2007.2002

Teske, A., and Sørensen, K. B. (2008). Uncultured archaea in deep marine subsurface sediments: have we caught them all? *ISME J.* 2, 3–18. doi: 10.1038/ismej.2007.90

Thamdrup, B., Rossello-Mora, R., and Amann, R. (2000). Microbial manganese and sulfate reduction in Black Sea shelf sediments. *Appl. Environ. Microbiol.* 66, 2888–2897. doi: 10.1128/AEM.66.7.2888-2897.2000

Thorseth, I. H., Torsvik, T., Torsvik, V., Daae, F. L., Pedersen, R. B., and Keldysh-98 Sci, P. (2001). Diversity of life in ocean floor basalt. *Earth Planet. Sci. Lett.* 194, 31–37. doi: 10.1016/S0012-821X(01)00537-4

Toner, B. M., Lesniewski, R. A., Marlow, J. J., Briscoe, L. J., Santelli, C. M., Bach, W., et al. (2013). Mineralogy drives bacterial biogeography of hydrothermally inactive seafloor sulfide deposits. *Geomicrobiol. J.* 30, 313–326. doi: 10.1080/01490451.2012.688925

Weisburg, W. G., Barns, S. M., Pelletier, D. A., and Lane, D. J. (1991). 16S ribosomal DNA amplification for phylogenetic study. *J. Bacteriol.* 173, 697–703.

Wheat, C. G., Jannasch, H., Kastner, M., Hulme, S., Cowen, J., Edwards, K. J., et al. (2011). "Fluid sampling from oceanic borehole observatories: design and methods for CORK activities (1990-2010)," in *Proceedings of the IODP,* Vol. 327. (Tokyo). doi: 10.2204/iodp.proc.327.109.2011

Wheat, C. G., Jannasch, H. W., Fisher, A. T., Becker, K., Sharkey, J., and Hulme, S. (2010). Subseafloor seawater-basalt-microbe reactions: Continuous sampling of borehole fluids in a ridge flank environment. *Geochem. Geophys. Geosyst.* 11:Q07011. doi: 10.1029/2010GC003057

Wheat, C. G., Jannasch, H. W., Kastner, M., Plant, J. N., and Decarlo, E. H. (2003a). Seawater transport and reaction in upper oceanic basaltic basement: chemical data from continuous monitoring of sealed boreholes in a ridge flank environment. *Earth Planet. Sci. Lett.* 216, 549–564. doi: 10.1016/S0012-821X(03)00549-1

Wheat, C. G., Jannasch, H. W., Kastner, M., Plant, J. N., Decarlo, E. H., and Lebon, G. (2004). Venting formation fluids from deep-sea boreholes in a ridge flank setting: ODP Sites 1025 and 1026. *Geochem. Geophys. Geosyst.* 5:Q08007. doi: 10.1029/2004GC000710

Wheat, C. G., McManus, J., Mottl, M. J., and Giambalvo, E. (2003b). Oceanic phosphorus imbalance: magnitude of the mid-ocean ridge flank hydrothermal sink. *Geophys. Res. Lett.* 30:1895. doi: 10.1029/2003gl017318

Wheat, C. G., and Mottl, M. J. (2000). Composition of pore and spring waters from Baby Bare: global implications of geochemical fluxes from a ridge flank hydrothermal system. *Geochim. Cosmochim. Acta* 64, 629–642. doi: 10.1016/S0016-7037(99)00347-6

Whitman, W. B., Coleman, D. C., and Wiebe, W. J. (1998). Prokaryotes: the unseen majority. *Proc. Natl. Acad. Sci. U.S.A.* 95, 6578–6583. doi: 10.1073/pnas.95.12.6578

Wirsen, C. O., Sievert, S. M., Cavanaugh, C. M., Molynaeux, S. J., Ahmad, A., Taylor, L. T., et al. (2002). Characterization of an autotrophic sulfide-oxidizing marine Arcobacter sp. that produces filamentous sulfur. *Appl. Environ. Microbiol.* 68, 316–325. doi: 10.1128/AEM.68.1.316-325.2002

Conflict of Interest Statement: The authors declare that the research was conducted in the absence of any commercial or financial relationships that could be construed as a potential conflict of interest.

frontiers in Microbiology

ORIGINAL RESEARCH
published: 06 October 2015
doi: 10.3389/fmicb.2015.01078

Temperature and pressure adaptation of a sulfate reducer from the deep subsurface

*Katja Fichtel[1†], Jörn Logemann[2†], Jörg Fichtel[2], Jürgen Rullkötter[2], Heribert Cypionka[1] and Bert Engelen[1]**

[1] *Paleomicrobiology Group, Institute for Chemistry and Biology of the Marine Environment, University of Oldenburg, Oldenburg, Germany,* [2] *Organic Geochemistry Group, Institute for Chemistry and Biology of the Marine Environment, University of Oldenburg, Oldenburg, Germany*

OPEN ACCESS

Edited by:
Jason B. Sylvan, Texas A&M University, USA

Reviewed by:
Gordon Webster, Cardiff University, UK
Aude Picard, Harvard University, USA
Alberto Robador, University of Southern California, USA

***Correspondence:**
Bert Engelen, Paleomicrobiology Group, Institute for Chemistry and Biology of the Marine Environment, University of Oldenburg, Carl-von-Ossietzky-Straße 9-11, 26129 Oldenburg, Germany
engelen@icbm.de

† These authors have contributed equally to this work.

Specialty section:
This article was submitted to Extreme Microbiology, a section of the journal Frontiers in Microbiology

Received: *20 May 2015*
Accepted: *21 September 2015*
Published: *06 October 2015*

Citation:
Fichtel K, Logemann J, Fichtel J, Rullkötter J, Cypionka H and Engelen B (2015) Temperature and pressure adaptation of a sulfate reducer from the deep subsurface. Front. Microbiol. 6:1078. doi: 10.3389/fmicb.2015.01078

Microbial life in deep marine subsurface faces increasing temperatures and hydrostatic pressure with depth. In this study, we have examined growth characteristics and temperature-related adaptation of the *Desulfovibrio indonesiensis* strain P23 to the *in situ* pressure of 30 MPa. The strain originates from the deep subsurface of the eastern flank of the Juan de Fuca Ridge (IODP Site U1301). The organism was isolated at 20°C and atmospheric pressure from ~61°C-warm sediments approximately 5 m above the sediment–basement interface. In comparison to standard laboratory conditions (20°C and 0.1 MPa), faster growth was recorded when incubated at *in situ* pressure and high temperature (45°C), while cell filamentation was induced by further compression. The maximum growth temperature shifted from 48°C at atmospheric pressure to 50°C under high-pressure conditions. Complementary cellular lipid analyses revealed a two-step response of membrane viscosity to increasing temperature with an exchange of unsaturated by saturated fatty acids and subsequent change from branched to unbranched alkyl moieties. While temperature had a stronger effect on the degree of fatty acid saturation and restructuring of main phospholipids, pressure mainly affected branching and length of side chains. The simultaneous decrease of temperature and pressure to ambient laboratory conditions allowed the cultivation of our moderately thermophilic strain. This may in turn be one key to a successful isolation of microorganisms from the deep subsurface adapted to high temperature and pressure.

Keywords: ***Desulfovibrio*, fatty acids, intact polar lipids, Juan de Fuca Ridge, ornithine, phospholipids**

Introduction

The volume of world's oceans 200 m below sea level constitutes more than 95% of all aquatic habitats (Michiels et al., 2008). Additionally, the subseafloor represents a large reservoir for prokaryotic life (Whitman et al., 1998; Kallmeyer et al., 2012) and even extends into the upper oceanic crust (Heberling et al., 2010; Edwards et al., 2011; Orcutt et al., 2011).

Most studies to identify the microbial diversity within the deep marine subsurface are based on cultivation-independent approaches (Marchesi et al., 2001; Kormas et al., 2003; Inagaki et al., 2006; Webster et al., 2006; Biddle et al., 2008). Cultivation attempts are increasing (Bale et al., 1997; Wellsbury et al., 2002; Batzke et al., 2007; Kobayashi et al., 2008; Miyazaki et al., 2012; Takai et al., 2013), but are still the exception. Even though novel high-throughput techniques such as

metagenomics or single cell genomics are important for predicting *in situ* ecological functions (Teske, 2006; Lauro and Bartlett, 2008), the isolation of microorganisms from deep ecosystems is seen as the "gold standard" to identify putative physiological capabilities and specific adaptation mechanisms (Giovannoni and Stingl, 2007) to subseafloor habitats. Thus, isolates are still indispensable to verify metabolic pathways that are only detected by *in silico* analysis.

One interesting aspect to be analyzed on deep subsurface microorganisms is their ability to live under elevated hydrostatic pressure. Taking the deep ocean, the marine subsurface and the oceanic crust into account, the majority of all prokaryotic cells in the environment are facing high-pressure conditions. High hydrostatic pressure has 'pervasive effects' (Eloe et al., 2011) on microbial physiology, influencing macromolecular structures or cellular processes such as metabolisms, cell growth, viability, and motility (Bartlett, 2002; Abe, 2007). Previous investigations of pressure adaptation of marine microorganisms were performed mainly on psychrophilic deep-sea bacteria (DeLong and Yayanos, 1985; Wirsen et al., 1986; Kato et al., 2008) and some data exist for thermophilic bacteria and hyperthermophilic archaea from hydrothermal vents (Jannasch et al., 1992; Alain et al., 2002). Physiological data on mesophilic piezophiles were limited to a few isolates (Kaneko et al., 2000; Alazard et al., 2003; Khelaifia et al., 2011). Recent studies on these bacteria include isolates affiliated to *Shewanella profunda* (Toffin et al., 2004; Picard et al., 2015), *Shewanella piezotolerans* (Xiao et al., 2007; Wang et al., 2009; Wu et al., 2013), *Desulfovibrio hydrothermalis* (Amrani et al., 2014), and *Desulfovibrio piezophilus* (Khelaifia et al., 2011; Pradel et al., 2013). Moreover, pressure studies on isolates from marine subsurface sediments are rare (Bale et al., 1997; Barnes et al., 1998; Mangelsdorf et al., 2005; Toffin et al., 2005). Generally, the adaptation capacity depends on the ability of microorganisms to regulate structure and organization of their cell membrane as a response to changes in temperature and pressure in order to maintain the membrane fluidity necessary for sustaining biological functions ('homeoviscous adaptation', see Sinensky, 1974; Macdonald, 1988; Somero, 1992; Kaye and Baross, 2004). The reorganization of membrane constituents and proteins influences the membrane lipid composition, the degree of saturation of membrane-bound fatty acids (FAs), as well as their chain length and branching (DeLong and Yayanos, 1985, 1986; Wirsen et al., 1986; Yano et al., 1998; Mangelsdorf et al., 2005).

In our previous study, we have isolated several sulfate-reducing bacteria from subsurface sediments of the Juan de Fuca Ridge (Fichtel et al., 2012). The isolates were obtained from depths down to 260 m below the seafloor, about 5 m above the sediment–basement interface. The sampling location (IODP Site U1301) was target of several microbiological investigations of the sediments (Lever et al., 2010) but much more of the oceanic crust below (Jungbluth et al., 2014; Robador et al., 2015). IODP site U1301 exhibited a water depth of 2656 m, corresponding to an *in situ* pressure of ∼30 MPa for the deepest sediments analyzed. At this site, highly compacted hemipelagic clay with a particle size of <2 μm and a bulk density of ∼2 g/cm^3 covers the basaltic crust (Zühlsdorff et al., 2005). The sediments serve as a hydrogeologic barrier for advective fluid-flow from the basaltic aquifer into the sediments and do not allow any transportation of larger particles such as microbial cells. On the other hand, low-temperature hydrothermal fluids diffuse from the underlying oceanic crust into the sediment column, resulting in a steep temperature gradient of 2 to 62°C from the ocean floor to the basement. These crustal fluids provide energy sources like sulfate (16 mM) from below, thus stimulating sulfate-reducing communities to thrive within this habitat (Engelen et al., 2008).

Pure cultures were obtained under standard laboratory conditions, i.e., at atmospheric pressure and 20°C. The sulfate-reducing bacteria isolated from the deepest sediments above the basement solely belonged to the Deltaproteobacteria, namely one *Desulfotignum balticum*-affiliated strain from 260 m below seafloor (mbsf) and three strains related to *Desulfovibrio indonesiensis* from 240, 252, and 260 mbsf. As members of the *Deltaproteobacteria* are not known for forming resting stages, they are presumed to belong to active microbial populations of the deep subsurface. Physiological characterization of the isolates revealed that the *D. indonesiensis*-affiliated strains have a temperature range of growth from 10 to 48°C, and exhibit both, a chemoheterotrophic and lithoautotrophic lifestyle (Fichtel et al., 2012). Interestingly, the temperature range of growth did not reach *in situ* temperatures of 56–61°C. As temperature and pressure can have opposing influence on the cell membrane, an insufficient combination of both parameters may result in an inhibition of cross-membrane processes or even the disintegration of cells (Mangelsdorf et al., 2005). Thus, the question arose whether incubation under *in situ* pressure would induce a shift in their temperature range of growth.

Six sulfate-reducing isolates from deep subsurface sediments of IODP Site U1301 were examined for growth under high pressure and various temperatures. For the present study, we chose *D. indonesiensis* strain P23 as a representative to be analyzed in more detail. The isolate derived from the deepest sediment sample and exhibited relatively fast growth both, under high hydrostatic pressure and high temperatures. Microbiological investigations such as microscopic analyses and measurements of growth rates at different combinations of temperatures and pressures were complemented by membrane-lipid analysis to identify a cellular response to changing incubation conditions.

Materials and Methods

Bacterial Strains, their Origin and Growth Conditions

Pure cultures of strictly anaerobic, sulfate-reducing bacteria used in this study were obtained from up to 260 m deep subseafloor sediments. Samples were collected in the northeast Pacific at the Eastern Flank of the Juan de Fuca Ridge, IODP Site U1301 (47°45.28′N, 127°45.80′W; water depth: 2656 m) during IODP Expedition 301 in 2004. Details on environmental conditions, sampling, and contamination tests have been reported previously (Expedition 301 Scientists, 2005; Lever et al., 2006; Engelen et al., 2008; Fichtel et al., 2012). Enrichment and isolation of pure

cultures were performed at ambient conditions, i.e., atmospheric pressure of ∼0.1 MPa and 20°C. Cultivation procedures and phylogenetic analyses of cultures obtained are given in Fichtel et al. (2012). Strain P23, affiliated to *D. indonesiensis* (99% 16S rRNA gene sequence similarity), was analyzed representatively for pressure and temperature adaptation in more detail.

Five additional isolates from the same sampling site (*D. indonesiensis* strain P12 from 252 mbsf, *D. indonesiensis* strain P34 from 240 mbsf, *D. aespoeensis* strain P20 from 1.3 mbsf, *Desulfotignum balticum* strain P18 from 260 mbsf, *Desulfosporosinus lacus* strain P26 from 1.3 mbsf), and the type strain of *D. indonesiensis* (Ind1^T, DSM 1512) were analyzed in less detail for comparison. All strains were pre-cultured to early stationary phase at atmospheric pressure and 25 to 35°C in sulfate-containing (28 mM) artificial seawater media that had originally been used for isolation (Fichtel et al., 2012). Lactate (10 mM) or betaine (5 mM) was used as carbon source. Growth was routinely followed by photometrical determination of sulfide in form of colloidal CuS at 480 nm (Cord-Ruwisch, 1985) and of cell protein concentrations at 595 nm after Bradford (1976) as well as by visual inspection of the cells using phase-contrast microscopy. Transmission electron microscopy (TEM) of strain P12 was performed with air-dried, unfixed cells as described by Fichtel et al. (2012).

General Setup for Pressure Incubations

All pure cultures were examined as to whether they were able to grow under pressure (10 to 40 MPa). Bacterial growth experiments were performed in 'high-pressure steel vessels' [High Pressure Equipment (HiP) Company, Linden, PA, USA]. Inoculations were done in 60 or 70 ml serum bottles containing freshly prepared culture media and sealed with rubber stopper and crimp caps. Pre-cultures (4% of final volume) were injected and bottles were completely filled with the respective media avoiding any gas bubbles. Three serum bottles were placed inside a pre-heated pressure vessel filled with distilled water. Samples were set under hydrostatic pressure by means of a hand operated 'high-pressure generator' (model 81-5.75-10, HiP) using distilled water as hydraulic fluid. For subsampling, the vessel was carefully depressurized (∼1 min). The bottles were subsampled (5–6 ml) for growth analyses as quickly as possible (15–30 min), refilled with media to get completely filled serum bottles and again compressed within a few minutes. Pressurized samples were incubated between 1 and 16 days depending on growth behavior. Growth at hydrostatic pressure was defined to be positive after two independent successful experiments. Growth at 0.1 MPa was assessed by using the same protocol except for pressurization. As the assays at 0.1 MPa were treated in the same way, an effect of dilution can be neglected. In general, all assays were carried out in triplicate and repeated at least twice.

Hydrostatic Pressure Effects on Growth of *D. indonesiensis* Strain P23

To record the growth behavior of *D. indonesiensis* strain P23, pressure incubations were performed as described above. Growth curves and specific growth rates in response to different hydrostatic pressures were assessed by comparing the amount of sulfide and protein formed during defined times of incubation at low and high temperature. Specific growth rates were calculated from three to five data points along the logarithmic slope of the exponential portion of sulfide and protein curves using linear regression analysis.

The upper temperature limit for growth of *D. indonesiensis* strain P23 under high pressure was determined as follows: In pre-experiments, growth was tested in the range of 45 to 62°C at 20, 26, and 30 MPa. To reach the upper limit, growth curves were finally recorded in parallels at both, 0.1 and 20 MPa with slowly increasing temperatures from 45 to 52°C. Cultures grown at 45°C were allowed to adapt to higher temperatures for nine hours before incubation at 48°C. Temperature was increased again to 50°C after 12 h and to 52°C after 36 h of incubation. Pressure vessels were decompressed for growth analyses at the end of each temperature step as described above. After subsampling, serum bottles were refilled with fresh medium to circumvent substrate limitation.

Cultivation and Extraction for Lipid Analysis

For determination of whole cellular FAs and intact polar lipids (IPLs) *D. indonesiensis* strain P23 was grown as described above at 20, 35, and 45°C at both, 0.1 and 30 MPa, in total culture volumes of 1.5 to 2.2 l. To obtain enough cell material, all pressure incubations were performed in parallels of up to 30 serum bottles using several pressure cylinders. To compensate for growth phase differences (Hamamoto et al., 1994; Allen et al., 1999), cells of each experiment were immediately harvested at late exponential growth phase, combined by centrifugation at 4°C, and stored at −20°C until further analyses. Total lipids were obtained by ultrasonic extraction from each washed cell pellet following a modified Bligh & Dyer procedure (Sturt et al., 2004) as described by Logemann et al. (2011). The lipid extracts were combined and evaporated to dryness under nitrogen at room temperature, stored at −20°C and analyzed by combined gas chromatography and mass spectrometry (GC–MS).

Cellular FAs

The technical procedures were adapted from Rütters et al. (2002). In detail, aliquots of the total lipid extracts were transesterified with trimethylsulfonium hydroxide as described by Müller et al. (1990). FA methyl esters obtained were quantified by using a gas chromatograph (7890A GC-System Agilent Technologies, Santa Clara, CA, USA) equipped with a flame ionization detector (FID) and a capillary column (DB-5HT, length 30 m, ID 0.25 mm, 0.1 μm film thickness; J&W Scientific, Folsom, CA, USA). Identification was performed on a GC-MS system consisting of an HP 5890 Series II gas chromatograph (Hewlett Packard, Waldbronn, Germany) equipped with a DB-5HT column and coupled to a Finnigan MAT SSQ 710B mass spectrometer (Finnigan-Thermoquest, San Jose, CA, USA). Helium with a constant pressure of 12 psi was used for both systems. The GC oven temperature was raised from 60°C (isothermal for 2 min) to 360°C at a rate of 3°C min^{-1} and held for 5 min. Mass spectra were collected in full scan mode (*m/z* 50–650, ionization energy 70 eV, and 230°C source temperature). Mass

spectrometric investigations were used to confirm the results obtained with GC-FID. FAs were identified by comparison of the retention times with those of known standards (Bacterial Acid Methyl Esters CP Mix; Supelco, Bellefonte, PA, USA).

Intact Polar Lipids

Intact polar lipids were analyzed from an aliquot of each cell extract using high-performance liquid chromatography (HPLC)–electrospray ionization (ESI)-MS in the negative ion mode as described by Logemann et al. (2011). MS/MS spectra and full scan mass spectra (*m/z* 100–2000) were used for identification of head groups, diacylglycerols (DAGs) or acyl/ether glycerol (AEG) core lipids as well as fatty acyl side chains. Quantification was achieved by using an external multipoint calibration via compound mass trace areas. Phosphatidic acid (PA), phosphatidylglycerol (PG), phosphatidylethanolamine (PE), and phosphatidylinositol (PI) [all from Avanti Polar Lipids, Alabaster, AL, USA; Matreya, Pleasant Gap, PA, USA; Sigma–Aldrich, München, Germany, or Lipid Products, Redhill, UK] were used as standard compounds representative for different IPL classes. Due to the lack of commercially available standards for ornithine lipids (OL) or unknown polar lipids, OL were quantified via the calibration curve for PG (Seidel et al., 2013), while for unknown lipids the average signal response of all standards at every concentration was used.

Results

Growth of Sulfate-reducing Strains under High Hydrostatic Pressure

All Gram-negative sulfate-reducing pure cultures we had previously isolated at atmospheric pressure from subseafloor sediments (Fichtel et al., 2012) exhibited growth under elevated hydrostatic pressure of up to 30 MPa and 35°C (Supplementary Table S1). This was also found for the type strain of *D. indonesiensis* (Ind1^T), which had originally been isolated from a corroding ship at the sea surface (Feio et al., 1998). In contrast, for *Desulfosporosinus lacus* strain P26, spore formation was induced by elevated pressure of up to 20 MPa. Only spores or sporulating cells were observed 10 days after incubation of freshly grown cells. This finding indicates that the original isolate may have been derived from a spore that germinated during the isolation procedure.

The combination of the highest pressure and temperature applied (40 MPa/45°C) severely affected the shape of *D. indonesiensis*-like strains P12 and P23. Instead of forming the typical motile, vibrio-shaped cells (**Figure 1A**) (Fichtel et al., 2012), cell division appeared to be incomplete, and both strains grew as long, straight, or twisted filaments (**Figures 1B–D**). Also, no cell motility was observed during microscopic inspection of the long filaments. Cultures of *D. indonesiensis* strain P23 grown at 45°C revealed a cell length from 1–1.7 μm (±0.17 μm) at atmospheric pressure which increased to an average of 14.7 μm (±5.18 μm) at 40 MPa ($n = 20$). Consequently, growth in further experiments was determined via sulfide formation and by measuring protein production rather than cell counting.

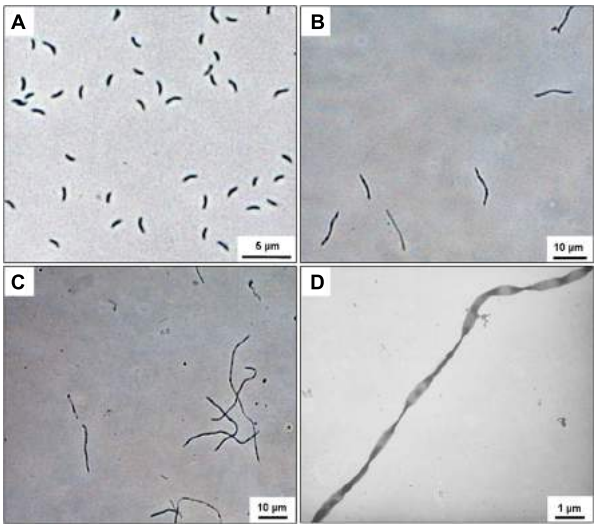

FIGURE 1 | Microscopic images of *Desulfovibrio indonesiensis* strains P12 and P23 grown at 45°C. Phase-contrast image of *D. indonesiensis* strain P23 grown at 0.1 MPa **(A)** and at 40 MPa **(B)**. Phase-contrast image **(C)** and transmission electron microscopy (TEM) **(D)** of *D. indonesiensis* strain P12 grown at 40 MPa.

Specific Growth Rates of *D. indonesiensis* Strain P23

During cultivation experiments with *D. indonesiensis* strain P23 at various pressures (0.1, 10, 20, 30, and 40 MPa) and low or high temperatures (20 or 45°C), we found that increasing pressure reduced the specific growth rate at 20°C. At 45°C and pressures between 10 and 30 MPa, growth appeared to be faster as higher protein contents were determined after a given incubation time (data not shown). Growth curves were recorded in detail for cultures grown to early stationary phase at 20 and 45°C both, at atmospheric conditions and 30 MPa (**Figure 2**). Based on protein production, growth at 20°C was twice as fast at 0.1 MPa as under high-pressure conditions. The exponential growth rate μ was calculated as 0.74 day^{-1} at atmospheric pressure and 0.38 day^{-1} at high pressure. In contrast, growth rates obtained at 45°C under high-pressure conditions (2.38 day^{-1}) were very similar to those at atmospheric pressure (2.24 day^{-1}). A similar trend was determined via sulfide measurement. Comparing all rates, fastest growth was found at 45°C and 30 MPa, indicating the stimulation of growth by both, high temperature and *in situ* pressure. Highest protein yields were obtained at combinations of low temperature and atmospheric pressure (62 mg l^{-1}) as well as high temperature and *in situ* pressure (53 mg l^{-1}). Interestingly, the opposite combination of low temperature and high pressure with ∼40 mg l^{-1} revealed a similarly low yield as at high temperature and low pressure.

Pressure-induced Shift of the Maximum Growth Temperature

During a cultivation experiment to determine the upper temperature limit of growth at elevated hydrostatic pressure (20 MPa), cells were allowed to adapt to slowly increasing

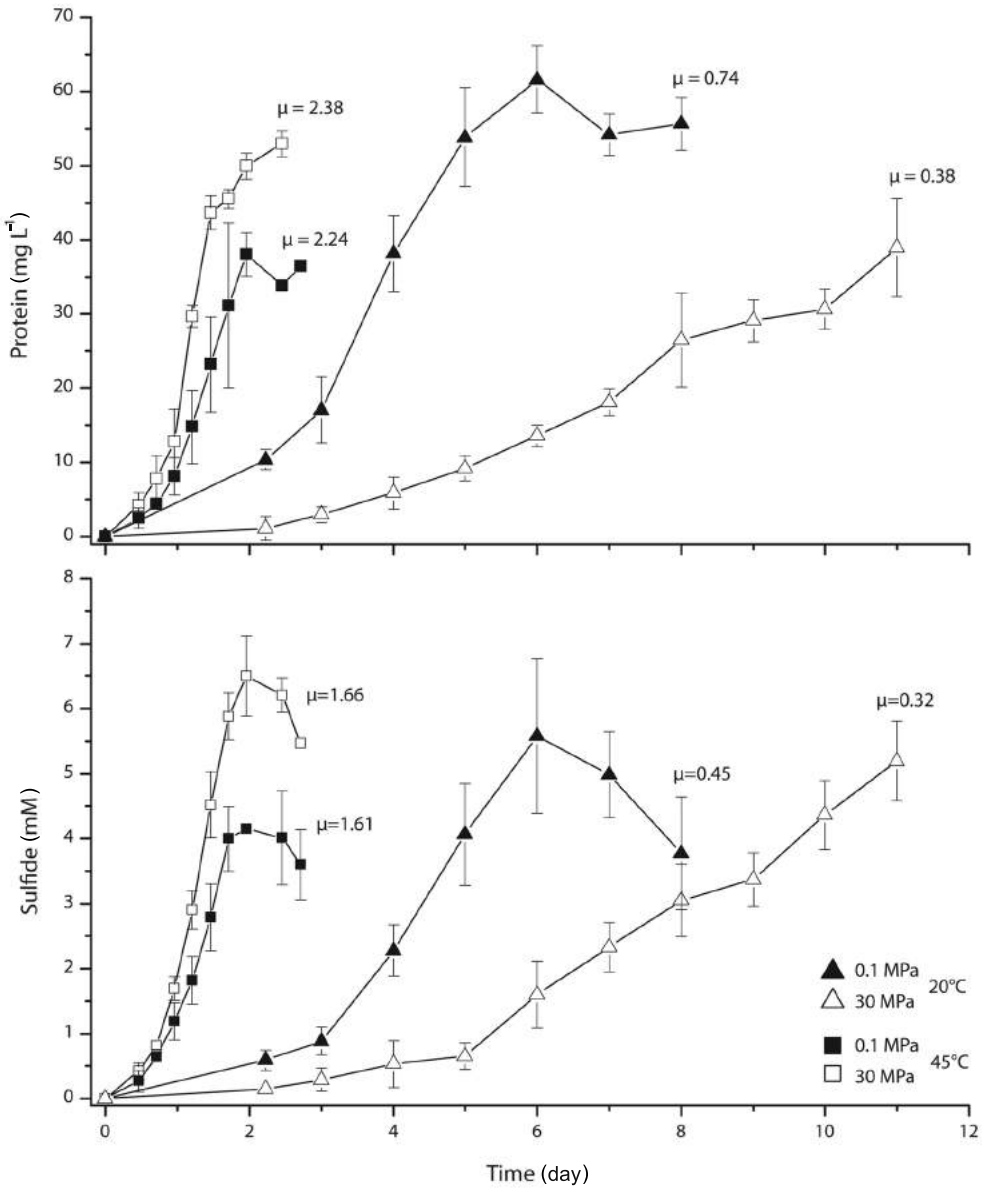

FIGURE 2 | Growth curves and specific growth rates μ (day^{-1}) of *D. indonesiensis* strain P23 grown at atmospheric and high hydrostatic pressure both at 20 and at 45°C. Values were calculated from photometrical measurements of protein and sulfide. Error bars indicate the standard deviation of three cultivation assays.

temperatures (Supplementary Figure S1). After 3 days of incubation in concert with a temperature shift to 50°C, cell counts in pressurized assays were highest at 50°C, reaching 4.04×10^8 cells ml^{-1}. In contrast, cells grown at 0.1 MPa reached their maximum at 48°C (2.23×10^8 cells ml^{-1}). Under these conditions, the previously determined maximum growth temperature of 48°C at atmospheric pressure was shifted to 50°C. At temperatures higher than 50°C, neither an ongoing protein production nor increasing sulfide formation was observed. This was confirmed in further test series that were inoculated with cells freshly grown at 50°C and 20 MPa. The upper temperature limit for growth was again indicated by the observation of highly elongated, non-motile, or deformed cells in comparison to the respective assays at 0.1 MPa.

Changes in Whole-cell FA Composition as a Response to Increasing Temperature and Elevated Pressure

The majority of whole cell FAs of *D. indonesiensis* strain P23 were branched and accounted for up to 79% under atmospheric pressure (Supplementary Table S2). Regardless of growth temperatures and pressures, major components were *iso*- and *anteiso*-branched 15:0 and *n*-18:0 FAs, which was already known for the type strain (Feio et al., 1998). Concerning

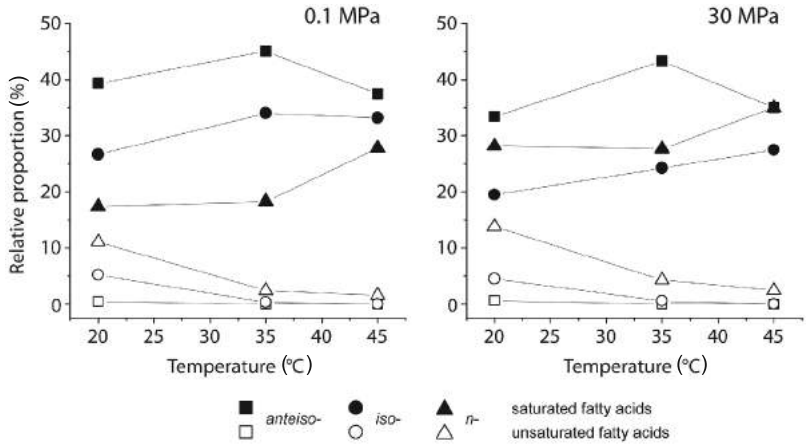

FIGURE 3 | Changes in relative amounts of whole cell fatty acids (FAs) of *D. indonesiensis* strain P23 grown at different temperatures and pressures.

the degree of unsaturation, only monounsaturated FAs were detected.

In comparison to cells grown at atmospheric conditions and 20°C, *D. indonesiensis* strain P23 showed strongly elevated levels of *n*-saturated FAs at the expense of branched-saturated FAs during incubation at the same temperature but high pressure (**Figure 3**; Supplementary Table S2). Under both pressure regimes, a two-step response of *D. indonesiensis* strain P23 was detected for increasing incubation temperatures. First, the relative amount of unsaturated FAs decreased strongly. Second, levels of *n*-saturated FAs increased mainly at the expense of *ai*-branched-saturated FAs. Comparing temperature-dependent incubations under atmospheric and under *in situ* pressure, pressure did not substantially increase the ratio of unsaturated to saturated FAs, but led to a higher *n*-saturation and concomitant decreased branching of FAs. Additionally, relative proportions of longer-chain FAs were substantially elevated under high-pressure conditions only (Supplementary Table S2).

Relative Distribution of Main IPLs Depending on Temperature and Pressure

Under all conditions tested, *D. indonesiensis* strain P23 contained two classes of IPLs: phospholipids (PG, PE, and PA) and the phosphorus- and glycerol-free OL (Supplementary Figure S2; Supplementary Table S3a). Phospholipids mainly contained a DAG-core lipid with ester-bound FA moieties as identified by MS–MS experiments. Additionally, PG was also detected as AEG with mixed ether/ester-bound side chains. Four additional IPLs with unidentified head groups were found (Un1-4). It appears likely that they represent yet unknown phospholipids as they were also detected as DAG or AEG (Supplementary Figures S3 and S4; Supplementary Table S3b).

Comparing the IPL compositions in almost all assays (exception 0.1 MPa and 45°C), the relative proportion of all phospholipids dominated over OLs. At high pressure, this behavior was more pronounced (Supplementary Table S4). For all other experiments at atmospheric pressure with increasing incubation temperatures, the amount of OL increased, while relative proportions of all other IPL except PG-AEG decreased (**Figure 4**). At pressures of 30 MPa, no clear trend in relative IPL proportions was observed. Major shifts with increasing temperatures were found for diacyl-phosphatidylglycerol (PG-DAG) and acyl-ether-phosphatidylglycerol (PG-AEG). While levels of PG-DAG dominated over PG-AEG at low temperature, the opposite ratio was found at higher temperatures. The values of total unknown IPLs (Σ Un 1–4) showed a response to temperature changes similar to that of the phospholipids. In high-pressure cultures, the effect of increasing temperature on the IPL composition was most pronounced between 20 and 35°C.

Composition and Length of IPL Side Chains Change with Cultivation Pressure and Temperature

The majority of analyzed IPLs contained a FA with 15 carbon atoms (Supplementary Table S3a). Moreover, the C_{15}-FA was the only FA component in IPLs with an AEG core. Polyunsaturated FAs were never detected. Ratios of unsaturated to saturated IPLs decreased with rising incubation temperature and were slightly higher in high-pressure assays. These findings are in good accordance with the whole cell FA data (Supplementary Table S2).

Side-chain combinations of PE and PG were quite similar with either C_{14}- or C_{15}-FA together with a C_{15}–C_{20}-moiety at the *sn*-2 position. Interestingly, two unknown IPLs (Un-1 and Un-2) contained either a fairly long FA chain or an ether-bound alkyl moiety of 21–23 carbon atoms. OLs had either 14:0 or 15:0 FAs together with a 3-hydroxy C_{16}–C_{20}-FAs.

Cell response of *D. indonesiensis* strain P23 to pressure and temperature was either reflected in changes of abundance, saturation, or carbon-number distribution of fatty acyl side chains in the three major polar lipids PE, PG, and OL. However, focusing on a single mass of an IPL without MS/MS experiments, several possibilities for the combination of ester- or ether-linked moieties arise. To simplify our data, we used the radyl value comprising the total carbon number of both side chains. As a result, PG generally had the greatest diversity of side chains, which was reflected in the broad range of radyl values from 28

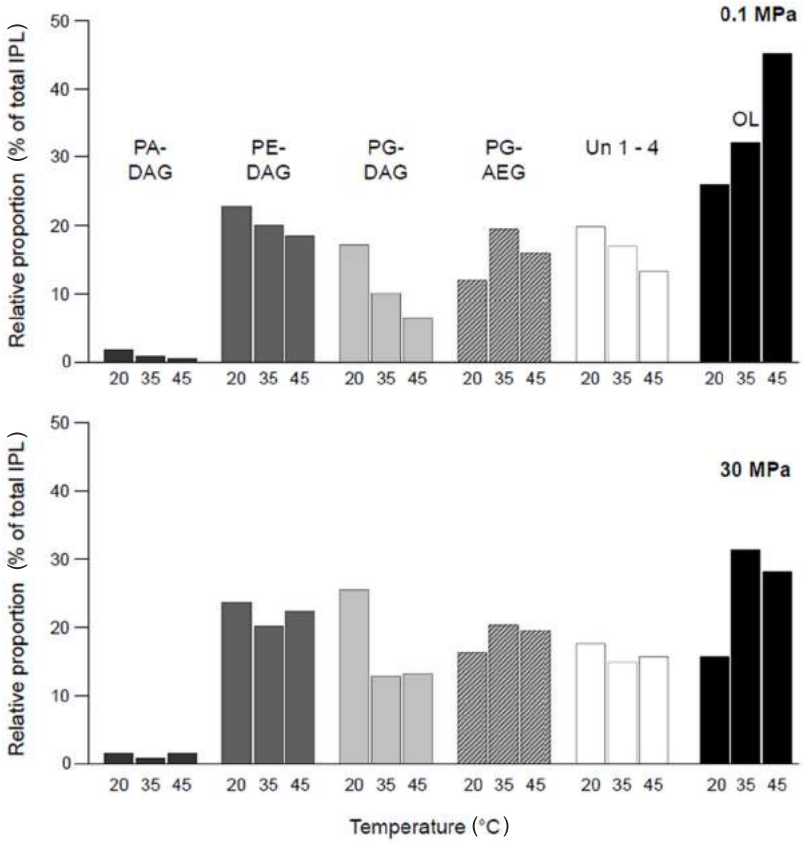

FIGURE 4 | Changes in relative amounts of major intact polar lipid (IPL) species of *D. indonesiensis* strain P23 depending on growth temperature and pressure.

to 37. Radyl values in PE varied between 30 and 36, and between 29 and 35 in OL. The radyl value pattern for PE and PG was dominated by 33 carbon atoms, resulting from high proportions of C_{15}- and C_{18}-FAs, while that of OL was dominated by 32, resulting from C_{15}- and 3-OH-C_{17}-FAs (**Figure 5**).

For PE and PG, higher incubation temperatures induced an increase of longer side chains at the expense of shorter ones. Additionally, at high-pressure incubations, the most abundant PE molecular species with a radyl value of 33 systematically decreased with temperature. Most strikingly, the radyl value pattern of OL was not affected by temperature during high-pressure incubations. Here, the distribution patterns were nearly identical and similar to that obtained at 20°C and 0.1 MPa. In contrast, major structural changes were found at atmospheric pressure and high temperatures with a dramatic increase of the relative proportion of the most dominant OL species with a radyl value of 32 carbon atoms.

In general, levels of unsaturated side chains in all major IPLs were highest at 20°C and decreased strongly with rising incubation temperature. While PE-DAG lipids contained the largest proportion of unsaturated moieties, PG lipids had the greatest diversity of side chains. As the PG pool even showed a temperature-induced restructuring with an internal shift from PG-DAG to PG-AEG, findings indicate that in *D. indonesiensis* strain P23 restructuring of PE and PG was relevant for bilayer stabilization, as a result of both, temperature and pressure changes.

Discussion

Reflecting the *in situ* conditions, our isolate P23 grew fastest at combined high pressure and high temperature. Remarkably, the cells responded to a temperature rise in a much more pronounced way than to elevated pressure. By decreasing pressure and temperature simultaneously, it was even possible to cultivate our moderately piezothermophilic strain from the warm deep subsurface at ambient conditions.

High-pressure Experiments Reveal the Piezothermophilic Nature of *D. indonesiensis* Strain P23

A high-pressure tolerance should demonstrate that microorganisms of the deep biosphere are well adapted to their pressurized subsurface habitat and that they do belong to the active part of deeply buried microbial communities (Bale et al., 1997). In this study, we demonstrated that *D. indonesiensis* strain P23 was able to grow under hydrostatic pressure of up to 40 MPa

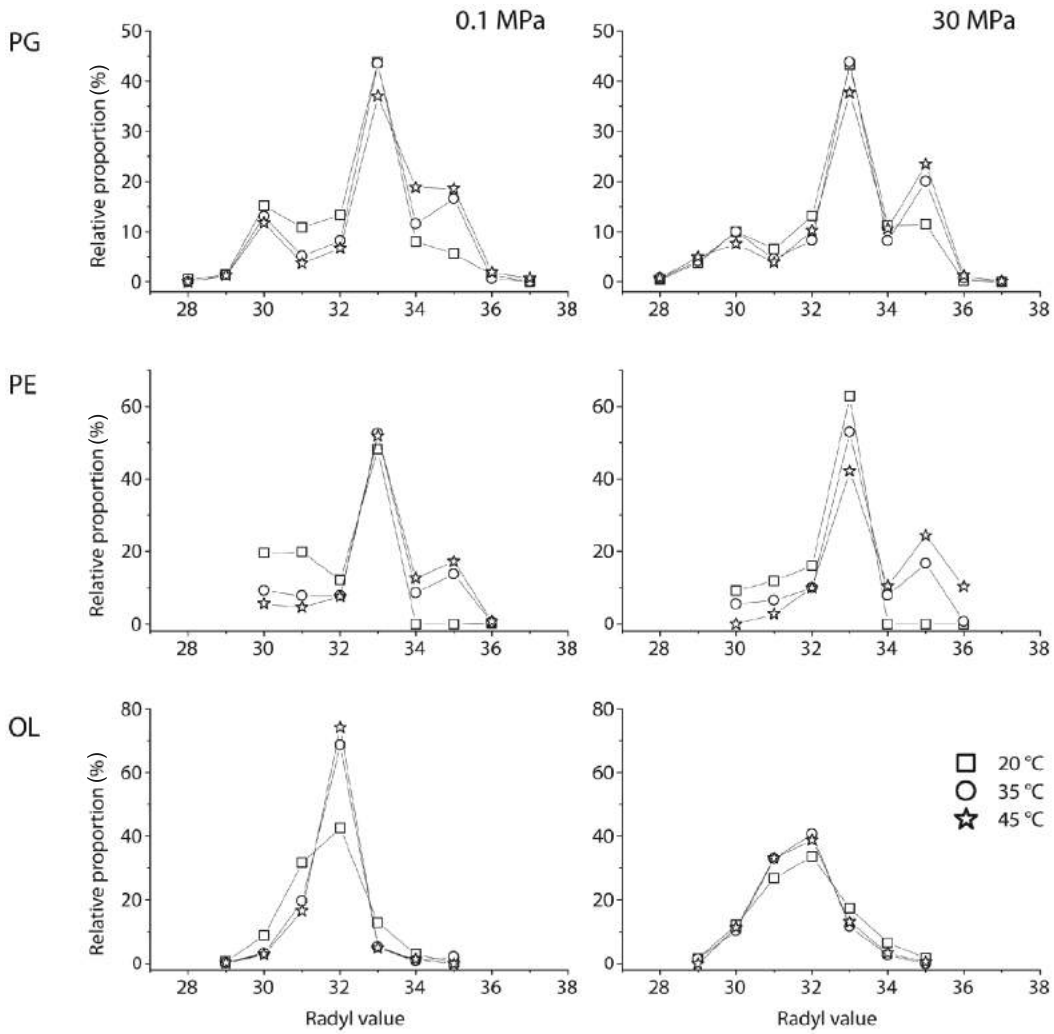

FIGURE 5 | IPLs inventory of strain P23 depending on different incubation conditions. Changes in fatty acyl side-chain length are expressed by radyl values, the combined number of carbon atoms of the two FA substituents of one IPL type. PG, phosphatidylglycerol; PE, phosphatidylethanolamine, and OL, ornithine lipid. PG data is based on the sum of PG-DAG and -AEG.

(*in situ* pressure ~30 MPa), even after cultivation at atmospheric pressure for more than 3 years. *D. indonesiensis* strain P23 obviously has not lost its piezophilic properties, which may be a common feature of pressurized deep-sea organisms sampled and isolated under decompressed conditions (Zobell and Johnson, 1949).

The degree of piezophily was strongly dependent on the incubation temperature (Zobell and Johnson, 1949; Kato et al., 1995). In our previous study (Fichtel et al., 2012), *D. indonesiensis* strain P23 was found to have an upper growth temperature of 48°C. At 20°C, *D. indonesiensis* strain P23 grew at both, atmospheric and elevated hydrostatic pressure with fastest growth rates at 0.1 MPa. In contrast, at higher temperatures, growth was accelerated by high hydrostatic pressure in the broad range from 10 to 30 MPa, and the maximum temperature of growth rose to 50°C only under pressure. Under these conditions, strain P23 would be considered to be moderately piezothermophilic (Yayanos, 1995; Kato and Bartlett, 1997) reflecting its adaptation to the *in situ* conditions present in its original warm subsurface habitat.

However, an increase of growth temperature does not necessarily improve the piezotolerance of microorganisms. For instance, in a study on typical atmosphere-adapted lactic acid bacteria, higher temperatures did not stimulate microbial growth under elevated pressure (Molina-Höppner et al., 2003). Unlike many pressure-adapted species, these lactic acid bacteria and other mesophiles may be unable to develop a specific pressure response in order to maintain membrane fluidity.

During growth at conditions above *in situ* pressure, the cell shape of our isolates changed. With increasing pressure and temperature, cells became more elongated and cell division was inhibited, indicating a typical stress response. Cell filamentation appears to be a characteristic pressure-related phenomenon in mesophilic bacteria (Zobell and Cobet, 1962, 1964; Lauro and

Bartlett, 2008). Pressure is believed to have a direct inhibitory effect on FtsZ ring formation, which is a prerequisite for membrane construction during cell division (Molina-Höppner et al., 2003; Ishii et al., 2004). Filament formation may also be mediated via a pressure-triggered SOS response involving the RecD protein, which is essential for DNA recombination and repair (Bidle and Bartlett, 1999; Aertsen et al., 2004). Interestingly, filamentation has frequently been shown to occur in piezophilic bacteria (e.g., *Marinitoga piezophila*) grown at atmospheric pressure (Alain et al., 2002). Our inverse finding may indicate that filamentation is a more general stress response that is triggered by pressure but works in both directions.

Pressure and Temperature Effects on Membrane Lipid Composition

While the whole cell FA analysis provides a fast overview on all cellular FAs, the analysis of IPLs directly targets the membrane building blocks. The results of both methods can be combined as FAs extracted from the membrane fraction are very similar to those extracted from whole cells (Pluschke and Overath, 1981; Allen et al., 1999; Kaneko et al., 2000).

Due to the theory of 'homeoviscous adaptation of membrane lipids' (Sinensky, 1974; Somero, 1992), it was expected that increasing growth temperature mainly results in a higher degree of saturation of membrane lipids to keep them appropriately fluid for integrity and cell function. For *D. indonesiensis* strain P23, this adaptation was detected with both analytical methods confirming previous studies on a variety of organisms (DeLong and Yayanos, 1985). Moreover, the cell response of *D. indonesiensis* strain P23 to changes in temperature apparently occurred stepwise. After changing the saturation level, as a subsequent response to higher incubation temperature *D. indonesiensis* strain P23 decreased its membrane fluidity by exchanging branched FAs with straight-chain FAs. This was most pronounced for *anteiso*-branched FAs, as they have lower melting points than *iso*-branched FAs; the effect is similar to that of saturation (Zhang and Rock, 2008). For *D. indonesiensis* strain P23, elevated initial proportions of straight-chain FAs under *in situ* pressure and 20°C were independent of the degree of saturation and indicated that pressure mostly diminished the branching of FAs. These findings are consistent with results obtained in previous studies on thermal adaptation of bacterial membranes (Rilfors et al., 1978; Nordström and Laakso, 1992; Koga, 2012). Comparing low and high-pressure incubations at the same temperatures, *D. indonesiensis* strain P23 reacted similarly as described for many other microorganisms with decreasing proportions of saturated FAs at high pressure (Fang et al., 2003). An initially higher ratio of unsaturated over saturated FAs (Wang et al., 2014) was not observed.

Another factor for membrane fluidity is the number of double bonds of unsaturated FAs. Polyunsaturated FAs were found in many piezopsychrophilic deep-sea bacteria, this regulatory capacity appears to be limited to psychrophilic microorganisms (DeLong and Yayanos, 1986; Wirsen et al., 1986; Kamimura et al., 1993; Yano et al., 1998) or mesophilic organisms from near-surface sediments (Freese et al., 2009). As *D. indonesiensis* strain P23 derives from a warm deep-sea habitat, the production of polyunsaturated FAs as a regulatory component may only become relevant when growth temperature falls below 20°C.

High Proportions of Ornithine-containing Lipids may Reflect Phosphate Limitation in the Original Habitat

Phosphorus-free ornithine-containing lipids are major membrane constituents in *D. indonesiensis* strain P23, as already described for other *Desulfovibrio* species (Makula and Finnerty, 1975; Seidel et al., 2013). The presence of OLs was found to be negatively correlated with available amounts of phosphate present in the culture medium (Geiger et al., 1999; Weissenmayer et al., 2002). Thus, the authors assumed that bacteria replaced phosphate-containing membrane lipids by phosphorus-free lipids such as OL, sulphoquinovosyl diacylglycerol (SQDG), or diacylglycerol trimethylhomoserine (DGTS). Although phosphate was not a limiting nutrient in our cultivation medium, *D. indonesiensis* strain P23 was isolated from phosphate-depleted sediment layers (Engelen et al., 2008). In this environment, the ability to produce phosphate-free membrane building blocks gives an advantage over other microorganisms that are not capable of this regulatory feature. Thus, it is possible, that this adaptation originally developed in the deep biosphere and was not lost when *D. indonesiensis* strain P23 was cultivated in phosphate-rich media.

Furthermore, our study indicates that OL may not only be a substitute for phosphate-containing membrane lipids. Cells grown at atmospheric pressure responded to increasing temperature with higher relative amounts of OL within the membrane, and FA chain-length variations. This temperature dependence corroborates recent findings by Seidel et al. (2013) who found elevated proportions of OL with increasing incubation temperature for several *D. acrylicus* strains. The authors suggested that changes in lipid composition of the cytoplasmic membrane may rather be important for the presence and activity of membrane-bound enzymes and do not necessarily influence viscosity. This assumption is supported by our results, as we found neither the expected decrease of OL levels with temperature in high-pressure incubations nor any obvious structural changes of OL moieties as an adaptation of membrane fluidity to high pressure.

Simultaneous Decrease of Pressure and Temperature Favors the Cultivation of Piezomesophiles from Deep Subsurface Sediments

To mimic environmental conditions, most enrichment cultures are incubated at *in situ* temperatures. In contrast, even for the cultivation of deep-sea microorganisms, pressure is normally not taken into account. This may be due to the high technical effort during sampling, storage, and microbial analyses (Parkes et al., 2009). While none of our enrichments from IODP Site U1301 that were performed at *in situ* temperatures and atmospheric pressure resulted in pure cultures, a great variety

of isolates were gained at ambient laboratory conditions (Fichtel et al., 2012). This can be explained by opposed effects of pressure and of temperature on general cell functions and the capability of microorganisms of adapting to these variations. Thus, a key for a successful isolation of piezomesophilic and other high-temperature-adapted prokaryotes from the subsurface under atmospheric pressure appears to be the decrease of cultivation temperature below the *in situ* temperature. For piezopsychrophiles in turn, this approach is not appropriate as *in situ* conditions of, e.g., 40 MPa and 2°C, the average values at the seafloor, would require an unrealistic incubation temperature of −2 to −6°C at atmospheric pressure (Chong and Cossins, 1983; Bartlett, 2002; Wang et al., 2009). On the other hand, pressure above *in situ* values may be advantageous for cultivating piezopsychrophiles at elevated temperatures, which generally accelerates growth (Kato et al., 1995).

In case of *D. indonesiensis* strain P23, applying the optimum hydrostatic pressure resulted in growth at 50°C but not at the respective *in situ* temperature of ∼60°C. However, this *in situ* temperature may not be precise. Temperatures at depth were estimated only by extrapolating heat flow data. They are estimated based on the assumption that heat transport within the sediment is vertical and conductive. This leads to uncertainties in temperatures estimated for the sediment–basement interface of ∼15–25% (Zühlsdorff et al., 2005). Another explanation why the *in situ* temperature was not reached is possibly due to the fact that the chemical composition of our media did not reproduce the chemical condition of the natural habitat. Alternatively, it may be explained by the effect of pressure on abiotic factors such as the solubility of gases. *D. indonesiensis* strain P23 turned out to be a chemolithoautotrophic sulfate reducer as it was able to grow on hydrogen and CO_2 as sole energy and carbon sources (Fichtel et al., 2012). In the present study, pressure incubation under autotrophic conditions was not performed, as this would have required a completely different technical equipment allowing cultivation with a gaseous headspace. However, pressure is an inevitable factor for isolating obligate piezophiles (Kato et al., 1996) or investigating the microbial utilization of gases or hydrocarbons in the subsurface.

Author Contributions

KF: Idea and concept, high-pressure experiments, data analyses (calculations, creation of tables and figures), microscopic pictures, data interpretation, first draft; JL: Idea and concept, analyses of whole-cell fatty acids and intact polar lipids, data analyses (calculations, creation of tables and figures), data interpretation, first draft; JF: Lipid analyses, data interpretation, revision; BE: Sampling, idea and concept, data interpretation, revision; HC: Idea and concept, data interpretation, revision; JR: Data interpretation, revision.

Acknowledgments

The authors are grateful to Friedrich Widdel and Christian Deusner for providing the high-pressure equipment and for technical advice. We appreciate Bernd Kopke and Michael Seidel for their help with lipid and data analysis. Erhard Rhiel is acknowledged for his help in preparing TEM photos. We would also like to thank the three reviewers for their valuable comments and suggestions. This research used samples provided by the Integrated Ocean Drilling Program (IODP) and was financially supported by the German Research Foundation (DFG). We dedicate this article to Katrina J. Edwards for her inspiring commitment to deep subsurface research.

Supplementary Material

The Supplementary Material for this article can be found online at: http://journal.frontiersin.org/article/10.3389/fmicb.2015.01078

References

Abe, F. (2007). Exploration of the effects of high hydrostatic pressure on microbial growth, physiology and survival: perspectives from piezophysiology. *Biosci. Biotechnol. Biochem.* 71, 2347–2357. doi: 10.1271/bbb.70015

Aertsen, A., Van Houdt, R., Vanoirbeek, K., and Michiels, C. W. (2004). An SOS response induced by high pressure in *Escherichia coli*. *J. Bacteriol.* 186, 6133–6141. doi: 10.1128/JB.186.18.6133-6141.2004

Alain, K., Marteinsson, V. T., Miroshnichenko, M. L., Bonch-Osmolovskaya, E. A., Prieur, D., and Birrien, J. L. (2002). *Marinitoga piezophila* sp. nov., a rod-shaped, thermo-piezophilic bacterium isolated under high hydrostatic pressure from a deep-sea hydrothermal vent. *Int. J. Syst. Evol. Microbiol.* 52, 1331–1339. doi: 10.1099/ijs.0.02068-0

Alazard, D., Dukan, S., Urios, A., Verhe, F., Bouabida, N., Morel, F., et al. (2003). *Desulfovibrio hydrothermalis* sp. nov., a novel sulfate-reducing bacterium isolated from hydrothermal vents. *Int. J. Syst. Evol. Microbiol.* 53, 173–178. doi: 10.1099/ijs.0.02323-0

Allen, E. E., Facciotti, D., and Bartlett, D. H. (1999). Monounsaturated but not polyunsaturated fatty acids are required for growth of the deep-sea bacterium *Photobacterium profundum* SS9 at high pressure and low temperature. *Appl. Environ. Microbiol.* 65, 1710–1720.

Amrani, A., Bergon, A., Holota, H., Tamburini, C., Garel, M., Ollivier, B., et al. (2014). Transcriptomics reveal several gene expression patterns in the piezophile *Desulfovibrio hydrothermalis* in response to hydrostatic pressure. *PLoS ONE* 9:e106831. doi: 10.1371/journal.pone.0106831

Bale, S. J., Goodman, K., Rochelle, P. A., Marchesi, J. R., Fry, J. C., Weightman, A. J., et al. (1997). *Desulfovibrio profundus* sp. nov, a novel barophilic sulfate-reducing bacterium from deep sediment layers in the Japan Sea. *Int. J. Syst. Bacteriol.* 47, 515–521. doi: 10.1099/00207713-47-2-515

Barnes, S. P., Bradbrook, S. D., Cragg, B. A., Marchesi, J. R., Weightman, A. J., Fry, J. C., et al. (1998). Isolation of sulfate-reducing bacteria from deep sediment layers of the Pacific Ocean. *Geomicrobiol. J.* 15, 67–83. doi: 10.1080/01490459809378066

Bartlett, D. H. (2002). Pressure effects on in vivo microbial processes. *Biochim. Biophys. Acta* 1595, 367–381. doi: 10.1016/S0167-4838(01)00357-0

Batzke, A., Engelen, B., Sass, H., and Cypionka, H. (2007). Phylogenetic and physiological diversity of cultured deep-biosphere bacteria from equatorial Pacific Ocean and Peru Margin sediments. *Geomicrobiol. J.* 24, 261–273. doi: 10.1080/01490450701456453

Biddle, J. F., Fitz-Gibbon, S., Schuster, S. C., Brenchley, J. E., and House, C. H. (2008). Metagenomic signatures of the Peru Margin subseafloor biosphere

show a genetically distinct environment. *Proc. Natl. Acad. Sci. U.S.A.* 105, 10583–10588. doi: 10.1073/pnas.0709942105

Bidle, K. A., and Bartlett, D. H. (1999). RecD function is required for high-pressure growth of a deep-sea bacterium. *J. Bacteriol.* 181, 2330–2337.

Bradford, M. M. (1976). A rapid and sensitive method for the quantitation of microgram quantities of protein utilizing the principle of protein-dye binding. *Anal. Biochem.* 72, 248–254.

Chong, P. L. G., and Cossins, A. R. (1983). A differential polarized phase fluorometric study of the effects of high hydrostatic pressure upon the fluidity of cellular membranes. *Biochemistry* 22, 409–415. doi: 10.1021/bi00271a026

Cord-Ruwisch, R. (1985). A quick method for the determination of dissolved and precipitated sulfides in cultures of sulfate-reducing bacteria. *J. Microbiol. Meth.* 4, 33–36. doi: 10.1016/0167-7012(85)90005-3

DeLong, E., and Yayanos, A. A. (1985). Adaptation of the membrane lipids of a deep-sea bacterium to changes in hydrostatic pressure. *Science* 228, 1101–1103. doi: 10.1126/science.3992247

DeLong, E. F., and Yayanos, A. A. (1986). Biochemical function and ecological significance of novel bacterial lipids in deep-sea prokaryotes. *Appl. Environ. Microbiol.* 51, 730–737.

Edwards, K. J., Wheat, C. G., and Sylvan, J. B. (2011). Under the sea: microbial life in volcanic oceanic crust. *Nat. Rev. Microbiol.* 9, 703–712. doi: 10.1038/nrmicro2647

Eloe, E. A., Malfatti, F., Gutierrez, J., Hardy, K., Schmidt, W. E., Pogliano, K., et al. (2011). Isolation and characterization of a psychropiezophilic *Alphaproteobacterium*. *Appl. Environ. Microbiol.* 77, 8145–8153. doi: 10.1128/AEM.05204-11

Engelen, B., Ziegelmüller, K., Wolf, L., Köpke, B., Gittel, A., Cypionka, H., et al. (2008). Fluids from the oceanic crust support microbial activities within the deep biosphere. *Geomicrobiol. J.* 25, 56–66. doi: 10.1080/01490450701829006

Expedition 301 Scientists (2005). "Site U1301," in *Proceedings of the IODP*, Vol. 301, eds A. T. Fisher, T. Urabe, A. Klaus, and the Exp. 301 Scientists (College Station, TX: IODP Management International, Inc.).

Fang, J. S., Chan, O. V., Kato, C., Sato, T., Peeples, T., and Niggemeyer, K. (2003). Phospholipid FA of piezophilic bacteria from the deep sea. *Lipids* 38, 885–887. doi: 10.1007/s11745-003-1140-7

Feio, M. J., Beech, I. B., Carepo, M., Lopes, J. M., Cheung, C. W. S., Franco, R., et al. (1998). Isolation and characterisation of a novel sulphate-reducing bacterium of the *Desulfovibrio* genus. *Anaerobe* 4, 117–130. doi: 10.1006/anae.1997.0142

Fichtel, K., Mathes, F., Könneke, M., Cypionka, H., and Engelen, B. (2012). Isolation of sulfate-reducing bacteria from sediments above the deep-subseafloor aquifer. *Front. Microbiol.* 3:65. doi: 10.3389/fmicb.2012.00065

Freese, E., Rütters, H., Köster, J., Rullkötter, J., and Sass, H. (2009). *Gammaproteobacteria* as a possible source of eicosapentaenoic acid in sediments. *Microb. Ecol.* 57, 444–454. doi: 10.1007/s00248-008-9443-2

Geiger, O., Röhrs, V., Weissenmayer, B., Finan, T., and Thomas-Oates, J. (1999). The regulator gene phoB mediates phosphate stress-controlled synthesis of the membrane lipid diacylglyceryl-N,N,N-trimethylhomoserine in *Rhizobium* (*Sinorhizobium*) *meliloti*. *Mol. Microbiol.* 32, 63–73. doi: 10.1046/j.1365-2958.1999.01325.x

Giovannoni, S., and Stingl, U. (2007). The importance of culturing bacterioplankton in the 'omics' age. *Nat. Rev. Microbiol.* 5, 820–826. doi: 10.1038/nrmicro1752

Hamamoto, T., Takata, N., Kudo, T., and Horikoshi, K. (1994). Effect of temperature and growth phase on fatty acid composition of the psychrophilic *Vibrio* sp. strain no. 5710. *FEMS Microbiol. Lett.* 119, 77–81. doi: 10.1111/j.1574-6968.1994.tb06870.x

Heberling, C., Lowell, R. P., Liu, L., and Fisk, M. R. (2010). Extent of the microbial biosphere in the oceanic crust. *Geochem. Geophys. Geosyst.* 11, 1–15. doi: 10.1029/2009GC002968

Inagaki, F., Nunoura, T., Nakagawa, S., Teske, A., Lever, M., Lauer, A., et al. (2006). Biogeographical distribution and diversity of microbes in methane hydrate-bearing deep marine sediments on the Pacific Ocean Margin. *Proc. Natl. Acad. Sci. U.S.A.* 103, 2815–2820. doi: 10.1073/pnas.0511033103

Ishii, A., Sato, T., Wachi, M., Nagai, K., and Kato, C. (2004). Effects of high hydrostatic pressure on bacterial cytoskeleton FtsZ polymers in vivo and in vitro. *Microbiology* 150, 1965–1972. doi: 10.1099/mic.0.26962-0

Jannasch, H. W., Wirsen, C. O., Molyneaux, S. J., and Langworthy, T. A. (1992). Comparative physiological studies on hyperthermophilic *Archaea* isolated from deep-sea hot vents with emphasis on *Pyrococcus* strain GB-D. *Appl. Environ. Microbiol.* 58, 3472–3481.

Jungbluth, S. P., Grote, J., Lin, H.-T., Cowen, J. P., and Rappe, M. S. (2014). Microbial diversity within basement fluids of the sediment-buried Juan de Fuca Ridge flank. *ISME J.* 7, 161–172. doi: 10.1038/ismej.2012.73

Kallmeyer, J., Pockalny, R., Adhikari, R. R., Smith, D. C., and D'Hondt, S. (2012). Global distribution of microbial abundance and biomass in subseafloor sediment. *Proc. Natl. Acad. Sci. U.S.A.* 109, 16213–16216. doi: 10.1073/pnas.1203849109

Kamimura, K., Fuse, H., Takimura, O., and Yamaoka, Y. (1993). Effects of growth pressure and temperature on fatty acid composition of a barotolerant deep-sea bacterium. *Appl. Environ. Microbiol.* 59, 924–926.

Kaneko, H., Takami, H., Inoue, A., and Horikoshi, K. (2000). Effects of hydrostatic pressure and temperature on growth and lipid composition of the inner membrane of barotolerant *Pseudomonas* sp. BT1 isolated from the deep-sea. *Biosci. Biotechnol. Biochem.* 64, 72–79. doi: 10.1271/bbb.64.72

Kato, C., and Bartlett, D. H. (1997). The molecular biology of barophilic bacteria. *Extremophiles* 1, 111–116. doi: 10.1007/s007920050023

Kato, C., Inoue, A., and Horikoshi, K. (1996). Isolating and characterizing deep-sea marine microorganisms. *Trends Biotechnol.* 14, 6–12. doi: 10.1016/0167-7799(96)80907-3

Kato, C., Nogi, Y., and Arakawa, S. (2008). "Isolation, cultivation, and diversity of deep-sea piezophiles," in *High-Pressure Microbiology*, eds C. Michiels, D. H. Bartlett, and A. Aertsen (Washington, DC: ASM Press).

Kato, C., Sato, T., and Horikoshi, K. (1995). Isolation and properties of barophilic and barotolerant bacteria from deep-sea mud samples. *Biodivers. Conserv.* 4, 1–9. doi: 10.1007/BF00115311

Kaye, J. Z., and Baross, J. A. (2004). Synchronous effects of temperature, hydrostatic pressure, and salinity on growth, phospholipid profiles, and protein patterns of four *Halomonas* species isolated from deep-sea hydrothermal-vent and sea surface environments. *Appl. Environ. Microbiol.* 70, 6220–6229. doi: 10.1128/AEM.70.10.6220-6229.2004

Khelaifia, S., Fardeau, M.-L., Pradel, N., Aussignargues, C., Garel, M., Tamburini, C., et al. (2011). *Desulfovibrio piezophilus* sp. nov., a piezophilic, sulfate-reducing bacterium isolated from wood falls in the Mediterranean Sea. *Int. J. Syst. Evol. Microbiol.* 61, 2706–2711. doi: 10.1099/ijs.0.028670-0

Kobayashi, T., Koide, O., Mori, K., Shimamura, S., Matsuura, T., Miura, T., et al. (2008). Phylogenetic and enzymatic diversity of deep subseafloor aerobic microorganisms in organics– and methane-rich sediments off Shimokita Peninsula. *Extremophiles* 12, 519–527. doi: 10.1007/s00792-008-0157-7

Koga, Y. (2012). Thermal adaptation of the archaeal and bacterial lipid membranes. *Archaea* 2012, 789652. doi: 10.1155/2012/789652

Kormas, K. A., Smith, D. C., Edgcomb, V., and Teske, A. (2003). Molecular analysis of deep subsurface microbial communities in Nankai Trough sediments (ODP Leg 190, Site 1176). *FEMS Microbiol. Ecol.* 45, 115–125. doi: 10.1016/S0168-6496(03)00128-4

Lauro, F. M., and Bartlett, D. H. (2008). Prokaryotic lifestyles in deep sea habitats. *Extremophiles* 12, 15–25. doi: 10.1007/s00792-007-0110-1

Lever, M. A., Alperin, M., Engelen, B., Inagaki, F., Nakagawa, S., Steinsbu, B. O., et al. (2006). Trends in basalt and sediment core contamination during IODP Expedition 301. *Geomicrobiol. J.* 23, 517–530. doi: 10.1080/01490450600897245

Lever, M. A., Alperin, M. J., Teske, A., Heuer, V. B., Schmidt, F., Hinrichs, K.-U., et al. (2010). Acetogenesis in deep subseafloor sediments of the Juan de Fuca Ridge flank: a synthesis of geochemical, thermodynamic, and gene-based evidence. *Geomicrobiol. J.* 27, 183–211. doi: 10.1080/01490450903456681

Logemann, J., Graue, J., Köster, J., Engelen, B., Rullkötter, J., and Cypionka, H. (2011). A laboratory experiment of intact polar lipid degradation in sandy sediments. *Biogeosciences* 8, 2547–2560. doi: 10.5194/bg-8-2547-2011

Macdonald, A. G. (1988). Application of the theory of homeoviscous adaptation to excitable membranes: pre-synaptic processes. *Biochem. J.* 256, 313–327. doi: 10.1042/bj2560313

Makula, R. A., and Finnerty, W. R. (1975). Isolation and characterization of an ornithine-containing lipid from *Desulfovibrio gigas*. *J. Bacteriol.* 123, 523–529.

Mangelsdorf, K., Zink, K. G., Birrien, J. L., and Toffin, L. (2005). A quantitative assessment of pressure dependent adaptive changes in the membrane lipids of piezosensitive deep sub-seafloor bacterium. *Org. Geochem.* 36, 1459–1479. doi: 10.1016/j.orggeochem.2005.08.002

Marchesi, J. R., Weightman, A. J., Cragg, B. A., Parkes, R. J., and Fry, J. C. (2001). Methanogen and bacterial diversity and distribution in deep gas hydrate sediments from the Cascadia Margin as revealed by 16S rRNA molecular analysis. *FEMS Microbiol. Ecol.* 34, 221–228. doi: 10.1111/j.1574-6941.2001.tb00773.x

Michiels, C., Bartlett, D. H., and Aertsen, A. (2008). *High-Pressure Microbiology*. Washington, DC: ASM Press.

Miyazaki, M., Koide, O., Kobayashi, T., Mori, K., Shimamura, S., Nunoura, T., et al. (2012). *Geofilum rubicundum* gen. nov., sp. nov., isolated from deep subseafloor sediment. *Int. J. Syst. Evol. Microbiol.* 62(Pt 5), 1075–1080. doi: 10.1099/ijs.0.032326-0

Molina-Höppner, A., Sato, T., Kato, C., Gänzle, M. G., and Vogel, R. F. (2003). Effects of pressure on cell morphology and cell division of lactic acid bacteria. *Extremophiles* 7, 511–516. doi: 10.1007/s00792-003-0349-0

Müller, K. D., Husmann, H., Nalik, H. P., and Schomburg, G. (1990). Trans-esterification of fatty acids from microorganisms and human blood serum by trimethylsulfonium hydroxide (TMSH) for GC analysis. *Chromatographia* 30, 245–248. doi: 10.1007/BF02319701

Nordström, K. M., and Laakso, S. V. (1992). Effect of growth temperature on fatty acid composition of ten *Thermus* strains. *Appl. Environ. Microbiol.* 58, 1656–1660.

Orcutt, B. N., Sylvan, J. B., Knab, N. J., and Edwards, K. J. (2011). Microbial ecology of the dark ocean above, at, and below the seafloor. *Microbiol. Mol. Biol. Rev.* 75, 361–422. doi: 10.1128/MMBR.00039-10

Parkes, R. J., Sellek, G., Webster, G., Martin, D., Anders, E., Weightman, A. J., et al. (2009). Culturable prokaryotic diversity of deep, gas hydrate sediments: first use of a continuous high-pressure, anaerobic, enrichment and isolation system for subseafloor sediments (DeepIsoBUG). *Environ. Microbiol.* 11, 3140–3153. doi: 10.1111/j.1462-2920.2009.02018.x

Picard, A., Testemale, D., Wagenknecht, L., Hazael, R., and Daniel, I. (2015). Iron reduction by the deep-sea bacterium *Shewanella profunda* LT13a under subsurface pressure and temperature conditions. *Front. Microbiol.* 5:796. doi: 10.3389/fmicb.2014.00796

Pluschke, G., and Overath, P. (1981). Function of phospholipids in *Escherichia coli*. Influence of changes in polar head group composition on the lipid phase transition and characterization of a mutant containing only saturated phospholipid acyl chains. *J. Biol. Chem.* 256, 3207–3212.

Pradel, N., Ji, B., Gimenez, G., Talla, E., Lenoble, P., Garel, M., et al. (2013). The first genomic and proteomic characterization of a deep-sea sulfate reducer: insights into the piezophilic lifestyle of *Desulfovibrio piezophilus*. *PLoS ONE* 8:e55130. doi: 10.1371/journal.pone.0055130

Rilfors, L., Wieslander, A., and Ståhl, S. (1978). Lipid and protein composition of membranes of Bacillus megaterium variants in the temperature range 5 to 70 degrees C. *J. Bacteriol.* 135, 1043–1052.

Robador, A., Jungbluth, S. P., LaRowe, D. E., Bowers, R. M., Rappe, M. S., Amend, J. P., et al. (2015). Activity and phylogenetic diversity of sulfate-reducing microorganisms in low-temperature subsurface fluids within the upper oceanic crust. *Front. Microbiol.* 5:748. doi: 10.3389/fmicb.2014.00748

Rütters, H., Sass, H., Cypionka, H., and Rullkötter, J. (2002). Phospholipid analysis as a tool to study complex microbial communities in marine sediments. *J. Microbiol. Meth.* 48, 149–160. doi: 10.1016/S0167-7012(01)00319-0

Seidel, M., Rütters, H., Rullkötter, J., and Sass, H. (2013). Phosphate-free ornithine lipid contents in *Desulfovibrio* spp. respond to growth temperature. *Org. Geochem.* 59, 133–142. doi: 10.1016/j.orggeochem.2013.04.004

Sinensky, M. (1974). Homeoviscous adaptation – A homeostatic process that regulates the viscosity of membrane lipids in *Escherichia coli*. *Proc. Natl. Acad. Sci. U.S.A.* 71, 522–525. doi: 10.1073/pnas.71.2.522

Somero, G. N. (1992). Adaptations to high hydrostatic pressure. *Annu. Rev. Physiol.* 54, 557–577. doi: 10.1146/annurev.ph.54.030192.003013

Sturt, H. F., Summons, R. E., Smith, K., Elvert, M., and Hinrichs, K. U. (2004). Intact polar membrane lipids in prokaryotes and sediments deciphered by high-performance liquid chromatography/electrospray ionization multistage mass spectrometry – New biomarkers for biogeochemistry and microbial ecology. *Rapid Commun. Mass Spectrom.* 18, 617–628. doi: 10.1002/rcm.1378

Takai, K., Abe, M., Miyazaki, M., Koide, O., Nunoura, T., Imachi, H., et al. (2013). *Sunxiuqinia faeciviva* sp. nov., a novel facultatively anaerobic, organoheterotrophic bacterium within the *Bacteroidetes* isolated from deep subseafloor sediment offshore Shimokita. *Jpn. Int. J. Syst. Evol. Microbiol.* 63, 1602–1609. doi: 10.1099/ijs.0.044065-0

Teske, A. P. (2006). Microbial communities of deep marine subsurface sediments: molecular and cultivation surveys. *Geomicrobiol. J.* 23, 357–368. doi: 10.1080/01490450600875613

Toffin, L., Bidault, A., Pignet, P., Tindall, B. J., Slobodkin, A., Kato, C., et al. (2004). *Shewanella profunda* sp. nov., isolated from deep marine sediment of the Nankai Trough. *Int. J. Syst. Evol. Microbiol.* 54, 1943–1949. doi: 10.1099/ijs.0.03007-0

Toffin, L., Zink, K., Kato, C., Pignet, P., Bidault, A., Bienvenu, N., et al. (2005). *Marinilactibacillus piezotolerans* sp. nov., a novel marine lactic acid bacterium isolated from deep sub-seafloor sediment of the Nankai Trough. *Int. J. Syst. Evol. Microbiol.* 55, 345–351. doi: 10.1099/ijs.0.63236-0

Wang, F., Xiao, X., Ou, H.-Y., Gai, Y., and Wang, F. (2009). Role and regulation of fatty acid biosynthesis in the response of *Shewanella piezotolerans* WP3 to different temperatures and pressures. *J. Bacteriol.* 191, 2574–2584. doi: 10.1128/JB.00498-08

Wang, J., Li, J., Dasgupta, S., Zhang, L., Golovko, M. Y., Golovko, S. A., et al. (2014). Alterations in membrane phospholipid fatty acids of gram-positive piezotolerant bacterium *Sporosarcina* sp dsk25 in response to growth pressure. *Lipids* 49, 347–356. doi: 10.1007/s11745-014-3878-7

Webster, G., John Parkes, R., Cragg, B. A., Newberry, C. J., Weightman, A. J., and Fry, J. C. (2006). Prokaryotic community composition and biogeochemical processes in deep subseafloor sediments from the Peru Margin. *FEMS Microbiol. Ecol.* 58, 65–85. doi: 10.1111/j.1574-6941.2006.00147.x

Weissenmayer, B., Gao, J.-L., López-Lara, I. M., and Geiger, O. (2002). Identification of a gene required for the biosynthesis of ornithine-derived lipids. *Mol. Microbiol.* 45, 721–733. doi: 10.1046/j.1365-2958.2002.03043.x

Wellsbury, P., Mather, I., and Parkes, R. J. (2002). Geomicrobiology of deep, low organic carbon sediments in the Woodlark Basin, Pacific Ocean. *FEMS Microbiol. Ecol.* 42, 59–70. doi: 10.1111/j.1574-6941.2002.tb00995.x

Whitman, W. B., Coleman, D. C., and Wiebe, W. J. (1998). Prokaryotes: the unseen majority. *Proc. Natl. Acad. Sci. U.S.A.* 95, 6578–6583. doi: 10.1073/pnas.95.12.6578

Wirsen, C. O., Jannasch, H. W., Wakeham, S. G., and Canuel, E. A. (1986). Membrane lipids of a psychrophilic and barophilic deep-sea bacterium. *Curr. Microbiol.* 14, 319–322. doi: 10.1007/BF01568697

Wu, W. F., Wang, F. P., Li, J. H., Yang, X. W., Xiao, X., and Pan, Y. X. (2013). Iron reduction and mineralization of deep-sea iron reducing bacterium *Shewanella piezotolerans* WP3 at elevated hydrostatic pressures. *Geobiology* 11, 593–601. doi: 10.1111/gbi.12061

Xiao, X., Wang, P., Zeng, X., Bartlett, D. H., and Wang, F. (2007). Shewanella psychrophila sp nov and *Shewanella piezotolerans* sp nov., isolated from west Pacific deep-sea sediment. *Int. J. Syst. Evol. Microbiol.* 57, 60–65. doi: 10.1099/ijs.0.64500-0

Yano, Y., Nakayama, A., Ishihara, K., and Saito, H. (1998). Adaptive changes in membrane lipids of barophilic bacteria in response to changes in growth pressure. *Appl. Environ. Microbiol.* 64, 479–485.

Yayanos, A. A. (1995). Microbiology to 10,500 Meters in the deep sea. *Annu. Rev. Microbiol.* 49, 777–805. doi: 10.1146/annurev.mi.49.100195.004021

Zhang, Y. M., and Rock, C. O. (2008). Membrane lipid homeostasis in bacteria. *Nat. Rev. Microbiol.* 6, 222–233. doi: 10.1038/nrmicro1839

Zobell, C. E., and Cobet, A. B. (1962). Growth, reproduction, and death rates of *Escherichia coli* at increased hydrostatic pressures. *J. Bacteriol.* 84, 1228–1236.

Zobell, C. E., and Cobet, A. B. (1964). Filament formation by *Escherichia coli* at increased hydrostatic pressures. *J. Bacteriol.* 87, 710–719.

Zobell, C. E., and Johnson, F. H. (1949). The influence of hydrostatic pressure on the growth and viability of terrestrial and marine bacteria. *J. Bacteriol.* 57, 179–189.

Zühlsdorff, L., Hutnak, M., Fisher, A. T., Spiess, V., Davis, E. E., Nedimovic, M., et al. (2005). "Site surveys related to IODP Expedition 301: imageFlux (S149) and RetroFlux (TN116) expeditions and earlier studies," in *Proceedings of the IODP*, Vol. 301, eds A. T. Fisher, T. Urabe, A. Klaus, and the Exp. 301 Scientists (College Station, TX: IODP Management International, Inc.).

Conflict of Interest Statement: The authors declare that the research was conducted in the absence of any commercial or financial relationships that could be construed as a potential conflict of interest.

frontiers in Microbiology

ORIGINAL RESEARCH
published: 22 December 2015
doi: 10.3389/fmicb.2015.01449

Key Factors Influencing Rates of Heterotrophic Sulfate Reduction in Active Seafloor Hydrothermal Massive Sulfide Deposits

Kiana L. Frank[1,2], Karyn L. Rogers[3], Daniel R. Rogers[4,5], David T. Johnston[5] and Peter R. Girguis[6]*

[1] Department of Molecular Biology, Harvard University, Cambridge, MA, USA, [2] Department of Oceanography, University of Hawaii, Honolulu, HI, USA, [3] Department of Earth and Environmental Sciences, Rensselaer Polytechnic Institute, Troy, NY, USA, [4] Department of Chemistry, Stonehill College, Easton, MA, USA, [5] Department of Earth and Planetary Sciences, Harvard University, Cambridge, MA, USA, [6] Department of Organismic and Evolutionary Biology, Harvard University, Cambridge, MA, USA

Hydrothermal vents are thermally and geochemically dynamic habitats, and the organisms therein are subject to steep gradients in temperature and chemistry. To date, the influence of these environmental dynamics on microbial sulfate reduction has not been well constrained. Here, via multivariate experiments, we evaluate the effects of key environmental variables (temperature, pH, H_2S, SO_4^{2-}, DOC) on sulfate reduction rates and metabolic energy yields in material recovered from a hydrothermal flange from the Grotto edifice in the Main Endeavor Field, Juan de Fuca Ridge. Sulfate reduction was measured in batch reactions across a range of physico-chemical conditions. Temperature and pH were the strongest stimuli, and maximum sulfate reduction rates were observed at 50°C and pH 6, suggesting that the *in situ* community of sulfate-reducing organisms in Grotto flanges may be most active in a slightly acidic and moderate thermal/chemical regime. At pH 4, sulfate reduction rates increased with sulfide concentrations most likely due to the mitigation of metal toxicity. While substrate concentrations also influenced sulfate reduction rates, energy-rich conditions muted the effect of metabolic energetics on sulfate reduction rates. We posit that variability in sulfate reduction rates reflect the response of the active microbial consortia to environmental constraints on *in situ* microbial physiology, toxicity, and the type and extent of energy limitation. These experiments help to constrain models of the spatial contribution of heterotrophic sulfate reduction within the complex gradients inherent to seafloor hydrothermal deposits.

Keywords: sulfate reduction, rate, energetics, hydrothermal deposits, microbial activity

OPEN ACCESS

Edited by:
Cara M. Santelli, University of Minnesota, USA

Reviewed by:
Andreas Teske, University of North Carolina at Chapel Hill, USA
Margaret Kingston Tivey, Woods Hole Oceanographic Institution, USA

****Correspondence:***
Kiana L. Frank
klfrank@hawaii.edu

Specialty section:
This article was submitted to Extreme Microbiology, a section of the journal Frontiers in Microbiology

Received: *15 July 2015*
Accepted: *04 December 2015*
Published: *22 December 2015*

Citation:
Frank KL, Rogers KL, Rogers DR, Johnston DT and Girguis PR (2015) Key Factors Influencing Rates of Heterotrophic Sulfate Reduction in Active Seafloor Hydrothermal Massive Sulfide Deposits. Front. Microbiol. 6:1449. doi: 10.3389/fmicb.2015.01449

INTRODUCTION

Sulfate-reducing bacteria and archaea gain energy by mediating the anaerobic oxidation of organic and inorganic substrates using sulfate as an electron acceptor. The electron donors utilized by sulfate reducers are quite variable, ranging from molecular hydrogen to aromatic compounds, although low molecular weight organic compounds including acetate, lactate, pyruvate, and ethanol

(prevalent in anaerobic environments as a result of the fermentative breakdown of biomass) are commonly used (Amend et al., 2004; Rabus et al., 2006; Tarpgaard et al., 2011).

Due to the high concentration of sulfate in seawater (28 mM; Dittmar, 1884), sulfate reduction (or SR) is an ubiquitous metabolism in hypoxic to anoxic marine habitats (Muyzer and Stams, 2008) such as oxygen minimum zone waters (Canfield et al., 2010), marine sediments (Kallmeyer et al., 2002; Robador et al., 2009), hydrocarbon seeps (Joye et al., 2004; Orcutt et al., 2005), marine hydrothermal vents (Jørgensen et al., 1992; Elsgaard et al., 1994a; Weber and Jørgensen, 2002; Frank et al., 2013), and the deep subsurface (D'Hondt et al., 2004; Engelen et al., 2008; Robador et al., 2015). As such, SR likely has a significant impact on the global carbon budget (Westrich and Berner, 1984; Canfield, 1989). Among 33 phylogenetically diverse sulfate-reducing microbial isolates, cell-specific SR rates vary by orders of magnitude in their respective thermal regimes (0.9 fmol cell^{-1} day^{-1} for *Desulfospira joergensenii* to 4340 fmol cell^{-1} day^{-1} for *Desulfohalobium retbaense*; Detmers et al., 2001). In marine sediments, estimates of cell-specific SR rates range from 10^{-4} to 10^{0} fmol cell^{-1} day^{-1} and are often lower than those of pure cultures by orders of magnitude (Jørgensen and Bak, 1991; Ravenschlag et al., 2000; Orcutt et al., 2005; Leloup et al., 2007, 2009; Holmkvist et al., 2011a,b). SR rates have also been shown to be highly heterogeneous within marine sediments due to variations in substrate and organic carbon availability, as well as other geochemical and physical factors (Canfield, 1989; Isaksen et al., 1994; Kallmeyer et al., 2002; Orcutt et al., 2005; Fike et al., 2008; Treude et al., 2009; Holmkvist et al., 2011a).

SR has been proposed to be one of the most thermodynamically favorable metabolic processes in marine hydrothermal ecosystems (McCollom and Shock, 1997; Tivey, 2004) because of the relative abundance of sulfate as an oxidant, as well as the relative abundance of appropriate reductants. Indeed, many sulfate-reducing microorganisms have been isolated from deep-sea hydrothermal ecosystems (Huber et al., 1997; Jeanthon et al., 2002; Alazard et al., 2003; Audiffrin et al., 2003). Data on the mass-specific SR rates in hydrothermal-influenced sediments (25–6600 nmol g-1 day-1, assuming an average sediment density of 2 g cm^{-3}; Elsgaard et al., 1994a,b; Weber and Jørgensen, 2002; Kallmeyer and Boetius, 2004), sulfide deposits (16–2700 nmol g^{-1} day^{-1}, Frank et al., 2013), and basaltic fluids (0.01–0.05 nmol ml^{-1} day^{-1}, Robador et al., 2015) underscore the biogeochemical and ecological relevance of microbial sulfate reduction in deep-sea hydrothermal ecosystems.

At hydrothermal vents, structures called chimneys develop as hydrothermal fluid mixes with cold seawater, providing a unique if not ideal habitat for a variety of bacteria and archaea that rely on vent- and seawater-derived compounds (Schrenk et al., 2003). However, the microorganisms within these porous mineral deposits are exposed, in varying degrees, to the dynamic and combined effects of high temperature, low pH, high concentrations of hydrogen sulfide, fluctuating amounts of carbon, and varying energy sources. Previous studies reveal differences in prokaryotic populations among individual sulfide deposits (Harmsen et al., 1997; Takai et al., 2001; Schrenk et al., 2003; Kormas et al., 2006; Pagé et al., 2008), but we know less about how physico-chemical gradients influence the rates of most key microbial metabolisms, including SR, within the walls of actively venting hydrothermal chimney structures.

The metabolic energy available for SR is likely influenced by the specific composition of the end-member fluids and ambient seawater (Tivey, 1995, 2004; Zhu et al., 2007) as well as temperature, among other factors. Microbial SR rates in hydrothermal vent systems are governed by a combination of thermodynamic driving forces and the kinetics of catabolic reactions. In energy-limited systems, metabolic reaction rates tend to decrease proportionally with catabolic energy yields, and the thermodynamic factor in the complete rate equation has been modeled either as a function of the energetic costs of ATP synthesis (Jin and Bethke, 2005) or the energetic requirements of maintaining a membrane potential (LaRowe et al., 2012). Application of these models to SR rates in hydrothermal vent environments and marine sediments suggests that SR rates can be significantly impacted by thermodynamic driving forces when substrates (e.g., SO_4^{2-}, CH_4, acetate) are limiting (Jin and Bethke, 2005; LaRowe et al., 2012). However, in environments with non-limiting sulfate or DOC concentrations, such as the experiments described here, heterotrophic SR rates can be modeled with standard Michaelis-Menten kinetics (Jin and Bethke, 2005). Even then, kinetic models depend on metabolism- and species-specific model parameters (Jin and Bethke, 2005; LaRowe et al., 2012). Model-predicted rates of hydrogenotrophic SR in hydrothermal chimneys (800 pmol cm^3 day^{-1}; LaRowe et al., 2014) are two to four orders of magnitude less than heterotrophic SR rates reported from Middle Valley chimneys (Frank et al., 2013), suggesting that kinetic models do not adequately capture the complexities of the natural environment. Although both thermodynamics and kinetics are functions of the physico-geochemical environment, the extent to which environmental factors—and their dynamics—influence SR rates remains unknown in hydrothermal chimneys and must be experimentally determined.

To better understand the parameters that affect SR rates within actively venting hydrothermal chimneys, we conducted a series of experiments that examined rates of microbial heterotrophic SR in batch incubations over a range of environmentally relevant chemical conditions (pH, H_2S, SO_4^{2-}, and organic carbon) and temperatures (4, 50, and 90°C) from hydrothermal flange recovered from the Grotto edifice at the Main Endeavor Field, Juan de Fuca Ridge. This vent was specifically selected to be the focus of this study because its geology, mineralogy (pyrrhotite and pyrite), and end-member fluid chemistry (pH of 4.2, 12.6 mmol kg^{-1} CO_2, 633 μmol kg^{-1} NH_3, 5.4 mmol kg^{-1} H_2S, 11 μM DOC) have been extensively studied over the past decade (Tivey and Delaney, 1986; Delaney et al., 1992; Butterfield et al., 1994; Tivey et al., 1999, 2002; Tivey, 2004; Lang et al., 2006; Zhu et al., 2007). While models infer that sulfate concentration may govern SR within sulfide deposits, the discrepancies between modeled and empirically derived rates lead us to conclude that other factors may be responsible for the observed SR rates. We therefore posit that SR rates in sulfide deposits are controlled by other factors, such as hydrogen sulfide concentration, pH, or

organic carbon availability. Here we present empirical evidence for SR activity within active hydrothermal chimneys and quantitatively constrain the magnitude of net heterotrophic SR activity across a gradient of environmentally-relevant physico-chemical regimes.

MATERIALS AND METHODS

Geologic Setting and Sampling of Hydrothermal Sulfide Deposits

The Main Endeavor vent field is located at 47°57′ N and 129°06 W (Tivey and Delaney, 1986) at a depth of 2220 m, the most shallow portion of the Endeavor segment of the Juan de Fuca ridge. This vent field is comparable in size and quantity of hydrothermal chimneys to most other hydrothermal areas, and is characterized by many (>15) large steep-walled active sulfide deposits (containing multiple high temperature spires and diffusing flanges) surrounded by a scattering of smaller inactive hydrothermal sulfide deposits in a roughly 400 m^2 area (Delaney et al., 1992; Robigou et al., 1993).

A single massive piece of hydrothermal deposit (∼100 kg in weight) was recovered from a flange on the Grotto vent (47.949, −129.098) at a depth of 2188.3 m (Dive J2-575, AT-18-08, *R/V Atlantis*) and brought up to the surface in the basket of the *ROV Jason II*. This sample will be hereafter referred to as a "flange." Once on board ship, tubeworms and other macrofauna were removed from the samples and the large pieces were broken into more manageable fragments (∼10–20 cm^3) with a flame-sterilized chisel and sledgehammer, with the user wearing sterile nitrile gloves. Samples were quickly transferred to 0.2 μm-filtered anaerobic (nitrogen-sparged) seawater. Samples were further broken down into smaller sizes while in anaerobic water, and subsamples from the interior of the fragments were immediately transferred to gastight jars (Freund Container Inc.) filled with sterile anaerobic seawater containing 2 mM sodium sulfide at pH 6, and stored at 4°C for incubations and analyses. The sterile sulfidic seawater in the gastight jars were refreshed periodically during storage at 4°C. The majority of the rate experiments (80%) were set up immediately on the ship using freshly collected samples. In parallel, subsamples (∼1 cm^3) from each flange were preserved aboard ship in glutaraldehyde (2.5% in phosphate buffered saline, PBS, pH 7.0), then prepared for electron microscopy via ethanol dehydration and critical point drying before being sputtered with a thin layer of gold-palladium to improve image resolution. Samples were imaged with a Zeiss model EVO Scanning Electron Microscope (SEM).

Measuring Sulfate Reduction Rates

Experimental Design and Incubation

Prior to incubation, each flange subsample was pulverized by hand for about 1 h to minimize fine-scale geological and microbial heterogeneity and facilitate more accurate experimental replication (akin to slurry experiments in sediments; Fossing and Jørgensen, 1989; Jørgensen et al., 1992; Weber and Jørgensen, 2002). Specifically, each subsample was pulverized with a flame-sterilized sledgehammer in sterile seawater actively bubbled with nitrogen within an anaerobic chamber. For each independent treatment, aliquots of 7.5 mL flange slurry (∼29 g wet weight and 20 g dry weight) were transferred into Balch tubes in an anaerobic chamber, and supplemented with 15 mL of sterile artificial seawater media designed to mimic the geochemical conditions within a hydrothermal flange (400 mM NaCl, 25 mM KCl, 30 mM $CaCl_2$, 2.3 mM $NaHCO_3$, 14 mM $NaSO_4^{2-}$, 1 mM H_2S, and 50 μM dissolved organic carbon—consisting of equimolar proportions 10 μM of pyruvate, citrate, formate, acetate, lactate) under a pure nitrogen headspace.

Concentrations of sulfide, sulfate and dissolved organic carbon (DOC) were varied independently to investigate concentration dependent effects on the rates of SR. The range of experimental conditions tested was determined from previously published concentration profiles of aqueous species modeled as functions of temperature and position within the Grotto vent structure (Tivey, 2004). Concentrations were varied by orders of magnitude within the modeled ranges to simulate conditions representative of different mixing regimes between seawater and vent fluid (**Table 1**). The range of DOC (which we approximate as a mix of pyruvate, citrate, formate, acetate, lactate—most of which have been identified to varying degrees within vent fluid and are known carbon sources for heterotrophic SR in culture) concentrations tested were based on the average DOC concentrations measured within diffuse fluids at the Main Endeavor Field (Lang et al., 2006, 2010). Hydrogen sulfide was present as H_2S (pK_a in seawater of 6.60) across all the conditions tested (Amend and Shock, 2001). Incubations were carried out at

TABLE 1 | Experimental media conditions.

Experiment	$[H_2S]$	[Sulfate]	[DOC][a]	pH[b]	Temperature °C	Innoculum[c]
Δ [Sulfide]	0 mM	14 mM	50 μM	4, 6	4, 50, 90	Fresh
	10 μM	14 mM	50 μM	4, 6	4, 50, 90	Fresh
	100 μM	14 mM	50 μM	4, 6	4, 50, 90	Fresh
	1 mM	14 mM	50 μM	4, 6	4, 50, 90	Fresh
Δ [DOC]	1 mM	14 mM	0 μM	4, 6	4, 50, 90	Stored
	1 mM	14 mM	0.5 μM	4, 6	4, 50, 90	Stored
	1 mM	14 mM	5 μM	4, 6	4, 50, 90	Stored
	1 mM	14 mM	50 μM	4, 6	4, 50, 90	Stored
Δ [Sulfate]	1 mM	10 nM	50 μM	4, 6	50	Stored
	1 mM	1 μM	50 μM	4, 6	50	Stored
	1 mM	10 μM	50 μM	4, 6	50	Stored
	1 mM	100 μM	50 μM	4, 6	50	Stored
	1 mM	1 mM	50 μM	4, 6	50	Stored

The base for each experiment was artificial seawater mix (KCl, CaCl2, NaCl) and 2.3 mM bicarbonate.

[a] Dissolved organic carbon amendments consisted of equimolar proportions of pyruvate, citrate, formate, acetate, and lactate.

[b] pH of media added to incubations.

[c] Homogenized hydrothermal flange used fresh (i.e., immediately after collection on the boat), or stored (used within 1 year of collection, storage in anaerobic sulfidic seawater at 4°C. SR rates measured 1 year after collection (stored) were not statistically different from sulfate reduction measurements made immediately after collection fresh).

pH 4 (to simulate the pH of end-member Grotto vent fluid and the average calculated pH of mixed fluids in highly reduced zones within the flange; Tivey, 2004) as well as pH 6 (representative of the calculated pH in fluid mixing zones; Tivey, 2004). All the results are presented and discussed in the context of the initial measured media conditions. During incubation, it is plausible that the dissolution or precipitation of sulfide minerals (or other chemical reactions) may have affected the pH and chemical composition of the media. Due to the presence of the radioactive tracer, fluid pH could not be readily measured throughout the course of the experiment. Estimates of final fluid conditions calculated with EQ3/6 support the observation that changes in fluid composition are likely consistent across samples incubated under the same conditions.

Sufficient $^{35}SO_4^{2-}$ was added to achieve 15 μCi of activity. Samples were incubated anaerobically for 1, 3, or 7 days at ambient seawater (4°C), thermophilic (50°C), and hyperthermophilic (90°C) temperatures. The range of temperatures considered was representative of different thermal regimes associated with the surface, outer layer and middle regions of hydrothermal chimneys (Schrenk et al., 2003; Tivey, 2004; Kormas et al., 2006). Negative controls consisted of samples amended with 28 mM molybdate to inhibit SR (Saleh et al., 1964; Newport and Nedwell, 1988). Three biological replicates were run for each treatment, and two biological replicates for each control.

Upon completion, reactions were quenched with the injection of 5 mL 25% zinc acetate, at pH 8 (i.e., 20-fold excess Zn), and all samples were frozen at −20°C for further analysis. Eighty percent of incubations were performed shipboard with freshly collected samples and the remaining 20% of incubations were completed within 1 year of collection. Select incubations performed on ship and replicated in the laboratory within 1 year of collection revealed no significant shift in observed SR rates due to the storage conditions (see **Figure 3**). However, even though the rates seemed unaffected, we have no data on the taxonomic composition of the sulfate reducing communities and cannot exclude the possibility that communities may have shifted during storage as has been shown to be the case for stored sediment cores (Lin et al., 2010).

Chromium Distillation Analysis

To determine SR rates, samples were thawed and the supernatant was removed and filtered through a 0.2 μm syringe filter. The homogenized flange that remained in the tube was washed three times with deionized water to remove any remaining sulfate. One gram (wet weight) of flange material was added to 10 mL of a 1:1 ethanol to water solution in the chromium distillation apparatus, and then degassed with nitrogen for 15 min to drive the environment anoxic. Hydrogen sulfide gas was evolved after the anaerobic addition of 8 mL of 12 N HCl and 10 mL of 1 M reduced chromium chloride, followed by 3 h of heating. The resulting hydrogen sulfide gas was carried via nitrogen gas through a condenser to remove HCl, and was then trapped as zinc sulfide in a 25% zinc acetate solution. While cold distillation methods for measuring SR using radiotracers have been developed and improved in recent years (Kallmeyer et al., 2004a; Røy et al., 2014), our experience has shown that—for metal-rich sulfide deposits—the hot chromium distillation method is sufficient in producing consistent results when run with the appropriate controls. To moderate potential artifacts of hot distillation methods including elevated rates in control samples, experiments were analyzed in triplicate, on different days and with different glassware to minimize cross-contamination, and any activity observed in "control" samples was deleted from the treatments. The radioactivity of the resulting sulfide ($Zn^{35}S$) and the remaining sulfate from the supernatant ($^{35}SO_4^{2-}$) were measured via liquid scintillation counter in Ultima Gold scintillation cocktail (ThermoFisher Inc., Waltham, MA).

Calculating Sulfate Reduction Rates

Rates were determined using the following calculation as in Fossing and Jørgensen (1989).

$$SRR = \frac{nSO_4^{2-} \cdot a \cdot 1.06}{(a + A) \cdot t} \quad (1)$$

Where nSO_4^{2-} is the quantity (in moles) of sulfate added to each incubation (14 mM * 15 mL = 210 μmol), a is the activity (dpm) of the trapped sulfide, 1.06 is the fractionation factor between the hydrogen sulfide and sulfate pools (Jørgensen and Fenchel, 1974), A is the activity of the sulfate pool at the completion of the incubation and t is the incubation time (days). The rates are presented in units of nmol S g^{-1} day^{-1}. As previously mentioned, SR rates are numerically presented as the difference in rates between experimental and the molybdate inhibited controls, further mitigating any potential artifacts caused by hot distillation methods.

Calculating V_{max}, K_m, and Assumptions

The Michaelis-Menten kinetic parameters of maximum rate (V_{max}) and half-saturation constant (K_m) were determined using a linearization of SR rate (V) vs. sulfate concentration [S] data via the Hanes Woolf plot (Equation 2),

$$\frac{[S]}{V} = \frac{V_{max}[S]}{K_m + [S]} \quad (2)$$

which is more accurate than the double reciprocal Lineweaver-Burk plot (Leskovac, 2003). The slope and X-intercept of the Hanes Woolf plot yield $\frac{1}{V_{max}}$ and K_m respectively. Sulfate concentrations plotted were initial concentrations as has been historically used when incubation conditions were short and sulfate concentrations were not depleted such that they significantly influenced SR rates (Pallud and Van Cappellen, 2006). Based on our previous study (Frank et al., 2013), we anticipated that the magnitude of SR rates would be on the order of nmol g^{-1} day^{-1}. Given that the input sulfate concentrations range from μM to mM—three orders of magnitude greater than the rate of consumption—and changes in sulfate concentration could not be resolved with our methods, the maximum input of SR activity on the concentration of sulfate is 0.03%. Consequently, we use the initial concentration here without concern.

Bioenergetic Calculations

Potential energy yields of the different metabolisms available in the incubations depend on temperature and fluid compositions. To quantify the energy yield from heterotrophic sulfate reduction (**Table 2**) in each incubation values of overall Gibbs energy (ΔG_r) were calculated according to:

$$\Delta G_r = \Delta G_r^0 + \mathrm{RT\,lnQ} \quad (3)$$

where ΔG_r^0 is the standard Gibbs energy of reaction at *in situ* temperature and pressure conditions, R is the gas constant, T is the temperature (Kelvin), and Q is the activity product, defined as

$$Q = \Pi a_i^{vi} \quad (4)$$

where a_i represents the activity of the *i*th species and $v_i$is the stoichiometric reaction coefficient, which is positive for products and negative for reactants. Values of ΔG_r^0 were calculated at 1 bar and incubation temperatures using the geochemical software package SUPCRT92 (Johnson et al., 1992) and additional thermodynamic data from Shock (1995). Activities of aqueous species were calculated using the geochemical speciation program EQ3 (Wolery, 1992a) based on the media composition described in Section Measuring Sulfate Reduction Rates and **Table 1**, with additional data from previously published work (Shock and Koretsky, 1993; Shock, 1995). For concentrations equal to zero, a value of 10^{-13} mol/kg was used as input. Resulting aqueous activities were used to calculate values of ΔG_r normalized for the number of electrons transferred in the redox for the reactions in **Table 2**. These reflect the metabolic energy available at the start of each incubation experiment for the complete oxidation of each organic acid, metabolisms that are documented among known sulfate reducers (Amend and Shock, 2001). Furthermore, to calculate the energy density in each incubation (as in Amend et al., 2011), it was assumed that the amended organic acids were the limiting reactant for all experiments when sulfate concentrations were in excess of 1 mM; otherwise sulfate was assumed to be limiting. While some sulfate reducers are known to produce carboxylic acid and alcohol intermediates, incomplete oxidation reactions were not considered here, as the goal of these calculations was to generate a broad understanding of sulfate reduction energetics, and not the metabolic potential for a particular species. Such an approach is common when comparing microbial metabolisms independent of species-specific pathways (e.g., Amend et al., 2004; Rogers and Amend, 2006; Skoog et al., 2007), although it should be noted that incomplete oxidation (fermentation) generally yields much less energy than complete oxidation (Rogers and Amend, 2006; Skoog et al., 2007).

To account for potential interactions between chimney-derived trace metals and amended sulfide, the saturation states of sulfide minerals were calculated as part of the initial fluid speciation (see above). Using reported concentrations of relevant trace metals (Fe, Zn, Cu, etc.) in end-member Grotto hydrothermal fluid (Butterfield et al., 1994), maximum aqueous activities of trace metals were calculated with the EQ3 geochemical speciation program (Wolery, 1992a,b). Several sulfide minerals commonly found in hydrothermal chimneys (e.g., pyrite, chalcocite, sphalerite) were supersaturated under incubation conditions, particularly for incubations with high concentrations of amended sulfide. The irreversible abiotic precipitation of mineral sulfides has the potential to draw down aqueous sulfide concentrations and impact sulfate reductions rates. Therefore, the geochemical reaction path program EQ6 (Wolery, 1992a; Wolery and Daveler, 1992) was used to constrain fluid compositions to equilibrium with these minerals phases. Using the single point model in EQ6, the Gibbs energy of the system was allowed to reach local minima by mineral precipitation, however redox reactions among carbon and sulfur species was suppressed with a custom thermodynamic database. The resulting fluid compositions were used to calculate metabolic reaction energetics as well as to evaluate the potential effects of metal speciation on sulfate reduction rates.

RESULTS

Physical Characteristics of the Study Site and Microscopy

Diffuse hydrothermal flow was observed on the surface of the hydrothermal flange of Grotto ranging in temperature from 2 to 18.1°C, while hot hydrothermal fluid (T_{max} = 215.6°C) was observed in pools accumulating on the underside of an overhanging flange. Sulfide minerals nearest to the hottest fluid were relatively friable, whereas the majority of the flange sampled was relatively solid, likely due to the precipitation of pyrrhotite, pyrite, and silica (Tivey and Delaney, 1986) in pore spaces at lower temperatures. An inner conduit-like channel was clearly present in the interior of the flange and densely lined with pyrite. Thick veins of anhydrite and channels of marcasite were also observed throughout the samples. Crystals of these minerals were imaged using scanning electron microscopy. Microbial cells were observed associated with mineral surfaces in low abundance

TABLE 2 | Heterotrophic sulfate reduction.

Carbon source	Reaction	e^-
Formate	$SO_4^{2-} + 4\ CH_2O_2 \rightarrow H_2S + 4\ HCO_3^- + 2\ H^+$	8
Acetate	$SO_4^{2-} + C_2H_4O_2 \rightarrow H_2S + 2\ HCO_3^-$	8
Pyruvate	$5\ SO_4^{2-} + 4\ C_3H_4O_3 + 4\ H_2O \rightarrow 5\ H_2S + 12\ HCO_3^- + 2\ H^+$	40
Lactate	$3\ SO_4^{2-} + 2\ C_3H_6O_3 \rightarrow 3\ H_2S + 6\ HCO_3^-$	24
Citrate	$9\ SO_4^{2-} + 4\ C_6H_5O_7^{3-} + 8\ H_2O + 6\ H^+ \rightarrow 9\ H_2S + 24\ HCO_3^-$	72

(Figure S1). There was no visual evidence of dense biofilms within the sample.

Sulfate Reduction Rates

Sulfate reduction was detected in incubations of flange material recovered from the Grotto vent at 4, 50, and 90°C over a range of environmentally-relevant chemical conditions (pH, H_2S, SO_4^{2-}, and organic carbon concentrations). Measured rates (except for those at low sulfate concentrations) are comparable in magnitude to those previously observed in hydrothermally-influenced sediments (e.g., Guaymas Basin or Lake Tanganyika; Elsgaard et al., 1994a,b; Weber and Jørgensen, 2002; Kallmeyer and Boetius, 2004). Among all treatments, the highest observed rate (3940 nmol g^{-1} day^{-1}) occurred at 100 μM H_2S, 14 mM SO_4^{2-}, 50 μM DOC, pH 6, and 50°C. The lowest observed rates (120 fmol g^{-1} day^{-1} – 1.5 nmol g^{-1} day^{-1}) were under conditions of most pronounced sulfate limitation (10–100 μM) in the presence of 1 mM H_2S, at pH 4 and 6, and at 50°C (it should be noted that we did not conduct these same sulfate limitation experiments at 4 and 90°C).

Control experiments were designed to inhibit biological sulfate reduction through the use of molybdate, a known inhibitor of SR. The SR rates in these controls were much lower than experimental samples (Mann-Whitney-Wilcox test, $p = 0.1$), though none of the samples were entirely inhibited, which is likely the result of mineral scavenging of molybdate (Bostick et al., 2003; Xu et al., 2006) or as an artifact of hot chromium distillation methods (Kallmeyer et al., 2004b). While we present rates for both experimental and molybdate-amended samples to provide a perspective on the relative contributions of abiotic vs. biotic sulfate reduction under varying environmental conditions (**Figures 2–4**), the subsequent analyses focus on a conservative measure of net biological rates, namely the difference in rates between experimental and the molybdate-inhibited controls. Additionally, because rates from 3-day to 7-day incubations were not significantly different from one another in these treatments ($n = 271$; Mann-Whitney-Wilcoxon, $p = 0.728$), they are being treated as pseudo-replicates. As has been previously observed (Frank et al., 2013), SR rates exhibited large standard deviations, presumably due to microscale sample heterogeneity (despite efforts to homogenize, mineral clasts ranged in size from 0.003 to 80 mm^3) among biological replicates. Such variation is consistent with the patterns we observed in previous SR rate measurements on Middle Valley vent deposits (with mineral sizes 0.001–7 mm^3; Frank et al., 2013).

The highest SR rates across all conditions tested were observed at 50°C (**Figure 1**). The average SR rates with 14 mM sulfate were 16.4 nmol g^{-1} day^{-1} at 4°C (3.99–66.8 nmol g^{-1} day^{-1}), 270 nmol g^{-1} day^{-1} at 50°C (10.0–1690 nmol g^{-1} day^{-1}), and 7.66 nmol g^{-1} day^{-1} at 90°C (0–24.9 nmol g^{-1} day^{-1} at 90°C). SR rates observed at 50°C were significantly higher than those measured at 4°C ($n = 152$; Mann-Whitney-Wilcoxon, $p < 0.0001$) and 90°C ($n = 151$; Mann-Whitney-Wilcoxon, $p < 0.0001$). Notably, 60% of samples incubated at 90°C show no biological sulfate reduction. Our data show that when temperature is varied independently from chemistry (under thermodynamically favorable conditions of excess sulfate and no oxygen), the highest rates of SR occur at 50°C. Furthermore, the distribution of rates with respect to temperature resembles distributions observed in hydrothermal sediments (Jørgensen et al., 1992; Elsgaard et al., 1994a; Weber and Jørgensen, 2002) and basaltic crustal fluids (Robador et al., 2015), where optimal temperatures range between 40 and 80°C, but it differs from those measured in vent structures from Middle Valley, where maximal rates were observed at 90°C (Frank et al., 2013).

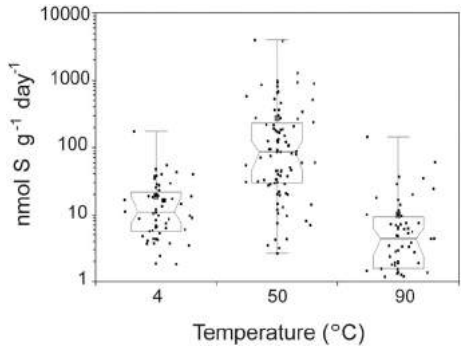

FIGURE 1 | Temperature dependence of sulfate reduction rates in crushed hydrothermal flange from Grotto vent (Main Endeavor, JdF). The median of 213 samples is plotted as a line, the 1st and 3rd quartiles as a box, and the minimum and maximum as whiskers with end caps. The 95% confidence interval of the median is represented by a notch on the box. The mean of the 213 samples is depicted as a gray square. Black squares indicate individual measurements. Note rates measured from sulfate gradient experiments were excluded in this figure because those experiments were only done at 50°C.

SR rates observed at pH 6 were significantly higher than those measured at pH 4 ($n = 271$; Mann-Whitney-Wilcoxon, $p = 0.0267$). The average SR rates at pH 6 were 149 nmol g^{-1} day^{-1} compared to 35.6 nmol g^{-1} day^{-1} at pH 4. Maximum SR rates at pH 6 seem incongruous with the pH of endmember hydrothermal fluid (4.2–4.7; Butterfield et al., 1994; Tivey, 2004), particularly in light of observations of Lake Tanganyika hydrothermal sediments, where maximum SR rates were observed at pH conditions near hydrothermal vent values (Elsgaard et al., 1994b). However, mixing models by Tivey (2004) predict fluid compositions with a pH of ∼6 at 50°C when mixing is driven by seawater advection, suggesting that microbial communities adapted to the 50°C niche in the Grotto flange also have an optimal pH range close to estimated *in situ* values.

While temperature and pH were the dominant factors influencing SR rates, media amendments were also correlated with rates, though to a lesser degree. SR rates were positively correlated ($p < 0.0001$) with sulfate concentration (10–14 mM) at both pH 6 and pH 4 (**Figure 2**). Over the entire range of sulfate concentrations tested (seven orders of magnitude), SR rates ranged from 50.1 fmol g^{-1} day^{-1} to 930 nmol g^{-1} day^{-1} at pH 6 (seven orders of magnitude) and from 9.8 fmol g^{-1} day^{-1} to 805 nmol g^{-1} day^{-1} at pH 4 (eight orders of magnitude). Furthermore, SR rates were slightly higher at pH 4 when sulfate concentrations were less than 14 mM. Michaelis-Menten Kinetics parameters determined using the Hanes-Woolf linearized form

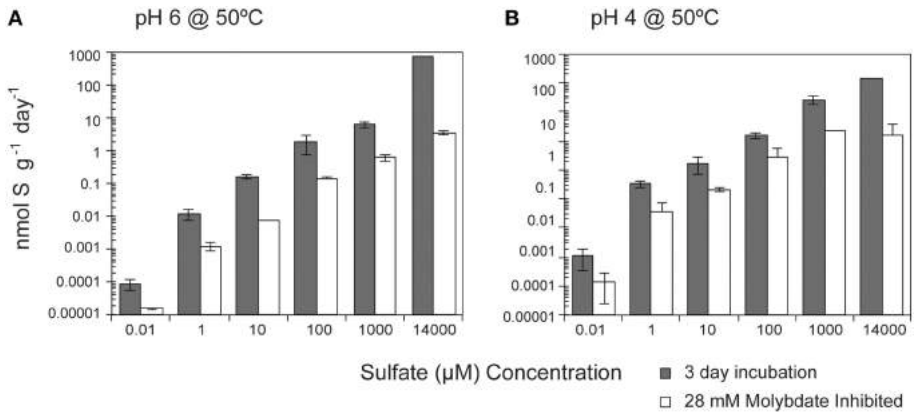

FIGURE 2 | Effect of sulfate concentration on sulfate reduction rates. The crushed flange from the Grotto hydrothermal deposits were incubated for 3 days (■) at 50°C at **(A)** pH 6 or **(B)** pH 4. 28 mM molybdate amended samples were incubated under all conditions (□) as controls. Error bars represent 1 standard deviation.

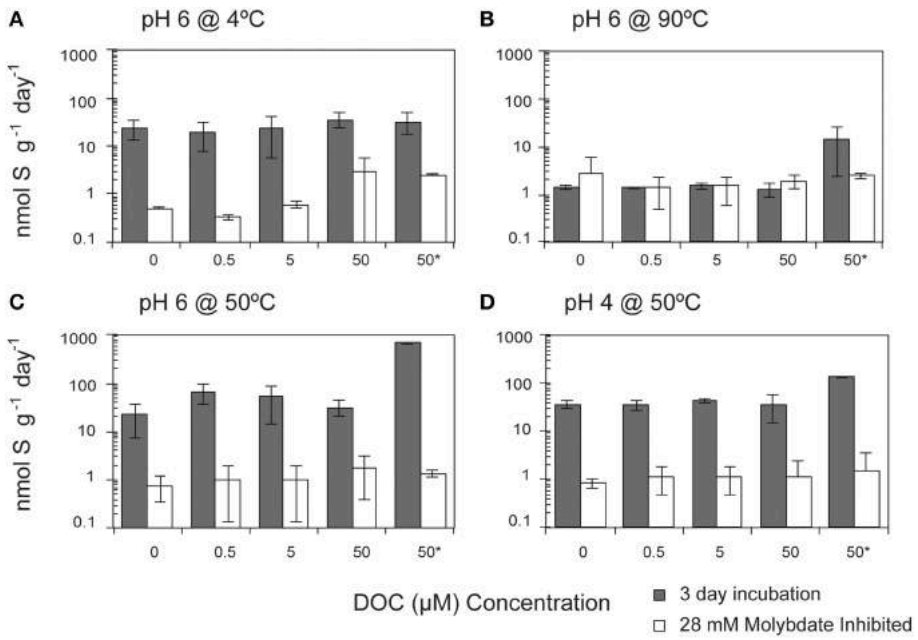

FIGURE 3 | Effect of dissolved organic carbon (DOC) concentrations on sulfate reduction rates. The crushed flange from the Grotto hydrothermal deposits were incubated for 3 days (■) in media of **(A)** pH 6 at 4°C, **(B)** pH 6 at 90°C, **(C)** pH 6 at 50°C, and **(D)** pH 4 at 50°C. While most of experiments were performed in laboratory using stored samples, concentrations identified with an asterisk (*) were done shipboard immediately after collection of hydrothermal chimney. 28 mM molybdate amended samples were incubated under all conditions (□) as controls. Error bars represent 1 standard deviation. Note the log scale on the y-axis.

of the Michaelis-Menten rate equation (Equation 2) revealed a K_m value of 7.1 mM and V_{max} of 298 nmol g^{-1} day^{-1} for SR at pH 6 ($r^2 = 0.441$) and a K_m value of 2.5 mM and V_{max} of 298 nmol g^{-1} day^{-1} at pH 4 ($r^2 = 0.513$). K_m, defined as the sulfate concentration at which SR rates are half-maximum, is a measure of affinity for sulfate (higher K_m corresponds to lower affinity). Given that the K_m values for most enzymes in the sulfate reduction pathways range roughly from 5 to 100 µM in cultured organisms (Trüper and Rogers, 1971; Ingvorsen et al., 1981; Ingvorsen and Jørgensen, 1984; Sonne-hansen and Westermann, 1999; Ramos et al., 2012), the pattern of SR rates observed in these experiments suggests that sulfate reduction enzymes do not reach saturation at the amended sulfate concentrations (plausible explanations for this observation are presented in the discussion). The apparent K_m value for SR at pH 6 is higher than the highest reported K_m values for thermophilic SR (3.17 ± 1.02 mM) from Yellowstone Mushroom Springs (Roychoudhury, 2004). Interestingly, the apparent K_m values for SR at pH 6 are higher than at pH 4, even though V_{max} remains constant under both conditions. Due to the low r^2 values for linear regressions,

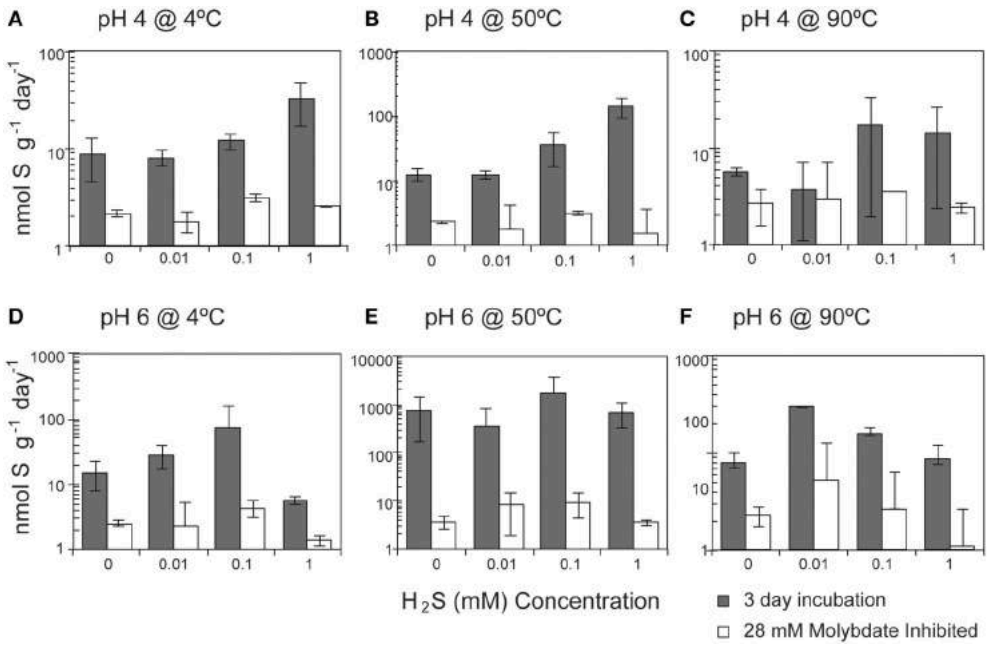

FIGURE 4 | Effect of sulfide concentration on sulfate reduction rates. The crushed flange from the Grotto hydrothermal deposits were incubated for 3 days (■) in media of **(A)** pH 4 at 4°C, **(B)** pH 4 at 50°C, **(C)** pH 4 at 90°C, **(D)** pH 6 at 4°C, **(E)** pH 6 at 50°C, and **(F)** pH 6 at 90°C. 28 mM molybdate amended samples were incubated under all conditions (□) as controls. Error bars represent 1 standard deviation. Note different scales for **(A,C)**.

future experiments should consider a wider range of sulfate concentrations to validate these values.

SR rates in the treatments without any exogenous DOC amendment were not significantly different from those incubated with DOC (pyruvate, citrate, formate, acetate, and lactate) at concentrations up to 50 μM (Pearson's correlation, $p = 0.565$; **Figure 3**). The observed rates suggest that the communities were not carbon limited and could have been utilizing organic carbon associated with flange materials. Given the common occurrence of macrofauna upon these chimneys, it is likely that endogenous organic carbon pools—such as from macrofaunal necromass—exist in these systems.

Overall, SR rates (ranging from 1.9 to 3936 nmol g^{-1} day^{-1}) were positively correlated with the concentration of hydrogen sulfide (Pearson's correlation, $n = 213$, $p = 0.04$; **Figure 4**). A strong correlation was observed at pH 4 at both 4°C ($p < 0.0001$) and 50°C ($p < 0.0001$), with SRR rates increasing between one and two orders of magnitude as the sulfide concentration increased from 0 to 1 mM (Table S1). In contrast, SR rates were not significantly correlated with the exogenous sulfide concentration at pH 6 (Pearson's correlation, $p = 0.354$).

Bioenergetic Models

The favorability of sulfate reduction in the incubation experiments, as estimated by overall Gibbs energy of reaction, ΔG_r, ranged from −6.41 kJ/mol e^- to −20.7 kJ/mol e^- over the range of sulfate, DOC, and sulfide concentrations tested. **Figure 5** shows ΔG_r, normalized for the number of electrons transferred, for the range of conditions in the 50°C, pH 6 experiments. Note that negative values of ΔG_r indicate exergonic reactions, and higher negative values (increasing on the y-axis) reflect increasing energy levels. While sulfate, DOC, and sulfide concentrations were varied by five orders of magnitude or more, values of ΔG_r only changed by 2–3 kJ/mol e^- at this temperature and pH, emphasizing that *in situ* concentrations of individual electron donors, acceptors, or products are not the largest contributor to free energy variations. However, varying the type of electron donor (in this case the species of organic acid) effected changes in ΔG_r up to ∼10 kJ/mol e^-. For example, at 0.1 mM sulfate, oxidation of acetate yields −7.76 kJ/mol e^-, while formate oxidation provides up to −17.79 kJ/mol e^-. Not surprisingly, the highest calculated energy yields were from formate oxidation under the maximum sulfate and minimum sulfide concentrations (**Figure 5Aiii**). The effect of temperature on metabolic energy availability was less pronounced than the effect of the organic acid species, with only 1–2 kJ/mol e^- variations in ΔG_r for any given reaction evaluated at 4, 50, and 90°C (e.g., At pH 6, 0.1 mM H_2S, 14 mM SO_4^{2-}, and 50 μM formate, ΔG_r ranged from −18.6 to −19.3 kJ/mol e^- from 4 to 90°C).

In batch experiments, like those described here, overall Gibbs energy values do not represent the amounts of substrate that might be limiting in closed systems. Accounting for the total amount of sulfate and DOC available for each incubation (by multiplying values of ΔG_r in kJ/mol rxn, by the concentration and stoichiometric reaction coefficient of the limiting substrate, as well as the volume of the incubation), it is possible to calculate the total amount of energy available (e.g., energy density; LaRowe and Amend, 2015) in each experiment (**Figure 5B**). Low concentrations of sulfate (SO_4^{2-}-limited conditions) or

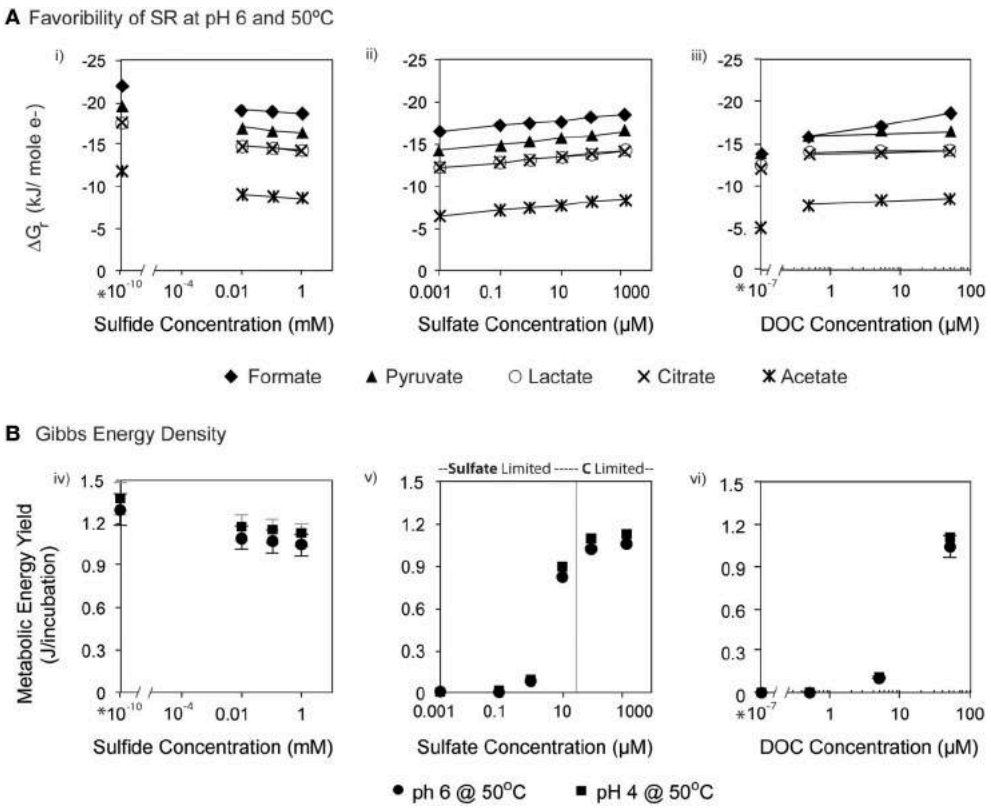

FIGURE 5 | (A) ΔG_r (kJ/mol e^-) calculated at pH 6 and 50°C for heterotrophic sulfate reduction via organic acids (formate, acetate, pyruvate, lactate and citrate) at varying concentrations of (i) sulfide, (ii) sulfate, and (iii) DOC. **(B)** The total energy available for sulfate reduction in each incubation at 50°C. Bars on each symbol represent the range of values for 4°C and 90°C. Asterisks (*) denote contrived values of zero that were inputted into the model for speciation calculation in EQ3.

DOC (organic carbon-limited conditions) both yielded minimal energy density ($\sim 10^{-6}$ kJ/incubation); however these values rose to nearly 1.2 kJ/incubation for concentrations of sulfate in excess of 1 mM and DOC at 50 μM (all under carbon limitation). Energy densities decreased minimally with increasing sulfide concentrations, consistent with expectations, as metabolic products are not limiting and therefore do not generally affect energy density.

While the species of electron donor, and—to a lesser extent—sulfate, sulfide, and individual organic acid concentrations, have some effect on overall metabolic energy yields, our calculations indicate that the largest contributor is the metabolic strategy itself. In general, ΔG_r values for both autotrophic and heterotrophic sulfate reduction occupy a small range of energetics over a broad range of environments compared to other metabolic strategies. For example, Rogers and Amend (2006) found that *in situ* ΔG_r values for SR coupled to oxidation of carboxylic acids ranged from −6.7 to −25.99 kJ/mol e^- in shallow marine hydrothermal vents, compared to −0.05 to −122.58 kJ/mol e^- for all other metabolic strategies considered (Amend et al., 2003; Rogers and Amend, 2006). Energy yields for heterotrophic SR from those shallow marine vents are very similar to values calculated here, despite having higher sulfate concentrations (up to 62 mM) and orders of magnitude lower sulfide (<400 μM) than the Grotto experiments. The metabolic energy yields calculated here are also similar to values predicted from seawater/hydrothermal fluid mixing models (McCollom and Shock, 1997; Rogers and Amend, 2006).

DISCUSSION

Physiological Constraints on SR Rates

The magnitude of SR rates within the Grotto flange is primarily governed by the temperature and, to a lesser extent, pH-dependent processes and their effect on the physiology of the native sulfate reducing microbial consortia (**Figures 1**, **2**, **4**, **6**). As previously noted, the maximum rates of SR occurred at 50°C and pH 6, and suggest that the native SR community is most active in a moderate (∼50°C) temperature and only slightly acidic pH regime. This is consistent with mixing models dominated by seawater advection, where a mixed fluid at 50°C had a pH of ∼6, high sulfate, low sulfide and limited oxygen (note that these calculated concentrations of dissolved O_2 do not take into consideration biotic or abiotic reactions that consume oxygen), providing ideal conditions for sulfate reduction in the outer region of the chimney (Tivey, 2004). The correspondence between our maximum SR rates and these mixing models suggests that advection of seawater into the wall of the vent may be an important factor for constraining the physiology of the native sulfate reducing community.

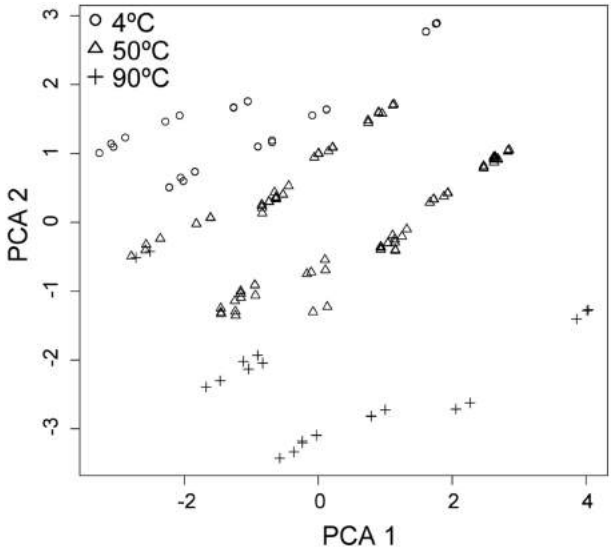

FIGURE 6 | Principal component analysis (PCA) of the variation between samples ($n = 274$) as a linear combination of standardized chemical (sulfate, sulfide, pH, DOC, Cu^{2+}, Fe^{2+}, and Zn^{2+}), thermal, rate and energetic parameters (variance within each parameter = 1). PCA 1 represents 28.5% and PCA 2 represents 19.9% of the variance within the data (PCA 3 and PCA 4, not shown, represent 12 and 10% respectively). Data are clustered most obviously by temperature at 4°C (◯), 50°C (Δ), and 90°C (+).

Previous work in other hydrothermal systems has also suggested that temperature is a primary factor in governing metabolic rates and, likely, community composition. For example, in basalt-hosted borehole fluids from Juan de Fuca Ridge maximum rates of SR occurred at temperatures near *in situ* conditions and were consistent with physiological tolerances of the native SR community (Robador et al., 2015). Similarly, in hydrothermal chimneys from Middle Valley vent field, Juan de Fuca Ridge, maximum SR rates were observed at temperatures (90°C) near the growth ranges for the *in situ* SR community (hyperthermophiles) (Frank et al., 2013). Considering that SR rates from Grotto and Middle Valley were measured under identical experimental conditions, differences in the thermal optima of SR between Grotto and Middle Valley are likely due to differences in the prokaryotic abundance and phylogenetic composition of associated consortia (Frank et al., 2013; Olins et al., 2013). This hypothesis is ecologically consistent with temperature being one of the main driving forces that shape the composition and abundance of hydrothermal vent microbial communities (Harmsen et al., 1997; Takai et al., 2001; Schrenk et al., 2003; Kormas et al., 2006; Pagé et al., 2008). Additionally, differences in density and composition within a chimney are a reflection of the mineralogy and physico-chemical conditions at each site. For example, deposits sampled at Middle Valley were physically smaller than Grotto, composed primarily of anhydrite (with no inner conduit like structures), and exposed to higher temperature end-member fluid (261°C). Thus, it is not surprising that the environment at Middle Valley selected for a hyperthermophilic community dominated by *Thermodesulfovibro* (Frank et al., 2013) or *Archaeoglobus*-like (Olins et al., 2013) organisms. On the other hand, Grotto is a very large hydrothermal deposit with a mature mineralogical structure (Tivey and Delaney, 1986), allowing for a greater range of habitable niches and more space for colonization. Because mesophillic, as well as slightly thermophilic phylotypes are often observed to colonize within the outer regions of hydrothermal vents (Takai et al., 2001; Hoek et al., 2003; Schrenk et al., 2003; Nakagawa et al., 2005; Kormas et al., 2006; Pagé et al., 2008), we posit that the majority of SR in the Grotto occurs in the outer to middle region of the flange and is dominated by thermophilic organisms.

Environmental Constraints on SR Rates

Environmental selection of physiologically adapted microbial communities applies not only to parameters such as temperature and pH, but also to geochemical constraints such as dissolved sulfide and metal toxicity. Some SR isolates can be inhibited by elevated sulfide (2–15 mM) (Reis et al., 1992; Okabe et al., 1995; Koschorreck, 2008), although vent isolates are known to tolerate a wider range of sulfide concentrations. For example, archaea isolated from of deep-sea hydrothermal vents such as *Methanocaldococcus jannaschii, Archaeoglobus profundus, Thermococcus fumicolans,* and isolates from the genus *Pyrococcus* and *Desulfurococcus* have high tolerance to hydrogen sulfide concentrations in the range of 40–100 mM (Jannasch et al., 1988; Lloyd et al., 2005). Our incubations experiments were amended with sulfide at concentrations (up to 1 mM), well below the values measured in in Grotto end-member fluids (5.4 mmol/kg at pH = 4.2; Butterfield et al., 1994). Assuming that native Grotto SR communities are adapted to tolerate *in situ* sulfide concentrations, it is unlikely that sulfide toxicity largely impacted SR rates in our experiments. This is consistent with experiments at optimal temperature and pH (50°C, pH 6), for which SR rates do not significantly depend on sulfide concentrations (Table S1, $p = 0.5$), despite the fact that increasing sulfide concentrations do decrease energy yields (**Figure 5Aiii**).

At 50°C and pH 4, measured SR rates increase with increasing sulfide (**Figure 4B**). The positive correlation of SR with sulfide concentration at pH 4 is surprising given that the favorability ($\Delta G_r°$) of SR decreases with increasing concentrations of sulfide. However, there are no significant correlations between rates of SR and ΔG_r in our sulfide amended incubations (**Figure 7A**; Pearson's correlation, $p > 0.2$) and no obvious patterns in energy density that might explain the differences attributable to pH. Accordingly, we investigated the possibility that sulfide amendments were poising the incubations at a redox potential favorable for SR (usually confined to E_h values of −0.3 to 0.0 V at circumneutral pH and slightly more positive under more acidic conditions; Lovley and Goodwin, 1988; Church et al., 2007). While the addition of sulfide at pH 4 does lower the E_h of the H_2S/SO_4^{2-} redox pair, this effect was pH invariant (Figure S2) and thus we posit that E_h is unlikely to be the parameter controlling increasing SR rates with increasing sulfide concentrations at pH 4 and 50°C.

Fluid pH, however, also affects mineral solubility, and at lower pH the toxicity of metals and organic acids are often

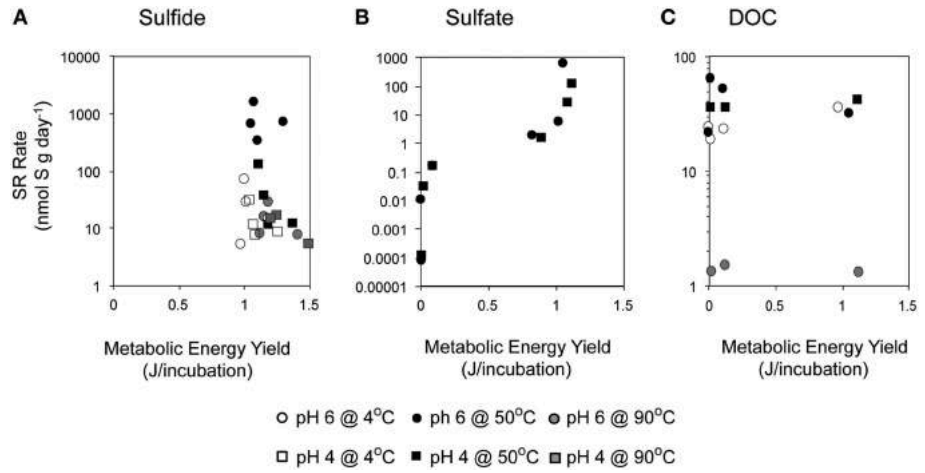

FIGURE 7 | Relationship between metabolic energy available from sulfate reduction and empirically measured rates of SR in incubations with varying concentrations of (A) sulfide, (B) sulfate, and (C) DOC are shown here at 4°C (white), 50°C (black), and 90°C (gray), and at pH 6 (circle) or pH 4 (square).

elevated as minerals are solubilized and organic acids become protonated (Ghose and Wiken, 1955; Oleszkiewicz et al., 1989; Giller et al., 1998; Gadd and Griffiths, 2013). For example, at low pH, the carboxyl groups of simple organic acids are primarily undissociated, allowing them to pass across the cell membrane where they can uncouple electrochemical gradients (Ghose and Wiken, 1955). Of particular concern in hydrothermal environments is the dissolution of metal sulfides, which is enhanced at lower pH and depends on sulfide concentrations. To evaluate the potential for metal toxicity in our incubations, we calculated *in situ* activities of Fe, Zn, and Cu (assuming *in situ* end-member concentrations; Butterfield et al., 1994), which are known to be toxic when dissolved and in sufficient concentration. The activities of Fe, Zn, and Cu were elevated at lower pH, and several metal sulfides and iron oxides were supersaturated under the high aqueous sulfide incubation conditions. We investigated the possibility that high sulfide amendments drew down trace metal concentration via mineral precipitation, thus explaining the increases in SR rates with increasing sulfide concentration. To account for mineral precipitation resulting from sulfide addition, we performed a single-point reaction path calculation to constrain the expected aqueous metal activities as functions of both pH and sulfide concentration. The fluid speciation models assumed initial trace metal concentrations from end-member fluid analyses (Butterfield et al., 1994) and allowed minerals to reach supersaturation resulting in aqueous activities of $\sim 10^{-5.3}$ and $\sim 10^{-3.7}$, Cu^{2+} and Fe^{2+} respectively. High sulfide concentrations likely led to abiotic mineral precipitation in the incubation experiments, leading to the drawdown of trace metal concentrations. Accounting for amended sulfide concentrations, *in situ* pH, and mineral precipitation (primarily pyrite, hematite and covellite), activities of Cu^{2+} and Fe^{2+}were reduced to 10^{-13} and $\sim 10^{-4.5}$, respectively, depending on pH (**Figure 8**). Precipitation of these metal sulfides also lowered the calculated fluid pH, an effect that was more pronounced for pH 6 incubations (final fluid pH ∼4 after mineral precipitation) than in pH 4 incubations (final pH ∼3.3). While we could not monitor pH during the radiolabeled experiments, these values are within the range expected for Grotto chimney environments, and the effect was minimal for pH 4 incubations.

Because the sulfate reducing organisms in this study are embedded within a metal sulfide matrix, the most feasible explanation for the pattern of increasing SR rates observed at pH 4 with increasing sulfide (**Figure 4B**) is attenuation of metal toxicity by metal-sulfide precipitation (**Figure 8**). In pure cultures of *Thermococcus fumicolans*, *Pyrococcus* strain GB-D, *Methanocaldococcus jannaschii*, sulfide additions were shown to attenuate the toxic effects of metal cations by forming metal-sulfide complexes (Edgcomb et al., 2004). In our incubation experiments, the reduction of aqueous Cu^{2+} (and to a lesser extent Fe^{2+}) via mineral precipitation, particularly at high sulfide concentrations, likely attenuated metal toxicity to native sulfate reducers. The free metal activities were below the ranges that have been found to be toxic to sulfate reducing bacteria (e.g., $10^{-3.1}$ to $10^{-4.33}$ for Cu^{2+} (Booth and Mercer, 1963; Saleh et al., 1964; Temple and Le Roux, 1964; Hao et al., 1994; Sani et al., 2001; Utgikar et al., 2002, 2003; **Figure 8A**). These patterns are particularly pronounced for Cu^{2+} and correlation between SR rates and aqueous Cu^{2+} activities suggests that metal-sulfide precipitation and the resulting decrease in metal toxicity can account for increasing SR rates at high sulfide concentrations (**Figure 8B**). The effect is even more apparent at pH 4 (e.g., a 10-fold decrease in SR rates as Cu^{2+} activities increase) likely because cells are already compromised by the low pH.

Energetic Constraints of SR Rates

Substrate availability and uptake mechanisms subtly influence the magnitude of SR rates in Grotto flanges. The Michaelis-Menten constants (or K_m, defined as the sulfate concentration at which the reaction rate is at half-maximum) calculated for Grotto are higher than the range of K_m values calculated for SR in marine sediments (0.204–1.63 mM; Boudreau and

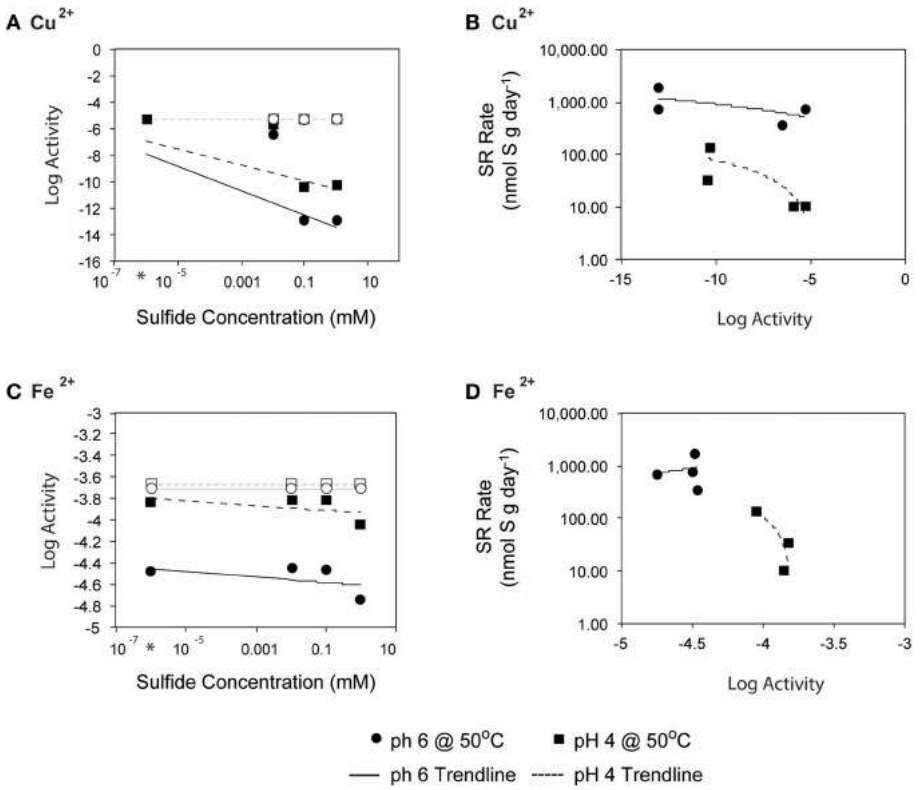

FIGURE 8 | Initial sulfide concentration and the log activities of (A) Cu^{2+} and (C) Fe^{2+} at 50°C (as calculated by EQ3/6) and pH of 4 (○) or 6 (■) are related. Linear regression lines are shown for pH 4 (- - -) and pH 6 (-). Average rates of SR at 50°C (from 0, 0.01, 0.1, and 1 mM H_2S additions experiments) are plotted with respect to log activities of **(B)** Cu^{2+} and **(D)** Fe^{2+}. Note that activity is a measure of the effective concentration of a species within a fluid.

Westrich, 1984; Kostka et al., 2002; Roychoudhury et al., 2003; Pallud and Van Cappellen, 2006), low sulfate environments (10–70 μM; Ingvorsen et al., 1981; Lovley et al., 1982), and marine sulfate reducers in pure culture (3.0–330 μM; Ingvorsen et al., 1981; Ingvorsen and Jørgensen, 1984; Sonne-hansen and Westermann, 1999). One plausible explanation for why K_m values for hydrothermal SR are higher than in other marine systems, is that the cellular uptake of sulfate is less efficient in hydrothermal sulfate reducers. Since all the enzymes required to catalyze sulfate into hydrogen sulfide are located in the interior of a cell (cytoplasm or associated with the inner surface of the cytoplasmic membrane), sulfate must be transported into the cells in order to be utilized. Due to the high sulfate concentration in seawater, marine SR communities often utilize low affinity transport mechanisms such as cation dependent passive transport (Cypionka and Konstanz, 1989; Kreke and Cypionka, 1992, 1994, 1995) but can switch to active transport via sulfate permeases (Piłsyk and Paszewski, 2009) under sulfate limitation (Tarpgaard et al., 2011). In comparison to marine systems, hydrothermal sulfide deposit environments have higher metal and H_2S loads, lower relative sulfate and experience higher temperature and lower pH fluids. Higher K_m values at vents may be a result of insoluble metal sulfides acting as barriers to prevent the transport of sulfate (or other substrate) into the cell (Utgikar et al., 2002). Hydrothermal communities may mediate the potentially inhibitory effects of high temperature, low pH and sulfate limitation by increasing the number or type of sulfate permeases per cell. Our data suggests that sulfate reducers have a higher affinity for sulfate at pH 4 than at pH 6 and may utilize different mechanisms (like increasing the number or type of sulfate permeases utilized) to overcome pH-induced constraints to maintain constant rates of SR.

It is also important to note that Michaelis-Menten kinetic models, and calculated values of K_m, are based on idealized growth conditions, including optimized physiological parameters, single limiting substrates (e.g., sulfate), the absence of inhibitory mechanisms, and no community members of competition in the community structure. For example, our values of K_m assume that sulfate is the sole limiting substrate, however calculated energy densities (**Figure 5Bv**) indicate this is not always, or even usually, the case in this system. Interestingly, the measured rates, at 14 mM sulfate, are comparable in magnitude to hydrothermally influenced sediments from Guaymas basin (high sulfate; Jørgensen et al., 1990; Elsgaard et al., 1994a) and Lake Tanganyika (low sulfate; Elsgaard et al., 1994b), which have strikingly different sulfate concentrations, suggesting that sulfate concentration alone may not govern the overall kinetics of SR. Considering this, it is more likely that energy availability in the context of substrate availability

is constraining the magnitude of rates and complicating the Michaelis-Menten kinetics pattern we might expect.

Substrate limitation is often concomitant with energy-limited conditions. Minimal energy requirements for autotrophic SR in marine sediments are inferred to be −19.1 kJ/mol SO_4^{2-} (Hoehler et al., 2001) and it has been suggested that these minimal requirements are always easily met for heterotrophic metabolisms (Lever et al., 2015). Regardless, our values of Gibbs free energy yields, normalized per mole of sulfate (ca. −100 to −150 kJ/mol SO_4^{2-}), greatly exceed the minimum energy requirements for autotrophic sulfate reduction. Thus, it is unlikely that metabolic energy availability was limiting in most conditions in our experiments. Nonetheless, SR rates are positively correlated with metabolic energy availability (**Figure 7B**; Kendal rank correlation $p < 0.005$), suggesting that energy availability still plays a role in microbial metabolic rates, even if it is not limiting microbial growth. Furthermore, the energy available for SR across most conditions within these incubations could support ∼10^5–10^6 cells•g matrix^{-1} [assuming that 10% of that energy supports growth, cellular synthesis requires 1434 J•g cell in anoxic environments (McCollom and Amend, 2005), the abundance of SR bacteria and archaea *in situ* is 10^3–10^4 cells•g matrix^{-1} (Frank et al., 2013), and cells have 1 *dsrA* gene copy (Klein et al., 2001; Kondo et al., 2004)]. Even at the lowest values of sulfate, 10 nM, the energy within the system could support ∼100 cells/g mineral.

Interestingly, high rates of SR were observed even when metabolic energy yield was assumed to be low, based on the exogenous DOC concentration provided in each batch reaction (**Figure 7C**). This suggests that we underestimated the energy yield provided in each batch reaction and did not take into consideration potential sources of endogenous carbon within the mineral inoculum. Heterotrophic SR utilizing a wide variety of metabolic products has been shown to be thermodynamically favorable in hydrothermal environments based on concentrations in diffuse fluid (Rogers and Amend, 2006). Mineral associated products of microbial respiration or fermentation and lysed cells are likely other sources of endogenous organic carbon. Perhaps more important is the contribution of remnants from associated macrofauna as the surface of the Grotto flange was heavily colonized by tubeworms. Tube worm growth provides structural scaffolding for the concentration and precipitation of minerals during the initial stages of hydrothermal chimney and flange formation (Kristall et al., 2006) and fossilized tube structures have been observed within mineralogical samples of Grotto deposits (Tivey et al., 1999). Reasonably, dead macrofauna—heterogeneously distributed within the walls of a hydrothermal deposit—may provide localized and concentrated sources of carbon for microbial utilization and sulfate reduction.

Currently, our assumptions of the amount of carbon available within the mineral matrix of hydrothermal vents is based solely on DOC measurements from end-member and diffuse flow (Lang et al., 2006, 2010). However, these fluid measurements may only place lower bounds on carbon availability in hydrothermal systems. Unfortunately, concentrations of mineral associated carbon (or total organic carbon) have not been evaluated, due to technical complications, in hydrothermal chimneys. The only measurements of the total organic carbon (TOC) in similar mineral hosted systems across the Juan de Fuca Ridge are in sediments and values (wt%) vary between 0.06 and 0.83% and hydrolysable amino acids account for up to 3.3% of this organic carbon (Andersson et al., 2000). If we assume a maximum density of 10^8 cells•g matrix^{-1} (Schrenk et al., 2003), and the average carbon content of 12.4 ± 6.3 fg C per oceanic bacterial cell (Fukuda et al., 1998) that's roughly 12.4 µg C•g matrix^{-1} (0.0012% by weight) that could be respired, and could support 0.0341 J•g matrix^{-1} of energy for sulfate reduction. Energy from the recycling of bacterial biomass alone would be enough to support 10^5 cells•g matrix^{-1}, and these calculations do not even include potential carbon estimations from eukaryotic input. Similarly, recent studies suggest that the degradation of subsurface microbial biomass may be an important source of organic matter in unsedimented hydrothermal systems and expands the types of heterotrophic metabolic strategies thought possible in these environments (Reeves et al., 2014). These data suggest that hydrothermal chimneys may contain a substantially greater amount of biologically available endogenous carbon to support heterotrophic metabolisms than has previously been considered by bioenergetic models. DOC and TOC measurements at vents are relatively sparse and a more thorough documentation of these values across vent fields would be incredibly valuable to re-evaluate the potential energy yields of heterotrophic metabolisms in hydrothermal systems.

We cannot overlook the possibility of substrate competition among *in situ* microorganisms utilizing alternate metabolisms. However, because these experiments were incubated in the absence of nitrate and hydrogen, potential competition with denitrifiers or any autotrophic metabolisms can be excluded in our reactions. Furthermore, data from numerous studies suggest that under these experimental conditions heterotrophic sulfate reducers would outcompete methanogenic bacteria (Oremland and Taylor, 1977; Oremland and Polcin, 1982; Lovley and Klug, 1986; Weijma et al., 2000). While many organisms capable of iron reduction have been isolated from vents (Takai et al., 2000; Kashefi et al., 2002; Hirayama et al., 2007; Sokolova et al., 2007; Slobodkina et al., 2009), the mineralogy of Grotto—reduced iron minerals (Tivey and Delaney, 1986; Delaney et al., 1992)- suggests limited influence from iron reducers under these experimental conditions.

CONCLUDING REMARKS

Multivariate experiments that couple empirically derived data and bioenergetic modeling can significantly advance our understanding of SR within complex hydrothermal systems by placing constraints on the factor(s) most likely governing SR activity at *in situ* conditions. Moving toward a better understanding of SR—and associated processes—in the natural world requires that processes are studied at conditions relevant to those found *in situ*. Indeed, the factors governing SR *in situ* are complex, sufficiently so as to make it difficult to establish causality with a high degree of certainty. That said, this work underscores the relevance of interactions among

physico-chemical conditions, water-rock reactions, microbial physiology, and metabolic energetics, and their combined effect on microbial activity. These findings suggest that the variability in sulfate reduction rates reflect the response of the active microbial consortia to environmental constraints on *in situ* microbial physiology, toxicity, and the type and extent of energy limitation. These results further emphasize that the effect of *in situ* metabolic reaction energetics is minimal under energy-rich conditions (Jin and Bethke, 2007), but likely play an important role under energy-limiting conditions and during competition. The data presented here highlight the significance of sulfate reduction in hydrothermal chimneys and provide a framework for continued studies of sulfur cycling along mid-ocean ridge systems.

It is important to recognize that geochemical models of metabolic energy availability, even when considering *in situ* fluid chemistry, cannot explain microbial activity, like SR rates, in all systems. Ideally future studies would couple fine-scale *in situ* redox measurements and microbial sampling with bioenergetic modeling and direct measurements of metabolic rates in order to more explicitly constrain microbial niches across steep redox gradients. Integrating analyses of the microbial community composition and structure, metagenomic reconstructions of energy metabolisms, and measured rates of metabolic activities of hydrothermal chimney microbes can provide specific evidence to test energetic hypothesizes. Only by concurrently assessing these biological and geochemical data can we begin to understand the relationship between vent geochemistry and the prolific and diverse communities observed therein, as well as their impact on global biogeochemical cycles of sulfur and carbon.

ACKNOWLEDGMENTS

Financial support for this research was provided by the Nation Science Foundation (OCE-0838107 and OCE-1061934 to PG), the National Aeronautic and Space Administration (NASA-ASTEP NNX09AB78G to C. Scholin and PG and NASA-ASTEP NNX07AV51G to A. Knoll and PG) and the Center for Dark Energy Biosphere Investigations (C-DEBI graduate fellowship support to KF). We are grateful for the expert assistance of the *R/V Atlantis* crews and the pilots and team of the *DSV Jason* for enabling the collections of hydrothermal deposits used in our experiments. We also thank Steve Sansone, Joseph Ring, Julie Hanlon, Colleen Cavanaugh, Heather Olins, John Skutnik, Mark Nielson and Victoria Bertics for providing assistance with various technical aspects of the experiments.

SUPPLEMENTARY MATERIAL

The Supplementary Material for this article can be found online at: http://journal.frontiersin.org/article/10.3389/fmicb.2015.01449

REFERENCES

Alazard, D., Dukan, S., Urios, A., Verhe, F., Bouabida, N., Morel, F., et al. (2003). *Desulfovibrio hydrothermalis* sp nov., a novel sulfate-reducing bacterium isolated from hydrothermal vents. *Int. J. Syst. Evol. Microbiol.* 53, 173–178. doi: 10.1099/ijs.0.02323-0

Amend, J. P., McCollom, T. M., Hentscher, M., and Bach, W. (2011). Catabolic and anabolic energy for chemolithoautotrophs in deep-sea hydrothermal systems hosted in different rock types. *Geochim. Cosmochim. Acta*, 75, 5736–5748. doi: 10.1016/j.gca.2011.07.041

Amend, J. P., and Rogers, K. L., Meyer-Dombard, D. R. (2004). "Microbially mediated sulfur-redox: energetics in marine hydrothermal vent systems," in *Sulfur Biogeochemistry: Past and Present*, eds J. P. Amend, K. J. Edwards, and T. W. Lyons (Boulder, CO: Geological Society of America), 17–34.

Amend, J. P., Rogers, K. L., Shock, E. L., Gurrieri, S., and Inguaggiato, S. (2003). Energetics of chemolithoautotrophy in the hydrothermal system of Vulcano Island, southern Italy. *Geobiology* 1, 37–58. doi: 10.1046/j.1472-4669.2003.00006.x

Amend, J. P., and Shock, E. L. (2001). Energetics of overall metabolic reactions of thermophilic and hyperthermophilic Archaea and Bacteria. *FEMS Microbiol. Rev.* 25, 175–243. doi: 10.1111/j.1574-6976.2001.tb00576.x

Andersson, E., Simoneit, B. R. T., and Holm, N. G. (2000). Amino acid abundances and stereochemistry in hydrothermally altered sediments from the Juan de Fuca Ridge, northeastern Pacific Ocean. *Appl. Geochem.* 15, 1169–1190. doi: 10.1016/S0883-2927(99)00110-9

Audiffrin, C., Cayol, J. L., Joulian, C., Casalot, L., Thomas, P., Garcia, J. L., et al. (2003). *Desulfonauticus submarinus* gen. nov., sp nov., a novel sulfate-reducing bacterium isolated from a deep-sea hydrothermal vent. *Int. J. Syst. Evol. Microbiol.* 53, 1585–1590. doi: 10.1099/ijs.0.02551-0

Booth, G. H., and Mercer, S. J. (1963). Resistance to copper of some oxidizing and reducing bacteria. *Nature* 199:622. doi: 10.1038/199622a0

Bostick, B. C., Fendorf, S., and Helz, G. R. (2003). Differential adsorption of molybdate and tetrathiomolybdate on pyrite (FeS_2). *Environ. Sci. Technol.* 37, 285–291. doi: 10.1021/es0257467

Boudreau, B., and Westrich, J. (1984). The dependence of bacterial sulfate reduction on sulfate concentration in marine sediments. *Geochim. Cosmochim.* 48, 2503–2516. doi: 10.1016/0016-7037(84)90301-6

Butterfield, D. A., McDuff, R. E., Mottl, M. J., Lilley, M. D., Lupton, J. E., and Massoth, G. J. (1994). Gradients in the composition of hydrothermal fluids from the Endeavour segment vent field: phase separation and brine loss. *J. Geophys. Res.* 99, 9561–9583. doi: 10.1029/93JB03132

Canfield, D. E. (1989). Sulfate Reduction and oxic respiration in marine-sediments- Implications for organic-carbon preservation in euxinic envrionments. *Deep Sea Res. A Oceanogr. Res. Pap.* 36, 121–138. doi: 10.1016/0198-0149(89)90022-8

Canfield, D. E., Stewart, F. J., Thamdrup, B., De Brabandere, L., Dalsgaard, T., Delong, E. F., et al. (2010). A cryptic sulfur cycle in oxygen-minimum-zone waters off the Chilean coast. *Science* 330, 1375–1378. doi: 10.1126/science.1196889

Church, C. D., Wilkin, R. T., Alpers, C. N., Rye, R. O., and McCleskey, R. B. (2007). Microbial sulfate reduction and metal attenuation in pH 4 acid mine water. *Geochem. Trans.* 8:10. doi: 10.1186/1467-4866-8-10

Cypionka, H., and Konstanz, U. (1989). Characterization of sulfate transport in *Desulfovibrio desulfuricans*. *Arch. Microbiol.* 152, 237–243. doi: 10.1007/BF00409657

D'Hondt, S., Jørgensen, B. B., Miller, D. J., Batzke, A., Blake, R., Cragg, B. A., et al. Guerin, G. (2004). Distributions of microbial activities in deep subseafloor sediments. *Science* 306, 2216–2221. doi: 10.1126/science.1101155

Delaney, J. R., Robigou, V., McDuff, R. E., and Tivey, M. K. (1992). Geology of a vigorous hydrothermal system on the Endeavor segment, Juan de Fuca ridge. *J. Geophys. Res. Earth* 97, 19663–19682. doi: 10.1029/92JB00174

Detmers, J., Brüchert, V., and Habicht, K. S. (2001). Diversity of sulfur isotope fractionations by sulfate-reducing prokaryotes. *Appl. Environ. Microbiol.* 67, 888–894. doi: 10.1128/AEM.67.2.888-894.2001

Dittmar, W. (1884). Report on researches into the composition of ocean water, collected by the HMS Challenger, during the years 1873-1876. *Rept. Sci. Results Voyag. H.M.S. Chall. (Phys. Chem.)*, 1, 1–251.

Edgcomb, V. P., Molyneaux, S. J., Saito, M. A., Lloyd, K., Böer, S., Wirsen, C. O., et al. (2004). Sulfide ameliorates metal toxicity for deep-sea hydrothermal vent

archaea. *Appl. Environ. Microbiol.* 70, 2551–2555. doi: 10.1128/AEM.70.4.2551-2555.2004

Elsgaard, L., Isaksen, M. F., Jørgensen, B. B., Alayse, A. M., and Jannasch, H. W. (1994a). Microbial sulfate reduction in deep-sea sediments at the Guaymas Basin hydrothermal vent area: influence of temperature and substrates. *Geochim. Cosmochim. Acta*, 58, 3335–3343. doi: 10.1016/0016-7037(94)90089-2

Elsgaard, L., Prieur, D., Mukwaya, G. M., and Jørgensen, B. B. (1994b). Thermophilic sulfate reduction in hydrothermal sediment of lake tanganyika, East Africa. *Appl. Environ. Microbiol.* 60, 1473–1480.

Engelen, B., Ziegelmüller, K., Wolf, L., Köpke, B., Gittel, A., Cypionka, H., et al. (2008). Fluids from the oceanic crust support microbial activities within the deep biosphere. *Geomicrobiol. J.* 25, 56–66. doi: 10.1080/01490450701829006

Fike, D. A., Gammon, C. L., Ziebis, W., and Orphan, V. J. (2008). Micron-scale mapping of sulfur cycling across the oxycline of a cyanobacterial mat: a paired nanoSIMS and CARD-FISH approach. *ISME J.* 2, 749–759. doi: 10.1038/ismej.2008.39

Fossing, H., and Jørgensen, B. B. (1989). Measurment of bacterial sulfate reduction in sediments- evaluation of a single-step chromium reduction method. *Biogeochemistry* 8, 205–222. doi: 10.1007/BF00002889

Frank, K. L., Rogers, D. R., Olins, H. C., Vidoudez, C., and Girguis, P. R. (2013). Characterizing the distribution and rates of microbial sulfate reduction at Middle Valley hydrothermal vents. *ISME* 7, 1391–1401. doi: 10.1038/ismej.2013.17

Fukuda, R., Ogawa, H., and Nagata, T. (1998). Direct determination of carbon and nitrogen contents of natural bacterial assemblages in marine environments. *Appl. Environ. Microbiol.* 64, 3352–3358.

Gadd, G. M., and Griffiths, A. J. (2013). Microorganisms and heavy metal toxicity. *Microb. Ecol.* 4, 303–317. doi: 10.1007/BF02013274

Ghose, T., and Wiken, T. (1955). Inhibition of bacterial sulphate-reduction in presence of short chain fatty acids. *Physiol. Plant.* 8, 116–134. doi: 10.1111/j.1399-3054.1955.tb08965.x

Giller, K. E., Witter, E., and McGrath, S. P. (1998). Toxicity of heavy metals to microorganisms and microbial processes in agricultural soils: a review. *Soil Biol. Biochem.* 30, 1389–1414. doi: 10.1016/S0038-0717(97)00270-8

Hao, O. J., Huang, L., Chen, J. M., and Buglass, R. L. (1994). Effects of metal additions on sulfate reduction activity in wastewaters. *Toxicol. Environ. Chem.* 46, 197–212. doi: 10.1080/02772249409358113

Harmsen, H. J. M., Prieur, D., and Jeanthon, C. (1997). Distribution of microorganisms in deep-sea hydrothermal vent chimneys investigated by whole-cell hybridization and enrichment culture of thermophilic subpopulations. *Appl. Environ. Microbiol.* 63, 2876–2883.

Hirayama, H., Sunamura, M., Takai, K., Nunoura, T., Noguchi, T., Oida, H., et al. Horikoshi, K. (2007). Culture-dependent and -independent characterization of microbial communities associated with a shallow submarine hydrothermal system occurring within a coral reef off Taketomi Island, Japan. *Appl. Environ. Microbiol.* 73, 7642–7656. doi: 10.1128/AEM.01258-07

Hoehler, T. M., Alperin, M. J., Albert, D. B., and Martens, C. S. (2001). Apparent minimum free energy requirements for methanogenic Archaea and sulfate-reducing bacteria in an anoxic marine sediment. *FEMS Microbiol. Ecol.* 38, 33–41. doi: 10.1111/j.1574-6941.2001.tb00879.x

Hoek, J., Banta, A., Hubler, F., and Reysenbach, A. L. (2003). Microbial diversity of a sulphide spire located in the Edmond deep-sea hydrothermal vent field on the Central Indian Ridge. *Geobiology* 1, 119–127. doi: 10.1046/j.1472-4669.2003.00015.x

Holmkvist, L., Ferdelman, T. G., and Jørgensen, B. B. (2011a). A cryptic sulfur cycle driven by iron in the methane zone of marine sediment (Aarhus Bay, Denmark). *Geochim. Cosmochim. Acta* 75, 3581–3599. doi: 10.1016/j.gca.2011.03.033

Holmkvist, L., Kamyshny, A. Jr., Vogt, C., Vamvakopoulos, K., Ferdelman, T. G., and Jørgensen, B. B. (2011b). Sulfate reduction below the sulfate-methane transition in Black Sea sediments. *Deep Sea Res. I Oceanogr. Res. Pap.* 58, 493–504. doi: 10.1016/j.dsr.2011.02.009

Huber, H., Jannasch, H., Rachel, R., Fuchs, T., and Stetter, K. O. (1997). *Archaeoglobus veneficus* sp nov, a novel facultative chemolithoautotrophic hyperthermophilic sulfite reducer, isolated from abyssal black smokers. *Syst. Appl. Microbiol.* 20, 374–380. doi: 10.1016/S0723-2020(97)80005-7

Ingvorsen, K., and Jørgensen, B. B. (1984). Kinetics of sulfate uptake by freshwater and marine species of *Desulfovibrio*. *Arch. Microbiol.* 139, 61–66. doi: 10.1007/BF00692713

Ingvorsen, K., Zeikus, J. G., and Brock, T. D. (1981). Dynamics of bacterial sulfate reduction in a eutrophic lake. *Appl. Environ. Microbiol.* 42, 1029–1036.

Isaksen, M. F., Bak, F., and Jørgensen, B. B. (1994). Thermophilic sulfate-reducing bacteria in cold marine sediment. *FEMS Microbiol. Ecol.* 14, 1–8. doi: 10.1111/j.1574-6941.1994.tb00084.x

Jannasch, H. W., Wirsen, C. O., Molyneaux, S. J., and Langworthy, T. A. (1988). Extremely thermophilic fermentative archaebacteria of the genus *Desulfurococcus* from deep-sea hydrothermal vents. *Appl. Environ. Microbiol.* 54, 1203–1209.

Jeanthon, C., Haridon, L., Cueff, V., Banta, A., Reysenbach, A., and Prieur, D. (2002). *Thermodesulfobacterium hydrogeniphilum* sp. nov., a thermophilic, chemolithoautotrophic, sulfate-reducing bacterium isolated from a deep-sea hydrothermal vent at Guaymas Basin. *Int. J. Syst. Evol. Microbiol.* 52, 765–772. doi: 10.1099/00207713-52-3-765

Jin, Q., and Bethke, C. M. (2007). The thermodynamics and kinetics of microbial metabolism. *Am. J. Sci.* 307, 643–677. doi: 10.2475/04.2007.01

Jin, Q. S., and Bethke, C. M. (2005). Predicting the rate of microbial respiration in geochemical environments. *Geochim. Cosmochim. Acta* 69, 1133–1143. doi: 10.1016/j.gca.2004.08.010

Johnson, J. W., Oelkers, E. H., and Helgeson, H. C. (1992). SUPCRT92: a software package for calculating the standard molal thermodynamic properties of minerals, gases, aqueous species, and reactions from 1 to 5000 bar and 0 to 1000°C. *Comput. Geosci.* 18, 899–947. doi: 10.1016/0098-3004(92)90029-Q

Jørgensen, B. B., and Bak, F. (1991). Pathways and microbiology of thiosulfate transformations and sulfate reduction in a marine sediment (Kattegat, Denmark). *Appl. Environ. Microbiol.* 57, 847–856.

Jørgensen, B. B., and Fenchel, T. (1974). The sulfur cycle of a marine sediment model system. *Mar. Biol.* 24, 189–201. doi: 10.1007/BF00391893

Jørgensen, B. B., Isaksen, M. F., and Jannasch, H. W. (1992). Bacterial sulfate reduction above 100-degrees-C in deep-sea hydrothermal vent sediments. *Science (80-.).* 258, 1756–1757. doi: 10.1126/science.258.5089.1756

Jørgensen, B. B., Zawacki, L. X., and Jannasch, H. W. (1990). Thermophilic bacterial sulfate reduction in deep-sea sediments at the Guaymas Basin hydrothermal vent site (Gulf of California). *Deep Sea Res. A Oceanogr. Res. Pap.* 37, 695–710. doi: 10.1016/0198-0149(90)90099-H

Joye, S. B., Boetius, A., Orcutt, B. N., Montoya, J. P., Schulz, H. N., Erickson, M. J., et al. (2004). The anaerobic oxidation of methane and sulfate reduction in sediments from Gulf of Mexico cold seeps. *Chem. Geol.* 205, 219–238. doi: 10.1016/j.chemgeo.2003.12.019

Kallmeyer, J., and Boetius, A. (2004). Effects of temperature and pressure on sulfate reduction and anaerobic oxidation of methane in hydrothermal sediments of Guaymas Basin. *Appl. Environ. Microbiol.* 70, 1231–1233. doi: 10.1128/AEM.70.2.1231-1233.2004

Kallmeyer, J., Ferdelman, T. G., and Jørgensen, B. B. (2002). Sulfate reduction rates in deeply, buried marine sediments. *Geochim. Cosmochim.* 66, A378.

Kallmeyer, J., Ferdelman, T. G., Weber, A., Fossing, H., and Jorgensen, B. B. (2004a). A cold chromium distillation procedure for radiolabeled sulfide applied to sulfate reduction measurements. *Limnol. Oceanogr.* 2, 171–180. doi: 10.4319/lom.2004.2.171

Kallmeyer, J., Ferdelman, T. G., Weber, A., Fossing, H., and Jørgensen, B. B. (2004b). Evaluation of a cold chromium distillation procedure for recovering very small amounts of radiolabeled sulfide related to sulfate reduction measurements. *Limnol. Oceanogr. Methods*, 2, 171–180. doi: 10.4319/lom.2004.2.171

Kashefi, K., Tor, J. M., Holmes, D. E., Gaw Van Praagh, C. V., Reysenbach, A.-L., and Lovley, D. R. (2002). *Geoglobus ahangari* gen. nov., sp. nov., a novel hyperthermophilic archaeon capable of oxidizing organic acids and growing autotrophically on hydrogen with Fe(III) serving as the sole electron acceptor. *Int. J. Syst. Evol. Microbiol.* 52, 719–728. doi: 10.1099/00207713-52-3-719

Klein, M., Friedrich, M., Roger, A. J., Hugenholtz, P., Fishbain, S., Abicht, H., et al. Linda, L. (2001). Multiple lateral transfers of dissimilatory sulfite reductase genes between major lineages of sulfate-reducing prokaryotes. *Appl. Environ. Microbiol.* 183 6028–6035. doi: 10.1128/jb.183.20.6028-6035.2001

Kondo, R., Nedwell, D. B., Purdy, K. J., and Silva, S. Q. (2004). Detection and enumeration of sulphate-reducing bacteria in estuarine sediments by competitive PCR. *Geomicrobiol. J.* 21, 145–157. doi: 10.1080/01490450490275307

Kormas, K. A., Tivey, M. K., Von Damm, K., and Teske, A. (2006). Bacterial and archaeal phylotypes associated with distinct mineralogical layers of a white

smoker spire from a deep-sea hydrothermal vent site (9 degrees N, East Pacific Rise). *Environ. Microbiol.* 8, 909–920. doi: 10.1111/j.1462-2920.2005.00978.x

Koschorreck, M. (2008). Microbial sulphate reduction at a low pH. *FEMS Microbiol. Ecol.* 64, 329–342. doi: 10.1111/j.1574-6941.2008.00482.x

Kostka, J. E., Roychoudhury, A., and Van Cappellen, P. (2002). Rates and controls of anaerobic microbial respiration across spatial and temporal gradients in saltmarsh sediments. *Biogeochemistry* 60, 49–76. doi: 10.1023/A:1016525216426

Kreke, B., and Cypionka, H. (1992). Protonmotive force in freshwater sulfate-reducing bacteria, and its role in sulfate accumulation in *Desulfobulbus propionicus*. *Arch. Microbiol.* 158, 183–187. doi: 10.1007/BF00290814

Kreke, B., and Cypionka, H. (1994). Role of sodium ions for sulfaate transport and energy metabolism in *Desulfovibrio salexigens*. *Arch. Microbiol.* 161, 55–61. doi: 10.1007/BF00248893

Kreke, B., and Cypionka, H. (1995). Energetics of sulfate transport in *Desulfomicrobium baculatum*. *Arch. Microbiol.* 163, 307–309. doi: 10.1007/BF00393385

Kristall, B., Kelley, D. S., Hannington, M. D., and Delaney, J. R. (2006). Growth history of a diffusely venting sulfide structure from the Juan de Fuca Ridge: a petrological and geochemical study. *Geochem. Geophys. Geosyst.* 7, 1–30. doi: 10.1029/2005gc001166

Lang, S. Q., Butterfield, D. A., Lilley, M. D., Johnson, H. P., and Hedges, J. I. (2006). Dissolved organic carbon in ridge-axis and ridge-flank hydrothermal systems. *Geochim. Cosmochim. Acta* 70, 3830–3842. doi: 10.1016/j.gca.2006.04.031

Lang, S. Q., Butterfield, D. A., Schulte, M., Kelley, D. S., and Lilley, M. D. (2010). Elevated concentrations of formate, acetate and dissolved organic carbon found at the Lost City hydrothermal field. *Geochim. Cosmochim. Acta* 74, 941–952. doi: 10.1016/j.gca.2009.10.045

LaRowe, D. E., and Amend, J. P. (2015). Power limits for microbial life. *Front. Microbiol.* 6:718. doi: 10.3389/fmicb.2015.00718

LaRowe, D. E., Dale, A. W., Aguilera, D. R., L'Heureux, I., Amend, J. P., and Regnier, P. (2014). Modeling microbial reaction rates in a submarine hydrothermal vent chimney wall. *Geochim. Cosmochim. Acta* 124, 72–97. doi: 10.1016/j.gca.2013.09.005

LaRowe, D. E., Dale, A. W., Amend, J. P., and Van Cappellen, P. (2012). Thermodynamic limitations on microbially catalyzed reaction rates. *Geochim. Cosmochim. Acta* 90, 96–109. doi: 10.1016/j.gca.2012.05.011

Leloup, J., Fossing, H., Kohls, K., Holmkvist, L., Borowski, C., and Jørgensen, B. B. (2009). Sulfate-reducing bacteria in marine sediment (Aarhus Bay, Denmark): abundance and diversity related to geochemical zonation. *Environ. Microbiol.* 11, 1278–1291. doi: 10.1111/j.1462-2920.2008.01855.x

Leloup, J., Loy, A., Knab, N. J., Borowski, C., Wagner, M., and Jørgensen, B. B. (2007). Diversity and abundance of sulfate-reducing microorganisms in the sulfate and methane zones of a marine sediment, Black Sea. *Environ. Microbiol.* 9, 131–142. doi: 10.1111/j.1462-2920.2006.01122.x

Leskovac, V. (2003). *Comprehensive Enzyme Kinetics*. New York, NY: Kluwer Academic Publishers.

Lever, M. A., Rogers, K. L., Lloyd, K. G., Overmann, J., Schink, B., Thauer, R. K., et al. (2015). Life under extreme energy limitation: a synthesis of laboratory- and field-based investigations. *FEMS Microbiol. Rev.* 39, 688–728. doi: 10.1093/femsre/fuv020

Lin, Y.-S., Biddle, J. F., Lipp, J. S., Orcutt, B. N., Holler, T., Teske, A., et al. (2010). Effect of storage conditions on archaeal and bacterial communities in subsurface marine sediments. *Geomicrobiol. J.* 27, 261–272. doi: 10.1080/01490450903410423

Lloyd, K. G., Edgcomb, V. P., Molyneaux, S. J., Böer, S., Wirsen, C. O., Atkins, M. S., et al. (2005). Effects of dissolved sulfide, pH, and temperature on growth and survival of marine hyperthermophilic archaea. *Appl. Environ. Microbiol.* 71, 6383–6387. doi: 10.1128/AEM.71.10.6383-6387.2005

Lovley, D. R., Dwyer, D. F., and Klug, M. J. (1982). Kinetic analysis of competition between sulfate reducers and methanogens for hydrogen in sediments. *Appl. Environ. Microbiol.* 43, 1373–1379.

Lovley, D. R., and Goodwin, S. (1988). Hydrogen concentrations as an indicator of the predominant terminal. *Geochim. Cosmochim. Acta* 52, 2993–3003. doi: 10.1016/0016-7037(88)90163-9

Lovley, R., and Klug, M. J. (1986). Model for the distribution of sulfate reduction and methanogenesis in freshwater sedimentst. *Geochim. Cosmochim. Acta* 50, 11–18. doi: 10.1016/0016-7037(86)90043-8

McCollom, T. M., and Amend, J. P. (2005). A thermodynamic assessment of energy requirements for biomass synthesis by chemolithoautotrophic micro-organisms in oxic and anoxic environments. *Geobiology* 3, 135–144. doi: 10.1111/j.1472-4669.2005.00045.x

McCollom, T. M., and Shock, E. L. (1997). Geochemical constraints on chemolithoautotrophic metabolism by microorganisms in seafloor hydrothermal systems. *Geochim. Cosmochim. Acta* 61, 4375–4391. doi: 10.1016/S0016-7037(97)00241-X

Muyzer, G., and Stams, A. J. M. (2008). The ecology and biotechnology of sulphate-reducing bacteria. *Nat. Rev Microbiol.* 6, 441–544. doi: 10.1038/nrmicro1892

Nakagawa, S., Takai, K., Inagaki, F., Hirayama, H., Nunoura, T., Horikoshi, K., et al. (2005). Distribution, phylogenetic diversity and physiological characteristics of epsilon-Proteobacteria in a deep-sea hydrothermal field. *Environ. Microbiol.* 7, 1619–1632. doi: 10.1111/j.1462-2920.2005.00856.x

Newport, P. J., and Nedwell, D. B. (1988). The mechanisms of inhibition of *Desulfovibrio* and *Desulfotomaculum* species by selenate and molybdate. *J. Appl. Microbiol.* 65, 419–423.

Okabe, S., Nielsen, P. H., Jones, W. L., and Characklis, W. G. (1995). Sulfide product inhibition of *Desulfovibrio desulfuricans* in batch and continuous cultures. *Water Res.* 29, 571–578. doi: 10.1016/0043-1354(94)00177-9

Oleszkiewicz, J. A., Marstaller, T., and McCartney, D. M. (1989). Effects of pH on sulfide toxicity to anaerobic processes. *Environ. Technol. Lett.* 10, 815–822. doi: 10.1080/09593338909384801

Olins, H. C., Rogers, D. R., Frank, K. L., Vidoudez, C., and Girguis, P. R. (2013). Assessing the influence of physical, geochemical and biological factors on anaerobic microbial primary productivity within hydrothermal vent chimneys. *Geobiology* 11, 279–293. doi: 10.1111/gbi.12034

Orcutt, B., Boetius, A., Elvert, M., Samarkin, V., and Joye, S. B. (2005). Molecular biogeochemistry of sulfate reduction, methanogenesis and the anaerobic oxidation of methane at Gulf of Mexico cold seeps. *Geochim. Cosmochim. Acta* 69, 4267–4281. doi: 10.1016/j.gca.2005.04.012

Oremland, R. S., and Polcin, S. (1982). Methanogenesis and sulfate reduction: competitive and noncompetitive substrates in estuarine sediments. *Appl. Environ. Microbiol.* 44, 1270–1276.

Oremland, R. S., and Taylor, B. F. (1977). Sulfate reduction and methanogenesis in marine sediments. *Geochim. Cosmochim.* 42, 209–214. doi: 10.1016/0016-7037(78)90133-3

Pagé, A., Tivey, M. K., Stakes, D. S., and Reysenbach, A. L. (2008). Temporal and spatial archaeal colonization of hydrothermal vent deposits. *Environ. Microbiol.* 10, 874–884. doi: 10.1111/j.1462-2920.2007.01505.x

Pallud, C., and Van Cappellen, P. (2006). Kinetics of microbial sulfate reduction in estuarine sediments. *Geochim. Cosmochim. Acta* 70, 1148–1162. doi: 10.1016/j.gca.2005.11.002

Piłsyk, S., and Paszewski, A. (2009). Sulfate permeases—phylogenetic diversity of sulfate transport. *Acta Biochim. Pol.* 56, 375–384.

Rabus, R., Hansen, T. A., and Widdel, F. (2006). Dissimilatory sulfate and sulfur reducing prokaryotes. *Prokaryotes* 2, 659–768. doi: 10.1007/0-387-30742-7_22

Ramos, A. R., Keller, K. L., Wall, J. D., and Pereira, I. A. C. (2012). The membrane QmoABC complex interacts directly with the dissimilatory adenosine 5' — phosphosulfate reductase in sulfate reducing bacteria. *Front. Microbiol.* 3:137. doi: 10.3389/fmicb.2012.00137

Ravenschlag, K., Sahm, K., Knoblauch, C., Jørgensen, B. B., and Amann, R. (2000). Community structure, cellular rRNA content, and activity of sulfate-reducing bacteria in marine Arctic sediments. *Appl. Environ. Microbiol.* 66, 3592–3602. doi: 10.1128/AEM.66.8.3592-3602.2000

Reeves, E. P., McDermott, J. M., and Seewald, J. S. (2014). The origin of methanethiol in midocean ridge hydrothermal fluids. *Proc. Natl. Acad. Sci. U.S.A.* 111, 5474–5479. doi: 10.1073/pnas.1400643111

Reis, M., a, Almeida, J. S., Lemos, P. C., and Carrondo, M. J. (1992). Effect of hydrogen sulfide on growth of sulfate reducing bacteria. *Biotechnol. Bioeng.* 40, 593–600. doi: 10.1002/bit.260400506

Robador, A., Brüchert, V., and Jørgensen, B. B. (2009). The impact of temperature change on the activity and community composition of sulfate-reducing bacteria in arctic versus temperate marine sediments. *Environ. Microbiol.* 11, 1692–1703. doi: 10.1111/j.1462-2920.2009.01896.x

Robador, A., Jungbluth, S. P., LaRowe, D. E., Bowers, R. M., Rappé, M. S., Amend, J. P., et al. (2015). Activity and phylogenetic diversity of sulfate-reducing

microorganisms in low-temperature subsurface fluids within the upper oceanic crust. *Front. Microbiol.* 5:748. doi: 10.3389/fmicb.2014.00748

Robigou, V., Delaney, J. R., and Stakes, D. S. (1993). Large massive sulfide deposits in a newly disocvered active hydrothermal system, the high rise field, endeavour segment Juan de Fuca ridge. *Geophys. Res. Lett.* 20, 1887–1890. doi: 10.1029/93GL01399

Rogers, K. L., and Amend, J. P. (2006). Energetics of potential heterotrophic metabolisms in the marine hydrothermal system of Vulcano Island, Italy. *Geochim. Cosmochim. Acta* 70, 6180–6200. doi: 10.1016/j.gca.2006.08.046

Roychoudhury, A. N. (2004). Sulfate respiration in extreme environments: a Kinetic Study. *Geomicrobiol. J.* 21, 33–43. doi: 10.1080/01490450490253446

Roychoudhury, A. N., Van Cappellen, P., Kostka, J. E., and Viollier, E. (2003). Kinetics of microbially mediated reactions: dissimilatory sulfate reduction in saltmarsh sediments (Sapelo Island, Georgia, USA). *Estuar. Coast. Shelf Sci.* 56, 1001–1010. doi: 10.1016/S0272-7714(02)00325-6

Røy, H., Weber, H. S., Tarpgaard, I. H., Ferdelman, T. G., and Jørgensen, B. B. (2014). Determination of dissimilatory sulfate reduction rates in marine sediment via radioactive 35S tracer. *Limnol. Oceanogr. Methods* 12, 196–211. doi: 10.4319/lom.2014.12.196

Saleh, A. M., Macpherson, R., and Miller, J. D. A. (1964). The effect of inhibitors on sulphate reducing bacteria: a compilation. *J. Appl. Microbiol.* 27, 281–293. doi: 10.1111/j.1365-2672.1964.tb04914.x

Sani, R. K., Sani, R. K., Peyton, B. M., Peyton, B. M., Brown, L. T., and Brown, L. T. (2001). Copper-induced inhibition of growth of Desulofovibrio desulfuricans G20: assessment of its toxicity and correlation with those of zinc and lead. *Appl. Environ. Microbiol.* 67, 4765–4772. doi: 10.1128/AEM.67.10.4765-4772.2001

Schrenk, M. O., Kelley, D. S., Delaney, J. R., and Baross, J. A. (2003). Incidence and diversity of microorganisms within the walls of an active deep-Sea sulfide chimney. *Appl. Environ. Microbiol.* 69, 3580–3592. doi: 10.1128/AEM.69.6.3580-3592.2003

Shock, E. L. (1995). Organic acid in hydrothermal solutions: standard molal thermodynamic properties of carboxylic acids and estimates of dissociation constants at high temperatures and pressures. *Am. J. Sci.* 295, 496–580. doi: 10.2475/ajs.295.5.496

Shock, E. L., and Koretsky, C. M. (1993). Metal-organic complexes in geochemical processes: calculation of standard partial molal thermodynamic properties of aqueous acetate complexes at high pressures and temperatures. *Geochim. Cosmochim. Acta* 57, 4899–4922. doi: 10.1016/0016-7037(93)90128-J

Skoog, A., Vlahos, P., Rogers, K. L., and Amend, J. P. (2007). Concentrations, distributions, and energy yields of dissolved neutral aldoses in a shallow hydrothermal vent system of Vulcano, Italy. *Org. Geochem.* 38, 1416–1430. doi: 10.1016/j.orggeochem.2007.03.005

Slobodkina, G. B., Kolganova, T. V., Querellou, J., Bonch-Osmolovskaya, E. A., and Slobodkin, A. I. (2009). *Geoglobus acetivorans* sp. nov., an iron(III)-reducing archaeon from a deep-sea hydrothermal vent. *Int. J. Syst. Evol. Microbiol.* 59, 2880–2883. doi: 10.1099/ijs.0.011080-0

Sokolova, T., Hanel, J., Onyenwoke, R. U., Reysenbach, A.-L., Banta, A., Geyer, R., et al. Wiegel, J. (2007). Novel chemolithotrophic, thermophilic, anaerobic bacteria *Thermolithobacter ferrireducens* gen. nov., sp. nov. and *Thermolithobacter carboxydivorans* sp. nov. *Extremophiles* 11, 145–157. doi: 10.1007/s00792-006-0022-5

Sonne-hansen, J., and Westermann, P. (1999). Kinetics of sulfate and hydrogen uptake by the thermophilic sulfate-reducing bacteria *Thermodesulfobacterium* sp. strain R1Ha3. *Appl. Environ. Microbiol.* 65, 1304–1307.

Takai, K., Komatsu, T., Inagaki, F., and Horikoshi, K. (2001). Distribution of archaea in a black smoker chimney structure. *Appl. Environ. Microbiol.* 67, 3618–3629. doi: 10.1128/AEM.67.8.3618-3629.2001

Takai, K., Sugai, A., Itoh, T., and Horikoshi, K. (2000). *Palaeococcus ferrophilus* gen. nov., sp. nov., a barophilic, hyperthermophilic archaeon from a deep-sea hydrothermal vent chimney. *Int. J. Syst. Evol. Microbiol.* 50, 489–500. doi: 10.1099/00207713-50-2-489

Tarpgaard, I. H., Roy, H., and Jørgensen, B. B. (2011). Concurrent low- and high-affinity sulfate reduction kinetics in marine sediment. *Geochim. Cosmochim. Acta* 75, 2997–3010. doi: 10.1016/j.gca.2011.03.028

Temple, K. L., and Le Roux, N. W. (1964). Syngenesis of sulfide ores; sulfate-reducing bacteria and copper toxicity. *Econ. Geol.* 59, 271–278. doi: 10.2113/gsecongeo.59.2.271

Tivey, M. (2004). "Environmental conditions within active seafloor vent structures: sensitivity to vent fluid composition and fluid flow," in *Subseafloor Biosphere at Mid-Ocean Ridges, Geophysical Monograph Series, No. 144*, eds W. Wilcock, C. Cary, E. DeLong, D. Kelley, and J. Baross (Washington, DC:American Geophysical Union), 137–152.

Tivey, M. A., Johnson, H. P., and Hole, W. (2002). Crustal magnetization reveals subsurface structure of Juan de Fuca Ridge hydrothermal vent fields. *Geology* 30, 979–982. doi: 10.1130/0091-7613(2002)030<0979:CMRSSO>2.0.CO;2

Tivey, M. K. (1995). The influence of hydrothermal fluid composition and advection rates on black smoker chimney mineralogy: insights from modeling transport and reaction. *Geochim. et Cosmochim. Acta* 59, 1933–1949. doi: 10.1016/0016-7037(95)00118-2

Tivey, M. K., and Delaney, J. R. (1986). Growth of large sulfide structures on the endeavour segment of the Juan de Fuca ridge. *Earth Planet. Sci. Lett.* 77, 303–317. doi: 10.1016/0012-821X(86)90142-1

Tivey, M. K., Stakes, D. S., Cook, T. L., Hannington, M. D., and Petersen, S. (1999). A model for growth of steep-sided vent structures on the Endeavour Segment of the Juan de Fuca Ridge: results of a petrologic and geochemical study. *J. Geophys. Res.* 104, 22859–22883. doi: 10.1029/1999JB900107

Treude, T., Smith, C., Wenzhöfer, F., Carney, E., Bernardino, A., Hannides, A., et al. (2009). Biogeochemistry of a deep-sea whale fall: sulfate reduction, sulfide efflux and methanogenesis. *Mar. Ecol. Prog. Ser.* 382, 1–21. doi: 10.3354/meps07972

Trüper, H. G., and Rogers, L. A. (1971). Purification and properties of adenylyl sulfate reductase from the phototrophic sulfur bacterium, Thiocapsa roseopersicina. *J. Bacteriol.* 108, 1112–1121.

Utgikar, V., Harmon, S. M., Chaudhary, N., Tabak, H. H., Govind, R., and Haines, J. R. (2002). Inhibition of sulfate-reducing bacteria by metal sulfide formation in bioremediation of acid mine drainage. *Environ. Toxicol.* 17, 40–48. doi: 10.1002/tox.10031

Utgikar, V. P., Tabak, H. H., Haines, J. R., and Govind, R. (2003). Quantification of toxic and inhibitory impact of copper and zinc on mixed cultures of sulfate-reducing bacteria. *Biotechnol. Bioeng.* 82, 306–312. doi: 10.1002/bit.10575

Weber, A., and Jørgensen, B. B. (2002). Bacterial sulfate reduction in hydrothermal sediments of the Guaymas Basin, Gulf of California, Mexico. *Deep. Res. I Oceanogr. Res. Pap.* 49, 827–841. doi: 10.1016/S0967-0637(01)00079-6

Weijma, J., Stams, A. J., Hulshoff Pol, L. W., and Lettinga, G. (2000). Thermophilic sulfate reduction and methanogenesis with methanol in a high rate anaerobic reactor. *Biotechnol. Bioeng.* 67, 354–363. doi: 10.1002/(SICI)1097-0290(20000205)67:3<354::AID-BIT12>3.0.CO;2-X

Westrich, J. T., and Berner, R. A. (1984). The role of sedimentary organic matter in bacterial sulfate reduction: the G model tested. *Limnol. Oceanogr.* 29, 236–249. doi: 10.4319/lo.1984.29.2.0236

Wolery, T. J. (1992a). *EQ3/6, A Software Package for Geochemical Modeling of Aqueous Systems: Package Overview and Installation Guide (Version 7. 0)*. Livermore, CA: Lawrence Livermore National Laboratory.

Wolery, T. J. (1992b). *EQ3NR, a Computer Program for Geochemical Aqueous Speciation-solubility Calculations: Theoretical Manual, User's Guide and Related Documentation (Version 7.0)*. Livermore, CA: Lawrence Livermore Laboratory, University of California.

Wolery, T. J., and Daveler, S. A. (1992). *EQ6, a Computer Program for Reaction Path Modeling of Aqueous Geochemical Systems: Theoretical Manual, User's Guide and Related Documentation (Version 7.0)*. Livermore, CA: Lawrence Livermore Laboratory, University of California.

Xu, N., Christodoulatos, C., and Braida, W. (2006). Adsorption of molybdate and tetrathiomolybdate onto pyrite and goethite: effect of pH and competitive anions. *Chemosphere* 62, 1726–1735. doi: 10.1016/j.chemosphere.2005.06.025

Zhu, W., Tivey, M. K., Gittings, H., and Craddock, P. R. (2007). Permeability-porosity relationships in seafloor vent deposits: dependence on pore evolution processes. *J. Geophys. Res.* 112, 1–15. doi: 10.1029/2006jb004716

Conflict of Interest Statement: The authors declare that the research was conducted in the absence of any commercial or financial relationships that could be construed as a potential conflict of interest.

frontiers in Microbiology

ORIGINAL RESEARCH
published: 24 September 2015
doi: 10.3389/fmicb.2015.00968

Biogeography and evolution of *Thermococcus* isolates from hydrothermal vent systems of the Pacific

Mark T. Price, Heather Fullerton and Craig L. Moyer *

Department of Biology, Western Washington University, Bellingham, WA, USA

Thermococcus is a genus of hyperthermophilic archaea that is ubiquitous in marine hydrothermal environments growing in anaerobic subsurface habitats but able to survive in cold oxygenated seawater. DNA analyses of *Thermococcus* isolates were applied to determine the relationship between geographic distribution and relatedness focusing primarily on isolates from the Juan de Fuca Ridge and South East Pacific Rise. Amplified fragment length polymorphism (AFLP) analysis and multilocus sequence typing (MLST) were used to resolve genomic differences in 90 isolates of *Thermococcus*, making biogeographic patterns and evolutionary relationships apparent. Isolates were differentiated into regionally endemic populations however there was also evidence in some lineages of cosmopolitan distribution. The biodiversity identified in *Thermococcus* isolates and presence of distinct lineages within the same vent site suggests the utilization of varying ecological niches in this genus. In addition to resolving biogeographic patterns in *Thermococcus*, this study has raised new questions about the closely related *Pyrococcus* genus. The phylogenetic placement of *Pyrococcus* type strains shows the close relationship between *Thermococcus* and *Pyrococcus* and the unresolved divergence of these two genera.

Keywords: *Thermococcus*, hydrothermal vents, subsurface microbiology, biogeography, evolution

OPEN ACCESS

Edited by:
Beth Orcutt, Bigelow Laboratory for Ocean Sciences, USA

Reviewed by:
Julie L. Meyer, University of Florida, USA
Sean Patrick Jungbluth, University of Hawaii, USA

***Correspondence:**
Craig L. Moyer, Department of Biology, Western Washington University, 516 High Street, MS #9160, Bellingham, WA 98225,USA
cmoyer@hydro.biol.wwu.edu

Specialty section:
This article was submitted to Extreme Microbiology, a section of the journal Frontiers in Microbiology

Received: *27 May 2015*
Accepted: *01 September 2015*
Published: *24 September 2015*

Citation:
Price MT, Fullerton H and Moyer CL (2015) Biogeography and evolution of Thermococcus isolates from hydrothermal vent systems of the Pacific. Front. Microbiol. 6:968. doi: 10.3389/fmicb.2015.00968

Introduction

Microorganisms constitute the majority of known life forms making up greater than two-thirds of the metabolic and genetic diversity of the planet (Whitaker, 2006). The evolutionary forces responsible for shaping this vast amount of microbial diversity have been a topic of debate. Historically, microorganisms were viewed as having panmictic distributions, being constrained only by environmental conditions (Baas-Becking, 1934). Contemporary research has shown that limited dispersal, geographic isolation, selection and genetic drift can lead to divergence in microbial populations (Cho and Tiedje, 2000). The significance of physical isolation on the population divergence of terrestrial hyperthermophiles has been well documented (Papke et al., 2003; Whitaker et al., 2003; Papke and Ward, 2004; Whitaker, 2006; Reno et al., 2009); however, it is unknown whether similar patterns of isolation can be observed in hyperthermophiles at marine hydrothermal vents or if there is greater dispersal in these marine environments.

Marine hydrothermal vents are unique environments with extreme chemical, nutrient and temperature gradients. The organisms inhabiting hydrothermal vents are dispersed along plate

boundaries and can be separated from other vent systems by thousands of kilometers creating island-like ecosystems. While there has been evidence in support of endemic community structure at hydrothermal vents (Opatkiewicz et al., 2009; Flores et al., 2012), descriptions of biogeography for individual microbial taxa have been uncommon (Escobar-Páramo et al., 2005; DeChaine et al., 2006; McAllister et al., 2011; Mino et al., 2013). The limited descriptions of microbial biogeography at hydrothermal vents can be mitigated through the isolation of microorganisms in culture and sequencing of individual genomes (Ramette and Tiedje, 2007; Meyer and Huber, 2014).

The hyperthermophilic archaea of the *Thermococcales* order are found at hydrothermal vents and can serve as model organisms for the study of biogeography and evolution. *Thermococcales* belong to the euryarchaeota phylum and consist of the three genera *Pyrococcus* (Fiala and Stetter, 1986), *Thermococcus* (Zillig et al., 1983), and *Paleococcus* (Takai et al., 2000). The genera *Thermococcus* and *Pyrococcus* are commonly found at hydrothermal vent systems and are readily isolated in culture allowing for comparisons among individual isolates (Jannasch et al., 1992; Erauso et al., 1993; Atomi et al., 2004; Bae et al., 2006; Teske et al., 2009). Genomic and phenotypic differences between *Thermococcus* and *Pyrococcus* delineate these two closely related genera, e.g., *Pyrococcus* has a higher optimum growth temperature (Garrity et al., 2001). Known *Thermococcus* isolates have a maximum growth temperature of 90°C, but some species have been shown to grow at temperatures as low as 45°C (Adams, 1993; Robb and Place, 1995; Summit and Baross, 1998). However, between these two genera, *Thermococcus* has the highest number of characterized isolates (Garrity et al., 2001; Holden et al., 2001; Teske et al., 2009; Zivanovic et al., 2009).

Thermococcus exhibit a variety of metabolic strategies; however, the majority are anaerobic heterotrophs that ferment organic compounds (Robb and Place, 1995; Teske et al., 2009). The addition of elemental sulfur enhances growth in *Thermococcus* and is required in some strains (Teske et al., 2009). Lithotrophic metabolic pathways have been shown as well, e.g., *T. onnurines* and other type strains, can oxidize carbon monoxide to CO_2 using carbon monoxide dehydrogenases or CODHs (Lee et al., 2008; Sokolova et al., 2009; Zivanovic et al., 2009; Oger et al., 2011). Growth via formate oxidation and H_2 production, representing one of the simplest forms of anaerobic respiration, has also been demonstrated in *Thermococcus* (Kim et al., 2010). The ability to use these low energy yielding metabolic pathways has been suggested to have important implications on survival in environments where energy supplies are at times transient or unavailable (Lee et al., 2008; Kim et al., 2010).

Biogeographic patterns have been observed in *Thermococcales* using Multilocus Sequence Typing (MLST) with populations of *Pyrococcus* from different regions shown to be genetically distinct (Escobar-Páramo et al., 2005). However, descriptions of population divergence and biogeography for *Thermococcus* have been inconclusive, therefore *Thermococcus* are described as being widespread and ubiquitous in hydrothermal habitats (Holden et al., 2001; Huber et al., 2006). Although there has been evidence suggestive of a correlation among *Thermococcus* diversity, environmental conditions, and geography (Holden et al., 2001; Summit and Baross, 2001; Huber et al., 2006; Teske et al., 2009), no strong biogeographic pattern has emerged. Analysis of *Thermococcus* by random amplified polymorphic DNA (RAPD) has identified diverse genomic profiles from the same sample site and similar profiles from different sites, illustrating both the biodiversity present and dispersal potential within a hydrothermal vent field (Lepage et al., 2004). While *Thermococcus* are commonly found in hydrothermal systems, the lack of evidence for biogeographic patterns has made it unclear whether populations are panmictic in their distribution or whether there is population structure at varying geographic scales.

With the exception of RAPD analysis, the genetic markers used in previous *Thermococcus* studies have not had a high degree of resolution. Two different and yet complementary DNA typing methods that utilize multiple sites from across the genome are MLST and Amplified Fragment Length Polymorphism (AFLP) analysis. MLST is a well-established DNA typing method using multiple loci spanning the genome to construct robust phylogenetic relationships among related microorganisms (Maiden et al., 1998). By applying MLST analysis to *Thermococcus* isolates their evolutionary relationships and biodiversity can be described more accurately, e.g., MLST analysis has delineated biogeographic patterns in *Sulfolobus* isolates sharing 99.8% sequence similarity for the SSU rRNA gene (Whitaker et al., 2003). MLST data have also provided a basis for defining species level boundaries through the comparison of loci and their average nucleotide identity or ANI (Konstantinidis and Tiedje, 2005). ANI comparisons of MLST loci, with sequence similarities of 95% or greater, have been correlated with species level ANI values determined from whole-genome comparisons in bacteria (Konstantinidis and Tiedje, 2005; Konstantinidis et al., 2006a,b).

In contrast to MLST analysis, AFLP analysis utilizes genome-wide restriction fragment lengths giving AFLP a higher discriminatory power allowing for the typing of microorganisms to the strain level (Lin et al., 1996; Olive and Bean, 1999; Savelkoul et al., 1999). AFLP genome fingerprints may vary as a result of nucleotide sequence divergence as well as the movement of transposable elements, insertions or deletions, or genome rearrangements. Due to these large scale genetic changes occurring at higher rates in comparison to nucleotide sequence divergence, AFLP fingerprints have the potential to resolve more recent genomic differentiation (Rademaker et al., 2000). Conserved loci used for MLST analysis are representative of the core genome while the genome-wide restriction fragments used in AFLP analysis may be more representative of variable regions associated with the dispensable or flexible genome, where gene acquisition and loss occurs more frequently (Medini et al., 2005; Tettelin et al., 2008; Cordero and Polz, 2014).

To address questions of biogeography, biodiversity and evolution in the oceanic crust, *Thermococcus* isolates from different hydrothermal regions were analyzed using MLST and AFLP. *Thermococcus* isolates from the Juan de Fuca Ridge (JdF) and East Pacific Rise (EPR) were the primary focus of this study with type strains and isolates from other hydrothermal habitats included for comparison.

Materials and Methods

Thermococcales Isolates and Type Strains

Sample material was collected from hydrothermal vent sites during research cruises between the years of 1988–2008. Study sites and sampling are as previously described (Holden et al., 2001; Summit and Baross, 2001; Huber et al., 2006; Davis and Moyer, 2008). Both submersible and remotely operated vehicles (ROV's) were used to collect a diversity of sample material that included plume samples, hot fluids, diffuse fluids, chimney walls, sulfide muds, and Alvinellid polychaete tissue samples. Sample material was used to inoculate liquid media for the enrichment of *Thermococcales*. Media formulations and methods are as previously described (Holden et al., 2001). Isolates in this culture collection were previously characterized through analysis of the SSU rRNA for genus level associations (Holden et al., 2001; Summit and Baross, 2001; Huber et al., 2006). The collection of 90 *Thermococcus* isolates contains representatives from the Juan de Fuca Ridge (JdF), Gorda Ridge, East Pacific Rise (EPR), Mid Atlantic Ridge (MAR), Mariana Arc and Loihi Seamount (**Table 1**). Sample sites within the JdF and EPR are at similar spatial distances providing nested sampling within these two regions (**Figure 1**). Distances among vents within regions range from ∼65 to ∼450 km, with distances between the main study sites, the JdF and EPR, up to ∼7000 km. *Thermococcus* isolates and type strains from other regions, as well as *Pyrococcus* type strains, were included for comparison. Table S1 lists *Thermococcus* type strains included in AFLP and MLST analysis. Cultures of the type strains *Thermococcus kodakarensis* (JCM 12380) and *Thermococcus onnurines* (JCM 13517) were acquired through the Riken BioResource Center (Ibaraki, Japan) and were cultured in the same manner as other isolates in the collection. Genomic DNA for the type strains *Thermococcus barophilus* and *Thermococcus peptonophilus* were acquired from the American Type Culture Collection (Manassas, VA).

DNA Extraction

Genomic DNA (gDNA) was extracted from freshly cultured cells. Cultured isolates were initially centrifuged at 750 × g for 5 min to pellet the sulfur. Supernatant was removed and centrifuged at 11,000 × g for 10 min in a chilled rotor (4°C). The resulting cell pellet was used for gDNA extraction with the DNeasy Tissue Kit (Qiagen, Valencia, CA) following manufacturer's protocols. A NanoDrop ND-1000 spectrophotometer (Thermo Scientific, Wilmington, DE) was used to check DNA concentration and purity.

TABLE 1 | *Thermococcus* isolates analyzed through AFLP and MLST and their corresponding vent segments ($n = 90$).

Juan de Fuca Ridge	**55**	**East Pacific rise**	**22**	**Gorda Ridge**	**5**
Middle valley	8	9° North	1	**Lō'ihi Seamount**	**4**
Endeavor segment	23	17.5° South	7	**Mid Atlantic Ridge**	**2**
Coaxial segment	4	18.5° South	5	**Mariana Arc**	**2**
Axial volcano	18	21.5° South	9		
Cleft segment	2				

Vent regions are in bold, vent segments are included as subsets for the two primary regions under study.

AFLP Reactions and Cluster Analysis

AFLP analysis was performed using the Applied Biosystems (ABI) AFLP Microbial Fingerprinting kit (Applied Biosystems, Carlsbad, CA). Reactions and PCR conditions were as described in kit protocols using the restriction enzymes EcoRI and MseI. Primers were designed for the selective amplification of restriction fragments of between 50 and 500 base pairs. Two selective primer sets were used in separate reactions to obtain two individual AFLP profiles (EcoRI-0 and MseI-CT; EcoRI-C and MseI-G). AFLP reactions were purified across Sephadex G-75 columns and dried down in a 96 well plate before being resuspended in 15 µl of a 1:30 dilution of Liz-500 (ABI) size standard in formamide. Fragment lengths were analyzed using an ABI Prism 3130XL Genetic Analyzer. Electropherograms were optimized with samples rerun or diluted when necessary for comparable peak heights among isolates. Electropherogram data were checked for quality using ABI Genemapper software, and imported into BioNumerics version 4.61 (Applied Maths, Sint-Martens-Latem, Belgium) for further analysis.

Cluster analysis of AFLP electropherogram data was performed using the Pearson product-moment correlation coefficient in BioNumerics (Häne et al., 1993). Cluster analyses of AFLP primer sets were combined and averaged to construct a dendogram with cophenetic correlation coefficients.

Multi Locus Sequence Typing

Primers for MLST analysis were designed using nucleotide alignments from the following six annotated genomes: *Thermococcus kodakaraensis* KOD1 (Fukui et al., 2005), *Thermococcus onnurineus* NA1 (Lee et al., 2008), *Thermococcus gammatolerans* EJ3 (Zivanovic et al., 2009), *Thermococcus* sp. AM4 (Oger et al., 2011), *Thermococcus barophilus* MP (Vannier et al., 2011), and *Thermococcus sibiricus* (Mardanov et al., 2009). Gene sequences retrieved through GenBank were aligned with ClustalW multiple sequence aligner using default parameters (Thompson et al., 1994). Candidate genes were screened for conserved regions suitable for the amplification of between 300 and 500 base pairs. Loci associated with information processing and metabolism were the focus in identifying MLST candidate genes, along with the distribution of loci across the genome. Gene loci positions in the six reference genomes were plotted to check distribution and compare gene synteny (Figure S1). A portion of the following seven loci were picked for MLST analysis: SSU rRNA, Elongation Factor 1 Alpha subunit, DNA topoisomerase VI Alpha subunit, DNA polymerase II large subunit, threonyl-tRNA synthetase, pyruvate ferredoxin oxidoreductase Beta subunit, and histone acetyltransferase. The primer design software Primer3 was used to design primers (Rozen and Skaletsky, 2000). Degenerate primers were designed for all loci, with the exception of the SSU rRNA gene, in order to account for the diversity present in the six reference genomes (Table S2).

The following PCR mix was used for the SSU rRNA and EF1α genes: 50 ng of gDNA template, 0.5 µl JumpStart Taq (2.5 U/µl;

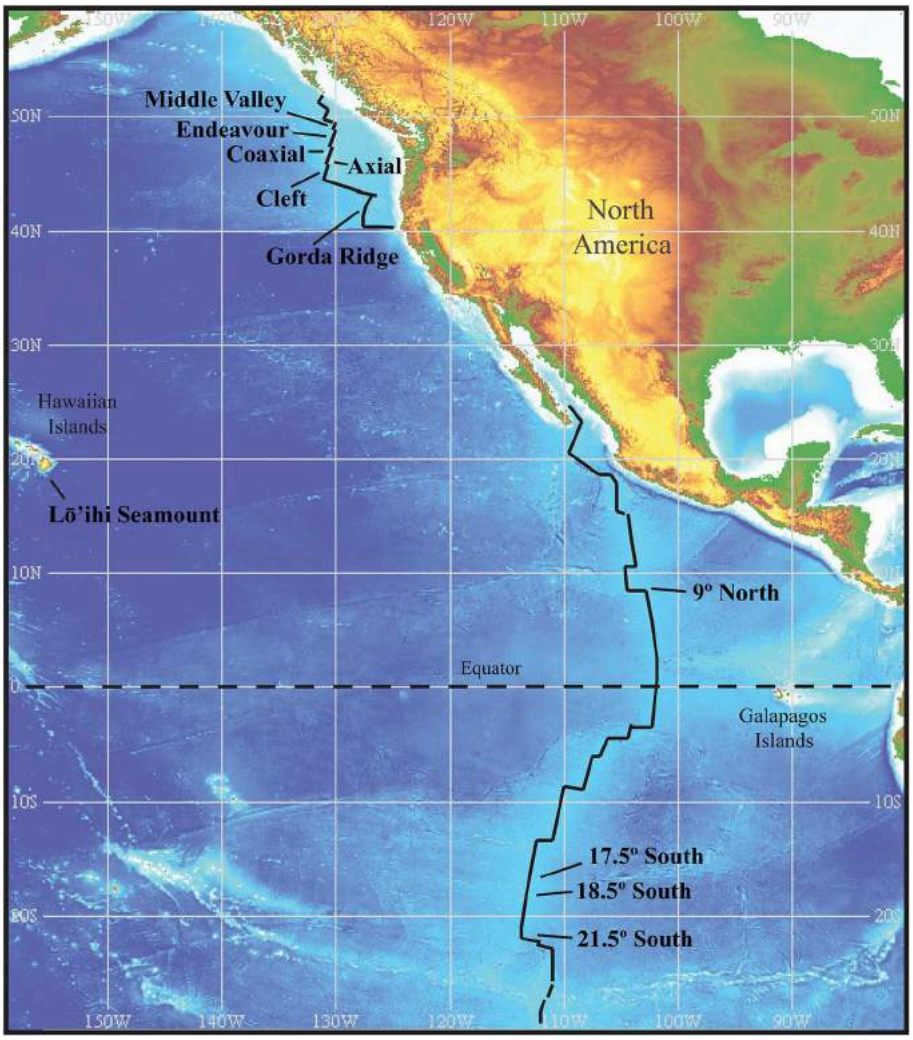

FIGURE 1 | Location of vents within the two main regions sampled. The Juan de Fuca Ridge and associated vent segments with the Gorda Ridge to the south, and the East Pacific Rise. Sample sites within these two regions are at comparable distances from one another and provide nested sampling within regions. Image reproduced from the GEBCO world map 2014, www.gebco.net.

Sigma, St. Louis, Mo), 1X Taq PCR buffer, 1.5 mM $MgCl_2$, 0.2 mM each deoxynucleoside triphosphate, 0.2 μM each forward and reverse primer, and molecular grade water to a total volume of 50 μl for each reaction. For the SSU rRNA genes the following PCR cycle was used: an initial 10 min hot start at 95°C, followed by 30 cycles of denaturation (95°C for 30 s), annealing (58°C for 30 s), and elongation (72°C for 30 s). This was followed by a final elongation step at 72°C for 7 min. For the EF1α genes the PCR cycle was the same as the above with the exception of a 56°C annealing temperature. For the remaining five genes the mixture and conditions were the same as the above with the exception of a 0.8 μM concentration for forward and reverse primers, and 55°C annealing temperature.

PCR amplicons were verified and checked for size through gel electrophoresis. Amplicons were sequenced using ABI BigDye Terminator v3.1, using an ABI Prism 3130XL Genetic Analyzer. Nucleotide sequences were contiguously assembled using BioNumerics and were verified via BLASTn (Altschul et al., 1990). The concatenated alignment of all seven amplicons following the masking of sequence data and removal of non-homologous positions resulted in 2648 bp of nucleotide sequence for analysis. Partial sequences for all loci were submitted to GenBank and assigned accession numbers (SSU rRNA: KP187908-KP187997, DNA polymerase II large subunit: KP187998-KP188087, DNA topoisomerase VI subunit A: KP188088-KP188177, elongation factor-1 alpha: KP188178-KP188267, histone acetyltransferase: KP188268-KP188357, pyruvate:ferredoxin oxidoreductase subunit beta: KP188358-KP188447, threonyl-tRNA synthetase: KP188448-KP188537).

The ExPASy translate tool (Swiss Institute of Bioinformatics) was used to determine the correct reading frame for protein coding genes before nucleotide sequences were translated into amino acid sequences using MEGA v5 (Tamura et al., 2011).

Sequences of individual loci were aligned by ClustalW in MEGA v5 with all gaps removed.

A sequence based test for selection was performed on each protein coding locus using the Datamonkey online server using the following parameters: Data type was codon, genetic code set to universal code, and the method used was SLAC (Pond and Frost, 2005). Non-synonymous verses synonymous (dN/dS) ratios were calculated on the in-frame nucleotide alignments of individual loci to determine if loci were under strong selection.

Phylogenetic Analysis

Maximum likelihood (ML) phylogenetic trees were constructed using the RAxML BlackBox online server (Stamatakis et al., 2008). A mixed/partition model was applied to the concatenated alignment of nucleotide (SSU rRNA) using the CAT model (Stamatakis, 2006; Stamatakis et al., 2008) and amino acid sequences, using the WAG (Whelan and Goldman, 2001) protein model, with per gene optimization of branch lengths and 100 bootstraps. The tree with the lowest log likelihood score was selected from 10 replicates. The concatenated ML tree was rooted using the *Crenarchea, Staphylothermus marinus* as an outgroup. Homologs in *Staphylothermus marinus* for six of the seven loci (no suitable homolog was found for DNA polymerase II) were used for phylogenetic analysis and rooting of the tree using the parameters described above. Clades were assigned to groupings of three or more isolates. Bootstrap values of 20 and above were reported. The ML tree for the SSU rRNA locus, with the inclusion of *Palaeococcus ferriphilus* and *Palaeococcus helgesonii* sequences (Takai et al., 2000; Amend et al., 2003), was also rooted using *Staphylothermus marinus* as an outgroup. For both trees, the choice of *Staphylothermus marinus* as an outgroup was made as it required minimal masking relative to the several other *Crenarcheaota* tested without changing position of the root.

MLST Clade Analysis

The 2648 bp concatenated nucleotide sequence was used for analysis of the Average Nucleotide Identity (ANI) of clades, as an estimate of species level boundaries (Konstantinidis and Tiedje, 2005; Konstantinidis et al., 2006a,b). ANI values were calculated through BLAST (bl2seq; NCBI BLAST) with the lowest similarity value in comparisons between isolates recorded as the ANI for a particular clade.

The six protein-coding loci were used for the analysis of GC-content of clades, an estimate of evolutionary history, using the Datamonkey online server as described above (Pond and Frost, 2005).

Linkage analysis was performed to test for evidence of recombination in MLST loci. In clonal organisms linkage among loci (linkage disequilibria) is expected with evidence of unlinked loci (linkage equilibria) associated with gene transfer or recombination events. Linkage among loci was tested using the Non-redundant database (NRDB; PubMLST) and Linkage Analysis (LIAN) v3.5 set to default parameters, e.g., Monte Carlo with 100 iterations. (Haubold and Hudson, 2000). Isolate loci were coded through NRDB and the null hypothesis of linkage equilibrium for clades was tested using LIAN v3.5 with the standardized index of association (I_A) reported.

Codon GC-content

Ratios of the GC-content for first and third codon positions were analyzed as a measure of gene history (Muto and Osawa, 1987). A two dimensional plot of codon ratios was constructed from the average GC-content of all six protein coding loci. The first and third codon positions of loci were calculated for individual clades and individual isolates and type strains when not associated with Clades I-X using MEGA v5 (Tamura et al., 2011). The first and third codon positions were plotted in a similar manner previously shown to differentiate genomic variation in bacteria (Kaplan and Fine, 1998).

Mantel Test

A Mantel test comparing geographic distance and genetic distance was performed using the statistical software zt (Bonnet and de Peer, 2002). Pairwise genetic distances for nucleotide sequence data were calculated using the Maximum Composite Likelihood model in MEGA v5 (Tamura et al., 2011). Geographic distances among vents were calculated from hydrothermal vent latitude and longitude. Matrices of isolate genetic and geographic distance were compared to test the null hypothesis of independence between matrices. A simple Mantel test with 10,000 randomizations was performed on all isolates, on isolates from the two main regions being investigated (JdF and EPR) and on closely associated phylogenetic clades.

Analysis of Molecular Variance

Analysis of Molecular Variance (AMOVA) was calculated in Arlequin version 3.11 (Excoffier et al., 2005) on the concatenated nucleotide sequences of all seven loci. AMOVA was used to test for correlations between sample type and sample site. Isolates were grouped by the sample type they were isolated from and by the hydrothermal vent site from which they were isolated, with the *p*-value significance test for variance carried out using 10,000 permutations.

Principal Component Analysis

Principal Component Analysis (PCA) was performed on AFLP band calling data using BioNumerics v4.61. Band calling data were collected through the automated selection of bands from both primer sets using the following parameters: a minimum profiling of 5% for primer set 1, a minimum profiling of 10% for primer set 2, with the optimization and position tolerances for selecting bands set to 0.10% for both primer sets. Band calling resulted in an average of 14 bands per isolate for primer set 1 and an average of 15 bands per isolate for primer set 2. Band calling data from both primer sets were combined and converted into a binary presence absence matrix. Default settings were applied for PCA in BioNumerics, subtracting the average for characters.

Results

AFLP Cluster Analysis

Through cluster analysis, isolate AFLP profiles are grouped by similarity. The cluster analysis dendogram topology is well supported by cophenetic correlation coefficients (Figure S2). Isolates from the JdF and EPR are differentiated at regional levels

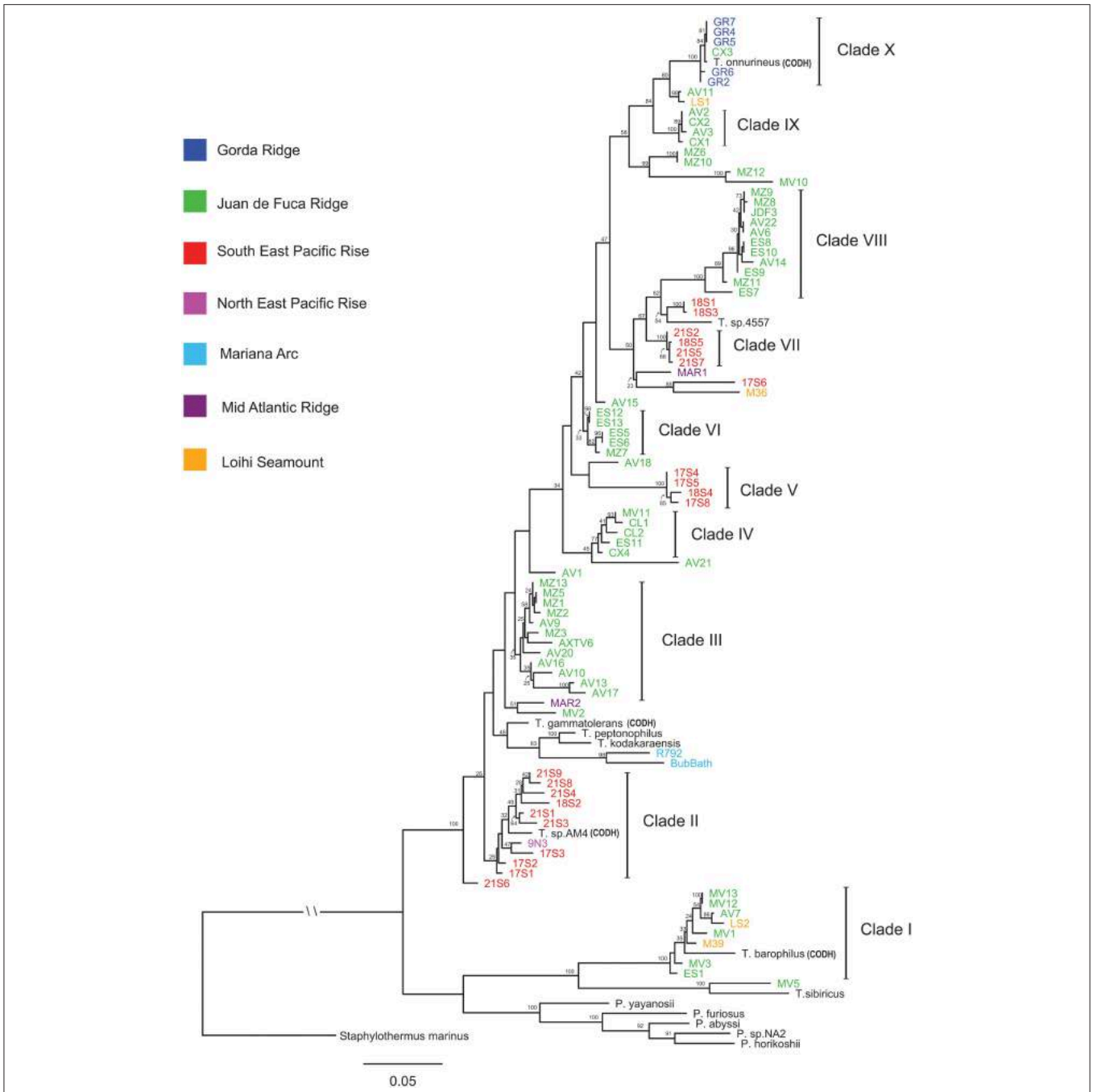

FIGURE 2 | Maximum likelihood phylogenetic tree of the concatenated amino acid and SSU rRNA sequences constructed using RAxML with a mixed/partitioned model and per gene optimization of branch lengths with 100 bootstraps. Bootstrap values of 20 and above are reported. The *Crenarchaeota Staphylothermus marinus* was used as an outgroup. Genomes containing carbon monoxide dehydrogenase genes are labeled CODH.

with no clustering of isolates between these two regions. Isolate diversity is exemplified by the number of clusters found within the JdF and EPR regions with up to five clusters identified for each. These clusters are made up of isolates from more than one vent site within a region, more than one sample type and for JdF isolates, from different sampling years. Isolate groupings illustrate the dispersal potential between vent sites within a region with clusters containing isolates from vents spread throughout a region. Isolates previously identified through SSU rRNA analysis as *Pyrococcus* clustered together with the exception of isolate MV7. Type strains and isolates from regions other than the JdF or EPR had low AFLP profile similarity with isolates in this study, with the exception of the type strain *Thermococcus onnurines*. This type strain (*T. onnurines*) was isolated from the Papua New

Guinea-Australia-Canada-Manus (PACMANUS) field (Bae et al., 2006) and had high similarity with the cluster containing Gorda Ridge isolates and isolate CX3 from the coaxial segment, with ≥ 68% AFLP profile similarity among these isolates.

MLST and Phylogenetic Analysis

Analysis of the individual alignments for the six protein coding loci did not show significant evidence for any of the loci undergoing strong selection (Table S3), making these loci suitable for MLST analysis. Ratios of dN/dS were consistent with dN/dS ratios reported for conserved genes under purifying selection (Kuhn et al., 2006).

The ML phylogeny of concatenated MLST loci differentiated isolates into clades that are in general agreement with isolate groupings through AFLP cluster analysis (**Figure 2** and Figure S2). Isolates from the JdF and EPR are differentiated into lineages that are phylogenetically related across these two regions (**Figure 2**). The regional divergence among phylogenetically related isolates is most apparent in the paraphyly observed between Clades VII and VIII. A general pattern of isolates differentiated by region was observed with individual clades made up of isolates from that same region. Regional groupings were most apparent in the isolates associated with the JDF and EPR; however, regional groupings were also observed in the two isolates from the Mariana Arc, the type strains *T. peptonophilus* and *T. kodakaraenis* both from Japan, and the type strains *T. sp.* 4557 and *T. sp.* AM4 isolated from the EPR (which both group with lineages also from the EPR). Exceptions to regional groupings are seen in Clades I and X, a pattern also observed through AFLP cluster analysis. Clade I contains isolates from the JdF Ridge, Loihi Seamount, and the type strain *T. barophilus* from the Mid Atlantic Ridge (MAR). Clade X contains isolates from the Gorda Ridge, an isolate from the CoAxial Segment (of the JdF), and the type strain *T. onnurines* from the PACMANUS Basin, with all of these isolates sharing 99% sequence identity. *Pyrococcus* type strains along with Clade I, the type strain *T. sibiricus* and isolate MV5 are placed in a basal position in the phylogenetic tree, ancestral to Clades II through X. The type strain *P. yayanosii* has the shortest distance, from these basal groups, to *Thermococcus* isolates in Clades II through X. The ancestral relationship between *Pyrococcus* type strains and *Thermococcus* isolates in the ML phylogeny of concatenated MLST loci remains unresolved.

The ML tree for the SSU rRNA gene, which includes *Palaeococcus* isloates and is rooted with *Staphylothermus marinus*, places the Clade I *Thermococcus* isolates in an ancestral position to *Pyrococcus* type strains and the *Thermococcus* isolates found in Clades II through X (**Figure 3**). This illustrates the paraphyletic associations among members of the *Thermococcus* and *Pyrococcus* genera. Several other *Crenarchaeota* were tested as an outgroup including: *Cenarchaeum symbiosum*, *Sulfolobus tokodaii*, *Nitrosopumilus maritimus*, and *Pyrobaculum aerophilum*. None of these other taxa changed the position of the root (data not shown).

MLST Clade Analysis

Analysis of clade ANI allowed for clade diversity to be estimated based on species level boundaries observed in bacteria (ANI ≥ 95%). Clades I, II, and III have ANI values below 95% reflecting diversity that is likely beyond the individual species level (**Table 2**). Clades IV through X have ANI values at or above 95% suggesting that these clades may represent individual species. Pairwise comparisons among all clades (data not shown) result in ANI values <95%, suggesting that individual clades represent distinct species.

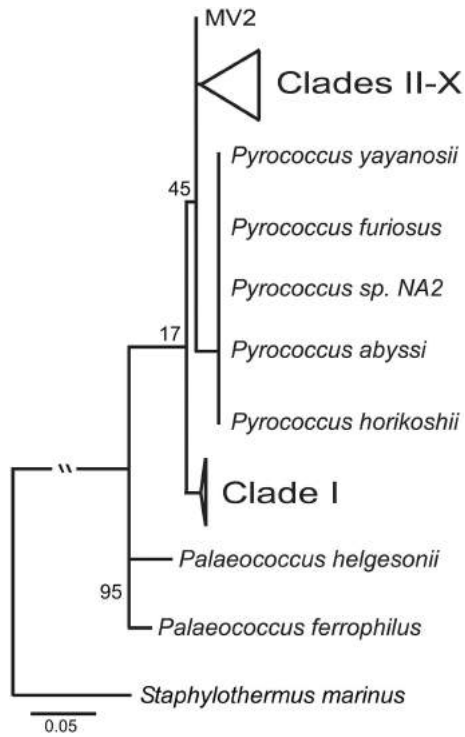

FIGURE 3 | Maximum likelihood phylogenetic tree of the SSU rRNA with the inclusion of *Palaeococcus* species and with *Staphylothermus marinus* as an outgroup. Clade I is ancestral to both *Pyrococcus* type strains and *Thermococcus* isolates in clades II–X. Numbers at nodes represent bootstrap values.

Variation in GC-content was observed among all clades (**Table 2**). Clade I at 45.50% had the lowest GC-content in comparison to other *Thermococcus* clades and was closer to GC values reported for *Pyrococcus* genera (Lecompte et al., 2001). Clade X with a GC-content of 55.93% had the next lowest percentage with clades II through IX having GC-content ratios between 57.03 and 59.64%.

Linkage analysis was applied to test for linkage among the MLST loci. Linkage analysis of individual clades rejected the null hypothesis of linkage equilibria, with the measure of linkage (I_A) significantly different from zero and/or not significant. Therefore, clade analysis did not show evidence of gene transfer or recombination in MLST loci examined.

Codon GC-content Ratios

A two dimensional plot of average GC-content at the first and third codon position illustrates differences in codon GC ratios for clades, isolates and type strains from the phylogenetic tree (Figure S3). *Thermococcus* isolates from Clade I along with the type strain *Thermococcus sibiricus* and isolate MV5 have codon

TABLE 2 | Clade analysis for Average Nucleotide Identity (ANI), GC-content and test for linkage among loci with the Index of association (I_A) and probability value reported.

Clade	ANI%	GC ratio	I_A	*p*-value
I	91	45.50	0.3667	0.001
II	94	57.65	0.0189	0.394
III	93	57.97	0.4845	0.001
IV	98	59.05	−0.0352	0.605
V	97	57.43	0.6179	0.001
VI	99	58.49	0.5873	0.001
VII	99	59.03	0.3644	0.001
VIII	95	59.64	0.0328	0.248
IX	99	57.03	0.1061	0.251
X	99	55.93	0.6356	0.001

GC ratios that are closer to *Pyrococcus* isolates and type strains, in agreement with our MLST phylogenetic tree (**Figure 2**). *Pyrococcus yayanosii*, which has been shown to have a higher GC content in comparison to other *Pyrococcus* (Jun et al., 2011), has a codon GC ratio closer to those calculated for the *Thermococcus* isolates found in Clades II through X.

Mantel Test

Mantel's analysis testing the correlation between genetic distance and geographic distance did not find a significant correlation when looking at all isolates or isolates from either the JdF or EPR regions separately (Table S4). The lack of a correlation at these scales is in part due to the degree of genetic diversity present within regions and within vent sites. Analysis of closely associated phylogenetic clades from the two main regions (JdF and EPR) did find a significant correlation between genetic distance and geographic distance. An exception to this is the analysis of Clades IX and X, where geographic distance and genetic distance are not correlated. In particular, Clade X contains isolates from disparate regions which share high sequence similarity.

Analysis of Molecular Variance

Variation in isolates grouped by sample type (1.1% of variation $P = 0.324$) and by sample site (16.2% of variation $P = 0.121$) showed no significant correlation using an AMOVA of MLST nucleotide data.

Principal Component Analysis

PCA revealed that the first three principal components described 16.8% of the variation in the AFLP data (**Figure 4**). Principal components 1 and 2 plotted on the X and Y axes respectively, differentiate isolates from Clade I and Clade X from other isolates in this study. Principal component 3 plotted on the Z axis differentiates isolates into larger regionally related groups, particularly the JdF isolates (northern-most) from the EPR isolates (southern-most).

Discussion

A comparison of *Thermococcus* isolates through AFLP and MLST analysis have made biogeographic patterns evident; however, phylogenetic analysis does not suggest a simple model of allopatric speciation. This suggests that there is high dispersal in the *Thermococcus* genus. The strongest biogeographic patterns were observed between northern isolates from the JdF and southern isolates from the EPR, most likely due to these regions having the highest representation (**Table 1**).

A barrier to dispersal between northern and southern hydrothermal regions developed as the North American Plate overrode the Pacific Plate. The discontinuous nature of the plate boundary and associated hydrothermal vents allowed for endemic populations to develop over time between the northern JdF and southern EPR. The paraphyletic association between Clades VII and VIII demonstrates the shared ancestry between these two lineages and their divergence when populations became isolated from one another. The limited mixing of water masses through circulating ocean currents may have also contributed to the isolation of these populations (Müller et al., 2014). Analysis of *Thermococcus* isolates from a more contiguous series of hydrothermal venting regions, like the Mid Atlantic Ridge, would be useful in further resolving the relationship between dispersal and genetic distance in this genus.

The high dispersal observed in *Thermococcus* may result from an ability to survive outside of the hydrothermal vent environment for extended periods of time. Thermophilic activity has been measured in equatorial deep-sea sediments hundreds of km away from any known hydrothermal activity, thereby hypothesizing long distance transport and survival from the EPR (Dobbs and Selph, 1997). Dispersal over great distances must be considered particularly when looking at the isolates found in Clade X, where high sequence and AFLP profile similarity was found in isolates from vent sites ∼9500 km apart (i.e., Gorda Ridge and Manus Basin). Explanations for the high similarity observed in these isolates may include: a population bottleneck or recent population divergence, increased dispersal potential resulting from the ability to survive outside of the vent environment, or possibly a niche-specific ecotype due to unique metabolic characteristics. Isolates in Clade X that were collected from the Gorda Ridge have already been shown to grow over an atypically broad range of temperatures (45–90°C) for hyperthermophiles (Summit and Baross, 1998). The discovery of the CODH gene cassette in the type strain *T. onnurines* (found in Clade X) and the occurrence of these genes in other distantly related type strains may be indicative of a gene transfer event providing a selective advantage. Isolates found in Clade X may also be representative of a subsurface ecotype, with five of the seven isolates in this clade isolated from a plume event (Summit and Baross, 1998). Hydrothermal fluids released from subseafloor reservoirs during a plume event are believed to have residence times of from months to years and hydrothermal fluids have been detected thousands of kilometers from their origin (Lupton, 1996; Lupton et al., 1998, 1999). This makes hydrothermal plumes a potential vehicle for the dispersal of microorganisms associated with subsurface hydrothermal habitats over great distances. Long distance dispersal has also been demonstrated in dormant thermophilic endospores through the circulation of ocean currents (Müller et al., 2014). Further investigation of Clade X will require full-genome comparisons against other

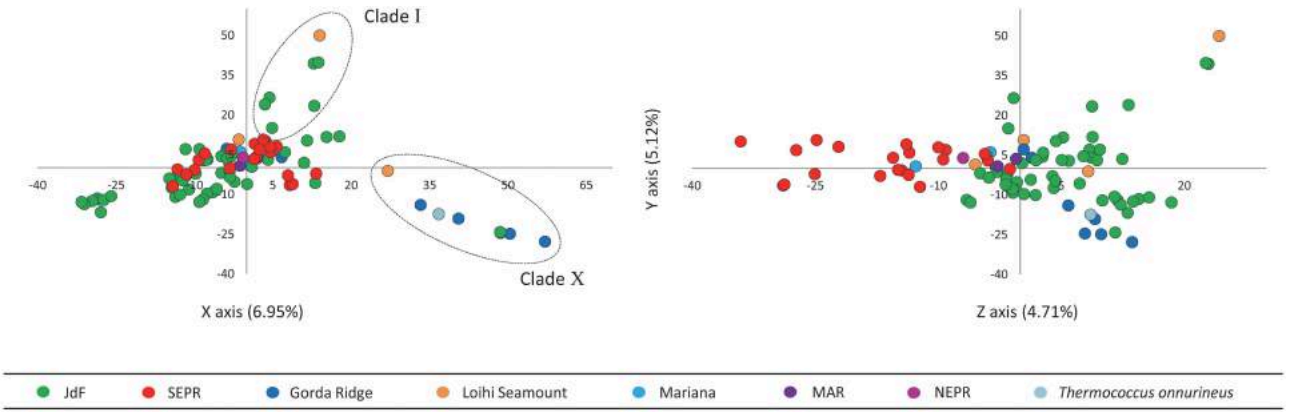

FIGURE 4 | Principal component analysis of AFLP data with the first three principal components describing the greatest variation plotted on the X, Y, and Z axes. Principal component 1 and 2 plotted on the X and Y axes differentiate isolates in Clade I and Clade X from other isolates in this study. Principal component 3 plotted on the Z axis differentiates isolates into larger regionally related groups.

Thermococcus genomes, to look for genes unique to this group that may allow for greater survival and dispersal outside the hydrothermal environment.

Clade I represents a group of *Thermococcus* that was unique in comparison to the other clades identified; however, Clade I like Clade X contained isolates from different regions (i.e., Loihi Seamount and Juan de Fuca Ridge). The most striking characteristic of the Clade I group was the phylogenetic distance between this group from other *Thermococcus* isolates as compared to their close proximity to several *Pyrococcus* type strains. This pattern was also observed in the GC-content analyses illustrating the divergence of the Clade I lineage with the *Pyrococcus* genus from the other *Thermococcus* isolates examined. In the SSU rRNA gene tree (**Figure 3**), Clade I was placed in an ancestral position relative to both *Pyrococcus* type strains and *Thermococcus* isolates from Clades II through X resulting in paraphyletic groupings of the *Thermococcus* and *Pyrococcus* genera. This topology has also been demonstrated in other phylogenetic analyses of the *Thermococcales* (Teske et al., 2009; Yilmaz et al., 2014). These data suggest that Clade I is a close sister lineage to *Pyrococcus* requiring reclassification.

Biodiversity in the *Thermococcus* genus has been made evident in this study through the identification of three or more lineages co-occurring within the same hydrothermal vent system. These divergent lineages have likely adapted to different ecological niches, allowing them to coexist at the same vent site. Previous research has shown a correlation between environmental habitat and phylogeny with the hydrothermal vent habitats of sulfide chimneys and subseafloor zones proposed as the differing environments involved in the maintenance of diversity (Summit and Baross, 2001). Although no significant correlation was found in our study between lineages and the environmental samples from which they were isolated, the broader divergence observed in the phylogenetic tree may well be due to the differing source habitats as previously described. These broader lineage groups, Clades II and III vs. Clades VII and VIII, may represent lineages adapted to different niches and present in both regions, which have diverged over time into regionally endemic populations. Determining the source environment for any of the lineages identified will be extremely difficult particularly when considering the continuous mixing of fluids within subsurface hydrothermal conduits and the limitations imposed by current sampling techniques. While it may not be possible to improve greatly on sampling techniques in the near future, the biodiversity described can be investigated more thoroughly through the genomic analysis of metabolic characteristics associated with different lineages and how these relate to the utilization of different habitats.

Horizontal gene transfer (HGT) and recombination are believed to play an important role in the mixing of microbial populations and shaping of diversity (Gogarten et al., 2002; Nesbø et al., 2006; Zhaxybayeva et al., 2006), however the role of HGT is unclear since there is a decrease in these events as geographic distance and genetic distance among microorganisms increase, e.g., extrinsic and intrinsic barriers to gene transfer and recombination (Whitaker et al., 2005; Reno et al., 2009; Cadillo-Quiroz et al., 2012). Genomic diversity in *Thermococcus* isolates was investigated through the analysis of AFLP and MLST data for evidence of genomic rearrangements and gene transfer events. The conserved nature of MLST loci evident in dN/dS ratios and through linkage analysis support the theory that conserved housekeeping genes making up the core genome are unlikely to undergo gene transfer or recombination (Medini et al., 2005; Tettelin et al., 2008; Cordero and Polz, 2014). The same lineages identified through MLST were also identified through AFLP, although AFLP analysis detected greater genomic variation. Analysis of AFLP data through PCA (**Figure 4**) provides evidence suggestive of regionally related recombination, with phylogenetically distinct lineages clustered into larger regionally related groups. This is in contrast to what is shown in the ML phylogenetic tree constructed from MLST data (**Figure 2**) where isolates from a shared region are often differentiated into distinct clades. Shared genomic characteristics within regions, between divergent lineages, may be detected in AFLP data as the genome

wide restriction fragment lengths are more representative of variable regions of the genome where gene acquisition and loss occur more frequently.

Biogeographic patterns in viruses and mobile genetic elements have been identified in both terrestrial and marine environments as exemplified by *Sulfolobus* and *Vibrio*, respectively (Held and Whitaker, 2009; Boucher et al., 2011). In the *Thermococcales*, geographically associated recombination has been reported with the identification of a shared 16 kb region flanked by insertion sequence (IS) elements, found in *Pyrococcus furiosus* and *Thermococcus litoralis* both of which were isolated from Vulcano Island, Italy (Diruggiero et al., 2000). To address regionally related recombination in *Thermococcus*, mobile genetic elements like insertion sequence elements and transposons (Diruggiero et al., 2000; Zivanovic et al., 2002; Escobar-Páramo et al., 2005; Fukui et al., 2005; Mardanov et al., 2009) along with viral related elements (Fukui et al., 2005; Mardanov et al., 2009; Portillo and Gonzalez, 2009; Zivanovic et al., 2009; Vannier et al., 2011) and extracellular vesicles (Choi et al., 2015) can be investigated within populations at regional levels and across regions, for further evidence in support of regionally related recombination.

This study begins to elucidate the level of genomic resolution required to track population divergence in isolates of *Thermococcus* at marine hydrothermal systems. These systems are thermodynamically energized by strong gradients (e.g., temperature, oxygen, etc.) fueling multiple potential habitats within the subsurface crustal environment (Edwards et al., 2011; Orcutt et al., 2011). The ability to observe divergence in microorganisms is largely dependent on the geographic scale investigated and level of genetic resolution applied. Biogeographic patterns shown in the archaeal genus *Thermococcus* demonstrate that even in microorganisms with dispersal over thousands of kilometers, divergence can occur when populations are isolated from one another. By identifying the appropriate scale and level of resolution required, the impact that geography and barriers to dispersal have on shaping microbial diversity are now being realized. Identifying the role and significance of mobile genetic elements in the shaping of microbial populations is the next step to understanding the evolutionary forces behind the planet's vast microbial diversity.

Acknowledgments

Many thanks to John Baross and his lab for allowing us access to this amazing collection and to the many undergraduate researchers in the Moyer lab who helped maintain the Zoo Collection of *Thermococcus*, with special thanks to Debbie Whitley for getting us started during her summer internship. This work was funded in part by WWU's Office of Research and Sponsored Programs and by the Center for Dark Energy Biosphere Investigations. This is C-DEBI Contribution 279.

Supplementary Material

The Supplementary Material for this article can be found online at: http://journal.frontiersin.org/article/10.3389/fmicb.2015.00968

References

Adams, M. W. (1993). Enzymes and proteins from organisms that grow near and above 100°C. *Annu. Rev. Microbiol.* 47, 627–658. doi: 10.1146/annurev.mi.47.100193.003211

Altschul, S. F., Gish, W., Miller, W., Myers, E. W., and Lipman, D. J. (1990). Basic local alignment search tool. *J. Mol. Biol.* 215, 403–410. doi: 10.1016/S0022-2836(05)80360-2

Amend, J. P., Meyer-Dombard, D. R., Sheth, S. N., Zolotova, N., and Amend, A. C. (2003). *Palaeococcus helgesonii* sp. nov., a facultatively anaerobic, hyperthermophilic archaeon from a geothermal well on Vulcano Island, Italy. *Arch. Microbiol.* 179, 394–401. doi: 10.1007/s00203-003-0542-7

Atomi, H., Fukui, T., Kanai, T., Morikawa, M., and Imanaka, T. (2004). Description of *Thermococcus kodakaraensis* sp. nov., a well studied hyperthermophilic archaeon previously reported as Pyrococcus sp. KOD1. *Archaea* 1, 263–267. doi: 10.1155/2004/204953

Baas-Becking, L. G. M. (1934). *Geobiologie of Inleiding tot de Milieukunde*. The Hague: Van Stockum, W. P., and N. V. Zoon.

Bae, S. S., Kim, Y. J., Yang, S. H., Lim, J. K., Jeon, J. H., Lee, H. S., et al. (2006). *Thermococcus onnurineus* sp. nov., a hyperthermophilic archaeon isolated from a deep-sea hydrothermal vent area at the PACMANUS field. *J. Microbiol. Biotechnol.* 16, 1826–1831.

Bonnet, E., and de Peer, Y. V. (2002). zt: a software tool for simple and partial Mantel tests. *J. Stat. Softw.* 7, 1–12.

Boucher, Y., Cordero, O. X., Takemura, A., Hunt, D. E., Schliep, K., Bapteste, E., et al. (2011). Local mobile gene pools rapidly cross species boundaries to create endemicity within global *Vibrio cholerae* populations. *mBio* 2, e00335–e00310. doi: 10.1128/mBio.00335-10

Cadillo-Quiroz, H., Didelot, X., Held, N. L., Herrera, A., Darling, A., Reno, M. L., et al. (2012). Patterns of gene flow define species of thermophilic Archaea. *PLoS Biol.* 10:e1001265. doi: 10.1371/journal.pbio.1001265

Cho, J. -C., and Tiedje, J. M. (2000). Biogeography and degree of endemicity of fluorescent *Pseudomonas* strains in soil. *Appl. Environ. Microbiol.* 66, 5448–5456. doi: 10.1128/AEM.66.12.5448-5456.2000

Choi, D. H., Kwon, Y. M., Chiura, H. X., Yang, E. C., Bae, S. S., Kang, S. G., et al. (2015). Extracellular vesicles of the hyperthermophilic archaeon *Thermococcus onnurineus* NA1^T. *Appl. Environ. Microbiol.* 81, 4591–4599. doi: 10.1128/AEM.00428-15

Cordero, O. X., and Polz, M. F. (2014). Explaining microbial genomic diversity in light of evolutionary ecology. *Nat. Rev. Microbiol.* 12, 263–273. doi: 10.1038/nrmicro3218

Davis, R. E., and Moyer, C. L. (2008). Extreme spatial and temporal variability of hydrothermal microbial mat communities along the Mariana Island Arc and southern Mariana back-arc system. *J. Geophys. Res.* 113, B08S15. doi: 10.1029/2007JB005413

DeChaine, E. G., Bates, A. E., Shank, T. M., and Cavanaugh, C. M. (2006). Off-axis symbiosis found: characterization and biogeography of bacterial symbionts of *Bathymodiolus* mussels from Lost City hydrothermal vents. *Environ. Microbiol.* 8, 1902–1912. doi: 10.1111/j.1462-2920.2005.01113.x

Diruggiero, J., Dunn, D., Maeder, D. L., Holley-Shanks, R., Chatard, J., Horlacher, R., et al. (2000). Evidence of recent lateral gene transfer among hyperthermophilic Archaea. *Mol. Microbiol.* 38, 684–693. doi: 10.1046/j.1365-2958.2000.02161.x

Dobbs, F. C., and Selph, K. A. (1997). Thermophilic bacterial activity in a deep-sea sediment from the Pacific Ocean. *Aquatic Microbiol. Ecol.* 13, 209–212. doi: 10.3354/ame013209

Edwards, K. J., Wheat, C. G., and Sylvan, J. B. (2011). Under the sea: microbial life in volcanic oceanic crust. *Nat. Rev. Microbiol.* 9, 703–712. doi: 10.1038/nrmicro2647

Erauso, G., Reysenbach, A. -L., Godfroy, A., Meunier, J. -R., Crump, B., Partensky, F., et al. (1993). *Pyrococcus abyssi* sp. nov., a new hyperthermophilic archaeon isolated from a deep-sea hydrothermal vent. *Arch. Microbiol.* 160, 338–349. doi: 10.1007/BF00252219

Escobar-Páramo, P., Ghosh, S., and DiRuggiero, J. (2005). Evidence for genetic drift in the diversification of a geographically isolated population of the hyperthermophilic archaeon *Pyrococcus*. *Mol. Biol. Evol.* 22, 2297–2303. doi: 10.1093/molbev/msi227

Excoffier, L., Laval, G., and Schneider, S. (2005). Arlequin (version 3.0): an integrated software package for population genetics data analysis. *Evol. Bioinform. Online* 1, 47–50.

Fiala, G., and Stetter, K. (1986). *Pyrococcus furiosus* sp. nov. represents a novel genus of marine heterotrophic archaebacteria growing optimally at 100°C. *Arch. Microbiol.* 145, 56–61. doi: 10.1007/BF00413027

Flores, G. E., Shakya, M., Meneghin, J., Yang, Z. K., Seewald, J. S., Wheat, C. G., et al. (2012). Inter-field variability in the microbial communities of hydrothermal vent deposits from a back-arc basin. *Geobiology* 10, 333–346. doi: 10.1111/j.1472-4669.2012.00325.x

Fukui, T., Atomi, H., Kanai, T., Matsumi, R., Fujiwara, S., and Imanaka, T. (2005). Complete genome sequence of the hyperthermophilic archaeon *Thermococcus kodakaraensis* KOD1 and comparison with *Pyrococcus* genomes. *Genome Res.* 15, 352–363. doi: 10.1101/gr.3003105

Garrity, G. M., Boone, D. R., and Castenholz, R. W. (2001). *Bergey's Manual of Systematic Bacteriology, Vol. 1: The Archaea and the Deeply Branching and Phototrophic Bacteria*. New York, NY: Springer.

Gogarten, J. P., Doolittle, W. F., and Lawrence, J. G. (2002). Prokaryotic evolution in light of gene transfer. *Mol. Biol. Evol.* 19, 2226–2238. doi: 10.1093/oxfordjournals.molbev.a004046

Häne, B. G., Jäger, K., and Drexler, H. G. (1993). The Pearson product-moment correlation coefficient is better suited for identification of DNA fingerprint profiles than band matching algorithms. *Electrophoresis* 14, 967–972. doi: 10.1002/elps.11501401154

Haubold, B., and Hudson, R. R. (2000). LIAN 3.0: detecting linkage disequilibrium in multilocus data. *Bioinformatics* 16, 847–848. doi: 10.1093/bioinformatics/16.9.847

Held, N. L., and Whitaker, R. J. (2009). Viral biogeography revealed by signatures in *Sulfolobus islandicus* genomes. *Environ. Microbiol.* 11, 457–466. doi: 10.1111/j.1462-2920.2008.01784.x

Holden, J. F., Takai, K., Summit, M., Bolton, S., Zyskowski, J., and Baross, J. A. (2001). Diversity among three novel groups of hyperthermophilic deep-sea *Thermococcus* species from three sites in the northeastern Pacific Ocean. *FEMS Microbiol. Ecol.* 36, 51–60. doi: 10.1111/j.1574-6941.2001.tb00825.x

Huber, J. A., Butterfield, D. A., and Baross, J. A. (2006). Diversity and distribution of subseafloor Thermococcales populations in diffuse hydrothermal vents at an active deep-sea volcano in the northeast Pacific Ocean. *J. Geophys. Res.* 111, G04016. doi: 10.1029/2005JG000097

Jannasch, H. W., Wirsen, C. O., Molyneaux, S. J., and Langworthy, T. A. (1992). Comparative physiological studies on hyperthermophilic Archaea isolated from deep-sea hot vents with emphasis on *Pyrococcus* strain GB-D. *Appl. Environ. Microbiol.* 58, 3472–3481.

Jun, X., Lupeng, L., Minjuan, X., Oger, P., Fengping, W., Jebbar, M., et al. (2011). Complete genome sequence of the obligate piezophilic hyperthermophilic archaeon *Pyrococcus yayanosii* CH1. *J. Bacteriol.* 193, 4297–4298. doi: 10.1128/JB.05345-11

Kaplan, J. B., and Fine, D. H. (1998). Codon usage in *Actinobacillus actinomycetemcomitans*. *FEMS Microbiol. Lett.* 163, 31–36. doi: 10.1111/j.1574-6968.1998.tb13022.x

Kim, Y. J., Lee, H. S., Kim, E. S., Bae, S. S., Lim, J. K., Matsumi, R., et al. (2010). Formate-driven growth coupled with H_2 production. *Nature* 467, 352–355. doi: 10.1038/nature09375

Konstantinidis, K. T., Ramette, A., and Tiedje, J. M. (2006a). Toward a more robust assessment of intraspecies diversity, using fewer genetic markers. *Appl. Environ. Microbiol.* 72, 7286–7293. doi: 10.1128/AEM.01398-06

Konstantinidis, K. T., Ramette, A., and Tiedje, J. M. (2006b). The bacterial species definition in the genomic era. *Philos. Trans. R. Soc. Lond. B Biol. Sci.* 361, 1929–1940. doi: 10.1098/rstb.2006.1920

Konstantinidis, K. T., and Tiedje, J. M. (2005). Genomic insights that advance the species definition for prokaryotes. *Proc. Natl. Acad. Sci. U.S.A.* 102, 2567–2572. doi: 10.1073/pnas.0409727102

Kuhn, G., Francioli, P., and Blanc, D. S. (2006). Evidence for clonal evolution among highly polymorphic genes in methicillin-resistant *Staphylococcus aureus*. *J. Bacteriol.* 188, 169–178. doi: 10.1128/JB.188.1.169-178.2006

Lecompte, O., Ripp, R., Puzos-Barbe, V., Duprat, S., Heilig, R., Dietrich, J., et al. (2001). Genome evolution at the genus level: comparison of three complete genomes of hyperthermophilic archaea. *Genome Res.* 11, 981–993. doi: 10.1101/gr.GR1653R

Lee, H. S., Kang, S. G., Bae, S. S., Lim, J. K., Cho, Y., Kim, Y. J., et al. (2008). The complete genome sequence of *Thermococcus onnurineus* NA1 reveals a mixed heterotrophic and carboxydotrophic metabolism. *J. Bacteriol.* 190, 7491–7499. doi: 10.1128/JB.00746-08

Lepage, E., Marguet, E., Gesline, C., Matte-Tailliez, O., Zillig, W., Forterre, P., et al. (2004). Molecular diversity of new *Thermococcales* isolates from a single area of hydrothermal deep-sea vents as revealed by randomly amplified polymorphic DNA fingerprinting and 16S rRNA gene sequence analysis. *Appl. Environ. Microbiol.* 70, 1277–1286. doi: 10.1128/AEM.70.3.1277-1286.2004

Lin, J. -J., Kuo, J., and Ma, J. (1996). A PCR-based DNA fingerprinting technique: AFLP for molecular typing of bacteria. *Nucleic Acids Res.* 24, 3649–3650. doi: 10.1093/nar/24.18.3649

Lupton, J. E. (1996). A far-field hydrothermal plume from Loihi Seamount. *Science* 272, 976–979. doi: 10.1126/science.272.5264.976

Lupton, J. E., Baker, E. T., Garfield, N., Massoth, G. J., Feely, R. A., Cowen, J. P., et al. (1998). Tracking the evolution of a hydrothermal event plume with a RAFOS neutrally buoyant drifter. *Science* 280, 1052–1055. doi: 10.1126/science.280.5366.1052

Lupton, J. E., Baker, E. T., and Massoth, G. J. (1999). Helium, heat, and the generation of hydrothermal event plumes at mid-ocean ridges. *Earth Planet. Sci. Lett.* 171, 343–350. doi: 10.1016/S0012-821X(99)00149-1

Maiden, M. C., Bygraves, J. A., Feil, E., Morelli, G., Russell, J. E., Urwin, R., et al. (1998). Multilocus sequence typing: a portable approach to the identification of clones within populations of pathogenic microorganisms. *Microbiology* 95, 3140–3145. doi: 10.1073/pnas.95.6.3140

Mardanov, A. V., Ravin, N. V., Svetlitchnyi, V. A., Beletsky, A. V., Miroshnichenko, M. L., Bonch-Osmolovskaya, E. A., et al. (2009). Metabolic versatility and indigenous origin of the archaeon *Thermococcus sibiricus*, isolated from a siberian oil reservoir, as revealed by genome analysis. *Appl. Environ. Microbiol.* 75, 4580–4588. doi: 10.1128/AEM.00718-09

McAllister, S. M., Davis, R. E., McBeth, J. M., Tebo, B. M., Emerson, D., and Moyer, C. L. (2011). Biodiversity and emerging biogeography of the neutrophilic iron-oxidizing *Zetaproteobacteria*. *Appl. Environ. Microbiol.* 77, 5445–5457. doi: 10.1128/AEM.00533-11

Medini, D., Donati, C., Tettelin, H., Masignani, V., and Rappuoli, R. (2005). The microbial pan-genome. *Curr. Opin. Genet. Dev.* 15, 589–594. doi: 10.1016/j.gde.2005.09.006

Meyer, J. L., and Huber, J. A. (2014). Strain-level genomic variation in natural populations of *Lebetimonas* from an erupting deep-sea volcano. *ISME J.* 8, 867–880. doi: 10.1038/ismej.2013.206

Mino, S., Makita, H., Toki, T., Miyazaki, J., Kato, S., Watanabe, H., et al. (2013). Biogeography of *Persephonella* in deep-sea hydrothermal vents of the Western Pacific. *Front. Microbiol.* 4:107. doi: 10.3389/fmicb.2013.00107

Müller, A. L., Rosa de Rezende, J. R., Hubert, C. R., Kjeldsen, K. U., Lagkouvardos, I., Berry, D., et al. (2014). Endospores of thermophilic bacteria as tracers of microbial dispersal by ocean currents. *ISME J.* 8, 1153–1165. doi: 10.1038/ismej.2013.225

Muto, A., and Osawa, S. (1987). The guanine and cytosine content of genomic DNA and bacterial evolution. *Proc. Natl. Acad. Sci. U.S.A.* 84, 166–169. doi: 10.1073/pnas.84.1.166

Nesbø, C. L., Dlutek, M., and Doolittle, W. F. (2006). Recombination in Thermotoga: implications for species concepts and biogeography. *Genetics* 172, 759–769. doi: 10.1534/genetics.105.049312

Oger, P., Sokolova, T. G., Kozhevnikova, D. A., Chernyh, N. A., Bartlett, D. H., Bonch-Osmolovskaya, E. A., et al. (2011). Complete genome sequence of the hyperthermophilic archaeon *Thermococcus* sp. strain AM4, capable of organotrophic growth and growth at the expense of hydrogenogenic or

sulfidogenic oxidation of carbon monoxide. *J. Bacteriol.* 193, 7019–7020. doi: 10.1128/JB.06259-11

Olive, D. M., and Bean, P. (1999). Principles and applications of methods for DNA-based typing of microbial organisms. *J. Clin. Microbiol.* 37, 1661–1669.

Opatkiewicz, A. D., Butterfield, D. A., and Baross, J. A. (2009). Individual hydrothermal vents at Axial Seamount harbor distinct subseafloor microbial communities. *FEMS Microbiol. Ecol.* 70, 413–424. doi: 10.1111/j.1574-6941.2009.00747.x

Orcutt, B. N., Sylvan, J. B., Knab, N. J., and Edwards, K. J. (2011). Microbial ecology of the dark ocean above, at, and below the seafloor. *Microbiol. Mol. Biol. Rev.* 75, 361–422. doi: 10.1128/MMBR.00039-10

Papke, R. T., Ramsing, N. B., Bateson, M. M., and Ward, D. M. (2003). Geographical isolation in hot spring cyanobacteria. *Environ. Microbiol.* 5, 650–659. doi: 10.1046/j.1462-2920.2003.00460.x

Papke, R. T., and Ward, D. M. (2004). The importance of physical isolation to microbial diversification. *FEMS Microbiol. Ecol.* 48, 293–303. doi: 10.1016/j.femsec.2004.03.013

Pond, S. L., and Frost, S. D. (2005). Datamonkey: rapid detection of selective pressure on individual sites of codon alignments. *Bioinformatics* 21, 2531–2533. doi: 10.1093/bioinformatics/bti320

Portillo, M. C., and Gonzalez, J. M. (2009). CRISPR elements in the Thermococcales: evidence for associated horizontal gene transfer in *Pyrococcus furiosus*. *J. Appl. Genet.* 50, 421–430. doi: 10.1007/BF03195703

Rademaker, J. L., Hoste, B., Louws, F. J., Kersters, K., Swings, J., Vauterin, L., et al. (2000). Comparison of AFLP and rep-PCR genomic fingerprinting with DNA-DNA homology studies: *Xanthomonas* as a model system. *Int. J. Syst. Evol. Microbiol.* 50, 665–677. doi: 10.1099/00207713-50-2-665

Ramette, A., and Tiedje, J. M. (2007). Biogeography: an emerging cornerstone for understanding prokaryotic diversity, ecology, and evolution. *Microb. Ecol.* 53, 197–207. doi: 10.1007/s00248-005-5010-2

Reno, M. L., Held, N. L., Fields, C. J., Burke, P. V., and Whitaker, R. J. (2009). Biogeography of the *Sulfolobus islandicus* pan-genome. *Proc. Natl. Acad. Sci. U.S.A.* 106, 8605–8610. doi: 10.1073/pnas.0808945106

Robb, F. T., and Place, A. R., (eds.) (1995). *Thermophiles: Archaea a Laboratory Manual*. Plainview, NY: Cold Spring Harbor Laboratory Press.

Rozen, S., and Skaletsky, H. (2000). Primer3 on the WWW for general users and for biologist programmers. *Methods Mol. Biol.* 132, 365–386. doi: 10.1385/1-59259-192-2:365

Savelkoul, P. H., Aarts, H. J., de Haas, J., Dijkshoorn, L., Duim, B., Otsen, M., et al. (1999). Amplified-fragment length polymorphism analysis: the state of an art. *J. Clin. Microbiol.* 37, 3083–3091.

Sokolova, T. G., Henstra, A. M., Sipma, J., Parshina, S. N., Stams, A. J., and Lebedinsky, A. V. (2009). Diversity and ecophysiological features of thermophilic carboxydotrophic anaerobes. *FEMS Microbiol. Ecol.* 68, 131–141. doi: 10.1111/j.1574-6941.2009.00663

Stamatakis, A. (2006). RAxML-VI-HPC: maximum likelihood-based phylogenetic analyses with thousands of taxa and mixed models. *Bioinformatics* 22, 2688–2690. doi: 10.1093/bioinformatics/btl446

Stamatakis, A., Hoover, P., and Rougemont, J. (2008). A rapid bootstrap algorithm for the RAxML web servers. *Syst. Biol.* 57, 758–771. doi: 10.1080/10635150802429642

Summit, M., and Baross, J. A. (1998). Thermophilic subseafloor microorganisms from the 1996 north Gorda Ridge eruption. *Deep Sea Res. II* 45, 2751–2766. doi: 10.1016/S0967-0645(98)00092-7

Summit, M., and Baross, J. A. (2001). A novel microbial habitat in the mid-ocean ridge subseafloor. *Proc. Natl. Acad. Sci. U.S.A.* 98, 2158–2163. doi: 10.1073/pnas.051516098

Takai, K., Sugai, A., Itoh, T., and Horikoshi, K. (2000). *Palaeococcus ferrophilus* gen. nov., sp. nov., a barophilic, hyperthermophilic archaeon from a deep-sea hydrothermal vent chimney. *Int. J. Syst. Evol. Microbiol.* 50, 489–500. doi: 10.1099/00207713-50-2-489

Tamura, K., Peterson, D., Peterson, N., Stecher, G., Nei, M., and Kumar, S. (2011). MEGA5: molecular evolutionary genetics analysis using maximum likelihood, evolutionary distance, and maximum parsimony methods. *Mol. Biol. Evol.* 28, 2731–2739. doi: 10.1093/molbev/msr121

Teske, A., Edgcomb, V., Rivers, A. R., Thompson, J. R., de Vera Gomez, A., Molyneaux, S. J., et al. (2009). A molecular and physiological survey of a diverse collection of hydrothermal vent *Thermococcus* and *Pyrococcus* isolates. *Extremophiles* 13, 905–915. doi: 10.1007/s00792-009-0278-7

Tettelin, H., Riley, D., Cattuto, C., and Medini, D. (2008). Comparative genomics: the bacterial pan-genome. *Curr. Opin. Microbiol.* 12, 472–477. doi: 10.1016/j.mib.2008.09.006

Thompson, J. D., Higgins, D. G., and Gibson, T. J. (1994). CLUSTAL W: improving the sensitivity of progressive multiple sequence alignment through sequence weighting, position-specific gap penalties and weight matrix choice. *Nucleic Acids Res.* 22, 4673–4680. doi: 10.1093/nar/22.22.4673

Vannier, P., Marteinsson, V. T., Fridjonsson, O. H., Oger, P., and Jebbar, M. (2011). Complete genome sequence of the hyperthermophilic, piezophilic, heterotrophic, and carboxydotrophic archaeon *Thermococcus barophilus* MP. *J. Bacteriol.* 193, 1481–1482. doi: 10.1128/JB.01490-10

Whelan, S., and Goldman, N. (2001). A general empirical model of protein evolution derived from multiple protein families using a maximum-likelihood approach. *Mol. Biol. Evol.* 18, 691–699. doi: 10.1093/oxfordjournals.molbev.a003851

Whitaker, R. (2006). Allopatric origins of microbial species. *Philos. Trans. R. Soc. Lond. B Biol. Sci.* 361, 1975–1984. doi: 10.1098/rstb.2006.1927

Whitaker, R. J., Grogan, D. W., and Taylor, J. W. (2003). Geographic barriers isolate endemic populations of hyperthermophilic archaea. *Science* 301, 976–978. doi: 10.1126/science.1086909

Whitaker, R. J., Grogan, D. W., and Taylor, J. W. (2005). Recombination shapes the natural population structure of the hyperthermophilic archaeon *Sulfolobus islandicus*. *Mol. Biol. Evol.* 22, 2354–2361. doi: 10.1093/molbev/msi233

Yilmaz, P., Parfrey, L. W., Yarza, P., Gerken, J., Pruesse, E., Quast, C., et al. (2014). The SILVA and "All-species living tree project (LTP)" taxonomic frameworks. *Nucleic Acids Res.* 42, D643–D648. doi: 10.1093/nar/gkt1209

Zhaxybayeva, O., Gogarten, J. P., Charlebois, R. L., Doolittle, W. F., and Papke, R. T. (2006). Phylogenetic analyses of cyanobacterial genomes: quantification of horizontal gene transfer events. *Genome Res.* 16, 1099–1108. doi: 10.1101/gr.5322306

Zillig, W., Holz, I., Janekovic, D., Schäfer, W., and Reiter, W. (1983). The archaebacterium *Thermococcus celer* represents, a novel genus within the thermophilic branch of the archaebacteria. *Syst. Appl. Microbiol.* 4, 88–94. doi: 10.1016/S0723-2020(83)80036-8

Zivanovic, Y., Armengaud, J., Lagorce, A., Leplat, C., Guérin, P., Dutertre, M., et al. (2009). Genome analysis and genome-wide proteomics of *Thermococcus gammatolerans*, the most radioresistant organism known amongst the Archaea. *Genome Biol.* 10:R70. doi: 10.1186/gb-2009-10-6-r70

Zivanovic, Y., Lopez, P., Philippe, H., and Forterre, P. (2002). *Pyrococcus* genome comparison evidences chromosome shuffling-driven evolution. *Nucleic Acids Res.* 30, 1902–1910. doi: 10.1093/nar/30.9.1902

Conflict of Interest Statement: The authors declare that the research was conducted in the absence of any commercial or financial relationships that could be construed as a potential conflict of interest.

frontiers in Microbiology

ORIGINAL RESEARCH
published: 18 February 2016
doi: 10.3389/fmicb.2016.00075

The Guaymas Basin Hiking Guide to Hydrothermal Mounds, Chimneys, and Microbial Mats: Complex Seafloor Expressions of Subsurface Hydrothermal Circulation

Andreas Teske[1], Dirk de Beer[2], Luke J. McKay[1,3], Margaret K. Tivey[4], Jennifer F. Biddle[5], Daniel Hoer[1], Karen G. Lloyd[1,6], Mark A. Lever[1,7], Hans Røy[8], Daniel B. Albert[1], Howard P. Mendlovitz[1] and Barbara J. MacGregor[1]*

[1] Department of Marine Sciences, University of North Carolina at Chapel Hill, Chapel Hill, NC, USA, [2] Microsensor Group, Max Planck Institute for Marine Microbiology, Bremen, Germany, [3] Center for Biofilm Engineering and Department of Land Resources and Environmental Sciences, Montana State University, Bozeman, MT, USA, [4] Department of Marine Chemistry and Geochemistry, Woods Hole Oceanographic Institution, Woods Hole, MA, USA, [5] School of Marine Science and Policy, University of Delaware, Lewes, DE, USA, [6] Department of Microbiology, University of Tennessee at Knoxville, Knoxville, TN, USA, [7] Department of Environmental Sciences, Eidgenössische Technische Hochschule, Zurich, Switzerland, [8] Center for Geomicrobiology, Aarhus University, Aarhus, Denmark

OPEN ACCESS

Edited by:
Jason B. Sylvan, Texas A&M University, USA

Reviewed by:
James F. Holden, University of Massachusetts Amherst, USA
Keir Becker, University of Miami, USA

***Correspondence:**
Andreas Teske
teske@email.unc.edu

Specialty section:
This article was submitted to Extreme Microbiology, a section of the journal Frontiers in Microbiology

Received: *01 October 2015*
Accepted: *15 January 2016*
Published: *18 February 2016*

Citation:
Teske A, de Beer D, McKay LJ, Tivey MK, Biddle JF, Hoer D, Lloyd KG, Lever MA, Røy H, Albert DB, Mendlovitz HP and MacGregor BJ (2016) The Guaymas Basin Hiking Guide to Hydrothermal Mounds, Chimneys, and Microbial Mats: Complex Seafloor Expressions of Subsurface Hydrothermal Circulation. Front. Microbiol. 7:75. doi: 10.3389/fmicb.2016.00075

The hydrothermal mats, mounds, and chimneys of the southern Guaymas Basin are the surface expression of complex subsurface hydrothermal circulation patterns. In this overview, we document the most frequently visited features of this hydrothermal area with photographs, temperature measurements, and selected geochemical data; many of these distinct habitats await characterization of their microbial communities and activities. Microprofiler deployments on microbial mats and hydrothermal sediments show their steep geochemical and thermal gradients at millimeter-scale vertical resolution. Mapping these hydrothermal features and sampling locations within the southern Guaymas Basin suggest linkages to underlying shallow sills and heat flow gradients. Recognizing the inherent spatial limitations of much current Guaymas Basin sampling calls for comprehensive surveys of the wider spreading region.

Keywords: Guaymas basin, hydrothermal circulation, hydrothermal sediment, *Beggiatoa* mat, *in situ* profiles, heatflow, porewater chemistry

INTRODUCTION

The Guaymas Basin in the Gulf of California is a young marginal rift basin characterized by active seafloor spreading and rapid deposition of organic-rich, diatomaceous sediments from highly productive overlying waters (Calvert, 1966). Organic-rich sediments of several hundred meters thickness overlie the spreading centers of Guaymas Basin and alternate with shallow intrusions of doleritic sills into the unconsolidated sediments (Einsele et al., 1980; Saunders et al., 1982). These magmatic intrusions into sediments produce organically derived thermogenic alteration products dominated by methane (Whelan et al., 1988), CO_2, low-molecular weight organic acids (Martens, 1990), ammonia (Von Damm et al., 1985), and a wide spectrum of hydrocarbons (Simoneit and Lonsdale, 1982; Simoneit, 1985; Bazylinski et al., 1988; Whelan et al., 1988) that are released into

sedimentary pore fluid and the ocean. Organic-rich fluids transported to the upper sediment column provide fossil carbon substrates to highly active, benthic microbial communities that oxidize and assimilate them (Pearson et al., 2005; Kniemeyer et al., 2007; Teske et al., 2014).

The two (northern and southern) axial troughs of Guaymas Basin are bounded by extensive systems of axial-parallel fault lines on both sides (Lonsdale and Becker, 1985; Fisher and Becker, 1991). Active hydrothermalism is predominantly found in the southern trough, where the hydrothermal sediments, mounds and chimneys form a complex hydrothermal landscape on the seafloor (Lonsdale and Becker, 1985). The conspicuous diversity of these seafloor features reflects different geochemical and temperature settings; their hydrothermal reactions, driven by underlying thermodynamic disequilibria, are modulated by location-specific reaction pathways in deep sediments or volcanic sills, and the variable residence times of hydrothermal liquid following these reaction pathways and hydrothermal circulation patterns (Gieskes et al., 1982; Kastner, 1982). Hydrothermal reactions generate and mobilize volatile hydrocarbons that migrate to the sediment surface (Peter et al., 1991; Lizarralde et al., 2011), under spatiotemporally variable temperature regimes that may limit or favor biological oxidation and assimilation (Biddle et al., 2012; McKay et al., 2012). This subsurface processing system produces a maze of subsurface flow pathways that ultimately reach the sediment surface, where they are evident in hydrothermal edifices of different developmental stages, hydrothermal mineral deposits, venting orifices emitting hot hydrothermal fluids, and hydrothermally active sediments.

The complex hydrothermal features at the Guaymas Basin seafloor were previously mapped and to a limited extent photographically documented, using a combination of dives with research submersible HOV *Alvin*, deep tow sonar records, and deep tow thermistor measurements (Koski et al., 1985; Lonsdale and Becker, 1985; Peter and Scott, 1988). The black and white photographs published in these early surveys permitted the first glimpses of the Guaymas Basin hydrothermal vent environment. Color images of hydrothermally active sediments with microbial mats and *Riftia* colonies were taken from HOV *Alvin*, and showed the distinct white, yellow, and orange coloration of the microbial mats, dominated by large filamentous sulfur-oxidizing bacteria, at that time ascribed to the genus *Beggiatoa* (Jannasch et al., 1989; Gundersen et al., 1992). Benthic communities and microbial mats revealing off-axis hydrothermal influence on the sedimented ridge flanks of Guaymas Basin were recorded by deep tow color photography (Lizarralde et al., 2011). Recent photos of well-documented Guaymas Basin hydrothermal sediments and microbial mats have accompanied published papers in online Supplementary Material (Holler et al., 2011; McKay et al., 2012), sometimes in edited form to show the location of temperature measurements (McKay et al., 2012), or they have appeared as small-scale figure inserts to illustrate sampling site context (Callac et al., 2013; MacGregor et al., 2013b). To our knowledge, only two publications have made an effort to document at least some of multiple Guaymas Basin sampling sites in color figures specifically for this purpose (Lizarralde et al., 2011; Meyer et al., 2013).

In contrast to the limited and widely scattered published image material, research cruises and individual cruise participants often accumulate a surprising amount of *in situ* observations and high-definition camera images, with varying degrees of scientific context and auxiliary data. Although these images provide the closest approximation of the *in situ* aspect of remote and rarely visited deep-sea hydrothermal vent environments, their context with respect to precise location, time, and observations linked to the site gets lost without detailed curation and documentation; all too often these important resources remain underused and serve merely as "decoration" for cruise blogs and occasional lectures. Here, we place detailed and previously unpublished *in situ* photographic surveys of microbial mats, hydrothermal mounds and chimneys collected by HOV *Alvin* during two cruises to the southern Guaymas Basin spreading center (AT15-40 and AT15-56) into the context of location, time, *in situ* data, and published studies that add to the thermal and geochemical site characterization (**Table 1**). In particular, *in situ* microprofiler deployments at several locations provide highly resolved chemical gradients at the sediment–water interface, where coinciding electron donors and acceptors provide energy for microbial mat growth.

We provide a baseline record of key locations and sampling sites that may be revisited on future research cruises, and be selected as targets for time-line studies of hydrothermal vent environments (**Figure 1**). We also place this frequently visited hydrothermal area into the context of underlying basalt sills emplaced into the sediment, and suggest that hydrothermal circulation patterns are not localized randomly; instead, this hydrothermal area and its hydrothermal flow paths follow specific boundaries of a shallow subsurface sill, or the fault lines through a sill (Lonsdale and Becker, 1985). This extended compilation may ultimately serve as a "hiking guide" that orients and familiarizes the reader and Guaymas Basin visitor with this uniquely complex seafloor landscape; like any guide, it will also lend itself to revisions, extensions, and updates that reflect ongoing and future research.

MATERIALS AND METHODS

Image Localization and Retrieval

Images were recorded during research cruises with RV *Atlantis* and HOV *Alvin* during two cruises to the southern spreading center of Guaymas Basin in the Gulf of California (AT15-40, December 6–18, 2008, and AT15-56, November 23–December 5, 2009). Site locations were based on local XY grid data, the gridding system used by the National Deep Submergence Facility (NSDF) as recorded on the *Alvin* framegrabber system[1] for the time and location of each observation. Local XY is a grid system (in meters) that is referenced to a local Latitude/Longitude origin. The conversion between Latitude/Longitude and Local XY use a simple flat-earth projection with East = X and

[1] www.whoi.edu/page.do?pid=11042

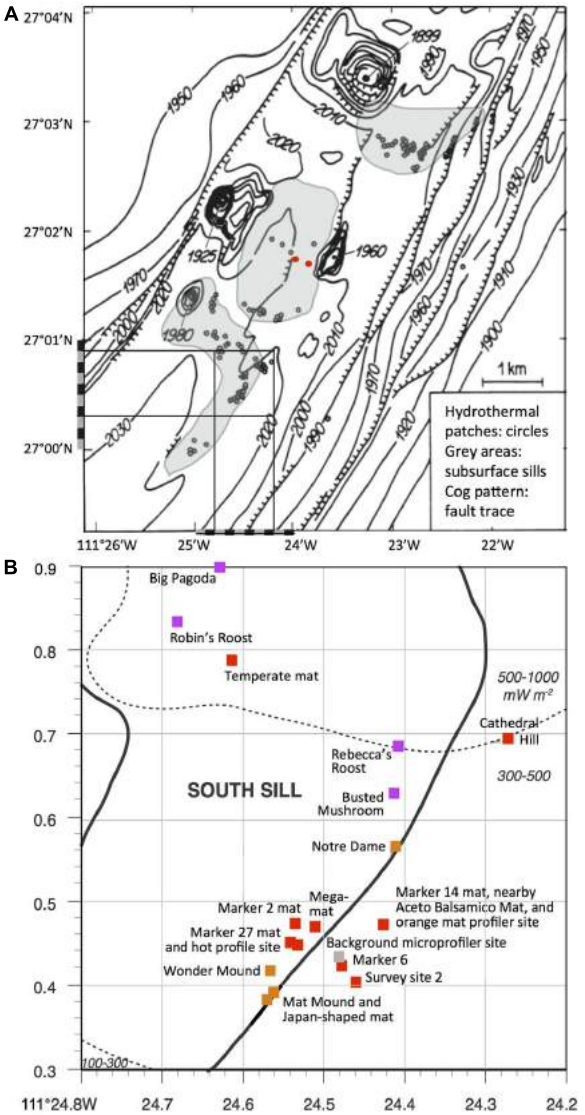

FIGURE 1 | Seafloor map of Guaymas Basin hydrothermal features. **(A)** The southern Guaymas trough with hydrothermal sites marked as small circles (Bazylinski et al., 1989, adapted from Simoneit and Lonsdale, 1982). The square in the southwestern corner of the chart corresponds to the seafloor area shown enlarged and in greater detail below. The positions of the two DSDP drilling holes 477 and 477A are marked by red dots. **(B)** Sampling area of Guaymas cruises AT15-40 and 15-56, with major hydrothermal features, superimposed on heat flow measurements of Guaymas seafloor sediments (Fisher and Becker, 1991) and subsurface sill positions indicated by gray-shaded areas (Peter and Shanks, 1992). Red squares indicate mat-dominated sites, sienna brown indicates hydrothermal mounds with diffusive venting, and purple indicates large edifices and chimneys with evidence for channelized flow. The bathymetric map is reused from Bazylinski et al. (1989) and the sill positions are redrawn from Peter and Shanks (1992) by permission of the publishers.

North = Y. It is used for relatively small areas (a few kilometers) where the distortion introduced by the projection is minimal[2]. Latitude/longitude positions of key locations were converted from XY grid data using the online NSDF coordinate conversion utility[3]. To allow for unambiguous retrieval of the original images, each framegrabber image is referenced in the figure legends with the *Alvin* heading in which the image was taken (0 = north; 90 = east; 180 = south, 270 = west), the submersible's depth in m, and the time point in Greenwich Mean Time (GMT). For higher-resolution images taken with *Alvin's* external still camera, only GMT is given, as imprinted on the image file. When possible, photos were complemented with 10 cm scale bars calibrated by two red laser beams emitted from *Alvin*, 10 cm parallel from each other.

Heat Flow Measurements

In situ temperature profiles at sampling sites were recorded using *Alvin*'s external heat flow temperature probe, a 0.6 m titanium tube containing a linear heater and five thermistors (type 44032, Omega Engineering, Inc.) at 10 cm intervals along the length of the tube (McKay et al., 2012). When fully inserted, this probe records the approach of probe temperatures to *in situ* temperatures at the sediment/water interface, and at 10, 20, 30, and 40 cm sediment depth. The probe was inserted for ca. 3–5 min during every measurement until the temperature readings stabilized.

Microprofiler Deployments

High resolution depth profiles were measured with an *in situ* microprofiler unit. The unit has an electronic cylinder with the amplifiers for the microsensors (11 total) and a computer for data storage and motor control. On the bottom plate of the electronic cylinder microsensors for H_2S, pH, O_2, redox potential and temperature were mounted (Revsbech and Ward, 1983; Jeroschewski et al., 1996; De Beer et al., 1997). The cylinder can be moved vertically in steps down to 25 μm. The microprofiler was adjusted to a buoyancy of 18 kg in water. It was carried by *Alvin* to the selected sites and precisely positioned by *Alvin's* hydraulic manipulator arm. The microprofiler was preprogrammed to measure profiles of 13 cm length with a step size of 250 μm. By gently pushing the profiler in the sediment, the sensor tips were adjusted to the starting position of ca. 3 cm above the sediment surface. A profile measurement was started by pushing the starter button with the arm of *Alvin*. Each profile measurement took ∼75 min, including a waiting time of 10 min to allow *Alvin* to leave the site and continue with other tasks. After completing a profile the sensors returned to the starting position and the unit was ready to be repositioned for new measurements. Results of *in situ* profiler measurements were compared to independent measurements of geochemical gradients, via porewater analysis, and to thermal profiles determined using the *Alvin* heat flow probe.

The pH and ORP microsensors were calibrated in standard buffers; the offset at the seafloor was obtained by comparing with values in a retrieved bottom water sample, obtained by *Alvin's* Niskin bottles. The H_2S microsensor was calibrated by adding 100-μL increments of a 500-mM Na_2S stock solution to

[2]http://www.marine-geo.org/references/descriptions/LocalXY.php

[3]http://www.whoi.edu/marine/ndsf/utility/NDSFutility.html

acidified seawater (pH < 3) at *in situ* temperature. Subsamples from the calibration solution were fixed immediately in 2% (wt/wt) zinc acetate, and the H_2S concentration was determined spectrophotometrically with the methylene blue method (Cline, 1969). The S_{tot} profiles *in situ* were calculated from the H_2S and pH profile using a pK_1 of 6.64 (Jeroschewski et al., 1996). The O_2 sensor was calibrated *in situ* using the signal in bottom water and in anoxic sediment (de Beer et al., 2006). The oxygen concentration in bottom water was determined from retrieved samples using Winkler titration (Hansen, 1999).

Thermocouple Arrays

The thermocouple arrays consist of eight ∼50 cm long Ti-sheathed 1/8th inch O.D. type-J thermocouples that are mounted on an open frame made from titanium to prevent corrosion when exposed to the hot vent fluid. The sensing ends of the thermocouples within a cylindrical open frame are placed over the vent orifice while the other end of the thermocouples are connected to two sensor modules that contain electronics and remain at a safe distance from hot fluid (Pagé et al., 2008).

Porewater Geochemical Analyses

Sulfate concentration measurements were completed shipboard; after centrifuging sediment-filled 15 ml tubes, the overlying porewater was filtered through 0.45 μm filters, acidified with 50 μl of 50% HCl and bubbled with nitrogen for 4 min to remove sulfide. Sulfate concentrations were then measured shipboard using a 2010i Dionex Ion Chromatograph (Sunnyvale, CA, USA) through Ag^+ exchange columns (Dionex) to remove Cl^- (Martens et al., 1999). For sulfide, 1 ml porewater samples were combined with 0.1 M zinc acetate and concentrations were analyzed spectrophotometrically on the ship (Cline, 1969). Porewater concentrations of dissolved organic acids were measured via HPLC (Albert and Martens, 1997). Briefly, we used a Beckman Model 332 gradient liquid chromatograph in combination with an ISCO V4 UV/VIS detector and a Shimadzu CR3-A integrator. The detector had an IO-mm flow cell and was operated at 400-nm wavelength. The column used was a 22-cm Brownlee C8 cartridge with a 1.5 cm C8 guard column and either a 1.5-cm C8 or polymeric reversed-phase guard cartridge in the sample loop as a concentrator (Albert and Martens, 1997).

RESULTS

The results are structured into three distinct sections. The first section provides an overview on the wide range of microbial mats that thrive on hydrothermal sediments, and situates previous microbiology studies of specific mat locations by recovering the *in situ* context, complemented by porewater geochemical profiles of mat-covered sediments when available. The second section focuses on microsensor *in situ* measurements in microbial mats and seafloor sediments, and their microbiological and geochemical context. The third section summarizes field observations on hydrothermal mounds and chimneys.

Microbial Mats on Hydrothermal Sediments

Among the wide range of hydrothermal vent sites, Guaymas Basin is distinguished by hydrothermal sediments that are permeated by fluids rich in sulfidic, methane, and dissolved inorganic carbon (DIC; Von Damm et al., 1985). Where these fluids reach the sediment surface, they sustain highly visible microbial mats of large, filamentous, vacuolated, sulfur-oxidizing bacteria within the family *Beggiatoaceae* (Jannasch et al., 1989; Nelson et al., 1989). These microbial mats often show a white fringe and an orange center, reminiscent of fried eggs, and contrast sharply against the surrounding brown–gray sediment (**Figure 2**). The orange center coincides with local maxima of temperature, carbon and energy sources; upward-shifted temperature zones and concentration peaks of hydrothermal energy sources characterize the underlying sediments. The white filaments are sustained by more gradual hydrothermal gradients on the periphery of the hydrothermal hot spot. Interestingly, noticeable temperature and chemical gradients extend into the surrounding bare sediments, but they become less steep and do not sustain thick mats (Supplementary Figure S1, and McKay et al., 2012). In these cases, essential components for seafloor mat sustenance appear to be lacking, or are not sufficient for colonization by mat-forming bacteria. The orange-colored and colorless filaments were placed near the genus-level candidate taxa Maribeggiatoa and Marithioploca, and the genus *Thiomargarita* based on 16S rRNA sequencing of individual filaments (McKay et al., 2012); the common literature designation of these organisms as *Beggiatoa* (Jannasch et al., 1989; Nelson et al., 1989) should be regarded as shorthand for what are actually several distinct genus-level lineages within the family *Beggiatoaceae* (Salman et al., 2011; Teske and Salman, 2015). Genome- and protein-based studies of the orange filament type indicate that they are versatile organisms with autotrophic and heterotrophic capabilities that can oxidize sulfide with nitrate as electron acceptor (MacGregor et al., 2013a,b). At a sediment depth of a few centimeters below these mats, thermotolerant, anaerobic methane-oxidizing archaea (ANME archaea) are frequently detected in 16S rRNA gene clone libraries and high-throughout sequencing surveys (Teske et al., 2002; Biddle et al., 2012; Ruff et al., 2015; Dowell et al., 2016). The ANME archaea show distribution patterns that are congruent with the high concentration of methane (several millimolar) in the hydrothermal sediments; they are in part represented by high-temperature adapted lineages in Guaymas Basin (Holler et al., 2011; Biddle et al., 2012; Kellermann et al., 2012). The combination of ANME archaea in anaerobic, reducing and methane-rich sediments, and of sulfide-oxidizing *Beggiatoa* mats or other sulfide-oxidizing bacteria on the surface of the same sediments, is highly characteristic of Guaymas Basin hydrothermal sediments (Teske et al., 2014).

The mat shown in **Figure 2C** was sampled during dive 4572 for a biogeochemical study of nitrate reduction in hydrothermal sediments of Guaymas Basin. Surficial (0–3 cm) sediments of four *Alvin* push cores in the white mat between the yellow and green heat flow gradients of Dive 4564 (near core 4564-1, plotted

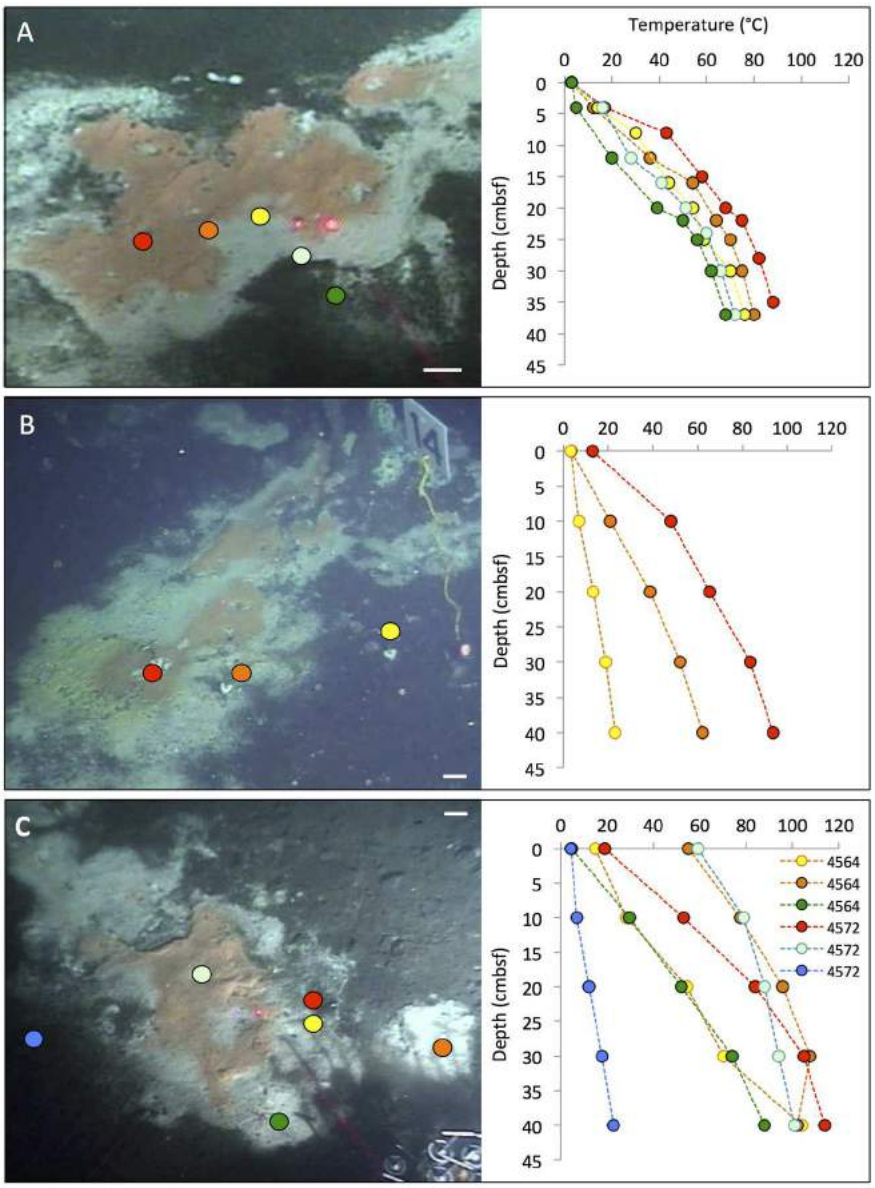

FIGURE 2 | Typical "fried egg" microbial mats. The orange *Beggiatoa* mats in the center tend toward pink in these frame grabber images; yet direct *in situ* observation and shipboard recovery show orange as the actual color. *In situ* temperature gradients in the color-marked positions are measured with *Alvin's* heat flow probe. The scale bar corresponds to 10 cm. **(A)** The Marker 2 mat was the first Guaymas Basin mat, where a temperature gradient from the center of the mat to the surrounding bare sediment was measured, using the *Alvin* high-temperature probe. *Alvin* heading 255, depth 2000.5 m, GMT 17:37:07, dive 4483, December 6, 2008. **(B)** The mat at Marker 14 was equipped with one temperature logger each in the orange center, the white fringe, and nearby bare sediment. *Alvin* heading 208, depth 2007.8 m, GMT 16:38:23, dive 4562, November 23, 2009. Geochemistry and temperature profiles of this mat are published (McKay et al., 2012); the temperature profiles are replotted here for comparison. **(C)** The large mat at Marker 27 is shown here before installment of temperature loggers or sampling. *Alvin* heading 36, depth 2002.5 m, GMT 22:02:30, dive 4564, November 25, 2009. Photographs courtesy of the Woods Hole Oceanographic Institution, from RV *Atlantis* cruises AT15-40 and AT 15-56.

in Supplementary Figure S1) were used to test the response of nitrate reduction to increased concentrations of nitrate (positive at 0.5 mM nitrate and higher), sulfide (negative at >0.5 mM sulfide), and DOC (no effect from 0 to 5 mM DOC carbon; Bowles et al., 2012). Therefore, high sulfide concentrations interfere with nitrate reduction in the hydrothermal sediments of Guaymas Basin, just as previously observed in coastal and estuarine sediments (Joye, 2002). Interestingly, a parallel 16S rRNA gene sequencing survey of these Guaymas mat sediments did not yield any members of the *Beggiatoaceae*, but mostly members of Delta- and Alphaproteobacteria, the Bacteroidetes, and some Gammaproteobacteria (Bowles et al., 2012). Due to their high cell volume, the *Beggiatoaceae* contribution to cell numbers and genomes in microbial mats lags behind that

of other abundant bacteria, and they easily elude sequence-based detection; capturing their 16S rRNA genes requires highly purified filaments (Jørgensen et al., 2010; McKay et al., 2012). Taken together, these studies indicate that by cell and genome number per volume, members of the *Beggiatoaceae* may not even be the most abundant bacteria that perform nitrate reduction in organic-rich, sulfide-rich mat sediments of Guaymas Basin mats and hydrothermal sediments; nitrate-reducing, sulfide- or hydrogen-oxidizing Epsilonproteobacteria are plausible candidates for this ecological role in hydrothermal environments (Campbell et al., 2006).

In some cases, the fried-egg appearance of a hydrothermal hot spot is modified when the central orange mat turns into an orange fringe mat surrounding a central crater-like region, where the smooth mat surface gives way to roughly textured sediment, often with a dusting of white particles, probably sulfur precipitates (**Figure 3**). In some cases, shimmering water could be observed rising from the exposed, cratered sediment surface, indicating that the hydrothermal temperature gradient has an advective component. *In situ* microsensor studies of thick mats have shown hydrothermal circulation patterns that alternate between injections of oxygenated seawater and ejections of anoxic hydrothermal fluid through the sediment–water interface (Gundersen et al., 1992). Episodic intensification of such pumping patterns could disrupt and sweep away a microbial mat and surficial sediment, or exterminate the bacterial mat by sudden upflow of hot hydrothermal fluid or lack of a consistent redox gradient. While Guaymas Basin *Beggiatoaceae* depend upon the hydrothermal hot spot as a source of electron donors, they appear to prefer cool *in situ* temperatures (on average 8 to 12°C) at the sediment surface (McKay et al., 2012).

Although hydrothermal hot spots with *Beggiatoa* mats are highly conspicuous, they are transient seafloor features that depend on the changeable course of hydrothermal flow paths in the subsurface. For example, a well-developed white and orange *Beggiatoa* mat overlying hydrothermally active sediment next to a healthy *Riftia* colony on a small hydrothermal mound (**Figure 4A**), visited in December 2008 and identified by placing a marker disk nearby, had almost entirely disappeared a year later (**Figure 4B**), along with the hydrothermal temperature gradient in the sediment (**Figure 4C**). The *Riftia* colony was decaying on its periphery, and scavengers (scale worms and

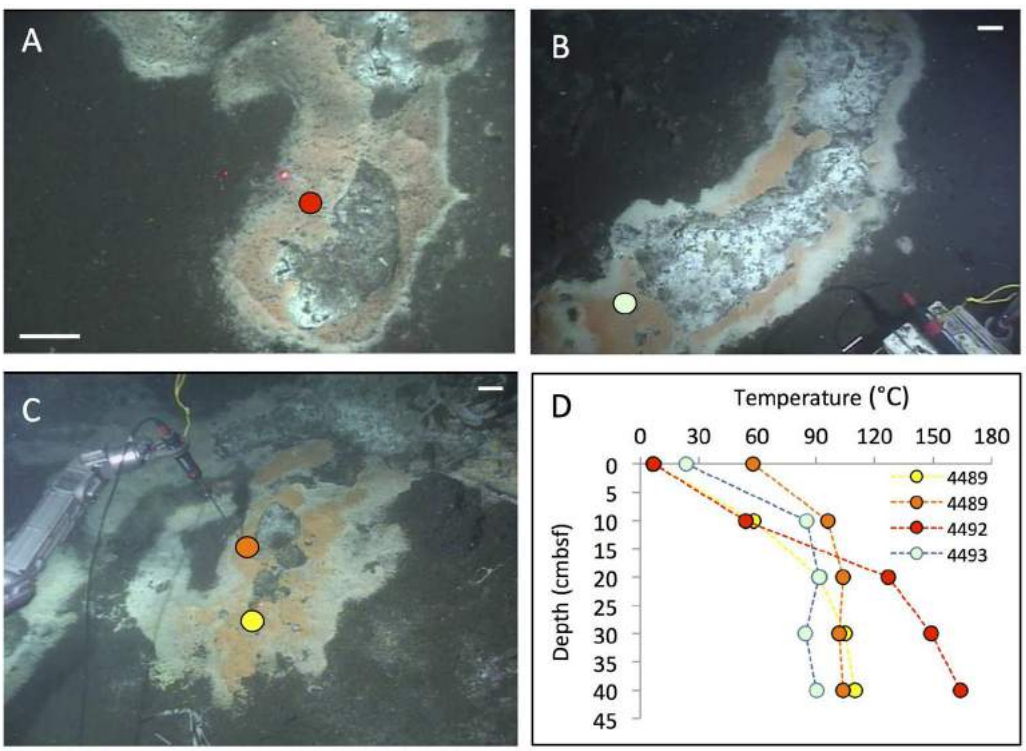

FIGURE 3 | Cratered microbial mats. Microbial mats with a white outer fringe, an orange layer, and a "cratered" central area with white-coated sediments, coinciding with shimmering water. *In situ* temperature gradients are measured with the *Alvin* heat flow probe. The scale bar corresponds to 10 cm. **(A)** Small elongated mat connected to a small mound outside of the top picture frame. Two cores have been sampled here under the moniker "Survey site 2" (Meyer et al., 2013). *Alvin* heading 334, depth 2011 m, GMT 19:58:15, dive 4492, December 16, 2008. **(B)** Elongated "Japan-shaped" mat was connected to a small mound outside of the upper picture frame. *Alvin* heading 237, depth 2004 m, GMT 20:13:25, dive 4493, December 17, 2008. Examination of the framegrabber record showed that this mat was also observed just before sighting Mat Mound (**Figure 13**) at GMT 18:34:40, with a heading of 306 on dive 4483. **(C)** The UNC mat, ca. 20 m southwest of Megamat (Biddle et al., 2012), contains a small cratered area in the center. *Alvin* heading 106, depth 2001 m, GMT 21:36:50, dive 4489, December 13, 2008. **(D)** The four temperature gradients from these cratered mats, plotted together. Photographs courtesy of the Woods Hole Oceanographic Institution, from RV *Atlantis* cruise AT 15-40.

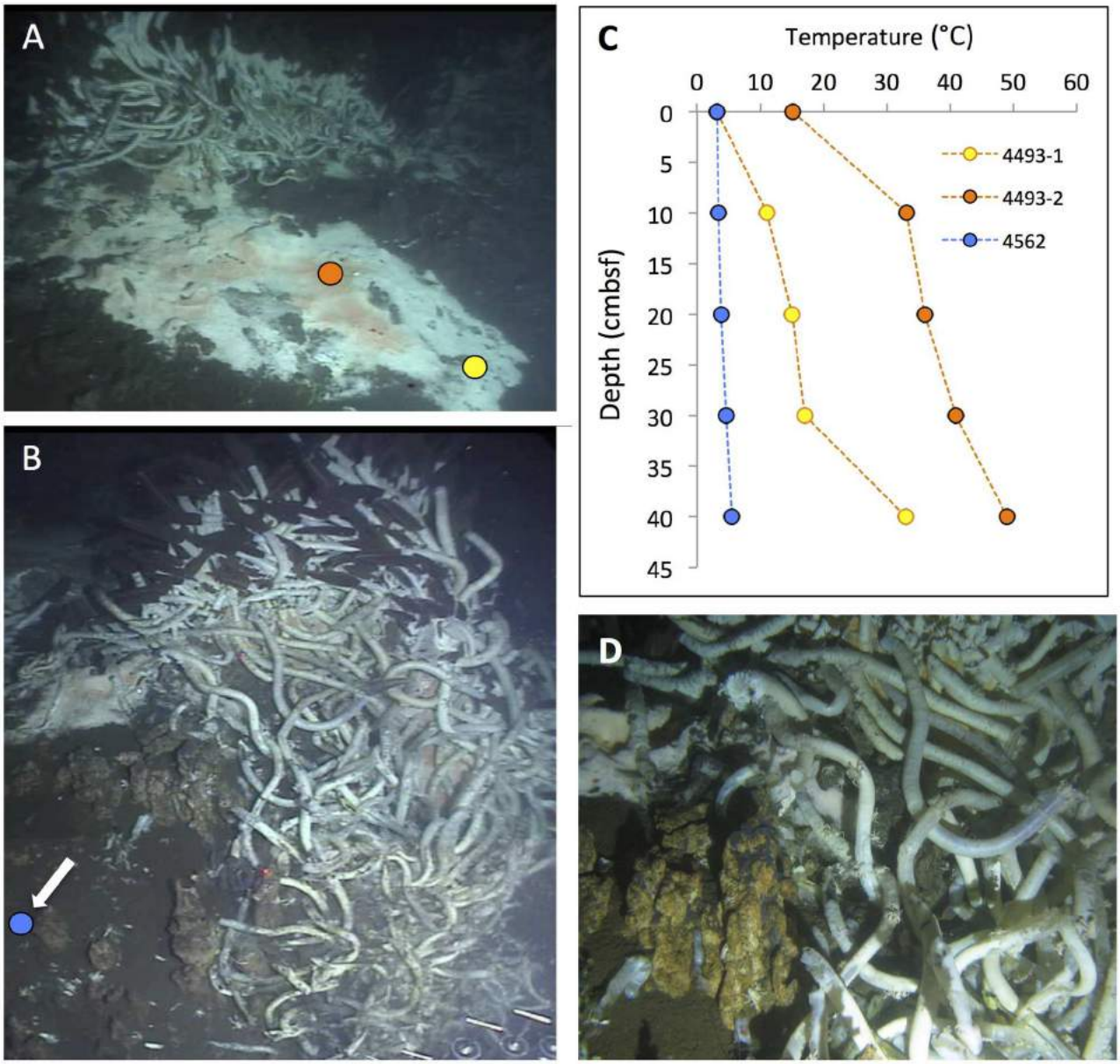

FIGURE 4 | Changing hydrothermal flux. The changing microbial mats and *Riftia* colonies at this small hydrothermal mound, termed "Marker 6," were documented during repeat visits in December 2008 and November 2009. **(A)** Framegrabber image of active *Beggiatoa* mat on sloping sediment next to thriving *Riftia* cluster on small mound. Two heat flow probe measurements revealed hydrothermal gradients in the white and orange mat. *Alvin* heading 123, depth 2003 m, GMT 22:19:44, dive 4484, December 7, 2008. **(B)** Composite framegrabber image of the same spot at a clockwise rotated angle, taken almost a year later. A cold heat flow profile (see arrow on left margin) measured at a spot between the two hot 2008 temperature profiles shows that the hydrothermal temperature gradient has almost disappeared. The *Beggiatoa* mat has receded to a small spot adjacent toward and into the center of the *Riftia* cluster; the sedimented slope is bare and much of the *Riftia* cluster has died, leaving empty sheaths dominated by scavenging isopods in the foreground. *Alvin* heading 91, depth 2006 m, GMT 17:47:25 (lower portion) and 17:47:55 (upper portion of composite image), Dive 4562, November 23, 2009. **(C)** Temperature gradient plots of the two active 2008 gradients and the cold 2009 gradient. **(D)** Closeup of decaying *Riftia* with abundant crabs and scale worms in the foreground of **(B)**; the image was taken with the external *Alvin* still camera. GMT 17:22:57. *Alvin* Dive 4562, November 23, 2009. Photographs courtesy of the Woods Hole Oceanographic Institution, from RV *Atlantis* cruise AT 15-56.

isopods) occurred in conspicuous abundance (**Figure 4D**). The rusty-brown color of the hydrothermal outcrops, especially visible in **Figure 4D**, indicate oxidizing conditions, the absence of microbial mat overgrowth, and the scarcity or absence of dissolved sulfide; such conditions are incompatible with active *Riftia* sp. (Luther et al., 2001), and have instead been documented as the declining stage of *Riftia* colonies (Shank et al., 1998).

In addition to the commonly encountered *Beggiatoa* mats associated with hotspots of reducing hydrothermal fluids migrating toward the sediment surface, several previously unreported types of mats and colorful surface precipitates have been found that remain to be investigated more closely (**Figure 5**). An unusually extensive hot mat was called "Megamat" for its size as well as its extremely hot temperatures, and repeatedly sampled in 2008 and 2009 (Biddle et al., 2012; Cardman, 2014). Most of this mat was covered with white precipitates; some marginal areas contained yellow and orange *Beggiatoa* mats (**Figure 5A**). The sediments of Megamat contained smaller proportions of methane-oxidizing archaea (ANME), but yielded abundant phylotypes of hyperthermophilic archaea, including the acidophilic, sulfur-reducing archaeon *Aciduliprofundum thermophilum* (Cardman, 2014). Based on multiple subsurface temperature gradients in the hottest region of Megamat, the temperature field within the underlying sediments was modeled in 3D, and showed temperature gradients steepening from the margins of the mat toward its central region, where 200°C was recorded at ca. 35 to 40 cm depth (McKay et al., 2012). Steep temperature gradients across the edge of Megamat were also found in 2009; within ca. 1 m distance, the temperature gradient of ca. 50°C over 40 cm depth in the bare sediment area adjacent to the mat doubles to ∼100°C over the same depth (**Figure 5A**). The porewater profiles of Megamat indicate methane- and DIC-rich sediments where sulfate decreases toward depletion and sulfide accumulates in the upper sediments layers (Supplementary Figure S2).

TABLE 1 | Site compilation including sampling or measurement locations, latitude/longitude, dive context, and relevant publications by the AT15-40 and AT15-56 science crew.

Site and Figure	Latitude and Longitude	Alvin Dive and Cruise Number, and localization context	Reference
Microbial mats			
Marker 2 mat, **Figure 2A**	27°00.468 N, 111°24.537 W	4483; AT15-40 shipboard xy fix	This publication
Marker 14 mat, **Figure 2B**	27°00.470 N, 111°24.431 W	4562; AT15-56 dive target position	McKay et al., 2012, 2015
Marker 27 mat, **Figure 2C**	27°00.445 N, 111°24.529 W	4564, 4572; AT15-56 dive target position	Bowles et al., 2012, McKay et al., 2012
Survey site 2 mat, **Figure 3A**	27°00.403 N, 111°24.459 W	4492; AT15-40 shipboard xy fix	Meyer et al., 2013
Japan-shaped mat near Mat Mound, **Figure 3B**	27°00.379 N; 111°24.566 W	4493; AT15-40 shipboard xy fix	This publication
UNC Mat, **Figure 3C**	27°00.445 N, 111°24.530 W	4489; AT15-40 shipboard xy fixes	Biddle et al., 2012, Ruff et al., 2015*
Marker 6 mat, **Figure 4**	27°00.423 N, 111°24.477 W	4484, 4562; AT15-40 shipboard xy fix	This publication
Megamat, **Figure 5A**	27°00.464 N, 111°24.512 W	4485, 4486, 4488, 4490, 4491, 4562; AT15-40 shipboard xy fix	Biddle et al., 2012, McKay et al., 2012, Ruff et al., 2015*
Cathedral Hill/Marker 24, **Figure 5B**	27°00.696 N, 111°24.265 W	4565; AT15-56 dive target position	This publication
Temperate mat, **Figure 5C**	27°00.786 N, 111°24.612 W	4574; AT15-56 frame grabber coordinates	This publication
Microprofiler sites			
Orange mat near Marker14, **Figure 6**	27°00.466 N, 111°24.425 W	4564; AT15-56 frame grabber coordinates	This publication
"AcetoBalsamico" mat near Marker 14, **Figure 7**	27°00.470 N, 111°24.427 W	4562, 4569, 4570, 4573; AT15-56 frame grabber coordinates	This publication
Hot profiler site near Marker 27, **Figures 8A,B**	27°00.448 N, 111°24.541 W	4566, 4567; AT15-56 frame grabber coordinates	This publication
Background sediment profiler site, **Figures 8C,D**	27°00.436 N, 111°24.480 W	4569; AT15-56 frame grabber coordinates	This publication
Hydrothermal structures			
Big Pagoda, **Figure 9**	27°00.909 N, 111°24.639 W	4574; AT15-56 frame grabber coordinates	This publication
Robins Roost, **Figure 10**	27°00.833 N, 111°24.679 W	4574; AT15-56 frame grabber coordinates	This publication
Rebecca's Roost, **Figure 11**	27°00.683 N; 111°24.404 W	4574; AT15-56 frame grabber coordinates	This publication
Busted Mushroom, **Figure 12**	27°00.63 N, 111°24.41 W	4555; 4557; 4571; AT15-56 dive target position	Pagé et al., 2008
Mat Mound, **Figure 13**	27°00.388 N, 111°24.560 W	4483, 4484; AT15-40 shipboard xy fix	Ruff et al., 2015*, Dowell et al., 2016
Wonder Mound, **Figure 14**	27°00.416 N, 111°24.563 W	4562; AT15-56 frame grabber coordinates	This publication
Notre Dame, **Figure 15**	27°N00.564 N,111°24.410 W	4573; AT15-56 frame grabber coordinates	This publication

**The Guaymas samples in Ruff et al., 2015 are from Mat Mound (GB1, GB4a, GB4b), Megamat (GB2), and the UNC Mat (GB3).*

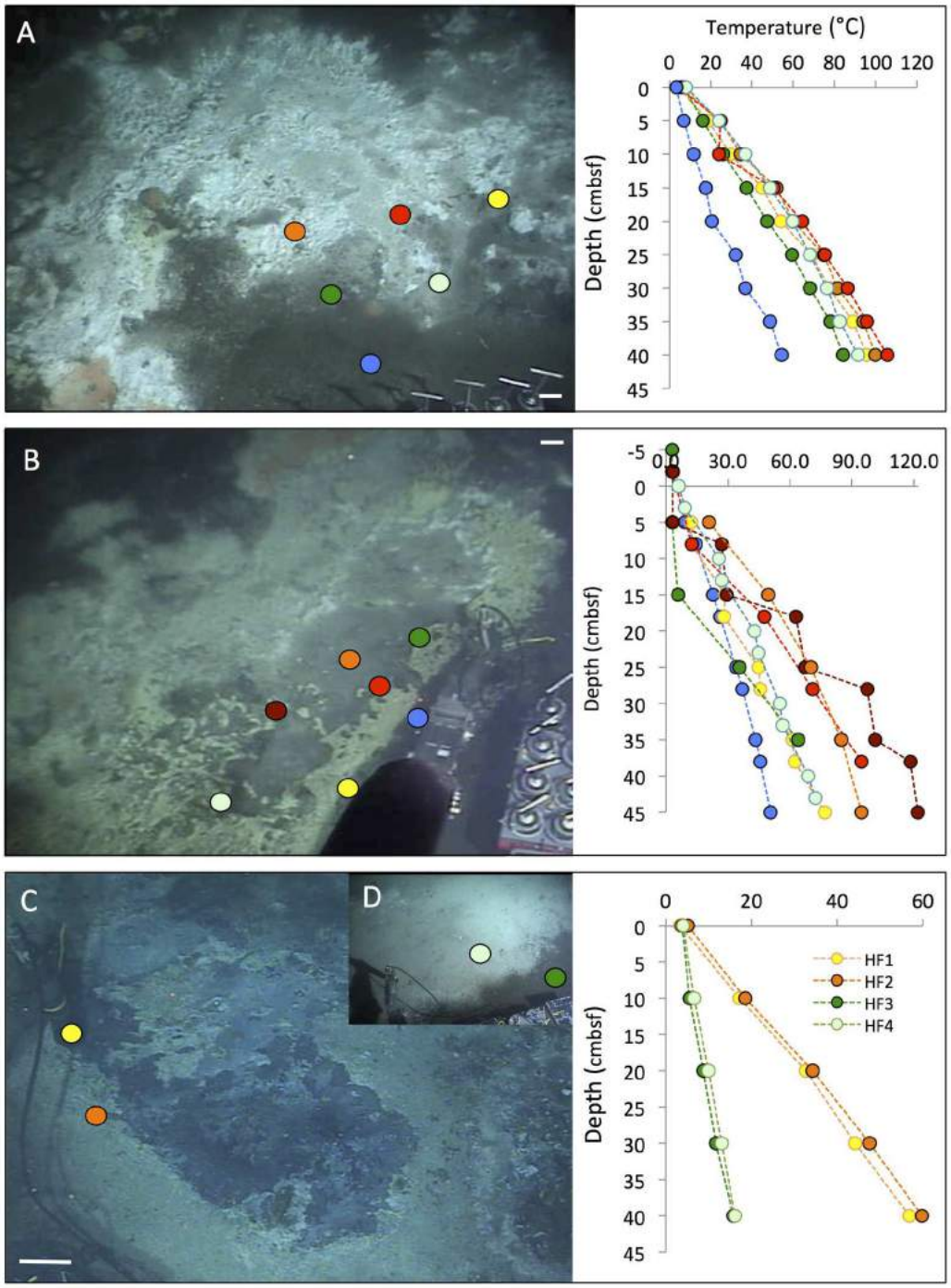

FIGURE 5 | Megamat and Cathedral Hill mats. Temperature profiles measured with the *Alvin* heat flow probe are marked with colored dots on the photos and plotted profiles in matching colors. The scale bar corresponds to 10 cm. **(A)** Partial view of hydrocarbon-rich Megamat before coring and sampling. The heat flow profiles show the thermal transition from mat-covered to bare sediment. Alvin *heading* 219, depth 2012 m, GMT 18:14:26, dive 4562, November 23, 2009. **(B)** Overview of the microbial mats area at the Cathedral Hill area, a complex of multiple white, gray, yellow, and orange mats next to a small hydrothermal massif. *Alvin* heading 174, depth 2020.3 m, GMT 18:33:10, dive 4565, November 26, 2009. Seven heat flow temperature gradients were measured on *Alvin* dive 4565 during a general survey of the area. **(C)** Temperate mats resembling the Cathedral Hill mats by yellow, white and gray surface colors. *Alvin* heading 126, depth 2021 m, GMT 18:37:07, dive 4574, December 5, 2009. **(D)** The small insert in the upper right corner shows a nearby, significantly cooler, white–gray and smooth mat area. *Alvin* heading 120, depth 2020.7 m, GMT 19:17:40, dive 4574, December 5, 2009. Photographs courtesy of the Woods Hole Oceanographic Institution, from RV *Atlantis* cruise AT 15-56.

A distinct mat complex near a group of small hydrothermal mounds and chimneys, called "Cathedral Hill," consisted of a complex mosaic of grayish-colored sediments partially covered by yellow precipitates (**Figure 5B**). This area was extensively mapped with seven temperature profiles and turned out to be consistently warm or hot, as the sediment gradients varied from ca. 50°C to 120°C at 40 cm depth (**Figure 5B**); matching porewater profiles indicated methane- and DIC-rich, highly sulfidic sediments with rapid sulfate depletion below the sediment surface (Supplementary Figure S3). The conspicuous yellow precipitates on the sediment surface are not *Beggiatoa* mats; microscopic examination of such a sediment core (core 4565-6, next to the thermal profile in yellow) revealed filamentous sulfur precipitates that are commonly produced by autotrophic sulfide-oxidizing bacteria of the genus *Arcobacter*, a member of the Epsilonproteobacteria (Pjevac et al., 2014). Since sulfur precipitates produced by *Arcobacter* sp. are usually bright white (Taylor et al., 1999), additional factors would be required to account for the yellowish color; a close investigation of these precipitates is certainly warranted.

Cooler sediments harbored similar, complex yellow-tinted or light-gray precipitates surrounded by brown seafloor sediments. These mats appeared as a thick but uneven carpet of precipitates, with an interconnected web of "ridges" and lower lying portions between these ridges (**Figure 5C**).

In Situ Microprofiler Measurements

Several mats were examined by *in situ* microprofiling, to obtain finely resolved thermal and chemical gradients across the mat surface on the millimeter and centimeter scale; the profiles shown here cover a vertical extent of 10 cm. We examined orange *Beggiatoa* mats overlying hydrothermally active sediments (**Figure 6**), yellow mats or precipitates overlying relatively cool sediments (**Figure 7**), sediments with advective flow of extremely hot hydrothermal fluid (**Figures 8A,B**), and cold background sediments without visible hydrothermal activity (**Figures 8C,D**). Shared features of these microprofiler measurements were the low oxygen concentrations recorded above the sediment surface, ranging from near 30 to ca. 60 μM, or ca. 10 to 20% of seawater saturation. These values, measured in cold bottom water above the sediment surface, are unlikely to represent measurement artifacts caused by hydrothermal impact on the probes, since the control measurements above cold, non-hydrothermal sediment also yielded bottom water oxygen concentrations near 40 μM, in the same range as above hydrothermal sediments (**Figure 8D**). Oxygen concentration profiles of the Guaymas Basin water column obtained over 50 years ago are consistent with the microsensor data and indicate strong oxygen depletion throughout the mid- and bottom water, toward ca. 20% of near-surface oxygen concentrations (Calvert, 1964).

The orange *Beggiatoa* mat (**Figure 6A**) and some of its associated microprofiler gradients (total sulfide, O_2 and NO_x) were previously published as "*Beggiatoa* Mat BM1" (Winkel et al., 2014), but are documented here in full. The local thermal gradients at the microprofiler site showed considerable spatial heterogeneity (**Figure 6B**). While the heat flow temperature gradient in yellow (**Figure 6A**) and the *in situ* temperature gradient determined by the *in situ* profiler (**Figure 6B**) resembled each other and showed a temperature increase of ∼1°C per cm almost linearly over the measurement range, the heat flow temperature gradient in red (**Figure 6A**) was considerably steeper and reaches higher temperatures, illustrating the high degree of spatial heterogeneity.

The orange *Beggiatoa* mat shows sharp chemical changes at the mat surface (**Figure 6B**). The concentrations of H_2S and total sulfide, which are not detectable in the bottom water and at the mat surface, increase sharply downcore. H_2S concentrations rose along a strong linear gradient within the upper sediment layers until they reached a concentration plateau of ca. 1 mM near 4 cm depth, indicating no net production or consumption. Total sulfide accumulated to a local maximum around 5 mM in the upper 2 cm before slowly decreasing (**Figure 6B**). The total sulfide peak indicates desulfurization reactions in the sediment, mobilization and upward migration of reduced sulfur, and precipitation and accumulation of these sulfur phases immediately below the sediment surface. The shape of the total sulfide profile, below the surficial total sulfide peak, indicated fluid upflow of ca. 50 cm/year (de Beer et al., 2006). The pH values showed a surface-associated maximum near pH 8, consistent with several possible explanations. Chemosynthetic activity and CO_2 uptake into microbial cells could deplete CO_2 locally, analogous to photosynthetic CO_2 depletion in benthic cyanobacterial mats (Jørgensen et al., 1983); however, chemosynthetic sulfur oxidation and its resulting acidification effects argue against this explanation. Electron transport and H^+ consumption by cable bacteria could account for this slightly alkaline peak at the sediment surface (Nielsen et al., 2010). Another contributing reaction for this pH could be the proton-consuming microbial oxidation of H_2S with nitrate to elemental sulfur and dinitrogen gas or ammonia; the reactants are available in the surficial sediment (Salman et al., 2015). The pH then decreased to near-neutral levels around 6.5 downcore, approaching the mildly acidic pH of 5.9 for carbonate-buffered hydrothermal fluids measured *ex situ* at Guaymas Basin (Von Damm et al., 1985). Combined nitrate and nitrite concentrations increased from bottom water background of ∼20 μM (most likely dominated by nitrate) to ca. 75 μM within the mat, possibly indicating intracellular nitrate accumulation and leakage by large, vacuolated *Beggiatoaceae* (McKay et al., 2012), and nitrifying activity by ammonia-oxidizing, nitrite-producing archaea that grow associated with the *Beggiatoaceae* filaments (Winkel et al., 2014). Oxygen was quickly consumed at the mat surface; a narrow local peak within the upper 1 cm of the mat may indicate advective transport, for example by hydrothermal pumping that re-introduces pockets of oxygenated seawater into shallow sediments near hydrothermal hot spots (Gundersen et al., 1992). Regardless of short-term oxygen spikes, the redox potential of the upper sediment decreased below 400 mV in the upper 2 cm, indicating consistently reduced conditions.

The sulfide profile determined by *in situ* profiler was consistent with the porewater profile of H_2S measured in core 4564-14 next to the *in situ* profiler; porewater sulfide reaches the 1 mM range between the midpoints of the 3–6 and 6–9 cm

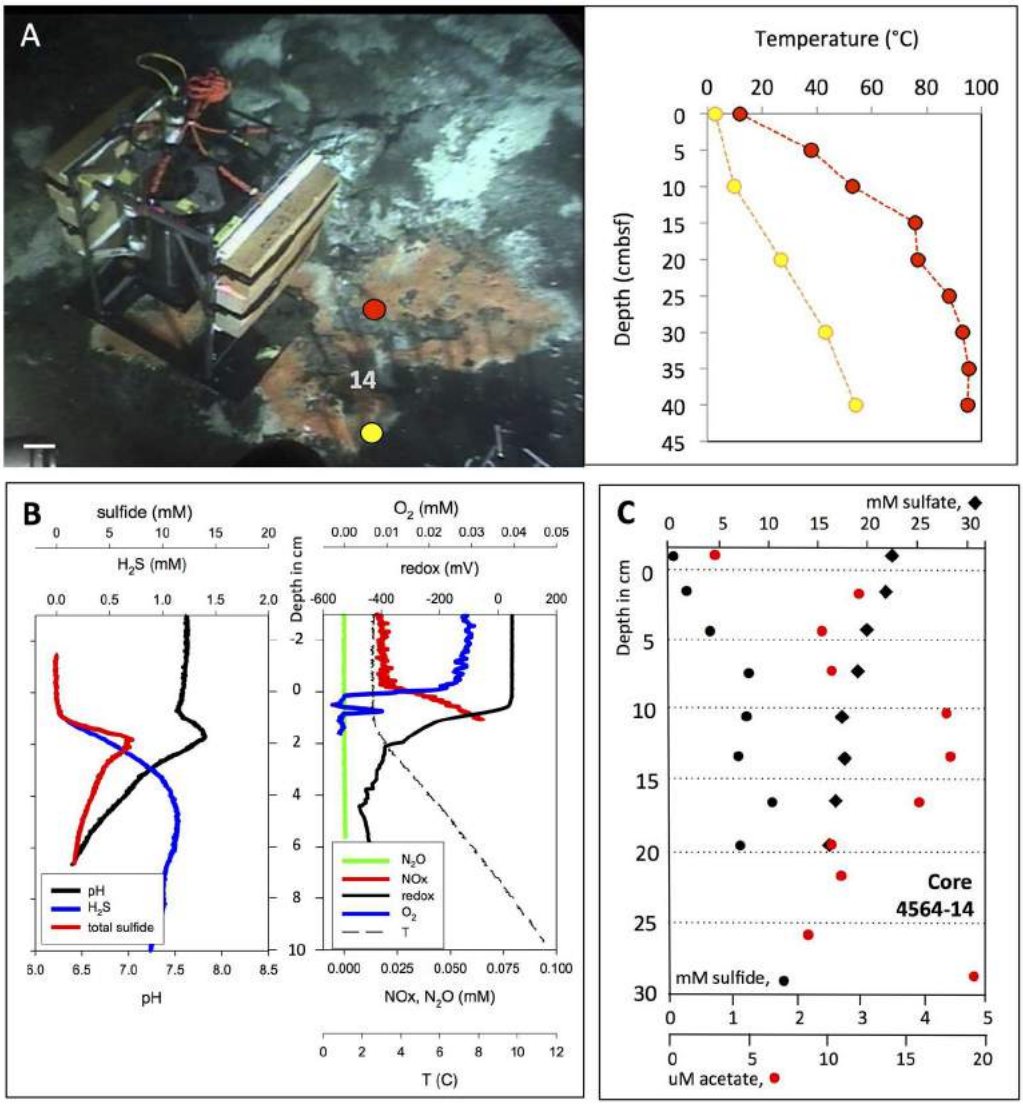

FIGURE 6 | *In situ* microprofiler survey of orange *Beggiatoa* mat. (A) *In situ* profiler after placement on an orange *Beggiatoa* mat near Marker 14. *Alvin* heading 96, depth 2008 m, GMT 16:36:50, dive 4564, November 25, 2009. Temperature gradients were measured with the heat flow probe in two spots near the base of the profiler. The microsensor temperature profile matches the near-surface heat flow temperature profile plotted in yellow, but it is cooler than the nearby heat flow profile in red. **(B)** *In situ* profiler measurement of temperature, redox potential, oxygen, nitrate/nitrite, N_2O, H_2S, and total sulfides at orange mat location. **(C)** Sulfate, sulfide, and acetate porewater gradients from *Alvin* core 4564-14 taken in orange mat-covered sediment, marked by the number 14 in panel **(A)**. Photographs courtesy of the Woods Hole Oceanographic Institution, from RV *Atlantis* cruise AT 15-56.

sediment layers, and remains generally between 1 and 1.5 mM throughout the remaining length of the core (**Figure 6C**). The lack of fine-scale resolution and the slightly lower H_2S porewater concentrations in the surficial sediments are consequences of porewater processing and potential sulfide loss due to oxidation.

An extensive yellow mat found during dive 4562 was characterized by similar yellow-colored surface precipitates as seen at Cathedral Hill, but showed moderate temperature gradients reaching 30°C (**Figure 7A**). This mat was investigated by microprofiler deployment (**Figure 7B**) and push coring followed by porewater analysis (**Figure 7C**). The geochemical and temperature gradients in this mat differed from those in the orange *Beggiatoaceae* mat examined on dive 4564. The *in situ* temperature microprofile started with the bottom water temperature (ca. 3.5°C, **Figure 7B**) at the sediment surface, whereas the heat flow probes started with ∼5°C higher temperatures (**Figure 7A**). This is a possible consequence of inserting the relatively thick heat flow probe into the sediment as it creates a flow channel during insertion into the sediment. After detecting high acetate porewater concentrations in its underlying sediment, represented here by an acetate porewater profile from core 4569-D (**Figure 7C**), the mat was nicknamed "Aceto Balsamico Mat." The geochemical gradients in this mat differ from those in the orange *Beggiatoaceae* mat examined on dive

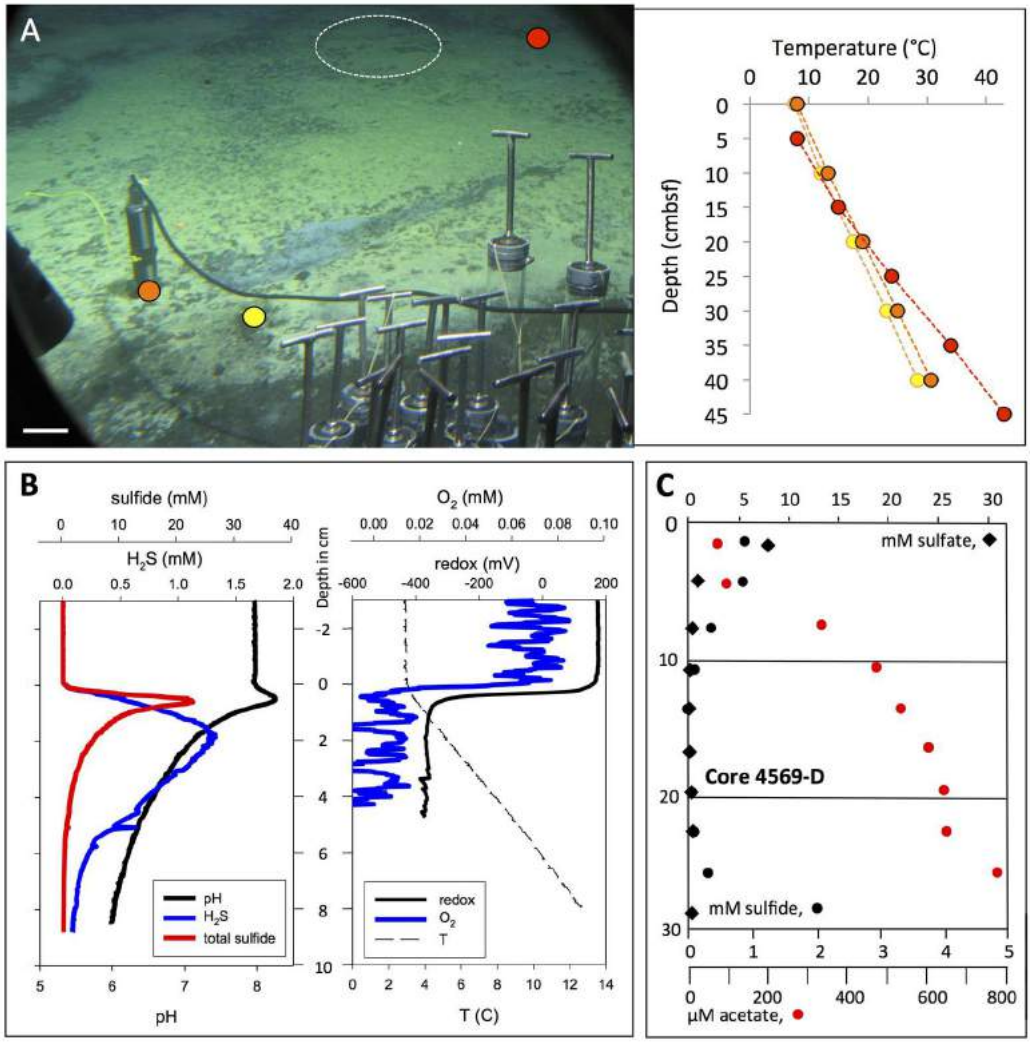

FIGURE 7 | *In situ* microprofiler survey of yellow "Aceto balsamico" mat. (A) This mat on moderately warm sediments resembles the yellow, sulfur-rich Cathedral Hill mats in sulfur color and surface texture; it is located ca. 10 m south of Marker 14. The scale bar corresponds to 10 cm. Corresponding frame grabber images: *Alvin* heading 218, 2009.5 m depth, GMT 16:59:05, dive 4562, November 23, 2009. Two heat flow probe measurements were made on dive 4562, marked in yellow and orange. The *in situ* microprofiler measurement was performed in the area marked by the circle during *Alvin* dive 4570 (November 24, 2009), and a heat flow measurement nearby (in red) was taken. **(B)** *In situ* microprofiler measurement of temperature, redox potential, oxygen, nitrate/nitrite, N_2O, H_2S, and total sulfides during *Alvin* dive 4570. **(C)** The sulfide, sulfate and acetate porewater profiles are from core D taken on dive 4569. Photographs courtesy of the Woods Hole Oceanographic Institution, from RV *Atlantis* cruise AT 15-56.

4564. The porewater acetate concentrations reaching >800 μM in the mat subsurface sediments exceeded the moderate acetate concentrations – in the range of 10–20 μM – that were found in the *Beggiatoa* mat sediments examined during dive 4564 (**Figure 6C**). The lower H_2S concentrations in the mat measured in core 4569-D were confirmed independently by *in situ* profiling during dive 4570. H_2S concentrations decreased from the 1 mM range at the sediment surface to detection background below 10 cm sediment depth. Total sulfide at the sediment/water interface reached 20 mM (**Figure 7B**). As porewater sulfide disappeared within the upper 10 cm, porewater sulfate was depleted toward background within the upper 10 cm (**Figure 7C**). This simultaneous disappearance of sulfate and sulfide is highly unusual among all Guaymas Basin sediment profiles; its explanation would call either for a sulfur-depleted subsurface fluid source, or incomplete sulfate reduction or sulfide oxidation to intermediate oxidation states of sulfur. The noisy oxygen profile (**Figure 7B**) was characterized by omnipresent irregular oscillations between individual measurement points, spaced by 250 μm, above and within the sediment. If taken literally, these oscillations would indicate strongly fluctuating oxygen concentrations on submillimeter vertical scales within the bottom water, which seems unlikely; instead, unidentified *in situ* conditions might have interfered with the stability of the oxygen probe readings. The oscillations were superimposed on a pattern of rapid oxygen consumption at the mat surface, a

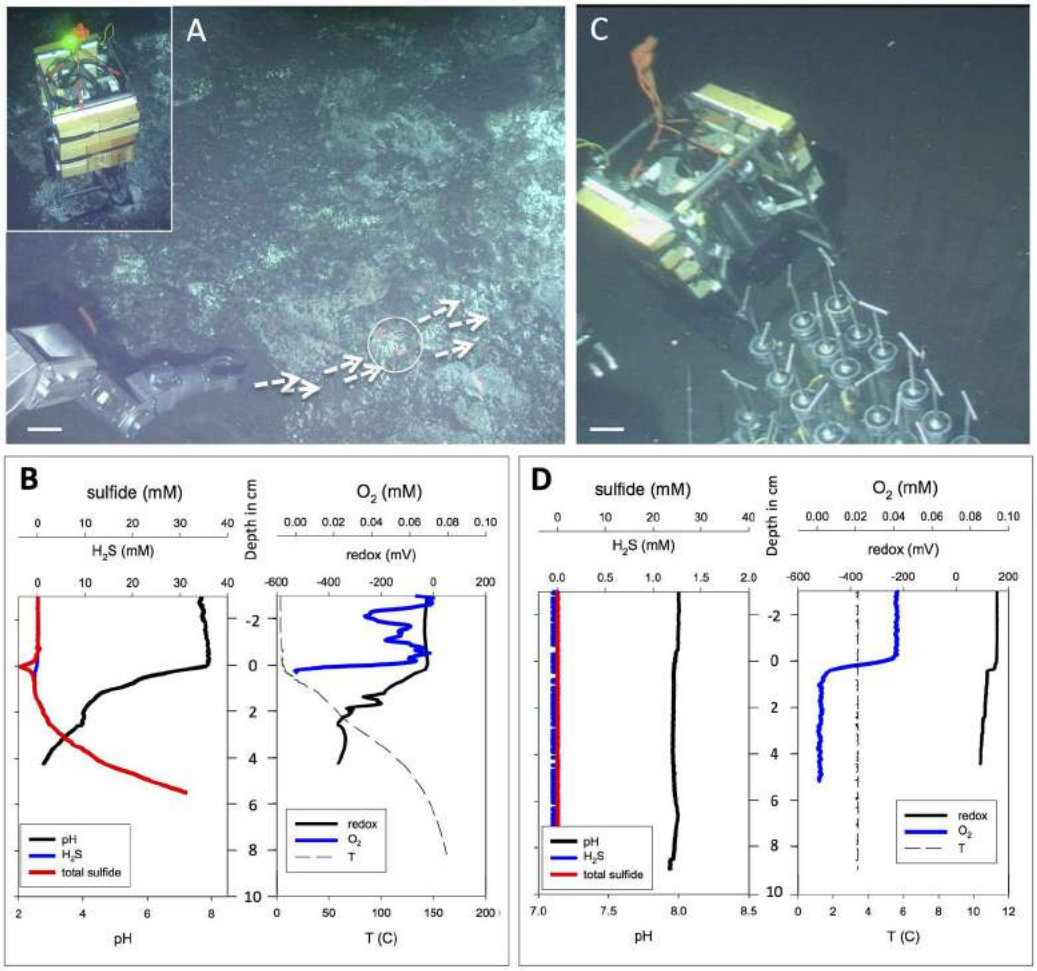

FIGURE 8 | Extremely hot versus background microprofiler deployments. Contrasting extremely hot and non-hydrothermal background microprofiler deployments. **(A)** *In situ* microprofiler deployment near Marker 27, on sediment with strong hydrothermal flow and schlieren patterns along the sediment–water interface. White arrows mark surface fluid flow; the circle marks the approximate area of the microprofiler measurement. The scale bar corresponds to 10 cm. *Alvin* heading 287, depth 2001 m; GMT is unknown due to *Alvin* frame grabber gap; dive 4566, November 27, 2009. The insert in the upper left corner shows the microprofiler just as it initiates the measurements at the hot spot, as indicated by a green light signal. The frame grabber record documents this profiler location again on the subsequent day: *Alvin* heading 160, depth 2001 m, GMT 20:59.32, dive 4567, November 28, 2009. **(B)** *In situ* profiler measurement of temperature, redox potential, oxygen, H_2S, and total sulfides at the hot flow spot during *Alvin* dive 4566. **(C)** *In situ* microprofiler deployment on bare olive-brown sediment without visible hydrothermal activity or microbial mats. The scale bar corresponds to 10 cm. *Alvin* heading 216, depth 2001 m, GMT 19:14:13, dive 4569, November 30, 2009. This deployment provides a negative control. A heat flow gradient taken next to the profiler showed cold seafloor temperatures between 2.8 and 3.0°C throughout its depth range. **(D)** *In situ* profiler measurement of temperature, redox potential, oxygen, H_2S, and total sulfides on cold, non-hydrothermal sediments during *Alvin* dive 4569. Photographs courtesy of Woods Hole Oceanographic Institution, from RV *Atlantis* cruise AT 15-56.

possible consequence of sulfide oxidation at the sediment surface. The redox profile remained smooth and changes from close to +200 mV in the bottom water to ∼–400 mV in the sediment (**Figure 7B**).

A microprofiler deployment into very hot sediment (**Figures 8A,B**) during Dive 4566 has to be regarded as exploratory, since the microelectrodes have not been tested and evaluated for extremely high temperatures. The sediment was covered by irregular white patches and crusts that do not resemble the thick white and orange *Beggiatoaceae* mats. Instead of gradual, diffusive hydrothermal seepage, advection seems to play a greater role here; swirl-like optical distortions or "schlieren patterns" in the bottom water rippling over the sediment surface (indicated by arrows in **Figure 8A**) indicate warm or hot fluid flow directly on the sediment surface and across the spot where these microprofiles were measured, marked by a circle. The shimmering effect can indicate escaping hydrothermal fluids, or convective heating from subsurface fluid conduits that cause convection from the heated sediment surface to the cold seawater. Sulfide concentrations reached 30 mM within 6 cm of the sediment surface; these extremely high sulfide concentrations require a strong hydrothermal contribution. Total sulfide and H_2S concentrations are expected to be identical, as the pH is far below the pK_1 value for H_2S/HS^-. Oxygen fluctuations in

the overlying water could be the equivalent of centimeter-scale perturbations of oxygen-depleted water rising from and moving along the sediment surface (**Figure 8B**). The oxygen probe did not work within the hot sediment. The extreme temperature gradient reaches ca. 160°C at 8 cm depth; and the associated pH gradient converges to at least pH 2.5 below 4 cm depth. Such pH extremes require the presence of strong acids under minimal alkalinity and low DIC, conditions that are at odds with the reported pH of 5.9 for carbonate-buffered Guaymas Basin hydrothermal fluid (Von Damm et al., 1985). If correct, this measurement would indicate the presence of unbuffered, strongly acidified hydrothermal fluids. It is also possible that the microsensor technology used here is running against its inherent limits at high *in situ* temperatures, and that alternative sensor materials, for example pressure- and temperature-stable iridium oxide sensors, are required (Kakooei et al., 2013).

Cold Guaymas Basin seafloor sediments without any visible mat cover were profiled as a negative control (**Figure 8C**); they showed the absence of sulfide, a consistent porewater pH near 8.0 (close to seawater pH), non-reducing conditions, and uniformly cold temperatures near 3.5°C in the sediment (**Figure 8D**). Under these cold, non-hydrothermal conditions, the microsensor signals remain smooth and do not show any unusual distortions or oscillations.

Hydrothermal Chimneys and Mounds

The hydrothermal edifices in Guaymas Basin show diverse morphologies that can be categorized into broad mounds, thick chimneys, and thin flutes and flanges; their complex composition represents a mixture of carbonates, sulfates, silicates, metal sulfides, and iron oxides, and further distinguishes them from the metal sulfide-dominated deposits and chimneys at sediment-free spreading centers (Koski et al., 1985; Lonsdale and Becker, 1985; Peter and Scott, 1988). Broad hydrothermal mounds with extensive talus slopes do not show conspicuous venting, but their surfaces, often sealed by amorphous silica precipitates, cover internal hydrothermal circulation. Hydrothermal chimneys with thick trunks of cemented hydrothermal sulfides and carbonates are often locally overgrown with microbial mats and *Riftia* clusters under suitable diffusive venting regimes. Extremely hot, fragile and highly active venting structures composed of hydrothermal sulfide minerals can take the shape of thin, vertically growing flutes or horizontally spreading eaves and flanges (Peter and Scott, 1988). These flutes and flanges often appear at the top or on the flanks of larger hydrothermal edifices where they mark locations of channelized hydrothermal outflow; generally they are too hot to allow growth of microbial mats.

A good example for a large hydrothermal edifice that combines a thick trunk with flanges on top is the "Big Pagoda" structure (**Figure 9**). Shown here is a section of ca. 3.5 m in vertical extent with microbial mats and *Riftia* colonies growing on the trunk, indicating diffuse venting (**Figures 9A,B**). The top of the edifice is covered with lobed extensions spreading approximately a meter sideways into the water column (**Figures 9C–E**). Broken-off inactive flanges appeared underneath larger, more recent flanges, indicating their continuous formation and extension concomitant with degradation and erosion (**Figure 9E**). Small chimneys appeared in the center of some flanges (**Figures 9A,D**), indicating that part of the hydrothermal flow seeps and rises through the center of these protuberances. The orange and white *Beggiatoa* mats that are abundant on the central trunk of "Pagoda" were missing on the flanges.

A smaller hydrothermal site termed "Robin's Roost" showed the highly localized hot venting area underneath an active flange, where an *in situ* temperature of 278.5°C was measured in shimmering vent fluids rising over its outer edge (**Figure 10**), using *Alvin's* high-temperature probe. The portion of the flange that is not directly exposed to the hot venting fluid shows *Beggiatoa* mat overgrowth.

Currently the largest hydrothermal edifice in the frequently visited hydrothermal sampling area of the southern Guaymas Basin, "Rebecca's Roost" reaches a height of ca. 20 m from the seafloor; the large size of this structure precluded attempts to construct composite images. The images of the top (**Figures 11A–C**) show the colorless, shimmering venting fluid emerging from a diffusively venting zone marked by a gray mineral matrix, visible slightly below a fragile and broken outer crust covered with *Beggiatoa* mats that appears to encase the venting zone like a broken eggshell. Extremely thin and fragile chimneys on the flanks of the trunk provided a jet-like outflow for light-gray (not black) hydrothermal fluid into the surrounding seawater (**Figures 11D,E**). These friable structures break off easily and could be penetrated with *Alvin's* high-temperature probe to measure the temperature of the hydrothermal outflow directly, here determined as 313.8°C (**Figure 11D**). These temperatures were close to those of hydrothermal fluids (315°C) originating from a shallow subsurface basaltic intrusion at the East Hill site, north of this sampling area; the East Hill fluids were among the hottest in Guaymas Basin, and the East Hill chimney sulfides showed an abiotic $\delta^{34}S$ signature near zero, consistent with an abiotic, strictly hydrothermal origin (Peter and Shanks, 1992). By inference, the large edifice of Rebecca's Roost may also function as the outlet for a hydrothermal flow path that does not allow for significant subsurface mixing and cooling.

South of Rebecca's Roost rises another tall but narrower hydrothermal edifice called "Busted Mushroom," named after the mushroom-like edifices present on its top and material from toppled mushroom edifices (**Figure 12A**). Orange/white *Beggiatoa* mats coated the surfaces of the mound at the base of the mushroom stems (**Figure 12B**). A study of microbial colonization of active mushroom-like chimneys carried out on this mound revealed compositional differences in archaeal communities associated with very young (4-day) and older (72-day) chimney material that grew within and around arrays of eight thermocouples within a Titanium frame placed over the active vent (Pagé et al., 2008). These archaeal communities underwent a shift from autotrophic, CO_2/H_2-dependent hyperthermophilic methanogens colonizing the 4-day chimney material (predominantly *Methanocaldococcus* sp.) toward methylotrophic/acetoclastic methanogens (*Methanosarcinales*) and fermentative heterotrophic thermophiles (*Korarchaeota*, *Aciduliprofundales*) in the 72-day old chimney material. In 2009, additional arrays were deployed during cruise AT15-55 to further investigate the timelines of microbial colonization on

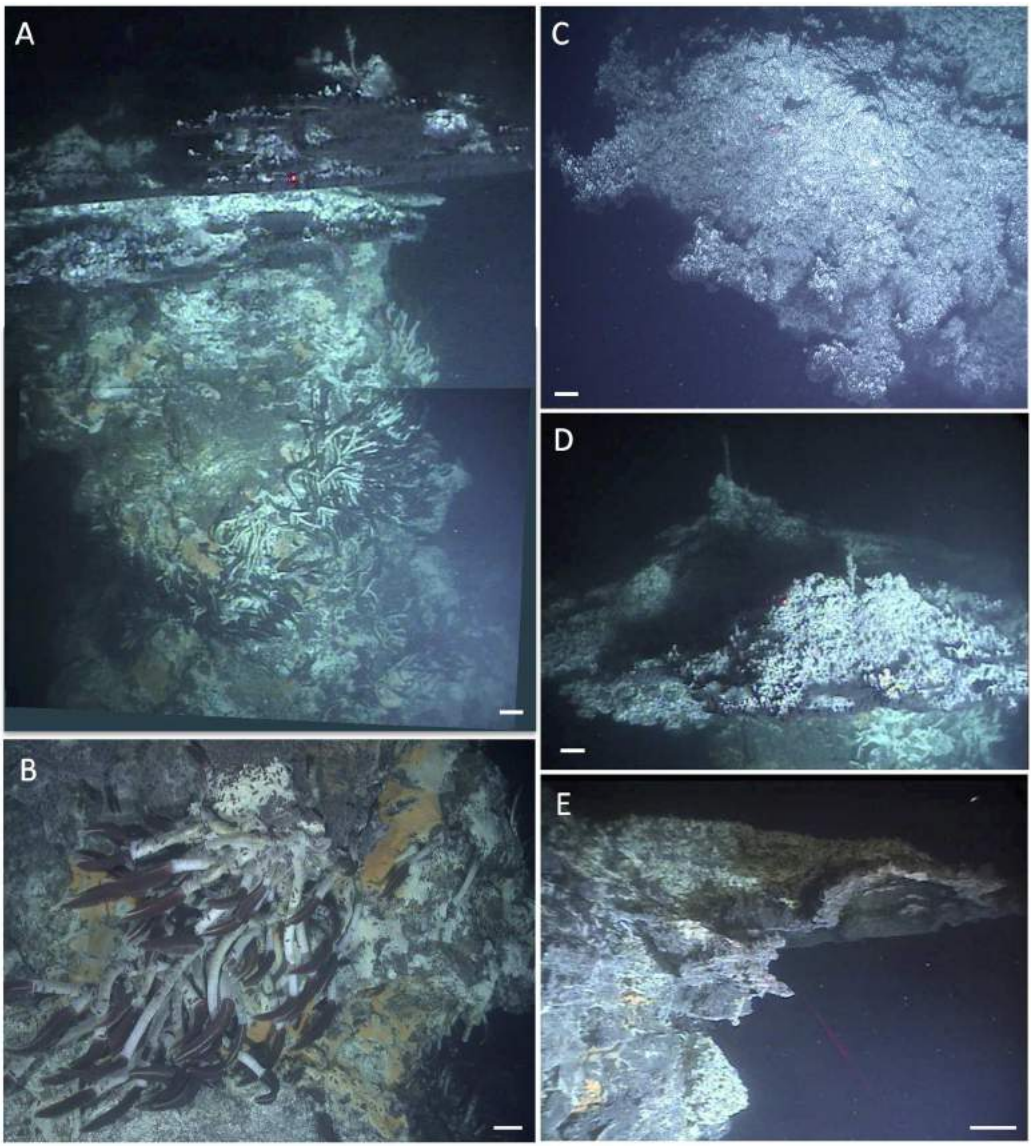

FIGURE 9 | Hydrothermal flanges at Big Pagoda. This large hydrothermal edifice, visited during dive 4574 on December 5, 2009, is termed "Big Pagoda" in reference to its flanges that are spreading like protruding pagoda roofs at the top of this structure. Scale bars correspond to 10 cm. **(A)** Composite image of Pagoda showing the flanges emerging from the top of the massive hydrothermal edifice, its trunk overgrown with microbial mats and *Riftia* clusters. The top section of this image has heading 172; depth 1979.7 m, GMT 16:37:05, and bottom image section has *Alvin* heading 179, depth 1980 m, GMT 16:36:35. **(B)** Close-up of faunal assemblage on Pagoda trunk, with *Riftia* clusters, orange and white *Beggiatoa* mats, and a profusion of grazing scale worms. GMT 16:44:43. **(C)** Top-down view of spreading flange, GMT 16:37:36. Photos **(B,C)** were taken with *Alvin's* still photo camera. **(D)** Side view of Pagoda top, with the same flange in the foreground. *Alvin* heading 156, depth 1979 m, GMT 16:38:05. **(E)** View of protruding flange section from below, as it emerges from the base of the hydrothermal edifice on the left. *Alvin* heading 23, depth 1980.3 m, GMT 16:43:05. Photographs courtesy of Woods Hole Oceanographic Institution, from RV *Atlantis* cruise AT 15-56.

new chimneys. Here, these experiments illustrate the extremely fast growth of hydrothermal chimneys within days. During Alvin dive 4555 on November 10, 2009, a small mushroom structure (foreground, **Figure 12A**) was razed and an array deployed to monitor time lines of mineral precipitation. Two days later, Alvin dive 4557 recovered this array and the fragile beehive chimney that had grown around it (**Figure 12B**). After several rounds of array deployments, the last array of cruise AT15-55 was deployed (November 17, 2009) over the orifice of the larger mushroom structure (which had fallen in the meantime), to be recovered on Alvin dive 4571 during the subsequent cruise (December 2, 2009). During this 15-day interval a mushroom edifice had grown through the array and the stem that developed had engulfed four of the eight thermocouples (**Figure 12C**). The chimney (mushroom stem) wall that developed within the array over the 15-day interval was similar in structure to the chimney walls recovered after 72 days in 2003; these were dominated by calcite and also contained variable amounts of barite, anhydrite,

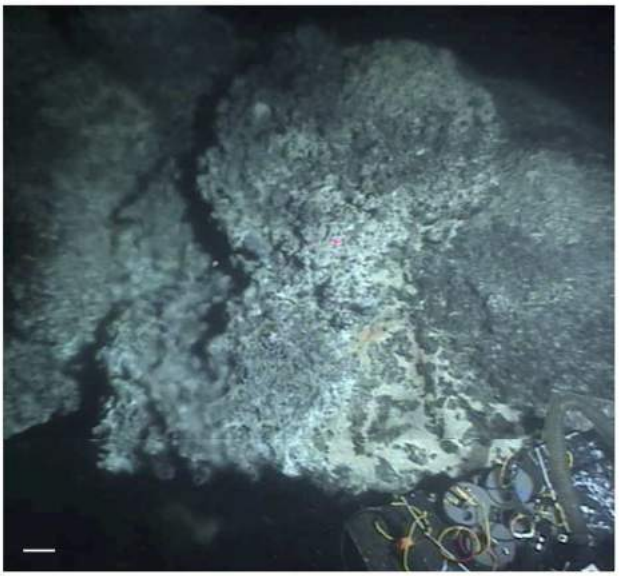

FIGURE 10 | Robin's Roost. This hydrothermal structure was visited during dive 4574 on December 5, 2009. Its top shows actively venting flanges, partially overgrown with *Beggiatoa* mats. Using *Alvin's* high-temperature probe, an *in situ* temperature of 278.5°C was measured in the shimmering vent fluids rising at and around the lip of the flange, on the left within this composite frame grabber image. Yellow and orange *Beggiatoa* mats are growing in protected spots on top of the flange, in the right center of the composite image. The sampling box in the lower right is ca. 50 cm wide. The scale bar corresponds to 10 cm. *Alvin* heading 151, depth 2000.5 m, GMT 18:18:07, and 18:17:07 for the bottom part of the image. Photographs courtesy of Woods Hole Oceanographic Institution, from RV *Atlantis* cruise AT 15-56.

and metal sulfides (Pagé et al., 2008). Temperature and microbial data from the 2009 deployments were compared to data from 2003 to provide information about how the chimneys grow, what the temperatures were at the different places sampled, and to investigate compositional differences in archaeal and bacterial communities as functions of temperature and time (Reysenbach and Tivey, pers. comm.).

A smaller hydrothermal structure, "Mat Mound" (**Figure 13A**), was investigated in detail with *Alvin* dives in December 2008. "Mat Mound" combined features of hydrothermal edifices such as "Big Pagoda" and "Rebecca's Roost," for example the steep, diffusively venting walls that were overgrown by *Beggiatoa* mats and young *Riftia* colonies (**Figure 13B**), with the characteristics of hydrothermal mounds, such as the extensive basal slopes that are surrounding the structure like a ring of talus debris originating from the steep walls. Some of these basal slopes are in themselves hydrothermally active (**Figure 13C**). Temperature point measurements showed a moderate thermal regime of cool temperatures on the mound walls (6 to 15°C), hot temperatures near the base of the mound (50–100°C), and cooler temperatures at the surface of the surrounding sediments nearby (10°C; Dowell et al., 2016). No evidence for channelized hydrothermal flow or a chimney-like orifice was found, and diffusive venting through the mound mineral matrix appeared to predominate. The contact zone between the mound and the surrounding sediment harbored thick microbial mats and the steepest temperature gradients, at and above 100°C at 40 cm sediment depth (Dowell et al., 2016). Mat-covered sediments surrounding "Mat Mound" were characterized geochemically and microbiologically; they turned out to be strongly sulfidic and reducing, and contained seawater sulfate coexisting with high methane concentrations, thus providing a suitable habitat for heat-tolerant, sulfate-dependent, methane-oxidizing microbial communities (Dowell et al., 2016). The bare sediments at a short distance (∼1 m) from the mound contained only minimal concentrations of porewater sulfide and methane, and the *in situ* temperatures down to 40 cm sediment depth were reduced to a range between 3 and 5°C; obviously, the hydrothermal gradients had dissipated a short distance from the mound.

Nearby, an even larger mound was visited on Alvin dive 4562 in November 2009, and termed "Wonder Mound" for its imposing and massive appearance, with an estimated height of ca. 4–5 m and a diameter of more than 10 m based on *in situ* observation (**Figure 14**). In contrast to "Mat Mound," *Riftia* colonies were either absent or reduced to small clumps (visible in the bottom left corner of **Figure 14A**). Orange and white *Beggiatoa* mats were well developed (**Figure 14B**) and could be harvested from the surface of the mound with *Alvin's* suction device, called the "slurp gun" (**Figure 14C**). The moderate *in situ* temperature regime on the mat-covered surface (8–24°C at three different spots in the orange *Beggiatoa* mat in **Figure 14B**) is compatible with diffuse venting of mixed fluids that permeate the outer walls of this mound. The pointed top of "Wonder Mound" and the thick flange-like lobes that followed contour lines around the peak and emitted shimmering water and/or rising particles, suggested a hydrothermal hot spot characterized by strong diffusive venting (**Figure 14A**).

The most visually dramatic hydrothermal edifice found during RV *Atlantis* cruises AT15-40 and AT15-56 was a wall of vertical hydrothermal chimneys, first observed during *Alvin* dive 4573 on December 4, 2009 (**Figure 15A**). This ∼2 m high structure, termed "Notre Dame" by the observers to prevent confusion with the "Cathedral Hill" location sampled previously on dive 4565, was almost entirely covered with white, yellow, and orange *Beggiatoa* mats (**Figure 15B**). The mats colonized exclusively the chimneys but ended exactly at their base, and did not extend into the surrounding sediments (**Figure 15C**). Due to time limitations, no *in situ* temperature measurements were made.

DISCUSSION

Subsurface Context of Hydrothermal Features

The diverse hydrothermal sediments, mats, mounds, and chimneys documented here show distinct distribution patterns across the Guaymas Basin seafloor that are ultimately linked to subsurface hydrothermal circulation and heat sources. Early Deep-tow sonar surveys of the central southern Guaymas trough indicated several sills buried at shallow depths (Lonsdale and

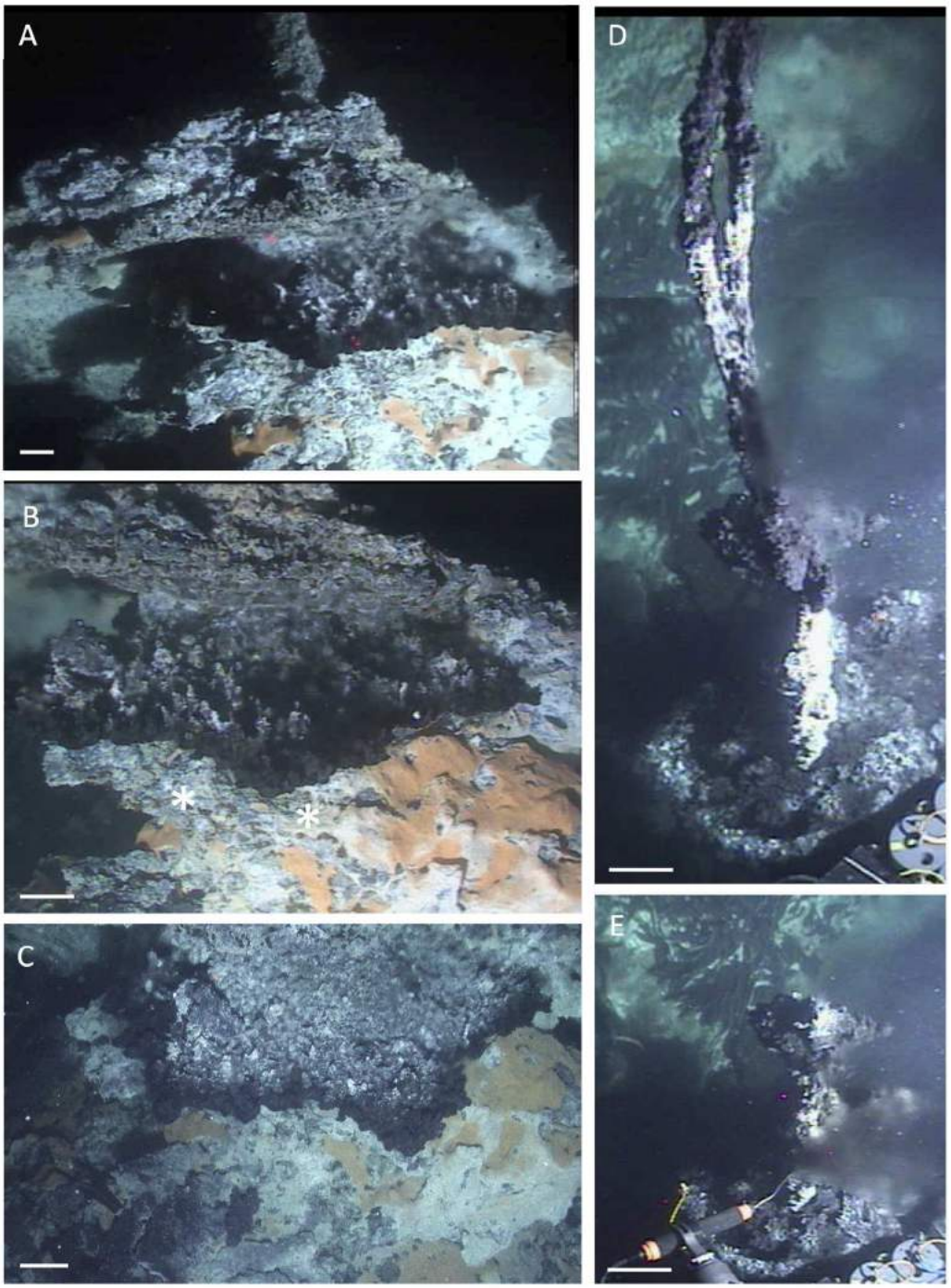

FIGURE 11 | Top of Rebecca's Roost. The large hydrothermal edifice "Rebecca's Roost" was visited on *Alvin* Dive 4574, December 5, 2009. The scale bars correspond to 10 cm. **(A)** Composite framegrabber image of top venting orifice of Rebecca's Roost as seen on *Alvin* Dive 4574, with shimmering fluid under flanges and mat-covered "lip" at the edge of the fluid source area. *Alvin* heading 163, depth 1989 m, GMT 20:23:11 and 20:22:41. **(B)** Framegrabber image of orange and white microbial mat right at the edge of the top venting orifice. *Alvin* heading 163, depth 1989 m, GMT 20:22:11. **(C)** *Alvin* external still camera photo showing "birds eye" view into the fluid source area, and mat-covered lip below. The mat-covered surface drops off near-vertically at the bottom of the photo. The photo was taken on the same *Alvin* dive shortly after photos **(A,B)**. Visual comparison of the orange *Beggiatoa* mats shows that two exposed rim pieces of the mat-covered lip (marked with asterisks in **B**) are missing here and were apparently broken off. **(D)** Composite framegrabber image of a peripheral thin chimney, viewed against the *Riftia*-covered walls of Rebecca's Roost. Upper portion of the image: Alvin heading 214, depth 1989.8 m, GMT 20:27:11; lower portion: *Alvin* heading 213, depth 1990 m, GMT 20:26.41. **(E)** After the highly fragile chimney top was broken off, a vent fluid *in situ* temperature of 313.8°C was measured with *Alvin's* high-temperature probe penetrating into the base of the friable chimney, marked by a jet of grayish, shimmering hydrothermal fluid. *Alvin* heading 214, depth 1989.8 m, GMT 20:31.42. Photographs courtesy of Woods Hole Oceanographic Institution, from RV *Atlantis* cruise AT 15-56.

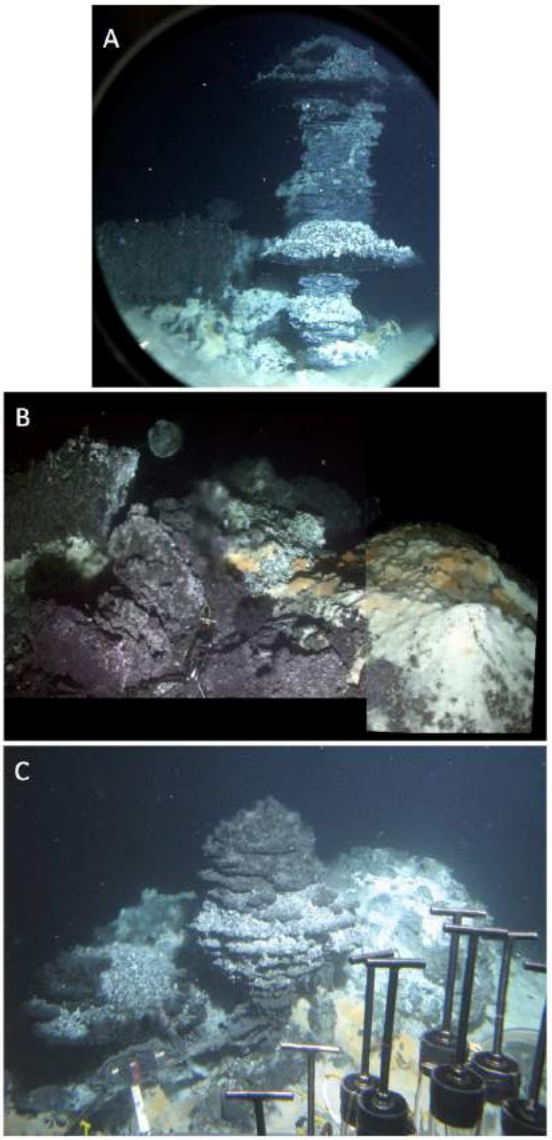

FIGURE 12 | Busted Mushroom. Mushroom-like deposits on the top of the "Busted Mushroom" hydrothermal edifice. **(A)** Two "mushrooms" photographed on November 10, 2009 during cruise AT15-55 (*Alvin* dive 4555); the tree-trunk-like stem of a previously toppled mushroom can be seen to the left of the standing mushrooms. Comparable frame grabber images: *Alvin* heading 326, depth 1990 m, GMT 19:05. **(B)** A 2-day old fragile beehive grew within and around the cylindrical end of the array that was placed over the vent that fed the shorter mushroom in **(A)**. New material engulfing the eight thermocouples is visible at end of the titanium frame in the lower left of photograph, beneath schlieren caused by hot fluid flow; pieces of the fallen stem of the taller mushroom in **(A)** are located to the immediate left of the titanium frame, in front of the older fallen stem. Microbial mats in the foreground coat much of the top of the edifice, which was significantly larger than the portion photographed here on November 12, 2009 (*Alvin* Dive 4557, cruise AT15-55). Corresponding frame grabber image: *Alvin* heading 310, depth of 1989.5, GMT 20:42:12. **(C)** As observed on *Alvin* dive 4571, a 15-day-old mushroom and stem grew through an array deployed at a second vent opening, to the taller mushroom shown in **(A)**. Corresponding frame grabber image: *Alvin* heading 180; depth 1990 m, GMT 17:17.45. All photographs courtesy of the Woods Hole Oceanographic Institution, from RV *Atlantis* cruises AT15-55 and AT 15-56.

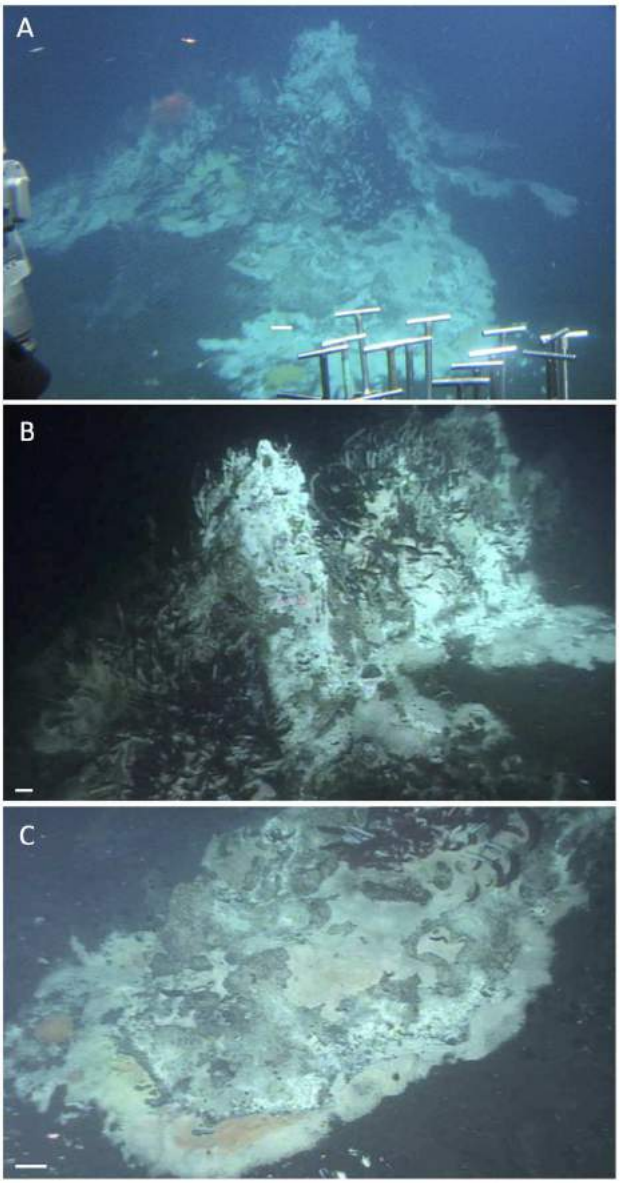

FIGURE 13 | Mat Mound, an extensive hydrothermal mound ca. 2.5 m high and several meters across. The scale bar corresponds to 10 cm. **(A)** Still photo from inside *Alvin* approaching Mat Mound from the east during *Alvin* dive 4483 (December 6, 2008). The photo shows the multiple pinnacles, extensive *Riftia* overgrowth, and downward sloping microbial mats growing on the hydrothermal flanks and surrounding sediments of Mat Mound. **(B)** The central pinnacle of Mat Mound in a framegrabber image from the subsequent dive. *Alvin* heading 285, depth 2002 m, GMT 21:45:18, dive 4484, December 7, 2008. **(C)** Extended slope of Mat Mound with *Riftia* colony higher up, and patchy white and orange *Beggiatoa* mats covering the lower slope and the sediment contact zone. *Alvin* heading 238, depth 2003 m, GMT 18:40:10, dive 4484, December 7, 2008. All photographs courtesy of the Woods Hole Oceanographic Institution, from RV *Atlantis* cruise AT 15-40.

Becker, 1985). Close to the hydrothermal area surveyed here, a shallow sub bottom intrusion (<100 mbsf) was interpreted as a thin sill; the approximate positions of this and a similar sill nearby

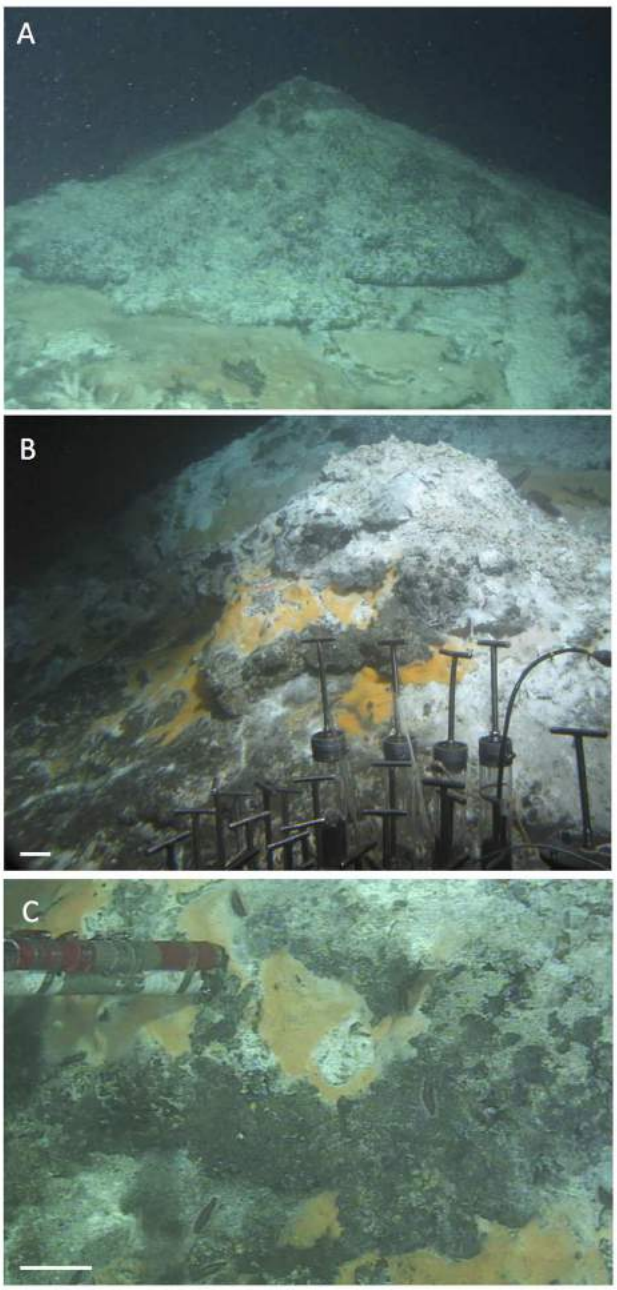

FIGURE 14 | Wonder Mound. This gently sloping hydrothermal mound with a single peak was overgrown with microbial mats but only few clusters of *Riftia*. Images are from *Alvin* dive 4562, November 23, 2009. The scale bars correspond to 10 cm. **(A)** Frame grabber image of the top of Wonder Mound; the peak is surrounded with lobed structures that could be incipient flanges, hugging the contours of the mound instead of protruding into the water. *Alvin* heading 108, depth 1997 m, GMT 22:09:31. **(B)** External still image of mound flanks with orange *Beggiatoa* mats. *Alvin* heading 108, depth 1997 m, GMT 22:06:14. *In situ* temperatures of 24°C, 8°C and 10°C, respectively, were measured with the high-temperature probe in surficial orange mats in the center of this image (GMT 22:06:30 to 22:09:01). **(C)** Frame grabber image of slurp gun sampling of orange *Beggiatoa* mats from the base of Wonder Mound. *Alvin* heading 108, depth 1997 m, GMT 22:13:01. All photographs courtesy of the Woods Hole Oceanographic Institution, from RV *Atlantis* cruise AT 15-56.

(based on Figure 2 in Lonsdale and Becker, 1985) were revised, extrapolated and combined into a continuous boomerang-shaped sill, the southernmost of three sills that are lined up in the center of southern Guaymas Trough (mapped in Peter et al., 1990 and Peter and Shanks, 1992). If these inferred sill positions are correct, the cluster of hydrothermal mounds and microbial mats sampled during *Atlantis* and *Alvin* cruises AT15-40 and AT15-56 would trace the southeastern arm of the boomerang-shaped, southernmost sill (**Figures 1A,B**), and confirm previous conclusions on the relationship between hydrothermal features and sill boundaries (Lonsdale and Becker, 1985). As a corollary, the hydrothermal fluids that migrated to the sediment surface within this sampling region would most likely originated from the same local hydrothermal circulation system linked to this sill. Some indirect geochemical evidence supports this scenario. The $\delta^{13}C$ baseline values of hydrothermal methane from hot sediments in this region (>150°C, to exclude biological imprint) form a tight cluster from –39.09 to –43.18‰; (McKay et al., 2015) that contrasts with the more variable $\delta^{13}C$ values between –51 and –43‰; for hydrothermal methane reported previously from different sites in Guaymas Basin (Welhan, 1988). Interestingly, lighter $\delta^{13}C$ values of –50.8 and –45.1‰; were obtained from hydrothermal fluid samples collected during *Alvin* dives 1169 and 1175 in the "North Hill" region of the southern Guaymas trough, several miles to the north near the northernmost of the three mapped sills; whereas a matching $\delta^{13}C$ value of –43.2‰; was obtained for a hydrothermal fluid sample collected on dive 1173 within the same sampling area as surveyed here (Welhan and Lupton, 1987). A wider-ranging chemical and isotopic survey of hydrothermal fluids in Guaymas Basin could obviously extend these initial data and allow the development of a spatially resolved regional database that could be useful in identifying and mapping subsurface hydrothermal circulation patterns. The hypothesis of a shared subsurface methane source for the commonly visited sampling area on the southern sill would be consistent with a localized, sill-to-surface hydrothermal circulation pattern, as proposed after Deep-Sea Drilling Program Leg 64 provided the first view of the Guaymas Basin subsurface (Kastner, 1982). The approximate depth range of this circulation pattern could be inferred from the depth of the middle sill mapped in **Figure 1** that was drilled twice during DSDP Leg 64. At these two adjacent locations (DSDP holes 477 and 477A, marked by red dots), the underlying sill extended from depths of 58 to 105.5 mbsf and 32.5 to 62.5 mbsf, respectively (Shipboard Scientific Party, 1982).

While the mat-rich area also includes diffusively venting hydrothermal mounts, the largest hydrothermal edifices characterized by channelized fluid flow (Big Pagoda, Rebecca's Roost) were located farther north (**Figure 1B**). This transition from mat-dominated hydrothermal sediments and hydrothermal mounds without channelized flow, toward actively venting chimneys and flange-lined chimney tops coincided with a north-trending increase in heat flux (Fisher and Becker, 1991) that ranged from 100 to 300 mW per m^2 southwest of the mat-dominated hydrothermal field, toward 300–600 mW per m^2 in the area with large hydrothermal chimneys to the North (**Figure 1B**). A comparison of the heat flow map of the southern Guaymas trough (Figure 2 in Fisher and Becker,

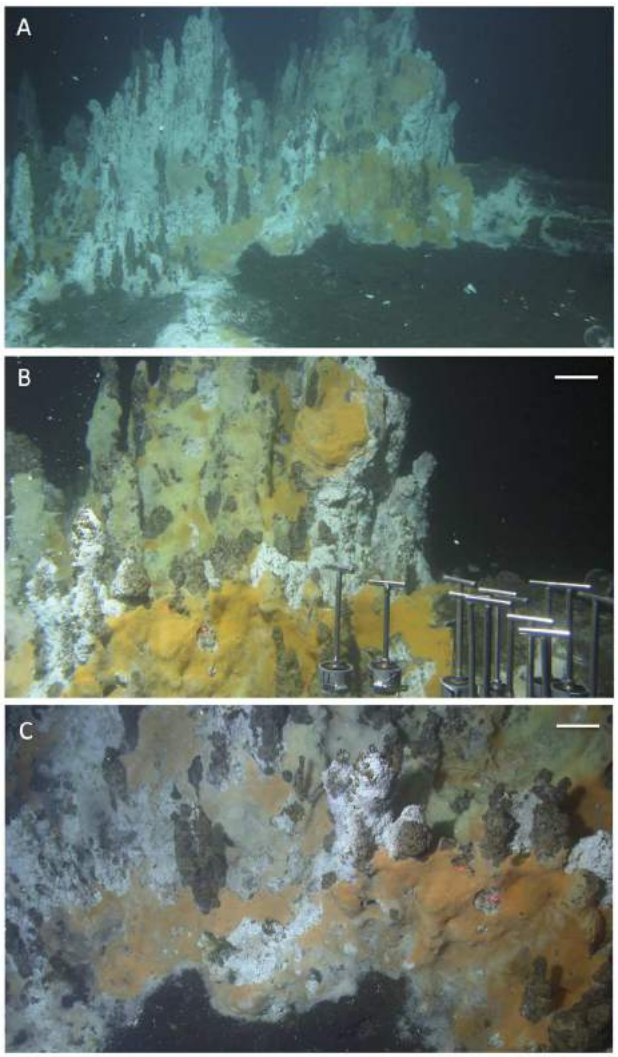

FIGURE 15 | Notre Dame, a multi-chimney hydrothermal edifice, ~3 m high. The site was named in reference to the soaring vertical lines and visual splendor of gothic cathedrals. All pictures were taken with the external still camera during *Alvin* dive 4573, December 4, 2009, depth 2012 m. Based on the framegrabber records, the corresponding *Alvin* headings are in the range of 116 to 133. **(A)** Overall view of the hydrothermal edifice, heading approximately Southeast, GMT 19:36:53. **(B)** Close up of microbial mat network on the tall chimneys; GMT 19:38:35. **(C)** Base of mound and bare sediment, GMT 19:37:26. The orange and yellow mats appear to overgrow the bare surfaces of the chimney-like edifices and their patchy white coating, possibly sulfur precipitates. All photographs courtesy of the Woods Hole Oceanographic Institution, from RV *Atlantis* cruise AT 15-56.

1991) and of the hydrothermal features and subseafloor sills compiled in **Figure 1A** shows that the areas of highest heat flux coincide broadly with the two mapped sill areas positioned further northeast along the trough axis. We also call attention to the observation that the largest hydrothermal features with channelized fluid flow (Big Pagoda, Rebecca's Roost) appear to be located over the central portion of the underlying sill, not on its periphery, suggesting localized hydrothermal flow through a fault line within the sill; this possibility was noted previously (Lonsdale and Becker, 1985).

To the best of our knowledge, the hydrothermal areas to the north of the commonly visited sampling area are currently neglected by *Alvin* dives, at least since early surveys of Guaymas Basin in the 1980s (Lonsdale and Becker, 1985); published sampling records in microbiological studies of Guaymas Basin indicate that the same well-known dive targets in the region described here are visited repeatedly by our own and by other microbiologically oriented cruises (Campbell et al., 2001, 2013). To obtain a greater diversity of hydrothermal samples from both the northern and southern Guaymas Basin troughs and their ridge flanks (Lizarralde et al., 2011), and to document a fuller range of hydrothermal habitats, new survey tools, such as the autonomous ROV *Sentry* appear highly promising.

An improved survey of Guaymas Basin would also provide a greater range of sampling sites to address open questions, such as fluid and gas transport through different types of hydrothermal sediments, and the overall budget of carbon, sulfur, nitrogen and other elemental fluxes across the sediment/water interface. Previous work appears to be limited to heat flow surveys (Williams et al., 1979; Lonsdale and Becker, 1985; Fisher and Becker, 1991), basin-wide studies of Helium-3 and manganese accumulation (Lupton, 1979; Campbell et al., 1988), and initial estimates of hydrothermal carbon mobilization and loss from the overall sediment volume affected by sill intrusion (Lizarralde et al., 2011); therefore, quantitative investigations of hydrothermal transport in Guaymas Basin represent a wide-open research field. Quantifications of microbially catalyzed biogeochemical processes in hydrothermal sediments of Guaymas Basin have so far focused on sulfate reduction (Elsgaard et al., 1994; Weber and Jørgensen, 2002; Meyer et al., 2013) and to a lesser extent on nitrate reduction (Bowles et al., 2012). These and other microbial activities could be linked to microbial gene expression studies on the level of specific functional genes, as demonstrated for archaeal methane oxidation in Guaymas Basin sediments (Biddle et al., 2012), or on the level of metatranscriptomes as shown for archaeal nitrification in hydrothermal plumes (Baker et al., 2012). Temperature regimes permitting, microbial processing of hydrothermal carbon and energy sources is not limited to the surface. Ultimately, recovering subsurface sediments and sill sections by deep coring and drilling would yield significant scientific returns about biological, chemical and hydrothermal gradients beyond the surficial sediment layers in Guaymas Basin (Teske et al., 2014).

AUTHOR CONTRIBUTIONS

AT compiled the figures, did the data archaeology, and wrote the paper; DD performed and plotted the *in situ* microprofiler measurements; LM compiled and plotted the heatflow probe temperature profiles; JB performed the 2008 and 2009 observations at Marker 6; MT performed the mineralogical analyses at Busted Mushroom and contributed the photos of this site; DH, KL, ML, HR, DA, and HM contributed *in situ*

observations and geochemical and thermal measurements of different hydrothermal sediments and mats, BM mapped the hydrothermal seafloor locations in the context of subsurface sill and heatflow locations.

ACKNOWLEDGMENTS

This survey of Guaymas Basin was supported by NSF Biological Oceanography grant OCE-0647633 to AT and BM. We thank the captain and crew of RV *Atlantis*, and the *Alvin* team for expert support above and below sea level during cruises AT15-40 and AT15-56 in December 2008 and November/December 2009, and the science crew for careful documentation of our *Alvin* dives and their published and unpublished results. Kudos also to the engineers at WHOI who developed and installed *Alvin's* framegrabber system and external still cameras; without these sophisticated documentation and imaging capabilities, this survey would have been impossible. AT acknowledges a W. Reynolds research leave from UNC, Guaymas-relevant support from the Center for Dark Energy Biosphere Investigations (C-DEBI) at the University of Southern California, and the hospitality and highly conducive writing environment provided at the Hanse Wissenschaftskolleg in Delmenhorst, Germany. This is C-DEBI manuscript No. 319.

SUPPLEMENTARY MATERIAL

The Supplementary Material for this article can be found online at: http://journal.frontiersin.org/article/10.3389/fmicb.2016.00075

REFERENCES

Albert, D. B., and Martens, C. S. (1997). Determination of low molecular weight organic acid concentrations in seawater and pore-water samples via HPLC. *Mar. Chem.* 56, 27–37. doi: 10.1016/S0304-4203(96)00083-7

Baker, B. J., Lesniewski, R. A., and Dick, G. J. (2012). Genome-enabled transcriptomics reveal archaeal populations that drive nitrification in a deep-sea hydrothermal plume. *ISME J.* 6, 2269–2279. doi: 10.1038/ismej.2012.64

Bazylinski, D. A., Farrington, J. W., and Jannasch, H. W. (1988). Hydrocarbons in surface sediments from a Guaymas Basin hydrothermal vent site. *Org. Geochem.* 12, 547–558. doi: 10.1016/0146-6380(88)90146-5

Bazylinski, D. A., Wirsen, C. O., and Jannasch, H. W. (1989). Microbial utilization of naturally occurring hydrocarbons at the Guaymas Basin hydrothermal vent site. *Appl. Environ. Microbiol.* 55, 2832–2836.

Biddle, J. F., Cardman, Z., Mendlovitz, H., Albert, D. B., Lloyd, K. G., Boetius, A., et al. (2012). Anaerobic oxidation of methane at different temperature regimes in Guaymas Basin hydrothermal sediments. *ISME J.* 6, 1018–1031. doi: 10.1038/ismej.2011.164

Bowles, M. W., Nigro, L. M., Teske, A. P., and Joye, S. B. (2012). Denitrification and environmental factors influencing nitrate removal in Guaymas Basin hydrothermally-altered sediments. *Front. Microbiol.* 3:377. doi: 10.3389/fmicb.2012.00377

Callac, N., Rommevaux-Jestin, C., Rouxel, O., Lesongeur, F., Liorzou, C., Bollinger, C., et al. (2013). Microbial colonization of basaltic glasses in hydrothermal organic-rich sediments at Guaymas Basin. *Front. Microbiol* 4:250. doi: 10.3389/fmicb.2013.00250

Calvert, S. E. (1964). "Factors affecting distribution of laminated diatomaceous sediments in the Gulf of California," in *Marine Geology of the Gulf of California*, Vol. 3, eds T. H. Van Andel and G. G. Jr. Shor (Tulsa: American Association of Petroleum Geologists Memoir), 311–330.

Calvert, S. E. (1966). Origin of diatom-rich, varved sediments from the Gulf of California. *J. Geol.* 74, 546–565. doi: 10.1086/627188

Campbell, A., Gieskes, J. M., Lupton, J. E., and Lonsdale, P. F. (1988). Manganese geochemistry in the Guaymas Basin, Gulf of California. *Geochim. Cosmochim. Acta* 52, 345–357. doi: 10.1038/ismej.2012.63

Campbell, B. J., Engel, A. S., Porter, M. L., and Takai, K. (2006). The versatile epsilon *proteobacteria*: key players in sulphidic habitats. *Nat. Rev. Microbiol.* 4, 458–468. doi: 10.1038/nrmicro1414

Campbell, B. J., Jeanthon, C., Kostka, J. E., Luther, G. W., and Cary, C. C. (2001). Growth and phylogenetic properties of novel bacteria belonging to the Epsilon subdivision of the *Proteobacteria* enriched from *Alvinella pompejana* and Deep-Sea hydrothermal vents. *Appl. Environ. Microbiol.* 67, 4566–4572. doi: 10.1128/AEM.67.10.4566-4572.2001

Campbell, B. J., Polson, S. W., Allen, L. Z., Williamson, S. J., Lee, C. K., Wommack, K. E., et al. (2013). Diffuse flow environments within basalt- and sediment-hosted hydrothermal vent ecosystems harbor specialized microbial communities. *Front. Microbiol.* 4:182. doi: 10.3389/fmicb.2013.00182

Cardman, Z. (2014). *Active Prokaryotic Communities Along a Thermally and Mat-covered, Geochemically Variable Transect in Guaymas Basin sediments*, Masters Science thesis, Department of Marine Sciences, University of North Carolina at Chapel Hill, Chapel Hill, CA.

Cline, J. D. (1969). Spectrophotometric determination of hydrogen sulfide in natural waters. *Limnol. Oceanogr.* 14, 454–458. doi: 10.4319/lo.1969.14.3.0454

de Beer, D., Sauter, E., Niemann, H., Kaul, N., Foucher, J. P., Witte, U., et al. (2006). In situ fluxes and zonation of microbial activity in surface sediments of the Håkon Mosby Mud Volcano. *Limnol. Oceanogr.* 51, 1315–1331. doi: 10.4319/lo.2006.51.3.1315

De Beer, D., Schramm, A., Santegoeds, C. M., and Kühl, M. (1997). A nitrite microsensor for profiling environmental biofilms. *Appl. Environ. Microbiol.* 63, 973–977.

Dowell, F., Cardman, Z., Dasarathy, S., Kellermann, M. Y., Lipp, J. S., Ruff, S. E., et al. (2016). Microbial communities in methane- and short chain alkane-rich hydrothermal sediments of Guaymas Basin. *Front. Microbiol.* 7:17. doi: 10.3389/fmicb.2016.00017

Einsele, G., Gieskes, J. M., Curray, J., Moore, D. M., Aguayo, E., Aubry, M.-P., et al. (1980). Intrusion of basaltic sills into highly porous sediments, and resulting hydrothermal activity. *Nature* 283, 441–445. doi: 10.1038/283441a0

Elsgaard, L., Isaksen, M. F., Jørgensen, B. B., Alayse, A.-M., and Jannasch, H. W. (1994). Microbial sulfate reduction in deep-sea sediments at the Guaymas Basin hydrothermal vent area: influence of temperature and sub- strates. *Geochim. Cosmochim. Acta* 58, 3335–3343. doi: 10.1016/0016-7037(94)90089-2

Fisher, A. T., and Becker, K. (1991). Heat flow, hydrothermal circulation and basalt intrusions in the Guaymas Basin, Gulf of California. *Earth Plan. Sci. Lett.* 103, 84–89. doi: 10.1016/0012-821X(91)90152-8

Gieskes, J. M., Kastner, M., Einsele, G., Kelts, K., and Niemitz, J. (1982). "Hydrothermal activity in the Guaymas Basin, Gulf of California: a synthesis," in *Initial Reports of the Deep Sea Drilling Project*, Vol. 64, eds J. R. Curray, J. Blakeslee, L. W. Platt, L. N. Stout, D. G. Moore, and J. E. Aguayo et al. (Washington, DC: U.S. Government Printing Office), 1159–1167.

Gundersen, J. K., Jørgensen, B. B., Larsen, E., and Jannasch, H. W. (1992). Mats of giant sulphur bacteria on deep-sea sediments due to fluctuating hydrothermal flow. *Nature* 360, 454–456. doi: 10.1038/360454a0

Hansen, H. P. (1999). "Determination of oxygen, Chapter 4," in *Methods of Seawater Analysis*, 3rd Edn, eds K. Grasshoff, K. Kremling, and M. Ehrhardt (Weinheim: Wiley Verlag), 75–89.

Holler, T., Widdel, F., Knittel, K., Amann, R., Kellermann, M. Y., Hinrichs, K.-U., et al. (2011). Thermophilic anaerobic oxidation of methane by marine microbial consortia. *ISME J.* 5, 1946–1956. doi: 10.1038/ismej.2011.77

Jannasch, H. W., Nelson, D. C., and Wirsen, C. O. (1989). Massive natural occurrence of unusually large bacteria (Beggiatoa sp.) at a hydrothermal deep-sea vent site. *Nature* 342, 834–836. doi: 10.1038/342834a0

Jeroschewski, P., Steukart, C., and Kühl, M. (1996). An amperometric microsensor for the determination of H_2S in aquatic environments. *Anal. Chem.* 68, 4351–4357. doi: 10.1021/ac960091b

Jørgensen, B. B., Dunker, R., Grünke, S., and Roy, H. (2010). Filamentous sulfur bacteria, Beggiatoa spp., in arctic marine sediments (Svalbard, 79 degrees N). *FEMS Microbiol. Ecol.* 73, 500–513. doi: 10.1111/j.1574-6941.2010.00918.x

Jørgensen, B. B., Revsbech, N. P., and Cohen, Y. (1983). Photosynthesis and structure of benthic microbial mats: microelectrode and SEM studies of four cyanobacterial communities. *Limnol. Oceanogr.* 28, 1075–1083. doi: 10.4319/lo.1983.28.6.1075

Joye, S. B. (2002). "Denitrification in the marine environment," in *Encyclopedia of Environmental Microbiology*, ed. G. Collins (New York, NY: John Wiley & Sons, Inc.), 1010–1019.

Kakooei, S., Ismail, M. C., and Ari-Wahjoedi, B. (2013). An overview of pH sensors based on iridium oxide: fabrication and application. *Int. J. Mater. Sci. Innovat.* 1, 62–72.

Kastner, M. (1982). "Evidence for two distinct hydrothermal systems in the Guaymas Basin," in *Initial Reports of the Deep Sea Drilling Project*, eds J. R. Curray, J. Blakeslee, L. W. Platt, L. N. Stout, D. G. Moore, and J. E. Aguayo, et al. (Washington, DC: U.S. Government Printing Office), 1143–1158.

Kellermann, M. Y., Wegener, G., Elvert, M., Yoshinaga, M. Y., Lin, Y. S., Holler, T., et al. (2012). Autotrophy as predominant mode of carbon fixation in thermophilic anaerobic methane-oxidizing microbial communities. *Proc. Natl. Acad. Sci. U.S.A.* 109, 19321–19326. doi: 10.1073/pnas.1208795109

Kniemeyer, O., Musat, F., Sievert, S. M., Knittel, K., Wilkes, H., Blumenberg, M., et al. (2007). Anaerobic oxidation of short-chain hydrocarbons by marine sulphate-reducing bacteria. *Nature* 449, 898–901. doi: 10.1038/nature06200

Koski, R. A., Lonsdale, P. F., Shanks, W. C., Berndt, M. E., and Howe, S. S. (1985). Mineralogy and geochemistry of a sediment-hosted hydrothermal sulfide deposit from the southern trough of Guaymas Basin, Gulf of California. *J. Geophys. Res.* 90, 6695–6707. doi: 10.1029/JB090iB08p06695

Lizarralde, D., Soule, A., Seewald, J., and Proskurowski, G. (2011). Carbon release by off-axis magmatism in a young sedimented spreading centre. *Nat. Geosci.* 4, 50–54. doi: 10.1038/ngeo1006

Lonsdale, P., and Becker, K. (1985). Hydrothermal plumes, hot springs, and conductive heat flow in the Southern Trough of Guaymas Basin. *Earth Planet. Sci. Lett.* 73, 211–225. doi: 10.1016/0012-821X(85)90070-6

Lupton, J. E. (1979). Helium-3 in the Guaymas Basin: evidence for injection of mantle volatiles in the Gulf of California. *J. Geophys. Res.* 84, 7446–7452. doi: 10.1029/JB084iB13p07446

Luther, G. W., Rozan, T., Taillefert, M., Nuzzio, D., DiMeo, C., Shank, T. M., et al. (2001). Chemical speciation drives hydrothermal vent ecology. *Nature* 410, 813–815. doi: 10.1038/35071069

MacGregor, B. J., Biddle, J. F., Harbort, C., Matthysse, A. G., and Teske, A. (2013a). Sulfide oxidation, nitrate respiration, carbon acquisition and electron transport pathways suggested by the draft genome of a single orange Guaymas Basin Beggiatoa (Cand. Maribeggiatoa) sp. filament. *Mar. Genomics* 11, 53–65. doi: 10.1016/j.margen.2013.08.001

MacGregor, B. J., Biddle, J. F., Siebert, J. R., Staunton, E., Hegg, E., Matthysse, A. G., et al. (2013b). Why orange Guaymas Basin *Beggiatoa* spp. are orange: single-filament genome-enabled identification of an abundant octaheme cytochrome with hydroxylamine oxidase, hydrazine oxidase and nitrite reductase activities. *Appl. Environ. Microbiol.* 79, 1183–1190. doi: 10.1128/AEM.02538-12

Martens, C. S. (1990). Generation of short chain organic acid anions in hydrothermally altered sediments of the Guaymas Basin, Gulf of California. *Appl. Geochem.* 5, 71–76. doi: 10.1016/0883-2927(90)90037-6

Martens, C. S., Albert, D. B., and Alperin, M. J. (1999). Stable isotopic tracing of anaerobic methane oxidation in the gassy sediments of Eckernförde Bay, German Baltic Sea. *Am. J. Sci.* 299, 589–610. doi: 10.2475/ajs.299.7-9.589

McKay, L., Klokman, V. W., Mendlovitz, H. P., LaRowe, D. E., Hoer, D. R., Albert, D., et al. (2015). Thermal and geochemical influences on microbial biogeography in the hydrothermal sediments of Guaymas Basin. *Environ. Microbiol. Rep.* doi: 10.1111/1758-2229.12365 [Epub ahead of print].

McKay, L. J., MacGregor, B. J., Biddle, J. F., Mendlovitz, H. P., Hoer, D., Lipp, J. S., et al. (2012). Spatial heterogeneity and underlying geochemistry of phylogenetically diverse orange and white Beggiatoa mats in Guaymas Basin hydrothermal sediments. *Deep Sea Res. I* 67, 21–31. doi: 10.1016/j.dsr.2012.04.011

Meyer, S., Wegener, G., Lloyd, K. G., Teske, A., Boetius, A., and Ramette, A. (2013). Microbial habitat connectivity across spatial scales and hydrothermal temperature gradients at Guaymas Basin. *Front. Microbiol.* 4:207. doi: 10.3389/fmicb.2013.00207

Nelson, D. C., Wirsen, C. O., and Jannasch, H. W. (1989). Characterization of large, auto- trophic Beggiatoa spp. abundant at hydrothermal vents of the Guaymas Basin. *Appl. Environ. Microbiol.* 55, 2909–2917.

Nielsen, L. P., Risgaard-Petersen, N., Fossing, H., Christensen, P. B., and Sayama, M. (2010). Electric currents couple spatially separated biogeochemical processes in marine sediment. *Nature* 463, 1071–1074. doi: 10.1038/nature08790

Pagé, A., Tivey, M. K., Stakes, D., and Reysenbach, A.-L. (2008). Temporal and spatial archaeal colonization of hydrothermal vent deposits. *Environ. Microbiol.* 10, 874–884. doi: 10.1111/j.1462-2920.2007.01505.x

Party. (1982). "Guaymas basin: sites 477, 478, and 481," in *Initial Reports of the Deep Sea Drilling Project*, Vol. 64, eds J. R. Curray, J. Blakeslee, L. W. Platt, L. N. Stout, D. G. Moore, and J. E. Aguayo, et al. (Washington, DC: U.S. Government Printing Office), 211–293.

Pearson, A., Seewald, J. S., and Eglinton, T. I. (2005). Bacterial incorporation of relict carbon in the hydrothermal environment of Guaymas Basin. *Geochim. Cosmochim. Acta* 69, 5477–5486. doi: 10.1016/j.gca.2005.07.007

Peter, J. M., Peltonen, P., Scott, S. D., Simoneit, B. R. T., and Kawka, O. E. (1991). 14C ages of hydrothermal petroleum and carbonate in Guaymas Basin, Gulf of California: implications for oil generation, expulsion, and migration. *Geology* 19, 253–256. doi: 10.1130/0091-7613(1991)019<0253:CAOHPA>2.3.CO;2

Peter, J. M., and Scott, S. D. (1988). Mineralogy, composition, and fluid-inclusion microthermometry of seafloor hydrothermal deposits in the southern trough of Guaymas Basin, Gulf of California. *Can. Mineral.* 26, 567–587.

Peter, J. M., and Shanks, W. C. III. (1992). Sulfur, carbon, and oxygen isotope variations in submarine hydrothermal deposits of Guaymas Basin, Gulf of California, USA [sic!] Geochim. *Cosmochim. Acta* 56, 2025–2040. doi: 10.1016/0016-7037(92)90327-F

Peter, J. M., Simoneit, B. R. T., Kawka, O. E., and Scott, S. D. (1990). Liquid hydrocarbon-bearing inclusions in modern hydrothermal chimneys and mounds from the southern trough of Guaymas Basin, Gulf of California. *Appl. Geochem.* 5, 51–63. doi: 10.1016/0883-2927(90)90035-4

Pjevac, P., Kamyshny, A., Dyksma, S., and Mussmann, M. (2014). Microbial consumption of zero-valence sulfur in marine benthic habitats. *Environ. Microbiol.* 16, 3416–3430. doi: 10.1111/1462-2920.12410

Revsbech, N. P., and Ward, D. M. (1983). Oxygen microelectrode that is insensitive to medium chemical composition: use in an acid microbial mat dominated by *Cyanidium caldarium*. *Appl. Environ. Microbiol.* 45, 755–759.

Ruff, S. E., Biddle, J. F., Teske, A., Knittel, K., Boetius, A., and Ramette, A. (2015). Global dispersion and local diversification of the methane seep microbiome. *Proc. Natl. Acad. Sci. U.S.A.* 112, 4015–4020. doi: 10.1073/pnas.1421865112

Salman, V., Amann, R., Girnth, A. C., Polerecky, L., Bailey, J. V., Høgslund, S., et al. (2011). A single-cell sequencing approach to the classification of large, vacuolated sulfur bacteria. *Syst. Appl. Microbiol.* 34, 243–259. doi: 10.1016/j.syapm.2011.02.001

Salman, V., Yang, T., Berben, T., Klein, F., Angert, E., and Teske, A. (2015). Calcite-accumulating large sulfur bacteria of the genus *Achromatium* in Sippewissett Salt Marsh. *ISME J.* 9, 2503–2514. doi: 10.1038/ismej.2015.62

Saunders, A., Fornari, D. J., Joron, J. L., Tarney, J., and Treuil, M. (1982). "Geochemistry of basic igneous rocks, Gulf of California," in *Initial Reports of the Deep Sea Drilling Project*, Vol. 64, eds J. Curray and D. Moore (Texas, TX: Ocean Drilling Program, College Station), 595–642.

Shank, T. M., Fornari, D. J., Von Damm, K. L., Lilley, M. D., Haymon, R. M., and Lutz, R. A. (1998). Temporal and spatial patterns of biological community development at nascent deep-sea hydrothermal vents along the East Pacific Rise. *Deep Sea Res.* 45, 465–515.

Simoneit, B. R. T. (1985). Hydrothermal petroleum: genesis, migration and deposition in Guaymas Basin. Gulf of California. *Can. J. Earth Sci.* 22, 1919–1929. doi: 10.1139/e85-208

Simoneit, B. R. T., and Lonsdale, P. E. (1982). Hydrothermal petroleum in mineralized mounds at the seabed of Guaymas Basin. *Nature* 295, 198–202. doi: 10.1038/295198a0

Taylor, C. D., Wirsen, C. O., and Gaill, F. (1999). Rapid microbial production of filamentous sulfur mats at hydrothermal vents. *Appl. Environ. Microbiol.* 65, 2253–2255.

Teske, A., Callaghan, A. V., and LaRowe, D. E. (2014). Biosphere frontiers of subsurface life in the sedimented hydrothermal system of Guaymas Basin. *Front. Microbiol.* 5:362. doi: 10.3389/fmicb.2014.00362

Teske, A., Hinrichs, K.-U., Edgcomb, V., de Vera Gomez, A., Kysela, D., Sylva, S. P., et al. (2002). Microbial diversity in hydrothermal sediments in the Guaymas Basin: evidence for anaerobic methanotrophic communities. *Appl. Environ. Microbiol.* 68, 1994–2007. doi: 10.1128/AEM.68.4.1994-2007.2002

Teske, A., and Salman, V. (2015). "The family Beggiatoaceae, Chap. 6," in *The Prokaryotes – Gammaproteobacteria. The Prokaryotes*, 4th Edn, eds E. Rosenberg, E. F. DeLong, F. Thompson, S. Lory, and E. Stackebrandt (Berlin: Springer-Verlag), 93–134.

Von Damm, K. L., Edmond, J. M., Measures, C. I., and Grant, B. (1985). Chemistry of submarine hydrothermal solutions at Guaymas Basin, Gulf of California. *Geochim. Cosmochim. Acta* 49, 2221–2237. doi: 10.1016/0016-7037(85)90223-6

Weber, A., and Jørgensen, B. B. (2002). Bacterial sulfate reduction in hydrothermal sediments of the Guaymas Basin, Gulf of California, Mexico. *Deep Sea Res. I* 149, 827–841. doi: 10.1016/S0967-0637(01)00079-6

Welhan, J. (1988). Origins of methane in hydrothermal systems. *Chem. Geol.* 71, 183–198. doi: 10.1016/0009-2541(88)90114-3

Welhan, J. A., and Lupton, J. E. (1987). Light hydrocarbon gases in Guaymas Basin hydrothermal fluids: *Thermogenic versus* abiogenic origin. *AAPG Bull.* 71, 215–233.

Whelan, J. K., Simoneit, B. R. T., and Tarafa, M. E. (1988). C1-C8 hydrocarbons in sediments from Guaymas Basin, Gulf of California – Comparison to Peru Margin, Japan Trench, and California Borderlands. *Org. Geochem.* 12, 171–194. doi: 10.1016/0146-6380(88)90253-7

Williams, D. L., Becker, K., Lawver, L. A., and Von Herzen, R. P. (1979). Heat flow at the spreading centers of the Guaymas Basin, Gulf of California. *J. Geophys. Res.* 84, 6757–6769. doi: 10.1029/JB084iB12p06757

Winkel, M., De Beer, D., Lavik, G., Peplies, J., and Mussmann, M. (2014). Close association of active nitrifyers with Beggiatoa mats covering deep-sea hydrothermal sediments. *Environ. Microbiol.* 16, 1612–1626. doi: 10.1111/1462-2920.12316

Conflict of Interest Statement: The authors declare that the research was conducted in the absence of any commercial or financial relationships that could be construed as a potential conflict of interest.

frontiers in Microbiology

ORIGINAL RESEARCH
published: 16 December 2015
doi: 10.3389/fmicb.2015.01397

Abundant Intergenic TAACTGA Direct Repeats and Putative Alternate RNA Polymerase β′ Subunits in Marine *Beggiatoaceae* Genomes: Possible Regulatory Roles and Origins

Barbara J. MacGregor *

Department of Marine Sciences, University of North Carolina–Chapel Hill, Chapel Hill, NC, USA

The genome sequences of several giant marine sulfur-oxidizing bacteria present evidence of a possible post-transcriptional regulatory network that may have been transmitted to or from two distantly related bacteria lineages. The draft genome of a *Cand.* "Maribeggiatoa" filament from the Guaymas Basin (Gulf of California, Mexico) seafloor contains 169 sets of TAACTGA direct repeats and one indirect repeat, with two to six copies per set. Related heptamers are rarely or never found as direct repeats. TAACTGA direct repeats are also found in some other *Beggiatoaceae*, *Thiocystis violascens*, a range of Cyanobacteria, and five Bacteroidetes. This phylogenetic distribution suggests they may have been transmitted horizontally, but no mechanism is evident. There is no correlation between total TAACTGA occurrences and repeats per genome. In most species the repeat units are relatively short, but longer arrays of up to 43 copies are found in several Bacteroidetes and Cyanobacteria. The majority of TAACTGA repeats in the *Cand.* "Maribeggiatoa" Orange Guaymas (BOGUAY) genome are within several nucleotides upstream of a putative start codon, suggesting they may be binding sites for a post-transcriptional regulator. Candidates include members of the ribosomal protein S1, Csp (cold shock protein), and Csr (carbon storage regulator) families. No pattern was evident in the predicted functions of the open reading frames (ORFs) downstream of repeats, but some encode presumably essential products such as ribosomal proteins. Among these is an ORF encoding a possible alternate or modified RNA polymerase beta prime subunit, predicted to have the expected subunit interaction domains but lacking most catalytic residues. A similar ORF was found in the *Thioploca ingrica* draft genome, but in no others. In both species they are immediately upstream of putative sensor kinase genes with nearly identical domain structures. In the marine *Beggiatoaceae*, a role for the TAACTGA repeats in translational regulation is suggested. More speculatively, the putative alternate RNA polymerase subunit could be a negative transcriptional regulator.

Keywords: heptamer repeats, DNA-directed RNA polymerase, beta prime subunit, *Beggiatoaceae*, Cyanobacteria, Bacteroidetes, orange Guaymas "Maribeggiatoa"

OPEN ACCESS

Edited by:
Beth Orcutt, Bigelow Laboratory for Ocean Sciences, USA

Reviewed by:
Jeremy Dodsworth, California State University, San Bernardino, USA
Emily J. Fleming, California State University, Chico, USA

***Correspondence:**
Barbara J. MacGregor
bmacgreg@unc.edu

Specialty section:
This article was submitted to Extreme Microbiology, a section of the journal Frontiers in Microbiology

Received: *28 August 2015*
Accepted: *23 November 2015*
Published: *16 December 2015*

Citation:
MacGregor BJ (2015) Abundant Intergenic TAACTGA Direct Repeats and Putative Alternate RNA Polymerase β′ Subunits in Marine Beggiatoaceae Genomes: Possible Regulatory Roles and Origins. Front. Microbiol. 6:1397. doi: 10.3389/fmicb.2015.01397

INTRODUCTION

Organic-rich sediments surrounding hydrothermal sites on the Guaymas Basin sea floor often host luxuriant microbial mats, visually dominated by large filamentous, vacuolated, orange-pigmented, and unpigmented *Beggiatoaceae* (Jannasch et al., 1989). From 16S rRNA data, these appear to belong to several distinct species. None of them are yet in culture, but physiological (McHatton et al., 1996) and genomic (MacGregor et al., 2013a) studies are consistent with a sulfur-oxidizing, nitrate-reducing metabolism. They are gradient dwellers, living between hot sulfidic fluids flowing up through the sediments below and cold, oxygenated overlying seawater. In general, the pigmented forms are found toward the center of mats, where flow rates (and temperature) are higher, while unpigmented forms are more concentrated at the periphery (McKay et al., 2012). The pigmentation is thought to be due to high concentrations of an octaheme cytochrome, possibly a nitrite reductase (MacGregor et al., 2013b). The Orange Guaymas *Cand.* "Maribeggiatoa" (BOGUAY) draft genome (MacGregor et al., 2013a) was obtained from a single orange filament cleaned of epibionts.

In the course of analyzing this genome, numerous short direct repeats of the heptanucleotide TAACTGA were noticed, particularly in intergenic regions directly upstream of translational start codons. The genomes of the marine *Beggiatoaceae Cand*. "Thiomargarita nelsonii" and *Thioploca ingrica,* and *Thiocystis violascens* (*Chromatiaceae*)—but not the freshwater *Beggiatoa alba*—also feature these repeats to varying degrees. Database searches further found TAACTGA direct repeats in some Cyanobacteria and a few Bacteroidetes, consistent with earlier evidence (MacGregor et al., 2013c) for genetic exchange between these groups and the *Beggiatoaceae*.

Tandem direct repeats of short nucleotide sequences have a very sporadic distribution in bacteria. In a comprehensive study, Mrázek et al. (2007) examined the distribution of what were termed long simple sequence repeats (LSSR) in prokaryotic genome sequences available at the time (2007). Repeat units of 1–11 nt were considered, and "long" was defined as series of repeats longer than statistically expected in a given genome. Species rich in LSSRs could be divided into those with repeat units primarily 1–4 or 5–11 nt long. They were phylogenetically scattered: for example, the 10 genomes identified with the most 5–11 nt repeats included four Betaproteobacteria (all *Burkholderia* spp.), two Cyanobacteria, three Actinobacteria, and one Gammaproteobacterium (*Xanthomonas campestris* ATCC 33913). Heptanucleotide repeats were the most abundant category in most genomes; it was proposed interaction of these with DNA polymerase might favor slippage and therefore duplications or deletions, and that 7 nt might be the length of sequence interacting with the polymerase. It was also noted that repeat units whose lengths are multiples of three were the most likely to be found within coding regions, presumably because series of them can be expanded and contracted without truncating a protein as long as they do not generate stop codons.

The same group went on to examine the genome-wide distribution of LSSR in several host-adapted pathogenic bacteria (Guo and Mrázek, 2008). Such repeats have been proposed and in some cases demonstrated to be involved in phase variation via slippage during DNA replication, turning on or off expression of virulence functions at either the transcriptional or the translational level. Some LSSR were in fact associated with antigenicity functions, such as envelope biogenesis genes, but COG classifications including these were not significantly overrepresented among the very diverse repeat-associated genes.

The genome-wide distribution of SSR (here abbreviating "simple satellite repeats") in *Escherichia coli* has also been examined (Gur-Arie et al., 2000), considering only 1–6 nt units. For tetranucleotides, the longest unit reported in this regard, 78.9% of repeats were found in coding regions—very nearly the same proportion of the whole genome that is coding (79.5%). The repeats in intergenic regions did not show any particular concentration near translational start sites.

The two experimentally studied examples of bacterial tandem repeats between a promoter and a start codon are both upstream of surface proteins involved in phase variation in the respiratory pathogen *Moraxella catarrhalis*. A tract of either 9 or 10 G residues occurs 30 nt upstream of the translational start for the UspA1 gene (Lafontaine et al., 2001), which allows adhesion of the bacterium to human epithelial cells. Nine-residue G tracts were associated with high expression and 10-residue tracts with low expression. The tetranucleotide AGAT is found in strain-dependent copy numbers (from 6 to 23) in the 5′ untranslated regions of mRNAs for UspA2 (Attia and Hansen, 2006), a surface protein conferring resistance to human serum. Mutational studies in one strain found highest UspA2 expression with 18 copies.

This study describes the distribution of TAACTGA heptamer repeats in the BOGUAY genome, and the limited number of other species in which they have been found. Possible roles in translational regulation and genome rearrangement will be considered, depending on the length and position of the different repeat arrays. A possible alternate or derived RNA polymerase beta prime subunit gene identified in the Orange Guaymas "Maribeggiatoa" and *Thioploca ingrica* genomes is also discussed.

MATERIALS AND METHODS

An orange tuft retrieved from core 4489-10 from RV *Atlantis*/HOV *Alvin* cruise AT15-40 (13 December 2008) at the UNC Gradient Mat site in Guaymas Basin, Gulf of California, Mexico (latitude 27° 0.450300′ N, longitude 111° 24.532320′ W, depth 2001 m) was cleaned of epibionts; its DNA amplified, tested for genetic purity, sequenced, assembled, and annotated; and the genome sequence checked for completeness, as previously described (MacGregor et al., 2013a,c). A total of 99.3% of the sequence was assembled into 822 contigs, suggesting good coverage was achieved. 4.7 Mb of sequence was recovered, with 80% of it forming large (≥15 kb) contigs. Throughout this paper, the genome is referred to as BOGUAY (from "*Beggiatoa* orange Guaymas") and annotated sequences are referred to by 5-digit contig and 4-digit open reading frame (ORF) numbers (e.g., 00024_0691) or by ORF number alone (e.g., BOGUAY_0691). Additional sequence analysis was carried out using a combination of the JCVI-supplied annotation,

TABLE 1 | Orientation of TAACTGA repeats in the BOGUAY genome.

Repeats	Orientation													Total
	Toward start codon, no RBS				Toward start codon, with RBS			Toward stop codon			Contig end	Other		
	Intergenic	Overlap	In ORF	Total	Intergenic	Overlap	Total	Intergenic	Overlap	In ORF	Total	Total	Intergenic	In ORF	Total	
2	40	3	3	46	10	1	11	8	–	–	8	2	–	1	1	68
2, split	15	–	–	15	1	–	1	1	–	–	1	–	1	–	1	18
3	27	4	1	32	2	1	3	1	1	1	3	2	–	–	–	40
3, split	11	1	1	13	–	–	–	–	–	–	–	–	–	1	1	14
4	15	3	1	19	–	–	–	–	–	–	–	–	–	–	–	19
4, split	4	–	–	4	–	–	–	–	–	–	–	2	–	–	–	6
5	2	–	–	2	–	–	–	–	–	–	–	–	–	–	–	2
5, split	–	–	–	–	–	–	–	–	–	–	–	–	–	1	1	1
6	1	–	–	1	–	–	–	–	–	–	–	–	–	–	–	1
Inverted repeat	–	–	–	–	–	–	–	–	–	–	–	–	–	1	1	1
Total	115	11	6	132	13	2	15	10	1	1	12	6	1	4	5	170

"Split" sets have a different but related 7-mer between two TAACTGA sequences.

the IMG/ER (Markowitz et al., 2009) and RAST (Aziz et al., 2008) platforms, and BLASTN, BLASTX, and BLASTP and PSIBLAST searches of the GenBank nr databases. Nucleic acid and amino acid sequence alignments were performed in MEGA5 (Tamura et al., 2011) using MUSCLE (Edgar, 2004) and small adjustments made manually. For identification of other TAACTGA-containing genomes, the GenBank nr database was searched with seven direct repeats of the TAACTGA sequence, using the default "short query" settings. For each strain with a sequence identified by this search, the genome sequence was searched for all TAACTGA direct repeats (in both orientations). RNA structure predictions are the first results from a minimum free energy calculation using the default settings of the MaxExpect algorithm from the RNAstructure Web Server (http://rna.urmc.rochester.edu/RNAstructureWeb/, Reuter and Mathews, 2010). Translations were done via the ExPASy portal of the Swiss Institute of Bioinformatics (Artimo et al., 2012). Protein domains were identified in CDD (Marchler-Bauer et al., 2011).

RESULTS AND DISCUSSION

Overview of Sequenced *Beggiatoaceae*

The *Beggiatoaceae* family of giant sulfur bacteria includes species with a range of morphologies and habitats, very few of which have as yet been cultivated. Their classification is still in progress (Salman et al., 2011, 2013), but it is clear that many strains formerly designated *Beggiatoa* should be reclassified. Genomic sequence data are currently available for a small but diverse selection of these: complete or near-complete genome sequences for *B. alba* B18LD (Lucas et al. unpublished), *Thioploca ingrica* (Kojima et al., 2015), and Orange Guaymas "Maribeggiatoa" (MacGregor et al., 2013a,b,c); a partial sequence for *Cand.* "Thiomargarita nelsonii" (Mußmann et al., unpublished); and very partial sequences for two single filaments from the Baltic Sea, designated *Cand.* "Isobeggiatoa" PS and SS (Mussmann et al., 2007). By 16S rRNA gene sequence analysis, *B. alba* is in a separate clade from the rest of these (Salman et al., 2013).

Abundance and Distribution of TAACTGA Repeats in the BOGUAY and Other *Beggiatoaceae* Genomes

The Orange Guaymas "Maribeggiatoa" (BOGUAY) genome, with ∼5330 annotated genes, contains some 169 sets of direct TAACTGA repeats and one indirect repeat, with between two and six copies per set (**Table 1**). Thirty-six of the sets are split by one or two different but related 7 bp sequences. Their distribution is not random: most are in a "forward" orientation upstream of a putative start codon, with the largest single category ending 1 nt upstream (**Figure 1**). All but 25 sets are completely intergenic. Of the rest, 14 overlap the end of an upstream ORF, with 13 in forward orientation to a downstream ORF; 10 are interior to ORFs in reverse orientation (Supplemental Table 1); and one is an inverted repeat near the end of an ORF, with the repeat units separated by one base pair (**Table 2**). There are an additional 819 singletons, whose distribution was not examined, for a total of 1357. TAACTGA repeats are also found in the "Isobeggiatoa"

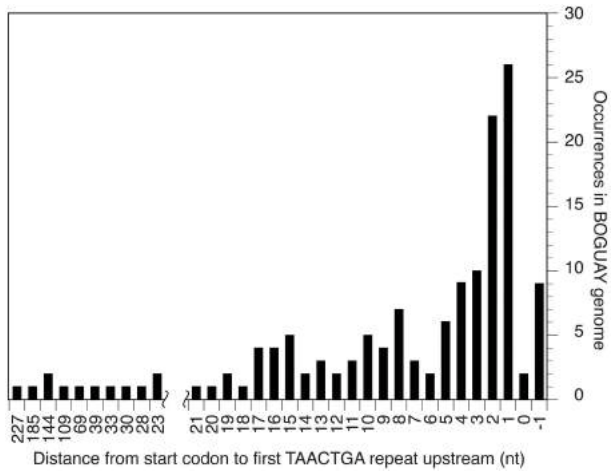

FIGURE 1 | Distance between start codon and first repeat for BOGUAY intergenic TAACTGA repeats.

sp. PS and SS genomes, but these are too incomplete for thorough comparison. Of other sequenced *Beggiatoaceae*, Cand. "Thiomargarita nelsonii" has a similar number of repeats, and a higher proportion of doublets and triplets, but fewer longer sets; *T. ingrica* has a similar number of TAACTGA copies, but very few as direct repeats; and *B. alba* has less than half as many total copies and no direct repeats (**Figures 2A,B**, Supplemental Table 2).

Direct Repeats of Sequences Similar to TAACTGA are Rare in the BOGUAY Genome

A survey of the BOGUAY genome for heptamers with a single-base difference to TAACTGA (**Table 3**) showed that while some of these are in similar or greater abundance than TAACTGA as singletons, the maximum number of doublets for any of them was six, and only two had any longer sets of direct repeats (one of four units, one of six). Several scrambled versions of TAACTGA were also searched; all are at lower to considerably lower abundance as singletons, and none is found as even a single direct repeat. Factors such as coding potential likely influence the distribution of each of these, and some permutations may be selected against as interfering with whatever function(s) TAACTGA repeats may have, but TAACTGA does appear to be a favored sequence.

Predicted Characteristics of RNA and Amino Acid Sequences that Might be Produced from TAACTGA Repeats

If the BOGUAY TAACTGA repeats have common function(s), these could be at the DNA, RNA, or in a few cases protein level. At the DNA level, repeat sequences can serve as recombinational and mutational hot spots (reviewed in Lovett, 2004; Zhou et al., 2014), or as binding sites for regulatory proteins. They could conceivably also mark the site of transposon excisions; some transposon insertions can generate 7 nt direct repeats (Sallam et al., 2006), although in the studied cases they seem usually to resolve to singletons upon excision (Foster et al., 1981).

At the RNA level, the repeats may again be protein-binding sites (or interrupt existing ones), and/or impart secondary structure. As direct repeats in up to six copies, however, TAACTGA is not predicted to generate any particular RNA secondary structure in either orientation (**Table 3**), unless by interaction with surrounding sequences.

At the protein level, translation of TAACTGA and its reverse complement (TCAGTTA) reveals what is probably a major factor controlling genomic distribution of these sequences. In the "forward" orientation, translation of TAACTGA repeats yields the repeating amino acid sequence LITDN–, where dashes represent stop codons. These can therefore overlap the end of coding sequences by no more than 18 nt, or two full repeats plus four nucleotides. If repeats are carried by mobile elements, their introduction into coding sequences in forward orientation will terminate the gene, and usually be deleterious. In some locations it might be tolerated however, for example between the subunits of modular proteins, or at the beginning or end of a protein. Possible examples will be discussed below.

Translation of repeats in the "reverse" orientation yields the repeating sequence LSVISYQ. At first glance, this suggests a leucine zipper dimerization domain (reviewed in Parry et al., 2008), with nonpolar residues in the first (L) and fourth (I) positions, but there are no charged amino acids for interactions on the other face of the predicted helix, and the nonpolar third position (V) is unusual. According to the algorithm of Bornberg-Bauer et al. (1998), this sequence does not have the requisite leucine zipper coiled-coil structure even when 20 or more amino acid repeats are included. *Ab initio* structure predictions (Xu and Zhang, 2012) for a peptide composed of seven LSVISYQ repeats (and several variants) suggest a structure dominated by antiparallel beta sheets (not shown), but structure in a real protein would depend on the number of repeats and on interactions with the rest of the protein.

Compared to other similar heptamers, TAACTGA has no obvious special features (**Table 3**): several have similar genomic abundances, many yield apparently similar local RNA conformations, a majority can be translated in "reverse" orientation, and all single-base mutants yield one or more stop codons in "forward" orientation. None of these properties shows a strong correlation with chromosomal abundance, or with occurrence as direct repeats. Assuming all relevant properties have been considered, this is consistent with TAACTGA repeats arising in one lineage and being horizontally transferred to others. The alternatives that this particular sequence became repeated independently in multiple isolated lineages, or was preserved as such in only a few, seem less likely.

Abundance and Distribution of TAACTGA Repeats in the Cyanobacteria and Bacteroidetes

A GenBank search for TAACTGA direct repeats found a very limited phylogenetic distribution (**Figure 2**). Outside of the *Beggiatoaceae*, considering only complete or near-complete

TABLE 2 | TAACTGA repeats within or overlapping BOGUAY ORFs.

A) Forward orientation

Upstream ORF with repeats		Repeat region sequence	Downstream ORF		
Description	COG group		Locus tag	Description	COG group
ATPase, histidine kinase-, DNA gyrase B-, and HSP90-like domain protein	T		00163_1011	response regulator receiver domain protein	T
adenylate and guanylate cyclase catalytic domain protein	T		00391_1539	hemerythrin HHE cation binding domain protein	T
PAS domain S-box	T		01232_0432	response regulator receiver domain protein	
Tol-Pal system-associated acyl-CoA thioesterase	R		00647_3823	TolQ	U
glycine cleavage system T protein	E		00883_3308	glycine cleavage system H protein	E
COG3222, DUF2064	S		00162_0503	homoserine kinase, ThrB	R
CheR methyltransferase, SAM binding domain protein	N, T		00806_2998	protein-glutamate methylesterase CheB	
ABC transporter, ATP-binding protein	G, M		00127_3139	methyltransferase domain protein	H
electron transport complex, RnfABCDGE type, E subunit	C		01035_2232	Uncharacterized protein conserved in bacteria COG3122	S
regulatory protein, FmdB family	S		00106_0256	aspartyl-tRNA synthetase	J
hypothetical protein			00614_2860	roadblock/LC7 domain protein	R
hypothetical protein			01005_2993	hypothetical protein	
hypothetical protein			00155_2445	hypothetical protein	
hypothetical protein			00472_0533	putative potassium uptake protein TrkA (on opposite strand, coming in from end of contig)	P

B) Reverse orientation

Repeat region sequence	ORF downstream of repeats (if any)		
	Locus tag	Description	COG group
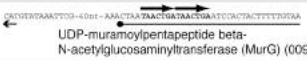 UDP-muramoylpentapeptide beta-N-acetylglucosaminyltransferase (MurG) (00938_0721)			
 hypothetical protein (00199_2704)	00199_2702	methyl-accepting chemotaxis protein signaling domain protein	N, T
 hypothetical protein (01017_0756)	01017_0755	Uncharacterized conserved protein	
 hypothetical protein (01192_0163)	01192_0161	glutamine synthetase, type I (>100 nt downstream)	E
 conserved domain protein (01153_1105)	01153_1104	receptor family ligand-binding protein	E
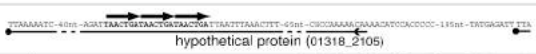 hypothetical protein (01318_2105)	01318_2106	conserved hypothetical protein (>200 nt downstream)	
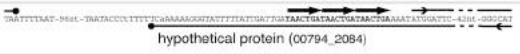 hypothetical protein (00794_2084)	00794_2083	putative proton/sodium-glutamate symport protein GltT	C
 putative corrinoid ABC transporter permease (00106_0223)	00106_0222	lipofamily protein	
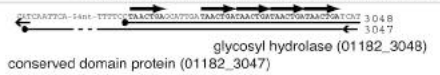 glycosyl hydrolase (01182_3048) conserved domain protein (01182_3047)			
DNA-directed RNA polymerase, beta' subunit (00100_0018)			

C) Inverted repeat

Upstream ORF			Downstream ORF		
Description	COG group		Locus tag	Description	COG group
segregation and condensation protein B			00780_1610	conserved hypothetical protein	

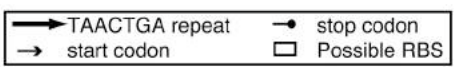

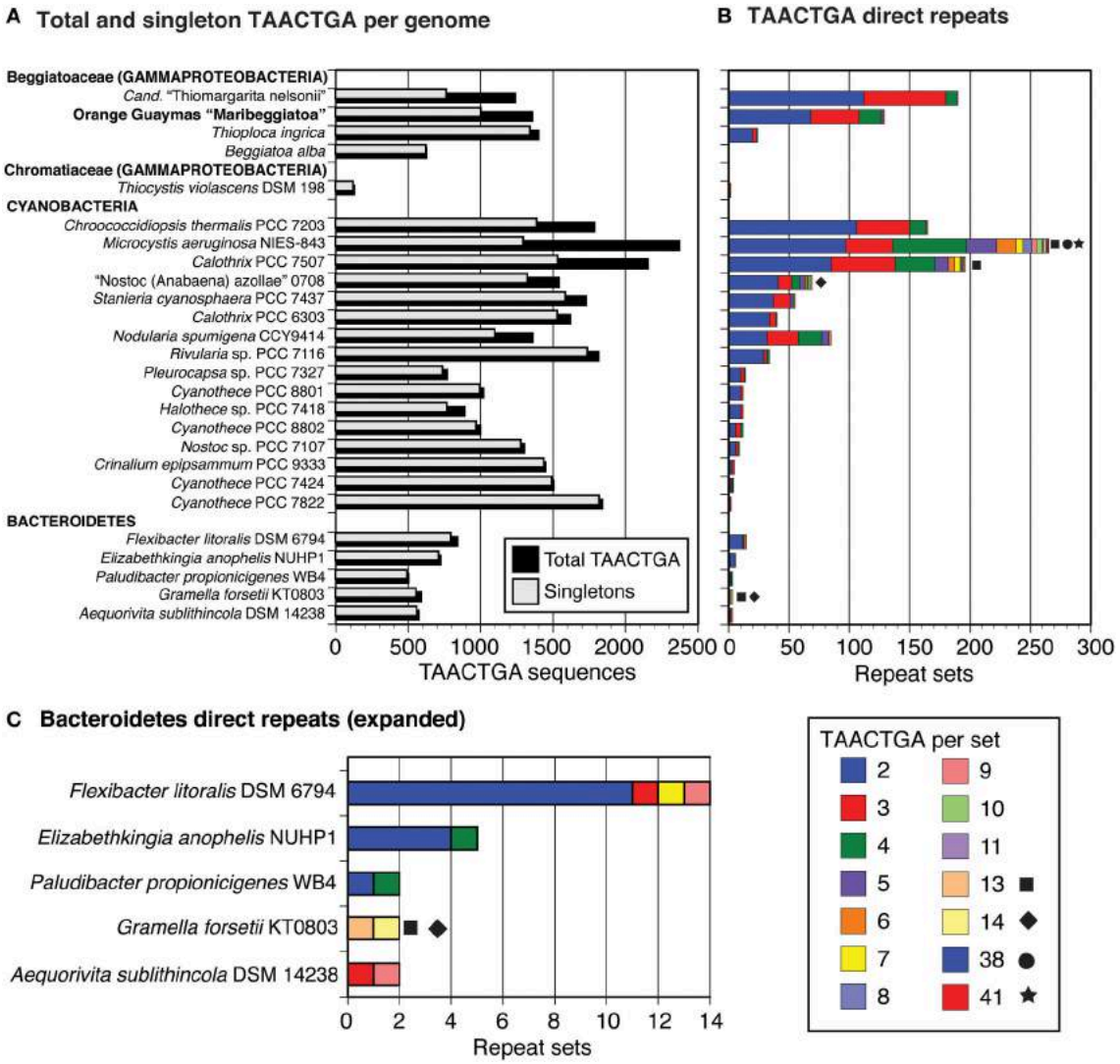

FIGURE 2 | Number and length of TAACTGA repeat sets in different species. The GenBank nr database was searched with seven direct repeats of the TAACTGA sequence, using the default "short query" settings. For each strain with a sequence identified by this search, the genome sequence was searched for all TAACTGA direct repeats (in both orientations), and these were classified by the number of repeats they contain. The strains were sorted in order of number of two-repeat copies within each phylogenetic group. *Beggiatoa alba* contains no sets of repeats, but was included to present a complete set of available *Beggiatoaceae* genomes. **(A)** Total and singleton repeats in all species. **(B)** Repeat sets, classified by length. Especially long sets are highlighted by symbols. **(C)** Expanded view for Bacteroidetes repeat sets.

genomes, TAACTGA repeats were identified in one other sulfur-oxidizing Gammaproteobacterium (*Thiocystis violascens* DSM 198), 15 Cyanobacteria, and 5 Bacteroidetes. This distribution is similar to that previously noted for the *fdxN* element excision-controlling factor proteins XisH and XisI (MacGregor et al., 2013c). An updated (May 2015) database search found that at least one of these was annotated in all cyanobacterial genomes with TAACTGA repeats except *Stanieria cyanosphaera* PCC 7437, but not in the Bacteroidetes represented (although they are found in some other genera in this group) and not in *T. ingricans* or *T. violascens* (Supplemental Table 7). The hypothetical protein BOGUAY_0693, which has 29 close matches in the BOGUAY genome, has matches in some but not all of the same cyanobacteria, the other *Beggiatoaceae*, and *Flexibacter litoralis*, but not in the remaining Bacteroidetes or *T. violascens* (Supplemental Table 7). Whether or not a common transfer mechanism is involved, this is consistent with a history of genetic exchange among some Cyanobacteria and *Beggiatoaceae*.

As in the *Beggiatoaceae*, there is no necessary correlation between number of singletons and number of repeats (**Figure 2**, Supplemental Table 2); for example, *Cyanothece* PCC 7424 has more singleton and nearly as many total copies as "Nostoc azollae" 0708, but 3 vs. 69 sets of repeats. There are no obvious morphologies, metabolic types, or habitats common to all the species found: for example, *Microcystis aeruginosa* NIES-843

TABLE 3 | TAACTGA-like sequences in the BOGUAY genome.

DNA sequence (forward)	Total and direct-repeat occurrences in BOGUAY genome						Predicted RNA minimum free energy structure for six direct repeats				Amino acid repeat unit	
	Total copies	Repeats in set					Forward		Reverse complement		Forward	Reverse complement
		2	3	4	5	6	Type	kcal mol^{-1}	Type	kcal mol^{-1}		
TAACTGA AND SINGLE-BASE MUTATIONS												
TAA***T***TGA	1908	6					Stem-loop	−4.3	One pair	3.5	LIIDN–	SIINYQL
TAA***A***TGA	1416	1					One pair	3.6	One pair	3.5	MINDK–	SFIIYHL
TAACTGA	1357	68	40	19	1	1	One pair	3.9	One pair	3.9	LITDN–	SVISYQL
AAACTGA	1354	4					One pair	3.9	One pair	3.9	KLKTEN-	SVFSFQF
TAACT***C***A	1206						One pair	3.9	Stem-loop	−10.2	LITHNS-	VMSYEL-
TAACT***T***A	1018						Stem-loop	−6.1	Stem-loop	−9.7	LITYNL-	VISYKL-
TA***T***CTGA	943						Stem-loop	−14.6	Stem-loop	−13.4	YLISDI-	SDIRYQI
CAACTGA	829	3					One pair	3.1	Stem-loop	−6.3	QLTTDN-	SVVSCQL
T***T***ACTGA	810					1	Stem-loop	−4.4	One pair	3.9	LLITDY-	SVISNQ-
TAACT***A***A	786	4		1			One pair	3.9	Stem-loop	−4.3	LITNN–	LLVISY-
T***C***ACTGA	786	1					Stem-loop	−15.1	Stem-loop	−21.2	SLITDH-	SVISDQ-
T***G***ACTGA	778						One pair	3.9	One pair	3.9	LMTDD–	SVISHQS
TAAC***G***GA	742	1					Stem-loop	−4.6	One pair	3.4	RITDNG-	SVIRYPL
TA***C***CTGA	701						One pair	3.9	Stem-loop	−11.0	YLIPDT-	SGIRYQV
TAA***G***TGA	632						One pair	3.2	One pair	3.9	VISDK–	SLITYHL
TAACTG***T***	625	1					Stem-loop	−12.8	Stem-loop	−11.8	LLTVNC-	QLTVNS-
GAACTGA	606						Stem-loop	−4.1	Stem-loop	−2.2	ELRTEN-	SVLSSQF
TA***G***CTGA	598						Stem-loop	−18.4	Stem-loop	−10.4	LIADS–	SAISYQL
TAAC***A***GA	544						One pair	3.9	One pair	3.8	QITDNR-	SVICYLL
TAACTG***G***	476						Stem-loop	−11.8	Stem-loop	−14.4	LVTGNW-	PVTSYQL
TAAC***C***GA	470	1					One pair	3.4	Stem-loop	−12.8	PITDNR-	SVIGYRL
TAACTG***C***	351						Stem-loop	−4.0	Stem-loop	−11.8	LLTANC-	QLAVSS-
SHUFFLED TAACTGA (SELECTION)												
ATATCAG	1030						Stem-loop	−13.4	Stem-loop	−14.0	ISDIRYQ	YLISDI-
ATAATCG	867						Stem-loop	−14.0	Stem-loop	−15.4	SIIDNR-	RLSIIDY
CTAAGTA	322						Stem-loop	−13.8	Stem-loop	−14.5	VLSTKY-	YLVLST-
TCGAATA	319						Stem-loop	−9.4	Stem-loop	−11.0	SNIEYRI	YSIFDIR
TAACTAG	160						Stem-loop	−16.6	Stem-loop	−15.6	LVTSN–	LLVTSY-

*DNA sequences are arranged by number of occurrences. The TAACTGA sequence itself is outlined. Single-base differences to it are in bold italics. For each DNA sequence, an RNA structure was predicted for six direct repeats. Amino acid sequences were predicted for 7 direct repeats, but only a single repeat unit is shown. Shaded boxes indicate amino acid sequences containing stop codons. RNA structure predictions are the first results from a minimum free energy calculation using the default settings of the MaxExpect algorithm from the RNAstructure Web Server [*http://ma.urmc.rochester.edu/RNAstructureWeb/*, (Reuter and Mathews, 2010)]. Translations were done via the ExPASy portal of the Swiss Institute of Bioinformatics (Artimo et al., 2012).*

(NC7) is a colonial freshwater cyanobacterium isolated in Japan (Otsuka et al., 2000); *Elizabethkingia anophelis* NUHP1 is a Gram negative rod from a mosquito midgut collected in The Gambia (Kämpfer et al., 2011); and *Aequorivita sublithincola* DSM 14238 is an endolithic Gram negative bacterium found as rods or filaments, isolated from within a quartz rock in Antarctica (Bowman and Nichols, 2002). This complicates the argument just made for horizontal transfer; characterization of other heptamer repeats and additional genomic sequencing may clarify this issue.

Cyanobacteria

Among the Cyanobacteria, the sequenced genomes of the freshwater, bloom-forming *M. aeruginosa*, particularly strains NIES-843 (Kaneko et al., 2007) and PCC 7806 (Frangeul et al., 2008), have high proportions of repeated sequences. This has been proposed to be part of an evolutionary strategy relying on genome plasticity, with a comparatively high number of horizontally acquired genes and repeated genes and sequences (Humbert et al., 2013). These include a range of repeating heptamers, with TAACTGA repeats often mixed with others. A complete analysis was not carried out here, but a small random sample of the 265 sets of *M. aeruginosa* NIES-843 TAACTGA repeats suggests that they may play more or different roles than in BOGUAY. Of 24 sets of repeats mapped in detail (Supplemental Table 3), 22 were intergenic and two in "reverse" orientation within ORFs encoding small hypothetical proteins. Of the intergenic sets, just six were in "forward" orientation relative to a downstream start codon, and at a range of distances (from 1 to 214 nt). Eight sets were in reverse origin relative to a start codon and eight were between stop codons. All of the latter are in the same orientation on the chromosome; it would be interesting to see whether this pattern holds throughout the genome. If this is a representative sample, it is a clear contrast to the BOGUAY genome, where most sets of repeats are intergenic and in "forward" orientation to a relatively nearby start codon. The chromosomal arrangement is not known because the genome is not closed.

Repeat distributions in four *Cyanothece* strains with relatively few TAACTGA copies were also compared (Supplemental Table 4). *Cyanothece* PCC 8801 and 8802 are very similar, with nine sets of repeats in matching positions in terms of flanking ORFs and only small intergenic sequence differences, mostly indels in 7 nt increments. Seven of these repeat sets are just upstream of a start codon, one just upstream of a putative Shine-Dalgarno (SD) sequence, and one in reverse orientation near the upstream ORF. PCC 8802 has an additional intergenic set relatively far upstream from a start codon; each strain has an intergenic plasmid-borne set, but between different ORFs; and PCC 8801 has one set in reverse orientation internal to an ORF. In PCC 7424, there are only three sets of repeats, none in positions matching the other two strains. All are intergenic and in "forward" orientation, at varying distances from the nearest start codon. The closest relatives of the flanking ORFs are all from strain PCC 7822, including those flanking its only set of repeats. Overall, whether TAACTGA and related repeats derive from a common cyanobacterial ancestor or are transmitted by some mobile element, they appear to have followed strain-specific paths here as in other lineages.

Bacteroidetes

The distribution of TAACTGA repeats in the Bacteroidetes (**Figure 2C**) suggests they could also have more than one role in this group. *F. litoralis* DSM 6794 is similar to BOGUAY, on a more limited scale. Of 14 repeat sets, 12 are intergenic and in the "forward" orientation relative to a start codon between 1 and 43 nt downstream (Supplemental Table 5). One set of seven repeats is located immediately downstream of a stop codon, in reverse orientation, and a set of two is located within a putative PurC (SAICAR synthase) gene, near its end. In *Paludibacter propionicigenes* WB4 there are just two sets of direct repeats, one close to a start codon and the other toward the center of a long intergenic region (Supplemental Table 5).

The remaining three Bacteroidetes strains have different distributions. *Gramella forsetii* KT0803 and *A. sublithincola* DSM 14238 have only two sets of TAACTGA direct repeats each, but three of these are quite long (**Figure 2C**). All are intergenic and in "forward" orientation relative to the downstream ORF, but only one is immediately upstream of a start codon, and the intergenic regions contain other heptamer direct repeats as well (Supplemental Figure 3). For both *A. sublithincola* sets and one of the *G. forsetii* ones, the closest matches to the upstream and downstream ORFs are found in the same close relative (*A. capsosiphonis* DSM 23843 and *G. echinicola* DSM 19838, respectively), which have shorter intergenic regions without obvious sets of repeats, although the immediate gene neighborhoods appear the same (Supplemental Figure 3A). In the second *G. forsetii* example (Supplemental Figure 3B), at least the downstream ORF may have been acquired by horizontal transfer. The closest match to the upstream ORF is from the Bacteroidetes strain *Gillisia limnaea* DSM 15749, which has a similar local gene neighborhood, except that instead of a homolog of the downstream ORF there is a short hypothetical protein encoded on the opposite strand. No sets of direct repeats are evident in this intergenic region. Downstream, the closest match to the *G. forsetii* ORF is from *Bacillus azotoformans* LMG9581, which has no other apparent local similarity to *G. forsetii*. A phylogenetic reconstruction for this ORF and a comparison of intergenic regions in other *Gramella, Gillisia*, and *Bacillus* strains would be needed to propose a history for this small region, but the pattern so far suggests a role in gene rearrangement for these intergenic repeats.

E. anophelis NUHP1 has sets of TAACTGA repeats between only three pairs of ORFs, which are not very long (four sets of two, one set of four), but in two cases they are part of nearly identical intergenic regions containing larger assemblages of heptamer repeats and flanked by ORFs encoding putative proteins with stretches of high identity (Supplemental Table 6). Comparisons with closest neighbors (all *Elizabethkingia* strains) were difficult because the contigs identified often end partway through the repeat region, likely because of assembly difficulties. The third repeat set is a single pair, found toward the center of a relatively long (295 bp) intergenic region with no other obvious repeats.

Canonical Ribosome Binding Sites are Rare in Repeat-Containing BOGUAY Intergenic Regions

The TAACTGA repeats in the BOGUAY genome are generally positioned close to start codons (**Figure 1**), overlapping the expected ribosome binding site. The Shine-Dalgarno (SD) sequence predicted from the 16S rRNA genes of BOGUAY and other sequenced *Beggiatoaceae* is the same as that of *E. coli* (AGGAGGU). With only one G residue per heptamer in either orientation, the repeat sequence itself has little SD character, so most of the ORFs downstream of them have no obvious ribosome binding site. For an overview of the genome, any four consecutive bases from the AGGAGGU sequence ending 4–13 nt upstream of a start codon was considered an SD, recognizing that this may lead to over- or undercounting. The number of such sequences was estimated at 1346 (Supplemental Table 8), accounting for 25% of the 5272 predicted protein-coding genes. This is toward the low side for bacteria overall, but by no means unmatched (Ma et al., 2002). Of intergenic regions with repeats, just 15 (∼10%) also include SD sequences (**Table 4**), with the repeats ending between 2 and 25 bp upstream of them.

Functional Classification of BOGUAY ORFs Downstream of TAACTGA Repeats

The COG (Clusters of Orthologous Groups; Tatusov et al., 1997) classifications of ORFs with and without upstream repeats were compared (**Table 5**). Categories F, D, Q, E, and J were particularly overrepresented among those with repeats, while only category A was as strongly underrepresented. Note however that 63% of all ORFs and 29% of those with repeats have not been classified at all, and some 8% more of each are in categories R (general function prediction only) and S (function unknown). No clear picture of a possible transcriptional or translational regulatory role for TAACTGA repeats is apparent at this level, particularly since it is not known whether regulation is positive or negative. Several concentrations of repeat sequences will be considered in more detail below.

TAACTGA Repeats within Open Reading Frames

While most of the TAACTGA repeats in the BOGUAY genome are intergenic, suggesting a regulatory role, there are exceptions. The coding regions of 25 putative BOGUAY proteins contain or overlap 24 sets of direct repeats, with one set found in overlapping ORFs (BOGUAY_3048 and _3047). In 13 of these, between one partial and two complete repeats overlap the stop codon of an upstream gene in "forward" orientation relative to a downstream gene (**Table 2A**); as mentioned above, forward repeats generate stop codons in all three reading frames, so these are necessarily at the end of ORFs. In only two of these was a recognizable SD sequence found between the end of the repeats and the start codon of the downstream ORF. In three more ORFs, sets of repeats were found within or overlapping one end or the other of the putative coding sequence, but not directly upstream of another (**Table 2B**). One example was also found of an indirect repeat near the end of an ORF, with one base pair separating the two copies (**Table 2C**).

The 11 ORFs containing "reverse" repeats (**Table 2B**) have no apparent amino acid sequence similarity outside the repeat-encoded region (Supplemental Figure 1). Seven are short hypothetical or conserved-domain proteins with no assigned functions. One of these overlaps a putative glycosyl hydrolase (BOGUAY 01182_3048); the repeat-encoded amino acids in the latter are near the C-terminal end of the predicted protein, with little homology to otherwise close database relatives and outside the CDD-defined glycosyl hydrolase domain that includes most of the rest of the ORF (not shown). The repeat-encoded amino acids of two of the other ORFs with assigned functions are likewise outside regions of assigned function, either toward the very beginning (corrinoid ABC permease, BOGUAY 00106_0223) or very end (MurG, BOGUAY 00938_0721) of their respective amino acid sequences. The exception is BOGUAY 00100_0018, an ORF encoding a putative protein similar to an RNA polymerase beta prime subunit, discussed below.

If the repeats were or are mobile within the genome, their insertion within coding sequences seems to have been successful primarily at the periphery of at least the primary structure of proteins. For repeats in "forward" orientation, this is a necessary consequence of their sequence, which encodes stop codons in all three reading frames. "Reverse" repeats could in principle occur anywhere, but most insertions are likely deleterious. Those at the end of proteins, or perhaps splitting a protein into two new functional proteins, are probably more likely to become fixed.

Direct TAACTGA repeats are also found within hypothetical proteins in *Beggiatoa* sp. PS and some cyanobacteria, particularly *M. aeruginosa* strains. A BLASTP search of the GenBank protein database with 7, 14, or 21 LSVISYQ repeats yielded mostly predicted amino acid sequences annotated as hypothetical proteins. The shorter variant yielded the most perfect matches (Supplemental Table 9). The phylogenetic distribution of at least the top hits was quite restricted: 61 cyanobacterial sequences, of which 25 were from *M. aeruginosa* and 25 from *Moorea producens*; 17 Gammaproteobacterial sequences, of which 12 were from *Pseudoalteromonas* spp. and 2 from *Beggiatoaceae*; 9 from the Betaproteobacterium *Burkholderia pseudomallei*; 6 from Alphaproteobacteria, of which 4 were from *Ehrlichia ruminantium*; and one reportedly from a bird. Interestingly, one of these was annotated as an FdxN element excision controlling factor protein-like protein (BAG05441.1 from *M. aeruginosa* NIES-843). However, given the large number of these in the database, and the fact that it has no BLASTP matches from this group, this is suspected to be a misannotation. Similarly, the *B. pseudomallei* predicted protein (KGC53376) described as a putative 60S ribosomal protein L19 does not seem to actually belong to this group.

TAACTGA Repeats in Putative Ribosomal Protein Operons

One COG category overrepresented among BOGUAY ORFs preceded by repeats is J (Translation) with 13 examples, including four upstream of putative genes for ribosomal proteins (S1, L3, S4, and S21; **Figure 3**) and five others within putative

TABLE 4 | BOGUAY ORFs preceded by both Shine-Dalgarno sequences and TAACTGA repeats.

Upstream ORF	Repeat region sequence	Downstream ORF		Downstream COG category
hypothetical protein	(>100 bp to next ORF) TTTGTGATTAGTGATAAAGCAACCTTATTTTTAACTGATAACTGACAAAGGAACAATTTATATG	00031_3793	pfam14072 (DndB - DNA sulfur modification-associated)	none
conserved domain protein, ABC transporter type 1, transmembrane domain	(>100 bp to next ORF) TCGTTTTTCAGATTGTTGGTTTTAGACTCTGATAACTGATAACTGAACTAAGGAGAATTAAATTATTATG	00848_4300	V-type H(+)-translocating pyrophosphatase	C
beta propeller domain	(>100 bp to next ORF) TTTATGTATACCTAATTAAAACAACACTGATAACTGATAACTGAACAATAAGGTAAAATTTCCCAATATG	01124_0963	succinate dehydrogenase flavoprotein subunit	C
Inner membrane protein CreD	CATGTTAAATATTAAGTGAA~66nt~ACTGATAATTAATAACTGATAACTGATAAGGAGATTACACCTTCAATG	01192_0212	ribosomal protein S21	J
hypothetical protein	(>100 bp to next ORF) TATAAGGTAACTCAAATTTGACTGACAAATATTTTAACTGATAACTGATAATTCAAAAGGAATATAGGTG	00666_1840	amino acid carrier protein	E
phosphoglycerate kinase family protein	TAATTTAAAGATG~70nt~AAAGTTGACTGATAACTGATAACTGATAACTTAATAGGAAAATTTTATG	00163_1000	fructose-bisphosphate aldolase, class II, Calvin cycle subtype	G
3-oxoacyl-(acyl-carrier-protein) reductase	(>100 bp to next ORF) TTATTATGAATGAATAACTGATAACTGACAACTGATAAATGATAATTGAAAAGAGGAGCTAATTTGTTATG	00396_2179	acyl carrier protein	I, Q
regulatory protein, FmdB family	ATGCCTATT~273nt~AGTTCAAGCACTGATAACTGATAACTGAATAAGGAAAATTATG	00106_0256	aspartyl-tRNA synthetase	J
sulfite reductase, dissimilatory-type alpha subunit	TGAATTAACTGATAACTAATAACTAATAACTGATAACTGAATTAGGAGGTTATTTATG	01191_1510	sulfite reductase, dissimilatory-type beta subunit	C
response regulator receiver domain protein	TAATTATTGGCATTAATTAACTGATAACTGACAACACTTAACTGATAACTTAAAAGGATATGATG	00362_1734	response regulator receiver domain protein	none
septum site-determining protein MinC	TGATTAATGGTTAATAGTTAACTGATAACTGATAACTTAAAACAGAATAACTGATACAGGAAAGTATTTTG	00127_3142	septum site-determining protein MinD	D
glycogen~starch synthases, ADP-glucose type	TAGTTAGTGTTCAGTTATCAGTTAACTGATAACTGATAACTGAACACTGATAACAAGAGGTTATTTTATG	00241_1023	glycosyl hydrolase, family 57	none
hypothetical protein	TAGTCATCAGTCTTGTTAAATGACACTGATAACTGATAACTGATAACTGATAAAGGAAAACATACGTATG	01295_4360	hypothetical protein	none
acetyl-CoA carboxylase, biotin carboxyl carrier protein	TAATAATTTATTAGTTATCAGTTATCAGTCAAAAAAACCTAACTGATAACTGATAACTGATATAGAGGTTAAAGTACATG	00861_2920	acetyl-CoA carboxylase, biotin carboxylase subunit	I
hypothetical protein	ATGCCAGAT~111nt~AAAGTCATGATAACTGATAACTGATAACTGATATAGGAGTACACAAAAATG	00614_2860	roadblock/LC7 domain protein	R

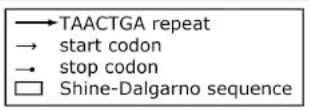

Shine-Dalgarno sequences are defined, here and throughout, as having 4 or more consecutive matches to the consensus sequence AGGAGGT. Entries are organized to highlight similar arrangements of SDs and repeats.

r-protein operons (*pnp*, *fusA*) or nearby (COG2976, *pheS*, BOGUAY_0218). Only one of these (S21, **Figure 3H**) also has a ribosome-binding site by the criteria used above. As described previously (MacGregor et al., 2013a), BOGUAY ribosomal protein genes are organized similarly to those in *E. coli* (see e.g., Fu et al., 2013 for an illustration) and many other bacteria. Where studied, these are transcribed as multigene operons, with translation generally regulated by a negative feedback loop involving one of the proteins encoded by the operon. Short noncoding RNAs transcribed within these operons may also play a role (Khayrullina et al., 2012). There is no experimental evidence regarding transcription of any BOGUAY genes, but it is worth noting that all TAACTGA repeats within BOGUAY r-protein operons are internal to the standard operons, suggesting a role in translational rather than transcriptional regulation. Insertion of a mobile element at such an internal site might also be favorable compared to insertion in a promoter region for these highly expressed operons, although given the essential role of ribosomes any insertion at all seems potentially disruptive.

This distribution has some overlap with the other *Beggiatoaceae* "T. nelsonii" and *T. ingrica*. In particular, all three species have TAACTGA repeats upstream of their putative S1 subunit genes (Supplemental Figure 2): BOGUAY has 5, beginning 1 nt upstream; "T. nelsonii" has three copies but with gaps between them, also beginning 1 nt upstream; and *T. ingrica* has 2 copies, beginning 21 nt upstream. The sequence of this gap is nearly identical (18 of 21 nt) to the *B. alba* sequence over this stretch; *B. alba* of course has no repeats. This shared sequence does not include a ribosome-binding site, by the definition used here, but does have an AGGG and an AGGGG run.

Three of the four putative BOGUAY r-protein genes preceded by repeats (S1, S4, and L3) are also among those with proposed extraribosomal functions in *E. coli* (reviewed in Aseev and Boni, 2011). During translation, S1 is involved in ribosome docking and in unfolding of structured mRNAs (Duval et al., 2013), interacting with AT-rich regions upstream of the SD sequence (if there is one), as well as with downstream sequences (Tzareva et al., 1994). In *E. coli*, S1 is required for translation of all mRNAs with leader sequences (reviewed in Hajnsdorf and Boni, 2012), while leaderless mRNAs can be translated by ribosomes lacking it (reviewed in Byrgazov et al., 2013). Like several other ribosomal proteins, it inhibits translation of its own operon: at least *in vitro*, free S1 competes with ribosome-bound S1 for mRNA binding upstream of the start codon (Boni et al., 2001). Again *in vitro*,

TABLE 5 | COG classification of BOGUAY ORFs downstream of TAACTGA repeats compared to whole genome.

COG category		Number of ORFs downstream of repeats	% of ORFs downstream of repeats	% of all ORFs	Fold difference (%repeats/%total)
OVERREPRESENTED DOWNSTREAM OF TAACTGA REPEATS					
F	Nucleotide metabolism and transport	6.5	4.55	0.82	5.6
D	Cell cycle control and mitosis	3	2.60	0.62	4.2
Q	Secondary metabolites	1.8	1.95	0.47	4.1
E	Amino acid metabolism and transport	12.5	9.09	2.36	3.9
J	Translation	13	8.44	2.39	3.5
H	Coenzyme metabolism	7.5	5.19	1.78	2.9
I	Lipid metabolism	2.8	1.95	0.80	2.4
O	Post-translational modification, protein turnover, chaperone functions	7	4.55	1.94	2.3
G	Carbohydrate metabolism and transport	4	2.60	1.16	2.2
M	Cell wall/membrane/envelope biogenesis	7	5.84	3.12	1.9
T	Signal transduction	7	4.55	2.48	1.8
C	Energy production and conversion	6.5	4.55	2.85	1.6
V	Defense mechanisms	1	0.65	0.45	1.4
K	Transcription	1.5	1.30	1.23	1.1
UNDERREPRESENTED					
U	Intracellular trafficking and secretion	2	1.30	1.49	0.9
L	Replication and repair	1.5	1.30	1.69	0.8
N	Cell motility	0.5	0.65	1.16	0.6
P	Inorganic ion transport and metabolism	1	0.65	1.83	0.4
A	RNA processing and modification	0	0.00	0.04	0.0
UNCATEGORIZED					
R	General functional prediction only	6.8	4.55	4.28	1.1
S	Function unknown	8	4.55	3.91	1.2
None assigned		46	29.22	63.16	0.5
TOTAL		147	100.00	100.00	

Fractional occurrences were used for ORFs assigned to more than one category.

it is reported to have a transcriptional role as well: *E. coli* S1 co-purifies with RNAP and stimulates transcriptional cycling (Sukhodolets et al., 2006).

The *E. coli* S4 ribosomal protein, in addition to negatively regulating translation of its own operon, is proposed to form part of transcriptional antitermination complexes that may also include L1, L3, and L4 (Torres et al., 2001), with S4 binding RNAP directly.

Candidate Repeat-Binding Proteins

The frequent position of the TAACTGA repeats upstream of and apparently replacing SD sequences, including five direct repeats directly upstream of the S1 gene (**Figure 3**), suggests that they might play a role in translation. Several categories of known translational regulatory proteins have properties that suggest them as candidates.

Ribosomal Protein S1

Interaction with the S1 subunit is one possibility. S1 has a relatively weak and reversible association with the ribosome, and is added last in assembly (Subramanian and Vanduin, 1977). In *E. coli* and many other Gram negative bacteria, it is composed of six linked oligonucleotide/oligosaccharide binding (OB)-fold domains; where studied, the four C-terminal domains are RNA-binding, while the two N-terminal domains make protein-protein contacts with ribosomal, and other proteins (reviewed in Hajnsdorf and Boni, 2012). The BOGUAY S1 protein is predicted to have a typical Gram negative S1 structure (not shown).

The *E. coli* S1 gene itself (*rpsA*) lacks a strong SD sequence and does not require one for expression (Boni et al., 2001). The upstream region forms three hairpins, which contribute to its translational efficiency (Boni et al., 2001; Skorski et al., 2006). Different secondary structures can be predicted for the intergenic region upstream of the BOGUAY S1 gene, depending how much of this and the coding sequence are included in the calculation (not shown), but they have no obvious similarity to those in *E. coli*. Without experimental evidence, or knowledge of the transcriptional start site, they cannot be assigned a function. One argument against a TAACTGA-binding role for S1 is the reported non-specificity of S1 RNA recognition, limited to a preference for AT-rich sequences (reviewed in Aseev and Boni, 2011). TAACTGA repeats are somewhat AT rich, but do not produce long polypyrimidine tracts.

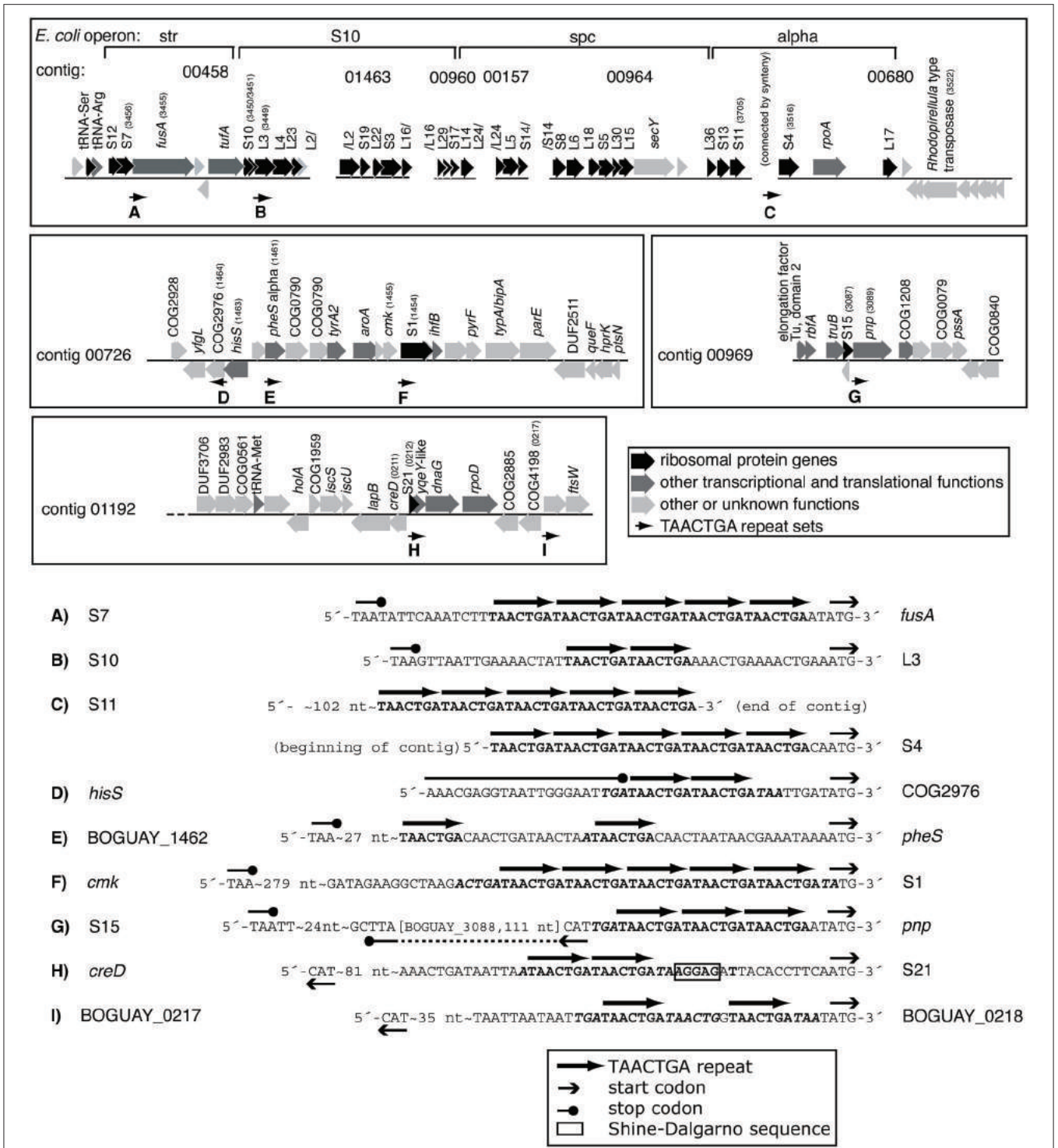

FIGURE 3 | TAACTGA repeats in and near putative BOGUAY ribosomal protein operons. Repeats are found upstream of putative genes for **(A)** *fusA* (elongation factor G); **(B)** ribosomal protein L3; **(C)** ribosomal protein S4; **(D)** a COG2976 protein; **(E)** *pheS* (phenylalanine-tRNA ligase, alpha subunit); **(F)** ribosomal protein S1; **(G)** *pnp* (polynucleotide phosphorylase); **(H)** ribosomal protein S1; and **(I)** ORF BOGUAY_0218.

Cold Shock Proteins

As a second possibility, the cold shock proteins (CSPs; since shown to include proteins with other roles) are OB-fold proteins with a single S1-like domain that can bind single-stranded RNA or DNA. Intriguingly, X-ray crystallography (Sachs et al., 2012) and microarray binding (Morgan et al., 2007) studies of *Bacillus subtilis* CspB have shown that it can bind heptamer direct repeats (reviewed in Horn et al., 2007), with one protein per heptamer,

although only weak sequence specificity (e.g., stronger binding to TTCTTTT than TTTTTT) has been demonstrated. During cold shock, CSPs bind both non-specifically to general RNA and specifically to the 5′ untranslated region of selected mRNAs; this selection has been proposed to rely more on secondary structure than primary sequence (Giuliodori et al., 2004), but limited work has been done on this question. It seems conceivable that some Csp-like proteins might bind in a sequence-specific manner.

There are several putative proteins with cold shock domains in the BOGUAY genome (Supplemental Table 10). Two include just a single cold shock domain, and are annotated as CspA and CspE; two have a downstream Excalibur calcium-binding domain; and one has a downstream DUF1264 domain. According to a CDD (Marchler-Bauer et al., 2011) search, the CSP-Excalibur architecture is found in 301 other proteins in the GenBank nr protein database, of which 298 are Proteobacterial; 256 of these are Gammaproteobacterial. Similarly, the CDS-DUF1264 architecture is found in 801 nr sequences, of which 766 are Proteobacterial and 614 Gammaproteobacterial. Cyanobacteria were the next largest group, but with just 13 examples. It is not uncommon for a single Gammaproteobacterial genome to encode more than one CSP domain protein (not shown).

PSORTb 3.0 (Yu et al., 2010) predicts the putative BOGUAY CspA and CspE to be cytoplasmic, by similarity to known proteins (Supplemental Table 10). The CSP-DUF1264 protein is predicted to possess four internal helices and be a cytoplasmic membrane protein, making it an unlikely translational regulatory protein. No prediction could be made for the two CSP-Excalibur putative proteins (while the name stands for "extracellular calcium-binding region," this is due to the proteins the domain was originally identified in Rigden et al. (2003); other proteins containing it may or may not be extracellular). At least two (the putative CspA and CspE) and possibly four of these CSP-like proteins are therefore candidates for TAACTGA binding. While so-called cold-shock domain proteins need not respond to temperature, temperature is likely an important environmental clue in the Guaymas Basin microbial mats, signaling the intensity of the hydrothermal flow that supplies sulfide to the sulfide-oxidizing BOGUAY strain and its relatives.

CsrA-Like Proteins

As a third possibility, CsrA (*E. coli* carbon storage regulatory protein) and related proteins bind to single-stranded RNA, in some cases inhibiting translation by competing with ribosomes for binding to Shine-Dalgarno sequences. They play a role in processes including motility, biofilm formation, quorum sensing, and virulence in a wide range of bacteria (reviewed in Romeo et al., 2013; Van Assche et al., 2015). The BOGUAY genome contains a *csrA* candidate (BOGUAY 00153_2343) with a strong possible SD site (AGGAG, 7 nt from the start codon), consistent with the autoregulation often found for these genes (Romeo et al., 2013). However, the known RNA binding sites for CsrA proteins, whether on target RNAs or on regulatory small RNAs, are centered on SD-like GGA motifs with more than 7 nt spacing (reviewed in Duss et al., 2014). These are not found in TAACTGA repeats in either orientation, making these unlikely to be recognized by a canonical CsrA.

Possible Secondary or Repurposed RNA Polymerase Beta Prime Subunits in BOGUAY and *Thioploca Ingrica*

The BOGUAY genome encodes two putative RNAP β′ subunits (MacGregor et al., 2013c), an unusual feature also found in the recently sequenced *T. ingrica* genome, but not in *B. alba*. The partial "Isobeggiatoa" PS sequence includes only one. The *Cand.* "Thiomargarita nelsonii" genome is annotated with two (OT06_22820, OT06_51635), each on short contigs with no surrounding ORFs, but their sequences are identical except that OT06_51635 is missing 214 C-terminal amino acids where its contig ends; if this is in fact a duplication, it would seem to be a fairly recent one. Of 100 top BLASTP hits to BOGUAY 00100_0018, the alternate beta prime gene, only one intraspecific pair of beta prime genes was found. *Nitrosococcus watsonii* C-113 has an apparent tandem duplication of its beta (Nwat_2177, Nwat_2165) and beta prime (Nwat_2176, Nwat_2164) genes along with surrounding ribosomal protein and other translation-related genes. The two putative beta prime subunit genes are 100% identical at the nucleotide level; again, if this is a duplication, it appears recent.

BOGUAY and *T. ingrica*, by contrast, each have two different beta prime-like genes (**Figure 4**). One of these (BOGUAY_3638, THII_2732) appears to include all the expected catalytic and subunit-interaction sites of a bacterial beta prime subunit, and is very similar to the single "Isobeggiatoa" PS sequence (BGP_5131). The other (BOGUAY_0018, THII_0330) has the N-terminal subunit interaction and DNA-binding sites expected for an RNA polymerase beta prime subunit, but the *T. ingrica* sequence has several active-site substitutions, and neither has a complete catalytic site D–D–D sequence. The N-terminal domains resemble other beta prime sequences, but the C-terminal domains differ from each other and their genomic partners in the variable S13 region. The BOGUAY ORF has three TAACTGA units in forward orientation just upstream of its start codon, interleaved with two TTACTGA sequences, and three in reverse orientation within the ORF, one direct TCAGTTA repeat and a third unit separated by the related 7-mer TCAATTA (**Figure 6A**, below). These encode the amino acid sequence LSVINYQLS and fall within a variable region of the predicted beta prime N-terminal domain (**Figure 4**), which in the *E. coli* crystal structure is in a surface loop near the alpha II subunit (Murakami, 2013).

The genomic context of the BOGUAY beta prime is unusual. Of the four *Beggiatoaceae* beta prime genes for which some surrounding sequence is available (**Figure 5A**), all but BOGUAY have beta and beta prime genes immediately adjacent, as do many if not most other bacteria (Dandekar et al., 1998). Upstream of the putative beta subunit gene, BOGUAY, *T. ingrica*, and *B. alba* each have a NusG and four ribosomal protein genes; the "Isobeggiatoa" PS contig does not extend upstream. Downstream, the BOGUAY beta and beta prime subunit genes have apparently become separated, being internal to separate contigs. Comparing the beta/beta prime intergenic regions in the other three species,

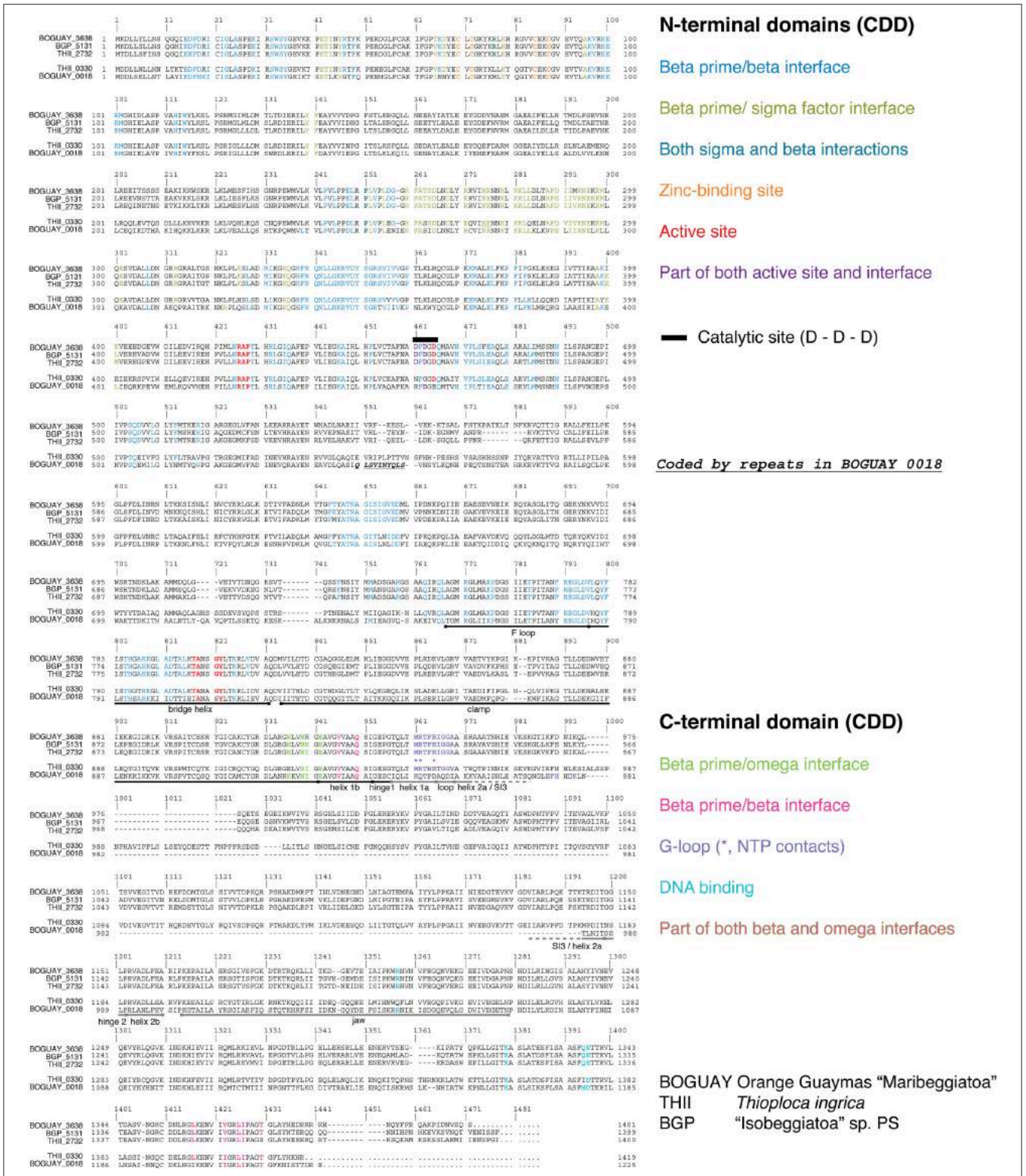

FIGURE 4 | Alignment of RNA polymerase beta prime and beta-prime like sequences from the BOGUAY, "Isobeggiatoa" PS, and *Thioploca ingrica* genomes. Sequences were aligned in MEGA5.2.2 (Tamura et al., 2011) using Muscle (Edgar, 2004). Trigger loop and SI3 annotation are after Windgassen et al. (2014), F loop and bridge loop annotation after Miropolskaya et al. (2014), jaw annotation after Opalka et al. (2010), and clamp annotation after Davis et al. (2007). Other putative domains were identified in CDD (Conserved Domain Database; Marchler-Bauer et al., 2011). Active-site and G-loop regions are boxed, and details of these shown to the right of the complete alignment.

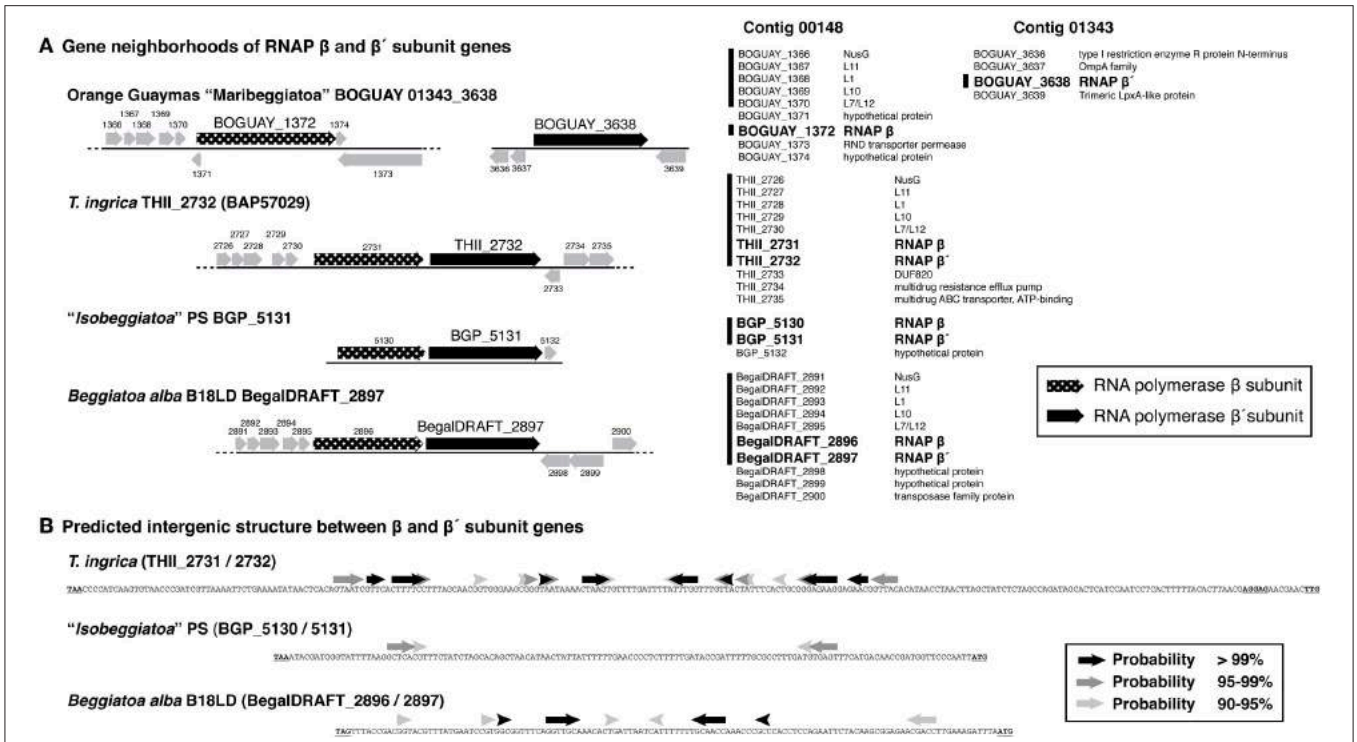

FIGURE 5 | Gene neighborhoods and intergenic sequence for putative RNA polymerase beta and beta prime subunit genes from *Beggiatoaceae* genome sequences. (A) Gene neighborhoods are shown as cartoons (left) and lists (right). Vertical lines alongside lists indicate ORF sequences common to at least three species (the "Isobeggiatoa" PS genome is very partial). RNA polymerase subunit genes are in bold. **(B)** Predicted stem-loop structures in the beta/beta prime intergenic region are the first results from a minimum free energy calculation using the default settings of the MaxExpect algorithm from the RNAstructure Web Server (http://rna.urmc.rochester.edu/RNAstructureWeb/, Reuter and Mathews, 2010), with arrows shaded by the probability of the interaction.

that in *T. ingrica* is longer (338 nt) than those in *B. alba* and BGP (126 and 133 nt, respectively). It also includes a stronger potential stem-loop structure (**Figure 5B**), possibly a transcriptional terminator. One scenario is that the two genes became transcriptionally uncoupled in a common ancestor of *T. ingrica* and the BOGUAY strain, making the intergenic region a viable site for genomic rearrangements and introduction (by whatever mechanism) of TAACTGA repeats. If the putative beta prime variants are in fact expressed, perhaps the separation of beta and beta prime allows the levels of the three proteins to be separately regulated.

Predicted Sensor Proteins are Immediately Downstream of the Putative Secondary Beta Prime Subunit Genes

Each of the variant beta prime genes is immediately followed by a predicted hybrid sensor kinase gene (**Figure 6**). These have nearly identical structures according to the Conserved Domain Database (CDD; Marchler-Bauer et al., 2011): a GAF-superfamily domain, four PAS domains, a histidine kinase, three REC domains, and an HPT domain. GAF domains, which include those in FhlA (formate hydrogen lyase transcriptional activator)-family proteins, bind and respond to cyclic-nucleotide second messengers (Aravind and Ponting, 1997). PAS domains are intracellular or periplasmic redox sensors responsive to various stimuli, including light and oxygen, with specificity determined partly by small-molecule cofactors such as a heme or flavin (Taylor and Zhulin, 1999; Kneuper et al., 2010). HisKA-HATPase_c (histidine kinase A—histidine-kinase-like ATPase) domains respond to sensor inputs by autophosphorylating on a histidine residue, which in turn typically phosphorylates a response regulator (REC) domain aspartate residue (Stock et al., 2000), changing its conformation and, for example, promoting dimerization and DNA binding. HPt (histidine-containing phosphotransfer) domains transfer phosphate groups to other proteins along phosphorylation cascades (Matsushika and Mizuno, 1998). Both the BOGUAY and *T. ingrica* putative sensor proteins are strongly predicted by PSORTb (Yu et al., 2010) to be inner-membrane proteins, by comparison with *E. coli* BarA, which was localized in a membrane proteomic survey (Daley et al., 2005). As is usual with the highly modular sensor proteins, neither has any other full-length matches in current databases, although each of the subdomains does. There is not yet enough known about sensor proteins to predict what stimuli these might respond to, or what their upstream and downstream interaction partners might be, but it can be hypothesized that they sense a condition in the periplasm and transmit that information to cytoplasmic elements via a phosphorylation cascade, which may directly or indirectly contact the variant beta prime.

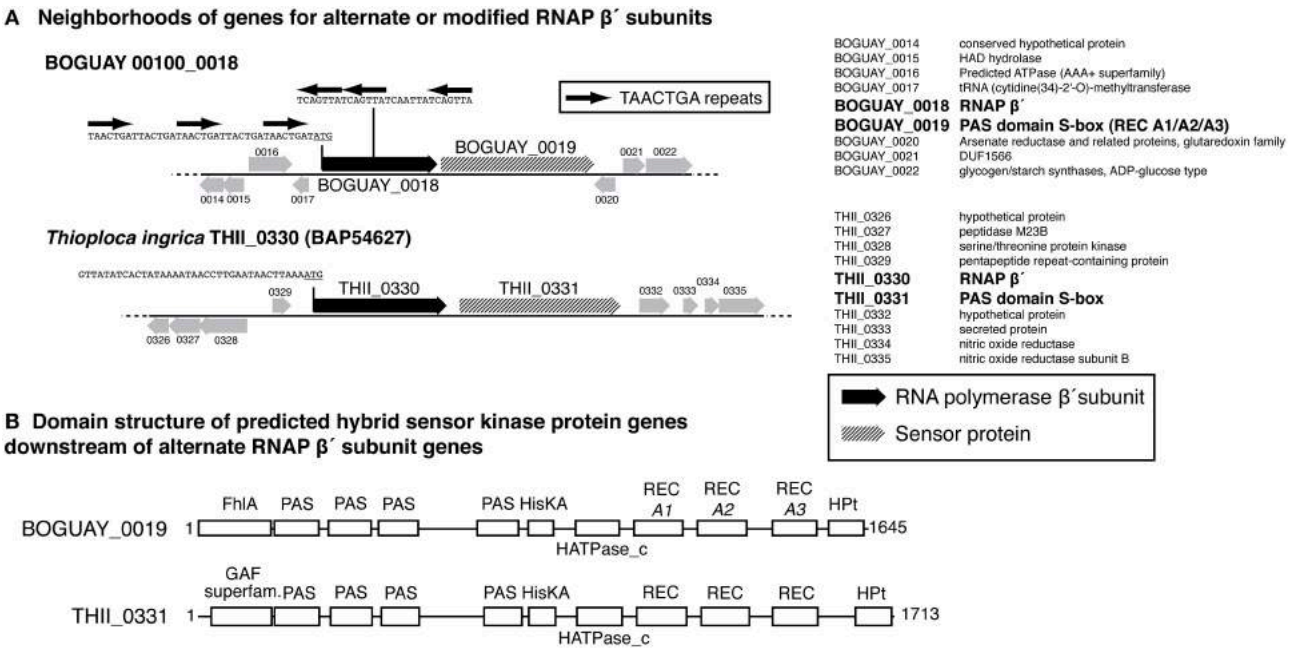

FIGURE 6 | (A) Gene neighborhoods for putative alternate RNA polymerase beta prime subunit genes from the BOGUAY and *Thioploca ingrica* genome sequences. Gene neighborhoods are shown as cartoons (left) and lists (right). Positions of TAACTGA repeats within and upstream of BOGUAY 00100_0018 are indicated; the corresponding upstream sequence from *T. ingrica,* which has no repeats in this region, is included for comparison. **(B)** Predicted domain structures of putative downstream sensor proteins. Domains were identified in CDD (Marchler-Bauer et al., 2011).

SUMMARY AND PERSPECTIVES

TAACTGA Repeats May Play Different Roles in Different Species

The draft genomes of Orange Guaymas "Maribeggiatoa" (BOGUAY) and *Cand.* "Thiomargarita nelsonii," and to a lesser extent *T. ingrica*, contain an unusually high number of TAACTGA direct repeats, while close relative *B. alba* and apparently all but one other sequenced Gammaproteobacterium (*T. violascens*, also a sulfur oxidizer) have none at all. TAACTGA direct repeats were also found in Cyanobacteria, especially in species known for harboring long repetitive arrays, and in a few Bacteroidetes. This is consistent with earlier evidence for genetic exchange among these groups (MacGregor et al., 2013c), particularly the Cyanobacteria and some *Beggiatoaceae*, although no exchange mechanism is obvious as yet. Once introduced into a genome, whether by exchange or mutation, the tolerated sites and orientations for repeats will be determined by sequence characteristics such as length, coding potential, and propensity to form secondary structures, and by their interaction with existing cellular machinery. For the BOGUAY intergenic TAACTGA repeats, a plausible scenario is that they were recognized by an existing nucleic acid-binding protein—perhaps a ribosomal subunit, perhaps a protein that interacts with these—and over time a regulatory network evolved by selection for individuals with favorable protein interaction(s) and combinations of insertions. The original introduction may have happened in the common ancestor of a branch of the *Beggiatoaceae*, with different networks evolving (or not) in each subsequent lineage. The very long arrays in species such as *M. aeruginosa* and *G. forsetii* suggest a role in genome rearrangement may have evolved in these. Acquisition of additional genome sequences for the *Beggiatoaceae* may help illuminate this history.

Another possibility is that a TAACTGA-binding protein is the mobile element. On entering a new species, it could interact with pre-existing "good-enough" RNA or DNA sequences, with closer matches and useful locations evolving over time. Identification of repeat-binding protein(s) in the BOGUAY genome and evaluation of their inferred phylogeny and gene neighborhoods in other species could help in evaluating this model.

TAACTGA Repeats May Play a Role in Translational Regulation in the BOGUAY Strain

In the BOGUAY genome, most of the TAACTGA repeats are in "forward" orientation immediately upstream of putative start codons and overlapping the expected ribosome-binding site, suggesting that they may have taken on a role in translational regulation in this species. Genes and ORFs lacking recognizable Shine-Dalgarno sequences are prevalent in BOGUAY and many other bacterial genomes (Ma et al., 2002), including such highly expressed genes as the *E. coli* ribosomal protein S1 gene (*rpsA*; Aseev and Boni, 2011); in BOGUAY, only a small proportion of these are preceded by TAACTGA repeats. Possibilities for the translational role of the BOGUAY repeats, not all mutually exclusive, include:

a) Canonical BOGUAY ribosomes are able to bind efficiently enough to the repeats for production of even highly translated proteins, despite the absence of sequence complementary to the 16S rRNA.
b) Ribosomes with different subunit compositions—in particular, those lacking S1—may have different binding sites, as already recognized for leaderless mRNAs; this could include TAACTGA repeats.
c) Repeats may be recognized by some other RNA-binding protein (e.g., a Csp-like one), which then recruits ribosomes.
d) Repeats are irrelevant, these genes are translated like leaderless mRNAs by ribosomes lacking S1.

Possible Function of Second RNA Polymerase Beta Prime Subunit-Like Proteins in BOGUAY and *Thioploca Ingrica*

Another unusual feature of the BOGUAY genome is a second RNA polymerase beta prime-like ORF, also found in *T. ingrica*, and immediately upstream of multisensor kinases in both. In BOGUAY, this putative alternate or modified gene is both preceded by and contains TAACTGA repeats. The BOGUAY genome has the additional peculiarity that the beta and "normal" beta prime genes are not adjacent, but rather internal to separate contigs. Assuming the beta prime-like gene is expressed, one possibility is that it associates with other RNA polymerase subunits, forming either a functional or a non-functional complex: the absence of key catalytic residues suggests it would be non-functional, but this would need experimental testing. This is somewhat supported by the physical separation of the beta and beta prime genes in BOGUAY, and their possible transcriptional separation in *T. ingrica*: if two proteins are competing for the beta prime role, it may be beneficial to regulate their production separately from that of their common partners. In BOGUAY, the TAACTGA repeats upstream of the beta prime-like ORF suggest that it may be part of their putative global regulatory network.

Perspectives

Experimental tests of these ideas will be challenging in an uncultivated, difficult to collect species. Some basic questions may be answerable by transcriptomic analysis of samples collected from different Guaymas Basin sites and/or preincubated under different conditions (temperature, oxygen, sulfide). Are ORFs preceded by repeats up- and downregulated in concert? Is the second beta-prime like ORF transcribed, and if so, under what conditions? How does its expression pattern compare with that of other RNA polymerase subunit genes? There are also indications from the partial "Isobeggiatoa" genome sequences that the more accessible Baltic Sea *Beggiatoaceae* may have similar repeat distributions. *In vitro* identification of repeat-binding proteins might be possible from total mat protein preparations, or by heterologous expression and isolation of cloned (or synthesized) genes for candidate proteins.

FUNDING

The Guaymas Basin project was funded by NSF OCE 0647633. Genome sequencing was performed by the J. Craig Venter Institute, with funding from The Gordon and Betty Moore Foundation Marine Microbial Genome Sequencing Project. The use of RAST was supported in part by the National Institute of Allergy and Infectious Diseases, National Institutes of Health, Department of Health and Human Services (NIAD) under contract HHSN266200400042C.

ACKNOWLEDGMENTS

Thanks to the captain and crews of R/V *Atlantis* and HOV *Alvin* for two enjoyable cruises to Guaymas Basin, and to Drs. Alecia Septer and Lisa Nigro for helpful comments on the manuscript. Genome comparisons were carried out in IMG/ER (https://img.jgi.doe.gov/cgi-bin/er/main.cgi).

SUPPLEMENTARY MATERIAL

The Supplementary Material for this article can be found online at: http://journal.frontiersin.org/article/10.3389/fmicb.2015.01397

REFERENCES

Aravind, L., and Ponting, C. P. (1997). The GAF domain: an evolutionary link between diverse phototransducing proteins. *Trends Biochem. Sci.* 22, 458–459. doi: 10.1016/S0968-0004(97)01148-1

Artimo, P., Jonnalagedda, M., Arnold, K., Baratin, D., Csardi, G., De Castro, E., et al. (2012). ExPASy: SIB bioinformatics resource portal. *Nucleic Acids Res.* 40, W597–W603. doi: 10.1093/nar/gks400

Aseev, L. V., and Boni, I. V. (2011). Extraribosomal functions of bacterial ribosomal proteins. *Mol. Biol.* 45, 739–750. doi: 10.1134/S0026893311050025

Attia, A. S., and Hansen, E. J. (2006). A conserved tetranucleotide repeat is necessary for wild-type expression of the *Moraxella catarrhalis* UspA2 protein. *J. Bacteriol.* 188, 7840–7852. doi: 10.1128/JB.01204-06

Aziz, R. K., Bartels, D., Best, A. A., Dejongh, M., Disz, T., Edwards, R. A., et al. (2008). The RAST Server: rapid annotations using subsystems technology. *BMC Genomics* 9:75. doi: 10.1186/1471-2164-9-75

Boni, I. V., Artamonova, V. S., Tzareva, N. V., and Dreyfus, M. (2001). Non-canonical mechanism for translational control in bacteria: synthesis of ribosomal protein S1. *EMBO J.* 20, 4222–4232. doi: 10.1093/emboj/20.15.4222

Bornberg-Bauer, E., Rivals, E., and Vingron, M. (1998). Computational approaches to identify leucine zippers. *Nucleic Acids Res.* 26, 2740–2746. doi: 10.1093/nar/26.11.2740

Bowman, J. P., and Nichols, D. S. (2002). Aequorivita gen. nov., a member of the family Flavobacteriaceae isolated from terrestrial and marine Antarctic habitats. *Int. J. Syst. Evol. Microbiol.* 52, 1533–1541. doi: 10.1099/00207713-52-5-1533

Byrgazov, K., Vesper, O., and Moll, I. (2013). Ribosome heterogeneity: another level of complexity in bacterial translation regulation. *Curr. Opin. Microbiol.* 16, 133–139. doi: 10.1016/j.mib.2013.01.009

Daley, D. O., Rapp, M., Granseth, E., Melén, K., Drew, D., and Von Heijne, G. (2005). Global topology analysis of the *Escherichia coli* inner membrane proteome. *Science* 308, 1321–1323. doi: 10.1126/science.1109730

Dandekar, T., Snel, B., Huynen, M., and Bork, P. (1998). Conservation of gene order: a fingerprint of proteins that physically interact. *Trends Biochem. Sci.* 23, 324–328. doi: 10.1016/S0968-0004(98)01274-2

Davis, C. A., Bingman, C. A., Landick, R., Record, M. T., and Saecker, R. M. (2007). Real-time footprinting of DNA in the first kinetically significant intermediate in open complex formation by *Escherichia coli* RNA polymerase. *Proc. Natl. Acad. Sci. U.S.A.* 104, 7833–7838. doi: 10.1073/pnas.0609888104

Duss, O., Michel, E., Konté, N. D. D., Schubert, M., and Allain, F. H. T. (2014). Molecular basis for the wide range of affinity found in Csr/Rsm protein-RNA recognition. *Nucleic Acids Res.* 42, 5332–5346. doi: 10.1093/nar/gku141

Duval, M., Korepanov, A., Fuchsbauer, O., Fechter, P., Haller, A., Fabbretti, A., et al. (2013). *Escherichia coli* ribosomal protein S1 unfolds structured mRNAs onto the ribosome for active translation initiation. *PLoS Biol.* 11:e1001731. doi: 10.1371/journal.pbio.1001731

Edgar, R. C. (2004). MUSCLE: multiple sequence alignment with high accuracy and high throughput. *Nucleic Acids Res.* 32, 1792–1797. doi: 10.1093/nar/gkh340

Foster, T. J., Lundblad, V., Hanley-Way, S., Halling, S. M., and Kleckner, N. (1981). Three Tn10-associated excision events: relationship to transposition and role of direct and inverted repeats. *Cell* 23, 215–227. doi: 10.1016/0092-8674(81)90286-5

Frangeul, L., Quillardet, P., Castets, A. M., Humbert, J. F., Matthijs, H. C. P., Cortez, D., et al. (2008). Highly plastic genome of *Microcystis aeruginosa* PCC 7806, a ubiquitous toxic freshwater cyanobacterium. *BMC Genomics* 9:274. doi: 10.1186/1471-2164-9-274

Fu, Y., Deiorio-Haggar, K., Anthony, J., and Meyer, M. M. (2013). Most RNAs regulating ribosomal protein biosynthesis in *Escherichia coli* are narrowly distributed to Gammaproteobacteria. *Nucleic Acids Res.* 41, 3491–3503. doi: 10.1093/nar/gkt055

Giuliodori, A. M., Brandi, A., Gualerzi, C. O., and Pon, C. L. (2004). Preferential translation of cold-shock mRNAs during cold adaptation. *RNA* 10, 265–276. doi: 10.1261/rna.5164904

Guo, X., and Mrázek, J. (2008). Long simple sequence repeats in host-adapted pathogens localize near genes encoding antigens, housekeeping genes, and pseudogenes. *J. Mol. Evol.* 67, 497–509. doi: 10.1007/s00239-008-9166-5

Gur-Arie, R., Cohen, C. J., Eitan, Y., Shelef, L., Hallerman, E. M., and Kashi, Y. (2000). Simple sequence repeats in *Escherichia coli*: abundance, distribution, composition, and polymorphism. *Genome Res.* 10, 62–71. doi: 10.1101/gr.10.1.62

Hajnsdorf, E., and Boni, I. V. (2012). Multiple activities of RNA-binding proteins S1 and Hfq. *Biochimie* 94, 1544–1553. doi: 10.1016/j.biochi.2012.02.010

Horn, G., Hofweber, R., Kremer, W., and Kalbitzer, H. R. (2007). Structure and function of bacterial cold shock proteins. *Cell. Mol. Life Sci.* 64, 1457–1470. doi: 10.1007/s00018-007-6388-4

Humbert, J. F., Barbe, V., Latifi, A., Gugger, M., Calteau, A., Coursin, T., et al. (2013). A tribute to disorder in the genome of the bloom-forming freshwater cyanobacterium *Microcystis aeruginosa*. *PLoS ONE* 8:e70747. doi: 10.1371/journal.pone.0070747

Jannasch, H. W., Nelson, D. C., and Wirsen, C. O. (1989). Massive natural occurrence of unusually large bacteria (*Beggiatoa* sp.) at a hydrothermal deep-sea vent site. *Nature* 342, 834–836. doi: 10.1038/342834a0

Kämpfer, P., Matthews, H., Glaeser, S. P., Martin, K., Lodders, N., and Faye, I. (2011). *Elizabethkingia anophelis* sp. nov., isolated from the midgut of the mosquito Anopheles gambiae. *Int. J. Syst. Evol. Microbiol.* 61, 2670–2675. doi: 10.1099/ijs.0.026393-0

Kaneko, T., Nakajima, N., Okamoto, S., Suzuki, I., Tanabe, Y., Tamaoki, M., et al. (2007). Complete genomic structure of the bloom-forming toxic cyanobacterium *Microcystis aeruginosa* NIES-843. *DNA Res.* 14, 247–256. doi: 10.1093/dnares/dsm026

Khayrullina, G. A., Raabe, C. A., Hoe, C. H., Becker, K., Reinhardt, R., Tang, T. H., et al. (2012). Transcription analysis and small non-protein coding RNAs associated with bacterial ribosomal protein operons. *Curr. Med. Chem.* 19, 5187–5198. doi: 10.2174/092986712803530485

Kneuper, H., Scheu, P. D., Etzkorn, M., Sevvana, M., Dünnwald, P., Becker, S., et al. (2010). "Sensing ligands by periplasmic sensing histidine kinases with sensory PAS domains," in *Sensory Mechanisms in Bacteria: Molecular Aspects of Signal Recognition,* eds S. Spiro and R. Dixon. (Norfolk, UK: Caister Academic Press), 39–59.

Kojima, H., Ogura, Y., Yamamoto, N., Togashi, T., Mori, H., Watanabe, T., et al. (2015). Ecophysiology of Thioploca ingrica as revealed by the complete genome sequence supplemented with proteomic evidence. *ISME J.* 9, 1166–1176. doi: 10.1038/ismej.2014.209

Lafontaine, E. R., Wagner, N. J., and Hansen, E. J. (2001). Expression of the *Moraxella catarrhalis* UspA1 protein undergoes phase variation and is regulated at the transcriptional level. *J. Bacteriol.* 183, 1540–1551. doi: 10.1128/JB.183.5.1540-1551.2001

Lovett, S. T. (2004). Encoded errors: mutations and rearrangements mediated by misalignment at repetitive DNA sequences. *Mol. Microbiol.* 52, 1243–1253. doi: 10.1111/j.1365-2958.2004.04076.x

Ma, J., Campbell, A., and Karlin, S. (2002). Correlations between Shine-Dalgarno sequences and gene features such as predicted expression levels and operon structures. *J. Bacteriol.* 184, 5733–5745. doi: 10.1128/JB.184.20.5733-5745.2002

MacGregor, B. J., Biddle, J. F., Harbort, C., Matthysse, A. G., and Teske, A. (2013a). Sulfide oxidation, nitrate respiration, carbon acquisition, and electron transport pathways suggested by the draft genome of a single orange Guaymas Basin *Beggiatoa* (*Cand. Maribeggiatoa)* sp. filament. *Mar. Genomics* 11, 53–65. doi: 10.1016/j.margen.2013.08.001

MacGregor, B. J., Biddle, J. F., Siebert, J. R., Staunton, E., Hegg, E. L., Matthysse, A. G., et al. (2013b). Why orange Guaymas Basin *Beggiatoa* (*Maribeggiatoa*) spp. are orange: single-filament genome-enabled identification of an abundant octaheme cytochrome with hydroxylamine oxidase, hydrazine oxidase, and nitrite reductase activities. *Appl. Environ. Microbiol.* 79, 1183–1190. doi: 10.1128/AEM.02538-12

MacGregor, B. J., Biddle, J. F., and Teske, A. (2013c). Mobile elements in a single-filament orange Guaymas Basin *Beggiatoa* (*Maribeggiatoa*) sp. draft genome: evidence for genetic exchange with cyanobacteria. *Appl. Environ. Microbiol.* 79, 3974–3985. doi: 10.1128/AEM.03821-12

Marchler-Bauer, A., Lu, S., Anderson, J. B., Chitsaz, F., Derbyshire, M. K., DeWeese-Scott, C., et al. (2011). CDD: a Conserved Domain Database for the functional annotation of proteins. *Nucleic Acids Res.* 39, D225–D229. doi: 10.1093/nar/gkq1189

Markowitz, V. M., Mavromatis, K., Ivanova, N. N., Chen, I.-M. A., Chu, K., and Kyrpides, N. C. (2009). IMG ER: a system for microbial genome annotation expert review and curation. *Bioinformatics* 25, 2271–2278. doi: 10.1093/bioinformatics/btp393

Matsushika, A., and Mizuno, T. (1998). The structure and function of the histidine-containing phosphotransfer (HPt) signaling domain of the *Escherichia coli* ArcB sensor. *J. Biochem.* 124, 440–445. doi: 10.1093/oxfordjournals.jbchem.a022132

McHatton, S. C., Barry, J. P., Jannasch, H. W., and Nelson, D. C. (1996). High nitrate concentrations in vacuolate, autotrophic marine *Beggiatoa* spp. *Appl. Environ. Microbiol.* 62, 954–958.

McKay, L. J., MacGregor, B. J., Biddle, J. F., Albert, D. B., Mendlovitz, H. P., Hoer, D. R., et al. (2012). Spatial heterogeneity and underlying geochemistry of phylogenetically diverse orange and white *Beggiatoa* mats in Guaymas Basin hydrothermal sediments. *Deep-Sea Res. I* 67, 21–31. doi: 10.1016/j.dsr.2012.04.011

Miropolskaya, N., Esyunina, D., Klimasauskas, S., Nikiforov, V., Artsimovitch, I., and Kulbachinskiy, A. (2014). Interplay between the trigger loop and the F loop during RNA polymerase catalysis. *Nucleic Acids Res.* 42, 544–552. doi: 10.1093/nar/gkt877

Morgan, H. P., Estibeiro, P., Wear, M. A., Max, K. E. A., Heinemann, U., Cubeddu, L., et al. (2007). Sequence specificity of single-stranded DNA-binding proteins: a novel DNA microarray approach. *Nucleic Acids Res.* 35:e75. doi: 10.1093/nar/gkm040

Mrázek, J., Guo, X., and Shah, A. (2007). Simple sequence repeats in prokaryotic genomes. *Proc. Natl. Acad. Sci. U.S.A.* 104, 8472–8477. doi: 10.1073/pnas.0702412104

Murakami, K. S. (2013). X-ray crystal structure of *Escherichia coli* RNA polymerase σ^{70} holoenzyme. *J. Biol. Chem.* 288, 9126–9134. doi: 10.1074/jbc.M112.430900

Mussmann, M., Hu, F. Z., Richter, M., de Beer, D., Preisler, A., Jørgensen, B. B., et al. (2007). Insights into the genome of large sulfur bacteria revealed by analysis of single filaments. *PLoS Biol.* 5:e230. doi: 10.1371/journal.pbio.0050230

Opalka, N., Brown, J., Lane, W. J., Twist, K. A., Landick, R., Asturias, F. J., et al. (2010). Complete structural model of *Escherichia coli* RNA polymerase from a hybrid approach. *PLoS Biol.* 8:e1000483. doi: 10.1371/journal.pbio.1000483

Otsuka, S., Suda, S., Li, R. H., Matsumoto, S., and Watanabe, M. M. (2000). Morphological variability of colonies of *Microcystis* morphospecies in culture. *J. Gen. Appl. Microbiol.* 46, 39–50. doi: 10.2323/jgam.46.39

Parry, D. A., Fraser, R. D., and Squire, J. M. (2008). Fifty years of coiled-coils and α-helical bundles: a close relationship between sequence and structure. *J. Struct. Biol.* 163, 258–269. doi: 10.1016/j.jsb.2008.01.016

Reuter, J. S., and Mathews, D. H. (2010). RNAstructure: software for RNA secondary structure prediction and analysis. *BMC Bioinformatics* 11:129. doi: 10.1186/1471-2105-11-129

Rigden, D. J., Jedrzejas, M. J., and Galperin, M. Y. (2003). An extracellular calcium-binding domain in bacteria with a distant relationship to EF-hands. *FEMS Microbiol. Lett.* 221, 103–110. doi: 10.1016/S0378-1097(03)00160-5

Romeo, T., Vakulskas, C. A., and Babitzke, P. (2013). Post-transcriptional regulation on a global scale: form and function of Csr/Rsm systems. *Environ. Microbiol.* 15, 313–324. doi: 10.1111/j.1462-2920.2012.02794.x

Sachs, R., Max, K. E. A., Heinemann, U., and Balbach, J. (2012). RNA single strands bind to a conserved surface of the major cold shock protein in crystals and solution. *RNA* 18, 65–76. doi: 10.1261/rna.02809212

Sallam, K. I., Mitani, Y., and Tamura, T. (2006). Construction of random transposition mutagenesis system in *Rhodococcus erythropolis* using IS1415. *J. Biotechnol.* 121, 13–22. doi: 10.1016/j.jbiotec.2005.07.007

Salman, V., Amann, R., Girnth, A. C., Polerecky, L., Bailey, J. V., Høgslund, S., et al. (2011). A single-cell sequencing approach to the classification of large, vacuolated sulfur bacteria. *Syst. Appl. Microbiol.* 34, 243–259. doi: 10.1016/j.syapm.2011.02.001

Salman, V., Bailey, J. V., and Teske, A. (2013). Phylogenetic and morphologic complexity of giant sulphur bacteria. *Antonie Van Leeuwenhoek* 104, 169–186. doi: 10.1007/s10482-013-9952-y

Skorski, P., Leroy, P., Fayet, O., Dreyfus, M., and Hermann-Le Denmat, S. (2006). The highly efficient translation initiation region from the *Escherichia coli rpsA* gene lacks a Shine-Dalgarno element. *J. Bacteriol.* 188, 6277–6285. doi: 10.1128/JB.00591-06

Stock, A. M., Robinson, V. L., and Goudreau, P. N. (2000). Two-component signal transduction. *Annu. Rev. Biochem.* 69, 183–215. doi: 10.1146/annurev.biochem.69.1.183

Subramanian, A. R., and Vanduin, J. (1977). Exchange of individual ribosomal proteins between ribosomes as studied by heavy-isotope transfer experiments. *Mol. Gen. Genet.* 158, 1–9. doi: 10.1007/BF00455113

Sukhodolets, M. V., Garges, S., and Adhya, S. (2006). Ribosomal protein S1 promotes transcriptional cycling. *RNA* 12, 1505–1513. doi: 10.1261/rna.2321606

Tamura, K., Peterson, D., Peterson, N., Stecher, G., Nei, M., and Kumar, S. (2011). MEGA5: molecular evolutionary genetics analysis using maximum likelihood, evolutionary distance, and maximum parsimony methods. *Mol. Biol. Evol.* 28, 2731–2739. doi: 10.1093/molbev/msr121

Tatusov, R. L., Koonin, E. V., and Lipman, D. J. (1997). A genomic perspective on protein families. *Science* 278, 631–637. doi: 10.1126/science.278.5338.631

Taylor, B. L., and Zhulin, I. B. (1999). PAS domains: internal sensors of oxygen, redox potential, and light. *Microbiol. Mol. Biol. Rev.* 63, 479–506.

Torres, M., Condon, C., Balada, J. M., Squires, C., and Squires, C. L. (2001). Ribosomal protein S4 is a transcription factor with properties remarkably similar to NusA, a protein involved in both non-ribosomal and ribosomal RNA antitermination. *EMBO J.* 20, 3811–3820. doi: 10.1093/emboj/20.14.3811

Tzareva, N. V., Makhno, V. I., and Boni, I. V. (1994). Ribosome-messenger recognition in the absence of the Shine-Dalgarno interactions. *FEBS Lett.* 337, 189–194. doi: 10.1016/0014-5793(94)80271-8

Van Assche, E., Van Puyvelde, S., Vanderleyden, J., and Steenackers, H. P. (2015). RNA-binding proteins involved in post-transcriptional regulation in bacteria. *Front. Microbiol.* 6:141. doi: 10.3389/fmicb.2015.00141

Windgassen, T. A., Mooney, R. A., Nayak, D., Palangat, M., Zhang, J. W., and Landick, R. (2014). Trigger-helix folding pathway and SI3 mediate catalysis and hairpin-stabilized pausing by *Escherichia coli* RNA polymerase. *Nucleic Acids Res.* 42, 12707–12721. doi: 10.1093/nar/gku997

Xu, D., and Zhang, Y. (2012). *Ab initio* protein structure assembly using continuous structure fragments and optimized knowledge-based force field. *Proteins* 80, 1715–1735. doi: 10.1002/prot.24065

Yu, N. Y., Wagner, J. R., Laird, M. R., Melli, G., Rey, S., Lo, R., et al. (2010). PSORTb 3.0: improved protein subcellular localization prediction with refined localization subcategories and predictive capabilities for all prokaryotes. *Bioinformatics* 26, 1608–1615. doi: 10.1093/bioinformatics/btq249

Zhou, K., Aertsen, A., and Michiels, C. W. (2014). The role of variable DNA tandem repeats in bacterial adaptation. *FEMS Microbiol. Rev.* 38, 119–141. doi: 10.1111/1574-6976.12036

Conflict of Interest Statement: The author declares that the research was conducted in the absence of any commercial or financial relationships that could be construed as a potential conflict of interest.

frontiers in Microbiology

HYPOTHESIS AND THEORY
published: 10 March 2017
doi: 10.3389/fmicb.2017.00363

Submarine Basaltic Glass Colonization by the Heterotrophic Fe(II)-Oxidizing and Siderophore-Producing Deep-Sea Bacterium *Pseudomonas stutzeri* VS-10: The Potential Role of Basalt in Enhancing Growth

Lisa A. Sudek[1], Greg Wanger[2], Alexis S. Templeton[3], Hubert Staudigel[4] and Bradley M. Tebo[1†]*

[1] Marine Biology Research Division, Scripps Institution of Oceanography, University of California, San Diego, La Jolla, CA, USA, [2] Jet Propulsion Laboratory, California Institute of Technology, University of Southern California, Pasadena, CA, USA, [3] Department of Geological Sciences, University of Colorado Boulder, Boulder, CO, USA, [4] Institute of Geophysics and Planetary Physics, Scripps Institution of Oceanography, University of California, San Diego, La Jolla, CA, USA

OPEN ACCESS

Edited by:
Jason B. Sylvan, Texas A&M University, USA

Reviewed by:
Annette Ruth Rowe, University of Southern California, USA
Pauline Audrey Henri, University of Delaware, USA

***Correspondence:**
Lisa A. Sudek
lisasudek@gmail.com

†Present address:
Bradley M. Tebo, Institute of Environmental Health, Oregon Health and Science University, Portland, OR, USA

Specialty section:
This article was submitted to Extreme Microbiology, a section of the journal Frontiers in Microbiology

Received: *06 May 2016*
Accepted: *21 February 2017*
Published: *10 March 2017*

Citation:
Sudek LA, Wanger G, Templeton AS, Staudigel H and Tebo BM (2017) Submarine Basaltic Glass Colonization by the Heterotrophic Fe(II)-Oxidizing and Siderophore-Producing Deep-Sea Bacterium Pseudomonas stutzeri VS-10: The Potential Role of Basalt in Enhancing Growth. Front. Microbiol. 8:363. doi: 10.3389/fmicb.2017.00363

Phylogenetically and metabolically diverse bacterial communities have been found in association with submarine basaltic glass surfaces. The driving forces behind basalt colonization are for the most part unknown. It remains ambiguous if basalt provides ecological advantages beyond representing a substrate for surface colonization, such as supplying nutrients and/or energy. *Pseudomonas stutzeri* VS-10, a metabolically versatile bacterium isolated from Vailulu'u Seamount, was used as a model organism to investigate the physiological responses observed when biofilms are established on basaltic glasses. In Fe-limited heterotrophic media, *P. stutzeri* VS-10 exhibited elevated growth in the presence of basaltic glass. Diffusion chamber experiments demonstrated that physical attachment or contact of soluble metabolites such as siderophores with the basaltic glass plays a pivotal role in this process. Electrochemical data indicated that *P. stutzeri* VS-10 is able to use solid substrates (electrodes) as terminal electron donors and acceptors. Siderophore production and heterotrophic Fe(II) oxidation are discussed as potential mechanisms enhancing growth of *P. stutzeri* VS-10 on glass surfaces. In correlation with that we discuss the possibility that metabolic versatility could represent a common and beneficial physiological trait in marine microbial communities being subject to oligotrophic and rapidly changing deep-sea conditions.

Keywords: biofilm, basalt, Fe(II) oxidation, microbial fuel cell, siderophores, diffusion chamber

INTRODUCTION

Microorganisms play a pivotal role in the geochemical cycling of elements and the overall ecological function of deep-sea aquatic systems (Deming and Baross, 1993; Edwards et al., 2005). In hydrothermally influenced deep-sea habitats, microbes have recently been shown to contribute a substantial fraction to the biogeochemical cycling of Fe, an essential element for almost all

living organisms (Li et al., 2013). As observed in surface waters, the bioavailability of Fe controls patterns of primary productivity and carbon cycling in the deep-sea and throughout the oceans (Moore et al., 2002; Boyd and Ellwood, 2010). While hydrothermally active deep-sea systems such as submarine volcanoes and mid-ocean ridge environments are significant sources of fluids enriched in Fe, aqueous Fe(II) rapidly oxidizes and precipitates as Fe(III) oxyhydroxides when mixed with deep, oxygenated seawater. Significant Fe resolubilization can then occur through microbial activity, such as through the chelation of Fe(III) by organic ligands. This "iron pump" was recently identified as an important mechanism for making Fe bioavailable both locally and globally (Statham et al., 2005; Bennett et al., 2008; Toner et al., 2009; Li et al., 2013).

Despite the rapid abiotic oxidation of Fe(II) and the low energetic yield compared to more favorable chemolithotrophic metabolisms such as sulfide oxidation (Edwards et al., 2005; Emerson et al., 2010), both autotrophic and heterotrophic Fe(II)-oxidizing bacteria (FeOB) have been shown to be part of phylogenetically and metabolically diverse deep-sea microbial communities (Edwards et al., 2003; Emerson et al., 2007; Sudek et al., 2009; Singer et al., 2013; Scott et al., 2015). They are thought to play an important role in redox transformations of Fe in deep-sea systems (Edwards et al., 2004), and they are commonly associated with diffuse seeps of Fe(II)-rich fluids (Emerson and Moyer, 2002; Edwards et al., 2011; Scott et al., 2015), as well as basaltic surfaces of varying age (Santelli et al., 2008; Sudek et al., 2009; Henri et al., 2016).

Basaltic glass comprising about 20% of the extrusive layer of the oceanic crust represents one of the most geochemically reactive sources of solid-phase Fe for microbial colonization in the deep-sea and in addition, contains a number of bio-essential elements including Mg, Ca, Mn, and P (Staudigel and Hart, 1983; Drechsel and Winkelmann, 1997). Recent phylogenetic studies have shown that deep-sea basalt surfaces harbor phylogenetically diverse microbial communities (Thorseth et al., 2001; Lysnes et al., 2004; Templeton et al., 2005; Mason et al., 2007, 2009; Santelli et al., 2008; Sudek et al., 2009). Quantitative polymerase chain reaction (qPCR) measurements of microbial communities associated with the glassy rims of young weathered basalts from the East Pacific Rise (EPR) have indicated total bacterial and archaeal cell densities between 3×10^6 and 1×10^9 cells per gram of rock (Santelli et al., 2008). In contrast, the total microbial cell numbers of deep ocean waters (>1000 m) range between 8×10^3 and 9×10^4 cells per ml of seawater (Santelli et al., 2008).

Bacterial metabolisms within such basalt surface communities have been shown to be versatile (Templeton et al., 2005; Mason et al., 2009, 2010; Sudek et al., 2009; Callac et al., 2013). Reduced forms of elements such as Fe(II), Mn(II) and S(-II) in basalts can serve as potential electron donors for chemolithotrophic communities (Christie et al., 2001; Bach and Edwards, 2003; Henri et al., 2016). In addition, chemolithoautotrophic Fe(II)-oxidizing organisms are widely assumed to fix carbon that at least part of the basalt community relies upon (Santelli, 2007).

Metal oxides often found on the basalt surface and formed through the abiotic and biotic oxidation of basalt can also serve as nutritional source of Fe for siderophore-producing bacteria. In fact, many of the microbial strains found in association with submarine basaltic glass surfaces have been shown to be capable of multiple metabolic functions (Sudek et al., 2009). It is unclear to what degree this metabolic plasticity may represent a niche adaptation response or what the advantages of basalt surface-associated growth may offer these communities. In particular it remains ambiguous whether the colonization process is directed toward fulfilling specific ecological advantages such as nutrient acquisition and/or energy generation. Little is known about the microbial ecology of glass colonization, including the key mechanisms that drive surface colonization. Finally it is unclear to what degree microbial activity can affect the dissolution rates of basaltic glasses and hence control the biogeochemical cycling of elements at the rock/water interface. Weathering structures on the surface of basaltic glass surfaces and the occurrence of palagonite have suggested a role of bacteria in the development of the structures (Thorseth et al., 1992, 1995). More recently laboratory batch experiments on basalt samples from near Axial Seamount indicated that basalt weathering (i.e., release of metals such as Fe, Mn and Ca) was increased in the presence of bacteria (Daughney et al., 2004). It was also shown that surface features and mineralogies of basalts weathered in the presence of bacteria were similar to those of natural weathered basalts (Daughney et al., 2004).

Here we investigate the role of submarine basaltic glass in the growth of the siderophore-producing and Fe(II)-oxidizing deep-sea bacterium *Pseudomonas stutzeri* VS-10. This Gammaproteobacterium was isolated from a submarine volcanic rock at Vailulu'u Seamount (Sudek et al., 2009) and, due to exhibiting increased growth in the presence of basalt, was used as a model for studying the characteristics of microbe/basalt interactions. Specifically, we explore the role of basalt as a source for either nutrients or energy and the importance of direct physical contact of the cells or soluble compounds produced by the bacterium with the basalt. In addition, we discuss the potential role of filamentous structures within *P. stutzeri* VS-10 biofilms in surface-related growth. This work provides new evidence for possible roles of submarine basaltic glass in supporting metabolically diverse deep-sea microbial communities.

MATERIALS AND METHODS

Volcanic Rocks and Minerals

The basaltic glass used in all experimental set-ups was originally collected at Kilauea volcano (Pu'U-o'O), Hawaii, USA in 2002 and had been re-melted as described elsewhere (Bailey et al., 2009). Fe(II) content in the basalt averaged 9–10 wt %. For all growth experiments, the basalt was crushed to an approximate grain size of 2–3 mm, washed several times in deionized water, washed twice in 0.1N HCl to remove potential surface Fe, and sonicated in deionized water for 40 min. After a final rinse with deionized water the glass grains were dried in sterile glass dishes, covered with aseptic aluminum foil at 40°C and then microwave sterilized in glass dishes for 10 min.

Organisms and Media

Pseudomonas stutzeri VS-10 was isolated from a rhyolitic rock surface exposed for 3 months to low-temperature, non-hydrothermally influenced conditions (Marker 2: 14 13.103°S / 169 04.106°W; 582 m water depth) at Vailulu'u Seamount. It was isolated as a siderophore producer through serial transfer of colonies on Chrome-Azurol-Sulfonate plates (Sudek et al., 2009) and was shown to grow well at room temperature. All experiments were subsequently carried out at room temperature to ensure reproducibility of results from different experimental set-ups. *Shewanella oneidensis* MR-1 was obtained from K. Nealson at the J. Craig Venter Institute where the electrochemical work was carried out.

Minimal Glycerol Medium

An artificial seawater medium amended with glycerol was used in Fe-limited growth experiments in the presence and absence of basalt. It was also used in diffusion chamber experiments to assess the cell's requirement for basalt as a nutrient source and microbial fuel cell (MFC) experiments to analyze *P. stutzeri* VS-10's ability to use electrodes as an electron acceptor. The medium contained: 100 mM $MgSO_4$, 20 mM $CaCl_2$, 600 mM NaCl, 20 mM KCl, 40 mM glycerol, 333 μM K_2HPO_4, 18.5 mM NH_4Cl and 50 mM HEPES (pH 7.4). To limit the potential contamination of the medium with Fe the medium (adjusted to pH 7.4) was passed through a column containing Chelex-100 resin (analytical grade 100–200 mesh sodium form, Bio-Rad cat. # 142-2832) prepared based on the methods of Price et al. (1989). The Chelex was loaded in a previously acid washed (10 % HCl, Fisher cat. # A144-212) 1.5 × 15 cm glass column (Kontes class company flex column, cat. # 420400-1515) equipped with a three-way nylon stopcock (Kontes cat. # 420 163-4503). The flow rate was adjusted to approximately one drop per second. The medium was subsequently filter-sterilized through 0.22 μm Stericups (Millipore cat. #: SCGPU05RELC) and the final pH was measured. To test for the role of basalt as a source for nutrients and energy no trace elements were added.

MR-1 Medium for Fuel Cell Experiments

For our MFC experiments we used two different media. Experiments testing for the reduction potential of *P. stutzeri* VS-10 were run on minimal glycerol medium (see Minimal Glycerol Medium With and Without Basalt) to allow for comparison of results to data from growth experiments. In contrast, experiments testing for the oxidation potential of strain VS-10 in combination with *S. oneidensis* MR-1 contained MR-1 defined medium that allowed for comparison of results to previously published data collected on *S. oneidensis* MR-1 (Bretschger et al., 2007). It contained 30 mM PIPES [piperazine-*N*,N^{prime}-bis(2-ethanesulfonic acid)] pH 7.2, 7.5 mM NaOH, 10 mM NH_4Cl, 1.34 mM KCl, 4.35 mM NaH_2PO_4, 30 mM NaCl with the addition of 10 ml/liter each of vitamin solution (Kieft et al., 1999), amino acid solution and trace mineral stock solution (Bretschger et al., 2007). A final concentration of 20 mM lactate was used as the sole carbon source.

Growth Experiments

Minimal Glycerol Medium With and Without Basalt

Prior to the inoculation of all minimal medium cultures with *P. stutzeri* VS-10, the strain was grown at 37°C overnight in Luria-Bertani (LB) medium (per L of ultrapure H_2O: 10 g Bacto Tryptone, 5 g Yeast Extract, 10 g NaCl, adjusted to pH 7.0). Cells were harvested by centrifugation at 8000 rpm for 10 min. and washed three times in 5 ml of minimal glycerol medium. The optical density at 600 nm (OD_{600}) of the final resuspension of cells was measured to estimate cell numbers. Fifteen ml glass tubes, previously washed in 10% HCl for 2 days, rinsed six times in deionized water and microwave-sterilized for 10 min., were used to determine growth of *P. stutzeri* VS-10 on minimal glycerol medium in the presence and absence of basalt. In the tubes containing basalt ∼0.5 g of basaltic rock grains were added to 5 ml of Chelexed medium. Except for abiotic (rock/water) controls each tube was subsequently inoculated with the washed cell suspension of *P. stutzeri* VS-10.

For the removal of biofilms from the interior of the glass tubes and the rock and mineral grains prior to spectrophotometric cell density measurements at 600 nm, the tubes were briefly vortexed and vigorously tapped onto a surface. Scanning electron microscopy (SEM) later showed the effectiveness of this method in removing bacterial cells from the rock surfaces. Due to the size and density of rock and mineral grains and their rapid settling after vortexing, they are unlikely to have interfered with the optical density measurements. To account for any contribution from abiotically derived alteration products, all cultures were compared with controls (rock/water, mineral/water), which represented less than 2% of the measured OD of the cultures. The interference of biologically derived secondary mineral deposits as well as small amounts of Fe hydroxides inside the culture containing $FeCl_2$ with OD_{600} measurements was considered insignificant.

Diffusion Chamber

The significance of direct attachment or proximity of cells or soluble compounds produced by the bacterium to the basalt surface for growth of *P. stutzeri* VS-10 was investigated in diffusion chambers, consisting of dual compartment borosilicate chambers similar to the one described in Bretschger et al. (2007). We use the term "proximity" in this manuscript to refer to the absence of a physical barrier between the cells and the basalt where soluble molecules such as siderophores or redox-active compounds could come in contact with the basalt surface. The diffusion chamber compartments were separated by a proton-exchange membrane (Nafion® 424, DuPont) which would be impermeable to small and large molecules and colloids but did not contain any electrodes. Prior to inoculation with *P. stutzeri* VS-10 cells, 5 g of sterile basalt was added to one of the compartments. The glass chambers were assembled, wrapped in aluminum foil and autoclaved at 121°C for 30 min. Upon cooling, 50 ml of filter sterilized minimal glycerol medium was added to both compartments. Nutrient-limited washed cells (see above) of *P. stutzeri* VS-10 were added to an initial OD_{600} of ∼0.05 to the compartment containing basalt grains in one set-up and to the opposite side in the other set-up. Cell

growth was subsequently monitored based on optical density measurement at 600 nm. The abiotic status of the uninoculated compartment was continuously monitored based on optical density measurements and microscopic analysis. A constant flow of filter-sterilized air was applied to both sides of each chamber to assure sufficient oxygen concentrations for the growth of the strain and to support homogenization of the solution prior to optical density measurements. Biofilm formation on the inside walls of the glass chamber was minimized by vigorous shaking and careful tapping, resulting in the visible detachment and homogenization of biofilms from the glass walls. Using sterile pipets the solution was again homogenized prior to sampling.

Scanning Electron Microscopy

Scanning electron microscopy was utilized to investigate biofilm formation and morphology of *P. stutzeri* VS-10 on basaltic glass surfaces. To preserve the cell integrity of all samples they were initially fixed in 2.5% glutaraldehyde (v/v) in 0.1 M sodium cacodylate buffer (pH 7, Fisher cat. # NC9842332) at 4°C overnight. To remove salts the samples were washed with 30 mM followed by 15 mM 2-[4-(2-sulfoethyl)piperazin-1-yl]dethanesulfonic acid (PIPES, pH 7.4). The samples were then gradually dehydrated by washing with a graded series of 10, 25, 50, 75, 90, and finally 100% ethanol for 5 min each. To prevent deformation and collapse of the surface structure and to conserve surface morphology samples were critical point dried. After mounting the samples on SEM stubs they were sputter-coated with gold/palladium (80/20) in a coating unit at V = 2.5 KV and I = 20 mA for 60 s. Samples were imaged on a Philips XL30 field emission SEM (FESEM) at the Nano3 facility of the University of California, San Diego.

Microbial Fuel Cells

Electrochemical properties of the *P. stutzeri* VS-10 biofilm under nutrient-limited conditions were investigated in MFCs. Current production was observed using dual chamber MFCs of the type shown in Bretschger et al. (2007). MFCs were assembled using proton-exchange membranes (Nafion® 424, DuPont) and electrodes. In MFC experiments testing for *P. stutzeri* VS-10's ability to use a cathode as a terminal electron donor (oxidation potential) both anode and cathode were constructed from graphite felt (GF-S6-06, Electrolytica). In experiments testing for the strain's reduction potential the anode was constructed from graphite felt (GF-S6-06, Electrolytica) while the cathode was graphite bonded to platinum wire (0.3 mm, Alfa-Aesar). The cathode electrodes in both experiments were electroplated with a platinum catalyst to drive the oxygen reduction reaction. The MFCs were autoclaved prior to the addition of 0.22 μm filtered media. Ag/AgCl reference electrodes were aseptically inserted into both the anode and cathode compartments after autoclaving. Anaerobic conditions were maintained on the MFC anode by continuously passing filtered nitrogen gas through the compartment at a rate of 20 mL/min. Aerobic conditions were maintained in the cathode compartment by continuously passing air at a rate of 40 mL/min (Manohar et al., 2008).

TABLE 1 | Experimental set-up of microbial fuel cells (MFCs) testing for the oxidation potential of *P. stutzeri* VS-10.

	Anode	Cathode
MFC 1	Abiotic	Abiotic
MFC 2	*S. oneidensis MR-1*	*S. oneidensis MR-1*
MFC 3	*S. oneidensis MR-1*	*P. stutzeri VS-10*

Oxidation Potential

The potential of *S. oneidensis* MR-1 and *P. stutzeri* VS-10 to use a cathode as an electron donor was tested. Three separate sets of MFCs were set up, one abiotic and two biotic. Prior to the experimental set-up the growth of *P. stutzeri* VS-10 on this medium was ensured. Each MFC contained 30 ml of sterile MR-1 defined medium containing 10 mM of lactate as the sole electron donor and carbon source. The anode compartments of these fuel cells were initially inoculated with *S. oneidensis* MR-1 at a density of OD_{600} of 0.6. After 100 h in which the cathode compartments of both MFCs had remained abiotic, the cathode compartments of each MFC was inoculated with, in one case, a culture of *S. oneidensis* MR-1, in the other case, a culture of *P. stutzeri* VS-10. MR-1 consumes the lactate and transfers the electrons to the anode which functions as the electron acceptor. The electrons are then passed on to the cathode where they serve as an electron source for either MR-1 or VS-10 in the cathode compartment. Both strains were grown on MR-1 defined medium, washed as described before (see above) and inoculated to an initial OD_{600} of ∼0.6 (**Table 1**).

Reduction Potential

The ability of *P. stutzeri* VS-10 to reduce an anode, and hence use a solid surface as a terminal electron acceptor, was determined. Thirty milliliters of 0.22 μm filter-sterilized minimal glycerol medium was added into each of the compartments of two MFCs. One served as an abiotic control while the other one was subsequently inoculated with a washed culture of *P. stutzeri* VS-10. Prior to inoculation of the anode compartment, *P. stutzeri* VS-10 was grown to exponential phase on LB medium, washed as described previously (see Growth Experiments) and inoculated to a final OD_{600} of ∼0.05. Throughout the experiment samples were taken through sterilized disposable borosilicate glass Pasteur pipettes (Fisher cat # 13-678-20C) and the OD_{600} of the culture was determined spectrophotometrically. Initially, aerobic conditions inside the cell were established by supplying filter-sterilized oxygen (0.22 μm) to both compartments close to the electrodes. After 73 h conditions were changed from aerobic to anaerobic conditions by replacing the oxygen flow to the anode compartment with filter-sterilized (0.22 μm) nitrogen.

Electrochemical Measurements

Microbial fuel cell voltage was measured every minute across a 100 Ω external resistor using a high-impedence digital multimeter (model 2700; Keithley Instruments). MFC polarization measurements were taken for both the oxidation (see Oxidation Potential) and reduction (see Reduction Potential) potentials by opening the circuit and allowing the cell potential to build to a maximum (i.e., Open Circuit Potential or OCP).

Once the OCP was reached, a potentiostat (Gamry Inc) was used to measure the polarization behavior of the MFC. During this process the external resistance is decreased from a maximum (infinite resistance) to a minimum (short circuit) and the corresponding current is measured. Current (I) is calculated from these data using Ohm's law (I = V/R) and Power (P) is calculated using P = I*V. The total surface area of the anode was 290 cm^2.

The MFCs were also evaluated in the experiment measuring the reduction potential using cyclic voltammetry (CV) to determine the redox activity of the abiotic components (e.g., electrodes) as well as the biotic components (e.g., bacteria). The voltammograms were obtained by sweeping the cell potential and measuring the corresponding current response. The voltage of the electrodes was swept at a scan rate of 25 mV/s from −500 mV to +500 mV vs. Ag/AgCl. At the termination of the experiments the electrodes were harvested, fixed in 2.5% glutaraldehyde (v/v) in 0.1 M sodium cacodylate buffer (pH 7, Fisher cat. # NC9842332) at 4°C overnight and visualized by SEM.

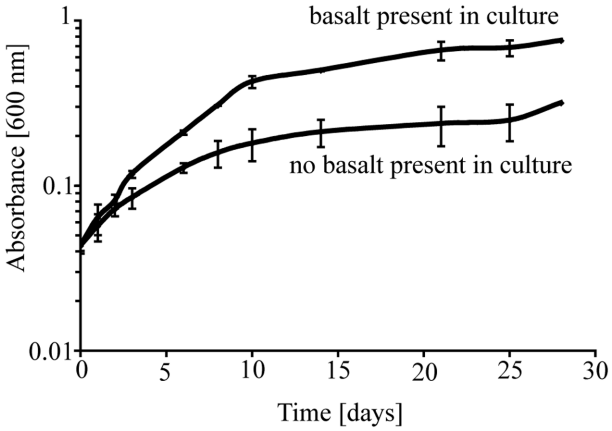

FIGURE 1 | Growth of *P. stutzeri* VS-10 on Chelex-treated minimal glycerol medium with or without basalt. Results are based on duplicate growth experiments for each condition. Error bars represent the standard deviation.

RESULTS

To investigate the potential role of basalt in supporting growth of *P. stutzeri* VS-10, we initially carried out two batch growth experiments at room temperature under aerobic Fe-limited conditions using a minimal medium containing glycerol as the sole carbon source, with and without basalt. In the batch experiments occurring over a period of ∼4 weeks, we observed various growth of *P. stutzeri* as measured spectroscopically by light absorption at 600 nm (**Figure 1**). The results showed that while there was some growth (increase from $OD_{600\ nm}$ of 0.046–0.316) on the glycerol medium alone, growth in the presence of glycerol and basalt was 2.4 times higher (from 0.045 to 0.754) after 28 days (**Figure 1**).

To test the importance of direct attachment or proximity (i.e., lack of a physical barrier) of cells to basaltic glass in contributing to the elevated growth of *P. stutzeri* VS-10, additional growth experiments were conducted in a diffusion chamber. *P. stutzeri* VS-10 was grown under Fe-limited conditions either in the presence of basaltic glass or physically separated from basaltic glass by a membrane. Under physical separation, growth of the bacterium is reduced (**Figure 2**), similar to the results of our first experiment when basalt was absent (**Figure 1**). In contrast, the presence of basalt leads to elevated growth, exceeding the growth observed in our batch experiment, a result likely due to larger amounts of basalt used in the diffusion chamber as well as more constant agitation. These results demonstrate that physical contact, or at least proximity of *P. stutzeri VS-10* to basaltic glass, increases growth.

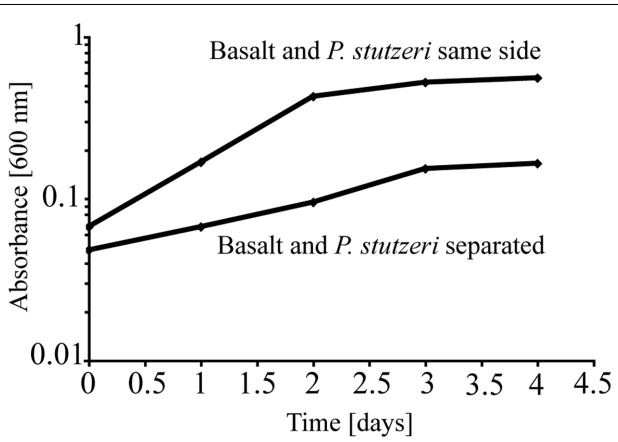

FIGURE 2 | Diffusion chamber experiments demonstrating growth of *P. stutzeri* VS-10 on Chelex-treated minimal glycerol medium in direct contact with and physically separated from basalt.

Morphological Appearance of *P. stutzeri* VS-10 Biofilms on Basaltic Glass Surfaces

Having demonstrated that physical contact and/or the exchange of soluble molecules between the bacterium and the glass has an important effect on growth we explored the morphological appearance of *P. stutzeri* in its biofilms ranging from monolayers of cells to more complex structures (**Figure 3**). The biofilm distribution appears to be extensive and not limited to natural depressions (e.g., cracks) in the rock surface (**Figure 3A**). Filamentous structures (with an approximate diameter of 10 nm) are a noticeable part of the VS-10 biofilm (**Figures 3B,C**). These filaments are similar in appearance to fiber-like structures recently described as extensions of the outer membrane in *Shewanella oneidensis* MR-1 (Pirbadian et al., 2014). Structures similar in appearance have also previously been described as artifacts stemming from the dehydration of EPS as part of the SEM preparation (Dohnalkova et al., 2011). Without a detailed compositional analysis a classification of these filaments is impossible.

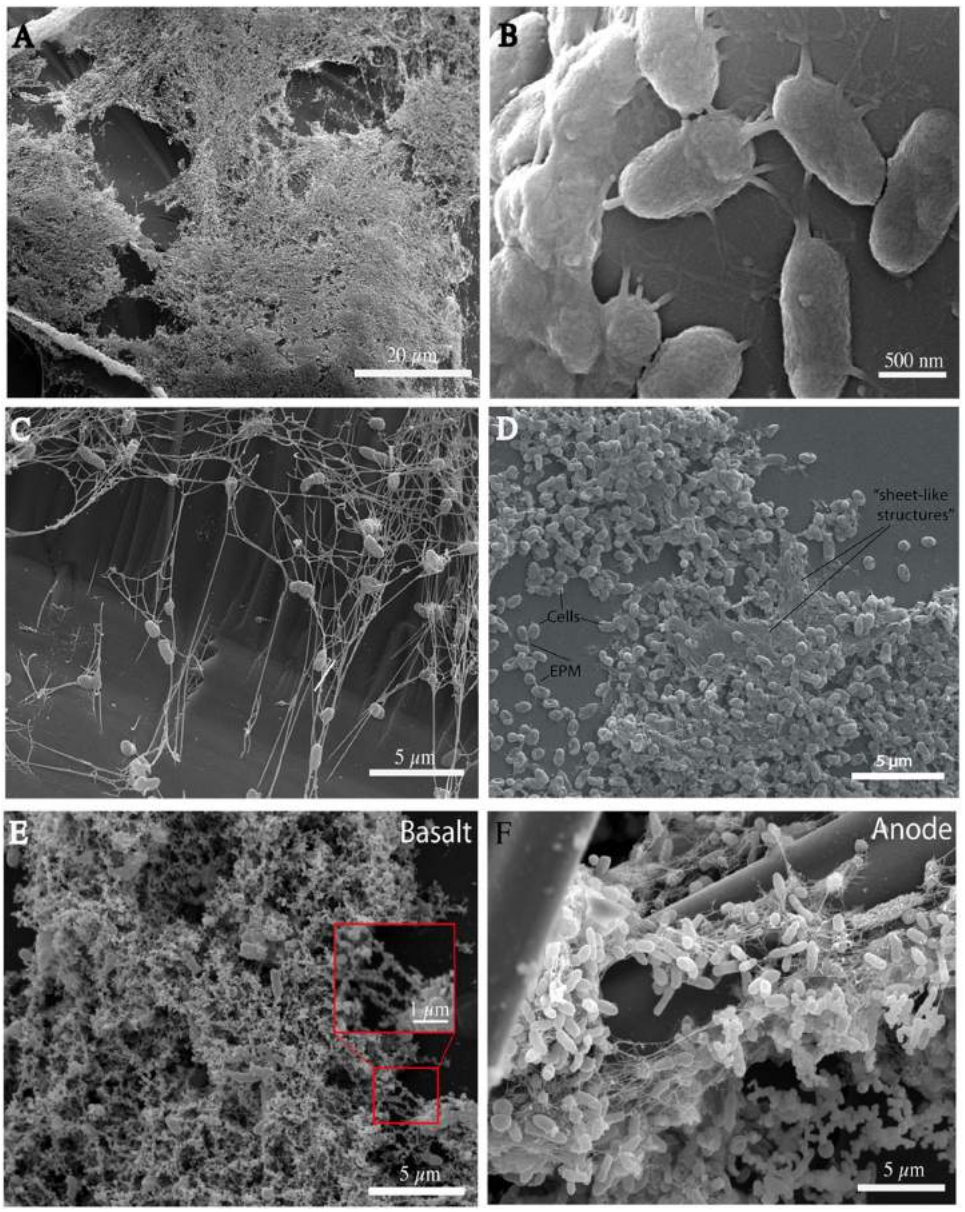

FIGURE 3 | Scanning electron micrographs (SEMs) of *P. stutzeri* VS-10 cells on basaltic glass taken at different time points. All cultures were grown on minimal glycerol medium. Basalt fragments used in the cultures (all but **F**) were all treated equally. Biofilm formation is extensive and not limited to natural depressions (**A**, 22 days of incubation). Filamentous structures may facilitate cell-to-cell and cell-to substrate adherence (**B,C**, 4 days of incubation). In thicker parts of the biofilm they appear almost "sheet-like" (**D**, 1 week of incubation). Encrustation of the filaments is apparent when grown in the presence of basalt (red box **E**, after 6 days of incubation). Encrustations appear significantly reduced in biofilms developed inside microbial fuel cells (**F**, anode biofilm).

The role of extensions in *P. stutzeri* VS-10 biofilms appears to be to facilitate both cell-to-cell and cell-to-glass interactions (**Figures 3B,C**). They vary in number ranging from 1 or 2 to up to ∼20 filaments per cell and are unevenly spread over the entire cell surface (**Figure 3B**). The number of appendages on each cell appears to depend on biofilm thickness. Single cells seem to adhere to the glass surface via a few (2–10) appendages (**Figure 3B**). Cells within thicker parts of the biofilm exhibit more and longer extensions or "sheet-like" structures (**Figure 3D**).

When grown on minimal glycerol medium in the presence of basalt the filaments and cells become mineral-encrusted (**Figure 3E**). Energy Dispersive Spectroscopy (EDS) identified iron and oxygen as the main elements present in the encrustations and traces of silica and titanium (data not shown). These analyses suggest that these encrustations likely represent secondary minerals [e.g., Fe(hydr)oxides, Fe(II)/(III)-silicate/oxides and possibly Fe(II)-bearing minerals] formed as a result of basalt weathering.

Electrochemical Properties of *P. stutzeri* VS-10

To further investigate the role of the biofilm in the elevated growth of *P. stutzeri* VS-10 on basalt, the electrochemical properties of the strain were investigated in MFCs. The oxidation/reduction potential of *P. stutzeri* VS-10 was measured and compared to data obtained from *S. oneidensis* MR-1, a known electrogenic bacterium (El-Naggar et al., 2010).

Oxidation Potential

In addition to a blank MFC (MFC1) the anode compartments of two MFCs (MFC2 and 3) were initially inoculated with cultures of *S. oneidensis* MR-1, a bacterium known to couple the oxidation of organic compounds to the reduction of an anode inside MFCs (Fitzgerald et al., 2012). At $t_{72\ h}$, when the cathode compartments were still abiotic, the circuit was opened and the potential of the fuel cell was allowed to build to a maximum open circuit potential (OCP). The initial OCP of both MFCs was similar, MFC2: +285 mV and MFC3: +270 mV vs. Ag/AgCl. At $t_{100\ h}$ the cathode compartments of MFC2 and MFC3 were inoculated with *S. oneidensis* MR-1 and *P. stutzeri* VS-10, respectively. At $t_{140\ h}$ the OCP of MFC2 (with MR-1) and MFC3 (with VS-10) had increased to +344 mV and +398 mV vs. Ag/AgCl respectively (**Table 2**).

The maximum current densities for both MFCs were also recorded before ($t_{72\ h}$) and after ($t_{140\ h}$) the inoculation of the cathode compartments with the respective strains. Maximum current densities of MFC2 containing *S. oneidensis* MR-1 on the cathode side increased from 7.45 $\mu A/m^2$ at $t_{72\ h}$ to 23.77 $\mu A/m^2$ at $t_{140\ h}$. Comparatively, the maximum current density in MFC3 containing *P. stutzeri* VS-10 on the cathode side increased from 6.49 $\mu A/m^2$ ($t_{72\ h}$) to 20.77 $\mu A/m^2$ ($t_{140\ h}$) (**Table 2**).

Reduction Potential

Pseudomonas stutzeri VS-10's ability to use an anode as a terminal electron acceptor and hence transfer electrons to a solid surface was investigated in MFCs under microaerobic conditions over 5 days. It was shown that *P. stutzeri* VS-10 produced an electrochemical current relative to a blank MFC operated under identical conditions (**Figure 4**).

The polarization curve of the MFC inoculated with strain VS-10 showed a maximum power density of 1.73×10^{-3} $\mu W/cm^2$ compared to the blank MFC (**Figure 4**). The maximum current densities for the MFC containing *P. stutzeri* VS-10 compared to the blank were 1.12×10^{-2} $\mu A/cm^2$ and 5.90×10^{-5} $\mu A/cm^2$, respectively. The apparent cell densities (based on optical density measurements at 600 nm) decreased significantly over the 120 h of the experiment (data not shown) most likely due to biofilm formation on the anode (**Figure 3F**), along the membrane and on the glass walls of the MFC.

Cyclic Voltammetry

Cyclic voltammetry was used to evaluate the redox activity of the anode and the type of extracellular electron transfer mechanisms of *P. stutzeri* VS-10 to the anode. CV is commonly used to study and characterize the electron transfer interactions between microorganisms or microbial biofilms and MFC anodes (Fricke et al., 2008). It is also used to distinguish between direct electron transfer (DET, e.g., via membrane bound cytochromes) and mediated electron transfer (MET, e.g., via conductive filamentous "nanowires" or via excretion of redox active components). CV measurements were performed toward the end of the MFC experiment. Because sweep rates were relatively low (∼25 mV/s) and cells were not depleted of the electron donor, we believe CV conditions to be within the turnover regime. This would indicate that at each potential, all the proteins involved in the pathway were oxidized and reduced multiple times (LaBelle and Bond, 2009).

Figure 5 shows the cyclic voltammograms of *P. stutzeri* VS-10 (red line) vs. a blank electrode (solid blue line). Data show that the rate of electron transfer increased after inoculation (red line). The voltammogram exhibited two oxidation (anodic) peaks in the upper portion of the current-voltage (I-V) trace that are matched with a light blue line to reduction (cathodic) peaks in the lower trace suggesting that the oxidation and reduction of the corresponding compounds are reversible. The estimated mid-point potentials (E1/2) of the two redox-active compounds are approximately −0.13V and +0.25V (vs. Ag/AgCl) and the difference between the mid-point potential and the anodic and cathodic peak potentials suggests a single electron transfer for both components. It is not known if these peaks represent compounds excreted by VS-10 (e.g., electron shuttles) or if they are directly attached to the cell surface including the filaments.

DISCUSSION

Weathering of deep ocean basalts has been shown to have a significant impact on local and global ocean chemistry (Hart,

TABLE 2 | Results from experiments testing for the oxidation potential of VS-10 in Microbial Fuel Cells (MFCs).

	MFC1	MFC2		MFC3	
Cathode/anode	**Abiotic/abiotic**	**MR-1/abiotic**	**MR-1/MR-1**	**MR-1/abiotic**	**MR-1/VS-10**
		$T_{72\ h}$	$T_{140\ h}$	$T_{72\ h}$	$T_{140\ h}$
Open circuit potential [mV]	–	+270	+344	+285	+398
Maximum current density [$\mu A/m^2$]	–	7.45	23.77	6.49	20.77

While MFC1 was run as an abiotic blank, both anode compartments of MFC2 and 3 were initially inoculated with a culture of S. oneidensis MR-1 while the cathode compartments remained sterile. At 100 h the cathode compartment of MFC2 was inoculated with another culture of S. oneidensis MR-1 while the cathode compartment of MFC3 was inoculated with a culture of P. stutzeri VS-10.

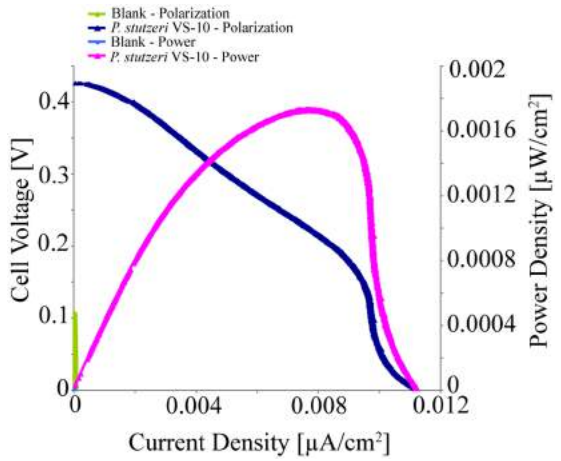

FIGURE 4 | Polarization and power curves for the microbial fuel cells (MFC) testing of *P. stutzeri* VS-10's potential to use an anode as a terminal electron acceptor. The maximum power density of the biotic MFC (pink line) is 1.73×10^{-3} µW/cm^2 compared to an un-inoculated fuel cell (blank) with a maximum power density of 3.07×10^{-6} mW/cm^2 (green line). The maximum current densities for the inoculated and un-inoculated MFCs were 1.12×10^{-2} µA/cm^2 (dark blue line) and 5.90×10^{-5} µA/cm^2 (light blue line, barely visible at the *x, y* origin).

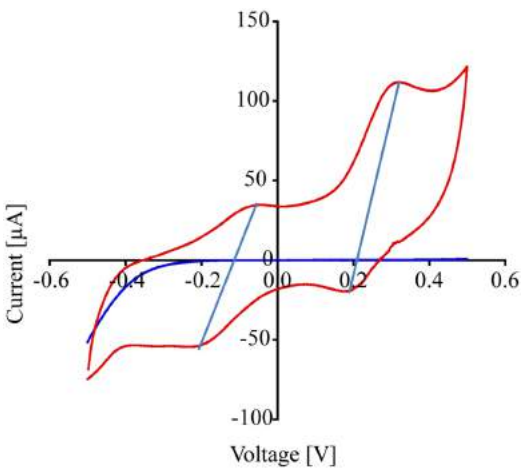

FIGURE 5 | Results from cyclic voltammogram measurements carried out on the MFC testing for the reduction potential of *P. stutzeri* VS-10. Cyclic voltammograms of the MFC inoculated with *P. stutzeri* VS-10 (red lines) and an uninoculated control (blank electrode, dark blue line). The presence of at least 2 redox-active components (in form of flat peaks) at ~ –0.05 V and at ~0.31 V becomes apparent. The two "peaks" in the upper portion of the current-voltage (I-V) trace are matched by peaks in the lower trace at –0.2 V and +0.18 V. The thin vertical light blue lines connect the peaks in the oxidation and the reduction sweep (a reversible redox reaction).

1970; Staudigel et al., 1995, Staudigel et al., 2006). Geological data suggest that seafloor weathering of the oceanic crust is likely to be mediated by microbial activity (Staudigel et al., 2008) but the interactions between submarine basaltic glasses and their associated microbial biofilm communities are, for the most part, unknown. Edwards et al. (2003) were the first to show that basaltic glass, as a source for Fe(II), could support the growth of gamma and alpha proteobacteria characterized as neutrophilic autotrophic FeOB. More recently, Henri et al. (2016) provided the most convincing data from seafloor and laboratory incubations that known lithotrophic FeOB such as the Zetaproteobacterium *Mariprofundus ferrooxydans* PV-1, can utilize structural Fe(II) in basaltic glass as their energy source for growth. While microbial communities associated with submarine basaltic glasses have been shown to be phylogenetically and metabolically diverse, other potential roles of basalt in supporting these communities and the forces that may drive colonization of basaltic glass haven't been explored in detail.

Basalt surface-related microbial communities show a variety morphological appearances ranging from cell clusters (surface-associated cells) to mature (robust) biofilms (Thorseth et al., 2001; Templeton et al., 2009). These structures have been speculated to correlate with successive stages of colonization starting with incipient microbial colonization by single cells, including many prosthecate organisms (Einen et al., 2006), and developing into more mature microbial communities (Thorseth et al., 1995).

Filamentous structures are often found within microbial biofilms and have more recently become the subject of electrochemical investigations. While microbial extracellular structures have been shown to play a role in electron transfer of microbial strains such as *Shewanella oneidensis* MR-1 and *Geobacter sulfurreducens* (Reguera et al., 2005; El-Naggar et al., 2010; Pirbadian et al., 2014), they were just recently characterized as extensions of the outer membrane in *S. oneidensis* MR-1 (Pirbadian et al., 2014), making them distinct from other extracellular polymeric substances (EPS) commonly excreted by microbes forming the biofilm matrix. The role of such filaments in surface related growth and potentially the electron transport chain of deep-sea bacteria, and heterotrophic FeOB in particular, is, so far, poorly understood.

While substrate associated growth is a dominant microbial lifestyle (i.e., biofilm vs. planktonic communities), it remains ambiguous whether basalt colonization provides an ecological advantage such as acquisition of nutrients and/or energy sources for the surface-associated microbes (Bailey et al., 2009). In addition, the mechanisms of microbial basalt colonization and how surface related bacteria may satisfy their metabolic needs are largely unknown.

To address some of these unknowns we investigated the physiology of an organism we isolated from seafloor volcanic rock, *P. stutzeri* VS-10, a heterotrophic Fe(II)-oxidizing and siderophore-producing bacterium (Sudek et al., 2009). Results from three lines of inquiry in this study provide new insights into the lifestyle of VS-10. First, we showed that *P. stutzeri* VS-10 grows noticeably better without a physical barrier to the basalt while little growth is observed when the organism is separated from the basalt by a permeable membrane that also prevents the diffusion of small molecules; this leads to the recognition that *P. stutzeri* must have mechanisms for acquiring Fe from basalt. Second we described the physical appearance of biofilms on glass surfaces, observing the formation of both filamentous and sheet-like structures, which generated questions regarding the role of such filaments within the biofilm. Finally, we measured some

of the electrochemical properties of the surface attached cells, enabling us to hypothesize about their possible role in electron transfer mediated by *P. stutzeri* VS-10.

Basalt as a Source for Nutritional Fe

Elevated growth under Fe-limited conditions in the presence of basaltic glass (**Figure 1**) suggests that the Fe supplied from the basalt is used by cells either as a nutrient and/or energy source. Based on diffusion chamber experiments, either direct attachment or at least physical proximity of cells to the glass surface is critical in this process (**Figure 2**).

Pseudomonas stutzeri VS-10 was originally isolated as a siderophore-producing bacterium. It was shown to produce a number of structurally related siderophores (amonabactins) when grown under Fe-limited conditions on a minimal glycerol medium (Sandy, 2011; Sudek, 2011). Basaltic glasses used in our study have the potential to provide nutritional Fe in two forms, directly as structurally-bound Fe(II) and Fe(III), or in the form of Fe(hydr)oxides formed in the presence of oxygen along the basalt surface. These Fe(hydr)oxides are commonly found on natural submarine basalt surfaces and are believed to be the result of both biotic and abiotic oxidation of the basalts.

Perez et al. (2016) recently demonstrated the essential role of siderophores in the *P. aeruginosa*-promoted dissolution processes of basaltic glasses. This work revealed that the Fe speciation in the glass could affect siderophore production, and in turn, *P. aeruginosa* could affect the basalt dissolution rates and take up released Fe as a required nutrient for growth. The role of siderophores produced by *P. stutzeri* VS-10 in providing nutritional Fe and subsequently supporting growth in our experiment is unknown. Results from diffusion chamber experiments (**Figure 2**) may indicate an involvement represented by a lower growth under conditions where siderophore diffusion through a membrane and subsequent complexation of Fe from basalt or Fe(hydr)oxides was prevented. If siderophores were indeed involved in nutritional Fe acquisition from basalt that would most likely affect basalt dissolution rates over time as described for *P. aeruginosa* (Perez et al., 2016).

Basalt as an Electron Source or Sink

Electrochemical data indicate that *P. stutzeri* VS-10 cells appear to be able to use solid surfaces both as an electron donor and a terminal electron acceptor (**Table 2** and **Figure 4**). Such properties could enable this strain to either use the basalt as an electron source, facilitating the oxidation of structural Fe(II), or to the use of Fe(III) oxides formed on the basalt surface as an electron sink. Both scenarios would benefit the growth of the bacterium energetically. Such physiological interactions are deserving of further study to determine the potential mechanisms of electron transfer from solid-phase Fe(II) and the resulting impact on the chemical properties of the basalt/microbe interface.

The role of filaments observed in the biofilm structure, and/or redox-active compounds such as electron shuttles in the establishment of a biofilm and in elevated growth of *P. stutzeri* VS-10 on the basalt surface is intriguing. We hypothesize that either one could be involved in oxidizing Fe(II) from basalt or reducing surface associated Fe(hydr)oxides. This would again be supported by our diffusion chamber experiments in which a direct attachment to the rock (filaments) or the diffusion of redox-active compounds through the membrane was prevented.

While soluble components, possibly redox shuttles or redox mediators as suggested by cyclic voltammograms of *P. stutzeri* VS-10 (**Figure 5**), could be used as part of the strain's electron transfer pathway, the exact structure of such putative compounds is unknown. Possible electron shuttles include organic heterocyclic and monocyclic compounds, sulfur species and hydrogen (Rabaey et al., 2007). Many of these chemical species have to be provided externally for the bacterium to be able to use them for shuttle-based electron transfer. However, *Pseudomonas* species commonly produce exogenous redox-active compounds such as the phenazines, pyocyanin and phenazine-1-carboxamide (Hernandez et al., 2004; Rabaey et al., 2005; Yong et al., 2014). Bacterial phenazines are commonly known to serve as electron shuttles to alternate terminal acceptors, to modify cellular redox states and to contribute to biofilm formation and architecture (Pierson and Pierson, 2010).

While the abundance of filamentous structures in bacterial biofilms from variable environmental habitats seems to be far more common than initially thought, the role of such filaments in metabolic processes remains for the most part unknown. The research presented here represents a first hypothesis on their role in supporting life on submarine basaltic glasses.

The lack of experimental replicates does not allow robust comparisons of our electrochemical results to previously published data on *S. oneidensis* MR-1, an electrogenic bacterium that has been studied in detail. However, comparisons between our polarization and maximum current density results for *P. stutzeri* VS-10 and *S. oneidensis* MR-1 were attempted to be made (**Table 2**). Overall these results suggest that *P. stutzeri* VS-10 is able to build a larger cathodic potential than *S. oneidensis* MR-1 (i.e., it has a higher oxidation potential than MR-1) while *S. oneidensis* MR-1 seems to be more efficient at stripping electrons from the cathode. The electrochemical similarities between *P. stutzeri* VS-10 and *S. oneidensis* MR-1 biofilms may indicate that the electron transport system of *P. stutzeri* VS-10 is expressed on the cell surface and that there are distinct electron pathways into and out of the cells as previously described in *S. oneidensis* MR-1 (Bretschger et al., 2007).

One phenomenon we observed in *P. stutzeri* VS-10 cultures containing basalt was the occurrence of what seems to be secondary mineral deposits (most likely metal oxides) along the filamentous structures. The encrustation is extensive and seems to correlate with biofilm thickness and/or length of growth. Single cells or monolayers often still appear clean after a few days (**Figures 3B,C**) in comparison to thicker parts of the biofilm that established over longer periods of times. In biofilms that had more time to develop, encrustation of filaments is intense while cells still appear comparatively clean (**Figures 3A,D**). Indication that these precipitates represent metal oxides derived from the alteration of basalt is the fact that they are lacking in cultures cultivated inside MFCs where electrons are provided from a cathode or attached to an anode (**Figure 3F**).

Precipitation of Fe(III)-oxides (generated as waste products) on the cell surface and the resulting encrustation of cells,

potentially impeding cell metabolism, represent a common problem for neutrophilic Fe(II)-oxidizing bacteria. The metal oxides may give rise to limited diffusion of nutrients and restricted transport of waste across the membrane resulting in a reduction in overall viability of the cell (Kappler et al., 2005). Potential strategies to avoid such encrustation and to ensure mineral deposition at a certain distance from the cell surface have been reviewed previously (Schaedler et al., 2009). The most common mechanism described is the precipitation of Fe(III)-minerals along extracellular organic matrixes (sheaths, stalks, filaments or fibers) which are considered precipitation templates or nuclei. Such precipitation has been described in several species of neutrophilic Fe(II)-oxidizing bacteria including *Rhodobacter ferrooxidans* strain SW2, *Gallionella* spp., *Chlorobium ferrooxidans* strain KoFox, *Leptothrix ochracea* and more recently *Mariprofundus ferrooxidans* PV-1 (Chan et al., 2004; Hallberg and Ferris, 2004; Summers et al., 2013).

Pseudomonas stutzeri VS-10's ability to accelerate Fe(II)-oxidation under heterotrophic conditions could represent a metabolic trait to ensure additional energy acquisition in oligotrophic environments. *P. stutzeri* VS-10 biofilm growth on basaltic glass has been shown to be substantial. Diffusion limitation within the biofilm as commonly described Stewart (2003) is likely. We speculate that basalt may serve as an additional energy source in *P. stutzeri* VS-10 biofilms. In particular, cells in direct contact with basalt are more likely to become subject to diffusion limitation. Biologically catalyzed Fe(II)-oxidation at this interface could therefore represent a metabolism that is thermodynamically and kinetically favorable for microbial utilization at the lower O_2 saturation within a biofilm. This correlates well with the enhanced growth characteristics of strain VS-10 when grown in close contact with basaltic rock and the ability to grow on the cathode in a MFC.

Summers et al. (2013) recently demonstrated that cathodes poised at a constant redox potential, designed to mimic the one of Fe(II) in the environment, could serve as an electron donor to the marine Fe(II)-oxidizing bacterium *Mariprofundus ferrooxydans* PV-1. In comparison to *P. stutzeri* VS-10, PV-1 cells were shown to be non-biofilm forming and appeared to attach to the cathode via single cell polysaccharide matrixes. However one phenomenon both strains have in common is the presence of Fe(III)-minerals along extracellular polymers (stalks in PV-1; filaments in VS-10) in cultures containing Fe and the absence of such in MFCs.

Based on our results we hypothesize that extracellular filaments, most likely representing an extension of the cells outer membrane and possibly being involved in the electron transport chain of bacteria, may be more common in marine heterotrophic Fe(II)-oxidizing microorganisms than currently appreciated. The potential role in electron-transfer reactions between rock surfaces and microbial biofilms may be critical for promoting important redox processes necessary to sustain a diverse deep-ocean biosphere.

Recently, Rowe et al. (2015) adopted a strategy to used poised electrodes as a cultivation approach to enrich for electrochemically active organisms from marine sediments, and to subsequently select for organisms that could use solid substrates as an electron donor. In that study, Fe(0) and FeS were used as the electron donors to isolate Fe-oxidizers from the genera *Halomonas*, *Marinobacter*, *Pseudomonas,* and *Idiomarina* from the electrode enrichments, which were then subjected to electrochemical tests. All of these isolates were shown to be heterotrophic as well as FeOB, and current production would occur through electrode oxidation in the presence of O_2. This study did not provide direct evidence for redox mediators, and attachment to the electrode was common. This work serves as another example where *Pseudomonas* strains have been shown to be metabolically versatile and capable of growing using an electrode as the electron donor.

We previously suggested that metabolic versatility in microorganisms is likely to represent a common trait in oligotrophic deep-sea environments (Sudek et al., 2009). Siderophore production is a mechanism developed to ensure nutritional Fe-availability in deep-sea waters where Fe solubility is commonly low. In contrast, the ability to harvest energy through the oxidation of both Fe(II) and organics could represent an adaptive mechanism enabling a mixotrophic lifestyle and providing the option to thrive under geochemically dynamic conditions. Similarly, the ability to use the anode as an electron acceptor suggests that oxidized metal species commonly found on basalt surfaces could represent accessible electron acceptors for microbes growing on surfaces in diffusion limited biofilms. The results presented here underscore the potential role of submarine basaltic glass to act both as a source for nutrients and for energy generation subsequently supporting the phylogenetically and metabolically versatile microbial communities within deep-sea ecosystems.

AUTHOR CONTRIBUTIONS

LS designed and performed all the experiments and interpreted the results. GW helped to design, run and interpret the electrochemical analyses (microbial fuel cells, conductivity measurements). LS wrote the manuscript. BT, AT, and HS substantially contributed to the experimental design, data interpretation, drafting and revising of the manuscript. LS, GW, AT, HS, and BT all agree to be accountable for all aspects of this work and approved the final version to be published.

FUNDING

Funding sources include the National Science Foundation Microbial Observatories (MCB-0348668/0742010), Biogeosciences (OCE-0433692), and the Ocean Sciences (OCE-0526285) programs and the Agouron Institute.

ACKNOWLEDGMENTS

The authors would like to thank Yuri Gorby for enabling the work done in microbial fuel cells. Thanks to Don Dingwell (LMU) who helped with the preparation of basalt glasses.

REFERENCES

Bach, W., and Edwards, K. J. (2003). Iron and sulfide oxidation within the basaltic ocean crust: implications for chemolithoautotrophic microbial biomass production. *Geochim. Cosmochim. Acta* 67, 3871–3887. doi: 10.1016/S0016-7037(03)00304-1

Bailey, B. E., Templeton, A. S., Staudigel, H., and Tebo, B. (2009). Utilization of substrate components during basaltic glass colonization by *Pseudomonas* and *Shewanella* isolates. *Geomicrobiol. J.* 26, 648–656. doi: 10.1080/01490450903263376

Bennett, S. A., Achterberg, E. P., Connelly, D. P., Statham, P. J., Fones, G. R., and German, C. R. (2008). The distribution and stabilisation of dissolved Fe in deep-sea hydrothermal plumes. *Earth Planet. Sci. Lett.* 270, 157–167. doi: 10.1016/j.epsl.2008.01.048

Boyd, P. W., and Ellwood, M. J. (2010). The biogeochemical cycle of iron in the ocean. *Nat. Geosci.* 3, 675–682. doi: 10.1038/ngeo964

Bretschger, O., Obraztsova, A., Sturm, C. A., Chang, I. S., Gorby, Y. A., Reed, S. B., et al. (2007). Current production and metal oxide reduction by *Shewanella oneidensis* MR-1 wild type and mutants. *Appl. Environ. Microbiol.* 73, 7003–7012. doi: 10.1128/AEM.01087-07

Callac, N., Rommevaux-Jestin, C., Rouxel, O., Lesongeur, F., Liorzou, C., Bollinger, C., et al. (2013). Microbial colonization of basaltic glasses in hydrothermal organic-rich sediments at Guaymas Basin. *Front. Microbiol.* 4:250. doi: 10.3389/fmicb.2013.00250

Chan, C. S., De Stasio, G., Welch, S. A., Girasole, M., Frazer, B. H., Nesterova, M. V., et al. (2004). Microbial polysaccharides template assembly of nanocrystal fibers. *Science* 303, 1656–1658. doi: 10.1126/science.1092098

Christie, D. M., Pedersen, R. S., and Miller, D. J. (2001). *Proceedings of the Ocean Drilling Program, Initial Reports, Leg 187 [CD-ROM]*. College Station TX: Ocean Drilling Program. doi: 10.2973/odp.proc.ir.187.2001

Daughney, C. J., Rioux, J.-P., Fortin, D., and Pichler, T. (2004). Laboratory investigation of the role of bacteria in the weathering of basalt near deep-sea hydrothermal vents. *Geomicrobiol. J.* 21, 21–31. doi: 10.1080/01490450490253437

Deming, J. W., and Baross, J. A. (1993). "The early diagenesis of organic matter: bacterial activity," in *Topics in Geobiology*, Vol. 11, eds M. H. Engel and S. A. Macko (New York, NY: Plenum Press).

Dohnalkova, A. C., Marshall, M. J., Arey, B. W., Williams, K. H., Buck, E. C., and Fredrickson, J. K. (2011). Imaging hydrated microbial extracellular polymers: comparative analysis by electron microscopy. *Appl. Environ. Microbiol.* 77, 1254–1262. doi: 10.1128/AEM.02001-10

Drechsel, H., and Winkelmann, G. (1997). "Iron chelation and siderophores," in *Transition Metals in Microbial Metabolism*, eds G. Winkelmann and C. J. Carrano (Amsterdam: Harwood Academic Publishers), 1–49.

Edwards, K. J., Bach, W., and McCollom, T. M. (2005). Geomicrobiology in oceanography: microbe–mineral interactions at and below the seafloor. *Trends Microbiol.* 13, 449–456. doi: 10.1016/j.tim.2005.07.005

Edwards, K. J., Bach, W., McCollom, T. M., and Rogers, D. R. (2004). Neutrophilic iron-oxidizing bacteria in the ocean: their habitats, diversity, and roles in mineral deposition, rock alteration, and biomass production in the deep-sea. *Geomicrobiol. J.* 21, 393–404. doi: 10.1080/01490450490485863

Edwards, K. J., Glazer, B. T., Rouxel, O. J., Bach, W., Emerson, D., Davis, R. E., et al. (2011). Ultra-diffuse hydrothermal venting supports Fe-oxidizing bacteria and massive umber deposition at 5000 m off Hawaii. *ISME J.* 5, 1748–1758. doi: 10.1038/ismej.2011.48

Edwards, K. J., Rogers, D. R., Wirsen, C. O., and McCollom, T. M. (2003). Isolation and characterization of novel psychrophilic, neutrophilic, Fe-oxidizing, chemolithoautotrophic alpha- and gamma-*Proteobacteria* from the deep-sea. *Appl. Environ. Microbiol.* 69, 2906–2913. doi: 10.1128/AEM.69.5.2906-2913.2003

Einen, J., Kruber, C., Øvreas, L., Thorseth, I. H., and Torsvik, T. (2006). Microbial colonization and alteration of basaltic glass. *Biogeosci. Discuss.* 3, 273–307. doi: 10.5194/bgd-3-273-2006

El-Naggar, M. Y., Wanger, G., Leung, K. M., Yuzvinsky, T. D., Southam, G., Yang, J., et al. (2010). Electrical transport along bacterial nanowires from *Shewanella oneidensis* MR-1. *Proc. Natl. Acad. Sci. U.S.A.* 107, 18127–18131. doi: 10.1073/pnas.1004880107

Emerson, D., Fleming, E. J., and McBeth, J. M. (2010). Iron-oxidizing bacteria: an environmental and genomic perspective. *Annu. Rev. Microbiol.* 64, 561–583. doi: 10.1146/annurev.micro.112408.134208

Emerson, D., and Moyer, C. L. (2002). Neutrophilic Fe-oxidizing bacteria are abundant at the Loihi Seamount hydrothermal vents and play a major role in Fe oxide deposition. *Appl. Environ. Microbiol.* 68, 3085–3093. doi: 10.1128/AEM.68.6.3085-3093.2002

Emerson, D., Rentz, J. A., Lilburn, T. G., Davis, R. E., Aldrich, H., Chan, C., et al. (2007). A novel lineage of *Proteobacteria* involved in formation of marine Fe-oxidizing microbial mat communities. *PLoS ONE* 2:e667. doi: 10.1371/journal.pone.0000667

Fitzgerald, L. A., Petersen, E. R., Ray, R. I., Little, B. J., Cooper, C. J., Howard, E. C., et al. (2012). *Shewanella oneidensis* MR-1 Msh pilin proteins are involved in extracellular electron transfer in microbial fuel cells. *Process. Biochem.* 47, 170–174. doi: 10.1016/j.procbio.2011.10.029

Fricke, K., Harnisch, F., and Schröder, U. (2008). On the use of cyclic voltammetry for the study of anodic electron transfer in microbial fuel cells. *Energy Environ. Sci.* 1, 144–147. doi: 10.1039/b802363h

Hallberg, R., and Ferris, F. G. (2004). Biomineralization by *Gallionella*. *Geomicrobiol. J.* 21, 325–330. doi: 10.1080/01490450490454001

Hart, R. A. (1970). Chemical exchange between sea water and deep ocean basalts. *Earth Planet. Sci. Lett.* 9, 269–279. doi: 10.1038/nature06899

Henri, P. A., Rommevaux-Jestin, C., Lesongeur, F., Mumford, A., Emerson, D., Godfroy, A., et al. (2016). Structural Iron (II) of basaltic glass as an energy source for zetaproteobacteria in an abyssal plain environment, off the mid atlantic ridge. *Front. Microbiol.* 6:1518. doi: 10.3389/fmicb.2015.01518

Hernandez, M. E., Kappler, A., and Newman, D. K. (2004). Phenazines and other redox-active antibiotics promote microbial mineral reduction. *Appl. Environ. Microbiol.* 70, 921–928. doi: 10.1128/AEM.70.2.921-928.2004

Kappler, A., Schink, B., and Newman, D. K. (2005). Fe(III) mineral formation and cell encrustation by the nitrate-dependent Fe(II)-oxidizing strain BoFeN1. *Geobiology* 3, 235–245. doi: 10.1111/j.1472-4669.2006.00056.x

Kieft, T. L., Fredrickson, J. K., Onstott, T. C., Gorby, Y. A., Kostandarithes, H. M., Bailey, T. J., et al. (1999). Dissimilatory reduction of Fe(III) and other electron acceptors by a Thermus isolate. *Appl. Environ. Microbiol.* 65, 1214–1221.

LaBelle, E., and Bond, D. R. (2009). "Cyclic voltammetry for the study of microbial electron transfer at electrodes," in *Bioelectrochemical Systems: From Extracellular Electron Tranfer to Biotechnological Application*, Chap. 9, eds K. Rabaey, O. L. Angenent, U. Schröder, and J. Keller (London: IWA Publishing).

Li, J., Peng, X., Zhou, H., Li, J., and Sun, Z. (2013). Molecular evidence for microorganisms participating in Fe, Mn and S biogeochemical cycling in two low-temperature hydrothermal fields at the Southwest Indian Ridge. *J. Geophys. Res. Biogeosci.* 118, 665–679. doi: 10.1002/jgrg.20057

Lysnes, K., Thorseth, I. H., Steinsbu, B. O., Øvreås, L., Torsvik, T., and Pedersen, R. B. (2004). Microbial community diversity in seafloor basalt from the Arctic spreading ridges. *FEMS Microbiol. Ecol.* 50, 213–230. doi: 10.1016/j.femsec.2004.06.014

Manohar, A. K., Bretschger, O., Nealson, K. H., and Mansfeld, F. (2008). The polarization behavior of the anode in a microbial fuel cell. *Electrochim. Acta* 53, 3508–3513. doi: 10.1016/j.electacta.2007.12.002

Mason, O. U., Di Meo-Savoie, C. A., Van Nostrand, J. D., Zhou, J., Fisk, M. R., and Giovannoni, S. J. (2009). Prokaryotic diversity, distribution, and insights into their role in biogeochemical cycling in marine basalts. *ISME J.* 3, 231–242. doi: 10.1038/ismej.2008.92

Mason, O. U., Nakagawa, T., Rosner, M., Van Nostrand, J. D., Zhou, J., Maruyama, A., et al. (2010). First investigation of the microbiology of the deepest layer of ocean crust. *PLoS ONE* 5:e15399. doi: 10.1371/journal.pone.0015399

Mason, O. U., Stingl, U., Wilhelm, L. J., Moeseneder, M. M., Di Meo-Savoie, C. A., Fisk, M. R., et al. (2007). The phylogeny of endolithic microbes associated with marine basalts. *Environ. Microbiol.* 9, 2539–2550. doi: 10.1111/j.1462-2920.2007.01372.x

Moore, J. K., Doney, S. C., Glover, D. M., and Fung, I. Y. (2002). Iron cycling and nutrient-limitation patterns in surface waters of the world. *Deep sea Res. Part II* 49, 463–507. doi: 10.1016/S0967-0645(01)00109-6

Perez, A., Rossano, S., Trcera, N., Huguenot, D., Fourdrin, C., Verney-Carron, A., et al. (2016). Bioalteration of synthetic Fe(III)-, Fe(II)-bearing

basaltic glasses and Fe-free glass in the presence of the heterotrophic bacteria strain *Pseudomonas aeruginosa*: impact of siderophores. *Geochim. Cosmochim. Acta* 188, 147–162. doi: 10.1016/j.gca.2016.05.028

Pierson, L. S. III, and Pierson, E. A. (2010). Metabolism and function of phenazines in bacteria: impacts on the behavior of bacteria in the environment and biotechnological processes. *Appl. Microbiol. Biotechnol.* 86, 1659–1670. doi: 10.1007/s00253-010-2509-3

Pirbadian, S., Barchinger, S. E., Leung, K. M., Byun, H. S., Jangir, Y., Bouhenni, R. A., et al. (2014). *Shewanella oneidensis* MR-1 nanowires are outer membrane and periplasmic extensions of the extracellular electron transport components. *Proc. Natl. Acad. Sci. U.S.A.* 111, 12883–12888. doi: 10.1073/pnas.1410551111

Price, N. M., Harrison, G. I., Hering, J. G., Hudson, R. J., Nirel, P. M. V., Palenik, B., et al. (1989). Preparation and chemistry of the artificial algal culture medium aquil. *Biol. Oceanogr.* 6, 443–461. doi: 10.1080/01965581.1988.10749544

Rabaey, K., Boon, N., Hofte, M., and Verstraete, W. (2005). Microbial phenazine production enhances electron transfer in biofuel cells. *Environ. Sci. Technol.* 39, 3401–3408. doi: 10.1021/es048563o

Rabaey, K., Rodriguez, J., Blackall, L. L., Keller, J., Gross, P., Batstone, D., et al. (2007). Microbial ecology meets electrochemistry: electricity-driven and driving communities. *ISME J.* 1, 9–18. doi: 10.1038/ismej.2007.4

Reguera, G., McCarthy, K. D., Mehta, T., Nicoll, J. S., Tuominen, M. T., and Lovley, D. R. (2005). Extracellular electron transfer via microbial nanowires. *Nature* 435, 1098–1101. doi: 10.1038/nature03661

Rowe, R. A., Chellamuthu, P., Lam, B., Okamoto, A., and Nealson, K. H. (2015). Marine sediments microbes capable of electrode oxidation as a surrogate for lithotrophic insoluble substrate metabolism. *Front. Microbiol.* 5:784. doi: 10.3389/fmicb.2014.00784

Sandy, M. (2011). *Isolation and Structure Characterization of New Bacterial Triscatecholate Siderophores*. Ph.D. dissertation, University of California, Santa Barbara, CA.

Santelli, C. M. (2007). *Geomicrobiology of the Ocean Crust: The Phylogenetic Diversity, Abundance, and Distribution of Microbial Communities Inhabiting Basalt and Implications for Rock Alteration Processes*. Ph. D. dissertation, Massachusetts Institute of Technology, Cambridge, MA. doi: 10.1575/1912/1735

Santelli, C. M., Orcutt, B. N., Banning, E., Bach, W., Moyer, C. L., Sogin, M. L., et al. (2008). Abundance and diversity of microbial life in ocean crust. *Nature* 453, 653–656. doi: 10.1038/nature06899

Schaedler, S., Burkhardt, C., Hegler, F., Straub, K. L., Miot, J., Benzerara, K., et al. (2009). Formation of Cell-Iron-Mineral aggregates by phototrophic and nitrate-reducing anaerobic Fe(II)-oxidizing bacteria. *Geomicrobiol. J.* 26, 93–103. doi: 10.1080/01490450802660573

Scott, J. J., Breier, J. A., Luther, G. W. III, and Emerson, D. (2015). Microbial iron mats at the mid-atlantic ridge and evidence that zetaproteobacteria may be restricted to iron-oxidizing marine systems. *PLoS ONE* 10:e0119284. doi: 10.1371/journal.pone.0119284

Singer, E., Heidelberg, J. F., Dhillon, A., and Edwards, K. J. (2013). Metagenomic insights into the dominant Fe (II) oxidizing zetaproteobacteria from an iron mat at Lô ́ihi, Hawai ́l. *Front. Microbiol.* 4:52. doi: 10.3389/fmicb.2013.00052

Statham, P., German, C., and Connelly, D. (2005). Iron (II) distribution and oxidation kinetics in hydrothermal plumes at the Kairei and Edmond vent sites, Indian Ocean. *Earth Planet. Sci. Lett.* 236, 588–596. doi: 10.1016/j.epsl.2005.03.008

Staudigel, H., Chastain, R., Yayanos, A., and Bourcier, R. (1995). Biologically mediated dissolution of glass. *Chem. Geol.* 2, 147–154. doi: 10.1016/0009-2541(95)00115-X

Staudigel, H., Furnes, H., Banerjee, N. R., Dilek, Y., and Muehlenbachs, K. (2006). Microbes and volcanoes: a tale from the oceans, ophiolites and greenstone belts. *GSA Today* 16, 4–10. doi: 10.1130/GSAT01610A.1

Staudigel, H., Furnes, H., McLoughlin, N., Banerjee, N. R., Connell, L. B., and Templeton, A. (2008). 3.5 billion years of glass bioalteration: Volcanic rocks as a basis for microbial life? *Earth Sci. Rev.* 89, 156–176. doi: 10.1016/j.earscirev.2008.04.005

Staudigel, H., and Hart, S. R. (1983). Alteration of basaltic glass: mechanisms and significance for the oceanic crust-seawater budget. *Geochim. Cosmochim. Acta* 47, 337–350. doi: 10.1016/0016-7037(83)90257-0

Stewart, P. S. (2003). Diffusion in biofilms. *J. Bacteriol.* 185, 1485–1491. doi: 10.1128/JB.185.5.1485-1491.2003

Sudek, L. A. (2011). *Ecology of Microbe/Basaltic Glass Interactions: Mechanisms and Diversity*. Ph. D. dissertation, University of California, San Diego, CA.

Sudek, L. A., Templeton, A. S., Tebo, B. M., and Staudigel, H. (2009). Microbial ecology of Fe (hydr)oxide mats and basaltic rock from Vailulu'u Seamount, American Samoa. *Geomicrobiol. J.* 26, 581–596. doi: 10.1080/01490450903263400

Summers, Z. M., Gralnick, J. A., and Bond, D. R. (2013). Cultivation of an obligate Fe(II)-oxidizing lithoautotrophic bacterium using electrodes. *MBio* 4:e420-12. doi: 10.1128/mBio.00420-12

Templeton, A. S., Knowles, E. J., Eldridge, D. L., Arey, B. W., Dohnalkova, A. C., Webb, S. M., et al. (2009). A seafloor microbial biome hosted within incipient ferromanganese crusts. *Nat. Geosci.* 2, 872–876. doi: 10.1038/ngeo696

Templeton, A. S., Staudigel, H., and Tebo, B. M. (2005). Diverse Mn(II)-oxidizing bacteria isolated from submarine basalts at Loihi Seamount. *Geomicrobiol. J.* 22, 127–139. doi: 10.1080/01490450590945951

Thorseth, I. H., Furnes, H., and Heldal, M. (1992). The importance of microbiological activity in the alteration of natural basaltic glass. *Geochim. Cosmochim. Acta* 56, 845–850. doi: 10.1016/0016-7037(92)90104-Q

Thorseth, I. H., Furnes, H., and Tumyr, O. (1995). Textural and chemical effects of bacterial activity on basaltic glass: an experimental approach. *Chem. Geol.* 119, 139–160. doi: 10.1016/0009-2541(94)00098-S

Thorseth, I. H., Torsvik, T., Torsvik, V., Daae, F. L., and Pedersen, R. B. (2001). Diversity of life in ocean floor basalts. *Earth Planet. Sci. Lett.* 194, 31–37. doi: 10.1038/nature06899

Toner, B. M., Fakra, S. C., Manganini, S. J., Santelli, C. M., Marcus, M. A., Moffett, J. W., et al. (2009). Preservation of iron(II) by carbon-rich matrices in a hydrothermal plume. *Nat. Geosci.* 2, 197–201. doi: 10.1038/ngeo433

Yong, X. Y., Shi, D. Y., Chen, Y. L., Feng, J., Xu, L., Zhou, J., et al. (2014). Enhancement of bioelectricity generation by manipulation of the electron shuttles synthesis pathway in microbial fuel cells. *Bioresour. Technol.* 152, 220–224. doi: 10.1016/j.biortech.2013.10.086

Conflict of Interest Statement: The authors declare that the research was conducted in the absence of any commercial or financial relationships that could be construed as a potential conflict of interest.

The reviewer AR declared a shared affiliation, though no other collaboration, with one of the authors GW to the handling Editor, who ensured that the process nevertheless met the standards of a fair and objective review.

frontiers in Microbiology

ORIGINAL RESEARCH
published: 21 January 2016
doi: 10.3389/fmicb.2015.01518

Structural Iron (II) of Basaltic Glass as an Energy Source for Zetaproteobacteria in an Abyssal Plain Environment, Off the Mid Atlantic Ridge

Pauline A. Henri[1], Céline Rommevaux-Jestin[1], Françoise Lesongeur[2], Adam Mumford[3], David Emerson[3], Anne Godfroy[2] and Bénédicte Ménez[1]*

[1] Institut de Physique du Globe de Paris, Sorbonne Paris Cité, Univ Paris Diderot, Centre National de la Recherche Scientifique, Paris, France, [2] Laboratoire de Microbiologie des Environnements Extrêmes, Ifremer, CNRS/UMR 6197, Plouzané, France, [3] Bigelow Laboratory for Ocean Sciences, East Boothbay, ME, USA

OPEN ACCESS

Edited by:
Cara M. Santelli, University of Minnesota, USA

Reviewed by:
Axel Schippers, Federal Institute for Geosciences and Natural Resources (BGR), Germany
Lisa Mayhew, University of Colorado – Boulder, USA

****Correspondence:***
Pauline A. Henri
henri@ipgp.fr

Specialty section:
This article was submitted to Extreme Microbiology, a section of the journal Frontiers in Microbiology

Received: *31 August 2015*
Accepted: *17 December 2015*
Published: *21 January 2016*

Citation:
Henri PA, Rommevaux-Jestin C, Lesongeur F, Mumford A, Emerson D, Godfroy A and Ménez B (2016) Structural Iron (II) of Basaltic Glass as an Energy Source for Zetaproteobacteria in an Abyssal Plain Environment, Off the Mid Atlantic Ridge. Front. Microbiol. 6:1518. doi: 10.3389/fmicb.2015.01518

To explore the capability of basaltic glass to support the growth of chemosynthetic microorganisms, complementary *in situ* and *in vitro* colonization experiments were performed. Microbial colonizers containing synthetic tholeitic basaltic glasses, either enriched in reduced or oxidized iron, were deployed off-axis from the Mid Atlantic Ridge on surface sediments of the abyssal plain (35°N; 29°W). *In situ* microbial colonization was assessed by sequencing of the 16S rRNA gene and basaltic glass alteration was characterized using Scanning Electron Microscopy, micro-X-ray Absorption Near Edge Structure at the Fe-K-edge and Raman microspectroscopy. The colonized surface of the reduced basaltic glass was covered by a rind of alteration made of iron-oxides trapped in a palagonite-like structure with thicknesses up to 150 μm. The relative abundance of the associated microbial community was dominated (39% of all reads) by a single operational taxonomic unit (OTU) that shared 92% identity with the iron-oxidizer *Mariprofundus ferrooxydans* PV-1. Conversely, the oxidized basaltic glass showed the absence of iron-oxides enriched surface deposits and correspondingly there was a lack of known iron-oxidizing bacteria in the inventoried diversity. *In vitro*, a similar reduced basaltic glass was incubated in artificial seawater with a pure culture of the iron-oxidizing *M. ferrooxydans* DIS-1 for 2 weeks, without any additional nutrients or minerals. Confocal Laser Scanning Microscopy revealed that the glass surface was covered by twisted stalks characteristic of this iron-oxidizing Zetaproteobacteria. This result supported findings of the *in situ* experiments indicating that the Fe(II) present in the basalt was the energy source for the growth of representatives of Zetaproteobacteria in both the abyssal plain and the *in vitro* experiment. In accordance, the surface alteration rind observed on the reduced basaltic glass incubated *in situ* could at least partly result from their activity.

Keywords: basaltic glass, Zetaproteobacteria, bio-mediated alteration, iron-oxidation, abyssal plain

INTRODUCTION

In the dark ocean, microbial communities must thrive either by using organic carbon coming from the photic zone as an energy source, thus by chemoorganotrophy or by chemolithotrophy. Chemolithotrophic microbes gain their energy by oxidizing a wide variety of reduced inorganic substrates such as sulfur and sulfides, ammonia, molecular hydrogen, and iron. Because iron is the fourth most abundant element in the Earth's crust, Fe(II) is potentially among the most abundant energy sources for life at the boundary between the oxygenated ocean and the reducing subsurface (Fortin and Langley, 2005). Nonetheless, the chemical oxidation of Fe(II) to less soluble Fe(III) and the subsequent precipitation of iron (oxyhydr)oxides occur rapidly in the presence of strong oxidants especially at non-acidic pH in well-oxygenated environments. The iron oxidizing bacteria (FeOB) that derive their energy from the oxidation of Fe(II) compete with this abiotic reaction; however, when the O_2 fugacity is low, specialized groups of FeOB can flourish.

Microbial Fe(II)-oxidation has a lower energetic yield (≈ -90 kJ·mol^{-1}; Emerson et al., 2010) compared to other chemolithotrophic metabolisms that are widespread at the ocean/seafloor interface such as sulfide oxidation (≈ -500 kJ·mol^{-1}; Edwards et al., 2005). Despite these poor energetics and a well oxygenated modern ocean, communities of marine FeOB are increasingly being described, especially in areas of hydrothermal venting, either at seamounts or at seafloor spreading centers, where anoxic and hot fluids enriched in Fe(II) discharge and mix with oxygenated cold seawater (Emerson and Moyer, 2002; Hodges and Olson, 2009; Kato et al., 2009; Sudek et al., 2009; Emerson et al., 2010). Among these FeOB, members of the newly described class formed by the Zetaproteobacteria (Emerson et al., 2007) were shown to be widely distributed and systematically associated with iron-rich marine environments (Scott et al., 2015). Zetaproteobacteria are able to grow via Fe-oxidation at circumneutral pH and under microaerophilic conditions, resulting in the precipitation of large amounts of Fe-oxyhydroxides. One cultured representative of this class, *Mariprofundus ferrooxydans* PV-1, produces characteristic twisted stalks of iron oxyhydroxides that also contain exopolymeric substances (Emerson and Moyer, 1997; Chan et al., 2009).

While the biological oxidation of Fe(II) is now well established in certain deep-sea benthic habitats, there are still open questions about the sources of Fe(II). Edwards et al. (2003) were the first to test the hypothesis that glassy basalt could support the growth of FeOB, acting as a substrate by constituting a solid Fe(II) source. They carried out *in vitro* experiments during which they isolated FeOB from deep sea, low-temperature weathering deposits recovered in the vicinity of the Juan de Fuca hydrothermal area. These bacteria were cultured on a variety of natural and synthetic solid rock and mineral substrates, including basaltic glass (at 10 wt% FeO) without any addition of other energy sources. It was shown that when the basaltic glass was used as substrate, it promoted the growth of neutrophilic autotrophic iron-oxidizing Gammaproteobacteria- and Alphaproteobacteria, suggesting a role for these organisms in primary production and basalt weathering at seafloor. However, neither the initial basalt substrate nor the obtained alteration by-products were characterized or discussed. In parallel, several studies that aimed at describing microbiota hosted in basalts, demonstrated that microbial communities of the oceanic crust are very diverse (Lysnes et al., 2004; Templeton et al., 2005; Mason et al., 2007, 2009; Einen et al., 2008; Santelli et al., 2008; Sudek et al., 2009; Orcutt et al., 2011). However, there have few attempts to link the inventory of the microbial communities with the description of the basalt alterations phases. It was shown that the microbial diversity positively correlates with the degree of basaltic glasses' alteration (Santelli et al., 2008), and that the composition of the microbial communities depended on the age of the basalts and therefore on their alteration state (Lysnes et al., 2004; Mason et al., 2009). Nonetheless these studies mainly focused on old basalts (of millions of years) recovered by drilling into the oceanic crust.

Few studies focused on young oceanic basaltic glasses. Those have shown that, although abundantly colonized by heterotrophic microorganisms, the glassy rims of the basaltic lavas were not significantly altered (Templeton et al., 2009; Cockell et al., 2010). Consequently, the basaltic glass was considered by these authors to be a surface habitat on which to grow, rather than as a direct source of energy to support microbial growth. In parallel, *in situ* and laboratory experiments have also demonstrated the capability of adhering microorganisms to directly alter silicates and hence to release elements from the basalt by producing protons, hydroxyl groups or organic ligands at the point of attachment. By modifying locally their environment through their metabolic by-products, microorganisms can then make bioavailable the nutrients and metals contained in silicates (Bennett et al., 2001; Brantley et al., 2001; Rogers and Bennett, 2004).

Here, we present the first direct evidence of the capability of structural Fe(II) from basaltic glass to serve as an energy source for FeOB belonging to the class of Zetaproteobacteria in an abyssal plain off the Mid Atlantic Ridge (MAR). In this context, bottom seawater contrasts with seafloor environments influenced by hydrothermal fluids, being typified by low temperatures, high chlorinity, high pH, high alkalinity, and low metal and hydrogen sulfide concentrations. The results reported here combine complementary *in situ* and *in vitro* colonization experiments whose products were characterized by a multidisciplinary approach that combined molecular ecology along with spectroscopy and microscopy techniques.

MATERIALS AND METHODS

Experimental Settings

In Situ Experiment

The *in situ* colonization experiment was carried out for 11 months in a sedimented abyssal plain, off the Mid Atlantic Ridge (N35°59,88; W29°02,949 at 3200 m below sea level – mbsl; **Figure 1**). The deployment of the colonization device was done during the Graviluck 06 cruise (R.V. *L'Atalante* with the *Nautile* submersible, 2006) and the recovery occurred during the MoMARDream 07 cruise (R.V. *Pourquoi Pas?* with the *Nautile*

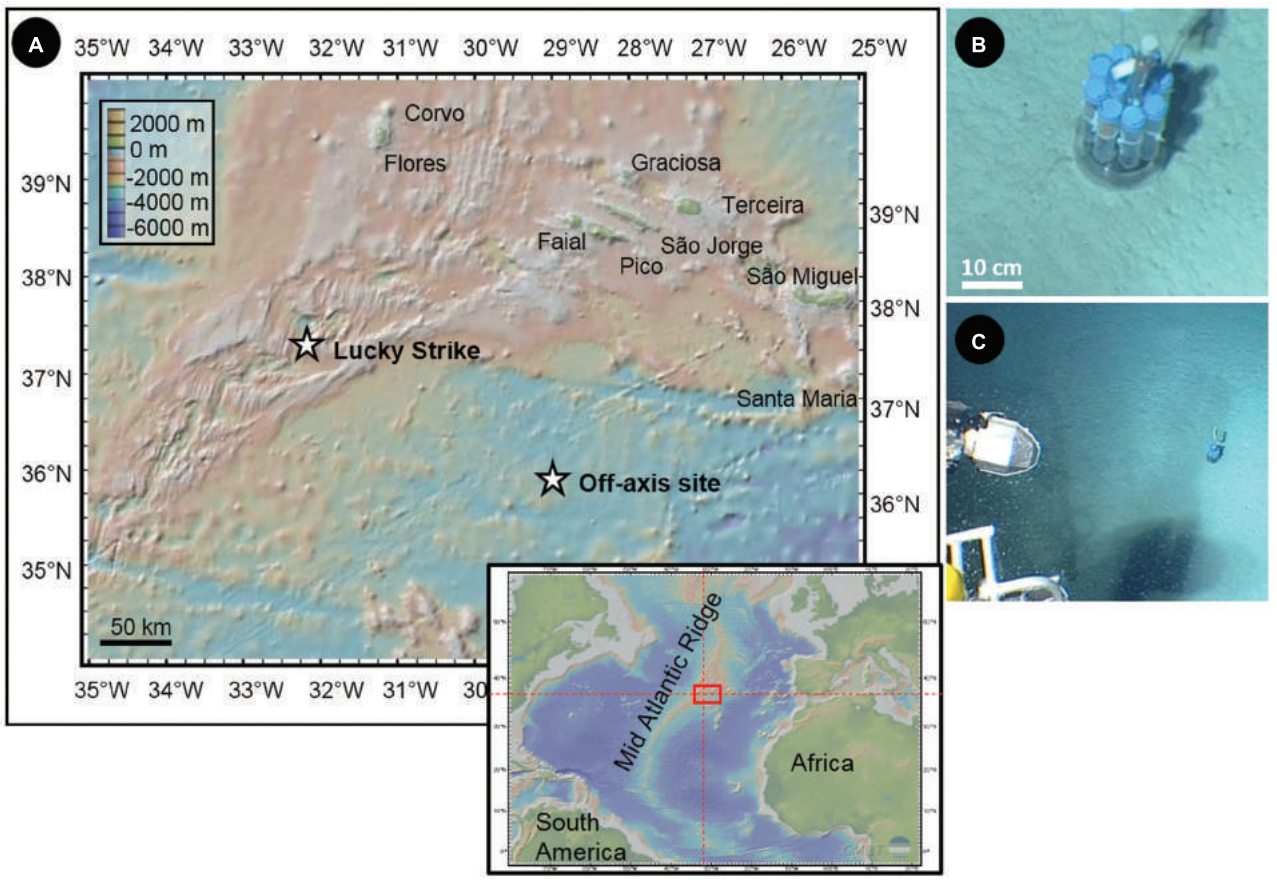

FIGURE 1 | (A) Location and associated bathymetry of the Lucky Strike hydrothermal field along the Mid-Atlantic Ridge (MAR) and of the off-axis site in the Atlantic abyssal plain (N35°59, 88; W29°02,949; 3200 mbsl) where incubations of synthetic basaltic glasses were carried out during 11 months. **(B)** and **(C)** Pictures of the microbial incubator deployed in the abyssal plain (taken in 2006 by the *Nautile* submersible).

submersible, 2007). During the Graviluck 06 cruise, a CTD profile was collected up to 2635 mbsl in the water column above the deployment location, in order to characterize the environmental conditions of the site.

The colonization modules consisted of a ballasted plastic holder that hosted up to twelve biological colonizers and abiotic controls distributed around an autonomous temperature probe. The biological incubators were made up of capped 50 ml DB Falcon^{TM} conical polypropylene tubes, in which ±20 holes of 1 mm in diameter were drilled to allow seawater circulation. Each colonizer was filled with chips of basaltic glass designed to serve as solid Fe-substrates. The basaltic glasses were synthesized at the Laboratoire de Géomatériaux et Environnement (Université de Marne-la-Vallée, France) from a mixture of different oxide and carbonate powders, resulting in a typical tholeiitic basalt composition (i.e., in weight%, 48.6 SiO_2, 15.7 Al_2O_3, 11.1 CaO, 7.7 MgO, 12.5 FeO/Fe_2O_3, 2.7 Na_2O, 0.2 K_2O, and 1.4 TiO_2). Two different types of synthesis were performed: (1) under a reducing atmosphere of H_2 to enrich the glass in Fe(II) (hereafter referred to as BH2) and (2) under an oxidizing atmosphere of O_2 to conversely enrich the glass in Fe(III) (hereafter referred to as BO2). The synthesis protocol is described in the Supplementary Material. Freshly synthetized basaltic glasses were cleaned in an ultrasonic bath filled with ethanol, and then air-dried before being packed in the colonizers. In order to benefit from abiotic controls, tubes without holes were also filled with basaltic glass chip and closed by a 0.22 μm cellulose filtration membrane (Millipore^{TM}) to allow exchanges with the surrounding fluid while avoiding microbial colonization. The filled colonizers were sterilized by autoclaving for 30 min at 121°C shipboard. The colonizer holder was cleaned up with a Desibac HPC$^{®}$ solution and rinsed with deionized water (MilliQ^{TM} 18 MΩ) then ethanol 96% prior to the assemblage. For the deployment by the Nautile submersible during the Graviluck cruise (2006), the full module was installed in a biobox that was cleaned with the same protocol as for the colonizer holder and filled with sterilized deionized water in order to avoid microbial contamination from the water column during operations. During the incubation period, *in situ* temperature was monitored every 5 min by using an autonomous temperature sensor (NKE SDT6000D-26001) set amongst the Falcon^{TM} tubes.

During the MoMARDream cruise (2007), the module was recovered in a biobox using the Nautile submersible and the incubated basaltic glass chips were preserved on board under

sterile conditions for different types of analysis. For DNA analysis, samples were stored in ethanol 96% at −20°C. About 2 L of ambient seawater from the seafloor was filtered onto 0.22 μm-pore-size membranes, which were then stored in ethanol 96% at −20°C for DNA analyses. Deep sea sediments were also sampled in the vicinity of the colonization module and similarly preserved for DNA analysis.

In Vitro Experiments

Two types of *in vitro* experiments were conducted. The first one aimed at reproducing in laboratory the conditions mimicking the abiotic control which did not succeed during the *in situ* experiment. For this purpose, fragments of reduced basaltic glass were autoclaved 20 min at 121°C and packed in 50 ml Falcon™ tubes containing sterile costal seawater (previously filtered onto 0.22 μm filtration membrane and autoclaved). One tube was incubated at 4°C whereas a second one stayed at ambient temperature, both during 1 year.

The second experiment aimed at testing the hypothesis that Zetaproteobacteria could thrive with the synthetic reduced basaltic glass as the only solid Fe(II) substrate. For this purpose a custom built flow through system was used. Briefly, this consisted of a 50 ml incubation chamber that was continuously flushed with sterile seawater, buffered with $NaHCO_3$ at pH 6.5 and gently bubbled with filtered air to avoid complete anaerobic conditions (Mumford and Emerson, unpublished results). Two sterilized chips of synthetic reduced basaltic glass were stuck on a glass slide with silicon glue. The slide was introduced vertically in the incubation chamber that was inoculated with 1 ml of a pure culture of the FeOB *M. ferrooxydans* DIS-1 that was originally isolated from mild steel, and is an obligate Fe-oxidizer. Prior to inoculation, abundance and shape of the cells were checked through fluorescent staining using the green-fluorescent nucleic acid stain SYTO® 13. The incubation lasted 2 weeks, without any addition of nutrient, chemical or minerals.

Methods and Data Analyses

Analysis of the 16s rRNA Gene Sequences

In order to characterize the microbial diversity, total genomic DNA was extracted using the UltraClean® Soil DNA Isolation Kit (MO BIO laboratories, Inc,) following the manufacturer protocol.

Sequencing of the 16S rRNA gene sequences of the community DNA extracted from the reduced and oxidized incubated basaltic glasses (BH2 and BO2, respectively), the abyssal plain sediment (SED) and the background seawater samples (H2O) was performed by conventional Sanger technique using universal primers: U1492R (5′-GGC TAC CTT GTT ACG ACT T-3′) as reverse primer and E8F (5′-AGA GTT TGA TCC TGG CTC AG-3′) or 27F (5′-AGA GTT TGA TCC TGG CTC AG-3′) as forward primers. Clone libraries were constructed using the TOPO® XL PCR Cloning Kit, with the One Shot® TOP10 Chemically Competent *Escherichia coli* kit (Invitrogen™) according to the manufacturer instructions. Plasmid extraction, purification and sequencing were carried out by GATC Biotech (Germany).

The microbial diversity of BH2 sample was additionally analyzed by 454-pyrosequencing through the amplification of the V2–V3 region of the 16S rRNA coding genes with 27F (5′-AGA GTT TGA TCC TGG CTC AG-3′) as forward primer and 533R (5′-TTA CCG CGG CTG CTG GCA C-3′) reverse. Pyrosequencing, demultiplexing, and contig assembly were carried out by Beckman Coulter genomics (Danvers, MA, USA) using the Roche GS FLX platform (454 Life Sciences, Branford, CT, USA) with the Titanium LIB-A kit for bi-directional amplicons sequencing (see Supplementary Material for further information).

Data processing was performed with Mothur (Schloss et al., 2009). For 454-pyrosequencing analyses, we only kept the sequences whose sizes ranged between 400 and 500 bp with no ambiguity and a maximum homopolymer length of 8 bp. A 50 bp sliding-window with an average quality of 35 was used for filtering, as recommended in (Schloss et al., 2011). For all sequences, the presence of chimeras for removal was checked by Uchime (Edgar et al., 2011). Taxonomic affiliations were made with the SILVA database (Pruesse et al., 2007; Quast et al., 2012). Sequences with bootstrap values below 95% have been considered as non-affiliated sequences. Sequence alignment, generation of the distance matrix from the aligned sequences and calculation of the rarefaction curves and richness indicators were performed with Mothur (v1.33.3). The sequence data reported in this study have been submitted to the GenBank nucleotide sequence database under accession number KM580076–KM580346 for the sequences obtained by Sanger sequencing and the BioProject ID PRJNA260775 for the sequences obtained by 454-pyrosequencing.

A distance level of 0.03 was used to compare sequences for both rarefaction and diversity indicators. Operational taxonomic units (OTUs) were similarly defined by a 0.03 distance level (i.e., sequences with ≥97% similarity are designated to a single OTU). Representative sequences of each sample along with closely related environmental clones and cultured species were selected for general phylogenetic tree construction. Tree topology and branch lengths were determined with MEGA 5 (Kumar et al., 2008), using maximum likelihood criterion for distance analysis. Maximum likelihood bootstrapping was carried out with 1,000 replicates.

Spectroscopy/Microscopy

Raman spectroscopy analyses were performed at IPGP with a Renishaw InVia spectrometer using the 514 nm wavelength argon laser (20 mW) focused through an Olympus BX61 microscope with 50× objective (numerical aperture: 0.75). The obtained planar resolution was about 1 μm, with a power delivered at the sample surface of 0.5 mW. The Raman signal was dispersed with a 1800 grooves/mm holographic grating and collected using a RENCAM CCD array detector. The obtained spectral data were acquired, visualized and the baselines were subtracted (by polynomial fitting) with the software Wire 3.3 (Renishaw).

Scanning Electron Microscopy (SEM) was performed at the "Service Commun de Microscopie Electronique à Balayage" (UPMC, Paris, France) with a Zeiss SUPRA 55 VP Field Emission Scanning Electron Microscope on carbon coated samples. Three secondary electron detectors (Everhart-Thornley for high voltage mode, VPSE for variable pressure mode and InLens for low

voltage mode) and a backscattered electron detector enabled the acquisition of high resolution images using analytical conditions that varied from 3 to 30 kV, 10 pA–1 nA, and 30–133 Pa with a 3.3–7.2 mm working distance. Elemental microanalyses were also performed using an Energy Dispersive X-ray (EDX) spectrometer (PGT Sahara).

To assess the redox state of iron in the synthetic basaltic glasses before and after the *in situ* incubation experiment, glass chips were embedded in LR White resin (4/5 araldite DBF epoxy resin, 1/5 hardener Huntsman containing triethylenetetramine) following the manufacturer protocol. Embedded chips were then cut and polished first with a silicon carbide polishing paper and then on tissue carpet with a solution of Mecaprex® diamond compounds up to a 1 μm grain until glass chips were outcropping. Synchrotron-based X-ray fluorescence measurements of elemental distributions and X-ray Absorption Near Edge Structure (XANES) spectra at the Fe K-edge were acquired on beamline LUCIA (Synchrotron Soleil, Saint Aubin, France) using Si (311) crystal monochromator (0.2 eV resolution for Fe) and a focused spot size of 2 μm × 2 μm. Several Fe-bearing compounds with various redox states were used as references (see Supplementary Table S1). The iron redox state of samples was evaluated following the procedure described by Wilke et al. (2001; see Supplementary Figure S2 and Table S2). Spectra collected on the alteration rind were fitted using linear combinations of the Fe K-edge XANES spectra collected on the reference compounds in order to determine the composition of the alteration layer.

Confocal Laser Scanning Microscopy (CLSM) was used to visualize basalt chip surfaces from the *in vitro* incubation experiments. Each sample was overlaid with a staining solution consisting of 1.5 μl at 2 mg/ml of rhodamine-conjugated *Ricinus communis* agglutinin I (Vector Labs), and 5 μl of SYTO® 13 in 144.5 μl 0.5% low-melting-point agarose in MilliQ reagent-grade water. They, respectively, stain carbohydrate linkages in polysaccharides, and nucleic acids. Following the application of the staining solution, a custom-made frame allowed for approximately 150 μm of clearance between the top of the basaltic glass chip and the underside of the coverslip (Mumford and Emerson, unpublished results). After the frames were applied, the slides were incubated with the dyes for 1 hour at 4°C, and then low melt agarose (0.5%) was added to stabilize the chips and covered with a glass coverslip. Observations were performed at Bigelow Laboratory with a Zeiss LSM 700/Axio Observer using an oil immersion C-Apochromat objective 40×/1.2 W. Fluorescence images were obtained following excitation at 488 and 555 nm, by collecting the emitted fluorescence between 300–550 and 578–800 nm, respectively.

Additional CLSM images were acquired at IPGP using an Olympus FluoView FV1000 Confocal Microscope, displaying a spectral resolution of 2 nm and a spatial resolution of 0.2 μm, on samples from the *in situ* experiment stained with green-fluorescent SYTO® 9 used at a working concentration of 50 μM. An oil immersion objective UPLSAPO 60XO (Olympus; 60× magnification, numerical aperture = 1.35) was used. Fluorescence image stacks were obtained with excitation at a wavelength of 488 nm, by collecting the emitted fluorescence between 300 and 500 nm. The three-dimensional images were acquired, visualized and processed using the F10-ASW FLUOVIEW software (Olympus).

RESULTS

The colonization module was deployed in the abyssal plain on carbonated sediments (**Figures 1B,C**). The oxygen concentration measured by the CTD probe at 2635 mbsl was 246.8 μmol/kg, attesting to a well-oxygenated environment. The temperature recorded by the probe installed in the colonization module revealed stable values during the entire incubation period (i.e., 11 months) with a mean value of 2.92°C (±0.02°C).

Phylogenetic Diversity and Distribution for the *In Situ* Experiment

For BH2, the incubated synthetic reduced basaltic glass for which both sequencing techniques were used, 454-pyrosequencing provided as expected more reads (3797) compared to the number of clones retrieved by Sanger sequencing (42). Because of this greater number of sequences, allowing a more representative assessment of the bacterial diversity and composition for BH2, we have focused on the 454-pyrosequencing results in the case of this sample. For comparison with the diversity results obtained for the three other samples that were only sequenced using the Sanger technique, we have only used percentages of the total number of the obtained sequences for each sample. Both sequencing techniques lead to comparable OTU distribution for BH2 (**Table 1**). Shannon indices were also comparable for the two sequencing techniques (**Table 2**).

The Shannon's indices estimated for each sample showed that the microbial diversity in the water sample was the lowest. Those of the two incubated basaltic glass were comparable with intermediate values, the greatest values being that of the sediment (**Table 2**). By considering only the Sanger results, the observed and predicted OTU richness also showed more diversity in the sediment, followed by seawater and then the two basaltic glass samples. The rarefaction curves depicting the number of OTUs as a function of the number of analyzed sequences (**Figure 2**), showed that for an equivalent sampling effort (<100 sequences, left part of the plot) the highest observed species richness was found in the sediment, its rarefaction curve being far from reaching an asymptote, while those of BH2 (for both Sanger and 454-pyrosequencing), BO2 and water were comparable.

For all samples, most of the sequences were not closely related to cultured microorganisms. The high level (phylum/class) taxonomic distribution of OTUs is shown in **Table 1**. The phylum *Proteobacteria* dominated in all the samples and represented 48% of the OTUs retrieved from sediment and BO2 and 72–87% of the OTUs of BH2 and water, respectively. The only classes represented in all the samples were Alphaproteobacteria, Deltaproteobacteria, Gammaproteobacteria, and *Actinobacteria*. The classes with the highest relative abundance were Alphaproteobacteria in water (80%) and BO2 (32%), Gammaproteobacteria in the sediment (23%) and Zetaproteobacteria for BH2 (39%). The incubated

TABLE 1 | Distribution of phyla and classes retrieved from the oxidized and the reduced basaltic glass incubated *in situ* (BO2 and BH2), the sediment (SED) and the water (H2O) samples using Sanger sequencing (Sang) and pyrosequencing (Pyr).

Phylum[1]	Class[1]	Number of OTUs					Percentage of total sequences				
		BH2		BO2	H2O	SED	BH2		BO2	H2O	SED
		Pyr	Sang	Sang	Sang	Sang	Pyr	Sang	Sang	Sang	Sang
Proteobacteria	α	90	10	6	12	7	18	36	32	80	13
	γ	88	3	3	3	13	6	12	10	3	23
	ζ	1	1				39	31			
	δ	11		3	1	4	0.5		6	1	6
	ε	30	2				7	7			
	β	10			1	2	0.4			1	3
	JTB23				1					1	
	Others	34			1	2	1			1	3
Bacteroidetes		111	4	8		1	21	12	23		2
Planctomycetes		37	1	3		9	2	2	11		14
Acidobacteria						2					3
Actinobacteria		3		1	3	1	0.2		2	7	2
Candidate_division_TG-1						1					2
Chloroflexi		2				3	0.1				6
Gemmatimonadetes						1					5
Nitrospirae						2					3
Verrucomicrobia		3		1			0.1		2		
Other classes[2]		12					0.4				
Non affiliated after the domain		63		3	2	9	3		12	5	16

α, γ, ζ, δ, ε, β *stand for Alphaproteobacteria, Gammaproteobacteria, Zetaproteobacteria, Deltaproteobacteria, Epsilonproteobacteria, and Betaproteobacteria, respectively.*
[1]*Representing more than 1% of the total sequences at least in one sample.*
[2]*Representing less than 1% of the total sequences in the samples.*

TABLE 2 | Number of OTUs retrieved in the oxidized and the reduced basaltic glass incubated *in situ,* the sediment and the water samples using Sanger sequencing and pyrosequencing (pyro) along with estimates of diversity and richness.

	Collected sequences	OTU observed	Shannon H′ (CI)	Chao1 (95% CI)
Water (Sanger)	87	24	2.51 (±0.25)	70 (36–195)
BO2 (Sanger)	81	28	3.11 (±0.18)	36 (31–52)
BH2 (Sanger)	42	21	2.77 (±0.33)	38 (27–74)
BH2 (pyro)	3797	495	3.23 (±0.08)	1161 (981–1408)
Sediment (Sanger)	64	57	4.00 (±0.18)	270 (145–570)

CI stands for confidence indices.

basaltic glasses BH2 and BO2 accounted for 21 and 23% of the retrieved *Bacteroidetes* sequences, respectively, while this phylum represented only 2% of the retrieved sequences in the sediment and was absent in water.

Basaltic Glass Samples

Zetaproteobacteria were only retrieved in the reduced iron basalt sample (BH2). A single OTU accounted for 39% of the total sequences retrieved from this sample, while the next most abundant OTU accounted for 21% of the sequences (**Table 1**). The 400 bp read for the Zetaproteobacteria OTU (sequence OA BH2 OTU 1 in **Figure 3**) obtained by 454-pyrosequencing was nearly identical to almost complete 16S rRNA gene sequence obtained by Sanger sequencing (OA BH2 clone 94 in **Figure 3**). It was 99% similar to a sequence identified as Zetaproteobacteria sampled from a hydrothermal fluid near the Southern Mariana trough (AB284832.1, **Figure 3**; Kato et al., 2009). The nearest cultured organism (with 92% similarity) was *M. ferrooxydans* PV-1, known to be a chemolithoautotrophic iron oxidizing bacterium (Emerson and Moyer, 1997).

Members of the Epsilonproteobacteria, also only present in BH2 sample (**Figure 3**), were taxonomically affiliated to the sulfide-oxidizing genera *Sulfurimonas* and *Sulfurovorum*. Sequences were related at 94 to 99% to endosymbionts of either *Osedax mucofloris* (FN773294.1) or *Alvinichonca* sp. from sunken woods (AB235231.1) or at 99% to uncultured bacteria from the Guaymas basin (FJ981070) and the Rainbow and Lucky Strike hydrothermal fields (AY354174.1 and HE576782.1, respectively).

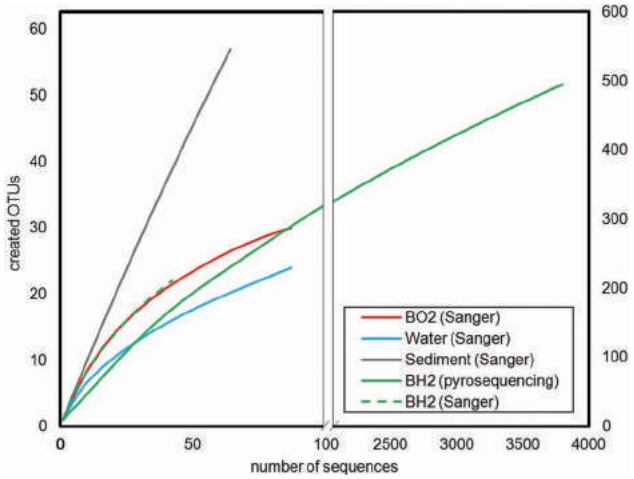

FIGURE 2 | Rarefaction curves calculated for a 0.03 distance level. The left part corresponds to an enlarged view of the number of OTUs created for a number of analyzed sequences below 100 in order to allow the comparison between the low number of sequences obtained by Sanger sequencing for seawater, sediment and basaltic glasses, and the high number of sequences obtained by 454-pyrosequencing for the reduced basaltic glass.

As shown in **Figure 3** and **Table 1**, Alphaproteobacteria showed the highest relative abundance in BO2 sample (32%) and represented 18% of the total sequences retrieved from BH2. In BO2 the majority of alphaproteobacterial sequences (22%) were closely related to uncultured bacteria hosted in macrofauna found on sunken wood (FM994678.1; HE663324.1). The other alphaproteobacterial sequences were closely related to sequences collected either in deep-sea sediment or in low-temperature hydrothermal precipitates (FN297835.1; EF067909.1). Six percent of the alphaproteobacterial sequences in BH2 sample were closely related to uncultured bacteria hosted by gastropods also found on sunken woods (FM994678.1), and four percent to a chemoorganotrophic endosymbiont of the bone-eater worm *O. mucofloris* (FN773293.1). Some sequences were related to *Caulobacter* sp. that are ubiquitous in seawater and mainly chemoorganotrophic aerobes, or to a *Rhodobacteraceae* (EF067909.1) from aerobic enrichment cultures inoculated with basalt. A few other sequences belonged to the microaerophilic *Rhodospirillales* order, known to be photoorganotrophic but able to growth also without light. Among these sequences, some were closely related to an uncultured bacterium from Fe-rich microbial mats and basaltic rocks from Vailulu'u seamount (FJ497642.1).

Within the *Bacteroidetes* whose cultured representatives are heterotrophs and mostly aerobes, most of the BH2 sequences belonged to the *Flavobacteria* class, whereas in BO2, *Sphingobacteria* were more frequently retrieved than *Flavobacteria*. In BH2, most of the flavobacterial sequences were related to sequences found associated with macrofauna (Supplementary Figure S1). In BO2, some of these sequences were related to uncultured *Bacteroidetes* from chimney-like structures with iron oxides (FJ905648.1) or hydrothermal vents of the Lau basin (AB247861.1). Other sequences were closely related to the strictly aerobic chemoheterotroph *Gaetbulibacter marinus* (AB681678.1) and to an uncultured bacterium from deep sea vent (AY373402.1).

In the basalts BO2 and BH2, the gammaproteobacterial sequences (10 and 6% of the total sequences, respectively; **Table 1**) were mainly affiliated to the genera *Colwellia* (aerobic chemoorganotroph; AY167311.1) and to sulfur-oxidizing *Leucothrix* (**Figure 3**). Other sequences were related to the sulfur-oxidizing symbiont of the clam *Lucina florida*. In BO2, the aerobic gender *Oleiphilus*, thriving only on hydrocarbons and derivates (Golyshin et al., 2002), was also represented with sequences close to an uncultured *Oleiphilus* sp. from surface water samples of an iron fertilization experiment.

The phylum *Planctomycetes* represented, respectively, 11–14% of BO2 and sediment diversity and only 2% for BH2 (**Table 1**). The cultured representatives of this phylum include aerobic or facultative anaerobic chemoheterotrophs. As shown in Supplementary Figure S1, BO2 sequences of *Planctomycetes* were mainly related to uncultured bacteria from low temperature hydrothermal oxides of the South West Indian Ridge (JN860365.1), or to a lower extent to uncultured bacteria hosted by the marine sponge *Haliclona* cf. *Gellius* sp. (EU236275.1).

Deltaproteobacteria (**Figure 3**) in BO2 (6%; **Table 1**) were related to genera *Haliangium* (cultured species are myxobacteria), *Kofleria* and *Bdellovibrio* sp (parasitic). The deltaproteobacterial sequences represented only less than 1% of the diversity of BH2 and water, respectively.

The actinobacterial sequences in BO2 (2.5%) are close to an uncultured bacterium from arctic surface sediment (Supplementary Figure S1). They were absent from BH2 sample.

Sediment and Water Samples

Gammaproteobacteria were dominant in the sediment (23%) whereas they represented less than 10% of the other samples' abundance. Numerous sediment gammaproteobacterial sequences were related to sequences retrieved from deep-sea polymetallic nodules and adjacent sediments (Wu et al., 2013). In the water sample, the 3% of Gammaproteobacteria were found either non-affiliated at the class level or as belonging to the oligotrophic marine cluster OM182.

The strong dominance of Alphaproteobacteria in the water sample was due to the affiliation of about 72% of the retrieved sequences to the heterotrophic SAR11 clade, widespread in oceanic environment and thriving on dissolved organic carbon and nitrogen from the water column (Morris et al., 2002). The water sample sequences were close to the SAR11 clade member Candidatus *Pelagibacter* (NR 074224.1, **Figure 3**). In the sediment alphaproteobacterial sequences (13%) belonged mostly to the families *Rhodobacteraceae* and *Rhodospirillaceae* and are closely related to sequences retrieved in deep sea polymetallic nodules or sediments.

The *Planctomycetes* sequences retrieved from the sediment (14%) are closely related to uncultured bacteria collected in marine sediment or abyssal plain water. *Planctomycetes* were absent in the water sample. The deltaproteobacterial sequences

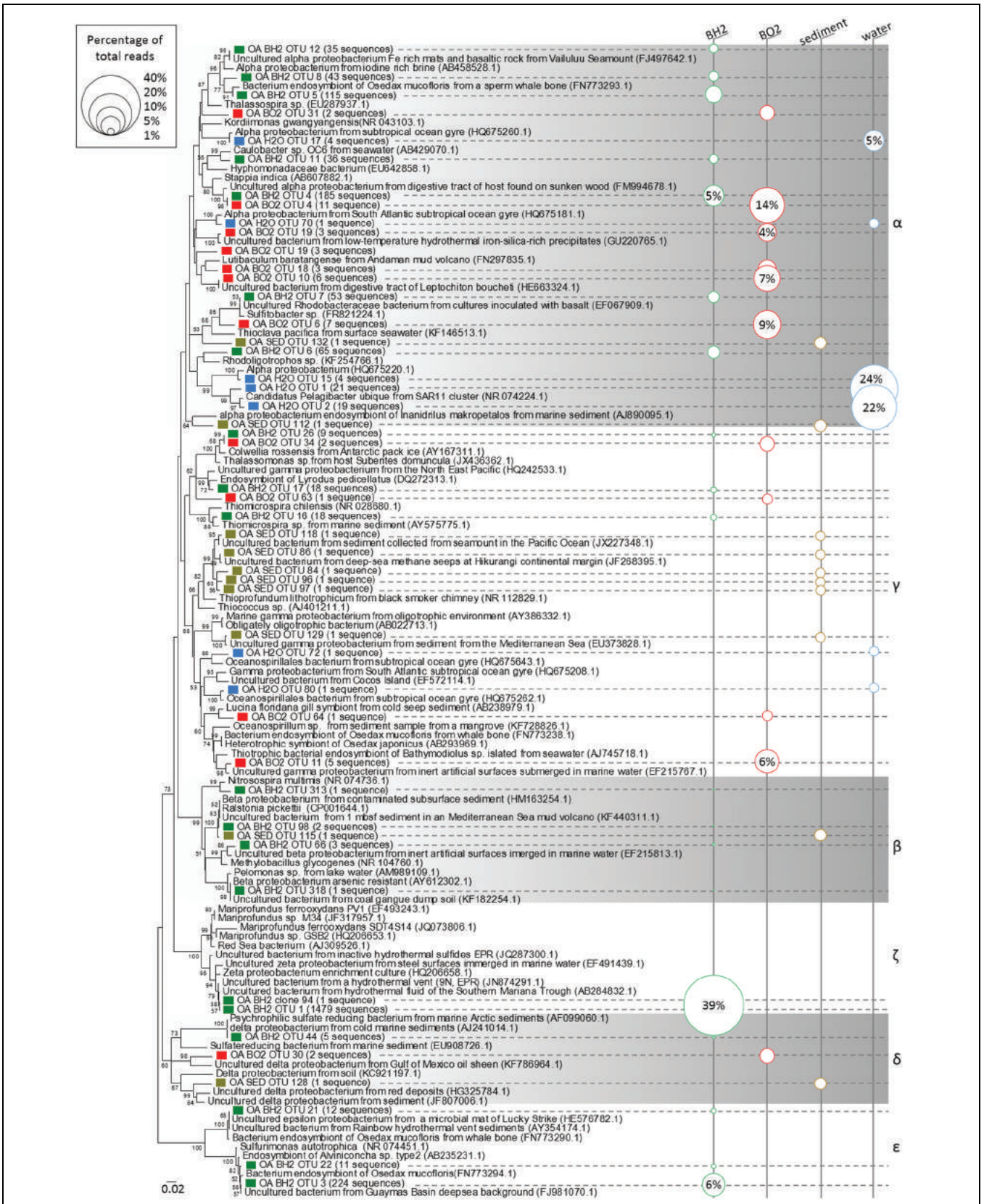

FIGURE 3 | Continued

FIGURE 3 | Continued

Phylogenetic relationships among the proteobacterial 16S rRNA gene sequences of representative OTUs of the oxidized (BO2) and reduced (BH2) basaltic glass incubated in the abyssal plain along with the seawater (H2O) and the sediment (SED). Sequences obtained in this study and designated by a prefix "OA" are indicated by a colored square; Green = BH2; Red = BO2; Blue = H2O; Bright brown = SED. The corresponding number of sequences obtained for each OTU is indicated after the name of the representative and the size of the circles in the right part figures the percentage represented by each OTU with respect to the total number of sequences. The numbers in the parentheses are the GenBank accession numbers for the NCBI sequences. The tree was determined by neighbor-joining analysis. Bootstrap values for nodes were obtained using 1,000 replicates, and only values >50% are indicated. The scale bar represents 0.02 substitutions per nucleotide position. α, γ, β, ζ, δ, and ε stand for Alphaproteobacteria, Gammaproteobacteria, Betaproteobacteria, Zetaproteobacteria, Deltaproteobacteria, and Epsilonproteobacteria, respectively.

retrieved from the sediment (6%) are related at 84 to 90% to cultured iron-reducing *Geobacter* sp. or *Desulfuromonas* sp. reducing elemental sulfur into sulfide. The *Bacteroidetes*, well represented in the basaltic glasses, represent only 2% of the sediment's OTUs and is absent in water. *Actinobacteria* were mainly represented in water (7%) with sequences affiliated to the *Acidimicrobineae* marine group and closely related to the cultured low GC content ultra-small marine *Actinobacteria,* namely Candidatus Actinomarina minuta (KC811150, Ghai et al., 2013), and to uncultured bacteria from surface seawater or the ultra-oligotrophic waters of the South Pacific gyre (JN985949.1).

Surface Analysis of the Basaltic Glass

Estimates of the initial Fe redox state of the basaltic glass, based on Fe K-edge XANES analysis, confirmed that after synthesis, the oxidized basaltic glass BO2 contained around 97% Fe(III) whereas the reduced BH2 contained around 82% Fe(II) (see Supplementary Table S2).

After incubation, the surfaces of the basaltic glass chips from the different experiments were observed using SEM and synchrotron X-ray fluorescence imaging. SEM observations revealed different features that depended upon the iron speciation in the initial basaltic glass (**Figure 4**). The BO2 samples from the *in situ* experiment did not show any traces of weathering (e.g., surface irregularities, dissolution pits) or secondary mineralization (**Figure 4A**), but cell-like structures and relics of diatoms and flagellates were observed that likely sank from the water column. Similarly, the *in vitro* abiotic control, performed using BH2, did not show any traces of cells or alteration features and only NaCl crystals formed during sample drying were noticeable (**Figure 4B**).

In contrast, the surface of BH2 incubated *in situ* had a quite uniformly thick (up to 150 μm) rust-colored rind that was evenly distributed on the surface compared to the *in vitro* incubated sample that had a thin rind sporadically distributed on the surface (**Figures 4C,D**, respectively). The BH2 rind was mainly enriched in iron and oxygen as indicated by EDX spectrum (**Figure 4E**) with less abundant Si, Al, K, Mn hence suggesting it was composed of iron oxides and silicates, likely clays, both being mineral phases composing palagonite that derives from glass alteration.

The fine texture of the alteration rind appeared similar in samples from the *in vitro* and *in situ* experiments, both presenting Fe-rich aggregated spherules covering the surface of the basalt (**Figures 5A,B**). These micron-sized spherules and the associated larger ball-like structures often displayed numerous cell imprints at their surface and were partly covered by a veil of organic matter (**Figures 5C,D**). Higher magnification revealed the stalks were associated with microspherules for the *in vitro* experiment (**Figure 5E**) while in the *in situ* experiment aggregates of microspherules were interspersed with rod-shaped microbial cells without stalks (**Figure 5F**).

Microbial cells were closely associated to the iron-rich rind as revealed by CLSM images of the SYTO® 9-stained BH2 sample from the *in situ* experiment (in green on **Figure 5H**). The reduced basaltic glass sample incubated in the laboratory flow-through system for 2 weeks with *M. ferrooxydans* exhibited a relatively high cell density and numerous Fe-bearing twisted stalks produced by the bacteria (**Figure 5G**). The laboratory incubation confirmed that microbial growth occurred presumably from Fe(II) supplied from the reduced basaltic glass, since it was the only iron source.

Similarly, the elemental distributions produced by the X-ray fluorescence microprobe on a transversal section of a BH2 fragment (**Figure 6A**) showed an enrichment in iron in the 150-μm thick iron-oxide rind (**Figures 6B,D**). To a lesser extent, Ti was also enriched in the alteration rind, compared to the intact basaltic glass while the presence of Al is quite comparable between the two phases and K seems slightly enriched at the interface (**Figure 6B**). The rind appeared chemically heterogeneous with a second phase depicted by the presence of Al, K, Ca, and Si that are colocalized and inversely correlated with Fe and Mn distributions (**Figure 6D**). The SEM-EDX results indicated a partially crystallized palagonite which is constituted by a mix of Ca-, and Si-bearing clays and zeolites along with Fe-, Mn-bearing oxides and results from low-temperature alteration of basaltic glass (Knowles et al., 2012).

XANES spectra at the K-Fe edge were acquired in the unaltered core of the basaltic glass fragment (point 1 on **Figure 6B**), at the interface between the basalt and the alteration rind, likely constituting the alteration front (point 2) and at different locations in the iron-enriched rind (points 3, 4, and 5). The pre-edge features of each spectra showed that the proportion of Fe(III) progressively increased from the unaltered basalt (where it initially reached 18%) to the external part of the rind (**Figure 6C**). Fitting of the most outer spectrum (spectrum 5) using linear combinations of pure components yielded a closest match with the following combinations: 49.9% BH2, 23.3% hypersthene (pyroxene with a 2+ valence state for iron), 21.5% hematite, and 5.5% biotite, a clay mineral (Supplementary Figure S3).

Raman spectroscopy was used to characterize the nature and mineralogy of the Fe-rich rind occurring at the surface of the chips of basaltic glass incubated both *in situ* and *in vitro*. As shown in **Figure 7**, the Raman spectrum of the basaltic glass typically exhibited a broad band around 975 cm^{-1}. Depending

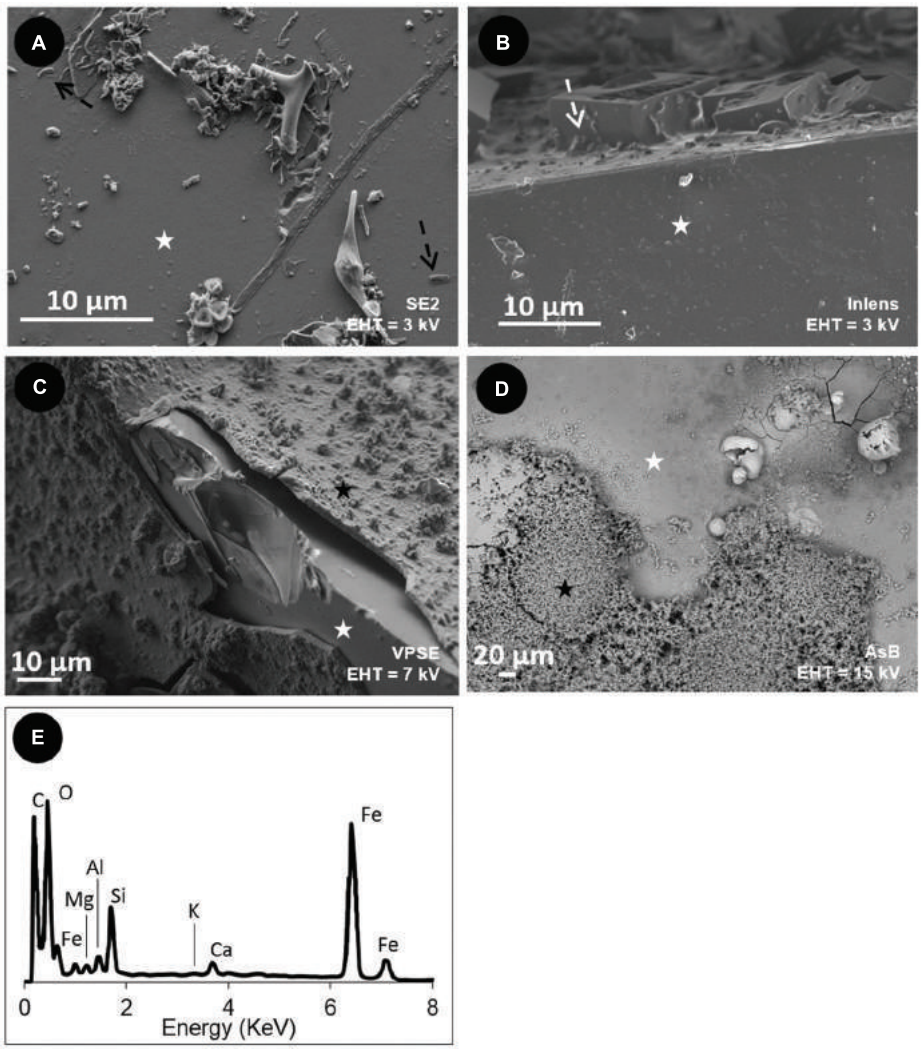

FIGURE 4 | Scanning Electron Microscopy (SEM) images of the surface of the basaltic glass chips incubated *in situ* in the abyssal plain (A,C) and *in vitro* (B,D). (A) oxidized basaltic glass incubated *in situ* (BO2; seen from above); **(B)** reduced basaltic glass abiotically incubated *in vitro* at 4°C and serving as control (side view); **(C)** reduced basaltic glass incubated *in situ* (BH2; side view); **(D)** reduced basaltic glass incubated *in vitro* with *Mariprofundus ferrooxydans* DIS-1 (seen from top). White stars = basaltic glass surface; black stars = iron oxides; black dotted arrows = cell-like structures; white dotted arrows = salt crystals. **(E)** EDX spectrum collected on the weathering rind at the surface of the reduced basaltic glass (BH2) incubated *in situ* and shown in **(C)**. Accelerating voltage (EHT) and detection modes (SE2, VPSE, Inlens = secondary electrons; AsB = backscattered electrons) used for each image are indicated.

on the thickness of the alteration rind, this band can be visible in some spectra showing also iron oxides' characteristic bands. The Raman spectra collected in these Fe-rich areas also showed broad bands at 1320 and 1590 cm^{-1}, identified as the *D* and *G* bands that are characteristic of poorly ordered carbonaceous material (Spötl et al., 1998) and interpreted as degraded organic matter according to previous studies (Maquelin et al., 2002; Callac et al., 2013). The comparison with spectra from reference compounds indicated the different iron (oxyhydr)oxides were either goethite [α FeO(OH)] for the Fe-Ox-3 point shown in **Figure 7** or biotic maghemite (γ Fe_2O_3) for the Fe-Ox-1 point. In other spectra, as the Fe-Ox-2 spectrum displayed in **Figure 7**, hematite (α Fe_2O_3) can be evidenced without any organic matter bands. Raman spectra of the Fe-bearing twisted stalks obtained during the *in vitro* experiment with *M. ferrooxydans* DIS-1 revealed a very close similarity with the Fe-Ox-1 spectrum obtained on the *in situ* incubated sample, both resembling the biotic maghemite standard. All these (oxyhydro)oxides are poorly crystallized, as revealed by their Raman band widths.

DISCUSSION

The mean temperature of 2.92°C recorded by the temperature probe for the entire duration of the incubation experiment (11 months) confirmed that the *in situ* incubation experiment was performed in a non-hydrothermally influenced environment, as expected for bottom seawater in an abyssal plain. Concordantly,

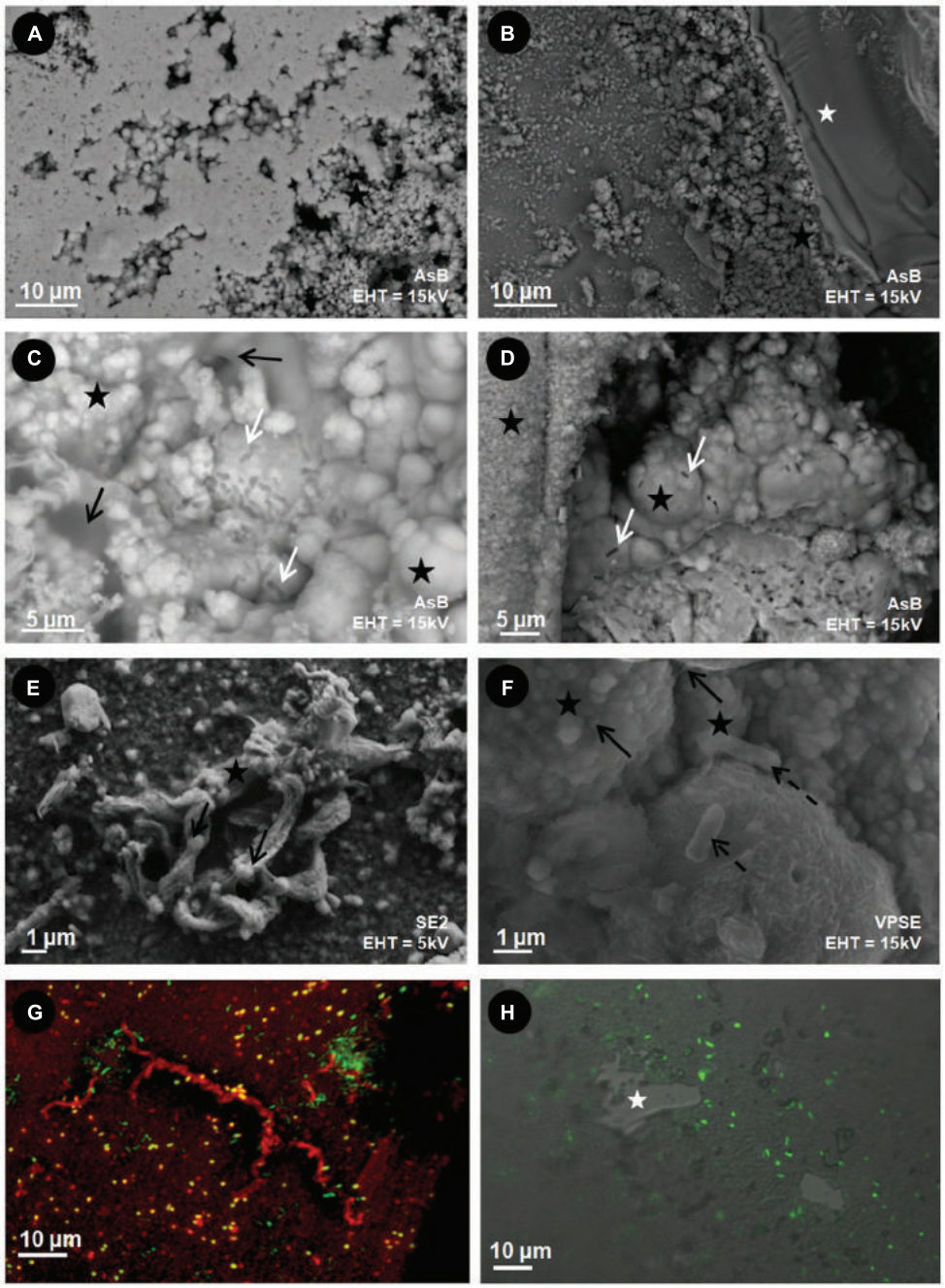

FIGURE 5 | Scanning Electron Microscopy (A–F) and CLSM (G,H) images of the surface of the reduced basaltic glass (BH2) incubated *in vitro* with *M. ferrooxydans* DIS-1 (left) and *in situ* in the abyssal plain (right). White stars = basaltic glass surface; black stars = iron oxides; black dotted arrows = cell-like structures; white arrow = cell imprints; black arrows = organic matter. **(G)** Composite CLSM image obtained with a sequential excitation at 488 and 555 nm and fluorescence emission collected between 300–550 and 578–800 nm, respectively; Green = SYTO® 13 (DNA dye); Red = rhodamine-conjugated *Ricinus communis* agglutinin I (aliphatic chains' marker); **(H)** CLSM image obtained with a excitation at a wavelength of 488 nm, by collecting the emitted fluorescence between 300 and 500 nm superimposed on an image obtained in Differential Interferential Contrast; Green = SYTO® 9 (DNA marker). Accelerating voltage (EHT) and detection modes (SE2, V PSE, Inlens = secondary electrons; AsB = backscattered electrons) used for each image are indicated.

the dominance of the SAR11 clade and the co-occurrence of other clones indicative of marine heterotrophs in the water sample were consistent with an ambient seawater community. Similarly, the important contribution in the sediment sample diversity of OTUs closely related to sequences from deep sea sediments and polymetallic nodules was also in agreement with such a sedimentary abyssal environment.

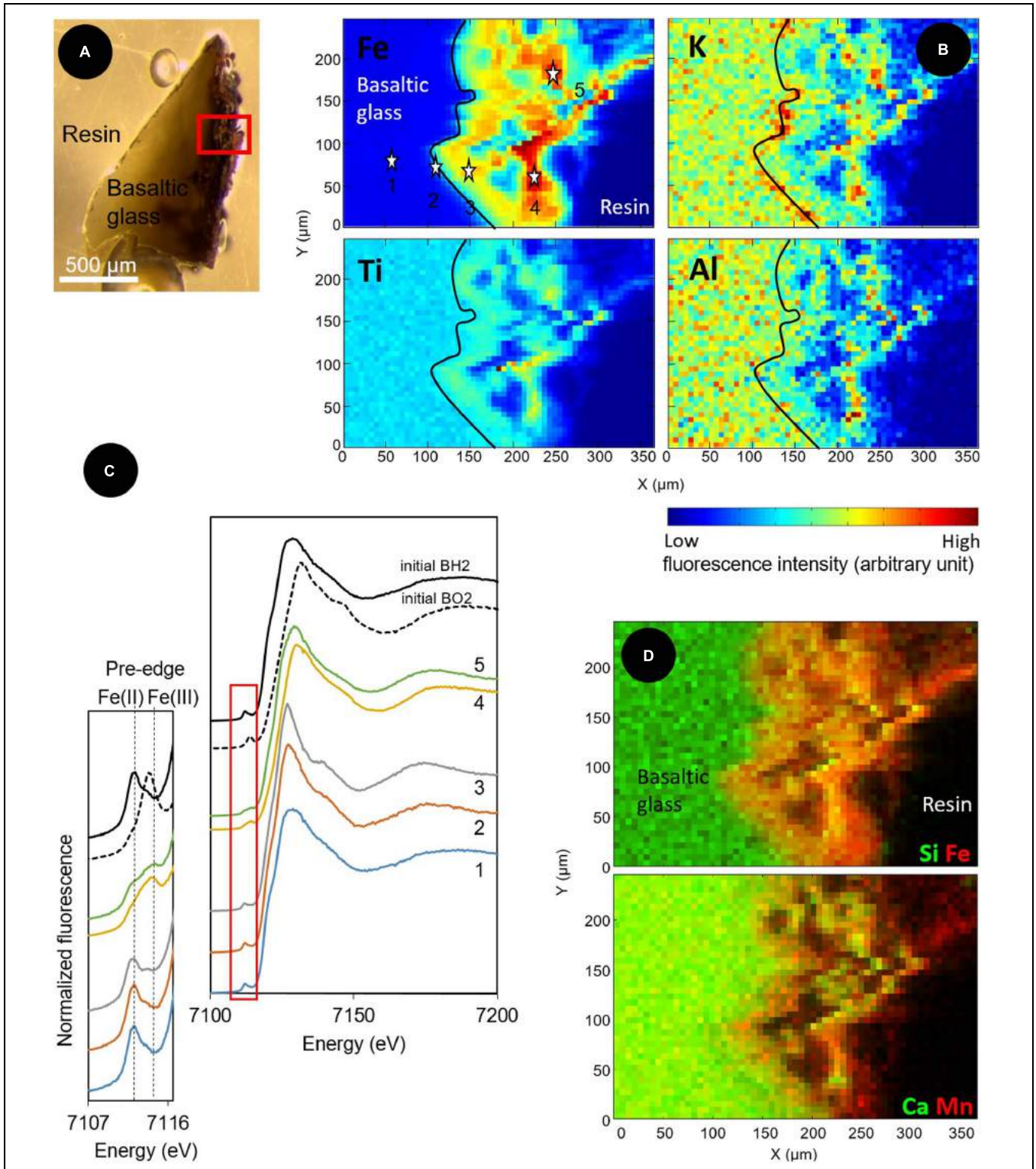

FIGURE 6 | Optical and X-ray fluorescence microprobe images along with XANES spectra at the Fe K-edge collected on a transversal section of a basaltic glass fragment incubated *in situ* in the abyssal plain. (A) Optical image in reflected light of the resin-embedded BH2 fragment; **(B)** X-ray fluorescence maps of Fe, Ti, Al, and K collected at 8 keV in the area indicated by a red square in **(A)**. The black line delineates the alteration front; **(C)** Associated Fe K-edge XANES spectra collected from 4 µm × 4 µm spots at the numbered stars' locations indicated on the Fe map in **(B)** and on unreacted reduced and oxidized basaltic glasses (BH2 and BO2) serving as references to demonstrate a change in oxidation state from Fe(II) in the basaltic glass to Fe(III) in the alteration rind.; **(D)** Red/Green maps of the distribution of Si (green) and Fe (red); and Ca (green) and Mn (red), showing the spatial colocation of Si and Ca, inversely correlated to the location of Fe and Mn.

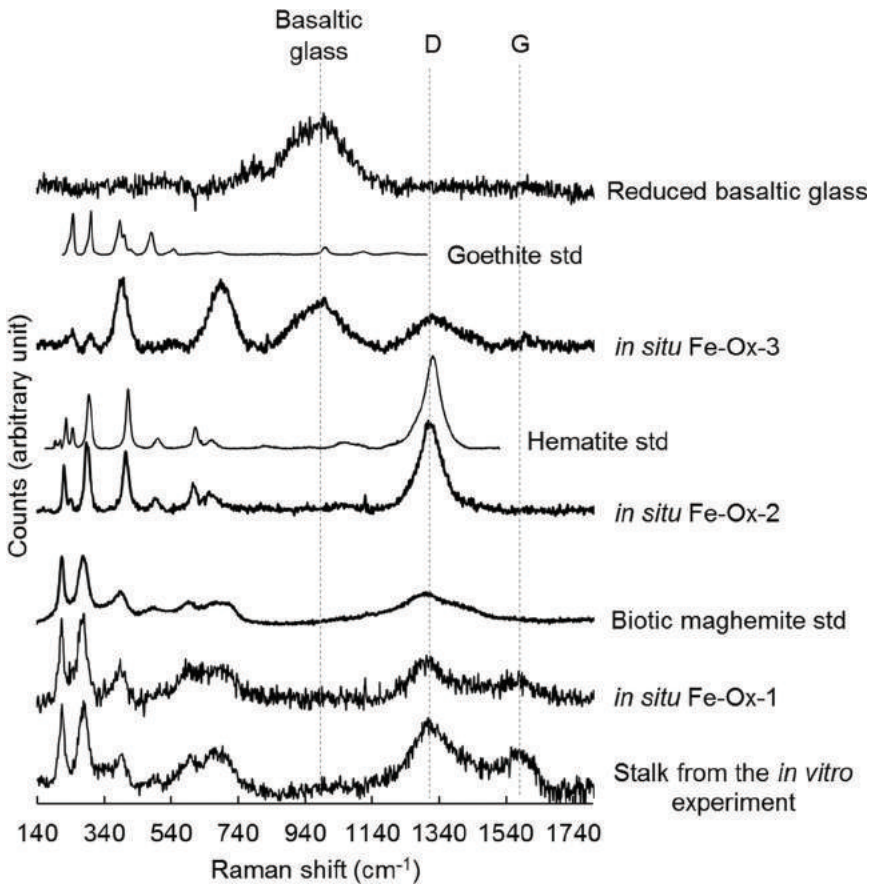

FIGURE 7 | Raman spectra collected at 514 nm excitation on iron oxides found in the alteration rind at the surface of the reduced basaltic glass incubated *in situ* in the abyssal plain and *in vitro* with *M. ferrooxydans* DIS-1, all compared to reference spectra of iron oxides (goethite, hematite, biogenic maghemite).

Conversely, the communities of bacteria on the *in situ* incubated basaltic glasses (both BO2 and BH2) were distinct from surrounding seawater. Indeed the SAR 11 clade that dominated in the water sample was absent in both basalts' surface communities. Instead, the sequences retrieved from the incubated basalts were related to those extracted from deep sea sediment or to marine symbiotic bacteria (of either wood boring bivalves or gastropods and chitons). Symbionts of *O. mucoflorix* were particularly represented, with relatives belonging to the Alphaproteobacteria, Gammaproteobacteria, and Epsilonproteobacteria classes that encompass sulfide oxidizers. The presence of Alphaproteobacteria (other than those from the SAR11 clade), Gammaproteobacteria, Epsilonproteobacteria (sulfide-oxidizers) along with *Planctomycetes* and *Bacteroidetes* is fully consistent with previous studies documenting microbial communities at the surface of relatively young outcropping basalts (Lysnes et al., 2004; Santelli et al., 2008; Mason et al., 2009; Sudek et al., 2009).

The occurrence and abundance of Zetaproteobacteria is, however, less common but seems also related to the presence of basalt. Indeed, numerous sequences, besides the Zetaproteobacteria sequences, retrieved from BH2 were similar to environmental sequences collected in hydrothermal environments and seamounts or in basalts from various locations. Orcutt et al. (2011) described both microbial communities at the surface of different colonized solids (including basalt) incubated *in situ* during 4 years at depths of 210 and 280 m below seafloor (mbsf) in a 3.5 Ma drilled basaltic crust, and the alteration phases present at the surface of the colonizable solids. In Orcutt's study, the surfaces of the incubated solids were mostly colonized by *Firmicutes*, the candidate class OP18 and Gammaproteobacteria whatever the type of minerals, and reflected an anaerobic community. Although not inventoried in the microbial diversity, the surfaces of basalt chips in those incubations showed evidence for helical filaments composed of iron oxides, resembling those produced by iron-oxidizing bacteria such as Zetaproteobacteria, suggesting the presence of iron-oxidizing organisms during the course of the colonization experiment, perhaps during an earlier, more aerobic phase of the experiment. In the present study, the samples were incubated hundreds of kilometers away from the nearest known hydrothermal field or from any fresh basalt outcroppings (associated with ridge processes). This suggests that there are either unrecognized resources that support the growth of these

basalt-adapted microbes on the seafloor, or that they are part of a dormant, rare biosphere that seed the deep ocean, and bloom when they encounter environmental conditions that support their growth.

The most remarkable difference between the reduced and oxidized basaltic glasses was the presence and high relative abundance of Zetaproteobacteria on the reduced glass, but their absence on the oxidized one along with the concomitant presence of an alteration rind. A recent meta-analysis of Zetaproteobacteria distribution found they were only present in high Fe(II) marine environments where they are assumed to be playing an important role in iron-oxidation under microaerophilic conditions (Scott et al., 2015). Their presence in this deep (3200 mbsl), cold and oxygenated environment with a low level of Fe(II) because far from any hydrothermal activity suggests they may have been recruited from cold sediments where a biogenic iron cycle is present. Although Fe-oxidizing Zetaproteobacteria were first described at low temperature, Fe-rich diffuse vents (Moyer et al., 1995; Davis et al., 2009; Rassa et al., 2009; Forget et al., 2010) more recent studies have documented their presence in diverse habitats including non-hydrothermal environments (McAllister et al., 2011; McBeth et al., 2011; Rubin-Blum et al., 2014). To account for the presence of Zetaproteobacteria in continental margin sediments with no hydrothermal activity, Rubin-Blum et al. (2014) proposed that the particulate Fe from the water column is likely reduced in microenvironments and thus become bioavailable for FeOB inhabiting the sediment. Nonetheless, in our study, Zetaproteobacteria were only retrieved from the reduced basaltic glass samples and were not detected on the oxidized basaltic glass, in the surrounding seawater or in the sediment. Rarefaction curves showed, however, that the sampling effort was likely insufficient, particularly for the sediment, to fully embrace the entire diversity. We thus propose that Zetaproteobacteria colonizing the BH2 sample could come from the sediment where Fe(II) concentrations are either too low, or too localized, to allow these organisms to sufficiently develop to be detected by classical Sanger sequencing. Interestingly, an enrichment experiment carried out in a near-shore environment of the Atlantic using mild steel also resulted in abundant growth of Zetaproteobacteria (McBeth et al., 2011). Similar to the results reported here, while the relative abundance of Zetaproteobacteria on the steel surface was high, the diversity was very low, being represented by only 1 or 2 OTUs. We suggest that they were recruited from a low abundance population of the surrounding seawater where a modest biologically driven iron cycle occurs as in the deep-sea sediments where our experiment was conducted.

We also propose the presence of Fe(II) in BH2 to be key in the specific colonization process, hence supporting growth of these FeOB. The 4–10 wt% Fe in the reduced basaltic glass, as determined by semi-quantitative EDX analyses, represented the most abundant source of Fe(II) in the *in situ* experiment. If Fe(II) would have come from another source (either as dissolved or particulate Fe(II) or as Fe(III) precipitates from seawater), the oxidized basalt would also have shown the presence of Zetaproteobacteria in its community along with an alteration rind as the one observed for BH2. The hypothesis that the source of iron was the structural Fe(II) of the reduced basaltic glass is also supported by the results obtained in the *in vitro* experiment where the Fe(II) from the reduced basalt was used by Zetaproteobacteria as the primary energy source for their growth. Regarding the relative abundance of Zetaproteobacteria in the *in situ* incubated samples, the enrichment in Fe(II) provided by the reduced basalt was sufficient to provoke a "bloom" of sediment-hosted Zetaproteobacteria.

After less than 1 year of incubation, the state of alteration in both the *in situ* and *in vitro* experiments is likely too early to show a strongly irregular basalt surface or noticeable hemispherical peats that could results from cells-basalts interactions as observed in numerous studies on old basalts (mostly older than 1 Ma; Wilke et al., 2005; Thorseth et al., 1992, 1995, 2001, 2003; Furnes and Staudigel, 1999; Staudigel et al., 2008). That is why we will further designate a significant alteration by the presence of an alteration rind of iron oxyhydroxides, since the secondary mineral phases resulting of the basalt alteration are mostly composed of iron oxyhydroxides and clays (Knowles et al., 2012).

The presence and relative abundance of Zetaproteobacteria in the BH2 sample correlated with the presence of a thick rind of alteration composed of poorly crystallized iron oxyhydroxides along with Si-Al-Ca-K bearing phases as evidenced by SEM-EDX and synchrotron X-ray fluorescence measurements. This alteration rind attests for the mobilization (dissolution and reprecipitation) of the basalt-forming elements into secondary phases. It shows striking similarities with palagonite, a byproduct of the low temperature alteration of basaltic glass, composed of amorphous or poorly crystallized iron (oxyhydr)oxides together with clay minerals. Nonetheless their biological or abiotic origin is often tricky to assess (Knowles et al., 2012). As confirmed by the CTD profile, the seawater at this depth is oxygenated and deep seawater pH in the North Atlantic is close to circumneutral values. Abiotic iron oxidation occurs rapidly under these conditions and the BH2 alteration rind could then have been formed at least partly abiotically. Nonetheless, both the SEM observations of the rind-hosted iron-oxides showing them associated to microbial cells and the Raman spectra of the Fe-oxides very often associated to organic matter, suggest a biological origin for these Fe-precipitates (**Figures 5** and **7**). Additionally, the abundant presence of microaerophilic Zetaproteobacteria in the reduced basaltic glass sample suggests that a low-oxygen micro-environment may have formed in the recesses of the stacked basaltic glass fragments likely due to weak circulation of oxygenated seawater. It is also possible that a biofilm aggregating the basalt chips or the alteration rind itself played the role of diffusion barrier for oxygen. This weakly oxygenated micro-environment could have permitted Fe(II) to be available for oxidation by Zetaproteobacteria. Coherently, during the abiotic *in vitro* incubation of the reduced basaltic glass at 4°C for a period of time that is comparable to the one of the *in situ* experiment, no alteration rind was observed (**Figure 4**). This suggest that no basalt dissolution occurred abiotically at seafloor temperatures over 1 year and that Zetaproteobacteria likely play a dynamical role in extracting Fe(II) from the basalt and hence in altering the glass.

The textures of the iron oxides observed at the surface of *in situ* incubated BH2 did not show the Fe-twisted stalks typifying *M. ferrooxydans* (Kato et al., 2009; Rassa et al., 2009; McBeth et al., 2011; Fleming et al., 2013; Rubin-Blum et al., 2014). However, several FeOB including *Sideroxydans* sp., and *Gallionella capsiferriformans* are known to produce amorphous iron oxides (Emerson and Moyer, 1997, 2002; Weiss et al., 2007); furthermore, a non-stalk-forming member of the Zetaproteobacteria that is an iron oxidizer was recently isolated from an Fe(II)-rich, diffuse hydrothermal vent site at TAG (Emerson, unpublished). The stalks produced by FeOB are coated by extracellular polymeric substances (EPS). The organic matter is presumed to be excreted by cells in order to bind and precipitate the Fe(III) produced by Fe(II) oxidation away from the cell to avoid encrustation (Chan et al., 2011). The same process has been suggested for FeOB that do not produce stalks (Miot et al., 2009). The association of organic matter with the poorly crystallized iron oxides evidenced by Raman spectroscopy in BH2 sample could be related to such a process. Moreover, the Raman spectra obtained on the stalk-organized iron oxides from the *in vitro* experiment with *M. ferrooxydans* DIS-1 were very similar to those obtained on the non-organized iron oxides from the *in situ* experiment (**Figure 7**). According to the phylogenetic distance with the cultured strains (**Figure 3**), the 16S rRNA gene sequence of Zetaproteobacteria retrieved in the abyssal plain could belong to a new genus able to oxidize Fe(II) and to embed in organic matter the produced Fe(III) to avoid cell incrustation but without creating twisted stalks. Another hypothesis derived from the similarity at low magnification of the alteration features in between the *in vitro* and the *in situ* incubated reduced basaltic glass (**Figures 5A–D**) is that the stalks have been formed, and then some processes led to their disappearance. They could have either been dissolved, re-crystallized, silicified (Li et al., 2013) or reduced by iron-reducing bacteria (Lee et al., 2013).

Overall, based on the results of both the *in situ* and *in vitro* experiments, we propose that the important rind of alteration observed solely at surface of the reduced basaltic glass BH2 derived from the development of iron-oxidizing Zetaproteobacteria. The basalt weathering has then been enhanced by their metabolic activity through the mechanisms depicted in **Figure 8**: the dissolution of the basaltic glass first occurred abiotically, hence releasing structural Fe(II) (1 on **Figure 8**); the dissolved Fe(II) was then quickly abiotically oxidized due to the oxygenated environment (2). The subsequent precipitation of insoluble Fe(III) could have been either bio-influenced (Decho, 2010) by the EPS produced by diverse microorganisms (3a) or abiotic, but in all cases would lead to the formation of an iron oxide alteration rind (3b). Microaerophilic conditions were then created either by (4a) the biofilm (the oxygen could have been consumed by diverse aerophilic

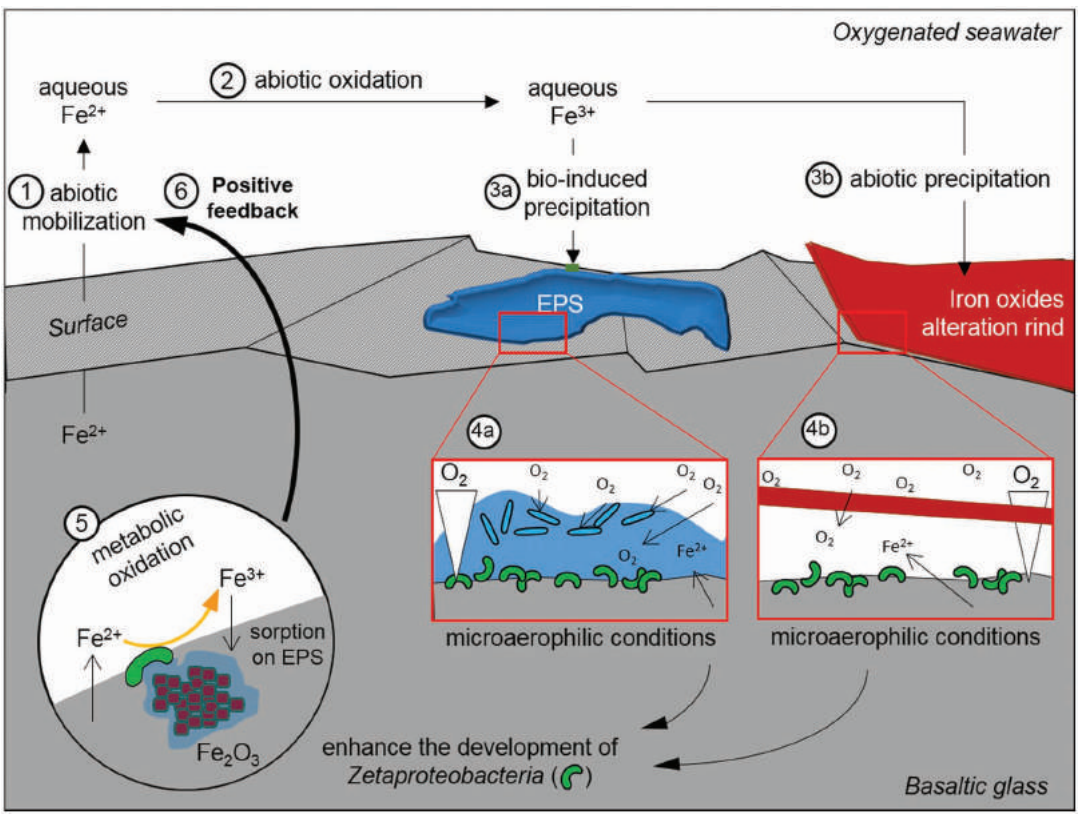

FIGURE 8 | Schematic representation of the postulated alteration process that has affected the reduced basaltic glass during the *in situ* incubation experiment in the abyssal plain. EPS stands for extracellular polymeric substances.

microorganisms on the top of the biofilm hence leading to a decreasing gradient of oxygen concentration up to the basalt surface (De Beer et al., 1994; Xu et al., 1998) or (4b) the thick alteration rind that formed a barrier of diffusion for the oxygen (Schott and Berner, 1983, 1985; Chou and Wollast, 1984). The microaerophilic conditions allowed the development of Zetaproteobacteria (5) that metabolically converted the structural Fe(II) into Fe(III). To avoid cell encrustation, Fe(III) was then quickly adsorbed on EPS (Banfield et al., 2000; Chan et al., 2009). EPS promoted precipitation through the presence of diverse functional groups negatively charged (e.g., hydroxyl, carboxyl) and acting as nucleation sites, but also inhibiting the growth of iron oxides, hence leading to small particles (Vollrath et al., 2013) as those observed coated by EPS (**Figure 5F**). Aggregation of these particles contributed to the alteration features observed at low magnification (**Figure 5B**). The removal of Fe(III) induced a positive feedback on Fe(II) dissolution by the modification of the system equilibrium, as observed with the acidophilic FeOB *Acidithiobacilus ferrooxydans* on basaltic glass by Navarrete et al. (2013).

CONCLUSION

In this study, we reported the abundant presence of Zetaproteobacteria on a reduced basaltic glass incubated a sedimentary abyssal plain and we demonstrated by both *in situ* and *in vitro* experiments that the structural Fe(II) of the basaltic glass can be used as the sole energy source for the development of FeOB in a non-hydrothermal environment. The outcropping pillows of fresh basalts at seafloor hence represent a potentially important habitat and energy source to sustain the development of FeOB and particularly Zetaproteobacteria. In terms of volume and contribution of these FeOB to the iron cycle and rock weathering at the interface between the oceanic lithosphere and the deep ocean this process could be very important in Earth history.

ACKNOWLEDGMENTS

The authors acknowledge the Graviluck 06 and MoMARDream 07 ship board cruise team: officers, crew, and technicians of the *R/V L'Atalante*, the DSV *Nautile* team and the scientific team, particularly the P.Is of the cruises Valérie Ballu and Javier Escartin. The authors thank Stéphanie Rossano (Laboratoire Géomatériaux et Environnement, Université de Marne-la-Vallée, France), who has allowed us to use her lab equipments and has shared with us her experience in the synthesis of MORB-type basaltic glasses. The authors want to thank Nicolas Trcera (SOLEIL synchrotron, France) for assistance during XANES experiment and for having shared with us his experience of the XANES data treatment. The authors want also thank Omar Boudouma for the SEM imaging. This work was supported by post-cruise funding (CNRS-INSU). Work in the laboratory DE was supported by a grant from ONR N00014-08-1-0334, and NSF grant OCE-1155754; writing and editing of the manuscript was supported in part by a grant from C-DEBI. This is C-DEBI contribution 290.

SUPPLEMENTARY MATERIAL

The Supplementary Material for this article can be found online at: http://journal.frontiersin.org/article/10.3389/fmicb.2015.01518

REFERENCES

Banfield, J. F., Welch, S. A., Zhang, H., Ebert, T. T., and Penn, R. L. (2000). Aggregation-based crystal growth and microstructure development in natural iron oxyhydroxide biomineralization products. *Science* 289, 751–754. doi: 10.1126/science.289.5480.751

Bennett, P., Rogers, J., Choi, W., and Hiebert, F. (2001). Silicates, silicate weathering, and microbial ecology. *Geomicrobiol. J.* 18, 3–19. doi: 10.1007/BF00171895

Brantley, S., Liermann, L., Bau, M., and Wu, S. (2001). Uptake of trace metals and rare earth elements from hornblende by a soil bacterium. *Geomicrobiol. J.* 18, 37–61. doi: 10.1080/01490450151079770

Callac, N., Rommevaux-Jestin, C., Rouxel, O., Lesongeur, F., Liorzou, C., and Bollinger, C. (2013). Microbial colonization of basaltic glasses in hydrothermal organic-rich sediments at Guaymas Basin. *Front. Microbiol.* 4:250. doi: 10.3389/fmicb.2013.00250

Chan, C. S., Fakra, S. C., Edwards, D. C., Emerson, D., and Banfield, J. F. (2009). Iron oxyhydroxide mineralization on microbial extracellular polysaccharides. *Geochim. Cosmochim. Acta* 73, 3807–3818. doi: 10.1016/j.gca.2009.02.036

Chan, C. S., Fakra, S. C., Emerson, D., Fleming, E. J., and Edwards, K. J. (2011). Lithotrophic iron-oxidizing bacteria produce organic stalks to control mineral growth: implications for biosignature formation. *ISME J.* 5, 717–727. doi: 10.1038/ismej.2010.173

Chou, L., and Wollast, R. (1984). Study of the weathering of albite at room temperature and pressure with a fluidized bed reactor. *Geochim. Cosmochim. Acta* 48, 2205–2217. doi: 10.1016/0016-7037(84)90217-5

Cockell, C. S., van Calsteren, P., Mosselmans, J. F. W., Franchi, I. A., Gilmour, I., and Kelly, L. (2010). Microbial endolithic colonization and the geochemical environment in young seafloor basalts. *Chem. Geol.* 279, 17–30. doi: 10.1016/j.chemgeo.2010.09.015

Davis, J. P., Youssef, N. H., and Elshahed, M. S. (2009). Assessment of the diversity, abundance, and ecological distribution of members of candidate division SR1 reveals a high level of phylogenetic diversity but limited morphotypic diversity. *Appl. Environ. Microbiol.* 75, 4139–4148. doi: 10.1128/AEM.00137-09

De Beer, D., Stoodley, P., Roe, F., and Lewandowski, Z. (1994). Effects of biofilm structures on oxygen distribution and mass transport. *Biotechnol. Bioeng.* 43, 1131–1138. doi: 10.1002/bit.260431118

Decho, A. W. (2010). Overview of biopolymer-induced mineralization: what goes on in biofilms? *Ecol. Eng.* 36, 137–144. doi: 10.1016/j.ecoleng.2009.01.003

Edgar, R. C., Haas, B. J., Clemente, J. C., Quince, C., and Knight, R. (2011). UCHIME improves sensitivity and speed of chimera detection. *Bioinformatics* 27, 2194–2200. doi: 10.1093/bioinformatics/btr381

Edwards, K. J., Bach, W., and McCollom, T. M. (2005). Geomicrobiology in oceanography: microbe–mineral interactions at and below the seafloor. *Trends Microbiol.* 13, 449–456. doi: 10.1016/j.tim.2005.07.005

Edwards, K. J., Bach, W., and Rogers, D. R. (2003). Geomicrobiology of the ocean crust: a role for chemoautotrophic Fe-bacteria. *Biol. Bull.* 204, 180–185. doi: 10.2307/1543555

Einen, J., Thorseth, I. H., and Øvreås, L. (2008). Enumeration of Archaea and Bacteria in seafloor basalt using real-time quantitative PCR and fluorescence microscopy. *FEMS Microbiol. Lett.* 282, 182–187. doi: 10.1111/j.1574-6968.2008.01119.x

Emerson, D., Fleming, E. J., and McBeth, J. M. (2010). Iron-oxidizing bacteria: an environmental and genomic perspective. *Annu. Rev. Microbiol.* 64, 561–583. doi: 10.1146/annurev.micro.112408.134208

Emerson, D., and Moyer, C. (1997). Isolation and characterization of novel iron-oxidizing bacteria that grow at circumneutral pH. *Appl. Environ. Microbiol.* 63, 4784–4792.

Emerson, D., and Moyer, C. L. (2002). Neutrophilic Fe-oxidizing bacteria are abundant at the Loihi Seamount hydrothermal vents and play a major role in Fe oxide deposition. *Appl. Environ. Microbiol.* 68, 3085–3093. doi: 10.1128/AEM.68.6.3085-3093.2002

Emerson, D., Rentz, J. A., Lilburn, T. G., Davis, R. E., Aldrich, H., Chan, C., et al. (2007). A novel lineage of *proteobacteria* involved in formation of marine Fe-oxidizing microbial mat communities. *PLoS ONE* 2:e667.

Fleming, E. J., Davis, R. E., McAllister, S. M., Chan, C. S., Moyer, C. L., and Tebo, B. M. (2013). Hidden in plain sight: discovery of sheath-forming, iron-oxidizing Zeta*proteobacteria* at Loihi Seamount, Hawaii, USA. *FEMS Microbiol. Ecol.* 85, 116–127. doi: 10.1111/1574-6941.12104

Forget, N., Murdock, S., and Juniper, S. (2010). Bacterial diversity in Fe-rich hydrothermal sediments at two South Tonga Arc submarine volcanoes. *Geobiology* 8, 417–432. doi: 10.1111/j.1472-4669.2010.00247.x

Fortin, D., and Langley, S. (2005). Formation and occurrence of biogenic iron-rich minerals. *Earth Sci. Rev.* 72, 1–19. doi: 10.1111/j.1472-4669.2007.00131.x

Furnes, H., and Staudigel, H. (1999). Biological mediation in ocean crust alteration: how deep is the deep biosphere? *Earth Planet. Sci. Lett.* 166, 97–103. doi: 10.1016/S0012-821X(99)00005-9

Ghai, R., Mizuno, C. M., Picazo, A., Camacho, A., and Rodriguez-Valera, F. (2013). Metagenomics uncovers a new group of low GC and ultra-small marine Actinobacteria. *Sci. Rep.* 3:2471. doi: 10.1038/srep02471

Golyshin, P. N., Chernikova, T. N., Abraham, W.-R., Lünsdorf, H., Timmis, K. N., and Yakimov, M. M. (2002). *Oleiphilaceae fam*. nov., to include *Oleiphilus messinensis* gen. nov., sp. nov., a novel marine bacterium that obligately utilizes hydrocarbons. *Int. J. Syst. Evol. Microbiol.* 52, 901–911. doi: 10.1099/00207713-52-3-901

Hodges, T. W., and Olson, J. B. (2009). Molecular comparison of bacterial communities within iron-containing flocculent mats associated with submarine volcanoes along the Kermadec Arc. *Appl. Environ. Microbiol.* 75, 1650–1657. doi: 10.1128/AEM.01835-08

Kato, S., Yanagawa, K., Sunamura, M., Takano, Y., Ishibashi, J., and Kakegawa, T. (2009). Abundance of Zeta*proteobacteria* within crustal fluids in back-arc hydrothermal fields of the Southern Mariana Trough. *Environ. Microbiol.* 11, 3210–3222. doi: 10.1111/j.1462-2920.2009.02031.x

Knowles, E., Wirth, R., and Templeton, A. (2012). A comparative analysis of potential biosignatures in basalt glass by FIB-TEM. *Chem. Geol.* 330–331, 165–175. doi: 10.1016/j.chemgeo.2012.08.028

Kumar, S., Nei, M., Dudley, J., and Tamura, K. (2008). MEGA: a biologist-centric software for evolutionary analysis of DNA and protein sequences. *Brief. Bioinform.* 9, 299–306. doi: 10.1093/bib/bbn017

Lee, J. S., McBeth, J. M., Ray, R. I., Little, B. J., and Emerson, D. (2013). Iron cycling at corroding carbon steel surfaces. *Biofouling* 29, 1243–1252. doi: 10.1080/08927014.2013.836184

Li, J., Peng, X., Zhou, H., Li, J., and Sun, Z. (2013). Molecular evidence for microorganisms participating in Fe, Mn, and S biogeochemical cycling in two low-temperature hydrothermal fields at the Southwest Indian Ridge. *J. Geophys. Res.* 118, 665–679.

Lysnes, K., Thorseth, I. H., Steinsbu, B. O., Øvreås, L., Torsvik, T., and Pedersen, R. B. (2004). Microbial community diversity in seafloor basalt from the Arctic spreading ridges. *FEMS Microbiol. Ecol.* 50, 213–230. doi: 10.1016/j.femsec.2004.06.014

Maquelin, K., Kirschner, C., Choo-Smith, L.-P., van den Braak, N., Endtz, H. P., and Naumann, D. (2002). Identification of medically relevant microorganisms by vibrational spectroscopy. *J. Microbiol. Methods* 51, 255–271. doi: 10.1016/S0167-7012(02)00127-6

Mason, O. U., Di Meo-Savoie, C. A., Van Nostrand, J. D., Zhou, J., Fisk, M. R., and Giovannoni, S. J. (2009). Prokaryotic diversity, distribution, and insights into their role in biogeochemical cycling in marine basalts. *ISME J.* 3, 231–242. doi: 10.1038/ismej.2008.92

Mason, O. U., Stingl, U., Wilhelm, L. J., Moeseneder, M. M., Meo-Savoie, D., and Carol, A. (2007). The phylogeny of endolithic microbes associated with marine basalts. *Environ. Microbiol.* 9, 2539–2550. doi: 10.1111/j.1462-2920.2007.01372.x

McAllister, S. M., Davis, R. E., McBeth, J. M., Tebo, B. M., Emerson, D., and Moyer, C. L. (2011). Biodiversity and emerging biogeography of the neutrophilic iron-oxidizing Zeta*proteobacteria*. *Appl. Environ. Microbiol.* 77, 5445–5457. doi: 10.1128/AEM.00533-11

McBeth, J. M., Little, B. J., Ray, R. I., Farrar, K. M., and Emerson, D. (2011). Neutrophilic iron-oxidizing "Zeta*proteobacteria*" and mild steel corrosion in nearshore marine environments. *Appl. Environ. Microbiol.* 77, 1405–1412. doi: 10.1128/AEM.02095-10

Miot, J., Benzerara, K., Obst, M., Kappler, A., Hegler, F., and Schädler, S. (2009). Extracellular iron biomineralization by photoautotrophic iron-oxidizing bacteria. *Appl. Environ. Microbiol.* 75, 5586–5591. doi: 10.1128/AEM.00490-09

Morris, R. M., Rappé, M. S., Connon, S. A., Vergin, K. L., Siebold, W. A., and Carlson, C. A. (2002). SAR11 clade dominates ocean surface bacterioplankton communities. *Nature* 420, 806–810. doi: 10.1038/nature01240

Moyer, C. L., Dobbs, F. C., and Karl, D. M. (1995). Phylogenetic diversity of the bacterial community from a microbial mat at an active, hydrothermal vent system, Loihi Seamount, Hawaii. *Appl. Environ. Microbiol.* 61, 1555–1562.

Navarrete, J. U., Cappelle, I. J., Schnittker, K., and Borrok, D. M. (2013). Bioleaching of ilmenite and basalt in the presence of iron-oxidizing and iron-scavenging bacteria. *Int. J. Astrobiol.* 12, 123–134. doi: 10.1017/S1473550412000493

Orcutt, B. N., Sylvan, J. B., Knab, N. J., and Edwards, K. J. (2011). Microbial ecology of the dark ocean above, at, and below the seafloor. *Microbiol. Mol. Biol. Rev.* 75, 361–422. doi: 10.1128/MMBR.00039-10

Pruesse, E., Quast, C., Knittel, K., Fuchs, B. M., Ludwig, W., and Peplies, J. (2007). SILVA: a comprehensive online resource for quality checked and aligned ribosomal RNA sequence data compatible with ARB. *Nucleic Acids Res.* 35, 7188–7196. doi: 10.1093/nar/gkm864

Quast, C., Pruesse, E., Yilmaz, P., Gerken, J., Schweer, T., and Yarza, P. (2012). The SILVA ribosomal RNA gene database project: improved data processing and web-based tools. *Nucleic Acids Res.* 41, D590–D596. doi: 10.1093/nar/gks1219

Rassa, A. C., McAllister, S. M., Safran, S. A., and Moyer, C. L. (2009). Zeta-*Proteobacteria* dominate the colonization and formation of microbial mats in low-temperature hydrothermal vents at Loihi Seamount, Hawaii. *Geomicrobiol. J.* 26, 623–638. doi: 10.1080/01490450903263350

Rogers, J. R., and Bennett, P. C. (2004). Mineral stimulation of subsurface microorganisms: release of limiting nutrients from silicates. *Chem. Geol.* 203, 91–108. doi: 10.1016/j.chemgeo.2003.09.001

Rubin-Blum, M., Antler, G., Tsadok, R., Shemesh, E., Austin, J. A., and Coleman, D. F. (2014). First evidence for the presence of iron oxidizing Zeta*proteobacteria* at the Levantine continental margins. *PLoS ONE* 9:e91456. doi: 10.1371/journal.pone.0091456

Santelli, C. M., Orcutt, B. N., Banning, E., Bach, W., Moyer, C. L., and Sogin, M. L. (2008). Abundance and diversity of microbial life in ocean crust. *Nature* 453, 653–656. doi: 10.1038/nature06899

Schloss, P. D., Gevers, D., and Westcott, S. L. (2011). Reducing the effects of PCR amplification and sequencing artifacts on 16S rRNA-based studies. *PLoS ONE* 6:e27310. doi: 10.1371/journal.pone.0027310

Schloss, P. D., Westcott, S. L., Ryabin, T., Hall, J. R., Hartmann, M., and Hollister, E. B. (2009). Introducing mothur: open-source, platform-independent, community-supported software for describing and comparing microbial communities. *Appl. Environ. Microbiol.* 75, 7537–7541. doi: 10.1128/AEM.01541-09

Schott, J., and Berner, R. A. (1983). X-ray photoelectron studies of the mechanism of iron silicate dissolution during weathering. *Geochim. Cosmochim. Acta* 47, 2233–2240. doi: 10.1016/0016-7037(83)90046-7

Schott, J., and Berner, R. A. (1985). Dissolution mechanisms of pyroxenes and olivines during weathering. *Chem. Weather.* 149, 35–53. doi: 10.1007/978-94-009-5333-8_3

Scott, J. J., Breier, J. A., Luther, G. W., and Emerson, D. (2015). Microbial iron mats at the Mid-Atlantic Ridge and evidence that Zeta*proteobacteria* may be restricted to iron-oxidizing marine systems. *PLoS ONE* 10:e0119284. doi: 10.1371/journal.pone.0119284

Spötl, C., Houseknecht, D. W., and Jaques, R. C. (1998). Kerogen maturation and incipient graphitization of hydrocarbon source rocks in the Arkoma

Basin, Oklahoma and Arkansas: a combined petrographic and Raman spectrometric study. *Org. Geochem.* 28, 535–542. doi: 10.1016/S0146-6380(98)00021-7

Staudigel, H., Furnes, H., McLoughlin, N., Banerjee, N. R., Connell, L. B., and Templeton, A. (2008). 3.5 billion years of glass bioalteration: volcanic rocks as a basis for microbial life? *Earth Sci. Rev.* 89, 156–176. doi: 10.1016/j.earscirev.2008.04.005

Sudek, L. A., Templeton, A. S., Tebo, B. M., and Staudigel, H. (2009). Microbial ecology of Fe (hydr) oxide mats and basaltic rock from Vailulu'u Seamount, American Samoa. *Geomicrobiol. J.* 26, 581–596. doi: 10.1080/01490450903263400

Templeton, A. S., Knowles, E. J., Eldridge, D. L., Arey, B. W., Dohnalkova, A. C., and Webb, S. M. (2009). A seafloor microbial biome hosted within incipient ferromanganese crusts. *Nat. Geosci.* 2, 872–876. doi: 10.1038/ngeo696

Templeton, A. S., Staudigel, H., and Tebo, B. M. (2005). Diverse Mn(II)-oxidizing bacteria isolated from submarine basalts at loihi seamount. *Geomicrobiol. J.* 22, 127–139. doi: 10.1080/01490450590945951

Thorseth, I. H., Furnes, H., and Heldal, M. (1992). The importance of microbiological activity in the alteration of natural basaltic glass. *Geochim. Cosmochim. Acta* 56, 845–850. doi: 10.1016/0016-7037(92)90104-Q

Thorseth, I. H., Pedersen, R. B., and Christie, D. M. (2003). Microbial alteration of 0–30-Ma seafloor and sub-seafloor basaltic glasses from the Australian Antarctic Discordance. *Earth Planet. Sci. Lett.* 215, 237–247. doi: 10.1016/S0012-821X(03)00427-8

Thorseth, I. H., Torsvik, T., Furnes, H., and Muehlenbachs, K. (1995). Microbes play an important role in the alteration of oceanic crust. *Chem. Geol.* 126, 137–146. doi: 10.1016/0009-2541(95)00114-8

Thorseth, I., Torsvik, T., Torsvik, V., Daae, F., and Pedersen, R. (2001). Diversity of life in ocean floor basalt. *Earth Planet. Sci. Lett.* 194, 31–37. doi: 10.1038/nature06899

Vollrath, S., Behrends, T., Koch, C. B., and Van Cappellen, P. (2013). Effects of temperature on rates and mineral products of microbial Fe (II) oxidation by *Leptothrix cholodnii* at microaerobic conditions. *Geochim. Cosmochim. Acta* 108, 107–124. doi: 10.1016/j.gca.2013.01.019

Weiss, J. V., Rentz, J. A., Plaia, T., Neubauer, S. C., Merrill-Floyd, M., and Lilburn, T. (2007). Characterization of Neutrophilic Fe (II)-Oxidizing Bacteria Isolated from the Rhizosphere of Wetland Plants and Description of *Ferritrophicum radicicola* gen. nov. sp. nov., and *Sideroxydans paludicola* sp. nov. *Geomicrobiol. J.* 24, 559–570. doi: 10.1080/01490450701670152

Wilke, M., Farges, F., Petit, P.-E., Brown, G. E., and Martin, F. (2001). Oxidation state and coordination of Fe in minerals: an Fe K-XANES spectroscopic study. *Am. Mineral.* 86, 714–730. doi: 10.2138/am-2001-5-612

Wilke, M., Partzsch, G. M., Bernhardt, R., and Lattard, D. (2005). Determination of the iron oxidation state in basaltic glasses using XANES at the K-edge. *Chem. Geol.* 220, 143–161. doi: 10.1016/j.chemgeo.2005.03.004

Wu, Y.-H., Liao, L., Wang, C.-S., Ma, W.-L., Meng, F.-X., Wu, M., et al. (2013). A comparison of microbial communities in deep-sea polymetallic nodules and the surrounding sediments in the Pacific Ocean. *Deep Sea Res. Part I Oceanogr. Res. Pap.* 79, 40–49. doi: 10.1016/j.dsr.2013.05.004

Xu, K. D., Stewart, P. S., Xia, F., Huang, C.-T., and McFeters, G. A. (1998). Spatial physiological heterogeneity in *Pseudomonas aeruginosa* biofilm is determined by oxygen availability. *Appl. Environ. Microbiol.* 64, 4035–4039.

Conflict of Interest Statement: The authors declare that the research was conducted in the absence of any commercial or financial relationships that could be construed as a potential conflict of interest.

frontiers in Microbiology

ORIGINAL RESEARCH
published: 24 May 2016
doi: 10.3389/fmicb.2016.00767

In Situ Microbial Community Succession on Mild Steel in Estuarine and Marine Environments: Exploring the Role of Iron-Oxidizing Bacteria

Joyce M. McBeth[1,2]* *and David Emerson*[1]

[1] Bigelow Laboratory for Ocean Sciences, East Boothbay, ME USA, [2] Department of Geological Sciences, University of Saskatchewan, Saskatoon, SK, Canada

Microbiologically influenced corrosion (MIC) is a complex biogeochemical process involving interactions between microbes, metals, minerals, and their environment. We hypothesized that sediment-derived iron-oxidizing bacteria (FeOB) would colonize and become numerically abundant on steel surfaces incubated in coastal marine environments. To test this, steel coupons were incubated on sediments over 40 days, and samples were taken at regular intervals to examine microbial community succession. The experiments were conducted at two locations: (1) a brackish salt marsh stream and (2) a coastal marine bay. We analyzed DNA extracted from the MIC biofilms for bacterial diversity using high-throughput amplicon sequencing of the SSU rRNA gene, and two coupons from the coastal site were single cell sorted and screened for the SSU rRNA gene. We quantified communities of Zetaproteobacteria, sulfate-reducing bacteria (SRB), and total bacteria and archaea using qPCR analyses. Zetaproteobacteria and SRB were identified in the sequencing data and qPCR analyses for samples collected throughout the incubations and were also present in adjacent sediments. At the brackish site, the diversity of Zetaproteobacteria was lower on the steel compared to sediments, consistent with the expected enrichment of FeOB on steel. Their numbers increased rapidly over the first 10 days. At the marine site, Zetaproteobacteria and other known FeOB were not detected in sediments; however, the numbers of Zetaproteobacteria increased dramatically within 10 days on the steel surface, although their diversity was nearly clonal. Iron oxyhydroxide stalk biosignatures were observed on the steel and in earlier enrichment culture studies; this is evidence that the Zetaproteobacteria identified in the qPCR, pyrosequencing, and single cell data were likely FeOB. In the brackish environment, members of freshwater FeOB were also present, but were absent in the fully marine site. This work indicates there is a successional pattern in the colonization of steel surfaces with FeOB being early colonizers; over time the MIC community matures to include other members

OPEN ACCESS

Edited by:
Cara M. Santelli,
University of Minnesota, USA

Reviewed by:
Trinity L. Hamilton,
University of Cincinnati, USA
Jinjun Kan,
Stroud Water Research Center, USA

***Correspondence:**
Joyce M. McBeth
joyce.mcbeth@usask.ca

Specialty section:
This article was submitted to Extreme Microbiology, a section of the journal Frontiers in Microbiology

Received: *14 January 2016*
Accepted: *06 May 2016*
Published: *24 May 2016*

Citation:
McBeth JM and Emerson D (2016) In Situ Microbial Community Succession on Mild Steel in Estuarine and Marine Environments: Exploring the Role of Iron-Oxidizing Bacteria. Front. Microbiol. 7:767. doi: 10.3389/fmicb.2016.00767

that may help accelerate corrosion. This work also shows there is a reservoir for Zetaproteobacteria in coastal sediment habitats, where they may influence the coastal iron cycle, and can rapidly colonize steel surfaces or other sources of Fe(II) when available.

Keywords: succession, Epsilonproteobacteria, Zetaproteobacteria, sulfate-reducing bacteria, MIC

INTRODUCTION

It is generally believed that the costs associated with corrosion are equivalent to about 3% of a nation's gross domestic product; corrosion of steel costs US taxpayers billions of dollars a year in damage to infrastructure (NACE International, 2002). In the marine environment, mild steel is used in everything from ship construction to docks to large moorings. Marine corrosion is mitigated through measures such as coatings (paint or metal) or cathodic protection (Chandler, 1985); nonetheless it is still a pervasive problem. A significant amount of corrosion is initiated and/or exacerbated by the presence of microorganisms, a process referred to as microbiologically influenced corrosion (MIC). A number of different groups of microbes carrying out metabolisms such as sulfate reduction, methanogenesis, and Fe-reduction have been implicated in MIC, and it is known that these processes can enhance dissolution of steel and produce cathodic conditions that cause surface pitting which leads to more rapid corrosion (Little and Lee, 2007). A particularly aggressive form of corrosion, accelerated low water corrosion (ALWC) is commonly associated with microorganisms (Little and Lee, 2007; Dang and Lovell, 2016).

While the physiological attributes of different members of the MIC community are generally understood, less is known about the ecology of the process. For example, the make-up of naturally occurring MIC communities is still relatively unknown. Even less is understood about how MIC communities vary through space and time, and if there are temporal, spatial, or geographical patterns in the membership of marine corrosion communities. Thus, unraveling the complex relationships between these microbes, the steel surfaces they inhabit, the minerals they produce, and how they affect the corrosion process are all important areas of study.

One group that is worthy of consideration in this context, is the lithoautotrophic Fe-oxidizing bacteria (FeOB) that can use the ferrous iron (Fe(II)) released from the steel surface as an electron donor for growth (e.g., McBeth et al., 2011). Despite the fact that Fe(II) is their primary energy source and they are frequently identified in corrosion biofilms, the role of this group in MIC is still not clear. Recent studies have shown FeOB are able to colonize and grow either on steel coupons introduced into the environment (Dang et al., 2011; McBeth et al., 2011; Jin et al., 2015), or are present on corroded steel associated with ALWC structures (Marty et al., 2014). Laboratory studies have shown FeOB enhance release of iron from mild steel coupon surfaces, and that in concert with Fe-reducing bacteria they promote roughening of the steel surface (Lee et al., 2013). However, there is no evidence that FeOB are responsible for pitting or accelerated corrosion (Lee et al., 2013).

The goal of this study was to examine the development and succession of marine corrosion communities, and explore the role of iron-oxidizing bacteria (FeOB) in these systems. We hypothesized that sediment-derived marine FeOB would colonize and become numerically abundant on steel surfaces incubated in coastal marine environments. To test this, we incubated steel samples at two locations and sampled them at regular intervals over a 40-day period: in a tidal salt marsh stream and in a nearshore marine environment. Steel biofilm microbial community composition and succession was examined using high-throughput amplicon sequencing, single cell genomics, qPCR, and image analyses.

MATERIALS AND METHODS

Sample Preparation, Deployment, and Sampling

Cold-finish 1018 mild carbon steel coupons (13 × 15 × 3 mm) were prepared as described in McBeth et al. (2011). Each coupon was contained in an individual subsampler, (see Supplemental Material Figure S2 in McBeth et al., 2011) that was composed of a cut off 15 ml conical tube with 9 μm mesh over the bottom and a black rubber stopper in the top. The subsamplers were contained in opaque PVC pipe holders with 1000 μm mesh bottom and opaque PVC caps. Samplers were sterilized by autoclaving and UV light illumination prior to addition of steel coupons and deployment at field sites.

The samplers were incubated at two locations. The GSB site was located in a tidal salt marsh on Great Salt Bay, Newcastle, ME (44° 2′29.73″N; 69°31′55.78″W). The GSB site study took place from 29 May to 9 July 2010 (sampled at 3, 6, 10, 14, 24, and 41 days). The second site location, designated the BBH site, was located just below the intertidal zone at the Maine Department of Marine Resources dock in West Boothbay Harbor, ME (43°50′39.50″N; 69°38′27.29″W) and took place from 16 August to 28 September 2011 (sampled at 3, 6, 9, 13, 17, 24, 31, 37, and 43 days). Tropical storm Irene moved through the region on 28 August 2011; however, the samplers remained in their original position and were undamaged. Samples for single cell genomics analyses were also deployed at the BBH site on 3 August 2011 and 16 August 2011 and were collected on 25 August 2011 (after 9- and 22-day incubations, respectively).

At each sampling timepoint, three steel coupons were collected and frozen for molecular analyses and a parallel coupon was collected and processed for imaging. Sediment samples immediately adjacent to the samplers were taken for comparative analysis. Corrosion products from each parallel coupon were examined using light microscopy to check for the presence

of mineral biosignatures indicative of FeOB growth (Emerson et al., 2010), and samples from these coupons were also fixed for scanning electron microscopy analyses [1 ml + 0.1 ml 50% glutaraldehyde (Electron Microscopy Sciences)]. At each sampling, the site pH was measured with a portable pH meter, salinity was determined with a refractometer, and the water, air temperature, and water depth were recorded. The average values and standard error for each of these parameters were calculated over the course of each experiment.

For DNA analysis, frozen coupons in MoBio Powerwater kit tubes were thawed and subjected to the Powerwater kit (MoBio) DNA extraction protocol and eluted with 100 μl of PW6 buffer (10 mM tris buffer, pH 8). The extracts were assessed for quality and quantified with a nanodrop spectrophotometer (Thermo Scientific) and Qubit fluorometer dsDNA HS kit (Invitrogen). DNA samples were stored at −80°C until further analysis.

Imaging

Scanning electron microscopy (SEM) samples were placed on filters and subjected to an ethanol dehydration series, mounted on aluminum stubs with carbon tape, critical point dried, and sputter coated with carbon. They were examined with a Zeiss Supra25 field emission SEM at a 10 kV accelerating voltage and 3 mm working distance. Samples of fresh biofilm from each series time point were examined using phase contrast light microscopy on an Olympus BX60 microscope with QICAM FAST CCD camera (QImaging, Surrey, BC, Canada).

SSU rRNA Gene Community Analysis

High-throughput amplicon sequencing of the SSU rRNA gene was used to assess community composition and diversity of both steel coupon biofilms and sediments. DNA extracts from selected time points were shipped to Research and Testing Laboratory (Lubbock, TX, USA) and analyzed using 454 tagged pyrosequencing. Samples were amplified using the primers 530F (5′-GTGCCAGCMGCNGCGG-3′) and 1100R (5′-GGGTTNCGNTCGTTG-3′) which target the V4 variable region of the SSU rRNA gene in Bacteria, as detailed in Dowd et al. (2008). The samples were sequenced using 454 Titanium chemistry (Roche). The sequencing data were analyzed using mothur v.1.33.3 and the mothur 454 standard operating procedure[1] (Schloss et al., 2009). Briefly, sequence barcodes and primers were removed, sequences were denoised with the mothur translation of the PyroNoise algorithm and trimmed to remove sequences if they contained ambiguous bases, homopolymers greater than 8, or less than 150 total bases. The remaining sequences were aligned to the SILVA bacterial database (alignment region start position 13858; Pruesse et al., 2007) and screened to remove sequences that were shorter than 250 bases without gaps. Remaining sequences were preclustered for sequences differing by a single base, and Uchime was used to detect chimeras (Edgar et al., 2011) measured against the Silva gold database. Chimeras were removed from the dataset. The resulting dataset was classified using the ribosomal database (RDP) classifier with a cutoff of 60% (Wang et al., 2007). The classifier database was modified with additional sequences and phylogenetic classification detail for the known FeOB (McBeth et al., 2013). The datasets from the 16 analyzed samples were normalized by random subsampling to include an equal number of reads (1173 each). The OTUs were clustered at a 97% similarity cutoff and classified. We calculated the Good's coverage estimate, number of OTUs, Chao1 richness estimate, and inverse Simpson diversity estimate for each sample. Yue and Clayton Theta distance matrix values were calculated between the sample communities (OTUs at 3% distance) and used to construct non-metric multidimensional scaling (NMDS) ordination plots for the samples from each study area.

Quantitative PCR

We conducted quantitative PCR (qPCR) analyses to assess the abundance of Zetaproteobacteria, sulfate-reducing bacteria (SRB), and Bacteria + Archaea in the DNA extracts from our samples. The primer sequences are summarized in **Table 1**; briefly, Zetaproteobacteria SSU rRNA gene copy numbers were quantified using primers designed by Kato et al. (2009), Bacteria + Archaea SSU rRNA gene copy numbers were obtained using primers designed by Takai and Horikoshi (2000), and SRB numbers were estimated using primers for the *DsrA* gene (Ben-Dov et al., 2007). The qPCR master mix contained Maxima SYBR Green qPCR Master Mix (Fermentas), primers at 0.3 μM, and 1 μl of template per reaction. Each reaction was prepared in triplicate and each plate also contained a standard dilution series of an amplified and quantified target gene, no template controls, and negative and positive control samples. For the Bacteria + Archaea and Zetaproteobacteria assays: standard series were prepared using amplified and quantified

[1]http://www.mothur.org

TABLE 1 | qPCR primers.

Target	Primers	5′-3′	Annealing/extension temperatures	Reference
Bacteria + Archaea (SSU rRNA gene)	Uni340F	CCT ACG GGR BGC ASC AG	55.8	Takai and Horikoshi, 2000
	Uni806R	GGA CTA CNN GGG TAT CTA AT		Takai and Horikoshi, 2000
Zetaproteobacteria (SSU rRNA gene)	Zeta672F	CGG AAT TCC GTG TGT AGC AGT	58	Kato et al., 2009
	Zeta837R	GCC ACW GYA GGG GTC GAT ACC		Kato et al., 2009
Sulfate-reducing bacteria (SRB) (*DsrA* gene)	RH1-dsr-F	GCC GTT ACT GTG ACC AGC C	55	Ben-Dov et al., 2007
	RH3-dsr-R	GGT GGA GCC GTG CAT GTT		Ben-Dov et al., 2007

Mariprofundus sp strain GSB2 SSU rRNA gene (27F to 1492R; HQ206653); negative controls were prepared using amplified *Desulfovibrio salexigens* (DSMZ 2638) *DsrA* gene and the SSU rRNA gene of a *Bacillus* isolate (unpublished strain SV-1; 100% match over 878 bases for *Bacillus galliciensis* strain MER_190, KT719772), respectively, and the positive control was prepared from amplified and quantified SSU rRNA gene sample from an estuarine iron mat collected in a previous study (Sample ID Site 1 (b, 2011) in McBeth et al. (2013)). For the *DsrA* gene assay, the standard series and positive controls were prepared from amplified *Desulfovibrio salexigens DsrA* gene, and the negative control was prepared using the estuarine iron mat amplified SSU rRNA gene detailed above. Analyses were performed on an iq5 Thermal cycler (Biorad) and a C1000 Thermal cycler with CFX96 RT PCR Detection System (Biorad) using the recommended protocol for the Maxima SYBR Green qPCR master mix. Copy numbers were normalized to DNA template concentration (ng of DNA in extract).

Single Cell Genomics

We single-cell sorted samples from the BBH site and conducted single-cell genomics analysis of the steel biofilms. The two sample points (9 and 22 days) were selected based on expected peak abundances of FeOB populations determined from our qPCR data observations from the GSB site time series. Each steel sample was placed in a 15 ml conical tube, 2 ml of filter sterilized seawater was added, the sample was gently agitated to dislodge flocculent microbial corrosion biofilm material from the coupon, and the biofilm material was transferred to a 2 ml centrifuge tube. The material was mixed five times with a 16G needle and syringe to break up particulates and microbes from the mineral matrix, and the material was gently homogenized using a vortex mixer. The samples were centrifuged briefly to remove large particles and diluted (1:10) in filtered seawater. The diluted samples were immediately sorted at the Bigelow Laboratory Single Cell Genomics Center (SCGC) for particles falling in the HNA region of the dot plot (medium sized particles of high fluorescence, likely to be bacteria). Samples were amplified using multiple displacement amplification (MDA), and screened for the presence of bacteria using the primers 27F (3′AGR GTT YGA TYM TGG CTC AG-5′) and 907R (3′-CCG TCA ATT CMT TTR AGT TT-5′) (Lane et al., 1985, 1991; Page et al., 2004). The amplicons were sequenced at the Beckman Coulter Genomics Facility[2] and the contigs were assembled in Sequencher (Gene Codes, Ann Arbor, MI, USA) and manually curated to correct mislabeled bases and remove sequences of poor quality. Sequences were aligned and classified using mothur as described for high-throughput amplicon sequencing analyses. Neighbor-joining trees were constructed for SSU rRNA gene data from Epsilonproteobacteria and Zetaproteobacteria single amplified genomes (SAGs) using Jukes–Cantor correction in ARB (v. 5.3, database 108). Percentages represent the bootstrap values at each node for 1000 replicate trees; percentages less than 50% are not shown. Cultured and uncultured nearest matches are presented in the trees to identify possible physiology/metabolism of SAGs.

[2]http://www.beckmangenomics.com

The high-throughput amplicon sequencing libraries and SAG sequence libraries were deposited at the European Nucleotide Archive (ENA) under the study accession numbers PRJEB12866 (sample accessions numbers ERS1068403 to ERS1068426) and PRJEB12879 (secondary accession number ERP014404; sample accession numbers 1069314 to ERS1069573), respectively.

RESULTS

Site Conditions

At the GSB saltmarsh site, the sampler was placed on soft sediments typical of a tidal saltmarsh. At the low water point, the sampler was above the water surface. The sampler was exposed to diurnal variations in temperature, salinity, and saturation (detailed in **Table 2**). We observed a salt wedge in the stream when the tide was high; higher salinity water inundating the salt marsh at high tide and freshwater flowed out in the stream at low tide. As the study progressed, the sample holders accumulated corrosion products and sediment particulates which caused them to retain water even during low tide.

At the BBH site, the samples were placed in a protected boat harbor on soft bottom, approximately 0.3 m below the extreme low water mark for the tides during the course of this study. The maximal tidal range during the study was on the order of 3.5 m. These samplers were exposed to only minor changes in salinity and temperature over the course of the study (**Table 2**).

Macroscopic Corrosion Evidence and Imaging Results

The steel coupons developed orange flocculent coatings within the 1st week of each incubation; by the end of each study the coatings were still predominantly orange but also included patches of black or greenish precipitates (**Figures 1E–G**). Stalk structures indicative of FeOB were observed in microscopy images of the steel corrosion products at timepoints throughout the incubations (**Figures 1A–D**).

High-throughput Amplicon Sequencing Results

Amplicon sequencing was used to understand the community dynamics of populations colonizing steel coupons over time at the brackish site and full strength seawater site. We obtained between 1,173 and 44,683 reads for each of the coupon and sediment samples. The results of replicate coupon and sediment analyses are shown in **Figures 2** and **3**. Two samples from the BBH site (one of the two 9-day coupons and the 43-day sediment sample) failed in PCR amplification, and so were eliminated from the dataset. Overall there were consistent patterns of taxonomic distributions between replicates, with one notable exception being the 43-day coupon samples from the BBH site, where unclassified reads dominated the total number of bacterial reads from one of the two replicate samples (**Figure 2B**) This sample was an outlier compared to the patterns in richness and diversity seen in the other 43-day coupon from this site, which was more consistent with the other BBH samples from the time-course.

TABLE 2 | Site conditions over the course of the studies.

Site	Parameter	Mean minimum	Mean maximum	Average	Maximum	Minimum	Total	Reference
GSB	Precipitation						352 mm	Newcastle, ME weather station (NOAA, 2015)
GSB	Air temperature	12.4°C	23.3°C		33°C	−2°C		Newcastle, ME weather station (NOAA, 2015)
GSB	Measured air temperature	18°C	27°C	22.2 ± 0.6°C				This study
BBH	Measured air temperature			19 ± 1°C	23°C	14°C		This study
GSB	Stream temperature			17 ± 0.8°C				This study
BBH	Sea surface temperature (±0.2°C)	16.3°C	18.5°C		21.4°C	13.4°C		(Maine DMR, 2015)
BBH	Measured water temperature			19 ± 1°C	21°C	13°C		This study
GSB	Stream pH			6.6 ± 0.1				This study
BBH	pH			8				This study
GSB	Stream salinity			6 ± 2‰	21‰ (high tide)	0‰ (low tide)		This study
BBH	Measured salinity			30.2 ± 0.5‰	32‰	27‰		This study
GSB	Stream depth				37 cm	1.5 cm		This study
GSB	Salinity at end of saltmarsh			26 ± 1‰				This study

At the phylum level, the corrosion biofilm and sediment communities in both series were dominated by Proteobacteria and Bacteriodetes (**Figures 2A,B**). Within the Proteobacteria, Zetaproteobacteria were present on the GSB site coupons throughout the experiment, as well as in sediments adjacent to the steel samples (**Figure 2E**). The presence of Zetaproteobacteria in the saltmarsh sediments was consistent with small but visible iron mats we observed adjacent to the incubation chamber at the GSB site. At the BBH site, sequences from the Zetaproteobacteria were present from 9 days onward, but were not observed in the sediments (**Figures 2D,F**).

A substantial difference between the GSB and BBH sites was the presence and relative abundance of the families Comamonadaceae and Gallionellaceae (both Betaproteobacteria) at the brackish GSB site, but their absence at the BBH site. At GSB, the most abundance genera within these families were related to *Hydrogenophaga, Rhodoferax, Nitrotoga,* and the known FeOB *Gallionella* and *Sideroxydans.*

Another notable difference between the sediment and steel biofilm community samples was the abundance of Epsilonproteobacteria. In the corrosion communities, Epsilonproteobacteria accounted for 2–17% (GSB site) and 0.1–2% (BBH site) of the total Proteobacteria reads, while in the sediment samples at both sites they were barely detectable, accounting for <1% of total Proteobacteria reads (**Figures 2C,D**). At the GSB site, the predominant genera of Epsilonproteobacteria were related to sulfur-oxidizers *Sulfurimonas*, *Sulfuricurvum*, and *Sulfurovum*. Relatives of a sulfide-oxidizing *Arcobacter* species also represented a large portion of the Epsilonproteobacteria in the early GSB biofilm samples, but their abundance decreased over the course of the incubation. In the BBH site steel biofilms relatives of *Sulfurimonas, Sulfurovum, and Arcobacter* were present.

The Deltaproteobacteria on the steel biofilms increased through time in each series and reads from this class were high in the sediment samples, as expected (**Figures 2C,D**). At the GSB site, many of these Deltaproteobacteria reads were Desulfobacterales (**Figure 2E**), Desulfuromonadales, and Myxococcales, and included relatives of known sulfate- and iron-reducing bacteria. At the BBH site, many of the reads also classified as Desulfobacterales (**Figure 2F**) and Myxococcales; however, fewer reads classified as Desulfuromonadales. These orders included reads that classified as relatives of the sulfate- and iron-reducing bacteria but in contrast to the GSB data, we did not observe reads classifying as *Geobacter* or *Geopsychrobacter* in the BBH site data.

The Alphaproteobacteria reads at both sites were dominated by the Rhodobacteriaceae; generally speaking, Alphaproteobacteria were richer in the GSB site samples in comparison with the BBH site samples. Gammaproteobacteria at the GSB site included relatives of methanotrophs, methane-oxidizers, and sulfur oxidizers, and at the BBH site we identified relatives of several known sulfur oxidizers. Reads classified as Shewanellaceae, potential iron-reducers, were identified in both data sets.

The amplicon results revealed members of the Bacteroidetes were remarkably abundant at the BBH site. In the BBH sediment sample, they accounted for nearly 80% of relative abundance of all the bacterial reads. These percentages are much higher than have been seen in other coastal sediments (Wang

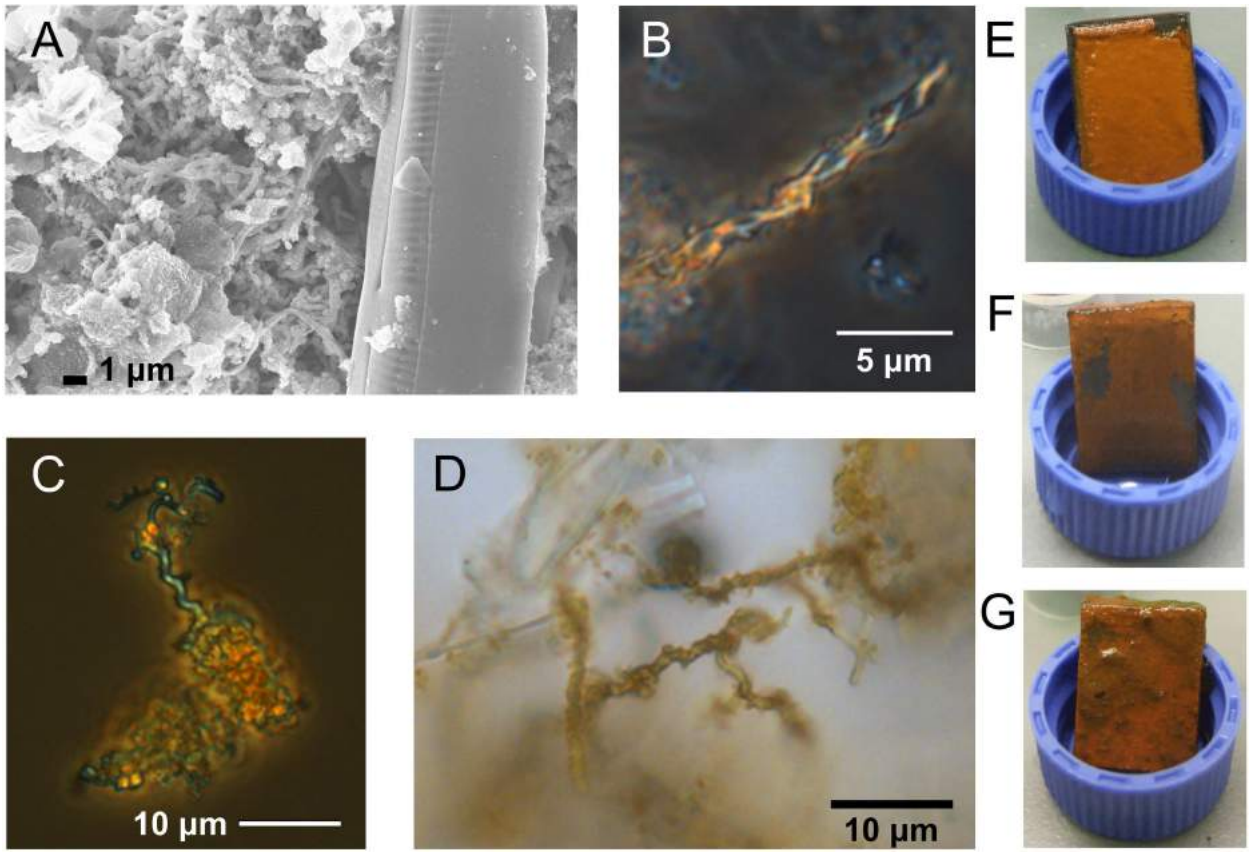

FIGURE 1 | Microscopy images of stalk structures characteristic of FeOB from field incubations and macroscopic images of corrosion biofilms. **(A)** SEM image from GSB site day 6, **(B)** light microscopy image from GSB site day 41, **(C)** light microscopy image from BBH site day 6, and **(D)** light microscopy image from BBH site day 13. Macroscopic images of BBH biofilms at: **(E)** day 9, **(F)** day 13, and **(G)** day 43.

et al., 2012). Consistent with the high sediment abundance of Bacteroidetes at the BBH site, the day 3 coupons at the BBH site had approximately 70% Bacteroidetes. Over time their relative abundance was variable but showed a general decline with biofilm age (**Figure 2B**). At the GSB site, the presence of this phylum was relatively constant and accounted for between 10 and 25% of the community. At both sites, the Bacteroidetes were dominated by the class Flavobacteria, which contains a diverse group of aerobic heterotrophs.

Alpha diversity results from the time series experiments are summarized in **Table 3**. The Good's coverage estimate indicated that the amplicon sequencing analyses captured between 63 and 98% of the sample community composition. Overall, the GSB site samples were richer and more diverse than the BBH samples. The sediment samples at the GSB site had particularly high diversity estimates, exceeding the other samples by nearly an order of magnitude. Zetaproteobacteria were richer at GSB (21 OTUs at 97% similarity) than at BBH (1 OTU).

Figures 3A,B contain the Beta diversity results. At both field sites we observed a trend in the community structure changes over the course of the experiments. As in the sequencing and qPCR data, we observed more variability in the replicate data and over the course of the experiment at the BBH study than at GSB. The initial timepoint samples from BBH clustered close to the sediment sample from that site.

qPCR Results

The low total DNA recoveries from the coupon surfaces (1–3 ng/ul for most GSB site samples and <1 ng/ul for most BBH site samples) made qPCR analyses challenging, and resulted in less than optimal replication between coupon samples. Nonetheless, for the coupons incubated at the GSB site, the Bacteria + Archaea SSU rRNA gene copies remained relatively constant over the course of the incubation at 10^5–10^6 gene copies per ng of DNA (**Figures 4A,B**) for both the coupons and the sediments. At the BBH site the Bacteria + Archaea SSU rRNA gene copy numbers on coupons spanned a broader range with 10^5–10^7 gene copies per ng of DNA, but were consistently on the order of 10^6 gene copies per ng of DNA in the sediments (**Figures 4C,D**).

Estimates of the abundance of Zetaproteobacteria on steel coupons at the GSB site based on qPCR indicated they were already detectable at 3 days, increased up to 10 days, and then declined gradually over the next 30 days. The copies of the *DsrA* gene (indicative of SRB) at the GSB site increased gradually over the course of the experiment from about 10^3 up to 10^4 gene copies per ng of DNA. The qPCR data for the GSB site sediment

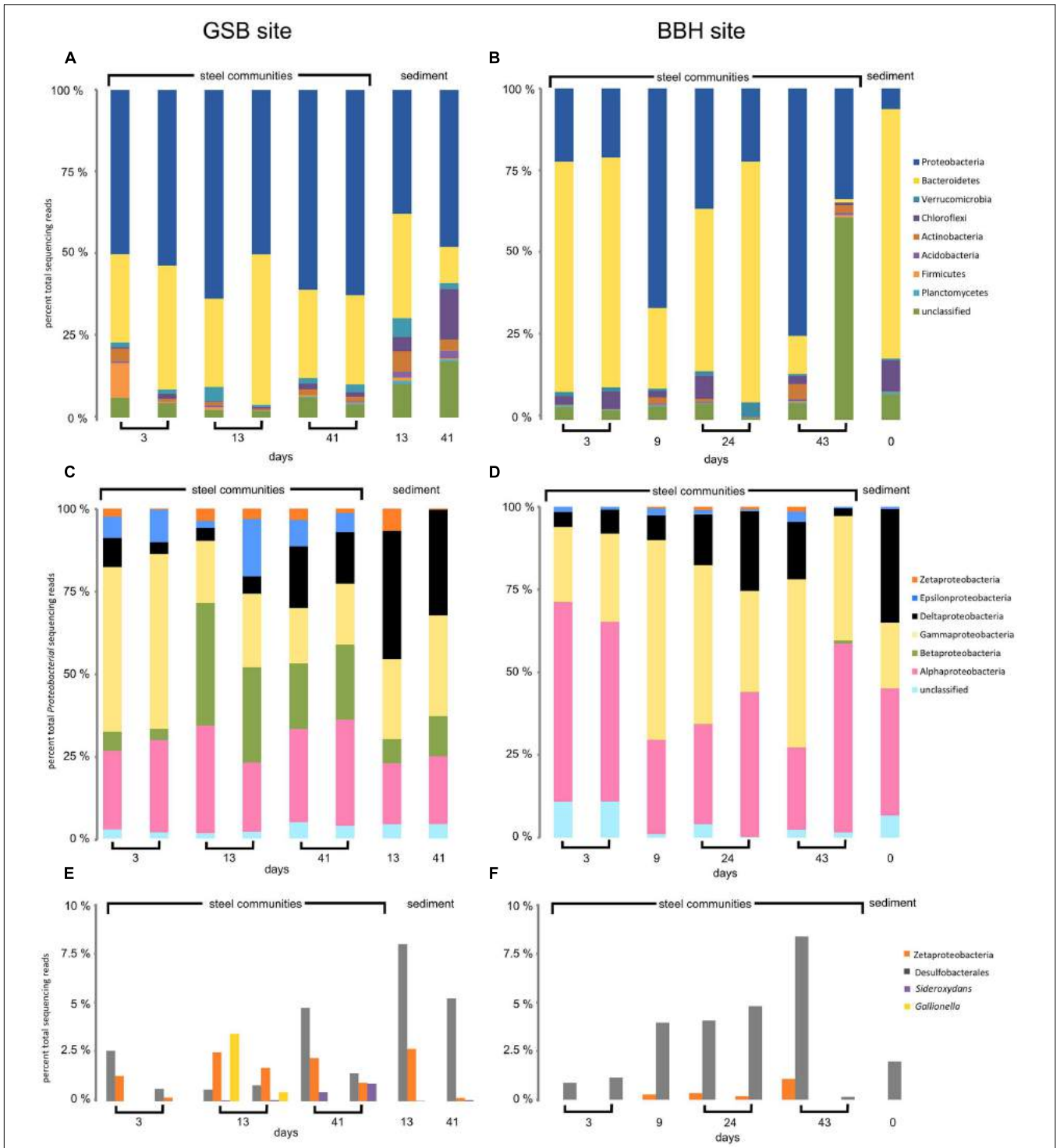

FIGURE 2 | High-throughput amplicon sequencing data for GSB saltmarsh and BBH harbor sites. (A,B) major phyla, **(C,D)** classes of Proteobacteria, and **(E,F)** sequences of FeOB relatives and Desulfobacterales.

was relatively constant, with Zetaproteobacteria about 1 to 2 orders of magnitude less abundant than SRB, and about 1 to 2 orders of magnitude less abundant than their maximal abundance measured on the coupons (at 10 days).

In contrast, at the BBH site the *DsrA* gene copies started out at about 10^6 gene copies per ng of DNA and decreased gradually over time, with a final concentration around 10^4 gene copies per ng of DNA. Here the Zetaproteobacteria abundance was

TABLE 3 | Alpha diversity results for high-throughput amplicon sequenced samples from GSB site and BBH site.

Site	Sample (days from start of time series, replicate)	Good's coverage estimate	Number of observed OTUs at 97%	Chao1 richness estimate	Inverse Simpson diversity estimate	Sample ID and ENA reference
GSB site	Steel (3, a)	0.86	351	566	115	GSB-FTS1-T1a.sff, ERS1068403
	Steel (3, b)	0.81	360	761	61	GSB-FTS1-T1b.sff, ERS1068404
	Steel (13, a)	0.79	384	933	62	GSB-FTS1-T4a.sff, ERS1068405
	Steel (13, b)	0.84	306	724	33	GSB-FTS1-T4b.sff, ERS1068406
	Steel (41, a)	0.79	398	908	70	GSB-FTS1-T6a.sff, ERS1068407
	Steel (41, b)	0.78	412	924	67	GSB-FTS1-T6b.sff, ERS1068408
	Sediment (13)	0.67	544	1592	111	GSB-FTS1-T4sed.sff, ERS1068409
	Sediment (41)	0.63	664	1436	467	GSB-FTS1-T6sed.sff, ERS1068410
BBH site	Steel (3, a)	0.94	156	247	11	BBH-FTS3-T1b.sff, ERS1068414
	Steel (3, b)	0.95	153	224	14	BBH-FTS3-T1c.sff, ERS1068415
	Steel (9)	0.88	288	490	61	BBH-FTS3-T3a.sff, ERS1068416
	Steel (24, a)	0.86	300	617	25	BBH-FTS3-T6a.sff, ERS1068418

All samples subsampled to 1173 sequences, and analyses were calculated for OTUs at 97% similarity.

essentially at or below the assay detection limit at 3 days, but then showed a large increase in abundance by days 6 and 13, followed by fluctuations and a general decline over time. In the BBH site sediments, Zetaproteobacteria were at concentrations at or below the detection limit of the assay throughout the study, and *DsrA* gene copies were on the order of 10^6 gene copies per ng of DNA. Note that the *DsrA* primers used in our study are known to overestimate the abundance of *DsrA* genes present which is a likely explanation for why these gene copies outnumber the total Bacteria + Archaea gene copies in **Figure 4D** (Ben-Dov et al., 2007).

SAG Results

Single cell sorts from the BBH site were successful and resulted in identifiable sequences from 148 cells (9-day sample) and 112 cells (22-day sample). Pie charts illustrating the proportions of taxa present in the SAG results are summarized in **Figure 5**. Zetaproteobacteria comprised 12% of the bacterial SAG library from the 9-day coupon sample, while at 22 days, only 0.9% of the SAG library were Zetaproteobacteria, indicating the proportion of Zetaproteobacteria in the biofilm communities decreased with time. Interestingly, the Zetaproteobacteria observed in both samples represented only two clonal sequences (**Figure 6**), both previously identified at this site and in other coastal enrichment studies (Genbank accession numbers HQ206658 and HQ206656; McBeth et al., 2011). No other relatives of known FeOB were identified in the SAG analyses.

Epsilonproteobacteria were numerically important corrosion community members in the SAG analyses (41 and 48% of the SAG libraries at 9 and 22 days, respectively; **Figure 5**). All of these SAGs grouped with relatives of the known sulfur-oxidizing genera *Sulfurimonas* and *Arcobacter*; in addition the day 9 SAG library had one *Sulfurovum* relative. Again, several clonal populations were observed in the SAG libraries (**Figure 7**). The Gammaproteobacteria (28–31% of the bacterial SAG libraries) were diverse at day 9 timepoint, but by 22 days the Gammaproteobacteria were reduced to relatives of *Thiomicrospira*. Alphaproteobacteria (7–17%) and Flavobacteria (3–5%) were also present. In addition to these recognized phylogenetic groups identified in the SAG libraries, 2 SAGs were only 90–92% matches to any know Genbank sequence.

DISCUSSION

The work presented here shows that mild steel corrosion communities are dynamic over time and there are successional patterns in the microbial communities. In both the brackish and seawater incubations, members of the Zetaproteobacteria that are presumptive FeOB were enriched on the steel surface, confirming earlier studies that FeOB are an important part of the MIC community (Dang et al., 2011; McBeth et al., 2011). At GSB, incubations were done in a locale where there was visible Fe-oxidation, and presumably Fe-reduction, occurring at the sediment interface in proximity to the steel coupons. In this case the Zetaproteobacteria were detectable in the sediments, but were enriched by 1 to 2 orders of magnitude on the coupons. The incubation site at the fully marine BBH site was on soft bottom

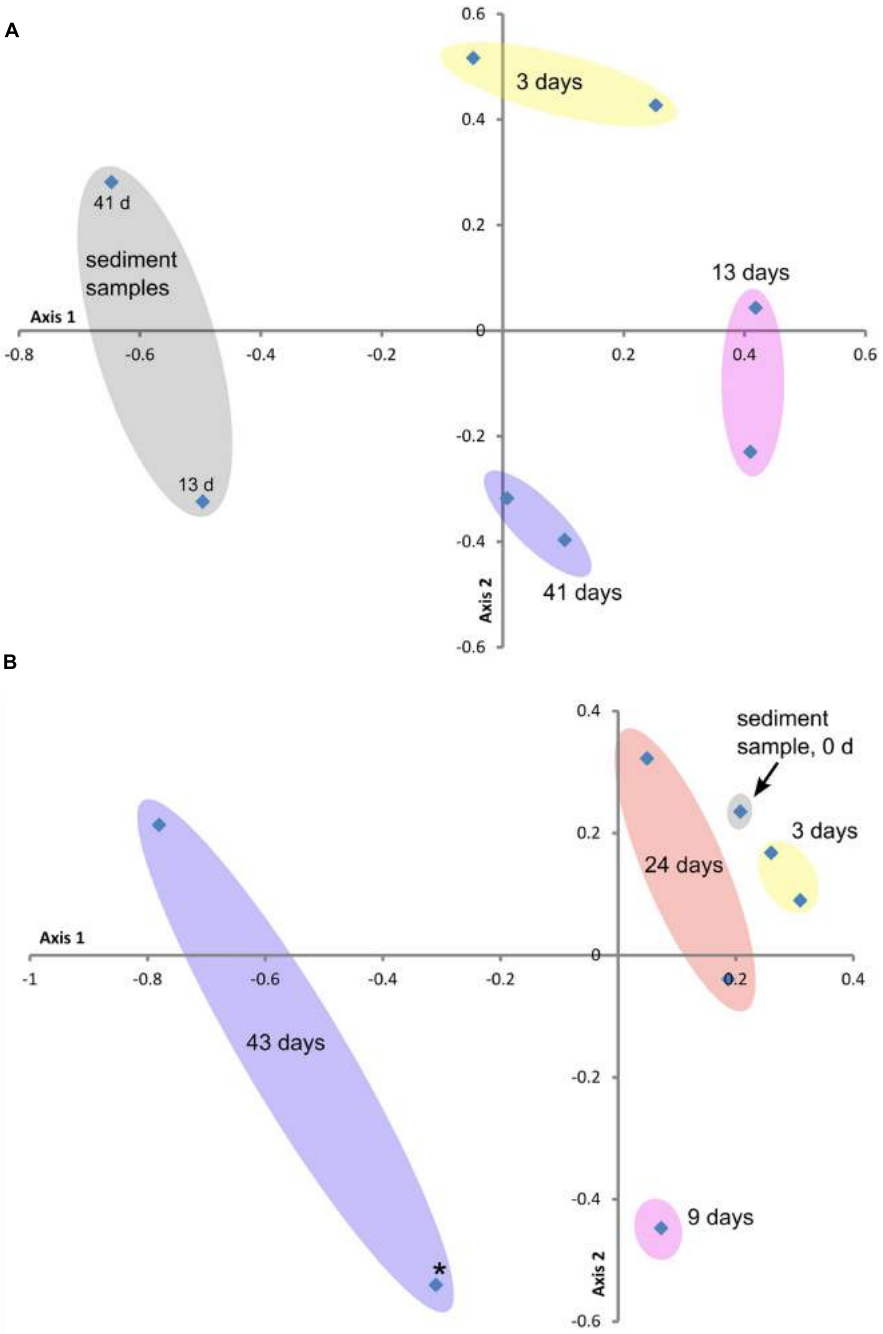

FIGURE 3 | Beta diversity ordination plots of sample communities from the two study sites: (A) GSB site and (B) BBH site. These non-metric multidimensional scaling plots (NMDS) are based on the Yue and Clayton Theta measure of dissimilarity values (distance matrix calculated at the 3% level), which assesses structural differences between the sample communities. Stress and R^2 values for these ordination plots were **(A)** 0.20 and 0.76 and **(B)** 0.09 and 0.97, respectively. Colored ovals encompass replicate samples where applicable. Point marked with star (*) in plot **(B)** represents outlier sample from **Table 3**.

sediment with no visible evidence for Fe-cycling (i.e., presence of iron mats or orange sediment), and qPCR assays did not detect Zetaproteobacteria in the surface sediments. Nonetheless, the same pattern of rapid colonization of the steel surface by FeOB occurred, and based on qPCR data, the abundance of Zetaproteobacteria on the steel surface reached a similar order of magnitude as for the brackish site at GSB. In both cases, it appeared the Zetaproteobacteria population reached an apex after 10–12 days and then declined. These results show that FeOB are early colonizers of steel surfaces, and are consistent with the findings of Dang et al. (2011). However, as the community develops, their relative abundance decreases, suggesting that the

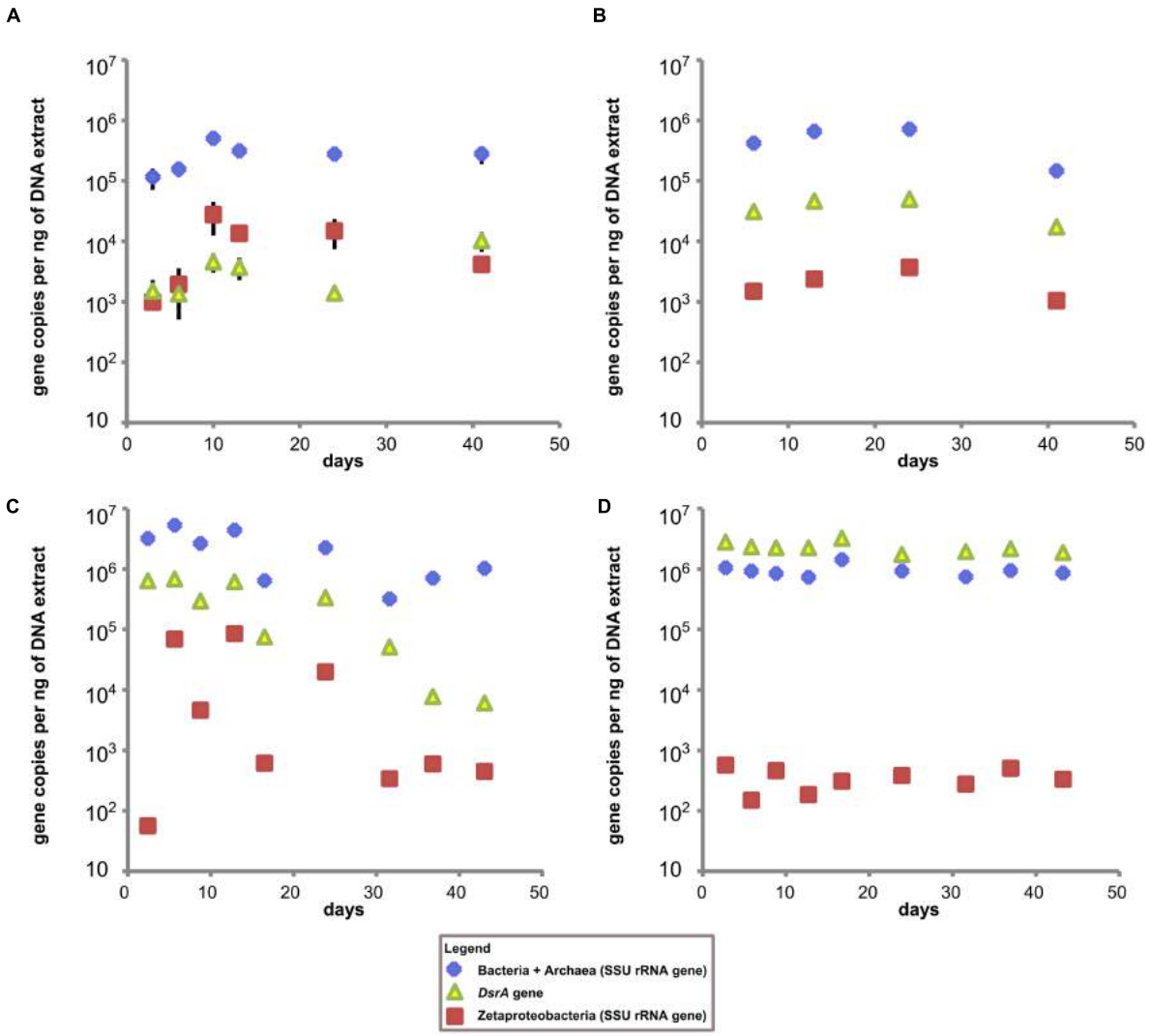

FIGURE 4 | Time series qPCR results. (A) Results from GSB site duplicate steel coupon extracts, **(B)** results from single stream sediment samples taken from sediment adjacent to the GSB site sampler, **(C)** results from BBH site triplicate steel coupon extracts, and **(D)** results from single sediment samples taken adjacent to the BBH site sampler. All data is gene copies per ng of DNA in extract. Error bars represent standard error of replicate samples where applicable; if not visible they fall within the boundaries of the symbol.

steel surface niche is changing to become a more mature biofilm with anoxic zones that support the growth of strict anaerobes like SRB. This is consistent with previously models for mature steel corrosion communities (Hamilton, 1985; Little and Lee, 2007).

This study is unique in looking at both brackish and marine environments with initiation of corrosion under fully aerobic conditions, nor are we aware of studies, aside from the work of Dang et al. (2011), that have investigated the *in situ* population dynamics of MIC communities. Over the 40-day incubation course of these experiments, the total diversity of the communities did not increase significantly; however, the population structure did change consistently through time (**Figure 3**). These dynamics indicate that the surface niche has not stabilized and that continued physicochemical changes may select for different populations, while at the same time ecological interactions between populations are also continuing to shape and alter the community. A longer time course would be necessary to determine if the MIC community reaches a stable composition. Deltaproteobacteria were expected to be part of the community, since this class includes a known sulfate- and Fe-reducing genera and both of these physiological groups have been previously observed in association with marine MIC communities (e.g., Dang et al., 2011; Enning et al., 2012). The relative abundance of Deltaproteobacteria, as assessed by amplicon sequencing, increased with time at both sites. The dynamics of SRB as specifically assessed by qPCR differed between GSB and BBH. At GSB, copy numbers of *DsrA* were low at 15 days and then increased over time, this is consistent with formation of a more mature biofilm with anoxic niches that could support sulfate-reduction. At BBH, *DsrA* copies were

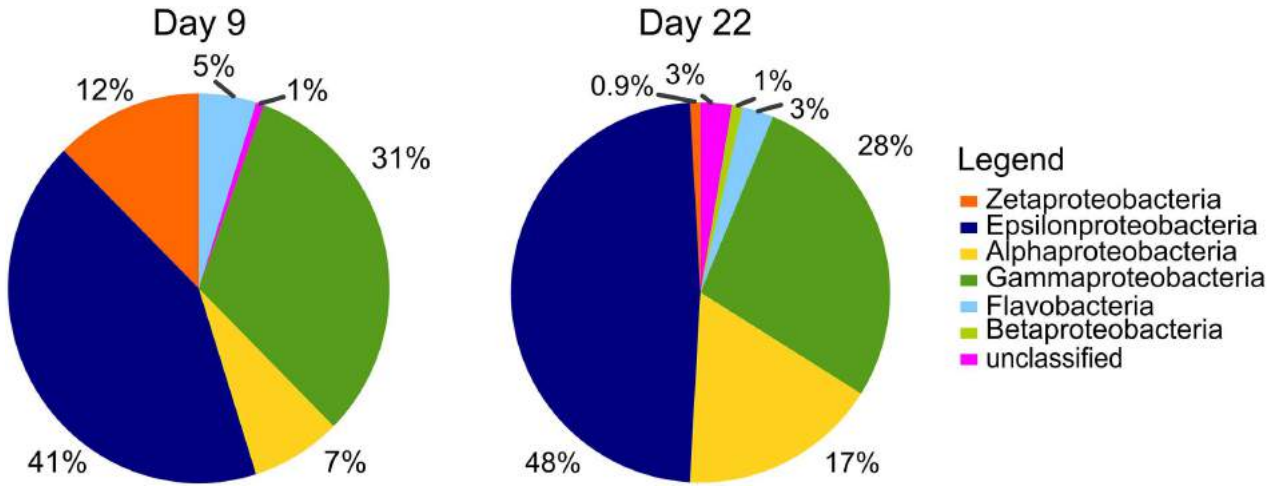

FIGURE 5 | Single amplified genome (SAG) results from BBH site, results from bacterial SSU rRNA gene screen of plates sorted from day 9 (148 SAGs) and day 22 (118 SAGs). Pie charts show percent of each class of Proteobacteria observed in each sample.

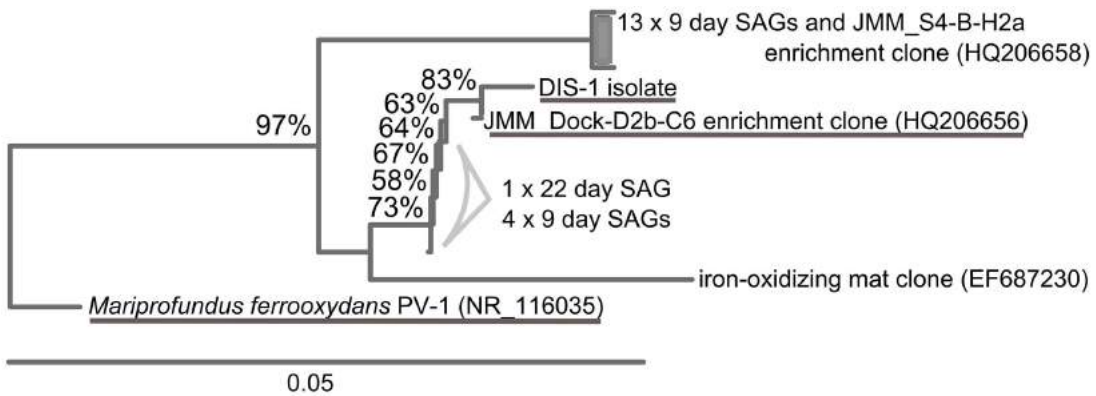

FIGURE 6 | Neighbor-joining tree showing SAGs classified as Zetaproteobacteria identified in the BBH site single cell sorts. Stalk-forming FeOB Zetaproteobacteria related to the SAGs are underlined.

relatively abundant initially, on a par with the sediments, and then decreased over time, while sediment numbers stayed quite constant. We do not have a good explanation for this pattern, and it is inconsistent with the relative increase in reads of Deltaproteobacteria in the amplicon analysis. One possibility is that Fe-reducing Deltaproteobacteria may have been a larger part of the community than SRB at the early timepoints, however, this is not reflected in the classification of the sequencing results. It has also recently been shown that some Alphaproteobacteria belonging to the *Roseobacter* clade contain *DsrA* genes and it is possible they may have also been targeted by the qPCR primers (Lenk et al., 2012).

The relatively high percentages (typically ranging from 25 to 75%) of Bacteroidetes in comparison with other sites (Wang et al., 2012) from sediment and coupon surface amplicon libraries was notable (**Figures 2** and **3**). The presence of Bacteroidetes on the BBH sampler coupons through most of the time course was especially pronounced. They accounted for nearly 70% of reads during the middle of the time-course, although they declined significantly by 43 days (**Figure 2**). A more detailed assessment of the SSU rRNA amplicon reads for this group indicated the closest known relatives were members of the Flavobacteriales that includes aerobic and facultative heterotrophs that are often saprophytic (Krieg et al., 2010). The work of Dang et al. (2011) also showed abundant Flavobacteriales on the surface of steel coupons incubated in coastal waters in China. The specific role of this group in the MIC community is difficult to ascertain, although it is possible they are taking advantage of primary production by chemolithotrophic Fe- and S-oxidizing bacteria. It is also known that members of the Flavobacteriales are efficient at colonizing surfaces and growing as biofilms (Doghri et al., 2015); thus, they may preferentially colonize substrates that are newly introduced into their environment. Another possible explanation for the high abundance of Bacteroidetes at the BBH site is that they are often excellent organic matter decomposers, and the environment was rich in particulate organic matter. More

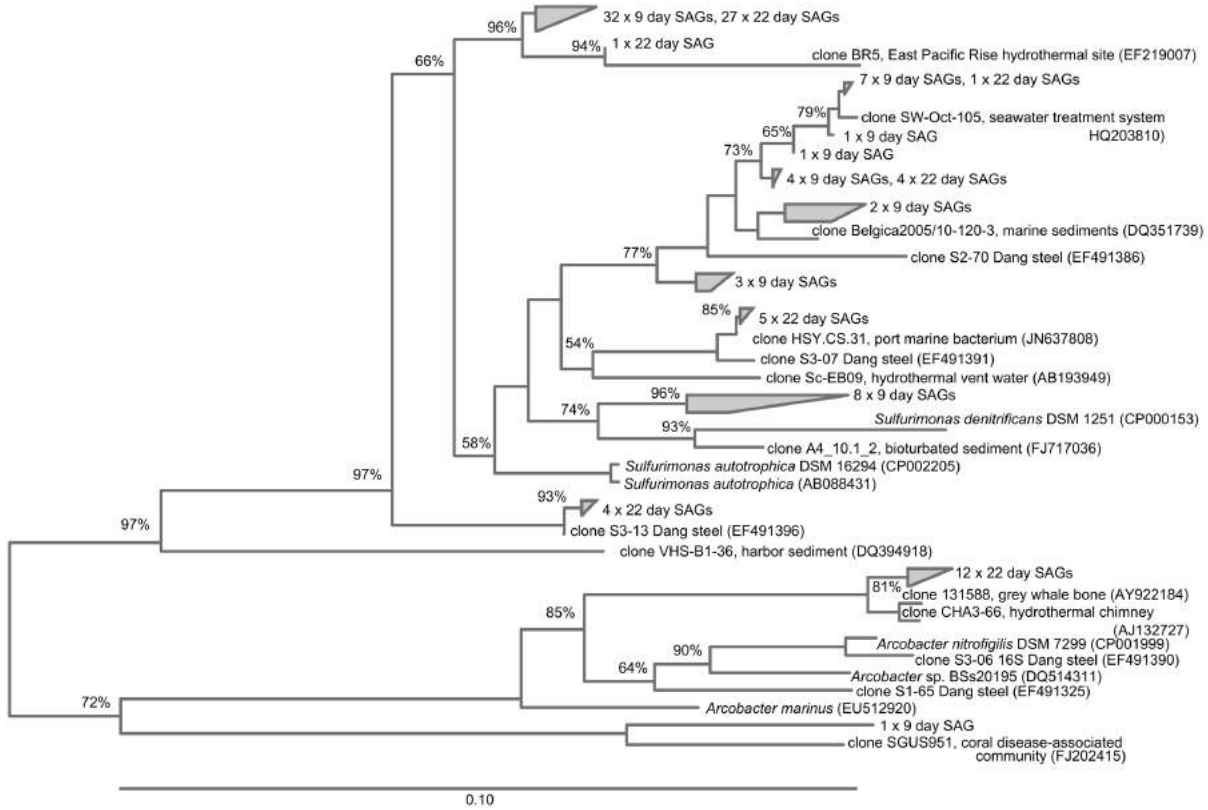

FIGURE 7 | Neighbor-joining tree showing SAGs classified as Epsilonproteobacteria identified in the BBH site single cell sorts.

specifically, there was a significant amount of seaweed in the vicinity of the sampler, although it was not in direct contact with the samples. This seaweed was starting to undergo senescence and degradation in late summer, which would likely promote the growth of saprophytic microbes (Thomas, 2015).

The high number of Epsilonproteobacteria identified in the SAG libraries at both time points was interesting. These represent absolute cell numbers in the sorted sample, which included cells from the loosely adhering portion of the biofilm. The Epsilonproteobacteria were consistently present in the amplicon libraries, but at a lower relative abundance. Members of the Epsilonproteobacteria are not commonly reported as being important members of the MIC community; however, Dang et al. (2011), also noted their relative abundance in steel colonization, and suggested they might be involved in S-oxidation, perhaps coupling their metabolism with the reduced S-products of sulfate reducers. Our findings are consistent with that report, as the identified genera included *Sulfurimonas* and *Arcobacter*, known S-oxidizers (Campbell et al., 2006). However, it cannot be ruled out that some of these organisms may also be carrying out H_2-oxidation (e.g., Takai et al., 2006), since H_2 production commonly occurs at steel surfaces (Little and Lee, 2007).

The presence and relative abundance of Zetaproteobacteria SAGs on the 9-day BBH samples in comparison with the samples taken at 22 days was consistent with the general decline in Zetaproteobacteria abundance observed from qPCR over the same timeline. It is worth noting we did not obtain any Deltaproteobacteria in the SAG libraries. Although it is possible this is bias of selecting a particular population of high nucleic acid cells via flow cytometry sort or bias against either lysis or amplication of this group in the SAG preparation, we believe a more likely explanation may have to do with the structure of the biofilm, and how it was sampled. The samples for SAG analysis were taken only from a comparatively loose surface layer of the biofilm, where more aerobic members of the community would be expected. For high-throughput amplicon sequencing and qPCR analyses the entire surface layer (consisting of the outer, loosely adherent layer, and an inner, more adherent layer) was used in order to obtain enough nucleic acid for the analyses. Thus it is possible the SAG libraries are selecting organisms with more aerobic metabolisms, which is consistent with the relative abundance of Zetaproteobacteria and Epsilonproteobacteria.

The population structure of FeOB within the biofilms showed important differences between brackish and fully marine conditions. At GSB, where the salinity fluctuated from between 0 and 21 ppt as a result of tidal influence, representatives of the freshwater FeOB, Gallionellaceae were found in addition to Zetaproteobacteria. This is consistent with an earlier study that looked at the distribution of FeOB along a salinity gradient and found overlap between these groups in brackish regions (McBeth et al., 2013). This also implies that freshwater FeOB are part of MIC communities in strictly freshwater habitats, and is consistent

with their presence on steel corrosion products in the Great Lakes (Hicks, 2007), scale from reclaimed wastewater (Jin et al., 2015), and from an incubation experiment (Rajala et al., 2015). Interestingly, the richness of Zetaproteobacteria was far greater at GSB – 21 OTUs at 97% similarity – than it was in fully marine BBH where only a single OTU was observed. In fact, our analysis of Zetaproteobacteria SAGs from BBH indicated a very low diversity with only two clones accounting for the abundance of Zetaproteobacteria on the samples. One explanation for this is that a low overall abundance of Zetaproteobacteria in the coastal ocean (at least at this location) leads to recruitment of only a few strains that become established on the steel surface and grow to abundance. This observation is supported by the clonal Zetaproteobacteria sequences we were able to amplify in a previous coastal study of corrosion biofilms (McBeth et al., 2011). Interestingly, basalt coupons incubated in the abyssal plain of the deep ocean are also known to recruit Zetaproteobacteria that presumably gain energy from the reduced iron within the basalt. These communities are also of low diversity, suggesting a similar mechanism of recruitment (Henri et al., 2015), as predicted by Edwards et al. (2004).

CONCLUSION

In this study, we have characterized the succession of mild steel corrosion communities over 40 days in both nearshore marine and estuarine salt marsh environments. This is the first time a detailed study of corrosion community succession has been conducted over a period of several weeks. We found that iron-oxidizing Zetaproteobacteria and Betaproteobacteria were able to rapidly colonize the steel surfaces over the first 10 days of the incubations; however, their numbers dropped after this initial colonization and as the corrosion community matured on the steel surfaces. Epsilonproteobacteria were also enriched on the steel samples over the course of these experiments, relative to background sediment samples. The iron-oxidizing Zetaproteobacteria were still able to achieve rapid colonization in the coastal marine environment where their ambient abundance was extremely low. This is further evidence of the amazing ability of these microbes to flourish on sources of reduced iron provided by transient niches as the opportunity arises – whether that niche consists of a steel structure or a fresh pillow basalt deposit.

AUTHOR CONTRIBUTIONS

This study was conceived by DE and designed by DE and JM. JM conducted the data acquisition, analysis, and interpretation, and manuscript preparation with assistance from DE. JM and DE wrote the manuscript, and have reviewed the final version for submission for publication. JM and DE agree to be accountable for all aspects of the work in ensuring that questions related to the accuracy or integrity of any part of the work are appropriately investigated and resolved.

FUNDING

Funding for this study was provided by the US Office of Naval Research, Grant #N00014-08-1-0334.

ACKNOWLEDGMENTS

We gratefully acknowledge the support of the Damariscotta River Association and the Maine Department of Marine Resources for allowing us access to the field sites at Great Salt Bay and the DMR Dock in West Boothbay Harbor, respectively. We thank the Bigelow Laboratory Single Cell Genomics Centre for assistance with sample processing and data analysis and use of their iq5 qPCR machine; Peter Countway for the use of his qubit, qPCR machines, and lab for sample preparation. We are grateful to Emily Fleming, Jennifer Fownes, Jarrod Scott, Nicole Poulton, Ramunas Stepanauskas, Wendy Korjeff Bellows, Brandon Swan, Erin Field, Jochen Nuester, Bob Anderson, Carlton Rauschenberg, Peter Larsen, and Andrew Hind for constructive discussions and assistance in the field and lab.

REFERENCES

Ben-Dov, E., Brenner, A., and Kushmaro, A. (2007). Quantification of sulfate-reducing bacteria in industrial wastewater, by real-time polymerase chain reaction (PCR) using dsrA and apsA genes. *Microb. Ecol.* 54, 439–451. doi: 10.1007/s00248-007-9233-2

Campbell, B. J., Engel, A. S., Porter, M. L., and Takai, K. (2006). The versatile ε-proteobacteria: key players in sulphidic habitats. *Nat. Rev. Microbiol.* 4, 458–468.

Chandler, K. A. (1985). *Marine and Offshore Corrosion*. New York: Butterworth-Heinemann Ltd.

Dang, H., Chen, R., Wang, L., Shao, S., Dai, L., Ye, Y., et al. (2011). Molecular characterization of putative biocorroding microbiota with a novel niche detection of Epsilon- and Zetaproteobacteria in Pacific Ocean coastal seawaters. *Environ. Microbiol.* 13, 3059–3074. doi: 10.1111/j.1462-2920.2011.02583.x

Dang, H., and Lovell, C. R. (2016). Microbial surface colonization and biofilm development in marine environments. *Microbiol. Mol. Biol. Rev.* 80, 91–138. doi: 10.1128/mmbr.00037-15

Doghri, I., Rodrigues, S., Bazire, A., Dufour, A., Akbar, D., Sopena, V., et al. (2015). Marine bacteria from the french atlantic coast displaying high forming-biofilm abilities and different biofilm 3D architectures. *BMC Microbiol.* 15:231. doi: 10.1186/s12866-015-0568-4

Dowd, S., Callaway, T., Wolcott, R., Sun, Y., McKeehan, T., Hagevoort, R., et al. (2008). Evaluation of the bacterial diversity in the feces of cattle using 16S rDNA bacterial tag-encoded FLX amplicon pyrosequencing (bTEFAP). *BMC Microbiol.* 8:125. doi: 10.1186/1471-2180-8-125

Edgar, R. C., Haas, B. J., Clemente, J. C., Quince, C., and Knight, R. (2011). UCHIME improves sensitivity and speed of chimera detection. *Bioinformatics* 27, 2194–2200. doi: 10.1093/bioinformatics/btr381

Edwards, K. J., Bach, W., McCollom, T. M., and Rogers, D. R. (2004). Neutrophilic iron-oxidizing bacteria in the ocean: their habitats, diversity, and roles in mineral deposition, rock alteration, and biomass production in the deep-sea. *Geomicrobiol. J.* 21, 393–404. doi: 10.1080/01490450490485863

Emerson, D., Fleming, E. J., and McBeth, J. M. (2010). Iron-oxidizing bacteria: an environmental and genomic perspective. *Annu. Rev. Microbiol.* 64, 561–583. doi: 10.1146/annurev.micro.112408.134208

Enning, D., Venzlaff, H., Garrelfs, J., Dinh, H. T., Meyer, V., Mayrhofer, K., et al. (2012). Marine sulfate-reducing bacteria cause serious corrosion of iron under electroconductive biogenic mineral crust. *Environ. Microbiol.* 14, 1772–1787. doi: 10.1111/j.1462-2920.2012.02778.x

Hamilton, A. W. (1985). The sulphate reducing bacteria and anaerobic corrosion. *Annu. Rev. Microbiol.* 39, 195–217. doi: 10.1146/annurev.mi.39.100185.001211

Henri, P. A., Rommevaux-Jestin, C., Lesongeur, F., Mumford, A., Emerson, D., Godfroy, A., et al. (2015). Structural iron (II) of basaltic glass as an energy source for Zetaproteobacteria in an abyssal plain environment, off the Mid Atlantic Ridge. *Front. Microbiol.* 6:1518. doi: 10.3389/fmicb.2015.01518

Hicks, R. E. (2007) *Department of Biology, University of Minnesota Duluth. Structure of Bacterial Communities Associated with Accelerated Corrosive Loss of Port Transportation Infrastructure*. Duluth, MN: Institute GLMR.

Jin, J., Wu, G., and Guan, Y. (2015). Effect of bacterial communities on the formation of cast iron corrosion tubercles in reclaimed water. *Water Res.* 71, 207–218. doi: 10.1016/j.watres.2014.12.056

Kato, S., Kobayashi, C., Kakegawa, T., and Yamagishi, A. (2009). Microbial communities in iron-silica-rich microbial mats at deep-sea hydrothermal fields of the Southern Mariana Trough. *Environ. Microbiol.* 11, 2094–2111. doi: 10.1111/j.1462-2920.2009.01930.x

Krieg, N., Ludwig, W., Euzéby, J., and Whitman, W. (2010). "Phylum XIV. Bacteroidetes phyl. nov.," in *Bergey's Manual of Systematic Bacteriology,* eds Krieg et al. (New York, NY: Springer).

Lane, D. J., Pace, B., Olsen, G. J., Stahl, D. A., Sogin, M. L., and Pace, N. R. (1985). Rapid determination of 16S ribosomal RNA sequences for phylogenetic analyses. *Proc. Natl. Acad. Sci. U.S.A.* 82, 6955–6959. doi: 10.1073/pnas.82.20.6955

Lane, D. J., Stackebrandt, E., and Goodfellow, M. (eds) (1991). *16S/23S rRNA Sequencing. In: Nucleic acid Techniques in Bacterial Systematics*. New York, NY: John Wiley & Sons.

Lee, J. S., McBeth, J. M., Ray, R. I., Little, B. J., and Emerson, D. (2013). Iron cycling at corroding carbon steel surfaces. *Biofouling* 29, 1243–1252. doi: 10.1080/08927014.2013.836184

Lenk, S., Moraru, C., Hahnke, S., Arnds, J., Richter, M., Kube, M., et al. (2012). Roseobacter clade bacteria are abundant in coastal sediments and encode a novel combination of sulfur oxidation genes. *ISME J.* 6, 2178–2187. doi: 10.1038/ismej.2012.66

Little, B. J., and Lee, J. S. (2007). *Microbiologically Influenced Corrosion. Microbiologically Influenced Corrosion*. Hoboken, NJ: Wiley-Interscience.

Maine DMR (2015). *Boothbay Harbor Environmental Data*. West Boothbay Harbor, ME: Maine Department of Marine Resources.

Marty, F., Gueuné, H., Malard, E., Sánchez-Amaya, J. M., Sjögren, L., Abbas, B., et al. (2014). Identification of key factors in accelerated low water corrosion through experimental simulation of tidal conditions: influence of stimulated indigenous microbiota. *Biofouling* 30, 281–297. doi: 10.1080/08927014.2013.864758

McBeth, J. M., Fleming, E. J., and Emerson, D. (2013). The transition from freshwater to marine iron-oxidizing bacterial lineages along a salinity gradient on the Sheepscot River, Maine, USA. *Environ. Microbiol. Rep.* 5, 453–463. doi: 10.1111/1758-2229.12033

McBeth, J. M., Little, B. J., Ray, R. I., Farrar, K. M., and Emerson, D. (2011). Neutrophilic iron-oxidizing "Zetaproteobacteria" and mild steel corrosion in nearshore marine environments. *Appl. Environ. Microbiol.* 77, 1405–1412. doi: 10.1128/AEM.02095-10

NACE International. (2002). Corrosion costs and preventive strategies in the united states [summary of the US FHWA publication No. FHWA-RD-01-156]. *Mater. Perform.* 41:12.

NOAA (2015). *Climate Data Online Data Tools*. Available at: http://www.ncdc.noaa.gov/cdo-web/datatools

Page, K. A., Connon, S. A., and Giovannoni, S. J. (2004). Representative freshwater bacterioplankton isolated from crater lake, oregon. *Appl. Environ. Microbiol.* 70, 6542–6550. doi: 10.1128/aem.70.11.6542-6550.2004

Pruesse, E., Quast, C., Knittel, K., Fuchs, B. M., Ludwig, W., Peplies, J., et al. (2007). SILVA: a comprehensive online resource for quality checked and aligned ribosomal RNA sequence data compatible with ARB. *Nucleic Acids Res.* 35, 7188–7196. doi: 10.1093/nar/gkm864

Rajala, P., Carpén, L., Vepsäläinen, M., Raulio, M., Sohlberg, E., and Bomberg, M. (2015). Microbially induced corrosion of carbon steel in deep groundwater environment. *Front. Microbiol.* 6:647. doi: 10.3389/fmicb.2015.00647

Schloss, P. D., Westcott, S. L., Ryabin, T., Hall, J. R., Hartmann, M., Hollister, E. B., et al. (2009). Introducing mothur: open-source, platform-independent, community-supported software for describing and comparing microbial communities. *Appl. Environ. Microbiol.* 75, 7537–7541. doi: 10.1128/aem.01541-09

Takai, K., and Horikoshi, K. (2000). Rapid detection and quantification of members of the archaeal community by quantitative PCR using fluorogenic probes. *Appl. Environ. Microbiol.* 66, 5066–5072. doi: 10.1128/aem.66.11.5066-5072.2000

Takai, K., Suzuki, M., Nakagawa, S., Miyazaki, M., Suzuki, Y., Inagaki, F., et al. (2006). *Sulfurimonas paralvinellae* sp. nov., a novel mesophilic, hydrogen- and sulfur-oxidizing chemolithoautotroph within the Epsilonproteobacteria isolated from a deep-sea hydrothermal vent polychaete nest, reclassification of Thiomicrospira denitrificans as Sulfurimonas denitrificans comb. nov. and emended description of the genus Sulfurimonas. *Int. J. Syst. Evol. Microbiol.* 56, 1725–1733. doi: 10.1099/ijs.0.64255-0

Thomas, T. (2015). A comprehensive analysis of the microbial communities of healthy and diseased marine macroalgae and the detection of known and potential bacterial pathogens. *Front. Microbiol.* 6:146. doi: 10.3389/fmicb.2015.00146

Wang, Q., Garrity, G. M., Tiedje, J. M., and Cole, J. R. (2007). Naive bayesian classifier for rapid assignment of rRNA sequences into the new bacterial taxonomy. *Appl. Environ. Microbiol.* 73, 5261–5267. doi: 10.1128/aem.00062-07

Wang, Y., Sheng, H.-F., He, Y., Wu, J.-Y., Jiang, Y.-X., Tam, N. F.-Y., et al. (2012). Comparison of the levels of bacterial diversity in freshwater, intertidal wetland, and marine sediments by using millions of illumina tags. *Appl. Environ. Microbiol.* 78, 8264–8271. doi: 10.1128/aem.01821-12

Conflict of Interest Statement: The authors declare that the research was conducted in the absence of any commercial or financial relationships that could be construed as a potential conflict of interest.

frontiers in Microbiology

ORIGINAL RESEARCH
published: 13 November 2015
doi: 10.3389/fmicb.2015.01265

Comparative Genomic Insights into Ecophysiology of Neutrophilic, Microaerophilic Iron Oxidizing Bacteria

Shingo Kato[1,2†], Moriya Ohkuma[2], Deborah H. Powell[3], Sean T. Krepski[1], Kenshiro Oshima[4], Masahira Hattori[4], Nicole Shapiro[5], Tanja Woyke[5] and Clara S. Chan[1*]*

[1] Department of Geological Sciences, University of Delaware, Newark, DE, USA, [2] Japan Collection of Microorganisms, RIKEN BioResource Center, Tsukuba, Japan, [3] Delaware Biotechnology Institute, University of Delaware, Newark, DE, USA, [4] Center for Omics and Bioinformatics, Graduate School of Frontier Sciences, University of Tokyo, Kashiwa, Japan, [5] Department of Energy Joint Genome Institute, Walnut Creek, CA, USA

OPEN ACCESS

Edited by:
Beth Orcutt,
Bigelow Laboratory for Ocean Sciences, USA

Reviewed by:
James Hemp,
California Institute of Technology, USA
Roman Barco,
University of Southern California, USA

***Correspondence:**
Shingo Kato
skato@jcm.riken.jp;
Clara S. Chan
cschan@udel.edu

†Present address:
Shingo Kato,
Seafloor Resources Research Project, Japan Agency for Marine-Earth Science and Technology, 2-15 Natsushima, Yokosuka 237-0061, Japan

Specialty section:
This article was submitted to Extreme Microbiology, a section of the journal Frontiers in Microbiology

Received: 02 September 2015
Accepted: 30 October 2015
Published: 13 November 2015

Citation:
Kato S, Ohkuma M, Powell DH, Krepski ST, Oshima K, Hattori M, Shapiro N, Woyke T and Chan CS (2015) Comparative Genomic Insights into Ecophysiology of Neutrophilic, Microaerophilic Iron Oxidizing Bacteria. Front. Microbiol. 6:1265. doi: 10.3389/fmicb.2015.01265

Neutrophilic microaerophilic iron-oxidizing bacteria (FeOB) are thought to play a significant role in cycling of carbon, iron and associated elements in both freshwater and marine iron-rich environments. However, the roles of the neutrophilic microaerophilic FeOB are still poorly understood due largely to the difficulty of cultivation and lack of functional gene markers. Here, we analyze the genomes of two freshwater neutrophilic microaerophilic stalk-forming FeOB, *Ferriphaselus amnicola* OYT1 and *Ferriphaselus* strain R-1. Phylogenetic analyses confirm that these are distinct species within Betaproteobacteria; we describe strain R-1 and propose the name *F. globulitus.* We compare the genomes to those of two freshwater Betaproteobacterial and three marine Zetaproteobacterial FeOB isolates in order to look for mechanisms common to all FeOB, or just stalk-forming FeOB. The OYT1 and R-1 genomes both contain homologs to *cyc2*, which encodes a protein that has been shown to oxidize Fe in the acidophilic FeOB, *Acidithiobacillus ferrooxidans.* This *c*-type cytochrome common to all seven microaerophilic FeOB isolates, strengthening the case for its common utility in the Fe oxidation pathway. In contrast, the OYT1 and R-1 genomes lack *mto* genes found in other freshwater FeOB. OYT1 and R-1 both have genes that suggest they can oxidize sulfur species. Both have the genes necessary to fix carbon by the Calvin–Benson–Basshom pathway, while only OYT1 has the genes necessary to fix nitrogen. The stalk-forming FeOB share *xag* genes that may help form the polysaccharide structure of stalks. Both OYT1 and R-1 make a novel biomineralization structure, short rod-shaped Fe oxyhydroxides much smaller than their stalks; these oxides are constantly shed, and may be a vector for C, P, and metal transport to downstream environments. Our results show that while different FeOB are adapted to particular niches, freshwater and marine FeOB likely share common mechanisms for Fe oxidation electron transport and biomineralization pathways.

Keywords: iron oxidation, iron-oxidizing bacteria, biomineralization, *Ferriphaselus*, Gallionellales

INTRODUCTION

Microorganisms have long been associated with Fe oxidation in the environment, but the extent of their contribution to Fe and other elemental cycles is still unknown. There is often a question about whether Fe(II) oxidation is driven by biotic or abiotic processes, especially in oxic environments. Studies of microaerophilic neutrophilic Fe-oxidizing bacteria (FeOB) have demonstrated that microbes can contribute to Fe(II) oxidation, especially at lower oxygen concentrations at which abiotic Fe(II) oxidation is slow enough for microbes to compete (Rentz et al., 2007; Druschel et al., 2008). At the interface where Fe(II)-rich fluids meet oxygenated waters, O_2 is often low; this is where we find abundant freshwater Betaproteobacterial FeOB and marine Zetaproteobacterial FeOB. Although traditionally studied in Fe microbial mats at groundwater seeps and hydrothermal vents, FeOB are being discovered in a variety of environments including rhizospheres, terrestrial aquifers, coastal sediments, and oceanic crustal boreholes (Emerson et al., 2007, 2010, 2015; Orcutt et al., 2011; McAllister et al., 2015), suggesting that microbes contribute significantly to Fe oxidation in these environments. It is intriguing that the microaerophilic neutrophilic FeOB mostly fall into two distinct classes of Proteobacteria; this presents the opportunity to learn about Fe oxidation in both freshwater and marine environments by comparing the physiology and genomes of Betaproteobacterial and Zetaproteobacterial FeOB.

In order to learn more about the roles of FeOB in nature, we need to determine the genes involved in the Fe oxidation electron transport system, which would then allow us to track FeOB activity. Difficulties in culturing FeOB have resulted in relatively few isolates and correspondingly few genomes: five genomes of microaerophilic FeOB reported thus far, two freshwater Betaproteobacteria and three marine Zetaproteobacteria (Singer et al., 2011; Emerson et al., 2013; Field et al., 2015). Comparative genomics, along with some initial genetic and proteomic work has led to candidate Fe oxidases and hypothetical models of Fe oxidation pathways (Singer et al., 2011; Liu et al., 2012; Emerson et al., 2013; Barco et al., 2015). The cytochrome MtoA from the freshwater FeOB *Sideroxydans lithotrophicus* was found to oxidize Fe *in vitro* (Liu et al., 2012). However, *mtoA* is rare in FeOB genomes, found in only the freshwater Betaproteobacteria *S. lithotrophicus* and *Gallionella capsiferriformans*, but not the marine Zetaproteobacteria, suggesting that it may be specific to freshwater FeOB. A proteomic/genomic study of the marine Zetaproteobacterium *Mariprofundus ferrooxydans* demonstrated high expression of a cytochrome *c*, $Cyc2_{PV\text{-}1}$, which shares homology with the outer membrane Fe oxidase of *Acidithiobacillus ferrooxidans*, an acidophilic FeOB (Castelle et al., 2008; Barco et al., 2015). This led to a proposed model for Fe oxidation by *M. ferrooxydans* in which $Cyc2_{PV\text{-}1}$ is the Fe oxidase, also involving a periplasmic cytochrome Cyc1 and the alternative complex III (ACIII) Act genes. The *cyc2* and *act* genes are attractive as potential markers of Fe oxidation because they are present in all of the sequenced FeOB genomes and are phylogenetically related. Further comparative genomics is needed to see if these genes are common across neutrophilic microaerophilic FeOB. FeOB genome analysis will also give us insight into how Fe oxidation fuels N, S, and C metabolisms, thus linking Fe and other major elemental cycles.

The primary way that FeOB affect the environment is through their biominerals. At circumneutral pH, Fe oxidation results in Fe(III) oxyhydroxides, which adsorb and coprecipitate organics, phosphate, arsenic, and other metals (e.g., Ferris, 2005; Borch et al., 2010). These oxides take the form of twisted ribbon-like stalks, hollow tubular sheaths, and granular (sometimes called "amorphous") oxides. These are often associated with polysaccharides, which may play a role in stalk morphology, as well as binding Fe(III) and removing it from the cell (Chan et al., 2009, 2011). Of the five currently available microaerophilic FeOB that have sequenced genomes, all of the stalk-formers are marine (*M. ferrooxydans* sp. PV-1, M34, and EKF-M39) (**Table 1**). Strikingly, freshwater FeOB *Gallionella ferruginea* and *Ferriphaselus* sp. also produce a very similar twisted stalk (Vatter and Wolfe, 1956; Krepski et al., 2012; Kato et al., 2014), suggesting that the stalk plays an important role in both freshwater and marine Fe oxidation. However, we are still learning about stalk function; it must not be completely necessary since many FeOB (e.g., *G. capsiferriformans* and *S. lithotrophicus*) lack stalks (Emerson and Moyer, 1997; Weiss et al., 2007), and stalk-formers themselves do not always form stalks (Hallbeck and Pedersen, 1995). To understand FeOB physiology and contributions to environmental geochemistry, we need better insight into stalk formation and how it differs from other oxide morphologies.

To better understand FeOB roles and mechanisms, we sequenced and analyzed the genomes of two freshwater stalk-forming FeOB, *Ferriphaselus amnicola* OYT1 and *Ferriphaselus* sp. R-1, within the order Gallionellales. We compare the OYT1 and R-1 genomes to other microaerophilic neutrophilic FeOB genomes to detect genes in common between (1) all seven aerobic FeOB genomes, focusing on electron carriers and Fe, C, N, and S metabolism, and (2) only the stalk-forming organisms OYT1, R-1, and *Mariprofundus* sp. We use electron microscopy to find novel Fe oxyhydroxide structures, which are much smaller than stalks. We suggest potential genes involved in each biomineral structure and discuss implications for the stalk's purpose, the mobility of biogenic oxides, and FeOB effects on Fe cycling.

MATERIALS AND METHODS

DNA Extraction, Sequencing, Assembly and Annotation

Genomic DNA of OYT1 and R-1 was extracted using a FastDNA spin kit for soil and the FastPrep instrument (MP Biomedicals) or a PowerSoil DNA isolation kit (MO-BIO) as previously described (Krepski et al., 2012; Kato et al., 2014). Whole-genome sequencing for OYT1 was performed using an Ion Torrent PGM system (Life Technologies) and 454 pyrosequencing (Roche) at the Center for Omics and Bioinformatics of the University of Tokyo, Japan. The generated reads were assembled using Newbler version 2.8 into 23 contigs with an N50 length of 423,423 bases. The draft genome sequences of OYT1 were annotated using Prokka (Seemann, 2014) that includes Prodigal (Hyatt et al., 2010), Aragorn (Laslett and Canback, 2004), Infernal

TABLE 1 | Overview of freshwater and marine neutrophilic microaerophilic FeOB genomes.

	Freshwater FeOB (Betaproteobacteria)				Marine FeOB (Zetaproteobacteria)		
	Stalk-formers		Non-stalk-formers		Stalk-formers		
	***Ferriphaselus amnicola* OYT1**	***Ferriphaselus* sp. R-1**	***Sideroxydans lithotrophicus* ES-1**	***Gallionella capsiferriformans* ES-2**	***Mariprofundus ferrooxydans* PV-1**	***Mariprofundus* sp. M34**	***Mariprofundus* sp. EKF-M39**
Status	Draft	Draft	Complete	Complete	Draft	Draft	Draft
# of Contigs	23	25	1	1	32	36	45
Megabase pairs	2.68	2.44	3.00	3.16	2.87	2.74	2.72
GC content (%)	55.9	60.7	57.5	52.8	54.0	53.9	51.9
# of protein-coding regions	2639	2361	3049	3006	2920	2733	2715
# of tRNA	45	50	44	51	48	44	43
Reference	This study	This study	Emerson et al., 2013	Emerson et al., 2013	Singer et al., 2011	Field et al., 2015	Field et al., 2015

(Nawrocki and Eddy, 2013) and RNAmmer (Lagesen et al., 2007) for detection of CDS, tRNA, non-coding RNA and rRNA, respectively. Whole-genome sequencing for R-1 was performed at the DOE Joint Genome Institute (JGI), USA, using the Illumina technology (Bennett, 2004). An Illumina Std shotgun library was constructed and sequenced on the Illumina HiSeq 2000 platform. Raw Illumina sequence data was artifact filtered and assembled via a hybrid approach using Velvet version 1.2.07 (Zerbino and Birney, 2008) and Allpaths-LG version r46652 (Gnerre et al., 2011). The final draft assembly of R-1 contained 25 contigs with an N50 length of 191,290 bases. The draft genome was annotated and integrated into the integrated microbial genomes (IMG) platform developed by the JGI (Markowitz et al., 2014).

Sequence Analyses

To determine the closest sequences (up to 10 sequences with e-value <0.01) to all the predicted protein-coding regions (CDS) of each of the two strains, BLASTP (Altschul et al., 1997) was performed against the non-redundant protein database collected from the NCBI website. Based on the BLASTP result, the top hits of each CDS was taxonomically classified using MEGAN (Huson et al., 2007). Usearch (Edgar, 2010) was used for clustering CDS at 50% identity to determine whether the CDS is shared among genomes or not. Mauve (Darling et al., 2010) was used for comparison and visualization of the gene order in the genomes among OYT1, R-1 and other iron-oxidizers. The prediction of metabolic pathways was performed using the Kyoto Encyclopedia of Genes and Genomes (KEGG) pathway tool (Ogata et al., 1999). PSORTb (Yu et al., 2010) was used to predict subcellular localization of proteins. Functional properties of proteins coded by genes were predicted using InterProScan (Zdobnov and Apweiler, 2001). Putative *c*-type cytochrome (Cyc) proteins were found with the InterProScan ID, IPR009056 (Cytochrome c-like domain).

To construct phylogenetic trees, sequences related to a target gene or protein sequence were searched using BLAST (Altschul et al., 1997) or HMMER (Finn et al., 2011), and collected from the databases. The collected sequences with the target sequences were aligned using MUSCLE (Edgar, 2004) or MAFFT (Katoh and Standley, 2013). Gap positions were removed from the alignments using Gblock (Castresana, 2000). Phylogenetic trees were constructed by PhyML (Guindon et al., 2010) with the LG + I + G model or Fasttree (Price et al., 2010) with the JTT + CAT model.

The average nucleotide identity (ANI) between the two strains were calculated using JSpecies (Richter and Rosselló-Móra, 2009). The value of *in silico* DNA–DNA hybridization between the two strains was determined using GGDC 2.0 (Meier-Kolthoff et al., 2013).

Time-lapse Imaging with Microslide Growth Chamber

Time-lapse experiments of OYT1 and R-1 were performed in microslide chambers as previously described by Krepski et al. (2013) with minor modifications. The modified Wolfe's minimal medium (MWMM) buffered with MES (adjusted to pH 6.2) was used as a basal medium as previously described (Kato et al., 2014). An FeS plug (without agar) was used as an iron source. Differential interference contrast images were captured every 5 min at 400x total magnification using a Zeiss AxioImager Z1 light microscope (Zeiss, Oberkochen, Germany) equipped with a Zeiss Axiocam Mrm camera. A Zeiss AxioVision software was used for image processing.

Fatty Acid Analysis, GC Content and Growth Test

The MWMM buffered with MES (adjusted to pH 6.2) was used as a basal medium to cultivate OYT1 an R-1 as previously described (Kato et al., 2014). FeS plug solidified with agar was used for an iron source. Fatty acid methyl esters and DNA base composition of R-1 were determined using the Microbial Identification System and HPLC method, respectively, as described (Kato et al., 2014).

For sulfide oxidation test, the basal medium solidified with low-melt-agarose (final 0.15% w/v) with Na_2S plug (10, 1, 0.1, 0.01 or 0.001 mM) instead of FeS was used for cultivation. For

the N_2 fixation test, the basal medium with no nitrogen source (i.e., no ammonium and nitrate) and a mixture of $N_2/CO_2/O_2$ gasses (95:4:1) in headspace was used for cultivation. A blank test with the mixture of $Ar/CO_2/O_2$ gasses in headspace was also performed. At least three transfers were conducted for the cultivation tests.

Electron Microscopy

Scanning electron microscopy (SEM) and transmission electron microscopy (TEM) for OYT1 and R-1 cultures were performed at the Delaware Biotechnology Institute (DBI) Bioimaging Center of University of Delaware, USA, as previously described (Kato et al., 2013). In brief, samples for SEM were mounted on a 0.2-μm-pore-size polycarbonate filter, rinsed with ultrapure water, air dried, and coated with gold/palladium or carbon. Energy dispersive X-ray (EDX) spectrometry equipped with the SEM was used to detect elements for the samples. Samples for TEM were mounted on a lacey-carbon-coated copper grid, washed with ultrapure water, air dried, and coated with carbon. OYT1 and R-1 were cultured in the basal medium with FeS plug at 22°C for 18 h.

Nucleotide Sequence Accession Numbers

The draft genome sequences of *Ferriphaselus* strains OYT1 and R-1 have been deposited in DDBJ/EMBL/GenBank under the accession numbers BBTH01000001-BBTH01000023 and JQKP01000001-JQKP01000025, respectively.

RESULTS AND DISCUSSION

Genomic Features and Phylogeny of OYT1 and R-1

An overview of the genome sequences of two freshwater neutrophilic microaerophilic stalk-forming FeOB, *Ferriphaselus amnicola* strain OYT1 (Kato et al., 2014) and *Ferriphaselus* sp. strain R-1 (Krepski et al., 2012), is shown in **Table 1**, along with freshwater non-stalk-forming and marine stalk-forming FeOB strains (Singer et al., 2011; Emerson et al., 2013; Field et al., 2015). All of the 139 conserved single copy genes among bacterial genomes (Rinke et al., 2013) were found in each draft genome of OYT1 and R-1, indicating that both draft genomes are nearly complete.

Our phylogenetic analysis of concatenated ribosomal proteins, shows that the OYT1 and R-1 are clustered with ES-1 and ES-2 in the order *Gallionellales* within the Betaproteobacteria (**Figure 1**), confirming previous phylogenetic analyses of 16S rRNA genes (Krepski et al., 2012; Kato et al., 2013). Various analyses suggest that OYT1 and R-1 are separate species within the same genus. The 16S rRNA gene similarity between OYT1 and R-1 (97.8%) is lower than 98.65% of a species definition level (Kim et al., 2014). The ANI of the OYT1 and R-1 genomes (81.5%) is much lower than 95–96% of a species definition level (Kim et al., 2014). The value of *in silico* DNA–DNA hybridization between the two strains was 25.10 ± 2.40%, which is much lower than the 70% species level definition. Differences in major cellular fatty acids

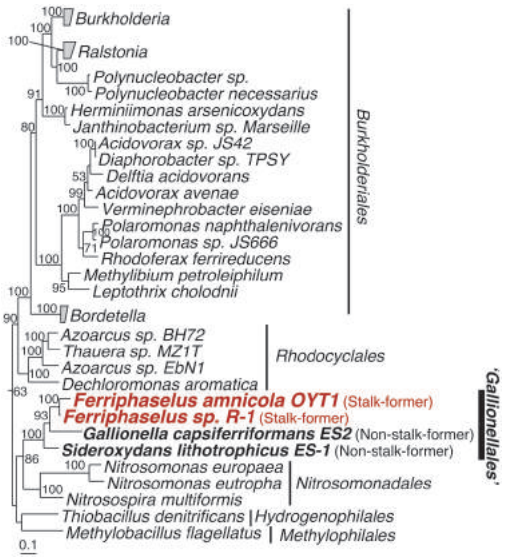

FIGURE 1 | Phylogenetic tree of concatenated amino acid sequences of 14 ribosomal proteins (RplA, RplB, RplC, RplD, RplE, RplF, RplK, RplM, RplN, RpsB, RpsC, RpsI, RpsJ and RpsS). Bootstrap values (>50 of 100 replicates) are shown at the branch points. The concatenated amino acid sequence of these proteins of *Escherichia coli* K12 was used as the out-group (not shown).

(Supplementary Table S1) and other phenotypic differences (see species description below) also support R-1 as a novel species, distinct from OYT1. Based on the previous work (Krepski et al., 2012; Kato et al., 2013), as well as the phylogenetic and taxonomic analyses presented here, we propose *Ferriphaselus globulitus* sp. nov., for strain R-1 as a novel species in the genus *Ferriphaselus*.

Almost all of the OYT1 and R-1 genes were classified into Proteobacterial classes, with over 60% of the total genes were classified into Betaproteobacteria, and over half of these classified into Gallionellales (**Figure 2**). In order to look for commonalities between all microaerophilic neutrophilic FeOB, we noted 21 genes that were present in all seven genomes and closely related to each other (i.e., found in top 10 hits by BLAST search; Supplementary Table S2). Of these, 15 are monophyletic, which is remarkable since some genes are from Betaproteobacteria and others belong to Zetaproteobacteria, suggesting an evolutionary relationship (i.e., horizontal transfer). Thirty-seven genes were closely related between freshwater and marine stalk formers, but not to non-stalk-formers; four of them are monophyletic. Below, we analyze some of these genes in more detail (**Table 2**), in the context of Fe oxidation-related electron transport and Fe oxide stalk formation. In addition, OYT1 and R-1 shared 373 genes with each other, but not the other five microaerophilic FeOB (Supplementary Table S3); some of them may be related to the novel biomineral morphology that we describe below.

Catabolism and Anabolism

Iron Oxidation and Electron Transport

The OYT1 and R-1 genomes both lack *mtoA* and *mtoB*, suggesting that these may be rare, and not part of a

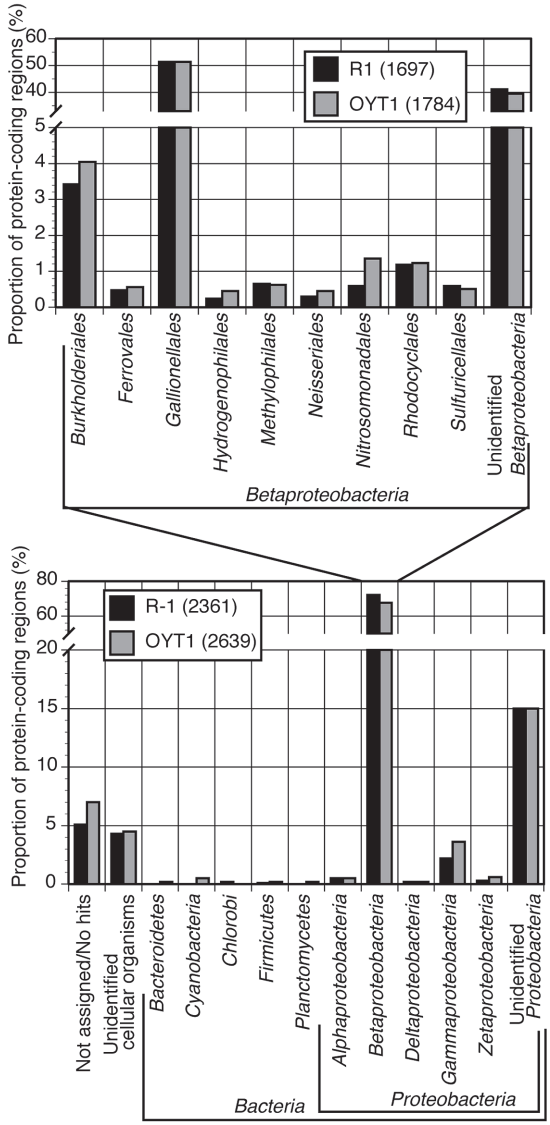

FIGURE 2 | Taxonomic classification of top hits of all CDS (genes) for OYT1 and R-1. Proportion of protein-coding regions classified into each taxon to the all **(lower panel)** or betaproteobacterial CDS **(upper panel)** are shown. The total numbers of CDS are 2639 for OYT1 and 2361 for R-1.

common mechanism of Fe oxidation amongst freshwater FeOB (**Table 3**). However, both genomes include homologs of *cyc2*$_{PV-1}$, a gene found in *M. ferrooxydans* PV-1 that encodes a Cyc2-like protein, which Barco et al. (2015) proposed as a candidate iron-oxidizing protein, based on high protein expression. Predicted to be an outer membrane *c*-type cytochrome, Cyc2$_{PV-1}$ has homologs encoded in all of the other neutrophilic microaerophilic FeOB genomes, as well as metagenomes containing *Gallionellales* and the *Zetaproteobacteria* (Barco et al., 2015). The presence in OYT1 and R-1 supports the hypothesis that this gene is required by microaerophilic FeOB, including both Beta- and Zetaproteobacteria.

In the OYT1 and R-1 genomes, the homologs of *cyc2*$_{PV-1}$ (CDS1) were not originally annotated as cytochromes due to the low similarity to previously known cytochromes; however, both contain a Cys-X-X-Cys-His heme-binding motif near the N terminus, as in PV-1. Cyc2$_{PV-1}$ homologs in neutrophilic chemolithotrophic FeOB generally cluster together, distinct from the Cyc2 of *A. ferrooxidans*, with Zetaproteobacteria in a separate grouping from the freshwater Gallionellales (**Figure 3**). However, the cluster of neutrophilic chemolithotrophic FeOB Cyc2 sequences also include several homologs from other organisms, including an iron-oxidizing phototroph *Chlorobium ferrooxidans*, as well as two sulfur-oxidizing species and two marine endosymbionts. The similarity to *C. ferrooxidans* and *A. ferrooxidans cyc2* suggests that this could be a common Fe oxidation mechanism across different types of Fe-oxidizing bacteria.

While OYT1 and R-1 share many other electron transport genes with PV-1 and other microaerophilic FeOB (see below), we did not find any homologs of *cyc1*$_{PV-1}$, the gene that encodes a periplasmic cytochrome, which was also implicated in Fe oxidation by its high expression in the PV-1 proteome (Barco et al., 2015); it is also missing in the genome of *Gallionella* ES-2, suggesting Cyc1 is not a common periplasmic electron carrier amongst FeOB. However, 16 genes encoding putative *c*-type cytochromes were found in the OYT1 genome, and 11 were found in the R-1 genome, in addition to the *cyc2* homolog (Supplementary Table S4); some of these Cyc (eight for OYT1, five for R-1) could serve as periplasmic electron carriers, substituting for Cyc1.

Once electrons are passed from the outer membrane electron carriers to periplasmic Cyc, some of the electrons must be used to produce NADH by reverse electron transport. Based on genes present in their genomes, OYT1 and R-1 can pass electrons to the cytochrome bc_1 complex (Complex III), which reduces a quinone, which in turn reduces NAD+ to NADH via the NADH dehydrogenase (Complex I) (**Figure 4**); this is similar to the model for all of the other sequenced microaerophilic FeOB as well as the acidophilic FeOB, *A. ferrooxidans* (Brasseur et al., 2002). Instead of Complex III, it is possible that OYT1 and R-1 use the alternative complex (AC) III to pass electrons to quinones. Like all other microaerophilic FeOB, OYT1 and R-1 genomes contain a gene cluster that show high similarity to *act* genes of ACIII (Yanyushin et al., 2005). ACIII and the related Qrc function as quinol oxidases or quinone reductases, as characterized in *Chloroflexus aurantiacus*, *Rhodothermus marinus*, and *Desulfovibrio vulgaris* (Pereira et al., 2007; Gao et al., 2009, 2013; Refojo et al., 2010; Venceslau et al., 2010) and as proposed for an uncultivated *Chromatiaceae* (Wang et al., 2015). Given the few studies on ACIII, its placement in FeOB electron transport systems is highly speculative.

The *act* gene clusters in both OYT1 and R-1 genomes each contain seven genes (CDS2–8; **Table 2**) related to *actAB1B2CDEF* (**Figure 5A**); *actB* is split into two subunits unlike in *R. marinus*. The closest relatives of all seven genes based on a homology search are those of FeOB (Supplementary Table S2), in addition to two Betaproteobacterial FeOB, i.e., *Ferrovum myxofaciens* (Johnson et al., 2014) and *Leptothrix ochracea* (Fleming et al.,

TABLE 2 | Temporary identification for the 20 CDS focused in this study.

ID	OYT1 locus_tag	R-1 locus_tag	Potential role	Gene name	Monophyly*
CDS1	OYT1_00168	DM08DRAFT_00346	Iron oxidation	*cyc2*	×
CDS2	OYT1_00085	DM08DRAFT_02259	Iron oxidation	*actA*	○
CDS3	OYT1_00084	DM08DRAFT_02260	Iron oxidation	*actB1*	○
CDS4	OYT1_00083	DM08DRAFT_02261	Iron oxidation	*actB2*	○
CDS5	OYT1_00082	DM08DRAFT_02262	Iron oxidation	*actC*	○
CDS6	OYT1_00081	DM08DRAFT_02263	Iron oxidation	*actD*	○
CDS7	OYT1_00080	DM08DRAFT_02264	Iron oxidation	*actE*	○
CDS8	OYT1_00079	DM08DRAFT_02265	Iron oxidation	*actF*	○
CDS9	OYT1_00167	DM08DRAFT_00347	Stalk formation	*bcsB*	○
CDS10	OYT1_00166	DM08DRAFT_00348	Stalk formation	*xagB*	○
CDS11	OYT1_00165	DM08DRAFT_00349	Stalk formation	*xagC*	○
CDS12	OYT1_00164	DM08DRAFT_00350	Unknown	*xagD*	○
CDS13	OYT1_00976	DM08DRAFT_01732	Dread formation	*bcsA*	–
CDS14	OYT1_00975	DM08DRAFT_01733	Dread formation	*bcsB*	–
CDS15	OYT1_00974	DM08DRAFT_01734	Dread formation	*bcsZ*	–
CDS16	OYT1_00296	DM08DRAFT_00247	Dread formation	*bcsC*	–
CDS17	OYT1_01454	DM08DRAFT_00108	Cell wall synthesis	*mltA*	○
CDS18	OYT1_01534	DM08DRAFT_01856	Cell wall synthesis	*ampG*	○
CDS19	OYT1_02351	DM08DRAFT_02295	Unknown	–	○
CDS20	OYT1_02621	DM08DRAFT_02432	Energy generation	*sthA*	○

* ○, *monophyletic clustering for FeOB;* ×, *non-monophyletic clustering for FeOB;* –, *found in only OYT1 and R-1.*

TABLE 3 | List of proteins potentially involved in iron oxidation pathway of the neutrophilic microaerophilic FeOB.

	Freshwater FeOB (Betaproteobacteria)				Marine FeOB (Zetaproteobacteria)			
	Stalk-formers		Non-stalk-formers		Stalk-formers			unknown
	Ferriphaselus		*Sideroxydans*	*Gallionella*	*Mariprofundus*			–
Proteins	**OYT1**	**R-1**	**ES-1**	**ES-2**	**PV-1**	**M34**	**EKF-M39**	**Zeta SAGs (24)[1]**
Cyc2	+[2]	+	+	+	+	+	+	9
MtoA	N.F.[3]	N.F.	+	+	N.F.	N.F.	N.F.	N.F.
Cyc1	N.F.	N.F.	+	–[4]	+	+	+	12
Alternative Complex III	+	+	+	+	+	+	N.F.	3
Cytochrome bc1 complex	+	+	+	–	+	+	+	10
Cytochrome bd quinol oxidase	+	N.F.	+	+	+	+	+	4
Cbb3-type cytochrome c oxidase	+	+	+	+	+	+	+	14
NADH dehydrogenase	+	+	+	+	+	+	+	19
Reference	This study	This study	Emerson et al., 2013	Emerson et al., 2013	Singer et al., 2011	Field et al., 2015	Field et al., 2015	Field et al., 2015

[1]*Numbers found in the total 24 single amplified genomes (SAGs) are indicated;* [2]*present;* [3]*not found in the incomplete genomes;* [4]*absent in the complete genome.*

2011) (Genbank accession number: AJUC00000000). Notably, the OYT1 and R-1 *act* genes are in the same order as in other FeOB genomes, with *actB* split into two: *actB1* with the [4Fe–4S] binding motif ($CX_2CX_3CX_{27}C$), which encodes a protein similar to a molybdopterin oxidoreductase, and *actB2*, which encodes a protein similar to an iron-sulfur protein, both within the complex iron-sulfur molybdoenzyme (CISM) super-family (**Figure 5B**) (Rothery et al., 2008). Each of the *act* genes of the Betaproteobacterial and Zetaproteobacterial FeOB isolates are clustered into a sub-clade within the ACIII-Qrc clade (*actB1*-like genes shown in **Figure 5C**; other *act* genes in Supplementary Figure S1). The phylogenetic analyses suggest a horizontal gene transfer between the Betaproteobacterial and Zetaproteobacterial FeOB.

Electrons not used in reverse ("uphill") electron transport would be directed toward a terminal oxidase ("downhill") in order to generate proton motive force (**Figure 4**). For OYT1, the terminal oxidase could either be the cbb_3-type

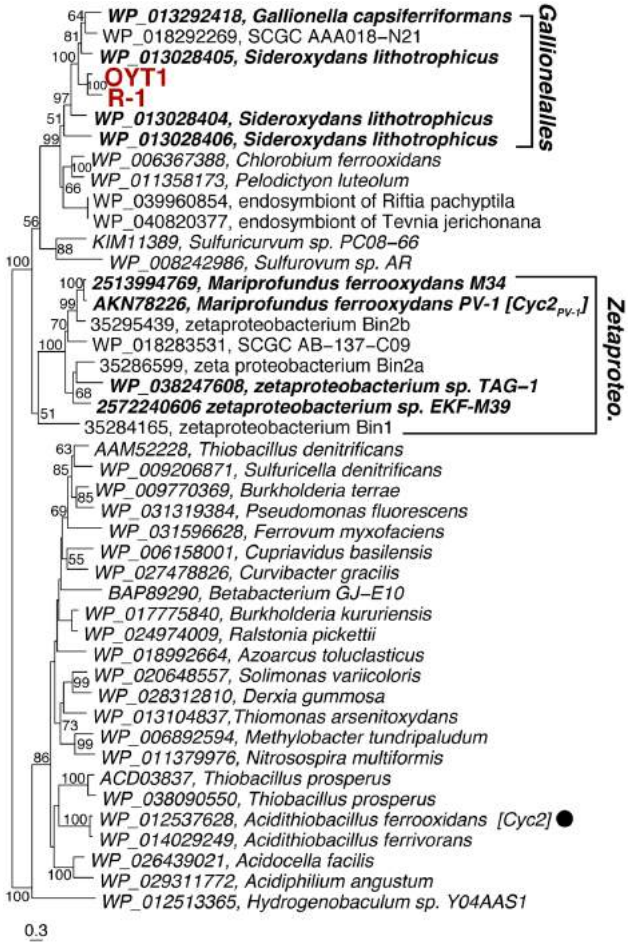

FIGURE 3 | Phylogenetic tree of $Cyc2_{PV-1}$ and its homologs corresponding to CDS1. The tree was constructed using an alignment dataset of the whole protein sequences without gap positions. Bootstrap values (>50 of 100 replicates) are shown at the branch points. Betaproteobacterial and Zetaproteobacterial neutrophilic FeOB are shown in bold. The filled circle following the species name indicates that the function of the protein has been identified.

cytochrome *c* oxidase (OYT1_00427, 00429, 00430) or the cytochrome *bd* quinol:O_2 oxidoreductase (OYT1_01855, 01856); the R-1 genome contained genes for the cbb_3-type complex (DM08DRAFT_00513, 00515, 00516) but not the cytochrome bd oxidase. Both types of terminal oxidases have high affinity for O_2 (Pitcher and Watmough, 2004; Borisov et al., 2011), consistent with the microaerophily of these FeOB. As expected, both OYT1 and R-1 genomes contain genes encoding an F-type ATPase (OYT1_01226–01233, DM08DRAFT_01947–01954) that converts the proton motive force to ATP.

Sulfur Oxidation

OYT1 and R-1 have thus far proven to be obligate Fe-oxidizers that do not grow by sulfide or thiosulfate oxidation (Krepski et al., 2012; Kato et al., 2014). The other FeOB isolates (*G. capsiferriformans* and *Mariprofundus* sp.) are also obligate Fe-oxidizers, except for *S. lithotrophicus*, which was shown to oxidize thiosulfate once genome analysis showed that it had *sox* genes needed for dissimilatory sulfur oxidation (Emerson et al., 2013). Given that culture tests have proven wrong in the past, we evaluated the OYT1 and R-1 genomes for sulfur metabolism genes, and also retested both strains for sulfide and thiosulfate oxidation. Although both strains failed to grow, genome analyses revealed genes involved in dissimilatory sulfur oxidation (*dsr*, *sqr*, *soe*) as described below, as well as sulfate assimilation (*cys*). Other genes related to sulfur oxidation (e.g., *sor*, *apr*, *sat,* and *sox*) were not found.

In both OYT1 and R-1 genomes, we found genes encoding sulfide:quinone oxidoreductase (Sqr), which oxidizes sulfide to elemental sulfur. Phylogenetic analysis indicates that the Sqr of OYT1 and R-1 is classified in Type I clade (Supplementary Figure S2; Marcia et al., 2010), along with other Betaproteobacterial SOB, including *Sideroxydans* ES-1. The Type I Sqr has affinity to sulfide at micromolar level, and plays a role in sulfide-dependent respiration, in addition to sulfide detoxification (Marcia et al., 2010).

Dissimilatory sulfite reductase (*dsr*) genes were found in the OYT1 and R-1 genomes (Supplementary Figure S3A), as well as in the *Sideroxydans* ES-1 genome (Emerson et al., 2013). Dsr catalyzes elemental sulfur oxidation to sulfite in some sulfur-oxidizing bacteria such as *Allochromatium vinosum* (Dahl et al., 2005) and, on the other hand, sulfite reduction to elemental sulfur in sulfate-reducing microorganisms (e.g., Wagner et al., 1998). The OYT1 and R-1 *dsr* gene clusters each contain 13 genes, *dsrABEFHCMKLJOPN*; as in ES-1, the cluster in the OYT1 is located near a sulfite oxidation *soe* gene cluster (Supplementary Figure S3A). DsrB of OYT1 and R-1 are closely related to *Sideroxydans* ES-1 and other Betaproteobacterial SOB (Supplementary Figure S4), suggesting that the Dsr complex plays a role in sulfur oxidation rather than sulfate reduction. In addition, a reverse DSR-associated gene cluster (rDAGC) was found upstream of the Dsr cluster in the OYT1 and R-1 genomes (Supplementary Figure S3A). The rDAGC has been found in the genomes of Betaproteobacterial SOB, including *Sideroxydans* ES-1 (Watanabe et al., 2014), and may be involved in the regulation of the *dsr* genes (Venceslau et al., 2014).

In the OYT1 and R-1 genomes, we found *soeABC* genes (Supplementary Figure S3A) encoding sulfite oxidizing enzyme (Soe), similar to that found in *A. vinosum* (Dahl et al., 2013). The Soe of OYT1 and R-1 cluster with other Soe within the CISM super-family (**Figure 5B**); this Soe cluster contains sulfide-, elemental sulfur-, and sulfite-oxidizing bacteria (SOB) including *Sideroxydans* ES-1 (Supplementary Figure S3B). In combination with Dsr, the Soe in OYT1 and R-1 may allow for elemental sulfur oxidation to sulfate, though S(0) oxidation has not yet been tested. Our findings suggest that further physiological experiments may confirm their ability to oxidize reduced sulfur species.

Carbon Fixation

Most microaerophilic FeOB isolated to date, including OYT1 and R-1, grow without an organic carbon source, so they are interpreted to be autotrophic (Kato et al., 2012;

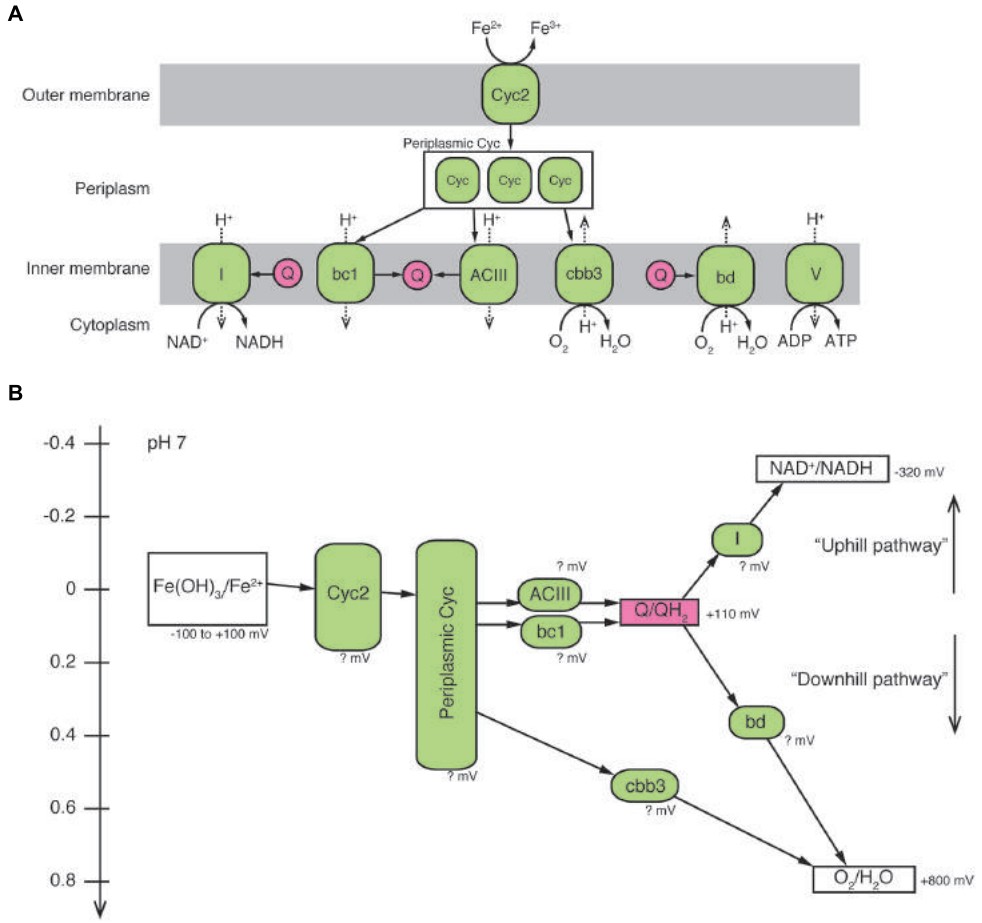

FIGURE 4 | A proposed model of electron pathway from Fe^{2+} to O_2 and generation of NADH and ATP in *Ferriphaselus* OYT1 and R-1. (A) Predicted locations of proteins (colored in green) potentially involved in the electron pathway. **(B)** Redox potentials of each reaction in the electron pathway. It should be noted that the redox potentials of all proteins of the FeOB are still unclear, and that the cytochrome *bd* complex was not found in the R-1 genome. I, Complex I (NADH dehydrogenase); bc1, cytochrome bc_1 complex; ACIII, alternative complex III; Q, quinone pool (colored in pink); Cyc, cytochrome *c*; bd, cytochrome *bd* complex; cbb3, cbb_3-type cytochrome *c* oxidase; V, Complex V (ATPase).

Krepski et al., 2012). Genomic analyses have supported this conclusion, as genes for carbon fixation via the Calvin–Benson–Basshom (CBB) pathway, including ribulose-1,5-bisphosphate carboxylase/oxygenase (RubisCO) genes are found in the genomes of *M. ferrooxydans* (Singer et al., 2011; Field et al., 2015) and *G. capsiferriformans* and *S. lithotrophicus* (Emerson et al., 2013), while *cbbM*-targeted PCR demonstrated the presence of RubisCO form II in OYT1 by PCR (Kato et al., 2013). Furthermore, RubisCO is significantly expressed in the *M. ferrooxydans* proteome (Barco et al., 2015). In this study, we found that both OYT1 and R-1 have all the genes necessary for the CBB pathway. A *cbbM* gene (indicative of RubisCO form II) is present in both OYT1 and R-1 genomes, while *cbbL* (indicative of RubisCO form I) is only found in R-1; there was no evidence of other carbon fixation pathways. The genes of RubisCO form II were found in all of the microaerophilic FeOB genomes; Form II is adapted to low O_2 and high CO_2 conditions (Badger and Bek, 2008), which is consistent with the microaerophilic lifestyle. RubisCO form I corresponds to higher O_2 and low CO_2 conditions (Badger and Bek, 2008); the FeOB that have both Form I and II (R-1, *S. lithotrophicus* ES-1, *M. ferrooxydans* PV-1 and M34) likely can survive in a wider range of O_2 and CO_2 conditions. Phylogeny of the FeOB CbbM and CbbL show that not all FeOB RubisCO are closely related (Supplementary Figure S5), suggesting a complex acquisition/evolutionary history.

Nitrogen Fixation

Thus far, there is genomic and physiological evidence of nitrogen fixation in some, though not all microaerophilic FeOB. The *nifH* gene has been also found in *Sideroxydans* ES-1 and *Mariprofundus* M34 and EKF-M39, but not *M. ferrooxydans* PV-1 or *G. capsiferriformans* ES-2. ES-1 can grow with N_2 as the sole N source, though it is the only one of those strains that has been tested. The OYT1 and R-1 genomes both possess *nif* genes for nitrogen fixation. The minimum set of *nif* genes (*nifHDKENB*) required for nitrogen fixation (Dos Santos et al., 2012) was found in the OYT1 genome, consistent with the cultivation result that OYT1 grew on N_2 as the sole nitrogen source. In

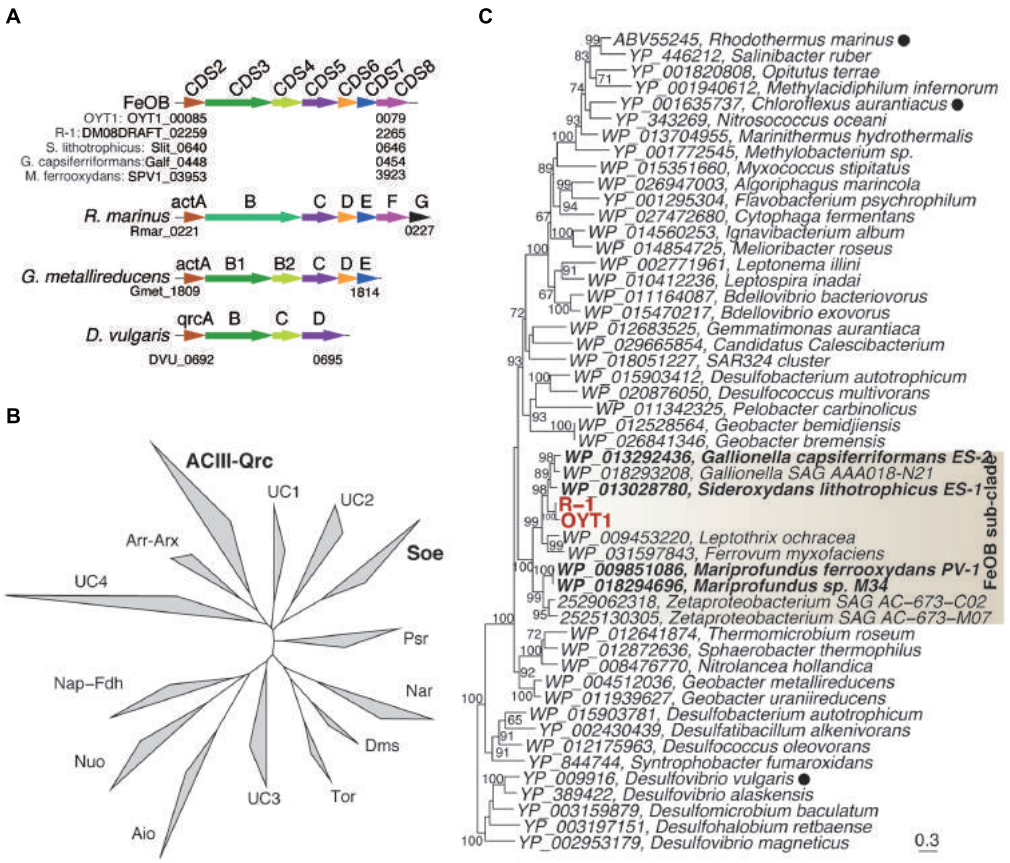

FIGURE 5 | The ACIII-like gene cluster. (A) Orders of protein-coding regions related to genes in the ACIII-like gene cluster. Homologs among the genomes are shown in the same color. Cyc, *c*-type cytochrome. **(B)** Phylogenetic tree for proteins corresponding to ActB1 in the complex iron-sulfur molybdoenzyme super-family including ACIII, Qrc, Aio, arsenite oxidase; Arr, arsenate respiratory reductase; Arx, alternative arsenite oxidase; Nap, periplasmic nitrate reductases; Fdh, formate dehydrogenases; Nuo, NADH:ubiquinone oxidoreductase; Tor, Trimethylamine *N*-oxide reductase; Dms, dimethyl sulfoxide reductase; Nar, respiratory nitrate reductase; Psr, polysulfide reductases; Soe, sulfite-oxidizing enzymes. UC indicate unclassified clades. **(C)** Phylogenetic tree for ActB1 and ActB1-like proteins corresponding to CDS3 in the ACIII-Qrc clade. Bootstrap values (>50 of 100 replicates) are shown at the branch points. Filled circles following the species names indicate that the function of the proteins has been identified.

contrast, *nifHDK* genes were not found in the R-1 genome, and the growth of R-1 on N_2 as the sole nitrogen source has not been observed in our tests. NifH (dinitrogenase reductase) is one of the key components of the nitrogenase enzyme complex and is a commonly used marker gene for nitrogen fixation. The NifH of the FeOB are all Type I, a group which contains aerobic and facultative anaerobes (Supplementary Figure S6) (Chien and Zinder, 1994). The presence of *nif* genes in several neutrophilic Fe-oxidizers, including OYT1, demonstrates a link between Fe oxidation and N_2 fixation in the environment at circumneutral pH.

Extracellular Structures

Many microorganisms have extracellular structures, such as pili and flagella, and secrete extracellular polymeric substances (EPS), that are involved in motility, attachment on surfaces, biofilm production and cell–cell interaction, and give the microorganisms competitive advantages (e.g., Mattick, 2002; Flemming and Wingender, 2010; Guttenplan and Kearns, 2013). FeOB stalks containing polysaccharides (Chan et al., 2009, 2011; Krepski et al., 2012; Kato et al., 2014) are one example of EPS. Furthermore, in this study, we found other extracellular structures that consisted of tens-nanometer-sized iron biominerals (nanoBIOS), morphologically distinct from the stalks, in OYT1 and R-1 cultures (**Figure 6**; Supplementary Figure S7). We call these structures "dreads" based on their morphology, which resembles the dreadlock hairstyle. Based on genomic analysis and microscopic observation, genes potentially involved in the formation of stalks and dreads and the ecophysiological roles of these structures are discussed.

Stalk Formation

Time-lapse imaging using microslide growth chambers showed that OYT1 and R-1 cells first attached to the glass surface, and then produced stalks (Video S1 for OYT1, data not shown for R-1). The average elongation rates were 1.4 (±0.4) μm/h and 1.2 (±0.6) μm/h for OYT1 and R-1 (n = 6 cells for each),

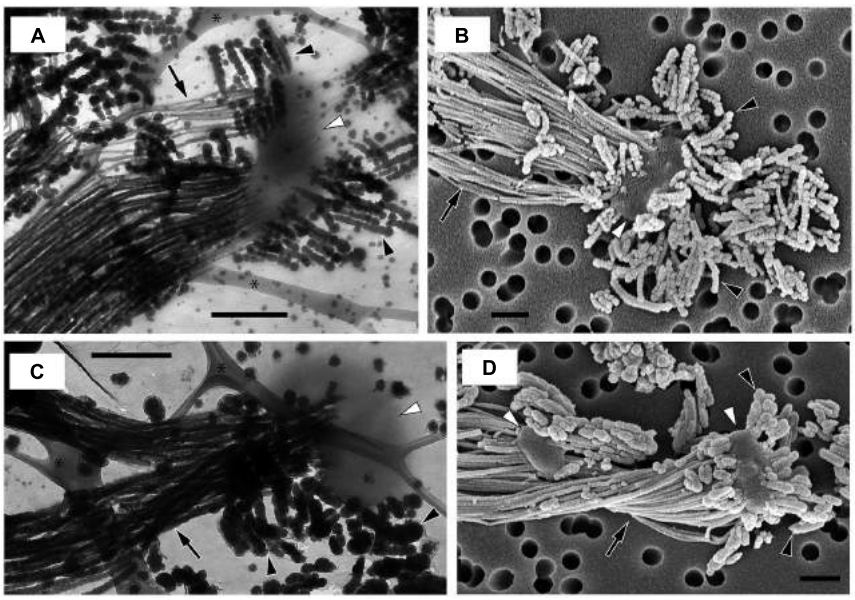

FIGURE 6 | Electron micrographs of strains OYT1 and R-1. (A,B) OYT1 and **(C,D)** R-1. **(A,C)** TEM and **(B,D)** SEM images. **(A,C)** asterisk (*) indicates lacey carbon on the TEM grids. White arrowheads, cells; black arrowheads, dreads; black arrows, stalks. Bars, 500 nm.

respectively, which are similar to that of *Mariprofundus* PV-1 (2.2 μm/h; Chan et al., 2011).

We found a cluster of four genes (CDS9–12; **Figure 7A**; **Table 2**, Supplementary Table S2) that was only present in the stalk forming FeOB (*Mariprofundus* and *Ferriphaselus* strains). Our phylogenetic analysis shows that each of CDS9–12 in the stalk forming FeOB is clustered into a distinct clade from the others, and that freshwater FeOB are clearly separated from those of the marine FeOB (**Figures 7B–E**). These results suggest that the genes were horizontally transferred between the common ancestor of the *Mariprofundus* and that of the *Ferriphaselus*.

CDS9 is annotated as a cellulose synthase regulator protein, classified in BcsB family (pfam ID: PF03170) that is involved in cellulose synthesis (Römling, 2002). CDS10–12 are similar to *xagBCD* genes, which are involved in extracellular polysaccharide production and biofilm formation in *Xanthomonas campestris* (Tao et al., 2010). The *xagB*-like CDS10 was annotated as beta-monoglucosyldiacylglycerol synthase, one of the glucosyltransferases that is needed to synthesize polysaccharides (Lairson et al., 2008). No CDS with considerable similarity to *xagA* gene was found in the OYT1 and R-1 genomes. Considering the monophyletic clustering of the genes of the stalk forming FeOB and the relatedness to extracellular polysaccharide production, the gene cluster of the CDS9–12 are good candidates for involvement in FeOB stalk production.

We found other genes related to polysaccharide synthesis in the OYT1 and R-1 genomes, which have already been reported in the other microaerophilic FeOB (Singer et al., 2011; Emerson et al., 2013; Bennett et al., 2014). Further studies are needed to reveal whether the cluster is related to the synthesis of extracellular polysaccharide or lipopolysaccharide of an outer membrane component.

Dreads Formation

We discovered new extracellular structures using a combination of light and electron microscopy of OYT1 and R-1 cultures. The time-lapse images (Supplementary Video S1) show that OYT1 cells produce amorphous extracellular structures distinct from stalks, although their morphology is unclear by the light microscopic images. The electron microscopy indicates that the amorphous structures are clusters of dreadlock-shaped minerals ("dreads") and that there are cells attached to the dreads, in addition to the stalk structure (**Figure 6**). These results provide evidence that the cells excrete dreads. The dreads extended from all sides of a cell, whereas the stalks were produced from only one side of the cell. The widths of dreads are larger and more varied than that of stalks in 1-day old cultures: stalks and dreads of OYT1 are 23 (± 6) nm and 63 (±16) nm wide, respectively; those of R-1 are 39 (±10) nm and 93 (±23) nm, respectively ($n \geq 20$ dreads or stalks of different cells). Dreads appeared segmented, especially in the OYT1 cultures (**Figure 6**; Supplementary Figure S7). The diameter of dread segments for both strains tends to be smaller (<30 nm, in some cases) nearer the cells, which may reflect the degree of mineralization. Dreads are typically <500 nm in length, clearly much shorter than that of stalks (>100 μm in many cases). SEM-EDX analysis shows that the dreads, as well as the stalks, of OYT1 and R-1 contain Fe and P (Supplementary Figure S8), likely representing phosphate adsorbed onto Fe oxyhydroxides. In the case of the stalks, this is consistent with the previous reports of the stalks of cultured and environmental *Gallionella* sp. and *Mariprofundus* PV-1 (Chan et al., 2009, 2011; Suzuki et al., 2011).

Dread-like structures have not previously been reported in other neutrophilic microaerophilic FeOB; however, it is possible that they have been overlooked. On re-examining

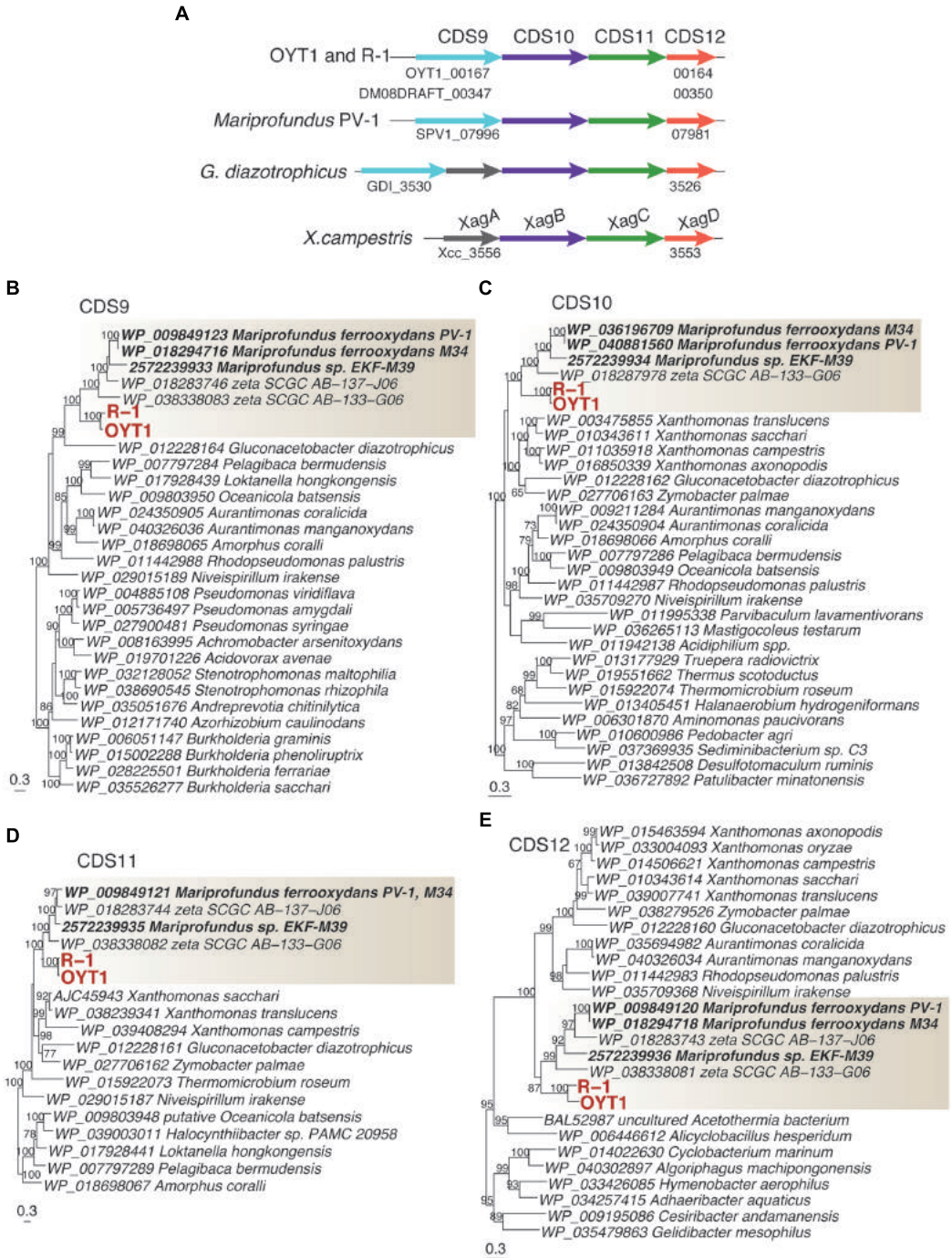

FIGURE 7 | The gene cluster containing *xag*-like genes. (A) Gene order in the gene cluster. Homologs among the genomes are shown in the same color. **(B)** Phylogenetic trees for proteins related to **(B)** CDS9 (BcsB-like), **(C)** CDS10 (XagB-like), **(D)** CDS11 (XagC-like) and **(E)** CDS12 (XagD-like). Bootstrap values (>50 of 100 replicates) are shown at the branch points. The gray box indicates a clade including FeOB isolates and SAGs of Betaproteobacteria and Zetaproteobacteria.

electron micrographs in the literature, we found dread-like precipitates associated with a stalk-forming *Gallionella ferruginea* (Figures 1 and 6 shown in Vatter and Wolfe, 1956). However, the authors thought that segmented, dread-like precipitates were ferrous sulfides used as the iron source for cultivation. The authors also found other precipitates called "granules" on the cells (Figures 8–10 shown in Vatter and Wolfe, 1956) and discussed that they might have been secreted inside the cell and were related to segmented stalk strands, or else were abiotic precipitates sorbed to the cell surface. We only observed stalks and dreads on

OYT1 and R-1 cells, but did not consistently see granules, so we can only confirm that dreads and stalks are distinct, but cannot conclude any relationship between dreads and granules.

If it is indeed the case that OYT1 and R-1 are the only dread-forming organisms, then we may identify genes potentially related to the production of dreads within the 373 genes (Supplementary Table S3) shared between the OYT1 and R-1 genomes, which were not detected in the other FeOB genomes; however, given the close relationship between OYT1 and R-1, that these are only two genomes, and the possibility that other FeOB make dread-like structures, there is a considerable amount of uncertainty here. Within these 373 genes, we found CDS13–16 related to *bcsABCZ* genes, which are involved in extracellular cellulose production (Römling, 2002; Mazur and Zimmer, 2011). Genes involved in synthesis of UDP-activated glucose and in gluconeogenesis, which are necessary to cellulose synthesis, were also found in the OYT1 and R-1 genomes. The set of *bcsABCZ*-like genes was not found in the other FeOB genomes, suggesting that the *bcsABCZ*-like genes found in only dread-forming FeOB are involved in the production of dreads. As described above, the other *bcsB*-like gene (CDS9) was found with *xag*-like genes (CDS10–12) in the OYT1 and R-1 genomes. Further organic chemical analysis are needed to determine if dreads and stalks contain cellulose.

Role of Stalk and Dreads

Why would neutrophilic microaerophilic FeOB produce two different biomineral morphologies? Stalk production was previously proposed as a mechanism(s) for avoiding encrustation by iron oxides (Chan et al., 2009, 2011). The *Ferriphaselus* OYT1 and R-1 dread structures appear to be easily shed, and therefore could play a role for avoiding Fe encrustation, leaving the stalks to play other roles. Stalks are associated with iron microbial mat formation. In this context, the stalks can serve as an anchor to attach on solid surfaces, preventing cells from being washed away in streams, groundwater seeps, or deep-sea vents. Attachment can also keep cells in the preferred microenvironment within opposing concentration gradients of oxygen and iron. Indeed, in gradient cultures, stalk-forming FeOB can attach to a glass surface and make colonies consisting of stalks and cells (Kucera and Wolfe, 1957; Kato et al., 2014). Previous studies showed that anchored *Mariprofundus* PV-1 cells can move by lengthening the stalks (Chan et al., 2011; Krepski et al., 2013). Such lifestyle of attachment and movement using extracellular slime from one side of a cell have been also reported from myxobacteria (Wolgemuth et al., 2002) and cyanobacteria (Hoiczyk and Baumeister, 1998).

Dreads may be more akin to the granular iron oxides produced by the many non-stalk-forming iron-oxidizers (e.g., Emerson and Moyer, 1997; Miot et al., 2009a,b). In contrast to the larger stalks, dreads and granules are small (∼10 s nm) and therefore likely mobile. So, while stalks represent a sink for Fe and any adsorbed or coprecipitated elements, the nanoparticulate dreads and granules (i.e., nanoBIOS) can be carried by groundwater and surface water, thereby redistributing Fe, along with associated heavy metals (e.g., Cu, Zn) and nutrients (e.g., C and P). In the environment, granular nanoBIOS are difficult to distinguish from abiotic oxides; however, the tapered, segmented dread morphology is much more recognizable and could therefore be used to help trace the fate of biogenic Fe oxides.

Attachment, Motility and Chemotaxis

Pili are involved in attachment on solid surfaces, twitching motility, and then in colonization or biofilm formation (Mattick, 2002). Genes related to Type IV pilus system proteins (PilACGHIJMNOPQSR) were found in the genomes of OYT1 and R-1, which are both organisms that are able to colonize the glass wall surface of a culture tube. Although direct evidence of the presence of pili of OYT1 and R-1 is still lacking, they have the genetic potential to produce pili, which could play a role in the attachment to surfaces.

The flagellum is one of the common constructs for bacterial mobility (Jarrell and McBride, 2008), and also plays a role in chemotaxis (Porter et al., 2011) and biofilm formation (Belas, 2014). Genes for all core proteins (Fli, Flg, and Flh proteins) of the bacterial flagellum complex (Macnab, 2003) were found in the OYT1 genome, and those except FliC were found in the R-1 genome. The presence of a polar flagellum has been microscopically confirmed in OYT1 (Kato et al., 2014), but not R-1. Genes for chemotaxis proteins (CheABDRWVYZ) and chemoreceptor proteins including aerotaxis receptor (Aer) were also found in the OYT1 and R-1 genomes. The genetic potential of aerotaxis is consistent with the obligate microaerophilic lifestyle of OYT1 and R1.

Genetic Marker Candidates for Neutrophilic Microaerophilic Iron-oxidizing Bacteria

To date, the presence and abundance of neutrophilic microaerophilic FeOB in a given environment has been based mainly on the detection of 16S rRNA genes closely related to the cultured FeOB (Kato et al., 2009a,b; Wang et al., 2009; Fleming et al., 2013). However, 16S rRNA genes do not necessarily correlate to metabolism. Although common microaerophilic FeOB fall within phylogenetic clusters (Gallionellales, Zetaproteobacteria), there is some uncertainty as to whether these clusters contain some non-FeOB. Gallionellales appears to be mostly comprised of FeOB, including many isolates of freshwater FeOB; however, the order also contains the nitrite-oxidizing bacterium '*Candidatus Nitrotoga arctica*' (Alawi et al., 2007), though culture-independent work suggests that Nitrotoga relatives form a distinguishable subclade (Lücker et al., 2015). In addition, there may be FeOB that we do not recognize by 16S rRNA gene identity because we have no related culture. If reliable functional gene-based markers could be developed for FeOB, we would be able to more confidently assess the spatial distribution, abundance, and activity of the FeOB in the environment. Below, we evaluate candidates of genetic markers for neutrophilic microaerophilic FeOB.

The ideal Fe oxidation genetic marker would be (1) required for Fe oxidation (ideally the Fe oxidase), (2) present in all neutrophilic microaerophilic FeOB, and (3) fall into a monophyletic cluster that does not include other organisms

(non-FeOB). We found 15 genes (CDS2–12 and 17–20) that meet criteria 2 and 3. We do not discuss CDS17–20 in detail, though the clustering (Supplementary Figure S9) suggests they are related to some unique physiological characteristics of the FeOB. Here we focus on the *act* genes (CDS2–8) and *cyc2* (CDS1), as promising candidates for genetic markers; as electron transport genes, they may meet the first criterion. Cyc2 is the leading candidate for an Fe oxidase; all neutrophilic microaerophilic FeOB have the gene, and the function has been demonstrated in an acidophilic FeOB. While the microaerophilic Cyc2 do form a phylogenetic cluster (**Figure 3**), it is not monophyletic, i.e., the cluster contains organisms with other metabolisms, though it is certainly possible, just not proven that these other organisms oxidize Fe(II). In contrast, the *act* genes are monophyletic (**Figure 4**, Supplementary Figure S1). They are present in all neutrophilic microaerophilic FeOB with genomes available, but the role in Fe oxidation is not clear. If it can be shown that Cyc2 and ACIII are necessary for Fe oxidation, then these genes could serve as genetic markers of microaerophilic Fe oxidation.

In summary, we have analyzed newly sequenced genomes from freshwater stalk-formers *Ferriphaselus* sp. OYT1 and R-1 to understand how microaerophilic FeOB function and contribute to biogeochemical cycling. Comparisons with the genomes of five existing Betaproteobacterial and Zetaproteobacterial FeOB show us patterns of gene presence and absence that advance our working hypotheses on Fe oxidation and biomineralization mechanisms. Analyzing genes specific to the genomes of the stalk-formers *Ferriphaselus* sp. and *Mariprofundus* sp. gives us some first insights into genes potentially involved in stalk structure, which would be useful in tracking Fe microbial mat formation. Differences between FeOB genomes, e.g., C, N, and S cycling genes and terminal oxidases, suggest that different FeOB are adapted to particular niches and contribute to other biogeochemical cycles in varied ways. Although we still need to demonstrate the function of the genes highlighted here, these genomic analyses begin to focus our picture of FeOB roles and mechanisms in Fe cycling in both freshwater and marine environments.

Description of *Ferriphaselus globulitus* sp. nov.

Ferriphaselus globulitus [glo.bu.li'tus. L. dim. n. globulus, a small sphere, globule; L. suff. -atus, suffix used with the sense provided with; N.L. masc. adj. globulitus, having small globules].

Cells are curved rods, or bean-shaped, 1.8–2.1 μm in length. Motile. Gram-negative. Do not form spores. Mesophilic and neutrophilic. Microaerobic, growing with opposing gradients of Fe(II) and O_2. Autotrophic. Capable of oxidizing Fe(II) as an energy source. Do not utilize thiosulfate, sulfide, nitrite, Mn(II), pyruvate, glucose or acetate as an energy source. Produces extracellular dreadlock-like iron oxides, in addition to twisted stalks. The major cellular fatty acids are C18:0, C16:0, C16:1v7c and/or C16:1v6c. Grows at 10–35°C (optimally at 25–30°C) and pH 5.6–7.0 (optimally at pH 5.6–6.1). Grows at low salt concentrations, below 0.3 g NaCl per L. The doubling time is 15 h. The type strain is R-1, isolated from an iron-rich floc in a groundwater seep in Christiana Creek, Newark, Delaware, United States of America. The total DNA G + C content of the type strain is 62.4 mol%.

AUTHOR CONTRIBUTIONS

SK and CC designed the study, analyzed the data, and wrote the paper. SK performed most of the experimentation, unless otherwise noted. DP performed the SEM imaging. STK cultured R-1 for various analyses. KO, MH, NS, and TW contributed to genome sequencing and annotation.

ACKNOWLEDGMENTS

We would like to thank Shannon Modla for help with TEM sample preparation. We are grateful to Tom Hanson, Erin Field, Cassandra Marnocha, Sean McAllister, Kevin Shuman, Jacob Hilzinger, Joshua Barnett, and Kara Hoppes for technical assistance, helpful comments and discussion. This work is supported by RIKEN Special Postdoctoral Researchers Program and the Japan Society for the Promotion of Science (JSPS) postdoctoral Fellowships for Research Abroad to SK. This work is also funded by NSF EAR-1151682 and NASA NNX12AG20G grants to CSC. The work conducted by the U.S. Department of Energy Joint Genome Institute, a DOE Office of Science User Facility, is supported by the Office of Science of the U.S. Department of Energy under Contract No. DE-AC02-05CH11231.

SUPPLEMENTARY MATERIAL

The Supplementary Material for this article can be found online at: http://journal.frontiersin.org/article/10.3389/fmicb.2015.01265

REFERENCES

Alawi, M., Lipski, A., Sanders, T., Eva Maria, P., and Spieck, E. (2007). Cultivation of a novel cold-adapted nitrite oxidizing betaproteobacterium from the siberian arctic. *ISME J.* 1, 256–264. doi: 10.1038/ismej.2007.34

Altschul, S. F., Madden, T. L., Schaffer, A. A., Zhang, J., Zhang, Z., Miller, W., et al. (1997). Gapped BLAST and PSI-BLAST: a new generation of protein database search programs. *Nucleic Acids Res.* 25, 3389–3402. doi: 10.1093/nar/25.17.3389

Badger, M. R., and Bek, E. J. (2008). Multiple rubisco forms in proteobacteria: their functional significance in relation to CO2 acquisition by the CBB cycle. *J. Exp. Bot.* 59, 1525–1541. doi: 10.1093/jxb/erm297

Barco, R. A., Emerson, D., Sylvan, J. B., Orcutt, B. N., Meyers, M. E. J., Ramíreza, G. A., et al. (2015). The proteomic profile of an obligate iron-oxidizing chemolithoautotroph reveals new insight into microbial iron oxidation. *Appl. Environ. Microbiol.* 81, 5927–5937. doi: 10.1128/AEM.01374-15

Belas, R. (2014). Biofilms, flagella, and mechanosensing of surfaces by bacteria. *Trends Microbiol.* 22, 517–527. doi: 10.1016/j.tim.2014.05.002

Bennett, S. (2004). Solexa ltd. *Pharmacogenomics* 5, 433–438. doi: 10.1517/14622416.5.4.433

Bennett, S. A., Toner, B. M., Barco, R., and Edwards, K. J. (2014). Carbon adsorption onto Fe oxyhydroxide stalks produced by a lithotrophic iron-oxidizing bacteria. *Geobiology* 12, 146–156. doi: 10.1111/gbi.12074

Borch, T., Kretzschmar, R., Kappler, A., Van Cappellen, P., Ginder-Vogel, M., Voegelin, A., et al. (2010). Biogeochemical redox processes and their impact on contaminant dynamics. *Environ. Sci. Technol.* 44, 15–23. doi: 10.1021/es9026248

Borisov, V. B., Gennis, R. B., Hemp, J., and Verkhovsky, M. I. (2011). The cytochrome bd respiratory oxygen reductases. *Biochim. Biophys. Acta* 1807, 1398–1413. doi: 10.1016/j.bbabio.2011.06.016

Brasseur, G. L., Bruscella, P., Bonnefoy, V., and Lemesle-Meunier, D. (2002). The bc1 complex of the iron-grown acidophilic chemolithotrophic bacterium *Acidithiobacillus ferrooxidans* functions in the reverse but not in the forward direction: is there a second bc1 complex? *Biochim. Biophys. Acta* 1555, 37–43. doi: 10.1016/S0005-2728(02)00251-7

Castelle, C., Guiral, M., Malarte, G., Ledgham, F., Leroy, G., Brugna, M., et al. (2008). A new iron-oxidizing/O2-reducing supercomplex spanning both inner and outer membranes, isolated from the extreme acidophile *Acidithiobacillus ferrooxidans*. *J. Biol. Chem.* 283, 25803–25811. doi: 10.1074/jbc.M802496200

Castresana, J. (2000). Selection of conserved blocks from multiple alignments for their use in phylogenetic analysis. *Mol. Biol. Evol.* 17, 540–552. doi: 10.1093/oxfordjournals.molbev.a026334

Chan, C. S., Fakra, S. C., Edwards, D. C., Emerson, D., and Banfield, J. F. (2009). Iron oxyhydroxide mineralization on microbial extracellular polysaccharides. *Geochim. Cosmochim. Acta* 73, 3807–3818. doi: 10.1016/j.gca.2009.02.036

Chan, C. S., Fakra, S. C., Emerson, D., Fleming, E. J., and Edwards, K. J. (2011). Lithotrophic iron-oxidizing bacteria produce organic stalks to control mineral growth: implications for biosignature formation. *ISME J.* 5, 717–727. doi: 10.1038/ismej.2010.173

Chien, Y. T., and Zinder, S. H. (1994). Cloning, DNA sequencing, and characterization of a nifD-homologous gene from the archaeon *Methanosarcina barkeri* 227 which resembles nifD1 from the eubacterium *Clostridium pasteurianum*. *J. Bacteriol.* 176, 6590–6598.

Dahl, C., Engels, S., Pott-Sperling, A. S., Schulte, A., Sander, J., LüBbe, Y., et al. (2005). Novel genes of the dsr gene cluster and evidence for close interaction of Dsr proteins during sulfur oxidation in the phototrophic sulfur bacterium *Allochromatium vinosum*. *J. Bacteriol* 187, 1392–1404. doi: 10.1128/JB.187.4.1392-1404.2005

Dahl, C., Franz, B., Hensen, D., Kesselheim, A., and Zigann, R. (2013). Sulfite oxidation in the purple sulfur bacterium *Allochromatium vinosum*: identification of SoeABC as a major player and relevance of SoxYZ in the process. *Microbiology* 159, 2626–2638. doi: 10.1099/mic.0.071019-0

Darling, A. E., Mau, B., and Perna, N. T. (2010). ProgressiveMauve: multiple genome alignment with gene gain, loss and rearrangement. *PLoS ONE* 5:e11147. doi: 10.1371/journal.pone.0011147

Dos Santos, P., Fang, Z., Mason, S., Setubal, J., and Dixon, R. (2012). Distribution of nitrogen fixation and nitrogenase-like sequences amongst microbial genomes. *BMC Genomics* 13:162. doi: 10.1186/1471-2164-13-162

Druschel, G. K., Emerson, D., Sutka, R., Suchecki, P., and Luther, G. W. III (2008). Low-oxygen and chemical kinetic constraints on the geochemical niche of neutrophilic iron(II) oxidizing microorganisms. *Geochim. Cosmochim. Acta* 72, 3358–3370. doi: 10.1016/j.gca.2008.04.035

Edgar, R. C. (2004). MUSCLE: multiple sequence alignment with high accuracy and high throughput. *Nucleic Acids Res.* 32, 1792–1797. doi: 10.1093/nar/gkh340

Edgar, R. C. (2010). Search and clustering orders of magnitude faster than BLAST. *Bioinformatics* 26, 2460–2461. doi: 10.1093/bioinformatics/btq461

Emerson, D., Field, E., Chertkov, O., Davenport, K., Goodwin, L., Munk, C., et al. (2013). Comparative genomics of freshwater Fe-oxidizing bacteria: implications for physiology, ecology, and systematics. *Front. Microbiol.* 4:254. doi: 10.3389/fmicb.2013.00254

Emerson, D., Fleming, E. J., and Mcbeth, J. M. (2010). Iron-oxidizing bacteria: an environmental and genomic perspective. *Annu. Rev. Microbiol.* 64, 561–583. doi: 10.1146/annurev.micro.112408.134208

Emerson, D., and Moyer, C. (1997). Isolation and characterization of novel iron-oxidizing bacteria that grow at circumneutral pH. *Appl. Environ. Microbiol.* 63, 4784–4792.

Emerson, D., Rentz, J. A., Lilburn, T. G., Davis, R. E., Aldrich, H., Chan, C., et al. (2007). A novel lineage of proteobacteria involved in formation of marine Fe-oxidizing microbial mat communities. *PLoS ONE* 2:e667. doi: 10.1371/journal.pone.0000667

Emerson, J. B., Thomas, B. C., Alvarez, W., and Banfield, J. F. (2015). Metagenomic analysis of a high CO2 subsurface microbial community populated by chemolithoautotrophs and bacteria and archaea from candidate phyla. *Environ. Microbiol.* doi: 10.1111/1462-2920.12817 [Epub ahead of print].

Ferris, F. G. (2005). Biogeochemical properties of bacteriogenic iron oxides. *Geomicrobiol. J.* 22, 79–85. doi: 10.1080/01490450590945861

Field, E. K., Sczyrba, A., Lyman, A. E., Harris, C. C., Woyke, T., Stepanauskas, R., et al. (2015). Genomic insights into the uncultivated marine Zetaproteobacteria at Loihi Seamount. *ISME J.* 9, 857–870. doi: 10.1038/ismej.2014.183

Finn, R. D., Clements, J., and Eddy, S. R. (2011). HMMER web server: interactive sequence similarity searching. *Nucleic Acids Res.* 39, W29–W37. doi: 10.1093/nar/gkr367

Fleming, E. J., Davis, R. E., Mcallister, S. M., Chan, C. S., Moyer, C. L., Tebo, B. M., et al. (2013). Hidden in plain sight: discovery of sheath-forming, iron-oxidizing Zetaproteobacteria at Loihi Seamount, Hawaii, USA. *FEMS Microbiol. Ecol.* 85, 116–127. doi: 10.1111/1574-6941.12104

Fleming, E. J., Langdon, A. E., Martinez-Garcia, M., Stepanauskas, R., Poulton, N. J., Masland, E. D. P., et al. (2011). What's new is old: resolving the identity of *Leptothrix ochracea* using single cell genomics, pyrosequencing and FISH. *PLoS ONE* 6:e17769. doi: 10.1371/journal.pone.0017769

Flemming, H.-C., and Wingender, J. (2010). The biofilm matrix. *Nat. Rev. Microbiol.* 8, 623–633.

Gao, X., Majumder, E. W., Kang, Y., Yue, H., and Blankenship, R. E. (2013). Functional analysis and expression of the mono-heme containing cytochrome c subunit of alternative complex III in *Chloroflexus aurantiacus*. *Arch. Biochem. Biophys.* 535, 197–204. doi: 10.1016/j.abb.2013.04.002

Gao, X., Xin, Y., and Blankenship, R. E. (2009). Enzymatic activity of the alternative complex III as a menaquinol: auracyanin oxidoreductase in the electron transfer chain of *Chloroflexus aurantiacus*. *FEBS Lett.* 583, 3275–3279. doi: 10.1016/j.febslet.2009.09.022

Gnerre, S., Maccallum, I., Przybylski, D., Ribeiro, F. J., Burton, J. N., Walker, B. J., et al. (2011). High-quality draft assemblies of mammalian genomes from massively parallel sequence data. *Proc. Natl. Acad. Sci. U.S.A.* 108, 1513–1518. doi: 10.1073/pnas.1017351108

Guindon, S., Dufayard, J.-F., Lefort, V., Anisimova, M., Hordijk, W., and Gascuel, O. (2010). New algorithms and methods to estimate maximum-likelihood phylogenies: assessing the performance of PhyML 3.0. *Syst. Biol.* 59, 307–321. doi: 10.1093/sysbio/syq010

Guttenplan, S. B., and Kearns, D. B. (2013). Regulation of flagellar motility during biofilm formation. *FEMS Microbiol. Rev.* 37, 849–871. doi: 10.1111/1574-6976.12018

Hallbeck, L., and Pedersen, K. (1995). Benefits associated with the stalk of *Gallionella ferruginea*, evaluated by comparison of a stalk-forming and a non-stalk-forming strain and biofilm studies in situ. *Microb. Ecol.* 30, 257–268. doi: 10.1007/BF00171933

Hoiczyk, E., and Baumeister, W. (1998). The junctional pore complex, a prokaryotic secretion organelle, is the molecular motor underlying gliding motility in cyanobacteria. *Curr. Biol.* 8, 1161–1168. doi: 10.1016/S0960-9822(07)00487-3

Huson, D. H., Auch, A. F., Qi, J., and Schuster, S. C. (2007). MEGAN analysis of metagenomic data. *Genome Res.* 17, 377–386. doi: 10.1101/gr.5969107

Hyatt, D., Chen, G.-L., Locascio, P., Land, M., Larimer, F., and Hauser, L. (2010). Prodigal: prokaryotic gene recognition and translation initiation site identification. *BMC Bioinformatics* 11:119. doi: 10.1186/1471-2105-11-119

Jarrell, K. F., and McBride, M. J. (2008). The surprisingly diverse ways that prokaryotes move. *Nat. Rev. Microbiol.* 6, 466–476. doi: 10.1038/nrmicro1900

Johnson, D. B., Hallberg, K. B., and Hedrich, S. (2014). Uncovering a microbial enigma: isolation and characterization of the streamer-generating, iron-oxidizing, acidophilic bacterium "*Ferrovum myxofaciens*." *Appl. Environ. Microbiol.* 80, 672–680. doi: 10.1128/AEM.03230-13

Kato, S., Chan, C., Itoh, T., and Ohkuma, M. (2013). Functional gene analysis of freshwater iron-rich flocs at circumneutral pH and isolation of a stalk-forming microaerophilic iron-oxidizing bacterium. *Appl. Environ. Microbiol.* 79, 5283–5290. doi: 10.1128/AEM.03840-12

Kato, S., Kobayashi, C., Kakegawa, T., and Yamagishi, A. (2009a). Microbial communities in iron-silica-rich microbial mats at deep-sea hydrothermal fields of the Southern Mariana Trough. *Environ. Microbiol.* 11, 2094–2111. doi: 10.1111/j.1462-2920.2009.01930.x

Kato, S., Yanagawa, K., Sunamura, M., Takano, Y., Ishibashi, J.-I., Kakegawa, T., et al. (2009b). Abundance of Zetaproteobacteria within crustal fluids in back-arc hydrothermal fields of the Southern Mariana Trough. *Environ. Microbiol.* 11, 3210–3222. doi: 10.1111/j.1462-2920.2009.02031.x

Kato, S., Krepski, S., Chan, C., Itoh, T., and Ohkuma, M. (2014). Ferriphaselus *Amnicola* gen. nov., sp. nov., a neutrophilic, stalk-forming, iron-oxidizing bacterium isolated from an iron-rich groundwater seep. *Int. J. Syst. Evol. Microbiol.* 64, 921–925. doi: 10.1099/ijs.0.058487-0

Kato, S., Nakawake, M., Ohkuma, M., and Yamagishi, A. (2012). Distribution and phylogenetic diversity of cbbM genes encoding RubisCO form II in a deep-sea hydrothermal field revealed by newly designed PCR primers. *Extremophiles* 16, 277–283. doi: 10.1007/s00792-011-0428-6

Katoh, K., and Standley, D. M. (2013). MAFFT multiple sequence alignment software version 7: improvements in performance and usability. *Mol. Biol. Evol.* 30, 772–780. doi: 10.1093/molbev/mst010

Kim, M., Oh, H.-S., Park, S.-C., and Chun, J. (2014). Towards a taxonomic coherence between average nucleotide identity and 16S rRNA gene sequence similarity for species demarcation of prokaryotes. *Int. J. Syst. Evol. Microbiol.* 64, 346–351. doi: 10.1099/ijs.0.059774-0

Krepski, S. T., Emerson, D., Hredzak-Showalter, P. L., Luther, G. W., and Chan, C. S. (2013). Morphology of biogenic iron oxides records microbial physiology and environmental conditions: toward interpreting iron microfossils. *Geobiology* 11, 457–471. doi: 10.1111/gbi.12043

Krepski, S. T., Hanson, T. E., and Chan, C. S. (2012). Isolation and characterization of a novel biomineral stalk-forming iron-oxidizing bacterium from a circumneutral groundwater seep. *Environ. Microbiol.* 14, 1671–1680. doi: 10.1111/j.1462-2920.2011.02652.x

Kucera, S., and Wolfe, R. S. (1957). A selective enrichment method for *Gallionella ferruginea*. *J. Bacteriol.* 74, 344–349.

Lagesen, K., Hallin, P., Rødland, E. A., Stærfeldt, H.-H., Rognes, T., and Ussery, D. W. (2007). RNAmmer: consistent and rapid annotation of ribosomal RNA genes. *Nucleic Acids Res.* 35, 3100–3108. doi: 10.1093/nar/gkm160

Lairson, L. L., Henrissat, B., Davies, G. J., and Withers, S. G. (2008). Glycosyltransferases: structures, functions, and mechanisms. *Annu. Rev. Biochem.* 77, 521–555. doi: 10.1146/annurev.biochem.76.061005.092322

Laslett, D., and Canback, B. (2004). Aragorn, a program to detect tRNA genes and tmRNA genes in nucleotide sequences. *Nucleic Acids Res.* 32, 11–16. doi: 10.1093/nar/gkh152

Liu, J., Wang, Z., Belchik, S. M., Edwards, M. J., Liu, C., Kennedy, D. W., et al. (2012). Identification and characterization of MtoA: a decaheme c-type cytochrome of the neutrophilic Fe(II)-oxidizing bacterium *Sideroxydans lithotrophicus* ES-1. *Front. Microbiol.* 3:37. doi: 10.3389/fmicb.2012.00037

Lücker, S., Schwarz, J., Gruber-Dorninger, C., Spieck, E., Wagner, M., and Daims, H. (2015). Nitrotoga-like bacteria are previously unrecognized key nitrite oxidizers in full-scale wastewater treatment plants. *ISME J.* 9, 708–720. doi: 10.1038/ismej.2014.158

Macnab, R. M. (2003). How bacteria assemble flagella. *Annu. Rev. Microbiol.* 57, 77–100. doi: 10.1146/annurev.micro.57.030502.090832

Marcia, M., Ermler, U., Peng, G., and Michel, H. (2010). A new structure-based classification of sulfide: quinone oxidoreductases. *Proteins* 78, 1073–1083. doi: 10.1002/prot.22665

Markowitz, V. M., Chen, I.-M. A., Palaniappan, K., Chu, K., Szeto, E., Pillay, M., et al. (2014). IMG 4 version of the integrated microbial genomes comparative analysis system. *Nucleic Acids Res.* 42, D560–D567. doi: 10.1093/nar/gkt963

Mattick, J. S. (2002). Type IV pili and twitching motility. *Annu. Rev. Microbiol.* 56, 289–314. doi: 10.1146/annurev.micro.56.012302.160938

Mazur, O., and Zimmer, J. (2011). Apo- and cellopentaose-bound structures of the bacterial cellulose synthase subunit BcsZ. *J. Biol. Chem.* 286, 17601–17606. doi: 10.1074/jbc.M111.227660

McAllister, S. M., Barnett, J. M., Heiss, J. W., Findlay, A. J., MacDonald, D. J., Dow, C. L., et al. (2015). Dynamic hydrologic and biogeochemical processes drive microbially enhanced iron and sulfur cycling within the intertidal mixing zone of a beach aquifer. *Limnol. Oceanogr.* 60, 329–345. doi: 10.1002/lno.10029

Meier-Kolthoff, J., Auch, A., Klenk, H.-P., and Goker, M. (2013). Genome sequence-based species delimitation with confidence intervals and improved distance functions. *BMC Bioinformatics* 14:60. doi: 10.1186/1471-2105-14-60

Miot, J., Benzerara, K., Morin, G., Kappler, A., Bernard, S., Obst, M., et al. (2009a). Iron biomineralization by anaerobic neutrophilic iron-oxidizing bacteria. *Geochim. Cosmochim. Acta* 73, 696–711. doi: 10.1016/j.gca.2008.10.033

Miot, J., Benzerara, K., Obst, M., Kappler, A., Hegler, F., Schädler, S., et al. (2009b). Extracellular iron biomineralization by photoautotrophic iron-oxidizing bacteria. *Appl. Environ. Microbiol.* 75, 5586–5591. doi: 10.1128/AEM.00490-09

Nawrocki, E. P., and Eddy, S. R. (2013). Infernal 1.1: 100-fold faster RNA homology searches. *Bioinformatics* 29, 2933–2935. doi: 10.1093/bioinformatics/btt509

Ogata, H., Goto, S., Sato, K., Fujibuchi, W., Bono, H., and Kanehisa, M. (1999). KEGG: kyoto encyclopedia of genes and genomes. *Nucleic Acids Res.* 27, 29–34. doi: 10.1093/nar/27.1.29

Orcutt, B. N., Bach, W., Becker, K., Fisher, A. T., Hentscher, M., Toner, B. M., et al. (2011). Colonization of subsurface microbial observatories deployed in young ocean crust. *ISME J.* 5, 692–703. doi: 10.1038/ismej.2010.157

Pereira, M. M., Refojo, P. N., Hreggvidsson, G. O., Hjorleifsdottir, S., and Teixeira, M. (2007). The alternative complex III from *Rhodothermus marinus* – a prototype of a new family of quinol: electron acceptor oxidoreductases. *FEBS Lett.* 581, 4831–4835. doi: 10.1016/j.febslet.2007.09.008

Pitcher, R. S., and Watmough, N. J. (2004). The bacterial cytochrome cbb3 oxidases. *Biochim. Biophys. Acta* 1655, 388–399. doi: 10.1016/j.bbabio.2003.09.017

Porter, S. L., Wadhams, G. H., and Armitage, J. P. (2011). Signal processing in complex chemotaxis pathways. *Nat. Rev. Microbiol.* 9, 153–165. doi: 10.1038/nrmicro2505

Price, M. N., Dehal, P. S., and Arkin, A. P. (2010). FastTree 2 – approximately maximum-likelihood trees for large alignments. *PLoS ONE* 5:e9490. doi: 10.1371/journal.pone.0009490

Refojo, P. C. N., Teixeira, M., and Pereira, M. M. (2010). The alternative complex III of *Rhodothermus marinus* and its structural and functional association with caa3 oxygen reductase. *Biochim. Biophys. Acta* 1797, 1477–1482. doi: 10.1016/j.bbabio.2010.02.029

Rentz, J. A., Kraiya, C., Luther, G. W. III, and Emerson, D. (2007). Control of ferrous iron oxidation within circumneutral microbial iron mats by cellular activity and autocatalysis. *Environ. Sci. Technol.* 41, 6084–6089. doi: 10.1021/es062203e

Richter, M., and Rosselló-Móra, R. (2009). Shifting the genomic gold standard for the prokaryotic species definition. *Proc. Natl. Acad. Sci. U.S.A.* 106, 19126–19131. doi: 10.1073/pnas.0906412106

Rinke, C., Schwientek, P., Sczyrba, A., Ivanova, N. N., Anderson, I. J., Cheng, J.-F., et al. (2013). Insights into the phylogeny and coding potential of microbial dark matter. *Nature* 499, 431–437. doi: 10.1038/nature12352

Römling, U. (2002). Molecular biology of cellulose production in bacteria. *Res. Microbiol.* 153, 205–212. doi: 10.1016/S0923-2508(02)01316-5

Rothery, R. A., Workun, G. J., and Weiner, J. H. (2008). The prokaryotic complex iron–sulfur molybdoenzyme family. *Biochim. Biophys. Acta* 1778, 1897–1929. doi: 10.1016/j.bbamem.2007.09.002

Seemann, T. (2014). Prokka: rapid prokaryotic genome annotation. *Bioinformatics* 30, 2068–2069. doi: 10.1093/bioinformatics/btu153

Singer, E., Emerson, D., Webb, E. A., Barco, R. A., Kuenen, J. G., Nelson, W. C., et al. (2011). Mariprofundus ferrooxydans PV-1 the first genome of a marine Fe(II) oxidizing zetaproteobacterium. *PLoS ONE* 6:e25386. doi: 10.1371/journal.pone.0025386

Suzuki, T., Hashimoto, H., Matsumoto, N., Furutani, M., Kunoh, H., and Takada, J. (2011). Nanometer-scale visualization and structural analysis of the inorganic/organic hybrid structure of *Gallionella ferruginea* twisted stalks. *Appl. Environ. Microbiol.* 77, 2877–2881. doi: 10.1128/AEM.02867-10

Tao, F., Swarup, S., and Zhang, L.-H. (2010). Quorum sensing modulation of a putative glycosyltransferase gene cluster essential for *Xanthomonas campestris* biofilm formation. *Environ. Microbiol.* 12, 3159–3170. doi: 10.1111/j.1462-2920.2010.02288.x

Vatter, A. E., and Wolfe, R. S. (1956). Electron microscopy of *Gallionella ferruginea*. *J. Bacteriol.* 72, 248–252.

Venceslau, S. S., Lino, R. R., and Pereira, I. A. C. (2010). The Qrc membrane complex, related to the alternative complex III, is a menaquinone reductase involved in sulfate respiration. *J. Biol. Chem.* 285, 22774–22783. doi: 10.1074/jbc.M110.124305

Venceslau, S. S., Stockdreher, Y., Dahl, C., and Pereira, I. A. C. (2014). The "Bacterial heterodisulfide" DsrC is a key protein in dissimilatory sulfur metabolism. *Biochim. Biophys. Acta* 1837, 1148–1164. doi: 10.1016/j.bbabio.2014.03.007

Wagner, M., Roger, A. J., Flax, J. L., Brusseau, G. A., and Stahl, D. A. (1998). Phylogeny of dissimilatory sulfite reductases supports an early origin of sulfate respiration. *J. Bacteriol.* 180, 2975–2982.

Wang, J., Muyzer, G., Bodelier, P. L. E., and Laanbroek, H. J. (2009). Diversity of iron oxidizers in wetland soils revealed by novel 16S rRNA primers targeting *Gallionella*-related bacteria. *ISME J.* 3, 715–725. doi: 10.1038/ismej.2009.7

Wang, Z., Leary, D. H., Malanoski, A. P., Li, R. W., Hervey, W. J., Eddie, B. J., et al. (2015). A previously uncharacterized, nonphotosynthetic member of the *Chromatiaceae* is the primary CO2-fixing constituent in a self-regenerating biocathode. *Appl. Environ. Microbiol.* 81, 699–712. doi: 10.1128/AEM.02947-14

Watanabe, T., Kojima, H., and Fukui, M. (2014). Complete genomes of freshwater sulfur oxidizers *Sulfuricella denitrificans* skB26 and *Sulfuritalea hydrogenivorans* sk43H: genetic insights into the sulfur oxidation pathway of betaproteobacteria. *Syst. Appl. Microbiol.* 37, 387–395. doi: 10.1016/j.syapm.2014.05.010

Weiss, J. V., Rentz, J. A., Plaia, T., Neubauer, S. C., Merrill-Floyd, M., Lilburn, T., et al. (2007). Characterization of neutrophilic Fe(II)-oxidizing bacteria isolated from the rhizosphere of wetland plants and description of *Ferritrophicum radicicola* gen. nov. sp. nov., and *Sideroxydans paludicola* sp. nov. *Geomicrobiol. J.* 24, 559–570. doi: 10.1080/01490450701670152

Wolgemuth, C., Hoiczyk, E., Kaiser, D., and Oster, G. (2002). How myxobacteria glide. *Curr. Biol.* 12, 369–377. doi: 10.1016/S0960-9822(02)00716-9

Yanyushin, M. F., Del Rosario, M. C., Brune, D. C., and Blankenship, R. E. (2005). New class of bacterial membrane oxidoreductases. *Biochemistry* 44, 10037–10045. doi: 10.1021/bi047267l

Yu, N. Y., Wagner, J. R., Laird, M. R., Melli, G., Rey, S. B., Lo, R., et al. (2010). PSORTb 3.0: improved protein subcellular localization prediction with refined localization subcategories and predictive capabilities for all prokaryotes. *Bioinformatics* 26, 1608–1615. doi: 10.1093/bioinformatics/btq249

Zdobnov, E. M., and Apweiler, R. (2001). InterProScan – an integration platform for the signature-recognition methods in InterPro. *Bioinformatics* 17, 847–848. doi: 10.1093/bioinformatics/17.9.847

Zerbino, D. R., and Birney, E. (2008). Velvet: algorithms for de novo short read assembly using de Bruijn graphs. *Genome Res.* 18, 821–829. doi: 10.1101/gr.074492.107

Conflict of Interest Statement: The authors declare that the research was conducted in the absence of any commercial or financial relationships that could be construed as a potential conflict of interest.

frontiers in Microbiology

ORIGINAL RESEARCH
published: 01 June 2016
doi: 10.3389/fmicb.2016.00796

The Architecture of Iron Microbial Mats Reflects the Adaptation of Chemolithotrophic Iron Oxidation in Freshwater and Marine Environments

Clara S. Chan[1,2]*, *Sean M. McAllister*[1,2], *Anna H. Leavitt*[3], *Brian T. Glazer*[4], *Sean T. Krepski*[2] and *David Emerson*[3]

[1] School of Marine Science and Policy, University of Delaware, Newark, DE, USA, [2] Geological Sciences, University of Delaware, Newark, DE, USA, [3] Bigelow Laboratory for Ocean Sciences, East Boothbay, ME, USA, [4] Department of Oceanography, University of Hawaii, Honolulu, HI, USA

Microbes form mats with architectures that promote efficient metabolism within a particular physicochemical environment, thus studying mat structure helps us understand ecophysiology. Despite much research on chemolithotrophic Fe-oxidizing bacteria, Fe mat architecture has not been visualized because these delicate structures are easily disrupted. There are striking similarities between the biominerals that comprise freshwater and marine Fe mats, made by Beta- and Zetaproteobacteria, respectively. If these biominerals are assembled into mat structures with similar functional morphology, this would suggest that mat architecture is adapted to serve roles specific to Fe oxidation. To evaluate this, we combined light, confocal, and scanning electron microscopy of intact Fe microbial mats with experiments on sheath formation in culture, in order to understand mat developmental history and subsequently evaluate the connection between Fe oxidation and mat morphology. We sampled a freshwater sheath mat from Maine and marine stalk and sheath mats from Loihi Seamount hydrothermal vents, Hawaii. Mat morphology correlated to niche: stalks formed in steeper O_2 gradients while sheaths were associated with low to undetectable O_2 gradients. Fe-biomineralized filaments, twisted stalks or hollow sheaths, formed the highly porous framework of each mat. The mat-formers are keystone species, with nascent marine stalk-rich mats comprised of novel and uncommon Zetaproteobacteria. For all mats, filaments were locally highly parallel with similar morphologies, indicating that cells were synchronously tracking a chemical or physical cue. In the freshwater mat, cells inhabited sheath ends at the growing edge of the mat. Correspondingly, time lapse culture imaging showed that sheaths are made like stalks, with cells rapidly leaving behind an Fe oxide filament. The distinctive architecture common to all observed Fe mats appears to serve specific functions related to chemolithotrophic Fe oxidation, including (1) removing Fe oxyhydroxide waste without entombing cells or clogging flow paths through the mat and (2) colonizing niches where Fe(II) and O_2 overlap. This work improves our understanding of Fe mat developmental history and how mat morphology links to metabolism. We can use these results to interpret biogenicity, metabolism, and paleoenvironmental conditions of Fe microfossil mats, which would give us insight into Earth's Fe and O_2 history.

Keywords: Fe-oxidizing bacteria, microbial mats, hydrothermal vents, Zetaproteobacteria, *Leptothrix ochracea*

OPEN ACCESS

Edited by:
Cara M. Santelli, University of Minnesota-Twin Cities, USA

Reviewed by:
John R. Spear, Colorado School of Mines, USA
Lotta Hallbeck, Microbial Analytics Sweden AB, Sweden

***Correspondence:**
Clara S. Chan
cschan@udel.edu

Specialty section:
This article was submitted to Extreme Microbiology, a section of the journal Frontiers in Microbiology

Received: *05 January 2016*
Accepted: *11 May 2016*
Published: *01 June 2016*

Citation:
Chan CS, McAllister SM, Leavitt AH, Glazer BT, Krepski ST and Emerson D (2016) The Architecture of Iron Microbial Mats Reflects the Adaptation of Chemolithotrophic Iron Oxidation in Freshwater and Marine Environments. Front. Microbiol. 7:796. doi: 10.3389/fmicb.2016.00796

INTRODUCTION

Microbial mats are intricately organized structures that provide functional advantage to their inhabitants (e.g., Stahl et al., 2013). Mat architecture reflects both ecology and physiology in that it promotes the metabolisms of the microbes that construct the mat. Chemolithotrophic microaerophilic Fe-oxidizing bacteria (FeOB) are well known for creating distinctive orange-rust colored mats where ferrous-rich fluids flow into oxygenated surface water (e.g., groundwater seeps, hydrothermal vents; Harder, 1919; Ghiorse, 1984; Emerson et al., 2010). These mats are often referred to as "flocs," and indeed, they easily break apart and flocculate, suggesting that coherence could result from random organization. These properties make it difficult to assess if Fe mats are the product of coordinated microbial behavior, yet knowing how and why FeOB develop certain mat architectures is important to understanding FeOB habitat and ecology, as well as interpreting Fe microfossils in the rock record.

Fe microbial mats range from small, millimeters- to centimeters-thick patches where groundwater trickles from rock faces (Emerson and Revsbech, 1994) to meter-deep, 100s m^2 fields where diffuse hydrothermal vents meet the deep sea floor (Edwards et al., 2011). In contrast to other microbial mats and biofilms, which typically include dense, tightly adherent masses of cells and extracellular polymers, Fe mats are instead composed of loosely aggregated Fe-mineralized filaments (twisted stalks, tubular sheaths) along with other morphologies. These biominerals easily disaggregate during sampling. As a result, despite much study on Fe mat community composition (e.g., McAllister et al., 2011; Baskar et al., 2012; Hegler et al., 2012; Scott et al., 2015) and mat-derived FeOB cultures (e.g., Hanert, 1973; Hallbeck et al., 1993; Emerson et al., 2007), we lack basic information about Fe mat architecture and how cells develop and inhabit the structures within natural settings.

Fe microbial mats have two compelling dichotomies, phylogenetic and morphologic (**Figure 1**), that enable comparative study. This provides a unique opportunity that could yield insights into how mat architectures are linked to microbial Fe oxidation. The bulk of Fe microbial mats is typically comprised of either stalks or sheaths (**Figure 1**). Stalks are formed by two groups of chemolithotrophic FeOB: (1) Betaproteobacteria of the family Gallionellaceae, in freshwater, (*Gallionella ferruginea*—Hanert, 1973; Hallbeck and Pedersen, 1990; *Ferriphaselus spp.*—Krepski et al., 2012; Kato et al., 2014) and (2) Zetaproteobacteria of the genus *Mariprofundus* in marine environments (Emerson et al., 2007; Chan et al., 2011). Stalk-forming isolates are all obligate chemolithoautotrophic microaerophilic FeOB that typically grow at micromolar to tens μM O_2 concentrations at the interfaces of steep Fe(II) and O_2 gradients (Emerson and Revsbech, 1994; Druschel et al., 2008; Glazer and Rouxel, 2009; Krepski et al., 2013; Fleming et al., 2014). Sheaths are formed either by (1) Betaproteobacteria *Leptothrix ochracea*, in freshwater (Harder, 1919; van Veen et al., 1978; Emerson and Revsbech, 1994; Fleming et al., 2014), or (2) Zetaproteobacteria in marine environments (Fleming et al., 2013). Sheath-formers tend to be found associated with higher O_2 concentrations (Fleming et al., 2014), though these have not been well constrained in the exact areas of active sheath growth. Since sheath-formers have not been isolated, the details of Fe and C metabolism are not certain. Nonetheless, the strong correlation between these organisms and relatively high Fe(II)-environments, as well as their copious production of Fe(III) oxyhydroxides strongly suggests that sheath-forming organisms oxidize Fe(II) as a key part of their metabolism. The striking parallel between terrestrial Betaproteobacteria and marine Zetaproteobacteria suggests that the filament-based mat structure plays specific roles in promoting microbial Fe oxidation. This would prove true if all types of filament-forming FeOB use their filaments to produce mats with similar architectures, despite the fact that stalk and sheath morphologies represent different O_2 niches, distinct cell-mineral spatial relationships (**Figure 1**), and likely distinct genetic mechanisms. Comparative study of the various Fe microbial mat types combined with niche characterization would help resolve whether metabolism or other factors most influence Fe mat architecture.

To understand Fe mat development, we must first understand how the individual biomineral filaments are formed. The stalk-formers are much better studied, largely because they have proven cultivable while the sheath-formers tend not to grow after a few transfers. For stalk-forming organisms, as a cell oxidizes Fe(II), it continually produces a rigid Fe(III) oxyhydroxide stalk with the cells always at the leading edge (**Figure 1A**; Hanert, 1973; Chan et al., 2011; Krepski et al., 2013). Thus, the stalk is a record of where cells were present and oxidizing Fe, making it possible to follow stalk morphology to determine a detailed history of mat development. Imaging of sheaths from freshwater has shown us that cells live as relatively short filaments within the sheaths, while producing copious amounts of sheath material; the end result being the sheaths are largely empty (**Figure 1B**; e.g., Mulder and van Veen, 1963; Emerson and Revsbech, 1994). However, detailed *in situ* analysis of sheath formation has not yet been performed. Understanding how individual sheaths form would allow us to visualize how sheath mats develop, which would then enable a more informed comparison of stalk- and sheath-based Fe mat architecture.

Thus, in this study, we combine observations of intact Fe microbial mats, both stalk and sheath-rich, with experiments on sheath formation in culture, in order to understand mat developmental history and subsequently evaluate the connection between Fe oxidation and mat morphology. We sampled mats from a representative freshwater system (Spruce Point Creek, Maine; sheath-rich) and deep sea hydrothermal vents (Loihi Seamount, Hawaii; stalk- and sheath-rich). We developed a new approach to sampling Fe mats in order to preserve the delicate structure, and analyzed the mats using light, confocal, and electron microscopy. Microscope chamber cultures of freshwater sheath-forming organisms allowed us to observe Fe oxidation and biomineralized sheath formation. Time lapse imaging showed that sheaths are made much like stalks are, with the cells growing at the leading edge, suggesting that both filaments serve common functions. All of the environmental Fe mats showed similarities in directionality and texture,

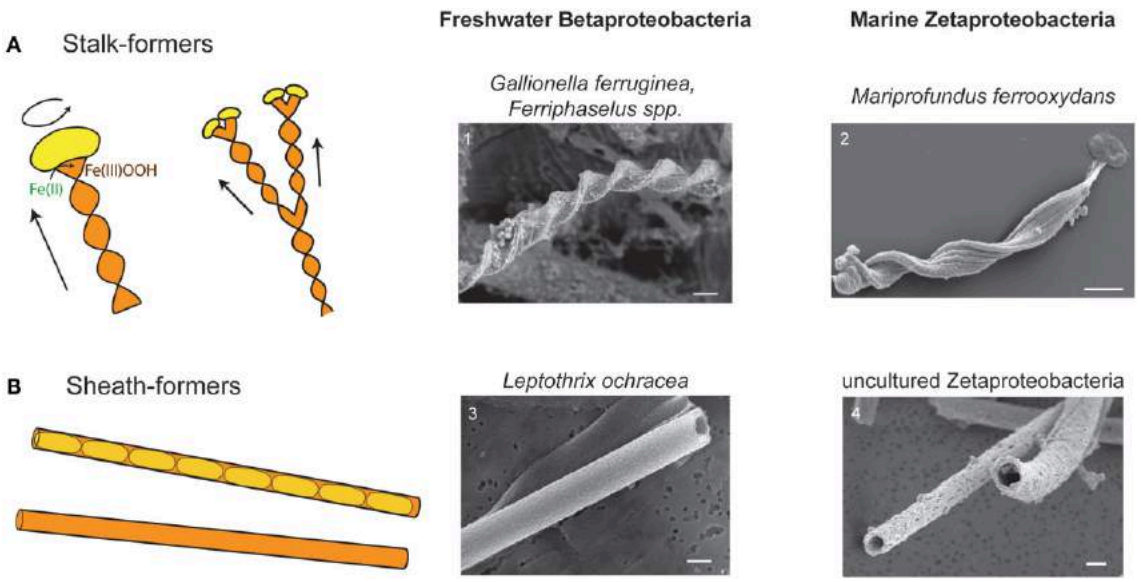

FIGURE 1 | Cartoons and SEM images of stalks and sheaths. (A) Cartoon of stalk formation: as cells (yellow) produce Fe oxyhydroxide (orange), they leave behind a ribbon-like stalk. Cell rotation causes stalk twisting. As cells divide and continue to form stalks, the stalk branches. Continued cell division results in multiple branching. SEM images of (1) *Gallionella* stalk from freshwater Fe mat, Piquette Mine, Wisconsin (Banfield et al., 2001) and (2) *M. ferrooxydans* PV-1 stalk. **(B)** Cartoon of sheaths showing cells inside sheath, and empty sheath (more typically observed). SEM images of (3) *L. ochracea* from freshwater Fe mat, Lakeside Drive, Maine (Fleming et al., 2011) and (4) sheath formed by an uncultured Zetaproteobacteria from Loihi Seamount, HI (Fleming et al., 2013). All scale bars = 1 μm.

suggesting that they have a similar developmental history. Coupled to field observations and geochemical measurements, we show that Fe mat structure appears to be a function of environmental niche and the distinct challenges of microbial Fe oxidation, including efficient Fe biomineralization without encrustation and maintaining position in Fe(II) and O_2 gradients.

METHODS

Overview of Field Sites and Analyses

Table 1 shows a summary of mat types sampled, with corresponding field sites and analyses. Descriptions of relevant site characteristics are included in the Results section.

Marine Mat Observations and Geochemical Measurements

Fe microbial mats were observed and collected during a cruise to the Loihi Seamount, Hawaii in March 2013, on the R/V Thompson, using the remotely operated vehicle (ROV) Jason II. *In situ* Fe(II) and O_2 analyses were performed using an *in situ* electrochemical analyzer (ISEA-III, Analytical Instrument Systems, Inc., Flemington, NJ, USA) connected to the ROV Jason-II similar to previously deployments (e.g., Luther et al., 2008; Glazer and Rouxel, 2009). Solid-state Au/Hg working electrodes, Ag/AgCl reference electrodes, and Pt counter electrodes were constructed from durable 3 mm diameter PEEK tubing and epoxy, and calibrated using standard electrochemical calibration methods (e.g., Brendel and Luther, 1995; Glazer et al., 2004; Luther et al., 2008). Parameters for individual voltammetric scans were: initial conditioning steps of −0.9 V for 5 s and −0.1 V for 2 s, then performing cyclic voltammeter by scanning from −0.1 to −1.85 V and back to −0.1 V at a scan rate of 500–2000 mV s^{-1}. Data were analyzed using a combination of the manufacturer's software (Advanced Analysis, AIS, Inc.), open-source voltammetric analysis software (Voltint; Bristow and Taillefert, 2008), and a custom auto-analysis package (Glazer, unpublished).

Marine Mat Sampling

For sampling, we targeted well-studied Fe-rich vent locations, where we have previously sampled mats with stalks and sheaths (e.g., Emerson and Moyer, 2002; McAllister et al., 2011; Fleming et al., 2013). Mats were sampled by ROV using either a suction sampler (where there was some cohesion) or a "scoop" sampler, which consisted of a 3″ plastic tube capped at both ends, one end with a ball valve. When handling the more delicate mats sampled with the scoop, samplers were opened in a bucket of seawater to minimize disturbance. The mat samples were eased out of the scoop sampler and collected in a sterile bowl. Subsamples for DNA analysis were frozen at –80°C. Intact pieces (∼a few cm^3) were carefully dissected with a scalpel to observe the internal structure and architecture. Dissected pieces were ∼0.5–2 cm in length by ∼0.5 cm in width and thickness. Samples for scanning electron microscopy (SEM) were fixed with 2.5% glutaraldehyde and washed with phosphate buffered saline (PBS). Samples for light microscopy were embedded in 0.5% high melt agarose, which was allowed to solidify at room temperature. Microscopy samples were stored at 4°C until further analysis.

TABLE 1 | Summary of samples and analyses.

Mat type	Sample sites	Geochemical analyses	Microscopy analyses	Molecular analyses
Marine, stalk-rich mat ("curd")	Loihi Seamount	*in situ* voltammetry for Fe(II) and O_2	Light, confocal, SEM	Pyrosequencing of SSU rRNA V1-V3
Marine, sheath-rich mat ("veil")	Loihi Seamount	*in situ* voltammetry for Fe(II) and O_2	Light, confocal, SEM	Pyrosequencing of SSU rRNA V1-V3
Freshwater, sheath-rich mat	Spruce Point, Maine	*in situ* O_2 optode; discrete sampling for Fe(II) by ferrozine	Light, confocal	
Freshwater, sheath-rich mat	Lakeside Drive, Maine		Time lapse light	
Freshwater, sheath-rich mat	Christina Creek, Delaware		Time lapse light	

Freshwater Mat Sampling and Measurements

At Spruce Point, Fe(II) profiles were obtained by taking discrete samples with a pipettor at 1 cm depth and horizontal intervals of 0.5 cm across the mat-water interface, and analyzing by the ferrozine method (Stookey, 1970). Oxygen concentrations were measured using a Pyroscience (Aachen, Germany) Firesting optical oxygen probe, as described by Emerson et al. (2015). The intact mats were sampled by gently scooping relatively cohesive mats directly into a 5 cm petri plate. Overlying water was removed and warm liquid 0.5% high melt agarose was added. These plates were placed on ice to solidify, which took 3–4 min, and then returned to the lab where they were fixed with gluteraldehyde within a few hours, then stored at 4°C until sectioning.

Sectioning and Staining of Intact Mat

Agarose-embedded samples were trimmed and sectioned to 100–250 μm thickness using a Leica VT 1000 vibratome, then stored at 4°C until imaged. Sections were stained to visualize iron oxides and cells, using the method modified from Krepski et al. (2013). Briefly, slices were stained with a rhodamine-labeled soybean agglutinin (SBA) lectin or Ricinus Communis Agglutinin (RCA) I (Vector Laboratories, Burlingame, CA, USA) by pipetting 1 μL of lectin per 100 μL of sample directly onto the agarose slice. One mL of deionized water was added to submerge the slice, and the sample was incubated in the dark at room temperature for a minimum of 2 h with gentle agitation every 15 min. The slice was washed twice in 1 mL of deionized water for 30 min each. To stain cells, 10 μL of nucleic acid dye Syto13 (Invitrogen) per 100ul of sample was added directly to the slice. Stained slices were then used immediately for imaging.

Light and Confocal Imaging

Mat slices were mounted on a microscope slide or tissue culture plate and imaged by brightfield and confocal fluorescence microscopy, either using a Zeiss Laser Scanning Microscope (LSM) 700 confocal scanning laser system coupled with a Zeiss Axiophot inverted microscope, or a Zeiss LSM 880-NLO with ZEN software (Zeiss, Jena, Germany). Slices were initially imaged by light microscopy to gain an understanding of general mat architecture, and photomosaics were obtained. On the LSM700, fluorescence imaging was performed using laser excitation at 488 and 555 nm, with a Plan-Neofluar 10 × 0.3 NA and C-Apochromat 40x (NA 1.2) water immersion objective, collecting the emitted fluorescence between 300–550 and 578–800 nm, respectively. On the LSM880, a 561 nm laser was used with a C-Apochromat 40x (NA 1.2) water immersion objective, with a 570–695 nm band pass filter.

Brightfield Light and Confocal Image Processing and Analysis

Brightfield mosaic images were stitched using the mosaicJ plugin for ImageJ. Confocal mosaic images were stitched in real time on the confocal microscope using ZEN 2. To display 3D information in 2D images, Z-stacks were merged using maximum intensity projection in ZEN 2011 (**Figures 4**, **5B–D**, **6C,E**, and **8B,D,E**). To highlight features, color-coded projection in ZEN 2011 was used to merge a Z-stack into a single image with color based on z-depth (**Figure 5A**, Supplemental Figure 2A). Other images were analyzed using the Fiji implementation of ImageJ (Schindelin et al., 2012). The number of cells was counted using the Analyze Particles function in ImageJ using thresholded maximum intensity projections of regions 2.42 to 9.10 × 10^{-5} cm^3. Directionality measurements were taken using the ImageJ 2.0.0 OrientationJ Measure plugin (Supplemental Figures 4–6). Orientation color surveys were created using this same plugin, with Finite Difference Hessian structure tensor approximation and default settings (**Figure 6D**). Manual filament coloring was performed in Adobe Photoshop (**Figures 4**, **5B**). 3D rendering of confocal images was done using Amira 5.6 (FEI, Hillsboro, Oregon, USA) (**Video 3**).

SEM Sample Preparation and Imaging

In the laboratory, samples were re-fixed with 2.5% glutaraldehyde and 1% OsO_4 for 1 h each in succession, with 3 washes with filtered deionized water after each step. Samples were dehydrated by a series of ethanol solutions: 10 min 25% EtOH, 20 min 50% EtOH, 30 min 75% EtOH, 30 min 95% EtOH, 2 × 30 min 100% EtOH. Samples were then critical point dried (Tousimis Autosamdri-815B, Rockville, MD), after which they were dissected and sputter coated with Au-Pd (Leica EM ACE600, Wetzlar, Germany). Samples were imaged in a Hitachi S-4700 field emission SEM equipped with a Oxford Instruments INCAx-act energy dispersive X-ray spectrometer. SEM images were imported into Adobe Photoshop for brightness and contrast adjustment.

Microslide Culturing

Enrichment cultures of *Leptothrix*-like organisms were grown in Fe(II)/O_2 gradients in either flat glass capillaries (Vitrocom, Mountain Lakes, NJ) or microscope growth chambers constructed from glass slides and coverslips, as described by Krepski et al. (2013). The inoculum was a sheath-rich freshwater mat sample collected from one of several sites (Christina Creek, Delaware (Krepski et al., 2012); White Clay Creek, Delaware; or Lakeside Drive stream, Maine (Fleming et al., 2014). Filtered environmental water was used as medium, and an opposing Fe(II)/O_2 gradient was constructed by adding FeS to one end and leaving the other end open to air. Still, mosaic, and time lapse imaging was performed either on an Olympus BX60 or Zeiss Axioimager microscope with Zeiss Axiovision.

DNA Extraction, Sequencing, and Analysis

DNA was extracted from two marine stalk-rich samples using the MoBio PowerSoil DNA Isolation kit. Tagged pyrosequencing of the V1-V3 region of the SSU rRNA gene was performed at the Research and Testing Laboratory (Lubbock, TX, USA). Sequences were classified using the SILVAngs pipeline against the SILVA reference database release 123 (Quast et al., 2013). Data were deposited at NCBI as short read archive accession number SRP072437. To avoid bias from microbes introduced during intact mat processing, we only analyzed and deposited Zetaproteobacterial sequences (876/4332, or 20% of high quality reads in Sample 1; 2777/7477, or 37% of Sample 2). Representatives from each OTU called by the SILVAngs pipeline were aligned against the Arb-SILVA database using the SINA Webaligner (Pruesse et al., 2012), added to a database of Zetaproteobacteria sequences, masked to 320 bp, and binned into OTUs using DOTUR (Schloss and Handelsman, 2005) to assign OTUs at 97% identity based on a curated alignment. Sequences were either assigned to known Zetaproteobacteria OTUs from McAllister et al. (2011) or considered new OTUs. Maximum likelihood phylogeny of our sequences was determined using RAxML 7.2.6 using the general time reversible (GTR) model with GAMMA approximation and 1000 bootstraps (Stamatakis, 2006).

RESULTS

Our previous work with natural Fe microbial mats taught us that the mats typically disaggregate under any significant shear force. Therefore, we developed a sampling and processing strategy in which we gently dislodge the mat from the substrate, minimizing disturbance during sample handling. Below, we describe the microstructure of two marine mats and one freshwater mat, in the context of their physical and chemical environments. Direct access to sheath-rich freshwater mats at Spruce Point allowed rapid fixation that maintained cells in their *in situ* positions. In combination with culturing in an Fe(II)/O_2 gradient microslide, we were able to show how sheathed FeOB make mats, which set the stage for a comparative analysis of stalk- and sheath-rich Fe mats.

Marine Stalk-Rich Fe Microbial Mat (Curd-Type), Loihi Seamount, Hawaii

The Fe-rich hydrothermal vents of the Loihi seamount host a range of Fe microbial mat types. Botryoidal mats are common on rock faces in close proximity to vent orifices (**Figure 2A**). Fe(II)-rich fluids flow diffusely through the mats and quickly across the face of the mats, with turbulent mixing entraining oxygen from surrounding waters. Here, aerobic microbial Fe oxidation corresponds to steep Fe(II)/O_2 gradients, meeting at the oxic/anoxic interface at or near the surface of the mat (**Table 2**).

These mats came apart in discrete chunks, and therefore are referred to as "curds." The curd-like mats formed in the path of venting fluid were smoother than the surrounding mats, and lighter in color, indicating they are less mineralized, which is typical of fresh mats. They easily disintegrate upon sampling; therefore a cylindrical ("scoop") sampler was used to gently dislodge and sample intact curds as shown in **Video 1**.

To get insight into the populations associated with newly-forming mats, we sequenced the small subunit (SSU) ribosomal RNA genes from subsamples of the intact curd mats and found that the Zetaproteobacteria mainly consisted of four operational taxonomic units (OTUs). Following Zetaproteobacterial OTU (ZOTU) designations outlined by McAllister et al. (2011), we found the normally rare ZOTU6 dominating the Zetaproteobacterial community in one intact curd sample (434 of 857, or 50.6% of Zetaproteobacterial sequences), while another sample was dominated by three novel ZOTUs, designated here as new ZOTU N1, N2, and N3 (combined, 1900 of 2735, or 69.5% of Zetaproteobacterial sequences) (Supplemental Figure 1).

Initial dissection revealed that the curd interior had a filamentous texture (**Figure 3A**). Microscopy revealed that an individual curd is composed of highly parallel stalks that all twisted in the same direction (**Figures 3B–E**). Continual branching produces more stalks, causing the radiation that results in the rounded shape of each curd (**Figures 2A**,

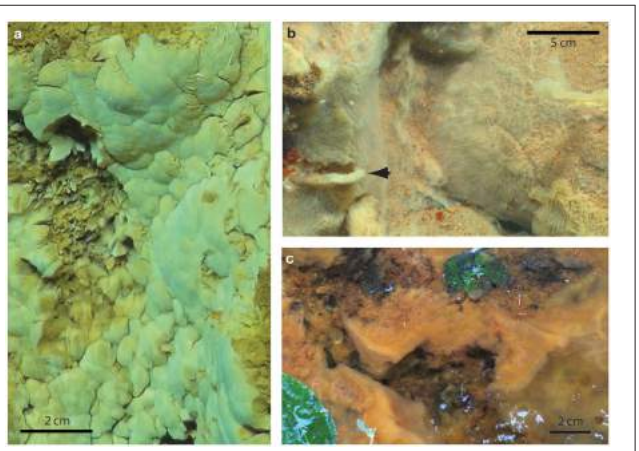

FIGURE 2 | Field pictures of Fe microbial mats. (A) Loihi marine curd mat (darker area on left side is an area where sample was removed), **(B)** Loihi marine veil mat; arrow denotes dislodged mat, showing thickness, **(C)** Spruce Point freshwater mat.

TABLE 2 | Oxygen concentration gradients in Loihi Fe mats.

Mat type, (location*)	$[O_2]$ at/near mat surface [μM]	$[O_2]$ below** mat surface [μM]	Fe(II) at/near mat surface [μM]	Fe(II) below** mat surface [μM]
Stalk-rich curd mat (Marker 38)	99.3	79.6	<10	<10
Stalk-rich curd mat (Marker 34)	32.7	<3	309	481
Stalk-rich curd mat (Marker 34)	24.6	10.5	<10	30.0
Sheath-rich veil mat (Marker 34)	37.7	33.1	<10	<10

Marker names correspond to sites described by Glazer and Rouxel (2009).

***For stalk-rich mats, measurements below mat surface were taken at ~7 cm depth. For sheath-rich mats, the measurement below the mat surface was taken at 1 cm depth, since the mats are much thinner.*

3C, **4**). Many stalks end at the boundaries between curds (**Figures 5A–C**). Using the branching patterns (e.g., **Figure 3D**), we were able to determine the direction of stalk growth, and therefore confirm that stalks grow toward the oxic exterior. Although we did not observe cells on the stalks, we deduce that they must have once been present at the stalk ends, at the leading edge of the mat. Many stalk ends thicken significantly just before termination (**Figures 5A,C,D**) or before thinning again (Supplemental Figure 2). We interpret this to be due to relatively rapid abiotic mineralization, since the stalks become featureless instead of showing the typical fibrillar structure observed with actively growing cells (Chan et al., 2011). This suggests that the environment temporarily became unfavorable, e.g., conditions that promote abiotic Fe oxidation, such as an increase in O_2 and/or Fe(II). These results demonstrate that an interplay of biotic and abiotic Fe oxidation contribute to overall mat structure.

While most of the stalks exhibit strong directionality, there are some exceptions (Supplemental Figures 3, 5, 6). At certain horizons of the curd mat, many or all stalks change direction, turning or coiling, overall exhibiting more random orientation (**Figures 5E–G**; see detailed documentation in Supplemental Figures 4–6). Such variation in stalk orientations has been observed in early stages of *M. ferrooxydans* culture, before strong gradients of Fe(II) and O_2 develop. These stalks likely record changes in some environmental cue; they may also contribute to the physical cohesiveness of the mat by acting essentially as a mesh that strengthens the mat fabric.

Marine Sheath-Rich Fe Microbial Mat (Veil-Type), Loihi Seamount, Hawaii

Although many Loihi mat samples are stalk-rich, sheaths have been observed as a minor component of bulk samples (Emerson and Moyer, 2002). In 2009, with improved lights and cameras aboard ROV Jason, we observed light orange-colored mat that appeared as a thin coating on other, darker orange microbial mats (**Figure 2B**). By sampling this approximately centimeter-thick surface layer, henceforth referred to as a "veil," we retrieved a mat that was dominated by sheaths. These sheaths bore a striking resemblance to *L. ochracea*; however, Fleming et al. (2013) demonstrated that these marine sheath-formers were Zetaproteobacteria, and not related to *L. ochracea*.

On previous cruises and in this study, we observed that veils typically form further away from focused vent flow, relative to the stalk-rich curd Fe mats. Away from vents, there is little to no visible flow, and correspondingly, shallow or undetectable chemical gradients. An O_2 concentration profile in a sheath-rich veil mat showed 38 μM O_2 at the surface, and 33 μM O_2 just below the surface. These mats appear fluffy and are typically thin (<2 cm thick), making it especially challenging to obtain discrete, intact mats from the seafloor. We sampled these mats either by using a suction sampler to carefully peel them away from their substrate, or by gently loosening the mat and then allowing it to fall into a tube ("scoop") sampler (**Video 2**).

As expected, the veils are composed primarily of sheaths of quite uniform width (**Figure 6**). In some areas, sheaths were parallel or subparallel (**Figure 6C**), while in other areas, it appeared there were two or more sets of sheaths interwoven, with bundles of parallel sheaths (**Figures 6D,E**). It is difficult to tell if sheathed cells grew contemporaneously in more than one direction, or if the woven pattern resulted from the growth of successive generations of sheath-formers that each move in a uniform direction. The texture is not an artifact of sampling; since the sheaths are delicate/brittle, damage typically causes a jumble of short, randomly-oriented sheaths, unlike the intact sheaths with significant directionality shown here (**Figure 6D**). In fact, we rarely observed sheath ends; instead, sheaths can often be traced entirely across the length of the sample. Sheaths are observed changing direction (i.e., turning), and there was not any significant thinning or thickening of sheath mineralization; both of these features suggest that sheathed communities experience more stable environmental conditions than the stalk-forming mats.

Colonization of Marine Mats by Other Fe-Mineralized Morphologies

Although a single morphology, stalk or sheath, comprised the primary framework of either curds or veils, both mat types included other morphologies. Because these morphologies are attached to stalks or sheaths, these likely represent secondary colonizers, and therefore can reveal insight into different ecological niches within a mat. For instance, some stalks are found colonizing sheath-rich mats (**Figure 7A**); however, we did not observe sheaths in the curd-mats. In all mats, stalks or sheaths were colonized by spherical structures; on closer

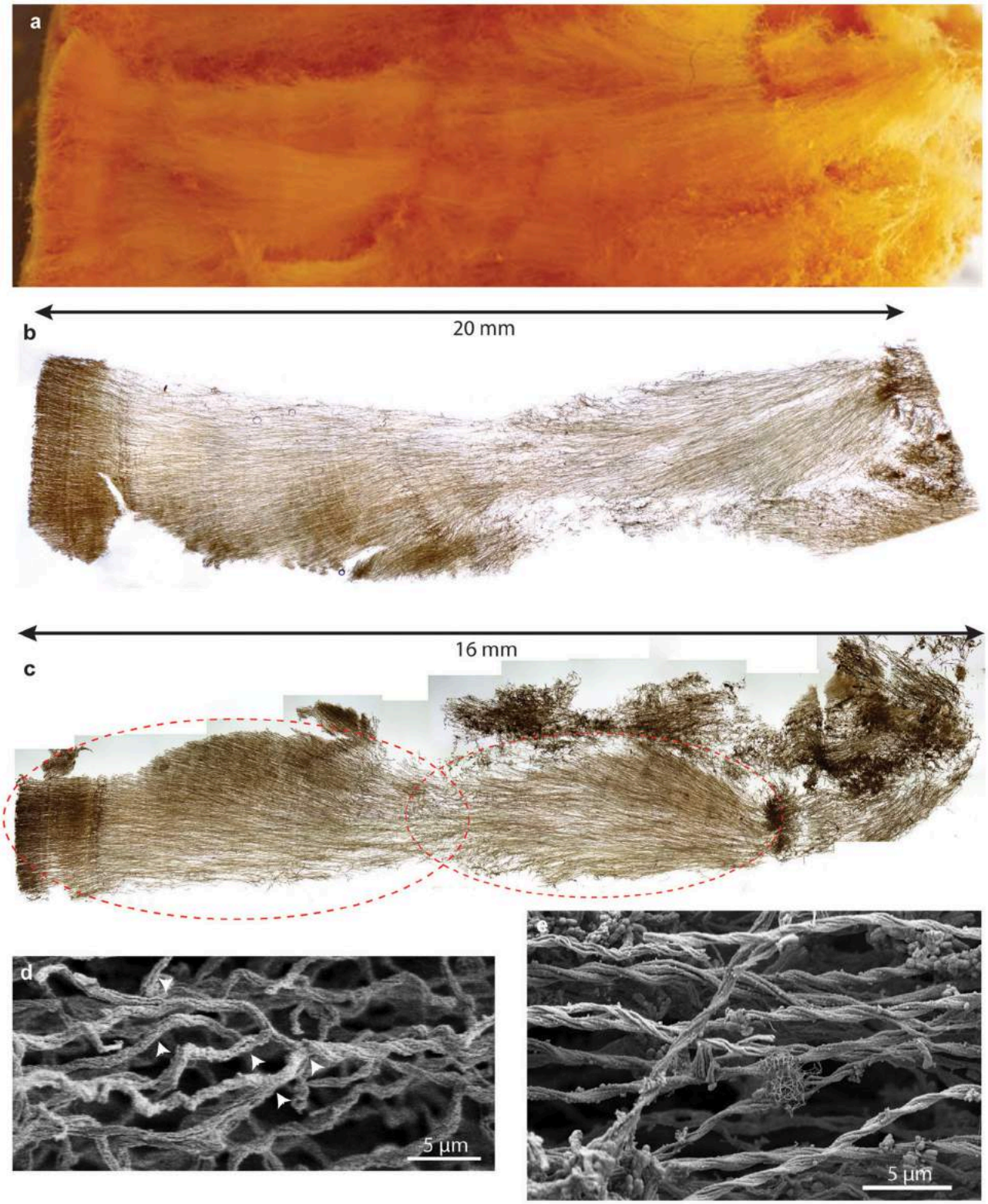

FIGURE 3 | Loihi stalk-rich curd mat. (A) Macroscopic view showing linear structure. **(B)** Thin section of mat similar to that shown in **(A)**; same scale. **(C)** Thin section of another curd mat showing curd structure as radiating filamentous sections. **(D,E)** SEM images showing multiple branch points **(D)**, which result in radiation. **(E)** parallel, uniform width stalks all twisting in the same direction, suggesting coordinated growth and biomineralization.

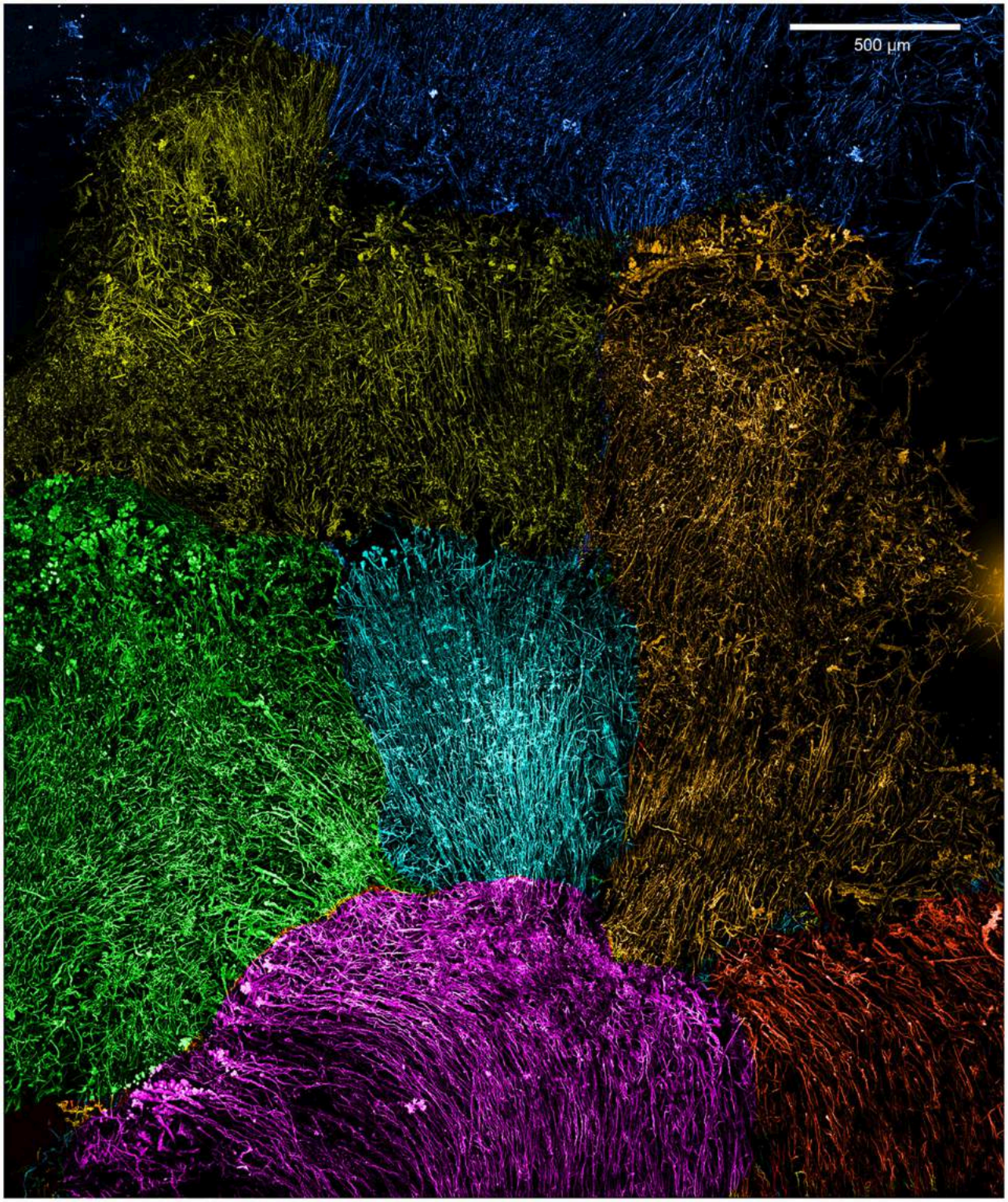

FIGURE 4 | Loihi stalk-rich curd mat confocal image, colored to highlight individual curds.

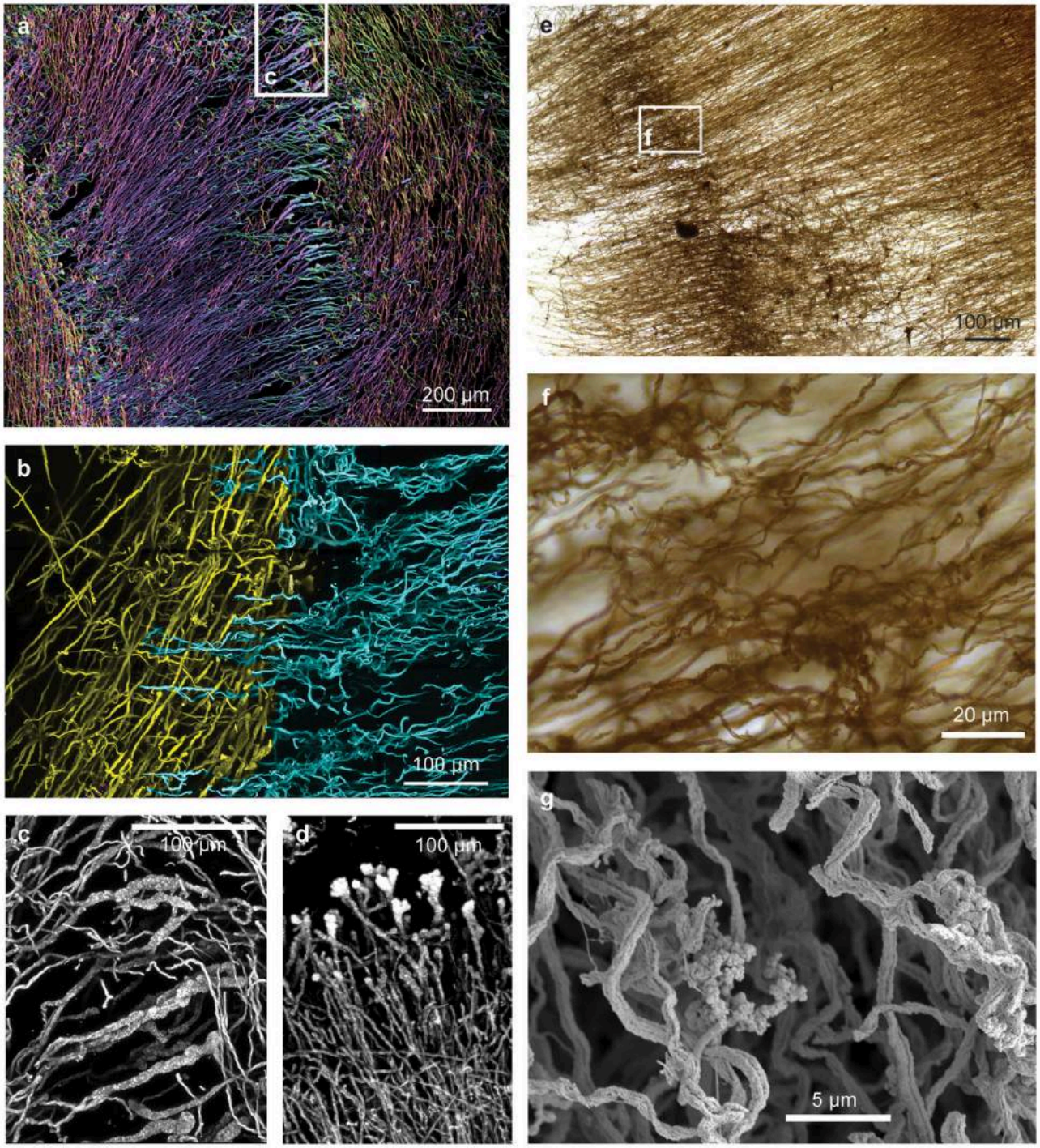

FIGURE 5 | Confocal and light microscopy images of Loihi curd mat stalks. (A) Changes in stalk directions define curd boundaries. Some stalks thicken before they terminate. This image is colorized based on depth within the sample slice. **(B)** Interfaces between areas of different stalk directions; Horizontal (blue) stalks have colonized vertical (yellow) stalks. **(C,D)** Stalks that thicken at the terminal ends. **(E–G)** Mat horizon, or band, in which stalks lose their strong directionality, and instead bend and coil. See Supplemental Figures 4–6 for more images and measurements of directionality.

examination by SEM, these structures are fibrillar, resembling rounded nests (**Figures 7A,B**). This is similar to *Siderocapsa*, a group of freshwater microbes morphologically defined by their Fe-mineralized capsules (Hanert, 2006). Like *Siderocapsa*, it is likely that a cell was at the center of the nests excreting Fe oxyhydroxide fibrils.

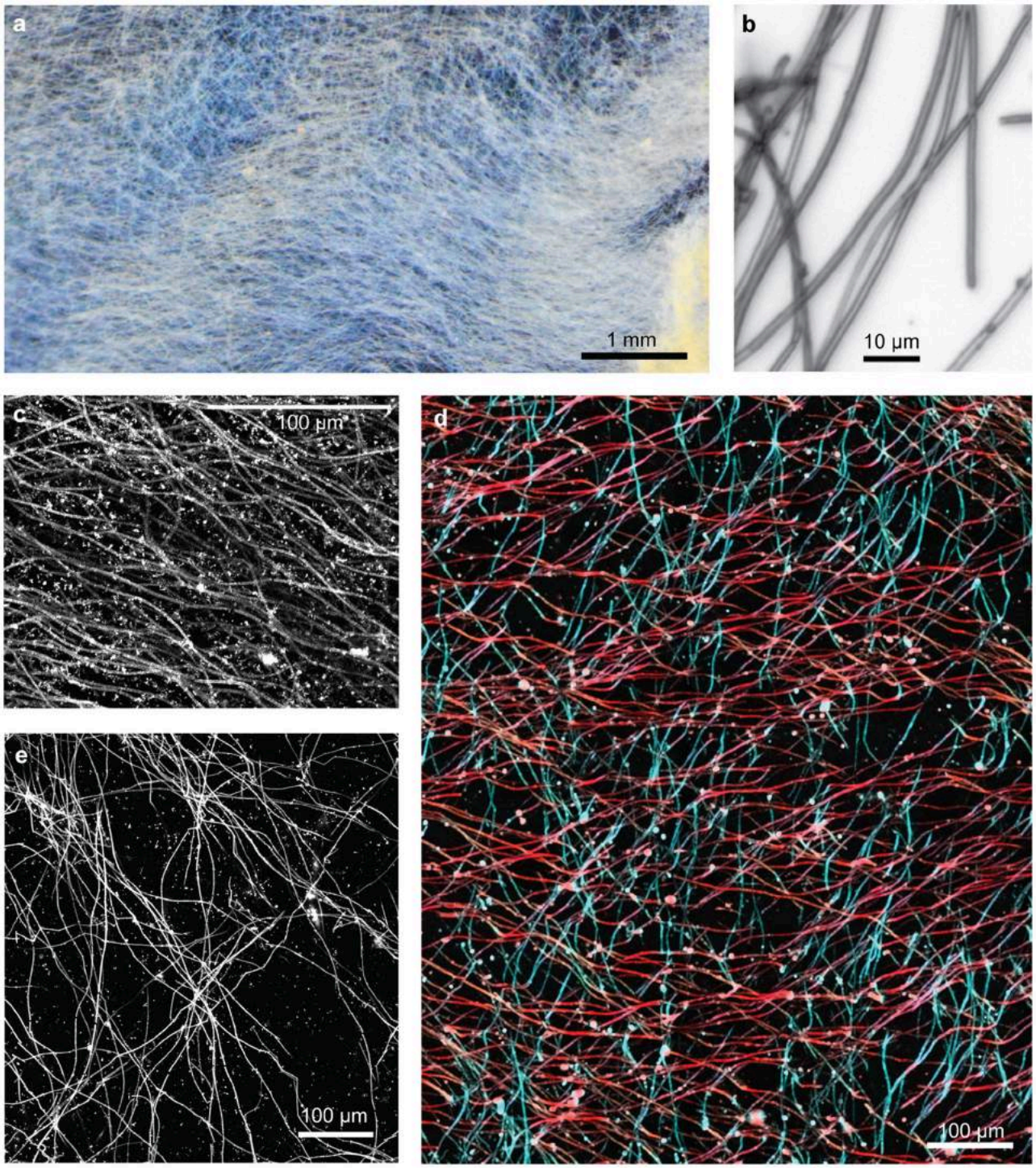

FIGURE 6 | Loihi sheath-rich veil mat. (A) Stereoscope image of embedded mat section showing an overall horizontal preferred orientation. **(B)** Light micrograph showing tubular sheaths. **(C–E)** Confocal images: **(C)** sheaths in a single orientation, **(D)** sheaths in two orientations, colored in red and blue, **(E)** bundles of sheaths in multiple orientations result in web-like structure.

Another structure that has commonly been observed in marine iron mats are short (∼5–50 µm) Y-shaped tubular filaments (Emerson and Moyer, 2010; Breier et al., 2012; Moeller et al., 2014; Peng et al., 2015). In the intact mats these structures were commonly observed colonizing either the sheaths or stalks (**Figure 6**). The Y's are composed of a flattened hollow tube made

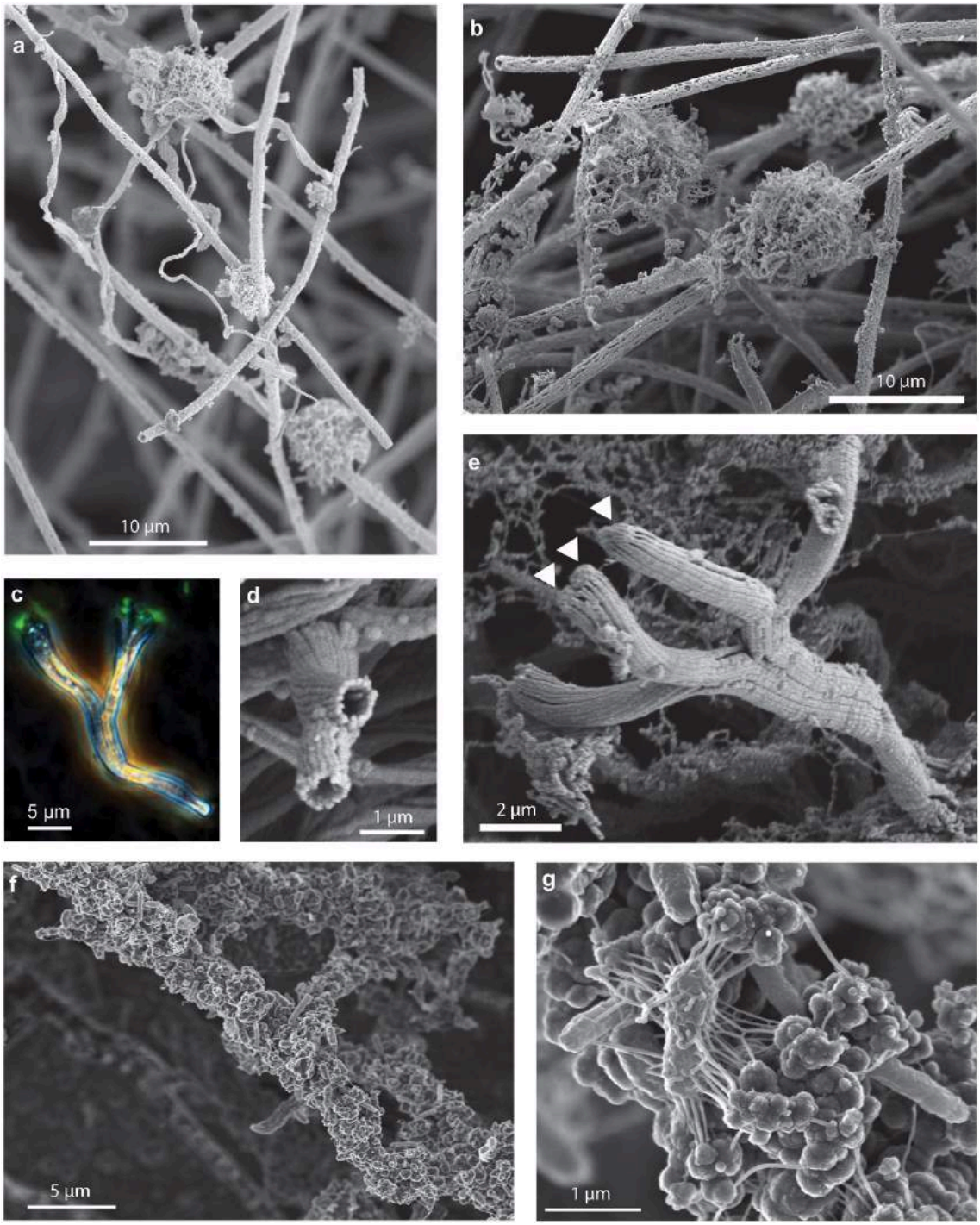

FIGURE 7 | Secondary colonizers include distinct Fe oxyhydroxide morphologies that colonize stalks and sheaths. SEM images of **(A)** stalks and fibrillar nests colonizing sheaths and **(B)** fibrillar nests on sheaths. **(C–E)** Branching tubes: **(C)** phase contrast/fluorescence image showing branching tubes with cells (arrows) on the end. **(D)** SEM image of end-view of branching tubes missing cells, **(E)** SEM image of branching tubes with cells (arrows) on the end, **(F,G)** filaments encrusted with amorphous oxides, cells, and EPS.

up of multiple Fe oxide fibrils. Much like stalks, a single cell can be found at the terminal end of the tube (**Figures 7C,E**), and when it divides the tube bifurcates producing the Y-structure; longer structures have been observed to twist. The different distributions of nests and Y's suggests that they colonize a particular geochemical niche distinct from that of the stalk- and

sheath-rich mat formers. Based on these observations, it is likely these secondary colonizers are adapted to grow at the lower O_2 concentrations that exist deeper in the mat.

Upon aging, mats become darker colored and often exhibit thicker mineralization. In these regions of the mat, filaments are thickly coated in amorphous mineralized structures and cells (**Figures 7F,G**), which probably represent other phylotypes and functional groups.

Freshwater Sheath-Rich Mat, Spruce Point, Maine

We sampled intact freshwater iron mats at Spruce Point, Maine, from a rock-lined ditch with water depths of 3–10 cm, and a slow flow rate on the order of 0.5 cm s^{-1}. The mats had complex morphologies including dams, small channels, and puffballs (**Figure 2C**) similar to those described by Schieber and Glamoclija (2007). Intact mat samples were collected at the leading edge of mats that had small channels (2–5 cm wide) of water flowing between them. The edge of the mat formed perpendicular to the flow of the water and was clearly visible as a lighter, whitish edge, in contrast to the more orange mats farther back from the channel. Oxygen concentrations at the mat surfaces do not differ much from those within the mat (**Table 3**). An Fe(II) transect showed that Fe(II) was present both in the mat and also the surrounding water, with a depletion in Fe(II) within the top centimeter of the mat (57 μM in top cm, vs. 111 μM outside mat, 190 μM inside mat; see full profile in Supplemental Figure 7).

TABLE 3 | Oxygen profiles in Spruce Point mats.

	1 cm in front of mat	Mat surface	1 cm inside mat
Closer to groundwater source	22 μM	21 μM	18 μM
Further downstream from source	58	58	57
Further downstream from source	59	58	60

The dominant morphotype in the Spruce Point mats was hollow sheaths typical of *L. ochracea* (**Figure 8**). Because we were able to embed and thus preserve the mat structure within minutes after sampling, we could image the native cell distribution. Remarkably, nearly all the filaments of *L. ochracea* cells were located at the leading edge of the mat. The bulk of the mat interior was composed of empty sheaths, colonized by other bacteria (**Figure 8**). The terminal ends of the sheaths were visibly less mineralized than the rest of the empty sheaths (**Figure 8A**). The sheaths are roughly parallel to one another (**Figures 8B,D,E**; see

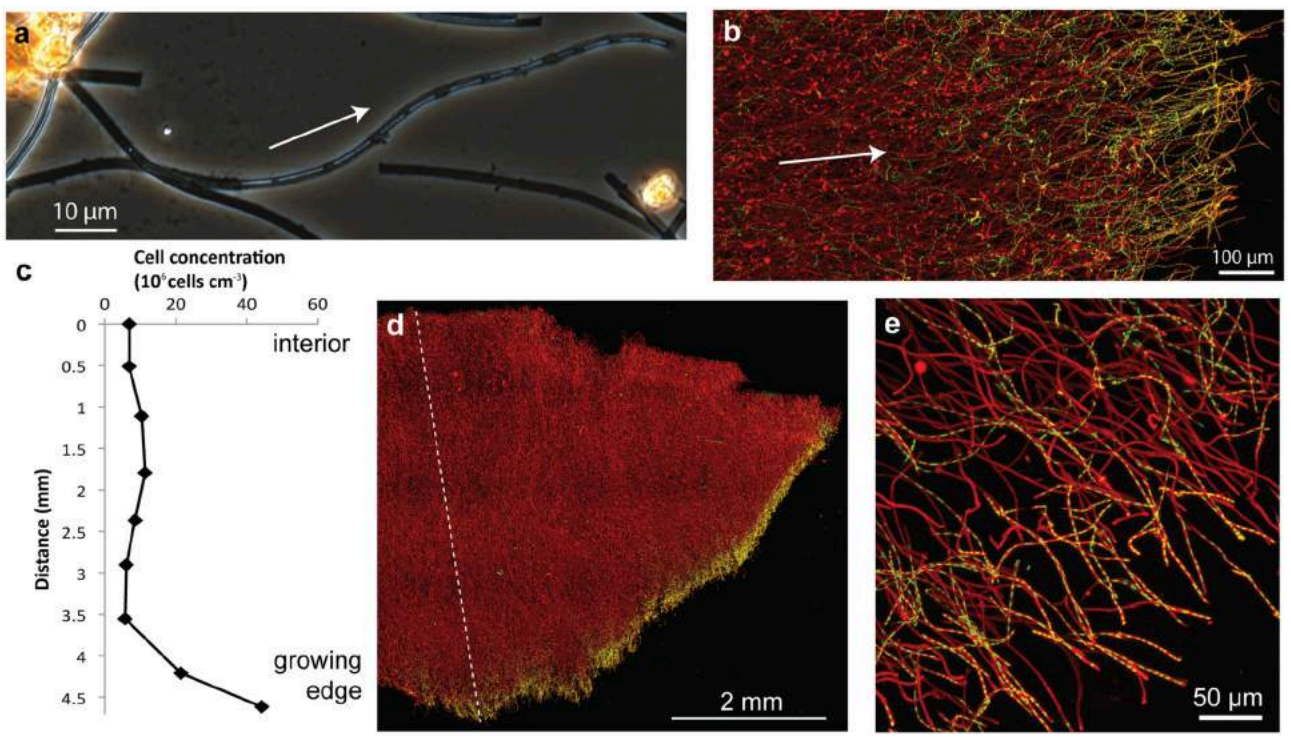

FIGURE 8 | Spruce Point mat confocal images and data showing that mat was produced by sheath-forming cells. Arrows show inferred direction of growth. **(A)** Phase contrast light micrograph showing cells at the ends of filaments, surrounded by sheath, which is lighter (less mineralized) than empty sheaths. **(B)** Confocal image of edge of mat showing many cell filaments parallel to the direction of growth, particularly those at the mat edges; but some cells filaments behind the leading edge are non-directional. Cells (green, SYTO) and Fe oxyhydroxides (red, rhodamine-conjugated SBA lectin) **(C)** Cell concentration in transect across mat shown in **(D)**. See dashed line for cell counting transect. **(D)** Overview of intact mat showing cells concentrated at growing edge of mat. **(E)** Cells inside the ends of tubular sheaths, at the edge of the mat.

Video 3 for 3D view of confocal data). Although most of the cell filaments are parallel to the overall direction of growth, a small proportion lack this directionality, which leads to some tangling that may help hold together the structure thus stabilizing the mat within stream flow.

Leptothrix Sheath Formation and Behavior

To better understand how sheath-forming FeOB make mats, and link behavior with morphology, we used time-lapse microscopy to observe cell growth and sheath formation in opposing Fe(II)/O_2 gradients. Using native mats as inoculum, we were able to image cells producing sheaths. Within 30–60 min of inoculation, filaments of cells were observed at the ends of sheaths (∼17 cells in **Figure 9A**). The cells rapidly left behind empty Fe oxyhydroxide coated sheath at the trailing end (**Figure 9A**, **Videos 4**–**7**). This confirms that multiple cells are responsible for the formation of each sheath. Since cells continuously leave behind the sheath, it is a record of *Leptothrix* cell growth, movement, and behavior.

In densely inoculated microslides, it was possible to follow the growth and response of a population of *L. ochracea* cells to opposing gradients of Fe(II) and O_2. Sheaths elongated away from the inoculum and FeS, toward O_2 (**Figures 9B,D** and **Video 7**). Initially, sheaths grew in this direction rapidly (rates varied, but measured at 19 μm/min in **Video 4**), and the filaments were relatively straight. After some time, the sheaths formed a denser band (**Figures 9B,C**), and the ensheathed cell filaments showed less directionality, instead coiling to different degrees (varying radius and pitch; **Figure 9E**). This may be akin to the loss of directionality in certain bands of the Loihi stalk-rich mat (**Figures 5E–G**).

DISCUSSION

The work presented here clearly demonstrates that FeOB produce organized microbial mats, rather than "Fe flocs," as they are commonly referred to, since flocculation implies aggregation of cells and minerals after precipitation. Instead, filament-producing FeOB grow in coordination to produce a highly structured, albeit delicate, mat comprised of Fe oxyhydroxide biominerals that are the direct result of their lithotrophic metabolism (**Figure 10**). The structure of any individual mat is likely driven by the physiological and behavioral responses of specific FeOB to a combination of hydrologic dynamics and fluxes of key substrates like O_2 and Fe(II). Obviously physiology and behavior have strong genetic components, but we observed remarkable commonalities in Fe mats produced by phylogenetically different FeOB in varied environments. Here we discuss the connections between the Fe oxidation metabolism

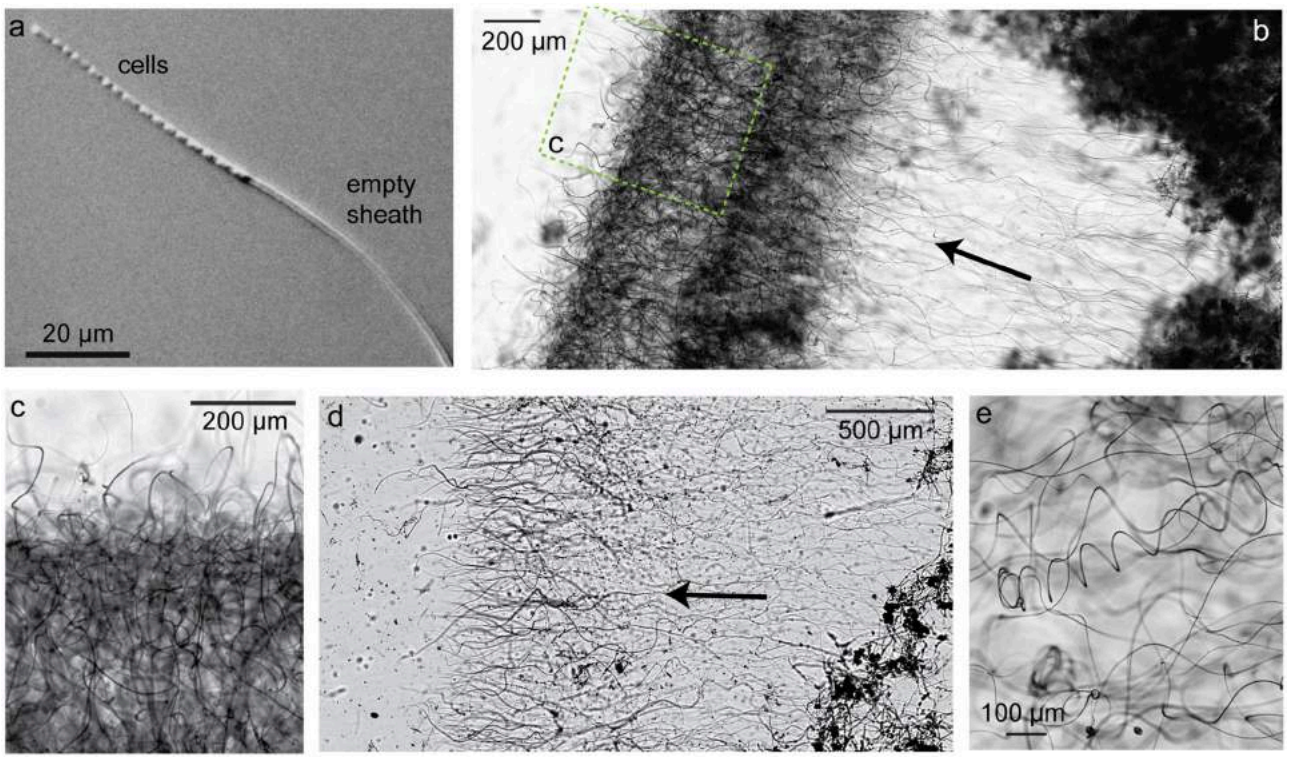

FIGURE 9 | Light micrographs of sheath-former *Leptothrix ochracea* enriched in a microslide growth chambers. Arrows indicate growth direction. **(A)** Individual *Leptothrix* sheath with cells at growing end. **(B)** Directional growth (arrow) from inoculum (dark material on right) and formation of dense growth band, likely at an optimal position in redox gradient. **(C)** Enlarged detail of denser growth band. **(D)** Directional growth in another microslide. **(E)** Within the growth band, some sheaths are coiled. See also **Videos 4**–**7**.

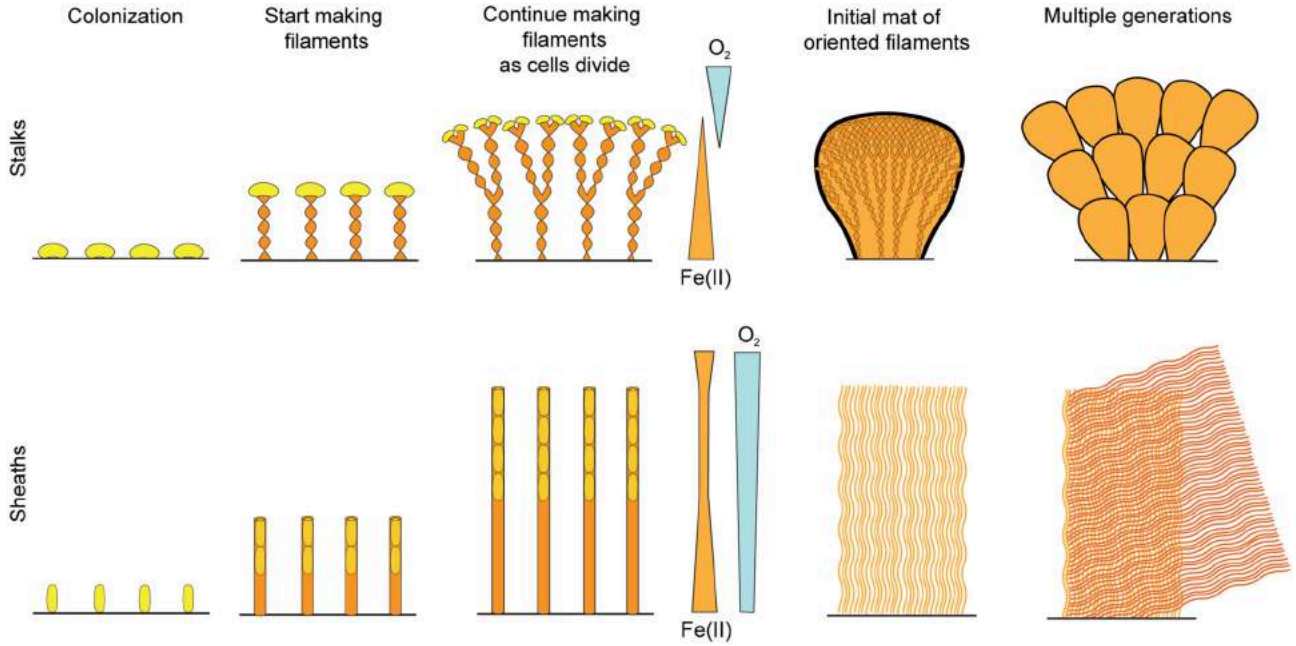

FIGURE 10 | Conceptual model of stalk- and sheath-rich mat development.

and mat structure, focusing on how adaptations could drive the common architecture between Fe microbial mats.

Sheath-Forming Organisms Use Biomineral Filaments to Attach to Surfaces and Remove Waste, Much Like Stalks

Our results show commonalities between Fe-mineralized stalks and sheaths that suggest they are used for similar purposes. As with stalks, *L. ochracea* sheaths are produced by cells growing at one end, leaving behind an Fe oxide mineralized filament (**Figure 10**). In both cases, one end of the filament is attached to a substrate, operating as a holdfast, while stalk/sheath production occurs as cells continuously produce Fe oxides. While sheaths are thought to serve as protection, e.g., from predation, dehydration, and harmful radiation (Ghiorse, 1984), such functions do not require such massive production of sheath, as is the case here. Thus, we observe that the cells use their mineral byproducts as an attachment and support structure; that is, both the twisted stalk and sheath, as well as the tubular Y structure, can be functionally considered a "stalk."

It has been noted that most Fe sheaths are empty (Mulder and van Veen, 1963; Emerson and Revsbech, 1994); similarly, stalks are more abundant than cells, by volume. This may be explained by the low free energy available from Fe(II) oxidation, about $-90\,kJ\ mol^{-1}$ Fe(II), which means a significant amount of Fe is required for C fixation (~43–70 mol of Fe(II) per mol C) (Neubauer et al., 2002; Sobolev and Roden, 2004). If all of the Fe is used to make stalks or sheaths, the consequence is relatively few cells leaving behind a comparatively large mineral-based structure. This is what we observed in the Spruce Point mat (**Figure 8**), where the *L. ochracea* cells primarily occupy the outer fringe of the mat, which is largely composed of empty sheaths (**Figure 8**). In the marine mats we were not able to image cells, but in the case of the stalk-based curd mat, we can infer that cells were present at stalk ends at the mat exterior. The structure of both the stalk and sheath mats are consistent with a strategy to remove Fe(III) waste products, leave the oxides behind in the mat, and thus prevent cell mineralization/encasement.

Both Sheath- and Stalk-Rich Fe Mats are the Result of Coordinated Growth and Motility/Taxis

A common feature of the mats and the *L. ochracea* culture is the highly parallel nature of the stalks and sheaths; in addition, stalks twist in the same direction. Together, this suggests that the mat-forming cells coordinate their movement and growth, advancing as a unified front. In part, the coordinated cellular response is likely driven by external stimuli, but it is also likely there is cell-cell communication within the mat. In the alternative scenario, with neither a stimulus or communication, stalks or sheaths would be randomly oriented, and cells would not be so concentrated at the mat edge. Instead, in the mats and cultures, random filament orientation is rare and confined to specific horizons/bands as discussed below, giving further evidence that orientation represents a community response.

This unified front of cells may be a response to gradients of Fe(II) and O_2, as seen in microslide growth experiments. The enrichments of *L. ochracea* sheaths grew in the direction of increasing O_2 (**Figure 9**, **Videos 4**–**7**), much like previous

observations of *M. ferrooxydans* stalk formation in microslides (Chan et al., 2011). Directional growth was also observed for *G. ferruginea*, though the direction of chemical gradients was not documented (Hanert, 1973). Once opposing Fe(II)/O_2 gradients developed and presumably stabilized (i.e., formed an Fe(II)/O_2 interface), the directional *L. ochracea* sheath growth ceased. At this point, we observed development of dense oxide bands that consisted of sheaths that either coiled tightly or turned perpendicular to the gradient; both strategies allow the sheath-formers to continue making the sheath while staying close to the narrow region in which they can access both Fe(II) and O_2. This further suggests that continuous sheath formation is necessary during Fe oxidation and growth; otherwise cell growth should continue without sheath formation. Similar bands were not observed in the sheath mats from Loihi or Spruce Point, but this likely corresponds to the shallow to non-existent gradients of Fe(II) and O_2 (see discussion in section Relationships between Filament Morphology, Niche, and Behavior). We do however, see thin bands of random orientation including some coiling in stalk mats. In this case, however, the directionality returns, raising the possibility that the mat is responding to changes in the flow and/or chemical composition of the vent fluid.

This brings us to the intriguing question of how cells move while also producing biominerals. In fact, *L. ochracea* cells appear to use biomineralization as a mechanism for motility, much like stalk-formers. In previous live culture imaging of *M. ferrooxydans*, we saw that a stalk was used to attach to substrate and then propel the cell forward (Chan et al., 2011). In the current study, we show a natural population of *L. ochracea* uses the sheath in a similar manner, but with the difference that tens of cells in a filament worked in coordination to produce a single sheath. While other organisms are known to assemble structures to propel themselves (e.g., Goldberg, 2001), a fascinating aspect of FeOB behavior is that the cells are entirely in the aqueous phase and not attached to any surface, i.e., they are not gliding along a surface or through a gel/matrix. In the case of the sheath, this raises interesting questions about how a sheathed filament of cells is able to propel itself. Cell movement would be constrained by the sheath, so are the cells extruding the sheath in such a way to direct their motion? If FeOB cells are somehow able to use production of a rigid sheath or stalk to translocate, this would represent a novel means of bacterial motility. If extrusion of biomineralized stalks and sheaths is indeed a form of motility, then the cells are cleverly using their Fe(III) waste to precisely control their position within the environment.

Fe Mat Formers Engineer Habitats That Promote Fe Oxidation

Although Fe microbial mats share basic characteristics with other microbial mats and biofilms, they also have fundamental differences that are likely related to Fe oxidation. The Fe mats most closely resemble mats produced by sulfur-oxidizing bacteria, including *Arcobacter sulfidicus*, a marine S-oxidizer that produces filamentous S(0)-structures (Taylor and Wirsen, 1997; Sievert et al., 2007). Sievert et al. suggest that the filamentous S(0) is an adaptation to rapid mineralization (in this case, detoxification of high sulfide levels) and maintaining position within the oxygen/sulfide interface. However, *A. sulfidicus* is unusual amongst the S-oxidizers; others such as *Beggiatoa, Thiothrix,* and various Epsilonbacteria form streamers and other mat-like structures, much like other microbes, in which cells themselves are the primary building block of the mat (Campbell et al., 2006; Teske and Salman, 2014). Another important group of mat-building microbes, the cyanobacteria, also produce a dense network of cells bound together by extracellular polymer substances (EPS) structures, sometimes also including sheaths (e.g., Fenchel and Kühl, 2000). Degradation of EPS by other microbes is thought to result in carbonate precipitation to produce a mineralized structure (e.g., Dupraz and Visscher, 2005), but this occurs below the zone of cyanobacterial growth. In contrast to the typical mats that are dense aggregates of cells and EPS, all of the Fe mats we analyzed are primarily built from Fe oxyhydroxide filamentous biominerals with little interstitial EPS, but a vast amount of open pore space. This distinctive architecture has benefits that meet the specific challenges of chemolithotrophic Fe oxidation metabolism, most notably the need to get rid of Fe oxhydroxide waste without entombing cells or clogging flow paths through the mat.

The mat-forming FeOB thus create a framework with high surface area and permeability, which presents an opportunity for other colonizing organisms. In fact, much of the the mat interior community is likely composed of secondary colonizers. These include FeOB, as evidenced by the Fe-mineralized structures shown in **Figure 7**. A prime example of this is the Y-shaped FeOB that we observed colonizing the stalks and sheaths at Loihi. These fascinating organisms produce unique flattened tubular Fe-oxyhydroxide casings that have been observed previously in marine Fe mats. But for the first time here, SEM (**Figure 7E**) reveals a detailed juxtaposition of cells and their mineral structure, suggesting that as these FeOB grow and divide, they produce Y-shaped branching structures similar to the branching stalks. These entire structures are relatively short with total lengths that typically range from 5–50 μm, which enables them to fit into the mat structure. Likewise, other colonizing structures (e.g., nests) are also more compact than the filaments. The porous framework structure constructed by the stalks and sheaths provides plenty of room for colonizing cells, polymers, and biominerals. In this way, the stalk- and sheath-forming FeOB are keystone species and ecological engineers. They are the first to colonize the Fe-rich environment, providing a physical habitat conducive to further Fe oxidation and likely other metabolisms.

Investigating the Identities of Mat-Forming FeOB

Although Fe stalk- and sheath-formation is the most well-known trait of neutrophilic FeOB, and clearly critical to Fe mat formation, it appears to be a task performed by many, but not all FeOB. For instance, freshwater stalk-formers are all members of Gallionellaceae within the Betaproteobacteria, but some Gallionellaceae (e.g., *G. capsiferriformans* and *Sideroxydans lithotrophicus*) do not make stalks or any organized extracellular structure (Emerson and Moyer, 1997). Marine stalk-forming

FeOB isolates are all members of the genus *Mariprofundus* within the Zetaproteobacteria (ZOTU11, as defined by McAllister et al., 2011), but new isolates of marine FeOB, including one that is nearly 97% similar by SSU rRNA to *Mariprofundus ferrooxydans*, do not form stalks either (Emerson and Barco unpublished data). These findings show that FeOB have alternative strategies for ridding themselves of Fe-oxyhydroxides (e.g., shedding smaller oxides; Kato et al., 2015; Field et al., in press), and suggest that stalk formation is a specialized task performed by specific members of the community.

Because there are not defined phylogenetic clusters of stalk- or sheath-formers, or genetic markers, we are still trying to determine the phylogenetic distribution of these organisms, to ultimately understand how these abilities evolved. Our molecular analysis of these relatively fresh, intact Loihi mats did not find members of the ZOTU 11 that includes the stalk-former *M. ferrooxydans*; instead ZOTU 6 and novel ZOTUs accounted for most of the Zetaproteobacteria. Thus it is possible that one or more of these OTUs, for which there are no cultured representatives, is a stalk former. However, as a note of caution, stalk-forming cells may be rarely observed in molecular studies since they are concentrated on the exterior of the mat (as seen in a freshwater mat; Mitsunobu et al., 2012), though we tried to include these cells by sampling the freshest mat possible. Another approach by Rassa et al. (2009) involved leaving sterile substrate near the vents for colonization. They found that ZOTU6 is a vanguard organism, consistent with our results, supporting the possibility that there are multiple groups of marine stalk-forming Zetaproteobacteria FeOB.

Relationships between Filament Morphology, Niche, and Behavior

We observed marine stalk-formers growing at the interface of steep Fe(II) and O_2 gradients (near vents), while sheath-formers appear to be associated with higher O_2 concentrations in low or undetectable gradients (e.g., at the periphery of vent sites at Loihi), consistent with previous studies (Fleming et al., 2013, 2014; Krepski et al., 2013). These contrasting niches can help explain differences in filament formation and resulting morphology. Specifically, how fast cells move likely corresponds to the type of gradients they prefer. *Leptothrix* sheath formation is much faster than Zetaproteobacteria stalk formation (19 μm min^{-1}, compared to 2 μm h^{-1} stalk formation rate observed for *M. ferrooxydans*), likely related to the number of cells involved. Because the sheath formers live in shallow gradients, they can likely move further than other FeOB while still maintaining their niche; this probably accounts for the lack of observable sheath ends/terminations in our centimeters-size samples. In contrast to sheaths and stalks, the branching tube "Y" structures are much shorter, which may correspond to a strategy in which they stop mineralizing and colonize elsewhere more frequently, suggesting they either have highly specific niche requirements or live in a less stable environment. Stalk twisting/coiling and sheath coiling may be related to gradient sensing and therefore chemotaxis; tighter coiling may represent efforts to minimize net motion. As we learn more about FeOB behavior, we will be able to translate morphology to environmental signals, and therefore niche. This behavior is instantly preserved as Fe oxhydroxide biominerals form, making Fe mats highly unusual in that their structure is a continuous record of FeOB metabolism.

Prospects for Interpreting Fe Microfossils

If Fe mats are rapidly encased in silica or carbonate, they can be preserved long term as microfossils, and thus serve as very specific records of metabolism and niches. Indeed, there are many instances of filamentous Fe microfossils in the rock record, ranging from recent to 1.7 Ga (Little et al., 2004; Slack et al., 2007; Crosby et al., 2014), many of which appear to be intact mats. Although there is a general sense that these are biogenic, we have until recently lacked detailed characterizations of modern equivalents. Such data can help determine if these microfossils represent aerobic Fe-oxidizing bacteria, and how to interpret paleoenvironmental chemistry and setting. Recent work on *M. ferrooxydans* gave us our first detailed observations of behavior and stalk morphology (width, branching, directionality), connecting biomineral textures to Fe oxidation metabolism and oxygen preferences for a single organism (Krepski et al., 2013). Here we have extended this to natural Fe mats, which show us examples of more complex texture that can be linked to environmental and perhaps ecological dynamics. Synthesizing our culture work with observations of natural mats improves our understanding of the developmental history of the mat. This allows us to look for uniquely biological features and read the mat morphologies as a history. Because the morphologies are specific to the aerobic Fe oxidation metabolism, finding and positively identifying Fe microfossils has the potential to improve our understanding of Earth's Fe and oxygen history.

AUTHOR CONTRIBUTIONS

CC conceived of the study and both CC and DE developed and directed the research. All authors participated in sampling, and conducted analyses, as follows: Light and confocal microscopy (SM, AL), SEM and molecular biology (SM), Loihi geochemistry (BG), Spruce point geochemistry (AL, DE), time lapse light microscopy (SK). CC wrote the manuscript, with major contributions from DE, and edits from all coauthors.

FUNDING

This work was funded by NSF grants OCE-1155290 to CSC, OCE-1155754 to DE, NASA grant NNX12AG20G to CSC and DE, and a Delaware Space Grant Fellowship to SMM (NASA Grant NNX10AN63H).

ACKNOWLEDGMENTS

We thank the crew of R/V Thompson and ROV Jason II for cruise/sampling assistance. Sample preparation and imaging were performed at the University of Delaware Bioimaging Facility, Bigelow Laboratory, and the Jackson Labortaory. We acknowledge Jean Ross and Mark Lessard for help with

vibratoming, Mike Moore, Jeff Caplan, and Adam Mumford for help with confocal imaging and image processing, and Deborah Powell for SEM imaging.

SUPPLEMENTARY MATERIAL

The Supplementary Material for this article can be found online at: http://journal.frontiersin.org/article/10.3389/fmicb.2016.00796

Video 1 | Sampling stalk-rich curd-type mat at Loihi seamount.

Video 2 | Sampling sheath-rich veil-type mats at Loihi seamount.

Video 3 | 3D rendering of confocal imaging of Spruce Point sheath-rich mat, showing directionality of sheaths.

Video 4 | Time lapse light micrograph series of sheath formation by multiple cells. Inoculum from Fe seep in Rittenhouse Park, Delaware.

Video 5 and 6 | Time lapse light micrograph series of a sheaths being formed by cells. Inoculum from Lakeside Drive, Maine Fe mat.

Video 7 | Time lapse light micrograph series of sheath formation, demonstrating growth towards higher oxygen concentration (left side of imaged area). Inoculum from Fe seep in White Clay Creek, Delaware.

REFERENCES

Banfield, J. F., Moreau, J. W., Chan, C. S., Welch, S. A., and Little, B. (2001). Mineralogical biosignatures and the search for life on Mars. *Astrobiology* 1, 447–465. doi: 10.1089/153110701753593856

Baskar, S., Baskar, R., Thorseth, I. H., Ovreås, L., and Pedersen, R. B. (2012). Microbially induced iron precipitation associated with a neutrophilic spring at Borra Caves, Vishakhapatnam, India. *Astrobiology* 12, 327–346. doi: 10.1089/ast.2011.0672

Breier, J. A., Gomez-Ibanez, D., Reddington, E., Huber, J. A., and Emerson, D. (2012). A precision multi-sampler for deep-sea hydrothermal microbial mat studies. *Deep Sea Res. Part I* 70, 83–90. doi: 10.1016/j.dsr.2012.10.006

Brendel, P. J., and Luther, G. W. (1995). Development of a gold amalgam voltammetric microelectrode for the determination of dissolved Fe, Mn, O2, and S(-II) in porewaters of marine and freshwater sediments. *Environ. Sci. Technol.* 29, 751–761. doi: 10.1021/es00003a024

Bristow, G., and Taillefert, M. (2008). VOLTINT: a matlab®-based program for semi-automated processing of geochemical data acquired by voltammetry. *Comput. Geosci.* 34, 153–162. doi: 10.1016/j.cageo.2007.01.005

Campbell, B. J., Engel, A. S., Porter, M. L., and Takai, K. (2006). The versatile epsilon-proteobacteria: key players in sulphidic habitats. *Nat. Rev. Microbiol.* 4, 458–468. doi: 10.1038/nrmicro1414

Chan, C. S., Fakra, S. C., Emerson, D., Fleming, E. J., and Edwards, K. J. (2011). Lithotrophic iron-oxidizing bacteria produce organic stalks to control mineral growth: implications for biosignature formation. *ISME J.* 5, 717–727. doi: 10.1038/ismej.2010.173

Crosby, C. H., Bailey, J. V., and Sharma, M. (2014). Fossil evidence of iron-oxidizing chemolithotrophy linked to phosphogenesis in the wake of the Great Oxidation Event. *Geology* 42, 1015–1018. doi: 10.1130/G35922.1

Druschel, G. K., Emerson, D., Sutka, R., Suchecki, P., and Luther, G. W. (2008). Low-oxygen and chemical kinetic constraints on the geochemical niche of neutrophilic iron(II) oxidizing microorganisms. *Geochim. Cosmochim. Acta* 72, 3358–3370. doi: 10.1016/j.gca.2008.04.035

Dupraz, C., and Visscher, P. T. (2005). Microbial lithification in marine stromatolites and hypersaline mats. *Trends Microbiol.* 13, 429–438. doi: 10.1016/j.tim.2005.07.008

Edwards, K. J., Glazer, B. T., Rouxel, O. J., Bach, W., Emerson, D., Davis, R. E., et al. (2011). Ultra-diffuse hydrothermal venting supports Fe-oxidizing bacteria and massive umber deposition at 5000 m off Hawaii. *ISME J.* 5, 1748–1758. doi: 10.1038/ismej.2011.48

Emerson, D., Fleming, E. J., and McBeth, J. M. (2010). Iron-oxidizing bacteria: an environmental and genomic perspective. *Annu. Rev. Microbiol.* 64, 561–583. doi: 10.1146/annurev.micro.112408.134208

Emerson, D., and Moyer, C. (1997). Isolation and characterization of novel iron-oxidizing bacteria that grow at circumneutral pH. *Appl Environ. Microbiol.* 63, 4784–4792.

Emerson, D., and Moyer, C. (2010). Microbiology of seamounts: common patterns observed in community structure. *Oceanography* 23, 148–163. doi: 10.5670/oceanog.2010.67

Emerson, D., and Moyer, C. L. (2002). Neutrophilic Fe-Oxidizing bacteria are abundant at the Loihi Seamount hydrothermal vents and play a major role in Fe oxide deposition. *Appl. Environ. Microbiol.* 68, 3085–3093. doi: 10.1128/AEM.68.6.3085-3093.2002

Emerson, D., Rentz, J. A., Lilburn, T. G., Davis, R. E., Aldrich, H., Chan, C., et al. (2007). A novel lineage of proteobacteria involved in formation of marine Fe-oxidizing microbial mat communities. *PLoS ONE* 2:e667. doi: 10.1371/journal.pone.0000667

Emerson, D., and Revsbech, N. P. (1994). Investigation of an iron-oxidizing microbial mat community located near Aarhus, Denmark - field studies. *Appl. Environ. Microbiol.* 60, 4022–4031.

Emerson, D., Scott, J. J., Benes, J., and Bowden, W. B. (2015). Microbial iron oxidation in the arctic tundra and its implications for biogeochemical cycling. *Appl. Environ. Microbiol.* 81, 8066–8075. doi: 10.1128/AEM.02832-15

Fenchel, T., and Kühl, M. (2000). Artificial cyanobacterial mats: growth, structure, and vertical zonation patterns. *Microbiol. Ecol.* 40, 85–93. doi: 10.1007/s002480000062

Field, E. K., Kato, S., Findlay, A. J., MacDonald, D. J., Luther, III, G. W., and Chan, C. S. (in press). Planktonic marine iron-oxidizers drive iron mineralization under low oxygen conditions. *Geobiol. J.* doi: 10.1111/gbi.12189

Fleming, E. J., Cetinić, I., Chan, C. S., Whitney King, D., and Emerson, D. (2014). Ecological succession among iron-oxidizing bacteria. *ISME J.* 8, 804–815. doi: 10.1038/ismej.2013.197

Fleming, E. J., Davis, R. E., McAllister, S. M., Chan, C. S., Moyer, C. L., Tebo, B. M., et al. (2013). Hidden in plain sight: discovery of sheath-forming, iron-oxidizing Zetaproteobacteria at Loihi Seamount, Hawaii, USA. *FEMS Microbiol. Ecol.* 85, 116–127. doi: 10.1111/1574-6941.12104

Fleming, E. J., Langdon, A. E., Martinez-Garcia, M., Stepanauskas, R., Poulton, N. J., Masland, E. D. P., et al. (2011). What's new is old: resolving the identity of *Leptothrix ochracea* using single cell genomics, pyrosequencing and FISH. *PLoS ONE* 6:e17769. doi: 10.1371/journal.pone.0017769

Ghiorse, W. (1984). Biology of iron-depositing and manganese-depositing bacteria. *Annu. Rev. Microbiol.* 38, 515–550. doi: 10.1146/annurev.mi.38.100184.002503

Glazer, B. T., Marsh, A. M., Stierhoff, K., and Luther, G. W. III (2004). The dynamic response of optical oxygen sensors and voltammetric electrodes to temporal changes in dissolved oxygen concentrations. *Anal. Chim. Acta* 518, 93–100. doi: 10.1016/j.aca.2004.05.040

Glazer, B. T., and Rouxel, O. J. (2009). Redox speciation and distribution within diverse iron-dominated microbial habitats at Loihi Seamount. *Geomicrobiol. J.* 26, 606–622. doi: 10.1080/01490450903263392

Goldberg, M. B. (2001). Actin-based motility of intracellular microbial pathogens. *Microbiol. Mol. Biol. Rev.* 65, 595–626, table of contents. doi: 10.1128/MMBR.65.4.595-626.2001

Hallbeck, L., and Pedersen, K. (1990). Culture parameters regulating stalk formation and growth rate of *Gallionella ferruginea*. *J. Gen. Microbiol.* 136, 1675–1680. doi: 10.1099/00221287-136-9-1675

Hallbeck, L., Ståhl, F., and Pedersen, K. (1993). Phylogeny and phenotypic characterization of the stalk-forming and iron-oxidizing bacterium *Gallionella ferruginea*. *J. Gen. Microbiol.* 139, 1531–1535. doi: 10.1099/00221287-139-7-1531

Hanert, H. (1973). Quantification of gallionella development under natural conditions. *Arch. Microbiol.* 88, 225–243.

Hanert, H. H. (2006). "The Genus Siderocapsa (and Other Iron- and Manganese-Oxidizing Eubacteria)," in *The Prokaryotes: Vol. 7: Proteobacteria: Delta, Epsilon Subclass, 3rd edn.* eds M. Dworkin, S. Falkow, E. Rosenberg, K.-H. Schleifer, and E. Stackebrandt (New York, NY: Springer), 1005–1015.

Harder, E. C. (1919). *Iron-Depositing Bacteria and Their Geological Relations*. Washington, DC: US Geological Survey Professional Paper 113.

Hegler, F., Lösekann-Behrens, T., Hanselmann, K., Behrens, S., and Kappler, A. (2012). Influence of seasonal and geochemical changes on the geomicrobiology of an iron carbonate mineral water spring. *Appl. Environ. Microbiol.* 78, 7185–7196. doi: 10.1128/AEM.01440-12

Kato, S., Krepski, S., Chan, C., Itoh, T., and Ohkuma, M. (2014). Ferriphaselus amnicola gen. nov., sp. nov., a neutrophilic, stalk-forming, iron-oxidizing bacterium isolated from an iron-rich groundwater seep. *Int. J. Syst. Evol. Microbiol.* 64, 921–925. doi: 10.1099/ijs.0.058487-0

Kato, S., Ohkuma, M., Powell, D. H., Krepski, S. T., Oshima, K., Hattori, M., et al. (2015). Comparative genomic insights into ecophysiology of neutrophilic, microaerophilic iron oxidizing bacteria. *Front. Microbiol.* 6:256. doi: 10.3389/fmicb.2015.01265

Krepski, S. T., Emerson, D., Hredzak-Showalter, P. L., Luther, G. W., and Chan, C. S. (2013). Morphology of biogenic iron oxides records microbial physiology and environmental conditions: toward interpreting iron microfossils. *Geobiology* 11, 457–471. doi: 10.1111/gbi.12043

Krepski, S. T., Hanson, T. E., and Chan, C. S. (2012). Isolation and characterization of a novel biomineral stalk-forming iron-oxidizing bacterium from a circumneutral groundwater seep. *Environ. Microbiol.* 14, 1671–1680. doi: 10.1111/j.1462-2920.2011.02652.x

Little, C., Glynn, S., and Mills, R. (2004). Four-hundred-and-ninety-million-year record of bacteriogenic iron oxide precipitation at sea-floor hydrothermal vents. *Geomicrobiol. J.* 21, 415–429. doi: 10.1080/01490450490485845

Luther, G. W. III., Glazer, B. T., Ma, S., Troubworst, R. E., Moore, T. S., Metzger, E., et al. (2008). Use of voltammetric solid-state (micro)electrodes for studying biogeochemical processes: laboratory measurements to real time measurements with an *in situ* electrochemical analyzer (ISEA). *Mar. Chem.* 108, 221–235. doi: 10.1016/j.marchem.2007.03.002

McAllister, S. M., Davis, R. E., McBeth, J. M., Tebo, B. M., Emerson, D., and Moyer, C. L. (2011). Biodiversity and emerging biogeography of the neutrophilic iron-oxidizing Zetaproteobacteria. *Appl. Environ. Microbiol.* 77, 5445–5457. doi: 10.1128/AEM.00533-11

Mitsunobu, S., Shiraishi, F., Makita, H., Orcutt, B. N., Kikuchi, S., Jorgensen, B. B., et al. (2012). Bacteriogenic Fe(III) (oxyhydr)oxides characterized by synchrotron microprobe coupled with spatially resolved phylogenetic analysis. *Environ. Sci. Technol.* 46, 3304–3311. doi: 10.1021/es203860m

Moeller, K., Schoenberg, R., Grenne, T., and Thorseth, I. H. (2014). Comparison of iron isotope variations in modern and Ordovician siliceous Fe oxyhydroxide deposits. *Geochim. Cosmochim. Acta.* 126, 422–440. doi: 10.1016/j.gca.2013.11.018

Mulder, E. G., and van Veen, W. L. (1963). Investigations on the Sphaerotilus-Leptothrix group. *Antonie Van Leeuwenhoek* 29, 121–153. doi: 10.1007/BF02046045

Neubauer, S. C., Emerson, D., and Megonigal, J. P. (2002). Life at the energetic edge: kinetics of circumneutral iron oxidation by lithotrophic iron-oxidizing bacteria isolated from the wetland-plant rhizosphere. *Appl. Environ. Microbiol.* 8, 3988–3995. doi: 10.1128/AEM.68.8.3988-3995.2002

Peng, X., Ta, K., Chen, S., Zhang, L., and Xu, H. (2015). Coexistence of Fe(II)- and Mn(II)-oxidizing Bacteria Govern the Formation of Deep Sea Umber Deposits. *Geochim. Cosmochim. Acta* 169, 200–216. doi: 10.1016/j.gca.2015.09.011

Pruesse, E., Peplies, J., and Glöckner, F. O. (2012). SINA: accurate high-throughput multiple sequence alignment of ribosomal RNA genes. *Bioinformatics* 28, 1823–1829. doi: 10.1093/bioinformatics/bts252

Quast, C., Pruesse, E., Yilmaz, P., Gerken, J., Schweer, T., Yarza, P., et al. (2013). The SILVA ribosomal RNA gene database project: improved data processing and web-based tools. *Nucleic Acids Res.* 41(D1):D590–D596. doi: 10.1093/nar/gks1219

Rassa, A., McAllister, S., Safran, S., and Moyer, C. (2009). Zeta-proteobacteria dominate the colonization and formation of microbial mats in low-temperature hydrothermal vents at Loihi Seamount, Hawaii. *Geomicrobiol. J.* 26, 623–638. doi: 10.1080/01490450903263350

Schieber, J., and Glamoclija, M. (2007). "Microbial mats built by iron bacteria: a modern example from southern Indiana," in *Atlas of Microbial Mat Features Preserved Within the Silicilastic Rock Record* eds J. Schieber, P. Bose, P. Eriksson, S. Banerjee, S. Sarkar, W. Altermann, and O. Catuneanu (New York, NY: Elsevier), 233–244.

Schindelin, J., Arganda-Carreras, I., Frise, E., Kaynig, V., Longair, M., Pietzsch, T., et al. (2012). Fiji: an open-source platform for biological-image analysis. *Nat. Methods* 9, 676–682. doi: 10.1038/nmeth.2019

Schloss, P. D., and Handelsman, J. (2005). Introducing DOTUR, a computer program for defining operational taxonomic units and estimating species richness. *Appl. Environ. Microbiol.* 71, 1501–1506. doi: 10.1128/AEM.71.3.1501-1506.2005

Scott, J. J., Breier, J. A., Luther, G. W. III., and Emerson, D. (2015). Microbial iron mats at the Mid-Atlantic Ridge and evidence that Zetaproteobacteria may be restricted to iron-oxidizing marine systems. *PLoS ONE* 10:e0119284. doi: 10.1371/journal.pone.0119284

Sievert, S. M., Wieringa, E. B. A., Wirsen, C. O., and Taylor, C. D. (2007). Growth and mechanism of filamentous-sulfur formation by Candidatus Arcobacter sulfidicus in opposing oxygen-sulfide gradients. *Environ. Microbiol.* 9, 271–276. doi: 10.1111/j.1462-2920.2006.01156.x

Slack, J. F., Grenne, T., Bekker, A., Rouxel, O. J., and Lindberg, P. A. (2007). Suboxic deep seawater in the late Paleoproterozoic: evidence from hematitic chert and iron formation related to seafloor-hydrothermal sulfide deposits, central Arizona, USA. *Earth Planet Sci. Lett.* 255, 243–256. doi: 10.1016/j.epsl.2006.12.018

Sobolev, D., and Roden, E. E. (2004). Characterization of a neutrophilic, chemolithoautotrophic Fe(II)-oxidizing b-proteobacterium from freshwater wetland sediments. *Geomicrobiol. J.* 21, 1–10. doi: 10.1080/01490450490253310

Stahl, D. A., Flowers, J. J., Hullar, M., and Davidson, S. (2013). "Structure and function of microbial communities," in *The Prokaryotes, 4th edn.* eds E. Rosenberg, E. DeLong, S. Lory, E. Stackebrandt, and F. Thompson (Berlin; Heidelberg: Springer), 3–30.

Stamatakis, A. (2006). RAxML-VI-HPC: maximum likelihood-based phylogenetic analyses with thousands of taxa and mixed models. *Bioinformatics* 22, 2688–2690. doi: 10.1093/bioinformatics/btl446

Stookey, L. (1970). Ferrozine—A new spectrophotometric reagent for iron. *Anal. Chem.* 42, 779–781. doi: 10.1021/ac60289a016

Taylor, C., and Wirsen, C. (1997). Microbiology and ecology of filamentous sulfur formation. *Science* 277, 1483–1485. doi: 10.1126/science.277.5331.1483

Teske, A., and Salman, V. (2014). "The Family Beggiatoaceae," in *The Prokaryotes, 4th edn.* eds E. Rosenberg, E. DeLong, S. Lory, E. Stackebrandt, and F. Thompson (Berlin; Heidelberg: Springer), 93–134.

van Veen, W. L., Mulder, E. G., and Deinema, M. H. (1978). The Sphaerotilus-Leptothrix group of bacteria. *Microbiol. Rev.* 42, 329–356.

Conflict of Interest Statement: The authors declare that the research was conducted in the absence of any commercial or financial relationships that could be construed as a potential conflict of interest.

frontiers in Microbiology

ORIGINAL RESEARCH
published: 10 May 2016
doi: 10.3389/fmicb.2016.00648

Iron Transformation Pathways and Redox Micro-Environments in Seafloor Sulfide-Mineral Deposits: Spatially Resolved Fe XAS and $\delta^{57/54}$Fe Observations

Brandy M. Toner[1], Olivier J. Rouxel[2], Cara M. Santelli[3], Wolfgang Bach[4] and Katrina J. Edwards[5†]*

[1] *Département des Ressources Physiques et Écosystèmes de Fond de Mer, Water, and Climate, University of Minnesota-Twin Cities, St. Paul, MN, USA,* [2] *Department of Deep-sea Physical Resources and Ecosystems, Centre de Brest, Institut Français de Recherche pour l'Exploitation de la Mer, Plouzané, France,* [3] *Department of Earth Sciences, University of Minnesota-Twin Cities, Minneapolis, MN, USA,* [4] *Department of Geosciences and MARUM, University of Bremen, Bremen, Germany,* [5] *Department of Biological Sciences, University of Southern California, Los Angeles, CA, USA*

Hydrothermal sulfide chimneys located along the global system of oceanic spreading centers are habitats for microbial life during active venting. Hydrothermally extinct, or inactive, sulfide deposits also host microbial communities at globally distributed sites. The main goal of this study is to describe Fe transformation pathways, through precipitation and oxidation-reduction (redox) reactions, and examine transformation products for signatures of biological activity using Fe mineralogy and stable isotope approaches. The study includes active and inactive sulfides from the East Pacific Rise 9°50′N vent field. First, the mineralogy of Fe(III)-bearing precipitates is investigated using microprobe X-ray absorption spectroscopy (μXAS) and X-ray diffraction (μXRD). Second, laser-ablation (LA) and micro-drilling (MD) are used to obtain spatially-resolved Fe stable isotope analysis by multicollector-inductively coupled plasma-mass spectrometry (MC-ICP-MS). Eight Fe-bearing minerals representing three mineralogical classes are present in the samples: oxyhydroxides, secondary phyllosilicates, and sulfides. For Fe oxyhydroxides within chimney walls and layers of Si-rich material, enrichments in both heavy and light Fe isotopes relative to pyrite are observed, yielding a range of δ^{57}Fe values up to 6‰. Overall, several pathways for Fe transformation are observed. Pathway 1 is characterized by precipitation of primary sulfide minerals from Fe(II)*aq*-rich fluids in zones of mixing between vent fluids and seawater. Pathway 2 is also consistent with zones of mixing but involves precipitation of sulfide minerals from Fe(II)*aq* generated by Fe(III) reduction. Pathway 3 is direct oxidation of Fe(II) aq from hydrothermal fluids to form Fe(III) precipitates. Finally, Pathway 4 involves oxidative alteration of pre-existing sulfide minerals to form Fe(III). The Fe mineralogy and isotope data do not support or refute a unique biological role in sulfide alteration. The findings reveal a dynamic range of Fe transformation pathways consistent with a continuum of micro-environments having variable redox conditions. These micro-environments likely support redox cycling of Fe and S and are consistent with culture-dependent and -independent assessments of microbial physiology and genetic diversity of hydrothermal sulfide deposits.

Keywords: hydrothermal, East Pacific Rise, X-ray absorption spectroscopy, stable isotopes, micro-environment, mineral alteration, iron, biosignature

OPEN ACCESS

Edited by:
Mark Alexander Lever, ETH Zürich, Switzerland

Reviewed by:
Aude Picard, Harvard University, USA
Julie L. Meyer, University of Florida, USA

****Correspondence:***
Brandy M. Toner
toner@umn.edu

† Deceased.

Specialty section:
This article was submitted to Extreme Microbiology, a section of the journal Frontiers in Microbiology

Received: *06 January 2016*
Accepted: *18 April 2016*
Published: *10 May 2016*

Citation:
Toner BM, Rouxel OJ, Santelli CM, Bach W and Edwards KJ (2016) Iron Transformation Pathways and Redox Micro-Environments in Seafloor Sulfide-Mineral Deposits: Spatially Resolved Fe XAS and $\delta^{57/54}$Fe Observations Front. Microbiol. 7:648. doi: 10.3389/fmicb.2016.00648

INTRODUCTION

Seafloor hydrothermal activity at oceanic spreading centers is one of the fundamental processes controlling the exchange of heat and chemical species between seawater and ocean rocks (Edmond et al., 1979; Stein and Stein, 1994; Elderfield and Schultz, 1996; Wheat et al., 2004). The altered rock and mineral deposits created by hydrothermal circulation are known to harbor microbial communities with ecological and functional characteristics corresponding to the chemistry of the host substrate (Santelli et al., 2008; Orcutt et al., 2011; Sylvan et al., 2012; Lever et al., 2013; Toner et al., 2013). In addition, it has been demonstrated that microorganisms interact with their rock/mineral environment by promoting mineral dissolution and precipitation (Holden and Adams, 2003; Houghton, 2007; Pagé et al., 2008; Templeton et al., 2009; Houghton and Seyfried, 2010). Investigations of the physiological and phylogenetic diversity of rock-hosted prokaryotes using both culture-based and molecular approaches show their important ecological roles in biogeochemical cycles of carbon (C), sulfur (S), nitrogen (N), and iron (Fe) (Reysenbach and Cady, 2001; Slobodkin et al., 2001; Edwards et al., 2003a; Byrne et al., 2009; Yamamoto and Takai, 2011).

The development of microbial habitats within hydrothermal chimney deposits is a combination of physical (temperature, porosity), chemical (dissolved and mineral), and biological factors (biofilms, mineral alteration). It is well-established that steep temperature and geochemical gradients form within the walls of actively venting chimneys (Tivey, 1995). Corresponding changes in microbial communities along physical and chemical gradients have been demonstrated at various levels of spatial resolution (Karl, 1995; Schrenk et al., 2003; Nakagawa et al., 2005; Pagé et al., 2008; Takai et al., 2008; Callac et al., 2015). The development of micro-environments within chimneys could explain the diverse genetic potential and wide range of metabolisms observed in organisms cultured from sulfide deposits. Analytical tools able to measure chemical, mineralogical, and isotopic information on the micron spatial scale are available, and the geoscience community has begun to apply them in concert (Marcus et al., 2015). Through the combination of these analytical approaches, one can now define the properties of micro-environments and gain the information needed to interpret micro-habitats or micro-niches within rock and mineral substrates.

In mid-ocean ridge (MOR) hydrothermal systems, Fe is a fundamental element (Emerson, 2016). Iron deserves special attention when considering the biogeochemistry of mid-ocean ridges because it: (1) is abundant in most vent fluids; (2) has dynamic solubility properties and precipitates with S to form part of the physical structure of sulfide deposits; (3) has dynamic oxidation-reduction (redox) properties and the ability to set and record redox conditions within fluid flow paths; and (4) is a potential substrate for microbial energy (Fe reduction) and respiration (Fe oxidation). In mid-ocean ridge systems, such as the East Pacific Rise at 9–10°N or Juan de Fuca Ridge Main Endeavor Field, the breadth of possible biogeochemical roles for Fe is fully populated. Hydrothermal sulfides are observed as active and inactive chimneys, massive sulfide deposits, and particles in hydrothermal plumes settling from the water column (Feely et al., 1992, 1994; Hannington et al., 1995; Tivey, 2007; Rouxel et al., 2008a; Toner et al., 2009a; Fouquet et al., 2010; Yucel et al., 2011; Breier et al., 2012). Iron (oxyhydr)oxide crusts form through the alteration of Fe-rich basalts and sulfides, and as microbial mats associated with diffuse venting (Alt, 1988; Mills and Elderfield, 1995; Wheat et al., 2000; Boyd and Scott, 2001; Emerson and Moyer, 2002; Edwards et al., 2011). The oxidizing conditions at the seafloor create a driving force for conversion of hydrothermally derived Fe(II)aq, as well as ferrous Fe in basalt and sulfide minerals, to Fe(III)-bearing minerals through chemical and biological means (Feely et al., 1994; Field and Sherrell, 2000; Edwards et al., 2003b; Toner et al., 2009b). In addition to the mineral forms of Fe, complexes with particulate and dissolved organic matter occur (Bennett et al., 2008; Toner et al., 2009a; Breier et al., 2012; Hawkes et al., 2013) and microorganisms take up hydrothermal Fe in plumes by a variety of mechanisms (Li et al., 2014).

Despite our understanding of the potential (bio)geochemical pathways for Fe transformation in hydrothermal systems, the actual Fe pools and most important mechanisms of transformation are difficult to measure and are an area of active research (Saito et al., 2013; Fitzsimmons et al., 2014; Resing et al., 2015). The strategic application of analytical tools over a range of spatial scales, from dissolved Fe species over a 1000 km to particulate Fe species within submicron aggregates, presents a way forward. In this contribution, we investigate the μm- to mm-scale chemistry of active and extinct hydrothermal sulfide deposits using micro-probe X-ray diffraction (μXRD), micro-probe Fe 1s X-ray absorption spectroscopy (μXAS), and spatially resolved Fe stable isotopes (laser ablation and micro-drilling). The main goal of this study is to describe the Fe transformation pathways in natural sulfide mineral deposits at the seafloor, and examine the products of alteration for indications or markers of biological activity. The research is an extension of incubation studies that subjected polished hydrothermal sulfide samples to seafloor conditions over a known period of time (Edwards et al., 2003b; Toner et al., 2009b) and Fe isotope studies of seafloor hydrothermal vents (Rouxel et al., 2004, 2008a). For our study of natural sulfide mineral alteration, we chose the East Pacific Rise (EPR) 9–10°N area because hydrothermally inactive sulfide deposits from this location are known to host microbial communities with the genetic potential to alter Fe- and S-bearing minerals through redox reactions (Sylvan et al., 2012; Toner et al., 2013). Our investigation reveals a suite of complex Fe transformation pathways, each of which can be partial or complete. We find that metastable Fe oxyhydroxide minerals persist in the samples despite strong evidence for dynamic Fe transformations, and that Fe isotopic fractionation creates very light isotopic signatures (δ^{57}Fe values as low as –7‰) for Fe oxyhydroxides in some samples but isotopically heavy in others. The most important outcome of this work is a record of micro-environments within active and inactive sulfide deposits. These micro-environments are consistent with the diverse genetic potential, and correspondingly wide range of potential metabolisms, observed in organisms cultured from

sulfide deposits. Micro-environments favorable to microbial Fe and S oxidation and reduction are supported by mineral and isotopic signatures. However, we did not identify any uniquely biological signatures and attribute this outcome to the complex interplay between biotic and abiotic reactions.

METHODS AND MATERIALS

Sample Collection and Processing

Hydrothermally active and inactive sulfide samples were collected from chimneys and massive sulfide deposits during an *R/V Atlantis—DSV Alvin* cruise to the East Pacific Rise (EPR) Clipperton and Siquieros Fracture Zones 9°28′N–9°51′N in 2004. On *Alvin* dives 4053, 4057, and 4059, samples rich in Zn and Fe were collected from: (1) K Vent; (2) north of Bio 9 Vent; (3) south east of Bio 9 Vent; and (4) an extinct, off-axis chimney (**Figures S1**, **S2**). Seafloor samples were collected in individual bio-boxes attached to Alvin's basket to avoid cross contamination and minimize exposure to surface sea water. Once on board, the samples were stored in the bio-boxes in the 4°C cooler until they were processed in the lab. The samples were placed on sterile Al-foil and sterile tools were used to split subsamples for microbiology and mineralogy studies. Samples for geochemical analysis were allowed to air-dry shipboard and were stored under ambient conditions until embedding and sectioning. Although residual reduced vent fluids in the active chimneys could oxidize during sample transport and handling, the amount of Fe in residual pore water relative to Fe in the overall sample is small. Therefore, transformations of Fe during sample transport and handling are not expected to affect the overall analysis of the samples. The sulfide mineral composition and associated microbial communities for the sample set has been described previously (Rouxel et al., 2008a; Sylvan et al., 2012; Toner et al., 2013). The samples for this study are listed in **Table S1**.

K Vent is an active sulfide mound hosting spires and relic chimney debris (i.e., rubble). K Vent samples have the unique identifier *EPR-4053-M* and the three samples were: EPR-4053-M3, rubble; EPR-4053-M1-A1, and EPR-4053-M1-A2, both are active spire samples (**Figure S3**). K Vent sulfides have central conduits of sphalerite (ZnS), marcasite (FeS_2), and silica-rich materials while the external walls are composed of sphalerite, pyrite (FeS_2), and silica (Rouxel et al., 2008a). The inactive massive sulfide samples (*EPR-4057-M2* and *EPR-4059-M3*) are from two different locations in the vicinity of Bio 9 Vent. EPR-4057-M2 has a relic central conduit of marcasite with finely disseminated sphalerite and pyrite throughout, and an external wall of marcasite and Fe oxyhydroxides. EPR-4059-M3 also has a marcasite conduit with sphalerite-pyrite core and sphalerite-pyrite lined fossil tube worms. The extinct, off-axis chimney *EPR-4059-M4* lacks a central conduit and has cm-thick sphalerite layers that transition to sphalerite-pyrite and an external wall covered with Fe oxides and silica.

Air-dry rock specimens were embedded in Epo-tek 301 two-part epoxy (Epoxy Technology). Cross-sections were cut with a wafering saw and adhered to standard glass microscope slides for polishing: producing coarsely polished thick sections (**Figure S4**). One sample, *EPR-4059-M3*, has a micro-probe quality polished section (30 μm; Spectrum Petrographics, Inc.). The polished sections were used for synchrotron radiation X-ray microprobe measurements while thick sections were used for laser-ablation and micro-drilling for isotope analysis.

Scanning Electron Microscopy (SEM)

Subsamples of several EPR sulfides were fixed in 4% paraformaldehyde at room temperature for 4 h, rinsed with a 1:1 phosphate buffer solution (PBS), and stored in PBS-ethanol at −20°C shipboard. Sample EPR-4059-M4 was subjected to critical point drying and platinum sputter coating prior to SEM imaging at the University of Minnesota, Characterization Facility with a field emission gun scanning electron microscope (JEOL 6500).

Synchrotron Microprobe X-Ray Absorption Spectroscopy (XAS) Analysis

Iron speciation was measured by Fe 1s XAS in fluorescence mode at the hard X-ray microprobe beamline 10.3.2, Advanced Light Source (ALS), Lawrence Berkeley National Laboratory, Berkeley, CA (Manceau et al., 2002; Marcus et al., 2004). The monochromator was calibrated by setting the inflection point of an Fe 1s XAS spectrum, collected from an Fe foil, to 7110.75 eV (Kraft et al., 1996). The distribution of elements in polished sections was determined by micro-focused X-ray fluorescence (μXRF) mapping using a seven-element Ge solid-state fluorescence detector (Canberra). X-ray fluorescence maps at multiple incident energies were collected to determine the distribution of elements, including Si, S, Ca, Mn, Fe, Co, Cu, Ni, Zn, and As. These XRF maps were then dead-time corrected, registered, and combined into a single composite map with custom beam-line software (Marcus et al., 2004). Composite XRF maps were used to locate sample locations for point Fe XAS data collection. XRF map measurements used $3 \times 3\ \mu m^2$ beam spot on the sample.

Iron 1s spectra in the X-ray absorption near edge structure (XANES) energy range were used to survey the oxidation state and mineral class of the Fe-bearing phases. Iron 1s spectra in the extended X-ray absorption fine structure (EXAFS) energy range were conducted in selected locations to better describe the type of Fe oxyhydroxide phases present. XANES and EXAFS measurements used $10 \times 3\ \mu m^2$ beam spot on the sample. Iron EXAFS data collection to a reciprocal space (k-space, $Å^{-1}$) value of 14.4 was attempted in all cases to provide adequate resolution for second shell Fe-Fe interatomic distances (Combes et al., 1989). However, the final usable EXAFS data range (based on signal to noise quality) extended to 11.75 to 12.6 $Å^{-1}$ and shell-by-shell fitting was not performed. All Fe 1s spectra were dead-time corrected, energy calibrated, averaged, pre-edge subtracted, and post-edge normalized. Iron EXAFS scans were spline subtracted and converted to reciprocal space (Marcus et al., 2004; Webb, 2005). Iron XANES spectra were corrected for over-absorption induced distortion:

$$\mu_{corrected} = \mu_{exp}/(1 + a\,(1 - \mu_{exp}))$$

where *a* was adjusted to obtain agreement between the corrected spectrum and high quality reference standards. Iron EXAFS data collection targeted sample locations with low over-absorption induced distortion; therefore, EXAFS spectra were not corrected for the phenomenon.

Iron XANES (43 spectra) and EXAFS (8 spectra) data were subjected to principal component (PCA) and target transformation (TTA) analysis using SixPack and BL10.3.2 software using methods described previously (Manceau et al., 2002; Webb, 2005; Toner et al., 2006; Breier et al., 2012). Subsequently, linear combination fitting (LCF) of experimental spectra was performed using a library of standards (Hansel et al., 2003; Marcus et al., 2008; Toner et al., 2009b) and custom beamline software (Marcus et al., 2004). A summary of the reference materials is presented in **Table S2**. The biogenic Fe oxyhydroxide reference spectrum was collected from an Fe-encrusted biofilm (composed of twisted-stalk microbial particles) formed on porous chimney sulfide chips during a 2 month incubation near the Juan de Fuca Ridge (Edwards et al., 2003b). Iron EXAFS was used to describe the Fe-precipitates as polymerized Fe(III) with short-range structure characterized by edge-sharing features and little three-dimensional ordering (Toner et al., 2009b). The best LCF was chosen based on the normalized sum square parameter (NSS):

$$NSS = 100 \times [\sum(\mu_{exp} - \mu_{fit})^2 / \sum(\mu_{exp})^2]$$

where the addition of a spectral component to the fit required a 10% or greater improvement in the NSS value. The Fe XAS reference materials deemed most appropriate for this dataset via PCA-TTA are listed in **Table S2**. The error on the percentages of species present is estimated to be ±10%.

Synchrotron Radiation X-Ray Diffraction

X-ray diffraction (XRD) patterns were collected for sample *EPR-4053-M2* from a polished thick section at the ALS, Lawrence Berkeley National Laboratory, Berkeley, CA, USA, on beamline 7.3.3 (Tamura et al., 2002). While Fe XANES and EXAFS are effective at distinguishing among mineralogical classes, in certain cases, they do not provide strong distinction among minerals within the same class (O'Day et al., 2004; Prietzel et al., 2007). For this sample, XRD was used to verify Fe XANES and EXAFS observations of the mineral goethite (α-FeOOH). The area of interest for XRD data collection was located using XRF mapping. The XRD patterns were collected with a CCD camera in reflection mode with a 6.3 keV incident energy and 15 × 8.5 μm^2 spot size at the sample. The diffraction patterns were processed with the software *XMAS* for comparison to standards (Tamura et al., 2003).

Multi-Collector Inductively Coupled Plasma Mass Spectrometry (MC-ICP-MS)

Fine scale variations of Fe and S isotope compositions of Fe-oxyhydroxides and pyrite across chimney walls were primarily analyzed using laser ablation technique coupled to multicollector inductively coupled plasma mass spectrometry (MC-ICP-MS). Micro-drilling was also used to allow matrix-free Fe-isotope analysis of mixed Fe-Si oxide and sulfide minerals after complete chemical purification following previously developed methods (Rouxel et al., 2005, 2008a).

For coupled Fe- and S-isotope analysis of pyrite, we adapted a technique previously used by (Craddock et al., 2008) for the determination of $^{34}S/^{32}S$ isotope ratios in S-bearing minerals. We used a Nd:YAG deep UV (213 nm) laser ablation system (NewWave™ UP213) coupled to MC-ICP-MS (Neptune, Thermo Scientific) operating at the Woods Hole Oceanographic Institution. The use of high resolution sector-field mass spectrometry removes major isobaric interferences on S-isotopes from O^{2+}, as already described in numerous studies (Mason et al., 2006; Craddock et al., 2008; Paris et al., 2013). A similar high-resolution approach was used for Fe-isotope analysis (Graham et al., 2004; Horn et al., 2006; Nishizawa et al., 2010). For the simultaneous analysis of both Fe- and S-isotope values in pyrite, our method involved data acquisition in two sequences (i.e., peak jumping mode) allowing the simultaneous determination of ^{32}S, ^{33}S, ^{34}S (sequence 1), and ^{52}Cr, ^{54}Fe, ^{57}Fe (sequence 2). This approach allows determining high-precision $^{34}S/^{32}S$ and $^{57}Fe/^{54}Fe$ and on-line correction of potential ^{54}Cr interference on ^{54}Fe using ^{52}Cr.

The laser setup was similar to a published method (Craddock et al., 2008): spot diameter of 60 μm, 10 Hz pulse rate, laser intensity 50–70%, energy density 9–10 j/cm^2. Note that under these conditions, ^{56}Fe signal intensity was found to be >50 V in some cases (i.e., maximum signal measurable on the Neptune Faraday cups), precluding the measurement of $\delta^{56}Fe$ values. For the determination of only Fe-isotope ratios in pyrite and Fe-oxyhydroxide, we also used a peak jumping mode as follows: ^{54}Fe, ^{56}Fe, ^{57}Fe, ^{58}Fe+^{58}Ni, ^{60}Ni, ^{61}Ni, ^{62}Ni (sequence 1), ^{52}Cr (sequence 2), ^{32}S (sequence 3), ^{28}Si (sequence 4). Using this approach, all Fe isotopes could be determined together with Ni isotopes ($^{62}Ni/^{60}Ni$) that are used for mass bias correction. ^{52}Cr was also measured to allow minor isobaric correction on ^{54}Fe. The measurements of ^{32}S and ^{28}Si also allowed us to check for the potential presence of silica (e.g., amorphous silica) and pyrite during analysis of Fe-oxyhydroxides. Operating parameters for laser analysis of Fe isotopes were optimized in order to provide the most stable signal intensities during ablation. The laser was operated under the same setup as for coupled S-Fe isotope measurements but with a smaller spot size of 25 μm to obtain a maximum signal on ^{56}Fe below 40V.

As discussed in Craddock et al., 2008, a line scan ("raster") protocol was used in preference to a single crater mode in order to obtain a higher and more uniform rate of material removal with respect to time. The raster mode utilizes a movable sample stage under a fixed laser beam to generate the desired raster pattern. The size of the trench formed during ablation was about 200 μm in cross-sectional area. A scan speed of 5 μm s^{-1} was used during ablation. Total acquisition time was about 4 min and results in ablation of about 15 μg of sample. The signal intensity was monitored to ensure that transport of sample into the ICP-MS does not significantly diminish as material is ablated during analysis.

The laser was connected directly to a PFA scott-type spray chamber (Savillex) via 3 mm internal diameter Tygon tubing and

used helium (He) as the carrier gas from the laser to the ICP. The setup was such that laser ablation and solution aspiration could be operated simultaneously to enable laser ablated particles to be efficiently mixed with an ultra-pure 0.28 M HNO_3 blank solution prior to injection into the ICP torch. Thus, particles were effectively analyzed as a "wet plasma" ensuring that ablated aerosols were closely matrix-matched to solution standards. Since solution and *in situ* laser analysis was performed interchangeably with identical instrumental setup, the correction of instrumental mass bias used a combination of the "sample-standard bracketing technique" as well as internal normalization technique (i.e., Ni isotopes). Here, we used Ni isotope standard NIST 986 of known isotope composition. For coupled Fe- and S-isotope analysis 34S) of pyrite, the data were calibrated against δ^{57}Fe and δ (i.e., aqueous standards prepared in appropriate matrix composition (molar S/Fe ratios at 2) and two internal pyrite standards GAV-18 and FL-19-09. The concentrations of Fe and S (i.e., sulfate form) solution prepared from internal standards (Spex Certiprep) in 0.28 M HNO_3 were adjusted to obtain similar signal intensity of the ablated sample and bracketing standard solution, typically with less than 20% difference g/g of Fe and S). When only Fe-isotope μ (corresponding to about 10 ^{57}Fe), bracketing standard solutions δ^{56}Fe and δ-values were measured (g/g). During each laser μg/g to 5 μ were prepared at a concentration of two analysis run, a Ni standard solution was introduced continuously in the spray chamber and mixed with sample aerosols to allow internal mass bias corrections as described elsewhere (Poitrasson and Freydier, 2005; Rouxel et al., 2005). An example laser isotopic run is presented in **Figure S5**.

We have examined and determined rigorous corrections for analytical difficulties such as instrumental mass bias, unresolved isobaric interferences, blanks, and laser ablation- and matrix-induced isotopic fractionation. By comparing raw Fe and S isotope ratios measured on standard minerals and calibrated against standard solutions, it was possible to determine the instrumental mass bias (i.e., isotope fractionation induced by laser ablation). Calibrated against the pure IRMM-14 solution, duplicated δ^{57}Fe analysis of GAV-18 pyrite standard yielded 0.48 ± 0.22‰ (2 sd, $n = 13$), which is about 0.17‰ lighter than bulk δ^{57}Fe value determined at 0.65 ± 0.14 (2 sd, $n = 2$). As already discussed for S isotopes using similar experimental setup (i.e., raster mode, Craddock et al., 2008), the isotopic compositions of the GAV-18 standard determined with both methods were identical within analytical uncertainties. This indicates that laser ablation introduced isotope fractionations that were within the analytical uncertainties (±0.2‰ at 2 sd).

To further evaluate whether Fe isotope analyses were potentially affected by the presence of S and Si impurities in Fe-oxyhydroxides, we added S and Si at various concentrations to pure standard solutions. The results show that, after appropriate corrections with Ni isotopes, no bias could be detected up to Si and S/Fe ratios (g/g) in solutions up to 0.7 and 2.5, respectively (**Figure S6**).

Although most advanced femtosecond ablation techniques enable matrix-independent calibration for Fe isotope analysis (Horn et al., 2006), our laser ablation technique may potentially be prone to significant fractionation during ablation and matrix effects that affect our accuracy and precision. Hence, we compared the Fe-isotope data obtained by laser ablation MC-ICP-MS with Fe-isotope data acquired through conventional MC-ICPMS technique after microdrilling and complete chromatographic purification. We collected powder micro-samples using a microdrill device (New Wave Micromill equipped with drill bit diameter of 700 μm) across the samples investigated by LA-MC-ICP-MS. Following the same protocols as for the bulk chimney samples (Rouxel et al., 2008a) we digested these micro-samples, separated Fe through anion-exchange chromatography procedure and measured Fe isotopes by MC-ICP-MS (Neptune, Thermo Scientific at Pole Spectrometry Ocean, Brest). The results on standards and comparison between laser-ablation and microdrilling techniques suggest that both approaches yield similar results within analytical uncertainties.

RESULTS

K Vent Diffuser Site

K Vent (**Figures S1A,B**) is an active diffuser site where active chimney spires (EPR-4053-M1-A1 and EPR-4053-M1-A2; **Figures S2A,B**) and inactive chimney rubble (EPR-4053-M3; **Figure S2C**) were collected. In the following paragraphs, for each of these samples, a description of the sample texture, Fe chemistry, and Fe (and in some cases S) isotopic composition is provided.

The seawater exposed surface of the actively diffusing spire (EPR-4053-M1-A1) is composed of an Fe-rich and S-depleted zone underlain by a Si-rich layer (**Figure 1A**). Linear combination fitting (LCF) results for Fe XANES and EXAFS spectra from this sample are consistent with ferrihydrite; 2-line and 6-line [$Fe_{10}O_{14}(OH)_2$ idealized formula (Michel et al., 2007); **Tables S3**, **S4**]. The Fe-rich and S-depleted zone in the actively diffusing spire sample EPR-4053-M1-A2 is displayed in **Figure 1B**). The Fe XANES and EXAFS data for this sample are consistent with an Fe(III)-rich biogenic-like Fe oxyhydroxide phase with ferrihydrite contributions: either 2-line or 6-line satisfies the LCF. Both samples investigated are from the base of the active spire of K Vent (**Figure S3**).

Two seawater-exposed surfaces of the K Vent inactive rubble (EPR-4053-M3) are shown in **Figures 1C,D**. Both regions of the sample are characterized by complex interweaved layers of Fe(III), Si, and sulfide. Petrographic observation and X-ray fluorescence maps (**Figure 2**) show the co-occurrence of Fe oxyhydroxide, silica (mainly amorphous silica) and pyrite with often rounded and colloform textures. Pyrite spherules (about 50–100 μm diameter) are particularly common along former pyritized worm tubes that are partially filled by silica and Fe oxyhydroxides. The Fe XANES data from both regions indicate that the Fe(III) layers are composed of a biogenic-like Fe oxyhydroxide (40–60 mol%; **Table S3**) and have varying contributions from goethite (α-FeOOH) or akaganeite (β-FeOOH). Fits to Fe XANES and EXAFS data are in good agreement (**Table S4**). Locations of coupled Fe and S isotope measurements for chimney wall pyrite, as well as colloform and spherulitic pyrite, using laser ablation are also shown in **Figure 2**

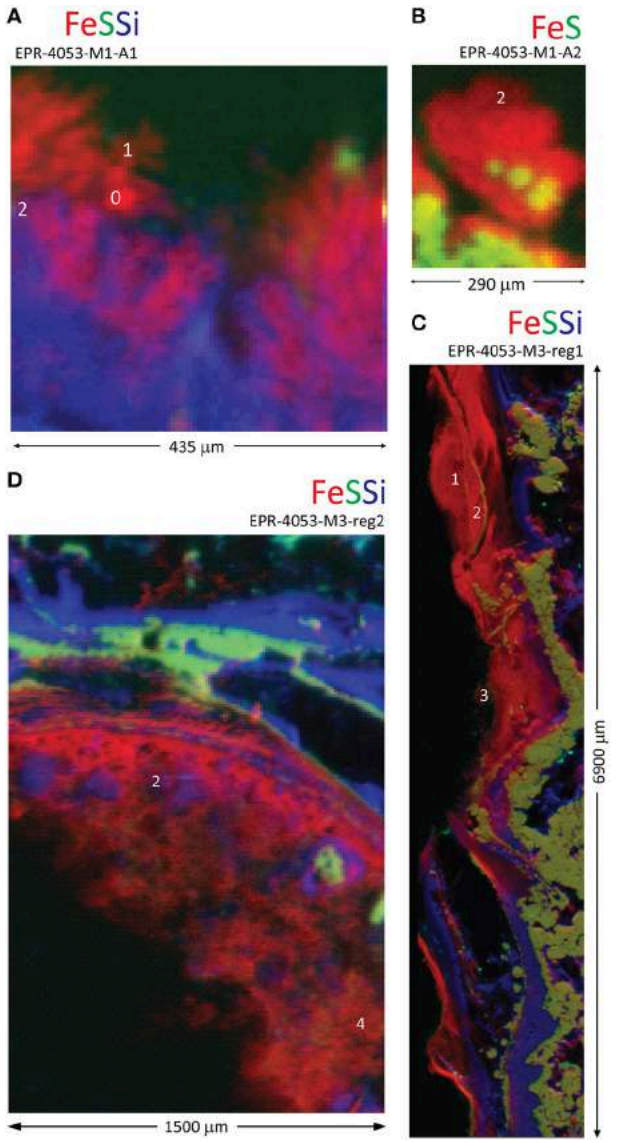

FIGURE 1 | Distribution of Fe, S, and Si in inactive spire and chimney rubble samples from K Vent. Red-green-blue (Fe-S-Si) tri-color X-ray fluorescence maps for **(A)** inactive spire (EPR-4053-M1-A1), **(B)** inactive spire (EPR-4053-M1-A2), **(C)** chimney rubble (EPR-4053-M3-reg1), and **(D)** chimney rubble (EPR-4053-M3-reg2). White numbers indicate locations for Fe X-ray absorption near edge structure (XANES; **Table S3**) or extended X-ray absorption fine structure (EXAFS; **Table S4**) data collection.

with results in **Table S5**. Results show relatively homogenous isotope values, with average $\delta^{57}Fe = -2.0 \pm 1.0‰$ (2 sd, $n = 8$) and $\delta^{34}S = 3.3 \pm 0.9‰$ (2 sd, $n = 8$) which is globally consistent with bulk chimney pyrite values ($\delta^{57}Fe = -1.49 \pm 0.16‰$ and $\delta^{34}S = 1.4 \pm 0.2‰$) (Rouxel et al., 2008a). Also in EPR-4053-M3-reg1, Fe oxyhyroxides occur in association with minor silica (**Figure 2**) forming a mm-thick external wall. Spatially resolved analyses using a microdrilling technique reveal a range of $\delta^{57}Fe$ values from $-0.32 \pm 0.10‰$ (2 sd) down to $-0.8 \pm 0.14‰$ (2 sd) which are similar, albeit slightly heavier, than laser ablation analysis ranging from $-0.44 \pm 0.14‰$ (2 sd) down to $-1.35 \pm 0.5‰$ (2 sd). Compared to colloform pyrite from the outer chimney wall, Fe oxyhydroxides show enrichments in heavy Fe isotopes by up to 2.3‰ (i.e., relative to $^{57}Fe/^{54}Fe$ ratios).

Bio 9 Massive Sulfide Deposits

Our sample set includes two massive sulfide deposits in the vicinity of Bio9 Vent (EPR-4057-M2 and EPR-4059-M3; **Figures S1C,D**). Both deposits exhibit Fe-rich and S-depleted zones at the seawater exposed surfaces with low (or undetectable) Si (**Figure 3**). The Fe XANES data for EPR-4057-M2 are dominated by the Fe(III) oxyhydroxide goethite with lesser contributions of a biogenic-like Fe oxyhydroxide signature (**Table S3**). The goethite phase assignment is supported by Fe EXAFS (**Table S4**) and micro-probe X-ray diffraction (**Figure S7**). One Fe XANES location is consistent with the Fe(III) oxyhydroxide lepidocrocite (spot 7). Where Fe XANES and EXAFS observations overlap for this sample, the observations are in agreement (**Table S4**). The Fe XANES data for the seawater exposed portion of massive sulfide EPR-4059-M3 reveal heterogeneous Fe-bearing mineralogy: consistent with 2-line ferrihydrite, goethite, akaganeite, and secondary phyllosilicates ("clay" minerals; **Table S3**). Despite the complexity in Fe-bearing phases, the Fe-rich and S-depleted phases are predominantly Fe(III).

Light micrographs and X-ray fluorescence maps of region 1 of sample EPR-4057-M2 (**Figure S8**; **Figure 4A**) show a relatively sharp contact between the external layer (i.e., alteration crust composed essentially of Fe oxyhydroxides) and the pyrite-rich interior. Disseminated Fe oxyhydroxides also occur as coatings and void filling between pyrite grains suggesting partial pyrite alteration. In this region, average $\delta^{57}Fe$ values by laser ablation analysis for Fe oxyhydroxides in the alteration layer and pyrite are $-1.93 \pm 0.20‰$ (2 sd, $n = 6$) and $-1.69 \pm 0.22‰$ (2 sd, $n = 4$), respectively. In other regions of the same sample similar average $\delta^{57}Fe$ values for Fe oxyhydroxides ($-1.64 \pm 0.32‰$) and pyrite (-2.37 ± 0.40 and $-2.12 \pm 0.60‰$) are obtained (**Table S6**). Average $\delta^{57}Fe$ values for pyrite are consistent with bulk values determined at $-2.58 \pm 0.09‰$ (Rouxel et al., 2008a). However, differences in $\delta^{57}Fe$ values from microdrilling another region of the sample are observed (region 3): $\delta^{57}Fe$ values ranging from -0.25 to $-0.44‰$ for Fe oxyhydroxides and $-1.09‰$ for pyrite (**Table S6**). These results suggest significant isotope heterogeneity of pyrite in this sample and show that Fe oxhydroxides may have either similar or slightly heavier $\delta^{57}Fe$ values relative to pyrite; which is in contrast with results obtained for sample EPR-4053-M3.

Inactive Off-Axis Chimney

An extinct, off-axis chimney structure (EPR-4059-M4) located 300 m east of the spreading center is part of our study (**Figure S1E**). Four regions of one grab sample show (**Figures 4B**, **5**) that the sample is characterized by a complex interweave of Fe(III)- and Si-rich layers. The seawater-exposed portion of the sample had bright orange and yellow precipitates (**Figure 6A**) composed of biological material (**Figures 6B,C**).

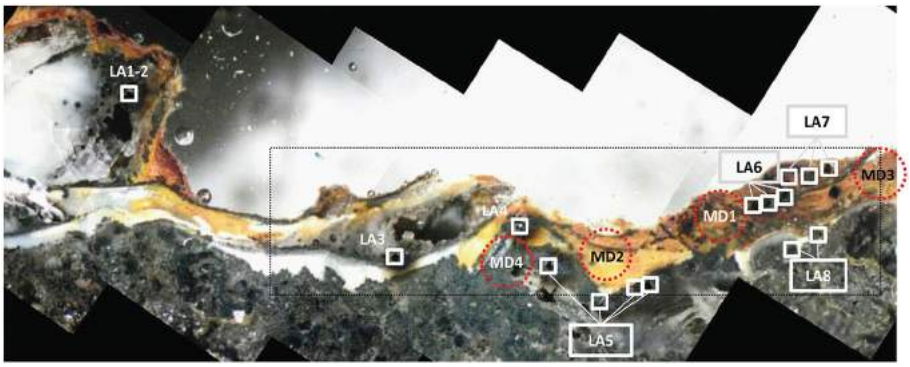

FIGURE 2 | Light microscope image for K Vent sample EPR-4053-M3-reg1. The area of the sample shown in **Figure 1C** is indicated by the black rectangle. Image is annotated with white boxes indicating laser ablation (LA) areas and red dashed circles indicating locations for micro-drilling (MD). Both laser ablation and micro-drilling produced samples for isotopic analysis (**Table S5**).

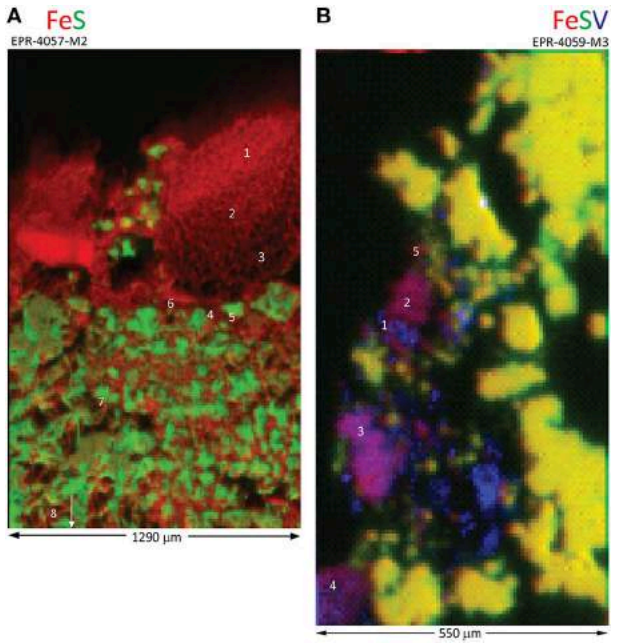

FIGURE 3 | Distribution of Fe, S, and V in massive sulfide deposits near Bio9 Vent. X-ray fluorescence maps for **(A)** EPR-4057-M2, and **(B)** red-green-blue (Fe-S-V) distribution for EPR-4059-M3. White numbers indicate locations for Fe X-ray absorption near edge structure (XANES) (**Table S3**) or extended X-ray absorption fine structure (EXAFS) (**Table S4**) data collection.

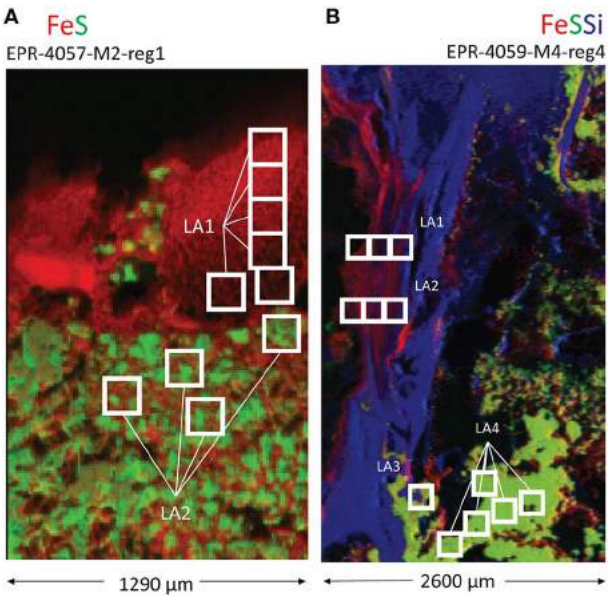

FIGURE 4 | Locations of laser ablation (LA) sampling for (A) a massive sulfide sample (EPR-4057-M2-reg1) and (B) an extinct, off-axis chimney sample (EPR-4059-M4-reg4). X-ray fluorescence (XRF) maps are annotated with white boxes indicating laser ablation areas corresponding to isotopic data in **Tables S6**, **S7**.

In region 1, the sulfides (pyrite) are overlain by a Si-rich layer, then an As-rich layer, and finally a Fe(III)-rich layer exposed to seawater(**Figure 5A**, spot 1; **Table S3**). The Fe XANES data indicate that the Fe(III) layer in region 1 was 70–100 mol% biogenic-like Fe oxyhydroxide with varying contributions from goethite and phyllosilicate (**Figure 5A**; spot5; **Table S3**). Laser ablation analyses of pyrite yield average δ^{57}Fe values of –2.9 ± 0.7‰ (2 sd, n = 7; **Table S7**; **Figure 7A**), which is within the range of δ^{57}Fe values for the bulk sample (δ^{57}Fe = –2.33 and –2.94‰) (Rouxel et al., 2008a). Iron isotope analysis of 3 areas enriched in Fe oxyhydroxides show contrasting Fe isotope values: (i) the external layer enriched in As has Fe isotope values similar to pyrite, with δ^{57}Fe = –2.1 ± 0.5‰ (2 sd, n = 4); (ii) the internal layer between pyrite and the external As-Fe-Si external crust shows very light Fe isotope values, with δ^{57}Fe = −4.6 ± 0.3‰ (2 sd, n = 4) which is even lighter than pyrite values; and (iii) average Fe oxyhydroxide layer (i.e., sampled by microdrilling) adjacent to the two others has a heavier value, δ^{57}Fe = –0.95 ± 0.04‰.

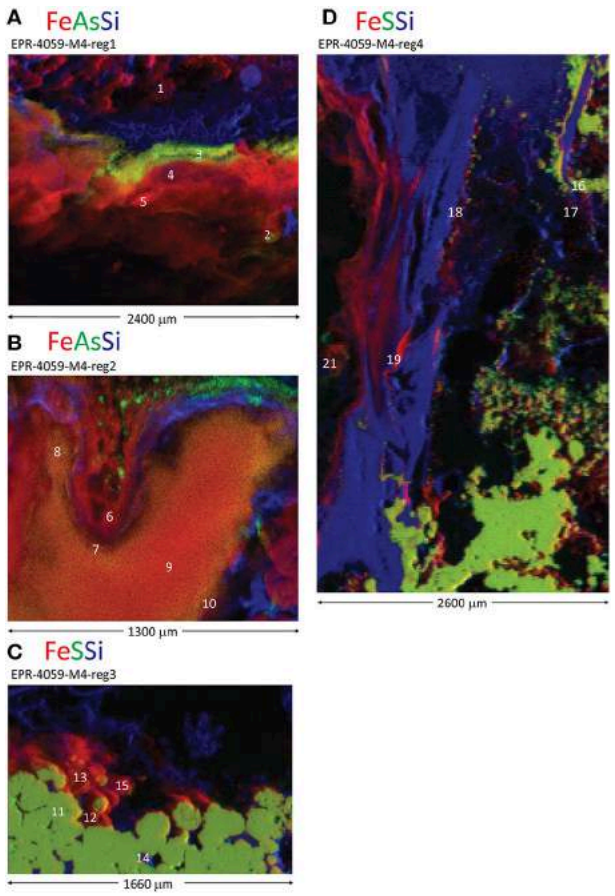

FIGURE 5 | Distribution of Fe, S, As, and Si in an inactive, off-axis chimney from the East Pacific Rise. Red-green-blue (Fe-S-Si or Fe-As-Si) tricolor X-ray fluorescence maps for four different regions of the sample: **(A)** EPR-4059-M4-reg1, **(B)** EPR-4059-M4-reg2, **(C)** EPR-4059-M4-reg3, and **(D)** EPR-4059-M4-reg4. White numbers indicate locations for Fe X-ray absorption near edge structure (XANES; **Table S3**) or extended X-ray absorption fine structure (EXAFS; **Table S4**) data collection.

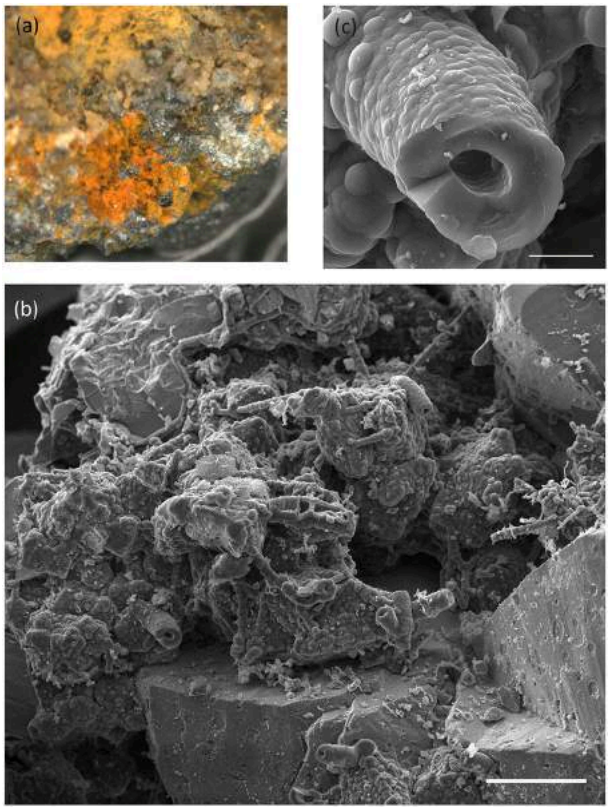

FIGURE 6 | Images of seawater exposed surface of East Pacific Rise off-axis, extinct chimney sample (EPR-4059-M4). (A) Binocular light microscope image of sample showing fine-grained orange and yellow alteration products. Field of view is ~0.5 cm. **(B)** Representative scanning electron microscope (SEM) image highlighting the abundance of biological materials. Scale bar is 100 μm. **(C)** A higher magnification image of a stalk-type structure prevalent in these materials. Scale bar is 10 μm.

Region 2 is internal to the grab sample and has Fe(III)-, As-, and S-rich layers (**Figure 5B**). The Fe oxyhydroxides in this region do not occur as a well-defined external crust along the outside layer of the chimney wall, but rather as filling material in a chimney cavity probably exposed to ambient seawater. The Fe XANES for the Fe(III)-rich materials are consistent with biogenic-like Fe oxyhydroxide, 2-line ferrihydrite, and goethite (**Table S3**). For region 2 spot 21, the best one component fit to the Fe EXAFS data is biogenic-like Fe oxyhydroxide (**Table S4**), and the best two component fit is biogenic-like Fe oxyhydroxide plus phyllosilicate. For the EXAFS LCF, the one component fit is chosen based on the *a priori* requirement that additional fit components require a 10% or greater improvement in the normalized sum square (NSS) parameter. The EXAFS results are overall consistent with the Fe XANES fitting. This region shows the lightest Fe isotope values obtained so far in natural samples with δ^{57}Fe values obtained by laser ablation ranging from −6.9 ± 0.7‰ (2 sd, n = 4) to −1.6 ± 0.3‰ while values from microdrilling ranging from −4.73 to −1.83‰ (**Figure 7B**; **Table S7**). This demonstrates a great heterogeneity of Fe isotopes values, characterized by δ^{57}Fe values both lighter and heavier than pyrite values from the adjacent area (δ^{57}Fe = −2.54‰ and −3.32 ± 0.4‰, microdrilling and laser ablation, respectively).

Region 3 has a thin layer of Fe(III) overlaying sulfides, with the seawater-exposed edge covered by a thin Si-rich layer (**Figure 5C**). The Fe XANES from the sulfide-Fe(III) transition indicate a variety of Fe(III)-bearing phases including biogenic-like Fe oxyhydroxide, goethite, and phyllosilicate (**Table S3**). No Fe isotope analysis was obtained from this region.

In region 4, sulfides (pyrite) are overlain by Si- and then Fe(III)-rich layers (**Figure 5D**, spot 16; **Table S3**). The Fe XANES indicate that the Fe(III)-bearing phases with spectral signatures consistent with 2-line ferrihydrite, goethite, akaganeite, and phyllosilicate (**Table S3**). Iron isotope values for pyrite obtained by laser ablation are relatively homogenous, with δ^{57}Fe = −3.25 ± 0.7‰ (2 sd, n = 12), which is similar within uncertainties

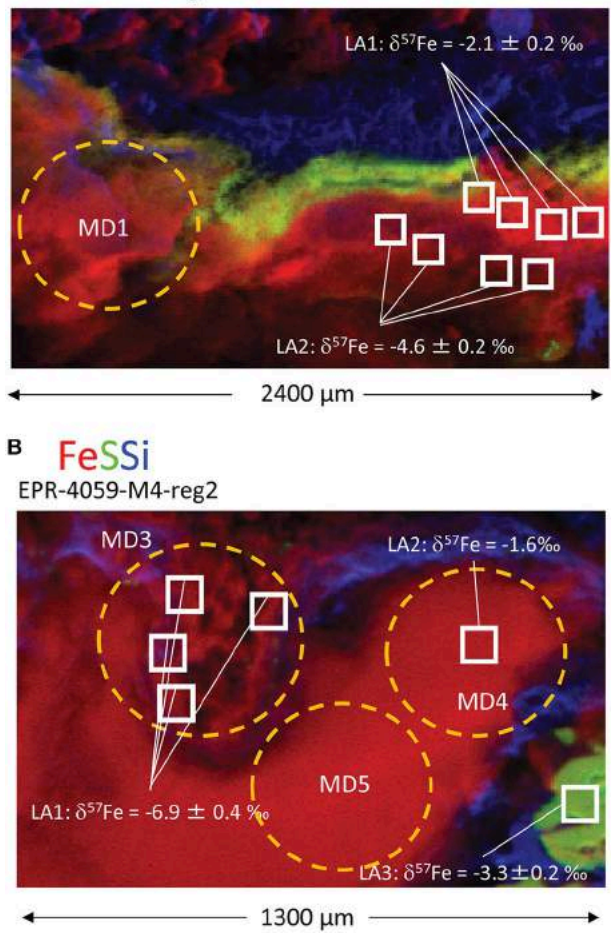

FIGURE 7 | Locations of laser ablation (LA) and micro-drilling (MD) samples for two regions within the extinct, off-axis chimney: (A) EPR-4059-M4-reg1 and (B) EPR-4059-M4-reg2. Both laser ablation and micro-drilling produced samples for isotopic analysis (**Table S7**).

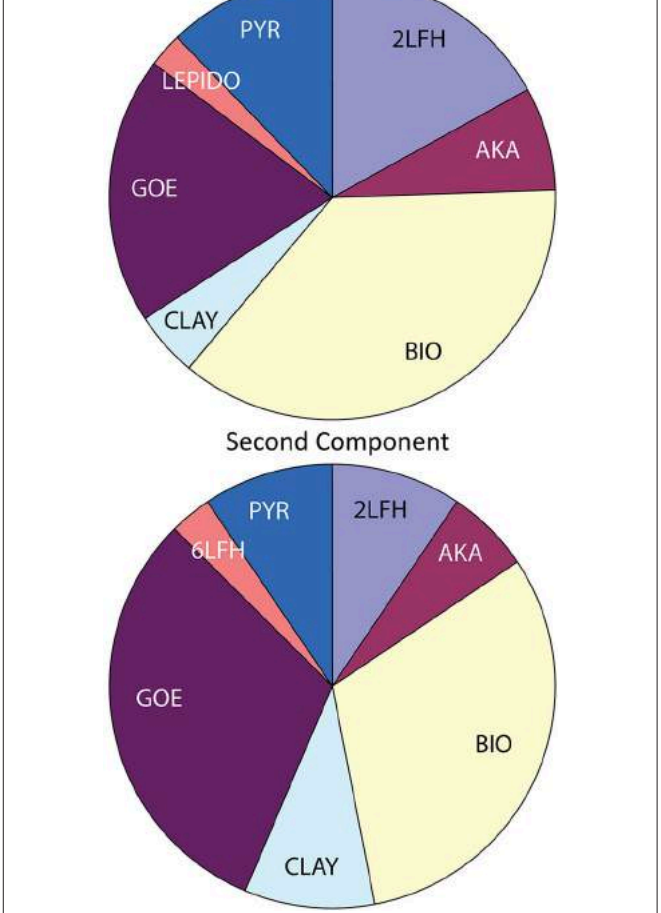

FIGURE 8 | Summary of linear combination fitting (LCF) results for Fe XANES spectra. Acronyms described in **Table S2** and full data set displayed in **Table S3**.

to the lower values obtained for microdrilled pyrite (δ^{57}Fe = −3.28‰) and bulk pyrite using (δ^{57}Fe = −2.33 and −2.94‰; **Table S7**; **Figure 4B**) (Rouxel et al., 2008a). Iron oxyhydroxides overlying the Si-rich layer show larger spread of δ^{57}Fe values, from −2.71 ± 0.12‰ (microdrilling) to −4.1 ± 0.8‰ (n = 3; laser ablation).

Diversity of Iron-Bearing Phases and Co-Located Elements

A summary of the linear least-squares fitting of spectra to combinations of reference spectra (LCF) is provided in **Table S3**. Principal component analysis (PCA) for the 43 Fe XANES spectra is consistent with eight different Fe species; as indicated by the minimum of the *IND* parameter (Manceau et al., 2002). The LCF results for Fe XANES spectra are in agreement with the PCA assessment of eight different Fe species among the 1st and 2nd fit components (**Table S3**; **Figure 8**). For 78% of the spectra, a second component in the fit is justified by a >10% improvement of the NSS parameter. For 32% of the spectra, a 3rd component is justified. These results indicate that in most cases, even at the 10-micron scale, a mixture of Fe-bearing minerals is present. The spectral components supported by PCA, target transformation analysis (TTA), and LCF are: pyrite (PYR); biogenic Fe oxyhydroxide (BIO); lepidocrocite (LEPIDO); 6-line ferrihydrite (6LFH); 2-line ferrihydrite (2LFH); nontronite (NONT); smectite (CLAY-S); goethite (GOE); and akaganeite (AKA) (**Table S2**). Note that Fe-bearing phyllosilicates nontronite and smectite components are binned as a single "clay" category (**Figure 8**). Three additional minor Fe-species (never exceeding 13 mole%) are supported by LCF as 3rd components: chromite (CHROM); richterite (RICHT); and pervoskite (PEROV). These fit results indicate that some additional Fe(II) is present in the sample, but are not interpreted as firm evidence for the specific mineral form.

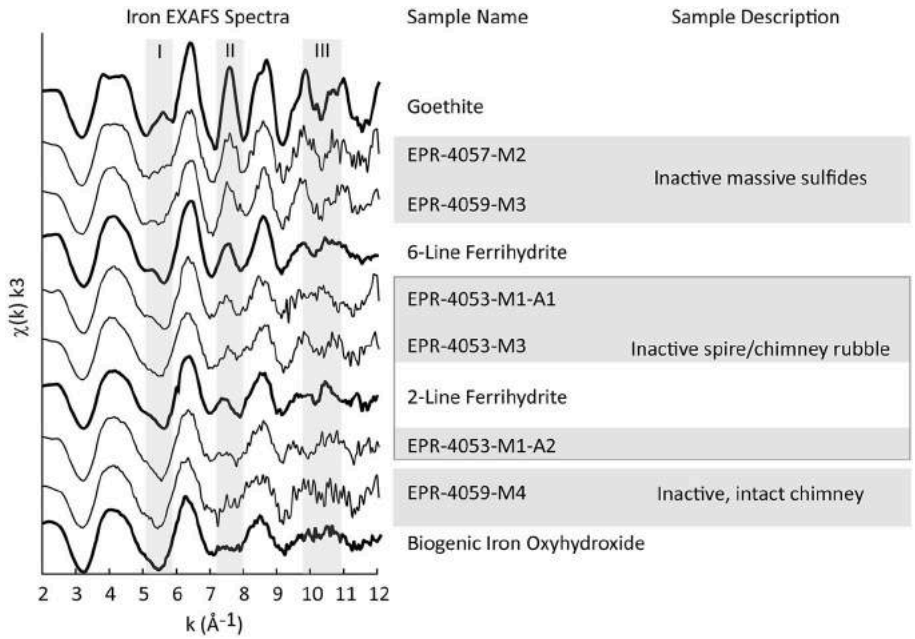

FIGURE 9 | Iron EXAFS spectra for EPR samples (fine lines) are plotted with spectra from Fe-bearing reference materials (bold lines). The location of Fe EXAFS data collection is recorded in **Table S4** with asterisks and annotated in **Figures 1**, **3**, **5**.

Comparison of Iron XANES and EXAFS Data

A full continuum of Fe oxyhydroxide phases, supported by Fe EXAFS data, are observed for the EPR sulfide deposits, from BIO-like phases lacking long-range structural order to well-crystallized goethite (**Figure 9**). Like the Fe XANES, Fe EXAFS spectra are subjected to LCF with reference spectra. Shell-by-shell fitting of the EXAFS data was not attempted due to the relatively short k-space range of the useable data (ca. 11 $Å^{-1}$). The results of the fitting are summarized in **Table S4**, and the LCFs are plotted with the EXAFS data in **Figure S9**. The fits to the EXAFS data agree well with XANES fits for the same locations on the samples. For example, the Fe EXAFS data from sample EPR-4057-M2 is best fit by 67% goethite (GOE) and 39% biogenic Fe oxyhydroxide (BIO) references. In this sample location, microprobe XRD was used to verify that goethite was present (**Figure S7**); this is an important methodological confirmation that the goethite reference spectrum is representative of goethite in the sample. The corresponding fit to the much shorter Fe XANES data region yields 62% goethite and 34% BIO. The comparisons of XANES and EXAFS data also show that spectroscopically similar phases can be difficult to distinguish using LCF. For example, the Fe EXAFS data from sample EPR-4053-M1-A2 is best fit by 55% BIO and 34% 6-line ferrihydrite (6LFH), while the corresponding Fe XANES data fit yields 47% BIO and 52% 2-line ferrihydrite (2LFH).

Comparison of Iron Isotope Compositions

The EPR chimney samples that exhibit complex interweaved layers of Fe(III), Si, and sulfide have a larger range of δ^{57}Fe values relative to massive sulfides (e.g., EPR-4057-M2). When Fe oxyhydroxides occur as filling materials within the chimney wall or as outside layer crusts in association with Si-rich material, enrichments in both heavy and light Fe isotopes relative to pyrite are possible. The range of values δ^{57}Fe is up to 6‰ which enlarges not only the range of Fe isotopes measured in hydrothermal vent environments (Rouxel et al., 2008a) but also in marine sediments (Severmann et al., 2006; Johnson et al., 2008; Rouxel et al., 2008b). In most cases, Fe-oxyhydroxides are enriched in light Fe isotopes relative to vent fluid sources (**Figure 10**).

DISCUSSION

Iron Isotope Systematics

Significant variability of Fe isotope composition in (oxyhydr)oxide precipitates is expected when Fe(II) is partially oxidized in conditions with slow rates of oxidation. Microbiological experiments have shown that Fe isotope fractionations are produced during dissimilatory Fe(III) reduction (Beard et al., 2003b; Icopini et al., 2004; Johnson and Beard, 2005) and anaerobic photosynthetic Fe(II) oxidation (Croal et al., 2004; Swanner et al., 2015). Iron isotopes can also be fractionated by abiotic Fe(II) oxidation, precipitation of ferric hydroxides (Bullen et al., 2001; Beard et al., 2010), and by sorption of aqueous Fe(II) onto Fe oxyhydroxides (Icopini et al., 2004; Wu et al., 2012). The largest equilibrium isotope fractionations (∼4.5‰ in $^{57}Fe/^{54}Fe$ ratios) observed and theoretically calculated are for coexisting Fe(III) and Fe(II) aqueous species (Welch et al., 2003; Anbar et al., 2005). Hence, in view of the variety of fractionating processes during Fe redox

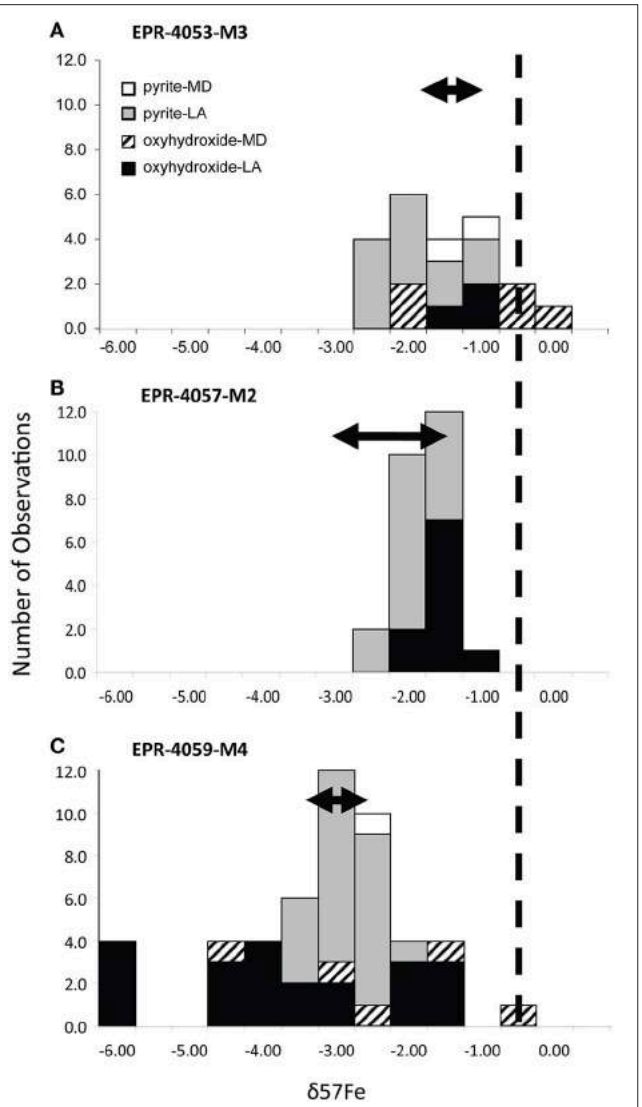

FIGURE 10 | Summary of δ^{57}Fe isotope values for (A) EPR-4053-M3 (K Vent rubble), (B) EPR-4057-M2 (Bio9 Area massive sulfide), and (C) EPR-4059-M4 (extinct, off-axis chimney). Micro-drilling (MD), laser ablation (LA), pyrite, and oxyhydroxides sample characteristics are indicated in the legend.

changes, it is not surprising that marked variations in Fe-isotope composition have been observed in Fe-rich marine environments (Severmann et al., 2006; Rouxel et al., 2008b). Large variations are also reported in banded iron formations (Johnson et al., 2003; Rouxel et al., 2005; Dauphas and Rouxel, 2006; Planavsky et al., 2012), hydrothermal fluids and precipitates (Sharma et al., 2001; Beard et al., 2003a; Rouxel et al., 2003, 2004), and ancient seafloor hydrothermal Fe-Si deposits (Planavsky et al., 2012; Moeller et al., 2014). Iron (oxyhydr)oxide particles within near-vent (buoyant) hydrothermal plumes at the Rainbow hydrothermal field (Mid Atlantic Ridge) have variable δ^{57}Fe values (0.15 to 1.65‰) relative to the original vent fluid, consistent with fractionation during partial oxidation of Fe(II)*aq* to Fe(III)*aq* in seawater (Severmann et al., 2004). In contrast, Fe (oxyhydr)oxide-rich sediments precipitated from non-buoyant hydrothermal plumes have δ^{57}Fe values that are indistinguishable from that of high-temperature hydrothermal fluids (Severmann et al., 2004). In a more recent study, low-temperature Fe (oxyhydr)oxide deposits from the Jan Mayen hydrothermal vent fields Norwegian-Greenland Sea yielded very light δ^{57}Fe values down to −2.8‰ (Moeller et al., 2014). These values are indistinguishable from low-temperature hydrothermal fluids from which they precipitated, suggesting that hydrothermal vent fluid underwent significant partial Fe(II) oxidation below seafloor leading to isotopically light Fe values for Fe(II), as previously proposed (Rouxel et al., 2003).

In our study, δ^{57}Fe values for Fe oxyhydroxides of the chimney wall are both heavier and lighter than the coeval pyrite or hydrothermal fluids. We propose that a reservoir effect is created during partial Fe(II) oxidation and can explain the diversity of values: (1) heavier values are consistent with small extent of Fe(II) oxidation; (2) lighter values are consistent with a greater extent of Fe(II) oxidation; and (3) lightest values are consistent with loss of Fe oxyhydroxides along a flow path (open system Fe oxidation) (Dauphas and Rouxel, 2006; Moeller et al., 2014). Extremely light Fe isotope values can be attained through Rayleigh-type fractionation and could explain the δ^{57}Fe values, as low as −7‰, we observe for Fe oxyhydroxides in sample EPR-4059-M4 (**Figure 10C**). Such partial Fe(II) oxidation probably required micro-aerobic conditions in which the rate of Fe(II) oxidation is slow enough to generate high variability of δ^{57}Fe values. Considering that such conditions are also favorable for the growth of Fe-oxidizing microorganisms (Druschel et al., 2008), the involvement of microorganisms in the Fe transformation pathways is likely. However, biotic Fe oxidation is not demonstrated in the present case because abiotic Fe oxidation can also produce these Fe isotope fractionation factors.

Iron Transformation Pathways in Sulfide Mineral Deposits

Summary of Transformation Pathways

The main goal of this study is to describe the Fe transformation pathways in natural sulfide mineral deposits at the seafloor, and examine the transformation products for indications or markers of biological activity. The hydrothermally inactive sulfide deposits of the EPR 9–10°N are known to host microbial communities with the genetic potential to alter Fe- and S-bearing minerals through redox reactions (Sylvan et al., 2012; Toner et al., 2013). Our investigation of the EPR sulfide deposits indicates that the alteration products are generated by at least four different pathways. Each pathway can be *complete and quantitative*, leading to an isotopic signature similar to the source Fe, or *partial*, leading to isotopic fractionation:

(Pathway 1) direct precipitation of Fe(II)*aq*, to form primary sulfide minerals, from hydrothermal fluids in zones of mixing between vent fluids and seawater;

(Pathway 2) precipitation of Fe(II)*aq*, to form sulfide minerals, from Fe(III) reduction in zones of mixing between vent fluids and seawater;

(Pathway 3) direct oxidation of Fe(II)*aq* from hydrothermal fluids, to form Fe(III) precipitates, in zones of mixing between vent fluids and seawater; and
(Pathway 4) oxidative alteration of pre-existing sulfide minerals to form Fe(III) precipitates.

Pathways Created by Vent Fluid-Seawater Mixing

In several sulfide deposits at the EPR, we observe layered zones of Fe(III)-, Si-, and sulfide-rich precipitates that are consistent with cooling vent fluids and low redox potential (e.g., **Figures 1A,D,C**, **5**). The precipitation of pyrite in the exterior chimney wall is probably a late-stage phenomenon reflecting a different pathway of mineral formation than the coarse-grained to euhedral pyrite composing the chimney wall. In many cases, we observe colloform and spherulitic pyrite textures on the chimney exterior in association with amorphous silica and often lining former worm tubes. Fine-grained to colloform pyrite with minor sphalerite may occur along fossil worm tubes (formed probably by *Alvinella*) (Little et al., 2007; Rouxel et al., 2008a). As discussed by Xu and Scott, 2005, spherulitic and colloform textures of pyrite reflect rapid crystallization (i.e., disequilibrium) with cooling caused by mixing between hot vent fluid and cold ambient seawater. Overall, for our samples, the texture and morphology of these pyrite-Si-oxyhydroxide zones is highly variable; we speculate that this is caused primarily by the wide range of fluid flow and redox regimes created in actively venting chimneys. For many of our samples, pyrite lined fossil worm tubes exhibit $\delta^{34}S$ and $\delta^{57}Fe$ values (4.3 to 3.0 and −1.8 to −1.2‰, respectively) typical of bulk pyrite from the chimney wall (Rouxel et al., 2008b), which is consistent with direct precipitation from hydrothermal fluids (Pathway 1).

In addition to Pathway 1, the presence of pyrite within layered zones of Fe(III)-, Si-, and sulfide-rich precipitates could be caused by reductive processes in the mixing zone (Pathway 2). For example, pyrite forming at low–temperature and in an open system in contact with sulfate-rich seawater creates the potential for microbial sulfate and Fe(III) reduction. This possibility has been proposed from studies of microbial diversity in hydrothermal chimneys (Callac et al., 2015), as well as metabolic energetic calculations (Amend et al., 2011). Sulfur isotope studies show the contribution of microbial sulfate reduction and sulfide formation at mid-oceanic ridges (Peters et al., 2010); however, a robust S isotope biosignature in hydrothermal chimney environments has not been demonstrated. Our results provide strong evidence for secondary and late-stage pyrite formation along the outside wall of the chimneys due to vent fluid-seawater mixing. This interpretation, based on isotope data, Fe speciation, and mineral textures, is also consistent with the observed enrichment in silica. In general, silica precipitation in seafloor hydrothermal chimneys requires some degree of conductive cooling due to the solubility of amorphous Si in simple mixing between hydrothermal fluids and seawater (Hannington et al., 1995).

Iron oxyhydroxides may also form in low-oxygen environments during hydrothermal-fluid mixing, although the expected slow rate of Fe oxidation in dilute hydrothermal fluids may limit the accumulation of Fe oxyhydroxides in the absence of microbial mediation. Localized Si and As enrichments within the Fe oxyhydroxides is common for our samples (**Figures 1A,C,D**, **5A–D**). In many cases, the layered Fe(III)-, Si-, and sulfide-rich zones exhibit $\delta^{57}Fe$ values that are consistently lighter than hydrothermal vent fluids (**Figure 10**). This observation cannot be explained by either partial or quantitative Fe(II) oxidation because the resulting Fe(III) should be enriched in heavy Fe isotopes relative to Fe(II), regardless of the mechanism and extent of Fe(II) oxidation. Therefore, it is likely that these Fe oxyhydroxides formed through a combination of quantitative oxidation of vent fluid Fe(II) (Pathway 3) and alteration (i.e., oxidation) of pyrite characterized by much lighter $\delta^{57}Fe$ values than vent fluids (Pathway 4).

In sample EPR-4053-M3-reg1 (**Figure 2**), $\delta^{57}Fe$ values are consistent with either partial oxidation of pyrite (*partial* Pathway 4) or direct and quantitative oxidation of late-stage vent fluid Fe(II) (Pathway 3). The $\delta^{57}Fe$ values of the Fe oxyhydroxides range from −0.32 to −1.59‰ which is heavier than associated pyrite by up to 2.3‰ but also within the range expected for hydrothermal vent fluids, especially low-temperature or late-stage vent fluids (Rouxel et al., 2008a; Moeller et al., 2014). In contrast, sample EPR-4059-M4-reg2 (**Figure 7B**) exhibits very light Fe isotope values for the Fe oxyhydroxides, which are up to 4.7‰ lighter than associated pyrite. These data cannot be explained by simple mixing between Fe(III) derived from local sulfide (pyrite) oxidation and Fe(II) from vent fluid. During partial Fe(II) oxidation, the remaining Fe(II) in solution is expected to become isotopically lighter due to the precipitation of isotopically heavy Fe-oxyhydroxide (*partial* Pathway 3). This mechanism, often referred to as a reservoir effect, has been shown to lead to isotopically light Fe(II) in sediment porewater ($\delta^{57}Fe$ down to −7.38‰) (Rouxel et al., 2008a) and likely occurs within cavities of hydrothermal chimneys. The fact that isotopically light Fe oxyhydroxides occur in association with significant Si enrichment (e.g., EPR-4059-M4-reg4; **Figure 4B**) and filling cavities of the chimney wall (EPR-4059-M4-reg2; **Figure 7B**) is consistent with this assumption. In this case, Fe(II) released during pyrite alteration (Pathway 4) or late-stage hydrothermal fluid undergoing partial oxidation in the chimney wall (*partial* Pathway 3), leads to the formation of isotopically light Fe(II) diffusing out of the chimney wall and ultimately precipitating as Fe oxyhydroxide.

Pathways Created by Complete and Direct Oxidation

In contrast to the Fe transformation pathways discussed in section Pathways Created by Vent Fluid-Seawater Mixing, the two massive sulfide deposits exhibit a simpler set of Fe reactions. For the EPR-4057-M2-reg1, the $\delta^{57}Fe$ values are very close to Fe in unaltered pyrite (−1.93 ± 0.20 vs. −1.69 ± 0.11‰), and are consistent with direct and complete oxidation of pyrite-Fe to goethite-Fe (Pathway 4; **Figure 4A**). While the incipient Fe oxyhydroxide phase is not known in this case, a short-term (2 months) chimney incubation study at the Juan de Fuca Ridge indicates the possibility of a biogenic-like Fe oxyhydroxide incipient phase (Toner et al., 2009b). The fact that the Fe oxyhydroxide is primarily goethite, with no co-located Si or As, is

suggestive of transformation of the initial precipitation products to the stable goethite phase over time in ambient deep ocean waters.

CONCLUSIONS

One of the main objectives of the present study is to determine whether alteration materials associated with seafloor sulfide deposits possess mineralogical or stable isotope biosignatures. In essence, we want to know the reactants, mechanisms, and products for reactions involving Fe. In light of the microbial community data (Sylvan et al., 2012; Toner et al., 2013), textural complexity noted in hand specimens (Rouxel et al., 2008a), and spatial scale of mineralogical variability in petrographic sections (this work), we chose a spatially resolved spectroscopic and isotopic approach to the study of the EPR sulfides. The spectroscopic approach provides the reaction products (and in some cases reactants) through measurement of the chemical form of Fe, as well as the identity of co-located elements: while the isotopic approach provides the source-Fe reactant(s) and the extent of the reaction. The application of these complementary tools at the 10–50 micron spatial scale certainly must have averaged over finer submicron geochemical information. However, the spatial scale of investigation did allow us to describe the diversity of mineral forms and isotopic signatures intrinsic to these sulfides, and demonstrates the synergy of spectroscopic and isotopic approaches.

Culture-independent microbiology results show that microbial communities of the EPR change when chimney structures become hydrothermally extinct (Sylvan et al., 2012). Once extinct, the EPR sulfide deposits host bacterial communities similar in composition and structure to mid-ocean ridge sulfides from far distant sites, such as the Indian Ocean (Toner et al., 2013). The presence of bacterial groups known for Fe and S cycling in EPR sulfide samples (e.g., β-Proteobacteria *Gallionella* sp. and ε-Proteobacteria *Sulfurimonas* sp.) indicates that microorganisms should be able to mediate the alteration of sulfide mineral substrates. As a result of S and/or Fe oxidation processes, Fe(III) reaction products are expected, and Fe(III)-bearing phases are abundant in the EPR sulfide deposits examined in this study. Overall, these findings provide evidence to support the idea that inactive sulfide deposits are more than passive surfaces for microbial attachment. However, only the genetic potential, not the metabolic capabilities, of microbial community members are measured by the sequencing approaches used to-date for this sample set.

While our analysis of Fe mineralogy and isotope values do not support or refute a unique biological role in Fe(III) oxyhydroxide precipitation during sulfide alteration, our findings do reveal complex reaction pathways of Fe—precipitation/dissolution and oxidation/reduction—in seafloor sulfide deposits. The variety of Fe transformation pathways we observe is consistent with the development of micro-environments within the sulfide deposits. By defining four pathways of Fe transformation, we can propose several micro-environments. We observe zones of mixing between vent fluids and seawater with both reducing (Pathways 1 and 2) and oxidizing conditions (Pathways 2 and 4). These micro-environments are consistent with the diverse genetic potential, and correspondingly wide range of potential metabolisms, observed in organisms cultured from sulfide deposits. The reducing-to-oxidizing range of mixing zones, in particular, could support micro-environments favorable to Fe and S oxidation and reduction within a single chimney deposit.

In contrast to the dynamic multi-step pathways revealed by Fe isotopes, the Fe XAS observations for these samples are consistent with stabilization of poorly ordered Fe(III) oxyhydroxide phases when Si and As are present. At first glance, it is surprising that multi-stage Fe oxidation and precipitation processes would preserve poorly ordered, and presumably, metastable Fe(III) oxyhydroxide phases. However, laboratory experiments have demonstrated that Fe atom replacement within Fe(III) oxyhydroxides, such as goethite, can produce the same mineral structure and particle morphology in the presence of Fe(II)*aq* (Handler et al., 2009). While there are many time-dependent factors that our measurements cannot assess—temperature, flow-rate, time-resolved vent fluid chemistry—the dynamic history supported by the Fe isotopes and static history supported by the mineralogy leads us to conclude that inorganic ligands (As, Si), and possibly biological material (Toner et al., 2009b, 2012), stabilize poorly ordered Fe(III) oxyhydroxide phases in these deposits. In addition, ligands appear to be retained by the deposit throughout a complex set of Fe transformation events and dynamic re-working of the Fe-bearing alteration products. It is possible that this mineral-stabilization outcome is driven by a decrease in permeability of the sulfide deposits as a function of time. Low-flow conditions could lead to the retention of ligands in pore spaces and preservation metastable phases despite continued alteration of the Fe-bearing minerals. The physical and chemical environments created by seafloor sulfide deposits do not appear to provide unique biosignatures. However, they do appear to be promising recorders of micro-environmental conditions present during hydrothermal activity.

AUTHOR CONTRIBUTIONS

Authors CS, OR, WB, and KE collected the samples, OR analyzed samples for Fe and S isotopes, BT and CS analyzed samples for Fe mineralogy, and BT, OR, CS, and WB prepared the manuscript.

ACKNOWLEDGMENTS

For financial support we thank: NASA for a small grant for laser ablation MC-ICP-MS measurements (BMT); the National Research Council Associate and NASA Postdoctoral Programs (BMT); RIDGE 2000 (OCE-0241791; KJE and WB); and CFANS University of Minnesota (BMT); LabexMer (ANR-10-LABX-19-01; OJR). For research support we thank: M. K. Tivey, G. A. Gaetani, and M. Sulanowska (Woods Hole Oceanographic Institution) for making laboratory space,

wafering saw, petrographic microscope, and polishing equipment available; M. A. Marcus for support at ALS BL10.3.2; N. Tamura for support at ALS BL 7.3.3; C. M. Hansel and S. Fendorf for providing iron EXAFS reference spectra; E. Ponzevera and Y. Germain for maintaining the mass spectrometry facility and clean lab at Ifremer; and L. J. Briscoe for scanning electron microscopy imaging. The Advanced Light Source (ALS) is supported by the Office of Science, Basic Energy Sciences, Division of Materials Science of the U.S. Department of Energy (DE-AC02-05CH11231). Part of this work was carried out at the Institute of Technology, Characterization Facility, University of Minnesota (an NSF-funded Materials Research Facilities Network).

SUPPLEMENTARY MATERIAL

The Supplementary Material for this article can be found online at: http://journal.frontiersin.org/article/10.3389/fmicb.2016.00648

Figure S1 | Seafloor photographs of sampling sites. (A,B) Location of K Vent samples EPR-4053-M2, EPR-4053-M1-A1, and EPR-4053-M1-A2. **(C,D)** Massive sulfide deposits in the Bio9 Vent area EPR-4057-M2 and EPR-4059-M3, respectively. **(E)** Off axis, extinct chimney sources of sample EPR-4059-M4. Images previously published in various forms in Rouxel et al., 2008a; Sylvan et al., 2012; Toner et al., 2013.

Figure S2 | Shipboard photographs of samples.

Figure S3 | Shipboard photographs of K Vent inactive spire showing the locations of EPR-4053-M1-A1 and EPR-4053-M1-A2. Portions of this figure are published in Rouxel et al., 2008b

Figure S4 | Photographs of polished thick sections showing the regions of the sample investigated.

Figure S5 | Example laser ablation run.

Figure S6 | Iron isotope values as a function of S:Fe and Si:Fe.

Figure S7 | (A) Synchrotron radiation microprobe X-ray diffraction data from spot 2 of EPR-4057-M2. **(B)** Data with goethite reference lines.

Figure S8 | Petrographic microscope images of sample EPR-4057-M2. (A) Iron oxyhydroxide accumulations at the seawater exposed surface of the massive sulfide deposit. **(B)** Oxidation of pyrrhotite crystals. **(C,D)** Sulfide minerals.

Figure S9 | Summary of Fe EXAFS data (dots) and best linear combination fit (solid lines). Goodness of fit parameters (**Table S4**) and key for reference materials (**Table S2**) are provided in the main text.

Table S1 | Summary of sample locations and naming conventions.

Table S2 | Summary of Fe-bearing reference materials used for linear combination fitting (LCF) of X-ray absorption spectra. The χ^2, *R*-value, and SPOIL parameters are derived from principal component (PCA) and target transformation analysis (TTA).

Table S3 | Linear combination fit results for Fe X-ray absorption near edge structure (XANES) spectra. Fit components are listed along with the mol% attributed to each component. The components (reference spectra) contributing to the best fit are described in **Table S2**. The normalized sum square (NSS) parameter is an indicator of the goodness of the fit. An * symbol indicates that extended X-ray absorption fine structure (EXAFS) spectra were also collected (**Table S4**). The "Over Absorption Correction" is defined in the Section Synchrotron Microprobe X-ray Absorption Spectroscopy (XAS) Analysis.

Table S4 | Linear combination fit results for Fe extended X-ray absorption fine structure (EXAFS) spectra. Fit components are listed along with the mol% attributed to each component. The components (reference spectra) contributing to the best fit are described in **Table S2**. The chi square parameter (χ^2) is an indicator of the goodness of the fit.

Table S5 | Iron and S isotope analyses for sample EPR-4053-M3-reg1 (K Vent). Laser ablation (LA) and micro-drill (MD) sampling are organized according to the dominant mineralogy at that location (pyrite and oxyhydroxide). Specific locations of sampling are displayed in **Figure 2**. One standard deviation (σ) is reported.

Table S6 | Iron isotope analyses for sample EPR-4057-M2 (Bio9 Area). Laser ablation (LA) and micro-drill (MD) sampling are organized according to the dominant mineralogy at that location (pyrite and oxyhydroxide). Specific locations of sampling are displayed in **Figure 4A**. One standard deviation (σ) is reported.

Table S7 | Iron isotope analyses for sample EPR-4059-M4 (off-axis chimney). Laser ablation (LA) and micro-drill (MD) sampling are organized according to the dominant mineralogy at that location (pyrite and oxyhydroxide). Specific locations of sampling are displayed in **Figures 4B**, **7A,B**. One standard deviation (σ) is reported.

REFERENCES

Alt, J. C. (1988). Hydrothermal oxide and nontronite deposits on seamounts in the eastern Pacific. *Mar. Geol.* 81, 227–239. doi: 10.1016/0025-3227(88)90029-1

Amend, J. P., McCollom, T. M., Hentscher, M., and Bach, W. (2011). Catabolic and anabolic energy for chemolithoautotrophs in deep-sea hydrothermal systems hosted in different rock types. *Geochim. Cosmochim. Acta* 75, 5736–5748. doi: 10.1016/j.gca.2011.07.041

Anbar, A. D., Jarzecki, A. A., and Spiro, T. G. (2005). Theoretical investigation of iron isotope fractionation between Fe(H2O)63+ and Fe(H2O)62+: implications for iron stable isotope geochemistry. *Geochim. Cosmochim. Acta* 69, 825–837. doi: 10.1016/j.gca.2004.06.012

Beard, B. L., Handler, R. M., Scherer, M. M., Wu, L. L., Czaja, A. D., Heimann, A., et al. (2010). Iron isotope fractionation between aqueous ferrous iron and goethite. *Earth Planet. Sci. Lett.* 295, 241–250. doi: 10.1016/j.epsl.2010.04.006

Beard, B. L., Johnson, C. M., Skulan, J. L., Nealson, K. H., Cox, L., and Sun, H. (2003b). Application of Fe isotopes to tracing the geochemical and biological cycling of Fe. *Chem. Geol.* 195, 87–117. doi: 10.1016/S0009-2541(02)00390-X

Beard, B. L., Johnson, C. M., Von Damm, K. L., and Poulson, R. L. (2003a). Iron isotope constraints on Fe cycling and mass balance in oxygenated Earth oceans. *Geology* 31, 629–632. doi: 10.1130/0091-7613(2003)031<0629:IICOFC>2.0.CO;2

Bennett, S. A., Achterberg, E. P., Connelly, D. P., Statham, P. J., Fones, G. R., and German, C. R. (2008). The distribution and stabilisation of dissolved Fe in deep-sea hydrothermal plumes. *Earth Planet. Sci. Lett.* 270, 157–167. doi: 10.1016/j.epsl.2008.01.048

Boyd, T. D., and Scott, S. D. (2001). Microbial and hydrothermal aspects of ferric oxyhydroxides and ferrosic hydroxides: the example of Franklin Seamount, Western Woodlark Basin, Papua New Guinea. *Geochem. Trans.* 2, 45. doi: 10.1039/b105277m

Breier, J. A., Toner, B. M., Fakra, S. C., Marcus, M. A., White, S. N., Thurnherr, A. M., et al. (2012). Sulfur, sulfides, oxides and organic matter aggregated in submarine hydrothermal plumes at 9°50′ N East Pacific Rise. *Geochim. Cosmochim. Acta* 88, 216–236. doi: 10.1016/j.gca.2012.04.003

Bullen, T. D., White A. F., Childs, C. W., Vivit, D. V., and Schultz, M. S. (2001). Demonstration of a significant iron isotope fractionation in nature. *Geology* 29, 699–702. doi: 10.1130/0091-7613(2001)029<0699:DOSAII>2.0.CO

Byrne, N., Strous, M., Crépeau, V., Kartal, B., Birrien, J.-L., Schmid, M., et al. (2009). Presence and activity of anaerobic ammonium-oxidizing bacteria at deep-sea hydrothermal vents. *ISME J.* 3, 117–123. doi: 10.1038/ismej.2008.72

Callac, N., Rouxel, O., Lesongeur, F., Liorzou, C., Bollinger, C., Pignet, P., et al. (2015). Biogeochemical insights into microbe–mineral–fluid interactions in hydrothermal chimneys using enrichment culture. *Extremophiles* 19, 597–617. doi: 10.1007/s00792-015-0742-5

Combes, J. M., Manceau, A., Calais, G., and Bottero, J. Y. (1989). Formation of ferric oxides from aqueous solutions: a polyhedral approach by X-ray absorption spectroscopy: I. Hydrolysis and formation of ferric gels. *Geochim. Cosmochim. Acta* 53, 583–594. doi: 10.1016/0016-7037(89)90001-x

Craddock, P. R., Rouxel, O. J., Ball, L. A., and Bach, W. (2008). Sulfur isotope measurement of sulfate and sulfide by high-resolution MC-ICP-MS. *Chem. Geol.* 253, 102–113. doi: 10.1016/j.chemgeo.2008.04.017

Croal, L. R., Johnson, C. M., Beard, B. L., and Newman, D. K. (2004). Iron isotope fractionation by Fe(II)-oxidizing photoautotrophic bacteria. *Geochim. Cosmochim. Acta* 68, 1227–1242. doi: 10.1016/j.gca.2003.09.011

Dauphas, N., and Rouxel, O. (2006). Mass spectrometry and natural variations of iron isotopes. *Mass Spectrom. Rev.* 25, 515–550. doi: 10.1002/mas.20078

Druschel, G. K., Emerson, D., Sutka, R., Suchecki, P., and Luther, I. I. I. G. W. (2008). Low-oxygen and chemical kinetic constraints on the geochemical niche of neutrophilic iron(II) oxidizing microorganisms. *Geochim. Cosmochim. Acta* 72, 3358–3370. doi: 10.1016/j.gca.2008.04.035

Edmond, J. M., Measures, C., McDuff, R. E., Chan, L. H., Collier, R., Grant, B., et al. (1979). Ridge crest hydrothermal activity and the balances of the major and minor elements in the ocean: the Galapagos data. *Earth Planet. Sci. Lett.* 46, 1–18. doi: 10.1016/0012-821X(79)90061-X

Edwards, K. J., Bach, W., and Rogers, D. R. (2003a). Geomicrobiology of the ocean crust: a role for chemolithoautotrophic Fe-bacteria. *Biol. Bull.* 204, 180–185. doi: 10.2307/1543555

Edwards, K. J., Glazer, B. T., Rouxel, O. J., Bach, W., Emerson, D., Davis, R. E., et al. (2011). Ultra-diffuse hydrothermal venting supports Fe-oxidizing bacteria and massive umber deposition at 5000 off Hawaii. *ISME J.* 5, 1–11. doi: 10.1038/ismej.2011.48

Edwards, K. J., McCollom, T. M., Konishi, H., and Buseck, P. R. (2003b). Seafloor bioalteration of sulfide minerals: results from *in situ* incubation studies. *Geochim. Cosmochim. Acta* 67, 2843–2856. doi: 10.1016/S0016-7037(03)00089-9

Elderfield, H., and Schultz, A. (1996). Mid-ocean ridge hydrothermal fluxes and the chemical composition of the ocean. *Annu. Rev. Earth Planet. Sci.* 24, 191–224. doi: 10.1146/annurev.earth.24.1.191

Emerson, D. (2016). The irony of iron – biogenic iron oxides as an iron source to the Ocean. *Front. Microbiol.* 6:1502. doi: 10.3389/fmicb.2015.01502

Emerson, D., and Moyer, C. L. (2002). Neutrophilic Fe-oxidizing bacteria are abundant at the Loihi seamount hydrothermal vents and play a major role in Fe oxide deposition. *Appl. Environ. Microbiol.* 68, 3085–3093. doi: 10.1128/AEM.68.6.3085-3093.2002

Feely, R. A., Gendron, J. F., and Baker, E. T. (1994). Hydrothermal plumes along the East Pacific Rise, 8 40′ to 11 50′N: particle distribution and composition. *Earth Planet. Sci. Lett.* 128, 19–36. doi: 10.1016/0012-821X(94)90023-X

Feely, R. A., Massoth, G. J., Baker, B. J., Lebon, G. T., and Geiselman, T. I. (1992). Tracking the dispersal of hydrothermal plumes from the Juan de Fuca Ridge using suspended matter compositions. *J. Geophys. Res.* 97, 3457–3468. doi: 10.1029/91JB03062

Field, M. P., and Sherrell, R. M. (2000). Dissolved and particulate Fe in a hydrothermal plume at 9 o 45′ N, East Pacific Rise: slow Fe(II) oxidation kinetics in Pacific plumes. *Geochim. Cosmochim. Acta* 64, 619–628. doi: 10.1016/s0016-7037(99)00333-6

Fitzsimmons, J. N., Boyle, E. A., and Jenkins, W. J. (2014). Distal transport of dissolved hydrothermal iron in the deep South Pacific Ocean. *Proc. Natl. Acad. Sci. U.S.A.* 111, 16654–16661. doi: 10.1073/pnas.1418778111

Fouquet, Y., Cambon, P., Etoubleau, J., Charlou, J. L., Ondreas, H., Barriga, F., et al. (2010). "Geodiversity of hydrothermal processes along the Mid-Atlantic Ridge—ultramafic-hosted mineralization: a new type of Oceanic Cu-Zn-Co-Au VMS deposit," in *Diversity of Hydrothermal Systems on Slow-spreading Ocean Ridges*, ed P. Rona (Washington DC: American Geophysical Union), 321–367.

Graham, S., Pearson, N. J., Jackson, S., Griffin, W., and O'Reilly, S. Y. (2004). Tracing Cu and Fe from source to porphyry: *in situ* determination of Cu and Fe isotope ratios in sulfides from the Grasberg Cu–Au deposit. *Chem. Geol.* 207, 147–169. doi: 10.1016/j.chemgeo.2004.02.009

Handler, R. M., Beard, B. L., Johnson, C. M., and Scherer, M. M. (2009). Atom exchange between Aqueous Fe (II) and Goethite : an Fe isotope tracer Study. *Environ. Sci. Technol.* 43, 1102–1107. doi: 10.1021/es802402m

Hannington, M. D., Jonasson, I. R., Herzig, P. M., and Peterson, S. (1995). "Physical and chemical processes of seafloor mineralization at Mid-Ocean ridges," in *Seafloor Hydrothermal Systems: Physical, Chemical, Biological, and Geological Interactions,* eds S. E. Humphris, R. A. Zierenberg, L. S. Mullineaux, and R. E. Thomson (Washington, DC: American Geophysical Union), 115–157.

Hansel, C. M., Benner, S. G., Neiss, J., Dohnalkova, A., Kukkadapu, R. K., and Fendorf, S. (2003). Secondary mineralization pathways induced by dissimilatory iron reduction of ferrihydrite under advective flow. *Geochim. Cosmochim. Acta* 67, 2977–2992. doi: 10.1016/S0016-7037(03)00276-X

Hawkes, J. A., Connelly, D. P., Gledhill, M., and Achterberg, E. P. (2013). The stabilization and transportation of dissolved iron from high temperature hydrothermal vent systems. *Earth Planet. Sci. Lett.* 375, 280–290. doi: 10.1016/j.epsl.2013.05.047

Holden, J., and Adams, M. W. W. (2003). Microbe–metal interactions in marine hydrothermal environments. *Curr. Opin. Chem. Biol.* 7, 160–165. doi: 10.1016/S1367-5931(03)00026-7

Horn, I., von Blanckenburg, F., Schoenberg, R., Steinhoefel, G., and Markl, G. (2006). *In situ* iron isotope ratio determination using UV-femtosecond laser ablation with application to hydrothermal ore formation processes. *Geochim. Cosmochim. Acta* 70, 3677–3688. doi: 10.1016/j.gca.2006.05.002

Houghton, J. L., and Seyfried, W. E. Jr. (2010). An experimental and theoretical approach to determining linkages between geochemical variability and microbial diversity in seafloor hydrothermal chimneys. *Geobiology* 8, 457–470. doi: 10.1111/j.1472-4669.2010.00255.x

Houghton, R. A. (2007). Balancing the global carbon budget. *Annu. Rev. Earth Planet. Sci.* 35, 313–347. doi: 10.1146/annurev.earth.35.031306.140057

Icopini, G. A., Anbar, A. D., Ruebush, S. S., Tien, M., and Brantley, S. L. (2004). Iron isotope fractionation during microbial reduction of iron: the importance of adsorption. *Geology* 32, 205–208. doi: 10.1130/G20184.1

Johnson, C. M., and Beard, B. L. (2005). Biogeochemical cycling of iron isotopes. *Science* 309, 1025–1027. doi: 10.1126/science.1112552

Johnson, C. M., Beard, B. L., Beukes, N. J., Klein, C., and O'Leary, J. M. (2003). Ancient geochemical cycling in the Earth as inferred from Fe isotope studies of banded iron formations from the Transvaal Craton. *Contrib. Mineral. Petrol.* 144, 523–547. doi: 10.1007/s00410-002-0418-x

Johnson, C. M., Beard, B. L., and Roden, E. E. (2008). The iron isotope fingerprints of redox and biogeochemical cycling in the modern and ancient Earth. *Annu. Rev. Earth Planet. Sci.* 36, 457–493. doi: 10.1146/annurev.earth.36.031207.124139

Karl, D. M. (1995). "Ecology of free-living, hydrothermal vent microbial communities," in *The Microbiology of Deep-Sea Hydrothermal Vents*, ed D. M. Karl (Boca Raton, FL: CRC Press), 35–124.

Kraft, S., Stümpel, J., Becker, P., and Kuetgens, U. (1996). High resolution x-ray absorption spectroscopy with absolute energy Calibration for the determination of absorption edge energies. *Rev. Sci. Instrum.* 67, 681–687. doi: 10.1063/1.1146657

Lever, M. A., Rouxel, O., Alt, J. C., Shimizu, N., Ono, S. H., Coggon, R. M., et al. (2013). Evidence for microbial carbon and sulfur cycling in deeply buried ridge flank basalt. *Science* 339, 1305–1308. doi: 10.1126/science.1229240

Li, M., Toner, B. M., Baker, B. J., Breier, J. A, Sheik, C. S., and Dick, G. J. (2014). Microbial iron uptake as a mechanism for dispersing iron from deep-sea hydrothermal vents. *Nat. Commun.* 5, 3192. doi: 10.1038/ncomms4192

Little, C. T. S., Magalashvili, A. G., and Banks, D. A. (2007). Neotethyan Late Cretaceous volcanic arc hydrothermal vent fauna. *Geology* 35, 835–838. doi: 10.1130/G23957A.1

Manceau, A., Marcus, M. A., and Tamura, N. (2002). Quantitative speciation of heavy metals in soils and sediments by synchrotron X-ray techniques. *Rev. Mineral. Geochem.* 49, 341–428. doi: 10.2138/gsrmg.49.1.341

Marcus, M. A., Edwards, K. J., Gueguen, B., Fakra, S. C., Horn, G., Jelinski, N., et al. (2015). Iron mineral structure, reactivity, and isotopic composition in a South Pacific Gyre ferromanganese nodule over 4 Ma. *Geochim. Cosmochim. Acta* 171, 61–79. doi: 10.1016/j.gca.2015.08.021

Marcus, M. A., MacDowell, A., Celestre, R., Manceau, A., Miller, T., Padmore, H. A., et al. (2004). Beamline 10.3.2 at ALS: a hard X-ray microprobe for

environmental and material sciences. *J. Synchrotron Rad.* 11, 239–247. doi: 10.1107/S0909049504005837

Marcus, M. A., Westphal, A. J., and Fakra, S. (2008). Classification of Fe-bearing species from K-edge XANES data using two-parameter correlation plots. *J. Synchrotron Rad.* 15, 463–468. doi: 10.1107/S0909049508018293

Mason, P. R. D., Kosler, J., de Hoog, J. C. M., Sylvester, P. J., Meffan-Main, S., Košler, J., et al. (2006). *In situ* determination of sulfur isotopes in sulfur-rich materials by laser ablation multiple-collector inductively coupled plasma mass spectrometry (LA-MC-ICP-MS). *J. Anal. At. Spectrom.* 21, 177–186. doi: 10.1039/B510883G

Michel, F. M., Ehm, L., Antao, S. M., Lee, P. L., Chupas, P. J., Liu, G., et al. (2007). The structure of ferrihydrite, a nanocrystalline material. *Science* 316, 1726–1729. doi: 10.1126/science.1142525

Mills, R. A., and Elderfield, H. (1995). Rare earth element geochemistry of hydrothermal deposits from the active TAG Mound, 26°N Mid-Atlantic Ridge. *Geochim. Cosmochim. Acta* 59, 3511–3524. doi: 10.1016/0016-7037(95)00224-N

Moeller, K., Schoenberg, R., Grenne, T., Thorseth, I. H., Drost, K., and Pedersen, R. B. (2014). Comparison of iron isotope variations in modern and Ordovician siliceous Fe oxyhydroxide deposits. *Geochim. Cosmochim. Acta* 126, 422–440. doi: 10.1016/j.gca.2013.11.018

Nakagawa, S., Takai, K., Inagaki, F., Hirayama, H., Nunoura, T., Horikoshi, K., et al. (2005). Distribution, phylogenetic diversity and physiological characteristics of epsilon-Proteobacteria in a deep-sea hydrothermal field. *Env. Microbiol.* 7, 1619–1632. doi: 10.1111/j.1462-2920.2005.00856.x

Nishizawa, M., Yamamoto, H., Ueno, Y., Tsuruoka, S., Shibuya, T., Sawaki, Y., et al. (2010). Grain-scale iron isotopic distribution of pyrite from Precambrian shallow marine carbonate revealed by a femtosecond laser ablation multicollector ICP-MS technique: possible proxy for the redox state of ancient seawater. *Geochim. Cosmochim. Acta* 74, 2760–2778. doi: 10.1016/j.gca.2010.02.014

O'Day, P. A., Rivera, N. Jr., Root, R., and Carroll, S. A. (2004). X-ray absorption spectroscopic study of Fe reference compounds for the analysis of natural sediments. *Am. Miner.* 89, 572–585. doi: 10.2138/am-2004-0412

Orcutt, B. N., Bach, W., Becker, K., Fisher, A. T., Hentscher, M., Toner, B. M., et al. (2011). Colonization of subsurface microbial observatories deployed in young ocean crust. *ISME J.* 5, 692–703. doi: 10.1038/ismej.2010.157

Pagé, A., Tivey, M. K., Stakes, D. S., and Reysenbach, A.-L. (2008). Temporal and spatial archaeal colonization of hydrothermal vent deposits. *Environ. Microbiol.* 10, 874–884. doi: 10.1111/j.1462-2920.2007.01505.x

Paris, G., Sessions, A. L., Subhas, A. V., and Adkins, J. F. (2013). MC-ICP-MS measurement of delta S-34 and delta S-33 in small amounts of dissolved sulfate. *Chem. Geol.* 345, 50–61. doi: 10.1016/j.chemgeo.2013.02.022

Peters, M., Strauss, H., Farquhar, J., Ockert, C., Eickmann, B., and Jost, C. L. (2010). Sulfur cycling at the Mid-Atlantic Ridge: a multiple sulfur isotope approach. *Chem. Geol.* 269, 180–196. doi: 10.1016/j.chemgeo.2009.09.016

Planavsky, N., Rouxel, O. J., Bekker, A., Hofmann, A., Little, C. T. S., and Lyons, T. W. (2012). Iron isotope composition of some Archean and Proterozoic iron formations. *Geochim. Cosmochim. Acta* 80, 158–169. doi: 10.1016/j.gca.2011.12.001

Poitrasson, F., and Freydier, R. (2005). Heavy iron isotope composition of granites determined by high resolution MC-ICP-MS. *Chem. Geol.* 222, 132–147. doi: 10.1016/j.chemgeo.2005.07.005

Prietzel, J., Thieme, J., Eusterhues, K., and Eichert, D. (2007). Iron speciation in soils and soil aggregates by synchrotron-based X-ray microspectroscopy (XANES, micro-XANES). *Eur. J. Soil Sci.* 58, 1027–1041. doi: 10.1111/j.1365-2389.2006.00882.x

Resing, J. A., Sedwick, P. N., German, C. R., Jenkins, W. J., Moffett, J. W., Sohst, B., et al. (2015). Basin-scale transport of hydrothermal dissolved metals across the South Pacific Ocean. *Nature* 523, 200–206. doi: 10.1038/nature14577

Reysenbach, A. L., and Cady, S. L. (2001). Microbiology of ancient and modern hydrothermal systems. *Trends Microbiol.* 9, 79–86. doi: 10.1016/S0966-842X(00)01921-1

Rouxel, O., Dobbek, N., Ludden, J., and Fouquet, Y. (2003). Iron isotope fractionation during oceanic crust alteration. *Chem. Geol.* 202, 155–182. doi: 10.1016/j.chemgeo.2003.08.011

Rouxel, O., Fouquet, Y., and Ludden, J. N. (2004). Subsurface processes at the lucky strike hydrothermal field, Mid-Atlantic ridge: evidence from sulfur, selenium, and iron isotopes. *Geochim. Cosmochim. Acta* 68, 2295–2311. doi: 10.1016/j.gca.2003.11.029

Rouxel, O., Shanks, W. C. III, Bach, W., and Edwards, K. J. (2008a). Integrated Fe- and S-isotope study of seafloor hydrothermal vents at East Pacific Rise 9–10°N. *Chem. Geol.* 252, 214–227. doi: 10.1016/j.chemgeo.2008.03.009

Rouxel, O., Sholkovitz, E., Charette, M., and Edwards, K. J. (2008b). Iron isotope fractionation in subterranean estuaries. *Geochim. Cosmochim. Acta* 72, 3413–3430. doi: 10.1016/j.gca.2008.05.001

Rouxel, O. J., Bekker, A., and Edwards, K. J. (2005). Iron isotope constraints on the Archean and Paleoproterozoic ocean redox state. *Science* 307, 1088–1091. doi: 10.1126/science.1105692

Saito, M. A., Noble, A. E., Tagliabue, A., Goepfert, T. J., Lamborg, C. H., and Jenkins, W. J. (2013). Slow-spreading submarine ridges in the South Atlantic as a significant oceanic iron source. *Nat. Geosci.* 6, 775–779. doi: 10.1038/ngeo1893

Santelli, C. M., Orcutt, B. N., Benning, E., Bach, W., Moyer, C. L., Sogin, M. L., et al. (2008). Abundance and diversity of microbial life in ocean crust. *Nature* 453, 653–657. doi: 10.1038/nature06899

Schrenk, M. O., Kelley, D. S., Delaney, J. R., and Baross, J. A. (2003). Incidence and diversity of microorganisms within the walls of an active deep-sea sulfide chimney. *Appl. Environ. Microbiol.* 69, 3580–3592. doi: 10.1128/AEM.69.6.3580-3592.2003

Severmann, S., Johnson, C. M., Beard, B. L., German, C. R., Edmonds, H. N., Chiba, H., et al. (2004). The effect of plume processes on the Fe isotope composition of hydrothermally derived Fe in the deep ocean as inferred from the Rainbow vent site, Mid-Atlantic Ridge, 36 degrees 14' N. *Earth Planet. Sci. Lett.* 225, 63–76. doi: 10.1016/j.epsl.2004.06.001

Severmann, S., Johnson, C. M., Beard, B. L., and McManus, J. (2006). The effect of early diagenesis on the Fe isotope compositions of porewaters and authigenic minerals in continental margin sediments. *Geochim. Cosmochim. Acta* 70, 2006–2022. doi: 10.1016/j.gca.2006.01.007

Sharma, M., Polizzotto, M., and Anbar, A. D. (2001). Iron isotopes in hot springs along the Juan de Fuca Ridge. *Earth Planet. Sci. Lett.* 194, 39–51. doi: 10.1016/S0012-821X(01)00538-6

Slobodkin, A., Campbell, B., Cary, S. C., Bonch-Osmolovskaya, E., and Jeanthon, C. (2001). Evidence for the presence of thermophilic Fe(III)-reducing microorganisms in deep-sea hydrothermal vents at 13°N (East Pacific Rise). *FEMs Microbiol. Ecol.* 36, 235–243. doi: 10.1016/s0168-6496(01)00138-6

Stein, C., and Stein, S. (1994). Constraints on hydrothermal Heat-Flux through the oceanic lithosphere from global heat-flow. *J. Geophys. Res.* 99, 3081–3095. doi: 10.1029/93JB02222

Swanner, E. D., Wu, W., Schoenberg, R., Byrne, J., Michel, F. M., Pan, Y., et al. (2015). Fractionation of Fe isotopes during Fe(II) oxidation by a marine photoferrotroph is controlled by the formation of organic Fe-complexes and colloidal Fe fractions. *Geochim. Cosmochim. Acta* 165, 44–61. doi: 10.1016/j.gca.2015.05.024

Sylvan, J. B., Toner, B. M., and Edwards, K. J. (2012). Life and death of deep-sea vents: bacterial diversity and ecosystem succession on inactive hydrothermal sulfides. *MBio* 3, 1–12. doi: 10.1128/mBio.00279-11

Takai, K., Nunoura, T., Ishibashi, J. I., Lupton, J., Suzuki, R., Hamasaki, H., et al. (2008). Variability in the microbial communities and hydrothermal fluid chemistry at the newly discovered Mariner hydrothermal field, southern Lau Basin. *J. Geophys. Res.* 113:G02031. doi: 10.1029/2007JG000636

Tamura, N., Celestre, R. S., MacDowell, A. A., Padmore, H. A., Spolenak, R., Valek, B. C., et al. (2002). Submicron x-ray diffraction and its application to problems in materials and environmental science. *Rev. Sci. Instrum.* 73, 1369–1372. doi: 10.1063/1.1436539

Tamura, N., MacDowell, A. A., Spolenak, R., Valek, B. C., Bravman, J. C., Brown, W. L., et al. (2003). Scanning X-ray Microdiffraction with submicron white beam for strain/stress and orientation mapping in thin films. *J. Synchrotron Radiat.* 10, 137–143. doi: 10.1107/S0909049502021362

Templeton, A. S., Knowles, E. J., Eldridge, D. L., Arey, B. W., Dohnalkova, A. C., Webb, S. M., et al. (2009). A seafloor microbial biome hosted within incipient ferromanganese crusts. *Nat. Geosci.* 2, 872–876. doi: 10.1038/ngeo696

Tivey, M. K. (1995). The influence of hydrothermal fluid composition and advection rates on black smoker chimney mineralogy: insights from modeling

transport and reaction. *Geochim. Cosmochim. Acta* 59, 1933–1949. doi: 10.1016/0016-7037(95)00118-2

Tivey, M. K. (2007). Generation of Seafloor Hydrothermal Vent Fluids and Associated Mineral Deposits. *Oceanography* 20, 50–65. doi: 10.5670/oceanog.2007.80

Toner, B., Manceau, A., Webb, S. M., and Sposito, G. (2006). Zinc sorption to biogenic hexagonal-birnessite particles within a hydrated bacterial biofilm. *Geochim. Cosmochim. Acta* 70, 27–43. doi: 10.1016/j.gca.2005.08.029

Toner, B. M., Berquo, T. S., Michel, F. M., Sorensen, J. V., Templeton, A. S., and Edwards, K. J. (2012). Mineralogy of iron microbial mats from Loihi Seamount. *Front. Microbiol. Chem.* 3:118. doi: 10.3389/fmicb.2012.00118

Toner, B. M., Fakra, S. C., Manganini, S. J., Santelli, C. M., Marcus, M. A., Moffett, J. W., et al. (2009a). Preservation of iron(II) by carbon-rich matrices in a hydrothermal plume. *Nat. Geosci.* 2, 197–201. doi: 10.1038/ngeo433

Toner, B. M., Lesniewski, R. A., Marlow, J. J., Briscoe, L. J., Santelli, C. M., Bach, W., et al. (2013). Mineralogy drives bacterial biogeography of hydrothermally inactive seafloor sulfide deposits. *Geomicrobiol. J.* 30, 313–326. doi: 10.1080/01490451.2012.688925

Toner, B. M., Santelli, C. M., Marcus, M. A., Wirth, R., Chan, C. S., McCollom, T. M., et al. (2009b). Biogenic iron oxyhydroxide formation at Mid-Ocean Ridge hydrothermal vents: juan de Fuca Ridge. *Geochim. Cosmochim. Acta* 73, 388–403. doi: 10.1016/j.gca.2008.09.035

Webb, S. M. (2005). SIXPACK: a graphical user interface for XAS analysis using IFEFFIT. *Phys. Scr.* T115, 1011–1014. doi: 10.1238/Physica.Topical.115a01011

Welch, S. A., Beard, B. L., Johnson, C. M., and Braterman, P. S. (2003). Kinetic and equilibrium Fe isotope fractionation between aqueous Fe(II) and Fe(III). *Geochim. Cosmochim. Acta* 67, 4231–4250. doi: 10.1016/S0016-7037(03)00266-7

Wheat, C. G., Jannasch, H. W., Plant, J. N., Moyer, C. L., Sansone, F. J., and McMurtry, G. M. (2000). Continuous sampling of hydrothermal fluids from Loihi Seamount after the 1996 event. *J. Geophys. Res. Earth* 105, 19353–19367. doi: 10.1029/2000JB900088

Wheat, C. G., Mottl, M. J., Fisher, A. T., Kadko, D., Davis, E. E., and Baker, E. (2004). Heat flow through a basaltic outcrop on a sedimented young ridge flank. *Geochem. Geophys. Geosyst.* 5:Q12006. doi: 10.1029/2004GC000700

Wu, L. L., Druschel, G., Findlay, A., Beard, B. L., and Johnson, C. M. (2012). Experimental determination of iron isotope fractionations among Fe-aq(2+)-FeSaq-Mackinawite at low temperatures: implications for the rock record. *Geochim. Cosmochim. Acta* 89, 46–61. doi: 10.1016/j.gca.2012.04.047

Xu, Q. D., and Scott, S. D. (2005). "Spherulitic pyrite in seafloor hydrothermal deposits: products of rapid crystallization from mixing fluids," in *Mineral Deposit Research Meeting the Global Challenge*, eds J. Mao and F. P. Bierlein (Berlin: Springer), 711–713.

Yamamoto, M., and Takai, K. (2011). Sulfur metabolisms in epsilon-and gamma-proteobacteria in deep-sea hydrothermal fields. *Front. Microbiol.* 2:192. doi: 10.3389/fmicb.2011.00192

Yucel, M., Gartman, A., Chan, C. S., and George, W., Luther, I. I. I. (2011). Hydrothermal vents as a kinetically stable source of iron-sulphide-bearing nanoparticles to the ocean. *Nat. Geosci.* 4, 367–371. doi: 10.1038/ngeo1148

Conflict of Interest Statement: The authors declare that the research was conducted in the absence of any commercial or financial relationships that could be construed as a potential conflict of interest.

Advantages of publishing in Frontiers

OPEN ACCESS
Articles are free to read, for greatest visibility

COLLABORATIVE PEER-REVIEW
Designed to be rigorous – yet also collaborative, fair and constructive

FAST PUBLICATION
Average 85 days from submission to publication (across all journals)

COPYRIGHT TO AUTHORS
No limit to article distribution and re-use

TRANSPARENT
Editors and reviewers acknowledged by name on published articles

SUPPORT
By our Swiss-based editorial team

IMPACT METRICS
Advanced metrics track your article's impact

GLOBAL SPREAD
5'100'000+ monthly article views and downloads

LOOP RESEARCH NETWORK
Our network increases readership for your article

Frontiers
EPFL Innovation Park, Building I • 1015 Lausanne • Switzerland
Tel +41 21 510 17 00 • Fax +41 21 510 17 01 • info@frontiersin.org
www.frontiersin.org

Find us on